

Bibliography of Lewis Research Center Technical Publications Announced in 1988

July 1989



NASA-102034-1
LEWIS RESEARCH CENTER
TECHNICAL PUBLICATIONS
ANNOUNCED IN 1988 (NASA) 771 000 000

10-1-77

unc125

02/02 0227052

**Bibliography of
Lewis Research Center
Technical Publications
Announced in 1988**



National Aeronautics and
Space Administration

Lewis Research Center
Cleveland, Ohio 44135

PREFACE

Editor's Note: *The Lewis Technical Publications Bibliography was first published in 1965 and has been published annually since 1976. The Bibliography is one of George Mandel's innovations—conceived and brought into being through his leadership, ideas, and dedication. George Mandel believed in the importance of the work being done at Lewis Research Center and wanted the knowledge gained through this research to be shared. He was proud to acknowledge and announce NASA Lewis publications and inventions, and was pleased to make these accomplishments accessible so that they could benefit others. This publication was about to go to print at the time of Mr. Mandel's untimely death in July 1989.*

In 1988, Lewis Research Center's 1216 research authors published 538 technical publications that were announced to and reached the worldwide scientific community. This was our highest number of technical publications in 16 years and a 10-percent increase over last year's high production of 493. The 538 papers included 252 symposium/seminar presentations and 77 articles sent directly to journals for publication. The number of seminar presentations was the highest in Lewis history (243 in 1987 and 226 in 1984), while the number of journal articles was the second highest in Lewis history (82 in 1986). Two other Center records were broken this year: there were 82 Lewis-hosted conference papers and 9 Lewis-authored theses.

In 1988, Lewis authors published approximately 61 percent of their research contributions in outside publications and the remainder as NASA research reports. Sixty-six percent of Lewis-authored society presentations and journal articles were addressed to members of the following ten technical societies: AIAA, 108 papers; ASME, 96 papers; SAE, 56 papers; IEEE, 34 papers; ASEE (American Society of Engineering Education), 30 papers; ACS (American Chemical Society), 26 papers; AIChE, 22 papers; ANS (American Nuclear Society), 20 papers; ACerS (American Ceramic Society), 16 papers; and ASM (American Society for Metals), 15 papers.

In 1988, 189 contractor-authored research reports were produced. In addition, nine patent applications were filed and seven patents were issued.

Lewis hosted eight research conferences and workshops in 1988. Five of these resulted in NASA Conference Publications, including

- NASA CP-10016, Free-Space Power Transmission, March 29-30
- NASA CP-3030, Space Photovoltaic Research and Technology (1988), April 19-21
- NASA CP-10018, Lunar Helium-3 and Fusion Power, April 25-26
- NASA CP-3003, Lewis Structures Technology—1988, May 24-25
- NASA CP-10025, HITEMP Review—1988, November 9-10

One of these conference publications was published at Lewis and made available to the attendees when they registered at the conference: the three-volume set of Lewis Structures Technology—1988. Other conferences and workshops hosted by Lewis in 1988 included

- NASA High Speed Civil Transport (HSCT) Community Noise Workshop, June 28-29
- Microgravity Materials Science Laboratory Workshop, September 7-8
- Oxidation of High-Temperature Intermetallics Workshop, September 22-23

In addition, the proceedings of one off-site workshop was published by Lewis:

- NASA CP-3026, Rotordynamic Instability Problems in High-Performance Turbomachinery—1988, May 16-18

Partly because of the dramatic increases in the number of technical publications and disclosures of inventions in 1988, Lewis was recently designated as a Quality Improvement Prototype by the Office of Management and Budget. Many Lewis authors and inventors have received awards for these contributions; among them are the following:

The 1988 Lewis Distinguished Paper Award was presented to C.F. Lorenzo, F.P. Chiaramonte, and C.M. Mehlic for their paper entitled "Determination of Compressor In-Stall Characteristics from Engine Surge Transients." ASME gave their 50th anniversary award of the Heat Transfer Division to Robert Graham, and AIAA gave their 1988 Wyld Propulsion Award to David Byers. (Byers has authored over 40 technical reports on space propulsion.) Hal Sliney received the Space Act Award for his invention of PS 200, which was patented this year, and R&D 100 Awards from Research & Development magazine were given for the development of the long-cycle-life nickel-hydrogen cell/battery and for the microprocessor-based system to detect and accommodate sensor failure.

The 1987 Robert J. Collier Trophy was awarded to Lewis and the NASA/Industry Advanced Turboprop (ATP) team this year, and the chief of the ATP Office, Keith Sievers, was named Northern Ohio Engineer of the Year. In addition, the Communications Technology Satellite (CTS) team received an Emmy award for developing the technology that improved television broadcasting throughout the world.

A few Lewis-authored publications are not included in this compilation because of FEDD (For Early Domestic Dissemination) and ITAR (International Traffic in Arms Regulations) considerations which limit their announcement and distribution.

All the publications in this collection were announced in the 1988 issues of STAR (Scientific and Technical Aerospace Reports) and IAA (International Aerospace Abstracts). Some 1988 publications will be announced in the 1989 issues of STAR and IAA and will thus appear in the 1989 Lewis Bibliography.

The arrangement of the material is by NASA subject category, as noted in the Contents. The various indexes will help locate specific publications by subject, author, contractor organization, contract number, and report number.

George Mandel
Chief, Technical Information Services Division

TABLE OF CONTENTS

PREFACE

i

AERONAUTICS

Includes aeronautics (general); aerodynamics; air transportation and safety; aircraft communications and navigation; aircraft design, testing and performance; aircraft instrumentation; aircraft propulsion and power; aircraft stability and control; and research and support facilities (air).

For related information see also *Astronautics*.

01 AERONAUTICS (GENERAL) 1

02 AERODYNAMICS 2

Includes aerodynamics of bodies, combinations, wings, rotors, and control surfaces; and internal flow in ducts and turbomachinery.

For related information see also *34 Fluid Mechanics and Heat Transfer*.

03 AIR TRANSPORTATION AND SAFETY 14

Includes passenger and cargo air transport operations; and aircraft accidents.

For related information see also *16 Space Transportation* and *85 Urban Technology and Transportation*.

04 AIRCRAFT COMMUNICATIONS AND NAVIGATION N.A.

Includes digital and voice communication with aircraft; air navigation systems (satellite and ground based); and air traffic control.

For related information see also *17 Space Communications, Spacecraft Communications, Command and Tracking* and *32 Communications and Radar*.

05 AIRCRAFT DESIGN, TESTING AND PERFORMANCE 16

Includes aircraft simulation technology.

For related information see also *18 Spacecraft Design, Testing and Performance* and *39 Structural Mechanics*. For land transportation vehicles see *85 Urban Technology and Transportation*.

06 AIRCRAFT INSTRUMENTATION 18

Includes cockpit and cabin display devices; and flight instruments.

For related information see also *19 Spacecraft Instrumentation* and *35 Instrumentation and Photography*.

07 AIRCRAFT PROPULSION AND POWER 18

Includes prime propulsion systems and systems components, e.g., gas turbine engines and compressors; and onboard auxiliary power plants for aircraft.

For related information see also *20 Spacecraft Propulsion and Power*, *28 Propellants and Fuels*, and *44 Energy Production and Conversion*.

08 AIRCRAFT STABILITY AND CONTROL 37

Includes aircraft handling qualities; piloting; flight controls; and autopilots.

For related information see also *05 Aircraft Design, Testing and Performance*.

09 RESEARCH AND SUPPORT FACILITIES (AIR) 39

Includes airports, hangars and runways; aircraft repair and overhaul facilities; wind tunnels; shock tubes; and aircraft engine test stands.

For related information see also *14 Ground Support Systems and Facilities (Space)*.

ASTRONAUTICS

Includes astronautics (general); astrodynamics; ground support systems and facilities (space); launch vehicles and space vehicles; space transportation; space communications, spacecraft communications, command and tracking; spacecraft design, testing and performance; spacecraft instrumentation; and spacecraft propulsion and power.

For related information see also *Aeronautics*.

12 ASTRONAUTICS (GENERAL) 41

For extraterrestrial exploration see *91 Lunar and Planetary Exploration*.

13 ASTRODYNAMICS 42

Includes powered and free-flight trajectories; and orbital and launching dynamics.

14 GROUND SUPPORT SYSTEMS AND FACILITIES (SPACE) 42

Includes launch complexes, research and production facilities; ground support equipment, e.g., mobile transporters; and simulators.

For related information see also *09 Research and Support Facilities (Air)*.

15 LAUNCH VEHICLES AND SPACE VEHICLES 44

Includes boosters; operating problems of launch/space vehicle systems; and reusable vehicles.

For related information see also *20 Spacecraft Propulsion and Power*.

16 SPACE TRANSPORTATION 44

Includes passenger and cargo space transportation, e.g., shuttle operations; and space rescue techniques.

For related information see also *03 Air Transportation and Safety* and *18 Spacecraft Design, Testing and Performance*. For space suits see *54 Man/System Technology and Life Support*.

17 SPACE COMMUNICATIONS, SPACECRAFT COMMUNICATIONS, COMMAND AND TRACKING 45

Includes telemetry; space communications networks; astronavigation and guidance; and radio blackout.

For related information see also *04 Aircraft Communications and Navigation* and *32 Communications and Radar*.

18 SPACECRAFT DESIGN, TESTING AND PERFORMANCE 46

Includes satellites; space platforms; space stations; spacecraft systems and components such as thermal and environmental controls; and attitude controls.

For life support systems see *54 Man/System Technology and Life Support*. For related information see also *05 Aircraft Design, Testing and Performance*, *39 Structural Mechanics*, and *16 Space Transportation*.

19 SPACECRAFT INSTRUMENTATION N.A.

For related information see also *06 Aircraft Instrumentation* and *35 Instrumentation and Photography*.

20 SPACECRAFT PROPULSION AND POWER 50

Includes main propulsion systems and components, e.g. rocket engines; and spacecraft auxiliary power sources.

For related information see also *07 Aircraft Propulsion and Power*, *28 Propellants and Fuels*, *44 Energy Production and Conversion*, and *15 Launch Vehicles and Space Vehicles*.

CHEMISTRY AND MATERIALS

Includes chemistry and materials (general); composite materials; inorganic and physical chemistry; metallic materials; nonmetallic materials; propellants and fuels; and materials processing.

23 CHEMISTRY AND MATERIALS (GENERAL) 68

24 COMPOSITE MATERIALS 69

Includes physical, chemical, and mechanical properties of laminates and other composite materials.

For ceramic materials see *27 Nonmetallic Materials*.

25 INORGANIC AND PHYSICAL CHEMISTRY 77

Includes chemical analysis, e.g., chromatography; combustion theory; electrochemistry; and photochemistry.

For related information see also *77 Thermodynamics and Statistical Physics*.

26 METALLIC MATERIALS 81

Includes physical, chemical, and mechanical properties of metals, e.g., corrosion; and metallurgy.

27 NONMETALLIC MATERIALS 95

Includes physical, chemical, and mechanical properties of plastics, elastomers, lubricants, polymers, textiles, adhesives, and ceramic materials.

For composite materials see *24 Composite Materials*.

28 PROPELLANTS AND FUELS 108

Includes rocket propellants, igniters and oxidizers; their storage and handling procedures; and aircraft fuels.

For related information see also *07 Aircraft Propulsion and Power*, *20 Spacecraft Propulsion and Power*, and *44 Energy Production and Conversion*.

29 MATERIALS PROCESSING 109

Includes space-based development of products and processes for commercial application.

For biological materials see *55 Space Biology*.

ENGINEERING

Includes engineering (general); communications and radar; electronics and electrical engineering; fluid mechanics and heat transfer; instrumentation and photography; lasers and masers; mechanical engineering; quality assurance and reliability; and structural mechanics.

For related information see also *Physics*.

31 ENGINEERING (GENERAL) 114

Includes vacuum technology; control engineering; display engineering; cryogenics; and fire prevention.

32 COMMUNICATIONS AND RADAR 115

Includes radar; land and global communications; communications theory; and optical communications.

For related information see also *04 Aircraft Communications and Navigation* and *17 Space Communications, Spacecraft Communications, Command and Tracking*. For search and rescue see *03 Air Transportation and Safety*, and *16 Space Transportation*.

33 ELECTRONICS AND ELECTRICAL ENGINEERING 121

Includes test equipment and maintainability; components, e.g., tunnel diodes and transistors; microminiaturization; and integrated circuitry.

For related information see also *60 Computer Operations and Hardware* and *76 Solid-State Physics*.

34 FLUID MECHANICS AND HEAT TRANSFER 131

Includes boundary layers; hydrodynamics; fluidics; mass transfer and ablation cooling.

For related information see also *02 Aerodynamics* and *77 Thermodynamics and Statistical Physics*.

35 INSTRUMENTATION AND PHOTOGRAPHY 156

Includes remote sensors; measuring instruments and gages; detectors; cameras and photographic supplies; and holography.

For aerial photography see *43 Earth Resources and Remote Sensing*. For related information see also *06 Aircraft Instrumentation* and *19 Spacecraft Instrumentation*.

36 LASERS AND MASERS 164

Includes parametric amplifiers.

For related information see also *76 Solid-State Physics*.

37 MECHANICAL ENGINEERING 164

Includes auxiliary systems (nonpower); machine elements and processes; and mechanical equipment.

38 QUALITY ASSURANCE AND RELIABILITY 176

Includes product sampling procedures and techniques; and quality control.

39 STRUCTURAL MECHANICS 180

Includes structural element design and weight analysis; fatigue; and thermal stress.

For applications see *05 Aircraft Design, Testing and Performance* and *18 Spacecraft Design, Testing and Performance*.

GEOSCIENCES

Includes geosciences (general); earth resources and remote sensing; energy production and conversion; environment pollution; geophysics; meteorology and climatology; and oceanography.

For related information see also *Space Sciences*.

42 GEOSCIENCES (GENERAL) N.A.

43 EARTH RESOURCES AND REMOTE SENSING N.A.

Includes remote sensing of earth resources by aircraft and spacecraft; photogrammetry; and aerial photography.

For instrumentation see *35 Instrumentation and Photography*.

44 ENERGY PRODUCTION AND CONVERSION 196

Includes specific energy conversion systems, e.g., fuel cells; global sources of energy; geophysical conversion; and windpower.

For related information see also *07 Aircraft Propulsion and Power*, *20 Spacecraft Propulsion and Power*, and *28 Propellants and Fuels*.

45 ENVIRONMENT POLLUTION N.A.

Includes atmospheric, noise, thermal, and water pollution.

46 GEOPHYSICS 204

Includes aeronomy; upper and lower atmosphere studies; ionospheric and magnetospheric physics; and geomagnetism.

For space radiation see *93 Space Radiation*.

47 METEOROLOGY AND CLIMATOLOGY N.A.

Includes weather forecasting and modification.

48 OCEANOGRAPHY N.A.

Includes biological, dynamic, and physical oceanography; and marine resources.

For related information see also *43 Earth Resources and Remote Sensing*.

LIFE SCIENCES

Includes life sciences (general); aerospace medicine; behavioral sciences; man/system technology and life support; and space biology.

51 LIFE SCIENCES (GENERAL) N.A.

52 AEROSPACE MEDICINE N.A.

Includes physiological factors; biological effects of radiation; and effects of weightlessness on man and animals.

53 BEHAVIORAL SCIENCES N.A.

Includes psychological factors; individual and group behavior; crew training and evaluation; and psychiatric research.

54 MAN/SYSTEM TECHNOLOGY AND LIFE SUPPORT 204

Includes human engineering; biotechnology; and space suits and protective clothing.

For related information see also *16 Space Transportation*.

55 SPACE BIOLOGY N.A.

Includes exobiology; planetary biology; and extraterrestrial life.

MATHEMATICAL AND COMPUTER SCIENCES

Includes mathematical and computer sciences (general); computer operations and hardware; computer programming and software; computer systems; cybernetics; numerical analysis; statistics and probability; systems analysis; and theoretical mathematics.

59 MATHEMATICAL AND COMPUTER SCIENCES (GENERAL) 204

60 COMPUTER OPERATIONS AND HARDWARE 205

Includes hardware for computer graphics, firmware, and data processing.

For components see *33 Electronics and Electrical Engineering*.

61 COMPUTER PROGRAMMING AND SOFTWARE 205

Includes computer programs, routines, algorithms, and specific applications, e.g., CAD/CAM.

62 COMPUTER SYSTEMS 208

Includes computer networks and special application computer systems.

63 CYBERNETICS 208

Includes feedback and control theory, artificial intelligence, robotics and expert systems.

For related information see also *54 Man/System Technology and Life Support*.

64 NUMERICAL ANALYSIS 209

Includes iteration, difference equations, and numerical approximation.

65 STATISTICS AND PROBABILITY N.A.

Includes data sampling and smoothing; Monte Carlo method; and stochastic processes.

66 SYSTEMS ANALYSIS 212

Includes mathematical modeling; network analysis; and operations research.

67 THEORETICAL MATHEMATICS N.A.

Includes topology and number theory.

PHYSICS

Includes physics (general); acoustics; atomic and molecular physics; nuclear and high-energy physics; optics; plasma physics; solid-state physics; and thermodynamics and statistical physics.

For related information see also *Engineering*.

70 PHYSICS (GENERAL) 212

For precision time and time interval (PTTI) see *35 Instrumentation and Photography*; for geophysics, astrophysics or solar physics see *46 Geophysics*, *90 Astrophysics*, or *92 Solar Physics*.

- 71 ACOUSTICS** **213**
Includes sound generation, transmission, and attenuation.
For noise pollution see *45 Environment Pollution*.
- 72 ATOMIC AND MOLECULAR PHYSICS** **N.A.**
Includes atomic structure, electron properties, and molecular spectra.
- 73 NUCLEAR AND HIGH-ENERGY PHYSICS** **217**
Includes elementary and nuclear particles; and reactor theory.
For space radiation see *93 Space Radiation*.
- 74 OPTICS** **217**
Includes light phenomena and optical devices.
For lasers see *36 Lasers and Masers*.
- 75 PLASMA PHYSICS** **218**
Includes magnetohydrodynamics and plasma fusion.
For ionospheric plasmas see *46 Geophysics*. For space plasmas see *90 Astrophysics*.
- 76 SOLID-STATE PHYSICS** **219**
Includes superconductivity.
For related information see also *33 Electronics and Electrical Engineering* and *36 Lasers and Masers*.
- 77 THERMODYNAMICS AND STATISTICAL PHYSICS** **222**
Includes quantum mechanics; theoretical physics; and Bose and Fermi statistics.
For related information see also *25 Inorganic and Physical Chemistry* and *34 Fluid Mechanics and Heat Transfer*.
- SOCIAL SCIENCES**
Includes social sciences (general); administration and management; documentation and information science; economics and cost analysis; law, political science, and space policy; and urban technology and transportation.
- 80 SOCIAL SCIENCES (GENERAL)** **N.A.**
Includes educational matters.
- 81 ADMINISTRATION AND MANAGEMENT** **223**
Includes management planning and research.
- 82 DOCUMENTATION AND INFORMATION SCIENCE** **223**
Includes information management; information storage and retrieval technology; technical writing; graphic arts; and micrography.
For computer documentation see *61 Computer Programming and Software*.
- 83 ECONOMICS AND COST ANALYSIS** **N.A.**
Includes cost effectiveness studies.

- 84 LAW, POLITICAL SCIENCE AND SPACE POLICY** **N.A.**
Includes NASA appropriation hearings; aviation law; space law and policy; international law; international cooperation; and patent policy.

- 85 URBAN TECHNOLOGY AND TRANSPORTATION** **223**
Includes applications of space technology to urban problems; technology transfer; technology assessment; and surface and mass transportation.
For related information see *03 Air Transportation and Safety*, *16 Space Transportation*, and *44 Energy Production and Conversion*.

SPACE SCIENCES

Includes space sciences (general); astronomy; astrophysics; lunar and planetary exploration; solar physics; and space radiation.
For related information see also *Geosciences*.

- 88 SPACE SCIENCES (GENERAL)** **225**

- 89 ASTRONOMY** **N.A.**
Includes radio, gamma-ray, and infrared astronomy; and astrometry.

- 90 ASTROPHYSICS** **225**
Includes cosmology; celestial mechanics; space plasmas; and interstellar and interplanetary gases and dust.
For related information see also *75 Plasma Physics*.

- 91 LUNAR AND PLANETARY EXPLORATION** **226**
Includes planetology; and manned and unmanned flights.
For spacecraft design or space stations see *18 Spacecraft Design, Testing and Performance*.

- 92 SOLAR PHYSICS** **N.A.**
Includes solar activity, solar flares, solar radiation and sunspots.
For related information see *93 Space Radiation*.

- 93 SPACE RADIATION** **227**
Includes cosmic radiation; and inner and outer earth's radiation belts.
For biological effects of radiation see *52 Aerospace Medicine*. For theory see *73 Nuclear and High-Energy Physics*.

GENERAL

Includes aeronautical, astronautical, and space science related histories, biographies, and pertinent reports too broad for categorization; histories or broad overviews of NASA programs.

- 99 GENERAL** **227**

Note: N.A. means that no abstracts were assigned to this category for this issue.

SUBJECT INDEX	A-1
PERSONAL AUTHOR INDEX	B-1
CORPORATE SOURCE INDEX	C-1
CONTRACT NUMBER INDEX	D-1
REPORT/ACCESSION NUMBER INDEX	E-1

Bibliography of Lewis Research Center Technical Publications Announced in 1988

01

AERONAUTICS (GENERAL)

A88-16749*# National Aeronautics and Space Administration. Langley Research Center, Hampton, VA.

RETOOLING CFD FOR HYPERSONIC AIRCRAFT

DOUGLAS L. DWOYER (NASA, Langley Research Center, Hampton, VA), PAUL KUTLER (NASA, Ames Research Center, Moffett Field, CA), and LOUIS A. POVINELLI (NASA, Lewis Research Center, Cleveland, OH) Aerospace America (ISSN 0740-722X), vol. 25, Oct. 1987, p. 32-35, 41.

The CFD facility requirements of hypersonic aircraft configuration design development are different from those thus far employed for reentry vehicle design, because (1) the airframe and the propulsion system must be fully integrated to achieve the desired performance; (2) the vehicle must be reusable, with minimum refurbishment requirements between flights; and (3) vehicle performance must be optimized for a wide range of Mach numbers. An evaluation is presently made of flow resolution within shock waves, transition and turbulence phenomenon tractability, chemical reaction modeling, and hypersonic boundary layer transition, with state-of-the-art CFD. O.C.

N88-21116*# National Aeronautics and Space Administration. Lewis Research Center, Cleveland, OH.

NUMERICAL ANALYSIS OF THREE-DIMENSIONAL VISCOUS INTERNAL FLOWS

RODRICK V. CHIMA and JEFFREY W. YOKOTA (Sverdrup Technology, Inc., Cleveland, Ohio.) 1988 10 p Proposed for presentation at the 1st National Fluid Dynamics Congress, Cincinnati, Ohio, 24-28 Jul. 1988; sponsored by AIAA, ASME, ASCE, SIAM and APS

(NASA-TM-100878; E-4112; NAS 1.15:100878) Avail: NTIS HC A02/MF A01 CSCL 01B

A 3-D Navier-Stokes code has been developed for analysis of turbomachinery blade rows and other internal flows. The Navier-Stokes equations are written in a Cartesian coordinate system rotating about the x-axis, and then mapped to a general body-fitted coordinate system. Streamwise viscous terms are neglected using the thin-layer assumption, and turbulence effects are modeled using the Baldwin-Lomax turbulence model. The equations are discretized using finite differences on stacked C-type grids and are solved using a multistage Runge-Kutta algorithm with a spatially-varying time step and implicit residual smoothing. Calculations have been made of a horseshoe vortex formed in front of a flat plate with a round leading edge standing in a turbulent endwall boundary layer. Comparisons are made with experimental data taken by Eckerle and Langston for a circular cylinder under similar conditions. Computer and measured results are compared in terms of endwall flow visualization pictures and total pressure loss contours and vector plots on the symmetry plane. Calculated details of the primary vortex show excellent agreement with the experimental data. The calculations also show a small secondary vortex not seen experimentally. Author

N88-23729*# National Aeronautics and Space Administration. Lewis Research Center, Cleveland, OH.

A NUMERICAL STUDY OF THE HOT GAS ENVIRONMENT AROUND A STOVL AIRCRAFT IN GROUND PROXIMITY

THOMAS J. VANOVERBEKE and JAMES D. HOLDEMAN 1988 28 p Prepared for presentation at the 24th Joint Propulsion Conference, Boston, Mass., 11-13 Jul. 1988; sponsored in part by AIAA, ASME, SAE, and ASEE (NASA-TM-100895; E-4138; NAS 1.15:100895; AIAA-88-2882) Avail: NTIS HC A03/MF A01 CSCL 01B

The development of Short Takeoff Vertical Landing (STOVL) aircraft has historically been an empirical- and experience-based technology. In this study, a 3-D turbulent flow CFD code was used to calculate the hot gas environment around an STOVL aircraft operating in ground proximity. Preliminary calculations are reported for a typical STOVL aircraft configuration to identify key features of the flow field, and to demonstrate and assess the capability of current 3-D CFD codes to calculate the temperature of the gases ingested at the engine inlet as a function of flow and geometric conditions. Author

N88-26328*# National Aeronautics and Space Administration. Lewis Research Center, Cleveland, OH.

FIBER OPTICS FOR ADVANCED AIRCRAFT

ROBERT J. BAUMBICK 1988 13 p Presented at the Fiber Optics, Optoelectronics and Laser Applications International Symposium and Exhibition, Boston, Mass., 6-9 Sep. 1988; sponsored by the Society of Photo-Optical Instrumentation Engineers

(NASA-TM-101294; E-4276; NAS 1.15:101294) Avail: NTIS HC A03/MF A01 CSCL 01B

The increased use of composites makes the digital control more susceptible to electromagnetic effects. In order to provide the protection to the digital control additional shielding will be required as well as protective circuitry for the electronics. This results in increased weight and reduced reliability. The advantages that fiber optic technology provides for advanced aircraft applications is recognized. The use of optical signals to carry information between the aircraft and the control module provides immunity from contamination by electromagnetic sources as well as other important benefits such as reduced weight and volume resulting from the elimination of the shielding and the replacement of metal conductors with low weight glass fibers. In 1975 NASA began work to develop passive optical sensors for use with fiber optics in aircraft control systems. The problem now is to choose the best optical sensor concepts and evaluate them for use. In 1985 NASA and DOD entered into a joint program, Fiber Optic Control System Integration (FOCSI), to look at optical technology specifically for use in advanced aircraft systems. The results of this program are discussed. The conclusion of the study indicated that the use of fiber optic technology in advanced aircraft systems is feasible and desirable. The study pointed to a lack of available sensors from vendors capable of operating in the adverse environments of advanced aircraft. Author

02 AERODYNAMICS

02

AERODYNAMICS

Includes aerodynamics of bodies, combinations, wings, rotors, and control surfaces; and internal flow in ducts and turbomachinery.

A88-10355*# National Aeronautics and Space Administration. Lewis Research Center, Cleveland, OH.
EXPLICIT MULTIGRID ALGORITHM FOR QUASI-THREE-DIMENSIONAL VISCOUS FLOWS IN TURBOMACHINERY

RODRICK V. CHIMA (NASA, Lewis Research Center, Cleveland, OH) Journal of Propulsion and Power (ISSN 0748-4658), vol. 3, Sept.-Oct. 1987, p. 397-405. Previously cited in issue 07, p. 828, Accession no. A86-19644. refs

A88-10369*# National Aeronautics and Space Administration. Langley Research Center, Hampton, VA.

GROUND TESTS CONFIRM THE PROMISE OF HYPERSONIC PROPULSION

GRIFFIN Y. ANDERSON (NASA, Langley Research Center, Hampton, VA), DANIEL P. BENCZE (NASA, Ames Research Center, Moffett Field, CA), and BOBBY W. SANDERS (NASA, Lewis Research Center, Cleveland, OH) Aerospace America (ISSN 0740-722X), vol. 25, Sept. 1987, p. 38-42.

The feasibility of developing a hypersonic hydrogen-fueled airbreathing vehicle capable of Mach 8 is examined. A modular dual-mode scramjet concept integrated with the airframe has been proposed. The research involved in the formation of this design is discussed. Particular attention is given to studies concerned with airframe integration; the evaluation of hypersonic inlets; and the analysis of viscous phenomena. The injector and combustor configurations of the modular engine, which is designed to operate as a ramjet and scramjet, are analyzed. The engine thrust performance of subscale engine modules was tested, and positive results were obtained. Simulation testing of a full-size model is being planned. I.F.

A88-10970*# National Aeronautics and Space Administration. Lewis Research Center, Cleveland, OH.

CHORDWISE PRESSURE MEASUREMENTS ON A BLADE OF MOD-2 WIND TURBINE

T. W. NYLAND (NASA, Lewis Research Center, Cleveland, OH) IN: Energy-Sources Technology Conference and Exhibition, Dallas, TX, Feb. 15-18, 1987, Proceedings. New York, American Society of Mechanical Engineers, 1987, p. 33-40.

Pressure measurements covering a range of wind velocities were made at one span location on a blade of the Mod-2 Wind Turbine. The data show the existence of higher pressure coefficients than would be expected from wind tunnel data. These high pressure coefficients may be the result of three-dimensional flow over the blade that delays flow separations. Data is presented showing the repetitiveness and abrupt changes in the pressure distribution that occurs as the blade rotates. Calculated values of suction and flap coefficients are also presented. Author

A88-11072*# National Aeronautics and Space Administration. Lewis Research Center, Cleveland, OH.

APPLICATION OF ADVANCED COMPUTATIONAL CODES IN THE DESIGN OF AN EXPERIMENT FOR A SUPERSONIC THROUGHFLOW FAN ROTOR

JERRY R. WOOD, JAMES F. SCHMIDT, RONALD J. STEINKE, RODRICK V. CHIMA, and WILLIAM G. KUNIK (NASA, Lewis Research Center, Cleveland, OH) ASME, International Gas Turbine Conference and Exhibition, 32nd, Anaheim, CA, May 31-June 4, 1987. 15 p. Previously announced in STAR as N87-22630. refs (ASME PAPER 87-GT-160)

Increased emphasis on sustained supersonic or hypersonic cruise has revived interest in the supersonic throughflow fan as a possible component in advanced propulsion systems. Use of a

fan that can operate with a supersonic inlet axial Mach number is attractive from the standpoint of reducing the inlet losses incurred in diffusing the flow from a supersonic flight Mach number to a subsonic one at the fan face. The design of the experiment using advanced computational codes to calculate the components required is described. The rotor was designed using existing turbomachinery design and analysis codes modified to handle fully supersonic axial flow through the rotor. A two-dimensional axisymmetric throughflow design code plus a blade element code were used to generate fan rotor velocity diagrams and blade shapes. A quasi-three-dimensional, thin shear layer Navier-Stokes code was used to assess the performance of the fan rotor blade shapes. The final design was stacked and checked for three-dimensional effects using a three-dimensional Euler code interactively coupled with a two-dimensional boundary layer code. The nozzle design in the expansion region was analyzed with a three-dimensional parabolized viscous code which corroborated the results from the Euler code. A translating supersonic diffuser was designed using these same codes. Author

A88-11121*# National Aeronautics and Space Administration. Lewis Research Center, Cleveland, OH.

A METHOD FOR CALCULATING TURBULENT BOUNDARY LAYERS AND LOSSES IN THE FLOW CHANNELS OF TURBOMACHINES

LAWRENCE F. SCHUMANN (NASA, Lewis Research Center; U.S. Army, Propulsion Directorate, Cleveland, OH) ASME, International Gas Turbine Conference and Exhibition, 32nd, Anaheim, CA, May 31-June 4, 1987. 10 p. Previously announced in STAR as N87-15944. refs (ASME PAPER 87-GT-225)

An interactive inviscid core flow-boundary layer method is presented for the calculation of turbomachine channel flows. For this method, a one-dimensional inviscid core flow is assumed. The end-wall and blade surface boundary layers are calculated using an integral entrainment method. The boundary layers are assumed to be collateral and thus are two-dimensional. The boundary layer equations are written in a streamline coordinate system. The streamwise velocity profiles are approximated by power law profiles. Compressibility is accounted for in the streamwise direction but not in the normal direction. Equations are derived for the special cases of conical and two-dimensional rectangular diffusers. For these cases, the assumptions of a one-dimensional core flow and collateral boundary layers are valid. Results using the method are compared with experiment and good quantitative agreement is obtained. Author

A88-11126*# Pratt and Whitney Aircraft, East Hartford, CT.
INTER AND INTRA BLADE ROW LASER VELOCIMETRY STUDIES OF GAS TURBINE COMPRESSOR FLOWS

M. CARLSON WILLIAMS (Pratt and Whitney, East Hartford, CT) ASME, International Gas Turbine Conference and Exhibition, 32nd, Anaheim, CA, May 31-June 4, 1987. 10 p. (Contract NAS3-20646) (ASME PAPER 87-GT-235)

The use of a two-component LDV to study the flow within gas turbine intrablade passages and air flow through multistage compressor rigs is investigated. The LDV, multistage compressor, and the data acquisition system employed in the experiments are described. The velocity magnitude and air angle as a function of rotor position were mapped; modulations in the multistage compressor data resulted in the application of spectral analysis techniques to identify and characterize the periodic fluctuations. It is noted that the two-component LDV is applicable to the characterization of the aerodynamics of flows. I.F.

A88-11186* National Aeronautics and Space Administration. Lewis Research Center, Cleveland, OH.

TRANSITION AND SEPARATION CONTROL ON A LOW-REYNOLDS NUMBER AIRFOIL

S. M. MANGALAM, A. BAR-SEVER (AS&M, Inc., Hampton, VA), K. B. M. Q. ZAMAN (NASA, Lewis Research Center, Cleveland, OH), and W. D. HARVEY (NASA, Langley Research Center,

Hampton, VA) IN: Aerodynamics at low Reynolds numbers Re greater than 10 to the 4th and less than 10 to the 6th; Proceedings of the International Conference, London, England, Oct. 15-18, 1986. Volume 1. London, Royal Aeronautical Society, 1986, p. 10.1-10.19. refs
(Contract NAS1-17670; NAS1-17683; NAS1-18235)

The major problem associated with the aerodynamic performance of airfoils at low Reynolds numbers is the presence of extensive laminar boundary-layer separation resulting in a large increase in pressure drag and a decrease in lift. The rapid deterioration in airfoil characteristics can be largely eliminated by artificially controlling the flow through the introduction of suitable disturbances in the boundary layer such that transition occurs ahead of the anticipated laminar separation. This paper presents the results of wind-tunnel tests conducted on a 10-cm model of LRN (1)-1007 airfoil with passive (roughness trips) and active (acoustic excitation) controls to trigger transition and suppress separation. Significant improvements in the aerodynamic characteristics of the airfoil were observed. Results of this study for a chord Reynolds number range of 40,000 to 250,000 are presented in this paper.

Author

A88-14155*# Dayton Univ., OH.
NUMERICAL SIMULATION OF SELF-SUSTAINED AND FORCED OSCILLATIONS IN JET SHEAR LAYERS

J. N. SCOTT (Dayton, University, OH) IN: Forum on Unsteady Flow Separation, Cincinnati, OH, June 14-17, 1987, Proceedings. New York, American Society of Mechanical Engineers, 1987, p. 123-130. refs
(Contract NAG3-526)

Excitation of axisymmetric jet shear layers has been investigated by solving the time-dependent compressible Navier-Stokes equations. MacCormack's explicit finite difference scheme is used in performing the computations on a CRAY X-MP computer. This work examines the influence of various means of excitation of the shear layer, to produce large scale vortex structures in such a manner that the mixing between two flows will be enhanced or diminished. While successful pressure excitation has been achieved in previous studies only limited success with temperature excitation at the inflow boundary has been accomplished. The current study focuses on the use of temperature excitation through the boundary layer immediately inside the jet lip. In order to achieve the required resolution significant grid refinement is necessary. The results of the computation with and without temperature excitation are analyzed and compared with results obtained using pressure excitation. The influence of amplitude and frequency on specific flow characteristics are also examined. The excitation frequency for both the temperature and pressure corresponds to a Strouhal number of .45 and the inflow jet Mach number is approximately .3. Author

A88-14459* National Aeronautics and Space Administration.
Lewis Research Center, Cleveland, OH.
EFFECT OF ACOUSTIC EXCITATION ON THE FLOW OVER A LOW-RE AIRFOIL

K. B. M. Q. ZAMAN (NASA, Lewis Research Center, Cleveland, OH), A. BAR-SEVER (NASA, Langley Research Center, Hampton, VA), and S. M. MANGALAM (NASA, Langley Research Center; AS & M, Inc., Hampton, VA) Journal of Fluid Mechanics (ISSN 0022-1120), vol. 182, Sept. 1987, p. 127-148. refs
(Contract NAS1-17670; NAS1-17683)

Wind-tunnel measurements of lift, drag, and wake velocity spectra were carried out under (tonal) acoustic excitation for a smooth airfoil in the chord-Reynolds-number $Re(c)$ range of 40,000-140,000. The data were supported by smoke-wire flow-visualization pictures. Small-amplitude excitation in a wide, low-frequency range is found to eliminate laminar separation that otherwise degrades the airfoil performance at low $Re(c)$ near the design angle of attack. Excitation at high frequencies eliminates a pre stall, periodic shedding of large-scale vortices. Significant improvement in lift is also achieved during post stall, but with large-amplitude excitation. Wind-tunnel resonances strongly

influence the results, especially in cases requiring large amplitudes. Author

A88-16567*# National Aeronautics and Space Administration.
Lewis Research Center, Cleveland, OH.

CONTROL OF SHEAR FLOWS BY ARTIFICIAL EXCITATION

E. J. RICE and K. B. M. Q. ZAMAN (NASA, Lewis Research Center, Cleveland, OH) AIAA, Aeroacoustics Conference, 11th, Sunnyvale, CA, Oct. 19-21, 1987. 11 p. Previously announced in STAR as N87-29420. refs
(AIAA PAPER 87-2722)

Investigations involving artificial excitation of various shear flows are reviewed. Potential applications of excitation in flow control, e.g., in enhancing mixing, and in delaying transition and separation are discussed. An account is given of the current activities at NASA Lewis Research Center in this regard. Author

A88-18654*# National Aeronautics and Space Administration.
Lewis Research Center, Cleveland, OH.

ON THE CORRELATION OF PLUME CENTERLINE VELOCITY DECAY OF TURBULENT ACOUSTICALLY EXCITED JETS

UWE H. VON GLAHN (NASA, Lewis Research Center, Cleveland, OH) AIAA, Aeroacoustics Conference, 11th, Sunnyvale, CA, Oct. 19-21, 1987. 35 p. refs
(AIAA PAPER 87-2692)

Acoustic excitation has been shown to alter the velocity decay and spreading characteristics of jet plumes by modifying the large-scale structures in the plume shear layer. The present work consists of reviewing and analyzing available published and unpublished experimental data in order to determine the importance and magnitude of the several variables that contribute to plume modification by acoustic excitation. Included in the study were consideration of the effects of internal or external acoustic excitation, excitation Strouhal number, acoustic excitation level, nozzle size and flow conditions. The last include jet Mach number and jet temperature. The effects of these factors on the plume centerline velocity decay are then summarized in an overall empirical correlation. Author

A88-18655*# National Aeronautics and Space Administration.
Lewis Research Center, Cleveland, OH.

ADVANCED TURBOPROP WING INSTALLATION EFFECTS MEASURED BY UNSTEADY BLADE PRESSURE AND NOISE

LAURENCE J. HEIDELBERG and RICHARD P. WOODWARD (NASA, Lewis Research Center, Cleveland, OH) AIAA, Aeroacoustics Conference, 11th, Sunnyvale, CA, Oct. 19-21, 1987. 23 p. Previously announced in STAR as N88-10008. refs
(AIAA PAPER 87-2719)

A single rotation model propeller (SR-7A) was tested at simulated takeoff/approach conditions (Mach 0.2), in the NASA Lewis 9- by 15-Ft Anechoic Wind Tunnel. Both unsteady blade surface pressures and noise measurements were made for a tractor configuration with propeller/straight wing and propeller alone configurations. The angle between the wing chord and propeller axis (droop angle) was varied along with the wing angle of attack to determine the effects on noise and unsteady loading. A method was developed that uses unsteady blade pressure measurements to provide a quantitative indication of propeller inflow conditions, at least for a uniform (across the propeller disk) inflow angle. The wing installation caused a nearly uniform upwash at the propeller inlet as evidenced by the domination of the pressure spectra by the first shaft order. This inflow angle increased at a rate of almost 150 percent of that of the wing angle-of-attack for a propeller-wing spacing of 0.54 wing chords at a constant droop angle. The flyover noise, as measured by the maximum blade passing frequency level, correlates closely with the propeller inflow angle (approx. 0.6 dB per degree of inflow angle) for all droop angles and wing angles of attack tested, including the propeller alone data. Large changes in the unsteady pressure responses on the suction surface of the blade were observed as the advance ratio was varied. The presence of a leading edge vortex may explain this behavior since changes in the location of this vortex would change with loading (advance ratio). Author

02 AERODYNAMICS

A88-18660*# National Aeronautics and Space Administration. Lewis Research Center, Cleveland, OH.

MEASUREMENTS OF THE UNSTEADY FLOW FIELD WITHIN THE STATOR ROW OF A TRANSONIC AXIAL-FLOW FAN. I - MEASUREMENT AND ANALYSIS TECHNIQUE

K. L. SUDER, A. J. STRAZISAR, J. J. ADAMCZYK (NASA, Lewis Research Center, Cleveland, OH), M. D. HATHAWAY (NASA, Lewis Research Center; U.S. Army, Propulsion Directorate, Cleveland, OH), and T. H. OKIISHI (Iowa State University of Science and Technology, Ames) ASME, Gas Turbine Conference and Exhibition, Anaheim, CA, May 31-June 4, 1987. 9 p. Previously announced in STAR as N87-16789. refs (ASME PAPER 87-GT-226)

This two-part paper presents laser anemometer measurements of the unsteady velocity field within the stator row of a transonic axial-flow fan. The objective is to provide additional insight into unsteady blade-row interactions within highspeed compressors which affect stage efficiency, energy transfer, and other design considerations. Part 1 describes the measurement and analysis techniques used for resolving the unsteady flow field features. The ensemble-average and variance of the measured velocities are used to identify the rotor wake generated and unresolved unsteadiness, respectively. (Rotor wake generated unsteadiness refers to the unsteadiness generated by the rotor wake velocity deficit and the term unresolved unsteadiness refers to all remaining contributions to unsteadiness such as vortex shedding, turbulence, mass flow fluctuations, etc.). A procedure for calculating auto and cross correlations of the rotor wake generated and unresolved unsteady velocity fluctuations is described. These unsteady-velocity correlations have significance since they also result from a decomposition of the Navier-Stokes equations. This decomposition of the Navier-Stokes equations resulting in the velocity correlations used to describe the unsteady velocity field will also be outlined in this paper. Author

A88-18661*# National Aeronautics and Space Administration. Lewis Research Center, Cleveland, OH.

MEASUREMENTS OF THE UNSTEADY FLOW FIELD WITHIN THE STATOR ROW OF A TRANSONIC AXIAL-FLOW FAN. II - RESULTS AND DISCUSSION

M. D. HATHAWAY (NASA, Lewis Research Center; U.S. Army, Propulsion Directorate, Cleveland, OH), K. L. SUDER, A. J. STRAZISAR, J. J. ADAMCZYK (NASA, Lewis Research Center, Cleveland, OH), and T. H. OKIISHI (Iowa State University of Science and Technology, Ames) ASME, Gas Turbine Conference and Exhibition, Anaheim, CA, May 31-June 4, 1987. 13 p. Previously announced in STAR as N87-16790. refs (ASME PAPER 87-GT-227)

Unsteady velocity field measurements made within the stator row of a transonic axial-flow fan are presented. Measurements were obtained at midspan for two different stator blade rows using a laser anemometer. The first stator row consists of double circular-arc airfoils with a solidity of 1.68. The second features controlled-diffusion airfoils with a solidity of 0.85. Both were tested at design-speed peak efficiency conditions. In addition, the controlled-diffusion stator was also tested at near stall conditions. The procedures developed here are used to identify the rotor wake generated and unresolved unsteadiness from the velocity measurements (rotor wake generated unsteadiness refers to the unsteadiness generated by the rotor wake velocity deficit and unresolved unsteadiness refers to all remaining unsteadiness which contributes to the spread in the distribution of velocities such as vortex shedding, turbulence, etc.). Auto and cross correlations of these unsteady velocity fluctuations are presented to show their relative magnitude and spatial distributions. Amplification and attenuation of both rotor wake generated and unresolved unsteadiness are shown to occur within the stator blade passage. Author

A88-20184*# National Aeronautics and Space Administration. Lewis Research Center, Cleveland, OH.

INITIAL TURBULENCE EFFECT ON JET EVOLUTION WITH AND WITHOUT TONAL EXCITATION

G. RAMAN (NASA, Lewis Research Center; Sverdrup Technology, Inc., Cleveland, OH), K. B. M. Q. ZAMAN, and E. J. RICE (NASA, Lewis Research Center, Cleveland, OH) AIAA, Aeroacoustics Conference, 11th, Sunnyvale, CA, Oct. 19-21, 1987. 17 p. Previously announced in STAR as N87-27627. refs (AIAA PAPER 87-2725)

The effect of initial turbulence level on the development of a jet and on the susceptibility of the jet to discrete tone excitation was experimentally investigated. Turbulence intensity was varied, over the range 0.15 to 5 percent, by using screens and grids placed upstream of an 8.8 cm diameter nozzle. Top-hat mean velocity profiles with approximately identical initial boundary layer states were ensured in all cases; the turbulence spectra were broadband. It was found, contrary to earlier reports, that the natural jet decay remained essentially unchanged for varying initial turbulence. For a fixed amplitude of the tonal excitation, increasing the initial turbulence damped out the growth of the instability wave; as a result, the excitability, assessed from the mean velocity decay on the axis, was found to diminish. However, the degree of damping in the amplification of the instability wave was only slight compared to the large increase in the initial turbulence. The jet with 5 percent turbulence could be measurably altered by excitation with a velocity perturbation amplitude as little as 0.25 percent of the jet velocity. The amplitude effect data indicate an upper bound of the extent to which a jet could be excited, and thus its plume shortened, by the plane wave, single frequency excitation. An additional data set with no grid or trip, yielding a nominally laminar boundary layer, re-emphasizes the profound effect of initial boundary layer state on jet evolution as well as on its excitability. This jet decayed the fastest naturally, and consequently, it was the least excitable in spite of its turbulence being the least. Author

A88-22078*# California State Univ., Long Beach.

THE CALCULATION OF FLOW OVER ICED AIRFOILS

TUNCER CEBECI (California State University, Long Beach) AIAA, Aerospace Sciences Meeting, 26th, Reno, NV, Jan. 11-14, 1988. 14 p. refs (Contract NAG3-601) (AIAA PAPER 88-0112)

Progress toward the development of a method for predicting the flowfield of an iced airfoil is described and shown to offer the prospect of a priori calculations of the effects of ice accretion and roughness on airfoil performance. The approach is based on interaction of inviscid flow solutions obtained by a panel method and improved upon by a finite-difference boundary-layer method which, operating in an inverse mode, incorporates viscous effects including those associated with separated flows. Results are presented for smooth, rough and iced airfoils as a function of angle of attack. Those for smooth and rough airfoils confirm the accuracy of the method and its applicability to surfaces with roughness similar to that associated with insect deposition and some forms of ice. Two procedures have been developed to deal with large ice accretion and their performance is examined and shown to be appropriate to the engineering requirements. Author

A88-22093*# National Aeronautics and Space Administration. Lewis Research Center, Cleveland, OH.

A NATURAL LOW FREQUENCY OSCILLATION IN THE WAKE OF AN AIRFOIL NEAR STALLING CONDITIONS

K. B. M. Q. ZAMAN and D. J. MCKINZIE (NASA, Lewis Research Center, Cleveland, OH) AIAA, Aerospace Sciences Meeting, 26th, Reno, NV, Jan. 11-14, 1988. 11 p. Previously announced in STAR as N88-10779. refs (AIAA PAPER 88-0131)

An unusually low frequency oscillation in the flow over an airfoil was explored experimentally. Wind tunnel measurements were carried out with a two dimensional airfoil model at a chord Reynolds number of 100,000. During deep stall the usual bluff-body shedding occurred at a Strouhal number. But at the onset of stall a low frequency periodic oscillation occurred, the corresponding Strouhal number being an order of magnitude lower. The phenomenon occurred in relatively unclean flow when the

freestream turbulence was raised to 0.4 percent, but did not in the cleaner flow with turbulence intensity of 0.1 percent. It could also be produced by certain high frequency acoustic excitation. Details of the flow field are compared between a case of low frequency oscillation at $\alpha = 15$ deg and a case of bluff-body shedding at $\alpha = 22.5$ deg. The origin of the low frequency oscillation traces to the upper surface of the airfoil and is seemingly associated with the periodic formation and breakdown of a large separation bubble. The intense flow fluctuations impart significant unsteady forces to the airfoil but diminish rapidly within a distance of one chord from the trailing edge. Author

A88-22364*# Pennsylvania State Univ., University Park.
SKIN FRICTION MEASUREMENTS BY LASER INTERFEROMETRY IN SWEEP SHOCK WAVE/TURBULENT BOUNDARY-LAYER INTERACTIONS

KWANG-SOO KIM and GARY S. SETTLES (Pennsylvania State University, University Park) AIAA, Aerospace Sciences Meeting, 26th, Reno, NV, Jan. 11-14, 1988. 11 p. refs (Contract AF-AFOSR-86-0082; NAG3-527) (AIAA PAPER 88-0497)

The laser interferometric skin friction meter was used to measure wall shear stress distributions in two interactions of fin-generated swept shock waves with turbulent boundary layers. The basic research configuration was an unswept sharp-leading-edge fin of variable angle mounted on a flatplate. The results indicate that such measurements are practical in high-speed interacting flows, and that a repeatability of + or - 6 percent or better is possible. Marked increases in wall shear were observed in both swept interactions tested. K.K.

A88-22444*# National Aeronautics and Space Administration. Lewis Research Center, Cleveland, OH.

NAVIER-STOKES CASCADE ANALYSIS WITH A STIFF K-EPSILON TURBULENCE SOLVER

JONG-SHANG LIU, PETER M. SOCKOL (NASA, Lewis Research Center, Cleveland, OH), and JOSEPH M. PRAHL (Case Western Reserve University, Cleveland, OH) AIAA, Aerospace Sciences Meeting, 26th, Reno, NV, Jan. 11-14, 1988. 10 p. Previously announced in STAR as N88-10778. refs (AIAA PAPER 88-0594)

The two dimensional, compressible, thin layer Navier-Stokes equations with the Baldwin-Lomax turbulence model and the kinetic energy-energy dissipation (k-epsilon) model are solved numerically to simulate the flow through a cascade. The governing equations are solved for the entire flow domain, without the boundary layer assumptions. The stiffness of the k-epsilon equations is discussed. A semi-implicit, Runge-Kutta, time-marching scheme is developed to solve the k-epsilon equations. The impact of the k-epsilon solver on the explicit Runge-Kutta Navier-Stokes solver is discussed. Numerical solutions are presented for two dimensional turbulent flow over a flat plate and a double circular arc cascade and compared with experimental data. Author

A88-22469*# Cornell Univ., Ithaca, NY.
EFFECTS OF NUMERICAL DISSIPATION ON FINITE-VOLUME SOLUTIONS OF COMPRESSIBLE FLOW PROBLEMS

DAVID A. CAUGHEY (Cornell University, Ithaca, NY) and ELI TURKEL (Tel Aviv University, Israel) AIAA, Aerospace Sciences Meeting, 26th, Reno, NV, Jan. 11-14, 1988. 10 p. refs (Contract NAG3-645; NAG2-373) (AIAA PAPER 88-0621)

The effects of numerical dissipation upon solutions to the Euler equations are considered, and results for transonic flows past airfoils are presented to demonstrate the effects of the dissipative terms. The equations are approximated using a finite-volume spatial approximation with added dissipation provided by an adaptive mixture of second and fourth differences. The resulting difference equations are solved using either an explicit multistage Runge-Kutta method or a diagonalized implicit method. It is found that errors in surface values can be introduced by the averaging required to calculate derived quantities of interest. R.R.

A88-22495*# Purdue Univ., West Lafayette, IN.
AERODYNAMIC INTERACTION BETWEEN PROPELLERS AND WINGS

DAVID WITKOWSKI, ALEX K. H. LEE, and JOHN P. SULLIVAN (Purdue University, West Lafayette, IN) AIAA, Aerospace Sciences Meeting, 26th, Reno, NV, Jan. 11-14, 1988. 13 p. refs (Contract NSG-3134) (AIAA PAPER 88-0665)

A combined computational/experimental investigation has been conducted to determine the time-averaged interactive performance of a propeller and wing in tractor configuration at Mach 0.1 and $Re = 470,000$, based on a wind tunnel model wing chord of 8 in. Wing angle-of-attack was varied from 0 to +13 deg, and propeller advance ratio ranged from 2.4 (windmilling) to 1.1 (maximum power). Both a semiempirical model and a vortex lattice simulation were used in the computational analysis. Good agreement has been obtained between theory and experiment. O.C.

A88-24825*# National Aeronautics and Space Administration. Lewis Research Center, Cleveland, OH.

NUMERICAL STUDY OF CHEMICALLY REACTING FLOWS USING AN LU SCHEME

JIAN SHUN SHUEN (NASA, Lewis Research Center; Sverdrup Technology, Inc., Cleveland, OH) and SEOKKWAN YOON (NASA, Ames Research Center, Moffett Field, CA) AIAA, Aerospace Sciences Meeting, 26th, Reno, NV, Jan. 11-14, 1988. 22 p. Previously announced in STAR as N88-14094. refs (AIAA PAPER 88-0436)

A new computational fluid dynamic code has been developed for the study of mixing and chemical reactions in the flow fields of ramjets and scramjets. The code employs an implicit finite volume, lower-upper symmetric successive overrelaxation scheme for solving the complete two-dimensional Navier-Stokes equations and species transport equations in a fully-coupled and very efficient manner. The combustion processes are modeled by an 8-species, 14-step finite rate chemistry model whereas turbulence is simulated by a Baldwin-Lomax algebraic model. The validity of the code is demonstrated by comparing the numerical calculations with both experimental data and previous calculations of a cold flow helium injection into a straight channel and premixed hydrogen-air reacting flows in a ramped duct. The code is then used to calculate the mixing and chemical reactions of a hydrogen jet transversely injected into a supersonic airstream. Results are presented describing the flow field, the recirculation regions in front and behind the injector, and the chemical reactions. Author

A88-27715*# National Aeronautics and Space Administration. Lewis Research Center, Cleveland, OH.

AN EXPLICIT RUNGE-KUTTA METHOD FOR UNSTEADY ROTOR/STATOR INTERACTION

PHILIP C. E. JORGENSEN and RODRICK V. CHIMA (NASA, Lewis Research Center, Cleveland, OH) AIAA, Aerospace Sciences Meeting, 26th, Reno, NV, Jan. 11-14, 1988. 15 p. refs (AIAA PAPER 88-0049)

A quasi-three-dimensional rotor/stator analysis has been developed for blade-to-blade flows in turbomachinery. The analysis solves the unsteady Euler or thin-layer Navier-Stokes equations in a body-fitted coordinate system. It accounts for the effects of rotation, radius change, and stream-surface thickness. The Baldwin-Lomax eddy-viscosity model is used for turbulent flows. The equations are integrated in time using a four-stage Runge-Kutta scheme with a constant timestep. Results are shown for the first stage of the Space Shuttle Main Engine high pressure fuel turbopump. Euler and Navier-Stokes results are compared on the scaled single- and multi-passage machine. The method is relatively fast and the quasi-three-dimensional formulation is applicable to a wide range of turbomachinery geometries. Author

A88-27717*# National Aeronautics and Space Administration. Lewis Research Center, Cleveland, OH.

NUMERICAL SIMULATION OF HYPERSONIC INLET FLOWS WITH EQUILIBRIUM OR FINITE RATE CHEMISTRY

SHENG-TAO YU, KWANG-CHUNG HSIEH, JIAN-SHUN SHUEN

02 AERODYNAMICS

(NASA, Lewis Research Center; Sverdrup Technology, Inc., Cleveland, OH), and BONNIE J. MCBRIDE (NASA, Lewis Research Center, Cleveland, OH) AIAA, Aerospace Sciences Meeting, 26th, Reno, NV, Jan. 11-14, 1988. 14 p. refs (AIAA PAPER 88-0273)

An efficient numerical program incorporated with comprehensive high temperature gas property models has been developed to simulate hypersonic inlet flows. The computer program employs an implicit lower-upper time marching scheme to solve the two-dimensional Navier-Stokes equations with variable thermodynamic and transport properties. Both finite-rate and local-equilibrium approaches are adopted in the chemical reaction model for dissociation and ionization of the inlet air. In the finite rate approach, eleven species equations coupled with fluid dynamic equations are solved simultaneously. In the local-equilibrium approach, instead of solving species equations, an efficient chemical equilibrium package has been developed and incorporated into the flow code to obtain chemical compositions directly. Gas properties for the reaction products species are calculated by methods of statistical mechanics and fit to a polynomial form for $C(p)$. In the present study, since the chemical reaction time is comparable to the flow residence time, the local-equilibrium model underpredicts the temperature in the shock layer. Significant differences of predicted chemical compositions in shock layer between finite rate and local-equilibrium approaches have been observed.

Author

A88-27718*# Sverdrup Technology, Inc., Cleveland, OH.
GLANCING SHOCK WAVE-TURBULENT BOUNDARY LAYER INTERACTION WITH BOUNDARY LAYER SUCTION

P. J. BARNHART (Sverdrup Technology, Inc., Cleveland, OH), I. GREBER (Case Western Reserve University, Cleveland, OH), and W. R. HINGST (NASA, Lewis Research Center, Cleveland, OH) AIAA, Aerospace Sciences Meeting, 26th, Reno, NV, Jan. 11-14, 1988. 11 p. refs (AIAA PAPER 88-0308)

Tests conducted to ascertain the stagnation pressure and flow angularity profiles of a turbulent boundary layer subjected to boundary layer suction (BLS) as it crosses a glancing sidewall shock wave have determined that the boundary layer does not separate upon crossing the shock wave. Without BLS, the upstream influence of the shock wave-induced wall static pressure rise was extensive, of the order of four boundary layer thicknesses; for the same case, with suction, the extent of upstream influence was 50 percent lower. In addition, flow angularities at the wall were found to be smaller with suction than without it.

O.C.

A88-30560* National Aeronautics and Space Administration.
Lewis Research Center, Cleveland, OH.

A NAVIER-STOKES SOLVER USING THE LU-SSOR TVD ALGORITHM

SEOKKWAN YOON (NASA, Lewis Research Center; Sverdrup Technology, Inc., Cleveland, OH) IN: Numerical methods in laminar and turbulent flow; Proceedings of the Fifth International Conference, Montreal, Canada, July 6-10, 1987. Volume 5, Part 2. Swansea, Wales, Pineridge Press, 1987, p. 1966-1976. Previously announced in STAR as N87-20243. refs

A new Navier-Stokes solver is developed by combining the efficiency of the LU-SSOR scheme and the accuracy of the flux-limited dissipation scheme. Application to laminar and turbulent flows and hypersonic flows proves the reliability of the new algorithm.

Author

A88-32314*# National Aeronautics and Space Administration,
Washington, DC.

APPLICATION OF A SEMIANALYTICAL TECHNIQUE FOR SENSITIVITY ANALYSIS OF UNSTEADY AERODYNAMIC COMPUTATIONS

DURBHA V. MURTHY (NASA, Washington, DC; Toledo, University, OH) and KRISHNA RAO V. KAZA (NASA, Lewis Research Center, Cleveland, OH) IN: Structures, Structural Dynamics and Materials Conference, 29th, Williamsburg, VA, Apr. 18-20, 1988, Technical

Papers. Part 3. Washington, DC, American Institute of Aeronautics and Astronautics, 1988, p. 1307-1316. refs (AIAA PAPER 88-2377)

A semianalytical approach is developed for the sensitivity analysis of linear unsteady aerodynamic loads. The semianalytical approach is easier to implement than the analytical approach. It is also computationally less expensive than the finite difference approach when used with panel methods which require a large number of panels. The semianalytical approach is applied to an isolated airfoil in a two-dimensional flow and rotating propfan blades in three-dimensional flow. Sensitivity coefficients with respect to nonshape-dependent variables are shown for some cases.

Author

A88-37220* McDonnell-Douglas Research Labs., Saint Louis, MO.

UNSTEADY FEATURES OF JETS IN LIFT AND CRUISE MODES FOR VTOL AIRCRAFT

V. KIBENS, K. R. SARIPALLI, R. W. WLEZIEN, and J. T. KEGELMAN (McDonnell Douglas Research Laboratories, Saint Louis, MO) IN: International Powered Lift Conference and Exposition, Santa Clara, CA, Dec. 7-10, 1987, Proceedings. Warrendale, PA, Society of Automotive Engineers, Inc., 1988, p. 543-552. refs (Contract NAS3-24621) (SAE PAPER 872359)

Experiments were performed to simulate jet plume effects associated with VTOL aircraft in takeoff and cruise modes. A water facility was used to investigate the influence of inclination angle and separation distance on the three-dimensional fountain flowfield generated by two impinging jets operating at a jet Reynolds number of 250,000. Substantial differences in the flow features were observed for different spacings between the jets. Plume effects in cruise mode were simulated by a supersonic unheated jet parallel to a wall. Variation of the distance between the wall and the edge of the plume is shown to have a major controlling effect on the supersonic screech instability.

Author

A88-40718*# Flow Research, Inc., Kent, WA.
OPTIMIZING ADVANCED PROPELLER DESIGNS BY SIMULTANEOUSLY UPDATING FLOW VARIABLES AND DESIGN PARAMETERS

MAGDI H. RIZK (Flow Research, Inc., Kent, WA) IN: AIAA Applied Aerodynamics Conference, 6th, Williamsburg, VA, June 6-8, 1988, Technical Papers. Washington, DC, American Institute of Aeronautics and Astronautics, 1988, p. 160-167. refs (Contract NAS3-24855) (AIAA PAPER 88-2532)

A scheme is developed for solving constrained optimization problems in which the objective function and the constraint function are dependent on the solution of the nonlinear flow equations. The scheme updates the design parameter iterative solutions and the flow variable iterative solutions simultaneously. It is applied to an advanced propeller design problem with the Euler equations used as the flow governing equations. The scheme's accuracy, efficiency and sensitivity to the computational parameters are tested.

Author

A88-42452*# Pennsylvania State Univ., University Park.
COMPARISON OF COMPUTATIONAL METHODS FOR THREE-DIMENSIONAL TURBULENT TURBOMACHINERY FLOWS

K. R. KIRTLEY, M. WARFIELD, and B. LAKSHMINARAYANA (Pennsylvania State University, University Park) Journal of Propulsion and Power (ISSN 0748-4658), vol. 4, May-June 1988, p. 207, 208. Previously cited in issue 20, p. 2916, Accession no. A86-42740. refs (Contract NSG-3266)

A88-44490*# National Aeronautics and Space Administration.
Lewis Research Center, Cleveland, OH.
POROUS WIND TUNNEL CORRECTIONS FOR COUNTERROTATION PROPELLER TESTING

GEORGE L. STEFKO and ROBERT J. JERACKI (NASA, Lewis Research Center, Cleveland, OH) AIAA, Aerodynamic Testing Conference, 15th, San Diego, CA, May 18-20, 1988. Previously announced in STAR as N88-22019. refs (AIAA PAPER 88-2055)

Wind tunnel interference corrections have direct impact on measured propeller efficiency. A systematic series of wind tunnel tests was done in the porous-wall NASA Lewis 8- by 6-Foot Wind Tunnel to determine the wind tunnel interference corrections to the NASA Lewis counterrotation propeller test data. The test results were compared with calculations from a potential flow code to determine the interference corrections. At a Mach number of 0.8, the interference corrections resulted in a -0.008 Mach number correction which reduced the counterrotation propeller net efficiency data by 0.46 percent at the reduced Mach number. Additional wind tunnel tests were done to measure the effect of propeller thrust on wind tunnel wall interference. No wall interference corrections due to propeller thrust were found necessary for the high speed counterrotation propeller data obtained in the porous wall NASA Lewis 8- by 6-Foot Wind Tunnel. Author

A88-44667* Sverdrup Technology, Inc., Middleburg Heights, OH.

HYPERSONIC TURBULENT WALL BOUNDARY LAYER COMPUTATIONS

S. C. KIM and G. J. HARLOFF (Sverdrup Technology, Inc., Middleburg Heights, OH) AIAA, ASME, SAE, and ASEE, Joint Propulsion Conference, 24th, Boston, MA, July 11-13, 1988. 8 p. refs

(Contract NAS3-25266)

(AIAA PAPER 88-2829)

The Baldwin-Lomax (1978) algebraic turbulence model was modified for hypersonic flow conditions. Two coefficients in the outer-layer eddy-viscosity model were determined as functions of Mach number and temperature ratio. By matching the solutions from the Baldwin-Lomax model to those from the Cebeci-Smith (1974) model for a flat plate at hypersonic speed, the new values of the coefficients were obtained. The results show that the values of C_{cp} and C_{kleb} are functions of both Mach number and wall temperature ratio. The C_{cp} and C_{kleb} variations with Mach number and wall temperature were used for the calculations of both a 4-deg wedge flow at Mach 18 and an axisymmetric Mach 20 nozzle flow. The Navier-Stokes equations with thin-layer approximation were solved for the above hypersonic flow conditions and the results were compared with existing experimental data. The agreement between the numerical solutions and the existing experimental data were good. The modified Baldwin-Lomax model thus is useful in the computations of hypersonic flows. Author

A88-44705* Virginia Polytechnic Inst. and State Univ., Blacksburg.

TURBULENCE MODELING IN HYPERSONIC INLETS

W. F. NG, A. C. TAYLOR, III (Virginia Polytechnic Institute and State University, Blacksburg), and K. AJMANI AIAA, ASME, SAE, and ASEE, Joint Propulsion Conference, 24th, Boston, MA, July 11-13, 1988. 11 p. refs

(Contract NAG3-676)

(AIAA PAPER 88-2957)

A study is conducted to analyze the performance of different turbulence models when applied to flow through a Mach 7.4 hypersonic inlet. The analysis, which is two-dimensional, is done by comparing computational results from a Parabolized Navier-Stokes code and a full Navier-Stokes code, with experimental data. The McDonald-Camarata (MC) and Baldwin-Lomax (BL) models were the two zero-equation models used in the study. The Turbulent Kinetic Energy (TKE) model was chosen as a representative higher order model. The MC model, when run with transition of flow, provides a solution which compares excellently with the data. Transition has a first order effect on the overall solution provided by the code. The BL model predicts separation of flow in the inlet, which contradicts experimental findings. The TKE model does not perform any better than the

MC and BL models, despite the fact that it is a higher order turbulence model. The BL and TKE models predict transition in the inlet at a location which is much earlier than observed in the experiment. This may be attributed to the empirical constants used to determine the point of transition. Author

A88-48758* National Aeronautics and Space Administration. Lewis Research Center, Cleveland, OH.

SUMMARY OF LOW-SPEED WIND TUNNEL RESULTS OF SEVERAL HIGH-SPEED COUNTERROTATION PROPELLER CONFIGURATIONS

CHRISTOPHER E. HUGHES (NASA, Lewis Research Center, Cleveland, OH) and JOHN A. GAZZANIGA (NASA, Lewis Research Center; Sverdrup Technology, Inc., Cleveland, OH) AIAA, ASME, SAE, and ASEE, Joint Propulsion Conference, 24th, Boston, MA, July 11-13, 1988. 34 p. Previously announced in STAR as N88-24597. refs

(AIAA PAPER 88-3149)

The low speed aerodynamic performance characteristics of several advanced counterrotation pusher propeller configurations with cruise design Mach numbers of 0.72 and 0.80 were investigated in the NASA Low Speed Wind Tunnel. The tests were conducted at Mach numbers representative of the takeoff and landing flight regime. The investigation included: (1) the propeller performance characteristics over a range of blade angle settings and rotational speeds at a Mach number of 0.20; (2) the effect on the propeller performance of varying the axial rotor spacing and mismatching the power and rotational speeds on the propeller rotors; and (3) determining the reverse thrust performance characteristics at Mach numbers of 0.0, 0.10, 0.15 and 0.20. The results of the investigation indicated that the overall low speed performance of the counterrotation propeller configurations was reasonable. Author

A88-48893* Kansas Univ., Lawrence.

EFFECT OF INITIAL TANGENTIAL VELOCITY DISTRIBUTION ON THE MEAN EVOLUTION OF A SWIRLING TURBULENT FREE JET

S. FAROKHI, R. TAGHAVI (Kansas, University, Lawrence), and E. J. RICE (NASA, Lewis Research Center, Cleveland, OH) IN: AIAA, ASME, SIAM, and APS, National Fluid Dynamics Congress, 1st, Cincinnati, OH, July 25-28, 1988, Technical Papers. Part 2. Washington, DC, American Institute of Aeronautics and Astronautics, 1988, p. 947-954. Previously announced in STAR as N88-24592. refs

(Contract NCC3-56)

(AIAA PAPER 88-3592)

An existing cold jet facility at NASA-Lewis was modified to produce swirling flows with controllable initial tangential velocity distribution. Distinctly different swirl velocity profiles were produced, and their effects on jet mixing characteristics were measured downstream of an 11.43 cm diameter convergent nozzle. It was experimentally shown that in the near field of a swirling turbulent jet, the mean velocity field strongly depends on the initial swirl profile. Two extreme tangential velocity distributions were produced. The two jets shared approximately the same initial mass flow rate of 5.9 kg/s, mass averaged axial Mach number and swirl number. Mean centerline velocity decay characteristics of the solid body rotation jet flow exhibited classical decay features of a swirling jet with $S = 0.48$ reported in the literature. It is concluded that the integrated swirl effect, reflected in the swirl number, is inadequate in describing the mean swirling jet behavior in the near field. Author

A88-48896* Lockheed Aeronautical Systems Co., Marietta, GA.

CENTERLINE MACH NUMBER CHARACTERISTICS OF HIGHLY HEATED FREE JETS

JAN LEPICOVSKY (Lockheed Aeronautical Systems Co., Marietta, GA) IN: AIAA, ASME, SIAM, and APS, National Fluid Dynamics Congress, 1st, Cincinnati, OH, July 25-28, 1988, Technical Papers. Part 2. Washington, DC, American Institute of Aeronautics and

02 AERODYNAMICS

Astronautics, 1988, p. 989-999. refs
(Contract NAS3-23708)
(AIAA PAPER 88-3612)

This paper describes a detailed experimental study of Mach number centerline characteristics of highly heated free jets. The jet characteristics were obtained at a range of jet Mach numbers from 0.1 to 0.9 and jet total temperatures up to 900 K. The results show that a strong correlation exists between nozzle-exit boundary-layer conditions and free-jet development. It is clear from this investigation that experimental data on free-jet development cannot be meaningfully compared from one facility to another without specific knowledge of nozzle exit conditions. It was concluded that direct effect of the jet operating conditions (elevated flow temperature) on free jet development is much less important than the indirect effect of changed nozzle-exit boundary-layer characteristics. Author

A88-48899*# National Aeronautics and Space Administration. Lewis Research Center, Cleveland, OH.

SATURATION AND THE LIMIT OF JET MIXING ENHANCEMENT BY SINGLE FREQUENCY PLANE WAVE EXCITATION - EXPERIMENT AND THEORY

GANESH RAMAN (NASA, Lewis Research Center; Sverdrup Technology, Inc., Cleveland, OH), EDWARD J. RICE (NASA, Lewis Research Center, Cleveland, OH), and REDA R. MANKBADI (Brown University, Providence, RI) IN: AIAA, ASME, SIAM, and APS, National Fluid Dynamics Congress, 1st, Cincinnati, OH, July 25-28, 1988, Technical Papers. Part 2. Washington, DC, American Institute of Aeronautics and Astronautics, 1988, p. 1000-1007. DARPA-supported research. Previously announced in STAR as N88-23732. refs

(Contract NAG3-673; NSF MSM-83-20307)
(AIAA PAPER 88-3613)

The limitations of single frequency plane wave excitation in mixing enhancement are investigated for a circular jet. Measurements made in an 8.8 cm diameter jet are compared with a theoretical model. The measurements are made to quantify mixing at excitation amplitudes up to 2 percent of the jet exit velocity. The initial boundary layer state, the exit mean and fluctuating velocity profiles and spectra are documented for all cases considered. The amplitude of the fundamental wave is recorded along the jet axis for various levels of excitation. As the amplitude of excitation is increased the jet spreading rate is increased, but beyond a saturation amplitude further increases have no effect on the spreading. The experimental results are compared with theoretical estimates. In the theory the flow is split into the mean flow, large scale motions, and fine scale turbulence. Shape assumptions for the mean flow, and fine scale turbulence along with the shape for the large scale motions obtained from a linear stability theory provide the closure. The experimental results compare reasonably well with predictions. Author

A88-48901*# Ohio State Univ., Columbus.

STRUCTURE OF A REATTACHING SUPERSONIC SHEAR FLOW

M. SAMIMY (Ohio State University, Columbus) and B. A. K. ABU-HIJLEH IN: AIAA, ASME, SIAM, and APS, National Fluid Dynamics Congress, 1st, Cincinnati, OH, July 25-28, 1988, Technical Papers. Part 2. Washington, DC, American Institute of Aeronautics and Astronautics, 1988, p. 1016-1021. refs
(Contract NAG3-764; N00014-87-K-0169)
(AIAA PAPER 88-3615)

A Mach 1.83 fully developed turbulent boundary layer with boundary layer thickness, free stream velocity, and Reynolds number of 7.5 mm, 476 m/s, and 6.2×10^6 to the 7th/m, respectively, was separated at a 25.4-mm backward step and formed a shear layer. Fast-response pressure transducers, schlieren photography, and LDV were used to study the structure of this reattaching shear flow. The preliminary results show that large-scale relatively organized structures with limited spanwise extent form in the free shear layer. Some of these structures appear to survive the recompression and reattachment processes, while others break down into smaller scales and the flow becomes increasingly

three-dimensional. The survived large-scale structures lose their organization through recompression/reattachment, but regain it after reattachment. The structures after reattachment form a 40-45-degree angle relative to the free stream and deteriorate gradually as they move downstream. Author

A88-50604*# National Aeronautics and Space Administration. Lewis Research Center, Cleveland, OH.

A COMPUTATIONAL ANALYSIS OF UNDER-EXPANDED JETS IN THE HYPERSONIC REGIME

ANDREW T. HSU and MENG-SING LIOU (NASA, Lewis Research Center, Cleveland, OH) IN: AIAA Atmospheric Flight Mechanics Conference, Minneapolis, MN, Aug. 15-17, 1988, Technical Papers. Washington, DC, American Institute of Aeronautics and Astronautics, 1988, p. 300-306. refs
(AIAA PAPER 88-4361)

Underexpanded axisymmetric jets are studied numerically using a full Navier-Stokes solver. Emphasis has been given to supersonic and hypersonic jets in supersonic and hypersonic ambient flows, a phenomenon previously being overlooked for the most part. The present work demonstrates that the shear layers and shock patterns in a jet plume can be captured without complicated viscous/inviscid and subsonic/supersonic coupling schemes. In addition, a supersonic pressure relief effect has been identified for underexpanded jets in supersonic ambient flows. While it is well known that an underexpanded jet in a quiescent ambience (or subsonic ambience) contains multiple shock cells, the present study shows that because of the supersonic pressure relief effect, an underexpanded jet in a supersonic or hypersonic ambience contains only one major shock cell. Author

A88-54189*# Flow Application Research, Fremont, CA.

DESIGN POINT VARIATION OF 3-D LOSS AND DEVIATION FOR AXIAL COMPRESSOR MIDDLE STAGES

WILLIAM B. ROBERTS (Flow Application Research, Fremont, CA), GEORGE K. SEROVY (Iowa State University of Science and Technology, Ames), and DONALD M. SANDERCOCK (NASA, Lewis Research Center, Cleveland, OH) ASME, Gas Turbine and Aeroengine Congress and Exposition, Amsterdam, Netherlands, June 6-9, 1988. 14 p. refs

(Contract NAG3-521)
(ASME PAPER 88-GT-57)

The available data on middle-stage research compressors operating near design point are used to derive simple empirical models for the spanwise variation of three-dimensional viscous loss coefficients for middle-stage axial compressor blading. The models make it possible to quickly estimate the total loss and deviation across the blade span when the three-dimensional distribution is superimposed on the two-dimensional variation calculated for each blade element. It is noted that extrapolated estimates should be used with caution since the correlations have been derived from a limited data base. V.L.

A88-54206*# National Aeronautics and Space Administration. Lewis Research Center, Cleveland, OH.

FLUTTER OF A FAN BLADE IN SUPERSONIC AXIAL FLOW

ROBERT E. KIELB and JOHN K. RAMSEY (NASA, Lewis Research Center, Cleveland, OH) ASME, Gas Turbine and Aeroengine Congress and Exposition, Amsterdam, Netherlands, June 6-9, 1988. 7 p. refs

(ASME PAPER 88-GT-78)

An application of a simple aeroelastic model to an advanced supersonic axial flow fan is presented. Lane's cascade theory is used to determine the unsteady aerodynamic loads. Parametric studies are performed to determine the effects of mode coupling, Mach number, damping, pitching axis location, solidity, stagger angle, and mistuning. The results show that supersonic axial flow fan and compressor blades are susceptible to a strong torsional mode flutter having critical reduced velocities which can be less than one. Author

N88-54375* National Aeronautics and Space Administration. Lewis Research Center, Cleveland, OH.

EXPERIMENTAL INVESTIGATION OF THE PERFORMANCE OF A SUPERSONIC COMPRESSOR CASCADE

T. L. TWEEDT (NASA, Lewis Research Center, Cleveland, OH), H. A. SCHREIBER, and H. STARKEN (DFVLR, Institut fuer Antriebstechnik, Cologne, Federal Republic of Germany) ASME, Gas Turbine and Aeroengine Congress and Exposition, Amsterdam, Netherlands, June 6-9, 1988. 13 p. refs
(ASME PAPER 88-GT-306)

Supersonic cascade wind tunnel results are presented for a linear, supersonic compressor cascade derived from the near-tip section of a high-throughflow axial flow compressor rotor over the inlet Mach number range of 1.30-1.71. Laser anemometry was used to obtain flow-velocity measurements showing the wave pattern in the entrance region. Attention is given to the unique-incidence relationship for this cascade, which relates the supersonic inlet Mach number to the inlet flow direction. An empirical correlation is obtained for the influence of the independent parameters of back pressure, axial velocity density ratio, and blade element performance. O.C.

N88-10008* National Aeronautics and Space Administration. Lewis Research Center, Cleveland, OH.

ADVANCED TURBOPROP WING INSTALLATION EFFECTS MEASURED BY UNSTEADY BLADE PRESSURE AND NOISE

LAURENCE J. HEIDELBERG and RICHARD P. WOODWARD 1987 23 p Presented at the 11th Aeroacoustics Conference, Sunnyvale, Calif., 19-21 Oct. 1987; sponsored by AIAA (NASA-TM-100200; E-3737; NAS 1.15:100200; AIAA-87-2719)
Avail: NTIS HC A03/MF A01 CSCL 01A

A single rotation model propeller (SR-7A) was tested at simulated takeoff/approach conditions (Mach 0.2), in the NASA Lewis 9- by 15-Ft Anechoic Wind Tunnel. Both unsteady blade surface pressures and noise measurements were made for a tractor configuration with propeller/straight wing and propeller alone configurations. The angle between the wing chord and propeller axis (droop angle) was varied along with the wing angle of attack to determine the effects on noise and unsteady loading. A method was developed that uses unsteady blade pressure measurements to provide a quantitative indication of propeller inflow conditions, at least for a uniform (across the propeller disk) inflow angle. The wing installation caused a nearly uniform upwash at the propeller inlet as evidenced by the domination of the pressure spectra by the first shaft order. This inflow angle increased at a rate of almost 150 percent of that of the wing angle-of-attack for a propeller-wing spacing of 0.54 wing chords at a constant droop angle. The flyover noise, as measured by the maximum blade passing frequency level, correlates closely with the propeller inflow angle (approx. 0.6 dB per degree of inflow angle) for all droop angles and wing angles of attack tested, including the propeller alone data. Large changes in the unsteady pressure responses on the suction surface of the blade were observed as the advance ratio was varied. The presence of a leading edge vortex may explain this behavior since changes in the location of this vortex would change with loading (advance ratio). Author

N88-10778* National Aeronautics and Space Administration. Lewis Research Center, Cleveland, OH.

NAVIER-STOKES CASCADE ANALYSIS WITH A STIFF KAPPA-EPSILON TURBULENCE SOLVER

JONG-SHANG LIU, PETER M. SOCKOL, and JOSEPH M. PRAHL (Case Western Reserve Univ., Cleveland, Ohio.) 1987 15 p Prepared for presentation at the 26th Aerospace Sciences Meeting, Reno, Nev., 11-14, 1988; sponsored by AIAA (NASA-TM-100218; ICOMP-87-6; E-3829; NAS 1.15:100218; AIAA-88-0594) Avail: NTIS HC A03/MF A01 CSCL 01A

The two dimensional, compressible, thin layer Navier-Stokes equations with the Baldwin-Lomax turbulence model and the kinetic energy-energy dissipation (k-epsilon) model are solved numerically to simulate the flow through a cascade. The governing equations are solved for the entire flow domain, without the boundary layer assumptions. The stiffness of the k-epsilon equations is discussed.

A semi-implicit, Runge-Kutta, time-marching scheme is developed to solve the k-epsilon equations. The impact of the k-epsilon solver on the explicit Runge-Kutta Navier-Stokes solver is discussed. Numerical solutions are presented for two dimensional turbulent flow over a flat plate and a double circular arc cascade and compared with experimental data. Author

N88-10779* National Aeronautics and Space Administration. Lewis Research Center, Cleveland, OH.

A NATURAL LOW FREQUENCY OSCILLATION IN THE WAKE OF AN AIRFOIL NEAR STALLING CONDITIONS

K. B. M. Q. ZAMAN and D. J. MCKINZIE 1987 17 p Prepared for presentation at the 26th Aerospace Sciences Meeting, Reno, Nev., 11-14 Jan. 1988; sponsored by AIAA (NASA-TM-100213; E-3822; NAS 1.15:100213; AIAA-88-0131)
Avail: NTIS HC A03/MF A01 CSCL 01A

An unusually low frequency oscillation in the flow over an airfoil was explored experimentally. Wind tunnel measurements were carried out with a two dimensional airfoil model at a chord Reynolds number of 100,000. During deep stall the usual bluff-body shedding occurred at a Strouhal number. But at the onset of stall a low frequency periodic oscillation occurred, the corresponding Strouhal number being an order of magnitude lower. The phenomenon occurred in relatively unclean flow when the freestream turbulence was raised to 0.4 percent, but did not in the cleaner flow with turbulence intensity of 0.1 percent. It could also be produced by certain high frequency acoustic excitation. Details of the flow field are compared between a case of low frequency oscillation at $\alpha = 15$ deg and a case of bluff-body shedding at $\alpha = 22.5$ deg. The origin of the low frequency oscillation traces to the upper surface of the airfoil and is seemingly associated with the periodic formation and breakdown of a large separation bubble. The intense flow fluctuations impart significant unsteady forces to the airfoil but diminish rapidly within a distance of one chord from the trailing edge. Author

N88-12461* National Aeronautics and Space Administration. Lewis Research Center, Cleveland, OH.

APPLICATION OF RUNGE KUTTA TIME MARCHING SCHEME FOR THE COMPUTATION OF TRANSONIC FLOWS IN TURBOMACHINES

S. V. SUBRAMANIAN and R. BOZZOLA (Avco Lycoming Div., Stratford, Conn.) 1987 19 p Presented at the 21st Joint Propulsion Conference, Monterey, Calif., 8-10 Jul. 1985; sponsored by AIAA, SAE and ASME Previously announced in IAA as A85-39728 (NASA-TM-86997; E-2543; NAS 1.15:86997) Avail: NTIS HC A03/MF A01 CSCL 01A

Numerical solutions of the unsteady Euler equations are obtained using the classical fourth order Runge Kutta time marching scheme. This method is fully explicit and is applied to the governing equations in the finite volume, conservation law form. In order to determine the efficiency of this scheme for solving turbomachinery flows, steady blade-to-blade solutions are obtained for compressor and turbine cascades under subsonic and transonic flow conditions. Computed results are compared with other numerical methods and wind tunnel measurements. The study also focuses on other important numerical aspects influencing the performance of the algorithm and the solution accuracy such as grid types, boundary conditions and artificial viscosity. For this purpose, H, O, and C type computational grids as well as characteristic and extrapolation type boundary conditions are included in solution procedures. Author

N88-13304* National Aeronautics and Space Administration. Lewis Research Center, Cleveland, OH.

AUTOMATED DESIGN OF CONTROLLED DIFFUSION BLADES

JOSE M. SANZ 1987 15 p Prepared for presentation at the 33rd International Gas Turbine and Aero-Engine Congress and Exposition, Amsterdam, The Netherlands, 5-9 Jun. 1988 (NASA-TM-100251; E-3877; NAS 1.15:100251) Avail: NTIS HC A03/MF A01 CSCL 01A

A numerical automation procedure has been developed to be

02 AERODYNAMICS

used in conjunction with an inverse hodograph method for the design of controlled diffusion blades. With this procedure a cascade of airfoils with a prescribed solidity, inlet Mach number, inlet air flow angle, and air flow turning can be produced automatically. The trailing edge thickness of the airfoil, an important quantity in inverse methods, is also prescribed. The automation procedure consists of a multidimensional Newton iteration in which the objective design conditions are achieved by acting on the hodograph input parameters of the underlying inverse code. The method, although more general in scope, is applied in this paper to the design of axial flow compressor blade sections, and a wide range of examples is presented. Author

N88-14966* # Ohio State Univ., Columbus. Dept. of Aeronautical and Astronautical Engineering.

A FLOW VISUALIZATION STUDY OF THE LEADING EDGE SEPARATION BUBBLE ON A NACA 0012 AIRFOIL WITH SIMULATED GLAZE ICE Final Report M.S. Thesis

ABDOLLAH KHODADOUST Jan. 1988 91 p
(Contract NAG3-28)
(NASA-CR-180846; NAS 1.26:180846) Avail: NTIS HC A05/MF A01 CSCL 01A

As a part of the ongoing research in aircraft icing, the leading edge separation bubble on the NACA 0012 model with a 5-min simulated glaze ice was investigated. The flow visualization methods used oil, tuft, splitter plate, smoke, and liquid crystals to get reattachment line data for the leading edge separation bubble on both surfaces of the airfoil. On the upper surface, the bubble was found to grow larger with increasing negative angles of attack and reduce in size with increasing angles of attack. The separated flow fails to reattach beyond 6 deg for the upper surface and -5 deg for the lower surface. The results of this study compared well with those of other experiments and computational results.

Author

N88-14967* # National Aeronautics and Space Administration. Lewis Research Center, Cleveland, OH.

AN EXPLICIT RUNGE-KUTTA METHOD FOR UNSTEADY ROTOR/STATOR INTERACTION

PHILIP C. E. JORGENSEN and RODRICK V. CHIMA Jan. 1988 15 p Prepared for presentation at the 26th Aerospace Sciences Meeting, Reno, Nev., 11-14 Jan. 1988; sponsored by AIAA (NASA-TM-100787; E-3959; NAS 1.15:100787; AIAA-88-0049) Avail: NTIS HC A03/MF A01 CSCL 01A

A quasi-three-dimensional rotor/stator analysis has been developed for blade-to-blade flows in turbomachinery. The analysis solves the unsteady Euler or thin-layer Navier-Stokes equations in a body-fitted coordinate system. It accounts for the effects of rotation, radius change, and stream-surface thickness. The Baldwin-Lomax eddy-viscosity model is used for turbulent flows. The equations are integrated in time using a four-stage Runge-Kutta scheme with a constant timestep. Results are shown for the first stage of the Space Shuttle Main Engine high pressure fuel turbopump. Euler and Navier-Stokes results are compared on the scaled single- and multi-passage machine. The method is relatively fast and the quasi-three-dimensional formulation is applicable to a wide range of turbomachinery geometries. Author

N88-15762* # Sverdrup Technology, Inc., Cleveland, OH.
CONSISTENT BOUNDARY CONDITIONS FOR REDUCED NAVIER-STOKES (RNS) SCHEME APPLIED TO 3-DIMENSIONAL INTERNAL VISCOUS FLOWS Final Report

D. R. REDDY and S. G. RUBIN Jan. 1988 20 p Presented at the 26th Aerospace Science Meeting, Reno, Nev., 11-14 Jan. 1988; sponsored by AIAA Prepared in cooperation with Cincinnati Univ., Ohio
(Contract NAS3-24105)
(NASA-CR-180874; E-3739-1; NAS 1.26:180874; AIAA-88-0714) Avail: NTIS HC A03/MF A01 CSCL 01A

A consistent and efficient set of boundary conditions is developed for the multi-sweep space-marching pressure-elliptic Reduced Navier-Stokes (RNS) scheme as applied for 3-D internal viscous flow problems. No-slip boundary conditions are directly

imposed on the solid walls. There is no iteration procedure required in the cross plane to ensure mass conservation across each marching plane. The finite difference equations forming the coefficient matrix are ordered such that the surface normal velocity is specified on all the solid walls; unlike external flows, a pressure boundary condition in the cross plane is not required. Since continuity is directly satisfied at all points in the flow domain, the first order momentum equations can be solved directly for the pressure without the need for a Poisson pressure correction equation. The procedure developed herein can also be applied with periodic boundary conditions. The analysis is given for general compressible flows. Incompressible flow solutions are obtained, for straight and curved ducts of square cross section, to validate the procedure. These solutions are used to demonstrate the applicability of the RNS scheme, with the improved boundary conditions for internal flows with strong interaction, as would be encountered in ducts and turbomachinery geometries. Author

N88-15766* # Ohio State Univ., Columbus. Dept. of Aeronautical and Astronautical Engineering.

AN EXPERIMENTAL MAPPING OF THE FLOW FIELD BEHIND A GLAZE ICE SHAPE ON A NACA 0012 AIRFOIL M.S. Thesis Final Report

SAMUEL A. SPRING Jan. 1988 84 p
(Contract NAG3-28)
(NASA-CR-180847; NAS 1.26:180847) Avail: NTIS HC A05/MF A01 CSCL 01A

The flow field about a NACA 0012 airfoil with a simulated glaze ice shape was studied. Split hot-film anemometry was used to measure the streamwise velocity component in the upper and lower separation bubbles aft of the glaze ice horns. Velocity profiles were presented as well as the boundary layer momentum and displacement thickness distributions through the bubbles. Data were presented at angles of attack of 0, 2 and 4 deg and clearly showed the large region of reverse flow. A detailed discussion of split hot-film acquisition and data reduction, and possible sources of error has been included. Author

N88-15769* # Sverdrup Technology, Inc., Cleveland, OH.

A MULTISTAGE MESH GENERATOR FOR SOLVING THE AVERAGE-PASSAGE EQUATION SYSTEM Final Report

RICHARD A. MULAC Jan. 1988 19 p
(Contract NAS3-24105)
(NASA-CR-179539; E-3928; NAS 1.26:179539) Avail: NTIS HC A03/MF A01 CSCL 01A

One means of numerically simulating the 3-D flow field within a multistage turbomachine is through the solution of the average-passage equation system. One requirement of a current algorithm used to solve this system of equations has been the ability to generate multiple blade row meshes which satisfy specific geometrical constraints. In addition to meeting this criterion, one desires a mesh generation code which requires minimal user input, utilizes variable mesh control parameters, generates diagnostics helpful to the user, and possesses the capability to handle widely varying geometries. A mesh generation code with these features was written and has been used in solving the inviscid form of the average-passing equation system for both ducted and unducted multiple blade row geometries. This paper serves as a user reference guide, with a description of the mesh generation algorithm, a sample input file, and examples of typical meshes generated. Author

N88-16679* # National Aeronautics and Space Administration. Lewis Research Center, Cleveland, OH.

CFD VALIDATION EXPERIMENTS FOR INTERNAL FLOWS

LOUIS A. POVINELLI 1988 22 p Proposed for presentation at the Symposium on Validation of Computational Fluid Dynamics, Lisbon, Portugal, 2-5 May 1988; sponsored by AGARD (NASA-TM-100797; E-3973; NAS 1.15:100797) Avail: NTIS HC A03/MF A01 CSCL 01A

Computational Fluid Dynamics (CFD) validation experiments at NASA Lewis Research Center are described. The material presented summarizes the research in three areas: Inlets, Ducts

and Nozzles; Turbomachinery; and Chemically Reacting Flows. The specific validation activities are concerned with shock-boundary layer interactions, vortex generator effects, large low speed centrifugal compressor measurements, transonic fan shock structure, rotor/stator kinetic energy distributions, stator wake shedding characteristics, boundary layer transition, multiphase flow and reacting shear layers. These experiments are intended to provide CFD validation data for the internal flow fields within aerospace propulsion system components. Author

N88-16681*# National Aeronautics and Space Administration. Lewis Research Center, Cleveland, OH.

ON THE CORRELATION OF PLUME CENTERLINE VELOCITY DECAY OF TURBULENT ACOUSTICALLY EXCITED JETS

UWE H. VONGLAHN 1987 35 p Presented at the 11th Aeroacoustics conference, Sunnyvale, Calif., 19-21 Oct. 1987; sponsored by AIAA Previously announced in IAA as A88-18654 (NASA-TM-100193; E-3780; NAS 1.26:100193; AIAA-87-2692) Avail: NTIS HC A03/MF A01 CSCL 01A

Acoustic excitation was shown to alter the velocity decay and spreading characteristics of jet plumes by modifying the large-scale structures in the plume shear layer. The present work consists of reviewing and analyzing available published and unpublished experimental data in order to determine the importance and magnitude of the several variables that contribute to plume modification by acoustic excitation. Included in the study were consideration of the effects of internal and external acoustic excitation, excitation Strouhal number, acoustic excitation level, nozzle size, and flow conditions. The last include jet Mach number and jet temperature. The effects of these factors on the plume centerline velocity decay are then summarized in an overall empirical correlation. Author

N88-17582*# Toledo Univ., OH. Coll. of Engineering.
NUMERICAL SIMULATION OF AXISYMMETRIC TURBULENT FLOW IN COMBUSTORS AND DIFFUSORS Ph.D. Thesis. Final Report

CHAIN NAN YUNG Feb. 1988 177 p
(Contract NAG3-355)
(NASA-CR-4115; E-3853; NAS 1.26:4115) Avail: NTIS HC A09/MF A01 CSCL 01A

A method for predicting turbulent flow in combustors and diffusers is developed. The Navier-Stokes equations, incorporating a turbulence kappa-epsilon model equation, were solved in a nonorthogonal curvilinear coordinate system. The solution applied the finite volume method to discretize the differential equations and utilized the SIMPLE algorithm iteratively to solve the differenced equations. A zonal grid method, wherein the flow field was divided into several subsections, was developed. This approach permitted different computational schemes to be used in the various zones. In addition, grid generation was made a more simple task. However, treatment of the zonal boundaries required special handling. Boundary overlap and interpolating techniques were used and an adjustment of the flow variables was required to assure conservation of mass, momentum and energy fluxes. The numerical accuracy was assessed using different finite differencing methods, i.e., hybrid, quadratic upwind and skew upwind, to represent the convection terms. Flows in different geometries of combustors and diffusers were simulated and results compared with experimental data and good agreement was obtained. Author

N88-20262*# National Aeronautics and Space Administration. Lewis Research Center, Cleveland, OH.

NUMERICAL SIMULATION OF SUBSONIC AND TRANSONIC PROPELLER FLOW Ph.D. Thesis

AARON SNYDER Apr. 1988 191 p
(NASA-TM-100163; E-3725; NAS 1.15:100163) Avail: NTIS HC A09/MF A01 CSCL 01A

The numerical simulation of 3-D transonic flow about a system of propeller blades is investigated. In particular, it is shown that the use of helical coordinates significantly simplifies the form of the governing equation when the propeller system is assumed to be surrounded by an irrotational flow field of an inviscid fluid. The

unsteady small disturbance equation, valid for lightly loaded blades and expressed in helical coordinates, is derived from the general blade-fixed potential equation, given for an arbitrary coordinate system. The use of a coordinate system which inherently adapts to the mean flow results in a disturbance equation requiring relatively few terms to accurately model the physics of the flow. Furthermore, the helical coordinate system presented here is novel in that it is periodic in the circumferential direction while, simultaneously, maintaining orthogonal properties at the mean blade locations. The periodic characteristic allows a complete cascade of blades to be treated, and the orthogonality property affords straightforward treatment of blade boundary conditions. An ADI numerical scheme is used to compute the solution of the steady flow as an asymptotic limit of an unsteady flow. As an example of the method, solutions are presented for subsonic and transonic flow about a 5 percent thick bicircular arc blade of an 8-bladed cascade. Both high and low advance ratio cases are computed and include a lifting as well as nonlifting cases. The nonlifting solutions obtained are compared to solutions from a Euler code. Author

N88-22019*# National Aeronautics and Space Administration. Lewis Research Center, Cleveland, OH.

POROUS WIND TUNNEL CORRECTIONS FOR COUNTERROTATION PROPELLER TESTING

GEORGE L. STEFKO and ROBERT J. JERACKI 1988 18 p
Presented at the 15th Aerodynamic Testing Conference, San Diego, Calif., 18-20 May 1988; sponsored by AIAA
(NASA-TM-100873; E-4099; NAS 1.15:100873) Avail: NTIS HC A03/MF A01 CSCL 01B

Wind tunnel interference corrections have direct impact on measured propeller efficiency. A systematic series of wind tunnel tests was done in the porous-wall NASA Lewis 8- by 6-Foot Wind Tunnel to determine the wind tunnel interference corrections to the NASA Lewis counterrotation propeller test data. The test results were compared with calculations from a potential flow code to determine the interference corrections. At a Mach number of 0.8, the interference corrections resulted in a -0.008 Mach number correction which reduced the counterrotation propeller net efficiency data by 0.46 percent at the reduced Mach number. Additional wind tunnel tests were done to measure the effect of propeller thrust on wind tunnel wall interference. No wall interference corrections due to propeller thrust were found necessary for the high speed counterrotation propeller data obtained in the porous wall NASA Lewis 8- by 6-Foot Wind Tunnel. Author

N88-23245*# Purdue Univ., West Lafayette, IN. School of Aeronautics and Astronautics.

THE 2-D AND 3-D TIME MARCHING TRANSONIC POTENTIAL FLOW METHOD FOR PROPPANS

MARC H. WILLIAMS /in NASA, Lewis Research Center, Lewis Structures Technology, 1988. Volume 1: Structural Dynamics p 263-271 May 1988
(Contract NAG3-499)

Avail: NTIS HC A20/MF A01 CSCL 01A

Recent efforts concentrated on the development of aerodynamic tools for the analysis of rotors at transonic speeds and of configurations involving relative rotation. Three distinct approaches were taken: (1) extension of the lifting surface method of Williams and Hwang (1986) to relative rotation; (2) development of a time marching linear potential method for counter rotation; and (3) development of 2 and 3 dimensional finite volume potential flow schemes for single rotation. Results from each of these approaches are described. Author

N88-23248*# Duke Univ., Durham, NC. Dept. of Mechanical Engineering and Materials Science.

REDUCED ORDER MODELS FOR NONLINEAR AERODYNAMICS

APARAJIT J. MAHAJAN, EARL H. DOWELL, and DONALD B. BLISS /in NASA, Lewis Research Center, Lewis Structures Technology, 1988. Volume 1: Structural Dynamics p 299-308 May

02 AERODYNAMICS

1988

(Contract NAG3-724)

Avail: NTIS HC A20/MF A01 CSCL 01A

Reduced order models are needed for reliable, efficient and accurate prediction of aerodynamic forces to analyze fluid structure interaction problems in turbomachinery, including propfans. Here, a finite difference, time marching Navier-Stokes code is validated for unsteady airfoil motion by comparing results with those from classical potential flow. The Navier-Stokes code is then analyzed for calculation of primitive and exact estimates of eigenvalues and eigenvectors associated with fluid-airfoil interaction. A variational formulation for the Euler equations and Navier-Stokes equations will be the basis for reduction of order through an eigenvector transformation. Author

N88-23732*# National Aeronautics and Space Administration, Lewis Research Center, Cleveland, OH.

SATURATION AND THE LIMIT OF JET MIXING ENHANCEMENT BY SINGLE FREQUENCY PLANE WAVE EXCITATION: EXPERIMENT AND THEORY

GANESH RAMAN, EDWARD J. RICE, and REDA R. MANKBADI (Brown Univ., Providence, R. I.) 1988 16 p Prepared for presentation at the 1st National Fluid Dynamics Congress, Cincinnati, Ohio, 24-28 Jul. 1988; sponsored in part by AIAA, ASME, ASCE, SIAM, and APS

(NASA-TM-100882; E-4115; NAS 1.15:100882) Avail: NTIS HC A03/MF A01 CSCL 01A

The limitations of single frequency plane wave excitation in mixing enhancement are investigated for a circular jet. Measurements made in an 8.8 cm diameter jet are compared with a theoretical model. The measurements are made to quantify mixing at excitation amplitudes up to 2 percent of the jet exit velocity. The initial boundary layer state, the exit mean and fluctuating velocity profiles and spectra are documented for all cases considered. The amplitude of the fundamental wave is recorded along the jet axis for various levels of excitation. As the amplitude of excitation is increased the jet spreading rate is increased, but beyond a saturation amplitude further increases have no effect on the spreading. The experimental results are compared with theoretical estimates. In the theory the flow is split into the mean flow, large scale motions, and fine scale turbulence. Shape assumptions for the mean flow, and fine scale turbulence along with the shape for the large scale motions obtained from a linear stability theory provide the closure. The experimental results compare reasonably well with predictions. Author

N88-23751*# Lockheed Aeronautical Systems Co., Marietta, GA.

ACOUSTICALLY EXCITED HEATED JETS. 1: INTERNAL EXCITATION Final Contractor Report

J. LEPICOVSKY, K. K. AHUJA, W. H. BROWN, M. SALIKUDDIN, and P. J. MORRIS (Pennsylvania State Univ., University Park.) Washington NASA Jun. 1988 135 p (Contract NAS3-23708)

(NASA-CR-4129-PT-1; E-4001; NAS 1.26:4129-PT-1; LG86ER0022-PT-1) Avail: NTIS HC A07/MF A01 CSCL 01A

The effects of relatively strong upstream acoustic excitation on the mixing of heated jets with the surrounding air are investigated. To determine the extent of the available information on experiments and theories dealing with acoustically excited heated jets, an extensive literature survey was carried out. The experimental program consisted of flow visualization and flowfield velocity and temperature measurements for a broad range of jet operating and flow excitation conditions. A 50.8-mm-diam nozzle was used for this purpose. Parallel to the experimental study, an existing theoretical model of excited jets was refined to include the region downstream of the jet potential core. Excellent agreement was found between theory and experiment in moderately heated jets. However, the theory has not yet been confirmed for highly heated jets. It was found that the sensitivity of heated jets to upstream acoustic excitation varies strongly with the jet operating conditions and that the threshold excitation level increases with increasing jet temperature. Furthermore, the preferential Strouhal

number is found not to change significantly with a change of the jet operating conditions. Finally, the effects of the nozzle exit boundary layer thickness appear to be similar for both heated and unheated jets at low Mach numbers. Author

N88-23752*# Lockheed Aeronautical Systems Co., Marietta, GA.

ACOUSTICALLY EXCITED HEATED JETS. 2: IN SEARCH OF A BETTER UNDERSTANDING Final Contractor Report

J. LEPICOVSKY, K. K. AHUJA, W. H. BROWN, M. SALIKUDDIN, and P. J. MORRIS (Pennsylvania State Univ., University Park.) Washington NASA Jun. 1988 90 p (Contract NAS3-23708)

(NASA-CR-4129-PT-2; E-4002; NAS 1.26:4129-PT-2; LG86ER0022-PT-2) Avail: NTIS HC A05/MF A01 CSCL 01A

The second part of a three-part report on the effects of acoustic excitation on jet mixing includes the results of an experimental investigation directed at resolving the question of poor excitability of some of the heated jets. The theoretical predictions discussed in Part 1 are examined to find explanations for the observed discrepancies between the measured and the predicted results. Additional testing was performed by studying the self excitation of the shock containing hot jets and also by exciting the jet by sound radiated through source tubes located externally around the periphery of the jet. The effects of nozzle-exit boundary layer conditions on jet excitability was also investigated. It is concluded that high-speed, heated jet mixing rates and consequently also the jet excitability strongly depends on nozzle exit boundary layer conditions. Author

N88-23753*# Lockheed Aeronautical Systems Co., Marietta, GA.

ACOUSTICALLY EXCITED HEATED JETS. 3: MEAN FLOW DATA Final Contractor Report

J. LEPICOVSKY, K. K. AHUJA, W. H. BROWN, M. SALIKUDDIN, and P. J. MORRIS (Pennsylvania State Univ., University Park.) Washington NASA Jun. 1988 116 p (Contract NAS3-23708)

(NASA-CR-4129-PT-3; E-4003; NAS 1.26:4129-PT-3; LG86ER0022-PT-3) Avail: NTIS HC A06/MF A01 CSCL 01A

This is Part 3 of a report on the excitability of heated jets under the influence of acoustic excitation. The effects of upstream internal acoustic excitation on jet mixing were described in Part 1. Part 2 described the effects of external excitation on flow mixing. Part 3 contains quantitative results from the measurements of mean Mach number and temperature and consists of radial profiles and centerline distributions measured at selected jet operating conditions for internally excited and unexcited jets. The mean flow data are presented in both graphical and tabulated forms. For the sake of completeness, this part contains temperature probe calibration curves also. Author

N88-24592*# National Aeronautics and Space Administration, Lewis Research Center, Cleveland, OH.

EFFECT OF INITIAL TANGENTIAL VELOCITY DISTRIBUTION ON THE MEAN EVOLUTION OF A SWIRLING TURBULENT FREE JET

S. FAROKHI, R. TAGHAVI (Kansas Univ., Lawrence.), and E. J. RICE 1988 10 p Prepared for presentation at the 1st National Fluid Dynamics Congress, Cincinnati, Ohio, 24-28 Jul. 1988; sponsored in part by AIAA, ASME, ASCE, SIAM, and ASP (Contract NCC3-56)

(NASA-TM-100934; E-4211; NAS 1.15:100934) Avail: NTIS HC A02/MF A01 CSCL 01A

An existing cold jet facility at NASA-Lewis was modified to produce swirling flows with controllable initial tangential velocity distribution. Distinctly different swirl velocity profiles were produced, and their effects on jet mixing characteristics were measured downstream of an 11.43 cm diameter convergent nozzle. It was experimentally shown that in the near field of a swirling turbulent jet, the mean velocity field strongly depends on the initial swirl profile. Two extreme tangential velocity distributions were produced. The two jets shared approximately the same initial mass flow rate

of 5.9 kg/s, mass averaged axial Mach number and swirl number. Mean centerline velocity decay characteristics of the solid body rotation jet flow exhibited classical decay features of a swirling jet with $S = 0.48$ reported in the literature. It is concluded that the integrated swirl effect, reflected in the swirl number, is inadequate in describing the mean swirling jet behavior in the near field.

Author

N88-25497*# National Aeronautics and Space Administration. Lewis Research Center, Cleveland, OH.
SUMMARY OF LOW-SPEED WIND TUNNEL RESULTS OF SEVERAL HIGH-SPEED COUNTERROTATION PROPELLER CONFIGURATIONS

CHRISTOPHER E. HUGHES and JOHN A. GAZZANIGA (Sverdrup Technology, Inc., Cleveland, Ohio.) 1988 35 p Presented at the 24th Joint Propulsion Conference, Boston, Mass., 11-13 Jul. 1988; sponsored by AIAA, ASME, SAE and ASEE (NASA-TM-100945; E-4234; NAS 1.15:100945; AIAA-88-3149) Avail: NTIS HC A03/MF A01 CSCL 01A

The low speed aerodynamic performance characteristics of several advanced counterrotation pusher propeller configurations with cruise design Mach numbers of 0.72 and 0.80 were investigated in the NASA Low Speed Wind Tunnel. The tests were conducted at Mach numbers representative of the takeoff and landing flight regime. The investigation included: (1) the propeller performance characteristics over a range of blade angle settings and rotational speeds at a Mach number of 0.20; (2) the effect on the propeller performance of varying the axial rotor spacing and mismatching the power and rotational speeds on the propeller rotors; (3) determining the reverse thrust performance characteristics at Mach numbers of 0.0, 0.10, 0.15 and 0.20. The results of the investigation indicated that the overall low speed performance of the counterrotation propeller configurations was reasonable.

Author

N88-25435*# National Aeronautics and Space Administration. Lewis Research Center, Cleveland, OH.

CORRELATIONS OF VELOCITY AND TEMPERATURE FLUCTUATIONS IN THE STAGNATION-POINT FLOW OF CIRCULAR CYLINDER IN TURBULENT FLOW

CHI R. WANG 1988 22 p Presented at the 1988 Winter Annual Meeting of the American Society of Mechanical Engineers, Chicago, Ill., 28 Nov. - 2 Dec. 1988 (NASA-TM-100930; E-4201; NAS 1.15:100930) Avail: NTIS HC A03/MF A01 CSCL 01A

Boundary layer flow and turbulence transport analyses to study the influence of the free-stream turbulence on the surface heat transfer rate and the skin friction around the stagnation point of a circular cylinder in a turbulent flow are presented. The analyses are formulated with the turbulent boundary layer equations, the Reynolds stress transport equations and the $k - \epsilon$ two-equation turbulence modeling. The analyses are used to calculate the time-averaged turbulence double correlations, the mean flow properties, the surface heat transfer rate and the skin friction with an isotropic turbulence in the freestream. The analytical results are described and compared with the existing experimental measurements. Depending on the free-stream turbulence properties, the turbulence kinetic energy can increase or decrease as the flow moves toward the surface. However, the turbulence kinetic energy induces large Reynolds normal stresses at the boundary layer edge. The Reynolds normal stresses change the boundary layer profiles of the time-averaged double correlations of the velocity and temperature fluctuations, the surface heat transfer rate and the skin friction. The free-stream turbulence dissipation rate can affect the stagnation-point heat transfer rate but the influence of the free-stream temperature fluctuation on the heat transfer rate is insignificant.

Author

N88-25445*# Avco-Everett Research Lab., MA.
IMPROVED NUMERICAL METHODS FOR TURBULENT VISCOUS RECIRCULATING FLOWS Final Report
 A. TURAN and J. P. VANDORMAAL Jul. 1988 245 p

(Contract NAS3-24351)

(NASA-CR-180852; NAS 1.26:180852) Avail: NTIS HC A11/MF A01 CSCL 01A

The performance of discrete methods for the prediction of fluid flows can be enhanced by improving the convergence rate of solvers and by increasing the accuracy of the discrete representation of the equations of motion. This report evaluates the gains in solver performance that are available when various acceleration methods are applied. Various discretizations are also examined and two are recommended because of their accuracy and robustness. Insertion of the improved discretization and solver accelerator into a TEACH mode, that has been widely applied to combustor flows, illustrates the substantial gains to be achieved.

Author

N88-26336*# Sverdrup Technology, Inc., Cleveland, OH.
HIGH SPEED INLET CALCULATIONS WITH REAL GAS EFFECTS Final Report

WILLIAM J. COIRIER Jul. 1988 8 p Presented at the 24th Joint Propulsion Conference, Boston, Mass., 11-13 Jul. 1988; sponsored in part by AIAA, ASME, SAE and ASEE (Contract NAS3-24105) (NASA-CR-182167; E-4287; NAS 1.26:182167; AIAA-88-3076) Avail: NTIS HC A02/MF A01 CSCL 01A

A 2-D steady-state Navier-Stokes solver has been upgraded to include the effects of frozen and equilibrium air chemistry for applications to high speed flight vehicles. To provide a computationally economical first order approximation to the high temperature physics, variable thermodynamic data is used for the chemically frozen mode to allow for a variation with temperature of the air specific heats and enthalpy. For calculations involving air in chemical equilibrium, a specially modified version of the NASA Lewis Chemical Equilibrium Code, CEC, is used to compute the chemical composition and resultant thermochemical properties. The upgraded solver is demonstrated by comparing results from calorically perfect ($C_p = \text{constant}$), thermally perfect (frozen) and equilibrium air calculations for a variety of geometries, and flight Mach numbers.

Author

N88-26340*# National Aeronautics and Space Administration. Lewis Research Center, Cleveland, OH.

A DIAGONALLY INVERTED LU IMPLICIT MULTIGRID SCHEME

JEFFREY W. YOKOTA, DAVID A. CAUGHEY (Cornell Univ., Ithaca, N.Y.), and RODRICK V. CHIMA 1988 11 p Presented at the 1st National Fluid Dynamics Congress, Cincinnati, Ohio, 24-28 Jul. 1988; sponsored by AIAA, ASME, ASCE, SIAM and APS (NASA-TM-100911; E-4163; NAS 1.15:100911; AIAA-88-3567) Avail: NTIS HC A03/MF A01 CSCL 01A

A new Diagonally Inverted LU Implicit scheme is developed within the framework of the multigrid method for the 3-D unsteady Euler equations. The matrix systems that are to be inverted in the LU scheme are treated by local diagonalizing transformations that decouple them into systems of scalar equations. Unlike the Diagonalized ADI method, the time accuracy of the LU scheme is not reduced since the diagonalization procedure does not destroy time conservation. Even more importantly, this diagonalization significantly reduces the computational effort required to solve the LU approximation and therefore transforms it into a more efficient method of numerically solving the 3-D Euler equations.

Author

N88-27174*# National Aeronautics and Space Administration. Lewis Research Center, Cleveland, OH.

A COMPUTATIONAL ANALYSIS OF UNDER-EXPANDED JETS IN THE HYPERSONIC REGIME

ANDREW T. HSU (Sverdrup Technology, Inc., Cleveland, Ohio.) and MENG-SING LIOU 1988 8 p Presented at the Atmospheric Flight Mechanics Conference, Minneapolis, Minn., 15-17 Aug. 1988; sponsored by AIAA (NASA-TM-101319; E-4317; NAS 1.15:101319) Avail: NTIS HC A02/MF A01 CSCL 01A

Underexpanded axisymmetric jets are studied numerically using a full Navier-Stokes solver. Emphasis has been given to supersonic

02 AERODYNAMICS

and hypersonic jets in supersonic and hypersonic ambient flows, a phenomenon previously overlooked. It is demonstrated that the shear layers and shock patterns in a jet plume can be captured without complicated viscous/inviscid and subsonic/supersonic coupling schemes. In addition, a supersonic pressure relief effect has been identified for underexpanded jets in supersonic ambient flows. While it is well known that an underexpanded jet in a quiescent ambience (or subsonic ambience) contains multiple shock cells, the present study shows that because of the supersonic pressure relief effect, an underexpanded jet in a supersonic or hypersonic ambience contains only one major shock cell. Author

N88-28041*# National Aeronautics and Space Administration. Lewis Research Center, Cleveland, OH.

INVESTIGATION OF OSCILLATING CASCADE AERODYNAMICS BY AN EXPERIMENTAL INFLUENCE COEFFICIENT TECHNIQUE

DANIEL H. BUFFUM and SANFORD FLEETER (Purdue Univ., West Lafayette, Ind.) Jul. 1988 25 p Presented at the 24th Joint Propulsion Conference, Boston, Mass., 11-13 Jul. 1988; sponsored in part by AIAA, ASME, SAE and ASEE (NASA-TM-101313; E-4308; NAS 1.15:101313; AIAA-88-2815) Avail: NTIS HC A03/MF A01 CSCL 01A

Fundamental experiments are performed in the NASA Lewis Transonic Oscillating Cascade Facility to investigate the torsion mode unsteady aerodynamics of a biconvex airfoil cascade at realistic values of the reduced frequency for all interblade phase angles at a specified mean flow condition. In particular, an unsteady aerodynamic influence coefficient technique is developed and utilized in which only one airfoil in the cascade is oscillated at a time and the resulting airfoil surface unsteady pressure distribution measured on one dynamically instrumented airfoil. The unsteady aerodynamics of an equivalent cascade with all airfoils oscillating at a specified interblade phase angle are then determined through a vector summation of these data. These influence coefficient determined oscillation cascade data are correlated with data obtained in this cascade with all airfoils oscillating at several interblade phase angle values. The influence coefficients are then utilized to determine the unsteady aerodynamics of the cascade for all interblade phase angles, with these unique data subsequently correlated with predictions from a linearized unsteady cascade model. Author

N88-29746*# National Aeronautics and Space Administration. Lewis Research Center, Cleveland, OH.

ANALYSIS AND OPTIMIZATION OF TRUNCATED SCARF NOZZLES SUBJECT TO EXTERNAL FLOW CONDITIONS M.S. Thesis - Toledo Univ.

RICKEY J. SHYNE Aug. 1988 88 p (NASA-TM-100955; E-4146; NAS 1.15:100955) Avail: NTIS HC A05/MF A01 CSCL 01A

Results of a calculation of an optimized truncated scarfed nozzle were compared. The truncated scarfed nozzle was designed for an exit Mach number of 6.0, i.e., the Mach number at the last nozzle characteristic is 6.0, with an external flow Mach number of 5.0. The nozzle was designed by the Rao method for optimum thrust nozzles modified for 2-D flow and truncated scarfed nozzle applications. This design was analyzed using a shock-fitting method for 2-D supersonic flows. Excellent agreement was achieved between the design and analysis. Truncation of the lower nozzle wall (cowl) revealed that there is an optimum length for truncating the cowl without degrading the nozzle performance. Truncation of the nozzle cowl past this optimal length should be analyzed in trade-off studies for thrust loss versus gross vehicle weight. Plots of the oblique shock wave equations were also identified which will allow computation of slip line angle, dynamic pressure coefficient, or ambient Mach number for various specific heat ratios. Author

N88-29771*# National Aeronautics and Space Administration. Lewis Research Center, Cleveland, OH.

EULER ANALYSIS OF A SWIRL RECOVERY VANE DESIGN FOR USE WITH AN ADVANCED SINGLE-ROTATION PROPFAN

CHRISTOPHER J. MILLER 1988 15 p Presented at the 24th Joint Propulsion Conference, Boston, Mass., 11-13 Jul. 1988; sponsored by AIAA, ASME, SAE and ASEE (NASA-TM-101357; E-4387; NAS 1.15:101357; AIAA-88-3152) Avail: NTIS HC A03/MF A01 CSCL 01A

Recent work has demonstrated the propulsive efficiency improvement available from single- and counter-rotation propfans as compared with current technology high bypass ratio turbofans. The concept known as swirl recovery vanes (SRV) is examined through the use of a 3-D Euler code. At high speed cruise conditions, the SRV can improve the efficiency level of a single-rotation propfan, but a concern is to have adequate hub choke margin. The SRV was designed with 2-D methods and was predicted to have hub choking at Mach 0.8 cruise. The 3-D Euler analysis properly accounts for sweep effects and 3-D relief, and predicts that at cruise the SRV will recover roughly 5 percent of the 10 percent efficiency loss due to swirl and have a good hub choke margin. Author

N88-29780*# National Aeronautics and Space Administration. Lewis Research Center, Cleveland, OH.

AN UNCONDITIONALLY STABLE RUNGE-KUTTA METHOD FOR UNSTEADY FLOWS

PHILIP C. E. JORGENSON and RODRICK V. CHIMA 1988 14 p Prepared for presentation at the 27th Aerospace Sciences Meeting, Reno, Nev., 9-12 Jan. 1989; sponsored in part by AIAA (NASA-TM-101347; E-4373; NAS 1.15:101347; AIAA-89-0205) Avail: NTIS HC A03/MF A01 CSCL 01A

A quasi-three dimensional analysis was developed for unsteady rotor-stator interaction in turbomachinery. The analysis solves the unsteady Euler or thin-layer Navier-Stokes equations in a body fitted coordinate system. It accounts for the effects of rotation, radius change, and stream surface thickness. The Baldwin-Lomax eddy viscosity model is used for turbulent flows. The equations are integrated in time using a four stage Runge-Kutta scheme with a constant time step. Implicit residual smoothing was employed to accelerate the solution of the time accurate computations. The scheme is described and accuracy analyses are given. Results are shown for a supersonic through-flow fan designed for NASA Lewis. The rotor:stator blade ratio was taken as 1:1. Results are also shown for the first stage of the Space Shuttle Main Engine high pressure fuel turbopump. Here the blade ratio is 2:3. Implicit residual smoothing was used to increase the time step limit of the unsmoothed scheme by a factor of six with negligible differences in the unsteady results. It is felt that the implicitly smoothed Runge-Kutta scheme is easily competitive with implicit schemes for unsteady flows while retaining the simplicity of an explicit scheme. Author

03

AIR TRANSPORTATION AND SAFETY

Includes passenger and cargo air transport operations; and aircraft accidents.

A88-22079*# Massachusetts Inst. of Tech., Cambridge.

INVESTIGATION OF SURFACE WATER BEHAVIOR DURING GLAZE ICE ACCRETION

R. JOHN HANSMAN, JR. and STEPHEN R. TURNOCK (MIT, Cambridge, MA) AIAA, Aerospace Sciences Meeting, 26th, Reno, NV, Jan. 11-14, 1988. 11 p. refs (Contract NAG3-666; NGL-22-009-640) (AIAA PAPER 88-0115)

Microvideo observations of glaze ice accretions on 1-in-diameter

cylinders in a closed-loop refrigerated wind tunnel were obtained to study factors controlling the behavior of unfrozen surface water during glaze ice accretion. Three zones of surface water behavior were noted, each with a characteristic roughness. The effect of substrate thermal and roughness properties on ice accretions was also studied. The contact angle and hysteresis were found to increase sharply at temperatures just below 0 C, explaining the high resistance to motion of water beads observed on accreting glaze ice surfaces. Based on the results, a simple multizone modification to the current glaze ice accretion model is proposed.

R.R.

A88-32714* Massachusetts Inst. of Tech., Cambridge.
**MEASUREMENT OF ICE THICKNESS (ICING) IN
 AERONAUTICS [MESURES DES EPAISSEURS DE GLACE
 (GIVRAGE) EN AERONAUTIQUE]**

R. JOHN HANSMAN and MARK S. JR. KIRBY (MIT, Cambridge, MA) *L'Aeronautique et l'Astronautique* (ISSN 0001-9275), no. 128, 1988, p. 57-68. In French. FAA-supported research.

(Contract NGL-22-009-640; NAG3-666)

Pulsed ultrasonic techniques have been used to measure the formation of ice in flight in an icing wind tunnel with a precision of + or - 0.5 mm. Two icing regimes, humid and dry, are identified. Both natural and artificial conditions are considered. On the basis of ice formation rates obtained by the ultrasound technique and the observed surface conditions, it is found that the heat transfer coefficients are larger in the wind tunnel tests than in actual flight, presumably due to the higher level of turbulence in the wind tunnel tests. Profiles obtained during flight under natural conditions are compared with mechanical-type measurements and with the results of stereographic analysis.

R.R.

A88-50910* Massachusetts Inst. of Tech., Cambridge.
**IN-FLIGHT MEASUREMENT OF AIRFOIL ICING USING AN
 ARRAY OF ULTRASONIC TRANSDUCERS**

R. JOHN HANSMAN, JR., MARK S. KIRBY (MIT, Cambridge, MA), ROBERT C. MCKNIGHT (NASA, Lewis Research Center, Cleveland, OH), and ROBERT L. HUMES (Calspan Corp., Arnold Air Force Station, TN) *Journal of Aircraft* (ISSN 0021-8669), vol. 25, June 1988, p. 531-537. FAA-supported research. Previously cited in issue 08, p. 1047, Accession no. A87-22464. refs

(Contract NGL-22-009-640; NAG3-666)

N88-12473* National Aeronautics and Space Administration.
 Lewis Research Center, Cleveland, OH.

**EXPERIMENTAL EVIDENCE FOR MODIFYING THE CURRENT
 PHYSICAL MODEL FOR ICE ACCRETION ON AIRCRAFT
 SURFACES**

W. OLSEN and E. WALKER 1986 47 p Film supplement
 (NASA-TM-87184; E-3658; NASA-MPD-1683; NAS 1.15:87184)

Avail: NTIS HC A03/MF A01; film supplement number

NASA-MPD-1683 available from NASA Lewis Research Center, Photographic and Printing Branch, Cleveland, Ohio CSCL 01C

Closeup movies, still photographs, and other experimental data suggest that the current physical model for ice accretion needs significant modification. At aircraft airspeeds there was no flow of liquid over the surface of the ice after a short initial flow, even at barely subfreezing temperatures. Instead, there were very large stationary drops on the ice surface that lose water from their bottoms by freezing and replenish their liquid by catching the microscopic cloud droplets. This observation disagrees with the existing physical model, which assumes there is a thin liquid film continuously flowing over the ice surface. With no such flow, the freezing-fraction concept of the model fails when a mass balance is performed on the surface water. Rime ice does, as the model predicts, form when the air temperature is low enough to cause the cloud droplets to freeze almost immediately on impact. However, the characteristic shapes of horn-glaze ice or rime ice are primarily caused by the ice shape affecting the airflow locally and consequently the droplet catch and the resulting ice shape. Ice roughness greatly increases the heat transfer coefficient, stops the movement of drops along the surface, and may also affect the airflow initially and thereby the droplet catch. At high subfreezing

temperatures the initial flow and shedding of surface drops have a large effect on the ice shape. At the incipient freezing limit, no ice forms.

Author

N88-13310* Wichita State Univ., KS.

**THEORETICAL ANALYSIS OF THE ELECTRICAL ASPECTS OF
 THE BASIC ELECTRO-IMPULSE PROBLEM IN AIRCRAFT
 DE-ICING APPLICATIONS Final Report**

ROBERT A. HENDERSON and ROBERT L. SCHRAG Nov. 1987 80 p

(Contract NAG3-284)

(NASA-CR-180845; NAS 1.26:180845) Avail: NTIS HC A05/MF A01 CSCL 01C

A method of modelling a system consisting of a cylindrical coil with its axis perpendicular to a metal plate of finite thickness, and a simple electrical circuit for producing a transient current in the coil, is discussed in the context of using such a system for de-icing aircraft surfaces. A transmission line model of the coil and metal plate is developed as the heart of the system model. It is shown that this transmission model is central to calculation of the coil impedance, the coil current, the magnetic fields established on the surfaces of the metal plate, and the resultant total force between the coil and the plate. FORTRAN algorithms were developed for numerical calculation of each of these quantities, and the algorithms were applied to an experimental prototype system in which these quantities had been measured. Good agreement is seen to exist between the predicted and measured results.

Author

N88-15778* Douglas Aircraft Co., Inc., Long Beach, CA. Aircraft Configuration and Performance Dept.

**EFFECTS OF ENVIRONMENTALLY IMPOSED ROUGHNESS
 ON AIRFOIL PERFORMANCE**

TUNCER CEBECI *In* Von Karman Inst. for Fluid Dynamics, Influence of Environmental Factors on Aircraft Wing Performance 43 p Feb. 1987

(Contract NAG3-601; NSF MEA-0818565)

Avail: NTIS HC A11/MF A01 CSCL 01C

The experimental evidence for the effects of rain, insects, and ice on airfoil performance are examined. The extent to which the available information can be incorporated in a calculation method in terms of change of shape and surface roughness is discussed. The methods described are based on the interactive boundary layer procedure of Cebeci or on the thin layer Navier Stokes procedure developed at NASA. Cases presented show that extensive flow separation occurs on the rough surfaces.

ESA

N88-15803* National Aeronautics and Space Administration.
 Lewis Research Center, Cleveland, OH.

THE NASA AIRCRAFT ICING RESEARCH PROGRAM

ROBERT J. SHAW and JOHN J. REINMANN *In its* Aeropropulsion '87. Session 5: Subsonic Propulsion Technology 27 p Nov. 1987

Avail: NTIS HC A08/MF A01 CSCL 01C

The objective of the NASA aircraft icing research program is to develop and make available to industry icing technology to support the needs and requirements for all weather aircraft designs. Research is being done for both fixed and rotary wing applications. The NASA program emphasizes technology development in two key areas: advanced ice protection concepts and icing simulation (analytical and experimental). The computer code development/validation, icing wind tunnel testing, and icing flight testing efforts which were conducted to support the icing technology development are reviewed.

Author

N88-16641* National Aeronautics and Space Administration.
 Lewis Research Center, Cleveland, OH.

NASA'S ROTORCRAFT ICING RESEARCH PROGRAM

ROBERT J. SHAW, JOHN J. REINMANN, and THOMAS L. MILLER (Sverdrup Technology, Inc., Cleveland, Ohio.) *In* NASA, Washington, NASA/Army Rotorcraft Technology. Volume 2: Materials and Structures, Propulsion and Drive Systems, Flight

03 AIR TRANSPORTATION AND SAFETY

Dynamics and Control, and Acoustics p 802-832 Feb. 1988
Avail: NTIS HC A25/MF A01 CSCL 01C

The objective of the NASA aircraft icing research program is to develop and make available icing technology to support the needs and requirements of industry for all weather aircraft designs. While a majority of the technology being developed is viewed to be generic (i.e., appropriate to all vehicle classes), vehicle specific emphasis is being placed on the helicopter due to its unique icing problems. In particular, some of the considerations for rotorcraft icing are indicated. The NASA icing research program emphasizes technology development in two key areas: ice protection concepts and icing simulation (analytical and experimental). The NASA research efforts related to rotorcraft icing in these two technology areas will be reviewed. Author

N88-18574*# Atmospheric Science Associates, Concord, MA.
THREE-DIMENSIONAL TRAJECTORY ANALYSES OF TWO DROP SIZING INSTRUMENTS: PMS OAP AND PMS FSSP Final Report

HILLYER G. NORMENT Washington NASA Feb. 1988
65 p
(Contract NAS3-24630)
(NASA-CR-4113; E-3851; NAS 1.26:4113; DOT/FAA/CT-87/30)
Avail: NTIS HC A04/MF A01 CSCL 01C

Flow induced distortions of water drop fluxes and speeds seen by the instruments were predicted by use of three dimensional flow and trajectory calculation methods. Sensitivities were determined for the instruments, in isolation and mounted under the wing of an airplane, to: water drop diameter (2 to 1000 microns), angle of attack and free stream air speed. For the optical array probe in isolation and on the airplane at 0 deg angle of attack, flux distortions of practical consequence are not found. At 4 deg airplane angle of attack, partial flow stagnation under the upturned wing causes significant decreases in both flux and speed for cloud size droplets. For the forward scattering spectrometer probe in isolation, only marginally significant sensitivities to free stream air speed are found, and no sensitivity is found to angle of attack. Both speed and flux of cloud size droplets are predicted to be undermeasured by from 12 to 24 percent depending on airplane angle of attack. For the wing-mounted instruments, effects of flow about the instruments themselves are found to be equal in importance to effects of flow about the airplane. Preferred orientation (canting) angles of distorted water drops are found to be functions of drop size, angle of attack and air speed. Author

N88-21143*# Massachusetts Inst. of Tech., Cambridge. Dept. of Aeronautics and Astronautics.

AN EXPERIMENTAL AND THEORETICAL STUDY OF THE ICE ACCRETION PROCESS DURING ARTIFICIAL AND NATURAL ICING CONDITIONS Final Contractor Report

MARK S. KIRBY and R. JOHN HANSMAN Apr. 1988 136 p
(Contract NAG3-666; NGL-22-009-640)
(NASA-CR-182119; NAS 1.26:182119; DOT/FAA/CT-87/17)
Avail: NTIS HC A07/MF A01 CSCL 01C

Real-time measurements of ice growth during artificial and natural icing conditions were conducted using an ultrasonic pulse-echo technique. This technique allows ice thickness to be measured with an accuracy of + or - 0.5 mm; in addition, the ultrasonic signal characteristics may be used to detect the presence of liquid on the ice surface and hence discern wet and dry ice growth behavior. Ice growth was measured on the stagnation line of a cylinder exposed to artificial icing conditions in the NASA Lewis Icing Research Tunnel (IRT), and similarly for a cylinder exposed in flight to natural icing conditions. Ice thickness was observed to increase approximately linearly with exposure time during the initial icing period. The ice accretion rate was found to vary with cloud temperature during wet ice growth, and liquid runback from the stagnation region was inferred. A steady-state energy balance model for the icing surface was used to compare heat transfer characteristics for IRT and natural icing conditions. Ultrasonic measurements of wet and dry ice growth observed in the IRT and in flight were compared with icing regimes predicted by a series of heat transfer coefficients. The heat transfer

magnitude was generally inferred to be higher for the IRT than for the natural icing conditions encountered in flight. An apparent variation in the heat transfer magnitude was also observed for flights conducted through different natural icing-cloud formations.

Author

N88-23717*# National Aeronautics and Space Administration. Lewis Research Center, Cleveland, OH.

IN-FLIGHT MEASUREMENT OF ICE GROWTH ON AN AIRFOIL USING AN ARRAY OF ULTRASONIC TRANSDUCERS

R. JOHN HANSMAN, JR., MARK S. KIRBY, ROBERT C. MCKNIGHT, and ROBERT L. HUMES (Calspan Corp., Arnold AFS, Tenn.) In NASA, Langley Research Center, Joint University Program for Air Transportation Research, 1986 p 7-15 Apr. 1988 Sponsored in cooperation with FAA
(Contract NGL-22-009-640; NAG3-666)
(AIAA-87-0178) Avail: NTIS HC A06/MF A01 CSCL 01C

Results of preliminary tests to measure ice growth on an airfoil during flight icing conditions are presented. Ultrasonic pulse echo measurements of ice thickness are obtained from an array of eight ultrasonic transducers mounted flush with the leading edge of the airfoil. These thickness measurements are used to document the evolution of the ice shape during the encounter in the form of successive ice profiles. Results from 3 research flights are presented and discussed. The accuracy of the ultrasonic measurements is found to be within 0.5 mm of mechanical and stereo photograph measurements of the ice accretion. Author

05

AIRCRAFT DESIGN, TESTING AND PERFORMANCE

Includes aircraft simulation technology.

A88-15227* Pratt and Whitney Aircraft, East Hartford, CT.

IN-FLIGHT THRUST DETERMINATION

ROBERT B. ABERNETHY (Pratt and Whitney, East Hartford, CT), GARY R. ADAMS (USAF, Wright-Patterson AFB, OH), JOHN C. ASCOUGH (Royal Aircraft Establishment, Farnborough, England), JENNIFER L. BAER-RIEDHART (NASA, Flight Research Center, Edwards, CA), GEORGE H. BALKCOM (General Dynamics Corp., Saint Louis, MO), THOMAS BIESIADNY (NASA, Lewis Research Center, Cleveland, OH) et al. (SAE Aerospace Information Report, SAE AIR 1703, Nov. 1985) IN: In-flight thrust determination and uncertainty. Warrendale, PA, Society of Automotive Engineers, Inc., 1986, 234 p. refs
(SAE AIR 1703)

The major aspects of processes that may be used for the determination of in-flight thrust are reviewed. Basic definitions are presented as well as analytical and ground-test methods for gathering data and calculating the thrust of the propulsion system during the flight development program of the aircraft. Test analysis examples include a single-exhaust turbofan, an intermediate-cowl turbofan, and a mixed-flow afterburning turbofan. K.K.

A88-15228* Pratt and Whitney Aircraft, East Hartford, CT.

UNCERTAINTY OF IN-FLIGHT THRUST DETERMINATION

ROBERT B. ABERNETHY (Pratt and Whitney, East Hartford, CT), GARY R. ADAMS (USAF, Wright-Patterson AFB, OH), JOHN W. STEURER (McDonnell Douglas Co., Saint Louis, MO), JOHN C. ASCOUGH (Royal Aircraft Establishment, Farnborough, England), JENNIFER L. BAER-RIEDHART (NASA, Flight Research Center, Edwards, CA), GEORGE H. BALKCOM (General Dynamics Corp., Saint Louis, MO), THOMAS BIESIADNY (NASA, Lewis Research Center, Cleveland, OH) et al. (SAE Aerospace Information Report, SAE AIR 1678, Aug. 1985) IN: In-flight thrust determination and uncertainty. Warrendale, PA, Society of Automotive Engineers, Inc., 1986, p. 243-338. refs
(SAE AIR 1678)

Methods for estimating the measurement error or uncertainty of in-flight thrust determination in aircraft employing conventional turbofan/turbojet engines are reviewed. While the term 'in-flight thrust determination' is used synonymously with 'in-flight thrust measurement', in-flight thrust is not directly measured but is determined or calculated using mathematical modeling relationships between in-flight thrust and various direct measurements of physical quantities. The in-flight thrust determination process incorporates both ground testing and flight testing. The present text is divided into the following categories: measurement uncertainty methodology and in-flight thrust measurement processes. K.K.

A88-15724* National Aeronautics and Space Administration. Lewis Research Center, Cleveland, OH.

A HEATER MADE FROM GRAPHITE COMPOSITE MATERIAL FOR POTENTIAL DEICING APPLICATION

CHING-CHEH HUNG (NASA, Lewis Research Center, Cleveland, OH), MICHAEL E. DILLEHAY, and MARK STAHL (Cleveland State University, OH) *Journal of Aircraft* (ISSN 0021-8669), vol. 24, Oct. 1987, p. 725-730. Previously cited in issue 09, p. 1197, Accession no. A87-24905. refs

A88-16748* National Aeronautics and Space Administration. Langley Research Center, Hampton, VA.

HYPERSONIC STRUCTURES AND MATERIALS - A PROGRESS REPORT

L. ROBERT JACKSON, SIDNEY C. DIXON, DARREL R. TENNEY (NASA, Langley Research Center, Hampton, VA), ALAN L. CARTER (NASA, Ames Research Center, Moffett Field, CA), and JOSEPH R. STEPHENS (NASA, Lewis Research Center, Cleveland, OH) *Aerospace America* (ISSN 0740-722X), vol. 25, Oct. 1987, p. 24, 25, 28-30.

The weight of a hypersonic, airbreathing SSTO vehicle may be more critical than for any previous aerospacecraft; an evaluation is accordingly made of the development status and applicability of intermetallic compounds, metal-matrix composites, carbon-carbon composites, ceramics, and ceramic-matrix composites applicable to SSTO craft primary structures. Aerothermal, aerothermoelastic, and acoustic loads are high because the airbreathing SSTO vehicle must follow a high dynamic pressure trajectory in order to achieve the requisite propulsive efficiency. Attention is given to the prospects for integral cryogenic tankage and actively hydrogen-cooled airframe and engine structures. O.C.

A88-22016* Wichita State Univ., KS.

ELECTRO-IMPULSE DE-ICING ELECTRODYNAMIC SOLUTION BY DISCRETE ELEMENTS

W. D. BERNHART and R. L. SCHRAG (Wichita State University, KS) *AIAA, Aerospace Sciences Meeting*, 26th, Reno, NV, Jan. 11-14, 1988. 10 p. refs

(Contract NAG3-284)

(AIAA PAPER 88-0018)

This paper describes a technique for analyzing the electrodynamic phenomena associated with electro-impulse deicing. The analysis is done in the time domain and utilizes a discrete element formulation concept expressed in state variable form. Calculated results include coil current, eddy currents in the target (aircraft leading edge skin), pressure distribution on the target, and total force and impulse on the target. Typical results are presented and described. Some comparisons are made between calculated and experimental results, and also between calculated values from other theoretical approaches. Application to the problem of a nonrigid target is treated briefly. Author

A88-22017* Wichita State Univ., KS.

ELECTRO-IMPULSE DE-ICING - A STATUS REPORT

G. W. ZUMWALT (Wichita State University, KS) *AIAA, Aerospace Sciences Meeting*, 26th, Reno, NV, Jan. 11-14, 1988. 6 p. refs

(Contract NAG3-284; DOT-FA03-86-C-00041)

(AIAA PAPER 88-0019)

The advantages and disadvantages of the Electro-Impulse De-Icing (EIDI) system are examined. The design and operation

of the EIDI are described. The effect of repeated impulsive loads on the structure and skin of the aircraft surface is investigated. It is observed that the wing skin directly over the coil receives the greatest stresses. Data from the testing of metal leading edges reveal that after 11,500 impulses cracks appear in the sheet brackets attaching the ribs to the coil beams. The composite leading edge was evaluated for fatigue, and after 20,000 impulses no cracks were detected. The advantages of the band-aid coil mount are discussed. I.F.

A88-22783* Texas A&M Univ., College Station.

MODEL HELICOPTER PERFORMANCE DEGRADATION WITH SIMULATED ICE SHAPES

ANA F. TINETTI and KENNETH D. KORKAN (Texas A & M University, College Station) *IN: AHS, Annual Forum*, 43rd, Saint Louis, MO, May 18-20, 1987, *Proceedings. Volume 2. Alexandria, VA, American Helicopter Society*, 1987, p. 765-780. refs

(Contract NAG3-626)

An experimental program using a commercially available model helicopter has been conducted in the Texas A&M University Subsonic Wind Tunnel to investigate main rotor performance degradation due to generic ice. The simulated ice, including both primary and secondary formations, was scaled by chord from previously documented artificial ice accretions. Base and iced performance data were gathered as functions of fuselage incidence, blade collective pitch, main rotor rotational velocity, and freestream velocity. It was observed that the presence of simulated ice tends to decrease the lift to equivalent drag ratio, as well as thrust coefficient for the range of velocity ratios tested. Also, increases in torque coefficient due to the generic ice formations were observed. Evaluation of the data has indicated that the addition of roughness due to secondary ice formations is crucial for proper evaluation of the degradation in main rotor performance. Author

N88-15811* National Aeronautics and Space Administration. Lewis Research Center, Cleveland, OH.

HIGH-SPEED INLET RESEARCH PROGRAM AND SUPPORTING ANALYSES

ROBERT E. COLTRIN *In its Aeropropulsion '87. Session 6: High-Speed Propulsion Technology* 20 p Nov. 1987

Avail: NTIS HC A06/MF A01 CSDL 01C

A Mach 5 cruise aircraft was studied in a joint program effort. The propulsion system chosen for this aircraft was an over-under turbojet/ramjet system. The ramjet portion of the inlet is to be tested in NASA Lewis' 10 x 10 SWT. Goals of the test program are to obtain performance data and bleed requirements, and also to obtain analysis code validation data. Supporting analysis of the inlet using a three-dimensional Navier-Stokes code (PEPSIS) indicates that sidewall shock/boundary layer interactions cause large separated regions in the corners underneath the cowl. Such separations generally lead to inlet unstart, and are thus a major concern. As a result of the analysis, additional bleed regions were added to the inlet model sidewalls and cowl to control separations in the corners. A two-dimensional analysis incorporating bleed on the ramp is also presented. Supporting experiments for the Mach 5 programs were conducted in the Lewis' 1 x 1 SWT. A small-scale model representing the inlet geometry up to the ramp shoulder and cowl lip was tested to verify the accelerator plate test technique and to obtain data on flow migration in the ramp and sidewall boundary layers. Another study explored several ramp bleed configurations to control boundary layer separations in that region. Design of a two-dimensional Mach 5 cruise inlet represents several major challenges including multimode operation and dual flow, high temperatures, and three-dimensional airflow effects. Author

N88-26360* Lockheed Aeronautical Systems Co., Marietta, GA.

PROFAN TEST ASSESSMENT TESTBED AIRCRAFT STABILITY AND CONTROL/PERFORMANCE 1/9-SCALE WIND TUNNEL TESTS Final Report

B. H. LITTLE, JR., K. H. TOMLIN, A. S. ALJABRI, and C. A. MASON May 1988 157 p

05 AIRCRAFT DESIGN, TESTING AND PERFORMANCE

(Contract NAS3-24339)
(NASA-CR-182121; NAS 1.26:182121; LG88ER0056) Avail:
NTIS HC A08/MF A01 CSCL 01C

One-ninth scale wind tunnel model tests of the Propfan Test Assessment (PTA) aircraft were performed in three different NASA facilities. Wing and propfan nacelle static pressures, model forces and moments, and flow field at the propfan plane were measured in these tests. Tests started in June 1985 and were completed in January 1987. These data were needed to assure PTA safety of flight, predict PTA performance, and validate analytical codes that will be used to predict flow fields in which the propfan will operate. Author

N88-28917*# Boeing Military Airplane Development, Wichita, KS.

MULTIPLE-PURPOSE SUBSONIC NAVAL AIRCRAFT (MPSNA): MULTIPLE APPLICATION PROPFAN STUDY (MAPS) Final Report

R. M. ENGELBECK, C. T. HAVEY, A. KLAMKA, C. L. MCNEIL, and M. A. PAIGE Sep. 1986 219 p
(Contract NAS3-24529)
(NASA-CR-175104; NAS 1.26:175104; D500-11313-1) Avail:
NTIS HC A10/MF A01 CSCL 01C

Study requirements, assumptions and guidelines were identified regarding carrier suitability, aircraft missions, technology availability, and propulsion considerations. Conceptual designs were executed for two missions, a full multimission aircraft and a minimum mission aircraft using three different propulsion systems, the Unducted Fan (UDF), the Propfan and an advanced Turbofan. Detailed aircraft optimization was completed on those configurations yielding gross weight performance and carrier spot factors. Propfan STOVL conceptual designs were exercised also to show the effects of STOVL on gross weight, spot factor and cost. An advanced technology research plan was generated to identify additional investigation opportunities from an airframe contractors standpoint. Life cycle cost analysis was accomplished yielding a comparison of the UDF and propfan configurations against each other as well as against a turbofan with equivalent state of the art turbo-machinery. Author

06

AIRCRAFT INSTRUMENTATION

Includes cockpit and cabin display devices; and flight instruments.

A88-51910*# Massachusetts Inst. of Tech., Cambridge.

ULTRASONIC TECHNIQUES FOR AIRCRAFT ICE ACCRETION MEASUREMENT

R. JOHN HANSMAN, JR., MARK S. KIRBY (MIT, Cambridge, MA), and FRED LICHTENFELTS (Simmonds Precision Products, Inc., Aircraft Systems Div., Vergennes, VT) AIAA, NASA, and AFWAL, Conference on Sensors and Measurements Techniques for Aeronautical Applications, Atlanta, GA, Sept. 7-9, 1988. 12 p. FAA-supported research.

(Contract NGL-22-009-640; NAG3-666)
(AIAA PAPER 88-4656)

Ultrasonic pulse-echo measurements of ice growth on cylinders and airfoils exposed to both artificial (icing wind tunnel) and natural (flight) icing conditions are presented. An accuracy of ± 0.5 mm is achieved with the present method. The ultrasonic signal characteristics associated with each of the two types of icing regimes identified, wet and dry ice growth, are discussed. Heat transfer coefficients are found to be higher in the wind tunnel environment than in flight. Results for ice growth on airfoils have also been obtained using an array of ultrasonic transducers. Icing profiles obtained during flight are compared with mechanical and stereo image measurements. R.R.

N88-28062*# National Aeronautics and Space Administration, Lewis Research Center, Cleveland, OH.

MODULATED-SPLITTING-RATIO FIBER-OPTIC TEMPERATURE SENSOR

GLENN BEHEIM, DONALD J. ANTHAN, JOHN R. RYS, KLAUS FRITSCH, and WALTER A. RUPPE (Case Western Reserve Univ., Cleveland, Ohio.) 1988 12 p Presented at Fiber Optic and Laser Sensors 6, Boston, Mass., 6-9 Sep. 1988; sponsored by Society of Photo-Optical Instrumentation Engineers (NASA-TM-101332; E-4344; NAS 1.15:101332) Avail: NTIS HC A03/MF A01 CSCL 01D

A fiber-optic temperature sensor is described, which uses a small silicon beamsplitter whose splitting ratio varies as a function of temperature. A four-beam technique is used to measure the sensor's temperature-indicating splitting ratio. This referencing method provides a measurement that is largely independent of the transmission properties of the sensor's optical fiber link. A significant advantage of this sensor, relative to other fiber-optic sensors, is its high stability, which permits the fiber-optic components to be readily substituted, thereby simplifying the sensor's installation and maintenance. Author

07

AIRCRAFT PROPULSION AND POWER

Includes prime propulsion systems and systems components, e.g., gas turbine engines and compressors; and onboard auxiliary power plants for aircraft.

A88-10998*# Princeton Univ., NJ.

LOCALIZATION OF NATURAL MODES OF VIBRATION IN BLADED DISKS

O. O. BENDIKSEN (Princeton University, NJ) and N. A. VALERO ASME, International Gas Turbine Conference and Exhibition, 32nd, Anaheim, CA, May 31-June 4, 1987. 11 p. refs
(Contract NAG3-308)
(ASME PAPER 87-GT-46)

A study is presented of the mode localization phenomenon in imperfect blade-disk and blade-shroud-disk assemblies. The results indicate that unshrouded blades mounted on stiff disks are especially susceptible, and even small blade imperfections within manufacturing tolerances are likely to trigger mode localization. Increasing the interblade coupling by adding shrouds or reducing the disk stiffness greatly reduces the localization susceptibility, although certain modes may still become localized if the shrouds are free to slip. Author

A88-11079*# Pratt and Whitney Aircraft, West Palm Beach, FL. **CONCEPTUAL DESIGN OF AN OPTIC BASED ENGINE CONTROL SYSTEM**

W. J. DAVIES (Pratt and Whitney, Engineering Div., West Palm Beach, FL), R. J. BAUMBICK (NASA, Lewis Research Center, Cleveland, OH), and R. W. VIZZINI (U.S. Navy, Naval Air Propulsion Test Center, Trenton, NJ) ASME, International Gas Turbine Conference and Exhibition, 32nd, Anaheim, CA, May 31-June 4, 1987. 8 p.
(ASME PAPER 87-GT-168)

Use of optics in the aircraft engine control systems would provide immunity to electromagnetic effects (such as lightning, radar, and nuclear pulses) for flight and propulsion control systems located throughout the aircraft and in need of communication and would result in weight reduction. This paper discusses a conceptual design of an optic engine control system that is being developed by the Fiber Optic Control System Integration (FOCSI) program. The features inherent in each of the optic-based components of the optic system, which includes the on-engine full authority digital electronic control, optic sensors, optic-based actuators, and an optic data bus for communication with the aircraft flight control system

are described in detail. The diagrams of the FOCSI control system and its components are included. I.S.

A88-15119*# Integral Technologies, Inc., Westmont, IL.
APPLICATION OF SEVERAL VARIABLE-VALVE-TIMING CONCEPTS TO AN LHR ENGINE

T. MOREL, R. KERIBAR (Integral Technologies, Inc., Westmont, IL), M. SAWLIVALA, and N. HAKIM (General Motors Corp., Detroit Diesel Allison Div., Romulus, MI) ASME, Transactions, Journal of Engineering for Gas Turbines and Power (ISSN 0022-0825), vol. 109, Oct. 1987, p. 402-409. DOE-supported research. (Contract DEN3-329) (ASME PAPER 87-ICE-29)

The paper discusses advantages provided by electronically controlled hydraulically activated valves (ECVs) when applied to low heat rejection (LHR) engines. The ECV concept provides additional engine control flexibility by allowing for a variable valve timing as a function of speed and load, or for a given transient condition. The results of a study carried out to assess the benefits that this flexibility can offer to an LHR engine indicated that, when judged on the benefits to BSFC, volumetric efficiency, and peak firing pressure, ECVs would provide only modest benefits in comparison to conventional valve profiles. It is noted, however, that once installed on the engine, the ECVs would permit a whole range of certain more sophisticated variable valve timing strategies not otherwise possible, such as high compression cranking, engine braking, cylinder cutouts, and volumetric efficiency timing with engine speed. I.S.

A88-19669*# Sverdrup Technology, Inc., Cleveland, OH.
ANALYTICAL DETERMINATION OF PROPELLER PERFORMANCE DEGRADATION DUE TO ICE ACCRETION

T. L. MILLER (Sverdrup Technology, Inc., Cleveland, OH), K. D. KORKAN (Texas A & M University, College Station), and R. J. SHAW (NASA, Lewis Research Center, Cleveland, OH) Journal of Aircraft (ISSN 0021-8669), vol. 24, Nov. 1987, p. 768-775. refs

A computer code capable of computing the propeller performance for clean, glaze, or rime ice propeller configurations to determine the performance degradation resulting from a given icing encounter has been developed. The inviscid, incompressible flowfield at each specified propeller radial location is first computed using the Theodorsen method. A droplet trajectory computation then calculates the droplet impingement points and airfoil collection efficiency for each radial location. User-selectable empirical correlations are available for determining the aerodynamic penalties due to ice accretion. Propeller performance is finally computed using strip analysis for either the clean or iced propeller. In the iced mode, the thrust and torque coefficient equations are modified by the drag and lift coefficient increments due to ice to obtain the appropriate iced values. Comparison with available experimental propeller icing data shows generally good agreement. The code's capability of properly predicting the thrust coefficient, power coefficient, and propeller efficiency of an iced propeller is shown to be dependent on the choice of empirical correlation employed as well as on the proper specification of the radial icing extent and propeller blade angle. Author

A88-20785*# National Aeronautics and Space Administration. Lewis Research Center, Cleveland, OH.

RESULTS OF NASA'S ENERGY EFFICIENT ENGINE PROGRAM

CARL C. CIEPLUCH (NASA, Lewis Research Center, Cleveland, OH), DONALD Y. DAVIS (General Electric Co., Evendale, OH), and DAVID E. GRAY (United Technologies Corp., Pratt and Whitney Div., East Hartford, CT) Journal of Propulsion and Power (ISSN 0748-4658), vol. 3, Nov.-Dec. 1987, p. 560-568. refs

The major activity undertaken in the NASA Energy Efficient Engine Program has been completed. This paper reports on the progress made toward achieving the program goal of developing advanced technology to significantly reduce fuel consumption and operating costs of future subsonic transport-type propulsion systems. An additional goal was that the advanced concepts be

compatible with future environmental regulations. Along with the results obtained, a brief overview of the design details of both the General Electric and Pratt and Whitney energy efficient engines and the overall program scope are presented. Overall, this program has been highly successful; the technology developed during its course is, and will continue to be, effectively employed in both current and future advance transport aircraft engine designs. Author

A88-22497*# Lockheed-Georgia Co., Marietta.
MEASUREMENT AND PREDICTION OF PROPELLER FLOW FIELD ON THE PTA AIRCRAFT AT SPEEDS OF UP TO MACH 0.85

ABDULLAH S. ALJABRI (Lockheed Aeronautical Systems Co., Marietta, GA) AIAA, Aerospace Sciences Meeting, 26th, Reno, NV, Jan. 11-14, 1988. 11 p. (Contract NAS3-24339) (AIAA PAPER 88-0667)

High speed subsonic transports powered by advanced propellers provide significant fuel savings compared to turbofan powered transports. Unfortunately, however, propfans must operate in aircraft-induced nonuniform flow fields which can lead to high blade cyclic stresses, vibration and noise. To optimize the design and installation of these advanced propellers, therefore, detailed knowledge of the complex flow field is required. As part of the NASA Propfan Test Assessment (PTA) program, a 1/9 scale semispan model of the Gulfstream II propfan test-bed aircraft was tested in the NASA-Lewis 8 x 6 supersonic wind tunnel to obtain propeller flow field data. Detailed radial and azimuthal surveys were made to obtain the total pressure in the flow and the three components of velocity. Data was acquired for Mach numbers ranging from 0.6 to 0.85. Analytical predictions were also made using a subsonic panel method, QUADPAN. Comparison of wind-tunnel measurements and analytical predictions show good agreement throughout the Mach range. Author

A88-27295*# Purdue Univ., West Lafayette, IN.
TRANSIENT ENGINE PERFORMANCE WITH WATER INGESTION

T. HAYKIN and S. N. B. MURTHY (Purdue University, West Lafayette, IN) Journal of Propulsion and Power (ISSN 0748-4658), vol. 4, Jan.-Feb. 1988, p. 81-88. Previously cited in issue 20, p. 2921, Accession no. A86-42755. refs (Contract NAG3-481)

A88-27296*# Clarkson Univ., Potsdam, NY.
SOOT LOADING IN A GENERIC GAS TURBINE COMBUSTOR

W. A. ECKERLE (Clarkson University, Potsdam, NY) and T. J. ROSFJORD (United Technologies Research Center, East Hartford, CT) Journal of Propulsion and Power (ISSN 0748-4658), vol. 4, Jan.-Feb. 1988, p. 89-96. Previously cited in issue 08, p. 1051, Accession no. A87-22544. refs (Contract NAS3-24223)

A88-30776* Teledyne CAE, Toledo, OH.
DESIGN AND EXPERIMENTAL EVALUATION OF A HIGH TEMPERATURE RADIAL TURBINE WITH A MOVEABLE SIDEWALL NOZZLE

CASIMIR ROGO (Teledyne, Inc., Teledyne CAE Div., Toledo, OH) and RICHARD J. ROELKE (NASA, Lewis Research Center, Cleveland, OH) SAE, Aerospace Technology Conference and Exposition, Long Beach, CA, Oct. 5-8, 1987. 13 p. Army-sponsored research. refs (SAE PAPER 871782)

The uncooled, 2.27 kg/sec mass flow radial turbine designed to operate at 1477 K in the gas generator of an advanced, variable-capacity 683 kW turboshaft engine was configured with a cooled, movable sidewall nozzle capable of changing the stage flow capacity from 50 to 100 percent of maximum. Overall performance test data were obtained in a turbine test rig that duplicated engine Reynolds numbers; attention is given to the changing of flow capacity by moving the hub or shroud sidewall, vane sidewall leakage, vaneless space sidewall geometry, and

07 AIRCRAFT PROPULSION AND POWER

nozzle-cooling injection. Data are presented in the form of turbine flow, efficiency, work parameter, and performance mappings.

O.C.

A88-30777* National Aeronautics and Space Administration. Lewis Research Center, Cleveland, OH.

DESIGN AND PERFORMANCE OF CONTROLLED-DIFFUSION STATOR COMPARED WITH ORIGINAL DOUBLE-CIRCULAR-ARC STATOR

THOMAS F. GELDER, JAMES F. SCHMIDT, KENNETH L. SUDER (NASA, Lewis Research Center, Cleveland, OH), and MICHAEL D. HATHAWAY (NASA, Lewis Research Center; U.S. Army, Aviation Research and Technology Activity, Cleveland, OH) SAE, Aerospace Technology Conference and Exposition, Long Beach, CA, Oct. 5-8, 1987. 15 p. Previously announced in STAR as N87-26910. refs

(SAE PAPER 871783)

The capabilities of two stators, one with controlled-diffusion (CD) blade sections and one with double-circular-arc (DCA) blade sections, were compared. A CD stator was designed and tested that had the same chord length but half the blades of the DCA stator. The same fan rotor (tip speed, 429 m/sec; pressure ratio, 1.65) was used with each stator row. The design and analysis system is briefly described. The overall stage and rotor performances with each stator are compared, as are selected blade element data. The minimum overall efficiency decrement across the stator was approximately 1 percentage point greater with the CD blade sections than with the DCA blade sections.

Author

A88-31608* National Aeronautics and Space Administration. Lewis Research Center, Cleveland, OH.

BLADED DISK ASSEMBLIES; PROCEEDINGS OF THE ELEVENTH BIENNIAL CONFERENCE ON MECHANICAL VIBRATION AND NOISE, BOSTON, MA, SEPT. 27-30, 1987

R. KIELB, ED. (NASA, Lewis Research Center, Cleveland, OH), E. CRAWLEY, ED. (MIT, Cambridge, MA), and J. C. SIMONIS, ED. (Southwest Research Institute, San Antonio, TX) Conference sponsored by ASME. New York, American Society of Mechanical Engineers, 1987, 122 p. For individual items see A88-31609 to A88-31618.

The present conference on bladed disk assemblies discusses aerodynamic indicial response and stability derivatives for a rotor annulus, an analysis of aerodynamically forced turbomachine vibration, the effect of downwash on the nonsteady forces in a turbomachine stage, the vibration of turbomachine blades with root flexibility effects, mistuned bladed disk assembly vibrations, and the model-generation and modal analysis of flexible bladed disk assemblies. Also discussed are the vibration characteristics of a mistuned bladed disk, free and forced vibrations associated with localization phenomena in mistuned assemblies with cyclic symmetry, steam turbine cyclic symmetry through constraint equations, and the interpretation of experimental and theoretical results predicting vibrating turbocharger blade mode shapes.

O.C.

A88-31610* Aerostructures, Inc., Arlington, VA.

AERODYNAMICALLY FORCED VIBRATION ANALYSIS OF TURBOMACHINES

V. ELCHURI (Aerostructure, Inc., Arlington, VA) and P. R. PAMIDI (RPK Corp., Columbia, MD) IN: Bladed disk assemblies; Proceedings of the Eleventh Biennial Conference on Mechanical Vibration and Noise, Boston, MA, Sept. 27-30, 1987. New York, American Society of Mechanical Engineers, 1987, p. 9-20. refs (Contract NAS3-24387)

An account is given of theoretical considerations for the determination of turbomachine response under aerodynamic excitation, as in the cases of advanced turboprop rotors with highly swept blades and axial flow compressors. Dynamic response is characterized in terms of the normal modal coordinates of tuned rotating cyclic structures for both rigid and flexible hubs/disks. Implementation of the scheme is in NASTRAN; coriolis and centripetal accelerations are included, together with differential

stiffness effects. Analytically predicted vibratory stresses for the blades of two different advanced turboprops are compared to those determined by wind tunnel tests conducted by NASA-Lewis.

O.C.

A88-32223* Akron Univ., OH.

PARAMETRIC STUDIES OF ADVANCED TURBOPROPS

D. G. FERTIS (Akron, University, OH), R. A. AIELLO, C. C. CHAMIS (NASA, Lewis Research Center, Cleveland, OH), and J. G. MASER IN: Structures, Structural Dynamics and Materials Conference, 29th, Williamsburg, VA, Apr. 18-20, 1988, Technical Papers. Part 1. Washington, DC, American Institute of Aeronautics and Astronautics, 1988, p. 431-440. refs (AIAA PAPER 88-2266)

The effects of geometric variables (sweep and twist) on the structural performance of advanced turboprops are investigated. The investigation is limited to aerodynamically efficient turboprops using an acceptable design configuration as a baseline. The baseline configuration is modified using a seven by seven array of independently varying sweep and twist parameters while maintaining acceptable aerodynamic efficiency. The turboprop structural performance is evaluated in terms of critical speeds, tip displacements, and vibration frequencies where geometric nonlinearities are included. The results obtained are presented in such a manner as to highlight the effects of sweep and twist on the structural performance of aerodynamically efficient turboprop configurations.

Author

A88-32277* Sverdrup Technology, Inc., Cleveland, OH.

APPLICATION OF STRUCTURAL TAILORING TO SPAR/SHELL TURBOPROPS

ROBERT RUBINSTEIN (Sverdrup Technology, Inc., Middleburg Heights, OH) and CHRISTOS C. CHAMIS (NASA, Lewis Research Center, Cleveland, OH) IN: Structures, Structural Dynamics and Materials Conference, 29th, Williamsburg, VA, Apr. 18-20, 1988, Technical Papers. Part 2. Washington, DC, American Institute of Aeronautics and Astronautics, 1988, p. 992-998. (AIAA PAPER 88-2333)

The problem of designing a swept advanced turboprop (ATP) blade for minimum noise output is discussed. Optimal sweep distributions are found using the computer code STAT (Structural Tailoring of Advanced Turboprops). The initial designs are unswept. The blade designs have minimum noise output while satisfying other blade design requirements. The STAT program and the modifications required during this work are described. Parameter studies of the effect of sweep on noise output are also presented.

Author

A88-32332* National Aeronautics and Space Administration. Lewis Research Center, Cleveland, OH.

EVALUATION OF A TURBINE BLADE DAMPER USING AN INTEGRAL APPROACH

ROBERT E. KIELB (NASA, Lewis Research Center, Cleveland, OH), JERRY H. GRIFFIN (Carnegie-Mellon University, Pittsburgh, PA), and CHAI-HSIANG MENQ (Ohio State University, Columbus) IN: Structures, Structural Dynamics and Materials Conference, 29th, Williamsburg, VA, Apr. 18-20, 1988, Technical Papers. Part 3. Washington, DC, American Institute of Aeronautics and Astronautics, 1988, p. 1495-1500. refs (AIAA PAPER 88-2400)

An integrated experimental/analytical approach to friction damper design optimization in cases where gas turbine blade-response data are unavailable under actual engine operating conditions is presently applied to the case of a damper designed to relieve a blade-cracking problem on a liquid fuel rocket engine's turbopump. Attention is given to the experimental methods and analytical models used, as well as to the predicted damper performance. The inclusion of macroslip, microslip, and variable normal load effects was found to be necessary.

O.C.

A88-35505* National Aeronautics and Space Administration. Lewis Research Center, Cleveland, OH.

DETERMINATION OF COMPRESSOR IN-STALL CHARACTERISTICS FROM ENGINE SURGE TRANSIENTS
CARL F. LORENZO, FRANCIS P. CHIARAMONTE, and CHARLES M. MEHALIC (NASA, Lewis Research Center, Cleveland, OH) Journal of Propulsion and Power (ISSN 0748-4658), vol. 4, Mar.-Apr. 1988, p. 133-143. Previously cited in issue 17, p. 2432, Accession no. A84-36959. refs

A88-35528* National Aeronautics and Space Administration. Lewis Research Center, Cleveland, OH.

EXPERIMENTAL CLASSICAL FLUTTER RESULTS OF A COMPOSITE ADVANCED TURBOPROP MODEL
O. MEHMED and K. R. V. KAZA (NASA, Lewis Research Center, Cleveland, OH) IN: Recent trends in aeroelasticity, structures, and structural dynamics; Proceedings of the R. L. Bisplinghoff Memorial Symposium, Gainesville, FL, Feb. 6, 7, 1986. Gainesville, FL, University Presses of Florida, 1987, p. 62-74. Previously announced in STAR as N86-29271.

Experimental results are presented that show the effects of blade pitch angle and number of blades on classical flutter of a composite advanced turboprop (propfan) model. An increase in the number of blades on the rotor or the blade pitch angle is destabilizing which shows an aerodynamic coupling or cascade effect between blades. The flutter came in suddenly and all blades vibrated at the same frequency but at different amplitudes and with a common predominant phase angle between consecutive blades. This further indicates aerodynamic coupling between blades. The flutter frequency was between the first two blade normal modes, signifying an aerodynamic coupling between the normal modes. Flutter was observed at all blade pitch angles from small to large angles-of-attack of the blades. A strong blade response occurred, for four blades at the two-per-revolution (2P) frequency, when the rotor speed was near the crossing of the flutter mode frequency and the 2P order line. This is because the damping is low near the flutter condition and the interblade phase angle of the flutter mode and the 2P response are the same.

Author

A88-35530* Princeton Univ., NJ.
RECENT DEVELOPMENTS IN FLUTTER SUPPRESSION TECHNIQUES FOR TURBOMACHINERY ROTORS

O. O. BENDIKSEN (Princeton University, NJ) IN: Recent trends in aeroelasticity, structures, and structural dynamics; Proceedings of the R. L. Bisplinghoff Memorial Symposium, Gainesville, FL, Feb. 6, 7, 1986. Gainesville, FL, University Presses of Florida, 1987, p. 87-100. refs
(Contract NAG3-308)

Recent research on passive flutter control techniques for rotors and cascades is reviewed. The proposed methods include the use of periodicity-breaking imperfections, aeroelastic tailoring, dry friction damping, and mode shape control. Numerical results are presented to illustrate the effectiveness of each method in controlling various types of flutter, and to evaluate the feasibility of incorporating the techniques in current and future technology rotors. Mistuning may be the only feasible approach for existing engines, but aeroelastic tailoring offers promising advantages for future engines.

Author

A88-36745* National Aeronautics and Space Administration. Lewis Research Center, Cleveland, OH.

ADVANCED COMPOSITE TURBOPROPS - MODELING, STRUCTURAL, AND DYNAMIC ANALYSES
R. A. AIELLO and S. CHI (NASA, Lewis Research Center, Cleveland, OH) ASME, Transactions, Journal of Engineering for Gas Turbines and Power (ISSN 0022-0825), vol. 110, April 1988, p. 306-311. refs
(ASME PAPER 87-GT-78)

This paper presents a structural and dynamic analysis of a scaled-down wind tunnel model propfan blade made from fiber composites. This blade is one of a series of propfan blades that have been tested at the NASA Lewis Research Center wind tunnel

facilities. The blade is highly swept and twisted and of the spar/shell construction. Due to the complexity of the blade geometry and its high performance, it is subjected to much higher loads and tends to be much less stable than conventional blades. The structural and dynamic analyses of the blade were performed using the NASA-Lewis COBSTRAN computer code. COBSTRAN is designed to generate the mesh and calculate the anisotropic material properties for composite blade analysis. Comparison of analytical and experimental mode shapes and frequencies are shown, verifying the model development and analysis techniques used. The methodologies and programs developed for this analysis are directly applicable to other propfan blades.

Author

A88-37199* National Aeronautics and Space Administration. Lewis Research Center, Cleveland, OH.

FLIGHT PROPULSION CONTROL INTEGRATION FOR V/STOL AIRCRAFT
JAMES R. MIHALOEWS (NASA, Lewis Research Center, Cleveland, OH) IN: International Powered Lift Conference and Exposition, Santa Clara, CA, Dec. 7-10, 1987, Proceedings. Warrendale, PA, Society of Automotive Engineers, Inc., 1988, p. 303-315. Previously announced in STAR as N88-11680. refs
(SAE PAPER 872330)

The goal of the propulsion community is to have the enabling propulsion technologies in place to permit a low risk decision regarding the initiation of a research STOVL supersonic attack fighter aircraft in the mid-1990's. This technology will effectively integrate, enhance, and extend the supersonic cruise, STOVL, and fighter/attack programs to enable U.S. industry to develop a revolutionary supersonic short takeoff vertical landing fighter/attack aircraft in the post-ATF period. The rationale, methods, and criteria used in developing a joint NASA Lewis and NASA Ames research program to develop the technology element for integrated flight propulsion control through integrated methodologies is presented. This program, the Supersonic STOVL integrated Flight Propulsion Controls Program, is part of the overall NASA Lewis Supersonic STOVL integrated approach to an integrated program to achieve integrated flight propulsion control technology.

Author

A88-37215* National Aeronautics and Space Administration. Lewis Research Center, Cleveland, OH.

NASA SUPERSONIC STOVL PROPULSION TECHNOLOGY PROGRAM
PETER G. BATTERTON and BERNARD J. BLAHA (NASA, Lewis Research Center, Cleveland, OH) IN: International Powered Lift Conference and Exposition, Santa Clara, CA, Dec. 7-10, 1987, Proceedings. Warrendale, PA, Society of Automotive Engineers, Inc., 1988, p. 483-494. Previously announced in STAR as N88-14093. refs
(SAE PAPER 872352)

Supersonic capable STOVL fighter/attack aircraft can provide capabilities for close support and air superiority which will be highly desirable in the future. Previous papers in this session described the historical aspects, trade-offs, and requirements for powered lift propulsion systems, and it is shown that propulsion technology is more key to the success of this type of aircraft than for any previous fighter/attack aircraft. The NASA Lewis Research Center program activities which address required propulsion technology development are discussed. Several elements of this program were initiated which address hot gas ingestion and ejector augmentor performance and some preliminary results are shown. In addition, some additional near-term research activity plans and the new Powered Lift Facility (PLF) research capability are presented.

Author

A88-37217* National Aeronautics and Space Administration. Lewis Research Center, Cleveland, OH.

TEST STAND PERFORMANCE OF A CONVERTIBLE ENGINE FOR ADVANCED V/STOL AND ROTORCRAFT PROPULSION
JACK G. MCARDLE (NASA, Lewis Research Center, Cleveland, OH) IN: International Powered Lift Conference and Exposition, Santa Clara, CA, Dec. 7-10, 1987, Proceedings. Warrendale, PA,

07 AIRCRAFT PROPULSION AND POWER

Society of Automotive Engineers, Inc., 1988, p. 507-517. Previously announced in STAR as N88-11679. refs
(SAE PAPER 872355)

A variable inlet guide vane (VIGV) convertible engine that could be used to power future high-speed V/STOL and rotorcraft was tested on an outdoor stand. The engine ran stably and smoothly in the turbofan, turboshaft, and dual (combined fan and shaft) power modes. In the turbofan mode with the VIGV open, fuel consumption was comparable to that of a conventional turbofan engine. In the turboshaft mode with the VIGV closed, fuel consumption was higher than that of present turboshaft engines because power was wasted in churning fan-tip air flow. In dynamic performance tests with a specially built digital engine control and using a waterbrake dynamometer for shaft load, the engine responded effectively to large steps in thrust command and shaft torque. Author

A88-37947* # General Electric Co., Cincinnati, OH.

SCALE MODEL ACOUSTIC TESTING OF COUNTERROTATING FANS

B. A. JANARDAN, S. CHUANG, P. Y. HO, and R. LEE (General Electric Co., Cincinnati, OH) IN: Aerodynamic Testing Conference, 15th, San Diego, CA, May 18-20, 1988, Technical Papers. Washington, DC, American Institute of Aeronautics and Astronautics, 1988, p. 402-411. refs
(Contract NAS3-24080)
(AIAA PAPER 88-2057)

The UDF contrarotating propfan has been subjected to scale model wind tunnel testing to ascertain both general performance and acoustic characteristics data bases. Model Propulsion Simulator test rigs able to mount contrarotating fan blades of up to 24.5-inch diameter were used, and one of these was installed in a large anechoic test chamber for acoustic measurement of conditions simulating representative takeoffs, power cutbacks, and landing approaches. Attention is presently given to the data acquisition/reduction systems, the scaling criteria used to obtain engine size acoustic data, and comparisons with demonstrator aircraft in-flight acoustic test results. O.C.

A88-39707* National Aeronautics and Space Administration. Lewis Research Center, Cleveland, OH.

TURBOFAN ENGINE CORE NOISE SOURCE DIAGNOSTICS

ALLEN M. KARCHMER (NASA, Lewis Research Center, Cleveland, OH) IN: NOISE-CON 87; Proceedings of the National Conference on Noise Control Engineering, State College, PA, June 8-10, 1987. Poughkeepsie, NY, Noise Control Foundation, 1987, p. 121-128. refs

The paper describes a turbofan-engine measurement program utilizing a variety of diagnostic techniques to identify a source of core-generated noise which contributes to the overall external engine noise characteristics. Included in the turbofan engine diagnostics are data examination, time domain correlation, and frequency domain analysis. It is found that the turbulent pressure fluctuations within the combustor are a source for core noise which propagates through the nozzle and radiates to the far-field. K.K.

A88-40554* National Aeronautics and Space Administration. Lewis Research Center, Cleveland, OH.

AN OVERVIEW OF ROTORCRAFT PROPULSION RESEARCH AT LEWIS RESEARCH CENTER

ROBERT C. BILL, GILBERT J. WEDEN (NASA, Lewis Research Center; U.S. Army, Propulsion Directorate, Cleveland, OH), and JOHN J. COY (NASA, Lewis Research Center, Cleveland, OH) Vertiflite (ISSN 0042-4455), vol. 34, May-June 1988, p. 24-31.

Rotorcraft propulsion research at Lewis Research Center is discussed, stressing programs in four areas of component research: compressors, combustors, turbines and transmissions, and three developmental programs: the Small Turboshaft Engine Research (STER) Project, the Advanced Rotorcraft Transmission (ART) program, and the Compound Cycle Engine (CCE) program. The component research emphasizes special problems of turboshaft engines in the 5 lb/sec to 30 lb/sec range. The objectives of the STER program are to evaluate the application of advanced

concepts to small turboshaft engine systems and to investigate system related phenomena, such as distortion effects and secondary flow phenomena. The goals of the ART program are to reduce transmission weight by 25 percent, noise generation by 10 dB and mean time between removal to 5,000 hrs. The CCE program is working to combine the airflow capacity and light-weight features of a gas turbine with the more efficient, but heavier diesel turbine. R.B.

A88-44706* # National Aeronautics and Space Administration. Lewis Research Center, Cleveland, OH.

SMALL ENGINE COMPONENTS TEST FACILITY TURBINE TESTING CELL

BRENT C. NOWLIN and VINCENT G. VERHOFF (NASA, Lewis Research Center, Cleveland, OH) AIAA, ASME, SAE, and ASEE, Joint Propulsion Conference, 24th, Boston, MA, July 11-13, 1988. 12 p. Previously announced in STAR as N88-22037. (AIAA PAPER 88-2962)

NASA Lewis Research Center has designed and constructed a new state-of-the-art test facility. This facility, called the Small Engine Components Test Facility (SECTF), is used to test gas turbines and compressors at conditions similar to actual engine conditions. The SECTF is comprised of two separate facilities - a turbine test cell and a compressor test cell. The paper will describe the turbine test cell. The capabilities of the facility make it unique - no other facility of its kind is capable of combining its pressure, speed, and temperature ranges. Turbine inlet air ranges up to 9 atm (125 psig). The turbine exhaust pressure ranges from 0.15 atm (2 psia) to atmospheric pressure. Turbine inlet air temperatures range from ambient to 700 K (1260 deg R). The controllable speed of the turbine rotor ranges from 4000 to 60,000 rpm and the maximum power absorbed by the facility dynamometer is 1250 hp. The data acquisition system scans up to 2000 channels/sec. This paper will discuss in detail the capabilities of the facility, overall facility design, instrumentation used in the facility, and the data acquisition system. Actual research data is not discussed. Author

A88-44727* # National Aeronautics and Space Administration. Lewis Research Center, Cleveland, OH.

EFFECT OF SPATIAL INLET TEMPERATURE AND PRESSURE DISTORTION ON TURBOFAN ENGINE STABILITY

CHARLES M. MEHALIC (NASA, Lewis Research Center, Cleveland, OH) AIAA, ASME, SAE, and ASEE, Joint Propulsion Conference, 24th, Boston, MA, July 11-13, 1988. 16 p. Previously announced in STAR as N88-21162. refs
(AIAA PAPER 88-3016)

The effects of circumferential and radial inlet temperature distortion, circumferential pressure distortion, and combined temperature and pressure distortion on the stability of an advanced turbofan engine were investigated experimentally at simulated altitude conditions. With circumferential and radial inlet temperature distortion, a flow instability generated by the fan operating near stall caused the high-pressure compressor to surge at, or near, the same time as the fan. The effect of combined distortion was dependent on the relative location of the high-temperature and low-pressure regions; high-pressure compressor stalls occurred when the regions coincided, and fan stalls occurred with the regions separated. Author

A88-45011* # General Motors Corp., Indianapolis, IN.

THE DESIGN OF AN AIR-COOLED METALLIC HIGH TEMPERATURE RADIAL TURBINE

PHILIP H. SNYDER (General Motors Corp., Allison Gas Turbine Div., Indianapolis, IN) and RICHARD J. ROELKE (NASA, Lewis Research Center, Cleveland, OH) AIAA, ASME, SAE, and ASEE, Joint Propulsion Conference, 24th, Boston, MA, July 11-13, 1988. 9 p. refs
(AIAA PAPER 88-2872)

Recent trends in small advanced gas turbine engines call for higher turbine inlet temperatures. Advances in radial turbine technology have opened the way for a cooled metallic radial turbine capable of withstanding turbine inlet temperatures of 2500 F while

meeting the challenge of high efficiency in this small flow size range. In response to this need, a small air-cooled radial turbine has been designed utilizing internal blade coolant passages. The coolant flow passage design is uniquely tailored to simultaneously meet rotor cooling needs and rotor fabrication constraints. The rotor flow-path design seeks to realize improved aerodynamic blade loading characteristics and high efficiency while satisfying rotor life requirements. An up-scaled version of the final engine rotor is currently under fabrication and, after instrumentation, will be tested in the warm turbine test facility at the NASA Lewis Research Center. Author

A88-48032*# National Aeronautics and Space Administration. Lewis Research Center, Cleveland, OH.

THE CHALLENGES AND OPPORTUNITIES OF SUPERSONIC TRANSPORT PROPULSION TECHNOLOGY

WILLIAM C. STRACK (NASA, Lewis Research Center, Cleveland, OH) and SHELBY J. MORRIS, JR. (NASA, Langley Research Center, Hampton, VA) AIAA, ASME, SAE, and ASEE, Joint Propulsion Conference and Exhibit, 24th, Boston, MA, July 11-13, 1988. 13 p. Previously announced in STAR as N88-23806. refs (AIAA PAPER 88-2985)

The major challenges confronting the propulsion community for civil supersonic transport applications are identified: high propulsion system efficiency at both supersonic and subsonic cruise conditions, low-cost fuel with adequate thermal stability at high temperatures, low noise cycles and exhaust systems, low emission combustion systems, and low drag installations. Both past progress and future opportunities are discussed in relation to perceived technology shortfalls for an economically successful airplane that satisfies environmental constraints. Author

A88-48752*# National Aeronautics and Space Administration. Lewis Research Center, Cleveland, OH.

A NUMERICAL STUDY OF THE HOT GAS ENVIRONMENT AROUND A STOVL AIRCRAFT IN GROUND PROXIMITY

THOMAS J. VANOVERBEKE and JAMES D. HOLDEMAN (NASA, Lewis Research Center, Cleveland, OH) AIAA, ASME, SAE, and ASEE, Joint Propulsion Conference, 24th, Boston, MA, July 11-13, 1988. 27 p. Previously announced in STAR as N88-23729. refs (AIAA PAPER 88-2882)

The development of Short Takeoff Vertical Landing (STOVL) aircraft has historically been an empirical- and experience-based technology. In this study, a 3-D turbulent flow CFD code was used to calculate the hot gas environment around an STOVL aircraft operating in ground proximity. Preliminary calculations are reported for a typical STOVL aircraft configuration to identify key features of the flow field, and to demonstrate and assess the capability of current 3-D CFD codes to calculate the temperature of the gases ingested at the engine inlet as a function of flow and geometric conditions. Author

A88-48759*# National Aeronautics and Space Administration. Lewis Research Center, Cleveland, OH.

EXPERIMENTAL VIBRATION DAMPING CHARACTERISTICS OF THE THIRD-STAGE ROTOR OF A THREE-STAGE TRANSONIC AXIAL-FLOW COMPRESSOR

FREDERICK A. NEWMAN (NASA, Lewis Research Center, Cleveland, OH) AIAA, ASME, SAE, and ASEE, Joint Propulsion Conference, 24th, Boston, MA, July 11-13, 1988. 23 p. Previously announced in STAR as N88-24642. refs (AIAA PAPER 88-3229)

Rotor blade aerodynamic damping is experimentally determined in a three-stage transonic axial flow compressor having design aerodynamic performance goals of 4.5:1 pressure ratio and 65.5 lbf/sec weight flow. The combined damping associated with each mode is determined by a least squares fit of a single degree of freedom system transfer function to the nonsynchronous portion of the rotor blade strain gage output power spectra. The combined damping consists of the aerodynamic damping and the structural and mechanical damping. The aerodynamic damping varies linearly with the inlet total pressure for a given corrected speed, weight flow, and pressure ratio while the structural and mechanical

damping is assumed to remain constant. The combined damping is determined at three inlet total pressure levels to obtain the aerodynamic damping. The third-stage rotor blade aerodynamic damping is presented and discussed for the design equivalent speed with the stator blades reset for maximum efficiency. The compressor overall performance and experimental Campbell diagrams for the third-stage rotor blade row are also presented. Author

A88-50783*# National Aeronautics and Space Administration. Lewis Research Center, Cleveland, OH.

AN EMPIRICAL MODEL OF THE EFFECTS OF CURVATURE AND CONVERGENCE ON DILUTION JET MIXING

JAMES D. HOLDEMAN (NASA, Lewis Research Center, Cleveland, OH), RAM SRINIVASEN, and GRAIG D. WHITE (Allied-Signal Aerospace Co., Garrett Engine Div., Phoenix, AZ) AIAA, ASME, SAE, and ASEE, Joint Propulsion Conference, 24th, Boston, MA, July 11-13, 1988. 19 p. Previously announced in STAR as N88-24640. refs (AIAA PAPER 88-3180)

An existing empirical model of the temperature field downstream of single and multiple rows of jets injected into a confined crossflow has been extended to model the effects of curvature and convergence on the mixing. This extension is based on the results of a numerical study of these effects using a 3-D turbulent flow computer code. Temperature distributions calculated with the empirical model are presented to show the effects of flow area convergence, radius of curvature, and inner and outer wall injection for single and opposed rows of jets. Author

A88-50785*# National Aeronautics and Space Administration. Lewis Research Center, Cleveland, OH.

TWO-DIMENSIONAL VISCOUS FLOW COMPUTATIONS OF HYPERSONIC SCRAMJET NOZZLE FLOWFIELDS AT DESIGN AND OFF-DESIGN CONDITIONS

G. J. HARLOFF, H. T. LAI, and E. S. NELSON (NASA, Lewis Research Center; Sverdrup Technology, Inc., Cleveland, OH) AIAA, ASME, SAE, and ASEE, Joint Propulsion Conference, 24th, Boston, MA, July 11-13, 1988. 12 p. Previously announced in STAR as N88-25459. refs (Contract NAS3-25266) (AIAA PAPER 88-3280)

The PARC2D code has been selected to analyze the flowfields of a representative hypersonic scramjet nozzle over a range of flight conditions from Mach 3 to 20. The flowfields, wall pressures, wall skin friction values, heat transfer values and overall nozzle performance are presented. Author

A88-52684*# Purdue Univ., West Lafayette, IN.

CONTROL OF ROTOR AERODYNAMICALLY FORCED VIBRATIONS BY SPLITTERS

SANFORD FLEETER, DAVID A. TOPP (Purdue University, West Lafayette, IN), and DANIEL HOYNIK (NASA, Lewis Research Center, Cleveland, OH) (Structures, Structural Dynamics and Materials Conference, 27th, San Antonio, TX, May 19-21, 1986, Technical Papers. Part 2, p. 77-88) Journal of Propulsion and Power (ISSN 0748-4658), vol. 4, Sept.-Oct. 1988, p. 445-451. Previously cited in issue 18, p. 2612, Accession no. A86-38892. refs

A88-53137*# National Aeronautics and Space Administration. Lewis Research Center, Cleveland, OH.

A PRELIMINARY DESIGN STUDY OF SUPERSONIC THROUGH-FLOW FAN INLETS

PAUL J. BARNHART (NASA, Lewis Research Center, Cleveland; Sverdrup Technology, Inc., Middleburg Heights, OH) AIAA, ASME, SAE, and ASEE, Joint Propulsion Conference, 24th, Boston, MA, July 11-13, 1988. 11 p. refs (Contract NAS3-24105) (AIAA PAPER 88-3075)

From Mach 3.20 cruise propulsion systems, preliminary design studies for two supersonic through-flow fan primary inlets and a single core inlet were undertaken. Method of characteristics and

07 AIRCRAFT PROPULSION AND POWER

one-dimensional performance techniques were applied to assess the potential improvements supersonic through-flow fan technology has over more conventional systems. A fixed geometry supersonic through-flow fan primary inlet was found to have better performance than a conventional inlet design on the basis of total pressure recovery, air flow, aerodynamic drag and size and weight.

Author

A88-54137* National Aeronautics and Space Administration. Lewis Research Center, Cleveland, OH.

TOWARD IMPROVED DURABILITY IN ADVANCED AIRCRAFT ENGINE HOT SECTIONS; PROCEEDINGS OF THE THIRTY-THIRD ASME INTERNATIONAL GAS TURBINE AND AEROENGINE CONGRESS AND EXPOSITION, AMSTERDAM, NETHERLANDS, JUNE 5-9, 1988

DANIEL E. SOKOLOWSKI, ED. (NASA, Lewis Research Center, Cleveland, OH) Congress and Exposition sponsored by ASME. New York, American Society of Mechanical Engineers, 1988, 128 p. For individual items see A88-54138 to A88-54146.

The present conference on durability improvement methods for advanced aircraft gas turbine hot-section components discusses NASA's 'HOST' project, advanced high-temperature instrumentation for hot-section research, the development and application of combustor aerothermal models, and the evaluation of a data base and numerical model for turbine heat transfer. Also discussed are structural analysis methods for gas turbine hot section components, fatigue life-prediction modeling for turbine hot section materials, and the service life modeling of thermal barrier coatings for aircraft gas turbine engines.

O.C.

A88-54138*# National Aeronautics and Space Administration. Lewis Research Center, Cleveland, OH.

NASA HOST PROJECT OVERVIEW

D. E. SOKOLOWSKI (NASA, Lewis Research Center, Cleveland, OH) IN: Toward improved durability in advanced aircraft engine hot sections; Proceedings of the Thirty-third ASME International Gas Turbine and Aeroengine Congress and Exposition, Amsterdam, Netherlands, June 5-9, 1988. New York, American Society of Mechanical Engineers, 1988, p. 1-4. refs

NASA's Hot Section Technology, or 'HOST', program has developed improved analytical models for the aerothermal environment, thermomechanical loading, material behavior, structural response, and service life of aircraft gas turbine engines' hot section components. These models, in conjunction with sophisticated computer codes, can be used in design analyses of critical combustor and turbine elements. Toward these ends, efforts were undertaken in instrumentation, combustion, turbine heat transfer, structural analysis, fatigue/fracture, and surface protection. Attention is presently given to the organization of HOST activities and their specific subject matter.

O.C.

A88-54140*# National Aeronautics and Space Administration. Lewis Research Center, Cleveland, OH.

ASSESSMENT, DEVELOPMENT, AND APPLICATION OF COMBUSTOR AEROTHERMAL MODELS

J. D. HOLDEMAN (NASA, Lewis Research Center, Cleveland, OH), H. C. MONGIA (General Motors Corp., Indianapolis, IN), and E. J. MULARZ (NASA, Lewis Research Center; U.S. Army, Propulsion Directorate, Cleveland, OH) IN: Toward improved durability in advanced aircraft engine hot sections; Proceedings of the Thirty-third ASME International Gas Turbine and Aeroengine Congress and Exposition, Amsterdam, Netherlands, June 5-9, 1988. New York, American Society of Mechanical Engineers, 1988, p. 23-37. Previously announced in STAR as N88-19469. refs

The gas turbine combustion system design and development effort is an engineering exercise to obtain an acceptable solution to the conflicting design trade-offs between combustion efficiency, gaseous emissions, smoke, ignition, restart, lean blowout, burner exit temperature quality, structural durability, and life cycle cost. For many years, these combustor design trade-offs have been carried out with the help of fundamental reasoning and extensive component and bench testing, backed by empirical and experience correlations. Recent advances in the capability of computational

fluid dynamics codes have led to their application to complex 3-D flows such as those in the gas turbine combustor. A number of U.S. Government and industry sponsored programs have made significant contributions to the formulation, development, and verification of an analytical combustor design methodology which will better define the aerothermal loads in a combustor, and be a valuable tool for design of future combustion systems. The contributions made by NASA Hot Section Technology (HOST) sponsored Aerothermal Modeling and supporting programs are described.

Author

A88-54141*# National Aeronautics and Space Administration. Lewis Research Center, Cleveland, OH.

REVIEW AND ASSESSMENT OF THE DATABASE AND NUMERICAL MODELING FOR TURBINE HEAT TRANSFER

H. J. GLADDEN and R. J. SIMONEAU (NASA, Lewis Research Center, Cleveland, OH) IN: Toward improved durability in advanced aircraft engine hot sections; Proceedings of the Thirty-third ASME International Gas Turbine and Aeroengine Congress and Exposition, Amsterdam, Netherlands, June 5-9, 1988. New York, American Society of Mechanical Engineers, 1988, p. 39-55. refs

The objectives of the HOST Turbine Heat Transfer subproject were to obtain a better understanding of the physics of the aerothermodynamic phenomena and to assess and improve the analytical methods used to predict the flow and heat transfer in high-temperature gas turbines. At the time the HOST project was initiated, an across-the-board improvement in turbine design technology was needed. A building-block approach was utilized and the research ranged from the study of fundamental phenomena and modeling to experiments in simulated real engine environments. Experimental research accounted for approximately 75 percent of the funding while the analytical efforts were approximately 25 percent. A healthy government/industry/university partnership, with industry providing almost half of the research, was created to advance the turbine heat transfer design technology base.

Author

A88-54146*# National Aeronautics and Space Administration. Lewis Research Center, Cleveland, OH.

VIEWS ON THE IMPACT OF HOST

J. B. ESGAR (NASA, Lewis Research Center; Sverdrup Technology, Inc., Cleveland, OH) and D. E. SOKOLOWSKI (NASA, Lewis Research Center, Cleveland, OH) IN: Toward improved durability in advanced aircraft engine hot sections; Proceedings of the Thirty-third ASME International Gas Turbine and Aeroengine Congress and Exposition, Amsterdam, Netherlands, June 5-9, 1988. New York, American Society of Mechanical Engineers, 1988, p. 117-123.

The Hot Section Technology (HOST) Project, which was initiated by NASA Lewis Research Center in 1980 and concluded in 1987, was aimed at improving advanced aircraft engine hot section durability through better technical understanding and more accurate design analysis capability. The project was a multidisciplinary, multiorganizational, focused research effort that involved 21 organizations and 70 research and technology activities and generated approximately 250 research reports. No major hardware was developed. To evaluate whether HOST had a significant impact on the overall aircraft engine industry in the development of new engines, interviews were conducted with 41 participants in the project to obtain their views. The summarized results of these interviews are presented.

Author

N88-10790*# National Aeronautics and Space Administration. Lewis Research Center, Cleveland, OH.

STABILITY RELATIONSHIP FOR WATER DROPLET CRYSTALLIZATION WITH THE NASA LEWIS ICING SPRAY

C. JOHN MAREK and C. SCOTT BARTLETT (Sverdrup Technology, Inc., Arnold Air Force Station, Tenn.) 1987 20 p Prepared for presentation at the 26th Aerospace Sciences Meeting, Reno, Nev., 11-14 Jan. 1988; sponsored by AIAA (NASA-TM-100220; E-3832; NAS 1.15:100220; AIAA-88-0289) Avail: NTIS HC A03/MF A01 CSCL 14B

In order to produce small droplets for icing cloud simulation,

high pressure air atomizing nozzles are used. For certain icing testing applications, median drop sizes as small as 5 mm are needed, which require air atomizing pressures greater than 3000 kPa. Isentropic expansion of the ambient temperature atomizing air to atmospheric pressure can result in air stream temperatures of -160 C which results in ice crystals forming in the cloud. To avoid such low temperatures, it is necessary to heat the air and water to high initial temperatures. An icing spray research program was conducted to map the temperatures below which ice crystals form. A soot slide technique was used to determine the presence of crystals in the spray. Author

N88-10791*# General Electric Co., Cincinnati, OH. Aircraft Engine Business Group.

BLADE LOSS TRANSIENT DYNAMICS ANALYSIS, VOLUME 1. TASK 2: TETRA 2 THEORETICAL DEVELOPMENT Final Report

VINCENTE C. GALLARDO and GERALD BLACK Nov. 1986 92 p
(Contract NAS3-24381)
(NASA-CR-179632; NAS 1.26:179632) Avail: NTIS HC A05/MF A01 CSCL 21E

The theoretical development of the forced steady state analysis of the structural dynamic response of a turbine engine having nonlinear connecting elements is discussed. Based on modal synthesis, and the principle of harmonic balance, the governing relations are the compatibility of displacements at the nonlinear connecting elements. There are four displacement compatibility equations at each nonlinear connection, which are solved by iteration for the principle harmonic of the excitation frequency. The resulting computer program, TETRA 2, combines the original TETRA transient analysis (with flexible bladed disk) with the steady state capability. A more versatile nonlinear rub or bearing element which contains a hardening (or softening) spring, with or without deadband, is also incorporated. Author

N88-10792*# General Electric Co., Cincinnati, OH. Aircraft Engine Business Group.

BLADE LOSS TRANSIENT DYNAMICS ANALYSIS, VOLUME 2. TASK 2: TETRA 2 USER'S MANUAL Final Report

GERALD BLACK and VINCENTE C. GALLARDO Nov. 1986 204 p
(Contract NAS3-24381)
(NASA-CR-179633; NAS 1.26:179633) Avail: NTIS HC A10/MF A01 CSCL 21E

This is the user's manual for the TETRA 2 Computer Code, a program developed in the NASA-Lewis Blade Loss Program. TETRA 2 calculates a turbine engine's dynamic structural response from applied stimuli. The calculation options are: (1) transient response; and (2) steady state forced response. Based on the method of modal syntheses, the program allows the use of linear, as well as nonlinear connecting elements. Both transient and steady state options can include: flexible Bladed Disk Module, and Nonlinear Connecting Elements (including deadband, hardening/softening spring). The transient option has the additional capability to calculate response with a squeeze film bearing module. TETRA 2 output is summarized in a plotfile which permits post processing such as FFT or graphical animation with the proper software and computer equipment. Author

N88-11679*# National Aeronautics and Space Administration. Lewis Research Center, Cleveland, OH.

TEST STAND PERFORMANCE OF A CONVERTIBLE ENGINE FOR ADVANCED V/STOL AND ROTORCRAFT PROPULSION

JACK G. MCARDLE 1987 22 p Presented at the International Powered Lift Conference, Santa Clara, Calif., 7-10 Dec. 1987; sponsored by the Society of Automotive Engineers
(NASA-TM-100211; E-3819; NAS 1.15:100211) Avail: NTIS HC A03/MF A01 CSCL 21E

A variable inlet guide vane (VIGV) convertible engine that could be used to power future high-speed V/STOL and rotorcraft was tested on an outdoor stand. The engine ran stably and smoothly in the turbofan, turboshaft, and dual (combined fan and shaft)

power modes. In the turbofan mode with the VIGV open, fuel consumption was comparable to that of a conventional turbofan engine. In the turboshaft mode with the VIGV closed, fuel consumption was higher than that of present turboshaft engines because power was wasted in churning fan-tip air flow. In dynamic performance tests with a specially built digital engine control and using a waterbrake dynamometer for shaft load, the engine responded effectively to large steps in thrust command and shaft torque. Author

N88-12490*# National Aeronautics and Space Administration. Lewis Research Center, Cleveland, OH.

PERFORMANCE AND COMBUSTION CHARACTERISTICS OF DIRECT-INJECTION STRATIFIED-CHARGE ROTARY ENGINES

HUNG LEE NGUYEN Dec. 1987 29 p
(NASA-TM-100134; E-3684; NAS 1.15:100134) Avail: NTIS HC A03/MF A01 CSCL 21A

Computer simulations of the direct-injection stratified-charge (DISC) Wankel engine have been used to calculate heat release rates and performance and efficiency characteristics of the 1007R engine. Engine pressure data have been used in a heat release analysis to study the effects of heat transfer, leakage, and crevice flows. Predicted engine performance data are compared with experimental test data over a range of engine speeds and loads. An examination of methods to improve the performance of the Wankel engine with faster combustion, reduced leakage, higher compression ratio, and turbocharging is presented. Author

N88-13338*# National Aeronautics and Space Administration. Lewis Research Center, Cleveland, OH.

COMBUSTION CHARACTERISTICS OF GAS TURBINE ALTERNATIVE FUELS

R. JAMES ROLLBUHLER Dec. 1987 20 p Presented at the 25th Automotive Technology Development Contractors' Coordination Meeting (ATD/CCM), Dearborn, Mich., 26-29 Oct. 1987; sponsored by the Society of Automotive Engineers
(Contract DE-A101-85CE-50111)
(NASA-TM-100247; E-3869; NAS 1.15:100247; DOE/NASA/50111-1) Avail: NTIS HC A03/MF A01 CSCL 21E

An experimental investigation was conducted to obtain combustion performance values for specific heavyend, synthetic hydrocarbon fuels. A flame tube combustor modified to duplicate an advanced gas turbine engine combustor was used for the tests. Each fuel was tested at steady-state operating conditions over a range of mass flow rates, fuel-to-air mass ratio, and inlet air temperatures. The combustion pressure, as well as the hardware, were kept nearly constant over the program test phase. Test results were obtained in regards to geometric temperature pattern factors as a function of combustor wall temperatures, the combustion gas temperature, and the combustion emissions, both as affected by the mass flow rate and fuel-to-air ratio. The synthetic fuels were reacted in the combustor such that for most tests their performance was as good, if not better, than the baseline gasoline or diesel fuel tests. The only detrimental effects were that at high inlet air temperature conditions, fuel decomposition occurred in the fuel atomizing nozzle passages resulting in blockage. And the nitrogen oxide emissions were above EPA limits at low flow rate and high operating temperature conditions. Author

N88-13345*# National Aeronautics and Space Administration. Lewis Research Center, Cleveland, OH.

REGRESSED RELATIONS FOR FORCED CONVECTION HEAT TRANSFER IN A DIRECT INJECTION STRATIFIED CHARGE ROTARY ENGINE

CHI M. LEE and HAROLD J. SCHOCK (Michigan State Univ., East Lansing.) 1988 24 p Proposed for presentation at the 1988 International Congress and Exposition, Detroit, Mich., 29 Feb. - 4 Mar. 1988; sponsored by the Society of Automotive Engineers, Inc.
(NASA-TM-100124; E-3689; NAS 1.15:100124) Avail: NTIS HC A03/MF A01 CSCL 20E

Currently, the heat transfer equation used in the rotary combustion engine (RCE) simulation model is taken from piston

07 AIRCRAFT PROPULSION AND POWER

engine studies. These relations have been empirically developed by the experimental input coming from piston engines whose geometry differs considerably from that of the RCE. The objective of this work was to derive equations to estimate heat transfer coefficients in the combustion chamber of an RCE. This was accomplished by making detailed temperature and pressure measurements in a direct injection stratified charge (DISC) RCE under a range of conditions. For each specific measurement point, the local gas velocity was assumed equal to the local rotor tip speed. Local physical properties of the fluids were then calculated. Two types of correlation equations were derived and are described in this paper. The first correlation expresses the Nusselt number as a function of the Prandtl number, Reynolds number, and characteristic temperature ratio; the second correlation expresses the forced convection heat transfer coefficient as a function of fluid temperature, pressure and velocity. Author

N88-13346* National Aeronautics and Space Administration. Lewis Research Center, Cleveland, OH.

UNSTEADY AERODYNAMICS OF AN OSCILLATING CASCADE IN A COMPRESSIBLE FLOW FIELD

DANIEL H. BUFFUM, DONALD R. BOLDMAN, and SANFORD FLEETER (Purdue Univ., West Lafayette, Ind.) 1987 22 p Presented at the 4th Symposium on Unsteady Aerodynamics and Aeroelasticity of Turbomachines and Propellers, Aachen, Fed. Republic of Germany, 6-10 Sep. 1987; sponsored by Aachen Univ.

(NASA-TM-100219; E-3830; NAS 1.15:100219) Avail: NTIS HC A03/MF A01 CSCL 20E

Fundamental experiments were performed in the NASA Lewis Transonic Oscillating Cascade Facility to investigate and quantify the unsteady aerodynamics of a cascade of biconvex airfoils executing torsion-mode oscillations at realistic reduced frequencies. Flush-mounted, high-response miniature pressure transducers were used to measure the unsteady airfoil surface pressures. The pressures were measured for three interblade phase angles at two inlet Mach numbers, 0.65 and 0.80, and two incidence angles, 0 and 7 deg. The time-variant pressures were analyzed by means of discrete Fourier transform techniques, and these unique data were then compared with predictions from a linearized unsteady cascade model. The experimental results indicate that the interblade phase angle had a major effect on the chordwise distributions of the airfoil surface unsteady pressure, and that reduced frequency, incidence angle, and Mach number had a somewhat less significant effect. Author

N88-13347* National Aeronautics and Space Administration. Lewis Research Center, Cleveland, OH.

A NUMERICAL STUDY OF THE EFFECTS OF CURVATURE AND CONVERGENCE ON DILUTION JET MIXING

J. D. HOLDEMAN, R. REYNOLDS, and C. WHITE (Garrett Turbine Engine Co., Phoenix, Ariz.) 1987 19 p Presented at the 23rd Joint Propulsion Conference, San Diego, Calif., 29 Jun. - 2 Jul. 1987; sponsored by AIAA, SAE, ASME and ASEE (NASA-TM-89878; E-3548; NAS 1.15:89878) Avail: NTIS HC A03/MF A01 CSCL 21E

An analytical program was conducted to assemble and assess a three-dimensional turbulent viscous flow computer code capable of analyzing the flow field in the transition liners of small gas turbine engines. This code is of the TEACH type with hybrid numerics, and uses the power law and SIMPLER algorithms, an orthogonal curvilinear coordinate system, and an algebraic Reynolds stress turbulence model. The assessments performed in this study, consistent with results in the literature, showed that in its present form this code is capable of predicting trends and qualitative results. The assembled code was used to perform a numerical experiment to investigate the effects of curvature and convergence in the transition liner on the mixing of single and opposed rows of cool dilution jets injected into a hot mainstream flow. Author

N88-14093* National Aeronautics and Space Administration. Lewis Research Center, Cleveland, OH.

NASA SUPERSONIC STOVL PROPULSION TECHNOLOGY PROGRAM

PETER G. BATTERTON and BERNARD J. BLAHA 1987 20 p Presented at the International Powered Lift Conference, Santa Clara, Calif., 7-10 Dec. 1987; sponsored by the Society of Automotive Engineers (NASA-TM-100227; E-3846; NAS 1.15:100227) Avail: NTIS HC A03/MF A01 CSCL 21E

Supersonic capable STOVL fighter/attack aircraft can provide capabilities for close support and air superiority which will be highly desirable in the future. Previous papers in this session described the historical aspects, trade-offs, and requirements for powered lift propulsion systems, and it is shown that propulsion technology is more key to the success of this type of aircraft than for any previous fighter/attack aircraft. The NASA Lewis Research Center program activities which address required propulsion technology development are discussed. Several elements of this program were initiated which address hot gas ingestion and ejector augmentor performance and some preliminary results are shown. In addition, some additional near-term research activity plans and the new Powered Lift Facility (PLF) research capability are presented. Author

N88-14094* National Aeronautics and Space Administration. Ames Research Center, Moffett Field, CA.

NUMERICAL STUDY OF CHEMICALLY REACTING FLOWS USING AN LU SCHEME Final Contractor Report

JIAN SHUN SHUEN (Sverdrup Technology, Inc., Cleveland, Ohio.) and SEOKKWAN YOON 1988 23 p Presented at the 26th Aerospace Sciences Meeting, Reno, Nev., 11-14 Jan. 1988; sponsored by AIAA (Contract NAS3-24105)

(NASA-CR-180882; E-3875; NAS 1.26:180882; AIAA-88-0436) Avail: NTIS HC A03/MF A01 CSCL 21E

A new computational fluid dynamic code has been developed for the study of mixing and chemical reactions in the flow fields of ramjets and scramjets. The code employs an implicit finite volume, lower-upper symmetric successive overrelaxation scheme for solving the complete two-dimensional Navier-Stokes equations and species transport equations in a fully-coupled and very efficient manner. The combustion processes are modeled by an 8-species, 14-step finite rate chemistry model whereas turbulence is simulated by a Baldwin-Lomax algebraic model. The validity of the code is demonstrated by comparing the numerical calculations with both experimental data and previous calculations of a cold flow helium injection into a straight channel and premixed hydrogen-air reacting flows in a ramped duct. The code is then used to calculate the mixing and chemical reactions of a hydrogen jet transversely injected into a supersonic airstream. Results are presented describing the flow field, the recirculation regions in front and behind the injector, and the chemical reactions. Author

N88-14095* Hamilton Standard, Windsor Locks, CT.

ANALYSIS AND TEST EVALUATION OF THE DYNAMIC STABILITY OF THREE ADVANCED TURBOPROP MODELS AT ZERO FORWARD SPEED Final Report

ARTHUR F. SMITH Dec. 1985 115 p (Contract NAS3-22755)

(NASA-CR-175025; NAS 1.26:175025; HSER-11054) Avail: NTIS HC A06/MF A01 CSCL 01A

Results of static stability wind tunnel tests of three 62.2 cm (24.5 in) diameter models of the Prop-Fan are presented. Measurements of blade stresses were made with the Prop-Fans mounted on an isolated nacelle in an open 5.5 m (18 ft) wind tunnel test section with no tunnel flow. The tests were conducted in the United Technology Research Center Large Subsonic Wind Tunnel. Stall flutter was determined by regions of high stress, which were compared with predictions of boundaries of zero total viscous damping. The structural analysis used beam methods for the model with straight blades and finite element methods for the models with swept blades. Increasing blade sweep tends to

suppress stall flutter. Comparisons with similar test data acquired at NASA/Lewis are good. Correlations between measured and predicted critical speeds for all the models are good. The trend of increased stability with increased blade sweep is well predicted. Calculated flutter boundaries generally coincide with tested boundaries. Stall flutter is predicted to occur in the third (torsion) mode. The straight blade test shows third mode response, while the swept blades respond in other modes. Author

N88-14096*# Hamilton Standard, Windsor Locks, CT.
ANALYSIS AND TEST EVALUATION OF THE DYNAMIC RESPONSE AND STABILITY OF THREE ADVANCED TURBOPROP MODELS AT LOW FORWARD SPEED Final Report

ARTHUR F. SMITH Dec. 1985 110 p
 (Contract NAS3-22755)
 (NASA-CR-175026; NAS 1.26:175026; HSER-11055) Avail: NTIS HC A06/MF A01 CSCL 01A

Results of wind tunnel tests at low forward speed for blade dynamic response and stability of three 62.2 cm (24.5 in) diameter models of the Prop-Fan, advanced turboprop, are presented. Measurements of dynamic response were made with the rotors mounted on an isolated nacelle, with varying tilt for nonuniform inflow. Low speed stall flutter tests were conducted at Mach numbers from 0.0 to 0.35. Measurements are compared to Eigen-solution flutter boundaries. Calculated 1P stress response agrees favorably with experiment. Predicted stall flutter boundaries correlate well with measured high stress regions. Stall flutter is significantly reduced by increased blade sweep. Susceptibility to stall flutter decreases rapidly with forward speed. Author

N88-14097*# Hamilton Standard, Windsor Locks, CT.
LARGE-SCALE ADVANCED PROP-FAN (LAP) BLADE DESIGN Contractor Report, Sep. 1983 - Mar. 1984

JOHN A. VIOLETTE, WILLIAM E. SULLIVAN, and JAY E. TURNBERG 1984 181 p
 (Contract NAS3-23051)
 (NASA-CR-174790; NAS 1.26:174790; HSER-9246) Avail: NTIS HC A09/MF A01 CSCL 01C

This report covers the design analysis of a very thin, highly swept, propeller blade to be used in the Large-Scale Advanced Prop-Fan (LAP) test program. The report includes: design requirements and goals, a description of the blade configuration which meets requirements, a description of the analytical methods utilized/developed to demonstrate compliance with the requirements, and the results of these analyses. The methods described include: finite element modeling, predicted aerodynamic loads and their application to the blade, steady state and vibratory response analyses, blade resonant frequencies and mode shapes, bird impact analysis, and predictions of stalled and unstalled flutter phenomena. Summarized results include deflections, retention loads, stress/strength comparisons, foreign object damage resistance, resonant frequencies and critical speed margins, resonant vibratory mode shapes, calculated boundaries of stalled and unstalled flutter, and aerodynamic and acoustic performance calculations. Author

N88-14985*# United Technologies Corp., East Hartford, CT.
FUEL-INJECTOR/AIR-SWIRL CHARACTERIZATION Final Report

J. B. MCVEY, J. B. KENNEDY, and S. RUSSELL Jan. 1988 58 p
 (Contract NAS3-24352)
 (NASA-CR-180864; NAS 1.26:180864) Avail: NTIS HC A04/MF A01 CSCL 21E

Experimental data on the characteristics of the spray produced by a gas-turbine engine airblast fuel injector are reported. The data acquired include the mass-flux distribution measured by use of a high-resolution spray patternator; the gas-phase velocity field measured by use of a two-component laser Doppler velocimeter, and the liquid droplet size and velocity distributions measured by use of a single-component phase-Doppler anemometer. The data

are intended for use in assessments of two-phase flow computational methods as applied to combustor design procedures. Author

N88-15785*# National Aeronautics and Space Administration, Lewis Research Center, Cleveland, OH.

AEROPROPULSION '87. SESSION 2: AEROPROPULSION STRUCTURES RESEARCH

Nov. 1987 52 p Conference held in Cleveland, Ohio, 17-19 Nov. 1987 Submitted for publication
 (NASA-CP-10003-SESS-2; E-3798-SESS-2; NAS 1.55:10003-SESS-2) Avail: NTIS HC A04/MF A01 CSCL 21E

Aeropropulsion systems present unique problems to the structural engineer. The extremes in operating temperatures, rotational effects, and behaviors of advanced material systems combine into complexities that require advances in many scientific disciplines involved in structural analysis and design procedures. This session provides an overview of the complexities of aeropropulsion structures and the theoretical, computational, and experimental research conducted to achieve the needed advances.

N88-15786*# National Aeronautics and Space Administration, Lewis Research Center, Cleveland, OH.

AEROPROPULSION STRUCTURES

LESTER D. NICHOLS *In its* Aeropropulsion '87. Session 2: Aeropropulsion Structures Research 10 p Nov. 1987
 Avail: NTIS HC A04/MF A01 CSCL 21E

The structural engineer is faced with unique problems when dealing with aeropropulsion systems. He is faced with extremes in operating temperatures, rotational effects, and behaviors of advanced material systems which combine into complexities that require advances in many scientific disciplines involved in structural analysis and design procedures. This presentation provides an overview of the complexities of aeropropulsion structures and the theoretical, computational, and experimental research conducted to achieve the needed advances. Author

N88-15787*# National Aeronautics and Space Administration, Lewis Research Center, Cleveland, OH.

DETERMINING STRUCTURAL PERFORMANCE

MICHAEL A. ERNST and LOUIS J. KIRALY *In its* Aeropropulsion '87. Session 2: Aeropropulsion Structures Research 14 p Nov. 1987
 Avail: NTIS HC A04/MF A01 CSCL 21E

An overview is given of the methods and concepts developed to enhance and predict structural dynamic characteristics of advanced aeropropulsion systems. Aeroelasticity, Vibration Control, Dynamic Systems, and Computational Structural Methods are four disciplines that make up the research program at NASA/Lewis Research Center. The Aeroelasticity program develops analytical and experimental methods to minimize flutter and forced vibration of aerospace propulsion systems. Both frequency domain and time domain methods have been developed for applications on the turbofan, turbopump, and advanced turboprop. To improve life and performance, the Vibration Control program conceives, analyzes, develops, and demonstrates new methods to control vibrations in aerospace systems. Active and passive vibration control is accomplished with electromagnetic dampers, magnetic bearings, and piezoelectric crystals to control rotor vibrations. The Dynamic Systems program analyzes and verifies the dynamics of interacting systems, as well as develops concepts and methods for high-temperature dynamic seals. The Computational Structural Methods program uses computer science to improve solutions of structural problems. Author

N88-15788*# National Aeronautics and Space Administration, Lewis Research Center, Cleveland, OH.

LIFE PREDICTION TECHNOLOGIES FOR AERONAUTICAL PROPULSION SYSTEMS

MICHAEL A. MCGAW *In its* Aeropropulsion '87. Session 2: Aeropropulsion Structures Research 12 p Nov. 1987
 Avail: NTIS HC A04/MF A01 CSCL 21E

07 AIRCRAFT PROPULSION AND POWER

Fatigue and fracture problems continue to occur in aeronautical gas turbine engines. Components whose useful life is limited by these failure modes include turbine hot-section blades, vanes and disks. Safety considerations dictate that catastrophic failures be avoided, while economic considerations dictate that non-catastrophic failures occur as infrequently as possible. The design decision is therefore in making the tradeoff between engine performance and durability. The NASA Lewis Research Center has contributed to the aeropropulsion industry in the areas of life prediction technology for 30 years, developing creep and fatigue life prediction methodologies for hot-section materials. Emphasis is placed on the development of methods capable of handling both thermal and mechanical fatigue under severe environments. Recent accomplishments include the development of more accurate creep-fatigue life prediction methods such as the total strain version of Lewis' Strainrange Partitioning (SRP) and the HOST-developed Cyclic Damage Accumulation (CDA) model. Other examples include the Double Damage Curve Approach (DDCA), which provides greatly improved accuracy for cumulative fatigue design rules. Author

N88-15789*# National Aeronautics and Space Administration. Lewis Research Center, Cleveland, OH.

INTEGRATED ANALYSIS AND APPLICATIONS

DALE A. HOPKINS *In its* Aeropropulsion '87. Session 2: Aeropropulsion Structures Research 12 p Nov. 1987

Avail: NTIS HC A04/MF A01 CSCL 21E

A select overview is provided of ongoing research focusing on the development and verification of integrated structural analysis and optimal design capabilities for advanced aerospace propulsion and power systems. Subjects discussed include the following: (1) Composites - analytical models (composite mechanics), integrated computational methods, and characterization of composite structural response and durability for resin-, metal-, and ceramic-matrix systems; (2) Advanced inelastic analysis - algorithm/numerical methods for more accurate and efficient analysis; (3) Constitutive modeling - theoretical formulation and characterization of thermoviscoplastic material behavior; (4) Computational simulation - engine structures from components to assembly, and up to an entire engine system subjected to simulated test-stand and mission load histories; (5) Probabilistic structural analysis - quantification of the effects of uncertainty in geometry, material, loads, and boundary conditions on structural response for true reliability assessment; and (6) Interdisciplinary optimization - incorporation of mathematical optimization and multidisciplinary analyses to provide streamlined, autonomous optimal design systems. Author

N88-15790*# National Aeronautics and Space Administration. Lewis Research Center, Cleveland, OH.

AEROPROPULSION '87. SESSION 3: INTERNAL FLUID MECHANICS RESEARCH

Nov. 1987 75 p Conference held in Cleveland, Ohio, 17-19 Nov. 1987 Submitted for publication

(NASA-CP-10003-SESS-3; E-3798-SESS-3; NAS

1.55:10003-SESS-3) Avail: NTIS HC A04/MF A01 CSCL 21E

Internal fluid mechanics research at Lewis is directed toward an improved understanding of the important flow physics affecting aerospace propulsion systems, and applying this improved understanding to formulate accurate predictive codes. To this end, research is conducted involving detailed experimentation and analysis. The presentations in this session summarize ongoing work and indicated future emphasis in three major research thrusts: namely, inlets, ducts, and nozzles; turbomachinery; and chemical reacting flows.

N88-15792*# National Aeronautics and Space Administration. Lewis Research Center, Cleveland, OH.

TURBOMACHINERY

ROBERT J. SIMONEAU, ANTHONY J. STRAZISAR, PETER M. SOCKOL, LONNIE REID, and JOHN J. ADAMCZYK *In its* Aeropropulsion '87. Session 3: Internal Fluid Mechanics Research

23 p Nov. 1987

Avail: NTIS HC A04/MF A01 CSCL 21E

The discipline research in turbomachinery, which is directed toward building the tools needed to understand such a complex flow phenomenon, is based on the fact that flow in turbomachinery is fundamentally unsteady or time dependent. Success in building a reliable inventory of analytic and experimental tools will depend on how the time and time-averages are treated, as well as on who the space and space-averages are treated. The raw tools at disposal (both experimentally and computational) are truly powerful and their numbers are growing at a staggering pace. As a result of this power, a case can be made that a situation exists where information is outstripping understanding. The challenge is to develop a set of computational and experimental tools which genuinely increase understanding of the fluid flow and heat transfer in a turbomachine. Viewgraphs outline a philosophy based on working on a stairstep hierarchy of mathematical and experimental complexity to build a system of tools, which enable one to aggressively design the turbomachinery of the next century. Examples of the types of computational and experimental tools under current development at Lewis, with progress to date, are examined. The examples include work in both the time-resolved and time-averaged domains. Finally, an attempt is made to identify the proper place for Lewis in this continuum of research. Author

N88-15794*# National Aeronautics and Space Administration. Lewis Research Center, Cleveland, OH.

AEROPROPULSION '87. SESSION 4: INSTRUMENTATION AND CONTROLS RESEARCH

Nov. 1987 77 p Conference held in Cleveland, Ohio, 17-19 Nov. 1987 Submitted for publication

(NASA-CP-10003-SESS-4; E-3798-SESS-4; NAS

1.55:10003-SESS-4) Avail: NTIS HC A05/MF A01 CSCL 21E

The Lewis Research Center has had a long history of research directed toward advancing the national capability in the areas of propulsion research instrumentation and propulsion controls. Some of the major advances from this research that are currently in use are highlighted as well as some of the ongoing and planned research that will strongly impact the future capabilities. The presentations will cover the efforts on research instrumentation and controls as well as the research on high temperature electronics. This introductory section will focus on the major drivers or needs of the aeropropulsion industry that have shaped the instrumentation and controls research programs. Also covered will be the technological opportunities that have greatly impacted the program and that permitted break-throughs in several areas.

N88-15799*# National Aeronautics and Space Administration. Lewis Research Center, Cleveland, OH.

DIRECTIONS IN PROPULSION CONTROL

CARL F. LORENZO *In its* Aeropropulsion '87. Session 4: Instrumentation and Controls Research 15 p Nov. 1987

Avail: NTIS HC A05/MF A01 CSCL 21E

The research needs in the area of propulsion control as driven by trends in advanced aircraft are considered. Ongoing propulsion control research at NASA Lewis is discussed. Special emphasis is made on research to improve control system reliability through the use of analytical redundancy to accommodate failed control sensors. In conclusion, a discussion of new research thrusts in the area of supersonic STOVL integrated control and intelligent system control is presented. Author

N88-15800*# National Aeronautics and Space Administration. Lewis Research Center, Cleveland, OH.

AEROPROPULSION '87. SESSION 5: SUBSONIC PROPULSION TECHNOLOGY

Nov. 1987 153 p Conference held in Cleveland, Ohio, 17-19 Nov. 1987 Submitted for publication

(NASA-CP-10003-SESS-5; E-3798-SESS-5; NAS

1.55:10003-SESS-5) Avail: NTIS HC A08/MF A01 CSCL 21E

NASA is conducting aeropropulsion research over a broad range of Mach numbers. In addition to the high-speed propulsion research described, major progress was recorded in research aimed at the

subsonic flight regimes of interest to many commercial and military users. Recent progress and future directions in such areas as small engine technology, rotorcraft transmissions, icing, Hot Section Technology (HOST) and the Advanced Turboprop Program (ATP) are covered.

N88-15801*# National Aeronautics and Space Administration. Lewis Research Center, Cleveland, OH.

SMALL ENGINE TECHNOLOGY PROGRAMS

RICHARD W. NIEDZWIECKI *In its* Aeropropulsion '87. Session 5: Subsonic Propulsion Technology 35 p Nov. 1987
 Avail: NTIS HC A08/MF A01 CSCL 21E

Small engine technology programs being conducted at the NASA Lewis Research Center are described. Small gas turbine research is aimed at general aviation, commutercraft, rotorcraft, and cruise missile applications. The Rotary Engine Program is aimed at supplying fuel flexible, fuel efficient technology to the general aviation industry, but also has applications to other missions. There is a strong element of synergism between the various programs in several respects. All of the programs are aimed towards highly efficient engine cycles, very efficient components, and the use of high temperature structural ceramics. This research tends to be generic in nature and has broad applications. The Heavy Duty Diesel Transport (HDDT), rotary technology, and the compound cycle programs are all examining approaches to minimum heat rejection, or adiabatic systems employing advanced materials. The Automotive Gas Turbine (AGT) program is also directed towards ceramics application to gas turbine hot section components. Turbomachinery advances in the gas turbines will benefit advanced turbochargers and turbo-compounders for the intermittent combustion systems, and the fundamental understandings and analytical codes developed in the research and technology programs will be directly applicable to the system projects. Author

N88-15804*# National Aeronautics and Space Administration. Lewis Research Center, Cleveland, OH.

AIRCRAFT ENGINE HOT SECTION TECHNOLOGY: AN OVERVIEW OF THE HOST PROJECT

DANIEL E. SOKOLOWSKI and MARVIN H. HIRSCHBERG *In its* Aeropropulsion '87. Session 5: Subsonic Propulsion Technology 10 p Nov. 1987
 Avail: NTIS HC A08/MF A01 CSCL 21E

NASA sponsored the Turbine Engine Hot Section Technology (HOST) Project to address the need for improved durability in advanced aircraft engine combustors and turbines. Analytical and experimental activities aimed at more accurate prediction of the aerothermal environment, the thermomechanical loads, the material behavior and structural responses to loads, and life predictions for cyclic high-temperature operation were underway for the last 7 years. The project has involved representatives from six engineering disciplines who are spread across three work sectors (industry, academia, and NASA). The HOST Project not only initiated and sponsored 70 major activities, but was also the keystone in joining the multiple disciplines and work sectors to focus on critical research needs. A broad overview of the project is given along with initial indications of the project's impact. Author

N88-15805*# National Aeronautics and Space Administration. Lewis Research Center, Cleveland, OH.

OVERVIEW OF NASA PTA PROPFAN FLIGHT TEST PROGRAM

EDWIN J. GRABER *In its* Aeropropulsion '87. Session 5: Subsonic Propulsion Technology 26 p Nov. 1987
 Avail: NTIS HC A08/MF A01 CSCL 21E

During the last several years high-speed propellers have made the transition from a wind tunnel curiosity to a very likely near-term, fuel-efficient propulsion system that could revolutionize the subsonic commercial air transport industry. A key ingredient in this remarkable progress is the advanced turboprop industry. Working together, NASA and industry have developed and flight tested two propeller propulsion systems to provide answers to key technical questions and concerns. An industry team is currently

developing a third propeller propulsion system for flight testing late this year. The progress of one of the NASA-industry flight test programs, called the Propfan Test Assessment (PTA) Program is reported. In PTA, a 9 foot diameter propfan was installed on the left wing of a Gulfstream GII executive jet and is undergoing extensive flight testing at Dobbins Air Force Base to evaluate propfan structural integrity, near and far field noise, and cabin interior noise characteristics. This research testing includes variations in propeller tip speed and power loading, nacelle tilt angle, and aircraft Mach number and altitude. As a result, extensive parametric data will be obtained to verify and improve computer codes for predicting propeller structural aeroelastic, aerodynamic, and acoustic characteristics. Over 600 measurements are being recorded for each of approximately 600 flight test conditions.

Author

N88-15806*# National Aeronautics and Space Administration. Lewis Research Center, Cleveland, OH.

ADVANCED PROPELLER RESEARCH

JOHN F. GROENEWEG and LAWRENCE J. BOBER *In its* Aeropropulsion '87. Session 5: Subsonic Propulsion Technology 30 p Nov. 1987
 Avail: NTIS HC A08/MF A01 CSCL 21E

Recent results of aerodynamic and acoustic research on both single and counter-rotation propellers are reviewed. Data and analytical results are presented for three propellers: SR-7A, the single rotation design used in the NASA Propfan Test Assessment (PTA); and F7-A7, the 8+8 counterrotating design used in the proof-of-concept Unducted Fan (UDF) engine. In addition to propeller efficiencies, cruise and takeoff noise, and blade pressure data, off-design phenomena involving formation of leading edge vortices are described. Aerodynamic and acoustic computational results derived from three-dimensional Euler and acoustic radiation codes are presented. Research on unsteady flows, which are particularly important for understanding counterrotation interaction noise, unsteady loading effects on acoustics, and flutter or forced response is described. The first results of three-dimensional unsteady Euler solutions are illustrated for a single rotation propeller at an angle of attack and for a counterrotation propeller. Basic experimental and theoretical results from studies of the unsteady aerodynamics of oscillating cascades are outlined. Finally, advanced concepts involving swirl recovery vanes and ultra bypass ducted propellers are discussed. Author

N88-15807*# National Aeronautics and Space Administration. Lewis Research Center, Cleveland, OH.

AEROPROPULSION '87. SESSION 6: HIGH-SPEED PROPULSION TECHNOLOGY

Nov. 1987 119 p Conference held in Cleveland, Ohio, 17-19 Nov. 1987 Submitted for publication
 (NASA-CP-10003-SESS-6; E-3798-SESS-6; NAS 1.55:10003-SESS-6) Avail: NTIS HC A06/MF A01 CSCL 21E

NASA is conducting aeronautical research over a broad range of Mach numbers. In addition to the advanced CTOL propulsion research described in a separate session, the Lewis Research Center has intensified its efforts towards propulsion technology for selected high-speed flight applications. In a companion program, the Langley Research Center has also accomplished excellent research in Supersonic Combustion Ramjet (SCRAM) propulsion. What is presented in this session is an unclassified review of some of the propulsion research results that are applicable for supersonic to hypersonic vehicles. Not only is a review provided for several key work areas, it also presents a viewpoint on future research directions by calling attention to cycles, components, and facilities involved in this rapidly expanding field of work.

N88-15808*# National Aeronautics and Space Administration. Lewis Research Center, Cleveland, OH.

SUPERSONIC STOVL PROPULSION TECHNOLOGY PROGRAM: AN OVERVIEW

BERNARD J. BLAHA and PETER G. BATTERTON *In its* Aeropropulsion '87. Session 6: High-Speed Propulsion Technology

07 AIRCRAFT PROPULSION AND POWER

23 p Nov. 1987

Avail: NTIS HC A06/MF A01 CSCL 21E

Planning activities are continuing between NASA, DOD, and two foreign governments to develop the technology and to demonstrate the design capability for advanced, supersonic, short-takeoff and vertical-landing (STOVL) aircraft by the mid-1990s. As a result, a Memorandum of Understanding (MOU) was established by the United Kingdom to jointly pursue the required technology; and an MOU with Canada is expected to be signed shortly. The NASA Lewis Research Center will play a lead role in the development of the required propulsion technologies which were identified as being critical to achieve viable STOVL aircraft. These planning activities have already resulted in initial research programs focused on technologies common to two or more of the proposed propulsion system concepts. An overview of the Lewis Research Center's role in the overall program plan and recent results in the development of the required propulsion technologies is presented. Author

N88-15809*# National Aeronautics and Space Administration. Lewis Research Center, Cleveland, OH.

PROPULSION CHALLENGES AND OPPORTUNITIES FOR HIGH-SPEED TRANSPORT AIRCRAFT

WILLIAM C. STRACK *In its* Aeropropulsion '87. Session 6: High-Speed Propulsion Technology 19 p Nov. 1987

Avail: NTIS HC A06/MF A01 CSCL 21E

For several years there was a growing interest in the subject of efficient sustained supersonic cruise technology applied to a high-speed transport aircraft. The major challenges confronting the propulsion community for supersonic transport (SST) applications are identified. Both past progress and future opportunities are discussed in relation to perceived technology shortfalls for an economically successful SST that satisfies environmental constraints. A very large improvement in propulsion system efficiency is needed both at supersonic and subsonic cruise conditions. Toward that end, several advanced engine concepts are being considered that, together with advanced discipline and component technologies, promise at least 40 percent better efficiency than the Concorde engine. The quest for higher productivity through higher speed is also thwarted by the lack of a conventional, low-priced fuel that is thermally stable at the higher temperatures associated with faster flight. Airport noise remains a tough challenge because previously researched concepts fall short of achieving FAR 36 Stage 3 noise levels. Innovative solutions may be necessary to reach acceptably low noise. While the technical challenges are indeed formidable, it is reasonable to assume that the current shortfalls in fuel economy and noise can be overcome through an aggressive propulsion research program. Author

N88-15810*# National Aeronautics and Space Administration. Lewis Research Center, Cleveland, OH.

SUPERSONIC THROUGHFLOW FANS FOR HIGH-SPEED AIRCRAFT

CALVIN L. BALL *In its* Aeropropulsion '87. Session 6: High-Speed Propulsion Technology 26 p Nov. 1987

Avail: NTIS HC A06/MF A01 CSCL 21E

Increased need for more efficient long-range supersonic flight has revived interest in the supersonic throughflow fan as a possible component for advanced high-speed propulsion systems. A fan that can operate with supersonic inlet axial Mach numbers would reduce the inlet losses incurred in diffusing the flow from supersonic Mach numbers to a subsonic one at the fan face. In addition, the size and weight of an all-supersonic inlet will be substantially lower than those of a conventional inlet. However, the data base for components of this type is practically nonexistent. Therefore, in order to furnish the required information for assessing the potential for this type of fan, the NASA Lewis Research Center has begun a program to design, analyze, build, and test a fan stage that is capable of operating with supersonic axial velocities from inlet to exit. The objectives are to demonstrate the feasibility and potential of supersonic throughflow fans, to gain a fundamental understanding of the flow physics associated with such systems,

and to develop an experimental data base for design and analysis code validation. A brief overview of past supersonic throughflow fan activities are provided; the technology needs discussed; the design of a supersonic throughflow fan stage, a facility inlet, and a downstream diffuser described; and the results from the analysis codes used in executing the design are presented. Also presented is an engine concept intended to permit establishing supersonic throughflow within the fan on the runway and maintaining the supersonic throughflow condition within the fan throughout the flight envelope. Author

N88-16637*# National Aeronautics and Space Administration. Lewis Research Center, Cleveland, OH.

TECHNOLOGY DEVELOPMENTS FOR A COMPOUND CYCLE ENGINE

GEORGE A. BOBULA, WILLIAM T. WINTUCKY, and J. G. CASTOR (Garrett Turbine Engine Co., Phoenix, Ariz.) *In* NASA, Washington, NASA/Army Rotorcraft Technology. Volume 2: Materials and Structures, Propulsion and Drive Systems, Flight Dynamics and Control, and Acoustics p 683-697 Feb. 1988

Avail: NTIS HC A25/MF A01 CSCL 21E

The Compound Cycle Engine (CCE) is a highly turbocharged, power compounded power plant which combines the light weight pressure rise capability of a gas turbine with the high efficiency of a diesel. When optimized for a rotorcraft, the CCE will reduce fuel burned for a typical 2 hour (plus 30 min reserve) mission by 30 to 40 percent when compared to a conventional advanced technology gas turbine. The CCE can provide a 50 percent increase in range-payload product on this mission. Results of recent activities in a program to establish the technology base for a CCE are presented. The objective of this program is to research and develop those critical technologies which are necessary for the demonstration of a multicylinder diesel core in the early 1990s. A major accomplishment was the initial screening and identification of a lubricant which has potential for meeting the material wear rate limits of the application. An in-situ wear measurement system also was developed to provide accurate, readily obtainable, real time measurements of ring and liner wear. Wear data, from early single cylinder engine tests, are presented to show correlation of the in-situ measurements and the system's utility in determining parametric wear trends. A plan to demonstrate a compound cycle engine by the mid 1990s is included. Author

N88-16638*# National Aeronautics and Space Administration. Lewis Research Center, Cleveland, OH.

SMALL GAS TURBINE ENGINE TECHNOLOGY

RICHARD W. NIEDZWIECKI and PETER L. MEITNER (Army Research and Technology Labs., Cleveland, Ohio.) *In* NASA, Washington, NASA/Army Rotorcraft Technology. Volume 2: Materials and Structures, Propulsion and Drive Systems, Flight Dynamics and Control, and Acoustics p 698-736 Feb. 1988

Avail: NTIS HC A25/MF A01 CSCL 21E

Performance of small gas turbine engines in the 250 to 1,000 horsepower size range is significantly lower than that of large engines. Engines of this size are typically used in rotorcraft, commutercraft, general aviation, and cruise missile applications. Principal reasons for the lower efficiencies of a smaller engine are well known: component efficiencies are lower by as much as 8 to 10 percentage points because of size effects. Small engines are designed for lower cycle pressures and temperatures because of smaller blading and cooling limitations. The highly developed analytical and manufacturing techniques evolved for large engines are not directly transferrable to small engines. Thus, it was recognized that a focused effort addressing technologies for small engines was needed and could significantly impact their performance. Recently, in-house and contract studies were undertaken at the NASA Lewis Research Center to identify advanced engine cycle and component requirements for substantial performance improvement of small gas turbines for projected year 2000 applications. The results of both in-house research and contract studies are presented. In summary, projected fuel savings of 22 to 42 percent could be obtained. Accompanying direct operating cost reductions of 11 to 17 percent, depending on fuel

cost, were also estimated. High payoff technologies are identified for all engine applications, and recent results of experimental research to evolve the high payoff technologies are described.

Author

N88-16639*# National Aeronautics and Space Administration. Lewis Research Center, Cleveland, OH.

THE CONVERTIBLE ENGINE: A DUAL-MODE PROPULSION SYSTEM

JACK G. MCARDLE *In* NASA, Washington, NASA/Army Rotorcraft Technology. Volume 2: Materials and Structures, Propulsion and Drive Systems, Flight Dynamics and Control, and Acoustics p 737-768 Feb. 1988

Avail: NTIS HC A25/MF A01 CSCL 21E

A variable inlet guide vane (VIGV) convertible engine that could be used to power future high-speed rotorcraft was tested on an outdoor stand. The engine ran stably and smoothly in the turbofan, turboshaft, and dual (combined fan and shaft) power modes. In the turbofan mode with the VIGV open, fuel consumption was comparable to that of a conventional turbofan engine. In the turboshaft mode with the VIGV closed, fuel consumption was higher than that of present turboshaft engines because power was wasted in churning fan-tip air flow. In dynamic performance tests with a specially built digital engine control and using a waterbrake dynamometer for shaft load, the engine responded effectively to large steps in thrust command and shaft torque. Previous mission analyses of a conceptual X-wing rotorcraft capable of 400-knot cruise speed were revised to account for more fan-tip churning power loss that was originally estimated. The calculations confirm that using convertible engines rather than separate life and cruise engines would result in a smaller, lighter craft with lower fuel use and direct operating cost.

Author

N88-16640*# National Aeronautics and Space Administration. Lewis Research Center, Cleveland, OH.

RESULTS OF NASA/ARMY TRANSMISSION RESEARCH

JOHN J. COY (Army Research and Technology Labs., Cleveland, Ohio.), DENNIS P. TOWNSEND, and HAROLD H. COE *In* NASA, Washington, NASA/Army Rotorcraft Technology. Volume 2: Materials and Structures, Propulsion and Drive Systems, Flight Dynamics and Control, and Acoustics p 769-801 Feb. 1988

Avail: NTIS HC A25/MF A01 CSCL 21E

Since 1970 the NASA Lewis Research Center and the U.S. Army Aviation Systems Command have shared an interest in advancing the technology for helicopter propulsion systems. In particular, that portion of the program that applies to the drive train and its various mechanical components are outlined. The major goals of the program were (and continue to be) to increase the life, reliability, and maintainability, reduce the weight, noise, and vibration, and maintain the relatively high mechanical efficiency of the gear train. Major historical milestones are reviewed, significant advances in technology for bearings, gears, and transmissions are discussed, and the outlook for the future is presented. The reference list is comprehensive.

Author

N88-16697*# National Aeronautics and Space Administration. Lewis Research Center, Cleveland, OH.

AEROPROPULSION '87. SESSION 1: AEROPROPULSION MATERIALS RESEARCH

Nov. 1987 121 p Conference held in Cleveland, Ohio, 17-19 Nov. 1987 Submitted for publication

(NASA-CP-10003-SESS-1; E-3798-SESS-1; NAS 1.55:10003-SESS-1) Avail: NTIS HC A06/MF A01 CSCL 21E

Topics addressed include: aeropropulsion research and technology impact; high temperature polymer matrix composites; creep and fatigue effects; self-lubricating coatings; and ceramics for engines.

N88-16698*# National Aeronautics and Space Administration. Lewis Research Center, Cleveland, OH.

IMPACT AND PROMISE OF NASA AEROPROPULSION TECHNOLOGY

NEAL T. SAUNDERS and DAVID N. BOWDITCH *In its*

Aeropropulsion '87. Session 1: Aeropropulsion Materials Research 30 p Nov. 1987

Avail: NTIS HC A06/MF A01 CSCL 21E

The aeropropulsion industry in the United States has established an enviable record of leading the world in aeropropulsion for commercial and military aircraft. The NASA aeropropulsion propulsion program (primarily conducted through the Lewis Research Center) has significantly contributed to that success through research and technology advances and technology demonstrations such as the Refan, Engine Component Improvement, and the Energy Efficient Engine Programs. Some past NASA contributions to engines in current aircraft are reviewed, and technologies emerging from current research programs for the aircraft of the 1990's are described. Finally, current program thrusts toward improving propulsion systems in the 2000's for subsonic commercial aircraft and higher speed aircraft such as the High-Speed Civil Transport and the National Aerospace Plane (NASP) are discussed.

Author

N88-17656*# National Aeronautics and Space Administration. Lewis Research Center, Cleveland, OH.

EXPERIMENTAL EVALUATION OF A TRANSLATING NOZZLE SIDEWALL RADIAL TURBINE

RICHARD J. ROELKE and CASIMIR ROGO (Teledyne CAE, Toledo, Ohio.) *In* AGARD Advanced Technology for Aero Gas Turbine Components 13 p Sep. 1987

Avail: NTIS HC A23/MF A01 CSCL 21E

An experimental performance evaluation was made of two movable sidewall variable area radial turbines. The turbine designs were representative of the gas generator turbine of a variable flow capacity rotorcraft engine. The first turbine was an uncooled design while the second turbine had a cooled nozzle but an uncooled rotor. The cooled nozzle turbine was evaluated both with and without coolant flow. The test results showed that the movable nozzle wall is a viable and efficient means to effectively control the flow capacity of a radial turbine. Peak efficiencies of the second turbine with and without nozzle coolant were 86.5 and 88 percent respectively. These values are comparable to pivoting vane variable geometry turbines; however, the decrease in efficiency as the flow was varied from the design value was much less for the movable wall turbine. Several design improvements which should increase the turbine efficiency one or two more points are identified. These design improvements include reduced leakage losses and relocation of the vane coolant ejection holes to reduce mainstream disturbance.

Author

N88-18594*# National Aeronautics and Space Administration. Lewis Research Center, Cleveland, OH.

LIQUID SPRAYS AND FLOW STUDIES IN THE DIRECT-INJECTION DIESEL ENGINE UNDER MOTORED CONDITIONS

HUNG LEE NGUYEN, MARK H. CARPENTER, JUAN I. RAMOS (Carnegie-Mellon Univ., Pittsburgh, Pa.), HAROLD J. SCHOCK, and JAMES D. STEGEMAN Mar. 1988 80 p

(NASA-TM-100135; E-3685; NAS 1.15:100135) Avail: NTIS HC A05/MF A01 CSCL 21E

A two dimensional, implicit finite difference method of the control volume variety, a two equation model of turbulence, and a discrete droplet model were used to study the flow field, turbulence levels, fuel penetration, vaporization, and mixing in diesel engine environments. The model was also used to study the effects of engine speed, injection angle, spray cone angle, droplet distribution, and intake swirl angle on the flow field, spray penetration and vaporization, and turbulence in motored two-stroke diesel engines. It is shown that there are optimum conditions for injection, which depend on droplet distribution, swirl, spray cone angle, and injection angle. The optimum conditions result in good spray penetration and vaporization and in good fuel mixing. The calculation presented clearly indicates that internal combustion engine models can be used to assess, at least qualitatively, the effects of injection characteristics and engine operating conditions on the flow field and on the spray penetration and vaporization in diesel engines.

Author

07 AIRCRAFT PROPULSION AND POWER

N88-19469*# National Aeronautics and Space Administration. Lewis Research Center, Cleveland, OH.

ASSESSMENT, DEVELOPMENT AND APPLICATION OF COMBUSTOR AEROTHERMAL MODELS

J. D. HOLDEMAN, H. C. MONGIA, and E. J. MULARZ (Army Aviation Research and Development Command, Cleveland, Ohio.) 1988 21 p Proposed for presentation at the 33rd International Gas Turbine and Aeroengine Congress and Exposition, Amsterdam, The Netherlands, 5-9 Jun. 1988; sponsored by ASME (NASA-TM-100290; E-3914; NAS 1.15:100290; AVSCOM-TM-88-C-001) Avail: NTIS HC A03/MF A01 CSCL 21E

The gas turbine combustion system design and development effort is an engineering exercise to obtain an acceptable solution to the conflicting design trade-offs between combustion efficiency, gaseous emissions, smoke, ignition, restart, lean blowout, burner exit temperature quality, structural durability, and life cycle cost. For many years, these combustor design trade-offs have been carried out with the help of fundamental reasoning and extensive component and bench testing, backed by empirical and experience correlations. Recent advances in the capability of computational fluid dynamics codes have led to their application to complex 3-D flows such as those in the gas turbine combustor. A number of U.S. Government and industry sponsored programs have made significant contributions to the formulation, development, and verification of an analytical combustor design methodology which will better define the aerothermal loads in a combustor, and be a valuable tool for design of future combustion systems. The contributions made by NASA Hot Section Technology (HOST) sponsored Aerothermal Modeling and supporting programs are described. Author

N88-20306*# Hamilton Standard, Windsor Locks, CT.

LARGE-SCALE ADVANCED PROP-FAN (LAP) Final Report

C. L. DEGEORGE 1988 255 p Original contains color illustrations (Contract NAS3-23051) (NASA-CR-182112; NAS 1.26:182112) Avail: NTIS HC A12/MF A01 CSCL 21E

In recent years, considerable attention has been directed toward improving aircraft fuel efficiency. Analytical studies and research with wind tunnel models have demonstrated that the high inherent efficiency of low speed turboprop propulsion systems may now be extended to the Mach .8 flight regime of today's commercial airliners. This can be accomplished with a propeller, employing a large number of thin highly swept blades. The term Prop-Fan has been coined to describe such a propulsion system. In 1983 the NASA-Lewis Research Center contracted with Hamilton Standard to design, build and test a near full scale Prop-Fan, designated the Large Scale Advanced Prop-Fan (LAP). This report provides a detailed description of the LAP program. The assumptions and analytical procedures used in the design of Prop-Fan system components are discussed in detail. The manufacturing techniques used in the fabrication of the Prop-Fan are presented. Each of the tests run during the course of the program are also discussed and the major conclusions derived from them stated. Author

N88-21160*# National Aeronautics and Space Administration. Lewis Research Center, Cleveland, OH.

UTILIZATION OF PARALLEL PROCESSING IN SOLVING THE INVISCID FORM OF THE AVERAGE-PASSAGE EQUATION SYSTEM FOR MULTISTAGE TURBOMACHINERY

RICHARD A. MULAC, MARK L. CELESTINA, JOHN J. ADAMCZYK, KENT P. MISEGADES, and JEF M. DAWSON (Cray Research, Inc., Mendota Heights, Minn.) 1987 13 p Prepared for the 8th Computational Fluid Dynamics Conference, Honolulu, Hawaii, 9-11 Jun. 1987; sponsored by AIAA Previously announced in IAA as A87-42057

(NASA-TM-89845; E-3508; NAS 1.15:89845) Avail: NTIS HC A03/MF A01 CSCL 21E

A procedure is outlined which utilizes parallel processing to solve the inviscid form of the average-passage equation system for multistage turbomachinery along with a description of its

implementation in a FORTRAN computer code, MSTAGE. A scheme to reduce the central memory requirements of the program is also detailed. Both the multitasking and I/O routines referred to are specific to the Cray X-MP line of computers and its associated SSD (Solid-State Disk). Results are presented for a simulation of a two-stage rocket engine fuel pump turbine. Author

N88-21161*# National Aeronautics and Space Administration. Lewis Research Center, Cleveland, OH.

NNEPQ: CHEMICAL EQUILIBRIUM VERSION OF THE NAVY/NASA ENGINE PROGRAM

LAURENCE H. FISHBACH and SANFORD GORDON (Gordon, Sanford, Cleveland, Ohio) 1988 10 p Proposed for presentation at the 1988 International Gas Turbine and Aerospace Congress, Amsterdam, Netherlands, 5-9 Jun. 1988; sponsored by ASME (NASA-TM-100851; E-4050; NAS 1.15:100851) Avail: NTIS HC A02/MF A01 CSCL 21E

The Navy NASA Engine Program, NNEP, currently is in use at a large number of government agencies, commercial companies and universities. This computer code has been used extensively to calculate the design and off-design (matched) performance of a broad range of turbine engines, ranging from subsonic turboprops to variable cycle engines for supersonic transports. Recently, there has been increased interest in applications for which NNEP was not capable of simulating, namely, high Mach applications, alternate fuels including cryogenics, and cycles such as the gas generator air-turbo-rocker (ATR). In addition, there is interest in cycles employing ejectors such as for military fighters. New engine component models had to be created for incorporation into NNEP, and it was found necessary to include chemical dissociation effects of high temperature gases. The incorporation of these extended capabilities into NNEP is discussed and some of the effects of these changes are illustrated. Author

N88-21162*# National Aeronautics and Space Administration. Lewis Research Center, Cleveland, OH.

EFFECT OF SPATIAL INLET TEMPERATURE AND PRESSURE DISTORTION ON TURBOFAN ENGINE STABILITY

CHARLES M. MEHALIC 1988 19 p Proposed for presentation at the 24th Joint Propulsion Conference, Boston, Mass., 11-13 Jul. 1988; sponsored by AIAA, ASME, ASME and SAE (NASA-TM-100850; E-4047; NAS 1.15:100850; AIAA-88-3016) Avail: NTIS HC A03/MF A01 CSCL 21E

The effects of circumferential and radial inlet temperature distortion, circumferential pressure distortion, and combined temperature and pressure distortion on the stability of an advanced turbofan engine were investigated experimentally at simulated altitude conditions. With circumferential and radial inlet temperature distortion, a flow instability generated by the fan operating near stall caused the high-pressure compressor to surge at, or near, the same time as the fan. The effect of combined distortion was dependent on the relative location of the high-temperature and low-pressure regions; high-pressure compressor stalls occurred when the regions coincided, and fan stalls occurred with the regions separated. Author

N88-21163*# National Aeronautics and Space Administration. Lewis Research Center, Cleveland, OH.

A MICROPROCESSOR-BASED REAL-TIME SIMULATOR OF A TURBOFAN ENGINE

JONATHAN S. LITT (Army Aviation Research and Development Command, Cleveland, Ohio.), JOHN C. DELAAT, and WALTER C. MERRILL 1988 16 p Presented at the 19th Annual Pittsburgh Conference on Modeling and Simulation, Pittsburgh, Pa., 5-6 May 1988; sponsored by ISA and IEEE

(NASA-TM-100889; E-4124; NAS 1.15:100889; AVSCOM-TR-88-C-011) Avail: NTIS HC A03/MF A01 CSCL 21E

A real-time digital simulator of a Pratt and Whitney F 100 engine is discussed. This self-contained unit can operate in an open-loop stand-alone mode or as part of a closed-loop control system. It can also be used in control system design and development. It

accepts five analog control inputs and its sixteen outputs are returned as analog signals. Author

N88-22037*# National Aeronautics and Space Administration. Lewis Research Center, Cleveland, OH.

SMALL ENGINE COMPONENTS TEST FACILITY TURBINE TESTING CELL

BRENT C. NOWLIN and VINCENT G. VERHOFF 1988 17 p
Prepared for presentation at the 24th Joint Propulsion Conference, Boston, Mass., 11-13 Jul. 1988; sponsored in part by AIAA, ASME, and SAE
(NASA-TM-100887; E-4120; NAS 1.15:100887; AIAA-88-2963)
Avail: NTIS HC A03/MF A01 CSCL 21E

NASA Lewis Research Center has designed and constructed a new state-of-the-art test facility. This facility, called the Small Engine Components Test Facility (SECTF), is used to test gas turbines and compressors at conditions similar to actual engine conditions. The SECTF is comprised of two separate facilities - a turbine test cell and a compressor test cell. The paper will describe the turbine test cell. The capabilities of the facility make it unique - no other facility of its kind is capable of combining its pressure, speed, and temperature ranges. Turbine inlet air ranges up to 9 atm (125 psig). The turbine exhaust pressure ranges from 0.15 atm (2 psia) to atmospheric pressure. Turbine inlet air temperatures range from ambient to 700 K (1260 deg R). The controllable speed of the turbine rotor ranges from 4000 to 60,000 rpm and the maximum power absorbed by the facility dynamometer is 1250 hp. The data acquisition system scans up to 2000 channels/sec. This paper will discuss in detail the capabilities of the facility, overall facility design, instrumentation used in the facility, and the data acquisition system. Actual research data is not discussed.

Author

N88-22383*# National Aeronautics and Space Administration. Lewis Research Center, Cleveland, OH.

HIGH-TEMPERATURE COMBUSTOR LINER TESTS IN STRUCTURAL COMPONENT RESPONSE TEST FACILITY

PAUL E. MOORHEAD *In its* Lewis Structures Technology, 1988. Volume 2: Structural Mechanics p 5-13 May 1988
Avail: NTIS HC A14/MF A01 CSCL 21E

Jet engine combustor liners were tested in the structural component response facility at NASA Lewis. In this facility combustor liners were thermally cycled to simulate a flight envelope of takeoff, cruise, and return to idle. Temperatures were measured with both thermocouples and an infrared thermal imaging system. A conventional stacked-ring louvered combustor liner developed a crack at 1603 cycles. This test was discontinued after 1728 cycles because of distortion of the liner. A segmented or float wall combustor liner tested at the same heat flux showed no significant change after 1600 cycles. Changes are being made in the facility to allow higher temperatures.

Author

N88-22384*# National Aeronautics and Space Administration. Lewis Research Center, Cleveland, OH.

LIFE ASSESSMENT OF COMBUSTOR LINER USING UNIFIED CONSTITUTIVE MODELS

M. T. TONG (Sverdrup Technology, Inc., Cleveland, Ohio.) and R. L. THOMPSON *In its* Lewis Structures Technology, 1988. Volume 2: Structural Mechanics p 15-25 May 1988
(Contract NAS3-24105)
Avail: NTIS HC A14/MF A01 CSCL 21E

Hot section components of gas turbine engines are subject to severe thermomechanical loads during each mission cycle. Inelastic deformation can be induced in localized regions leading to eventual fatigue cracking. Assessment of durability requires reasonably accurate calculation of the structural response at the critical location for crack initiation. In recent years nonlinear finite element computer codes have become available for calculating inelastic structural response under cyclic loading. NASA-Lewis sponsored the development of unified constitutive material models and their implementation in nonlinear finite element computer codes for the structural analysis of hot section components. These unified models were evaluated with regard to their effect on the life prediction of

a hot section component. The component considered was a gas turbine engine combustor liner. A typical engine mission cycle was used for the thermal and structural analyses. The analyses were performed on a CRAY computer using the MARC finite element code. The results were compared with laboratory test results, in terms of crack initiation lives. Author

N88-22390*# National Aeronautics and Space Administration. Lewis Research Center, Cleveland, OH.

THE COMPOSITE BLADE STRUCTURAL ANALYZER (COBSTRAN)

ROBERT A. AIELLO *In its* Lewis Structures Technology, 1988. Volume 2: Structural Mechanics p 83-97 May 1988
Avail: NTIS HC A14/MF A01 CSCL 21E

The use and application of the COBSTRAN (COmposite BLADE STRuctural ANALyzer) computer code is presented. COBSTRAN was developed at NASA-Lewis and is currently being used for the design and analysis of aircraft engine ducted and unducted fan blades. The features of COBSTRAN are demonstrated for the modeling and analysis of a scaled down wind tunnel model propfan blade made from fiber composites. Comparison of analytical and experimental mode shapes and frequencies are shown, verifying the model development and analysis techniques used. The methodologies and programs developed for this analysis are directly applicable to other propfan blades. Author

N88-22394*# MARC Analysis Research Corp., Palo Alto, CA.

MHOST: AN EFFICIENT FINITE ELEMENT PROGRAM FOR INELASTIC ANALYSIS OF SOLIDS AND STRUCTURES

S. NAKAZAWA *In* NASA. Lewis Research Center, Lewis Structures Technology, 1988. Volume 2: Structural Mechanics p 131-140 May 1988
(Contract NAS3-23698)

Avail: NTIS HC A14/MF A01 CSCL 21E

An efficient finite element program for 3-D inelastic analysis of gas turbine hot section components was constructed and validated. A novel mixed iterative solution strategy is derived from the augmented Hu-Washizu variational principle in order to nodally interpolate coordinates, displacements, deformation, strains, stresses and material properties. A series of increasingly sophisticated material models incorporated in MHOST include elasticity, secant plasticity, infinitesimal and finite deformation plasticity, creep and unified viscoplastic constitutive model proposed by Walker. A library of high performance elements is built into this computer program utilizing the concepts of selective reduced integrations and independent strain interpolations. A family of efficient solution algorithms is implemented in MHOST for linear and nonlinear equation solution including the classical Newton-Raphson, modified, quasi and secant Newton methods with optional line search and the conjugate gradient method.

Author

N88-22399*# National Aeronautics and Space Administration. Lewis Research Center, Cleveland, OH.

COMPUTATIONAL STRUCTURAL MECHANICS FOR ENGINE STRUCTURES

CHRISTOS C. CHAMIS *In its* Lewis Structures Technology, 1988. Volume 2: Structural Mechanics p 189-203 May 1988
Avail: NTIS HC A14/MF A01 CSCL 21E

The computational structural mechanics (CSM) program at Lewis encompasses the formulation and solution of structural mechanics problems and the development of integrated software systems to computationally simulate the performance, durability, and life of engine structures. It is structured to supplement, complement, and, whenever possible, replace costly experimental efforts. Specific objectives are to investigate unique advantages of parallel and multiprocessing for reformulating and solving structural mechanics and formulating and solving multidisciplinary mechanics and to develop integrated structural system computational simulators for predicting structural performance, evaluating newly developed methods, and identifying and prioritizing improved or missing methods. Author

07 AIRCRAFT PROPULSION AND POWER

N88-22431*# National Aeronautics and Space Administration. Lewis Research Center, Cleveland, OH.

REVIEW AND ASSESSMENT OF THE HOST TURBINE HEAT TRANSFER PROGRAM

HERBERT J. GLADDEN *In its* Lewis Structures Technology, 1988. Volume 3: Structural Integrity Fatigue and Fracture Wind Turbines HOST p 349-367 May 1988

Avail: NTIS HC A16/MF A01 CSCL 21E

The objectives of the HOST Turbine Heat Transfer subproject were to obtain a better understanding of the physics of the aerothermodynamic phenomena occurring in high-performance gas turbine engines and to assess and improve the analytical methods used to predict the fluid dynamics and heat transfer phenomena. At the time the HOST project was initiated, an across-the-board improvement in turbine design technology was needed. Therefore, a building-block approach was utilized, with research ranging from the study of fundamental phenomena and analytical modeling to experiments in simulated real-engine environments. Experimental research accounted for 75 percent of the project, and analytical efforts accounted for approximately 25 percent. Extensive experimental datasets were created depicting the three-dimensional flow field, high free-stream turbulence, boundary-layer transition, blade tip region heat transfer, film cooling effects in a simulated engine environment, rough-wall cooling enhancement in a rotating passage, and rotor-stator interaction effects. In addition, analytical modeling of these phenomena was initiated using boundary-layer assumptions as well as Navier-Stokes solutions. Author

N88-22902*# National Aeronautics and Space Administration. Lewis Research Center, Cleveland, OH.

NASA ADVANCED TURBOPROP RESEARCH AND CONCEPT VALIDATION PROGRAM

JOHN B. WHITLOW, JR. and G. KEITH SIEVERS 1988 23 p Proposed for presentation at the 1988 Conference and Exposition on Future Transportation Technology, San Francisco, Calif., 8-11 Aug. 1988; sponsored by the Society of Automotive Engineers (NASA-TM-100891; E-4129; NAS 1.15:100891) Avail: NTIS HC A03/MF A01 CSCL 21E

NASA has determined by experimental and analytical effort that use of advanced turboprop propulsion instead of the conventional turbofans in the older narrow-body airline fleet could reduce fuel consumption for this type of aircraft by up to 50 percent. In cooperation with industry, NASA has defined and implemented an Advanced Turboprop (ATP) program to develop and validate the technology required for these new high-speed, multibladed, thin, swept propeller concepts. This paper presents an overview of the analysis, model-scale test, and large-scale flight test elements of the program together with preliminary test results, as available. Author

N88-23247*# Army Aviation Systems Command, Cleveland, OH. Structural Dynamics Branch.

AEROELASTIC FORCED RESPONSE ANALYSIS OF TURBOMACHINERY

TODD E. SMITH (Sverdrup Technology, Inc., Cleveland, Ohio.) *In* NASA, Lewis Research Center, Lewis Structures Technology, 1988. Volume 1: Structural Dynamics p 287-297 May 1988 (Contract NAS3-24105)

Avail: NTIS HC A20/MF A01 CSCL 21E

An introduction is given to the research activity that is underway to enable the prediction of turbomachinery aeroelastic forced response. An effort is being made to assemble a computer program (FREPS) which incorporates the aeroelastic structural models, unsteady aerodynamic models, and forcing function models. The structural and aerodynamic models are currently well developed. The forcing function models are at a primitive level. A significant activity has begun to identify the forcing functions due to stator-rotor aerodynamic interaction. Author

N88-23806*# National Aeronautics and Space Administration. Lewis Research Center, Cleveland, OH.

THE CHALLENGES AND OPPORTUNITIES OF SUPERSONIC TRANSPORT PROPULSION TECHNOLOGY

WILLIAM C. STRACK and SHELBY J. MORRIS, JR. (National Aeronautics and Space Administration. Langley Research Center, Hampton, Va.) Jul. 1988 18 p Prepared for presentation at the 24th Joint Propulsion Conference, Boston, Mass., 11-13, Jul. 1988

(NASA-TM-100921; E-4178; NAS 1.15:100921; AIAA-88-2985)

Avail: NTIS HC A03/MF A01 CSCL 21E

The major challenges confronting the propulsion community for civil supersonic transport applications are identified: high propulsion system efficiency at both supersonic and subsonic cruise conditions, low-cost fuel with adequate thermal stability at high temperatures, low noise cycles and exhaust systems, low emission combustion systems, and low drag installations. Both past progress and future opportunities are discussed in relation to perceived technology shortfalls for an economically successful airplane that satisfies environmental constraints. Author

N88-24639*# National Aeronautics and Space Administration. Lewis Research Center, Cleveland, OH.

PARTICLE-LADEN WEAKLY SWIRLING FREE JETS: MEASUREMENTS AND PREDICTIONS

DANIEL L. BULZAN, JIAN-SHUN SHUEN, and GERARD M. FAETH (Michigan Univ., Ann Arbor.) 1988 22 p Presented at the 24th Joint Propulsion Conference, Boston, Mass., 11-13 Jul. 1988; sponsored by AIAA, ASEE, ASME and SAE

(NASA-TM-100920; E-4176; NAS 1.15:100920; AIAA-88-3138)

Avail: NTIS HC A03/MF A01 CSCL 21E

A theoretical and experimental investigation of particle-laden, weakly swirling, turbulent free jets was conducted. Glass particles, having a Sauter mean diameter of 39 microns with a standard deviation of 15 microns, were used. A single loading ratio of 0.2 was used in the experiments. Measurements are reported for three swirl numbers, ranging from 0.0 to 0.3. The measurements included mean and fluctuating velocities of both phases, and particle mass flux distributions. Measurements were compared with predictions from three types of multiphase flow analysis: locally homogeneous flow (LHF); deterministic separated flow (DSF); and stochastic separated flow (SSF). For the particle-laden jets, the LHF and DSF models did not provide very satisfactory predictions. The LHF model generally overestimated the rate of decay of particle mean axial and angular velocities with streamwise distance, due to the neglect of particle inertia. The LHF model predictions of particle mass flux also showed poor agreement with measurements due to the assumption of no-slip between phases. The DSF model also performed quite poorly for predictions of particle mass flux, because turbulent dispersion of the particles was neglected. The SSF model, which accounts for both particle inertia and turbulent dispersion of the particles, yielded reasonably good predictions throughout the flow field for the particle-laden jets. Author

N88-24640*# National Aeronautics and Space Administration. Lewis Research Center, Cleveland, OH.

AN EMPIRICAL MODEL OF THE EFFECTS OF CURVATURE AND CONVERGENCE ON DILUTION JET MIXING

JAMES D. HOLDEMAN, RAM SRINIVASAN, and CRAIG D. WHITE (Garrett Engine Co., Phoenix, Ariz.) 1988 20 p Presented at the 24th Joint Propulsion Conference, Boston, Mass., 11-13 Jul. 1988; sponsored in part by AIAA, ASME, SAE and ASEE Original document contains color illustrations

(NASA-TM-100896; E-4143; NAS 1.15:100896; AIAA-88-3180)

Avail: NTIS HC A03/MF A01 CSCL 21E

An existing empirical model of the temperature field downstream of single and multiple rows of jets injected into a confined crossflow has been extended to model the effects of curvature and convergence on the mixing. This extension is based on the results of a numerical study of these effects using a 3-D turbulent flow computer code. Temperature distributions calculated with the empirical model are presented to show the effects of flow area convergence, radius of curvature, and inner and outer wall injection for single and opposed rows of jets. Author

N88-24641*# National Aeronautics and Space Administration. Lewis Research Center, Cleveland, OH.

NASA/INDUSTRY ADVANCED TURBOPROP TECHNOLOGY PROGRAM

JOSEPH A. ZIEMIANSKI and JOHN B. WHITLOW, JR. 1988 26 p Prepared for presentation at the 16th Congress of the International Council of Aeronautical Sciences, Jerusalem, Israel, 28 Aug. - 2 Sep. 1988

(NASA-TM-100929; E-4198; NAS 1.15:100929) Avail: NTIS HC A03/MF A01 CSCL 21E

Experimental and analytical effort shows that use of advanced turboprop (propfan) propulsion instead of conventional turbofans in the older narrow-body airline fleet could reduce fuel consumption for this type of aircraft by up to 50 percent. The NASA Advanced Turboprop (ATP) program was formulated to address the key technologies required for these thin, swept-blade propeller concepts. A NASA, industry, and university team was assembled to develop and validate applicable design codes and prove by ground and flight test the viability of these propeller concepts. Some of the history of the ATP project, an overview of some of the issues, and a summary of the technology developed to make advanced propellers viable in the high-subsonic cruise speed application are presented. The ATP program was awarded the prestigious Robert J. Collier Trophy for the greatest achievement in aeronautics and astronautics in America in 1987. Author

N88-24642*# National Aeronautics and Space Administration. Lewis Research Center, Cleveland, OH.

EXPERIMENTAL VIBRATION DAMPING CHARACTERISTICS OF THE THIRD-STAGE ROTOR OF A THREE-STAGE TRANSONIC AXIAL-FLOW COMPRESSOR

FREDERICK A. NEWMAN 1988 24 p Presented at the 24th Joint Propulsion Conference, Boston, Mass., 11-13 Jul. 1988; sponsored in part by AIAA, ASME, SAE and ASEE

(NASA-TM-100948; E-4240; NAS 1.15:100948; AIAA-88-3229) Avail: NTIS HC A03/MF A01 CSCL 21E

Rotor blade aerodynamic damping is experimentally determined in a three-stage transonic axial flow compressor having design aerodynamic performance goals of 4.5:1 pressure ratio and 65.5 lbm/sec weight flow. The combined damping associated with each mode is determined by a least squares fit of a single degree of freedom system transfer function to the nonsynchronous portion of the rotor blade strain gage output power spectra. The combined damping consists of the aerodynamic damping and the structural and mechanical damping. The aerodynamic damping varies linearly with the inlet total pressure for a given corrected speed, weight flow, and pressure ratio while the structural and mechanical damping is assumed to remain constant. The combined damping is determined at three inlet total pressure levels to obtain the aerodynamic damping. The third-stage rotor blade aerodynamic damping is presented and discussed for the design equivalent speed with the stator blades reset for maximum efficiency. The compressor overall performance and experimental Campbell diagrams for the third-stage rotor blade row are also presented.

Author

N88-25458*# National Aeronautics and Space Administration. Lewis Research Center, Cleveland, OH.

OVERVIEW OF NASA RESEARCH IN FIBER OPTICS FOR AIRCRAFT CONTROLS

GARY T. SENG 1988 9 p Proposed for presentation at the ISA/88 International Conference and Exhibit, Houston, Tex., 16-21 Oct. 1988; sponsored by the Instrument Society of America

(NASA-TM-100919; E-4156; NAS 1.15:100919) Avail: NTIS HC A02/MF A01 CSCL 01C

The challenge of those involved in aircraft control system hardware development is to accommodate an ever-increasing complexity in aircraft control, while limiting the size and weight of the components and improving system reliability. A technology that displays promise towards this end is fiber optics. The primary advantages of employing optical fibers, passive optical sensors and optically controlled actuators are weight/volume reduction, immunity from electromagnetic effects, high bandwidth capabilities

and freedom from short circuits/sparking contacts. Since 1975, NASA Lewis has been performing in-house, contract and grant research in fiber optic sensors, high temperature electro-optic switches and fly-by-light control system architecture. Passive optical sensor development is an essential yet challenging area of work and has therefore received much attention during this period. A major effort to develop fly-by-light control system technology, known as the Fiber Optic Control System Integration (FOCSI) program, was initiated in 1985 as a cooperative effort between NASA and DOD. Phase 1 of FOCSI, completed in 1986, was aimed at the design of a fiber optic integrated propulsion/flight control system. Phase 2 will provide subcomponent and system development and system testing. In addition to a summary of the benefits of fiber optics, the FOCSI program, sensor advances, and future directions in the NASA Lewis program are discussed.

Author

N88-25459*# Sverdrup Technology, Inc., Cleveland, OH.
TWO-DIMENSIONAL VISCOUS FLOW COMPUTATIONS OF HYPERSONIC SCRAMJET NOZZLE FLOWFIELDS AT DESIGN AND OFF-DESIGN CONDITIONS Final Report

G. J. HARLOFF, H. T. LAI, and E. S. NELSON Jun. 1988 18 p Presented at the 24th Joint Propulsion Conference, Boston, Mass., 11-13 Jul. 1988; sponsored in part by AIAA, ASME, SAE, and ASEE

(Contract NAS3-25266)

(NASA-CR-182150; E-4190; NAS 1.26:182150) Avail: NTIS HC A03/MF A01 CSCL 21E

The PARC2D code has been selected to analyze the flowfields of a representative hypersonic scramjet nozzle over a range of flight conditions from Mach 3 to 20. The flowfields, wall pressures, wall skin friction values, heat transfer values and overall nozzle performance are presented.

Author

N88-25460*# National Aeronautics and Space Administration. Lewis Research Center, Cleveland, OH.

RECENT ADVANCES IN CAPACITANCE TYPE OF BLADE TIP CLEARANCE MEASUREMENTS

JOHN P. BARRANGER 1988 18 p Prepared for presentation at the Conference on Sensors and Measurement Techniques for Aeronautical Applications, Atlanta, Ga., 7-9 Sep. 1988; sponsored by AIAA

(NASA-TM-101291; E-4271; NAS 1.15:101291) Avail: NTIS HC A03/MF A01 CSCL 21E

Two recent electronic advances at NASA-Lewis that meet the blade tip clearance needs of a wide class of fans, compressors, and turbines are described. The first is a frequency modulated (FM) oscillator that requires only a single low cost ultrahigh frequency operational amplifier. Its carrier frequency is 42.8 MHz when used with a 61 cm long hermetically sealed coaxial cable. The oscillator can be calibrated in the static mode and has a negative peak frequency deviation of 400 kHz for a typical rotor blade. High temperature performance tests of the probe and 13 cm of the adjacent cable show good accuracy up to 600 C, the maximum which produces a clearance error of + or - 10 microns at a clearance of 500 microns. In the second advance, a guarded probe configuration allows a longer cable capacitance. The capacitance of the probe is part of a small time constant feedback in a high speed operational amplifier. The solution of the governing differential equation is applied to a ramp type of input. The results show an amplifier output that contains a term which is proportional to the derivative of the feedback capacitance. The capacitance is obtained by subtracting a balancing reference channel followed by an integration stage.

Author

N88-27200*# National Aeronautics and Space Administration. Lewis Research Center, Cleveland, OH.

EXPERIMENTAL DETERMINATION OF AERODYNAMIC DAMPING IN A THREE-STAGE TRANSONIC AXIAL-FLOW COMPRESSOR M.S. Thesis - Case Western Reserve Univ.

FREDERICK A. NEWMAN Aug. 1988 113 p

(NASA-TM-100953; E-4267; NAS 1.15:100953) Avail: NTIS HC A06/MF A01 CSCL 21E

07 AIRCRAFT PROPULSION AND POWER

Rotor blade aerodynamic damping is experimentally determined in a three-stage transonic axial flow compressor having design aerodynamic performance goals of 4.5:1 pressure ratio and 65.5 lbf/sec weight flow. The combined damping associated with each mode is determined by a least squares fit of a single degree of freedom system transfer function to the nonsynchronous portion of the rotor blade strain gauge output power spectra. The combined damping consists of aerodynamic and structural and mechanical damping. The aerodynamic damping varies linearly with the inlet total pressure for a given equivalent speed, equivalent mass flow, and pressure ratio while structural and mechanical damping are assumed to be constant. The combined damping is determined at three inlet total pressure levels to obtain the aerodynamic damping. The third stage rotor blade aerodynamic damping is presented and discussed for 70, 80, 90, and 100 percent design equivalent speed. The compressor overall performance and experimental Campbell diagrams for the third stage rotor blade row are also presented. Author

N88-27201*# National Aeronautics and Space Administration. Lewis Research Center, Cleveland, OH.

DOCUMENTATION OF THE BENSON DIESEL ENGINE SIMULATION PROGRAM

JON VANGERPEN Aug. 1988 136 p Prepared in cooperation with Army Aviation Research and Technical Command, Cleveland, Ohio
(Contract DA PROJ. 1L1-61102-AH-45)
(NASA-TM-100940; E-4221; NAS 1.15:100940;
AVSCOM-TR-88-C-025) Avail: NTIS HC A07/MF A01 CSCL 21E

This report documents the Benson Diesel Engine Simulation Program and explains how it can be used to predict the performance of diesel engines. The program was obtained from the Garrett Turbine Engine Company but has been extensively modified since. The program is a thermodynamic simulation of the diesel engine cycle which uses a single zone combustion model. It can be used to predict the effect of changes in engine design and operating parameters such as valve timing, speed and boost pressure. The most significant change made to this program is the addition of a more detailed heat transfer model to predict metal part temperatures. This report contains a description of the sub-models used in the Benson program, a description of the input parameters and sample program runs. Author

N88-28074*# Pratt and Whitney Aircraft, East Hartford, CT.
STRUCTURAL TAILORING OF ADVANCED TURBOPROPS (STAT) Interim Report
KENNETH W. BROWN Aug. 1988 67 p
(Contract NAS3-23941)
(NASA-CR-180861; NAS 1.26:180861; PWA-5967-46) Avail: NTIS HC A04/MF A01 CSCL 21E

This interim report describes the progress achieved in the structural Tailoring of Advanced Turboprops (STAT) program which was developed to perform numerical optimizations on highly swept propfan blades. The optimization procedure seeks to minimize an objective function, defined as either direct operating cost or aeroelastic differences between a blade and its scaled model, by tuning internal and external geometry variables that must satisfy realistic blade design constraints. This report provides a detailed description of the input, optimization procedures, approximate analyses and refined analyses, as well as validation test cases for the STAT program. In addition, conclusions and recommendations are summarized. Author

N88-28927*# Hamilton Standard, Windsor Locks, CT.
EXPERIMENTAL AND ANALYTICAL EVALUATION OF THE EFFECTS OF SIMULATED ENGINE INLETS ON THE BLADE VIBRATORY STRESSES OF THE SR-3 MODEL PROP-FAN Final Report
PREM N. BANSAL Sep. 1985 118 p
(Contract NAS3-24222)
(NASA-CR-174959; NAS 1.26:174959) Avail: NTIS HC A06/MF A01 CSCL 21E

A cooperative wind tunnel test program, referred to as GUN-3, had been conducted previously to assess the effect of inlet configuration and location on the inlet face pressure recovery and inlet drag in the presence of a high-speed advanced turboprop. These tests were conducted with the inlets located just downstream of the SR-3 model Prop-Fan, a moderately swept, eight-bladed 62.2 cm (24.5 inch) diameter advanced, high-speed turboprop model fabricated from titanium. During these tests, two blades of the SR-3 model Prop-Fan were strain gaged to measure the vibratory blade stresses occurring during the inlet aerodynamic test program. The purpose of the effort reported herein was to reduce and analyze the test results related to the vibratory strain gage measurements obtained. Three inlet configurations had been tested. These were: (1) single scoop, (2) twin scoop, and (3) annular. Each of the three inlets was tested at a position just behind the rotor. The single scoop inlet was also tested at a position further aft. Tests were also done without an inlet. These results emphasize the importance of avoiding critical speeds in the continuous operating range. B.W.

N88-28928*# Hamilton Standard, Windsor Locks, CT.
SR-7A AEROELASTIC MODEL DESIGN REPORT
D. NAGLE, S. AUYEUNG, and J. TURNBERG Washington, D.C. Oct. 1986 118 p
(Contract NAS3-23051)
(NASA-CR-174791; NAS 1.26:174791; HSER-9251) Avail: NTIS HC A06/MF A01 CSCL 21E

A scale model was designed to simulate the aeroelastic characteristics and performance of the 2.74 meter (9 ft.) diameter SR-7L blade. The procedures used in this model blade design are discussed. Included in this synopsis is background information concerning scaling parameters and an explanation of manufacturing limitations. A description of the final composite model blade, made of titanium, fiberglass, and graphite, is provided. Analytical methods for determining the blade stresses, natural frequencies and mode shapes, and stability are discussed at length. Author

N88-28929*# General Electric Co., Cincinnati, OH. Aircraft Engine Business Group.
E3 10C COMPRESSOR TEST ANALYSIS OF HIGH-SPEED POST-STALL DATA
S. D. DVORAK, W. M. HOSNY, and W. G. STEENKEN Oct. 1986 109 p
(Contract NAS3-24211)
(NASA-CR-179521; NAS 1.26:179521; R86AEB564) Avail: NTIS HC A06/MF A01 CSCL 21E

In-stall characteristics from high-speed post-stall transients are determined. The transient, surge-cycle nature of high-speed post-stall operation precludes the possibility of obtaining in-stall characteristics in a steady-state manner, as is possible during low-speed post-stall operation, which is characterized by quasi-steady rotating-stall behavior. Maximum likelihood parameter estimation techniques were used to obtain the quasi-steady high-speed characteristics from transient data. The necessary data was first obtained from a specially instrumented compressor that was tested well beyond its limits of normal operation. The unsteady, post-stall data thus obtained was then digitized and processed through a simplified analytical model to construct the input-output relationship necessary for estimation. In-stall characteristics were determined using this estimation procedure at two different high-speed conditions, 90 and 98.5 percent corrected speed. The estimated characteristics were found to be robust in the presence of measurement noise and unmodelled system dynamics, but the compressor response-time constants, also estimated, were more sensitive to these same disturbances. The experimentally determined low-speed in-stall characteristics and the estimated high-speed in-stall characteristics were then incorporated into a one-dimensional compressor simulation model developed as a parallel effort to the compressor testing and data reduction effort, which yielded predictable results. Author

N88-28930*# United Technologies Corp., East Hartford, CT.
THE EFFECTS OF INLET TURBULENCE AND ROTOR/STATOR INTERACTIONS ON THE AERODYNAMICS AND HEAT TRANSFER OF A LARGE-SCALE ROTATING TURBINE MODEL. VOLUME 3: HEAT TRANSFER DATA TABULATION 65 PERCENT AXIAL SPACING Final Report
 R. P. DRING, M. F. BLAIR, and H. D. JOSLYN Washington, D.C. May 1986 235 p
 (Contract NAS3-23717)
 (NASA-CR-179468; NAS 1.26:179468; UTRC/R86-956480-VOL-3)
 Avail: NTIS HC A11/MF A01 CSDL 21E

This is Volume 3 - Heat Transfer Data Tabulation (65 percent Axial Spacing) of a combined experimental and analytical program which was conducted to examine the effects of inlet turbulence on airfoil heat transfer. The experimental portion of the study was conducted in a large-scale (approximately 5X engine), ambient temperature, rotating turbine model configured in both single stage and stage-and-a-half arrangements. Heat transfer measurements were obtained using low-conductivity airfoils with miniature thermocouples welded to a thin, electrically heated surface skin. Heat transfer data were acquired for various combinations of low or high inlet turbulence intensity, flow coefficient, first-stator/rotor axial spacing, Reynolds number and relative circumferential position of the first and second stators. Author

N88-29804*# United Technologies Corp., East Hartford, CT.
THE EFFECTS OF INLET TURBULENCE AND ROTOR/STATOR INTERACTIONS ON THE AERODYNAMICS AND HEAT TRANSFER OF A LARGE-SCALE ROTATING TURBINE MODEL. VOLUME 2: HEAT TRANSFER DATA TABULATION. 15 PERCENT AXIAL SPACING Final Report
 R. P. DRING, M. F. BLAIR, and H. D. JOSLYN Washington, D.C. May 1986 242 p
 (Contract NAS3-23717)
 (NASA-CR-179467; NAS 1.26:179467; UTRC-R86-956480-VOL-2)
 Avail: NTIS HC A11/MF A01 CSDL 21E

A combined experimental and analytical program was conducted to examine the effects of inlet turbulence on airfoil heat transfer. The experimental portion of the study was conducted in a large-scale (approx 5X engine), ambient temperature, rotating turbine model configured in both single stage and stage-and-a-half arrangements. Heat transfer measurements were obtained using low-conductivity airfoils with miniature thermocouples welded to a thin, electrically heated surface skin. Heat transfer data were acquired for various combinations of low or high inlet turbulence intensity, flow coefficient, first-stator/rotor axial spacing, Reynolds number and relative circumferential position of the first and second stators. Aerodynamic measurements obtained as part of the program include distributions of the mean and fluctuating velocities at the turbine inlet and, for each airfoil row, midspan airfoil surface pressures and circumferential distributions of the downstream steady state pressures and fluctuating velocities. Analytical results include airfoil heat transfer predictions produced using existing 2-D boundary layer computation schemes and an examination of solutions of the unsteady boundary layer equations. The results are reported in four separate volumes, of which this is Volume 2: Heat Transfer Data Tabulation; 15 Percent Axial Spacing. Author

N88-29807*# National Aeronautics and Space Administration. Lewis Research Center, Cleveland, OH.
AEROELASTIC RESPONSE OF METALLIC AND COMPOSITE PROPPAN MODELS IN YAWED FLOW
 KRISHNA RAO V. KAZA, MARC H. WILLIAMS, ORAL MEHMED, and G. V. NERAYANAN (Sverdrup Technology, Inc., Cleveland, Ohio.) 1988 26 p Presented at the 24th Joint Propulsion Conference, Boston, Mass., 11-13 Jul. 1988; sponsored in part by AIAA, ASEE, ASME and SAE
 (NASA-TM-100964; E-4229; NAS 1.15:100964; AIAA-88-3154)
 Avail: NTIS HC A03/MF A01 CSDL 21E

An analytical investigation of aeroelastic response of metallic and composite propfan models in yawed flow was performed. The analytical model is based on the normal modes of a rotating blade and the three dimensional unsteady lifting surface aerodynamic

theory including blade mistuning. The calculated blade stresses or strains are compared with published wind tunnel data on two metallic and three composite propfan wind tunnel models. The comparison shows a good agreement between theory and experiment. Additional parametric results indicate that blade response is very sensitive to the blade stiffness and also to blade frequency and mode shape mistuning. From these findings, it is concluded that both frequency and mode shape mistuning should be included in aeroelastic response analysis. Furthermore, both calculated and measured strains show that combined blade frequency and mode shape mistuning has beneficial effects on response due to yawed flow. Author

N88-29811*# Southwest Research Inst., San Antonio, TX. Dept. of Materials Sciences.

CONSTITUTIVE MODELING FOR ISOTROPIC MATERIALS Final Report

K. S. CHAN, U. S. LINDHOLM, and S. R. BODNER Jun. 1988 155 p
 (Contract NAS3-23925; SWRI PROJ. 06-7576)
 (NASA-CR-182132; NAS 1.26:182132) Avail: NTIS HC A08/MF A01 CSDL 21E

The third and fourth years of a 4-year research program, part of the NASA HOST Program, are described. The program goals were: (1) to develop and validate unified constitutive models for isotropic materials, and (2) to demonstrate their usefulness for structural analysis of hot section components of gas turbine engines. The unified models selected for development and evaluation were those of Bodner-Partom and of Walker. The unified approach for elastic-viscoplastic constitutive equations is a viable method for representing and predicting material response characteristics in the range where strain rate and temperature dependent inelastic deformations are experienced. This conclusion is reached by extensive comparison of model calculations against the experimental results of a test program of two high temperature Ni-base alloys, B1900+Hf and Mar-M247, over a wide temperature range for a variety of deformation and thermal histories including uniaxial, multiaxial, and thermomechanical loading paths. The applicability of the Bodner-Partom and the Walker models for structural applications has been demonstrated by implementing these models into the MARC finite element code and by performing a number of analyses including thermomechanical histories on components of hot sections of gas turbine engines and benchmark notch tensile specimens. The results of the 4-year program have been published in four annual reports. The results of the base program are summarized in this report. The tasks covered include: (1) development of material test procedures, (2) thermal history effects, and (3) verification of the constitutive model for an alternative material. Author

08

AIRCRAFT STABILITY AND CONTROL

Includes aircraft handling qualities; piloting; flight controls; and autopilots.

A88-50272*# National Aeronautics and Space Administration. Lewis Research Center, Cleveland, OH.
COOPERATIVE SYNTHESIS OF CONTROL AND DISPLAY AUGMENTATION FOR A STOL AIRCRAFT IN THE APPROACH AND LANDING TASK

SANJAY GARG (NASA, Lewis Research Center; Sverdrup Technology, Inc., Middleburg Heights, OH) and DAVID K. SCHMIDT (Purdue University, West Lafayette, IN) IN: AIAA Guidance, Navigation and Control Conference, Minneapolis, MN, Aug. 15-17, 1988, Technical Papers. Part 2. Washington, DC, American Institute of Aeronautics and Astronautics, 1988, p. 1071-1082. Research supported by Honeywell Inc. refs

08 AIRCRAFT STABILITY AND CONTROL

(Contract NAG4-1; F33615-86-C-3615)
(AIAA PAPER 88-4182)

Application of the Cooperative methodology to synthesize control/display augmentation systems for the piloted longitudinal landing task with a modern, statically-unstable, fighter aircraft is considered. Starting with a control augmentation law which yields augmented vehicle dynamics that meet Level I handling qualities specifications, the effect of time-delay in the Head-up-display is studied using model-based criterion. This evaluation showed that even with 'good' conventional dynamics, a realistic value of display time-delay will cause significant deterioration in pilot workload and piloted-system performance. Application of the Cooperative methodology to control augmentation alone resulted in augmented vehicle dynamics which provide direct control of the flight path from the pilot stick. Analytical evaluation of these dynamics indicates that such dynamics might lead to improved pilot ratings over conventional dynamics, especially in the presence of time-delays in the system. Also, application of the methodology to simultaneous synthesis of control augmentation and flight director laws revealed that it might be advantageous to consider the control/display trade-off in the early design stages. Author

N88-11680*# National Aeronautics and Space Administration. Lewis Research Center, Cleveland, OH.

FLIGHT PROPULSION CONTROL INTEGRATION FOR V/STOL AIRCRAFT

JAMES R. MIHALOEWS 1987 22 p. Presented at the International Powered Lift Conference, Santa Clara, Calif., 7-10 Dec. 1987; sponsored by the Society of Automotive Engineers (NASA-TM-100226; E-3845; NAS 1.15:100226) Avail: NTIS HC A03/MF A01 CSCL 01C

The goal of the propulsion community is to have the enabling propulsion technologies in place to permit a low risk decision regarding the initiation of a research STOVL supersonic attack fighter aircraft in the mid-1990's. This technology will effectively integrate, enhance, and extend the supersonic cruise, STOVL, and fighter/attack programs to enable U.S. industry to develop a revolutionary supersonic short takeoff vertical landing fighter/attack aircraft in the post-ATF period. The rationale, methods, and criteria used in developing a joint NASA Lewis and NASA Ames research program to develop the technology element for integrated flight propulsion control through integrated methodologies is presented. This program, the Supersonic STOVL Integrated Flight Propulsion Controls Program, is part of the overall NASA Lewis Supersonic STOVL integrated approach to an integrated program to achieve integrated flight propulsion control technology. Author

N88-16643*# National Aeronautics and Space Administration. Lewis Research Center, Cleveland, OH.

ROTORCRAFT FLIGHT-PROPULSION CONTROL INTEGRATION

JAMES R. MIHALOEWS, MARK G. BALLIN, and D. G. C. RUTLEDGE (Sikorsky Aircraft, Stratford, Conn.) In NASA, Washington, NASA/Army Rotorcraft Technology. Volume 2: Materials and Structures, Propulsion and Drive Systems, Flight Dynamics and Control, and Acoustics p 900-928 Feb. 1988 Avail: NTIS HC A25/MF A01 CSCL 01C

The NASA Ames and Lewis Research Centers, in conjunction with the Army Research and Technology Laboratories have initiated and completed, in part, a joint research program focused on improving the performance, maneuverability, and operating characteristics of rotorcraft by integrating the flight and propulsion controls. The background of the program, its supporting programs, its goals and objectives, and an approach to accomplish them are discussed. Results of the modern control governor design of the T700 and the Rotorcraft Integrated Flight-Propulsion Control Study, which were key elements of the program, are also presented. Author

N88-16647*# National Aeronautics and Space Administration. Lewis Research Center, Cleveland, OH.

IDENTIFICATION AND PROPOSED CONTROL OF HELICOPTER TRANSMISSION NOISE AT THE SOURCE

JOHN J. COY, ROBERT F. HANDSCHUH, DAVID G. LEWICKI (Army Research and Technology Labs., Cleveland, Ohio.), RONALD G. HUFF, EUGENE A. KREJSA, and ALLAN M. KARCHMER In NASA, Washington, NASA/Army Rotorcraft Technology. Volume 2: Materials and Structures, Propulsion and Drive Systems, Flight Dynamics and Control, and Acoustics p 1045-1065 Feb. 1988 Previously announced as N87-16816

Avail: NTIS HC A25/MF A01 CSCL 01C

Helicopter cabin interiors require noise treatment which is expensive and adds weight. The gears inside the main power transmission are major sources of cabin noise. Work conducted by the NASA Lewis Research Center in measuring cabin interior noise and in relating the noise spectrum to the gear vibration of the Army OH-58 helicopter is described. Flight test data indicate that the planetary gear train is a major source of cabin noise and that other low frequency sources are present that could dominate the cabin noise. Companion vibration measurements were made in a transmission test stand, revealing that the single largest contributor to the transmission vibration was the spiral bevel gear mesh. The current understanding of the nature and causes of gear and transmission noise is discussed. It is believed that the kinematical errors of the gear mesh have a strong influence on that noise. The completed NASA/Army sponsored research that applies to transmission noise reduction is summarized. The continuing research program is also reviewed. Author

N88-19475*# National Aeronautics and Space Administration. Lewis Research Center, Cleveland, OH.

ROTORCRAFT FLIGHT-PROPULSION CONTROL INTEGRATION: AN ECLECTIC DESIGN CONCEPT

JAMES R. MIHALOEWS, MARK G. BALLIN, and D. G. C. RUTLEDGE (Sikorsky Aircraft, Stratford, Conn.) Apr. 1988 34 p

(NASA-TP-2815; E-3812; NAS 1.60:2815) Avail: NTIS HC A03/MF A01 CSCL 01C

The NASA Ames and Lewis Research Centers, in conjunction with the Army Research and Technology Laboratories, have initiated and partially completed a joint research program focused on improving the performance, maneuverability, and operating characteristics of rotorcraft by integrating the flight and propulsion controls. The background of the program, its supporting programs, its goals and objectives, and an approach to accomplish them are discussed. Results of the modern control governor design of the General Electric T700 engine and the Rotorcraft Integrated Flight-Propulsion Control Study, which were key elements of the program, are also presented. Author

N88-23249*# Georgia Inst. of Tech., Atlanta.

APPLICATION OF NAVIER-STOKES ANALYSIS TO STALL FLUTTER

J. C. WU, R. SRIVASTAVA, and L. N. SANKAR In NASA, Lewis Research Center, Lewis Structures Technology, 1988. Volume 1: Structural Dynamics p 309-320 May 1988

(Contract NAG3-730)

Avail: NTIS HC A20/MF A01 CSCL 01A

A solution procedure was developed to investigate the two-dimensional, one- or two-dimensional flutter characteristics of arbitrary airfoils. This procedure requires a simultaneous integration in time of the solid and fluid equations of motion. The fluid equations of motion are the unsteady compressible Navier-Stokes equations, solved in a body-fitted moving coordinate system using an approximate factorization scheme. The solid equations of motion are integrated in time using an Euler implicit scheme. Flutter is said to occur if small disturbances imposed on the airfoil attitude lead to divergent oscillatory motions at subsequent times. The flutter characteristics of airfoils in subsonic speed at high angles of attack and airfoils in high subsonic and transonic speeds at low angles of attack are investigated. The stall flutter characteristics are also predicted using the same procedure. Author

09 RESEARCH AND SUPPORT FACILITIES (AIR)

N88-26376*# National Aeronautics and Space Administration. Lewis Research Center, Cleveland, OH.

COMPUTER SIMULATION OF A SINGLE PILOT FLYING A MODERN HIGH-PERFORMANCE HELICOPTER

MARK E. ZIPF, WILLIAM G. VOGT, MARLIN H. MICKLE, RONALD G. HOELZEMAN, FEI KAI, and JAMES R. MIHALOEW (Pittsburgh Univ., Pa.) Jul. 1988 25 p

(Contract NAG3-729)

(NASA-TM-100182; E-3759; NAS 1.15:100182) Avail: NTIS HC A03/MF A01 CSCL 01C

Presented is a computer simulation of a human response pilot model able to execute operational flight maneuvers and vehicle stabilization of a modern high-performance helicopter. Low-order, single-variable, human response mechanisms, integrated to form a multivariable pilot structure, provide a comprehensive operational control over the vehicle. Evaluations of the integrated pilot were performed by direct insertion into a nonlinear, total-force simulation environment provided by NASA Lewis. Comparisons between the integrated pilot structure and single-variable pilot mechanisms are presented. Static and dynamically alterable configurations of the pilot structure are introduced to simulate pilot activities during vehicle maneuvers. These configurations, in conjunction with higher level, decision-making processes, are considered for use where guidance and navigational procedures, operational mode transfers, and resource sharing are required. Author

N88-26377*# National Aeronautics and Space Administration. Lewis Research Center, Cleveland, OH.

COMPUTER SIMULATION OF MULTIPLE PILOTS FLYING A MODERN HIGH PERFORMANCE HELICOPTER

MARK E. ZIPF, WILLIAM G. VOGT, MARLIN H. MICKLE, RONALD G. HOELZEMAN, FEI KAI, and JAMES R. MIHALOEW (Pittsburgh Univ., Pa.) Jul. 1988 32 p

(Contract NAG3-729)

(NASA-TM-100183; E-3760; NAS 1.15:100183) Avail: NTIS HC A03/MF A01 CSCL 01C

A computer simulation of a human response pilot mechanism within the flight control loop of a high-performance modern helicopter is presented. A human response mechanism, implemented by a low order, linear transfer function, is used in a decoupled single variable configuration that exploits the dominant vehicle characteristics by associating cockpit controls and instrumentation with specific vehicle dynamics. Low order helicopter models obtained from evaluations of the time and frequency domain responses of a nonlinear simulation model, provided by NASA Lewis Research Center, are presented and considered in the discussion of the pilot development. Pilot responses and reactions to test maneuvers are presented and discussed. Higher level implementation, using the pilot mechanisms, are discussed and considered for their use in a comprehensive control structure. Author

09

RESEARCH AND SUPPORT FACILITIES (AIR)

Includes airports, hangars and runways; aircraft repair and overhaul facilities; wind tunnels; shock tubes; and aircraft engine test stands.

A88-22121*# Clemson Univ., SC.

DEVELOPMENT OF A SPECIAL-PURPOSE TEST SURFACE GUIDED BY UNCERTAINTY ANALYSIS - INTRODUCTION OF A NEW UNCERTAINTY ANALYSIS STEP

T. WANG (Clemson University, SC) and T. W. SIMON (Minnesota, University, Minneapolis) AIAA, Aerospace Sciences Meeting, 26th, Reno, NV, Jan. 11-14, 1988. 10 p. Research supported by the University of Minnesota and South Carolina Energy Research and Development Center. refs

(Contract NAG3-286)

(AIAA PAPER 88-0169)

Development of a recent experimental program to investigate the effects of streamwise curvature on boundary layer transition required making a bendable, heated and instrumented test wall, a rather nonconventional surface. The present paper describes this surface, the design choices made in its development and how uncertainty analysis was used, beginning early in the test program, to make such design choices. Published uncertainty analysis techniques were found to be of great value; but, it became clear that another step, one herein called the pre-test analysis, would aid the program development. Finally, it is shown how the uncertainty analysis was used to determine whether the test surface was qualified for service. Author

A88-30778* National Aeronautics and Space Administration. Lewis Research Center, Cleveland, OH.

EXPERIMENTAL EVALUATION OF CORNER VANES - SUMMARY

ROYCE MOORE, DONALD BOLDMAN, RYCKEY SHYNE, and THOMAS GELDER (NASA, Lewis Research Center, Cleveland, OH) SAE, Aerospace Technology Conference and Exposition, Long Beach, CA, Oct. 5-8, 1987. 19 p. Previously announced in STAR as N87-28571. refs (SAE PAPER 871784)

Two types of turning vane airfoils (a controlled-diffusion shape and a circular arc shape) have been evaluated in the high-speed and fan-drive corners of a 0.1-scale model of NASA Lewis Research Center's proposed Altitude Wind Tunnel. The high-speed corner was evaluated with and without a simulated engine exhaust removal scoop. The fan-drive corner was evaluated with and without the high-speed corner. Flow surveys of pressure and flow angle were taken for both the corners and the vanes to determine their respective losses. The two-dimensional vane losses were low; however, the overall corner losses were higher because three-dimensional flow was generated by the complex geometry resulting from the turning vanes intersecting the end wall. The three-dimensional effects were especially pronounced in the outer region of the circular corner. Author

A88-32188*# National Aeronautics and Space Administration. Lewis Research Center, Cleveland, OH.

THERMOSTRUCTURAL ANALYSIS WITH EXPERIMENTAL VERIFICATION IN A HIGH HEAT FLUX FACILITY OF A SIMULATED COWL LIP

MATTHEW E. MELIS and HERBERT J. GLADDEN (NASA, Lewis Research Center, Cleveland, OH) IN: Structures, Structural Dynamics and Materials Conference, 29th, Williamsburg, VA, Apr. 18-20, 1988, Technical Papers. Part 1. Washington, DC, American Institute of Aeronautics and Astronautics, 1988, p. 106-115. (AIAA PAPER 88-2222)

Three-dimensional FEM analyses using the NASTRAN and MARC codes have been used to predict the thermal and structural response of active cooling schemes proposed for a hypersonic vehicle's propulsion system cowl lip under high aerothermodynamic heating loads. In order to experimentally verify these analyses, a hydrogen/oxygen rocket engine has been modified to employ the exhaust stream as a high enthalpy/high heat flux source for the evaluation of various actively cooled, simulated cowl lip segments as well as flat structural segments. O.C.

A88-33065*# National Aeronautics and Space Administration. Lewis Research Center, Cleveland, OH.

A DISTRIBUTED DATA ACQUISITION SYSTEM FOR AERONAUTICS TEST FACILITIES

DENNIS L. FRONEK, ROBERT N. SETTER, PHILIP Z. BLUMENTHAL, and ROBERT R. SMALLEY (NASA, Lewis Research Center, Cleveland, OH) IN: International Instrumentation Symposium, 33rd, Las Vegas, NV, May 3-8, 1987, Proceedings. Research Triangle Park, NC, Instrument Society of America, 1987, p. 167-172. Previously announced in STAR as N87-16851.

The NASA Lewis Research Center is in the process of installing a new data acquisition and display system. This new system will

09 RESEARCH AND SUPPORT FACILITIES (AIR)

provide small and medium sized aeronautics test facilities with a state-of-the-art real-time data acquisition and display system. The new data system will provide for the acquisition of signals from a variety of instrumentation sources. They include analog measurements of temperatures, pressures, and other steady state voltage inputs; frequency inputs to measure speed and flow; discrete I/O for significant events, and modular instrument systems such as multiplexed pressure modules or electronic instrumentation with a IEEE 488 interface. The data system is designed to acquire data, convert it to engineering units, compute test dependent performance calculations, limit check selected channels or calculations, and display the information in alphanumeric or graphical form with a cycle time of one second for the alphanumeric data. This paper describes the system configuration, its salient features, and the expected impact on testing. Author

A88-37926* Syracuse Univ., NY.

AN ISENTROPIC COMPRESSION HEATED LUDWIG TUBE TRANSIENT WIND TUNNEL

PATRICK J. MAGARI and JOHN E. LAGRAFF (Syracuse University, NY) IN: Aerodynamic Testing Conference, 15th, San Diego, CA, May 18-20, 1988, Technical Papers. Washington, DC, American Institute of Aeronautics and Astronautics, 1988, p. 179-188. refs (Contract NAG3-621) (AIAA PAPER 88-2019)

Syracuse University's Ludwig tube with isentropic compression facility is a transient wind tunnel employing a piston drive that incorporates isentropic compression heating of the test gas located ahead of a piston. The facility is well-suited for experimental investigations concerning supersonic and subsonic vehicles over a wide range of pressures, Reynolds numbers, and temperatures; all three parameters can be almost independently controlled. Work at the facility currently includes wake-induced stagnation point heat transfer and supersonic boundary layer transition. O.C.

A88-44820* National Aeronautics and Space Administration. Lewis Research Center, Cleveland, OH.

AN EXPERIMENTAL INVESTIGATION OF THE EFFECT OF TEST-CELL PRESSURE ON THE PERFORMANCE OF RESISTOJET

D. H. MANZELLA (NASA, Lewis Research Center; Sverdrup Technology, Inc., Cleveland, OH), P. F. PENKO (NASA, Lewis Research Center, Cleveland, OH), K. J. DE WITT, and T. G. KEITH, JR. (Toledo, University, OH) AIAA, ASME, SAE, and ASEE, Joint Propulsion Conference, 24th, Boston, MA, July 11-13, 1988. 8 p. NASA-supported research. refs (AIAA PAPER 88-3286)

The effect of test-cell pressure on the performance of two resistojets was investigated. Tests were conducted in a vacuum facility at pressures ranging from 0.000043 to 0.54 torr for two resistojet configurations: a laboratory model and an engineering model for the Space Station. The tests showed that for each thruster there was a decline in performance when tested in vacuum pressures above 0.001 torr. Measurements were made of surface temperature, thrust, and exit-plane pitot pressure over the range of test-cell pressures. From these measurements, the decline in performance of the laboratory-model resistojet at higher cell pressures was attributed to heat losses due to convection. For the engineering-model resistojet, the decline in performance was found to be a combination of heat loss and an effect of cell pressure on the nozzle flow. Author

N88-15814* National Aeronautics and Space Administration. Lewis Research Center, Cleveland, OH.

EXPERIMENTAL INVESTIGATION OF THE SUBSONIC HIGH-ALTITUDE OPERATION OF THE NASA LEWIS 10- BY 10-FOOT SUPERSONIC WIND TUNNEL

CHRISTOPHER E. HUGHES and ROBERT J. JERACKI Jan. 1988 26 p (NASA-TM-100214; E-3823; NAS 1.15:100214) Avail: NTIS HC A03/MF A01 CSCL 14B

An experimental investigation was conducted in the NASA Lewis 10- by 10-Foot Supersonic Wind Tunnel during subsonic

tunnel operation in the aerodynamic cycle to determine the test section flow characteristics near the Advanced Turboprop Project propeller model plane of rotation. The investigation used an eight-probe pitot static flow survey rake to measure total and static pressures at two locations in the wind tunnel: the test section and the bellmouth section (upstream of the two-dimensional flexible-wall nozzle). A cone angularity probe was used to measure any flow angularity in the test section. The evaluation was conducted at tunnel Mach numbers from 0.10 to 0.35 and at three operating altitudes from 2,000 to 50,000 ft. which correspond to tunnel reference total pressures from 1960 to 245 psfa, respectively. The results of this experimental investigation indicate a total-pressure loss area in the center of the test section and a static-pressure gradient from the test section centerline to the wall. These total and static pressure differences were observed at all tunnel operating altitudes and diminished at lower tunnel velocities. The total-pressure loss area was also found in the bellmouth section, which indicates that the loss mechanism is not the tunnel flexible-wall nozzle. The flow in the test section is essentially axial since very small flow angles were measured. The results also indicate that a correction to the tunnel total and static pressures must be applied in order to determine accurate freestream conditions at the test section centerline. Author

N88-17686* National Aeronautics and Space Administration. Lewis Research Center, Cleveland, OH.

EXPERIMENTAL EVALUATION OF TURNING VANE DESIGNS FOR HIGH-SPEED AND COUPLED FAN-DRIVE CORNERS OF 0.1-SCALE MODEL OF NASA LEWIS RESEARCH CENTER'S PROPOSED ALTITUDE WIND TUNNEL

THOMAS F. GELDER, ROYCE D. MOORE, RICKEY J. SHYNE, and DONALD R. BOLDMAN May 1987 54 p Microfiche available as supplement (NASA-TP-2681; E-3218; NAS 1.60:2681) Avail: NTIS HC A04/MF A01 CSCL 14B

Two turning vane designs were experimentally evaluated for the fan-drive corner (corner 2) coupled to an upstream diffuser and the high-speed corner (corner 1) of the 0.1 scale model of NASA Lewis Research Center's proposed Altitude Wind Tunnel. For corner 2 both a controlled-diffusion vane design (vane A4) and a circular-arc vane design (vane B) were studied. The corner 2 total pressure loss coefficient was about 0.12 with either vane design. This was about 25 percent less loss than when corner 2 was tested alone. Although the vane A4 design has the advantage of 20 percent fewer vanes than the vane B design, its vane shape is more complex. The effects of simulated inlet flow distortion on the overall losses for corner 1 or 2 were small. Author

N88-25464* National Aeronautics and Space Administration. Lewis Research Center, Cleveland, OH.

TECHNIQUES UTILIZED IN THE SIMULATED ALTITUDE TESTING OF A 2D-CD VECTORING AND REVERSING NOZZLE

H. BRUCE BLOCK, LIVELY BRYANT, JOHN H. DICUS, ALLAN S. MOORE, MAUREEN E. BURNS, ROBERT F. SOLOMON, and IRVING SHEER Jun. 1988 43 p (NASA-TM-100872; E-4096; NAS 1.15:100872) Avail: NTIS HC A03/MF A01 CSCL 14B

Simulated altitude testing of a two-dimensional, convergent-divergent, thrust vectoring and reversing exhaust nozzle was accomplished. An important objective of this test was to develop test hardware and techniques to properly operate a vectoring and reversing nozzle within the confines of an altitude test facility. This report presents detailed information on the major test support systems utilized, the operational performance of the systems and the problems encountered, and test equipment improvements recommended for future tests. The most challenging support systems included the multi-axis thrust measurement system, vectored and reverse exhaust gas collection systems, and infrared temperature measurement systems used to evaluate and monitor the nozzle. The feasibility of testing a vectoring and reversing nozzle of this type in an altitude chamber was successfully demonstrated. Supporting systems performed as required. During reverser operation, engine exhaust gases were successfully

captured and turned downstream. However, a small amount of exhaust gas spilled out the collector ducts' inlet openings when the reverser was opened more than 60 percent. The spillage did not affect engine or nozzle performance. The three infrared systems which viewed the nozzle through the exhaust collection system worked remarkably well considering the harsh environment.

Author

N88-28939* National Aeronautics and Space Administration. Lewis Research Center, Cleveland, OH.

ARCJET POWER SUPPLY AND START CIRCUIT Patent

ROBERT P. GRUBER, inventor (to NASA) 30 Aug. 1988 5 p
Filed 10 Jun. 1987 Supersedes N87-25335 (25 - 19, p 2573)
(NASA-CASE-LEW-14374-1; US-PATENT-4,766,724;
US-PATENT-APPL-SN-060200; US-PATENT-CLASS-60-203.1;
US-PATENT-CLASS-219-383; US-PATENT-CLASS-363-97)
Avail: US Patent and Trademark Office CSCL 14B

A dc power supply for spacecraft arcjet thrusters has an integral automatic starting circuit and an output averaging inductor. The output averaging inductor, in series with the load, provides instantaneous current control, and ignition pulse and an isolated signal proportional to the arc voltage. A pulse width modulated converter, close loop configured, is also incorporated to give fast response output current control.

Official Gazette of the U.S. Patent and Trademark Office

N88-29825*# Southwest Research Inst., San Antonio, TX.

SPRAY AUTOMATED BALANCING OF ROTORS: METHODS AND MATERIALS Final Report

ANTHONY J. SMALLEY, RICHARD M. BALDWIN, and WILBUR R. SCHICK Aug. 1988 122 p
(Contract NAS3-25069; DA PROJ. 1L1-62209-AH-76)
(NASA-CR-182151; NAS 1.26:182151; AVSCOM-TR-88-C-018)
Avail: NTIS HC A06/MF A01 CSCL 14B

The work described consists of two parts. In the first part, a survey is performed to assess the state of the art in rotor balancing technology as it applies to Army gas turbine engines and associated power transmission hardware. The second part evaluates thermal spray processes for balancing weight addition in an automated balancing procedure. The industry survey reveals that: (1) computerized balancing equipment is valuable to reduce errors, improve balance quality, and provide documentation; (2) slow-speed balancing is used exclusively, with no foreseeable need for production high-speed balancing; (3) automated procedures are desired; and (4) thermal spray balancing is viewed with cautious optimism whereas laser balancing is viewed with concern for flight propulsion hardware. The FARE method (Fuel/Air Repetitive Explosion) was selected for experimental evaluation of bond strength and fatigue strength. Material combinations tested were tungsten carbide on stainless steel (17-4), Inconel 718 on Inconel 718, and Triballoy 800 on Inconel 718. Bond strengths were entirely adequate for use in balancing. Material combinations have been identified for use in hot and cold sections of an engine, with fatigue strengths equivalent to those for hand-ground materials.

Author

12

ASTRONAUTICS (GENERAL)

A88-16215*# Ford Aerospace and Communications Corp., Palo Alto, CA.

ECONOMIC BENEFITS OF THE SPACE STATION TO COMMERCIAL COMMUNICATION SATELLITE OPERATORS

KENT M. PRICE, JOHN E. DIXSON, and CHARLES J. WEYANDT (Ford Aerospace and Communications Corp., Western Development Laboratories Div., Palo Alto, CA) IAF, International Astronautical Congress, 38th, Brighton, England, Oct. 10-17, 1987.

8 p.

(Contract NAS3-24253)

(IAF PAPER 87-622)

The economic and financial aspects of newly defined space-based activities, procedures, and operations (APOs) and associated satellite system designs are presented that have the potential to improve economic performance of future geostationary communications satellites. Launch insurance, launch costs, and the economics of APOs are examined. Retrieval missions and various Space Station scenarios are addressed. The potential benefits of the new APOs to the commercial communications satellite system operator are quantified.

C.D.

A88-22405*# Wyle Labs., Inc., Huntsville, AL.

EXPERIMENTS TO ENSURE SPACE STATION FIRE SAFETY - A CHALLENGE

W. W. YOUNGBLOOD and K. M. SEISER (Wyle Laboratories, Inc., Huntsville, AL) AIAA, Aerospace Sciences Meeting, 26th, Reno, NV, Jan. 11-14, 1988. 10 p. refs

(Contract NAS3-25067)

(AIAA PAPER 88-0540)

Three experiments have been formulated in order to address prominent fire safety requirements aboard the NASA Space Shuttle; these experiments are to be conducted as part of a Space Station-based Technology Development Mission for the growth phase of Space Station construction and operation. The experiments are: (1) an investigation of the flame-spread rate and combustion-product evolution in the burning of typical spacecraft materials in low gravity; (2) an evaluation of the interaction of fires and candidate fire extinguishers in low gravity; and (3) an investigation of the persistence and propagation of smoldering and deep-seated combustion in low gravity.

O.C.

A88-28583* Air Force Academy, CO.

LOW COST GET-AWAY-SPECIAL (GAS) FURNACE

GLON D. TURNER, FRED A. ANTOON (U.S. Air Force Academy, Colorado Springs, CO), and HENRY C. DEGROH (NASA, Lewis Research Center, Cleveland, OH) IN: Materials processing in the reduced gravity environment of space; Proceedings of the Symposium, Boston, MA, Dec. 1-3, 1986. Pittsburgh, PA, Materials Research Society, 1987, p. 305-311. USAF-supported research.

A simple and inexpensive Space Shuttle experimental apparatus to conduct microgravity melting and solidification is presented. A GAS space furnace was initially developed as a student design project at the USAF Academy and further refined at NASA Lewis. The experiment package consists of a melting chamber, battery power system, temperature data recording systems, and electronic controller. The melting chamber is a thin-walled tube wrapped by heating resistance wire. Thermocouples are used to record the specimen thermal history. Power is supplied by 2-V batteries wired to produce 360 W. The mV output of the thermocouples is amplified, cold-junction compensated, and converted to a frequency which is then recorded on an off-the-shelf cassette tape recorder. A backup data recording system which digitizes the amplified signal and records the data on EEPROMs has also been included. This experimental device demonstrates that basic science research can be kept simple and inexpensive.

Author

A88-52331* National Aeronautics and Space Administration. Lewis Research Center, Cleveland, OH.

TECHNOLOGIES FOR PROTECTION OF THE SPACE STATION POWER SYSTEM SURFACES IN ATOMIC OXYGEN ENVIRONMENT

HENRY K. NAHRA and SHARON K. RUTLEDGE (NASA, Lewis Research Center, Cleveland, OH) IN: Space Congress, 25th, Cocoa Beach, FL, Apr. 26-29, 1988, Proceedings. Cape Canaveral, FL, Canaveral Council of Technical Societies, 1988, p. 5-1 to 5-8. refs

Technologies for protecting Space Station surfaces from degradation caused by atomic oxygen are discussed, stressing protection of the power system surfaces. The Space Station power system is described and research concerning the solar array surfaces and radiator surfaces is examined. The possibility of

13 ASTRODYNAMICS

coating the solar array surfaces with a sputter deposited thin film of silicon oxide containing small concentrations of polytetrafluoroethylene is presented. Hexamethyldisiloxane coating for these surfaces is also considered. For the radiator surfaces, possible coatings include silver teflon thermal coating and zinc orthotitanate. R.B.

13

ASTRODYNAMICS

Includes powered and free-flight trajectories; and orbital and launching dynamics.

A88-10957*# Ford Aerospace and Communications Corp., Palo Alto, CA.

NEW NON-GEOSYNCHRONOUS ORBITS FOR COMMUNICATIONS SATELLITES TO OFF-LOAD DAILY PEAKS IN GEOSTATIONARY TRAFFIC

A. E. TURNER (Ford Aerospace and Communications Corp., Palo Alto, CA) AAS and AIAA, Astrodynamics Specialist Conference, Kalispell, MT, Aug. 10-13, 1987. 26 p.

(Contract NAS3-24891)

(AAS PAPER 87-547)

The potential for satellites in two orbits, the sun-synchronous 12-hour equatorial orbit (STET) and the apogee at constant time-of-day equatorial orbit (ACE), to off-load peaks in the CONUS geostationary communications traffic is discussed. These orbits are found to require maneuvers of smaller magnitudes for insertion than geostationary orbits. Advantages of the ACE orbit over the STET orbit are discussed, including larger satellite mass capability for a given launch vehicle, lower slant ranges, and larger angular separation from the geostationary arc for a nonequatorial ground observer. R.R.

A88-50406*# Illinois Univ., Urbana.

OPTIMAL COOPERATIVE TIME-FIXED IMPULSIVE RENDEZVOUS

KOOROSH MIRFAKHRAIE, BRUCE A. CONWAY, and JOHN E. PRUSSING (Illinois, University, Urbana) IN: AIAA/AAS Astrodynamics Conference, Minneapolis, MN, Aug. 15-17, 1988, Technical Papers. Washington, DC, American Institute of Aeronautics and Astronautics, 1988, p. 469-479. refs

(Contract NAG3-805)

(AIAA PAPER 88-4279)

A method has been developed for determining optimal, i.e., minimum fuel, trajectories for the fixed-time cooperative rendezvous of two spacecraft. The method presently assumes that the vehicles perform a total of three impulsive maneuvers with each vehicle being active, that is, making at least one maneuver. The cost of a feasible 'reference' trajectory is improved by an optimizer which uses an analytical gradient developed using primer vector theory and a new solution for the optimal terminal (rendezvous) maneuver. Results are presented for a large number of cases in which the initial orbits of both vehicles are circular but in which the initial positions of the vehicles and the allotted time for rendezvous are varied. In general, the cost of the cooperative rendezvous is less than that of rendezvous with one vehicle passive. Further improvement in cost may be obtained in the future when additional, i.e., midcourse, impulses are allowed and inserted as indicated for some cases by the primer vector histories which are generated by the program. Author

A88-50435*# Stanford Univ., CA.

LOW THRUST POWER-LIMITED TRANSFER FOR A POLE SQUATTER

J. V. BREAKWELL (Stanford University, CA) and O. M. GOLAN IN: AIAA/AAS Astrodynamics Conference, Minneapolis, MN, Aug. 15-17, 1988, Technical Papers. Washington, DC, American Institute

of Aeronautics and Astronautics, 1988, p. 717-722.

(Contract NAG3-286)

(AIAA PAPER 88-4310)

The problem of minimum fuel transfer in a central gravity field for power-limited low thrust propulsion has been studied by several investigators. Orbital averaging was used by Edelbaum in the co-axial and co-planar cases, and by Marec and Vinh for the general transfer between elliptical orbits. The co-latus rectum transfer, which has a complete analytical solution, can be applied to the Pole Squatter. Typical results for the evolution of the orbit parameters and the variation of the thrust acceleration along the orbit are shown. Author

N88-14110*# Ohio State Univ., Columbus. ElectroScience Lab. ENGINEERING CALCULATIONS FOR THE DELTA S METHOD OF SOLVING THE ORBITAL ALLOTMENT PROBLEM

P. A. KOHNHORST, C. A. LEVIS, and E. K. WALTON Oct. 1987 224 p

(Contract NAG3-159)

(NASA-CR-182372; NAS 1.26:182372; ESL-TR-718688-6) Avail: NTIS HC A10/MF A01 CSCL 22A

The method of calculating single-entry separation requirements for pairs of satellites is extended to include the interference on the top link as well as on the down link. Several heuristic models for analyzing the effects of shaped-beam antenna designs on required satellite separations are introduced and demonstrated with gain contour plots. The calculation of aggregate interference is extended to include the effects of up-link interference. The relationship between the single-entry C/I requirements, used in determining satellite separation constraints for various optimization procedures, and the aggregate C/I values of the resulting solutions is discussed. Author

14

GROUND SUPPORT SYSTEMS AND FACILITIES (SPACE)

Includes launch complexes, research and production facilities; ground support equipment, e.g., mobile transporters; and simulators.

A88-15954*# Rockwell International Corp., Canoga Park, CA.

OPTICAL MEASUREMENTS PERTAINING TO SPACE STATION SOLAR DYNAMIC POWER SYSTEMS

S. HOLLY, T. SPRINGER (Rockwell International Corp., Rocketdyne Div., Canoga Park, CA), and K. S. JEFFERIES (NASA, Lewis Research Center, Cleveland, OH) IAF, International Astronautical Congress, 38th, Brighton, England, Oct. 10-17, 1987. 16 p.

(IAF PAPER 87-229)

The Space Station solar dynamic power system is a hybrid of solar photovoltaic and solar dynamic systems, the latter of which uses a parabolic reflector to collect solar energy. This paper describes analytical results of an off-axis solar illumination on the intensity distribution in arbitrary target planes perpendicular to the axis of a parabolic reflector. Such computational capability would make it possible to predict optical intensity distributions resulting from off-axis angles of incident radiation on such target planes. To validate the computer code, experimental optical measurements were performed on the multifaceted paraboloidal collector at the Solar Dynamic Test Facility at Rocketdyne's Santa Susana Field Laboratory. The experimental data compared reasonably well with the calculated values. I.S.

A88-48038*# Rockwell International Corp., Canoga Park, CA.

AN EXPERT SYSTEM APPROACH TO TURBOPUMP HEALTH MONITORING

JOHN G. PERRY, JAY P. RIECHEL, ARNIE M. NORMAN (Rockwell International Corp., Rocketdyne Div., Canoga Park, CA), and

GEORGE MADSZAR (NASA, Lewis Research Center, Cleveland, OH) AIAA, ASME, SAE, and ASEE, Joint Propulsion Conference and Exhibit, 24th, Boston, MA, July 11-13, 1988. 7 p.
(Contract NAS3-25279)
(AIAA PAPER 88-3117)

A preliminary report is presented on the development of a system for monitoring the High Pressure Oxidizer Turbopump of the SSME. System development will proceed by defining the degradation mechanism of the turbopump, identifying those conventional and advanced sensor measurements that can monitor these mechanisms, and determining the digital processing requirements for these measurements. Once the failures and associated measurements have been defined, an expert system will be developed that can make both diagnostic and prognostic inferences about the condition and performance of the turbopump. Author

A88-52364* National Aeronautics and Space Administration. Lewis Research Center, Cleveland, OH.

GROUND BASED MATERIALS SCIENCE EXPERIMENTS

M. B. MEYER, J. C. JOHNSTON, and T. K. GLASGOW (NASA, Lewis Research Center, Cleveland, OH) IN: Space Congress, 25th, Cocoa Beach, FL, Apr. 26-29, 1988, Proceedings. Cape Canaveral, FL, Canaveral Council of Technical Societies, 1988, p. 10-15 to 10-25.

The facilities at the Microgravity Materials Science Laboratory (MMSL) at the Lewis Research Center, created to offer immediate and low-cost access to ground-based testing facilities for industrial, academic, and government researchers, are described. The equipment in the MMSL falls into three categories: (1) devices which emulate some aspect of low gravitational forces, (2) specialized capabilities for 1-g development and refinement of microgravity experiments, and (3) functional duplicates of flight hardware. Equipment diagrams are included. I.S.

N88-12515*# National Aeronautics and Space Administration. Lewis Research Center, Cleveland, OH.

OPTICAL ALIGNMENT OF CENTAUR'S INERTIAL GUIDANCE SYSTEM

ANDREW L. GORDAN Dec. 1987 108 p
(NASA-TM-88844; E-3226; NAS 1.15:88844) Avail: NTIS HC A06/MF A01 CSCL 14B

During Centaur launch operations the launch azimuth of the inertial platform's U-accelerometer input axis must be accurately established and maintained. This is accomplished by using an optically closed loop system with a long-range autotheodolite whose line of sight was established by a first-order survey. A collimated light beam from the autotheodolite intercepts a reflecting Porro prism mounted on the platform azimuth gimbal. Thus, any deviation of the Porro prism from its predetermined heading is optically detected by the autotheodolite. The error signal produced is used to torque the azimuth gimbal back to its required launch azimuth. The heading of the U-accelerometer input axis is therefore maintained automatically. Previously, the autotheodolite system could not distinguish between vehicle sway and rotational motion of the inertial platform unless at least three prisms were used. One prism was mounted on the inertial platform to maintain azimuth alignment, and two prisms were mounted externally on the vehicle to track sway. For example, the automatic azimuth-laying theodolite (AALT-SV-M2) on the Saturn vehicle used three prisms. The results of testing and modifying the AALT-SV-M2 autotheodolite to simultaneously monitor and maintain alignment of the inertial platform and track the sway of the vehicle from a single Porro prism. Author

N88-21186*# National Aeronautics and Space Administration. Lewis Research Center, Cleveland, OH.

MIXING FUEL PARTICLES FOR SPACE COMBUSTION RESEARCH USING ACOUSTICS

ROBERT J. BURNS, JEROME A. JOHNSON, and ROBERT B. KLIMEK 1988 16 p Presented at the 2nd International Symposium on Experimental Methods for Microgravity Materials Science Research, Phoenix, Ariz., 25-29 Jan. 1988; sponsored by

the Metallurgical Society of AIME

(NASA-TM-100295; E-3943; NAS 1.15:100295; AIME-A88-23)

Avail: NTIS HC A03/MF A01 CSCL 21B

Part of the microgravity science to be conducted aboard the Shuttle (STS) involves combustion using solids, particles, and liquid droplets. The central experimental facts needed for characterization of premixed quiescent particle cloud flames cannot be adequately established by normal gravity studies alone. The experimental results to date of acoustically mixing a prototypical particulate, lycopodium, in a 5 cm diameter by 75 cm long flame tube aboard a Learjet aircraft flying a 20 sec low gravity trajectory are described. Photographic and light detector instrumentation combine to measure and characterize particle cloud uniformity. Author

N88-24659*# National Aeronautics and Space Administration. Lewis Research Center, Cleveland, OH.

EXPERIMENTAL RADIO FREQUENCY LINK FOR KA-BAND COMMUNICATIONS APPLICATIONS

GENE FUJIKAWA, MARTIN J. CONRAY, ALAN L. SAUNDERS, and DALE E. POPE Jun. 1988 16 p
(NASA-TM-100824; E-4012; NAS 1.15:100824) Avail: NTIS HC A03/MF A01 CSCL 17B

An experimental radio frequency link has been demonstrated to provide two-way communication between a remote user ground terminal and a ground-based Ka-band transponder. Bit-error-rate performance and radio frequency characteristics of the communication link were investigated. Author

N88-26385# National Aeronautics and Space Administration. Lewis Research Center, Cleveland, OH.

APPLICATION OF SUPERCONDUCTING TECHNOLOGY TO EARTH-TO-ORBIT ELECTROMAGNETIC LAUNCH SYSTEMS

J. R. HULL (Argonne National Lab., Ill.) and L. M. CARNEY 1988 15 p Presented at the Conference on Superconductivity and Applications, Buffalo, N.Y., 18 Apr. 1988
(Contract W-31109-ENG-38)
(NASA-TM-101134; NAS 1.15:101134; DE88-009955; CONF-880466-1) Avail: NTIS HC A03/MF A01

Benefits may occur by incorporating superconductors, both existing and those currently under development, in one or more parts of a large-scale electromagnetic launch (EML) system that is capable of delivering payloads from the surface of the Earth to space. The use of superconductors for many of the EML components results in lower system losses; consequently, reductions in the size and number of energy storage devices are possible. Applied high-temperature superconductivity may eventually enable novel design concepts for energy distribution and switching. All of these technical improvements have the potential to reduce system complexity and lower payload launch costs. DOE

N88-28942*# National Aeronautics and Space Administration. Lewis Research Center, Cleveland, OH.

LEWIS RESEARCH CENTER SPACE STATION ELECTRIC POWER SYSTEM TEST FACILITIES

ARTHUR G. BIRCHENOUGH and DONALD F. MARTIN 28 Apr. 1988 30 p
(NASA-TM-100924; E-3904; NAS 1.15:100924) Avail: NTIS HC A03/MF A01 CSCL 14B

NASA Lewis Research Center facilities were developed to support testing of the Space Station Electric Power System. The capabilities and plans for these facilities are described. The three facilities which are required in the Phase C/D testing, the Power Systems Facility, the Space Power Facility, and the EPS Simulation Lab, are described in detail. The responsibilities of NASA Lewis and outside groups in conducting tests are also discussed. Author

15 LAUNCH VEHICLES AND SPACE VEHICLES

15

LAUNCH VEHICLES AND SPACE VEHICLES

Includes boosters; operating problems of launch/space vehicle systems; and reusable vehicles.

A88-18631*# Jet Propulsion Lab., California Inst. of Tech., Pasadena.

MODAL TEST/ANALYSIS CORRELATION FOR THE CENTAUR G PRIME LAUNCH VEHICLE

J. CHEN, T. M. ROSE, M. TRUBERT, B. WADA (California Institute of Technology, Jet Propulsion Laboratory, Pasadena), and F. SHAKER (NASA, Lewis Research Center, Cleveland, OH) (Structures, Structural Dynamics and Materials Conference, 27th, San Antonio, TX, May 19-21, 1986, Technical Papers, Part 2, p. 621-633) Journal of Spacecraft and Rockets (ISSN 0022-4650), vol. 24, Sept.-Oct. 1987, p. 423-429. Previously cited in issue 18, p. 2615, Accession no. A86-38943. refs
(Contract NAS7-918)

N88-17715*# National Aeronautics and Space Administration. Lewis Research Center, Cleveland, OH.

SIMULATION TEST BEDS FOR THE SPACE STATION ELECTRICAL POWER SYSTEM

GERALD G. SADLER Mar. 1988 20 p
(NASA-TM-100786; E-3958; NAS 1.15:100786) Avail: NTIS HC A03/MF A01 CSCL 22B

NASA Lewis Research Center and its prime contractor are responsible for developing the electrical power system on the space station. The power system will be controlled by a network of distributed processors. Control software will be verified, validated, and tested in hardware and software test beds. Current plans for the software test bed involve using real time and nonreal time simulations of the power system. This paper will discuss the general simulation objectives and configurations, control architecture, interfaces between simulator and controls, types of tests, and facility configurations. Author

N88-25470*# National Aeronautics and Space Administration. Lewis Research Center, Cleveland, OH.

WEIGHT SAVINGS IN AEROSPACE VEHICLES THROUGH PROPELLANT SCAVENGING

STEVEN J. SCHNEIDER and BRIAN D. REED 1988 25 p
Presented at the 47th Annual Conference on Mass Properties Engineering, Plymouth, Mich., 23-25 May 1988; sponsored by the Society of Allied Weight Engineers, Inc.
(NASA-TM-100900; E-4079; NAS 1.15:100900; SAWE-1818)
Avail: NTIS HC A03/MF A01 CSCL 22B

Vehicle payload benefits of scavenging hydrogen and oxygen propellants are addressed. The approach used is to select a vehicle and a mission and then select a scavenging system for detailed weight analysis. The Shuttle 2 vehicle on a Space Station rendezvous mission was chosen for study. The propellant scavenging system scavenges liquid hydrogen and liquid oxygen from the launch propulsion tankage during orbital maneuvers and stores them in well insulated liquid accumulators for use in a cryogenic auxiliary propulsion system. The fraction of auxiliary propulsion propellant which may be scavenged for propulsive purposes is estimated to be 45.1 percent. The auxiliary propulsion subsystem dry mass, including the proposed scavenging system, an additional 20 percent for secondary structure, an additional 5 percent for electrical service, a 10 percent weight growth margin, and 15.4 percent propellant reserves and residuals is estimated to be 6331 kg. This study shows that the fraction of the on-orbit vehicle mass required by the auxiliary propulsion system of this Shuttle 2 vehicle using this technology is estimated to be 12.0 percent compared to 19.9 percent for a vehicle with an earth-storable bipropellant system. This results in a vehicle with the capability of delivering an additional 7820 kg to the Space Station. Author

N88-29833*# National Aeronautics and Space Administration. Lewis Research Center, Cleveland, OH.

THE EFFECT OF THE NEAR EARTH MICROMETEOROID ENVIRONMENT ON A HIGHLY REFLECTIVE MIRROR SURFACE

MICHAEL J. MIRTICH, HERMAN MARK, and WILLIAM R. KERSLAKE 1988 40 p Presented at the 26th Aerospace Sciences Meeting, Reno, Nev., 11-14 Jan. 1988; sponsored by AIAA
(NASA-TM-101307; E-4233; NAS 1.15:101307) Avail: NTIS HC A03/MF A01 CSCL 22B

A resurgence of interest in placing large solar concentrator solar dynamic systems in space for power generation has brought up again a concern for maintaining the integrity of the optical properties of highly specular reflecting surfaces in the near earth space environment. One of the environmental hazards needing evaluation is the micrometeoroid environment. It has been shown that highly reflective polished metals and thin film coatings degrade when exposed to simulated micrometeoroids in the lab. At NASA-Lewis, a shock tube was used to simulate the phenomenon of micrometeoroid impact by accelerating micron sized particles to hypervelocities. Any changes in the optical properties of surfaces exposed to this impact were then evaluated. The degradation of optical properties of polished metals and thin metallic films after exposure to simulated micrometeoroids was determined as a function of impacting kinetic energy area of the particles. A calibrated sensor was developed to not only detect the micrometeoroid environment, but also to evaluate the degradation of the optical properties of thin aluminum films in space. Results of the simulation are presented and discussed. Author

N88-29835*# General Dynamics Corp., San Diego, CA. **CENTAUR OPERATIONS AT THE SPACE STATION: COST AND TRANSPORTATION ANALYSIS Final Report**

10 Aug. 1988 241 p
(Contract NAS3-24900)
(NASA-CR-182128; NAS 1.26:182128; GDSS-SP-88-006) Avail: NTIS HC A11/MF A01 CSCL 22B

A study was conducted to expand on the results of an initial study entitled Centaur Operations at the Space Station. The previous study developed technology demonstration missions (TDMs) that utilized the Centaur G-prime upper stage to advance OTV technologies required for accommodations and operations at the Space Station. An initial evaluation was performed of the cost to NASA for TDM implementation. Due to the potential for commercial communication satellite operation utilizing the TDM hardware, an evaluation of the Centaur's transportation potential was also performed. Author

16

SPACE TRANSPORTATION

Includes passenger and cargo space transportation, e.g., shuttle operations; and space rescue techniques.

A88-27584*# Ford Aerospace and Communications Corp., Palo Alto, CA.

THE ECONOMICS OF SATELLITE RETRIEVAL

KENT M. PRICE (Ford Aerospace and Communications Corp., Space Systems Div., Palo Alto, CA) and JOEL S. GREENBERG (Princeton Synergetics, Inc., NJ) IN: AIAA International Communication Satellite Systems Conference, 12th, Arlington, VA, Mar. 13-17, 1988, Technical Papers. Washington, DC, American Institute of Aeronautics and Astronautics, 1988, p. 496-510.
(Contract NAS3-24253)
(AIAA PAPER 88-0843)

The economics of space operations with and without the Space Station have been studied in terms of the financial performance of a typical communications-satellite business venture. A stochastic

17 SPACE COMM., SPACECRAFT COMM., COMMAND & TRACKING

Monte-Carlo communications-satellite business model is employed which includes factors such as satellite configuration, random and wearout failures, reliability of launch and space operations, stand-down time resulting from failures, and insurance by operation. Financial performance impacts have been evaluated in terms of the magnitude of investment, net present value, and return on investment. R.R.

N88-12520* # National Aeronautics and Space Administration. Lewis Research Center, Cleveland, OH.

SPACECRAFT FIRE SAFETY

JANICE M. MARGLE, ed. (Pennsylvania State Univ., Abington.) 1987 134 p Workshop held in Cleveland, Ohio, 20-21 Aug. 1986

(NASA-CP-2476; E-3464; NAS 1.55:2476) Avail: NTIS HC A07/MF A01 CSCL 22B

Fire detection, fire standards and testing, fire extinguishment, inerting and atmospheres, fire-related medical science, aircraft fire safety, Space Station safety concerns, microgravity combustion, spacecraft material flammability testing, and metal combustion are among the topics considered.

N88-18612* # National Bureau of Standards, Gaithersburg, MD. Center for Fire Research.

SPACECRAFT FIRE DETECTION AND EXTINGUISHMENT: A BIBLIOGRAPHY Final Report

NORA H. JASON Feb. 1988 64 p

(Contract NASA ORDER C-32000-J)

(NASA-CR-180880; NAS 1.26:180880; NBSIR-88/3712;

PB88-178553) Avail: NTIS HC A04/MF A01 CSCL 22B

Pertinent fire detection and extinguishment references have been identified to further the knowledge of spacecraft fire safety. To broaden the scope of the bibliography, other unusual environments, e.g., aircraft, submarine, ship, have been included. In addition, for a more comprehensive view of the spacecraft fire safety problem, selected subjects are included, e.g., materials flammability, smoke, human behavior. The references will provide the researcher with access to state-of-the-art and historic works. Selected references from the 1960's have been included, but the emphasis is on references published from 1975 to 1987. The references are arranged by very broad categories. Often a paper will cover more than one topic, but for the purposes of this bibliography it will be cited only once. Author

17

SPACE COMM., SPACECRAFT COMM., COMMAND & TRACKING

Includes telemetry; space communications networks; astronavigation and guidance; and radio blackout.

A88-27544* # Communications Satellite Corp., Clarksburg, MD. COST-EFFECTIVE INTERSATELLITE LINK APPLICATIONS TO THE FIXED SATELLITE SERVICES

Y. S. LEE (COMSAT Laboratories, Clarksburg, MD) IN: AIAA International Communication Satellite Systems Conference, 12th, Arlington, VA, Mar. 13-17, 1988, Technical Papers. Washington, DC, American Institute of Aeronautics and Astronautics, 1988, p. 167-173. refs

(Contract NAS3-24884)

(AIAA PAPER 88-0770)

Potential cost-effective applications of intersatellite links (ISLs) to domestic, regional, and global fixed satellite services are presented, addressing traffic forecast and service demands for the year 2001. To determine the cost advantages and other systems benefits of ISLs, selected satellite network architectures were derived for ISL and corresponding non-ISL systems. The cost analysis was performed using payload sizing based on

state-of-the-art ISL technology, both optical and microwave.

Author

A88-35251* National Aeronautics and Space Administration. Lewis Research Center, Cleveland, OH.

OPTICAL TECHNOLOGIES FOR SPACE COMMUNICATION SYSTEMS; PROCEEDINGS OF THE MEETING, LOS ANGELES, CA, JAN. 15, 16, 1987

KUL BHASIN, ED. (NASA, Lewis Research Center, Cleveland, OH) and GERHARD A. KOEPF, ED. (Ball Corp., Ball Aerospace Systems Div., Boulder, CO) Meeting sponsored by SPIE. Bellingham, WA, Society of Photo-Optical Instrumentation Engineers (SPIE Proceedings. Volume 756), 1987, 190 p. For individual items see A88-35252 to A88-35275.

(SPIE-756)

The conference presents papers on optical communications in space, diode laser transmitters, lasercom link transmission characteristics, lasercom systems and technologies, high frequency optical components, and optically controlled phased array antennas. Particular attention is given to a deep space optical communications development program, 0.87-micron CSP diode lasers for spaceborne communications, performance measurements of a diode laser optical communications link with Q = 4 PPM signaling, the optical communications link design for the tracking and data acquisition system, and a cost-performance model for ground-based optical communications receiving telescopes. Other topics include optoelectronic componentry for the direct transmission of microwave signals over optical fiber, applications of monolithic detectors, and optical control considerations for phased array antennas. K.K.

A88-35274* Drexel Univ., Philadelphia, PA.

SYSTEM ARCHITECTURE OF MMIC-BASED LARGE APERTURE ARRAYS FOR SPACE APPLICATIONS

P. R. HERCZFELD, M. KAM (Drexel University, Philadelphia, PA), R. R. KUNATH, K. B. BHASIN (NASA, Lewis Research Center, Cleveland, OH), and NICK LA PRADE (RCA, RCA Astro-Electronics Div., Hightstown, NJ) IN: Optical technologies for space communication systems; Proceedings of the Meeting, Los Angeles, CA, Jan. 15, 16, 1987. Bellingham, WA, Society of Photo-Optical Instrumentation Engineers, 1987, p. 164-172. Research supported by the Commonwealth of Pennsylvania. Previously announced in STAR as N87-20468. refs

The persistent trend to use millimeter-wave frequencies for satellite communications presents the challenge to design large-aperture phased arrays for space applications. These arrays, which comprise 100 to 10,000 elements, are now possible due to the advent of lightwave technology and the availability of monolithic microwave integrated circuits. In this paper, system aspects of optically controlled array design are studied. In particular, two architectures for a 40 GHz array are outlined, and the main system-related issues are examined: power budget, synchronization in frequency and phase, and stochastic effects. Author

N88-19565* # National Aeronautics and Space Administration. Lewis Research Center, Cleveland, OH.

HIGH EFFICIENCY, LONG LIFE TRAVELING WAVE TUBES FOR FUTURE COMMUNICATIONS SATELLITES

JAMES A. DAYTON, JR. 1988 10 p Presented at the 12th International Communication Satellite Systems Conference, Arlington, Va., 13-17 Mar. 1988; sponsored by AIAA Previously announced in IAA as A88-27578

(NASA-TM-100837; E-3935; NAS 1.15:100837) Avail: NTIS HC A02/MF A01 CSCL 09F

Electron beam devices, primarily traveling wave tubes (TWTs), have been used as the power amplifiers in almost all space communications and data transmission systems. Based on the technology that is presently available and the expected success of current research efforts, it is reasonable to predict the development of a new class of microwave TWTs with efficiencies in excess of 60 percent and lifetimes of at least 10 years. Because of this rapid advance of technology, the TWT is expected to remain the dominant device for power amplifiers in space. Author

17 SPACE COMM., SPACECRAFT COMM., COMMAND & TRACKING

N88-22919*# National Aeronautics and Space Administration. Lewis Research Center, Cleveland, OH.

NUMERICAL ARC SEGMENTATION ALGORITHM FOR A RADIO CONFERENCE: A SOFTWARE TOOL FOR COMMUNICATION SATELLITE SYSTEMS PLANNING

W. A. WHYTE, A. O. HEYWARD, D. S. PONCHAK, R. L. SPENCE, and J. E. ZUZEK 1988 16 p Presented at the 12th International Communications Satellite Systems Conference, Arlington, Va., 13-17 Mar. 1988; sponsored by AIAA Previously announced in IAA as A88-27531

(NASA-TM-100789; E-3962; NAS 1.15:100789; AIAA-88-0788)
Avail: NTIS HC A03/MF A01 CSCL 09F

The Numerical Arc Segmentation Algorithm for a Radio Conference (NASARC) provides a method of generating predetermined arc segments for use in the development of an allotment planning procedure to be carried out at the 1988 World Administrative Radio Conference (WARC) on the Use of the Geostationary Satellite Orbit and the Planning of Space Services Utilizing It. Through careful selection of the predetermined arc (PDA) for each administration, flexibility can be increased in terms of choice of system technical characteristics and specific orbit location while reducing the need for coordination among administrations. The NASARC software determines pairwise compatibility between all possible service areas at discrete arc locations. NASARC then exhaustively enumerates groups of administrations whose satellites can be closely located in orbit, and finds the arc segment over which each such compatible group exists. From the set of all possible compatible groupings, groups and their associated arc segments are selected using a heuristic procedure such that a PDA is identified for each administration. Various aspects of the NASARC concept and how the software accomplishes specific features of allotment planning are discussed. Author

N88-22920*# National Aeronautics and Space Administration. Lewis Research Center, Cleveland, OH.

THE BIT-ERROR RATE PERFORMANCE OF A SATELLITE MICROWAVE MATRIX SWITCH

ROBERT J. KERCZEWSKI 1988 14 p Presented at the 12th International Communication Satellite Systems Conference, Arlington, Va., 13-17 Mar. 1988; sponsored by AIAA Previously announced in IAA as A88-27572

(NASA-TM-100285; E-3925; NAS 1.15:100285; AIAA-88-0826)
Avail: NTIS HC A03/MF A01 CSCL 09F

The matrix switch is a critical element of communications satellites using multiple-beam antennas and on-board switching. Two proof-of-concept models of a microwave matrix switch have been developed under NASA-sponsored contracts. These switches have undergone extensive testing at NASA Lewis Research Center to determine their operating characteristics in a system environment. The results of these tests indicate the effect of the matrix switch on the overall system operation. Author

N88-24663*# National Aeronautics and Space Administration. Lewis Research Center, Cleveland, OH.

SERVICE OFFERINGS AND INTERFACES FOR THE ACTS NETWORK OF EARTH STATIONS

THOM A. CONEY 1988 22 p Presented at the 12th International Communication Satellite Systems Conference, Arlington, Va., 13-17 Mar. 1988; sponsored by AIAA
(NASA-TM-100809; E-3989; NAS 1.15:100809) Avail: NTIS HC A03/MF A01 CSCL 09F

The Advanced Communications Satellite (ACTS) is capable of two modes of communication. Mode 1 is a mesh network of Earth stations using baseband-switched, time-division multiple-access (BBS-TDMA) and hopping beams. Mode 2 is a mesh network using satellite-switched, time-division multiple-access (SS-TDMA) and fixed (or hopping) beams. The purpose of this paper is to present the functional requirements and the design of the ACTS Mode 1 Earth station terrestrial interface. Included among the requirements are that: (1) the interface support standard telecommunications service offerings (i.e., voice, video and data at rates ranging from 9.6 kbps to 44 Mbps); (2) the interface

support the unique design characteristics of the ACTS communications systems (e.g., the real time demand assignment of satellite capacity); and (3) the interface support test hardware capable of validating ACTS communications processes. The resulting interface design makes use of an appropriate combination of T1 or T3 multiplexers and a small central office (maximum capacity 56 subscriber lines per unit). Author

18

SPACECRAFT DESIGN, TESTING AND PERFORMANCE

Includes satellites; space platforms; space stations; spacecraft systems and components such as thermal and environmental controls; and attitude controls.

A88-11737*# Alabama Univ., Huntsville.

RECORD CHARGING EVENTS FROM APPLIED TECHNOLOGY SATELLITE 6

R. C. OLSEN (Alabama, University, Huntsville) Journal of Spacecraft and Rockets (ISSN 0022-4650), vol. 24, July-Aug. 1987, p. 362-366. refs

(Contract NAS8-33982; NAG3-620)

Applied Technology Satellite 6 regularly charged to large negative potentials in sunlight and eclipse in the earth's midnight to dawn region. This geosynchronous satellite normally reached potentials of -100 to -1000 V in sunlight, and potentials of -100 to -10,000 V in eclipse. The largest potential recorded in eclipse for this satellite was -19 kV, in an environment characterized by an electron temperature of 18 keV. The most negative potential recorded in sunlight was -2 kV, at local dawn, while immersed in an 11-keV electron population. These are the most negative potentials reported from the geosynchronous orbit to date for eclipse and sunlight, respectively. The magnitudes of these potentials indicate the need for methods of potential control on satellites at these altitudes, particularly those with shadowed insulating surfaces. Author

A88-27553*# Communications Satellite Corp., Clarksburg, MD.

FUTURE SWITCHING SATELLITES

S. JOSEPH CAMPANELLA, BENJAMIN A. PONTANO, and HARVEY CHALMERS (COMSAT Laboratories, Clarksburg, MD) IN: AIAA International Communication Satellite Systems Conference, 12th, Arlington, VA, Mar. 13-17, 1988, Technical Papers. Washington, DC, American Institute of Aeronautics and Astronautics, 1988, p. 264-273.

(Contract NAS3-24886)

(AIAA PAPER 88-0802)

Communications satellites of the future are likely to use much narrower beams in order to increase the uplink G/T and the downlink EIRP so that small earth terminals of the VSAT class can achieve full mesh connectivity. These satellites will need onboard switches to route traffic from originating upbeams to destination downbeams. This paper presents a new approach to accomplishing this rerouting using destination-directed packets that inherently carry the information needed to control the onboard switch connections and to adjust the traffic flow among the beams and the stations. The method also inherently provides channel multiplication and DAMA advantages which result in maximally efficient utilization of the space segment resource. C.D.

A88-27583*# Ford Aerospace and Communications Corp., Palo Alto, CA.

COMMUNICATIONS SATELLITES IN NON-GEOSTATIONARY ORBITS

KENT M. PRICE, WEN DOONG, TUAN Q. NGUYEN, ANDREW E. TURNER, and CHARLES WEYANDT (Ford Aerospace and Communications Corp., Space Systems Div., Palo Alto, CA) IN: AIAA International Communication Satellite Systems Conference,

12th, Arlington, VA, Mar. 13-17, 1988, Technical Papers. Washington, DC, American Institute of Aeronautics and Astronautics, 1988, p. 485-495.
(Contract NAS3-24891)
(AIAA PAPER 88-0842)

The design of a satellite communications system in an orbit lower than GEO is described. Two sun-synchronous orbits which lie in the equatorial plane have been selected: (1) the apogee at constant time-of-day equatorial orbit, a highly eccentric orbit with five revolutions per day, which allows 77-135 percent more satellite mass to be placed in orbit than for GEO; and (2) the sun-synchronous 12-hour equatorial orbit, a circular orbit with two revolutions per day, which allows 23-29 percent more mass. The results of a life cycle economic analysis illustrate that nongeostationary satellite systems could be competitive with geostationary satellite systems. R.R.

A88-31396* National Aeronautics and Space Administration. Lewis Research Center, Cleveland, OH.

STRUCTURAL ASSESSMENT OF A SPACE STATION SOLAR DYNAMIC HEAT RECEIVER THERMAL ENERGY STORAGE CANISTER

M. T. TONG (NASA, Lewis Research Center; Sverdrup Technology, Inc., Cleveland, OH), T. W. KERSLAKE, and R. L. THOMPSON (NASA, Lewis Research Center, Cleveland, OH) IN: AIAA SDM Issues of the International Space Station, Conference, Williamsburg, VA, Apr. 21, 22, 1988, Technical Papers. Washington, DC, American Institute of Aeronautics and Astronautics, 1988, p. 162-172. refs (AIAA PAPER 88-2487)

This paper assesses the structural performance of a Space Station thermal energy storage (TES) canister subject to orbital solar flux variation and engine cold start-up operating conditions. The impact of working fluid temperature and salt-void distribution on the canister structure are assessed. Both analytical and experimental studies were conducted to determine the temperature distribution of the canister. Subsequent finite-element structural analyses of the canister were performed using both analytically and experimentally obtained temperatures. The Arrhenius creep law was incorporated into the procedure, using secondary creep data for the canister material, Haynes-188 alloy. The predicted cyclic creep strain accumulations at the hot spot were used to assess the structural performance of the canister. In addition, the structural performance of the canister based on the analytically-determined temperature was compared with that based on the experimentally-measured temperature data. Author

A88-40013* Naval Postgraduate School, Monterey, CA.

AN UNUSUAL CHARGING EVENT ON ISEE 1

R. C. OLSEN (U.S. Naval Postgraduate School, Monterey, CA) and E. C. WHIPPLE (California, University, La Jolla) Journal of Geophysical Research (ISSN 0148-0227), vol. 93, June 1, 1988, p. 5568-5578. refs
(Contract NAG3-542; NAG3-620)

Electrostatic cleanliness requirements on ISEE 1 were expected to prevent negative charging in sunlight. This has largely been true, but on three occasions, ISEE 1 has been observed to charge to significant negative potentials in sunlight. Data from the two electric field experiments and from the plasma composition experiment on ISEE 1 show that the spacecraft charged to close to -70 V in sunlight at about 0700 UT on March 17, 1978. Data from the electron spectrometer experiment show that there was a potential barrier of some -10 to -20 V about the spacecraft during this event. The potential barrier was effective in turning back emitted photoelectrons to the spacecraft. Potential barriers can be formed by differential charging on the spacecraft or by the presence of excess space charge in the plasma. The shape of the barrier suggests that it is due to the former, even though electrostatic cleanliness specifications imposed on ISEE were intended to eliminate differential charging. Modeling of this event showed that the barrier could not be produced by the presence of space charge but that it was most likely produced by differential charging of the solar arrays. Author

A88-46799* Alabama Univ., Huntsville.

ELECTRON BEAM EXPERIMENTS AT HIGH ALTITUDES

R. C. OLSEN (Alabama, University, Huntsville) and H. A. COHEN (W. J. Schafer Associates, Inc., Arlington, VA) (COSPAR, URSI, and IAGA, Plenary Meeting, 26th, Symposium on Active Experiments, 1st, Toulouse, France, June 30-July 11, 1986) Advances in Space Research (ISSN 0273-1177), vol. 8, no. 1, 1988, p. 161-164. Previously announced in STAR as N87-26946. refs
(Contract NAG3-620)

Experiments with the electron gun on the SCATHA satellite produced evidence of beam-plasma interactions, and heating of the low energy electrons around the satellite. These experiments were conducted near geosynchronous orbit, in the dusk bulge, and plasma sheet, with one short operation in the lobe regions, providing a range of ambient plasma densities. The electron gun was operated at 50 eV, with beam currents of 1, 10, and 100 micro-A. Data from electrostatic analyzers and the DC electric field experiment show that the satellite charged to near the beam energy in sunlight, if the beam current was sufficient. Higher ambient densities required higher beam currents. The electrostatic analyzers showed distribution functions which had peaks, or plateaus, at energies greater than the satellite potential. These measurements indicate heating of the ambient plasma at several Debye lengths from the satellite, with the heated plasma then accelerated into the satellite. It is likely that the ambient plasma is in fact the photoelectron sheath generated by the satellite. Author

A88-47972* Iowa Univ., Iowa City.

GASEOUS ENVIRONMENT OF THE SHUTTLE EARLY IN THE SPACELAB 2 MISSION

JOLENE S. PICKETT, GERALD B. MURPHY, and WILLIAM S. KURTH (Iowa, University, Iowa City) Journal of Spacecraft and Rockets (ISSN 0022-4650), vol. 25, March-Apr. 1988, p. 169-174. refs

(Contract NAG3-449; NAS8-32807)

A cold-cathode ionization gage was flown on Space Shuttle flight STS-51F as part of the Spacelab 2 payload. Neutral pressure data that were taken in the payload bay during the first few hours on orbit are presented. These data show that when the payload bay is oriented such that the atmospheric gases are ramming into it, the pressure rises to a peak of 4×10^{-6} Torr. Pressure is also slightly higher during the sunlit portion of each orbit. Outgassing of the payload bay causes the pressure to be elevated to a few times 10^{-6} Torr early in the mission. In addition, several effects on pressure have been identified that are due to chemical releases. Substantial increases (50-150 percent) are seen during another experiment's gas purge. Orbiter chemical-release effects include: pressure increases of 200 percent up to 7×10^{-6} Torr due to Orbital Maneuvering System burns, minor perturbations in pressure due to vernier thruster firings and little or no increase in pressure due to water dumps. In the case of vernier thruster firings, effects are seen only from down-firing thrusters in the back of the Orbiter, which are probably due to reflection of thruster gases off Orbiter surfaces. Author

A88-53182* General Dynamics Corp., San Diego, CA.

DESIGN, DEVELOPMENT, AND TEST OF SHUTTLE/CENTAUR G-PRIME CRYOGENIC TANKAGE THERMAL PROTECTION SYSTEMS

PETER N. MACNEIL, JAMES E. ENGLAND (General Dynamics Corp., Space Systems Div., San Diego, CA), and RICHARD H. KNOLL (NASA, Lewis Research Center, Cleveland, OH) IN: Advances in cryogenic engineering. Volume 33 - Proceedings of the Cryogenic Engineering Conference, Saint Charles, IL, June 14-18, 1987. New York, Plenum Press, 1988, p. 341-348. refs

The thermal protection systems (TPS) for the Shuttle/Centaur were designed to provide fail-safe thermal protection during prelaunch, launch ascent, and on-orbit operations as well as during potential abort, where the Shuttle and Centaur would return to earth. The TPS selected used a helium-purged polyimide foam beneath three radiation shields for the liquid-hydrogen (LH2) tank and radiation shields only for the liquid-oxygen (LO2) tank. A

18 SPACECRAFT DESIGN, TESTING AND PERFORMANCE

double-walled vacuum bulkhead separated the two tanks. The LH2 tank had one 1.9 cm-thick layer of foam on the forward bulkhead and two layers on the larger-area sidewall. Full scale tests of the flight vehicle in a simulated Shuttle cargo bay gave total prelaunch heating rates of 29.5 and 12.9 kW for the LH2 and LO2 tanks, respectively. Calorimeter tests on a representative sample of the LH2 tank sidewall TPS indicated that the measured unit heating one would rapidly decrease from the prelaunch rate of about 300 W/sq m to a desired rate less than 4 W/sq m once on-orbit.

Author

N88-10084*# National Aeronautics and Space Administration. Lewis Research Center, Cleveland, OH.
SPACECRAFT 2000

Jul. 1986 236 p Workshop held in Cleveland, Ohio, 29-31 Jul. 1986

(NASA-CP-2473; E-3358; NAS 1.55:2473) Avail: NTIS HC A11/MF A01 CSCL 22B

The objective of the Workshop was to focus on the key technology area for 21st century spacecraft and the programs needed to facilitate technology development and validation. Topics addressed include: spacecraft systems; system development; structures and materials; thermal control; electrical power; telemetry, tracking, and control; data management; propulsion; and attitude control.

N88-10085*# National Aeronautics and Space Administration. Lewis Research Center, Cleveland, OH.

SPACECRAFT 2000 PROGRAM OVERVIEW

ROBERT W. BERCAW *In its Spacecraft 2000* p 1-6 Jul. 1986
Avail: NTIS HC A11/MF A01 CSCL 22B

The goals are to identify the critical need and technologies for spacecraft of the 21st century, and to recommend technology development and validation programs and possible government/industrial roles and partnerships. The objectives of the workshop are to increase awareness and exchange ideas among participants, highlight the spacecraft as a focal point for technology, and facilitate industry-government coordination. B.G.

N88-10092*# National Aeronautics and Space Administration. Lewis Research Center, Cleveland, OH.

SYSTEM DEVELOPMENT WORKING GROUP REPORT

WILLIAM L. SMITH (TRW Space Technology Labs., Redondo Beach, Calif.) and WILLIAM J. BIFANO *In its Spacecraft 2000* p 109-116 Jul. 1986

Avail: NTIS HC A11/MF A01 CSCL 22B

The critical need is the need for funding and testing as bridging support for highly leveraged technology of Spacecraft 2000 to promote flight development introduction and acceptance. Critical needs are foreseen to augment these capabilities to satisfy specific enabling technology validation and to flight qualify selected technologies. Recommendations are summarized. This presentation is represented by figures. B.G.

N88-10095*# National Aeronautics and Space Administration. Lewis Research Center, Cleveland, OH.

ELECTRICAL POWER WORKING GROUP REPORT

GERRIT VANOMMERING (Ford Aerospace and Communications Corp., Palo Alto, Calif.) and IRA T. MYERS *In its Spacecraft 2000* p 149-163 Jul. 1986

Avail: NTIS HC A11/MF A01 CSCL 22B

The status of and need for power technologies for Spacecraft 2000 were assessed and development programs required to establish an achievable and competitive technology base for spacecraft of the 21st century were identified. The results are summarized, including the recommendations and the underlying rationale. B.G.

N88-10100*# National Aeronautics and Space Administration. Lewis Research Center, Cleveland, OH.

SPACE STATION ASSEMBLY/SERVICING CAPABILITIES

JOSEPH JOYCE *In its Spacecraft 2000* p 77-84 Jul. 1986
Avail: NTIS HC A11/MF A01 CSCL 22B

The aim is to place a permanently manned space station on-orbit around the Earth, which is international in scope. The program is nearing the close of the system definition and preliminary design phase. The first shuttle launch for space station assembly on-orbit is estimated for January 1993. Topics perceived to be important to on-orbit assembly and servicing are discussed. This presentation is represented by charts. B.G.

N88-16794*# Ford Aerospace and Communications Corp., Palo Alto, CA. Space Systems Div.

COMMUNICATIONS SATELLITE SYSTEMS OPERATIONS WITH THE SPACE STATION. VOLUME 3: SUPPLEMENTARY TECHNICAL REPORT Final Report, Feb. - Dec. 1987

K. M. PRICE, P. RUSSELL, and C. WEYANDT Feb. 1988 221 p

(Contract NAS3-24253)

(NASA-CR-180875; NAS 1.26:180875) Avail: NTIS HC A10/MF A01 CSCL 22B

The NASA space station has the potential to provide significant economic benefits to commercial communications satellite operators. The initial reports quantified the benefits of space-based activities and assessed the impacts on the satellite design and the space station. Results are given for the following additional tasks: quantify the value of satellite retrievability operations and define its operational aspects; evaluate the use of expendable launch vehicles for transportation of satellites from the Earth to the space station; and quantify the economic value of modular satellites that are assembled and serviced in space. Author

N88-17728*# National Aeronautics and Space Administration. Lewis Research Center, Cleveland, OH.

MAGNETIC EMISSIONS TESTING OF THE SPACE STATION ENGINEERING MODEL RESISTOJET

DANIEL BRIEHL Feb. 1988 11 p

(NASA-TM-100788; E-3961; NAS 1.15:100788) Avail: NTIS HC A03/MF A01 CSCL 22B

The engineering model resistojets intended for altitude maintenance onboard the space station was tested for magnetic radiation emissions in the Radio Frequency Interference (RFI) facility at the Goddard Space Flight Center. The resistojets heater was supplied with power at 20 kHz and low voltage through a power controller. The resistojets was isolated from its power supply in the RFI enclosure, and the magnetic emission measured at three locations around the resistojets at various heater currents. At a heater current of 18.5 A the maximum magnetic emission was 61 dBpt at a distance of 1 m from the resistojets and at a location at the rear of the thruster. Calculations indicate that the case and heat shields provided a minimum of 4 dB of attenuation at a current of 18.5 A. Maximum radiation was measured at the rear of the resistojets along its major axis and was thought to be due to the magnetic radiation from the power leads. At a distance of 37 cm from the resistojets the maximum magnetic radiation measured was 73 dBpt at a current of 11.2 A. The power input leads were also a source of magnetic radiation. The engineering model resistojets requires about 20 dB of additional shielding. Author

N88-20353*# Wyle Labs., Inc., Huntsville, AL.

SPACECRAFT FIRE-SAFETY EXPERIMENTS FOR SPACE STATION: TECHNOLOGY DEVELOPMENT MISSION Final Contractor Report

WALLACE W. YOUNGBLOOD Apr. 1988 111 p

(Contract NAS3-25067)

(NASA-CR-182114; NAS 1.26:182114; WYLE-68300-1) Avail: NTIS HC A06/MF A01 CSCL 22B

Three concept designs for low-gravity, fire-safety related experiments are presented, as selected for the purpose of addressing key issues of enhancing safety and yet encouraging access to long-duration, manned spacecraft such as the NASA space station. The selected low-gravity experiments are the following: (1) an investigation of the flame-spread rate and combustion-product evolution of the burning of typical thicknesses of spacecraft materials in very low-speed flows; (2) an evaluation

of the interaction of fires and candidate extinguishers in various fire scenarios; and (3) an investigation of the persistence and propagation of smoldering and deep-seated combustion. Each experiment is expected to provide fundamental combustion-science data, as well as the fire-safety applications, and each requires the unique long-duration, low-gravity environment of the space station. Two generic test facilities, i.e., the Combustion Tunnel Facility and the Combustion Facility, are proposed for space station accommodation to support the selected experiments. In addition, three near-term, fire-safety related experiments are described along with other related precursor activities. Author

N88-21243* Hughes Research Labs., Malibu, CA.
SPACECRAFT DIELECTRIC SURFACE CHARGING PROPERTY DETERMINATION Final Report, Sep. 1980 - Nov. 1981
 W. S. WILLIAMSON Oct. 1987 84 p
 (Contract NAS3-22540)
 (NASA-CR-180879; NAS 1.26:180879) Avail: NTIS HC A05/MF A01 CSCL 22B

The charging properties of 127 micron thick polyimide, (a commonly used spacecraft dielectric material) was measured under conditions of irradiation by a low-current-density electron beam with energy between 2 and 14 keV. The observed charging characteristics were consistent with predictions of the NASCAP computer model. The use of low electron current density results in a nonlinearity in the sample-potential versus beam-energy characteristic which is attributed to conduction leakage through the sample. Microdischarges were present at relatively low beam energies. Author

N88-21245* National Aeronautics and Space Administration. Lewis Research Center, Cleveland, OH.
SPACE STATION POWER SYSTEM REQUIREMENTS
 JOHN W. DUNNING, JR. 1988 11 p Proposed for presentation at the 23rd Intersociety Energy Conversion Engineering Conference, Denver, Colo., 31 Jul. - 5 Aug. 1988; sponsored by ASME, AIAA, ANS, SAE, IEEE, ASC and AIChE
 (NASA-TM-100886; E-4119; NAS 1.15:100886) Avail: NTIS HC A03/MF A01 CSCL 22B

Presented is an overview of the requirements on which the Space Station Electric Power System is based as well as a summary of the design itself. The current design, which is based on silicon photovoltaic arrays, NiH₂ batteries, and 20 kHz distribution technology, meets all of the requirements. Author

N88-25473* General Dynamics/Astronautics, San Diego, CA. Space Systems Div.
CENTAUR OPERATIONS AT THE SPACE STATION Final Report, Sep. 1986 - Feb. 1987
 J. PORTER, W. THOMPSON, F. BENNETT, and J. HOLDRIDGE
 15 Feb. 1987 155 p
 (Contract NAS3-24900)
 (NASA-CR-179593; NAS 1.26:179593; GDSS-SP-87-003) Avail: NTIS HC A08/MF A01 CSCL 22B

A study was conducted on the feasibility of using a Centaur vehicle as a testbed to demonstrate critical OTV technologies at the Space Station. Two Technology Demonstration Missions (TDMs) were identified: (1) Accommodations, and (2) Operations. The Accommodations TDM contained: (1) berthing, (2) checkout, maintenance and safing, and (3) payload integration missions. The Operations TDM contained: (1) a cryogenic propellant resupply mission, and (2) Centaur deployment activities. A modified Space Station Co-Orbiting Platform (COP) was selected as the optimum refueling and launch node due to safety and operational considerations. After completion of the TDMs, the fueled Centaur would carry out a mission to actually test deployment and help offset TDM costs. From the Station, the Centaur could carry a single payload in excess of 20,000 pounds to geosynchronous orbit or multiple payloads. Author

N88-28082* National Aeronautics and Space Administration. Lewis Research Center, Cleveland, OH.

EXPERIMENTS APPLICATIONS GUIDE: ADVANCED COMMUNICATIONS TECHNOLOGY SATELLITE (ACTS)

Jul. 1988 42 p
 (NASA-TM-100265; ACT-101; NAS 1.15:100265) Avail: NTIS HC A03/MF A01 CSCL 22B

This applications guide first surveys the capabilities of the Advanced Communication Technology Satellite (ACTS) system (both the flight and ground segments). This overview is followed by a description of the baseband processor (BBP) and microwave switch matrix (MSM) operating modes. Terminals operating with the baseband processor are referred to as low burst rate (LBR); and those operating with the microwave switch matrix, as high burst rate (HBR). Three very small-aperture terminals (VSATs), LBR-1, LBR-2, and HBR, are described for various ACTS operating modes. Also described is the NASA Lewis link evaluation terminal. A section on ACTS experiment opportunities introduces a wide spectrum of network control, telecommunications, system, and scientific experiments. The performance of the VSATs is discussed in detail. This guide is intended as a catalyst to encourage participation by the telecommunications, business, and science communities in a broad spectrum of experiments. Author

N88-28959* National Aeronautics and Space Administration. Lewis Research Center, Cleveland, OH.

ASSESSMENT OF THE EFFECTS OF SPACE DEBRIS AND METEOROIDS ENVIRONMENT ON THE SPACE STATION SOLAR ARRAY ASSEMBLY

HENRY K. NAHRA Sep. 1988 11 p Presented at the 20th Photovoltaic Specialists Conference, Las Vegas, Nev., 26-30 Sep. 1988; sponsored in part by IEEE
 (NASA-TM-101315; E-4310; NAS 1.15:101315) Avail: NTIS HC A03/MF A01 CSCL 22B

The methodology used to assess the probability of no impact of space debris and meteoroids on a spacecraft structure is applied to the Space Station solar array assembly. Starting with the space debris and meteoroids flux models, the projected surface area of the solar cell string circuit of the solar array panel and the mast longeron, and the design lifetime, the possibility of no impact on the solar array mast and solar cell string circuits was determined as a function of particle size. The probability of no impact on the cell string circuits was used to derive the probability of no open circuit panel. The probability of meeting a certain power requirement at the end of the design lifetime was then calculated as a function of impacting particle size. Coupled with a penetration and damage models/correlations which relate the particle size to the penetration depth and damage, the results of this analysis can be used to determine the probability of meeting the lower power requirement given a degree of redundancy, and the probability of no impact on the solar array mast. Author

N88-29845* National Aeronautics and Space Administration. Lewis Research Center, Cleveland, OH.

TECHNOLOGY REQUIREMENTS FOR AN ORBITING FUEL DEPOT: A NECESSARY ELEMENT OF A SPACE INFRASTRUCTURE

R. M. STUBBS, R. R. CORBAN, and A. J. WILLOUGHBY (Analex Corp., Cleveland, Ohio.) 1988 10 p Presented at the 39th Annual Astronautical Congress of the International Astronautical Federation, Bangalore, India, 8-15 Oct. 1988
 (NASA-TM-101370; E-4414; NAS 1.15:101370) Avail: NTIS HC A02/MF A01 CSCL 22B

Advanced planning within NASA has identified several bold space exploration initiatives. The successful implementation of these missions will require a supporting space infrastructure which would include a fuel depot, an orbiting facility to store, transfer and process large quantities of cryogenic fluids. In order to adequately plan the technology development programs required to enable the construction and operation of a fuel depot, a multidisciplinary workshop was convened to assess critical technologies and their state of maturity. Since technology requirements depend strongly on the depot design assumptions,

20 SPACECRAFT PROPULSION AND POWER

several depot concepts are presented with their effect on criticality ratings. Over 70 depot-related technology areas are addressed.

Author

20

SPACECRAFT PROPULSION AND POWER

Includes main propulsion systems and components, e.g., rocket engines; and spacecraft auxiliary power sources.

A88-11038*# National Aeronautics and Space Administration. Lewis Research Center, Cleveland, OH.

REAL GAS PROPERTIES AND SPACE SHUTTLE MAIN ENGINE FUEL TURBINE PERFORMANCE PREDICTION

G. J. HARLOFF (NASA, Lewis Research Center; Sverdrup Technology, Inc., Cleveland, OH) ASME, International Gas Turbine Conference and Exhibition, 32nd, Anaheim, CA, May 31-June 4, 1987. 12 p. refs

(Contract NAS3-24105)

(ASME PAPER 87-GT-106)

The H₂/H₂O mixture thermodynamic and transport properties variations for the Space Shuttle Main Engine (SSME) fuel turbine over a range of temperatures and pressures are examined. The variation of molecular viscosity, specific heat at constant pressure, and Prandtl number for the hydrogen/steam mixture are fitted using polynomial relationships for future turbine performance use. The mixture property variations are calculated using GASP and WASP computer programs. The air equivalent performance of the SSME fuel turbine is computed. I.F.

A88-11738*# System Science and Software, San Diego, CA. **THRESHOLD-DETERMINING MECHANISMS FOR DISCHARGES IN HIGH-VOLTAGE SOLAR ARRAYS**

D. E. PARKS, G. A. JONGEWARD, I. KATZ, and V. A. DAVIS (Systems Science and Software, La Jolla, CA) Journal of Spacecraft and Rockets (ISSN 0022-4650), vol. 24, July-Aug. 1987, p. 367-371. Previously cited in issue 07, p. 863, Accession no. A86-19834. refs

(Contract NAS3-23881)

A88-11782*# National Aeronautics and Space Administration. Lewis Research Center, Cleveland, OH.

SPACE STATION ELECTRIC POWER SYSTEM REQUIREMENTS AND DESIGN

FRED TEREN (NASA, Lewis Research Center, Cleveland, OH) IN: IECEC '87; Proceedings of the Twenty-second Intersociety Energy Conversion Engineering Conference, Philadelphia, PA, Aug. 10-14, 1987. Volume 1. New York, American Institute of Aeronautics and Astronautics, 1987, p. 39-47. Previously announced in STAR as N87-22001.

An overview of the conceptual definition and design of the Space Station Electric Power System (EPS) is given. Responsibilities for the design and development of the EPS are defined. The EPS requirements are listed and discussed, including average and peak power requirements, contingency requirements, and fault tolerance. The most significant Phase B trade study results are summarized, and the design selections and rationale are given. Finally, the power management and distribution system architecture is presented. Author

A88-11785*# National Aeronautics and Space Administration. Lewis Research Center, Cleveland, OH.

RECENT DEVELOPMENTS IN INDIUM PHOSPHIDE SPACE SOLAR CELL RESEARCH

DAVID J. BRINKER and IRVING WEINBERG (NASA, Lewis Research Center, Cleveland, OH) IN: IECEC '87; Proceedings of the Twenty-second Intersociety Energy Conversion Engineering Conference, Philadelphia, PA, Aug. 10-14, 1987. Volume 1. New

York, American Institute of Aeronautics and Astronautics, 1987, p. 58-63. Previously announced in STAR as N87-26141. refs

Recent developments and progress in indium phosphide solar cell research for space application are reviewed. Indium phosphide homojunction cells were fabricated in both the n + p and p + n configurations with total area efficiencies of 17.9 and 15.9 percent (air mass 0 and 25 C) respectively. Organometallic chemical vapor deposition, liquid phase epitaxy, ion implantation and diffusion techniques were employed in InP cell fabrication. A theoretical model of a radiation tolerant, high efficiency homojunction cell was developed. A realistically attainable AM0 efficiency of 20.5 percent was calculated using this model with emitter and base doping of 6 x 10 to the 17th power and 5 x 10 to the 16th power/cm, respectively. Cells of both configurations were irradiated with 1 MeV electrons and 37 MeV protons. For both proton and electron irradiation, the n + p cells are more radiation resistant at higher fluences than the p + n cells. The first flight module of four InP cells was assembled for the Living Plume Shield III satellite. Author

A88-11794*# Sundstrand Corp., Rockford, IL.

TOLUENE STABILITY SPACE STATION RANKINE POWER SYSTEM

V. N. HAVENS, D. R. RAGALLER, L. SIBERT (Sundstrand Corp., Rockford, IL), and D. MILLER (NASA, Lewis Research Center, Cleveland, OH) IN: IECEC '87; Proceedings of the Twenty-second Intersociety Energy Conversion Engineering Conference, Philadelphia, PA, Aug. 10-14, 1987. Volume 1. New York, American Institute of Aeronautics and Astronautics, 1987, p. 121-126. refs

A dynamic test loop is designed to evaluate the thermal stability of an organic Rankine cycle working fluid, toluene, for potential application to the Space Station power conversion unit. Samples of the noncondensable gases and the liquid toluene were taken periodically during the 3410 hour test at 750 F peak temperature. The results obtained from the toluene stability loop verify that toluene degradation will not lead to a loss of performance over the 30-year Space Station mission life requirement. The identity of the degradation products and the low rates of formation were as expected from toluene capsule test data. Author

A88-11798*# Rockwell International Corp., Canoga Park, CA.

ADVANCED SPACE SOLAR DYNAMIC POWER SYSTEMS BEYOND IOC SPACE STATION

WAYNE E. WALLIN (Rockwell International Corp., Rocketdyne Div., Canoga Park, CA) and MILES O. DUSTIN (NASA, Lewis Research Center, Cleveland, OH) IN: IECEC '87; Proceedings of the Twenty-second Intersociety Energy Conversion Engineering Conference, Philadelphia, PA, Aug. 10-14, 1987. Volume 1. New York, American Institute of Aeronautics and Astronautics, 1987, p. 145-155. refs

(Contract NAS3-24864)

Three different solar dynamic power cycle systems were evaluated for application to missions projected beyond the IOC Space Station. All three systems were found to be superior to two photovoltaic systems (a planar silicon array and a GaAs concentrator array), with both lower weight and area. The alkali-metal Rankine cycle was eliminated from consideration due to low performance, and the Stirling cycle was found to be superior to the closed Brayton cycle in both weight and area. LiF salt, which establishes peak cycle temperatures for both of the considered cycles at about 1090 K, was shown to be the most suitable material for Thermal Energy Storage. R.R.

A88-11799*# National Aeronautics and Space Administration. Lewis Research Center, Cleveland, OH.

SOLAR CONCENTRATOR ADVANCED DEVELOPMENT PROJECT

ROBERT D. CORRIGAN (NASA, Lewis Research Center, Cleveland, OH) and DERIK T. EHRESMAN (Harris Corp., Melbourne, FL) IN: IECEC '87; Proceedings of the Twenty-second Intersociety Energy Conversion Engineering Conference, Philadelphia, PA, Aug. 10-14, 1987. Volume 1. New York, American Institute of Aeronautics and Astronautics, 1987, p. 156-161.

A solar dynamic concentrator design developed for use with a solar-thermodynamic power generation module intended for the Space Station is considered. The truss hexagonal panel reflector uses a modular design approach and is flexible in attainable flux profiles and assembly techniques. Preliminary structural, thermal, and optical analysis results are discussed. Accuracy of the surface reflectors should be within 5 mrad rms slope error, resulting in the need for close fabrication tolerances. Significant fabrication issues to be addressed include the facet reflective and protective coating processes and the surface specularity requirements.

R.R.

A88-11800* # Sanders Associates, Inc., Nashua, NH.

ADVANCED SOLAR RECEIVER CONCEPTUAL DESIGN STUDY
J. B. KESSELI (Sanders Associates, Inc., Nashua, NH) and D. E. LACY (NASA, Lewis Research Center, Cleveland, OH) IN: IECEC '87; Proceedings of the Twenty-second Intersociety Energy Conversion Engineering Conference, Philadelphia, PA, Aug. 10-14, 1987. Volume 1. New York, American Institute of Aeronautics and Astronautics, 1987, p. 162-168. refs

High temperature solar dynamic Brayton and Stirling receivers are investigated as candidate electrical power generating systems for future LEO missions. These receivers are smaller and more efficient than conventional receivers, and they offer less structural complexity and fewer thermal stress problems. Use of the advanced Direct Absorption Storage Receiver allows many of the problems associated with working with high-volumetric-change phase-change materials to be avoided. A specific mass reduction of about 1/3 with respect to the baseline receiver has been realized.

R.R.

A88-11805* # National Aeronautics and Space Administration. Lewis Research Center, Cleveland, OH.

IMPACT OF THERMAL ENERGY STORAGE PROPERTIES ON SOLAR DYNAMIC SPACE POWER CONVERSION SYSTEM MASS

ALBERT J. JUHASZ, CAROLYN E. COLES-HAMILTON, and DOVIE E. LACY (NASA, Lewis Research Center, Cleveland, OH) IN: IECEC '87; Proceedings of the Twenty-second Intersociety Energy Conversion Engineering Conference, Philadelphia, PA, Aug. 10-14, 1987. Volume 1. New York, American Institute of Aeronautics and Astronautics, 1987, p. 202-207. Previously announced in STAR as N87-22802.

A 16 parameter solar concentrator/heat receiver mass model is used in conjunction with Stirling and Brayton Power Conversion System (PCS) performance and mass computer codes to determine the effect of thermal energy storage (TES) material property changes on overall PCS mass as a function of steady state electrical power output. Included in the PCS mass model are component masses as a function of thermal power for: concentrator, heat receiver, heat exchangers (source unless integral with heat receiver, heat sink, regenerator), heat engine units with optional parallel redundancy, power conditioning and control (PC and C), PC and C radiator, main radiator, and structure. Critical TES properties are: melting temperature, heat of fusion, density of the liquid phase, and the ratio of solid-to-liquid density. Preliminary results indicate that even though overall system efficiency increases with TES melting temperature up to 1400 K for concentrator surface accuracies of 1 mrad or better, reductions in the overall system mass beyond that achievable with lithium fluoride (LiF) can be accomplished only if the heat of fusion is at least 800 kJ/kg and the liquid density is comparable to that of LiF (1800 kg/cu m).

Author

A88-11812* # National Aeronautics and Space Administration. Lewis Research Center, Cleveland, OH.

DEVELOPMENT OF AN ADVANCED PHOTOVOLTAIC CONCENTRATOR SYSTEM FOR SPACE APPLICATIONS

MICHAEL F. PISZCZOR, JR. (NASA, Lewis Research Center, Cleveland, OH) and MARK J. O'NEILL (ENTECH, Inc., Dallas, TX) IN: IECEC '87; Proceedings of the Twenty-second Intersociety Energy Conversion Engineering Conference, Philadelphia, PA, Aug. 10-14, 1987. Volume 1. New York, American Institute of Aeronautics

and Astronautics, 1987, p. 248-253. Previously announced in STAR as N87-24531. refs

Recent studies indicate that significant increases in system performance (increased efficiency and reduced system mass) are possible for high power space based systems by incorporating technological developments with photovoltaic power systems. The Advanced Photovoltaic Concentrator Program is an effort to take advantage of recent advancements in refractive optical elements. By using a domed Fresnel lens concentrator and a prismatic cell cover, to eliminate metallization losses, dramatic reductions in the required area and mass over current space photovoltaic systems are possible. The advanced concentrator concept also has significant advantages when compared to solar dynamic Organic Rankine Cycle power systems in Low Earth Orbit applications where energy storage is required. The program is currently involved in the selection of a material for the optical element that will survive the space environment and a demonstration of the system performance of the panel design.

Author

A88-11823* # Toledo Univ., OH.

A STUDY OF SCHWARZ CONVERTERS FOR NUCLEAR POWERED SPACECRAFT

THOMAS A. STUART (Toledo, University, OH) and GENE E. SCHWARZE (NASA, Lewis Research Center, Cleveland, OH) IN: IECEC '87; Proceedings of the Twenty-second Intersociety Energy Conversion Engineering Conference, Philadelphia, PA, Aug. 10-14, 1987. Volume 1. New York, American Institute of Aeronautics and Astronautics, 1987, p. 313-320. Previously announced in STAR as N87-23903. refs

(Contract NAG3-708)

High power space systems which use low dc voltage, high current sources such as thermoelectric generators, will most likely require high voltage conversion for transmission purposes. This study considers the use of the Schwarz resonant converter for use as the basic building block to accomplish this low-to-high voltage conversion for either a dc or an ac spacecraft bus. The Schwarz converter has the important assets of both inherent fault tolerance and resonant operation; parallel operation in modular form is possible. A regulated dc spacecraft bus requires only a single stage converter while a constant frequency ac bus requires a cascaded Schwarz converter configuration. If the power system requires constant output power from the dc generator, then a second converter is required to route unneeded power to a ballast load.

Author

A88-11827* # Virginia Polytechnic Inst. and State Univ., Blacksburg.

COMPUTER MODELING AND SIMULATION OF A 20KHZ AC DISTRIBUTION SYSTEM FOR SPACE STATION

FU-SHENG TSAI and FRED C. LEE (Virginia Polytechnic Institute and State University, Blacksburg) IN: IECEC '87; Proceedings of the Twenty-second Intersociety Energy Conversion Engineering Conference, Philadelphia, PA, Aug. 10-14, 1987. Volume 1. New York, American Institute of Aeronautics and Astronautics, 1987, p. 338-344. refs

(Contract NAG3-551)

A computer model of a 20 kHz, ac distribution testbed for Space Station is presented. The system consists of six resonant inverters, a one-hundred-meter transmission line, and three load receivers: a dc receiver, a bidirectional receiver, and an ac receiver. A model library is generated characterizing all system components. The system's local and global behaviors are investigated using the EASY5 dynamic analysis program.

Author

A88-11829* # General Dynamics Corp., San Diego, CA.
CONTROL CONSIDERATIONS FOR HIGH FREQUENCY, RESONANT, POWER PROCESSING EQUIPMENT USED IN LARGE SYSTEMS

J. W. MILDICE, K. E. SCHREINER (General Dynamics Corp., Space Systems Div., San Diego, CA), and F. WOLFF (NASA, Lewis Research Center, Cleveland, OH) IN: IECEC '87; Proceedings of the Twenty-second Intersociety Energy Conversion Engineering

20 SPACECRAFT PROPULSION AND POWER

Conference, Philadelphia, PA, Aug. 10-14, 1987. Volume 1. New York, American Institute of Aeronautics and Astronautics, 1987, p. 350-355. Previously announced in STAR as N87-23690.

Addressed is a class of resonant power processing equipment designed to be used in an integrated high frequency (20 KHz domain), utility power system for large, multi-user spacecraft and other aerospace vehicles. It describes a hardware approach, which has been the basis for parametric and physical data used to justify the selection of high frequency ac as the PMAD baseline for the space station. This paper is part of a larger effort undertaken by NASA and General Dynamics to be sure that all potential space station contractors and other aerospace power system designers understand and can comfortably use this technology, which is now widely used in the commercial sector. In this paper, we will examine control requirements, stability, and operational modes; and their hardware impacts from an integrated system point of view. The current space station PMAD system will provide the overall requirements model to develop an understanding of the performance of this type of system with regard to: (1) regulation; (2) power bus stability and voltage control; (3) source impedance; (4) transient response; (5) power factor effects; and (6) limits and overloads. Author

A88-11830*# National Aeronautics and Space Administration. Lewis Research Center, Cleveland, OH.

EMC AND POWER QUALITY STANDARDS FOR 20-KHZ POWER DISTRIBUTION

IRVING G. HANSEN (NASA, Lewis Research Center, Cleveland, OH) IN: IECEC '87; Proceedings of the Twenty-second Intersociety Energy Conversion Engineering Conference, Philadelphia, PA, Aug. 10-14, 1987. Volume 1. New York, American Institute of Aeronautics and Astronautics, 1987, p. 356-359. Previously announced in STAR as N87-22004.

The Space Station Power Distribution System has been baselined as a sinusoidal single phase, 440 VRMS system. This system has certain unique characteristics directly affecting its application. In particular, existing systematic description and control documents were modified to reflect the high operating frequency. This paper will discuss amendments made on Mil STD 704 (Electrical Power Characteristics), and Mil STD 461-B (Electromagnetic Emission and Susceptibility Requirements for the Control of Electromagnetic Interference). In some cases these amendments reflect changes of several orders of magnitude. Implications and impacts of these changes are discussed. Author

A88-11846*# National Aeronautics and Space Administration. Lewis Research Center, Cleveland, OH.

SP-100 ADVANCED TECHNOLOGY PROGRAM

RONALD J. SOVIE (NASA, Lewis Research Center, Cleveland, OH) IN: IECEC '87; Proceedings of the Twenty-second Intersociety Energy Conversion Engineering Conference, Philadelphia, PA, Aug. 10-14, 1987. Volume 1. New York, American Institute of Aeronautics and Astronautics, 1987, p. 449-456. Previously announced in STAR as N87-23027.

The goal of the triagency SP-100 Program is to develop long-lived, compact, lightweight, survivable nuclear reactor space power systems for application to the power range 50 kWe to 1 MWe. The successful development of these systems should enable or significantly enhance many of the future NASA civil and commercial missions. The NASA SP-100 Advanced Technology Program strongly augments the parallel SP-100 Ground Engineering System Development program and enhances the chances for success of the overall SP-100 program. The purpose of this paper is to discuss the key technical elements of the Advanced Technology Program and the progress made in the initial year and a half of the project. Author

A88-11853*# National Aeronautics and Space Administration. Lewis Research Center, Cleveland, OH.

AN INTEGRATED APPROACH TO SPACE STATION POWER SYSTEM AUTONOMOUS CONTROL

JAMES L. DOLCE (NASA, Lewis Research Center, Cleveland,

OH) IN: IECEC '87; Proceedings of the Twenty-second Intersociety Energy Conversion Engineering Conference, Philadelphia, PA, Aug. 10-14, 1987. Volume 1. New York, American Institute of Aeronautics and Astronautics, 1987, p. 499-508. refs

Space Station electrical power management must be accomplished autonomously in order to decrease both airborne and ground support costs. Attention is presently given to the augmentation of terrestrial utility algorithmic decision aids for power dispatching for space station use, using expert systems to direct power demand analyses and the integration of results into operational decisions. Functions to be thus managed encompass power scheduling, energy allocation, failure cause diagnoses, goal proposal and plan preparation, consequence evaluation, and execution plan selection. The operating states of the system are normal, preventive, emergency, and restorative. O.C.

A88-11861*# National Aeronautics and Space Administration. Lewis Research Center, Cleveland, OH.

LERC POWER SYSTEM AUTONOMY PROGRAM 1990 DEMONSTRATION

KARL A. FAYMON, GALE R. SUNDBERG, ROBERT R. BERCAW (NASA, Lewis Research Center, Cleveland, OH), and DAVID J. WEEKS (NASA, Marshall Space Flight Center, Huntsville, AL) IN: IECEC '87; Proceedings of the Twenty-second Intersociety Energy Conversion Engineering Conference, Philadelphia, PA, Aug. 10-14, 1987. Volume 1. New York, American Institute of Aeronautics and Astronautics, 1987, p. 547-551.

The NASA Lewis Research Center has undertaken a program for the development of space systems automation, with a view to increased reliability, safety, payload capability, and decreased operational costs. The NASA Space Station is a primary area of application for the techniques thus developed. Attention is presently given to the activities associated with the Power Systems Autonomy Demonstration Project, which has a projected demonstration date in 1990 and will integrate knowledge-based systems into a real-time environment. Two coordinated systems under expert system control will be demonstrated. O.C.

A88-11870*# National Aeronautics and Space Administration. Lewis Research Center, Cleveland, OH.

A SYSTEMS ENGINEERING APPROACH TO AUTOMATED FAILURE CAUSE DIAGNOSIS IN SPACE POWER SYSTEMS

JAMES L. DOLCE and KARL A. FAYMON (NASA, Lewis Research Center, Cleveland, OH) IN: IECEC '87; Proceedings of the Twenty-second Intersociety Energy Conversion Engineering Conference, Philadelphia, PA, Aug. 10-14, 1987. Volume 1. New York, American Institute of Aeronautics and Astronautics, 1987, p. 590-600. refs

Automatic failure-cause diagnosis is a key element in autonomous operation of space power systems such as Space Station's. A rule-based diagnostic system has been developed for determining the cause of degraded performance. The knowledge required for such diagnosis is elicited from the system engineering process by using traditional failure analysis techniques. Symptoms, failures, causes, and detector information are represented with structured data; and diagnostic procedural knowledge is represented with rules. Detected symptoms instantiate failure modes and possible causes consistent with currently held beliefs about the likelihood of the cause. A diagnosis concludes with an explanation of the observed symptoms in terms of a chain of possible causes and subcauses. Author

A88-11904*# International Fuel Cells Corp., South Windsor, CT. **REGENERATIVE FUEL CELL STUDY FOR SATELLITES IN GEO ORBIT**

LESLIE VAN DINE, ALEXANDER LEVY (International Fuel Cells Corp., South Windsor, CT), and OLGA GONZALEZ-SANABRIA (NASA, Lewis Research Center, Cleveland, OH) IN: IECEC '87; Proceedings of the Twenty-second Intersociety Energy Conversion Engineering Conference, Philadelphia, PA, Aug. 10-14, 1987. Volume 2. New York, American Institute of Aeronautics and Astronautics, 1987, p. 797-802.

The results of a 12 month study to identify high performance

regenerative hydrogen-oxygen fuel cell concepts for geosynchronous satellite application are summarized. Emphasis was placed on concepts with the potential for high energy density and passive means for water and heat management to maximize system reliability. Both polymer membrane and alkaline electrolyte fuel cells were considered, with emphasis on the alkaline cell because of its high performance, advanced state of development, and proven ability to operate in a launch and space environment. Three alkaline system concepts were studied. Results indicate that using near term technology energy densities between 46 and 52 watt-hour/lb can be achieved at efficiencies of 55 percent. Using advanced light weight cell construction which was achieved in experimental cells, composite tankage material for the reactant gases and the reversible stack concept, system energy densities of 115 watt-hours/lb can be projected. Author

A88-11913*# National Aeronautics and Space Administration. Lewis Research Center, Cleveland, OH.

EFFECT OF COMPONENT COMPRESSION ON THE INITIAL PERFORMANCE OF AN IPV NICKEL-HYDROGEN CELL

RANDALL F. GAHN (NASA, Lewis Research Center, Cleveland, OH) IN: IECEC '87; Proceedings of the Twenty-second Intersociety Energy Conversion Engineering Conference, Philadelphia, PA, Aug. 10-14, 1987. Volume 2. New York, American Institute of Aeronautics and Astronautics, 1987, p. 857-863. Previously announced in STAR as N87-24838.

An experimental method was developed for evaluating the effect of component compression on the charge and discharge voltage characteristics of a 3 1/2 in. diameter boiler plate cell. A standard boiler plate pressure vessel was modified by the addition of a mechanical feedthrough on the bottom of the vessel which permitted different compressions to be applied to the components without disturbing the integrity of the stack. Compression loadings from 0.94 to 27.4 psi were applied by suspending weights from the feedthrough rod. Cell voltages were measured for 0.96-C, 55-min charge and for 1.37-C, 35-min and 2-C, 24-min discharges. An initial change in voltage performance on both charge and discharge as the loading increased was attributed to seating of the components. Subsequent variation of the compression from 2.97 to 27.4 psi caused only minor changes in either the charge or the discharge voltages. Several one month open-circuit voltage stands and 1100 cycles under LEO conditions at the maximum loading have produced no change in performance. Author

A88-11917*# National Aeronautics and Space Administration. Lewis Research Center, Cleveland, OH.

EFFECT OF STORAGE AND LEO CYCLING ON MANUFACTURING TECHNOLOGY IPV NICKEL-HYDROGEN CELLS

JOHN J. SMITHRICK (NASA, Lewis Research Center, Cleveland, OH) IN: IECEC '87; Proceedings of the Twenty-second Intersociety Energy Conversion Engineering Conference, Philadelphia, PA, Aug. 10-14, 1987. Volume 2. New York, American Institute of Aeronautics and Astronautics, 1987, p. 878-881. Previously announced in STAR as N87-22308.

Yardney Manufacturing Technology (MANTECH) 50 A-hr space weight individual pressure vessel nickel-hydrogen cells were evaluated. This consisted of investigating: the effect of storage and charge/discharge cycling on cell performance. For the storage test the cells were precharged with hydrogen, by the manufacturer, to a pressure of 14.5 psia. After undergoing activation and acceptance tests, the cells were discharged at C/10 rate (5A) to 0.1 V or less. The terminals were then shorted. The cells were shipped to NASA Lewis Research Center where they were stored at room temperature in the shorted condition for 1 year. After storage, the acceptance tests were repeated at NASA Lewis. A comparison of test results indicate no significant degradation in electrical performance due to 1 year storage. For the cycle life test the regime was a 90 minute low earth orbit at deep depths of discharge (80 and 60 percent). At the 80 percent DOD the three cells failed on the average at cycle 741. Failure for this test was defined to occur when the cell voltage degraded to 1 V prior

to completion of the 35 min discharge. The DOD was reduced to 60 percent. The cycle life test was continued. Author

A88-11942*# National Aeronautics and Space Administration. Lewis Research Center, Cleveland, OH.

1987 OVERVIEW OF FREE-PISTON STIRLING TECHNOLOGY FOR SPACE POWER APPLICATION

JACK G. SLABY and DONALD L. ALGER (NASA, Lewis Research Center, Cleveland, OH) IN: IECEC '87; Proceedings of the Twenty-second Intersociety Energy Conversion Engineering Conference, Philadelphia, PA, Aug. 10-14, 1987. Volume 3. New York, American Institute of Aeronautics and Astronautics, 1987, p. 1371-1377.

The Lewis Research Center program concerned with the development of a free-piston Stirling engine for space-power applications is examined. The system mass of a Stirling system is compared to that of a Brayton system for the same peak temperature and output power; the advantages of the Stirling system are discussed. The predicted and experimental performances of the 25 kWe opposed-piston space power demonstrator engine are evaluated. It is determined that in order to enhance performance the regenerator needs to be modified, and the gas bearing flow between the displacer and power piston needs to be isolated in order to increase the operating stroke. Identification and correction of the energy losses, the design and operation of the linear alternator, and heat exchange concepts are considered. The design parameters and conceptual design characteristics for a 25 kWe single-cylinder free-piston Stirling space-power converter are described. I.F.

A88-11943*# National Aeronautics and Space Administration. Lewis Research Center, Cleveland, OH.

A COMPARISON OF STIRLING ENGINES FOR USE WITH A 25 KW DISH-ELECTRIC CONVERSION SYSTEM

RICHARD K. SHALTENS (NASA, Lewis Research Center, Cleveland, OH) IN: IECEC '87; Proceedings of the Twenty-second Intersociety Energy Conversion Engineering Conference, Philadelphia, PA, Aug. 10-14, 1987. Volume 3. New York, American Institute of Aeronautics and Astronautics, 1987, p. 1378-1385. refs

Two designs for an advanced Stirling conversion system (ASCS) are described. The objective of the ASCS is to generate about 25 kW of electric power to an electric utility grid at an engine/alternator target cost of \$300.00/kW at the manufacturing rate of 10,000 unit/yr. Both designs contain a free-piston Stirling engine (FPSE), a heat transport system, solar receiver, a means to generate electric power, the necessary auxiliaries, and a control system. The major differences between the two concepts are: one uses a 25 kWe single-piston FPSE which incorporates a linear alternator to directly convert the energy to electricity on the utility grid; and in the second design, electrical power is generated indirectly using a hydraulic output to a ground based hydraulic motor coupled to a rotating alternator. Diagrams of the two designs are presented. I.F.

A88-15958*# National Aeronautics and Space Administration. Lewis Research Center, Cleveland, OH.

SPACE STATION ELECTRICAL POWER SYSTEM

THOMAS L. LABUS and THOMAS H. COCHRAN (NASA, Lewis Research Center, Cleveland, OH) IAF, International Astronautical Congress, 38th, Brighton, England, Oct. 10-17, 1987. 12 p. Previously announced in STAR as N87-26144. (IAF PAPER 87-234)

The purpose of this paper is to describe the design of the Space Station Electrical Power System. This includes the Photovoltaic and Solar Dynamic Power Modules as well as the Power Management and Distribution System (PMAD). In addition, two programmatic options for developing the Electrical Power System will be presented. One approach is defined as the Enhanced Configuration and represents the results of the Phase B studies conducted by the NASA Lewis Research Center over the last two years. Another option, the Phased Program, represents

20 SPACECRAFT PROPULSION AND POWER

a more measured approach to reaching about the same capability as the Enhanced Configuration. Author

A88-15975*# Space Industries, Inc., Webster, TX.
WATER-PROPELLANT RESISTOJETS FOR MAN-TENDED PLATFORMS

ALLEN J. LOUVIERE (Space Industries, Inc., Webster, TX), ROBERT E. JONES, W. EARL MORREN, and JAMES S. SOVEY (NASA, Lewis Research Center, Cleveland, OH) IAF, International Astronautical Congress, 38th, Brighton, England, Oct. 10-17, 1987. 11 p. Previously announced in STAR as N87-26135. refs (IAF PAPER 87-259)

The selection of a propulsion system for a man-tended platform has been influenced by the planned use of resistojets for drag make-up on the manned Space Station. For that application a resistojet has been designed that is capable of operation with a wide variety of propellants, including water. The reasons for the selection of water as the propellant and the performance of water as a propellant are discussed. The man-tended platform and its mission requirements are described. Author

A88-16441* National Aeronautics and Space Administration. Lewis Research Center, Cleveland, OH.

PROBABILISTIC STRUCTURAL ANALYSIS METHODS FOR SPACE PROPULSION SYSTEM COMPONENTS

CHRISTOS C. CHAMIS (NASA, Lewis Research Center, Cleveland, OH) Probabilistic Engineering Mechanics (ISSN 0266-8920), vol. 2, June 1987, p. 100-110. Previously announced in STAR as N87-13794. refs

The development of a three-dimensional inelastic analysis methodology for the Space Shuttle main engine (SSME) structural components is described. The methodology is composed of: (1) composite load spectra, (2) probabilistic structural analysis methods, (3) the probabilistic finite element theory, and (4) probabilistic structural analysis. The methodology has led to significant technical progress in several important aspects of probabilistic structural analysis. The program and accomplishments to date are summarized. Author

A88-18230* Harris Corp., Melbourne, FL.

DEVELOPMENT OF COMPOSITE FACETS FOR THE SURFACE OF A SPACE-BASED SOLAR DYNAMIC CONCENTRATOR

SCHUYLER R. AYERS, DONALD E. MOREL, and JAMES A. SANBORN (Harris Corp., Government Aerospace Systems Div., Melbourne, FL) IN: Advanced composites: The latest developments; Proceedings of the Second Conference, Dearborn, MI, Nov. 18-20, 1986. Metals Park, OH, ASM International, 1986, p. 55-60.

(Contract NAS3-24670)

An account is given of the composite fabrication techniques envisioned for the production of mirror-quality substrates furnishing the specular reflectance required for the NASA Space Station's solar dynamic concentrator energy system. The candidate materials were graphite fiber-reinforced glass, aluminum, and polymer matrices whose surfaces would be coated with thin metal layers and with atomic oxygen degradation-inhibiting protective coatings to obtain the desired mirror surface. Graphite-epoxy mirror substrate samples have been found to perform satisfactorily for the required concentrator lifetime. O.C.

A88-18523* National Aeronautics and Space Administration. Lewis Research Center, Cleveland, OH.

OXIDATION-RESISTANT REFLECTIVE SURFACES FOR SOLAR DYNAMIC POWER GENERATION IN NEAR EARTH ORBIT

DANIEL A. GULINO (NASA, Lewis Research Center, Cleveland, OH), ROBERT A. EGGER (Cleveland State University, OH), and WILLIAM F. BANHOLZER (General Electric Co., Schenectady, NY) Journal of Vacuum Science and Technology A (ISSN 0734-2101), vol. 5, July-Aug. 1987, p. 2737-2741. Previously announced in STAR as N87-10960. refs

Reflective surfaces for Space Station power generation systems are required to withstand the atomic oxygen-dominated

environment of near earth orbit. Thin films of platinum and rhodium, which are corrosion resistant reflective metals, have been deposited by ion beam sputter deposition onto various substrate materials. Solar reflectances were then measured as a function of time of exposure to a RF-generated air plasma. Author

A88-21255* National Aeronautics and Space Administration. Lewis Research Center, Cleveland, OH.

SPACE STATION PROPULSION SYSTEM TECHNOLOGY

ROBERT E. JONES, PHILLIP R. MENG, STEVEN J. SCHNEIDER, JAMES S. SOVEY, and ROBERT R. TACINA (NASA, Lewis Research Center, Cleveland, OH) Acta Astronautica (ISSN 0094-5765), vol. 15, Sept. 1987, p. 673-683. Previously announced in STAR as N87-25422. refs

Two propulsion systems have been selected for the Space Station: O/H rockets for high thrust applications and the multipropellant resistojets for low thrust needs. These thruster systems integrate very well with the fluid systems on the station. Both thrusters will utilize waste fluids as their source of propellant. The O/H rocket will be fueled by electrolyzed water and the resistojets will use stored waste gases from the environmental control system and the various laboratories. This paper presents the results of experimental efforts with O/H and resistojet thrusters to determine their performance and life capability. Author

A88-32868*# Rockwell International Corp., Canoga Park, CA.

PROGRESS TOWARD AN ADVANCED CONDITION

MONITORING SYSTEM FOR REUSABLE ROCKET ENGINES

J. MARAM and S. BARKHOUDARIAN (Rockwell International Corp., Rocketdyne Div., Canoga Park, CA) Joint Army-Navy-NASA-Air Force Interagency Propulsion Committee, Propulsion Meeting, San Diego, CA, Dec. 15-17, 1987, Paper. 6 p. refs

(Contract NAS3-23349)

A new generation of advanced sensor technologies will allow the direct measurement of critical/degradable rocket engine components' health and the detection of degraded conditions before component deterioration affects engine performance, leading to substantial improvements in reusable engines' operation and maintenance. When combined with a computer-based engine condition-monitoring system, these sensors can furnish a continuously updated data base for the prediction of engine availability and advanced warning of emergent maintenance requirements. Attention is given to the case of a practical turbopump and combustion device diagnostic/prognostic health-monitoring system. O.C.

A88-43721*# Manhattan Coll., New York.

THREE DIMENSIONAL THERMAL ANALYSIS OF ROCKET THRUST CHAMBERS

M. H. N. NARAGHI (Manhattan College, Riverdale, NY) and E. S. ARMSTRONG (NASA, Lewis Research Center, Cleveland, OH) AIAA, Thermophysics, Plasmadynamics and Lasers Conference, San Antonio, TX, June 27-29, 1988. 11 p. refs

(Contract NAG3-759)

(AIAA PAPER 88-2643)

A numerical model for the three-dimensional thermal analysis of rocket thrust chambers and nozzles has been developed. The input to the model consists of the composition of the fuel/oxidant mixture and flow rates, chamber pressure, coolant entrance temperature and pressure, dimensions of the engine, materials and the number of nodes in different parts of the engine. The model allows for temperature variation in three dimensions: axial, radial and circumferential directions and by implementing an iterative scheme, it provides nodal temperature distribution, rates of heat transfer, hot gas and coolant thermal and transport properties. Author

A88-46220*# Michigan State Univ., East Lansing.

ELECTROTHERMAL PROPULSION OF SPACECRAFT WITH MILLIMETER AND SUBMILLIMETER ELECTROMAGNETIC ENERGY

L. L. FRASCH, R. FRITZ, and J. ASMUSSEN (Michigan State

University, East Lansing) Journal of Propulsion and Power (ISSN 0748-4658), vol. 4, July-Aug. 1988, p. 334-340. refs
(Contract NAG3-305)

The concept of millimeter and submillimeter wave electrothermal propulsion is considered. State-of-the-art radiation sources from 30-1000 GHz are examined to determine their applicability to electrothermal propulsion systems. The problem of energy conversion and power conditioning in this frequency range is also addressed. The potential advantage of utilizing power beaming with millimeter and submillimeter systems is examined. Finally, areas of future research and development are indicated. Author

A88-48037*# Rockwell International Corp., Canoga Park, CA.
IMPROVED MAINTAINABILITY OF SPACE-BASED REUSABLE ROCKET ENGINES

S. BARKHOUDARIAN, B. SZEMENYEI, R. S. NELSON, R. PAUCKERT, and T. HARMON (Rockwell International Corp., Rocketdyne Div., Canoga Park, CA) AIAA, ASME, SAE, and ASEE, Joint Propulsion Conference and Exhibit, 24th, Boston, MA, July 11-13, 1988. 5 p. refs
(Contract NAS3-23773)
(AIAA PAPER 88-3113)

Advanced, noninferential, noncontacting, in situ measurement technologies, combined with automated testing and expert systems, can provide continuous, automated health monitoring of critical space-based rocket engine components, requiring minimal disassembly and no manual data analysis, thus enhancing their maintainability. This paper concentrates on recent progress of noncontacting combustion chamber wall thickness condition-monitoring technologies. Author

A88-48753*# National Aeronautics and Space Administration, Lewis Research Center, Cleveland, OH.

INTERNAL EROSION RATES OF A 10-KW XENON ION THRUSTER

VINCENT K. RAWLIN (NASA, Lewis Research Center, Cleveland, OH) AIAA, ASME, SAE, and ASEE, Joint Propulsion Conference, 24th, Boston, MA, July 11-13, 1988. 29 p. Previously announced in STAR as N88-24688. refs
(AIAA PAPER 88-2912)

A 30 cm diameter divergent magnetic field ion thruster, developed for mercury operation at 2.7 kW, was modified and operated with xenon propellant at a power level of 10 kW for 567 h to evaluate thruster performance and lifetime. The major differences between this thruster and its baseline configuration were elimination of the three mercury vaporizers, use of a main discharge cathode with a larger orifice, reduction in discharge baffle diameter, and use of an ion accelerating system with larger acceleration grid holes. Grid thickness measurement uncertainties, combined with estimates of the effects of reactive residual facility background gases gave a minimum screen grid lifetime of 7000 h. Discharge cathode orifice erosion rates were measured with three different cathodes with different initial orifice diameters. Three potential problems were identified during the wear test: the upstream side of the discharge baffle eroded at an unacceptable rate; two of the main cathode tubes experienced oxidation, deformation, and failure; and the accelerator grid impingement current was more than an order of magnitude higher than that of the baseline mercury thruster. The charge exchange ion erosion was not quantified in this test. There were no measurable changes in the accelerator grid thickness or the accelerator grid hole diameters. Author

A88-48755*# National Aeronautics and Space Administration, Lewis Research Center, Cleveland, OH.

EVALUATION OF THE COMMUNICATIONS IMPACT OF A LOW POWER ARCJET THRUSTER

LYNNETTE M. CARNEY (NASA, Lewis Research Center, Cleveland, OH) AIAA, ASME, SAE, and ASEE, Joint Propulsion Conference, 24th, Boston, MA, July 11-13, 1988. 25 p. Previously announced in STAR as N88-24682. refs
(AIAA PAPER 88-3105)

The interaction of a 1 kW arcjet thruster plume with a

communications signal is evaluated. A two-parameter, source flow equation has been used to represent the far flow field distribution of the arcjet plume in a realistic spacecraft configuration. Modeling the plume as a plasma slab, the interaction of the plume with a 4 GHz communications signal is then evaluated in terms of signal attenuation and phase shift between transmitting and receiving antennas. Except for propagation paths which pass very near the arcjet source, the impacts to transmission appear to be negligible. The dominant signal loss mechanism is refraction of the beam rather than absorption losses due to collisions. However, significant reflection of the signal at the sharp vacuum-plasma boundary may also occur for propagation paths which pass near the source.

Author

A88-48756*# National Aeronautics and Space Administration, Lewis Research Center, Cleveland, OH.

AN EXTENDED LIFE AND PERFORMANCE TEST OF A LOW-POWER ARCJET

FRANCIS M. CURRAN and THOMAS W. HAAG (NASA, Lewis Research Center, Cleveland, OH) AIAA, ASME, SAE, and ASEE, Joint Propulsion Conference, 24th, Boston, MA, July 11-13, 1988. 22 p. Previously announced in STAR as N88-24687. refs
(AIAA PAPER 88-3106)

An automated, cyclic life test was performed to demonstrate the reliability and endurance of a low power dc cycle arcjet thruster. Over 1000 hr and 500 on-off cycles were accumulated which would represent the requirements for about 15 years of on-orbit lifetime. A hydrogen/nitrogen propellant mixture was used to simulate decomposed hydrazine propellant and the power level was nominally 1.2 kW after the burn-in period. The arcjet operated in a very repeatable fashion from cycle to cycle. The steady state voltage increased by approximately 6 V over the first 300 hr, and then by only 3 V through the remainder of the test. Thrust measurements taken before, during, and after the test verified that the thruster performed in a consistent fashion throughout the tests at a specific impulse of 450 to 460 sec. Post-test component evaluation revealed limited erosion on both the anode and cathode. Other thruster components, including graphite seals, appeared undamaged. Author

A88-48761*# National Aeronautics and Space Administration, Lewis Research Center, Cleveland, OH.

RECENT ADVANCES IN LOW-THRUST PROPULSION TECHNOLOGY

JAMES R. STONE (NASA, Lewis Research Center, Cleveland, OH) AIAA, ASME, SAE, and ASEE, Joint Propulsion Conference, 24th, Boston, MA, July 11-13, 1988. 26 p. Previously announced in STAR as N88-25260. refs
(AIAA PAPER 88-3283)

The NASA low-thrust propulsion technology program is aimed at providing high performance options to a broad class of near-term and future missions. Major emphases of the program are on storable and hydrogen/oxygen low-thrust chemical, low-power (auxiliary) electrothermal, and high-power electric propulsion. This paper represents the major accomplishments of the program and discusses their impact. Author

A88-48765*# National Aeronautics and Space Administration, Lewis Research Center, Cleveland, OH.

THERMODYNAMIC MODELING OF THE NO-VENT FILL METHODOLOGY FOR TRANSFERRING CRYOGENS IN LOW GRAVITY

DAVID J. CHATO (NASA, Lewis Research Center, Cleveland, OH) AIAA, ASME, SAE, and ASEE, Joint Propulsion Conference, 24th, Boston, MA, July 11-13, 1988. 9 p. Previously announced in STAR as N88-24686. refs
(AIAA PAPER 88-3403)

The filling of tanks with cryogenics in the low-gravity environment of space poses many technical challenges. Chief among these is the inability to vent only vapor from the tank as the filling proceeds. As a potential solution to this problem, the NASA Lewis Research Center is researching a technique known as No-Vent Fill. This technology potentially has broad application. The focus is the

20 SPACECRAFT PROPULSION AND POWER

fueling of space based Orbital Transfer Vehicles. The fundamental thermodynamics of the No-Vent Fill is described. The model is then used to conduct a parametric investigation of the key parameters: initial tank wall temperature, liquid-vapor interface heat transfer rate, liquid inflow rate, and inflowing liquid temperatures. Liquid inflowing temperature and the liquid-vapor interface heat transfer rate seem to be the most significant since they influence the entire fill process. The initial tank wall temperature must be sufficiently low to prevent a rapid pressure rise during the initial liquid flashing state, but then becomes less significant. Author

A88-49659* Southwest Research Inst., San Antonio, TX.
PROBABILISTIC STRUCTURAL ANALYSIS METHODS FOR SELECT SPACE PROPULSION SYSTEM STRUCTURAL COMPONENTS (PSAM)

T. A. CRUSE, O. H. BURNSIDE, Y.-T. WU, E. Z. POLCH (Southwest Research Institute, San Antonio, TX), and J. B. DIAS (MARC Analysis Research Corp., Palo Alto, CA) Computers and Structures (ISSN 0045-7949), vol. 29, no. 5, 1988, p. 891-901. Previously announced in STAR as N87-22784. refs (Contract NAS3-24389)

The objective is the development of several modular structural analysis packages capable of predicting the probabilistic response distribution for key structural variables such as maximum stress, natural frequencies, transient response, etc. The structural analysis packages are to include stochastic modeling of loads, material properties, geometry (tolerances), and boundary conditions. The solution is to be in terms of the cumulative probability of exceedance distribution (CDF) and confidence bounds. Two methods of probability modeling are to be included as well as three types of structural models - probabilistic finite-element method (PFEM); probabilistic approximate analysis methods (PAAM); and probabilistic boundary element methods (PBEM). The purpose in doing probabilistic structural analysis is to provide the designer with a more realistic ability to assess the importance of uncertainty in the response of a high performance structure. Probabilistic Structural Analysis Method (PSAM) tools will estimate structural safety and reliability, while providing the engineer with information on the confidence that should be given to the predicted behavior. Perhaps most critically, the PSAM results will directly provide information on the sensitivity of the design response to those variables which are seen to be uncertain. Author

A88-52333* National Aeronautics and Space Administration. Lewis Research Center, Cleveland, OH.

SPACE STATION PHOTOVOLTAIC POWER MODULES

CHARLES A. TATRO (NASA, Lewis Research Center, Cleveland, OH) IN: Space Congress, 25th, Cocoa Beach, FL, Apr. 26-29, 1988, Proceedings. Cape Canaveral, FL, Canaveral Council of Technical Societies, 1988, p. 5-21 to 5-33. refs

Silicon cell Photovoltaic (PV) power modules are key components of the Space Station Electrical Power System (EPS) scheduled to begin deployment in 1994. Four PV power modules, providing 75 KWe of user ac power, form the cornerstone of the EPS; which is comprised of Photovoltaic (PV) power modules, Solar Dynamic (SD) power modules, and the Power Management and Distribution (PMAD) system. The PV modules are located on rotating outboard sections of the Space Station (SS) structure and each module incorporates its own nickel-hydrogen energy storage batteries, its own thermal control system, and some autonomous control features. The PV modules are a cost-effective and technologically mature approach for providing reliable SS electrical power and are a solid base for EPS growth, which is expected to reach 300 KWe by the end of the Space Station's 30-year design lifetime. Author

A88-53101* Rockwell International Corp., Canoga Park, CA.

25-LBF GO2/GH2 SPACE STATION THRUSTER

L. E. FINDEN, G. L. BRILEY, and R. S. IACABUCCI (Rockwell International Corp., Rocketdyne Div., Canoga Park, CA) AIAA, ASME, SAE, and ASEE, Joint Propulsion Conference, 24th, Boston, MA, July 11-13, 1988. 8 p.

(Contract NAS3-25142; NAS8-36418)
(AIAA PAPER 88-2793)

Multiple 25-lbf oxygen/gaseous hydrogen thruster assemblies for the Space Station propulsion application were designed and fabricated by Rocketdyne and endurance tested at the NASA/Marshall Space Flight Center. The thrusters incorporate a regeneratively cooled thrust chamber with a nozzle area ratio of 30, a 12-element coaxial injector, an ignition system, and close-coupled propellant valves. The various thruster configurations comprised of mating different injectors and thrust chambers. Over 2 million lbf-sec of impulse was demonstrated at mixture ratios from 3 to 8.4 at vacuum conditions. A thruster was subjected to over 10,000 pulses during which minimum impulse bits of less than 0.5 lb/sec were repeatedly and reliably demonstrated. A total operating time of 25.6 hr was accumulated on the thruster assemblies with one 6.1-hr. continuous firing duration. The thrusters operated between a thrust range of 11.2 and 36.6 lbf. The test results indicate that all major technology issues for long-life gaseous oxygen/gaseous hydrogen thrusters for the Space Station application have been resolved. Author

A88-55361* Cleveland State Univ., OH.

MODELLING THE PERFORMANCE OF THE TAPERED ARTERY HEAT PIPE DESIGN FOR USE IN THE RADIATOR OF THE SOLAR DYNAMIC POWER SYSTEM OF THE NASA SPACE STATION

AUSTIN LEWIS EVANS (Cleveland State University, OH) IAF, International Astronautical Congress, 39th, Bangalore, India, Oct. 8-15, 1988. 6 p. refs (Contract NCC3-50)
(IAF PAPER 88-213)

The paper presents a computer program developed to model the steady-state performance of the tapered artery heat pipe for use in the radiator of the solar dynamic power system of the NASA Space Station. The program solves six governing equations to ascertain which one is limiting the maximum heat transfer rate of the heat pipe. The present model appeared to be slightly better than the LTV model in matching the 1-g data for the standard 15-ft test heat pipe. K.K.

N88-10106* Hughes Research Labs., Malibu, CA.

AN 8-CM ION THRUSTER CHARACTERIZATION

Supplementary Final Report, Mar. 1982 - Feb. 1983

F. J. WESSEL, D. J. HANCOCK, C. R. DULGEROFF, and W. S. WILLIAMSON Oct. 1987 57 p (Contract NAS3-22447)
(NASA-CR-180819; NAS 1.26:180819; HAC-E7324) Avail: NTIS HC A04/MF A01 CSCL 21H

The performance of the Ion Auxiliary Propulsion System (IAPS) thruster was increased to thrust $T = 32$ mN, specific impulse $I_{sp} = 4062$ s, and thrust-to-power ratio $T/P = 33$ mN/kW. This performance was obtained by increasing the discharge power, accelerating voltage, propellant flow rate, and chamber magnetic field. Adding a plenum and main vaporizer for propellant distribution was the only major change required in the thruster. The modified thruster characterization is presented. A cathode magnet assembly did not improve performance. A simplified power processing unit was designed and evaluated. This unit decreased the parts count of the IAPS power processing unit by a factor of ten. Author

N88-10886* Hughes Aircraft Co., Los Angeles, CA. Space and Communications Group.

AUXILIARY PROPULSION SYSTEM FLIGHT PACKAGE Final

Report, 16 Jan. 1978 - 31 Dec. 1986

C. R. COLLETT Nov. 1987 73 p (Contract NAS3-21055)
(NASA-CR-180828; NAS 1.26:180828) Avail: NTIS HC A04/MF A01 CSCL 21C

Hughes Aircraft Company developed qualified and integrated flight, a flight test Ion Auxiliary Propulsion System (IAPS), on an Air Force technology satellite. The IAPS Flight Package consists of two identical Thruster Subsystems and a Diagnostic Subsystem. Each thruster subsystem (TSS) is comprised of an 8-cm ion

Thruster-Gimbal-Beam Shield Unit (TGBSU); Power Electronics Unit; Digital Controller and Interface Unit (DCIU); and Propellant Tank, Valve and Feed Unit (PTVFU) plus the requisite cables. The Diagnostic Subsystem (DSS) includes four types of sensors for measuring the effect of the ion thrusters on the spacecraft and the surrounding plasma. Flight qualifications of IAPS, prior to installation on the spacecraft, consisted of performance, vibration and thermal-vacuum testing at the unit level, and thermal-vacuum testing at the subsystem level. Mutual compatibility between IAPS and the host spacecraft was demonstrated during a series of performance and environmental tests after the IAPS Flight Package was installed on the spacecraft. After a spacecraft acoustic test, performance of the ion thrusters was reverified by removing the TGBSUs for a thorough performance test at Hughes Research Laboratories (HRL). The TGBSUs were then reinstalled on the spacecraft. The IAPS Flight Package is ready for flight testing when Shuttle flights are resumed. Author

N88-11745*# National Aeronautics and Space Administration. Lewis Research Center, Cleveland, OH.

PHOTOVOLTAIC POWER MODULES FOR NASA'S MANNED SPACE STATION

CHARLES A. TATRO 1987 13 p Proposed for presentation at the 1988 Solar Energy Conference, Golden, Colo., 10-14 Apr. 1988; sponsored by ASME (NASA-TM-100229; E-3850; NAS 1.15:100229) Avail: NTIS HC A03/MF A01 CSCL 10C

The capability and the safety of manned spacecraft are largely dependent upon reliable electric power systems. Two similar space power systems able to survive the low Earth orbit environment, are being considered for NASA's Manned Space Station (SS), scheduled to begin operation in the mid 1990's. The Space Station Electric Power System (EPS) is composed of Photovoltaic (PV) Power Modules, Solar Dynamic (SD) Power Modules, and the Power Management and Distribution (PMAD) System. One EPS configuration will deliver 37.5 kW of PV based, utility grade, ac power to SS users. A second 75 kW PV based EPS option is also being considered for SS deployment. The two EPS options utilize common modules and differ only in the total number of PV Power Modules used. Each PV Power Module supplies 18.75 kW of ac power and incorporates its own energy storage and thermal control. The general requirements and the current preliminary design configuration of the Space Station PV Power Modules are examined. Author

N88-11746*# National Aeronautics and Space Administration. Lewis Research Center, Cleveland, OH.

SPACE STATION PROPULSION

ROBERT E. JONES, W. EARL MORREN, JAMES S. SOVEY, and ROBERT R. TACINA 1987 19 p Presented at the 1987 JANNAF Propulsion Conference, San Diego, Calif., 15-17 Dec. 1987 (NASA-TM-100216; E-3825; NAS 1.15:100216) Avail: NTIS HC A03/MF A01 CSCL 21H

Two propulsion systems have been selected for the space station: gaseous H₂O rockets for high thrust applications and the multipropellant resistojets for low thrust needs. These two thruster systems integrate very well with the fluid systems on the space station, utilizing waste fluids as their source of propellant. The H₂O rocket will be fueled by electrolyzed water and the resistojets will use waste gases collected from the environmental control system and the various laboratories. The results are presented of experimental efforts with H₂O and resistojets to determine their performance and life capability, as well as results of studies to determine the availability of water and waste gases. Author

N88-11747*# National Aeronautics and Space Administration. Lewis Research Center, Cleveland, OH.

SPRE 1 FREE-PISTON STIRLING ENGINE TESTING AT NASA LEWIS RESEARCH CENTER

JAMES E. CAIRELLI 1987 15 p Proposed for presentation at the 1988 Solar Energy Conference, Golden, Colo., 10-14 Apr. 1988;

sponsored by ASME

(NASA-TM-100241; E-3865; NAS 1.15:100241) Avail: NTIS HC A03/MF A01 CSCL 10B

As part of the NASA funded portion of the SP-100 Advanced Technology Program the Space Power Research Engine (SPRE 1) was designed and built to serve as a research tool for evaluation and development of advanced Stirling engine concepts. The SPRE 1 is designed to produce 12.5 kW electrical power when operated with helium at 15 MPa and with an absolute temperature ratio of two. The engine is now under test in a new test facility which was designed and built at NASA Lewis specifically to test the SPRE 1. The SPRE 1, the NASA test facility, the initial SPRE 1 test results, and future SPRE 1 test plans are described. Author

N88-11748*# National Aeronautics and Space Administration. Lewis Research Center, Cleveland, OH.

A LOW-POWER ARCJET CYCLIC LIFETEST

FRANCIS M. CURRAN, TERRY L. HARDY, and THOMAS W. HAAG 1987 15 p Presented at the 1987 JANNAF Propulsion Conference, San Diego, Calif., 15-17 Dec. 1987 (NASA-TM-100233; E-3858; NAS 1.15:100233) Avail: NTIS HC A03/MF A01 CSCL 21H

A cyclic lifetest of a low power dc arcjet thruster using a hydrogen/nitrogen propellant mixture simulating hydrazine is currently in progress. Over 300 hr of operation have been accumulated to date in 2 hr duty cycles at a power level of about 1.15 kW, approximating that available on commercial communications satellites. A burn-in period was carried out before consistent operation was attained. After this period, the arcjet operated in a very stable fashion from cycle to cycle. At the beginning of each cycle, there was a brief starting transient followed by a rapid rise to a steady-state voltage. The steady-state voltage increased by about 5 V over the first 95 cycles. After this, it increased by only 1 V through the remainder of the test. Thrust measurements taken before the life test and again after the completion of the 144th cycle showed that both thrust, specific impulse, and arc voltage had increased over this period of operation. No life limiting mechanisms were observed during the course of the testing. Author

N88-11749*# Page (R. J.) Co., Santa Ana, CA.

SLIP CASTING AND EXTRUDING SHAPES OF RHENIUM WITH METAL OXIDE ADDITIVES. PART 2: DEVELOPMENT OF GRAIN STABILIZED RHENIUM PARTS FOR RESISTOJETS Final Report

FRANCIS A. BARR and RUSSELL J. PAGE Nov. 1987 22 p (Contract NAS3-24651) (NASA-CR-180851; NAS 1.26:180851) Avail: NTIS HC A03/MF A01 CSCL 21H

The adaptation of the powdered particle process used for pure metal oxides to the coprocessing of rhenium oxides suitable to produce pure miniature resistojets hardware has been successful. Both slip casting and extrusion processes were used. The metal oxide ZrO₂ was stabilized into the cubic phase with Y₂O₃, for use as a potentially grain stabilizing additive to rhenium. Straight meter long tubing in two sizes are reported. Tubing suitable for resistojets ohmic heater use of fully fired dimensions of nominally 3.8 mm o.d. x 2.2 mm i.d. and 1.26 mm o.d. x .45 mm i.d. with 0, 0.5, 1.0 and 5.0% zirconia additives were produced for further study. Photomicrographs of these are discussed. The addition of the metal oxide zirconia to rhenium resulted in more dense and less porous parts. The additions of phase stabilized zirconia most likely act as a sintering aid. Tubes of varying diameter were slip cast which were representative of miniature pressure cases. Author

N88-11750*# National Aeronautics and Space Administration. Lewis Research Center, Cleveland, OH.

A LIFE TEST OF A 22-NEWTON (5-LBF) HYDRAZINE ROCKET P. R. MENG, S. J. SCHNEIDER, C. J. MORGAN, R. E. JONES, and D. A. PAHL (Rocket Research Corp., Redmond, Wash.) 1987 12 p Prepared for presentation at the JANNAF Propulsion

20 SPACECRAFT PROPULSION AND POWER

Conference, San Diego, Calif., 15-17 Dec. 1987
(NASA-TM-100232; E-3857; NAS 1.15:100232) Avail: NTIS HC
A03/MF A01 CSCL 21H

Life tests were conducted on a 22-N (5-lb) hydrazine rocket thruster which incorporates the latest technology to obtain long life from the catalyst bed. A spring mechanism surrounding the catalyst bed continually applies compression to the catalyst bed to prevent the formation of any void channels. The research rocket thruster was tested over an operational cycle of both steady state and pulse firing which simulated a possible space station duty cycle. The thruster ran as expected for about 40 hours, or 3.2 times 10 to the 6th power N-sec (7.2 times 10 to the 5th power lb-sec) total impulse. Subsequently, some thrust chamber pressure decreases were noted during long steady state test periods. After 60.2 hours of run time, tests had to be terminated due to a blockage in the propellant injector tube which occurred during heating of the thruster by a heat lamp. A chemical analysis of the catalyst indicated that iron and nickel metals had poisoned some of the catalyst, thereby causing a degradation in performance. It was determined that a contaminated barrel of hydrazine was the source of the metal poisoning. Author

N88-12538*# National Aeronautics and Space Administration. Lewis Research Center, Cleveland, OH.

COMPATABILITY OF DISPERSION-STRENGTHENED PLATINUM WITH RESISTOJET PROPELLANTS

MARGARET V. WHALEN and MICHAEL V. NATHAL Oct. 1987
29 p
(NASA-TP-2765; E-3738; NAS 1.60:2765) Avail: NTIS HC
A03/MF A01 CSCL 21H

Resistojets for the Space Station require long life and multipropellant capability. The choice of available materials to meet these requirements is limited. Dispersion-strengthened platinum was selected. Past results indicated that it should be sufficiently inert in candidate propellant environments and should be capable of operating at moderate temperatures for extended periods. A series of propellant compatibility tests was done with platinum strengthened with either yttria or zirconia. Data presented included the results of 1000-hr tests in CO₂, H₂, ammonia (NH₃), N₂, steam, hydrazine (N₂H₄), and methane (CH₄); and 2000-hr tests in H₂ and NH₃. The platinum samples were tested at 1400 C in CO₂, H₂, NH₃, N₂, steam, and N₂H₄; at 500 C in CH₄; and at 800 C in N₂H₄. The mass-loss results indicated material life, extrapolated from experimental mass-loss data, in excess of 100 000 hr in all environments except steam and N₂H₄, where it was greater than or = 45000 hr. Generally, on the basis of mass loss, there were no compatibility concerns in any of the environments considered. Optical and scanning electron microscopy were used to determine the effect of propellants on the material surface and to evaluate material stability. Author

N88-12539*# National Aeronautics and Space Administration. Lewis Research Center, Cleveland, OH.

A TWO-DIMENSIONAL FINITE DIFFERENCE PROGRAM FOR THERMAL ANALYSIS OF ROCKET THRUST CHAMBERS

MOHAMMAD H. NARAGHI Sep. 1987 53 p
(Contract NAG3-672)
(NASA-TM-100191; E-3773; NAS 1.15:100191) Avail: NTIS HC
A04/MF A01 CSCL 21H

A two-dimensional finite difference computer model for thermal analysis of rocket thrust chambers has been developed. The model uses an iterative scheme for calculating the temperature distribution within the chamber wall and implements a successive overrelaxation formula for a quick convergence. The inputs of the models are the dimensions of the thrust chamber wall, types of materials used, heat transfer coefficients and temperatures of the hot gas and the coolant. The resulting output of the program consists of the nodal temperature distribution, heat transfer to the coolant and heat transfer from the hot gas. Author

N88-12541*# Rockwell International Corp., Canoga Park, CA. Rocketdyne Div.

SPACE STATION RESISTOJET SYSTEM REQUIREMENTS AND INTERFACE DEFINITION STUDY Final Report, Jun. 1986 - Jun. 1987

L. E. FINDEN Nov. 1987 120 p
(Contract NAS3-24658)
(NASA-CR-180832; NAS 1.26:180832; RI/RD-87-211) Avail:
NTIS HC A06/MF A01 CSCL 21H

A conceptual design study of the resistojet orbital replacement unit (ORU) was conducted. The ORU consists of four 500-W multipropellant resistojets, fluid components downstream of the waste fluid storage subsystem, a power controller, structure, and micrometeorite shielding. The fluid components include latch valves, a water vaporizer, two pressure regulators or flow control valves, filters, check valves, fluid tubing, and interface couplings. Separate fluid components are provided for oxidizing fluids, reducing fluids and water. Different flow and power control methods were studied. The most promising methods consist of a constant pressure/on-off power control and a constant power/variable pressure control. The closed-loop power control incorporates a feedback signal which is proportional to resistojet heater temperature. Author

N88-12542*# National Aeronautics and Space Administration. Lewis Research Center, Cleveland, OH.

HIGH POWER ION THRUSTER PERFORMANCE

VINCENT K. RAWLIN and MICHAEL J. PATTERSON 1987 14 p
Presented at the Fourth Symposium on Space Nuclear Power Systems, Albuquerque, N. Mex., 12-16 Jan. 1987
(NASA-TM-100127; E-3676; NAS 1.15:100127) Avail: NTIS HC
A03/MF A01 CSCL 21C

The ion thruster is one of several forms of space electric propulsion being considered for use on future SP-100-based missions. One possible major mission ground rule is the use of a single Space Shuttle launch. Thus, the mass in orbit at the reactor activation altitude would be limited by the Shuttle mass constraints. When the spacecraft subsystem masses are subtracted from this available mass limit, a maximum propellant mass may be calculated. Knowing the characteristics of each type of electric thruster allows maximum values of total impulse, mission velocity increment, and thrusting time to be calculated. Because ion thrusters easily operate at high values of efficiency (60 to 70%) and specific impulse (3000 to 5000 sec), they can impart large values of total impulse to a spacecraft. They also can be operated with separate control of the propellant flow rate and exhaust velocity. This paper presents values of demonstrated and projected performance of high power ion thrusters used in an analysis of electric propulsion for an SP-100 based mission. Author

N88-14127*# National Aeronautics and Space Administration. Lewis Research Center, Cleveland, OH.

AUXILIARY PROPULSION TECHNOLOGY FOR ADVANCED EARTH-TO-ORBIT VEHICLES

STEVEN J. SCHNEIDER 1987 16 p
Presented at the 1987 JANNAF Propulsion Conference, San Diego, Calif., 15-17 Dec. 1987
(NASA-TM-100237; E-3783; NAS 1.15:100237) Avail: NTIS HC
A03/MF A01 CSCL 21H

The payload which can be delivered to orbit by advanced Earth-to-Orbit vehicles is significantly increased by advanced subsystem technology. Any weight which can be saved by advanced subsystem design can be converted to payload at Main Engine Cut Off (MECO) given the same launch vehicle performance. The auxiliary propulsion subsystem and the impetus for the current hydrogen/oxygen technology program is examined. A review of the auxiliary propulsion requirements of advanced Earth-to-Orbit (ETO) vehicles and their proposed missions is given first. Then the performance benefits of hydrogen/oxygen auxiliary propulsion are illustrated using current shuttle data. The proposed auxiliary propulsion subsystem implementation includes liquid hydrogen/liquid oxygen (LH₂/LO₂) primary Reaction Control System (RCS) engines and gaseous hydrogen/gaseous oxygen

(GH2/GO2) vernier RCS engines. A distribution system for the liquid cryogenics to the engines is outlined. The possibility of providing one dual-phase engine that can operate on either liquid or gaseous propellants is being explored, as well as the simultaneous firing of redundant primary RCS thrusters to provide Orbital Maneuvering System (OMS) level impulse. Scavenging of propellants from integral main engine tankage is proposed to utilize main engine tank residuals and to combine launch vehicle and subsystem reserves. Author

N88-15006*# Martin Marietta Aerospace, Denver, CO.

SPACE STATION ONBOARD PROPULSION SYSTEM: TECHNOLOGY STUDY Final Report

J. G. MCALLISTER, R. S. RUDLAND, L. R. REDD, D. H. BEEKMAN, S. M. CUFFIN, C. M. BEER, and K. K. MCCARTHY Jan. 1987 106 p

(Contract NAS3-23893)

(NASA-CR-179233; NAS 1.26:179233; MCR-87-500) Avail: NTIS HC A06/MF A01 CSCL 21H

The objective was to prepare for the design of the space station propulsion system. Propulsion system concepts were defined and schematics were developed for the most viable concepts. A dual model bipropellant system was found to deliver the largest amount of payload. However, when resupply is considered, an electrolysis system with 10 percent accumulators requires less resupply propellant, though it is penalized by the amount of time required to fill the accumulators and the power requirements for the electrolyzer. A computer simulation was prepared, which was originally intended to simulate the water electrolysis propulsion system but which was expanded to model other types of systems such as cold gas, monopropellant and bipropellant storable systems. J.P.B.

N88-15838*# National Aeronautics and Space Administration. Lewis Research Center, Cleveland, OH.

STATUS OF 20 KHZ SPACE STATION POWER DISTRIBUTION TECHNOLOGY

IRVING G. HANSEN Jan. 1988 12 p Presented at the Applied Power Electronics Conference and Exposition (APEC 88), New Orleans, La., 1-5 Feb. 1988; sponsored by IEEE

(NASA-TM-100781; E-3951; NAS 1.15:100781) Avail: NTIS HC A03/MF A01 CSCL 10B

Power Distribution on the NASA Space Station will be accomplished by a 20 kHz sinusoidal, 440 VRMS, single phase system. In order to minimize both system complexity and the total power conversion steps required, high frequency power will be distributed end-to-end in the system. To support the final design of flight power system hardware, advanced development and demonstrations have been made on key system technologies and components. The current status of this program is discussed. Author

N88-17731*# Sverdrup Technology, Inc., Cleveland, OH.

COMPONENT DATA BASE FOR SPACE STATION RESISTOJET AUXILIARY PROPULSION Final Report

CLAYTON H. BADER Jan. 1988 62 p Microfiche included as supplement

(Contract NAS3-24105)

(NASA-CR-180834; E-3856; NAS 1.26:180834) Avail: NTIS HC A04/MF A01 CSCL 21H

The resistojets were baselined for Space Station auxiliary propulsion because of its operational versatility, efficiency, and durability. This report was conceived as a guide to designers and planners of the Space Station auxiliary propulsion system. It is directed to the low thrust resistojets concept, though it should have application to other station concepts or systems such as the Environmental Control and Life Support System (ECLSS), Manufacturing and Technology Laboratory (MTL), and the Waste Fluid Management System (WFMS). The information will likely be quite useful in the same capacity for other non-Space Station systems including satellite, freeflyers, explorers, and maneuvering vehicles. The report is a catalog of the most useful information

for the most significant feed system components and is organized for the greatest convenience of the user. Author

N88-17732*# Aerojet TechSystems Co., Sacramento, CA.

ARCJET THRUSTER RESEARCH AND TECHNOLOGY Final Report

DARBY B. MAKEL and GORDON L. CANN (Technion, Inc., Irvine, Calif.) Feb. 1988 300 p

(Contract NAS3-24842)

(NASA-CR-180865; NAS 1.26:180865; RPT/BB0642) Avail:

NTIS HC A13/MF A01 CSCL 21H

The design, analysis, and performance testing of an advanced lower power arcjet is described. A high impedance, vortex stabilized 1-kw class arcjet has been studied. A baseline research thruster has been built and endurance and performance tested. This advanced arcjet has demonstrated long lifetime characteristics, but lower than expected performance. Analysis of the specific design has identified modifications which should improve performance and maintain the long life time shown by the arcjet. Author

N88-20361*# Rockwell International Corp., Canoga Park, CA. Rocketdyne Div.

SOLAR DYNAMIC POWER SYSTEM DEFINITION STUDY Final Report

WAYNE E. WALLIN and JERRY M. FRIEFELD Mar. 1988 322 p Prepared for presentation at the National Aerospace and Electronics Conf., Dayton, Ohio, 18-22 May 1987

(Contract NAS3-24864)

(NASA-CR-180877; NAS 1.26:180877; RI/RD87-250) Avail:

NTIS HC A14/MF A01 CSCL 10B

The solar dynamic power system design and analysis study compared Brayton, alkali-metal Rankine, and free-piston Stirling cycles with silicon planar and GaAs concentrator photovoltaic power systems for application to missions beyond the Phase 2 Space Station level of technology for all power systems. Conceptual designs for Brayton and Stirling power systems were developed for 35 kWe and 7 kWe power levels. All power systems were designed for 7-year end-of-life conditions in low Earth orbit. LiF was selected for thermal energy storage for the solar dynamic systems. Results indicate that the Stirling cycle systems have the highest performance (lowest weight and area) followed by the Brayton cycle, with photovoltaic systems considerably lower in performance. For example, based on the performance assumptions used, the planar silicon power system weight was 55 to 75 percent higher than for the Stirling system. A technology program was developed to address areas wherein significant performance improvements could be realized relative to the current state-of-the-art as represented by Space Station. In addition, a preliminary evaluation of hardenability potential found that solar dynamic systems can be hardened beyond the hardness inherent in the conceptual designs of this study. Author

N88-21249*# National Aeronautics and Space Administration. Lewis Research Center, Cleveland, OH.

ADVANCED SENSIBLE HEAT SOLAR RECEIVER FOR SPACE POWER

TIMOTHY J. BENNETT (Sverdrup Technology, Inc., Cleveland, Ohio.) and DOVIE E. LACY 1988 12 p Proposed for presentation at the 23rd Intersociety Energy Conversion Engineering Conference, Denver, Colo., 31 Jul. - 5 Aug. 1988; sponsored by ASME, AIAA, ANS, SAE, IEEE, ASC and AIChE

(NASA-TM-100847; E-4008; NAS 1.15:100847) Avail: NTIS HC A03/MF A01 CSCL 10B

NASA Lewis, through in-house efforts, has begun a study to generate a conceptual design of a sensible heat solar receiver and to determine the feasibility of such a system for space power applications. The sensible heat solar receiver generated in this study uses pure lithium as the thermal storage medium and was designed for a 7 kWe Brayton (PCS) operating at 1100 K. The receiver consists of two stages interconnected via temperature sensing variable conductance sodium heat pipes. The lithium is contained within a niobium vessel and the outer shell of the receiver

20 SPACECRAFT PROPULSION AND POWER

is constructed of third generation rigid, fibrous ceramic insulation material. Reradiation losses are controlled with niobium and aluminum shields. By nature of design, the sensible heat receiver generated in this study is comparable in both size and mass to a latent heat system of similar thermal capacitance. The heat receiver design and thermal analysis was conducted through the combined use of PATRAN, SINDA, TRASYS, and NASTRAN software packages. Author

N88-21250*# National Aeronautics and Space Administration. Lewis Research Center, Cleveland, OH.

SPACE STATION SOLAR CONCENTRATOR MATERIALS RESEARCH

DANIEL A. GULINO May 1988 15 p
(NASA-TM-100862; E-4074; NAS 1.15:100862) Avail: NTIS HC A03/MF A01 CSCL 10B

The Space Station will represent the first time that a solar dynamic power system will be used to generate electrical power in space. In a system such as this, sunlight is collected and focused by a solar concentrator onto the receiver of a heat engine which converts the energy into electricity. The concentrator must be capable of collecting and focusing as much of the incident sunlight as possible, and it must also withstand the atomic oxygen bombardment which occurs in low Earth orbit (LEO). This has led to the development of a system of thin film coatings applied to the concentrator facet surface in a chamber designed especially for this purpose. The system of thin film coatings employed gives both the necessary degree of reflectance and the required protection from the LEO atomic oxygen environment. Author

N88-21251*# National Aeronautics and Space Administration. Lewis Research Center, Cleveland, OH.

POWER TRANSMISSION STUDIES FOR TETHERED SP-100

DAVID J. BENTS 1988 16 p Proposed for presentation at the 23rd Intersociety Energy Conversion Engineering Conference, Denver, Colo., 31 Jul. - 5 Aug. 1988; sponsored by ASME, AIAA, ANS, SAE, IEEE, ASC and AIChE
(NASA-TM-100864; E-4081; NAS 1.15:100864) Avail: NTIS HC A03/MF A01 CSCL 10B

The tether and/or transmission line connecting the SP-100 to space station presents some unorthodox challenges in high voltage engineering, power transmission, and distribution. The line, which doubles as a structural element of this unusual spacecraft, will convey HVDC from SP-100 to the platform in low Earth orbit, and environment where the local plasma is sufficient to cause breakdown of exposed conductors at potentials of only a few hundred volts. Its anticipated several years operation, and continuously accumulating exposure to meteoroids and debris, raises an increasing likelihood that mechanical damage, including perforation, will be sustained in service. The present concept employs an array of gas insulated solid wall aluminum coaxial tubes; a conceptual design which showed basic feasibility of the SP-100 powered space station. Practical considerations of launch, deployment and assembly have lead to investigation of reel deployable, dielectric insulated coaxial cables. To be competitive, the dielectric would have to operate reliably in a radiation environment under electrical stresses exceeding 50 kV/cm. The SP-100 transmission line high voltage interfaces are also considered. Author

N88-21252*# National Aeronautics and Space Administration. Lewis Research Center, Cleveland, OH.

FINITE AREA COMBUSTOR THEORETICAL ROCKET PERFORMANCE

SANFORD GORDON (Gordon, Sanford, Cleveland, Ohio) and BONNIE J. MCBRIDE Apr. 1988 18 p
(NASA-TM-100785; E-3975; NAS 1.15:100785) Avail: NTIS HC A03/MF A01 CSCL 21H

Previous to this report, the computer program of NASA SP-273 and NASA TM-86885 was capable of calculating theoretical rocket performance based only on the assumption of an infinite area combustion chamber (IAC). An option was added to this program which now also permits the calculation of rocket performance based

on the assumption of a finite area combustion chamber (FAC). In the FAC model, the combustion process in the cylindrical chamber is assumed to be adiabatic, but nonisentropic. This results in a stagnation pressure drop from the injector face to the end of the chamber and a lower calculated performance for the FAC model than the IAC model. Author

N88-21253*# National Aeronautics and Space Administration. Lewis Research Center, Cleveland, OH.

AN EXPERIMENTAL INVESTIGATION OF AN ARCJET THRUSTER EXHAUST USING LANGMUIR PROBES M.S.

Thesis

LYNNETTE M. CARNEY Apr. 1988 26 p
(NASA-TM-100258; E-3883; NAS 1.15:100258) Avail: NTIS HC A03/MF A01 CSCL 21H

Electrostatic (Langmuir) probes of both spherical and cylindrical geometry have been used to obtain electron number density and temperature in the exhaust of a laboratory arcjet. The arcjet thruster operated on nitrogen and hydrogen mixtures to simulate fully decomposed hydrazine in a vacuum environment with background pressures less than 5×10^{-2} Pa. The exhaust appears to be only slightly ionized (less than 1 percent) with local plasma potentials near facility ground. The current-voltage characteristics of the probes indicate a Maxwellian temperature distribution. Plume data are presented as a function of arcjet operating condition and also position in the exhaust. Author

N88-21254*# National Aeronautics and Space Administration. Lewis Research Center, Cleveland, OH.

POWER SYSTEMS FOR PRODUCTION, CONSTRUCTION, LIFE SUPPORT AND OPERATIONS IN SPACE

RONALD J. SOVIE 1988 16 p Proposed for presentation at Space '88, Albuquerque, N. Mex., 29-31 Aug. 1988; sponsored by the American Society of Civil Engineers
(NASA-TM-100838; E-4026; NAS 1.15:100838) Avail: NTIS HC A03/MF A01 CSCL 22B

As one looks to man's future in space it becomes obvious that unprecedented amounts of power are required for the exploration, colonization, and exploitation of space. Activities envisioned include interplanetary travel and LEO to GEO transport using electric propulsion, Earth and lunar observatories, advance space stations, free-flying manufacturing platforms, communications platforms, and eventually evolutionary lunar and Mars bases. These latter bases would start as camps with modest power requirements (kWes) and evolve to large bases as manufacturing, food production, and life support materials are developed from lunar raw materials. These latter activities require very robust power supplies (MWes). The advanced power system technologies being pursued by NASA to fulfill these future needs are described. Technologies discussed will include nuclear, photovoltaic, and solar dynamic space power systems, including energy storage, power conditioning, power transmission, and thermal management. The state-of-the-art and gains to be made by technology advancements will be discussed. Mission requirements for a variety of applications (LEO, GEO, lunar, and Martian) will be treated, and data for power systems ranging from a few kilowatts to megawatt power systems will be represented. In addition the space power technologies being initiated under NASA's new Civilian Space Technology Initiative (CSTI) and Space Leadership Planning Group Activities will be discussed. Author

N88-22080*# National Aeronautics and Space Administration. Lewis Research Center, Cleveland, OH.

RAY TRACING OPTICAL ANALYSIS OF OFFSET SOLAR COLLECTOR FOR SPACE STATION SOLAR DYNAMIC SYSTEM

KENT S. JEFFERIES 1988 20 p Prepared for presentation at the 23rd Intersociety Energy Conversion Engineering Conference, Denver, Colo., 31 Jul. - 5 Aug. 1988; sponsored in part by ASME, AIAA, ANS, SAE, IEEE, ACS, and AIChE
(NASA-TM-100853; E-4056; NAS 1.15:100853) Avail: NTIS HC A03/MF A01 CSCL 10A

OFFSET, a detailed ray tracing computer code, was developed at NASA Lewis Research Center to model the offset solar collector for the Space Station solar dynamic electric power system. This model traces rays from 50 points on the face of the Sun to 10 points on each of the 456 collector facets. The triangular facets are modeled with spherical, parabolic, or toroidal reflective surface contour and surface slope errors. The rays are then traced through the receiver aperture to the walls of the receiver. Images of the collector and of the Sun within the receiver produced by this code provide insight into the collector receiver interface. Flux distribution on the receiver walls, plotted by this code, is improved by a combination of changes to aperture location and receiver tilt angle. Power loss by spillage at the receiver aperture is computed and is considerably reduced by using toroidal facets. Author

N88-22404*# National Aeronautics and Space Administration. Lewis Research Center, Cleveland, OH.
THERMAL-STRUCTURAL ANALYSES OF SPACE SHUTTLE MAIN ENGINE (SSME) HOT SECTION COMPONENTS
 ALI ABDUL-AZIZ (Sverdrup Technology, Inc., Cleveland, Ohio.) and ROBERT L. THOMPSON /in its Lewis Structures Technology, 1988. Volume 2: Structural Mechanics p 255-264 May 1988
 Avail: NTIS HC A14/MF A01 CSCL 21H

Three dimensional nonlinear finite element heat transfer and structural analyses were performed for the first stage high pressure fuel turbopump (HPFTP) blade of the space shuttle main engine (SSME). Directionally solidified (DS) MAR-M 246 and single crystal (SC) PWA-1480 material properties were used for the analyses. Analytical conditions were based on a typical test stand engine cycle. Blade temperature and stress strain histories were calculated by using the MARC finite element computer code. The structural response of an SSME turbine blade was assessed and a greater understanding of blade damage mechanisms, convective cooling effects, and thermal mechanical effects was gained. Author

N88-22933*# National Aeronautics and Space Administration. Lewis Research Center, Cleveland, OH.
DESCRIPTION OF AN OSCILLATING FLOW PRESSURE DROP TEST RIG
 J. GARY WOOD, ERIC L. MILLER, DAVID R. GEDEON, and GARY E. KOESTER (Sunpower, Inc., Athens, Ohio.) 1988 8 p
 Presented at the 23rd Intersociety Energy Conversion Engineering Conference, Denver, Colo., 31 Jul. - 5 Aug. 1988; sponsored in part by ASME, AIAA, ANS, SAE, IEEE, ACS and AIChE
 (NASA-TM-100905; E-4102; NAS 1.15:100905) Avail: NTIS HC A02/MF A01 CSCL 10B

A test rig designed to generate heat exchanger pressure drop information under oscillating flow conditions is described. This oscillating flow rig is based on a variable stroke and variable frequency linear drive motor. A frequency capability of 120 hertz and a mean test pressure up to 15 mPA (2200 psi) allows for testing at flow conditions found in modern high specific power Stirling engines. An important design feature of this rig is that it utilizes a single close coupled dynamic pressure transducer to measure the pressure drop across the test sample. This eliminates instrumentation difficulties associated with the pressure sensing lines common to differential pressure transducers. Another feature of the rig is that it utilizes a single displacement piston. This allows for testing of different sample lengths and configurations without hardware modifications. All data acquisition and reduction for the rig is performed with a dedicated personal computer. Thus the overall system design efficiently integrates the testing and data reduction procedures. The design methodology and details of the test rig is described. Author

N88-22934*# National Aeronautics and Space Administration. Lewis Research Center, Cleveland, OH.
THE 1988 OVERVIEW OF FREE-PISTON STIRLING TECHNOLOGY FOR SPACE POWER AT THE NASA LEWIS RESEARCH CENTER
 JACK G. SLABY 1988 11 p Prepared for presentation at the 4th International Conference on Stirling Engines, Tokyo, Japan, 7-10 Nov. 1988; sponsored by the Japan Society of Mechanical

Engineers
 (NASA-TM-100795; E-3971; NAS 1.15:100795) Avail: NTIS HC A03/MF A01 CSCL 10B

The completion of the Space Power Demonstrator Engine (SPDE) testing is discussed, terminating with the generation of 25 kW of engine power from a dynamically-balanced opposed-piston Stirling engine at a temperature ratio of 2.0. Engine efficiency was greater than 22 percent. The SPDE recently was divided into 2 separate single cylinder engines, Space Power Research Engine (SPRE), that serves as test beds for the evaluation of key technology disciplines, which include hydrodynamic gas bearings, high efficiency linear alternators, space qualified heat pipe heat exchangers, oscillating flow code validation, and engine loss understanding. The success of the SPDE at 650 K has resulted in a more ambitious Stirling endeavor, the design, fabrication, test, and evaluation of a designed-for-space 25 kW per cylinder Stirling Space Engine (SSE) to operate at a hot metal temperature of 1050 K using superalloy materials. This design is a low temperature confirmation of the 1300 K design. It is the 1300 K free-piston Stirling power conversion system that is the ultimate goal. The first two phases of this program, the 650 K SPDE and the 1050 K SSE are emphasized. Author

N88-22935*# National Aeronautics and Space Administration. Lewis Research Center, Cleveland, OH.
AN INTEGRATED AND MODULAR DIGITAL MODELING APPROACH FOR THE SPACE STATION ELECTRICAL POWER SYSTEM DEVELOPMENT
 FRANK J. GOMBOS (Rockwell International Corp., Canoga Park, Calif.) and NARAYAN DRAVID 1988 9 p Presented at the 23rd Intersociety Energy Conversion Engineering Conference, Denver, Colo., 31 Jul. - 5 Aug. 1988; sponsored in part by ASME, AIAA, ANS, SAE, IEEE, ACS, and AIChE
 (NASA-TM-100904; E-4155; NAS 1.15:100904) Avail: NTIS HC A02/MF A01 CSCL 10B

An electrical power system for the Space Station was designed, developed and built. This system provides for electrical power generation, conditioning, storage, and distribution. The initial configuration uses photovoltaic power generation. The power system control is based on a hierarchical architecture to support the requirements of automation. In the preliminary design and technology development phase of the program, various modeling techniques and software tools were evaluated for the purpose of meeting the Space Station power system modeling requirements. Rocketdyne and LeRC jointly selected the EASY5 simulation software, developed by Boeing Computer Services, as a system level modeling tool. The application of the selected analytical modeling approach to represent the entire power system is described. Typical results of model predictions are also summarized. The equipment modeled includes solar arrays, dc to ac converters, resonant inverters, battery storage system, alternator, transmission line, switch gear, and system level microprocessor controls. During the advanced development phase of this program, several models were developed using this approach. Author

N88-22939*# National Aeronautics and Space Administration. Lewis Research Center, Cleveland, OH.
THE APPLICATION OF HIGH TEMPERATURE SUPERCONDUCTORS TO SPACE ELECTRICAL POWER DISTRIBUTION COMPONENTS
 PAUL R. ARON and IRA T. MYERS 1988 8 p Proposed for presentation at the 23rd Intersociety Energy Conversion Engineering Conference, 31 Jul. - 5 Aug. 1988; sponsored by ASME, AIAA, ANS, SAE, IEEE, ACS and AIChE
 (NASA-TM-100901; E-4153; NAS 1.15:100901) Avail: NTIS HC A02/MF A01 CSCL 10B

Some important space based electrical power distribution systems and components are examined to determine what might be achieved with the introduction of high temperature superconductors (HTS). Components that are compared in a before and after fashion include transformers, transmission lines, and capacitors. It is concluded that HTS has its greatest effect on the

20 SPACECRAFT PROPULSION AND POWER

weight associated with transmission lines, where the weight penalty could be reduced by as much as 130 kg/kW/km of cable. Transformers, because 28 percent of their mass is in the conductor, are reduced in weight by the same factor. Capacitors are helped the least with only negligible savings possible. Finally, because HTS can relax the requirement to use alternating current in order to reduce conductor mass, it will be possible to generate significant savings by eliminating most transformers and capacitors. J.P.B.

N88-23829*# National Aeronautics and Space Administration. Lewis Research Center, Cleveland, OH.

A CYCLIC GROUND TEST OF AN ION AUXILIARY PROPULSION SYSTEM: DESCRIPTION AND OPERATIONAL CONSIDERATIONS

JERRI S. LING and EDWARD H. KRAMER Jun. 1988 54 p (NASA-TM-100870; E-3251; NAS 1.15:100870) Avail: NTIS HC A04/MF A01 CSCL 21H

The Ion Auxiliary Propulsion System (IAPS) experiment is designed for launch on an Air Force Space Test Program satellite (NASA-TM-78859; AIAA Paper No. 78-647). The primary objective of the experiment is to flight qualify the 8 cm mercury ion thruster system for stationkeeping applications. Secondary objectives are measuring the interactions between operating ion thruster systems and host spacecraft, and confirming the design performance of the thruster systems. Two complete 8 cm mercury ion thruster subsystems will be flown. One of these will be operated for 2557 on and off cycles and 7057 hours at full thrust. Tests are currently under way in support of the IAPS flight experiment. In this test an IAPS thruster is being operated through a series of startup/run/shut-down cycles which simulate thruster operation during the planned flight experiment. A test facility description and operational considerations of this testing using an engineering model 8 cm thruster (S/N 905) is the subject of this paper. Final results will be published at a later date when the ground test has been concluded. Author

N88-23830*# Rocket Research Corp., Redmond, WA.
ARCJET THRUSTER RESEARCH AND TECHNOLOGY, PHASE 1 Final Report

STEVEN C. KNOWLES 30 Sep. 1987 145 p (Contract NAS3-24631) (NASA-CR-182107; NAS 1.26:182107; REPT-87-R-1175) Avail: NTIS HC A07/MF A01 CSCL 21H

The objectives of Phase 1 were to evaluate analytically and experimentally the operation, performance, and lifetime of arcjet thrusters operating between 0.5 and 3.0 kW with catalytically decomposed hydrazine (N₂H₄) and to begin development of the requisite power control unit (PCU) technology. Fundamental analyses were performed of the arcjet nozzle, the gas kinetic reaction effects, the thermal environment, and the arc stabilizing vortex. The VNAP2 flow code was used to analyze arcjet nozzle performance with non-uniform entrance profiles. Viscous losses become dominant beyond expansion ratios of 50:1 because of the low Reynolds numbers. A survey of vortex phenomena and analysis techniques identified viscous dissipation and vortex breakdown as two flow instabilities that could affect arcjet operation. The gas kinetics code CREK1D was used to study the gas kinetics of high temperature N₂H₄ decomposition products. The arc/gas energy transfer is a non-equilibrium process because of the reaction rate constants and the short gas residence times. A thermal analysis code was used to guide design work and to provide a means to back out power losses at the anode fall based on test thermocouple data. The low flow rate and large thermal masses made optimization of a regenerative heating scheme unnecessary. Author

N88-24295*# National Aeronautics and Space Administration. Lewis Research Center, Cleveland, OH.

HIGH POWER ION THRUSTER PERFORMANCE

VINCENT K. RAWLIN and MICHAEL J. PATTERSON /in New Mexico Univ., Transactions of the Fourth Symposium on Space Nuclear Power Systems p 173-176 1987 Previously announced

as N88-12542

Avail: NTIS HC A22/MF A01 CSCL 21H

The ion thruster is one of several forms of space electric propulsion being considered for use on future SP-100 based missions. One possible major mission ground rule is the use of single Space Shuttle launch. Thus, the mass in orbit at the reactor activation altitude would be limited by the Shuttle mass constraints. When the spacecraft subsystem masses are subtracted from this available mass limit, a maximum propellant mass may be calculated. Knowing the characteristics of each type of electric thruster allow maximum values of total impulse, mission velocity increment, and thrusting time to be calculated. Because ion thrusters easily operate at high values of efficiency (60 to 70 percent) and specific impulse (3000 to 5000 sec), they can impart large values of total impulse to a spacecraft. They also can be operated with separate control of the propellant flow rate and exhaust velocity. Values are presented of demonstrated and projected performance of high power ion thrusters used in an analysis of electric propulsion for an SP-100 based mission. Author

N88-24296*# National Aeronautics and Space Administration. Lewis Research Center, Cleveland, OH.

ELECTRIC PROPULSION OPTIONS FOR THE SP-100 REFERENCE MISSION

TERRY L. HARDY, VINCENT K. RAWLIN, and MICHAEL J. PATTERSON /in New Mexico Univ., Transactions of the Fourth Symposium on Space Nuclear Power Systems p 177-180 1987 Avail: NTIS HC A22/MF A01 CSCL 21H

A study was conducted to compare resistojets, arcjet and ion thruster systems for use as an active load on a flight demonstration of the SP-100 nuclear power system. The dry masses of each propulsion system were calculated and assessments were made of the mission capabilities of each system based on the capabilities of a single Shuttle launch. From the analyses it was found that, for most systems, the dry mass accounted for less than 20 percent of the total propulsion system mass. The maximum velocity increments of the systems were up to 2300 m/s for resistojets, 4500 m/s for arcjet, and 24000 m/s for ion. The maximum thrusting times were up to 16 days for resistojets, 53 days for arcjet, and 853 days for ion thruster systems. Author

N88-24351*# National Aeronautics and Space Administration. Lewis Research Center, Cleveland, OH.

ANALYSIS OF CLOSED CYCLE MEGAWATT CLASS SPACE POWER SYSTEMS WITH NUCLEAR REACTOR HEAT SOURCES

A. J. JUHASZ and B. I. JONES /in New Mexico Univ., Transactions of the Fourth Symposium on Space Nuclear Power Systems p 423-426 1987 Avail: NTIS HC A22/MF A01 CSCL 21H

The analysis and integration studies of multimewatt nuclear power conversion systems for potential SDI applications is presented. A study is summarized which considered 3 separate types of power conversion systems for steady state power generation with a duty requirement of 1 yr at full power. The systems considered are based on the following conversion cycles: direct and indirect Brayton gas turbine, direct and indirect liquid metal Rankine, and in core thermionic. A complete mass analysis was performed for each system at power levels ranging from 1 to 25 MWe for both heat pipe and liquid droplet radiator options. In the modeling of common subsystems, reactor and shield calculations were based on multiparameter correlation and an in-house analysis for the heat rejection and other subsystems. Author

N88-24388*# National Aeronautics and Space Administration. Lewis Research Center, Cleveland, OH.

ELECTROMAGNETIC POWERED VEHICLES (EMPV) FOR MARS EXPLORATION

JOSE L. CHRISTIAN, JR. and IRA T. MYERS /in New Mexico Univ., Transactions of the Fifth Symposium on Space Nuclear Power Systems p 67-70 1988 Avail: NTIS HC A99/MF A01 CSCL 21H

Special attention has been given to manned missions to the Moon and Mars not only for exploration, but to establish permanent manned outposts. In order to fulfill such ambitious plans, it is necessary to establish technology bases in the areas of transportation, robotics, life support, and power generation. In the latter area, major progress has been made in solar dynamics, photovoltaics, heat cycle engines, thermionics, and nuclear space power generation. At the level of the present technology, massive structures are required for power generation, cooling, and shielding. The great mass of these systems will hinder a manned mission from obtaining a reasonable mobility over a planetary surface. For planetary exploration, small wheeled vehicles driven by batteries or fuel cells have been proposed, although other types such as solar or nuclear powered could potentially be used. Author

N88-24443* National Aeronautics and Space Administration. Lewis Research Center, Cleveland, OH.

STATUS OF HIGH POWER ELECTRIC PROPULSION TECHNOLOGY

DAVID C. BYERS and JAMES R. STONE In New Mexico Univ., Transactions of the Fifth Symposium on Space Nuclear Power Systems p 337-340 1988
 Avail: NTIS HC A99/MF A01 CSCL 21F

The growing emphasis on very challenging missions and the anticipated availability of high power levels in space have led to renewed interest in high power electric propulsion. The status of high power electric propulsion technology and its applicability to various missions are reviewed. The major thruster and system technology issues are identified which must be addressed in a focussed program in order to assure technology readiness for these missions. Author

N88-24682* National Aeronautics and Space Administration. Lewis Research Center, Cleveland, OH.

EVALUATION OF THE COMMUNICATIONS IMPACT OF A LOW POWER ARCJET THRUSTER

LYNNETTE M. CARNEY 1988 26 p Presented at the 24th Joint Propulsion Conference, Boston, Mass., 11-13 Jul. 1988; sponsored by AIAA, ASME, SAE and ASEE (NASA-TM-100926; E-4179; NAS 1.15:100926; AIAA-88-3105)
 Avail: NTIS HC A03/MF A01 CSCL 21H

The interaction of a 1 kW arcjet thruster plume with a communications signal is evaluated. A two-parameter, source flow equation has been used to represent the far flow field distribution of the arcjet plume in a realistic spacecraft configuration. Modelling the plume as a plasma slab, the interaction of the plume with a 4 GHz communications signal is then evaluated in terms of signal attenuation and phase shift between transmitting and receiving antennas. Except for propagation paths which pass very near the arcjet source, the impacts to transmission appear to be negligible. The dominant signal loss mechanism is refraction of the beam rather than absorption losses due to collisions. However, significant reflection of the signal at the sharp vacuum-plasma boundary may also occur for propagation paths which pass near the source. Author

N88-24686* National Aeronautics and Space Administration. Lewis Research Center, Cleveland, OH.

THERMODYNAMIC MODELING OF THE NO-VENT FILL METHODOLOGY FOR TRANSFERRING CRYOGENS IN LOW GRAVITY

DAVID J. CHATO 1988 10 p Prepared for presentation at the 24th Joint Propulsion Conference, Boston, Mass., 11-13 Jul. 1988; sponsored in part by AIAA, ASME, SAE, and ASEE (NASA-TM-100932; E-4206; NAS 1.15:100932; AIAA-88-3403)
 Avail: NTIS HC A02/MF A01 CSCL 21H

The filling of tanks with cryogenics in the low-gravity environment of space poses many technical challenges. Chief among these is the inability to vent only vapor from the tank as the filling proceeds. As a potential solution to this problem, the NASA Lewis Research Center is researching a technique known as No-Vent Fill. This technology potentially has broad application. The focus is the fueling of space based Orbital Transfer Vehicles. The fundamental

thermodynamics of the No-Vent Fill process to develop an analytical model of No-Vent Fill is described. The model is then used to conduct a parametric investigation of the key parameters: initial tank wall temperature, liquid-vapor interface heat transfer rate, liquid inflow rate, and inflowing liquid temperatures. Liquid inflowing temperature and the liquid-vapor interface heat transfer rate seem to be the most significant since they influence the entire fill process. The initial tank wall temperature must be sufficiently low to prevent a rapid pressure rise during the initial liquid flashing stage, but then becomes less significant. Author

N88-24687* National Aeronautics and Space Administration. Lewis Research Center, Cleveland, OH.

AN EXTENDED LIFE AND PERFORMANCE TEST OF A LOW-POWER ARCJET

FRANCIS M. CURRAN and THOMAS W. HAAG 1988 23 p Presented at the 24th Joint Propulsion Conference, Boston, Mass., 11-13 Jul. 1988; sponsored by AIAA, ASME, SAE and ASEE (NASA-TM-100942; E-4230; NAS 1.15:100942; AIAA-88-3106)
 Avail: NTIS HC A03/MF A01 CSCL 21C

An automated, cyclic life test was performed to demonstrate the reliability and endurance of a low power dc cycle arcjet thruster. Over 1000 hr and 500 on-off cycles were accumulated which would represent the requirements for about 15 years of on-orbit lifetime. A hydrogen/nitrogen propellant mixture was used to simulate decomposed hydrazine propellant and the power level was nominally 1.2 kW after the burn-in period. The arcjet operated in a very repeatable fashion from cycle to cycle. The steady state voltage increased by approximately 6 V over the first 300 hr, and then by only 3 V through the remainder of the test. Thrust measurements taken before, during, and after the test verified that the thruster performed in a consistent fashion throughout the tests at a specific impulse of 450 to 460 sec. Post-test component evaluation revealed limited erosion on both the anode and cathode. Other thruster components, including graphite seals, appeared undamaged. Author

N88-24688* National Aeronautics and Space Administration. Lewis Research Center, Cleveland, OH.

INTERNAL EROSION RATES OF A 10-KW XENON ION THRUSTER

VINCENT K. RAWLIN 1988 30 p Presented at the 24th Joint Propulsion Conference, Boston, Mass., 11-23 Jul. 1988; sponsored in part by AIAA, ASME, SAE, and ASEE (NASA-TM-100954; E-4228; NAS 1.15:100954; AIAA-88-2912)
 Avail: NTIS HC A03/MF A01 CSCL 21C

A 30 cm diameter divergent magnetic field ion thruster, developed for mercury operation at 2.7 kW, was modified and operated with xenon propellant at a power level of 10 kW for 567 h to evaluate thruster performance and lifetime. The major differences between this thruster and its baseline configuration were elimination of the three mercury vaporizers, use of a main discharge cathode with a larger orifice, reduction in discharge baffle diameter, and use of an ion accelerating system with larger acceleration grid holes. Grid thickness measurement uncertainties, combined with estimates of the effects of reactive residual facility background gases gave a minimum screen grid lifetime of 7000 h. Discharge cathode orifice erosion rates were measured with three different cathodes with different initial orifice diameters. Three potential problems were identified during the wear test: the upstream side of the discharge baffle eroded at an unacceptable rate; two of the main cathode tubes experienced oxidation, deformation, and failure; and the accelerator grid impingement current was more than an order of magnitude higher than that of the baseline mercury thruster. The charge exchange ion erosion was not quantified in this test. There were no measurable changes in the accelerator grid thickness or the accelerator grid hole diameters. Author

N88-24689* National Aeronautics and Space Administration. Lewis Research Center, Cleveland, OH.

CATALYTIC IGNITION OF HYDROGEN AND OXYGEN PROPELLANTS

20 SPACECRAFT PROPULSION AND POWER

ROBERT L. ZURAWSKI and JAMES M. GREEN (Sverdrup Technology, Inc., Arnold Air Force Station, Tenn.) 1988 20 p Presented at the 24th Joint Propulsion Conference, Boston, Mass., 11-13 Jul. 1988; sponsored in part by AIAA, ASME, SAE, and ASEE (NASA-TM-100957; E-4104; NAS 1.15:100957; AIAA-88-3300) Avail: NTIS HC A03/MF A01 CSCL 21B

An experimental program was conducted to evaluate the catalytic ignition of gaseous hydrogen and oxygen propellants. Shell 405 granular catalyst and a monolithic sponge catalyst were tested. Mixture ratio, mass flow rate, propellant temperature, and back pressure were varied parametrically in testing to determine the operational limits of the catalytic igniter. The test results show that the gaseous hydrogen and oxygen propellant combination can be ignited catalytically using Shell 405 catalyst over a wide range of mixture ratios, mass flow rates, and propellant injection temperatures. These operating conditions must be optimized to ensure reliable ignition for an extended period of time. A cyclic life of nearly 2000, 2 sec pulses at nominal operating conditions was demonstrated with the catalytic igniter. The results of the experimental program and the established operational limits for a catalytic igniter using the Shell 405 catalyst are presented.

Author

N88-24690*# National Aeronautics and Space Administration. Lewis Research Center, Cleveland, OH.

THRUST CHAMBER THERMAL BARRIER COATING TECHNIQUES

RICHARD J. QUENTMEYER 1988 19 p Prepared for presentation at the 72nd Specialists' Meeting of the Propulsion and Energetics Panel, Bath, England, 3-5 Oct. 1988; sponsored by AGARD (NASA-TM-100933; E-4204; NAS 1.15:100933) Avail: NTIS HC A03/MF A01 CSCL 21H

Methods for applying thermal barrier coatings to the hot-gas side wall of rocket thrust chambers in order to significantly reduce the heat transfer in high heat flux regions was the focus of technology efforts for many years. This paper describes a successful technique developed by the Lewis Research Center that starts with the coating of a mandrel and then builds the thrust chamber around it by electroforming appropriate materials. This results in a smooth coating with exceptional adherence, demonstrated in hot fire rig tests. The low cycle fatigue life of chambers with coatings applied in this manner was increased dramatically compared to uncoated chambers.

Author

N88-25474*# Minnesota Mining and Mfg. Co., Saint Paul. **DESIGN AND DEMONSTRATION OF A SYSTEM FOR THE DEPOSITION OF ATOMIC-OXYGEN DURABLE COATINGS FOR REFLECTIVE SOLAR DYNAMIC POWER SYSTEM CONCENTRATORS Final Contractor Report**

DONALD J. MCCLURE Jul. 1988 68 p (Contract NAS3-25075) (NASA-CR-4158; E-4150; NAS 1.26:4158) Avail: NTIS HC A04/MF A01 CSCL 22B

A system for the vacuum deposition of atomic-oxygen durable coatings for reflective solar dynamic power systems (SDPS) concentrators was designed and demonstrated. The design issues pertinent to SDPS were developed by the Government Aerospace Systems Division of the Harris Corporation and are described in NASA-CR-179489. Both design and demonstration phases have been completed. At the time of this report the deposition system was ready for coating of facets for SDPS concentrators. The materials issue relevant to the coating work were not entirely resolved. These issues can only be resolved when substrates which are comparable to those which will be used in flight hardware are available. The substrates available during the contract period were deficient in the areas of surface roughness and contamination. These issues are discussed more thoroughly in the body of the report.

Author

N88-25475*# National Aeronautics and Space Administration. Lewis Research Center, Cleveland, OH.

THERMAL DISTORTION ANALYSIS OF THE SPACE STATION SOLAR DYNAMIC CONCENTRATOR

JEFFREY J. TRUDELL, VITHAL DALSANIA, JOSEPH F. BAUMEISTER (Analex Corp., Cleveland, Ohio.), and KENT S. JEFFERIES 1988 25 p Presented at the 23rd Intersociety Energy Conversion Engineering Conference, Denver, Colo., 31 Jul. - 5 Aug. 1988; sponsored by ASME, AIAA, SAE, ANS, IEEE, ASC and AIChE (NASA-TM-100868; E-4090; NAS 1.15:100868) Avail: NTIS HC A03/MF A01 CSCL 10B

A method was developed to evaluate the thermal distortion of the Space Station Solar Dynamic Concentrator and the effects of thermal distortion on concentrator optical performance. The analytical method includes generating temperature distributions with TRASYS and SINDA models, interfacing the SINDA results with the SINDA-NASTRAN Interface Program (SNIP), calculating thermal distortion with a NASTRAN/PATRAN finite element model, and providing flux distribution maps within the receiver with the ray tracing OFFSET program. Temperature distributions, thermally induced slope errors, and flux distribution maps within the receiver are discussed. Results during a typical orbit indicate that temperatures of the hexagonal panels and triangular facets range between -18 and 99 C (-1 to 210 F), facet rotations are less than 0.2 mrad, and a change in facet radius due to thermal flattening is less than 5 percent. The predicted power loss with thermal distortion effects was less than 0.3 percent. The thermal distortion of the Solar Dynamic concentrator has negligible effect on the flux distribution within the receiver cavity.

Author

N88-25476*# National Aeronautics and Space Administration. Lewis Research Center, Cleveland, OH.

COMPONENT IMPROVEMENT OF FREE-PISTON STIRLING ENGINE KEY TECHNOLOGY FOR SPACE POWER

DONALD L. ALGER 1988 13 p Prepared for presentation at the 4th International Conference on Stirling Engines, Tokyo, Japan, 7-10 Nov. 1988; sponsored by Japan Society of Mechanical Engineers (NASA-TM-100950; E-4243; NAS 1.15:100950) Avail: NTIS HC A03/MF A01 CSCL 10B

The successful performance of the 25 kW Space Power Demonstrator (SPD) engine during an extensive testing period has provided a baseline of free piston Stirling engine technology from which future space Stirling engines may evolve. Much of the success of the engine was due to the initial careful selection of engine materials, fabrication and joining processes, and inspection procedures. Resolution of the few SPD engine problem areas that did occur has resulted in the technological advancement of certain key free piston Stirling engine components. Derivation of two half-SPD, single piston engines from the axially opposed piston SPD engine, designated as Space Power Research (SPR) engines, has made possible the continued improvement of these engine components. The two SPR engines serve as test bed engines for testing of engine components. Some important fabrication and joining processes are reviewed. Also, some component deficiencies that were discovered during SPD engine testing are described and approaches that were taken to correct these deficiencies are discussed. Potential component design modifications, based upon the SPD and SPR engine testing, are also reported.

Author

N88-25477*# National Aeronautics and Space Administration. Lewis Research Center, Cleveland, OH.

MOVING BELT RADIATOR DEVELOPMENT STATUS

K. ALAN WHITE Jul. 1988 24 p Presented at the 23rd Intersociety Energy Conversion Engineering Conference, Denver, Colo., 31 Jul. - 5 Aug. 1988; sponsored in part by ASME, AIAA, ANS, SAE, IEEE, ACS and AIChE (NASA-TM-100909; E-4140; NAS 1.15:100909) Avail: NTIS HC A03/MF A01 CSCL 22A

Development of the Moving Belt Radiator (MBR) as an advanced space radiator concept is discussed. The relative merits of Solid Belt (SBR), Liquid Belt (LBR), and Hybrid Belt (HBR)

Radiators are described. Analytical and experimental efforts related to the dynamics of a rotating belt in microgravity are reviewed. The development of methods for transferring heat to the moving belt is discussed, and the results from several experimental investigations are summarized. Limited efforts related to the belt deployment and stowage, and to fabrication of a hybrid belt, are also discussed. Life limiting factors such as seal wear and micrometeoroid resistance are identified. The results from various MBR point design studies for several power levels are compared with advanced Heat Pipe Radiator technology. MBR designs are shown to compare favorably at both 300 and 1000 K temperature levels. However, additional effort will be required to resolve critical technology issues and to demonstrate the advantage of MBR systems. Author

N88-25580* National Aeronautics and Space Administration. Lewis Research Center, Cleveland, OH.
A DETAILED DESCRIPTION OF THE UNCERTAINTY ANALYSIS FOR HIGH AREA RATIO ROCKET NOZZLE TESTS AT THE NASA LEWIS RESEARCH CENTER
 KENNETH J. DAVIDIAN, RONALD H. DIECK (Pratt and Whitney Aircraft, West Palm Beach, Fla.), and ISAAC CHUANG In Johns Hopkins Univ., The 24th JANNAF Combustion Meeting, Volume 2 p 291-318 Oct. 1987 Previously announced as N87-28602
 Avail: NTIS HC A17/MF A01 CSCL 21H

A preliminary uncertainty analysis was performed for the High Area Ratio Rocket Nozzle test program which took place at the altitude test capsule of the Rocket Engine Test Facility at the NASA Lewis Research Center. Results from the study establish the uncertainty of measured and calculated parameters required for the calculation of rocket engine specific impulse. A generalized description of the uncertainty methodology used is provided. Specific equations and a detailed description of the analysis is presented. Verification of the uncertainty analysis model was performed by comparison with results from the experimental program's data reduction code. Final results include an uncertainty for specific impulse of 1.30 percent. The largest contributors to this uncertainty were calibration errors from the test capsule pressure and thrust measurement devices. Author

N88-26401* National Aeronautics and Space Administration. Lewis Research Center, Cleveland, OH.
A REUSABLE ROCKET ENGINE INTELLIGENT CONTROL
 WALTER C. MERRILL and CARL F. LORENZO Jul. 1988 11 p
 Presented at the 24th Joint Propulsion Conference, Boston, Mass., 11-13 Jul. 1988; sponsored in part by AIAA, ASME, SAE, and ASEE
 (NASA-TM-100963; E-4256; NAS 1.15:100963; AIAA-88-3114)
 Avail: NTIS HC A03/MF A01 CSCL 21H

An intelligent control system for reusable space propulsion systems for future launch vehicles is described. The system description includes a framework for the design. The framework consists of an execution level with high-speed control and diagnostics, and a coordination level which marries expert system concepts with traditional control. A comparison is made between air breathing and rocket engine control concepts to assess the relative levels of development and to determine the applicability of air breathing control concepts to future reusable rocket engine systems. Author

N88-26402* National Aeronautics and Space Administration. Lewis Research Center, Cleveland, OH.
ADVANCED PHOTOVOLTAIC POWER SYSTEM TECHNOLOGY FOR LUNAR BASE APPLICATIONS
 DAVID J. BRINKER and DENNIS J. FLOOD 1988 10 p
 Presented at the Lunar Bases and Space Activities in the 21st Century Symposium, Houston, Tex., 5-7 Apr. 1988; sponsored by NASA, AIAA, Lunar and Planetary Inst., American Geophysical Unions, ANS, ASCE, Space Studies Inst. and National Space Society
 (NASA-TM-100965; E-4258; NAS 1.15:100965) Avail: NTIS HC A02/MF A01 CSCL 21H

Advanced photovoltaic/electrochemical (batteries or re-

generative fuel cells for storage) power system options for a lunar base are discussed and compared. Estimated system masses are compared with those projected for the SP-100 nuclear system. The results of the comparison are quantified in terms of the mass saved in a scenario which assembles the initial base elements in Low Earth Orbit (LEO) and launches from there to the lunar surface. A brief summary is given of advances in photo-voltaic/electrochemical power system technologies currently under development in the NASA/OAST program. A description of the planned focussed technology program for surface power in the new Pathfinder initiative is also provided. Author

N88-28087* Nielsen Engineering and Research, Inc., Mountain View, CA.
INVESTIGATION OF THE VALIDITY OF REYNOLDS AVERAGED TURBULENCE MODELS AT THE FREQUENCIES THAT OCCUR IN TURBOMACHINERY Final Contractor Report
 GARY D. KUHN Jul. 1988 114 p
 (Contract NAS3-24618; AFOSR-ISSA-86-0030)
 (NASA-CR-182162; NAS 1.26:182162; NEAR-TR-381) Avail:
 NTIS HC A06/MF A01 CSCL 09B

Turbulent flows subjected to various kinds of unsteady disturbances were simulated using a large-eddy-simulation computer code for flow in a channel. The disturbances were: a normal velocity expressed as a traveling wave on one wall of the channel; staggered blowing and suction distributions on the opposite walls of the channel; and oscillations of the mean flow through the channel. The wall boundary conditions were designed to simulate the effects of wakes of a stator stage passing through a rotor channel in a turbine. The oscillating flow simulated the effects of a pressure pulse moving over the rotor blade boundary layer. The objective of the simulations was to provide better understanding of the effects of time-dependent disturbances on the turbulence of a boundary layer and of the underlying physical phenomena regarding the basic interaction between the turbulence and external disturbances of the type found in turbomachinery. Results showed that turbulence is sensitive to certain ranges of frequencies of disturbances. However, no direct connection was found between the frequency of imposed disturbances and characteristic burst frequency of turbulence. New insight into the nature of turbulence at high frequencies was found. The viscous phenomena near solid walls was found to be the dominant influence for high frequency perturbations. At high frequencies, the turbulence was found to be undisturbed, remaining the same as for the steady mean flow. A transition range exists between the high frequency range and the low, or quasi-steady, range in which the turbulence is not predictable by either quasi-steady models or the steady flow model. The limiting lowest frequency for use of the steady flow turbulence model is that for which the viscous Stokes layer based on the blade passing frequency is thicker than the laminar sublayer. Author

N88-28088* National Aeronautics and Space Administration. Lewis Research Center, Cleveland, OH.
PERFORMANCE OF 10-KW CLASS XENON ION THRUSTERS
 MICHAEL J. PATTERSON and VINCENT K. RAWLIN 1988 30 p
 Presented at the 24th Joint Propulsion Conference, Boston, Mass., 11-13 Jul. 1988; AIAA, ASME, SAE and ASEE
 (NASA-TM-101292; E-4272; NAS 1.15:101292; AIAA-88-2914)
 Avail: NTIS HC A03/MF A01 CSCL 21C

Presented are performance data for laboratory and engineering model 30 cm-diameter ion thrusters operated with xenon propellant over a range of input power levels from approximately 2 to 20 kW. Also presented are preliminary performance results obtained from laboratory model 50 cm-diameter cusp- and divergent-field ion thrusters operating with both 30 cm- and 50 cm-diameter ion optics up to a 20 kW input power. These data include values of discharge chamber propellant and power efficiencies, as well as values of specific impulse, thruster efficiency, thrust and power. The operation of the 30 cm- and 50 cm-diameter ion optics are also discussed. Author

20 SPACECRAFT PROPULSION AND POWER

N88-28090*# National Aeronautics and Space Administration. Lewis Research Center, Cleveland, OH.

COMPARATIVE ANALYSIS OF THE SPACE POWER ARCHITECTURE STUDIES

RONALD J. SOVIE 1988 15 p Presented at the 23rd Intersociety Energy Conversion Engineering Conference, Denver, Colo., 31 Jul. - 5 Aug. 1988; sponsored by ASME, AIAA, ANS, SAE, IEEE, ACS and AIChE (NASA-TM-100977; E-4268; NAS 1.15:100977) Avail: NTIS HC A03/MF A01 CSCL 21H

The Strategic Defense Initiative Organization (SDIO) has recently completed the initial phase of Space Power Architecture Studies (SPAS). The initial effort consisted of three major contracted efforts and a comparative analysis performed by the SDIO Independent Evaluation Group (IEG) and the IEG Field Support Team. The purpose of the SPAS effort was to evaluate a wide range of power systems for SDIO applications using a wide range of attributes other than power-system mass and volume. Open cycle, closed cycle, and closed power system/weapon platform concepts were studied. The purpose of this paper is to summarize the salient results of these studies, identify important trends and future study needs. Author

N88-29658*# Aerojet TechSystems Co., Sacramento, CA. **ORBITAL TRANSFER VEHICLE 3000 LBF THRUST CHAMBER ASSEMBLY HOT FIRE TEST PROGRAM Interim Report** JUDY SCHNEIDER and WARREN R. HAYDEN Sep. 1988 235 p

(Contract NAS3-23772) (NASA-CR-182145; NAS 1.26:182145) Avail: NTIS HC A11/MF A01 CSCL 21H

The Aerojet Orbital Transfer Vehicle (OTV) Thrust Chamber Assembly (TCA) concept consists of a hydrogen cooled chamber, and annular injector, and an oxygen cooled centerbody. The hot fire testing of a heat sink version of the chamber with only the throat section using hydrogen cooling is documented. Hydraulic performance of the injector and cooled throat were verified by water flow testing prior to TCA assembly. The cooled throat was proof tested to 3000 psia to verify the integrity of the codeposited EF nickel-cobalt closeout. The first set of hot fire tests were conducted with a heat sink throat to obtain heat flux information. After demonstration of acceptable heat fluxes, the heat sink throat was replaced with the LH2 cooled throat section. Fourteen tests were conducted with a heat sink chamber and throat at chamber pressures of 85 to 359 psia. The injector face was modified at this time to add more face coolant flow. Ten tests were then conducted at chamber pressures of 197 to 620 psia. Actual heat fluxes at the higher chamber pressure range were 23 percent higher than the average of 10 Btu/in² predicted. Author

N88-29860*# National Aeronautics and Space Administration. Lewis Research Center, Cleveland, OH.

PERFORMANCE AND LIFETIME ASSESSMENT OF MPD ARC THRUSTER TECHNOLOGY

JAMES S. SOVEY and MARIS A. MANTENIEKS 1988 35 p Presented at the 24th Joint Propulsion Conference, Boston, Mass., 11-13 Jul. 1988; sponsored by AIAA, ASME, SAE and ASEE (NASA-TM-101293; E-4274; NAS 1.15:101293; AIAA-88-3211) Avail: NTIS HC A03/MF A01 CSCL 21H

A summary of performance and lifetime characteristics of pulsed and steady-state magnetoplasmadynamic (MPD) thrusters is presented. The technical focus is on cargo vehicle propulsion for exploration-class missions to the Moon and Mars. Relatively high MPD thruster efficiencies of 0.43 and 0.69 have been reported at about 5000 s specific impulse using hydrogen and lithium, respectively. Efficiencies of 0.10 to 0.35 in the 1000 to 4500 s specific impulse range have been obtained with other propellants (e.g., Ar, NH₃, N₂). Thermal efficiency data in excess of 0.80 at MW power levels using pulsed thrusters indicate the potential of high MPD thruster performance. Extended tests of pulsed and steady-state MPD thrusters yield total impulses at least two to three orders of magnitude below that necessary for cargo vehicle propulsion. Performance tests and diagnostics for life-limiting

mechanisms of megawatt-class thrusters will require high fidelity test stands which handle in excess of 10 kA and a vacuum facility whose operational pressure is less than 3 x 10 to the -4 torr.

Author

N88-29863*# Sundstrand Energy Systems, Rockford, IL. **STUDY OF TOLUENE STABILITY FOR AN ORGANIC RANKINE CYCLE (ORC) SPACE-BASED POWER SYSTEM Final Report** VANCE HAVENS and DANA RAGALLER Jul. 1988 292 p (Contract NAS3-24663)

(NASA-CR-180884; NAS 1.26:180884) Avail: NTIS HC A13/MF A01 CSCL 21H

The design, fabrication, assembly, and endurance operation of a dynamic test loop, built to evaluate the thermal stability of a proposed Organic Rankine Cycle (ORC) working fluid, is discussed. The test fluid, toluene, was circulated through a heater, simulated turbine, regenerator, condenser and pump to duplicate an actual ORC system. The maximum nominal fluid temperature, 750 F, was at the turbine simulator inlet. Samples of noncondensable gases and liquid toluene were taken periodically during the test. The samples were analyzed to identify the degradation products formed and the quantity of these products. From these data it was possible to determine the degradation rate of the working fluid and the generation rate of noncondensable gases. A further goal of this work was to relate the degradation observed in the dynamic operating loop to degradation obtained in isothermal capsule tests. This relationship was the basis for estimating the power loop degradation in the Space Station Organic Rankine Cycle system. Author

N88-29867*# Pratt and Whitney Aircraft, West Palm Beach, FL. Government Engine Business.

BREADBOARD RL10-2B LOW-THRUST OPERATING MODE (SECOND ITERATION) TEST REPORT Topical Report, Dec. 1987 - Jan. 1988

PAUL G. KANIC, RAYMOND B. KALDOR, and PIA M. WATKINS Aug. 1988 51 p

(Contract NAS3-25052) (NASA-CR-182160; NAS 1.26:182160; FR-20311-1) Avail: NTIS HC A04/MF A01 CSCL 21H

Cryogenic rocket engines requiring a cooling process to thermally condition the engine to operating temperature can be made more efficient if cooling propellants can be burned. Tank head idle and pumped idle modes can be used to burn propellants employed for cooling, thereby providing useful thrust. Such idle modes required the use of a heat exchanger to vaporize oxygen prior to injection into the combustion chamber. During December 1988, Pratt and Whitney conducted a series of engine hot firing demonstrating the operation of two new, previously untested oxidizer heat exchanger designs. The program was a second iteration of previous low thrust testing conducted in 1984, during which a first-generation heat exchanger design was used. Although operation was demonstrated at tank head idle and pumped idle, the engine experienced instability when propellants could not be supplied to the heat exchanger at design conditions. Author

N88-29868*# National Aeronautics and Space Administration. Lewis Research Center, Cleveland, OH.

EXPERIMENTAL EVALUATION OF RESISTOJET THRUSTER PLUME SHIELDS

LYNNETTE M. CARNEY and ALLAN B. BAILEY (Calspan Corp., Arnold AFS, Tenn.) 1988 27 p Presented at the 20th International Electric Propulsion Conference, Garmisch-Partenkirchen, Fed. Republic of Germany, 3-6 Oct. 1988; sponsored by DGLR, AIAA and JSASS (NASA-TM-101363; E-4356; NAS 1.15:101363; IEPC-88-091) Avail: NTIS HC A03/MF A01 CSCL 21H

The exhaust of an engineering model resistojet has been investigated using rotary pitot probes and a rotary quartz crystal microbalance. The resistojet operated on CO₂ propellant at a mass flow rate of 0.29 g/sec in both heated and unheated flows. Measurements of local flow angles in the near field of a conical plume shield indicated that the shield was not wholly effective in

confining the flow to the region upstream of its exit plane. However, the absolute levels of the measured mass flux into the backflow region were very low, on the order of 7×10 to the -7 power g/sqcm/sec or less. The use of a circular disk at the exit plane of the existing conical shield showed some benefit in decreasing the amount of backflow by a factor of two. Lastly, a detached shield placed upstream of the resistojet exit plane demonstrated a small degree of local shielding for the region directly behind it.

Author

N88-29869*# National Aeronautics and Space Administration. Lewis Research Center, Cleveland, OH.

THE DC POWER CONTROL FOR A LIQUID-FED RESISTOJET
ROBERT P. GRUBER 1988 12 p Prepared for presentation at the 20th International Electric Propulsion Conference, Garmisch-Partenkirchen, (Fed. Republic of Germany), 3-6 Oct. 1988; sponsored in part by DGLR, AIAA and JSASS (NASA-TM-101326; E-4337; NAS 1.15:101326; IEPC-88-045)
Avail: NTIS HC A03/MF A01 CSCL 21H

A simple breadboard power controller was designed and demonstrated for a new liquid-fed water resistojet. The 1-piece laboratory model thruster has an integrated vaporizer/superheater using a single heating element. Heater temperature was maintained at or near a preset reference value with the closed loop controller providing pulse width modulated (PWM) dc power into the thruster heater. A combined thruster, temperature readout, PWM transfer function was experimentally determined. This transfer function was used to design a proportional plus integral controller that demonstrated zero steady state error, conservative stability margins and adequate transient response to step changes in propellant flow rate, input voltage and temperature reference. Initial turn-on temperature overshoot from room temperature to a 650 C setpoint was 80 C. In addition, EMI was alleviated by reducing heater dI/dt and dV/dt using a simple diode-inductor-capacitor network. Based on limited initial tests, thruster preheat with no propellant flow was necessary to achieve stable system operation during startup. Breadboard power efficiency was 99 percent at 1 kW, and component mass was 0.4 kg excluding the power loss and mass of an input filter required for spacecraft integration. Author

N88-29872*# Sundstrand Energy Systems, Rockford, IL.
STUDY OF TOLUENE ROTARY FLUID MANAGEMENT DEVICE AND SHEAR FLOW CONDENSER PERFORMANCE FOR A SPACE-BASED ORGANIC RANKINE POWER SYSTEM Final Report

VANCE HAVENS and DANA RAGALLER Jul. 1988 103 p (Contract NAS3-24663)
(NASA-CR-180885; NAS 1.26:180885) Avail: NTIS HC A06/MF A01 CSCL 10B

Management of two-phase fluid and control of the heat transfer process in microgravity is a technical challenge that must be addressed for an orbital Organic Rankine Cycle (ORC) application. A test program was performed in 1-g that satisfactorily demonstrated the two-phase management capability of the rotating fluid management device (RFMD) and shear-flow condenser. Operational tests of the RFMD and shear flow condenser in adverse gravity orientations, confirmed that the centrifugal forces in the RFMD and the shear forces in the condenser were capable of overcoming gravity forces. In a microgravity environment, these same forces would not have to compete against gravity and would therefore be dominant. The specific test program covered the required operating range of the Space Station Solar Dynamic Rankine Cycle power system. Review of the test data verified that: fluid was pumped from the RFMD in all attitudes; subcooled states in the condenser were achieved; condensate was pushed uphill against gravity; and noncondensable gases were swept through the condenser. Author

N88-29873*# National Aeronautics and Space Administration. Lewis Research Center, Cleveland, OH.

SUCCESSFUL COMPLETION OF A CYCLIC GROUND TEST OF A MERCURY ION AUXILIARY PROPULSION SYSTEM
DAVID R. FRANCISCO, CHARLES A. LOW, JR., and JOHN L.

POWER 1988 13 p Prepared for presentation at the 20th International Electric Propulsion Conference, Garmisch-Partenkirchen, (Fed. Republic of Germany), 3-6 Oct. 1988; sponsored in part by DGLR, AIAA and JSASS (NASA-TM-101351; E-4378; NAS 1.15:101351; IEPC-88-035)
Avail: NTIS HC A03/MF A01 CSCL 21H

An engineering model Ion Auxiliary Propulsion System (IAPS) 8-cm thruster (S/N 905) has completed a life test at NASA Lewis Research Center. The mercury ion thruster successfully completed and exceeded the test goals of 2557 on/off cycles and 7057 hr of operation at full thrust. The final 1200 cycles and 3600 hr of the life test were conducted using an engineering model of the IAPS power electronics unit (PEU) and breadboard digital controller and interface unit (DCIU). This portion of the test is described in this paper with a charted history of thruster operating parameters and off-normal events. Performance and operating characteristics were constant throughout the test with only minor variations. The engineering model power electronics unit operated without malfunction; the flight software in the digital controller and interface unit was exercised and verified. Post-test inspection of the thruster revealed facility enhanced accelerator grid erosion but overall the thruster was in good condition. It was concluded that the thruster performance was not drastically degraded by time or cycles. Additional cyclic testing is currently under consideration. Author

N88-29874*# National Aeronautics and Space Administration. Lewis Research Center, Cleveland, OH.

IRIDIUM-COATED RHENIUM THRUSTERS BY CVD

JOHN T. HARDING, JOHN M. KAZAROFF, and MARSHALL A. APPEL (Jet Propulsion Lab., California Inst. of Tech., Pasadena.) 1988 12 p Presented at the 2nd International Conference on Surface Modification Technologies, Chicago, Ill., 25-29 Sep. 1988; sponsored by AIME and ASM (NASA-TM-101309; E-4304; NAS 1.15:101309) Avail: NTIS HC A03/MF A01 CSCL 21H

Operation of spacecraft thrusters at increased temperature reduces propellant requirements. Inasmuch as propellant comprises the bulk of a satellite's mass, even a small percentage reduction makes possible a significant enhancement of the mission in terms of increased payload. Because of its excellent high temperature strength, rhenium is often the structural material of choice. It can be fabricated into free-standing shapes by chemical vapor deposition (CVD) onto an expendable mandrel. What rhenium lacks is oxidation resistance, but this can be provided by a coating of iridium, also by CVD. This paper describes the process used by Ultramet to fabricate 22-N (5-lbf) and, more recently, 445-N (100-lbf) Ir/Re thrusters; characterizes the CVD-deposited materials; and summarizes the materials effects of firing these thrusters. Optimal propellant mixture ratios can be employed because the materials withstand an oxidizing environment up to the melting temperature of iridium, 2400 C (4350 F). Author

N88-29876*# Pratt and Whitney Aircraft, West Palm Beach, FL. Government Engine Business.

OXIDIZER HEAT EXCHANGER COMPONENT TEST Final Report

P. G. KANIC Sep. 1988 120 p (Contract NAS3-24738)
(NASA-CR-182159; NAS 1.26:182159; PW-FR-19602) Avail: NTIS HC A06/MF A01 CSCL 21H

The RL10-11B engine, is capable of multimode thrust operation. The engine operates at two low-thrust levels: tank head idle (THI), approximately 1 to 2 percent of full thrust; and pumped idle, 10 percent of full thrust. Operation at THI provides vehicle propellant settling thrust and efficient thermal conditioning; PI operation provides vehicle tank prepressurization and maneuver thrust for low-g deployment. Stable combustion of the RL10-11B engine during the low-thrust operating modes can be accomplished by using a heat exchanger to supply gaseous oxygen to the propellant injector. The oxidized heat exchanger (OHE) vaporizes the liquid oxygen using hydrogen as the energy source. This report summarizes the test activity and post-test data analysis for two possible heat exchangers, each of which employs a completely different design

23 CHEMISTRY AND MATERIALS (GENERAL)

philosophy. One design makes use of a low-heat transfer (PHT) approach in combination with a volume to attenuate pressure and flow oscillations. The test data showed that the LHT unit satisfied the oxygen exit quality of 0.95 or greater in both the THI and PI modes while maintaining stability. The HHT unit fulfilled all PI requirements; data for THI satisfactory operation is implied from experimental data that straddle the exact THI operating point.

Author

23

CHEMISTRY AND MATERIALS (GENERAL)

A88-11801* National Aeronautics and Space Administration. Lewis Research Center, Cleveland, OH.

SELECTION OF HIGH TEMPERATURE THERMAL ENERGY STORAGE MATERIALS FOR ADVANCED SOLAR DYNAMIC SPACE POWER SYSTEMS

DOVIE E. LACY, CAROLYN COLES-HAMILTON, and ALBERT JUHASZ (NASA, Lewis Research Center, Cleveland, OH) IN: IECEC '87; Proceedings of the Twenty-second Intersociety Energy Conversion Engineering Conference, Philadelphia, PA, Aug. 10-14, 1987. Volume 1. New York, American Institute of Aeronautics and Astronautics, 1987, p. 169-174. Previously announced in STAR as N87-22174. refs

Under the direction of NASA's Office of Aeronautics and Technology (OAST), the NASA Lewis Research Center has initiated an in-house thermal energy storage program to identify combinations of phase change thermal energy storage media for use with a Brayton and Stirling Advanced Solar Dynamic (ASD) space power system operating between 1070 and 1400 K. A study has been initiated to determine suitable combinations of thermal energy storage (TES) phase change materials (PCM) that result in the smallest and lightest weight ASD power system possible. To date the heats of fusion of several fluoride salt mixtures with melting points greater than 1025 K have been verified experimentally. The study has indicated that these salt systems produce large ASD systems because of their inherent low thermal conductivity and low density. It is desirable to have PCMs with high densities and high thermal conductivities. Therefore, alternate phase change materials based on metallic alloy systems are also being considered as possible TES candidates for future ASD space power systems.

Author

A88-28624* National Aeronautics and Space Administration. Lewis Research Center, Cleveland, OH.

IMPROVED PERFLUOROALKYL ETHER FLUID DEVELOPMENT

WILLIAM R. JONES, JR. (NASA, Lewis Research Center, Cleveland, OH), KAZIMIERA J. L. PACIOREK, JAMES H. NAKAHARA, MARK E. SMYTHE, and REINHOLD H. KRATZER (Ultrasystems, Inc., Irvine, CA) I & EC - Industrial and Engineering Chemistry Research (ISSN 0888-5885), vol. 26, no. 9, 1987, p. 1930-1935. Previously announced in STAR as N86-25474. refs

The feasibility of transforming a commercial linear perfluoroalkylether fluid into a material stable in the presence of metals and metal alloys in oxidizing atmospheres at 300 C without the loss of the desirable viscosity temperature characteristics was determined. The approach consisted of thermal oxidative treatment in the presence of catalyst to remove weak links, followed by transformation of the created functional groups into phospho-s-triazine linkages. It is found that the experimental material obtained in 66 percent yield from the commercial fluid exhibits, over an 8 hr period at 300 C in the presence of Ti(4Al, 4Mn) alloy, thermal oxidative stability better by a factor of 2.6 x 1000 based on volatiles evolved than the commercial product. The viscosity and molecular weight of the developed fluid are

unchanged and are essentially identical with the commercial material. No metal corrosion occurs with the experimental fluid at 300 C.

E.A.K.

A88-51393* National Aeronautics and Space Administration. Lewis Research Center, Cleveland, OH.

SOLAR DYNAMIC CONCENTRATOR DURABILITY IN ATOMIC OXYGEN AND MICROMETEOROID ENVIRONMENTS

DANIEL A. GULINO (NASA, Lewis Research Center, Cleveland, OH) Journal of Spacecraft and Rockets (ISSN 0022-4650), vol. 25, May-June 1988, p. 244-249. Previously cited in issue 08, p. 1062, Accession no. A87-22417. refs

A88-54350* Solar Turbines, Inc. San Diego, CA.

POROSITY DETERMINATION OF THERMAL BARRIER COATINGS

MARK VAN ROODE (Solar Turbines, Inc., San Diego, CA) and BRAD BEARDSLEY (Caterpillar, Inc., Peoria, IL) ASME, Gas Turbine and Aeroengine Congress and Exposition, Amsterdam, Netherlands, June 6-9, 1988, 8 p. refs

(Contract DEN3-332)

(ASME PAPER 88-GT-278)

Coating porosity is believed to be a critical factor for the thermal conductivity of thermal barrier coatings (TBCs). A number of different techniques have been used to determine the porosities of thermal barrier coatings for diesel applications as part of a NASA/DOE sponsored study. A comparison is made between methods based on water immersion, optical microscopy, eddy current thickness measurements, and Archimedes principle for TBC porosity determination.

Author

A88-54353* Southwest Research Inst., San Antonio, TX.

THERMAL BARRIER COATING LIFE PREDICTION MODEL DEVELOPMENT

T. A. CRUSE, S. E. STEWART (Southwest Research Institute, San Antonio, TX), and M. ORTIZ (Pratt and Whitney, East Hartford, CT) ASME, Gas Turbine and Aeroengine Congress and Exposition, Amsterdam, Netherlands, June 6-9, 1988, 8 p. Research supported by United Technologies Corp.

(Contract NAS3-23944)

(ASME PAPER 88-GT-284)

A life prediction model for correlating the spallation life of ceramic thermal barrier coatings is developed which includes both cyclic and time-dependent damage. The cyclic damage is related to the calculated cyclic inelastic strain range, while the time-dependent damage is related to the oxidation kinetics at the bond-ceramic interface. The cyclic inelastic strain range is calculated using a modified form of the Walker viscoplastic material model; calculation of the oxidation kinetics is based on traditional oxidation algorithms using experimentally determined parameters. The correlation between the actual and predicted spallation lives is within a factor of 3.

V.L.

A88-54988* National Aeronautics and Space Administration. Lewis Research Center, Cleveland, OH.

ATOMIC-OXYGEN DURABILITY OF IMPACT-DAMAGED SOLAR REFLECTORS

DANIEL A. GULINO (NASA, Lewis Research Center, Cleveland, OH) Journal of Spacecraft and Rockets (ISSN 0022-4650), vol. 25, Jan.-Feb. 1988, p. 39-44. Previously cited in issue 08, p. 1062, Accession no. A87-22417. refs

N88-12543* National Aeronautics and Space Administration. Lewis Research Center, Cleveland, OH.

SURFACE CATALYTIC DEGRADATION STUDY OF TWO LINEAR PERFLUOROPOLYALKYLETHERS AT 345 C

WILFREDO MORALES Nov. 1987 12 p
(NASA-TP-2774; E-3395; NAS 1.60:2774) Avail: NTIS HC A03/MF A01 CSCL 07A

Thin-liquid-film degradation studies of two commercially available perfluoropolyalkylether fluids (PFAE) were performed at 345 C, in nitrogen and air atmospheres, on iron and 440 C stainless steel surfaces. It was found that one fluid degraded on both iron

and 440 C stainless steel surfaces in an air atmosphere, whereas the other fluid did not degrade. Chemical analysis revealed that the test fluid degraded to lower molecular weight products and that the degradation was accompanied by the formation of a brownish deposit on both the iron and 440 C stainless steel surfaces. Surface analysis of the deposit revealed a substantial amount of iron oxide (Fe_2O_3). It was hypothesized that the fluid which degraded did so because of its acetal structure. The other fluid, lacking the acetal structure, did not degrade. Author

N88-13385* National Aeronautics and Space Administration. Lewis Research Center, Cleveland, OH.

PHASE PURITY OF NiCo_2O_4 , A CATALYST CANDIDATE FOR ELECTROLYSIS OF WATER

J. SINGER, W. L. FIELDER, R. G. GARLICK, and T. NEGAS (Trans Tech, Frederick, Md.) Dec. 1987 11 p (NASA-TM-100239; E-3754; NAS 1.15:100239) Avail: NTIS HC A03/MF A01 CSCL 07A

NiCo_2O_4 is shown to be difficult to obtain as a pure phase, and may never have been so obtained. High resolution x-ray diffractometry is required for its precise characterization. Film XRD is not likely to show the asymmetry in the spinel diffraction lines, caused by poorly crystallized NiO , as seen in diffractometer traces. The Co_3O_4 which is expected to accompany NiO as an impurity in NiCo_2O_4 syntheses has the same diffraction pattern as the binary oxide. Firings of the co-precipitated hydroxides at 300, 350, and 400 C, including one in pure O_2 , failed to produce single phase cobaltate. Scanning electron microscopy showed all the sintered products to range over several orders of magnitude in agglomerate/particle size. Surface areas by BET were all in the range 40 to 110 m^2/g , equivalent to particles of 200 to 100 Angstrom diameter. The spinel diffraction line breadths were compatible with those approximate dimensions. Author

N88-26404* National Aeronautics and Space Administration. Lewis Research Center, Cleveland, OH.

SUBSTITUTED 1,1,1-TRIARYL-2,2,2-TRIFLUOROETHANES AND PROCESSES FOR THEIR SYNTHESIS Patent

WILLIAM B. ALSTON, inventor (to NASA) and ROY F. GRATZ, inventor (to NASA) 19 Jul. 1988 12 p Filed 29 Oct. 1986 Supersedes N87-14432 (25 - 06, p 0739) Sponsored by NASA (NASA-CASE-LEW-14345-1; US-PATENT-4,758,380; US-PATENT-APPL-SN-924474; US-PATENT-CLASS-260-389; US-PATENT-CLASS-260-386; US-PATENT-CLASS-260-395; US-PATENT-CLASS-549-241) Avail: US Patent and Trademark Office CSCL 07A

Synthetic procedures are described for tetraalkyls, tetraacids and dianhydrides substituted 1,1,1-triaryl-2,2,2-trifluoroethanes which comprises: (1) 1,1-bis(dialkylaryl)-1 aryl-2,2,2-trifluoroethane; (2) 1,1-bis(dicarboxyaryl)-1 aryl-2,2,2-trifluoroethane; or (3) cyclic dianhydride or diamine of 1,1-bis(dialkylaryl)-1 aryl-2,2,2-trifluoroethanes.

Official Gazette of the U.S. Patent and Trademark Office

N88-28966* National Aeronautics and Space Administration. Lewis Research Center, Cleveland, OH.

THIN FILM COATINGS FOR SPACE ELECTRICAL POWER SYSTEM APPLICATIONS

DANIEL A. GULINO Sep. 1988 16 p Presented at the 2nd International Conference on Surface Modification Technologies, Chicago, Ill., 25-28 Sep. 1988; sponsored in part by The Metallurgical Society of AIME (NASA-TM-101325; E-4336; NAS 1.15:101325) Avail: NTIS HC A03/MF A01 CSCL 07C

This paper examines some of the ways in which thin film coatings can play a role in aerospace applications. Space systems discussed include photovoltaic and solar dynamic electric power generation systems, including applications in environmental protection, thermal energy storage, and radiator emittance enhancement. Potential applications of diamondlike films to both atmospheric and space based systems are examined. Also, potential uses of thin films of the recently discovered

high-temperature superconductive materials are discussed.

Author

24

COMPOSITE MATERIALS

Includes physical, chemical, and mechanical properties of laminates and other composite materials.

A88-12599* National Aeronautics and Space Administration. Lewis Research Center, Cleveland, OH.

SILSESQUIOXANES AS PRECURSORS TO CERAMIC COMPOSITES

F. I. HURWITZ, L. HYATT, J. GORECKI, and L. D'AMORE (NASA, Lewis Research Center, Cleveland, OH) Ceramic Engineering and Science Proceedings (ISSN 0196-6219), vol. 8, July-Aug. 1987, p. 732-743. Previously announced in STAR as N87-25432.

Silsesquioxanes having the general structure $\text{RSiO}(1.5)$, where R = methyl, propyl, or phenyl, melt flow at 70 to 100 C. Above 100 C, free OH groups condense. At 225 C further crosslinking occurs, and the materials form thermosets. Pyrolysis, with accompanying loss of volatiles, takes place at nominally 525 C. At higher temperatures, the R group serves as an internal carbon source for carbo-thermal reduction to SiC accompanied by the evolution of CO. By blending silsesquioxanes with varying R groups, both the melt rheology and composition of the fired ceramic can be controlled. Fibers can be spun from the melt which are stable in argon in 1400 C. The silsesquioxanes also were used as matrix precursors for Nicalon and alpha-SiC platelet reinforced composites. Author

A88-13158* National Aeronautics and Space Administration. Lewis Research Center, Cleveland, OH.

CERAMIC MATRIX AND RESIN MATRIX COMPOSITES - A COMPARISON

FRANCES I. HURWITZ (NASA, Lewis Research Center, Cleveland, OH) IN: Advanced materials technology '87; Proceedings of the Thirty-second International SAMPE Symposium and Exhibition, Anaheim, CA, Apr. 6-9, 1987. Covina, CA, Society for the Advancement of Material and Process Engineering, 1987, p. 433-443. Previously announced in STAR as N87-18615. refs

The underlying theory of continuous fiber reinforcement of ceramic matrix and resin matrix composites, their fabrication, microstructure, physical and mechanical properties are contrasted. The growing use of organometallic polymers as precursors to ceramic matrices is discussed as a means of providing low temperature processing capability without the fiber degradation encountered with more conventional ceramic processing techniques. Examples of ceramic matrix composites derived from particulate-filled, high char yield polymers and silsesquioxane precursors are provided. Author

A88-16965* National Aeronautics and Space Administration. Lewis Research Center, Cleveland, OH.

FRACTURE CHARACTERISTICS OF ANGLEPLYED LAMINATES FABRICATED FROM OVERAGED GRAPHITE/EPOXY PREPREG

CAROL A. GINTY and CHRISTOS C. CHAMIS (NASA, Lewis Research Center, Cleveland, OH) IN: Fractography of modern engineering materials: Composites and metals. Philadelphia, PA, American Society for Testing and Materials, 1987, p. 101-130. Previously announced in STAR as N86-25417. refs

A series of angleplyed graphite/epoxy laminates was fabricated from overaged prepreg and tested in tension to investigate the effects of overaged or advanced cure material on the degradation of laminate strength. Results, which include fracture stresses, indicate a severe degradation in strength. In addition, the fracture surfaces and microstructural characteristics are distinctly unlike any features observed in previous tests of this prepreg and laminate

24 COMPOSITE MATERIALS

configuration. Photographs of the surfaces and microstructures reveal flat morphologies consisting of alternate rows of fibers and hackles. These fracture surface characteristics are independent of the laminate configurations. The photomicrographs are presented and compared with data from similar studies to show the unique characteristics produced by the overage prepreg. Analytical studies produced results which agreed with those from the experimental investigations. Author

A88-29455* Purdue Univ., West Lafayette, IN.
DYNAMIC DELAMINATION FRACTURE TOUGHNESS OF A GRAPHITE/EPOXY LAMINATE UNDER IMPACT
C. T. SUN (Purdue University, West Lafayette, IN) and J. E. GRADY (NASA, Lewis Research Center, Cleveland, OH; Purdue University, West Lafayette, IN) Composites Science and Technology (ISSN 0266-3538), vol. 31, no. 1, 1988, p. 55-72. refs (Contract NAG3-211)

Dynamic delamination fracture toughness in a (90/0)5s T300/934 graphite/epoxy laminate was investigated using impact loading. Delamination cracks of three different sizes were embedded at the midplane of the composite specimen. The threshold impact velocity that causes propagation of the delamination crack was used in the dynamic analysis with the finite element method. From the finite element solution, the time-history of the strain energy release rate was calculated. The critical strain energy release rate was taken to equal the maximum value of the response history. Author

A88-31687* National Aeronautics and Space Administration. Lewis Research Center, Cleveland, OH.

SIC REINFORCED ALUMINIDE COMPOSITES
PAMELA K. BRINDLEY (NASA, Lewis Research Center, Cleveland, OH) IN: High-temperature ordered intermetallic alloys II; Proceedings of the Second Symposium, Boston, MA, Dec. 2-4, 1986. Pittsburgh, PA, Materials Research Society, 1987, p. 419-424. refs

The tensile properties of SiC fiber, Ti3Al+Nb and SiC/Ti3Al+Nb composite have been determined from 300 to 1365 K. The composite results compared favorably to rule-of-mixtures (ROM) predictions in the intermediate temperature regime of 475 to 700 K. Deviations from ROM are discussed. Composite tensile results were compared on a strength/density basis to wrought superalloys and found to be superior. Fiber-matrix compatibility was characterized for the composite at 1250 and 1365 K for 1 to 100 hours. Author

A88-31770* State Univ. of New York, Buffalo.
THERMAL CYCLING OF TUNGSTEN-FIBRE-REINFORCED SUPERALLOY COMPOSITES

ROBERT C. WETHERHOLD (New York, State University, Buffalo) and LEONARD J. WESTFALL (NASA, Lewis Research Center, Cleveland, OH) Journal of Materials Science (ISSN 0022-2461), vol. 23, Feb. 1988, p. 713-717. refs

The thermal cycling of a tungsten-fiber-reinforced superalloy (TFRS) composite is typical of its application in high-temperature engine environments. The mismatch in thermal expansion coefficients between fiber and matrix causes substantial longitudinal (0 deg) stresses in the composite, which can produce inelastic damage-producing matrix strains. The case of thermal fatigue is explored as a 'worst case' of the possible matrix damage, in comparison with specimens which are also mechanically loaded in tension. The thermally generated cyclic stresses and the attendant matrix plasticity may be estimated using a nonlinear finite-element program, by proposing a physical analog to the micromechanics equations. A damage metric for the matrix is proposed using the Coffin-Manson criterion, which metric can facilitate comparisons of damage among different candidate materials, and also comparisons for a given material subjected to different temperature cycles. An experimental program was carried out for thermal cycling of a 37 vol pct TFRS composite to different maximum temperatures. The results confirm the prediction that thermal cycling produces matrix degradation and composite strength reduction, which become more pronounced with increasing

maximum cyclic temperature. The strength of the fiber is shown to be identical for the as-fabricated and thermally cycled specimens, suggesting that the reduction in composite strength is due to the loss of matrix contribution and also to notching effects of the matrix voids on the fiber. Author

A88-35945* National Aeronautics and Space Administration. Lewis Research Center, Cleveland, OH.

MAST MATERIAL TEST PROGRAM (MAMATEP)
MICHAEL L. CIANCONE and SHARON K. RUTLEDGE (NASA, Lewis Research Center, Cleveland, OH) AIAA SDM Issues of the International Space Station, Conference, Williamsburg, VA, Apr. 21, 22, 1988. 12 p. refs (AIAA PAPER 88-2475)

The MAMATEP program, which is aimed at verifying the need for and evaluating the performance of various protection techniques for the solar array assembly mast of the Space Station photovoltaic power module, is discussed. Coated and uncoated mast material samples have been environmentally tested and evaluated, before and after testing, in terms of mass and bending modulus. The protective coatings include CV-1144 silicone, a Ni/Al/InSn eutectic, and an open-weave Al braid. Long-term plasma asher results from unprotected samples indicate that, even though fiberglass-epoxy samples degrade, a protection technique may not be necessary to ensure structural integrity. A protection technique, however, may be desirable to limit or contain the amount of debris generated by the degradation of the fiberglass-epoxy. V.L.

A88-36775* National Aeronautics and Space Administration. Lewis Research Center, Cleveland, OH.

HIGH TEMPERATURE POLYMER MATRIX COMPOSITES
TITO T. SERAFINI, ED. (NASA, Lewis Research Center, Cleveland, OH) Park Ridge, NJ, Noyes Data Corp., 1987, 429 p. Previously announced in STAR as N86-11260.

These are the proceedings of the High Temperature Polymer Matrix Composites Conference held at the NASA Lewis Research Center on March 16 to 18, 1983. The purpose of the conference is to provide scientists and engineers working in the field of high temperature polymer matrix composites an opportunity to review, exchange, and assess the latest developments in this rapidly expanding area of materials technology. Technical papers are presented in the following areas: (1) matrix development; (2) adhesive development; (3) Characterization; (4) environmental effects; and (5) applications. Author

A88-36945* Case Western Reserve Univ., Cleveland, OH.
CRACK DIFFUSION COEFFICIENT - A CANDIDATE FRACTURE TOUGHNESS PARAMETER FOR SHORT FIBER COMPOSITES

M. A. MULL, A. CHUDNOVSKY, and A. MOET (Case Western Reserve University, Cleveland, OH) IN: International Conference on Composite Materials, 6th, and European Conference on Composite Materials, 2nd, London, England, July 20-24, 1987, Proceedings. Volume 3. London and New York, Elsevier Applied Science, 1987, p. 3.337-3.345. refs (Contract NAG3-585-2)

In brittle matrix composites, crack propagation occurs along random trajectories reflecting the heterogeneous nature of the strength field. Considering the crack trajectory as a diffusive process, the 'crack diffusion coefficient' is introduced. From fatigue crack propagation experiments on a set of identical SEN polyester composite specimens, the variance of the crack tip position along the loading axis is found to be a linear function of the effective 'time'. The latter is taken as the effective crack length. The coefficient of proportionality between variance of the crack trajectory and the effective crack length defines the crack diffusion coefficient D which is found in the present study to be 0.165 mm. This parameter reflects the ability of the composite to deviate the crack from the energetically most efficient path and thus links fracture toughness to the microstructure. Author

A88-42437* National Aeronautics and Space Administration. Lewis Research Center, Cleveland, OH.

HYGROTHERMOMECHANICAL FIBER COMPOSITE FATIGUE - COMPUTATIONAL SIMULATION

C. A. GINTY and C. C. CHAMIS (NASA, Lewis Research Center, Cleveland, OH) IN: Materials - Pathway to the future; Proceedings of the Thirty-third International SAMPE Symposium and Exhibition, Anaheim, CA, Mar. 7-10, 1988. Covina, CA, Society for the Advancement of Material and Process Engineering, 1988, p. 1709-1720. refs

The technology of advanced fiber composites has matured to the point where these composites are prime contenders for various structural applications. One of the major design considerations for prolonged service of these composites is fatigue due to cyclic hygral (moisture), thermal and mechanical (hygrothermomechanical) loading conditions. Recent research activities at the Lewis Research Center have led to the development of formal procedures for predicting, using computational simulation, fatigue in fiber composites due to cyclic hygrothermomechanical loading conditions. These formal procedures have subsequently been programmed into a computer module and embedded into the Integrated Composites Analyzer (ICAN) computer code. The objective of this paper is to present and describe results obtained using the augmented ICAN computer code. Author

A88-44745*# National Aeronautics and Space Administration. Lewis Research Center, Cleveland, OH.

HIGH TEMPERATURE METAL MATRIX COMPOSITES FOR FUTURE AEROSPACE SYSTEMS

JOSEPH R. STEPHENS (NASA, Lewis Research Center, Cleveland, OH) AIAA, ASME, SAE, and ASEE, Joint Propulsion Conference, 24th, Boston, MA, July 11-13, 1988. 11 p. Previously announced in STAR as N88-10938. (AIAA PAPER 88-3059)

Research was conducted on metal matrix composites and intermetallic matrix composites to understand their behavior under anticipated future operating conditions envisioned for aerospace power and propulsion systems of the 21st century. Extremes in environmental conditions, high temperature, long operating lives, and cyclic conditions dictate that the test evaluations not only include laboratory testing, but simulated flight conditions. The various processing techniques employed to fabricate composites are discussed along with the basic research underway to understand the behavior of high temperature composites, and the relationship of this research to future aerospace systems. Author

A88-47214* National Aeronautics and Space Administration. Lewis Research Center, Cleveland, OH.

MEASUREMENT OF IMPACT-INDUCED DELAMINATION BUCKLING IN COMPOSITE LAMINATES

J. E. GRADY (NASA, Lewis Research Center, Cleveland, OH) and K. J. DEPAOLA IN: Dynamic failure; Proceedings of the 1987 SEM Fall Conference, Savannah, GA, Oct. 25-28, 1987. Bethel, CT, Society for Experimental Mechanics, Inc., 1987, p. 160-168. refs

High-velocity impact tests were performed on graphite/epoxy laminates with embedded delaminations. High-speed photography of the transversely impacted laminates shows that dynamic local buckling of the sublaminates region formed by the delamination can cause a mode-I-dominated propagation of that delamination. Simultaneous recordings of the dynamic strain histories at several locations in the buckled sublaminates region are used to measure the laminate and sublaminates responses to the impact loading. Flexural motion resulting from transverse impact is shown to reduce local buckling of the sublaminates. This buckling causes a progressive separation of the delaminated surfaces and subsequent extension of the delamination in a mode-I dominated fashion. Author

N88-10120*# National Aeronautics and Space Administration. Lewis Research Center, Cleveland, OH.

PRESSURE EFFECTS ON THE THERMAL STABILITY OF SiC FIBERS

MARTHA H. JASKOWIAK and JAMES A. DICARLO 1986 16 p Presented at the 88th Annual Meeting of the American Ceramic Society, Chicago, Ill. 27 Apr. - 1 May 1986

(NASA-TM-100146; E-3704; NAS 1.15:100146) Avail: NTIS HC A03/MF A01 CSCL 11D

Commercially available polymer derived SiC fibers were treated at temperatures from 1000 to 2200 C in vacuum and argon gas pressure of 1 and 1360 atm. Effects of gas pressure on the thermal stability of the fibers were determined through property comparison between the pressure treated fibers and vacuum treated fibers. Investigation of the thermal stability included studies of the fiber microstructure, weight loss, grain growth, and tensile strength. The 1360 atm argon gas treatment was found to shift the onset of fiber weight loss from 1200 to above 1500 C. Grain growth and tensile strength degradation were correlated with weight loss and were thus also inhibited by high pressure treatments. Additional heat treatment in 1 atm argon of the fibers initially treated at 1360 atm argon caused further weight loss and tensile strength degradation, thus indicating that high pressure inert gas conditions would be effective only in delaying fiber strength degradation. However, if the high gas pressure could be maintained throughout composite fabrication, then the composites could be processed at higher temperatures. Author

N88-10121*# National Aeronautics and Space Administration. Lewis Research Center, Cleveland, OH.

MECHANICAL PROPERTIES CHARACTERIZATION OF COMPOSITE SANDWICH MATERIALS INTENDED FOR SPACE ANTENNA APPLICATIONS

KENNETH J. BOWLES and RAYMOND D. VANNUCCI 1986 17 p Presented at Test Methods and Design Allowables for Fiber Composites: 2nd Symposium, Phoenix, Ariz., 3-4 Nov. 1986; sponsored by the American Society for Testing and Materials (NASA-TM-88893; E-3310; NAS 1.15:88893) Avail: NTIS HC A03/MF A01 CSCL 11D

The composite materials proposed for use in the Advanced Communications Technology Satellite (ACTS) Program contains a new, high modulus graphite fiber as the reinforcement. A study was conducted to measure certain mechanical properties of the new fiber-reinforced material as well as of a composite-faced aluminum honeycomb sandwich structure. Properties were measured at -157, 22, and 121 C. Complete characterization of this material was not intended. Longitudinal tensile, picture-frame shear, short-beam shear, and flexural tests were performed on specimens of the composite face-sheet materials. Unidirectional, cross-plyed, and quasi-isotropic fiber composite ply layup designs were fabricated and tested. These designs had been studied by using NASA's Integrated Composite Analyzer (ICAN) computer program. Flexural tests were conducted on (+/- 60/0 deg) sub s composite-faced sandwich structure material. Resistance strain gages were used to measure strains in the tensile, picture-frame, and sandwich flexural tests. The sandwich flexural strength was limited by the core strength at -157 and 22 C. The adhesive bond strength was the limiting factor at 121 C. Adhesive mechanical properties are reflected in sandwich structure flexural properties when the span-to-depth ratio is great enough to allow a significant shear effect on the load-deflection behavior of the sandwich beam. Most measured properties agreed satisfactorily with the properties predicted by ICAN. Author

N88-10896*# Case Western Reserve Univ., Cleveland, OH. Dept. of Physics.

DEGRADATION MECHANISMS OF MATERIALS FOR LARGE SPACE SYSTEMS IN LOW EARTH ORBIT Final Report, 6 Oct. 1982 - 5 Jan. 1985

WILLIAM L. GORDON and R. W. HOFFMAN Nov. 1987 32 p (Contract NAG3-352) (NASA-CR-181472; NAS 1.26:181472) Avail: NTIS HC A03/MF A01 CSCL 11D

24 COMPOSITE MATERIALS

Degradation was explored of various materials used in aerospace vehicles after severe loss of polymeric material coatings (Kapton) was observed on an early shuttle flight in low Earth orbit. Since atomic oxygen is the major component of the atmosphere at 300 km, and the shuttle's orbital velocity produced relative motion corresponding to approx. 5 eV of oxygen energy, it was natural to attribute much of this degradation to oxygen interaction. This assumption was tested using large volume vacuum systems and ion beam sources, in an exploratory effort to produce atomic oxygen of the appropriate energy, and to observe mass loss from various samples as well as optical radiation. Several investigations were initiated and the results of these investigations are presented in four papers. These papers are summarized. They are entitled: (1) The Space Shuttle Glow; (2) Laboratory Degradation of Kapton in a Low Energy Oxygen Ion Beam; (3) The Energy Dependence and Surface Morphology of Kapton Degradation Under Atomic Oxygen Bombardment; and (4) Surface Analysis of STS 8 Samples. Author

N88-10899*# National Aeronautics and Space Administration. Lewis Research Center, Cleveland, OH.

THE EFFECT OF BROMINATION OF CARBON FIBERS ON THE COEFFICIENT OF THERMAL EXPANSION OF GRAPHITE FIBER-EPOXY COMPOSITES

D. A. JAWORSKE and C. MACIAG (Cleveland State Univ., Ohio.) Nov. 1987 6 p
(NASA-TM-100236; E-3665-1; NAS 1.15:100236) Avail: NTIS HC A02/MF A01 CSCL 11D

To examine the effect of bromination of carbon fibers on the coefficient of thermal expansion (CTE) of carbon fiber epoxy composites, several pristine and brominated carbon fiber-epoxy composite samples were subjected to thermomechanical analysis. The CTE's of these samples were measured in the uniaxial and transverse directions. The CTE was dominated by the fibers in the uniaxial direction, while it was dominated by the matrix in the transverse directions. Bromination had no effect on the CTE of any of the composites. In addition, the CTE of fiber tow was measured in the absence of a polymer matrix, using an extension probe. The results from this technique were inconclusive. Author

N88-11758*# National Aeronautics and Space Administration. Lewis Research Center, Cleveland, OH.

TRANSPLY CRACK DENSITY DETECTION BY ACOUSTO-ULTRASONICS

JOHN H. HEMANN, KENNETH J. BOWLES, HAROLD KAUTZ, and PAUL CAVANO (Cleveland State Univ., Ohio.) 1987 10 p
Presented at Acousto-Ultrasonics: Theory and Application, Blacksburg, Va., 12-15 Jul. 1987
(NASA-TM-100224; E-3843; NAS 1.15:100224) Avail: NTIS HC A02/MF A01 CSCL 11D

The acousto-ultrasonic method was applied to a PMR-15 8-harness, satin Celion 3000 fabric composite to determine the extent of transply cracking. A six-ply 0/90 laminate was also subjected to mechanical loading, which induced transply cracking. The stress wave factor (SWF) is defined as the energy contained in the received signal from a 2.25-MHz center frequency transducer. The correlation of the SWF with transply crack density is shown. Author

N88-12551*# National Aeronautics and Space Administration. Lewis Research Center, Cleveland, OH.

FREE-EDGE DELAMINATION: LAMINATE WIDTH AND LOADING CONDITIONS EFFECTS

P. L. N. MURTHY (Cleveland State Univ., Ohio.) and C. C. CHAMIS Dec. 1987 28 p
(NASA-TM-100238; E-3862; NAS 1.15:100238) Avail: NTIS HC A03/MF A01 CSCL 11D

The width and loading conditions effects on free-edge stress fields in composite laminates are investigated using a three-dimensional finite element analysis. This analysis includes a special free-edge region refinement or superelement with progressive substructuring (mesh refinement) and finite thickness interply layers. The different loading conditions include in-plane and out-of-plane

bending, combined axial tension and in-plane shear, twisting, uniform temperature and uniform moisture. Results obtained indicate that: axial tension causes the smallest magnitude of interlaminar free edge stress compared to other loading conditions; free-edge delamination data obtained from laboratory specimens cannot be scaled to structural components; and composite structural components are not likely to delaminate. Author

N88-12552*# National Aeronautics and Space Administration. Lewis Research Center, Cleveland, OH.

COMPOSITE MECHANICS FOR ENGINE STRUCTURES

CHRISTOS C. CHAMIS 1987 35 p
Presented at the 32nd International Gas Turbine Conference and Exhibition, Anaheim, Calif., 31 May - 4 Jun. 1987; sponsored by ASME
(NASA-TM-100176; E-3750; NAS 1.15:100176) Avail: NTIS HC A03/MF A01 CSCL 11D

Recent research activities and accomplishments at Lewis Research Center on composite mechanics for engine structures are summarized. The activities focused mainly on developing procedures for the computational simulation of composite intrinsic and structural behavior. The computational simulation encompasses all aspects of composite mechanics, advanced three-dimensional finite-element methods, damage tolerance, composite structural and dynamic response, and structural tailoring and optimization. Author

N88-13409*# National Aeronautics and Space Administration. Lewis Research Center, Cleveland, OH.

FIBER COMPOSITE STRUCTURAL DURABILITY AND DAMAGE TOLERANCE: SIMPLIFIED PREDICTIVE METHODS

CHRISTOS C. CHAMIS and CAROL A. GINTY 1987 28 p
Presented at the 2nd Symposium on Composite Materials: Fatigue and Fracture, Cincinnati, Ohio, 26 Apr. - 1 May 1987; sponsored by the American Society for Testing and Materials
(NASA-TM-100179; E-3755; NAS 1.15:100179) Avail: NTIS HC A03/MF A01 CSCL 11D

Simplified predictive methods and models (theory) to evaluate fiber/polymer-matrix composite material for determining structural durability and damage tolerance are presented and described. This theory includes equations for (1) fatigue and fracture of composites without and with defects, (2) impact resistance and residual strength after impact, (3) thermal fatigue, and (4) combined stress fatigue. Several examples are included to illustrate applications of the theory and to identify significant parameters and sensitivities. Comparisons with limited experimental data are made. Author

N88-14150*# Case Western Reserve Univ., Cleveland, OH. Dept. of Material Science and Engineering.

STRESS RUPTURE BEHAVIOR OF SILICON CARBIDE COATED, LOW MODULUS CARBON/CARBON COMPOSITES

M.S. Thesis
GARY A. ROZAK and JOHN F. WALLACE Jan. 1988 98 p
(Contract NAG3-464)
(NASA-CR-180863; E-3708; NAS 1.26:180863) Avail: NTIS HC A05/MF A01 CSCL 11D

The disadvantages of carbon-carbon composites, in addition to the oxidation problem, are low thermal expansion, expensive fabrication procedures, and poor off axis properties. The background of carbon-carbon composites, their fabrication, oxidation, oxidation protection and mechanical testing in flexure are discussed. Author

N88-15018*# National Aeronautics and Space Administration. Lewis Research Center, Cleveland, OH.

IMPROVING THE INTERLAMINAR SHEAR STRENGTH OF CARBON FIBER-EPOXY COMPOSITES THROUGH CARBON FIBER BROMINATION

DONALD A. JAWORSKE and CAROLYN MACIAG (Cleveland State Univ., Ohio.) Dec. 1987 11 p
(NASA-TM-100248; E-3870; NAS 1.15:100248) Avail: NTIS HC A03/MF A01 CSCL 11D

The use of bromine to improve the interlaminar shear strength of PAN-based carbon fibers was investigated. Composite test

specimens fabricated from brominated T-300 fibers and a MY720 matrix exhibited on average a 30% improvement in ILSS over their pristine counterparts. Mass, electrical resistivity, density, contact angle, and scanning Auger microscopy results suggested a mechanism in which the bromine was covalently bonded to the surface of the fiber, and this resulted in an increased van der Waal's adhesion between fiber and matrix. Author

N88-15020*# National Aeronautics and Space Administration. Lewis Research Center, Cleveland, OH.

SIMPLIFIED PROCEDURES FOR DESIGNING COMPOSITE BOLTED JOINTS

CHRISTOS C. CHAMIS Feb. 1988 15 p Prepared for the 43rd Annual Conference of the Society of the Plastics Industry, Cincinnati, Ohio, 1-5 Feb. 1988 (NASA-TM-100281; E-3922; NAS 1.15:100281) Avail: NTIS HC A03/MF A01 CSCL 11D

Simplified procedures are described to design and analyze single and multi-bolt composite joints. Numerical examples illustrate the use of these methods. Factors affecting composite bolted joints are summarized. References are cited where more detailed discussion is presented on specific aspects of composite bolted joints. Design variables associated with these joints are summarized in the appendix. Author

N88-16700*# National Aeronautics and Space Administration. Lewis Research Center, Cleveland, OH.

HIGH TEMPERATURE POLYMER MATRIX COMPOSITES

MICHAEL A. MEADOR *In its* Aeropropulsion '87. Session 1: Aeropropulsion Materials Research 15 p Nov. 1987 Avail: NTIS HC A06/MF A01 CSCL 11D

With the increased emphasis on high performance aircraft the need for lightweight, thermal/oxidatively stable materials is growing. Because of their ease of fabrication, high specific strength, and ability to be tailored chemically to produce a variety of mechanical and physical properties, polymers and polymer matrix composites present themselves as attractive materials for a number of aeropropulsion applications. In the early 1970s researchers at the NASA Lewis Research Center developed a highly processable, thermally stable (600 F) polyimide, PMR-15. Since that time, PMR-15 has become commercially available and has found use in military aircraft, in particular, the F-404 engine for the Navy's F/A-18 strike fighter. The NASA Lewis' contributions to high temperature polymer matrix composite research will be discussed as well as current and future directions. Author

N88-16702*# National Aeronautics and Space Administration. Lewis Research Center, Cleveland, OH.

DEVELOPMENT OF A NEW GENERATION OF HIGH-TEMPERATURE COMPOSITE MATERIALS

PAMELA K. BRINDLEY *In its* Aeropropulsion '87. Session 1: Aeropropulsion Materials Research 15 p Nov. 1987 Avail: NTIS HC A06/MF A01 CSCL 11D

There are ever-increasing demands to develop low-density materials that maintain high strength and stiffness properties at elevated temperatures. Such materials are essential if the requirements for advanced aircraft, space power generation, and space station plans are to be realized. Metal matrix composites and intermetallic matrix composites are currently being investigated at NASA Lewis for such applications because they offer potential increases in strength, stiffness, and use temperature at a lower density than the most advanced single-crystal superalloys presently available. Today's discussion centers around the intermetallic matrix composites proposed by Lewis for meeting advanced aeropropulsion requirements. The fabrication process currently being used at Lewis to produce intermetallic matrix composites will be reviewed, and the properties of one such composite, SiC/Ti3Al + Nb, will be presented. In addition, the direction of future research will be outlined, including plans for enhanced fabrication of aluminide composites by the arc spray technique and fiber development by the floating-zone process. Author

N88-16828*# National Aeronautics and Space Administration. Lewis Research Center, Cleveland, OH.

DESIGN PROCEDURES FOR FIBER COMPOSITE BOX BEAMS CHRISTOS C. CHAMIS and PAPPU L. N. MURTHY (Cleveland State Univ., Ohio.) Feb. 1988 25 p (NASA-TM-100296; E-3296; NAS 1.15:100296) Avail: NTIS HC A03/MF A01 CSCL 11D

Step-by-step procedures are described which can be used for the preliminary design of fiber composite box beams subjected to combined loadings. These procedures include a collection of approximate closed-form equations so that all the required calculations can be performed using pocket calculators. Included is an illustrated example of a tapered cantilever box beam subjected to combined loads. The box beam is designed to satisfy strength, displacement, buckling, and frequency requirements. Author

N88-17744*# National Aeronautics and Space Administration. Lewis Research Center, Cleveland, OH.

MECHANICS OF COMPOSITE MATERIALS: PAST, PRESENT AND FUTURE

CHRISTOS C. CHAMIS 1988 41 p Presented at the 21st Annual Meeting of the Society for Engineering Science, Blacksburg, Va., 15-17 Oct. 1984 (NASA-TM-100793; E-3936; NAS 1.15:100793) Avail: NTIS HC A03/MF A01 CSCL 11D

Composite mechanics disciplines are presented and described at their various levels of sophistication and attendant scales of application. Correlation with experimental data is used as the prime discriminator between alternative methods and level of sophistication. Major emphasis is placed on: (1) where composite mechanics has been; (2) what it has accomplished; (3) where it is headed, based on present research activities; and (4) at the risk of being presumptuous, where it should be headed. The discussion is developed using selected, but typical examples of each composite mechanics discipline identifying degree of success, with respect to correlation with experimental data, and problems remaining. The discussion is centered about fiber/resin composites drawn mainly from the author's research activities/experience spanning two decades at Lewis. Author

N88-17745*# National Aeronautics and Space Administration. Lewis Research Center, Cleveland, OH.

FINITE ELEMENT SUBSTRUCTURING METHODS FOR COMPOSITE MECHANICS

PAPPU L. N. MURTHY (Cleveland State Univ., Ohio.) and CHRISTOS C. CHAMIS 1988 17 p Presented at the International Conference on Composite Materials and Structures, Madras, India, 6-9 Jan. 1988; sponsored by India Inst. of Technology (NASA-TM-100297; E-3946; NAS 1.15:100297) Avail: NTIS HC A03/MF A01 CSCL 11D

Finite element substructuring strategies are presented to obtain numerical solutions for three typical problems of interest to the composites community: (1) impact and toughness characterization of composites using Charpy's impact test specimen; (2) free-edge stress analysis of composite laminates; and (3) fracture toughness predictions of composites for individual and combined fracture of modes I, II, and III. The key issue common to these problems is the presence of singular or near singular stress fields. The regions prone to see steep stress gradients are substructured with progressively refined meshes to study the local response simultaneously with the global response. The results from the select examples indicate that finite element substructuring methods are computationally effective for composite singularity mechanics. J.P.B.

N88-18640*# National Aeronautics and Space Administration. Lewis Research Center, Cleveland, OH.

ETHYNYLATED AROMATICS AS HIGH TEMPERATURE MATRIX RESINS

FRANCES I. HURWITZ Oct. 1986 12 p Presented at the 18th National SAMPE Technical Conference, Seattle, Wash., 7-9 Oct. 1986 Previously announced as A87-34850

24 COMPOSITE MATERIALS

(NASA-TM-89829; E-3480; NAS 1.15:89829) Avail: NTIS HC A03/MF A01 CSCL 11D

Difunctional and trifunctional arylacetylenes were used as monomers to form thermoset matrix resin composites. Composites can be hot pressed at 180 C to react 80 percent of the acetylene groups. Crosslinking is completed by postcuring at 350 C. The postcured resins are thermally stable to nominally 460 C in air. As a result of their high crosslink density, the matrix exhibits brittle failure when uniaxial composites are tested in tension. Failure of both uniaxial tensile and flexural specimens occurs in shear at the fiber matrix interface. Tensile fracture stresses for 0 deg composites fabricated with 60 v/o Celion 6K graphite fiber were 827 MPa. The strain to failure was 0.5 percent. Composites fabricated with 8 harness satin Celion cloth (Fiberite 1133) and tested in tension also failed in shear at tensile stresses of 413 MPa. Author

N88-19592*# National Aeronautics and Space Administration. Lewis Research Center, Cleveland, OH.

MAST MATERIAL TEST PROGRAM (MAMATEP)

MICHAEL L. CIANCONE and SHARON K. RUTLEDGE 1988 13 p Presented at Issues of the International Space Station, Williamsburg, Va., 21-22 Apr. 1988; sponsored by AIAA (NASA-TM-100821; E-4005; NAS 1.15:100821; AIAA-88-2475)

Avail: NTIS HC A03/MF A01 CSCL 11D

The Mast Material Test Program (MAMATEP) at NASA Lewis is discussed. Objectives include verifying the need for, and evaluating the performance of, various protection techniques for the Solar Array Assembly mast of the Space Station Photovoltaic Power Module. Mast material samples were evaluated in terms of mass and bending modulus, measured before and after environmental exposure. Test environments included atomic oxygen exposure (RF plasma asher), thermal cycling, and mechanical flexing. Protective coatings included CV-1144 silicon, a Ni/Au/InSn eutectic, and an open weave, Al braid. Results indicate that unprotected samples degrade in an atomic oxygen environment at a steady rate. Open weave, Al braid offers little protection for the fiberglass-epoxy sample in an asher environment. Ni/Au/InSn eutectic offers excellent protection in an asher environment prior to thermal cycling and mechanical flexing. Long duration asher results from unprotected samples indicate that, even though the fiberglass-epoxy degrades, a protection technique may not be necessary to ensure structural integrity. However, a protection technique may be desirable to limit or contain the amount of debris generated by the degradation of the fiberglass-epoxy. Author

N88-21257*# National Aeronautics and Space Administration. Lewis Research Center, Cleveland, OH.

HYGROTHERMOMECHANICAL FIBER COMPOSITE FATIGUE: COMPUTATIONAL SIMULATION

CAROL A. GINTY and CHRISTOS C. CHAMIS 1988 13 p Presented at the 33rd International SAMPE Symposium and Exhibition, Anaheim, Calif., 7-10 Mar. 1988

(NASA-TM-100840; E-4029; NAS 1.15:100840) Avail: NTIS HC A03/MF A01 CSCL 11D

The technology of advanced composites has matured to the point where these composites are prime contenders for various structural applications. One of the major design considerations for prolonged service of these composites is fatigue due to cyclical hygral (moisture), thermal, and mechanical (hygrothermomechanical) loading conditions. Recent research activities at the NASA Lewis Research Center have led to the development of formal procedures for predicting, using computational simulation, fatigue in fiber composites due to cyclic hygrothermomechanical loading conditions. These formal procedures have subsequently been programmed into a computer module and embedded into the Integrated Composites Analyzer (ICAN) computer code. The objective of this paper is to present and describe results obtained using the augmented ICAN computer code. Author

N88-22367*# Akron Univ., OH.

UNIFIED CONSTITUTIVE MODEL DEVELOPMENT FOR METAL MATRIX COMPOSITES AT HIGH TEMPERATURE

D. N. ROBINSON In NASA. Lewis Research Center, Lewis Structures Technology, 1988. Volume 2: Structural Mechanics p 49-56 May 1988

(Contract NAG3-379)

Avail: NTIS HC A14/MF A01 CSCL 11D

Structural alloys used in high temperature applications exhibit complex thermomechanical behavior that is time dependent and hereditary. Recent attention is being focused on metal matrix composite materials for high temperature applications where they exhibit all the complexities of conventional alloys and their strong anisotropy adds further complexities. Here, a proven constitutive model for isotropic materials in which the inelastic strain rate and internal state are expressible as gradients of a dissipation potential is taken to depend on invariants that reflect local transverse isotropy. Applications illustrate the capability of the theory of representing the time dependent, hereditary, anisotropic behavior typical of these materials at high temperature. Author

N88-22391*# National Aeronautics and Space Administration. Lewis Research Center, Cleveland, OH.

FEATURES AND APPLICATIONS OF THE INTEGRATED COMPOSITES ANALYZER (ICAN) CODE

CAROL A. GINTY In its Lewis Structures Technology, 1988. Volume 2: Structural Mechanics p 99-112 May 1988 Previously announced as N87-16880

Avail: NTIS HC A14/MF A01 CSCL 11D

The thermal behavior of composite spacecraft antenna reflectors was investigated with the Integrated Composites Analyzer (ICAN) computer code. Parametric studies were conducted on the face sheets and honeycomb core which constitute the sandwich-type structures. Selected thermal and mechanical properties of the composite faces and sandwich structures are presented graphically as functions of varying fiber volume ratio, laminate configuration, fabrication factors, and environmental conditions. Author

N88-22395*# National Aeronautics and Space Administration. Lewis Research Center, Cleveland, OH.

METCAN: THE METAL MATRIX COMPOSITE ANALYZER

DALE A. HOPKINS and PAPPU L. N. MURTHY (Cleveland State Univ., Ohio.) In its Lewis Structures Technology, 1988. Volume 2: Structural Mechanics p 141-156 May 1988

(Contract NAG3-550)

Avail: NTIS HC A14/MF A01 CSCL 11D

Metal matrix composites (MMC) are the subject of intensive study and are receiving serious consideration for critical structural applications in advanced aerospace systems. MMC structural analysis and design methodologies are studied. Predicting the mechanical and thermal behavior and the structural response of components fabricated from MMC requires the use of a variety of mathematical models. These models relate stresses to applied forces, stress intensities at the tips of cracks to nominal stresses, buckling resistance to applied force, or vibration response to excitation forces. The extensive research in computational mechanics methods for predicting the nonlinear behavior of MMC are described. This research has culminated in the development of the METCAN (METal Matrix Composite ANalyzer) computer code. Author

N88-22402*# National Aeronautics and Space Administration. Lewis Research Center, Cleveland, OH.

IMPACT DAMAGE IN COMPOSITE LAMINATES

JOSEPH E. GRADY In its Lewis Structures Technology, 1988. Volume 2: Structural Mechanics p 235-243 May 1988

Avail: NTIS HC A14/MF A01 CSCL 11D

Damage tolerance requirements have become an important consideration in the design and fabrication of composite structural components for modern aircraft. The ability of a component to contain a flaw of a given size without serious loss of its structural integrity is of prime concern. Composite laminates are particularly

susceptible to damage caused by transverse impact loading. The ongoing program described is aimed at developing experimental and analytical methods that can be used to assess damage tolerance capabilities in composite structures subjected to impulsive loading. Some significant results of this work and the methodology used to obtain them are outlined. Author

N88-23888*# National Aeronautics and Space Administration. Lewis Research Center, Cleveland, OH.

CERAMIC MATRIX COMPOSITES

JAMES A. DICARLO *In its* Structural Ceramics p 181-187 May 1986

Avail: NTIS HC A11/MF A01 CSCL 11D

An overview is presented covering NASA Lewis research efforts aimed at materials and processing development for structurally reliable fiber-reinforced ceramic matrix composites (FRC). With the primary goal of developing technology for strong, tough Si-based FRC with use-temperatures above 1400 C, guidelines for optimum material properties and current problems in achieving these properties are discussed. Brief descriptions of particular research projects directed toward solving these problems are presented. Particular emphasis is placed on those efforts addressing the critical need of developing high performance SiC fibers with stability above 1400 C and with proper coatings for optimum composite structural performance. Based on current results for fiber and matrix development, concluding remarks are made concerning future directions of FRC studies. Author

N88-23890*# National Aeronautics and Space Administration. Lewis Research Center, Cleveland, OH.

POLYMER PRECURSORS FOR CERAMIC COMPOSITES

FRANCES I. HURWITZ *In its* Structural Ceramics p 199-202 May 1986

Avail: NTIS HC A11/MF A01 CSCL 11D

The fiber composite approach to reinforced ceramics provides the possibility of achieving ceramics with high fracture toughness relative to monolithics. Fabrication of ceramic composites, however, demands low processing temperatures to avoid fiber degradation. Formation of complex shapes further requires small diameter fibers as well as techniques for infiltrating the matrix between fibers. Polymers offer low temperature processability, control of rheology not available with ceramic powders, and should serve as precursors to matrix fibers. In recent years, a number of polysilanes and polysiloxanes were investigated as potential precursors. A review of candidate polymers is presented, including recent studies of silsesquioxanes. Author

N88-23892*# National Aeronautics and Space Administration. Lewis Research Center, Cleveland, OH.

SIC FIBER REINFORCED REACTION-BONDED Si3N4 COMPOSITES

RAMAKRISHNA T. BHATT *In its* Structural Ceramics p 213-222 May 1986

Avail: NTIS HC A11/MF A01 CSCL 11D

A technique for fabricating strong and tough SiC fiber reinforced reaction bonded Si3N4 matrix composites (SiC/RBSN) was developed. Using this technique, composites containing approximately 23, 30, and 40 volume fractions of aligned 140 micron diameter, chemically vapor deposited SiC fibers were fabricated. The room temperature physical and mechanical properties were evaluated. The results for composite tensile strength, bend strength, and fracture strain indicate that the composite displays excellent properties when compared with the unreinforced matrix of comparable porosity. The composite stress at which the matrix first cracks and the ultimate composite fracture strength increase with increasing volume fraction of fibers, and the composite fails gracefully. The mechanical property data of this ceramic composite are compared with similar data for unreinforced commercially available Si3N4 materials and for SEP SiC/SiC composites. Author

N88-24427*# National Aeronautics and Space Administration. Lewis Research Center, Cleveland, OH.

CREEP BEHAVIOR OF TUNGSTEN/NIOBIUM AND TUNGSTEN/NIOBIUM-1 PERCENT ZIRCONIUM COMPOSITES

D. W. PETRASEK and R. H. TITRAN *In* New Mexico Univ., Transactions of the Fifth Symposium on Space Nuclear Power Systems p 267-272 1988

Avail: NTIS HC A99/MF A01 CSCL 11D

A study was conducted to determine the feasibility of using tungsten fiber reinforced niobium or niobium-1 percent zirconium matrix composites to meet the anticipated increased temperature and creep resistance requirements imposed by advanced space power systems. The results obtained on the short time tensile properties indicated that W/Nb composites showed significant improvements in high temperature strength and offer significant mass reductions for high temperature space power systems. The prime material requirement for space power systems applications is long time creep resistance. A study was conducted to determine the effect of high temperature exposure on the properties of these composites, with emphasis upon their creep behavior at elevated temperatures. Author

N88-24712*# National Aeronautics and Space Administration. Lewis Research Center, Cleveland, OH.

THE 700 F PROPERTIES OF AUTOCLAVE CURED PMR-2 COMPOSITES

RAYMOND D. VANNUCCI and DIANE CIFANI 1988 17 p Proposed for presentation at the 20th International SAMPE Technical Conference, Minneapolis, Minn., 27-29 Sep. 1988; sponsored by the Society for Advancement of Material and Processing Engineering

(NASA-TM-100923; E-4186; NAS 1.15:100923) Avail: NTIS HC A03/MF A01 CSCL 11D

Studies were conducted to develop autoclave processing parameters for graphite reinforced PMR-2 resin composite materials intended for use in applications at temperatures up to 371 degrees (700 F). The effect of resin composition on autoclaveability was investigated. The effect of various graphite fibers and resin composition on 343 C (650 F) and 371 C (700 F) thermo-oxidative stability and mechanical properties was also investigated. The results of the processing studies show that PMR-2 resin composites can be easily fabricated under autoclave conditions. Autoclaved laminates exposed to 1 atm of air at 343 C (650 F) and 371 C (700 F) exhibited less than 5 percent weight loss after 750 hr exposure to 650 F air and 8 percent weight loss during exposure to 700 F air for 500 hr. After 500 hr exposure, autoclaved laminates exhibited greater than 90 percent retention of initial 650 and 700 F flexural and interlaminar shear strengths. The effect of resin formulated molecular weight and postcure conditions on laminate glass transition temperature is also discussed. Author

N88-25479*# Los Alamos National Lab., NM. Tritium Science and Technology Group.

SOLID-STATE COMBUSTION SYNTHESIS OF CERAMICS AND ALLOYS IN REDUCED GRAVITY Final Report

S. M. VALONE and R. G. BEHRENS Jul. 1988 85 p

(Contract NASA ORDER C-80011-F)

(NASA-CR-4163; E-4086; NAS 1.26:4163) Avail: NTIS HC A05/MF A01 CSCL 21B

Possible microgravity effects are explored in the combustion synthesis of ceramics and alloys from their constituent elements. Molten intermediates are typically present during the combustion process, thereby offering the chance for natural convection to take place. Numerical simulations suggest that the combustion front in concert with gravity may act as a partial zone-refinement mechanism which is attempting to sweep out porosity in the sample. Contrary to suggestions by dimensional analysis, no effects on the combustion rate are seen. An analytical model of the combustion velocity as a function of the gravitational field and the spreading rate of molten material gives the correct order of magnitude of the gravity effect as measured by centrifuge experiments. Author

24 COMPOSITE MATERIALS

N88-25483*# National Aeronautics and Space Administration. Lewis Research Center, Cleveland, OH.

A THERMALLY MODIFIED POLYMER MATRIX COMPOSITE MATERIAL WITH STRUCTURAL INTEGRITY TO 371 C

KENNETH J. BOWLES 1988 12 p Proposed for presentation at the 20th International SAMPE Technical Conference, Minneapolis, Minn., 27-29 Sep. 1988; sponsored by the Society for Advancement of Material and Processing Engineering (NASA-TM-100922; E-4182; NAS 1.15:100922) Avail: NTIS HC A03/MF A01 CSCL 11D

The potential for utilizing surface coatings to inhibit the thermal oxidation of polymer matrix composites was studied. Isothermal, inert gas exposures of graphite/PMR-15 composites indicated that after an initial loss of weight, no significant amounts of thermal degradation products are given off during high temperature exposures in the absence of oxygen. As long as a coating remains effective, the composite material should remain stable. It was also found that the glass transition temperature $T_{sub g}$ of the matrix resin could be increased to values in excess of 400 C. This resulted in measured short beam shear strengths of 75.9 MPa (11 Ksi), flexural strengths of 1172 MPa (170 Ksi) and flexural moduli of 141 GPa (20.5 Msi) for the material at a test temperature of 371 C. The treatment that was used caused a decrease in the PMR-15 resin density from 1.31 to 1.29 gm/cc. It was concluded that state-of-the-art composites, protected by oxygen-impermeous coatings, can be used as materials of construction with structural integrity to at least 371 C and possibly above. Author

N88-25487*# National Aeronautics and Space Administration. Lewis Research Center, Cleveland, OH.

AUGER ANALYSIS OF A FIBER/MATRIX INTERFACE IN A CERAMIC MATRIX COMPOSITE

FRANK S. HONEY (Case Western Reserve Univ., Cleveland, Ohio.) and STEPHEN V. PEPPER 1988 10 p Presented at the Spring Meeting of the Materials Research Society, Reno, Nev., 4-9 Apr. 1988 (NASA-TM-100892; E-4130; NAS 1.15:100892) Avail: NTIS HC A02/MF A01 CSCL 11D

Auger electron spectroscopy (AES) depth profiling was used to characterize the fiber/matrix interface of an SiC fiber, reaction bonded Si₃N₄ matrix composite. Depth profiles of the as received double coated fiber revealed concentration oscillations which disappeared after annealing the fiber in the environment used to fabricate the composite. After the composite was fractured, the Auger depth profiles showed that failure occurred in neither the Beta-SiC fiber body nor in the Si₃N₄ matrix but, concurrently, at the fiber coating/matrix interface and within the fiber coating itself. Author

N88-28094*# National Aeronautics and Space Administration. Lewis Research Center, Cleveland, OH.

PROBABILISTIC STRUCTURAL ANALYSIS TO QUANTIFY UNCERTAINTIES ASSOCIATED WITH TURBOPUMP BLADES

VINOD K. NAGPAL, ROBERT RUBINSTEIN (Sverdrup Technology, Inc., Cleveland, Ohio.), and CHRISTOS C. CHAMIS Feb. 1988 14 p Previously announced in IAA as A87-33581 (NASA-TM-100278; E-3919; NAS 1.15:100278) Avail: NTIS HC A03/MF A01 CSCL 11D

A probabilistic study of turbopump blades has been in progress at NASA Lewis Research Center for over the last two years. The objectives of this study are to evaluate the effects of uncertainties in geometry and material properties on the structural response of the turbopump blades to evaluate the tolerance limits on the design. A methodology based on probabilistic approach was developed to quantify the effects of the random uncertainties. The results indicate that only the variations in geometry have significant effects. Author

N88-28095*# National Aeronautics and Space Administration. Lewis Research Center, Cleveland, OH.

AS-RECEIVED MICROSTRUCTURE OF A SiC/Ti-15-3 COMPOSITE

BRADLEY A. LERCH, DAVID R. HULL, and TODD A. LEONHARDT

(Sverdrup Technology, Inc., Cleveland, Ohio.) Aug. 1988 27 p (NASA-TM-100938; E-4218; NAS 1.15:100938) Avail: NTIS HC A03/MF A01 CSCL 11D

A silicon carbide fiber reinforced titanium (Ti-15V-3Cr-3Sn-3Al) composite is metallographically examined. Several methods for examining composite materials are investigated and documented. Polishing techniques for this material are described. An interference layering method is developed to reveal the structure of the fiber, the reaction zone, and various phases within the matrix. Microprobe and transmission electron microscope (TEM) analyses are performed on the fiber/matrix interface. A detailed description of the fiber distribution as well as the microstructure of the fiber and matrix are presented. Author

N88-28980*# National Aeronautics and Space Administration. Lewis Research Center, Cleveland, OH.

INVESTIGATION OF A SiC/Ti-24Al-11Nb COMPOSITE

P. K. BRINDLEY, P. A. BARTOLOTTA, and S. J. KLIMA 1988 30 p Presented at the 117th TMS-AIME Annual Meeting, Phoenix, Ariz., 25-29 Jan. 1988; sponsored by the American Society for Metals (NASA-TM-100956; E-4253; NAS 1.15:100956) Avail: NTIS HC A03/MF A01 CSCL 11D

A summary of ongoing research on the characterization of a continuous fiber reinforced SiC/Ti-24Al-11Nb (at percent) composite is presented. The powder metallurgy fabrication technique is described as are the nondestructive evaluation results of the as-fabricated composite plates. Tensile properties of the SiC fiber, the matrix material, and the 0-deg SiC/Ti-24Al-11Nb composite (fibers oriented unidirectionally, parallel to the loading axis) from room temperature to 1100 C are presented and discussed with regard to the resultant fractography. The as-fabricated fiber-matrix interface has been examined by scanning transmission electron microscopy and the compounds present in the reaction zone have been identified. Fiber-matrix interaction and stability of the matrix near the fiber is characterized at 815, 985, and 1200 C from 1 to 500 hr. Measurements of the fiber-matrix reaction, the loss of C-rich coating from the surface of the SiC fiber, and the growth of the Beta depleted zone in the matrix adjacent to the fiber are presented. These data and the difference in coefficient of thermal expansion between the fiber and the matrix are discussed in terms of their likely effects on mechanical properties. Author

N88-28981*# University of Southern California, Los Angeles. Dept. of Materials Science.

THE HIGH TEMPERATURE CREEP DEFORMATION OF Si₃N₄-6Y₂O₃-2Al₂O₃

J. A. TODD and ZHI-YUE XU 1988 32 p (Contract NAG3-685) (NASA-CR-183204; NAS 1.26:183204) Avail: NTIS HC A03/MF A01 CSCL 11D

The creep properties of silicon nitride containing 6 wt percent yttria and 2 wt percent alumina have been determined in the temperature range 1573 to 1673 K. The stress exponent, n , in the equation $\epsilon = A \sigma^n \exp(-Q/RT)$ varies as σ sup n , was determined to be 2.00 + or - 0.15 and the true activation energy was found to be 692 + or - 25 kJ/mol. Transmission electron microscopy studies showed that deformation occurred in the grain boundary glassy phase accompanied by microcrack formation and cavitation. The steady state creep results are consistent with a diffusion controlled creep mechanism involving nitrogen diffusion through the grain boundary glassy phase. Author

N88-29888*# National Aeronautics and Space Administration. Lewis Research Center, Cleveland, OH.

BROMINATED GRAPHITE FIBERS AND METHOD OF PRODUCING THE SAME Patent Application

CHING-CHEH HUNG, inventor (to NASA) 14 Jul. 1988 9 p (NASA-CASE-LEW-14698-1; NAS 1.71:LEW-14698-1; US-PATENT-APPL-SN-219016) Avail: NTIS HC A02/MF A01 CSCL 11D

Highly graphitized as well as commercially available less

graphitized fibers are brominated in a relatively low temperature range. For liquid bromination, this range is between the melting point of bromine and room temperature. For vaporous bromination, this range is between -15 C and 0 C. The brominated fibers are then reacted with fluorine. NASA

25

INORGANIC AND PHYSICAL CHEMISTRY

Includes chemical analysis, e.g., chromatography; combustion theory; electrochemistry; and photochemistry.

A88-10963* National Aeronautics and Space Administration. Lewis Research Center, Cleveland, OH.

THERMAL DESORPTION STUDY OF PHYSICAL FORCES AT THE PTFE SURFACE

D. R. WHEELER and S. V. PEPPER (NASA, Lewis Research Center, Cleveland, OH) IN: Surface and colloid science in computer technology. New York, Plenum Publishing Corp., 1987, p. 309-320. refs

Thermal desorption spectroscopy (TDS) of the polytetrafluoroethylene (PTFE) surface was successfully employed to study the possible role of physical forces in the enhancement of metal-PTFE adhesion by radiation. The thermal desorption spectra were analyzed without assumptions to yield the activation energy for desorption over a range of xenon coverage from less than 0.1 monolayer to more than 100 monolayers. For multilayer coverage, the desorption is zero-order with an activation energy equal to the sublimation energy of xenon. For submonolayer coverages, the order for desorption from the unirradiated PTFE surface is 0.73 and the activation energy for desorption is between 3.32 and 3.36 kcal/mol; less than the xenon sublimation energy. The effect of irradiation is to increase the activation energy for desorption to as high as 4 kcal/mol at low coverage. Author

A88-11167* National Bureau of Standards, Gaithersburg, MD.
QUANTITATIVE CHARACTERIZATION OF THE VISCOSITY OF A MICROEMULSION

ROBERT F. BERG, MICHAEL R. MOLDOVER (NBS, Thermophysics Div., Gaithersburg, MD), and JOHN S. HUANG (Exxon Research and Engineering Co., Annandale, NJ) Journal of Chemical Physics (ISSN 0021-9606), vol. 87, Sept. 15, 1987, p. 3687-3691. refs
(Contract NASA ORDER C-86129-D)

The viscosity of the three-component microemulsion water/decane/AOT has been measured as a function of temperature and droplet volume fraction. At temperatures well below the phase-separation temperature the viscosity is described by treating the droplets as hard spheres suspended in decane. Upon approaching the two-phase region from low temperature, there is a large (as much as a factor of four) smooth increase of the viscosity which may be related to the percolation-like transition observed in the electrical conductivity. This increase in viscosity is not completely consistent with either a naive electroviscous model or a simple clustering model. The divergence of the viscosity near the critical point (39 C) is superimposed upon the smooth increase. The magnitude and temperature dependence of the critical divergence are similar to that seen near the critical points of binary liquid mixtures. Author

A88-16076*# Princeton Univ., NJ.
SOOTING AND DISRUPTION IN SPHERICALLY

SYMMETRICAL COMBUSTION OF DECANE DROPLETS IN AIR
F. L. DRYER, F. A. WILLIAMS (Princeton University, NJ), J. B. HAGGARD, JR. (NASA, Lewis Research Center, Cleveland, OH), and B. D. SHAW IAF, International Astronautical Congress, 38th, Brighton, England, Oct. 10-17, 1987. 7 p. refs
(Contract NAS3-24640)
(IAF PAPER 87-403)

The paper presents the results of experiments on the burning of individual 1-2 mm decane droplets in air at room temperature and atmospheric pressure. The NASA Lewis 2.2 s drop tower was used as well as a newly designed droplet-combustion apparatus that promotes nearly spherically symmetrical combustion. Unanticipated disruptions related to sooting behavior were encountered. K.K.

A88-16497*# National Aeronautics and Space Administration. Lewis Research Center, Cleveland, OH.

A THEORETICAL ANALYSIS OF THE EXTINCTION LIMITS OF A METHANE-AIR OPPOSED-JET DIFFUSION FLAME

S. L. OLSON (NASA, Lewis Research Center, Cleveland, OH) and J. S. T'EN (Case Western Reserve University, Cleveland, OH) Combustion and Flame (ISSN 0010-2180), vol. 70, Nov. 1987, p. 161-170. refs
(Contract NSF MEA-81-15339)

A theoretical analysis is described for a methane-air diffusion flame stabilized in the forward stagnation region of a porous metal cylinder in a forced convective flow. The analysis includes effects of radiative heat loss from the porous metal surface and finite rate kinetics but neglects the effects of gravity. The theoretically predicted extinction limits compare well with experimentally observed extinction limits from the literature. After the predicted limits compared well with the experimental limits, a parametric study of the effect of fuel surface emissivity and Lewis number was conducted with the numerical model. It was found that the computed blowoff limit is independent of radiative heat loss for high fuel blowing velocities but is a strong function of Lewis number. At low fuel blowing velocities, the extinction limit varies with both radiative heat loss and Lewis number. It is discovered, however, that even if thermal losses from the fuel surface are absent, the flame can extinguish at the fuel surface independently of Lewis number due to excessive reaction zone thinning. Author

A88-16643* Bowling Green State Univ., OH.
EVALUATION STUDIES ON CARBON SUPPORTED CATALYSTS FOR OXYGEN REDUCTION IN ALKALINE MEDIUM

VAKULA S. SRINIVASAN (Bowling Green State University, OH) and JOSEPH SINGER (NASA, Lewis Research Center, Cleveland, OH) IN: International Power Sources Symposium, 32nd, Cherry Hill, NJ, June 9-12, 1986, Proceedings. Pennington, NJ, Electrochemical Society, Inc., 1986, p. 580-589. refs

This paper describes tests designed to predict the performance of fuel cell electrodes, as applied to an alkaline oxygen-fuel cell having specially fabricated porous-carbon electrodes with various amounts of dispersed platinum or gold as active catalysts. The tests are based on information obtained from the techniques of cyclic voltammetry and polarization. The parameters obtained from cyclic voltammetry were of limited use in predicting fuel cell performance of the cathode. On the other hand, half-cell polarization measurements offered close simulation of the oxygen electrode, although a predictor of the electrode life is still lacking. The very low polarization of the Au-10 percent Pt catalytic electrode suggests that single-phase catalysts should be considered. I.S.

A88-17218* Purdue Univ., West Lafayette, IN.
FEASIBILITY OF HYDROXYL CONCENTRATION MEASUREMENTS BY LASER-SATURATED FLUORESCENCE IN HIGH-PRESSURE FLAMES

CAMPBELL D. CARTER, GALEN B. KING, NORMAND M. LAURENDEAU (Purdue University, West Lafayette, IN), and J. THADDEUS SALMON (Lawrence Livermore National Laboratory, Livermore, CA) Applied Optics (ISSN 0003-6935), vol. 26, Nov. 1, 1987, p. 4551-4562. USAF-supported research. refs
(Contract NAG3-351)

The effect of pressure on the laser-saturated fluorescence method for measuring OH concentration in high-pressure flames is studied using calculations for the burned-gas region of a stoichiometric H₂-O₂ flame at 2000 K. A numerical model of the excitation dynamics of OH is developed to explore the validity of the balanced cross-rate model at higher pressures. It is shown

that depopulation of the laser-coupled levels is sensitive to collisions which depopulate v-double-prime (VDP) = 0 and to rate coefficients for rotational transfer in the ground state which are smaller than those in the excited state. In particular, it is shown that the depopulation of VDP = 0, and hence the laser-coupled levels, depends on the probability of electronic quenching to vibrational levels for which VDP is greater than 0 and vibrational relaxation to VDP = 0. C.D.

A88-19233* National Aeronautics and Space Administration, Lewis Research Center, Cleveland, OH.

INTEGRATING COMBUSTION KINETIC RATE EQUATIONS BY SELECTIVE USE OF STIFF AND NONSTIFF METHODS

KRISHNAN RADHAKRISHNAN (NASA, Lewis Research Center, Cleveland, OH) AIAA Journal (ISSN 0001-1452), vol. 25, Nov. 1987, p. 1449-1455. Previously cited in issue 07, p. 874, Accession no. A85-19607. refs
(Contract NAG3-294; NAS3-24105)

A88-25023* National Aeronautics and Space Administration, Lewis Research Center, Cleveland, OH.

CHEMICAL DURABILITY OF HIGH-TEMPERATURE SUPERCONDUCTOR YBA₂CU₃O_{7-x} IN AQUEOUS ENVIRONMENTS

NAROTTAM P. BANSAL and ANN L. SANDKUHL (NASA, Lewis Research Center, Cleveland, OH) Applied Physics Letters (ISSN 0003-6951), vol. 52, Jan. 25, 1988, p. 323-325. refs

The stability of YBa₂Cu₃O_{7-x} in water and 100-percent humidity has been investigated at three temperatures, using pH measurements, X-ray diffraction, and scanning electron microscopy. The oxide-ceramic superconductor is highly unstable; it reacts rapidly with water and degrades in moisture. Dissolution of the oxide perovskite in water is highly incongruent. The corrosion products are found to be BaCO₃, CuO, O₂, etc. Barium hydroxide is first formed and further reacts with atmospheric CO₂ to form needle-shaped crystals of BaCO₃. For any practical applications, devices made from these materials would have to be protected with an impermeable coating to prevent deterioration from atmosphere. Author

A88-27722* Science Applications International Corp., Chatsworth, CA.

LAMINAR DIFFUSION FLAMES UNDER MICRO-GRAVITY CONDITIONS

RAYMOND B. EDELMAN, YOUSEF BAHADORI (Science Applications International Corp., Chatsworth, CA), SANDRA L. OLSON, and DENNIS P. STOCKER (NASA, Lewis Research Center, Cleveland, OH) AIAA, Aerospace Sciences Meeting, 26th, Reno, NV, Jan. 11-14, 1988. 11 p. refs
(Contract NAS3-22822)
(AIAA PAPER 88-0645)

Laminar methane and propane gas-jet diffusion flames have been theoretically and experimentally studied at NASA-Lewis under microgravity conditions. It is noted that laminar diffusion flames are strongly affected by the combined effects of kinetics, radiation, and such transient phenomena as flame ignition, stabilization, and extinction. Observations on the distinctive nature of the flame color and luminosity parameters in microgravity are presented, and flame behavior under transient, high-deceleration rates is discussed. Test hardware and instrumentation design are described. O.C.

A88-38532* Illinois Univ., Urbana.

THE EFFECT OF GRAVITY ON PREMIXED FLAME PROPAGATION AND EXTINCTION IN A VERTICAL STANDARD FLAMMABILITY TUBE

ROGER A. STREHLOW, KURT A. NOE, and BRIAN L. WHERLEY (Illinois University, Urbana) IN: Symposium (International) on Combustion, 21st, Munich, Federal Republic of Germany, Aug. 3-8, 1986, Proceedings. Pittsburgh, PA, Combustion Institute, 1988, p. 1899-1908. refs
(Contract NCC3-35)

The effect of gravity on the upward and downward flame propagation in lean methane/air and lean propane/air mixtures

was studied using plexiglass flammability tubes with ignition at the open-end gravity levels which ranged from microgravity (0 + or - 0.1 g) to 1.77 g. The lean limits were found to be about 5.25, 5.25, and 5.85 percent methane in air; and about 2.15, 2.06, and 2.20 percent propane in air for 1 g upward propagation, 0 g, and 1 g downward propagation, respectively. The propane/air flames observed were stable, irrespective of the g level. On the other hand, lean methane/air flames were found to be sporadically unstable for upward propagation at g levels less than 0.5 g, and for downward propagation at g = 1.0. The extinction process observed was the same for both systems studied: at g = 0, the flame extinguished from the edge toward the center, while at g of 1 and above, the flame extinguished from the center toward the edge. I.S.

A88-43018* California Univ., Berkeley.

TEMPERATURE AND VELOCITY PROFILES IN SOOTING FREE CONVECTION DIFFUSION FLAMES

JAMES A. ANG, PATRICK J. PAGNI, THOMAS G. MATAGA (California University, Berkeley), JANICE M. MARGLE, and VALERIE J. LYONS (NASA, Lewis Research Center, Cleveland, OH) AIAA Journal (ISSN 0001-1452), vol. 26, March 1988, p. 323-329. Previously cited in issue 07, p. 870, Accession no. A86-19962. refs
(Contract NBS-60-NANB5D-0552)

A88-44424* National Aeronautics and Space Administration, Lewis Research Center, Cleveland, OH.

SIGNIFICANCE OF VAPOR PHASE CHEMICAL REACTIONS ON CVD RATES PREDICTED BY CHEMICALLY FROZEN AND LOCAL THERMOCHEMICAL EQUILIBRIUM BOUNDARY LAYER THEORIES

SULEYMAN A. GOKOGLU (NASA, Lewis Research Center, Cleveland, OH) Electrochemical Society, Journal (ISSN 0013-4651), vol. 135, June 1988, p. 1562-1570. refs

This paper investigates the role played by vapor-phase chemical reactions on CVD rates by comparing the results of two extreme theories developed to predict CVD mass transport rates in the absence of interfacial kinetic barrier: one based on chemically frozen boundary layer and the other based on local thermochemical equilibrium. Both theories consider laminar convective-diffusion boundary layers at high Reynolds numbers and include thermal (Soret) diffusion and variable property effects. As an example, Na₂SO₄ deposition was studied. It was found that gas phase reactions have no important role on Na₂SO₄ deposition rates and on the predictions of the theories. The implications of the predictions of the two theories to other CVD systems are discussed. I.S.

A88-44425* Ohio State Univ., Columbus.

DIRECT MASS SPECTROMETRIC IDENTIFICATION OF SILICON OXYCHLORIDE COMPOUNDS

JOHN E. MARRA, ERIC R. KREIDLER (Ohio State University, Columbus), NATHAN S. JACOBSON, and DENNIS S. FOX (NASA, Lewis Research Center, Cleveland, OH) Electrochemical Society, Journal (ISSN 0013-4651), vol. 135, June 1988, p. 1571-1574. Research supported by the Edward Orton Junior Ceramic Foundation. refs
(Contract DAAG29-82-K-0149)

Silicon oxychloride compounds formed during the high temperature reaction of Si and SiC with Cl₂/O₂ mixtures at 930 and 950 C have been directly observed with an atmospheric pressure mass spectrometer sampling system. Molecules with the formulas Si₂OCl₆ and Si₃OCl₈ have been identified. These compounds are very likely formed by a gas phase reaction between the oxygen gas in the system and silicon tetrachloride which is produced by chlorination of the silicon-based material. Author

A88-46499* Case Western Reserve Univ., Cleveland, OH.

MODELLING IGNITION CHARACTERISTICS OF RICH H₂/O₂ MIXTURE IN A MONOLITHIC CATALYTIC REACTOR

TA-CHING TIEN and JAMES S. TIEN (Case Western Reserve University, Cleveland, OH) AIAA, ASME, SAE, and ASEE, Joint

Propulsion Conference, 24th, Boston, MA, July 11-13, 1988. 10 p. refs

(Contract NAG3-809)
(AIAA PAPER 88-3224)

Ignition of rich hydrogen-oxygen mixture in a monolithic catalytic reactor is studied using a transient combustion model. The model assumes a quasi-steady gas phase and a thermally-thin substrate. The ignition time lag is due to the thermal inertia of the substrate. One-step global chemical reaction is assumed both on the surface and in the gas phase. An effectiveness factor is introduced to account for the transition from a kinetically-limited catalytic surface reaction to a diffusion-limit one during ignition. Results presented include a catalytic ignition boundary, ignition delay time and the transient response in the catalytic bed. Author

N88-10132*# National Aeronautics and Space Administration. Lewis Research Center, Cleveland, OH.

EFFECT OF NASA ADVANCED DESIGNS ON THERMAL BEHAVIOR OF NI-H₂ CELLS

OLGA D. GONZALEZ-SANABRIA 1987 16 p Presented at the Annual Meeting of the American Institute of Chemical Engineers, New York, N.Y., 15-20 Nov. 1987

(NASA-TM-100197; E-3790; NAS 1.15:100197) Avail: NTIS HC A03/MF A01 CSCL 10C

As part of an overall effort to advance the technology of nickel-hydrogen batteries for low Earth orbit (LEO) applications, advanced designs for individual pressure vessel (IPV) nickel-hydrogen cells have been conceived. These designs incorporate alternative methods of oxygen recombination which affect the thermal behavior of the cells. The effect of these oxygen recombination methods on the cell temperature profiles is examined. Author

N88-11775*# National Aeronautics and Space Administration. Lewis Research Center, Cleveland, OH.

DETAILED MECHANISM OF BENZENE OXIDATION

DAVID A. BITTKER Oct. 1987 24 p
(NASA-TM-100202; E-3797; NAS 1.15:100202) Avail: NTIS HC A03/MF A01 CSCL 07D

A detailed quantitative mechanism for the oxidation of benzene in both argon and nitrogen diluted systems is presented. Computed ignition delay time for argon diluted mixtures are in satisfactory agreement with experimental results for a wide range of initial conditions. An experimental temperature versus time profile for a nitrogen diluted oxidation was accurately matched and several concentration profiles were matched qualitatively. Application of sensitivity analysis has given approximate rate constant expressions for the two dominant heat release reactions, the oxidation of C₆H₅ and C₅H₅ radicals by molecular oxygen. Author

N88-13428*# National Aeronautics and Space Administration. Lewis Research Center, Cleveland, OH.

DETAILED MECHANISM OF TOLUENE OXIDATION AND COMPARISON WITH BENZENE

DAVID A. BITTKER 1988 26 p Proposed for presentation at the 22nd International Symposium on Combustion, Seattle, Wash., 14-18 Aug. 1988; sponsored by the Combustion Inst.

(NASA-TM-100261; E-3889; NAS 1.15:100261) Avail: NTIS HC A03/MF A01 CSCL 07D

A detailed mechanism for the oxidation of toluene in both argon and nitrogen diluents is presented. The mechanism was used to compute experimentally ignition delay times for shock-heated toluene-oxygen-argon mixtures with reasonably good success over a wide range of initial temperatures and pressures. Attempts to compute experimentally measured concentration profiles for toluene oxidation in a turbulent reactor were partially successful. An extensive sensitivity analysis was performed to determine the reactions which control the ignition process and the rates of formation and destruction of various species. The most important step was found to be the reaction of toluene with molecular oxygen, followed by the reactions of hydroperoxyl and atomic oxygen with benzyl radicals. These findings contrast with the benzene oxidation, where the benzene-molecular oxygen

reaction is quite unimportant and the reaction of phenyl with molecular oxygen dominates. In the toluene mechanism the corresponding reaction of benzyl radicals with oxygen is unimportant. Two reactions which are important in the oxidation of benzene also influence the oxidation of toluene for several conditions. These are the oxidations of phenyl and cyclopentadienyl radicals by molecular oxygen. The mechanism presented successfully computes the decrease of toluene concentration with time in the nitrogen diluted turbulent reactor. This fact, in addition to the good prediction of ignition delay times, shows that this mechanism can be used for modeling the ignition and combustion process in practical, well-mixed combustion systems. Author

N88-15036*# National Aeronautics and Space Administration. Lewis Research Center, Cleveland, OH.

THE CARBON DIOXIDE CHAPERON EFFICIENCY FOR THE REACTION $H + O_2 + M \rightarrow HO_2 + M$ FROM IGNITION DELAY TIMES BEHIND REFLECTED SHOCK WAVES

THEODORE A. BRABBS and THOMAS F. ROBERTSON May 1987 15 p Presented at the Central States Meeting of the Combustion Inst., Argonne, Ill., 11-13 May 1987

(NASA-TM-100125; E-3489; NAS 1.15:100125) Avail: NTIS HC A03/MF A01 CSCL 21B

Ignition delay times for stoichiometric hydrogen-oxygen in argon with and without carbon dioxide were measured behind reflected shock waves. A 20-reaction kinetic mechanism models the measured hydrogen-oxygen delay times over the temperature range 950 to 1300 K. The chaperon efficiency for carbon dioxide determined for the hydrogen-oxygen carbon dioxide mixture was 7.0. This value is in agreement with literature values but much less than a recent value obtained from flow tube experiments. Delay times measured behind a reflected shock wave were about 20% longer than those measured behind incident shock waves. The kinetic mechanism successfully modeled the high-pressure data of Skinner and the hydrogen-air data of Slack. It is suggested that the lowest temperature points for the hydrogen-air data of Slack are unreliable and that the 0.27-atm data may illustrate a case where vibrational relaxation of nitrogen is important. The reaction pathway $HO_2 \rightarrow H_2O_2 \rightarrow OH$ yields H was required to model the high-pressure data of Skinner. The successful modeling of the stoichiometric hydrogen-air data demonstrates the appropriateness of deriving kinetic models from data for gas mixtures highly diluted with argon. The technique of reducing a detailed kinetic mechanism to only the important reactions for a limited range of experimental data may render the mechanism useless for other test conditions. Author

N88-15793*# National Aeronautics and Space Administration. Lewis Research Center, Cleveland, OH.

CHEMICAL REACTING FLOWS

EDWARD J. MULARZ and PETER M. SOCKOL *In its* Aeropropulsion '87. Session 3: Internal Fluid Mechanics Research 20 p Nov. 1987

Avail: NTIS HC A04/MF A01 CSCL 21B

Future aerospace propulsion concepts involve the combination of liquid or gaseous fuels in a highly turbulent internal air stream. Accurate predictive computer codes which can simulate the fluid mechanics, chemistry, and turbulence combustion interaction of these chemical reacting flows will be a new tool that is needed in the design of these future propulsion concepts. Experimental and code development research is being performed at Lewis to better understand chemical reacting flows with the long term goal of establishing these reliable computer codes. The approach to understanding chemical reacting flows is to look at separate simple parts of this complex phenomena as well as to study the full turbulent reacting flow process. As a result research on the fluid mechanics associated with chemical reacting flows was initiated. The chemistry of fuel-air combustion is also being studied. Finally, the phenomena of turbulence-combustion interaction is being investigated. This presentation will highlight research, both experimental and analytical, in each of these three major areas. Author

25 INORGANIC AND PHYSICAL CHEMISTRY

N88-15851*# Ultrasonics, Inc., Irvine, CA.

IMPROVED PERFLUOROALKYLETHER FLUID DEVELOPMENT Final Report, 1 Mar. 1985 - 30 Sep. 1987

K. L. PACIOREK, S. R. MASUDA, J. H. NAKAHARA, and R. H. KRATZER 30 Nov. 1987 55 p
(Contract NAS3-24632)

(NASA-CR-180872; SN-3504-F; NAS 1.26:180872) Avail: NTIS HC A04/MF A01 CSCL 07D

The objective of this program was to optimize and scale up the linear perfluoroalkylether stabilization process and to provide test data regarding the fluids' thermal oxidative stability in the presence of metal alloys. The stabilization of Fomblin Z-25 was scaled up to 300 g of fluid. The modified fluid was stable at 316 C in oxygen in the presence of M-50 alloy for more than 24 hrs but less than 40 hrs; the amount of volatiles produced after 24 hrs was 5.5 mg/g. In the presence of Ti(4Al,4Mn) alloy, under the above conditions, following an exposure of 24 hrs, the amount of volatiles formed was 6.2 mg/g; 56 hrs exposure yielded 13.9 mg/g. The commercial fluid at 288 C (in oxygen) in the presence of M-50 after 15 hrs of exposure decomposed extensively, 342 mg/g; in the presence of Ti(4Al,4Mn) alloy after only 8 hrs at 288 C, the amount of volatiles was 191 mg/g. Formulation of the commercial fluid with C2PN3 additive was not as effective as the stabilization processing. All the perfluoroalkylether fluids studied were stable in nitrogen at 343 C. The thermal oxidative stability in the absence of metal alloys varied, with Aflunox exhibiting the best behavior. All the fluids were degraded in oxygen at 316 C during 24 hrs exposure to Ti(4Al,4Mn) alloy with the exception of a perfluoroalkylether substituted triazine and the modified Z-25.

Author

N88-15853*# National Aeronautics and Space Administration, Lewis Research Center, Cleveland, OH.

THE EFFECT OF MICROGRAVITY ON FLAME SPREAD OVER A THIN FUEL M.S. Thesis, Case Western Reserve Univ., Cleveland, Ohio, Aug. 1987

SANDRA L. OLSON Dec. 1987 49 p
(NASA-TM-100195; E-3785; NAS 1.15:100195) Avail: NTIS HC A03/MF A01 CSCL 21B

A flame spreading over a thermally thin cellulose fuel was studied in a quiescent microgravity environment. Flame spread over two different fuel thicknesses was studied in ambient oxygen-nitrogen environments from the limiting oxygen concentration to 100 percent oxygen at 1 atm pressure. Comparative normal-gravity tests were also conducted. Gravity was found to play an important role in the mechanism of flame spread. In lower oxygen environments, the buoyant flow induced in normal gravity was found to accelerate the flame spread rate as compared to the microgravity flame spread rates. It was also found to stabilize the flame in oxidizer environments, where microgravity flames in a quiescent environment extinguish. In oxygen-rich environments, however, it was determined that gravity does not play an important role in the flame spread mechanism. Fuel thickness influences the flame spread rate in both normal gravity and microgravity. The flame spread rate varies inversely with fuel thickness in both normal gravity and in an oxygen-rich microgravity environment. In lower oxygen microgravity environments, however, the inverse relationship breaks down because finite-rate kinetics and heat losses become important. Two different extinction limits were found in microgravity for the two thicknesses of fuel. This is in contrast to the normal-gravity extinction limit, which was found to be independent of fuel thickness. In microgravity the flame is quenched because of excessive thermal losses, whereas in normal gravity the flame is extinguished by blowoff.

Author

N88-18672*# National Aeronautics and Space Administration, Lewis Research Center, Cleveland, OH.

MASS TRANSPORT PHENOMENA BETWEEN BUBBLES AND DISSOLVED GASES IN LIQUIDS UNDER REDUCED GRAVITY CONDITIONS

KENNETH J. DEWITT, JONATHAN L. BROCKWELL (Union Carbide Corp., South Charleston, W.Va.), CHAIN-NAN YUNG, AN-TI CHAI, JOHN B. MCQUILLEN, RAYMOND G. SOTOS, and ERIC

S. NEUMANN Jan. 1988 10 p Presented at the 26th Aerospace Sciences Meeting, Reno, Nev., 11-14 Jan. 1988; sponsored by AIAA

(NASA-TM-100273; E-3912; AIAA-88-0450; NAS 1.15:100273)

Avail: NTIS HC A02/MF A01 CSCL 07D

The experimental and analytical work that was done to establish justification and feasibility for a shuttle middeck experiment involving mass transfer between a gas bubble and a liquid is described. The experiment involves the observation and measurement of the dissolution of an isolated immobile gas bubble of specified size and composition in a thermostatted solvent liquid of known concentration in the reduced gravity environment of earth orbit. Methods to generate and deploy the bubble were successful both in normal gravity using mutually buoyant fluids and under reduced gravity conditions in the NASA Lear Jet. Initialization of the experiment with a bubble of a prescribed size and composition in a liquid of known concentration was accomplished using the concept of unstable equilibrium. Subsequent bubble dissolution or growth is obtained by a step increase or decrease in the liquid pressure. A numerical model was developed which simulates the bubble dynamics and can be used to determine molecular parameters by comparison with the experimental data. The primary objective of the experiment is the elimination of convective effects that occur in normal gravity.

Author

N88-20397*# Ohio State Univ., Columbus. ElectroScience Lab. **MATERIAL PARAMETER MEASUREMENTS AT HIGH TEMPERATURES**

A. DOMINEK, A. PARK, and L. PETERS, JR. Mar. 1988 24 p
(Contract NAG3-784)

(NASA-CR-182707; NAS 1.26:182707; OS-TR-719300-2) Avail: NTIS HC A03/MF A01 CSCL 07D

Alternate fixtures of techniques for the measurement of the constitutive material parameters at elevated temperatures are presented. The technique utilizes scattered field data from material coated cylinders between parallel plates or material coated hemispheres over a finite size groundplane. The data acquisition is centered around the HP 8510B Network Analyzer. The parameters are then found from a numerical search algorithm using the Newton-Raphson technique with the measured and calculated fields from these canonical scatters. Numerical and experimental results are shown.

Author

N88-26430*# National Aeronautics and Space Administration, Lewis Research Center, Cleveland, OH.

PERFORMANCE OF LIGHTWEIGHT NICKEL ELECTRODES

DORIS L. BRITTON 1988 8 p Presented at the 33rd International Power Sources Symposium, Cherry Hill, N.J., 13-16 Jun. 1988; sponsored by the Dept. of the Army

(NASA-TM-100958; E-4252; NAS 1.15:100958) Avail: NTIS HC A02/MF A01 CSCL 07D

The NASA Lewis Research Center is currently developing nickel electrodes for nickel-hydrogen (Ni-H₂) batteries. These electrodes are lighter in weight and have higher energy densities than the heavier state-of-the-art (SOA) sintered nickel electrodes. In the present approach, lightweight materials or plaques are used as conductive supports for the nickel hydroxide active material. These plaques (fiber and felt, nickel plated plastic and graphite) are commercial products that are fabricated into nickel electrodes by electrochemically impregnating them with active material. Evaluation is performed in half cells structured in the bipolar configuration. Initial performance tests include capacity measurements at five discharge levels, C/2, 1.0C 1.37C, 2.0C and 2.74C. The electrodes that pass the initial tests are life cycle tested in a low Earth orbit regime at 80 percent depth of discharge. Different formulations of nickel fiber materials obtained from several manufacturers are currently being tested as possible candidates for nickel electrodes. One particular lightweight fiber mat electrode has accumulated over 3000 cycles to date, with stable capacity and voltage. Life and performance data of this electrode were investigated and presented. Good dimensional stability and active material adherence have been demonstrated in electrodes made from this lightweight plaque.

Author

N88-27267*# National Aeronautics and Space Administration. Lewis Research Center, Cleveland, OH.

ALKALINE FUEL CELL PERFORMANCE INVESTIGATION

R. E. MARTIN (International Fuel Cells Corp., South Windsor, Conn.) and M. A. MANZO 5 Aug. 1988 10 p Presented at the 23rd Intersociety Energy Conversion Engineering Conference, Denver, Colo., 31 Jul. - 5 Aug. 1988; sponsored in part by ASME, AIAA, ANS, SAE, IEEE, ACS, and AIChE (NASA-TM-100937; E-4217; NAS 1.15:100937) Avail: NTIS HC A02/MF A01 CSCL 07D

An exploratory experimental fuel cell test program was conducted to investigate the performance characteristics of alkaline laboratory research electrodes. The objective of this work was to establish the effect of temperature, pressure, and concentration upon performance and evaluate candidate cathode configurations having the potential for improved performance. The performance characterization tests provided data to empirically establish the effect of temperature, pressure, and concentration upon performance for cell temperatures up to 300 F and reactant pressures up to 200 psia. Evaluation of five gold alloy cathode catalysts revealed that three doped gold alloys had more than two times the surface areas of reference cathodes and therefore offered the best potential for improved performance. Author

N88-28109*# National Aeronautics and Space Administration. Lewis Research Center, Cleveland, OH.

THE EFFECT OF COMPRESSION ON INDIVIDUAL PRESSURE VESSEL NICKEL/HYDROGEN COMPONENTS

MICHELLE A. MANZO and MARLA E. PEREZ-DAVIS Aug. 1988 12 p Presented at the 23rd Intersociety Energy Conversion Engineering Conference, Denver, Colo., 31 Jul. - 5 Aug. 1988; sponsored in part by ASME, AIAA, ANS, SAE, IEEE, ACS and AIChE (NASA-TM-101312; E-4305; NAS 1.15:101312) Avail: NTIS HC A03/MF A01 CSCL 10C

Compression tests were performed on representative Individual Pressure Vessel (IPV) Nickel/Hydrogen cell components in an effort to better understand the effects of force on component compression and the interactions of components under compression. It appears that the separator is the most easily compressed of all of the stack components. It will typically partially compress before any of the other components begin to compress. The compression characteristics of the cell components in assembly differed considerably from what would be predicted based on individual compression characteristics. Component interactions played a significant role in the stack response to compression. The results of the compression tests were factored into the design and selection of Belleville washers added to the cell stack to accommodate nickel electrode expansion while keeping the pressure on the stack within a reasonable range of the original preset. Author

N88-29952*# National Aeronautics and Space Administration. Lewis Research Center, Cleveland, OH.

ELECTROCATALYTIC REDUCTION OF OXYGEN ON MODIFIED OXIDE SURFACES M.S. Thesis

SCOTT A. CHAFFINS, VAKULA S. SRINIVASAN (Bowling Green State Univ., Ohio.), and JOSEPH SINGER Sep. 1988 84 p (Contract NGT-36-002-800) (NASA-TM-101333; E-4345; NAS 1.15:101333) Avail: NTIS HC A05/MF A01 CSCL 07D

A first step which frequently occurs in the reduction of dioxygen, e.g., at the cathode of the alkaline fuel cell, is the two-electron reduction to the peroxy ion, HO bar 2. For the efficiency of the fuel cell, this ion must be further reduced, or decomposed, to OH(-). Rate constants for HO bar 2 decomposition have been determined in 31 percent KOH at 25 C for the following catalysts in the form of suspended powders and Teflon-bonded electrodes: Pt, Au, cobalt tetrametoxyl phenyl porphyrin (CoTMPP), and La sub 0.5Pb sub 0.5MnO3. Rates were normalized to unit surface area measured by several methods as suitable. Where possible, four methods were used to measure rate constants: gasometric, oxygen probe, rotating disk electrode, and open-circuit potential

decay. Steady-state polarization was also tried but was not as satisfactory. Comparisons are given for the methods in regard to reliability, applicability to the material, and convenience. Author

26

METALLIC MATERIALS

Includes physical, chemical, and mechanical properties of metals, e.g., corrosion; and metallurgy.

A88-10028* National Aeronautics and Space Administration. Lewis Research Center, Cleveland, OH.

EFFECT OF ALLOY COMPOSITION ON THE SODIUM-SULFATE INDUCED HOT CORROSION ATTACK OF CAST NICKEL-BASE SUPERALLOYS AT 900 C

C. A. STEARNS, D. L. DEADMORE, and C. A. BARRETT (NASA, Lewis Research Center, Cleveland, OH) IN: Alternate alloying for environmental resistance; Proceedings of the Symposium, New Orleans, LA, Mar. 2-6, 1986. Warrendale, PA, Metallurgical Society, Inc., 1987, p. 131-143. refs

The effects of Cr, Al, Ti, Mo, Ta, Nb, and W content on the hot corrosion of Ni-base alloys were examined experimentally. The superalloys were tested for 300 1-hr cycles at 900 C in a Mach 0.3 burner rig flame containing 0.5 ppmw sodium. The data reveal that the best corrosion resistance is obtained when the Cr content is greater than 12 percent; however, good resistance is detected in some alloys with Cr content less than 10 percent provided that the Al content is less than 2.5 wt pct and the Ti content is less than 4 wt pct. It is observed that the influence of W, Ta, Mo, and Nb content on resistance is dependent on Al and Ti contents. The derivation of an equation for estimating hot corrosion attack as a function of alloy composition using multiple linear regression analysis is described. The applicability of the equation is tested using various data sets of alloys. It is noted that the equation can be used to explain the effects of alloy composition on attack rates. I.F.

A88-10029* United Technologies Research Center, East Hartford, CT.

HIGH-TEMPERATURE OXIDATION/CORROSION OF IRON-BASED SUPERALLOYS

F. D. LEMKEY, J. G. SMEGGIL, R. S. BAILEY (United Technologies Research Center, East Hartford, CT), J. C. SCHUSTER (Wien, Universitaet, Vienna, Austria), and H. NOWOTNY (Connecticut, University, Storrs) IN: Alternate alloying for environmental resistance; Proceedings of the Symposium, New Orleans, LA, Mar. 2-6, 1986. Warrendale, PA, Metallurgical Society, Inc., 1987, p. 145-155. DOE-sponsored research. refs (Contract DEN3-282)

The oxidation and sulfidation of several novel iron-base superalloys were evaluated in high-temperature cyclic tests. The experimental austenitic alloys examined were modifications of NASAUT-4GA which were developed for Stirling-engine application. The weight gains and resulting surface scales were measured and analyzed. Mixed oxide scales were found to form on all specimens exposed above 871 C. The build-up of these scales led to a depletion of Mn and Cr in a zone adjacent to the oxides. In addition, the initial oxidation of the Fe-rich alloy was inhibited by a thin but tenacious Si layer which formed at the interface between oxides and the parent layer. Sulfidation tests using Na2SO4 coatings resulted in the formation of a protective spinel and alpha-Fe2O3 phases. Preferential attack of the carbide phase by hydrogen was not observed after 350 h at 871 C. Author

A88-10030* National Aeronautics and Space Administration. Lewis Research Center, Cleveland, OH.

ROLE OF MOLYBDENUM IN THE NA2SO4 INDUCED CORROSION OF SUPERALLOYS AT HIGH TEMPERATURE

A. K. MISRA (NASA, Lewis Research Center, Cleveland, OH) IN:

Alternate alloying for environmental resistance; Proceedings of the Symposium, New Orleans, LA, Mar. 2-6, 1986. Warrendale, PA, Metallurgical Society, Inc., 1987, p. 187-208. Previously announced in STAR as N86-21658. refs

Sodium sulfate induced corrosion of a molybdenum containing nickel-base superalloy, Udimet 700, was studied in laboratory furnace test and in a high velocity (Mach 0.3) burner rig. The effect of SO₂ content in the atmosphere on the corrosion behavior in the laboratory furnace tests was determined. catastrophic corrosion occurs only when the melt contains MoO₃ in addition to Na₂SO₄ and Na₂MoO₄. The conditions under which catastrophic corrosion occurs are identified and a mechanism is described to explain the catastrophic corrosion. Author

A88-10031* National Aeronautics and Space Administration. Lewis Research Center, Cleveland, OH.

THE EFFECT OF VARIATIONS OF COBALT CONTENT ON THE CYCLIC OXIDATION RESISTANCE OF SELECTED NI-BASE SUPERALLOYS

CHARLES A. BARRETT (NASA, Lewis Research Center, Cleveland, OH) IN: Alternate alloying for environmental resistance; Proceedings of the Symposium, New Orleans, LA, Mar. 2-6, 1986. Warrendale, PA, Metallurgical Society, Inc., 1987, p. 211-231. Previously announced in STAR as N86-31702.

Cobalt levels were systematically varied in the Ni-base turbine alloys U-700 (cast), U-700m (PM/HIP), Waspaloy, Mar-M-247, In-738, Nimonic-115, U-720, and SX-R-150. the cobalt levels ranged from 0 wt pct to the nominal commercial content in each alloy. the alloys were tested in cyclic oxidation in static air at 1000, 1100 and 1150 C for 500, 200, and 100 hr, respectively. An oxidation attack parameter, K_a, derived from the specific weight change versus time data was used to evaluate the oxidation behavior of the alloys along with X-ray diffraction analysis of the surface oxides. The alloys tend to form either Cr₂O₃/chromite spinel or Al₂O₃/aluminate spinel depending on the Cr/Al ratio in the alloys. Alloys with a ratio of 3.5 or higher tend to favor the Cr oxides while those under 3.0 form mostly Al oxides. In general the Al₂O₃/aluminate spinel forming alloys have the better oxidation resistance. Increased cobalt content lowers the scaling resistance of the higher Cr alloys while a 5.0 wt pct Co content is optimum for the Al controlling alloys. The refractory metals, particularly Ta, appear beneficial to both types of oxides, perhaps due to the formation of the omnipresent trirutile Ni(Ta, Nb, Mo, W)₂O₆. Both scales break down as increasing amounts of NiO are formed.

Author

A88-10043* Case Western Reserve Univ., Cleveland, OH.
COMPRESSIVE CREEP BEHAVIOR OF ALLOYS BASED ON B2 FEAL

N. MANTRAVADI, K. VEDULA (Case Western Reserve University, Cleveland, OH), D. GAYDOSH, and R. H. TITRAN (NASA, Lewis Research Center, Cleveland, OH) IN: Alternate alloying for environmental resistance; Proceedings of the Symposium, New Orleans, LA, Mar. 2-6, 1986. Warrendale, PA, Metallurgical Society, Inc., 1987, p. 465-477. NASA-supported research. Previously announced in STAR as N86-28165. refs

Alloys based on FeAl are attractive alternative materials for environmental resistance at intermediate temperatures. Addition of small amounts of Nb, Hf, Ta, Mo, Zr, and B were shown to improve the compressive creep of this alloy at 1100 K. Boron, in particular, was found to have a synergistic effect along with Zr in providing properties substantially better than the binary alloy. This improvement seems to be related to the higher activation energy found for this alloy, suggesting a modification in the diffusion behavior due to the alloying additions. Author

A88-14567* National Aeronautics and Space Administration. Lewis Research Center, Cleveland, OH.

PRELIMINARY INVESTIGATION OF INERTIA FRICTION WELDING B2 ALUMINIDES

J. DANIEL WHITTENBERGER, THOMAS J. MOORE (NASA, Lewis Research Center, Cleveland, OH), and DANIEL L. KURUZAR

(Manufacturing Technology, Inc., Mishawaka, IN) Journal of Materials Science Letters (ISSN 0261-8028), vol. 6, Sept. 1987, p. 1016-1018. refs

An attempt is made to achieve inertia friction-welding in FeAl and NiAl samples, taking into account their intermetallics' compositions, extrusion parameters, and microstructural data. The energy required for the weld is stored in a rotating flywheel mass attached to one of the two pieces to be joined; when enough energy is introduced, the flywheel is disconnected and an axial load is applied which forces the spinning piece against the stationary one, converting the energy into heat by means of friction. Due to the inherent brittleness of the aluminides, a step-load program was used in which an initial, low-pressure heat buildup increased the work pieces' ductility. O.C.

A88-18528* Illinois Inst. of Tech., Chicago.

PRECIPITATION IN A RAPIDLY SOLIDIFIED AND AGED NI-AL-MO ALLOY

P. NASH (Illinois Institute of Technology, Chicago) and T. K. GLASGOW (NASA, Lewis Research Center, Cleveland, OH) Acta Metallurgica (ISSN 0001-6160), vol. 35, Nov. 1987, p. 2627-2635. refs

The early stages of decomposition of a highly supersaturated nickel-base alloy have been studied using TEM, SEM, and X-ray diffraction. The material was produced as a metastable solid solution by chill-block melt-spinning. On aging, the material exhibited a number of decomposition products appearing in series or concomitantly. Some of the decomposition products of this alloy, Ni₄Mo, Ni₃Mo, and Ni₂Mo, are related to those found in Ni-Mo binary alloys. Alpha-Mo formed during solidification was distinguished from that formed by precipitation in the solid state by orientation relationships. Author

A88-18884* National Aeronautics and Space Administration. Lewis Research Center, Cleveland, OH.

EFFECT OF INITIAL GAMMA PRIME SIZE ON THE ELEVATED TEMPERATURE CREEP PROPERTIES OF SINGLE CRYSTAL NICKEL BASE SUPERALLOYS

M. V. NATHAL (NASA, Lewis Research Center, Cleveland, OH) Metallurgical Transactions A - Physical Metallurgy and Materials Science (ISSN 0360-2133), vol. 18A, Nov. 1987, p. 1961-1970. refs

The influence of initial gamma-prime size and shape on the high-temperature creep properties of two single-crystal Ni-base superalloys was investigated. The two alloys were chosen to represent different magnitudes of gamma/gamma-prime lattice mismatch. A range of initial microstructures was produced by various quenching and aging treatments. Creep-rupture testing at 1000 C was performed under stresses where gamma-prime directionally coarsens to form gamma/gamma-prime lamellae in the early portion of the creep life. Both alloys exhibited a peak in creep resistance as a function of initial gamma-prime size. The peak corresponded to an initial microstructure consisting of cuboidal precipitates aligned along 001 line directions. These aligned cuboidal gamma-prime particles directionally coarsened into a relatively perfect lamellar gamma/gamma-prime structure in the early stages of creep, whereas the more irregularly shaped and distributed gamma-prime particles in both under- and overaged material formed more irregular lamellae with more imperfections. The alloy with a lower magnitude of mismatch was less sensitive to initial gamma-prime size and shape. Author

A88-18886* Arizona Univ., Tucson.

A THERMODYNAMIC PREDICTION FOR MICROPOROSITY FORMATION IN ALUMINUM-RICH AL-CU ALLOYS

D. R. POIRIER, K. YEUM (Arizona, University, Tucson), and A. L. MAPLES Metallurgical Transactions A - Physical Metallurgy and Materials Science (ISSN 0360-2133), vol. 18A, Nov. 1987, p. 1979-1987. refs
(Contract NAG3-723)

A computer model is used to predict the formation and degree of microporosity in a directionally solidified Al-4.5 wt pct Cu alloy, considering the interplay between solidification shrinkage and gas

porosity. Macroseggregation theory is used to determine the local pressure within the interdendritic liquid. Results show interdendritic porosity for initial hydrogen contents in the 0.03-1 ppm range, and none below contents of 0.03. An increase in either the thermal gradient or the solidification rate is shown to decrease the amount of interdendritic porosity. R.R.

A88-19958* Case Western Reserve Univ., Cleveland, OH.
CRYSTALLIZATION BEHAVIOR OF A MELT-SPUN FE-NI BASED STEEL

G. M. MICHAL, V. LAXMANAN (Case Western Reserve University, Cleveland, OH), and T. K. GLASGOW (NASA, Lewis Research Center, Cleveland, OH) IN: Undercooled alloy phases; Proceedings of the Hume-Rothery Memorial Symposium, New Orleans, LA, Mar. 2-6, 1986. Warrendale, PA, Metallurgical Society, Inc., 1987, p. 95-107. refs

Whether Fe-Ni-based alloys solidify with a bcc or fcc structure has been observed by many investigators to be a stronger function of kinetics and undercooling than strictly free-energy minimization. Such behavior has been observed in an Fe(52.8)-Ni(28.7)Al(3.4)Ti(6.1)B(9.0) alloy. The alloy was cast as ribbons about 45 microns thick using a dual free-jet variation of chillback melt spinning against a Cu wheel. Optical, X-ray, and electron analyses of the as-cast and annealed ribbons were performed. A microstructure of at least four layers containing combinations of ecc, bcc, and amorphous phases in differing proportions was observed in the as-cast ribbon. The midthickness layer had the most unusual features, containing fcc grains about 75 nm in size encompassing spherulitic regions as large as 15 microns comprised of fcc grains about 25 nm in size. The crystallization sequence responsible for the as-cast microstructure is discussed in terms of the competition between the formation of bcc and fcc phases as influenced by undercooling, recalescence, and variations in cooling rate experienced by the as-cast ribbon.

Author

A88-19960* National Aeronautics and Space Administration.
 Lewis Research Center, Cleveland, OH.

UNDERCOOLED AND RAPIDLY QUENCHED NI-MO ALLOYS

S. N. TEWARI and T. K. GLASGOW (NASA, Lewis Research Center, Cleveland, OH) IN: Undercooled alloy phases; Proceedings of the Hume-Rothery Memorial Symposium, New Orleans, LA, Mar. 2-6, 1986. Warrendale, PA, Metallurgical Society, Inc., 1987, p. 145-162. Research supported by the National Research Council. Previously announced in STAR as N86-21659. refs

Hypoeutectic, eutectic, and hypereutectic nickel-molybdenum alloys were rapidly solidified by both bulk undercooling and melt spinning techniques. Alloys were undercooled in both electromagnetic levitation and differential thermal analysis equipment. The rate of recalescence depended upon the degree of initial undercooling and the nature (faceted or nonfaceted) of the primary nucleating phase. Alloy melts were observed to undercool more in the presence of primary Beta (NiMo intermetallic) phase than in gamma (fcc solid solution) phase. Melt spinning resulted in an extension of molybdenum solid solubility in gamma nickel, from 28 to 37.5 at. pct Mo. Although the microstructures observed by undercooling and melt spinning were similar, the microseggregation pattern across the gamma dendrites was different. The range of microstructures evolved was analyzed in terms of the nature of the primary phase to nucleate, its subsequent dendritic growth, coarsening and fragmentation, and final solidification of interdendritic liquid.

Author

A88-19966* National Aeronautics and Space Administration.
 Lewis Research Center, Cleveland, OH.

DENDRITIC GROWTH IN A SUPERCOOLED ALLOY MELT

V. LAXMANAN (NASA, Lewis Research Center; Case Western Reserve University, Cleveland, OH) IN: Undercooled alloy phases; Proceedings of the Hume-Rothery Memorial Symposium, New Orleans, LA, Mar. 2-6, 1986. Warrendale, PA, Metallurgical Society, Inc., 1987, p. 453-496. refs

A simple model which describes the growth of an 'array' of dendrites into a supercooled, binary, alloy melt is presented. Solute

diffusion is calculated by superposing the solutions given by Flemings and Zener, and also, by superposing the solutions given by Ivantsov and Flemings. A general expression for the transport solution is suggested from which all other dendrite growth models presented earlier may be obtained as special cases. It is shown that both 'free' and 'constrained' growth may be described by a single transport solution, which indicates that (1) both thermal and solutal effects will be important during 'free' growth in dilute alloys, (2) only solutal effects are predominant during 'free' growth in concentrated alloys and during 'constrained' growth. An examination of the relevant dimensionless parameters also suggests that all dendrite growth models, regardless of the assumptions used to determine the tip radius (marginal stability, minimum undercooling, maximum velocity, minimum entropy production) should predict the experimentally observed extrema in tip radius and growth velocity in dilute alloys, during 'free' dendritic growth. Experimental data in binary H₂O-NaCl and succinonitrile-acetone solutions are shown to be in good agreement with the model. Author

A88-20199* National Aeronautics and Space Administration.
 Lewis Research Center, Cleveland, OH.

SIMULATING THE COOLING OF AN IMMISCIBLE ALLOY

H. B. PROBST (NASA, Lewis Research Center, Cleveland, OH) Advanced Materials and Processes (ISSN 0882-7958), vol. 132, Nov. 1987, p. 46-49. refs

A computer program to simulate the cooling of immiscible alloys is described, and the Pb-Zn system is presented as an example. The program permits the user to calculate various compositions of immiscible alloys. Illustrations are presented which depict the sequence of computer-monitor displays generated by the program. C.D.

A88-20266* National Aeronautics and Space Administration.
 Lewis Research Center, Cleveland, OH.

SODIUM SULFATE-INDUCED CORROSION OF PURE NICKEL AND SUPERALLOY UDIMET 700 IN A HIGH VELOCITY BURNER RIG AT 900 C

A. K. MISRA (NASA, Lewis Research Center; Case Western Reserve University, Cleveland, OH) Corrosion (ISSN 0010-9312), vol. 43, July 1987, p. 440-450. refs

Sodium sulfate-induced corrosion of pure nickel and a commercial nickel-base superalloy, Udimet 700 (U-700), were studied at 900 C in a Mach 0.3 burner rig with different Na levels in the combustor. The corrosion rate of Ni was independent of the Na level in the combustor and considerably lower than that measured in laboratory salt spray tests. The lower rates are associated with the deposition of only a small amount of Na₂SO₄ on the surface of the NiO scale. Corrosion of U-700 was observed to occur in two stages. During the first stage, the corrosion proceeds by reaction of Cr₂O₃ scale with the Na₂SO₄ and evaporation of the Na₂CrO₄ reaction product from the surface of the corroding sample. Cr depletion in the alloy occurs and small sulfide particles are formed in the Cr depletion zone. Extensive sulfidation occurs during the second state of corrosion, and a thick scale forms. The relationship between the corrosion rate of U-700 and the Na level in the combustor gives a good correlation in the range of 0.3 to 1.5 ppm by weight Na. Very low levels of Na in the combustor cause accelerated oxidation of U-700 without producing the typical hot corrosion morphology. Author

A88-20269* Dartmouth Coll., Hanover, NH.

DYNAMIC RECRYSTALLIZATION AND GRAIN BOUNDARY MIGRATION IN B2 FEAL

I. BAKER (Dartmouth College, Hanover, NH) and D. J. GAYDOSH (NASA, Lewis Research Center, Cleveland, OH) Metallography (ISSN 0026-0800), vol. 20, 1987, p. 347-357. refs

Transmission electron microscopy and optical microscopy were used to examine polycrystalline specimens of the B2-structured alloy FeAl strained under tension to fracture at elevated temperature. Strain-induced grain boundary migration was observed above 900 K and dynamic recrystallization was found at 1000 K

26 METALLIC MATERIALS

and 1100 K. Little evidence of dynamic recovery was evident but some networks were formed at 1100 K. Author

A88-22700* National Aeronautics and Space Administration. Lewis Research Center, Cleveland, OH.

THERMAL AGING EFFECTS IN REFRACTORY METAL ALLOYS

JOSEPH R. STEPHENS (NASA, Lewis Research Center, Cleveland, OH) IN: Space nuclear power systems 1986; Proceedings of the Third Symposium, Albuquerque, NM, Jan. 13-16, 1986. Malabar, FL, Orbit Book Co., Inc., 1987, p. 291-304. Previously announced in STAR as N86-16334. refs

The alloys of niobium and tantalum are attractive from a strength and compatibility viewpoint for high operating temperatures required in materials for fuel cladding, liquid metal transfer, and heat pipe applications in space power systems that will supply from 100 kWe to multi-megawatts for advanced space systems. To meet the system requirements, operating temperatures ranging from 1100 to 1600 K have been proposed. Expected lives of these space power systems are from 7 to 10 yr. A program is conducted at NASA Lewis to determine the effects of long-term, high-temperature exposure on the microstructural stability of several commercial tantalum and niobium alloys. Variables studied in the investigation include alloy composition, pre-age annealing temperature, aging time, temperature, and environment (lithium or vacuum), welding, and hydrogen doping. Alloys are investigated by means of cryogenic bend tests and tensile tests. Results show that the combination of tungsten and hafnium or zirconium found in commercial alloys such as T-111 and Cb-752 can lead to aging embrittlement and increased susceptibility to hydrogen embrittlement of ternary and more complex alloys. Modification of alloy composition helps to eliminate the embrittlement problem.

Author

A88-24037*# Southwest Research Inst., San Antonio, TX. **PHENOMENOLOGICAL MODELING OF HARDENING AND THERMAL RECOVERY IN METALS**

K. S. CHAN, U. S. LINDHOLM (Southwest Research Institute, San Antonio, TX), and S. R. BODNER (Technion - Israel Institute of Technology, Haifa) ASME, Transactions, Journal of Engineering Materials and Technology (ISSN 0094-4289), vol. 110, Jan. 1988, p. 1-8. Research supported by the Southwest Research Institute. refs

(Contract NAS3-23925)

Modeling of hardening and thermal recovery in metals is considered within the context of unified elastic-viscoplastic theories. Specifically, the choices of internal variables and hardening measures, and the resulting hardening response obtained by incorporating saturation-type evolution equations into two general forms of the flow law are examined. Based on the analytical considerations, a procedure for delineating directional and isotropic hardening from uniaxial hardening data has been developed for the Bodner-Partom model and applied to a nickel-base superalloy, B1900 + Hf. Predictions based on the directional hardening properties deduced from the monotonic loading data are shown to be in good agreement with results of cyclic tests. Author

A88-24485*# National Aeronautics and Space Administration. Lewis Research Center, Cleveland, OH.

INTERDIFFUSION IN NI-RICH, NI-CR-AL ALLOYS AT 1100 AND 1200 C. I - DIFFUSION PATHS AND MICROSTRUCTURES. II - DIFFUSION COEFFICIENTS AND PREDICTED CONCENTRATION PROFILES

J. A. NESBITT (NASA, Lewis Research Center, Cleveland, OH) and R. W. HECKEL (Michigan Technological University, Houghton) Metallurgical Transactions A - Physical Metallurgy and Materials Science (ISSN 0360-2133), vol. 18A, Dec. 1987, p. 2061-2086. refs

(Contract NAG3-244)

Interdiffusion in Ni-rich Ni-Cr-Al alloys is investigated experimentally after annealing at 1100 and 1200 C using gamma/gamma, gamma/gamma + beta, gamma/gamma + gamma prime, and gamma/gamma + alpha diffusion couples. The amount

and location of Kirkendall porosity suggests that Al diffuses more rapidly than Cr which diffuses more rapidly than Ni in the gamma phase of Ni-Cr-Al alloys. The location and extent of maxima and minima in the concentration profiles of the diffusion couples indicate that both cross-term diffusion coefficients are positive. Measurements are also presented of the ternary interdiffusion coefficients of the gamma phase in the Ni-Cr-Al system. It is shown that the interdiffusion coefficients can be accurately predicted by using a ternary finite-difference interdiffusion model. V.L.

A88-24486*# National Aeronautics and Space Administration. Lewis Research Center, Cleveland, OH.

PREDICTING DIFFUSION PATHS AND INTERFACE MOTION IN GAMMA/GAMMA + BETA, NI-CR-AL DIFFUSION COUPLES

J. A. NESBITT (NASA, Lewis Research Center, Cleveland, OH) and R. W. HECKEL (Michigan Technological University, Houghton) Metallurgical Transactions A - Physical Metallurgy and Materials Science (ISSN 0360-2133), vol. 18A, Dec. 1987, p. 2087-2094. refs

(Contract NAG3-244)

A simplified model has been developed to predict Beta recession and diffusion paths in ternary gamma/gamma + beta diffusion couples (gamma:fcc, beta: NiAl structure). The model was tested by predicting beta recession and diffusion paths for four gamma/gamma + beta, Ni-Cr-Al couples annealed for 100 hours at 1200 C. The model predicted beta recession within 20 percent of that measured for each of the couples. The model also predicted shifts in the concentration of the gamma phase at the gamma/gamma + beta interface within 2 at. pct Al and 6 at. pct Cr of that measured in each of the couples. A qualitative explanation based on simple kinetic and mass balance arguments has been given which demonstrates the necessity for diffusion in the two-phase region of certain gamma/gamma + beta, Ni-Cr-Al couples. Author

A88-24490* National Aeronautics and Space Administration. Lewis Research Center, Cleveland, OH.

CYCLIC HARDENING MECHANISMS IN NIMONIC 80A

B. A. LERCH (NASA, Lewis Research Center, Cleveland, OH) and V. GEROLD (Stuttgart, Universitaet; Max-Planck-Institut fuer Metallforschung, Federal Republic of Germany) Metallurgical Transactions A - Physical Metallurgy and Materials Science (ISSN 0360-2133), vol. 18A, Dec. 1987, p. 2135-2141. refs

A nickel base superalloy was fatigued under constant plastic strain range control. The hardening response was investigated as a function of plastic strain range and particle size of the gamma prime phase. Hardening was found to be a function of the slip band spacing. Numerous measurements of the slip band spacing and other statistical data on the slip band structures were obtained. Interactions between intersecting slip systems were shown to influence hardening. A Petch-Hall model was found to describe best this relationship between the response stress and the slip band spacing. Author

A88-24521* Hahn-Meitner-Inst. fuer Kernforschung, Berlin (Germany, F.R.).

ON THE CYCLIC STRESS-STRAIN BEHAVIOUR OF A NI-BASE SUPERALLOY AT ROOM TEMPERATURE

VAKIL SINGH, R. P. WAHL (Hahn-Meitner-Institut fuer Kernforschung Berlin GmbH, Federal Republic of Germany), W. CHEN (Berlin, Technische Universitaet, Federal Republic of Germany), and H. M. YUN (NASA, Lewis Research Center, Cleveland, OH) Scripta Metallurgica (ISSN 0036-9748), vol. 22, Jan. 1988, p. 77-79. Research supported by the Stiftung Volkswagenwerk. refs

The cyclic stress-strain behavior of Nimonic alloy PE16 was studied at room temperature and at different aging conditions to determine whether the plateau in the cyclic stress-strain curve (CSSC) reported by Arbutnot (1982) is typical of the room temperature behavior and/or some specific initial microstructural states. Specimen blanks were heat-treated in batches in Ar/H₂ (98/2) atmosphere to produce gamma-prime precipitates of different average sizes, but with the volume fraction of

gamma-prime precipitates kept constant at about 7 percent at all the heat-treatment conditions. Total axial strain controlled LCF tests were conducted under fully reversed loading ($R = -1$) at a constant strain rate of 0.004/s, using a servohydraulic machine. The load response in tension and compression was recorded continually, and stress-strain hysteresis loops were recorded at frequent intervals. In the present investigation, the CSSCs of the P16 alloy at room temperature did not display the plateaus reported by Arbuthnot. I.S.

A88-28902* National Aeronautics and Space Administration. Lewis Research Center, Cleveland, OH.

DIFFUSIONAL TRANSPORT DURING THE CYCLIC OXIDATION OF GAMMA + BETA, NI-CR-AL(Y, ZR) ALLOYS

J. A. NESBITT (NASA, Lewis Research Center, Cleveland, OH) and R. W. HECKEL (Michigan Technological University, Houghton) Oxidation of Metals (ISSN 0030-770X), vol. 29, Feb. 1988, p. 75-102. refs (Contract NSG-3215)

The cyclic oxidation behavior of several cast gamma + beta, Ni-Cr-Al(Y, Zr) alloys and one low-pressure plasma spraying gamma + beta, Ni-Co-Cr-Al(Y) alloy was studied. Cyclic oxidation was found to result in a decreasing Al concentration at the oxide-metal interface due to a high rate of Al consumption coupled with oxide scale cracking and spalling. Diffusion paths plotted on the ternary phase diagram showed higher Ni concentrations with increasing cyclic oxidation exposures. The alloy with the highest rate of Al consumption and the highest Al content underwent breakaway oxidation following 500 1-hr cycles at 1200 C. R.R.

A88-29098* National Aeronautics and Space Administration. Lewis Research Center, Cleveland, OH.

THE INFLUENCE OF GRAIN SIZE AND COMPOSITION ON 1000 TO 1400 K SLOW PLASTIC FLOW PROPERTIES OF NIAL

J. DANIEL WHITTENBERGER (NASA, Lewis Research Center, Cleveland, OH) Journal of Materials Science (ISSN 0022-2461), vol. 23, Jan. 1988, p. 235-240. refs

The compressive slow plastic flow behavior of several B2 crystal structure NiAl intermetallics has been studied in air between 1000 and 1400 K. Small grain-sized Ni-48.25 at. pct Al (of about 10 microns) was found to be stronger than the previously studied 17 microns diameter material. While grain refinement improved the strength at all test temperatures, the exact mechanism is not clear. Experiments at lower temperature revealed that composition as well as grain size can be an important factor, since Ni-49.2Al was weaker than Ni-48.25Al. Pronounced yield points were found during slow strain-rate testing at 1000 K; however, continued deformation appears to take place by the same mechanism(s) as found at high temperatures. Small changes in thermomechanical processing (TMP) schedules to fabricate Ni-49.2Al indicated that basic deformation characteristics (stress exponent and activation energy) are not affected; however, the preexponential term could be modified if TMP alters the grain structure. Author

A88-30269* National Aeronautics and Space Administration. Lewis Research Center, Cleveland, OH.

ADHERENT AL₂O₃ SCALES PRODUCED ON UNDOPED NICRAL ALLOYS

JAMES L. SMIALEK (NASA, Lewis Research Center, Cleveland, OH) Metallurgical Society of AIME and ASM, Symposium on Oxidation of Metals and Associated Mass Transport, Orlando, FL, Oct. 6, 7, 1986, Paper. 18 p. refs

Repeated oxidation and polishing of high purity Ni-15Cr-13Al has dramatically changed its cyclic oxidation behavior from nonadherent to adherent. No apparent change in scale phase, morphology or interface structure occurred during this transition, dismissing any mechanism based on pegging, vacancy sink, or growth stress. The principle change that did occur was a reduction in the sulfur content from 10 ppmw to 3 ppmw after 25 cycles at 1120 C. These observations are used to support the model of Al₂O₃ scale adherence put forth by Smeggil et al. which claims

that Al₂O₃ scale spallation occurs due to sulfur segregation and bond deterioration at the oxide-metal interface. Author

A88-31679* Dartmouth Coll., Hanover, NH.

THE MICROSTRUCTURE AND TENSILE PROPERTIES OF EXTRUDED MELT-SPUN RIBBONS OF IRON-RICH B2 FEAL

I. BAKER (Dartmouth College, Hanover, NH) and D. J. GAYDOSH (NASA, Lewis Research Center, Cleveland, OH) IN: High-temperature ordered intermetallic alloys II; Proceedings of the Second Symposium, Boston, MA, Dec. 2-4, 1986. Pittsburgh, PA, Materials Research Society, 1987, p. 315-320. refs

The microstructure of extruded rods of iron-rich FeAl (B2-structure), as characterized by TEM, SEM, optical microscopy and x-ray diffractometry, consisted of elongated grains with a 111-line fibre texture containing a high dislocation density. Numerous oxide particles were found, mostly in lines which reflected the matrix flow during extrusion. In addition, some large inclusions were present. Tensile testing of annealed, relatively dislocation-free specimens as a function of increasing temperature found increasing ductility up to 900K, above which a ductility drop occurred accompanied by a change in fracture mode, from transgranular cleavage to intergranular fracture. The yield strength, which was independent of temperature up to 800K (at about 500MPa), also decreased rapidly as diffusion became more important. The predominant slip vector changed from 111-line to 100-line around 700K. Author

A88-31684* Case Western Reserve Univ., Cleveland, OH.

B2 ALUMINIDES FOR HIGH TEMPERATURE APPLICATIONS

K. VEDULA (Case Western Reserve University, Cleveland, OH) and J. R. STEPHENS (NASA, Lewis Research Center, Cleveland, OH) IN: High-temperature ordered intermetallic alloys II; Proceedings of the Second Symposium, Boston, MA, Dec. 2-4, 1986. Pittsburgh, PA, Materials Research Society, 1987, p. 381-391. refs

The structure, phase composition, and mechanical properties of B2 FeAl and NiAl aluminides are investigated. It is noted that, in both alloys, the room temperature brittleness is of primary concern. In the case of FeAl, significant tensile ductilities of up to 8 percent have been obtained at room temperature in iron-rich alloys. In the case of polycrystalline NiAl, attempts to improve ductility have not so far been successful. Possible solutions to this problem are examined. V.L.

A88-31694* Case Western Reserve Univ., Cleveland, OH.

ROOM TEMPERATURE TENSILE DUCTILITY IN POWDER PROCESSED B2 FEAL ALLOYS

M. A. CRIMP, K. M. VEDULA (Case Western Reserve University, Cleveland, OH), and D. J. GAYDOSH (NASA, Lewis Research Center, Cleveland, OH) IN: High-temperature ordered intermetallic alloys II; Proceedings of the Second Symposium, Boston, MA, Dec. 2-4, 1986. Pittsburgh, PA, Materials Research Society, 1987, p. 499-504. refs

It has been shown that it is possible to obtain significant room temperature tensile ductility in FeAl alloys using iron-rich deviations from stoichiometry. A comparison of the room temperature tensile and compressive behaviors of Fe-50 at. pct Al and Fe-40 at. pct Al shows that FeAl is brittle at higher Al contents because it fractures along grain boundaries before general yielding. Lower aluminum contents reduce the yield stress substantially and hence some ductility is observed before fracture. Addition of boron results in measurable improvements in ductility of Fe-40 at. pct Al and is accompanied by an increase in transgranular tearing on the fracture surface, suggesting a grain boundary strengthening mechanism. Increasing the cooling rate following annealing at 1273 K results in a large increase in the yield strength and a corresponding decrease in ductility. Author

A88-32357*# Cincinnati Univ., OH.

ANISOTROPIC CONSTITUTIVE MODELING FOR NICKEL BASE SINGLE CRYSTAL SUPERALLOYS USING A CRYSTALLOGRAPHIC APPROACH

D. C. STOUFFER (Cincinnati, University, OH) and M. Y. SHEH

IN: Structures, Structural Dynamics and Materials Conference, 29th, Williamsburg, VA, Apr. 18-20, 1988, Technical Papers, Part 3. Washington, DC, American Institute of Aeronautics and Astronautics, 1988, p. 1719-1725. refs
(Contract NAG3-511)
(AIAA PAPER 88-2440)

A micromechanical model based on crystallographic slip theory was formulated for nickel-base single crystal superalloys. The current equations include both drag stress and back stress state variables to model the local inelastic flow. Specially designed experiments have been conducted to evaluate the effect of back stress in single crystals. The results showed that (1) the back stress is orientation dependent; and (2) the back stress state variable in the inelastic flow equation is necessary for predicting anelastic behavior of the material. The model also demonstrated improved fatigue predictive capability. Model predictions and experimental data are presented for single crystal superalloy Rene N4 at 982 C. Author

A88-32887* Aluminum Co. of America, Alcoa Center, PA.
DENDRITIC GROWTH OF UNDERCOOLED NICKEL-TIN. III
Y. WU (Aluminum Company of America, Alcoa Center, PA), T. J. PICCONE, Y. SHIOHARA, and M. C. FLEMINGS (MIT, Cambridge, MA) Metallurgical Transactions A - Physical Metallurgy and Materials Science (ISSN 0360-2133), vol. 19A, April 1988, p. 1109-1119. refs
(Contract NSG-7645; NAG3-597)

The paper is concerned with structures and microsegregations in undercooled droplets of Ni-25 wt pct Sn and eutectic Ni-32.5 wt pct Sn alloys. An analysis of experimental results suggests that all samples solidify dendritically and that the final structures are largely the result of ripening. Experimental data on minimum solute composition in the samples produced are bounded by two curves both of which assume equilibrium at all liquid-solid interfaces during recalescence and subsequent cooling. The eutectic alloy samples often show a dendritic structure over the surface in areas where shrinkage is present. This structure appears to be the remnant of an original growth structure in which only limited ripening occurred, due to the rapid removal of interdendritic liquid by shrinkage. V.L.

A88-35901* General Electric Co., Schenectady, NY.
LOW CYCLE FATIGUE

H. D. SOLOMON, ED., L. R. KAISAND, ED. (General Electric Co., Schenectady, NY), G. R. HALFORD, ED. (NASA, Lewis Research Center, Cleveland, OH), and B. N. LEIS, ED. (Battelle Columbus Laboratories, OH) Philadelphia, PA, American Society for Testing and Materials, 1988, 1305 p. For individual items see A88-35902 to A88-35938.
(ASTM STP-942)

The papers contained in this volume focus on various aspects of low cycle fatigue, including cyclic deformation, crack propagation, high-temperature low cycle fatigue, microstructural defects, multiaxial and variable amplitude loading, and life prediction. Papers are presented on the low cycle fatigue of some aluminum alloys, prediction of crack growth under creep-fatigue loading conditions, high-temperature low cycle fatigue behavior and lifetime prediction of a nickel-base ODS alloy, and an integrated approach to creep-fatigue life prediction. Other topics discussed include thermal fatigue testing of coated monocrystalline superalloys, low cycle fatigue of Al-Mg-Si alloys, and the effect of superimposed stresses at high frequency on low cycle fatigue. V.L.

A88-35905* Battelle Columbus Labs., OH.
A NONLINEAR HISTORY-DEPENDENT DAMAGE MODEL FOR LOW CYCLE FATIGUE

B. N. LEIS (Battelle Columbus Laboratories, OH) IN: Low cycle fatigue. Philadelphia, PA, American Society for Testing and Materials, 1988, p. 143-159. Research supported by Battelle Memorial Institute. refs
(Contract NAS3-22825)

A nonlinear damage postulate that embodies the dependence of the damage rate on cycle-dependent changes in the bulk

microstructure and the surface topography is examined. The postulate is analytically formulated in terms of the deformation history dependence of the bulk behavior. This formulation is used in conjunction with baseline data in accordance with the damage postulate to predict the low cycle fatigue resistance of OFE copper. Close comparison of the predictions with experimentally observed behavior suggests that the postulate offers a viable basis for nonlinear damage analysis. Author

A88-35908* National Aeronautics and Space Administration. Lewis Research Center, Cleveland, OH.

FATIGUE CRACK PROPAGATION OF NICKEL-BASE SUPERALLOYS AT 650 DEG C

J. GAYDA, T. P. GABB, and R. V. MINER (NASA, Lewis Research Center, Cleveland, OH) IN: Low cycle fatigue. Philadelphia, PA, American Society for Testing and Materials, 1988, p. 293-309. Previously announced in STAR as N86-12294. refs

The 650 C fatigue crack propagation behavior of two nickel-base superalloys, Rene 95 and Waspaloy, is studied with particular emphasis placed on understanding the roles of creep, environment, and two key grain boundary alloying additions, boron and zirconium. Comparison of air and vacuum data shows the air environment to be detrimental over a wide range of frequencies for both alloys. More in-depth analysis on Rene 95 shows at lower frequencies, such as 0.02 Hz, failure in air occurs by intergranular, environmentally-assisted creep crack growth, while at higher frequencies, up to 5.0 Hz, environmental interaction are still evident but creep effects are minimized. The effect of B and Zr in Waspaloy is found to be important where environmental and/or creep interactions are presented. In those instances, removal of B and Zr dramatically increases crack growth and it is therefore plausible that effective dilution of these elements may explain a previously observed trend in which crack growth rates increase with decreasing grain size. Author

A88-35910* National Aeronautics and Space Administration. Lewis Research Center, Cleveland, OH.

AN UPDATE OF THE TOTAL-STRAIN VERSION OF SRP

JAMES F. SALTSMAN and GARY R. HALFORD (NASA, Lewis Research Center, Cleveland, OH) IN: Low cycle fatigue. Philadelphia, PA, American Society for Testing and Materials, 1988, p. 329-340; Discussion, p. 340, 341. Previously announced in STAR as N86-12295. refs

An updated procedure for characterizing an alloy and predicting cyclic life by using the total strain range version of strainrange partitioning (TS-SRP) has been developed. The principal feature of this update is a new procedure for determining the intercept of time dependent elastic strain range versus cyclic life lines. The procedure is based on an established relation between failure and the cyclic stress-strain response of an alloy. The stress-strain response is characterized by empirical equations presented in this report. These equations were determined with the aid of a cyclic constitutive model. The procedures presented herein reduce the testing required to characterize an alloy. Failure testing is done only in the high strain, low life regime; cyclic stress-strain response is determined from tests conducted in both the high and low strain regimes. These tests are carried out to stability of the stress-strain hysteresis loop but not to failure. Thus both the time and costs required to characterize an alloy are greatly reduced. This approach was evaluated and verified for two nickel base superalloys, AF2-1DA and Inconel 718. Author

A88-35911* National Aeronautics and Space Administration. Lewis Research Center, Cleveland, OH.

CREEP-FATIGUE BEHAVIOR OF NICOCRALY COATED PWA 1480 SUPERALLOY SINGLE CRYSTALS

R. V. MINER, J. GAYDA, and M. G. HEBUR (NASA, Lewis Research Center, Cleveland, OH) IN: Low cycle fatigue. Philadelphia, PA, American Society for Testing and Materials, 1988, p. 371-384. Previously announced in STAR as N86-10311. refs

Single crystal specimens of a Ni base superalloy, PWA 1480, with a low pressure plasma sprayed NiCoCrAlY coating were tested in various 0.1 Hz fatigue and creep fatigue cycles both at 1015

and 1050 C. Creep fatigue tests of the cp, pc, and cc types were conducted with various constant total strain ranges employing creep dwells at various constant stresses. Considerable cyclic softening occurred as was evidenced particularly by rapidly increasing creep rates in the creep fatigue tests. The cycle time in the creep fatigue tests typically decreased by more than 80 percent at 0.5 N sub f. Though cyclic life did correlate with delta epsilon sub in a better correlation existed with sub f for both the fatigue and creep fatigue tests, and poor correlations were observed with either sigma sub max or the average cycle time. A model containing both delta sigma and delta sigma (sub in), N sub f = alpha delta sigma (sub in) beta delta sigma gamma, with best fit values of sigma for each cycle type, but the same values of beta and gamma, was found to provide good correlations. Life lines were not greatly different among the cycle types, differing only by a factor of about three. The cp cycle life line was lowest for both test temperatures, however among the other three cycle types there was no consistent ranking. For all test types failure occurred predominately by multiple internal cracking originating at pores. The strong correlation of life with delta sigma may reflect a significant crack growth period in the life of the specimens. Author

A88-35913* Massachusetts Inst. of Tech., Cambridge.
A MODEL FOR LIFE PREDICTIONS OF NICKEL-BASE SUPERALLOYS IN HIGH-TEMPERATURE LOW CYCLE FATIGUE

GLENN R. ROMANOSKI, REGIS M. PELLOUX (MIT, Cambridge, MA), and STEPHEN D. ANTOLOVICH (Georgia Institute of Technology, Atlanta) IN: Low cycle fatigue. Philadelphia, PA, American Society for Testing and Materials, 1988, p. 456-467; Discussion, p. 468, 469. refs
 (Contract NSG-3263)

Extensive characterization of low-cycle fatigue damage mechanisms was performed on polycrystalline Rene 80 and IN100 tested in the temperature range from 871 to 1000 C. Low-cycle fatigue life was found to be dominated by propagation of microcracks to a critical size governed by the maximum tensile stress. A model was developed which incorporates a threshold stress for crack extension, a stress-based crack growth expression, and a failure criterion. The mathematical equivalence between this mechanistically based model and the strain-life low-cycle fatigue law was demonstrated using cyclic stress-strain relationships. The model was shown to correlate the high-temperature low-cycle fatigue data of the different nickel-base superalloys considered in this study. Author

A88-35918* National Aeronautics and Space Administration. Lewis Research Center, Cleveland, OH.

BITHERMAL FATIGUE - A LINK BETWEEN ISOTHERMAL AND THERMOMECHANICAL FATIGUE

GARY R. HALFORD, MICHAEL A. MCGAW, ROBERT C. BILL, and PAOLO D. FANTI (NASA, Lewis Research Center, Cleveland, OH) IN: Low cycle fatigue. Philadelphia, PA, American Society for Testing and Materials, 1988, p. 625-637. refs

A technique for bithermal fatigue testing is presented in which the tensile and compressive halves of the cycle are conducted isothermally at two significantly different temperatures. With reference to experimental results obtained for a nickel-base superalloy, B1900 + Hf, it is shown that bithermal fatigue testing is a simple alternative to thermomechanical fatigue and can provide a conservative determination of thermomechanical fatigue life for creep damage dominated failure modes. Bithermal fatigue results can be directly related to thermomechanical fatigue results through the use of an appropriate damage rule. V.L.

A88-35919* Massachusetts Inst. of Tech., Cambridge.
THERMAL-MECHANICAL CYCLIC STRESS-STRAIN RESPONSES OF CAST B-1900 + HF

N. MARCHAND, R. M. PELLOUX (MIT, Cambridge, MA), and G. L'ESPERANCE (Montreal, Universite, Montreal, Canada) IN: Low cycle fatigue. Philadelphia, PA, American Society for Testing and Materials, 1988, p. 638-656. refs
 (Contract NAG3-280)

The fatigue response of B-1900 + Hf superalloy is investigated experimentally under combined thermal and mechanical strain cycling in air, and the results are compared with the existing thermomechanical data on B-1900 + Hf and with the results of a comprehensive study of the fatigue behavior of the alloy under isothermal conditions. It is found that the cyclic stress-strain behavior of the alloy under thermomechanical fatigue is different from the isothermal behavior, with more hardening observed both at high and low temperatures. It is concluded that the synergistic coupling between cyclic strains and temperature cannot be ignored in predicting the cyclic stress-strain behavior of the alloy under realistic conditions. V.L.

A88-35922* Georgia Inst. of Tech., Atlanta.
EFFECT OF TEMPERATURE, MICROSTRUCTURE, AND STRESS STATE ON THE LOW CYCLE FATIGUE BEHAVIOR OF WASPALOY

D. R. STAHL, S. D. ANTOLOVICH (Georgia Institute of Technology, Atlanta), M. MIRDAMADI, and S. Y. ZAMRIK (Pennsylvania State University, University Park) IN: Low cycle fatigue. Philadelphia, PA, American Society for Testing and Materials, 1988, p. 728-750. refs
 (Contract NAG3-264)

Specimens of Waspaloy of two different microstructures were tested in uniaxial and torsional low-cycle fatigue at 24 and 649 C. For all specimens, deformation and failure mechanisms are found to be independent of stress state at 24 C; in both microstructures, failure is associated with the formation of shear cracks. At 649 C, deformation and failure mechanisms for the fine-grain large gamma-prime specimens are independent of stress state, and the mechanisms are similar to those observed at 24 C. For the coarse-grain small gamma-prime specimens, however, failure occurs on principal planes in torsion and on shear plane in uniaxial tension. The results are interpreted in terms of deformation mode and microstructural instability. V.L.

A88-35938* Syracuse Univ., NY.
GRAIN BOUNDARY OXIDATION AND AN ANALYSIS OF THE EFFECTS OF OXIDATION ON FATIGUE CRACK NUCLEATION LIFE

Y. OSHIDA and H. W. LIU (Syracuse University, NY) IN: Low cycle fatigue. Philadelphia, PA, American Society for Testing and Materials, 1988, p. 1199-1217. Previously announced in STAR as N86-21654. refs
 (Contract NAG3-348)

The effects of preoxidation on subsequent fatigue life were studied. Surface oxidation and grain boundary oxidation of a nickel-base superalloy (TAZ-8A) were studied at 600 to 1000 C for 10 to 1000 hours in air. Surface oxides were identified and the kinetics of surface oxidation was discussed. Grain boundary oxide penetration and morphology were studied. Pancake type grain boundary oxide penetrates deeper and its size is larger, therefore, it is more detrimental to fatigue life than cone-type grain boundary oxide. Oxide penetration depth, a (sub m), is related to oxidation temperature, T, and exposure time, t, by an empirical relation of the Arrhenius type. Effects of T and t on statistical variation of a (sub m) were analyzed according to the Weibull distribution function. Once the oxide is cracked, it serves as a fatigue crack nucleus. Statistical variation of the remaining fatigue life, after the formation of an oxide crack of a critical length, is related directly to the statistical variation of grain boundary oxide penetration depth. Author

A88-37158* Case Western Reserve Univ., Cleveland, OH.
POWDER PROCESSING OF NICKEL AND OTHER ALUMINIDES BY HOT CONSOLIDATION

K. VEDULA (Case Western Reserve University, Cleveland, OH) and J. R. STEPHENS (NASA, Lewis Research Center, Cleveland, OH) IN: 1987 Annual Powder Metallurgy Conference, Dallas, TX, May 17-20, 1987, Proceedings. Princeton, NJ, Metal Powder Industries Federation, 1987, p. 561-573. refs

Alloys based on FeAl, NiAl, and Ni3Al have been processed by extrusion of powders over a range of compositions, powder

26 METALLIC MATERIALS

characteristics, and extrusion parameters. It is found that extrusion leads to dynamic recrystallization and that the grain size of the extrusions depends on the powder size, extrusion temperature, and extrusion ratio. Prior particle boundary oxides play an important role in controlling the grain size and uniformity by acting as obstacles to grain growth. Hot isostatic pressing and vacuum hot pressing can be used for powder densification, but prior particle oxides are not effectively broken up due to insufficient shearing deformation. V.L.

A88-38936* Arizona Univ., Tucson.

ANALYSIS OF PLASMA NITRIDED STEELS

J. SALIK (Arizona, University, Tucson), J. FERRANTE, F. HONEYCY (NASA, Lewis Research Center, Cleveland, OH), and R. HOFFMAN, JR. (Case Western Reserve University, Cleveland, OH) IN: Ion nitriding; Proceedings of the International Conference, Cleveland, OH, Sept. 15-17, 1986. Metals Park, OH, ASM International, 1987, p. 127-138. Previously announced in STAR as N87-21078.

The analysis of plasma nitrided steels can be divided to two main categories - structural and chemical. Structural analysis can provide information not only on the hardening mechanisms but also on the fundamental processes involved. Chemical analysis can be used to study the kinetics for the nitriding process and its mechanisms. In this paper preliminary results obtained by several techniques of both categories are presented and the applicability of those techniques to the analysis of plasma-nitrided steels is discussed. Author

A88-40329* National Aeronautics and Space Administration. Lewis Research Center, Cleveland, OH.

MICROSTRUCTURE-PROPERTY RELATIONSHIPS IN DIRECTIONALLY SOLIDIFIED SINGLE-CRYSTAL NICKEL-BASE SUPERALLOYS

REBECCA A. MACKAY and MICHAEL V. NATHAL (NASA, Lewis Research Center, Cleveland, OH) IN: MiCon 86: Optimization of processing, properties, and service performance through microstructural control; Proceedings of the Symposium, Philadelphia, PA, May 15, 16, 1986. Philadelphia, PA, American Society for Testing and Materials, 1988, p. 202-221; Discussion, p. 221. refs

This paper discusses some of the microstructural features which influence the creep properties of directionally solidified and single-crystal nickel-base superalloys. Gamma prime precipitate size and morphology, gamma-gamma (prime) lattice mismatch, phase instability, alloy composition, and processing variations are among the factors considered. Recent experimental results are reviewed and related to the operative deformation mechanisms and to the corresponding mechanical properties. Special emphasis is placed on the creep behavior of single-crystal superalloys at high temperatures, where directional gamma (prime) coarsening is prominent, and at lower temperatures, where gamma (prime) coarsening rates are significantly reduced. It can be seen that very subtle changes in microstructural features can have profound effects on the subsequent properties of these materials. Author

A88-40332* National Aeronautics and Space Administration. Lewis Research Center, Cleveland, OH.

ALLOY CHEMISTRY AND MICROSTRUCTURAL CONTROL TO MEET THE DEMANDS OF THE AUTOMOTIVE STIRLING ENGINE

JOSEPH R. STEPHENS (NASA, Lewis Research Center, Cleveland, OH) IN: MiCon 86: Optimization of processing, properties, and service performance through microstructural control; Proceedings of the Symposium, Philadelphia, PA, May 15, 16, 1986. Philadelphia, PA, American Society for Testing and Materials, 1988, p. 271-289. Previously announced in STAR as N86-20541. refs

The automotive Stirling engine now under development by DOE/NASA as an alternative to the internal combustion engine, imposes severe materials requirements for the hot portion of the engine. Materials selected must be low cost and contain a minimum of strategic elements so that availability is not a problem. Heater head tubes contain high pressure hydrogen on the inside and are exposed to hot combustion gases on the outside surface. The

cylinders and regenerator housings must be readily castable into complex shapes having varying wall thicknesses and be amenable to brazing and welding operations. Also, high strength, oxidation resistance, resistance to hydrogen permeation, cyclic operation, and long-life are required. A research program conducted by NASA Lewis focused on alloy chemistry and microstructural control to achieve the desired properties over the life of the engine. Results of alloy selection, characterization, evaluation, and actual engine testing of selected materials are presented. Author

A88-40588* Marko Materials, Inc., North Billerica, MA.

DISPERSION STRENGTHENED NIAL ALLOYS PRODUCED BY RAPID SOLIDIFICATION PROCESSING

S. C. JHA and R. RAY (Marko Materials, Inc., North Billerica, MA) Journal of Materials Science Letters (ISSN 0261-8028), vol. 7, March 1988, p. 285-288. refs
(Contract NAS3-25132)

Initial experimental results are presented concerning the relationship between microstructure and properties in rapidly solidified NiAl alloys whose melting point is of the order of 1900 K. When the dispersoid content of NiAl alloys is increased, the dispersoids begin to populate the grain boundaries, rendering them weak, so that failure must propagate intergranularly. It is concluded that NiAl alloys' strength can be significantly increased through dispersoid additions without sacrifice of high temperature ductility. O.C.

A88-40790* National Aeronautics and Space Administration. Lewis Research Center, Cleveland, OH.

WEAR OF IRON AND NICKEL IN CORROSIVE LIQUID ENVIRONMENTS

KAZUHISA MIYOSHI (NASA, Lewis Research Center, Cleveland, OH) and GEORGE W. P. RENGSTORFF National Association of Corrosion Engineers, International Corrosion Forum, Saint Louis, MO, Mar. 21-25, 1988, Paper. 15 p. Previously announced in STAR as N88-11817. refs

Friction and wear behavior of Fe and Ni sliding on aluminum oxide in aerated sulfuric acid and hydrochloric acid were investigated. The results show that the concentration of acid is an important factor in controlling the metal loss caused by wear corrosion processes in the acids. At very dilute acid concentration (10 to the -4 N), Fe behaves differently from Ni. Fe develops a soft, friable deposit, while Ni develops no corrosion layer. The formation and removal of the corrosion deposit on Fe resulted in high metal loss and coefficient of friction, as compared to the relatively low metal loss and coefficient of friction observed for Ni. At slightly higher acid concentration (10 to the -3 and 10 to the -2 N), no corrosion products were produced on both Fe and Ni. Wear of Fe and Ni was generally at a minimum. At higher acid concentration (10 to the -1 N and above), loss of Fe and Ni increased as the acid concentration increased. In sulfuric acid the maximum loss of both Fe and Ni was at 7.5 N (30 percent) concentration, and the metal losses of both Fe and Ni dropped markedly at 15 N (50 percent) and above. In hydrochloric acid, however, the Fe loss continued to increase with the increase of acid concentration, and the maximum Fe loss occurred in the most concentrated acid (12.1 N, 37 percent). There were variations in loss with Ni from specimen to specimen examined in hydrochloric acids (10 to the -1 N and above). The coefficient of friction for Ni increased slightly with an increase in acid concentration up to 10 to the -2 N. When corrosion started to dominate in the wear-corrosion process, the coefficient of friction decreased in both sulfuric and hydrochloric acids at 10 to the -1 N and above. Author

A88-41653* Wisconsin Univ., Madison.

RAPID SOLIDIFICATION OF HIGHLY UNDERCOOLED LIQUIDS

J. H. PEREPEZKO, J. A. GRAVES, and B. A. MUELLER (Wisconsin, University, Madison) IN: Processing of structural metals by rapid solidification; Proceedings of the Symposium on Enhanced Properties in Structural Metals via Rapid Solidification, Orlando, FL, Oct. 6-9, 1986. Metals Park, OH, ASM International, 1987, p.

13-29. refs

(Contract NAG3-436; DAAL03-86-K-0114)

Melt undercooling is considered as a fundamental processing parameter for powders and for melt-spun and surface-melted samples. With reference to experimental results for Mn, Al, Al-Be, Al-Fe, and InSb-Sb powders, it is shown that the undercooling behavior in droplets is influenced by powder size, coating, melt superheat, and cooling rate. Droplet sample microstructures can be compared directly with those of rapidly quenched powders to establish the application of laboratory-scale studies to large-scale processing. V.L.

A88-41654* National Aeronautics and Space Administration. Lewis Research Center, Cleveland, OH.

ON PRODUCING AN ALLOY OF UNIFORM COMPOSITION DURING RAPID SOLIDIFICATION PROCESSING

V. LAXMANAN (NASA, Lewis Research Center; Case Western Reserve University, Cleveland, OH) IN: Processing of structural metals by rapid solidification; Proceedings of the Symposium on Enhanced Properties in Structural Metals via Rapid Solidification, Orlando, FL, Oct. 6-9, 1986. Metals Park, OH, ASM International, 1987, p. 41-56. refs

The fundamental mechanisms responsible for both micro scale and macro scale compositional variations during cellular and dendritic solidification are discussed. It is shown that presently available models for cellular and dendritic growth in alloys predict only the elimination of macrosegregation during rapid solidification but that microsegregation still persists even in this regime. A simple model is proposed here to describe the complete elimination of microsegregation in the rapid solidification regime. A solid of ideally uniform composition can be produced with no micro or macro segregation at both very low large solidification rates. Author

A88-41655* Cleveland State Univ., OH.

PRIMARY ARM SPACING IN CHILL BLOCK MELT SPUN NI-MO ALLOYS

S. N. TEWARI (Cleveland State University, OH) and T. K. GLASGOW (NASA, Lewis Research Center, Cleveland, OH) IN: Processing of structural metals by rapid solidification; Proceedings of the Symposium on Enhanced Properties in Structural Metals via Rapid Solidification, Orlando, FL, Oct. 6-9, 1986. Metals Park, OH, ASM International, 1987, p. 57-66. Research supported by the U.S. National Research Council and NASA. Previously announced in STAR as N87-11875. refs

Chill block melt spun ribbons of Ni-Mo binary alloys containing 8.0 to 41.8 wt pct Mo have been prepared under carefully controlled processing conditions. The growth velocity has been determined as a function of distance from the quench surface from the observed ribbon thickness dependence on the melt puddle residence time. Primary arm spacing measured at the midribbon thickness locations show a dependence on growth velocity and alloy composition which is expected from dendritic growth models for binary alloys directionally solidified in a positive temperature gradient. Author

A88-46030* Cleveland State Univ., OH.

EFFECT OF MELT SPINNING ON GRAIN SIZE AND TEXTURE IN NI-MO ALLOYS

S. N. TEWARI (Cleveland State University, OH) Metallurgical Transactions A - Physical Metallurgy and Materials Science (ISSN 0360-2133), vol. 19A, July 1988, p. 1711-1720. Research supported by the U.S. National Research Council. refs (Contract NCC3-60)

Chill-block melt-spun ribbons of Ni-Mo alloys with Mo contents of 8 to 41.8 wt pct have been examined for microstructure and texture dependence on processing conditions. Linear features observed in grains solidified with a planar liquid-solid interface at the quench side of the ribbons have been identified to be due to the twins on the (111) γ plane formed during solidification. Grain size variation with the wheel surface speed and the alloy composition has been studied. The crystallographic texture on the quench side and the free surface side of the ribbons has been investigated. Author

A88-46038* Michigan Technological Univ., Houghton.

CHANNEL FORMATION IN PB-SN, PB-SB, AND PB-SN-SB ALLOY INGOTS AND COMPARISON WITH THE SYSTEM NH₄CL-H₂O

A. HELLAWELL (Michigan Technological University, Houghton) and J. R. SARAZIN Metallurgical Transactions A - Physical Metallurgy and Materials Science (ISSN 0360-2133), vol. 19A, July 1988, p. 1861-1871. refs

(Contract NAG3-560)

The formation of segregation channels during the unidirectional solidification of base chilled ingots has been studied as a function of composition in binary Pb-Sn and Pb-Sb and ternary Pb-Sn-Sb alloys. The patterns of channel distribution were characterized in the binary and ternary systems and are described as functions of temperature gradients, growth rates, dendrite spacings, and interdendritic permeabilities. Channels appear to nucleate at random across a dendritic front and subsequently to interact as they propagate, decreasing in density across the front. Assuming that the interdendritic spacing is the characteristic distance for a liquid perturbation, yields critical effective Rayleigh numbers which lie within a factor of $\times 40$ for both metallic and aqueous systems. This correlation is close, considering the sensitivity to any assumed dimension and the range of material properties involved, and is taken to support a model for channel nucleation occurring close to the dendritic growth front. Author

A88-47687* National Aeronautics and Space Administration. Lewis Research Center, Cleveland, OH.

ACCELERATED CRACK GROWTH RATE AT LOW DELTA K IN A SINGLE CRYSTAL SUPERALLOY

JACK TELESMA (NASA, Lewis Research Center, Cleveland, OH) and LOUIS GHOSN (Cleveland State University, OH) International Journal of Fracture (ISSN 0376-9429), vol. 37, May 1988, p. R19-R22. refs

The low Delta K crack growth behavior of a single crystal of the PWA 1480 nickel-based superalloy was investigated. The crystal was tested in the near (100) orientation with the side faces being in the near (001) orientation. Although in the higher Delta K region the fatigue crack growth (FCG) behavior is rather normal, at Delta K of about 8 MPa sq rt m, a transition occurs where the FCG rate appears to be independent of Delta K. This region is found to continue until Delta K of about 2.5 MPa sq rt m, where the FCG rate again decreases with decreasing Delta K. R.R.

A88-48182* Cincinnati Univ., OH.

A CRYSTALLOGRAPHIC MODEL FOR NICKEL BASE SINGLE CRYSTAL ALLOYS

L. T. DAME (International TechneGroup, Inc., Milford, OH) and D. C. STOUFFER (Cincinnati University, OH) ASME, Transactions, Journal of Applied Mechanics (ISSN 0021-8936), vol. 55, June 1988, p. 325-331. refs (Contract NAG3-511)

The purpose of this research is to develop a tool for the mechanical analysis of nickel-base single-crystal superalloys, specifically Rene N4, used in gas turbine engine components. This objective is achieved by developing a rate-dependent anisotropic constitutive model and implementing it in a nonlinear three-dimensional finite-element code. The constitutive model is developed from metallurgical concepts utilizing a crystallographic approach. An extension of Schmid's law is combined with the Bodner-Partom equations to model the inelastic tension/compression asymmetry and orientation-dependence in octahedral slip. Schmid's law is used to approximate the inelastic response of the material in cube slip. The constitutive equations model the tensile behavior, creep response and strain-rate sensitivity of the single-crystal superalloys. Methods for deriving the material constants from standard tests are also discussed. The model is implemented in a finite-element code, and the computed and experimental results are compared for several orientations and loading conditions. Author

26 METALLIC MATERIALS

A88-51318* National Aeronautics and Space Administration. Lewis Research Center, Cleveland, OH.

LATTICE PARAMETER VARIATIONS DURING AGING IN NICKEL-BASE SUPERALLOYS

M. V. NATHAL, R. A. MACKAY, and R. G. GARLICK (NASA, Lewis Research Center, Cleveland, OH) Scripta Metallurgica (ISSN 0036-9748), vol. 22, Sept. 1988, p. 1421-1424. refs

The importance of the state of coherency on measurements of gamma/gamma-prime lattice mismatch has been experimentally demonstrated during aging at 1000 C of specimens of an alloy with composition Ni-(8.6)Cr-(5.3)Al-(10.1)Co-(11.7)W-(1.2)Ti-(0.7)Mo (wt pct). Lattice parameter measurements are given as a function of aging time, and the corresponding sample microstructures are presented. The results show that changes of the two phases during aging did not influence the lattice parameter measurements, indicating that aging specimens to produce a semicoherent gamma/gamma-prime structure provides a good approximation of the true, unconstrained lattice mismatch. R.R.

A88-51736* National Aeronautics and Space Administration. Lewis Research Center, Cleveland, OH.

BITHERMAL LOW-CYCLE FATIGUE BEHAVIOR OF A NICOAL-COATED SINGLE CRYSTAL SUPERALLOY

J. GAYDA, T. P. GABB, R. V. MINER, and G. R. HALFORD (NASA, Lewis Research Center, Cleveland, OH) IN: Effects of load and thermal histories on mechanical behavior of materials; Proceedings of the Symposium, Denver, CO, Feb. 25, 26, 1987. Warrendale, PA, Metallurgical Society, Inc., 1987, p. 179-198. Previously announced in STAR as N87-20408. refs

Specimens of a single crystal superalloy, PWA 1480, both bare and coated with a NiCoAlCrAlY alloy, PWA 276, were tested in low-cycle fatigue at 650 and 1050 C, and in bithermal thermomechanical fatigue tests. In the two bithermal test types, tensile strain was imposed at one of the two temperatures and reversed in compression at the other. In the high-strain regime, lives for both bithermal test types approached that for the 650 C isothermal test on an inelastic strain basis, all being controlled by the low ductility of the superalloy at 650 C. In the low-strain regime, coating cracking reduced life in the 650 C isothermal test. The bithermal test imposing tension at 650 C, termed out-of-phase, also produced rapid surface cracking, but in both coated and bare specimens. Increased crack growth rates also occurred for the out-of-phase test. Increased lives in vacuum suggested that there is a large environmental contribution to damage in the out-of-phase test due to the 1050 C exposure followed by tensile straining at the low temperature. Author

A88-54145* National Aeronautics and Space Administration. Lewis Research Center, Cleveland, OH.

LIFE MODELING OF THERMAL BARRIER COATINGS FOR AIRCRAFT GAS TURBINE ENGINES

R. A. MILLER (NASA, Lewis Research Center, Cleveland, OH) IN: Toward improved durability in advanced aircraft engine hot sections; Proceedings of the Thirty-third ASME International Gas Turbine and Aeroengine Congress and Exposition, Amsterdam, Netherlands, June 5-9, 1988. New York, American Society of Mechanical Engineers, 1988, p. 109-115. Previously announced in STAR as N88-15060. refs

Thermal barrier coating life models developed under the NASA Lewis Research Center's Hot Section Technology (HOST) Program are summarized. An initial laboratory model and three design-capable models are discussed. Current understanding of coating failure mechanisms are also summarized. Author

N88-10938* National Aeronautics and Space Administration. Lewis Research Center, Cleveland, OH.

HIGH TEMPERATURE METAL MATRIX COMPOSITES FOR FUTURE AEROSPACE SYSTEMS

JOSEPH R. STEPHENS Oct. 1987 18 p Presented at the ASM International Composite Session, Cincinnati, Ohio, 13-15 Oct. 1987

(NASA-TM-100212; E-3821; NAS 1.15:100212) Avail: NTIS HC A03/MF A01 CSCL 11F

Research was conducted on metal matrix composites and intermetallic matrix composites to understand their behavior under anticipated future operating conditions envisioned for aerospace power and propulsion systems of the 21st century. Extremes in environmental conditions, high temperature, long operating lives, and cyclic conditions dictate that the test evaluations not only include laboratory testing, but simulated flight conditions. The various processing techniques employed to fabricate composites are discussed along with the basic research underway to understand the behavior of high temperature composites, and the relationship of this research to future aerospace systems.

Author

N88-10939* National Aeronautics and Space Administration. Lewis Research Center, Cleveland, OH.

A MICROSTRUCTURAL LATTICE MODEL FOR STRAIN ORIENTED PROBLEMS: A COMBINED MONTE CARLO FINITE ELEMENT TECHNIQUE

J. GAYDA and D. J. SROLOVITZ Nov. 1987 32 p (NASA-TM-100215; E-3824; NAS 1.15:100215) Avail: NTIS HC A03/MF A01 CSCL 11F

A specialized, microstructural lattice model, termed MCFET for combined Monte Carlo Finite Element Technique, was developed which simulates microstructural evolution in material systems where modulated phases occur and the directionality of the modulation is influenced by internal and external stresses. In this approach, the microstructure is discretized onto a fine lattice. Each element in the lattice is labelled in accordance with its microstructural identity. Diffusion of material at elevated temperatures is simulated by allowing exchanges of neighboring elements if the exchange lowers the total energy of the system. A Monte Carlo approach is used to select the exchange site while the change in energy associated with stress fields is computed using a finite element technique. The MCFET analysis was validated by comparing this approach with a closed form, analytical method for stress assisted, shape changes of a single particle in an infinite matrix. Sample MCFET analytical for multiparticle problems were also run and in general the resulting microstructural changes associated with the application of an external stress are similar to that observed in Ni-Al-Cr alloys at elevated temperature. Author

N88-10940* National Aeronautics and Space Administration. Lewis Research Center, Cleveland, OH.

THE EFFECT OF SULFUR AND ZIRCONIUM CO-DOPING ON THE OXIDATION OF NICRAL

JAMES L. SMIALEK Oct. 1987 18 p Presented at the 172nd Meeting of the Electrochemical Society, Honolulu, Hawaii, 18-23 Oct. 1987

(NASA-TM-100209; E-3814; NAS 1.15:100209) Avail: NTIS HC A03/MF A01 CSCL 11F

The adhesion behavior of Al₂O₃ scales formed on NiCrAl+Zr alloys was examined as a function of both sulfur and zirconium doping levels. In general, very high levels of zirconium were required to counteract the detrimental effects of sulfur. A sulfur-zirconium adherence map was constructed, as determined from the oxidation and spalling behavior in 1100 C cyclic tests. For low sulfur alloys, the amount of zirconium required for adherence at any given sulfur level can be described by Zr greater than 600 S sup 0.2 (in ppm). These results underscore the importance of sulfur to adhesion mechanisms and suggests that sulfur gettering is a first order effect of reactive element additions to MCrAl alloys.

Author

N88-11168* Cincinnati Univ., OH.

CONSTITUTIVE MODELING FOR SINGLE CRYSTAL SUPERALLOYS

DONALD C. STOUFFER, L. THOMAS DAME, and N. JAYARAMAN IN: NASA. Lewis Research Center, Turbine Engine Hot Section Technology, 1985 p 271-276 Oct. 1985 Prepared in cooperation with General Electric Co., Cincinnati, Ohio

(Contract NAG3-511)

Avail: NTIS HC A19/MF A01 CSCL 11F

A crystallographic approach to constitutive modeling of single crystal superalloys is discussed. The approach is based on identifying the active slip planes and slip directions. The shear stresses are computed on each of the slip planes from applied stress components. The slip rate is then computed on each slip system and the microscopic inelastic strain rates are the sum of the slip in the individual slip systems. The constitutive model was implemented in a finite element code using twenty noted isoparametric solid elements. Constants were determined for octahedral and cube slip systems. These constants were then used to predict tension-compression asymmetry and fatigue loops. Other data was used to model the tensile and creep response.

Author

N88-11169*# Connecticut Univ., Storrs.

CONSTITUTIVE MODELING OF SUPERALLOY SINGLE CRYSTALS WITH VERIFICATION TESTING

ERIC JORDAN and KEVIN P. WALKER (Engineering Science Software, Inc., Smithfield, R.I.) *In* NASA. Lewis Research Center, Turbine Engine Hot Section Technology, 1985 p 277-286 Oct. 1985

(Contract NAG3-512)

Avail: NTIS HC A19/MF A01 CSCL 11F

The goal is the development of constitutive equations to describe the elevated temperature stress-strain behavior of single crystal turbine blade alloys. The program includes both the development of a suitable model and verification of the model through elevated temperature-torsion testing. A constitutive model is derived from postulated constitutive behavior on individual crystallographic slip systems. The behavior of the entire single crystal is then arrived at by summing up the slip on all the operative crystallographic slip systems. This type of formulation has a number of important advantages, including the prediction orientation dependence and the ability to directly represent the constitutive behavior in terms which metallurgists use in describing the micromechanisms. Here, the model is briefly described, followed by the experimental set-up and some experimental findings to date.

Author

N88-11178*# Yale Univ., New Haven, CT. High Temperature Chemical Reaction Engineering Lab.

TURBINE AIRFOIL DEPOSITION MODELS AND THEIR HOT CORROSION IMPLICATIONS

D. E. ROSNER and R. NAGARAJAN *In* NASA. Lewis Research Center, Turbine Engine Hot Section Technology, 1985 p 373-381 Oct. 1985

(Contract NAG3-590)

Avail: NTIS HC A19/MF A01 CSCL 11F

This research project deals with the prediction of single- and multi-component salt-(solution) deposition, flow and oxide dissolution and their effects on the lifetime of turbine blades. Goals include rationalizing and helping to predict corrosion patterns on operational gas turbine (GT) rotor blades and stator vanes, and ultimately providing some of the tools required to design laboratory simulators and future corrosion resistant high-performance engines. Necessary background developments are reviewed. Results and tentative conclusions for single species (Na sub 2 SO sub 4 (1)) condensation, binary salt-solution (Na sub 2 SO sub 4-K sub 2 SO sub 4) condensation, and burner-rig testing of alloy materials are outlined.

Author

N88-11179*# National Aeronautics and Space Administration. Lewis Research Center, Cleveland, OH.

EXPERIMENTAL VERIFICATION OF VAPOR DEPOSITION RATE THEORY IN HIGH VELOCITY BURNER RIGS

SULEYMAN A. GOKOGLU (Case Western Reserve Univ., Cleveland, Ohio.) and GILBERT J. SANTORO *In* its Turbine Engine Hot Section Technology, 1985 p 383-390 Oct. 1985

Avail: NTIS HC A19/MF A01 CSCL 11F

The main objective has been the experimental verification of the corrosive vapor deposition theory in high-temperature,

high-velocity environments. Towards this end a Mach 0.3 burner-rig apparatus was built to measure deposition rates from salt-seeded (mostly Na salts) combustion gases on the internally cooled cylindrical collector. Deposition experiments are underway.

Author

N88-11180*# General Electric Co., Cincinnati, OH.

EFFECTS OF SURFACE CHEMISTRY ON HOT CORROSION LIFE

R. E. FRYXELL and G. E. LEESE *In* NASA. Lewis Research Center, Turbine Engine Hot Section Technology, 1985 p 391-396 Oct. 1985

(Contract NAS3-23926)

Avail: NTIS HC A19/MF A01 CSCL 11F

This program has its primary objective: the development of hot corrosion life prediction methodology based on a combination of laboratory test data and evaluation of field service turbine components which show evidence of hot corrosion. The laboratory program comprises burner rig testing by TRW. A summary of results is given for two series of burner rig tests. The life prediction methodology parameters to be appraised in a final campaign of burner rig tests are outlined.

Author

N88-11817*# National Aeronautics and Space Administration. Lewis Research Center, Cleveland, OH.

WEAR OF IRON AND NICKEL IN CORROSIVE LIQUID ENVIRONMENTS

KAZUHISA MIYOSHI and GEORGE W. P. RENGSTORFF (Toledo Univ., Ohio.) 1987 20 p Proposed for presentation at Corrosion '88, St. Louis, Mo., 21-25 Mar. 1988; sponsored by the National Association of Corrosion Engineers

(NASA-TM-100246; E-3861; NAS 1.15:100246) Avail: NTIS HC A03/MF A01 CSCL 11F

Friction and wear behavior of Fe and Ni sliding on aluminum oxide in aerated sulfuric acid and hydrochloric acid were investigated. The results show that the concentration of acid is an important factor in controlling the metal loss caused by wear corrosion processes in the acids. At very dilute acid concentration (10 to the -4 N), Fe behaves differently from Ni. Fe develops a soft, friable deposit, while Ni develops no corrosion layer. The formation and removal of the corrosion deposit on Fe resulted in high metal loss and coefficient of friction, as compared to the relatively low metal loss and coefficient of friction observed for Ni. At slightly higher acid concentration (10 to the -3 and 10 to the -2 N), no corrosion products were produced on both Fe and Ni. Wear of Fe and Ni was generally at a minimum. At higher acid concentration (10 to the -1 N and above), loss of Fe and Ni increased as the acid concentration increased. In sulfuric acid the maximum loss of both Fe and Ni was at 7.5 N (30%) concentration, and the metal losses of both Fe and Ni dropped markedly at 15 N (50%) and above. In hydrochloric acid, however, the Fe loss continued to increase with the increase of acid concentration, and the maximum Fe loss occurred in the most concentrated acid (12.1 N, 37%). There were variations in loss with Ni from specimen to specimen examined in hydrochloric acids (10 to the -1 N and above). The coefficient of friction for Ni increased slightly with an increase in acid concentration up to 10 to the -2 N. When corrosion started to dominate in the wear-corrosion process, the coefficient of friction decreased in both sulfuric and hydrochloric acids at 10 to the -1 N and above.

Author

N88-14179*# National Aeronautics and Space Administration. Lewis Research Center, Cleveland, OH.

ION-BEAM NITRIDING OF STEELS Patent

JOSHUA SALIK, inventor (to NASA) and THEODORE E. HUBBELL, inventor (to NASA) 3 Nov. 1987 7 p Filed 29 Jan. 1986 Supersedes N86-32556 (24 - 24, p 3708) Continuation-in-part of US-Patent-Appl-SN-661481, filed 16 Oct. 1984, abandoned (NASA-CASE-LEW-14104-2; US-PATENT-4,704,168; US-PATENT-APPL-SN-823713; US-PATENT-CLASS-148-16.6; US-PATENT-CLASS-204-192.31; US-PATENT-CLASS-427-38; US-PATENT-APPL-SN-661481) Avail: US Patent and Trademark Office CSCL 11F

26 METALLIC MATERIALS

A surface of a steel substrate is nitrided without external heating by exposing it to a beam of nitrogen ions under low pressure, a pressure much lower than that employed for ion-nitriding. An ion source is used instead of a glow discharge. Both of these features reduce the introduction of impurities into the substrate surface.

Official Gazette of the U.S. Patent and Trademark Office

N88-15060*# National Aeronautics and Space Administration. Lewis Research Center, Cleveland, OH.

LIFE MODELING OF THERMAL BARRIER COATINGS FOR AIRCRAFT GAS TURBINE ENGINES

ROBERT A. MILLER 1988 11 p Prepared for the 33rd International Gas Turbine and Aeroengine Congress and Exposition, Amsterdam, The Netherlands, 5-9 Jun. 1988; sponsored by ASME

(NASA-TM-100283; E-3921; NAS 1.15:100283) Avail: NTIS HC A03/MF A01 CSCL 11F

Thermal barrier coating life models developed under the NASA Lewis Research Center's Hot Section Technology (HOST) program are summarized. An initial laboratory model and three design-capable models are discussed. Current understanding of coating failure mechanisms are also summarized. Author

N88-18707*# National Aeronautics and Space Administration. Lewis Research Center, Cleveland, OH.

CREEP BEHAVIOR OF TUNGSTEN/NIOBIUM AND TUNGSTEN/NIOBIUM-1 PERCENT ZIRCONIUM COMPOSITES Final Report

DONALD W. PETRASEK and ROBERT H. TITRAN 1988 25 p Presented at the 5th Symposium on Space Nuclear Power Systems, Albuquerque, N. Mex., 11-14 Jan. 1988; sponsored by New Mexico Univ.

(Contract DE-AI03-86SF-16310)

(NASA-TM-100804; DOE/NASA/16310-5; E-3984; NAS 1.15:100804) Avail: NTIS HC A03/MF A01 CSCL 11F

The creep behavior and microstructural stability of tungsten fiber reinforced niobium and niobium 1 percent zirconium was determined at 1400 and 1500 K in order to assess the potential of this material for use in advanced space power systems. The creep behavior of the composite materials could be described by a power law creep equation. A linear relationship was found to exist between the minimum creep rate of the composite and the inverse of the composite creep rupture life. The composite materials had an order of magnitude increase in stress to achieve 1 percent creep strain and in rupture strength at test temperatures of 1400 and 1500 K compared to unreinforced material. The composite materials were also stronger than the unreinforced materials by an order of magnitude when density was taken into consideration. Results obtained on the creep behavior and microstructural stability of the composites show significant potential improvement in high temperature properties and mass reduction for space power system components. Author

N88-19610*# National Aeronautics and Space Administration. Lewis Research Center, Cleveland, OH.

THE CYCLIC STRESS-STRAIN BEHAVIOR OF A SINGLE CRYSTAL NICKEL-BASE SUPERALLOY Ph.D. Thesis

TIMOTHY P. GABB Feb. 1988 219 p

(NASA-TM-100269; E-3775; NAS 1.15:100269) Avail: NTIS HC A10/MF A01 CSCL 11F

The cyclic stress-strain response and similar deformation structures of the single crystal nickel based superalloy was described under a specific set of conditions. The isothermal low cycle fatigue response and deformation structures were described at a typical intermediate temperature and at high temperature. Specimens oriented near the (001) and (111) crystallographic orientations were tested at 1050 C, where more moderate orientation effects were expected. This enabled the description of the deformation structures at each of the 2 temperatures and their relationship to the observed cyclic stress-strain behavior. The initial yield strength of all specimens tested at 650 C was controlled by the shearing of the gamma prime precipitates by dislocation pairs. Low cycle fatigue tests at 650 C had cyclic hardening, which

was associated with dislocation interactions in the gamma matrix. The initial yield strength of specimens tested at 1050 C was associated with dislocation bypassing of the gamma prime precipitates. Low cycle fatigue tests at 1050 C had cyclic softening, associated with extensive dislocation recovery at the gamma-gamma prime interfaces along with some gamma prime precipitate coarsening. Author

N88-19613*# Garrett Processing Co., Torrance, CA. Metals Casting Div.

CAST IRON-BASE ALLOY FOR CYLINDER/REGENERATOR HOUSING Final Report

STEWART L. WITTER, HAROLD E. SIMMONS, and MICHAEL J. WOULDs Aug. 1985 142 p

(Contract DEN3-234; DE-AI01-85CE-50112)

(NASA-CR-182116; DOE/NASA/0234-1; NAS 1.26:182116)

Avail: NTIS HC A07/MF A01 CSCL 11F

NASACC-1 is a castable iron-base alloy designed to replace the costly and strategic cobalt-base X-40 alloy used in the automotive Stirling engine cylinder/generator housing. Over 40 alloy compositions were evaluated using investment cast test bars for stress-rupture testing. Also, hydrogen compatibility and oxygen corrosion resistance tests were used to determine the optimal alloy. NASACC-1 alloy was characterized using elevated and room temperature tensile, creep-rupture, low cycle fatigue, heat capacity, specific heat, and thermal expansion testing. Furthermore, phase analysis was performed on samples with several heat treated conditions. The properties are very encouraging. NASACC-1 alloy shows stress-rupture and low cycle fatigue properties equivalent to X-40. The oxidation resistance surpassed the program goal while maintaining acceptable resistance to hydrogen exposure. The welding, brazing, and casting characteristics are excellent. Finally, the cost of NASACC-1 is significantly lower than that of X-40. Author

N88-20417*# National Aeronautics and Space Administration. Lewis Research Center, Cleveland, OH.

INTERFACIAL ADHESION: THEORY AND EXPERIMENT

JOHN FERRANTE, GUILLERMO H. BOZZOLO, CLARENCE W. FINLEY (Pennsylvania State Univ., New Kensington.), and AMITAVA BANERJEA 1988 32 p Presented at the Spring Meeting of the Materials Research Society, Reno, Nev., 5-9 Apr. 1988

(NASA-TM-100830; E-4019; NAS 1.15:100830) Avail: NTIS HC A03/MF A01 CSCL 11F

Adhesion, the binding of different materials at an interface, is of general interest to many branches of technology, e.g., microelectronics, tribology, manufacturing, construction, etc. However, there is a lack of fundamental understanding of such diverse interfaces. In addition, experimental techniques generally have practical objectives, such as the achievement of sufficient strength to sustain mechanical or thermal effects and/or have the proper electronic properties. In addition, the theoretical description of binding at interfaces is quite limited, and a proper data base for such theoretical analysis does not exist. This presentation will review both experimental and theoretical aspects of adhesion in nonpolymer materials. The objective will be to delineate the critical parameters needed, governing adhesion testing along with an outline of testing objectives. A distinction will be made between practical and fundamental objectives. Examples are given where interfacial bonding may govern experimental consideration. The present status of theory is presented along with recommendations for future progress and needs. Author

N88-21295*# Case Western Reserve Univ., Cleveland, OH.

PROCESSING, PHYSICAL METALLURGY AND CREEP OF NIAL + TA AND NIAL + NB ALLOYS Ph.D. Thesis. Final Contractor Report

VIREN M. PATHARE Apr. 1988 190 p

(Contract NAG3-387)

(NASA-CR-182113; NAS 1.26:182113) Avail: NTIS HC A09/MF A01 CSCL 11F

Powder processed NiAl + Ta alloys containing 1, 2, and 4.5

at percent tantalum and NiAl + Nb alloys containing 1 and 2 at percent niobium were developed for improved creep properties. In addition, a cast alloy with 5 at percent tantalum was also studied. Hot extrusion parameters for processing alloys with 1 and 2 at percent of tantalum or niobium were designed. The NiAl + 4.5 at percent Ta alloy could be vacuum hot pressed successfully, even though it could not be extruded. All the phases in the multiphase alloys were identified and the phase transformations studied. The Ni₂AlTa in NiAl + 4.5 at percent Ta alloy transforms into a liquid phase above 1700 K. Solutionizing and annealing below this temperature gives rise to a uniform distribution of fine second phase precipitates. Compressive creep properties were evaluated at 1300 K using constant load and constant velocity tests. In the higher strain rate region single phase NiAl + 1 at percent Ta and NiAl + 1 at percent Nb alloys exhibit a stress exponent of 5 characteristic of climb controlled dislocation creep. In slower strain rate regime diffusional creep becomes important. The two phase alloys containing 2 to 5 at percent Ta and 2 at percent Nb show considerable improvement over binary NiAl and single phase alloys. Loose dislocation networks and tangles stabilized by the precipitates were found in the as crept microstructure. The cast alloy which has larger grains and a distribution of fine precipitates shows the maximum improvement over binary NiAl. Author

N88-21510* Cincinnati Univ., OH. Dept. of Aerospace Engineering and Engineering Mechanics.

A CONSTITUTIVE MODEL WITH DAMAGE FOR HIGH TEMPERATURE SUPERALLOYS

J. A. SHERWOOD and D. C. STOFFER In NASA. Lewis Research Center, Nonlinear Constitutive Relations for High Temperature Applications, 1986 p 187-200 Apr. 1988 Sponsored in part by AF (Contract NAG3-511)

Avail: NTIS HC A21/MF A01 CSCL 11F

A unified constitutive model is searched for that is applicable for high temperature superalloys used in modern gas turbines. Two unified inelastic state variable constitutive models were evaluated for use with the damage parameter proposed by Kachanov. The first is a model (Bodner, Partom) in which hardening is modeled through the use of a single state variable that is similar to drag stress. The other (Ramaswamy) employs both a drag stress and back stress. The extension was successful for predicting the tensile, creep, fatigue, torsional and nonproportional response of Rene' 80 at several temperatures. In both formulations, a cumulative damage parameter is introduced to model the changes in material properties due to the formation of microcracks and microvoids that ultimately produce a macroscopic crack. A back stress/drag stress/damage model was evaluated for Rene' 95 at 1200 F and is shown to predict the tensile, creep, and cyclic loading responses reasonably well. Author

N88-22168* National Aeronautics and Space Administration. Lewis Research Center, Cleveland, OH.

BITHERMAL FATIGUE OF A NICKEL-BASE SUPERALLOY SINGLE CRYSTAL

MICHAEL J. VERRILLI May 1988 15 p (NASA-TM-100885; E-4118; NAS 1.15:100885) Avail: NTIS HC A03/MF A01 CSCL 11F

The thermomechanical fatigue behavior of a nickel-base superalloy single crystal was investigated using a bithermal test technique. The bithermal fatigue test was used as a simple alternative to the more complex thermomechanical fatigue test. Both in-phase and out-of-phase bithermal tests were performed on (100)-oriented coated and bare Rene N4 single crystals. In out-of-plane bithermal tests, the tensile and compressive halves of the cycle were applied isothermally at 760 and 982 C, respectively, while for the in-phase bithermal tests the temperature-loading sequence was reversed. The bithermal fatigue lives of bare specimens were shorter than the isothermal fatigue lives at either temperature extreme when compared on an inelastic strain basis. Both in-phase and out-of-phase bithermal fatigue life curves converged in the large strain regime and diverged in the small strain regime, out-of-phase resulting in the shortest lives.

The coating had no effect on life for specimens cycled in-phase; however, the coating was detrimental for isothermal fatigue at 760 C and for out-of-phase fatigue under large strains. Author

N88-22427* Pratt and Whitney Aircraft, East Hartford, CT.

FATIGUE DAMAGE MODELING FOR COATED SINGLE CRYSTAL SUPERALLOYS

DAVID M. NISSLEY In NASA. Lewis Research Center, Lewis Structures Technology, 1988. Volume 3: Structural Integrity Fatigue and Fracture Wind Turbines HOST p 259-270 May 1988 (Contract NAS3-23939)

Avail: NTIS HC A16/MF A01 CSCL 11F

A high temperature, low-cycle fatigue life prediction method for coated single crystal nickel-base superalloys is being developed. The method is being developed for use in predicting crack initiation life of coated single crystal turbine airfoils. Although the models are being developed using coated single crystal PWA 1480, they should be readily adaptable to other coated nickel-base single crystal materials. The coatings chosen for this effort were of two generic types: a low pressure plasma sprayed NiCoCrAlY overlay, designated PWA 286, and an aluminide diffusion, designated PWA 273. In order to predict the useful crack initiation life of airfoils, the constitutive and failure behavior of the coating/substrate combination must be taken into account. Coatings alter the airfoil surface microstructure and are a primary source from which cracks originate. The adopted life prediction approach addresses this complexity by separating the coating and single crystal crack initiation regimes. This provides a flexible means for using different life model formulations for the coating and single crystal materials. At the completion of this program, all constitutive and life model formulations will be available in equation form and as software. The software will use the MARC general purpose finite element code to drive the constitutive models and calculate life parameters. Author

N88-22981* National Aeronautics and Space Administration. Lewis Research Center, Cleveland, OH.

CHARACTERIZATION OF PRECIPITATES IN A NIOBIUM-ZIRCONIUM-CARBON ALLOY Final Report

T. L. GROBSTEIN and R. H. TITRAN 1986 18 p Presented at the Metallurgical Society Fall Meeting, Orlando, Fla., 5-9 Oct. 1986; sponsored by AIME

(Contract DE-AL03-86SF-16310)

(NASA-TM-100848; DOE/NASA/16310-6; E-4041; NAS 1.15:100848) Avail: NTIS HC A03/MF A01 CSCL 11F

A niobium alloy with 1 percent zirconium and 0.063 percent carbon by weight was investigated in the as-rolled and annealed conditions, and after high-temperature (1350 and 1400 K) exposure with and without an applied stress. In the as-rolled and annealed conditions, large metastable carbides were observed in addition to a regular distribution of small particles. During the high-temperature exposure, the majority of the large carbides were dissolved and a more stable carbide phase formed. This finely dispersed phase had a composition determined to be approximately 70 percent ZrC and approximately 30 percent NbC and showed some evidence of an orientation relationship with the matrix. The precipitates appeared to coarsen slightly after approximately 5000 hr exposure in the presence of an applied stress resulted in a decrease in the size and in the interparticle spacing of the stable precipitates. However, the composition of the precipitate phase and its ability to pin dislocations were not affected by the temperature or stress conditions. Author

N88-22986* National Aeronautics and Space Administration. Lewis Research Center, Cleveland, OH.

FATIGUE CRACK GROWTH BEHAVIOR OF A SINGLE CRYSTAL ALLOY AS OBSERVED THROUGH AN IN SITU FATIGUE LOADING STAGE

JACK TELESMA and PETER KANTZOS 1988 19 p Proposed for presentation at the SAMPE Metals Processing Conference, Dayton, Ohio, 2-4 Aug. 1988

(NASA-TM-100863; E-4080; NAS 1.15:100863) Avail: NTIS HC A03/MF A01 CSCL 11F

26 METALLIC MATERIALS

An in situ fatigue loading stage inside a scanning electron microscope (SEM) was used to determine the fatigue crack growth behavior of a PWA 1480 single-crystal nickel-based superalloy. The loading stage permits real-time viewing of the fatigue damage processes at high magnification. The PWA 1480 single-crystal, single-edge notch specimens were tested with the load axis parallel to the (100) orientation. Two distinct fatigue failure mechanisms were identified. The crack growth rate differed substantially when the failure occurred on a single slip system in comparison to multislip system failure. Two processes by which crack branching is produced were identified and are discussed. Also discussed are the observed crack closure mechanisms. Author

N88-22987*# Syracuse Univ., NY. Dept. of Mechanical and Aerospace Engineering.

THE ANALYSIS OF FATIGUE CRACK GROWTH MECHANISM AND OXIDATION AND FATIGUE LIFE AT ELEVATED TEMPERATURES Final Contractor Report

H. W. LIU May 1988 12 p

(Contract NAG3-348)

(NASA-CR-182129; NAS 1.26:182129) Avail: NTIS HC A03/MF A01 CSCL 11F

Two quantitative models based on experimentally observed fatigue damage processes have been made: (1) a model of low cycle fatigue life based on fatigue crack growth under general-yielding cyclic loading; and (2) a model of accelerated fatigue crack growth at elevated temperatures based on grain boundary oxidation. These two quantitative models agree very well with the experimental observations. Author

N88-24279*# National Aeronautics and Space Administration. Lewis Research Center, Cleveland, OH.

PRELIMINARY STUDY OF NIOBIUM ALLOY CONTAMINATION BY TRANSPORT THROUGH HELIUM

C. M. SCHEUERMANN, T. J. MOORE, and D. R. WHEELER In New Mexico Univ., Transactions of the Fourth Symposium on Space Nuclear Power Systems p 103-106 1987 Sponsored by DOE, Washington, D.C. and DOD, Washington, D. C.

Avail: NTIS HC A22/MF A01 CSCL 11F

Transport of gaseous contaminants through the working fluid to or from sensitive refractory alloys is theoretically possible during long time operation of Brayton and Stirling space power generation systems which use a gas as the working fluid. A test was designed which could give an answer to whether transport of contaminants through the working fluid was a potential major problem. The findings of that preliminary study are summarized. Author

N88-24749*# National Aeronautics and Space Administration. Lewis Research Center, Cleveland, OH.

STATUS AND PROGNOSIS FOR ALTERNATIVE ENGINE MATERIALS

JOSEPH R. STEPHENS and MICHAEL V. NATHAL 1988 16 p Proposed for presentation at the 6th International Symposium on Superalloys, Champion, Pa., 18-22 Sep. 1988; sponsored by TMS-AIME

(NASA-TM-100903; E-4154; NAS 1.15:100903) Avail: NTIS HC A03/MF A01 CSCL 11F

The current state of research and development of new materials for advanced aircraft engines is reviewed. The advantages and disadvantages of intermetallic compounds and refractory metals as replacements for today's nickel-base alloys are discussed along with some results of research directed at overcoming some of the problems which restrict their application. It is concluded that continuous fiber reinforced intermetallic matrix composites offer one of the best chances for success. However, major technical barriers still exist, especially in the development of suitable fibers. The introduction of these materials into aircraft engines is expected to take in excess of 5 to 10 years. Author

N88-24754*# National Aeronautics and Space Administration. Lewis Research Center, Cleveland, OH.

ARC-TEXTURED METAL SURFACES FOR HIGH THERMAL EMITTANCE SPACE RADIATORS

BRUCE A. BANKS, SHARON K. RUTLEDGE, MICHAEL J. MIRTICH, TRACY BEHREND, DEBORAH HOTES, MICHAEL KUSSMAUL, JENNIFER BARRY, CURTIS STIDHAM, THOMAS STUEBER, and FRANK DIFILIPPO (Case Western Reserve Univ., Cleveland, Ohio.) 1988 11 p Presented at the International Conference on Metallurgical Coatings, San Diego, Calif., 11-15 Apr. 1988; sponsored by the American Vacuum Society (NASA-TM-100894; E-4135; NAS 1.15:100894) Avail: NTIS HC A03/MF A01 CSCL 11F

Carbon arc electrical discharges struck across the surfaces of metals such as Nb-1 percent Zr, alter the morphology to produce a high thermal emittance surface. Metal from the surface and carbon from the arc electrode vaporize during arcing, and then condense on the metal surface to produce a microscopically rough surface having a high thermal emittance. Quantitative spectral reflectance measurements from 0.33 to 15 microns were made on metal surfaces which were carbon arc treated in an inert gas environment. The resulting spectral reflectance data were then used to calculate thermal emittance as a function of temperature for various methods of arc treatment. The results of arc treatment on various metals are presented for both ac and dc arcs. Surface characterization data, including thermal emittance as a function of temperature, scanning electron microscopy, and atomic oxygen durability, are also presented. The ac arc texturing was found to increase the thermal emittance at 800 K from 0.05 to 0.70.

Author

N88-24766*# National Aeronautics and Space Administration. Lewis Research Center, Cleveland, OH.

ISOTHERMAL AND BITHERMAL THERMOMECHANICAL FATIGUE BEHAVIOR OF A NICOCRALY-COATED SINGLE CRYSTAL SUPERALLOY

J. GAYDA, T. P. GABB, and R. V. MINER 1988 14 p Prepared for presentation at the 6th International Conference on Superalloys, Seven Springs, Pa., 18-22 Sep. 1988; sponsored by the American Inst. of Mining Metallurgical and Petroleum Engineers

(NASA-TM-100907; E-4077; NAS 1.15:100907) Avail: NTIS HC A03/MF A01 CSCL 11F

Specimens of single crystal PWA 1480 with group of zone axes (100) orientation, bare, or with NiCoCrAlY coating PWA 276, were tested in low cycle fatigue (LCF) at 650, 870, and 1050 C, and in simplified bithermal thermomechanical fatigue (TMF) tests between these temperatures. These tests were examined as a bridge between isothermal LCF and general TMF. In the bithermal test, an inelastic strain is applied at one temperature, T sub max, and reversed at T sub min. The out-of-phase (OP) test type imposing tension at T sub min and compression at T sub max received most study, since it was more damaging than the in-phase type. Specifically investigated were the effects of: inelastic strain range, the coating, delta T, T sub max, T sub min, and the environment.

Author

N88-25531*# Case Western Reserve Univ., Cleveland, OH. Dept. of Materials Science and Engineering.

FRACTION EUTECTIC MEASUREMENTS IN SLOWLY COOLED PB - 15 WT PERCENT SN ALLOYS Final Report

ANTHONY C. STUDER and V. LAXMANAN Jun. 1988 22 p Presented at the 1987 Fall Meeting of the Metallurgical Society, Cincinnati, Ohio, 12-14 Oct. 1987

(Contract NCC3-74)

(NASA-CR-180830; E-3762; NAS 1.26:180830) Avail: NTIS HC A03/MF A01 CSCL 11F

A space shuttle experiment employing the General Purpose Furnace in its isothermal mode of operation is currently manifested for flight circa 1989. The aim of this experiment was to investigate the role of gravity in a slowly, and isothermally, cooled sample of a binary Pb - 15 wt percent Sn alloy. Ground based work in support of the microgravity experiment is discussed. In particular, it is shown that fraction eutectic measurements using an image analyzer, can be used to satisfactorily describe macrosegregation occurring in these slowly cooled ingots.

Author

N88-26436* National Aeronautics and Space Administration. Lewis Research Center, Cleveland, OH.

ACCELERATED FATIGUE CRACK GROWTH BEHAVIOR OF PWA 1480 SINGLE CRYSTAL ALLOY AND ITS DEPENDENCE ON THE DEFORMATION MODE

JACK TELESMA and LOUIS J. GHOSN (Cleveland State Univ., Ohio.) Jun. 1988 16 p Proposed for presentation at the 6th International Conference on Superalloys, Seven Springs, Pa., 18-22 Sep. 1988; sponsored by the American Inst. of Mining, Metallurgical and Petroleum Engineers (NASA-TM-100943; E-4231; NAS 1.15:100943) Avail: NTIS HC A03/MF A01 CSCL 11F

An investigation of the fatigue crack growth (FCG) behavior of PWA 1480 single crystal nickel base superalloy was conducted. Typical Paris region behavior was observed above a delta K of 8 MPa sq rt of m. However, below that stress intensity range, the alloy exhibited highly unusual behavior. This behavior consisted of a region where the crack growth rate became essentially independent of the applied stress intensity. The transition in the FCG behavior was related to a change in the observed crack growth mechanisms. In the Paris region, fatigue failure occurred along (111) facets; however, at the lower stress intensities, (001) fatigue failure was observed. A mechanism was proposed, based on barriers to dislocation motion, to explain the changes in the observed FCG behavior. The FCG data were also evaluated in terms of a recently proposed stress intensity parameter, K_{sub} . This parameter, based on the resolved shear stresses on the slip planes, quantified the crack driving force as well as the mode I delta K, and at the same time was also able to predict the microscopic crack path under different stress states. Author

N88-27310* National Aeronautics and Space Administration. Lewis Research Center, Cleveland, OH.

REFRACTORY METAL ALLOYS AND COMPOSITES FOR SPACE POWER SYSTEMS

JOSEPH R. STEPHENS, DONALD W. PETRASEK, and ROBERT H. TITRAN 1988 31 p Presented at the Spring Meeting of the Materials Research Society, Reno, Nev., 4-9 Apr. 1988 (NASA-TM-100946; E-4237; NAS 1.15:100946) Avail: NTIS HC A03/MF A01 CSCL 11F

Space power requirements for future NASA and other U.S. missions will range from a few kilowatts to megawatts of electricity. Maximum efficiency is a key goal of any power system in order to minimize weight and size so that the space shuttle may be used a minimum number of times to put the power supply into orbit. Nuclear power has been identified as the primary source to meet these high levels of electrical demand. One way to achieve maximum efficiency is to operate the power supply, energy conversion system, and related components at relatively high temperatures. NASA Lewis Research Center has undertaken a research program on advanced technology of refractory metal alloys and composites that will provide baseline information for space power systems in the 1900's and the 21st century. Basic research on the tensile and creep properties of fibers, matrices, and composites is discussed. Author

N88-29961* Cincinnati Univ., OH. Dept. of Aerospace Engineering and Engineering Mechanics.

ANISOTROPIC CONSTITUTIVE MODELING FOR NICKEL-BASE SINGLE CRYSTAL SUPERALLOYS Ph.D. Thesis

MICHAEL Y. SHEH 1988 190 p (Contract NAG3-511) (NASA-CR-182157; NAS 1.26:182157) Avail: NTIS HC A09/MF A01 CSCL 11F

An anisotropic constitutive model was developed based on crystallographic slip theory for nickel base single crystal superalloys. The constitutive equations developed utilizes drag stress and back stress state variables to model the local inelastic flow. Specially designed experiments were conducted to evaluate the existence of back stress in single crystal superalloy Rene N4 at 982 C. The results suggest that: (1) the back stress is orientation dependent; and (2) the back stress state variable is required for the current model to predict material anelastic recovery behavior. The model

was evaluated for its predictive capability on single crystal material behavior including orientation dependent stress-strain response, tension/compression asymmetry, strain rate sensitivity, anelastic recovery behavior, cyclic hardening and softening, stress relaxation, creep and associated crystal lattice rotation. Limitation and future development needs are discussed. Author

27

NONMETALLIC MATERIALS

Includes physical, chemical, and mechanical properties of plastics, elastomers, lubricants, polymers, textiles, adhesives, and ceramic materials.

A88-12587* Case Western Reserve Univ., Cleveland, OH.

INTERFACE ROUGHNESS EFFECT ON STRESSES IN CERAMIC COATINGS

ROBERT L. MULLEN (Case Western Reserve University, Cleveland, OH), ROBERT C. HENDRICKS, and GLEN MCDONALD (NASA, Lewis Research Center, Cleveland, OH) Ceramic Engineering and Science Proceedings (ISSN 0196-6219), vol. 8, July-Aug. 1987, p. 559-571.

This paper presents an analysis of the interface stress in plasma-sprayed zirconia coatings. The stress distributions along smooth and rough interfaces were calculated for perfectly bonded materials. The effect of mechanical interlock along the interface was also calculated. The interface stresses for noninterlocking interfaces were consistently higher; the interlocking interfaces showed high stresses in small regions only. Author

A88-12588* Akron Univ., OH.

THERMOMECHANICAL BEHAVIOR OF PLASMA-SPRAYED ZR02-Y203 COATINGS INFLUENCED BY PLASTICITY, CREEP, AND OXIDATION

J. PADOVAN, B. T. F. CHUNG (Akron, University, OH), GLEN E. MCDONALD, and ROBERT C. HENDRICKS (NASA, Lewis Research Center, Cleveland, OH) Ceramic Engineering and Science Proceedings (ISSN 0196-6219), vol. 8, July-Aug. 1987, p. 572-582. Previously announced in STAR as N87-18784.

Thermocycling of ceramic-coated turbomachine components produces high thermomechanical stresses that are mitigated by plasticity and creep but aggravated by oxidation, with residual stresses exacerbated by all three. These residual stresses, coupled with the thermocyclic loading, lead to high compressive stresses that cause the coating to spall. A ceramic-coated gas path seal is modeled with consideration given to creep, plasticity, and oxidation. The resulting stresses and possible failure modes are discussed. Author

A88-12589* Case Western Reserve Univ., Cleveland, OH.

SOME ADHESION/COHESION CHARACTERISTICS OF PLASMA-SPRAYED ZR02-Y203 UNDER TENSILE LOADING

ROBERT L. MULLEN (Case Western Reserve University, Cleveland, OH), BRIAN L. VLCEK (Rensselaer Polytechnic Institute, Troy, NY), ROBERT C. HENDRICKS, and GLEN MCDONALD (NASA, Lewis Research Center, Cleveland, OH) Ceramic Engineering and Science Proceedings (ISSN 0196-6219), vol. 8, July-Aug. 1987, p. 583-595.

A set of 12.7 mm diameter stainless steel tubes were coated with ceramic and expanded. The bond cast was 0.08 to 0.13 mm NiCrAlY with 0.38 mm of ZrO₂-8Y₂O₃ ceramic. Upon pressurization, the tube substrate yielded and overstressed the coatings in tension. The coatings cracked (i.e., they failed) but did not come off the tube. These results demonstrate that tensile failure of plasma-sprayed coatings is not catastrophic as is compressive failure, which leads to spallation. Author

27 NONMETALLIC MATERIALS

A88-12602* General Motors Corp., Indianapolis, IN.
DYNAMIC AND STATIC FATIGUE BEHAVIOR OF SINTERED SILICON NITRIDES

J. CHANG, P. KHANDELWAL, and P. W. HEITMAN (General Motors Corp., Allison Gas Turbine Div., Indianapolis, IN) Ceramic Engineering and Science Proceedings (ISSN 0196-6219), vol. 8, July-Aug. 1987, p. 766-777. DOE-supported research. refs (Contract DEN3-168)

The dynamic and static fatigue behavior of Kyocera SN220M sintered silicon nitride at 1000 C was studied. Fractographic analysis of the material failing in dynamic fatigue revealed the presence of slow crack growth (SCG) at stressing rates below 41 MPa/min. Under conditions of static fatigue this material also displayed SCG at stresses below 345 MPa. SCG appears to be controlled by microcracking of the grain boundaries. The crack velocity exponent (n) determined from both dynamic and static fatigue tests ranged from 11 to 16. Author

A88-13172* National Aeronautics and Space Administration. Lewis Research Center, Cleveland, OH.

PMR POLYIMIDE COMPOSITIONS FOR IMPROVED PERFORMANCE AT 371 C

RAYMOND D. VANNUCCI (NASA, Lewis Research Center, Cleveland, OH) IN: Advanced materials technology '87; Proceedings of the Thirty-second International SAMPE Symposium and Exhibition, Anaheim, CA, Apr. 6-9, 1987. Covina, CA, Society for the Advancement of Material and Process Engineering, 1987, p. 602-612. Previously announced in STAR as N87-16071.

Studies were conducted to identify matrix resins which have potential for use at 371 C (700 F). Utilizing PMR methodology, neat resin moldings were prepared with various monomer reactants and screened for thermo-oxidative stability at 371 C (700 F) under both ambient and a four-atmosphere air pressure. The results of the resin screening studies indicate that high molecular weight (HMW) formulated resins of first (PMR-15) and second (PMR-II) generation PMR materials exhibit lower levels of weight loss at 371 C (700) than PMR-15 and PMR-II resins. The resin systems which exhibited the best overall balance of processability, T_g and thermo-oxidative stability at 371 C were used to prepare unidirectional Celion 6000 and T-40R graphite fiber laminates. Laminates were evaluated for thermo-oxidative stability and 371 C mechanical properties. Results of the laminate evaluation studies indicate that two of the resin compositions have potential for use in 371 C applications. The most promising resin composition provided laminates which exhibited no drop in 371 C mechanical properties and only 11 percent weight loss after 200 hr exposure to atmospheres of air at 371 C. Author

A88-14568* Case Western Reserve Univ., Cleveland, OH.

CURVILINEAR CRACK LAYER PROPAGATION

ALEXANDER CHUDNOVSKY, KAMEL CHAOUI, and ABDELSAMIE MOET (Case Western Reserve University, Cleveland, OH) Journal of Materials Science Letters (ISSN 0261-8028), vol. 6, Sept. 1987, p. 1033-1038. refs (Contract NAG3-5852)

An account is given of an experiment designed to allow observation of the effect of damage orientation on the direction of crack growth in the case of crack layer propagation, using polystyrene as the model material. The direction of crack advance under a given loading condition is noted to be determined by a competition between the tendency of the crack to maintain its current direction and the tendency to follow the orientation of the crazes at its tip. The orientation of the crazes is, on the other hand, determined by the stress field due to the interaction of the crack, the crazes, and the hole. The changes in craze rotation relative to the crack define the active zone rotation. O.C.

A88-15120*# National Aeronautics and Space Administration. Lewis Research Center, Cleveland, OH.

PROGRESS TOWARD LIFE MODELING OF THERMAL BARRIER COATINGS FOR AIRCRAFT GAS TURBINE ENGINES

R. A. MILLER (NASA, Lewis Research Center, Cleveland, OH)

ASME, Transactions, Journal of Engineering for Gas Turbines and Power (ISSN 0022-0825), vol. 109, Oct. 1987, p. 448-451. refs (ASME PAPER 87-ICE-18)

Progress toward developing life models for simulating the behavior of thermal barrier coatings in aircraft gas turbine engines is discussed. A preliminary laboratory model is described as are current efforts to develop engine-capable models. Current understanding of failure mechanisms is also summarized. Author

A88-17214* Nebraska Univ., Lincoln.

ELECTRICAL RESISTIVITY (4K TO 2100K) OF ANNEALED VAPOR GROWTH CARBON FIBERS

AKHTER U. AHMED, MARTIN C. ROST, DUANE MEYER, RODNEY O. DILLON, JOHN A. WOOLLAM (Nebraska, University, Lincoln) et al. Applied Physics Communications (ISSN 0277-9374), vol. 7, no. 3, 1987, p. 135-155. Research supported by Applied Sciences, Inc. and Space Power, Inc. refs (Contract NAG3-95)

Carbon fibers have been grown from methane gas, on iron seeded substrates at 1370 K, and subsequently annealed to a series of temperatures between 2800 K and 3475 K. The subsequent measurement of the electrical resistivity are reported as a function of temperature from 4 K to 2100 K. The two band model for the resistivity of graphite is well fit to the data, and results in physically reasonable parameters of the fits. The resistivity vs temperature results for two boron doped fibers are reported as well. The product of the resistivity times density for these fibers is lower than that product for any refractory metal, for temperatures above about 1000 K, suggesting the usefulness of these fibers as high temperature materials in space applications. Author

A88-17368* Nebraska Univ., Lincoln.

ELECTRON-SPIN-RESONANCE STUDIES OF VAPOR-GROWN CARBON FIBERS

B. MARSHIK, D. MEYER, and T. APPLE (Nebraska, University, Lincoln) Journal of Applied Physics (ISSN 0021-8979), vol. 62, Nov. 1, 1987, p. 3947-3952. refs (Contract NAG3-95)

The effects of annealing temperature and fiber diameter on the degree of disorder of vapor-grown carbon fibers were investigated by analyzing the electron-spin-resonance (ESR) line shapes of fibers annealed at six various temperatures up to 3375 K. The diameter of fibers, grown from methane gas, ranged from 10 to 140 microns with most fibers between 20 and 50 microns. It was found that the degree of disorder of vapor-grown fibers decreases upon annealing to higher temperature; standard angular deviation between the fiber axis and the crystallite basal planes could vary from 35 deg (for annealing temperature of 2275 K) to 12 deg (for 3375 K). With respect to fiber diameter, order parameters were found to be higher for fibers of smaller diameters. I.S.

A88-18361* National Aeronautics and Space Administration. Lewis Research Center, Cleveland, OH.

GLASS PROPERTIES IN THE YTTRIA-ALUMINA-SILICA SYSTEM

M. J. HYATT (NASA, Lewis Research Center, Cleveland, OH; Missouri-Rolla, University, Rolla) and D. E. DAY (Missouri-Rolla, University, Rolla) American Ceramic Society, Communications (ISSN 0002-7820), vol. 70, Oct. 1987, p. C-283 to C-287. Research supported by the University of Missouri-Rolla. refs

The glass formation region in the yttria-alumina-silica system was investigated. Properties of glasses containing 25 to 55 wt pct yttria were measured and the effect of the composition was determined. The density, refractive index, thermal-expansion coefficient, and microhardness increased with increasing yttria content. The dissolution rate in 1N HCl increased with increasing yttria content and temperature. These glasses were also found to have high electrical resistivity. Author

A88-19056* National Aeronautics and Space Administration. Lewis Research Center, Cleveland, OH.

SIMPLE PROCESSING METHOD FOR HIGH-STRENGTH SILICON CARBIDE

JANET B. HURST and SUNIL DUTTA (NASA, Lewis Research Center, Cleveland, OH) American Ceramic Society, Communications (ISSN 0002-7820), vol. 70, Nov. 1987, p. C-303 to C-308. refs

Silicon carbide test bars were made by a simple wet-processing technique. The pressure casting method used the same equipment as conventional dry-pressing, but with a modified die. This casting technique was employed in order to produce test bars with improved strength and smaller fracture flaws than produced by dry-pressing. This was accomplished by eliminating pore clusters which were present in dry-pressed specimens and identified as a common source of failure in SiC MOR test bars. Author

A88-20257* National Aeronautics and Space Administration. Lewis Research Center, Cleveland, OH.

THERMAL CONDUCTIVITY OF PRISTINE AND BROMINATED HIGHLY GRAPHITIZED PITCH BASED CARBON FIBERS

CHING-CHEH HUNG (NASA, Lewis Research Center, Cleveland, OH) and JOHN MILLER (Kenyon College, Gambier, OH) Carbon (ISSN 0008-6223), vol. 25, no. 5, 1987, p. 679-684. Previously announced in STAR as N87-11893. refs

Thermal conductivity of brominated and pristine Union Carbide P-100 graphite fibers in the 30 to 160 C temperature range was determined by measuring thermal conductivities of graphite fiber epoxy composite samples and then excluding the epoxy contribution. A comparative thermal conductivity instrument was used to measure the thermal conductivity of the samples containing fibers. Results showed that the thermal conductivity values were 225 to 370 W/m-K and 215 to 340 W/m-K for pristine and brominated fibers, respectively. Furthermore, the thermal conductivity ratio of brominated to pristine P-100 fibers was 0.89, 0.91, and 0.92 at 55 to 80 C; 108 and 130 C, respectively. Such decrease in thermal conductivity results almost entirely from the 10 percent increase in fiber cross sectional area due to bromination. This result suggests that bromination effects on P-100 fiber structure is small, and that some structural changes, presumably the sharp-angled domain wall becomes less sharp, occurring in the 80 to 108 C temperature range. Author

A88-20278* National Aeronautics and Space Administration. Lewis Research Center, Cleveland, OH.

A COMPARISON OF THE BROMINATION DYNAMICS OF VARIOUS CARBON AND GRAPHITE FIBERS

JAMES R. GAIER (NASA, Lewis Research Center, Cleveland, OH) Synthetic Metals (ISSN 0379-6779), vol. 22, 1987, p. 15-22. refs

The electrical resistance of four grades of pitch-based graphite fibers and three experimental organic vapor-derived fibers was determined in situ during bromination and subsequent exposure to ambient laboratory air. The results show that the least graphitic pitch-based fiber does not brominate significantly, and that bromination and debromination reactions proceed much slower for vapor-derived fibers than for pitch-based ones. It is suggested that this decreased reaction rate is primarily due to the differences in graphene plane orientation between the fiber types. The results also imply that the vapor-derived and pitch-based fibers produce true intercalation compounds. R.R.

A88-20300* Case Western Reserve Univ., Cleveland, OH.
ION BEAM DEPOSITION OF AMORPHOUS CARBON FILMS WITH DIAMOND LIKE PROPERTIES

JOHN C. ANGUS (Case Western Reserve University, Cleveland, OH), MICHAEL J. MIRTICH, and EDWIN G. WINTUCKY (NASA, Lewis Research Center, Cleveland, OH) IN: Metastable materials formation by ion implantation. Amsterdam, Elsevier Science Publishing Co., Inc., 1982, p. 433-440. refs

Carbon films were deposited on silicon, quartz, and potassium bromide substrates from an ion beam. Growth rates were approximately 0.3 micron/hour. The films were featureless and

amorphous and contained only carbon and hydrogen in significant amounts. The density and carbon/hydrogen ratio indicate the film is a hydrogen deficient polymer. One possible structure, consistent with the data, is a random network of methylene linkages and tetrahedrally coordinated carbon atoms. Author

A88-26154* Ford Motor Co., Dearborn, MI.

STRENGTH CHARACTERIZATION OF YTTRIA/ALUMINA-DOPED SINTERED SILICON NITRIDE

R. K. GOVILA (Ford Motor Co., Ceramic Materials Dept., Dearborn, MI) International Journal of High Technology Ceramics (ISSN 0267-3762), vol. 3, no. 3, 1987, p. 179-197. refs (Contract DAAG46-77-C-0028; DEN3-167)

The flexural strength of yttria/alumina-doped sintered silicon nitride (Ford Material-RM 20) was measured as a function of temperature (20 to 1400 deg C), applied stress and time. Flexural stress rupture testing at 800 and 1000 deg C indicated that the material can sustain 344 MPa and 276 MPa, respectively, without failure, for a limited time (less than or equal to 100 h). The RM 20 material was susceptible to both oxidation and early stages of creep deformation at temperatures above 1000 deg C and displayed extensive creep deformation and degradation in strength above 1300 deg C. Author

A88-26222* National Aeronautics and Space Administration. Lewis Research Center, Cleveland, OH.

MOLTEN-SALT CORROSION OF SILICON NITRIDE. I - SODIUM CARBONATE. II - SODIUM SULFATE

DENNIS S. FOX and NATHAN S. JACOBSON (NASA, Lewis Research Center, Cleveland, OH) American Ceramic Society, Journal (ISSN 0002-7820), vol. 71, Feb. 1988, p. 128-138. refs

An experimental study of the corrosion of Si₃N₄ under thin films of Na₂CO₃ at 1000 C has been conducted using both pure Si₃N₄ and Si₃N₄ with various additives. The reaction mechanism is shown to consist of: (1) the decomposition of Na₂CO₃ and the formation of Na₂SiO₃; (2) rapid oxidation; and (3) the formation of a protective silica layer below the silicate. In the second part, the corrosion mechanism of Si₃N₄ + Na₂SO₄/O₂ at 1000 C was studied for both pure and additive-containing Si₃N₄. The reaction of Si₃N₄ + Na₂SO₄ was found to involve an initial period of slow weight loss (due to Na₂SO₄ vaporization and oxidation-dissolution) followed by further oxidation or the near termination of the reaction, depending on the Si₃N₄ additive. R.R.

A88-26963* National Aeronautics and Space Administration. Lewis Research Center, Cleveland, OH.

SYNTHESIS, ELECTRICAL AND THERMAL CONDUCTIVITIES, AND POTENTIAL APPLICATIONS OF GRAPHITE FLUORIDE FIBERS

CHING-CHEH HUNG (NASA, Lewis Research Center, Cleveland, OH), MARTIN LONG, and MARK STAHL (Cleveland State University, OH) SAMPE Quarterly (ISSN 0036-0821), vol. 19, Jan. 1988, p. 12-18. refs

Graphite fluoride fibers can be produced by fluorinating pristine or intercalated graphite fibers. The higher the degree of graphitization of the fibers, the higher the temperature needed to reach the same degree of fluorination. Structural damage during high temperature fluorination can be reduced or eliminated by pretreating the fibers with bromine and/or fluorine. The electrical resistivity of the fibers was in the 0.01 to 10 to the 11th ohm-cm range. The thermal conductivity of these fibers ranged from 5 to 75 W/m-K, which is much larger than the thermal conductivity of glass (1.1 W/m-K), the commonly used fiber in epoxy composites. A composite made from graphite fluoride fibers and epoxy or PTFE may be highly thermally conducting and electrically insulating or semiconducting. The electrically insulating product may be used as heat sinks for electrical or electronic instruments. Author

A88-29714* National Aeronautics and Space Administration. Lewis Research Center, Cleveland, OH.

EFFECT OF HIGH-TEMPERATURE HYDROGEN EXPOSURE ON SINTERED ALPHA-SiC

27 NONMETALLIC MATERIALS

GARY W. HALLUM and THOMAS P. HERBELL (NASA, Lewis Research Center, Cleveland, OH) *Advanced Ceramic Materials* (ISSN 0883-5551), vol. 3, March 1988, p. 171-175. Previously announced in STAR as N87-14518. refs

Sintered alpha-silicon carbide was exposed to pure, dry hydrogen at high temperatures for times up to 500 hr. Weight loss and corrosion were seen after 50 hr at temperatures as low as 1000 C. Corrosion of SiC by hydrogen produced grain boundary deterioration at 1100 C and a mixture of grain and grain boundary deterioration at 1300 C. Statistically significant strength reductions were seen in samples exposed to hydrogen for times greater than 50 hr and temperatures above 1100 C. Critical fracture origins were identified by fractography as either general grain boundary corrosion at 1100 C or as corrosion pits at 1300 C. A maximum strength decrease of approximately 33 percent was seen at 1100 and 1300 C after 500 hr exposure to hydrogen. A computer assisted thermodynamic program was also used to predict possible reaction species of SiC and hydrogen. Author

A88-31023* Case Western Reserve Univ., Cleveland, OH.
**MICROSCOPY OF EPITAXIALLY GROWN BETA-SiC ON
001-PLANE SILICON**

P. PIROUZ, C. M. CHOREY, T. T. CHENG (Case Western Reserve University, Cleveland, OH), and J. A. POWELL (NASA, Lewis Research Center, Cleveland, OH) *IN: Microscopy of semiconducting materials 1987; Proceedings of the Conference, Oxford, England, Apr. 6-8, 1987. Bristol, England, IOP Publishing, Ltd., 1987, p. 175-180. refs*

Various defects occurring in epitaxially grown layers of beta-SiC are characterized by TEM, and the mechanisms of growth and defect formation are discussed. In particular, attention is given to the following types of defects: misfit dislocations, interfacial twins, antiphase boundaries, threading dislocations, and wide stacking faults. Details of the experimental procedure are given. V.L.

A88-32372* National Aeronautics and Space Administration.
Lewis Research Center, Cleveland, OH.
**THE EFFECTS OF ATMOSPHERE ON THE TRIBOLOGICAL
PROPERTIES OF A CHROMIUM CARBIDE BASED COATING
FOR USE TO 760 C**

CHRISTOPHER DELLACORTE and HAROLD E. SLINEY (NASA, Lewis Research Center, Cleveland, OH) *Lubrication Engineering* (ISSN 0024-7154), vol. 44, April 1988, p. 338-343; Discussion, p. 343, 344. Previously announced in STAR as N87-16140. refs

The effect of atmosphere on the tribological properties of a plasma-sprayed chromium carbide based self-lubricating coating is reported. The coating contains bonded chromium carbide as the wear resistant base stock to which the lubricants silver and barium fluoride/calcium fluoride eutectic are added. It has been denoted as NASA PS200. Potential applications for the PS200 coating are cylinder wall/piston ring couples Stirling engines and foil bearing journal lubrication. Friction and wear studies were performed in helium, hydrogen, and moist air at temperatures from 25 to 760 C. In general, the atmosphere had a significant effect on both the friction and the wear of the coating and counterface material. Specimens tested in hydrogen, a reducing environment, exhibited the best tribological properties. Friction and wear increased in helium and air but are still within acceptable limits for intended applications. A variety of X-ray analyses was performed on the test specimens in an effort to explain the results. The following conclusions are made: (1) As the test atmosphere becomes less reducing, the coating experiences a higher concentration level of chromic oxide at the sliding interface which increases both the friction and wear. (2) Beneficial silver transfer from the parent coating to the counter-face material is less effective in air than in helium or hydrogen. (3) There may be a direct relationship between chromic oxide level present at the sliding interface and the friction coefficient. Author

A88-32853* National Aeronautics and Space Administration.
Lewis Research Center, Cleveland, OH.
**SPECIFIC HEAT OF PRISTINE AND BROMINATED GRAPHITE
FIBERS, COMPOSITES AND HOPG**

CHING-CHEN HUNG (NASA, Lewis Research Center, Cleveland, OH) and CAROLYN MACIAG (Cleveland State University, OH) *Carbon* (ISSN 0008-6223), vol. 25, no. 6, 1987, p. 837, 838. refs

Differential scanning calorimetry was used to obtain specific heat values of pristine and brominated P-100 graphite fibers and brominated P-100/epoxy composite as well as pristine and brominated highly oriented pyrolytic graphite (HOPG) for comparison. Based on the experimental results obtained, specific heat values are calculated for several different temperatures, with a standard deviation estimated at 1.4 percent of the average values. The data presented here are useful in designing heat transfer devices (such as airplane de-icing heaters) from bromine fibers. V.L.

A88-32854* National Aeronautics and Space Administration.
Lewis Research Center, Cleveland, OH.
**DIFFERENTIAL SCANNING CALORIMETRIC SURVEY OF
BROMINATED PAN, PITCH-BASED AND VAPOR-GROWN
FIBERS**

D. A. JAWORSKE, J. R. GAIER (NASA, Lewis Research Center, Cleveland, OH), C. MACIAG, and M. E. SLABE (Cleveland State University, OH) *Carbon* (ISSN 0008-6223), vol. 25, no. 6, 1987, p. 779-782. refs

A differential scanning calorimetric survey of brominated PAN, pitch-based and vapor-grown fibers revealed that only vapor-grown fibers heat-treated to temperatures of 2250 C or above exhibited the phase change at 100 C associated with the two-dimensional melting of bromine, similar to that observed in HOPG. All the pitch-based fibers tested, as well as vapor-grown fibers annealed to 2250 C, showed a substantial decrease in resistivity upon bromination but gave no indication of a phase change, suggesting that the bromine in these fibers does not have the long-range order needed to undergo two-dimensional melting. The brominated PAN fibers and unannealed vapor-grown fibers showed no phase change and no change in resistivity, indicating that these fibers do not intercalate bromine. Author

A88-32866* National Aeronautics and Space Administration.
Lewis Research Center, Cleveland, OH.
**MECHANICAL STRENGTH AND TRIBOLOGICAL BEHAVIOR
OF ION-BEAM-DEPOSITED BORON NITRIDE FILMS ON
NON-METALLIC SUBSTRATES**

KAZUHIISA MIYOSHI, JOHN J. POUCH, SAMUEL A. ALTEROVITZ, HAROLD E. SLINEY (NASA, Lewis Research Center, Cleveland, OH), and DONALD H. BUCKLEY (Case Western Reserve University, Cleveland, OH) *Surface and Coatings Technology* (ISSN 0257-8972), vol. 33, 1987, p. 221-233. Previously announced in STAR as N87-18668. refs

An investigation was conducted to examine the mechanical strength and tribological properties of boron nitride (BN) films ion-beam deposited on silicon (Si), fused silica (SiO₂), gallium arsenide (GaAs), and indium phosphide (InP) substrates in sliding contact with a diamond pin under a load. The results of the investigation indicate that BN films on nonmetallic substrates, like metal films on metallic substrates, deform elastically and plastically in the interfacial region when in contact with a diamond pin. However, unlike metal films and substrates, BN films on nonmetallic substrates can fracture when they are critically loaded. Not only does the yield pressure (hardness) of Si and SiO₂ substrates increase by a factor of 2 in the presence of a BN film, but the critical load needed to fracture increases as well. The presence of films on the brittle substrates can arrest crack formation. The BN film reduces adhesion and friction in the sliding contact. BN adheres to Si and SiO₂ and forms a good quality film, while it adheres poorly to GaAs and InP. The interfacial adhesive strengths were 1 GPa for a BN film on Si and appreciably higher than 1 GPa for a BN film on SiO₂. Author

A88-35565* National Aeronautics and Space Administration.
Lewis Research Center, Cleveland, OH.
**TRIBOLOGICAL PROPERTIES OF POLYMER FILMS AND
SOLID BODIES IN A VACUUM ENVIRONMENT**

ROBERT L. FUSARO (NASA, Lewis Research Center, Cleveland, OH) STLE Tribology Transactions (ISSN 0569-8197), vol. 31, April 1988, p. 174-180; Discussion, p. 181. Previously announced in STAR as N87-17906. refs

The tribological properties of ten different polymer based materials were evaluated in a vacuum environment to determine their suitability for possible lubrication applications in a space environment, such as might be encountered on the proposed Space Station. A pin-on-disk tribometer was used and the polymer materials were evaluated either as solid body disks or as films applied to 440C HT stainless steel disks. A 440C HT stainless steel hemispherically tipped pin was slid against the polymer materials. For comparison, similar tests were conducted in a controlled air atmosphere of 50 percent relative humidity air. In most instances, the polymer materials lubricated much better under vacuum conditions than in air. Thus, several of the materials show promise as lubricants for vacuum applications. Friction coefficients of 0.05 or less and polymer material wear rates of up to 2 orders of magnitude less than in air were obtained. One material showed considerable promise as a traction drive material. Relative high friction coefficients (0.36 to 0.52) and reasonably low wear rates were obtained in vacuum. Author

A88-35568* Rensselaer Polytechnic Inst., Troy, NY.
INVESTIGATION OF PTFE TRANSFER FILMS BY INFRARED EMISSION SPECTROSCOPY AND PHASE-LOCKED ELLIPSOMETRY

JAMES L. LAUER, BRUCE G. BUNTING (Rensselaer Polytechnic Institute, Troy, NY), and WILLIAM R. JONES, JR. (NASA, Lewis Research Center, Cleveland, OH) STLE Tribology Transactions (ISSN 0569-8197), vol. 31, April 1988, p. 282-288. Previously announced in STAR as N87-20421. refs
 (Contract DAAL03-86-K-0076; DAAL03-86-K-0042)

When a PTFE sheet was rubbed unidirectionally over a smooth surface of stainless steel an essentially monomolecular transfer film was formed. by ellipsometric and emission infrared spectroscopic techniques it was shown that the film was 10 to 15 Å thick and birefringent. From the intensity differences of infrared bands obtained with a polarizer passing radiation polarized in mutually perpendicular planes, it was possible to deduce transfer film orientation with the direction of rubbing. After standing in air for several weeks the transfer films apparently increased in thickness by as much as threefold. At the same time both the index of refraction and the absorption index decreased. Examination of the surfaces by optical and electron microscopies showed that the films had become porous and flaky. These observations were consistent with previous tribological measurements. The coefficients of friction decreased with the formation of the transfer film but increased again as the film developed breaks. The applicability of the ellipsometric and polarized infrared emission techniques to the identification of monomolecular tribological transfer films of polymers such as PTFE has been demonstrated. Author

A88-38318* National Aeronautics and Space Administration. Lewis Research Center, Cleveland, OH.

IMPROVED PROCESSING OF ALPHA-SiC

SUNIL DUTTA (NASA, Lewis Research Center, Cleveland, OH) Advanced Ceramic Materials (ISSN 0883-5551), vol. 3, May 1988, p. 257-262. refs

Dry pressing/sintering, slurry pressing/sintering, and hot isostatic pressing have been investigated with a view to developing an optimum processing technique to produce high-strength SiC for high-temperature structural applications. A baseline strength of 348 MPa was achieved by dry pressing and sintering. When slurry pressing was used to minimize agglomerates in the powder, a baseline strength of 428 MPa was obtained. An additional improvement in strength (655 MPa) was obtained by hot isostatic pressing, which prevented the formation of critical flaws resulting from residual agglomerates in the powder. It is expected that surface finish, such as lapping, polishing, and heat treatment, may further improve the strength and Weibull modulus of hot isostatically pressed alpha-sic. V.L.

A88-40792* National Aeronautics and Space Administration. Lewis Research Center, Cleveland, OH.

SILICON CARBIDE - PROGRESS IN CRYSTAL GROWTH

J. ANTHONY POWELL (NASA, Lewis Research Center, Cleveland, OH) IN: Novel refractory semiconductors. Pittsburgh, PA, Materials Research Society (MRS Symposium Proceedings. Volume 97), 1987, p. 159-170. refs

Recent progress in the development of two processes for producing large-area high-quality single crystals of SiC is described: (1) a modified Lely process for the growth of the alpha polytypes (e.g., 6H SiC) initially developed by Tairov and Tsvetkov (1978, 1981) and Ziegler et al. (1983), and (2) a process for the epitaxial growth of the beta polytype on single-crystal silicon or other substrates. Growth of large-area cubic SiC on Si is described together with growth of defect-free beta-SiC films on alpha-6H SiC crystals and TiC lattice. Semiconducting qualities of silicon carbide crystals grown by various techniques are discussed. I.S.

A88-40794* National Aeronautics and Space Administration. Lewis Research Center, Cleveland, OH.

BORON NITRIDE - COMPOSITION, OPTICAL PROPERTIES, AND MECHANICAL BEHAVIOR

JOHN J. POUCH, SAMUEL A. ALTEROVITZ, KAZUHISA MIYOSHI, and JOSEPH D. WARNER (NASA, Lewis Research Center, Cleveland, OH) (Materials Research Society, Spring Meeting, Anaheim, CA, Apr. 21-25, 1987) IN: Materials modification and growth using ion beams. Pittsburgh, PA, Materials Research Society (MRS Symposia Proceedings. Volume 93), 1987, p. 323-328. Previously announced in STAR as N87-25017. refs

A low energy ion beam deposition technique was used to grow boron nitride films on quartz, germanium, silicon, gallium arsenide, and indium phosphate. The film structure was amorphous with evidence of a hexagonal phase. The peak boron concentration was 82 at. percent. The carbon and oxygen impurities were in the 5 to 8 at. percent range. Boron-nitrogen and boron-boron bonds were revealed by X-ray photoelectron spectroscopy. The index of refraction varied from 1.65 to 1.67 for films deposited on III-V compound semiconductors. The coefficient of friction for boron nitride in sliding contact with diamond was less than 0.1. The substrate was silicon. Author

A88-41796*# National Aeronautics and Space Administration. Lewis Research Center, Cleveland, OH.

CHEMICAL VAPOR DEPOSITED SILICA COATINGS FOR SOLAR MIRROR PROTECTION

DANIEL A. GULINO (NASA, Lewis Research Center, Cleveland, OH), THERESA M. DEVER (Cleveland State University, OH), and WILLIAM F. BANHOLZER (General Electric Co., Schenectady, NY) AIAA, Aerospace Sciences Meeting, 26th, Reno, NV, Jan. 11-14, 1988. 9 p. Previously announced in STAR as N88-21306. refs
 (AIAA PAPER 88-0027)

A variety of techniques is available to apply protective coatings to oxidation susceptible spacecraft components, and each has associated advantages and disadvantages. Film applications by means of chemical vapor deposition (CVD) has the advantage of being able to be applied conformally to objects of irregular shape. For this reason, a study was made of the oxygen plasma durability of thin film (less than 5000 Å) silicon dioxide coatings applied by CVD. In these experiments, such coatings were applied to silver mirrors, which are strongly subject to oxidation, and which are proposed for use on the space station solar dynamic power system. Results indicate that such coatings can provide adequate protection without affecting the reflectance of the mirror. Scanning electron micrographs indicated that oxidation of the silver layer did occur at stress crack locations, but this did not affect the measured solar reflectances. Oxidation of the silver did not proceed beyond the immediate location of the crack. Such stress cracks did not occur in thinner silica films, and hence such films would be desirable for this application. Author

27 NONMETALLIC MATERIALS

A88-44743*# Allied-Signal Aerospace Co., Phoenix, AZ.
ELEVATED TEMPERATURE DURABILITY OF CERAMIC MATERIALS

LAURA J. LINDBERG (Allied-Signal Aerospace Co., Phoenix, AZ) AIAA, ASME, SAE, and ASEE, Joint Propulsion Conference, 24th, Boston, MA, July 11-13, 1988. 9 p. DOE-supported research. (Contract DEN3-167; DEN3-27) (AIAA PAPER 88-3055)

Fast fracture, stress rupture, and cyclic high temperature durability characterizations have been conducted for advanced silicon carbide and silicon nitride ceramics applicable to gas turbine hot section components. The fast fracture and stress rupture tests were conducted in four-point flexure at temperatures of up to 1540 C; the durability tests involved cycling specimens to temperatures of 1370 C and air quenching at 200 C for up to 3500 hrs. Materials with further reliability improvements are noted to be required for gas turbine hot section component applications. O.C.

A88-47562* Georgia Inst. of Tech., Atlanta.
SHEAR RHEOLOGICAL CHARACTERIZATION OF MOTOR OILS

SCOTT BAIR and WARD O. WINER (Georgia Institute of Technology, Atlanta) (STLE, Annual Meeting, 42nd, Anaheim, CA, May 11-14, 1987) STLE Tribology Transactions (ISSN 0569-8197), vol. 31, July 1988, p. 317-324. refs (Contract DOT-RS56-80-C-00015; NSG-3106)

Measurements of high pressure viscosity, traction coefficient, and EHD film thickness were performed on twelve commercial automotive engine oils, a reference oil, two unformulated base oils and two unformulated base oil and polymer blends. An effective high shear rate inlet viscosity was calculated from film thickness and pressure viscosity coefficient. The difference between measured and effective viscosity is a function of the polymer type and concentration. Traction measurements did not discriminate mileage formulated oils from those not so designated. Author

A88-47563* National Aeronautics and Space Administration. Lewis Research Center, Cleveland, OH.
SPUTTERED SILVER FILMS TO IMPROVE CHROMIUM CARBIDE BASED SOLID LUBRICANT COATINGS FOR USE TO 900 C

CHRISTOPHER DELLACORTE, HAROLD E. SLINNEY, and DANIEL L. DEADMORE (NASA, Lewis Research Center, Cleveland, OH) (STLE, Annual Meeting, 43rd, Cleveland, OH, May 9-12, 1988) STLE Tribology Transactions (ISSN 0569-8197), vol. 31, July 1988, p. 329-334. Previously announced in STAR as N88-15885. refs

Thin silver films, 250 to 3500 Å thick, were sputtered onto PS200, a plasma sprayed, chromium carbide based solid lubricant coating, to reduce run-in wear and improve tribological properties. The coating contains bonded chromium carbide as the wear resistant base stock with silver and barium fluoride/calcium fluoride eutectic added as low and high temperature lubricants, respectively. Potential applications for the PS200 coating are cylinder wall/piston ring lubrication for Stirling engines and foil bearing journal lubrication. In this preliminary program, the silver film overlay thickness was optimized based on tests using a pin-on-disk tribometer. The friction and wear studies were performed in a helium atmosphere at temperatures from 25 to 760 C with a sliding velocity of 2.7 m/s under a 4.9 N load. Films between 1000 and 1500 Å provide the best lubrication of the counterface material. The films enrich the sliding surface with lubricant and reduce the initial abrasiveness of the as ground, plasma-sprayed coating surface, thus reducing wear. Author

A88-48031*# Akron Univ., OH.
COMPUTERIZED LIFE AND RELIABILITY MODELLING FOR TURBOPROP TRANSMISSIONS

M. SAVAGE (Akron, University, OH), K. C. RADIL, D. G. LEWICKI (U.S. Army, Propulsion Directorate, Cleveland, OH), and J. J. COY (NASA, Lewis Research Center, Cleveland, OH) AIAA, ASME, SAE, and ASEE, Joint Propulsion Conference and Exhibit, 24th,

Boston, MA, July 11-13, 1988. 11 p. Previously announced in STAR as N88-23220. refs (AIAA PAPER 88-2979)

A generalized life and reliability model is presented for parallel shaft geared prop-fan and turboprop aircraft transmissions. The transmission life and reliability model is a combination of the individual reliability models for all the bearings and gears in the main load paths. The bearing and gear reliability models are based on classical fatigue theory and the two parameter Weibull failure distribution. A computer program was developed to calculate the transmission life and reliability. The program is modular. In its present form, the program can analyze five different transmission arrangements. However, the program can be modified easily to include additional transmission arrangements. An example is included which compares the life of a compound two-stage transmission with the life of a split-torque, parallel compound two-stage transmission as calculated by the computer program. Author

A88-49105* National Aeronautics and Space Administration. Lewis Research Center, Cleveland, OH.

SOL-GEL SYNTHESIS OF MAGNESIUM OXIDE-SILICON DIOXIDE GLASS COMPOSITIONS

NAROTTAM P. BANSAL (NASA, Lewis Research Center, Cleveland, OH) American Ceramic Society, Journal (ISSN 0002-7820), vol. 71, Aug. 1988, p. 666-672. Previously announced in STAR as N87-23750. refs

MgO-SiO₂ glasses containing up to 15 mol pct MgO, which could not have been prepared by the conventional glass melting method due to the presence of stable liquid-liquid immiscibility, were synthesized by the sol-gel technique. Clear and transparent gels were obtained from the hydrolysis and polycondensation of silicon tetraethoxide (TEOS) and magnesium nitrate hexahydrate when the water/TEOS mole ratio was four or more. The gelling time decreased with increase in magnesium content, water/TEOS ratio, and reaction temperature. Magnesium nitrate hexahydrate crystallized out of the gels containing 15 and 20 mol pct MgO on slow drying. This problem was partially alleviated by drying the gels quickly at higher temperatures. Monolithic gel samples were prepared using glycerol as the drying control additive. The gels were subjected to various thermal treatments and characterized by several methods. No organic groups could be detected in the glasses after heat treatments to approx. 800 C, but trace amounts of hydroxyl groups were still present. No crystalline phase was found from X-ray diffraction in the gel samples to approx. 890 C. At higher temperatures, alpha quartz precipitated out as the crystalline phase in gels containing up to 10 mol pct MgO. The overall activation energy for gel formation in 10MgO-90SiO₂ (mol pct) system for water/TEOS mole ratio of 7.5 was calculated to be 58.7 kJ/mol. Author

A88-49403* National Aeronautics and Space Administration. Lewis Research Center, Cleveland, OH.

STABILITY OF THE ELECTRICAL RESISTIVITY OF BROMINE, IODINE MONOCHLORIDE, COPPER(II) CHLORIDE, AND NICKEL(II) CHLORIDE INTERCALATED PITCH-BASED GRAPHITE FIBERS

JAMES R. GAIER (NASA, Lewis Research Center, Cleveland, OH), MELISSA E. SLABE (Cleveland State University, OH), and NANETTE SHAFFER (Intercal Co., Port Huron, MI) Carbon (ISSN 0008-6223), vol. 26, no. 3, 1988, p. 381-387. refs

A88-51300* National Aeronautics and Space Administration. Lewis Research Center, Cleveland, OH.

COMPARISON OF THE TRIBOLOGICAL PROPERTIES OF FLUORINATED COKES AND GRAPHITES

ROBERT L. FUSARO (NASA, Lewis Research Center, Cleveland, OH) STLE, Annual Meeting, 43rd, Cleveland, OH, May 9-12, 1988. 12 p. Previously announced in STAR as N87-29679. refs (STLE PREPRINT 88-AM-7F-1)

The friction, wear, endurance life, and surface morphology of rubbed (burnished) fluorinated graphite and fluorinated coke materials were studied. Two different coke powders, a graphitic

carbon powder, and a graphite powder were fluorinated and then tribologically investigated. In addition, one of the coke powders was reduced in size before fluorinating to evaluate the effect of a finer particle size on the tribological properties. For comparison, graphite and coke powders which were not fluorinated were also tribologically evaluated. Elemental analysis by emission spectroscopy was performed on each sample to determine the impurity content and X-ray diffraction analysis was performed to determine the crystallinity. Coke was found to have very little lubricating ability, but fluorinated coke did possess good lubricating properties. However, the fluorinated graphite and fluorinated graphitic carbon (which gave equivalent results) gave superior results to those obtained with the fluorinated cokes. No tribological benefit was found for using small versus a larger particle size of coke, at least when evaluated as a rubbed film. Author

A88-51307* Air Force Armament Lab., Eglin AFB, FL.
PRODUCTION AND CHARACTERIZATION OF CDCL₂ INTERCALATED GRAPHITE FIBERS

CLARENCE E. GOODEN (USAF, Armament Laboratory, Eglin AFB, FL), CHUONG PHAM, STEVE NAUD (U.S. Navy, Naval Coastal Systems Center, Panama City, FL), and JAMES R. GAIER (NASA, Lewis Research Center, Cleveland, OH) *Journal of Applied Physics* (ISSN 0021-8979), vol. 64, Sept. 1, 1988, p. 2384-2388. Navy-supported research. refs

Graphite fibers were intercalated using CdCl₂ as a Cl source and Cl₂ as carrier gas. Fibers were synthesized with a resistivity-density figure of merit comparable to that of copper. These fibers can withstand practical electrical current densities as high as 54,000 A/sq cm. Their thermal coefficient of resistivity is 0.0016 C, which is approximately 41 percent of those for copper and aluminum. Author

A88-54294*# Utah Univ., Salt Lake City.
MICROSTRUCTURAL EFFECTS ON FRACTURE TOUGHNESS OF POLYCRYSTALLINE CERAMICS IN COMBINED MODE I AND MODE II LOADING

D. SINGH and D. K. SHETTY (Utah, University, Salt Lake City) *ASME, Gas Turbine and Aeroengine Congress and Exposition, Amsterdam, Netherlands, June 6-9, 1988*. 7 p. refs (Contract NAG3-789) (ASME PAPER 88-GT-208)

Fracture toughness of polycrystalline alumina and ceria partially-stabilized tetragonal zirconia (CeO₂-TZP) ceramics were assessed in combined mode I and mode II loading using precracked disk specimens in diametral compression. Stress states ranging from pure mode I, combined mode I and mode II, and pure mode II were obtained by aligning the center crack at specific angles relative to the loading diameter. The resulting mixed-mode fracture toughness envelope showed significant deviation to higher fracture toughness in mode II relative to the predictions of the linear elastic fracture mechanics theory. Critical comparison with corresponding results on soda-lime glass and fracture surface observations showed that crack surface resistance arising from grain interlocking and abrasion was the main source of the increased fracture toughness in mode II loading of the polycrystalline ceramics. The normalized fracture toughness for pure mode II loading, (K_{II}/K_{IC}), increased with increasing grain size for the CeO₂-TZP ceramics. Quantitative fractography confirmed an increased percentage of transgranular fracture of the grains in mode II loading. Author

A88-54976*# Purdue Univ., West Lafayette, IN.
LINEAR AND NONLINEAR MECHANICAL PROPERTIES OF A SERIES OF EPOXY RESINS

D. B. CURLISS and J. M. CARUTHERS (Purdue University, West Lafayette, IN) *IN: Developments in Mechanics. Volume 14(c) - Midwestern Mechanics Conference, 20th, West Lafayette, IN, Aug. 31-Sept. 2, 1987, Proceedings. West Lafayette, IN, Purdue University, 1987, p. 1254-1259*. refs (Contract NAG3-599)

The linear viscoelastic properties have been measured for a series of bisphenol-A-based epoxy resins cured with the diamine DDS. The linear viscoelastic master curves were constructed via

time-temperature superposition of frequency dependent G-prime and G-double-prime isotherms. The G-double-prime master curves exhibited two sub-Tg transitions. Superposition of isotherms in the glass-to-rubber transition (i.e., alpha) and the beta transition at -60 C was achieved by simple horizontal shifts in the log frequency axis; however, in the region between alpha and beta, superposition could not be effected by simple horizontal shifts along the log frequency axis. The different temperature dependency of the alpha and beta relaxation mechanisms causes a complex response of G-double-prime in the so called alpha-prime region. A novel numerical procedure has been developed to extract the complete relaxation spectra and its temperature dependence from the G-prime and G-double-prime isothermal data in the alpha-prime region. Author

A88-55044* National Aeronautics and Space Administration.
 Lewis Research Center, Cleveland, OH.

ACOUSTIC IMAGING OF SUBTLE POROSITY VARIATIONS IN CERAMICS

E. R. GENERAZIO, D. J. ROTH, and G. Y. BAAKLINI (NASA, Lewis Research Center, Cleveland, OH) *Materials Evaluation* (ISSN 0025-5327), vol. 46, Sept. 1988, p. 1338-1343. refs

Acoustic images of silicon carbide ceramic disks were obtained using a precision scanning contact pulse-echo technique. Phase and cross-correlation velocity and attenuation maps were used to form color images of microstructural variations. These acoustic images reveal microstructural variations not observable with X-radiography. Author

N88-10188*# National Aeronautics and Space Administration.
 Lewis Research Center, Cleveland, OH.

EFFECT OF HIGH-TEMPERATURE ANNEALING ON THE MICROSTRUCTURE AND THERMOELECTRIC PROPERTIES OF GAP DOPED SIGE M.S. Thesis

SUSAN L. DRAPER Oct. 1987 23 p
 (NASA-TM-100164; E-3729; NAS 1.15:100164) Avail: NTIS HC A03/MF A01 CSCL 11G

Annealing of GaP doped SiGe will significantly alter the thermoelectric properties of the material resulting in increased performance as measured by the figure of merit Z and the power factor P. The microstructures and corresponding thermoelectric properties after annealing in the 1100 to 1300 C temperature range have been examined to correlate performance improvement with annealing history. The figure of merit and power factor were both improved by homogenizing the material and limiting the amount of cross-doping. Annealing at 1215 C for 100 hr resulted in the best combination of thermoelectric properties with a resultant figure of merit exceeding 1x10 to the -3 deg C to the -1 and a power factor of 44 microW/cm/deg C sq for the temperature range of interest for space power: 400 to 1000 C. Author

N88-11838*# National Aeronautics and Space Administration.
 Lewis Research Center, Cleveland, OH.

STRUCTURE AND GRAIN COARSENING DURING THE PROCESSING OF ENGINEERING CERAMICS Ph.D. Thesis - Leeds Univ., United Kingdom

NANCY J. SHAW Nov. 1987 178 p
 (NASA-TM-100235; E-3860; NAS 1.15:100235) Avail: NTIS HC A09/MF A01 CSCL 11B

Studies have been made of three ceramic systems (Al₂O₃, Y₂O₃/MgO, and SiC/C/B), both to explore a surface area/density diagram approach to examining the coarsening processes during sintering and to explore an alternative coarsening parameter, i.e., the grain boundary surface area (raising it at a given value of the density) and not the pore surface area; therefore, pinning of the grain boundaries by solid-solution drag is the only function evidenced by these results. The importance of such pinning even at densities as low as 75% of theoretical is linked to the existence of microstructural inhomogeneities. The early stages of sintering of Y₂O₃ powder have been examined using two techniques, BET surface area analysis and transmission electron microscopy. Each has given some insight into the process occurring and, used together, have provided some indication of the effect of MgO on

27 NONMETALLIC MATERIALS

coarsening during sintering. Attempts to further elucidate effects of MgO on the coarsening behavior of Y₂O₃ by the surface area/density diagram approach were unsuccessful due to masking effects of contaminating reactions during sintering and/or thermal etching. The behavior of the undoped SiC which only coarsens can be clearly distinguished by the surface area/density diagram from that of SiC/C/B which also concurrently densifies. Little additional information was obtainable by this method due to unfavorable sample etching characteristics. The advantages, disadvantages, and difficulties of application of these techniques to the study of coarsening during sintering are discussed. Author

N88-13453*# National Aeronautics and Space Administration. Lewis Research Center, Cleveland, OH.

COATINGS FOR HIGH-TEMPERATURE BEARINGS AND SEALS Final Report

HAROLD E. SLINEY Jul. 1987 14 p Presented at the Workshop on Coatings for Advanced Heat Engines, Castine, Me., 26-30 Jul. 1987; sponsored by DOE (Contract DE-AI01-85CE-50112) (NASA-TM-100249; E-3871; NAS 1.15:100249; DOE/NASA/50112-71) Avail: NTIS HC A01/MF A01 CSCL 11G

Criteria are discussed for predicting the probable lubricating ability of candidate solid materials from a consideration of their basic chemical and physical properties. The properties considered to be important in the model are thermochemical potential, adhesion, low hardness, plasticity, yield strength in shear, and brittle-to-ductile transition characteristics. A review of the selection and tribological testing of materials, which were selected for use in self-lubricating composite coatings by employing this model, is given. Two series of plasma-sprayed coatings with good tribological properties over a wide temperature spectrum are described. The PS 100 series of coatings contain oxidatively stable solid lubricants in a nichrome matrix. The PS 200 series contains the same solid lubricants in a very wear resistant metal-bonded chromium carbide matrix. Examples are given of applications of these coatings in high speed shaft seals, sliding contact bearings, and Stirling engine cylinder liners. Author

N88-14206*# National Aeronautics and Space Administration. Lewis Research Center, Cleveland, OH.

THE EFFECT OF TEXTURE ON THE CRACK GROWTH RESISTANCE OF ALUMINA

JONATHAN A. SALEM, JOHN L. SHANNON, JR., and RICHARD C. BRADT (Washington Univ., Seattle.) 1987 25 p Presented at the 89th Annual Meeting of the American Ceramic Society, Pittsburgh, Pa., 27-30 Apr. 1987 (NASA-TM-100250; E-3873; NAS 1.15:100250; REPT-167-B-87) Avail: NTIS HC A03/MF A01 CSCL 11B

The crack growth resistance of a textured, extruded alumina body was compared with that of an isotropic, isopressed body of similar grain size, density, and chemistry. R-curve levels reflected the preferred orientation; however, R-curve slopes (dK sub IR/d Delta a) were the same in all instances, implying a similar crack growth resistive mechanism. Three orthogonal orientations of crack growth in the two structures exhibited similar forms of K sub IR versus Delta-a curves, for which a schematic diagram for polycrystalline ceramics is proposed. Author

N88-15872*# National Aeronautics and Space Administration. Lewis Research Center, Cleveland, OH.

HOT PISTON RING/CYLINDER LINER MATERIALS: SELECTION AND EVALUATION Final Report

HAROLD E. SLINEY 1988 19 p Proposed for presentation at the 1988 International Congress and Exposition, Detroit, Mich., 29 Feb. - 4 Mar. 1988; sponsored by the Society of Automotive Engineers, Inc. (Contract DE-AI01-85CE-50112) (NASA-TM-100276; DOE/NASA/50112-73; E-3917; NAS 1.15:100276) Avail: NTIS HC A03/MF A01 CSCL 11B

In current designs of the automotive (kinematic) Stirling engine, the piston rings are made of a reinforced polymer and are located

below the pistons because they cannot withstand the high temperatures in the upper cylinder area. Theoretically, efficiency could be improved if hot piston rings were located near the top of the pistons. Described is a program to select piston ring and cylinder coating materials to test this theory. Candidate materials were screened, then subjected to a pin or disk friction and wear test machine. Tests were performed in hydrogen at specimen temperatures up to 760 C to simulate environmental conditions in the region of the hot piston ring reversal. Based on the results of these tests, a cobalt based alloy, Stellite 6B, was chosen for the piston rings and PS200, which consists of a metal-bonded chromium carbide matrix with dispersed solid lubricants, was chosen as the cylinder coating. Tests of a modified engine and a baseline engine showed that the hot ring reduced specific fuel consumption by up to 7 percent for some operating conditions and averaged about 3 percent for all conditions evaluated. Related applications of high-temperature coatings for shaft seals and as back-up lubricants are also described. Author

N88-15885*# National Aeronautics and Space Administration. Lewis Research Center, Cleveland, OH.

SPUTTERED SILVER FILMS TO IMPROVE CHROMIUM CARBIDE BASED SOLID LUBRICANT COATINGS FOR USE TO 900 C

CHRISTOPHER DELLACORTE, HAROLD E. SLINEY, and DANIEL L. DEADMORE 1988 17 p Prepared for the Annual Meeting of the Society of Tribologists and Lubrication Engineers, Cleveland, Ohio, 8-12 May 1988 (NASA-TM-100783; E-3955; NAS 1.15:100783) Avail: NTIS HC A03/MF A01 CSCL 11H

Thin silver films, 250 to 3500 A thick, were sputtered onto PS200, a plasma sprayed, chromium carbide based solid lubricant coating, to reduce run-in wear and improve tribological properties. The coating contains bonded chromium carbide as the wear resistant base stock with silver and barium fluoride/calcium fluoride eutectic added as low and high temperature lubricants respectively. Potential applications for the PS200 coating are cylinder wall/piston ring lubrication for Stirling engines and foil bearing journal lubrication. In this preliminary program, the silver film overlay thickness was optimized based on tests using a pin-on-disk tribometer. The friction and wear studies were performed in a helium atmosphere at temperatures from 25 to 760 C with a sliding velocity of 2.7 m/s under a 4.9 N load. Films between 1000 and 1500 A provide the best lubrication of the counterface material. The films enrich the sliding surface with lubricant and reduce the initial abrasiveness of the as ground, plasma-sprayed coating surface, thus reducing wear. Author

N88-15886*# AiResearch Casting Co., Torrance, CA. **IMPROVED SILICON NITRIDE FOR ADVANCED HEAT ENGINES Annual Technical Report, 26 Sep. 1984 - 30 Sep. 1985**

H. C. YEH, J. M. WIMMER, H. H. HUANG, M. E. RORABAUGH, J. SCHIENLE, and K. H. STYHR 15 Oct. 1985 149 p (Contract NAS3-24385) (NASA-CR-175006; NAS 1.26:175006; REPT-85-22592) Avail: NTIS HC A07/MF A01 CSCL 11B

The AiResearch Casting Company baseline silicon nitride (92 percent GTE SN-502 Si sub 3 N sub 4 plus 6 percent Y sub 2 O sub 3 plus 2 percent Al sub 2 O sub 3) was characterized with methods that included chemical analysis, oxygen content determination, electrophoresis, particle size distribution analysis, surface area determination, and analysis of the degree of agglomeration and maximum particle size of elutriated powder. Test bars were injection molded and processed through sintering at 0.68 MPa (100 psi) of nitrogen. The as-sintered test bars were evaluated by X-ray phase analysis, room and elevated temperature modulus of rupture strength, Weibull modulus, stress rupture, strength after oxidation, fracture origins, microstructure, and density from quantities of samples sufficiently large to generate statistically valid results. A series of small test matrices were conducted to study the effects and interactions of processing parameters which

included raw materials, binder systems, binder removal cycles, injection molding temperatures, particle size distribution, sintering additives, and sintering cycle parameters. Author

N88-16703*# National Aeronautics and Space Administration. Lewis Research Center, Cleveland, OH.

SELF-LUBRICATING COATINGS FOR HIGH-TEMPERATURE APPLICATIONS

HAROLD E. SLINEY *In its* Aeropropulsion '87. Session 1: Aeropropulsion Materials Research 13 p Nov. 1987
Avail: NTIS HC A06/MF A01 CSCL 11C

Some present-day aeropropulsion systems impose severe demands on the thermal and oxidative stability of lubricant, bearing, and seal materials. These demands will be much more severe for operational systems around the turn of the century. Solid lubricants with maximum temperature capabilities of about 1100 C are known. Unfortunately, none of the solid lubricants with the highest temperature capabilities are effective below approximately 400 C. However, research shows that silver and stable fluorides, such as calcium and barium fluoride act synergistically to provide lubrication from below room temperature to approximately 900 C. Plasma-sprayed, self-lubricating composite coatings that were developed at Lewis are described. Background information is given on coatings, designed as PS100 and PS101, that contain the solid lubricants in a Nichrome matrix. These coatings have low friction coefficients over a wide temperature range, but they have inadequate wear resistance for some long-duration applications. Wear resistance was dramatically improved in a recently developed coating PS200, by replacing the Nichrome matrix material with metal-bonded chromium carbide containing dispersed silver and calcium fluoride/barium fluoride eutectic (CaF₂/BaF₂). The lubricants control friction and the carbide matrix provides excellent wear resistance. Successful tests of these coatings are discussed. Author

N88-16704*# National Aeronautics and Space Administration. Lewis Research Center, Cleveland, OH.

CERAMICS FOR ENGINES

JAMES D. KISER, STANLEY R. LEVINE, and JAMES A. DICARLO *In its* Aeropropulsion '87. Session 1: Aeropropulsion Materials Research 18 p Nov. 1987
Avail: NTIS HC A06/MF A01 CSCL 11C

Structural ceramics were under nearly continuous development for various heat engine applications since the early 1970s. These efforts were sustained by the properties that ceramics offer in the areas of high-temperature strength, environmental resistance, and low density and the large benefits in system efficiency and performance that can result. The promise of ceramics was not realized because their brittle nature results in high sensitivity to microscopic flaws and catastrophic fracture behavior. This translated into low reliability for ceramic components and thus limited their application in engines. For structural ceramics to successfully make inroads into the terrestrial heat engine market requires further advances in low cost, net shape fabrication of high reliability components, and improvements in properties such as toughness, and strength. These advances will lead to very limited use of ceramics in noncritical applications in aerospace engines. For critical aerospace applications, an additional requirement is that the components display markedly improved toughness and noncatastrophic or graceful fracture. Thus the major emphasis is on fiber-reinforced ceramics. Author

N88-16868*# General Motors Corp., Indianapolis, IN. Gas Turbine Div.

NONDESTRUCTIVE EVALUATION OF STRUCTURAL CERAMICS BY PHOTOACOUSTIC MICROSCOPY Final Report

PRAMOD K. KHANDELWAL Jun. 1987 110 p
(Contract NAS3-24390)
(NASA-CR-180858; NAS 1.26:180858; EDR-12815) Avail: NTIS HC A06/MF A01 CSCL 11B

A photoacoustic microscopy (PAM) digital imaging system was developed and utilized to characterize silicon nitride material at the various stages of the ceramic fabrication process. Correlation

studies revealed that photoacoustic microscopy detected failure initiating defects in substantially more specimens than microradiography and ultrasonic techniques. Photoacoustic microscopy detected 10 to 100 micron size surface and subsurface pores and inclusions, respectively, up to 80 microns below the interrogating surface in machined sintered silicon nitride. Microradiography detected 50 micron diameter fracture controlling pores and inclusions. Subsurface holes were detected up to a depth of 570 microns and 1.00 mm in sintered silicon nitride and silicon carbide, respectively. Seeded voids of 20 to 30 micron diameters at the surface and 50 microns below the interrogating surface were detected by photoacoustic microscopy and microradiography with 1 percent X-ray thickness sensitivity. Tight surface cracks of 96 micron length x 48 micron depth were detected by photoacoustic microscopy. PAM volatilized and removed material in the green state which resulted in linear shallow microcracks after sintering. This significantly limits the use of PAM as an in-process NDE technique. M.G.

N88-16877*# National Aeronautics and Space Administration. Lewis Research Center, Cleveland, OH.

CORRELATIONS OF NORBORNENYL CROSSLINKED POLYIMIDE RESIN STRUCTURES WITH RESIN THERMO-OXIDATIVE STABILITY, RESIN GLASS TRANSITION TEMPERATURE AND COMPOSITE INITIAL MECHANICAL PROPERTIES

WILLIAM B. ALSTON 1988 5 p Presented at the Multidisciplinary Workshop on Chemistry and Properties of High Performance Composites, Jackson, Wyo., 28-31 Mar. 1988; sponsored by the American Chemical Society
(NASA-TM-100791; E-3966; NAS 1.15:100791; AVSCOM-TR-88-C-004; AD-A193313) Avail: NTIS HC A02/MF A01 CSCL 11B

PMR (polymerization of monomeric reactants) methodology was used to prepare 70 different polyimide oligomeric resins and 30 different unidirectional graphite fiber/polyimide composites. Monomeric composition as well as chain length between sites of crosslinks were varied to examine their effects on resin thermo-oxidative stability and glass transition temperature (T_g) of the cured/postcured resins. A linear correlation of decreasing 316 C resin weight loss/surface area versus (1) decreasing aliphatic content, or (2) increasing benzylic/aliphatic content stoichiometry ratio over a wide range of resin compositions was observed. An almost linear correlation of T_g versus molecular distance between the crosslinks was also observed. An attempt was made to correlate T_g with initial composite mechanical properties (flexural strength and interlaminar shear strength). However, the scatter in mechanical strength data prevented obtaining a clear correlation. Instead, only a range of composite mechanical properties was obtained at 25, 288, and 316 C. Perhaps more importantly, what did become apparent during the correlation study was (1) the PMR methodology could be used to prepare composites from resins containing a wide variety of monomer modifications, (2) that these composites almost invariably provided satisfactory initial mechanical properties as long as the resins formulated exhibited satisfactory processing flow, and (3) that PMR resins exhibited predictable rates of 316 C weight loss/surface area based on their benzylic/aliphatic stoichiometry ratio. Author

N88-17796*# National Aeronautics and Space Administration. Lewis Research Center, Cleveland, OH.

FRICTION AND WEAR OF MONOLITHIC AND FIBER REINFORCED SILICON-CERAMICS SLIDING AGAINST IN-718 ALLOY AT 25 TO 800 C IN ATMOSPHERIC AIR AT AMBIENT PRESSURE

DANIEL L. DEADMORE and HAROLD E. SLINEY Feb. 1988 31 p
(NASA-TM-100294; E-3942; NAS 1.15:100294) Avail: NTIS HC A03/MF A01 CSCL 11B

The friction and wear of monolithic and fiber reinforced Si-ceramics sliding against the nickel base alloy IN-718 at 25 to 800 C was measured. The monolithic materials tested were silicon carbide (SiC), fused silica (SiO₂), sialon, silicon nitride (Si₃N₄)

27 NONMETALLIC MATERIALS

with W and Mg additives, and Si₃N₄ with Y₂O₃ additive. At 25 C fused silica had the lowest friction while Si₃N₄ (W,Mg type) had the lowest wear. At 800 C sialon had the lowest friction while Si₃N₄ (W,Mg type) and sialon had the lowest wear. The SiC/IN-718 couple had the lowest total wear at 25 C. At 800 C the fused silica/IN-718 couple exhibited the least total wear. SiC fiber reinforced reaction bonded silicon nitride (RBSN) composite material with a porosity of 32 percent and a fiber content of 23 vol percent had a lower coefficient of friction and wear when sliding parallel to the fiber direction than in the perpendicular at 25 C. The coefficient of friction for the carbon fiber reinforced borosilicate composite was 0.18 at 25 C. This is the lowest of all the couples tested. Wear of this material was about two decades smaller than that of the monolithic fused silica. This illustrates the large improvement in tribological properties which can be achieved in ceramic materials by fiber reinforcement. At higher temperatures the oxidation products formed on the IN-718 alloy are transferred to the ceramic by sliding action and forms a thin, solid lubricant layer which decreases friction and wear for both the monolithic and fiber reinforced composites. Author

N88-17801*# National Aeronautics and Space Administration. Lewis Research Center, Cleveland, OH.

ADHESION, FRICTION AND MICROMECHANICAL PROPERTIES OF CERAMICS

KAZUHISA MIYOSHI 1988 24 p Proposed for presentation at the 15th International Conference on Metallurgical Coatings, San Diego, Calif., 11-15 Apr. 1988; sponsored by American Vacuum Society (NASA-TM-100782; E-3954; NAS 1.15:100782) Avail: NTIS HC A03/MF A01 CSCL 11C

The adhesion, friction, and micromechanical properties of ceramics, both in monolithic and coating form, are reviewed. Ceramics are examined in contact with themselves, other harder materials, and metals. For the simplicity of discussion, the tribological properties of concern in the processes are separated into two parts. The first part discusses the pull-off force (adhesion) and the shear force required to break the interfacial junctions between contacting surfaces. The role of chemical bonding in adhesion and friction, and the effects of surface contaminant films and temperature on tribological response with respect to adhesion and friction are discussed. The second part deals with abrasion of ceramics. Elastic, plastic, and fracture behavior of ceramics in solid state contact is discussed. The scratch technique of determining the critical load needed to fracture interfacial adhesive bonds of ceramic deposited on substrates is also addressed. Author

N88-18726*# National Aeronautics and Space Administration. Lewis Research Center, Cleveland, OH.

TRIBOLOGICAL PROPERTIES OF ALUMINA-BORON-SILICATE FABRIC FROM 25 TO 850 C Final Report

CHRISTOPHER DELLACORTE Mar. 1988 15 p (Contract DE-AL01-86CE-50162) (NASA-TM-100806; E-3986; DOE/NASA/50162-2; NAS 1.15:100806) Avail: NTIS HC A03/MF A01 CSCL 11B

Demanding tribological properties are required of the materials used for the sliding seal between the sidewalls and the lower wall of the variable area hypersonic engine. Temperatures range from room temperature and below to operating temperatures of 1000 C in an environment of air, hydrogen, and water vapor. Candidate sealing materials for this application are an alumina-boria-silicate, ceramic, fabric rope sliding against the engine walls which may be made from copper- or nickel-based alloys. Using a pin-on-disk tribometer, the friction and wear properties of some of these potential materials and possible lubrication methods are evaluated. The ceramic fabric rope displayed unacceptably high friction coefficients (0.6 to 1.3) and, thus, requires lubrication. Sputtered thin films of gold, silver, and CaF₂ reduced the friction by a factor of two. Sprayed coatings of boride nitride did not effectively lubricate the fabric. Static heat treatment tests at 950 C indicate that the fabric is chemically attacked by large quantities of silver,

CaF₂, and boron nitride. Sputtered films or powder impregnation of the fabric with gold may provide adequate lubrication up to 1000 C without showing any chemical attack. Author

N88-18734*# National Aeronautics and Space Administration. Lewis Research Center, Cleveland, OH.

OXIDATION AND PROTECTION OF FIBERGLASS-EPOXY COMPOSITE MASTS FOR PHOTOVOLTAIC ARRAYS IN THE LOW EARTH ORBITAL ENVIRONMENT

SHARON K. RUTLEDGE, PHILLIP E. PAULSEN, JOYCE A. BRADY (Cleveland State Univ., Ohio.), and MICHAEL L. CIANCONE 1988 12 p Presented at the Spring Meeting of the Materials Research Society, Reno, Nev., 5-9 Apr. 1988 (NASA-TM-100839; E-4027; NAS 1.15:100839) Avail: NTIS HC A03/MF A01 CSCL 11B

Fiberglass-epoxy composites are considered for use as structural members for the mast of the space station solar array panel. The low Earth orbital environment in which space station is to operate is composed mainly of atomic oxygen, which has been shown to cause erosion of many organic materials and some metals. Ground based testing in a plasma asher was performed to determine the extent of degradation of fiberglass-epoxy composites when exposed to a simulated atomic oxygen environment. During exposure, the epoxy at the surface of the composite was oxidized, exposing individual glass fibers which could easily be removed. Several methods of protecting the composite were evaluated in an atomic oxygen environment and with thermal cycling and flexing. The protection techniques evaluated to date include an aluminum braid covering, an indium-tin eutectic and a silicone based paint. The open aluminum braid offered little protection while the CV-1144 coating offered some initial protection against atomic oxygen, but appears to develop cracks which accelerate degradation when flexed. Coatings such as the In-Sn eutectic may provide adequate protection by containing the glass fibers even though mass loss still occurs. Author

N88-20454*# National Aeronautics and Space Administration. Lewis Research Center, Cleveland, OH.

DEVELOPMENT OF A TORSION BALANCE FOR ADHESION MEASUREMENTS

KAZUHISA MIYOSHI, CHIKAYOSHI MAEDA, and RYUICHI MASUO (Osaka Inst. of Tech., Japan) 1988 21 p Proposed for presentation at IMEKO 11, Houston, Tex., 16-21 Oct. 1988; sponsored by Instrument Society of America (NASA-TM-100799; E-3977; NAS 1.15:100799) Avail: NTIS HC A03/MF A01 CSCL 11B

A new torsion balance for study of adhesion in ceramics is discussed. A torsion wire and a linear variable differential transformer are used to monitor load and to measure pull-off force (adhesion force). The investigation suggests that this torsion balance is valuable in studying the interfacial properties of ceramics in controlled environments such as in ultrahigh vacuum. The pull-off forces measured in dry, moist, and saturated nitrogen atmosphere demonstrate that the adhesion of silicon nitride contacts remains low at humidities below 80 percent but rises rapidly above that. The adhesion at saturation is 10 times or more greater than that below 80 percent relative humidity. The adhesion in a saturated atmosphere arises primarily from the surface tension effects of a thin film of water adsorbed on the surface. The surface tension of the water film was 58 x 10 to the minus 5 to 65 x 10 to the minus 5 power. The accepted value for water is 72.7 x 10 to the minus 5 power N/cm. Adhesion characteristics of silicon nitride in contact with metals, like the friction characteristics of silicon carbide to metal contacts, can be related to the relative chemical activity of metals in ultrahigh vacuum. The more active the metal, the higher the adhesion. Author

N88-20455*# National Aeronautics and Space Administration. Lewis Research Center, Cleveland, OH.

AVAILABILITY AND COST ESTIMATE OF A HIGH NAPHTHENE, MODIFIED AVIATION TURBINE FUEL

GEORGE M. PROK Apr. 1988 9 p

(NASA-TM-100823; E-4011; NAS 1.15:100823) Avail: NTIS HC A02/MF A01 CSCL 11B

Information from an Air Force study was used to determine the potential availability and cost of a modified conventional fuel with a naphthene content which could have a thermal stability near that of JP-7 for high-speed civil transports. Results showed sufficient capacity for a fuel made of a blend of 50 percent naphthenic straight run kerosene and 50 percent hydrocracked product, assuming a near-term requirement of 210,000 BBL per day. Fuel cost would be as low as 62.5 to 64.5 cents per gallon, assuming 20 dollars per barrel for crude. Author

N88-21306*# National Aeronautics and Space Administration. Lewis Research Center, Cleveland, OH.

CHEMICAL VAPOR DEPOSITED SILICA COATINGS FOR SOLAR MIRROR PROTECTION

DANIEL A. GULINO, THERESE M. DEVER, and WILLIAM F. BANHOLZER (General Electric Co., Schenectady, N.Y.) Jan. 1988 9 p Presented at the 26th Aerospace Sciences Meeting, Reno, Nev., 11-14 Jan. 1988; sponsored by AIAA (NASA-TM-100834; E-4023; NAS 1.15:100834; AIAA-88-0027) Avail: NTIS HC A02/MF A01 CSCL 11C

A variety of techniques is available to apply protective coatings to oxidation susceptible spacecraft components, and each has associated advantages and disadvantages. Film applications by means of chemical vapor deposition (CVD) has the advantage of being able to be applied conformally to objects of irregular shape. For this reason, a study was made of the oxygen plasma durability of thin film (less than 5000 Å) silicon dioxide coatings applied by CVD. In these experiments, such coatings were applied to silver mirrors, which are strongly subject to oxidation, and which are proposed for use on the space station solar dynamic power system. Results indicate that such coatings can provide adequate protection without affecting the reflectance of the mirror. Scanning electron micrographs indicated that oxidation of the silver layer did occur at stress crack locations, but this did not affect the measured solar reflectances. Oxidation of the silver did not proceed beyond the immediate location of the crack. Such stress cracks did not occur in thinner silica films, and hence such films would be desirable for this application. Author

N88-21525*# Pratt and Whitney Aircraft, East Hartford, CT.

A CONSTITUTIVE MODEL FOR AN OVERLAY COATING

D. M. NISSLEY and G. A. SWANSON /in NASA. Lewis Research Center, Nonlinear Constitutive Relations for High Temperature Applications, 1986 p 419-436 Apr. 1988 (Contract NAS3-23939) Avail: NTIS HC A21/MF A01 CSCL 11C

Coatings are frequently applied to gas turbine blades and vanes to provide protection against oxidation and corrosion. The results of an experimental and analytical study to develop a constitutive model for an overlay coating is presented. Specimens were machined from a hot isostatically pressed billet of PWA 286. The tests consisted of isothermal stress relaxation cycles with monotonically increasing maximum strain and were conducted at various temperatures. The results were used to calculate the constants for various constitutive models, including the classical, the Walker isotropic, a simplified Walker, and Stowell models. A computerized regression analysis was used to calculate model constants from the data. The best fit was obtained for the Walker model, with the simplified Walker and classical models close behind. Author

N88-22197*# Illinois Univ., Urbana-Champaign. Dept. of Materials Science and Engineering.

HAFNIA-RICH MIXED OXIDE CERAMICS OF THE SYSTEM HFO₂-ZRO₂-TiO₂ FOR HEATERS AND HEAT EXCHANGERS IN ELECTROTHERMAL THRUSTERS: THE EFFECTS OF TITANIA ON SELECTED ELECTRICAL AND MECHANICAL PROPERTIES OF HAFNIA-RICH MIXED OXIDES IN THE SYSTEM HAFNIA-ZIRCONIA-TITANIA, VOLUME 1

PAUL RUSSELL STASZAK, G. P. WIRTZ, M. BERG, and S. D. BROWN May 1988 146 p

(Contract NAG3-495)

(NASA-CR-182800-VOL-1; NAS 1.26:182800-VOL-1) Avail: NTIS HC A07/MF A01 CSCL 11B

A study of the effects of titania on selected properties of hafnia-rich mixed oxides in the system hafnia-zirconia-titania (HZT) was made in the region 5 to 20 mol percent titania. The studied properties included electrical conductivity, thermal expansion, and fracture strength and toughness. The effects of titania on the properties were studied for the reduced state as well as the oxidized state of the sintered mixed oxides. X-ray analysis showed that the materials were not always single phase. The oxidized compositions went from being monoclinic solid solutions at low titania additions to having three phases (two monoclinic and a titanate phase) at high additions of titania. The reduced compositions showed an increasing cubic phase presence mixed with the monoclinic phase as titania was added. The electrical conductivity increased with temperature at approximately 0.1 mhos/cm at 1700 C for all compositions. The thermal expansion coefficient decreased with increasing titania as did the monoclinic to tetragonal transformation temperature. The fracture strength of the oxidized bars tended to decrease with the addition of titania owing to the presence of the second phase titania. The fracture strength of the reduced bars exhibited a minimum corresponding to a two-phase region of monoclinic and cubic phases. When the second phases were suppressed, the titania tended to increase the fracture strength slightly in both the oxidized and reduced states. The fracture toughness followed similar trends. Author

N88-22409*# National Aeronautics and Space Administration. Lewis Research Center, Cleveland, OH.

MONOLITHIC CERAMIC ANALYSIS USING THE SCARE PROGRAM

JANE M. MANDERSCHIED /in its Lewis Structures Technology, 1988. Volume 3: Structural Integrity Fatigue and Fracture Wind Turbines HOST p 5-20 May 1988 Avail: NTIS HC A16/MF A01 CSCL 11B

The Structural Ceramics Analysis and Reliability Evaluation (SCARE) computer program calculates the fast fracture reliability of monolithic ceramic components. The code is a post-processor to the MSC/NASTRAN general purpose finite element program. The SCARE program automatically accepts the MSC/NASTRAN output necessary to compute reliability. This includes element stresses, temperatures, volumes, and areas. The SCARE program computes two-parameter Weibull strength distributions from input fracture data for both volume and surface flaws. The distributions can then be used to calculate the reliability of geometrically complex components subjected to multiaxial stress states. Several fracture criteria and flaw types are available for selection by the user, including out-of-plane crack extension theories. The theoretical basis for the reliability calculations was proposed by Batdorf. These models combine linear elastic fracture mechanics (LEFM) with Weibull statistics to provide a mechanistic failure criterion. Other fracture theories included in SCARE are the normal stress averaging technique and the principle of independent action. The objective of this presentation is to summarize these theories, including their limitations and advantages, and to provide a general description of the SCARE program, along with example problems. Author

N88-22410*# Cleveland State Univ., OH.

WHISKER-REINFORCED CERAMIC COMPOSITES FOR HEAT ENGINE COMPONENTS

STEPHEN F. DUFFY /in NASA. Lewis Research Center, Lewis Structures Technology, 1988. Volume 3: Structural Integrity Fatigue and Fracture Wind Turbines HOST p 21-40 May 1988 (Contract NCC3-81)

Avail: NTIS HC A16/MF A01 CSCL 11B

Much work was undertaken to develop techniques of incorporating SiC whiskers into either a Si₃N₄ or SiC matrix. The result was the fabrication of ceramic composites with ever-increasing fracture toughness and strength. To complement this research effort, the fracture behavior of whisker-reinforced ceramics is studied so as to develop methodologies for the analysis

27 NONMETALLIC MATERIALS

of structural components fabricated from this toughened material. The results, outlined herein, focus on the following areas: the use of micromechanics to predict thermoelastic properties, theoretical aspects of fracture behavior, and reliability analysis. Author

N88-22411*# Cleveland State Univ., OH.
CONTINUOUS FIBER CERAMIC MATRIX COMPOSITES FOR HEAT ENGINE COMPONENTS

DAVID E. TRIPP *In* NASA. Lewis Research Center, Lewis Structures Technology, 1988. Volume 3: Structural Integrity Fatigue and Fracture Wind Turbines HOST p 41-61 May 1988

(Contract NCC3-81)

Avail: NTIS HC A16/MF A01 CSCL 11B

High strength at elevated temperatures, low density, resistance to wear, and abundance of nonstrategic raw materials make structural ceramics attractive for advanced heat engine applications. Unfortunately, ceramics have a low fracture toughness and fail catastrophically because of overload, impact, and contact stresses. Ceramic matrix composites provide the means to achieve improved fracture toughness while retaining desirable characteristics, such as high strength and low density. Materials scientists and engineers are trying to develop the ideal fibers and matrices to achieve the optimum ceramic matrix composite properties. A need exists for the development of failure models for the design of ceramic matrix composite heat engine components. Phenomenological failure models are currently the most frequently used in industry, but they are deterministic and do not adequately describe ceramic matrix composite behavior. Semi-empirical models were proposed, which relate the failure of notched composite laminates to the stress a characteristic distance away from the notch. Shear lag models describe composite failure modes at the micromechanics level. The enhanced matrix cracking stress occurs at the same applied stress level predicted by the two models of steady state cracking. Finally, statistical models take into consideration the distribution in composite failure strength. The intent is to develop these models into computer algorithms for the failure analysis of ceramic matrix composites under monotonically increasing loads. The algorithms will be included in a postprocessor to general purpose finite element programs.

Author

N88-23872*# National Aeronautics and Space Administration. Lewis Research Center, Cleveland, OH.

STRUCTURAL CERAMICS

May 1986 226 p Workshop held in Cleveland, Ohio, 20-21 May 1986 Sponsored by NASA, Washington (NASA-CP-2427; E-3063; NAS 1.55:2427) Avail: NTIS HC A11/MF A01 CSCL 11B

This publication is a compilation of abstracts and slides of papers presented at the NASA Lewis Structural Ceramics Workshop. Collectively, these papers depict the scope of NASA Lewis' structural ceramics program. The technical areas include monolithic SiC and Si₃N₄ development, ceramic matrix composites, tribology, design methodology, nondestructive evaluation (NDE), fracture mechanics, and corrosion.

This publication is a compilation of abstracts and slides of papers presented at the NASA Lewis Structural Ceramics Workshop. Collectively, these papers depict the scope of NASA Lewis' structural ceramics program. The technical areas include monolithic SiC and Si₃N₄ development, ceramic matrix composites, tribology, design methodology, nondestructive evaluation (NDE), fracture mechanics, and corrosion. Author

N88-23873*# National Aeronautics and Space Administration. Lewis Research Center, Cleveland, OH.

CERAMICS FOR TURBINE ENGINES

STANLEY R. LEVINE *In* its Structural Ceramics p 1-13 May 1986

Avail: NTIS HC A11/MF A01 CSCL 11C

The Ceramics for Turbine Engines Project is comprised of three main research programs with major elements as indicated: materials and processing (monolithics and fiber reinforcement), design methodology (design code and tribology), and life prediction

(environmental effects, nondestructive evaluation, fracture and fatigue, and time dependent behavior). From the NASA perspective an enhanced ceramics technology base directly supports aeronautics initiatives in small engine technology, high-performance turbine engine technology, and hypersonics. An overview of the program, which includes the technical objectives and content of each program, is provided. B.G.

N88-23874*# National Aeronautics and Space Administration. Lewis Research Center, Cleveland, OH.

FRICTION AND WEAR OF CERAMICS

DONALD H. BUCKLEY *In* its Structural Ceramics p 15-22 May 1986

Avail: NTIS HC A11/MF A01 CSCL 11C

The adhesion, friction, wear, and lubricated behaviors of both oxide and non-oxide ceramics are reviewed. Ceramics are examined in contact with themselves, other harder materials, and metals. Elastic, plastic, and fracture behavior of ceramics in solid state contact is discussed. The contact load necessary to initiate fracture in ceramics is shown to be appreciably reduced with tangential motion. Both friction and wear of ceramics are anisotropic and relate to crystal structure as with metals. Grit size effects in two and three body abrasive wear are observed for ceramics. Both the free energy of oxide formation and the d valence bond character of metals are related to the friction and wear characteristics for metals in contact with ceramics. Surface contaminants affect friction and adhesive wear. For example, carbon on silicon carbide and chlorine on aluminum oxide reduce friction while oxygen on metal surfaces in contact with ceramics increases friction. Lubrication increases the critical load necessary to initiate fracture of ceramics both in indentation and with sliding or rubbing. Author

N88-23875*# National Aeronautics and Space Administration. Lewis Research Center, Cleveland, OH.

SOME DESIGN CONSIDERATIONS FOR CERAMIC COMPONENTS IN HEAT ENGINE APPLICATIONS

JOHN P. GYEKENYESI *In* its Structural Ceramics p 23-33 May 1986

Avail: NTIS HC A11/MF A01 CSCL 11C

The design methodology for brittle material structures which is being developed and used at the Lewis Research Center for sizing ceramic components in heat engine applications is reviewed. Theoretical aspects of designing with structural ceramics are discussed, and a general purpose reliability program for predicting fast fracture response due to volume distributed flaws is described. Statistical treatment of brittle behavior, based on the Weibull model, is reviewed and its advantages, as well as drawbacks, are listed. A mechanistic statistical fracture theory, proposed by Batdorf to overcome the Weibull model limitations and based on Griffith fracture mechanics, is summarized. Failure probability predictions are made for rotating annular Si₃N₄ disks using various fracture models, and the results are compared to actual failure data. The application of these design methods to Government funded ceramics engine demonstration programs is surveyed. The uncertainty in observed component performance emphasizes the need for proof testing and improved nondestructive evaluation to guarantee adequate structural integrity. Author

N88-23879*# Ford Motor Co., Dearborn, MI.

IMPROVED SILICON CARBIDE FOR ADVANCED HEAT ENGINES

THOMAS J. WHALEN and J. A. MANGELS *In* NASA, Lewis Research Center, Structural Ceramics p 63-88 May 1986 (Contract NAS3-24384)

Avail: NTIS HC A11/MF A01 CSCL 11C

The development of silicon carbide materials of high strength was initiated and components of complex shape and high reliability were formed. The approach was to adapt a beta-SiC powder and binder system to the injection molding process and to develop procedures and process parameters capable of providing a sintered silicon carbide material with improved properties. The initial effort was to characterize the baseline precursor materials, develop

mixing and injection molding procedures for fabricating test bars, and characterize the properties of the sintered materials. Parallel studies of various mixing, dewaxing, and sintering procedures were performed in order to distinguish process routes for improving material properties. A total of 276 modulus-of-rupture (MOR) bars of the baseline material was molded, and 122 bars were fully processed to a sinter density of approximately 95 percent. Fluid mixing techniques were developed which significantly reduced flaw size and improved the strength of the material. Initial MOR tests indicated that strength of the fluid-mixed material exceeds the baseline property by more than 33 percent. the baseline property by more than 33 percent. B.G.

N88-23880*# National Aeronautics and Space Administration. Lewis Research Center, Cleveland, OH.

STRENGTH OPTIMIZATION OF ALPHA-SiC BY IMPROVED PROCESSING

SUNIL DUTTA *In its Structural Ceramics* p 89-98 May 1986
 Avail: NTIS HC A11/MF A01 CSCL 11C

Silicon carbide is of great interest for structural use in aircraft and automobile engines. This ceramic combines high thermal conductivity and low coefficient of thermal expansion, and consequently has good thermal shock resistance. However, like other ceramics, silicon carbide shows strength variability due to processing flaws such as large voids, shrinkage cracks, and inclusions. Agglomerates in the starting powder seem to be the predominant cause of such defects. Improved processing techniques such as slurry pressing and hot isostatic pressing (HIP) were employed to minimize these defects and to improve strength and reliability in the fabricated material. For this purpose 2-inch diameter disks were fabricated by various consolidation techniques. These include: dry pressing and sintering, slurry pressing and sintering, and slurry pressing and HIPing. The results are discussed. Author

N88-23882*# National Aeronautics and Space Administration. Lewis Research Center, Cleveland, OH.

IMPROVED PROCESSING OF Si₃N₄

WILLIAM A. SANDERS and GEORGE Y. BAAKLINI (Cleveland State Univ., Ohio.) *In its Structural Ceramics* p 119-127 May 1986

Avail: NTIS HC A11/MF A01 CSCL 11C

A sintered Si₃N₄-SiO₂-Y₂O₃ composition, NASA 6Y, was developed that reached four-point flexural average strength/standard deviation values of 857/36, 544/33, and 462/59 MPa at room temperature, 1200, and 1370 C, respectively. These strengths represented improvements of 56, 38, and 21 percent over baseline properties at the three test temperatures. At room temperature the standard deviation was reduced by more than a factor of three. These accomplishments were realized by the iterative utilization of conventional X-radiography to characterize structural (density) uniformity as affected by systematic changes in powder processing and sintering parameters. Accompanying the improvement in mechanical properties was a change in the type of flaw causing failure from a pore to a large columnar beta-Si₃N₄ grain typically 40 to 80 microns, 10 to 30 microns wide, and with an aspect ratio of 5:1. Author

N88-23883*# Case Western Reserve Univ., Cleveland, OH.

COLLOIDAL CHARACTERIZATION OF SILICON NITRIDE AND SILICON CARBIDE

DONALD L. FEKE *In NASA, Lewis Research Center, Structural Ceramics* p 129-138 May 1986
 (Contract NAG3-468)

Avail: NTIS HC A11/MF A01 CSCL 11C

The colloidal behavior of aqueous ceramic slips strongly affects the forming and sintering behavior and the ultimate mechanical strength of the final ceramic product. The colloidal behavior of these materials, which is dominated by electrical interactions between the particles, is complex due to the strong interaction of the solids with the processing fluids. A surface titration methodology, modified to account for this interaction, was developed and used to provide fundamental insights into the

interfacial chemistry of these systems. Various powder pretreatment strategies were explored to differentiate between true surface chemistry and artifacts due to exposure history. The colloidal behavior of both silicon nitride and carbide is dominated by silanol groups on the powder surfaces. However, the colloid chemistry of silicon nitride is apparently influenced by an additional amine group. With the proper powder treatments, silicon nitride and carbide powder can be made to appear colloiddally equivalent. The impact of these results on processing control will be discussed. Author

N88-23885*# National Aeronautics and Space Administration. Lewis Research Center, Cleveland, OH.

MOLTEN SALT CORROSION OF SiC AND Si₃N₄

N. S. JACOBSON, J. L. SMIALEK, and D. S. FOX *In its Structural Ceramics* p 147-162 May 1986

Avail: NTIS HC A11/MF A01 CSCL 11C

The most severe type of corrosion encountered in heat engines is corrosion by molten sodium sulfate, formed by the reaction of ingested sodium chloride and sulfur impurities in the fuel. This problem was studied extensively for superalloys, but only recently examined for ceramics. This problem is addressed with laboratory studies to understand the fundamental reaction mechanisms and with burner studies to provide a more realistic simulation of the conditions encountered in a heat engine. In addition the effect of corrosion on the strengths of these materials was assessed. Each of these aspects will be reviewed and some ideas toward possible solutions will be discussed. Author

N88-23891*# National Aeronautics and Space Administration. Lewis Research Center, Cleveland, OH.

SiC FIBER ANALYSIS

MARTHA H. JASKOWIAK *In its Structural Ceramics* p 203-212 May 1986

Avail: NTIS HC A11/MF A01 CSCL 11C

Polymer derived Nicalon SiC fibers are known to be thermally unstable at temperatures beyond 1200 C. In an effort to further understand the mechanisms of fiber degradation, Nicalon fibers were heat treated at temperatures up to 2200 C and argon gas pressures varying from 0 to 1360 atm. The effects of gas pressure on the thermal stability of the fibers were determined through property comparisons between the pressure-treated fibers and vacuum-treated fibers. Investigation of the thermal stability included studies of the fiber microstructure and mechanical and physical properties before and after treatments. Author

N88-26482*# National Aeronautics and Space Administration. Lewis Research Center, Cleveland, OH.

FRACTURE RESISTANCE OF A TiB₂ PARTICLE/SiC MATRIX COMPOSITE AT ELEVATED TEMPERATURE

MICHAEL G. JENKINS, JONATHAN A. SALEM, and SRINIVASA G. SESHADRI Jun. 1988 18 p

(NASA-TM-100967; E-3842-1; NAS 1.15:100967) Avail: NTIS HC A03/MF A01 CSCL 11C

The fracture resistance of a commercial TiB₂ particle/SiC matrix composite was evaluated at temperatures ranging from 20 to 1400 C. A laser interferometric strain gauge (LISG) was used to continuously monitor the crack mouth opening displacement (CMOD) of the chevron-notched and straight-notched, three-point bend specimens used. Crack growth resistance curves (R-curves) were determined from the load versus displacement curves and displacement calibrations. Fracture toughness, work-of-fracture, and R-curve levels were found to decrease with increasing temperature. Microstructure, fracture surface, and oxidation coat were examined to explain the fracture behavior. Author

N88-28142*# Garrett Turbine Engine Co., Phoenix, AZ.

THERMAL BARRIER COATING LIFE-PREDICTION MODEL DEVELOPMENT Annual Report No. 2

T. E. STRANGMAN, J. NEUMANN, and A. LIU 20 Oct. 1986 91 p

(Contract NAS3-23945)

(NASA-CR-179507; GTEC-21-5988; NAS 1.26:179507) Avail: NTIS HC A05/MF A01 CSCL 11C

27 NONMETALLIC MATERIALS

The program focuses on predicting the lives of two types of strain-tolerant and oxidation-resistant thermal barrier coating (TBC) systems that are produced by commercial coating suppliers to the gas turbine industry. The plasma-sprayed TBC system, composed of a low-pressure plasma-spray (LPPS) or an argon shrouded plasma-spray (ASPS) applied oxidation resistant NiCrAlY or (CoNiCrAlY) bond coating and an air-plasma-sprayed yttria partially stabilized zirconia insulative layer, is applied by both Chromalloy, Klock, and Union Carbide. The second type of TBC is applied by the electron beam-physical vapor deposition (EB-PVD) process by Temescal. The second year of the program was focused on specimen procurement, TMC system characterization, non-destructive evaluation methods, life prediction model development, and TFE731 engine testing of thermal barrier coated blades. Materials testing is approaching completion. Thermomechanical characterization of the TBC systems, with toughness, and spalling strain tests, was completed. Thermochemical testing is approximately two-thirds complete. Preliminary materials life models for the bond coating oxidation and zirconia sintering failure modes were developed. Integration of these life models with airfoil component analysis methods is in progress. Testing of high pressure turbine blades coated with the program TBC systems is in progress in a TFE731 turbofan engine. Eddy current technology feasibility was established with respect to nondestructively measuring zirconia layer thickness of a TBC system. Author

N88-28151*# Case Western Reserve Univ., Cleveland, OH.
DIAMOND LIKE CARBON COATINGS: CATEGORIZATION BY ATOMIC NUMBER DENSITY Final Report, 21 Dec. 1983 - 20 Dec. 1984

JOHN C. ANGUS 10 Nov. 1986 26 p
(Contract NAG3-505)
(NASA-CR-174895; NAS 1.26:174895) Avail: NTIS HC A03/MF A01 CSCL 11C

Dense diamond-like hydrocarbon films grown at the NASA Lewis Research Center by radio frequency self bias discharge and by direct ion beam deposition were studied. A new method for categorizing hydrocarbons based on their atomic number density and elemental composition was developed and applied to the diamond-like hydrocarbon films. It was shown that the diamond-like hydrocarbon films are an entirely new class of hydrocarbons with atomic number densities lying between those of single crystal diamond and adamantanes. In addition, a major review article on these new materials was completed in cooperation with NASA Lewis Research Center personnel. Author

N88-29984*# National Aeronautics and Space Administration. Lewis Research Center, Cleveland, OH.

NOVEL LADDER POLYMERS FOR USE AS HIGH TEMPERATURE STABLE RESINS OR COATINGS Patent Application

MARY ANN MEADOR, inventor (to NASA) 11 Aug. 1988 21 p
(NASA-CASE-LEW-14203-1; NAS 1.71:LEW-14203-1; US-PATENT-APPL-SN-231026) Avail: NTIS HC A03/MF A01 CSCL 11C

An object of the invention is to synthesize a new class of ladder and partial ladder polymers. In accordance with the invention, the new class of ladder and partial ladder polymers are synthesized by polymerizing a bis-dienophile with a bis-diene. Another object of the invention is to provide a fabricated, electrically conducting, void free composite comprising the new class of the ladder and partial ladder polymers described above. The novelty of the invention relates to a new class of ladder and partial ladder polymers and a process for synthesizing these polymers. These polymers are soluble in common organic solvents and are characterized with a unique dehydration property at temperatures of 300 to 400 C to provide thermo-oxidatively stable pentiptycene units along the polymeric backbone. These polymers are further characterized with high softening points and good thermo-oxidative stability properties. Thus these polymers have potential as processable, matrix resins for high temperature composite applications. NASA

28

PROPELLANTS AND FUELS

Includes rocket propellants, igniters, and oxidizers; their storage and handling procedures; and aircraft fuels.

A88-27720*# Pennsylvania State Univ., University Park.
VELOCITY-COUPLED FLOW OSCILLATIONS IN A SIMULATED SOLID-PROPELLANT ROCKET ENVIRONMENT

VIGOR YANG (Pennsylvania State University, University Park), KWANG-CHUNG HSIEH (NASA, Lewis Research Center; Sverdrup Technology, Inc., Cleveland, OH), and JESSE I. S. TSENG AIAA, Aerospace Sciences Meeting, 26th, Reno, NV, Jan. 11-14, 1988. 12 p. refs
(Contract F04611-86-K-0082)
(AIAA PAPER 88-0543)

A comprehensive numerical analysis has been carried out to study the unsteady flowfields in a simulated rocket-motor environment. The model is based on the time-dependent compressible Navier-Stokes equations with a two-equation turbulence closure scheme. Various important aspects of the coupling between acoustic oscillations and mean flowfields, including flow reversal, modification of transport properties, etc., are addressed. Results indicate that multi-dimensional effects play important roles in determining local flow structures and wave characteristics. In much of the domain, acoustic velocity nodal points are observed in the near-wall region. The classical one-dimensional theory fails to describe several important mechanisms associated with velocity-induced flow instabilities. Author

A88-27721*# National Aeronautics and Space Administration. Lewis Research Center, Cleveland, OH.

NUMERICAL STUDY OF MULTICOMPONENT DROPLET VAPORIZATION AT NEAR CRITICAL CONDITIONS

KWANG-CHUNG HSIEH, JIAN-SHUN SHUEN (NASA, Lewis Research Center; Sverdrup Technology, Inc., Cleveland, OH), and VIGOR YANG (Pennsylvania State University, University Park) AIAA, Aerospace Sciences Meeting, 26th, Reno, NV, Jan. 11-14, 1988. 9 p. refs
(AIAA PAPER 88-0637)

A comprehensive numerical analysis of multicomponent droplet vaporization at near critical conditions has been carried out. The model is based on the full time-dependent conservation equations and accommodates various important high-pressure phenomena. As an example, the case involving a two-component (n-pentane and n-octane) fuel droplet in nitrogen gas is studied. The influences of transient effects, surface regression, ambient gas solubility, and phase-equilibrium relations on vaporization mechanisms are examined in detail. Author

A88-44268* Drexel Univ., Philadelphia, PA.

MODIFIED REACTION MECHANISM OF AERATED N-DODECANE LIQUID FLOWING OVER HEATED METAL TUBES

K. T. REDDY, N. P. CERNANSKY (Drexel University, Philadelphia, PA), and R. S. COHEN (Temple University, Philadelphia, PA) Journal of Energy and Fuels (ISSN 0887-0624), vol. 2, no. 2, 1988, p. 205-213. Research supported by Drexel University. refs
(Contract NAG3-183)

The degradation mechanism of the n-dodecane was studied using a modified jet fuel thermal oxidation tester containing a sample withdrawal system as a reaction vessel. The reaction products were identified using gas chromatography and mass spectrometry. The soluble products were found to consist mainly of C5-C10 n-alkanes and 1-alkenes, C7-C10 aldehydes, tetrahydrofuran derivatives, dodecanol and dodecanone isomers, dodecyl hydroperoxide (ROOH) decomposition products, and C24 alkane isomers. The data from the experiments agreed with those of Hazlett et al. (1977). It was found that alkyl peroxide radical

reactions dominate in the autooxidation temperature regime (at T not above 300 C); the dominant path is for the alkyl peroxy radical to react bimolecularly with fuel to yield primarily alkyl hydroperoxides. The alkyl peroxide radical also undergoes self-termination and unimolecular isomerization and decomposition reactions, to yield smaller amounts of C12 alcohol plus ketone products and tetrahydrofuran derivatives, respectively. I.S.

A88-48751* # National Aeronautics and Space Administration. Lewis Research Center, Cleveland, OH.

CHARACTERIZATION OF ALUMINUM/RP-1 GEL PROPELLANT PROPERTIES

DOUGLAS C. RAPP (NASA, Lewis Research Center; Sverdrup Technology, Inc., Cleveland, OH) and ROBERT L. ZURAWSKI (NASA, Lewis Research Center, Cleveland, OH) AIAA, ASME, SAE, and ASEE, Joint Propulsion Conference, 24th, Boston, MA, July 11-13, 1988. 22 p. Previously announced in STAR as N88-24808. refs (AIAA PAPER 88-2821)

Research efforts are being conducted by the NASA Lewis Research Center to formulate and characterize the properties of Al/RP-1 and RP-1 gelled propellants for rocket propulsion systems. Twenty four different compositions of gelled fuels were formulated with 5 and 16 micron, atomized aluminum powder in RP-1. The total solids concentration in the propellant varied from 5 to 60 wt percent. Tests were conducted to evaluate the stability and rheological characteristics of the fuels. Physical separation of the solids occurred in fuels with less than 50 wt percent solids concentration. The rheological characteristics of the Al/RP-1 fuels varied with solids concentration. Both thixotropic and rheopectic gel behavior were observed. The unmetallized RP-1 gels, which were formulated by a different technique than the Al/RP-1 gels, were highly viscoelastic. A history of research efforts which were conducted to formulate and characterize the properties of metallized propellants for various applications is also given.

Author

A88-48764* # National Aeronautics and Space Administration. Lewis Research Center, Cleveland, OH.

CATALYTIC IGNITION OF HYDROGEN AND OXYGEN PROPELLANTS

ROBERT L. ZURAWSKI (NASA, Lewis Research Center, Cleveland, OH) and JAMES M. GREEN (NASA, Lewis Research Center; Sverdrup Technology, Inc., Cleveland, OH) AIAA, ASME, SAE, and ASEE, Joint Propulsion Conference, 24th, Boston, MA, July 11-13, 1988. 19 p. Previously announced in STAR as N88-24689. refs (AIAA PAPER 88-3300)

An experimental program was conducted to evaluate the catalytic ignition of gaseous hydrogen and oxygen propellants. Shell 405 granular catalyst and a monolithic sponge catalyst were tested. Mixture ratio, mass flow rate, propellant temperature, and back pressure were varied parametrically in testing to determine the operational limits of the catalytic igniter. The test results show that the gaseous hydrogen and oxygen propellant combination can be ignited catalytically using Shell 405 catalyst over a wide range of mixture ratios, mass flow rates, and propellant injection temperatures. These operating conditions must be optimized to ensure reliable ignition for an extended period of time. A cyclic life of nearly 2000, 2 sec pulses at nominal operating conditions was demonstrated with the catalytic igniter. The results of the experimental program and the established operational limits for a catalytic igniter using the Shell 405 catalysts are presented.

Author

N88-15940* # Washington Univ., Saint Louis, MO.

COMPUTATIONAL PREDICTION OF PROPELLANT REORIENTATION

JOHN I. HOCHSTEIN /in NASA, Lewis Research Center, Cleveland, Ohio. Cryogenic Fluid Management Technology Workshop. Volume 1: Presentation Material and Discussion p 317-344 Sep. 1987

(Contract NAG3-578)

Avail: NTIS HC A17/MF A01 CSCL 211

Viewgraphs from a presentation on computational prediction of propellant reorientation are given. Information is given on code verification, test conditions, predictions for a one-quarter scale cryogenic tank, pulsed settling, and preliminary results. R.J.F.

N88-24808* # National Aeronautics and Space Administration. Lewis Research Center, Cleveland, OH.

CHARACTERIZATION OF ALUMINUM/RP-1 GEL PROPELLANT PROPERTIES

DOUGLAS C. RAPP (Sverdrup Technology, Inc., Cleveland, Ohio.) and ROBERT L. ZURAWSKI 1988 23 p Presented at the 24th Joint Propulsion Conference, Boston, Mass., 11-13 Jul. 1988; sponsored by AIAA, ASME, SAE and ASEE (NASA-TM-100951; E-4242; NAS 1.15:100951; AIAA-88-2821) Avail: NTIS HC A03/MF A01 CSCL 211

Research efforts are being conducted by the NASA Lewis Research Center to formulate and characterize the properties of Al/RP-1 and RP-1 gelled propellants for rocket propulsion systems. Twenty four different compositions of gelled fuels were formulated with 5 and 16 micron, atomized aluminum powder in RP-1. The total solids concentration in the propellant varied from 5 to 60 wt percent. Tests were conducted to evaluate the stability and rheological characteristics of the fuels. Physical separation of the solids occurred in fuels with less than 50 wt percent solids concentration. The rheological characteristics of the Al/RP-1 fuels varied with solids concentration. Both thixotropic and rheopectic gel behavior were observed. The unmetallized RP-1 gels, which were formulated by a different technique than the Al/RP-1 gels, were highly viscoelastic. A history of research efforts which were conducted to formulate and characterize the properties of metallized propellants for various applications is also given.

Author

29

MATERIALS PROCESSING

Includes space-based development of products and processes for commercial applications.

A88-13163* National Aeronautics and Space Administration. Lewis Research Center, Cleveland, OH.

SIMULATION OF FLUID FLOWS DURING GROWTH OF ORGANIC CRYSTALS IN MICROGRAVITY

GARY D. ROBERTS, JAMES K. SUTTER, R. BALASUBRAMANIAM (NASA, Lewis Research Center, Cleveland, OH), WILLIAM FOWLIS (NASA, Marshall Space Flight Center, Huntsville, AL), M. D. RADCLIFFE (3M Co., Saint Paul, MN) et al. IN: Advanced materials technology '87; Proceedings of the Thirty-second International SAMPE Symposium and Exhibition, Anaheim, CA, Apr. 6-9, 1987. Covina, CA, Society for the Advancement of Material and Process Engineering, 1987, p. 497-505. refs

The improvements in crystal size and quality obtained in counterdiffusion-type crystal growth experiments in space are sometimes attributed to the reduction of natural convection in microgravity. Attention is presently given to the results of both the Space Shuttle-conducted and terrestrial versions of the Diffusive Mixing of Organic Solution experiments. Extensive mixing by natural convection is noted to occur even under microgravity conditions, in keeping with the results of a simple scaling analysis. O.C.

A88-13164* National Aeronautics and Space Administration. Lewis Research Center, Cleveland, OH.

RESEARCH OPPORTUNITIES IN MICROGRAVITY SCIENCE AND APPLICATIONS DURING SHUTTLE HIATUS

BRUCE N. ROSENTHAL, THOMAS GLASGOW (NASA, Lewis Research Center, Cleveland, OH), RICHARD E. BLACK (NASA, Marshall Space Flight Center, Huntsville, AL), and DANIEL E.

29 MATERIALS PROCESSING

ELLEMAN (California Institute of Technology, Jet Propulsion Laboratory, Pasadena) IN: Advanced materials technology '87; Proceedings of the Thirty-second International SAMPE Symposium and Exhibition, Anaheim, CA, Apr. 6-9, 1987. Covina, CA, Society for the Advancement of Material and Process Engineering, 1987, p. 506-516. Previously announced in STAR as N87-16917. refs

The opportunity to conduct microgravity and related research still exists, even with the temporary delay in the U.S. Space Shuttle program. Several ground-based facilities are available, and use of these facilities is highly recommended for the preparation of near and far term Shuttle or Space Station experiments. Drop tubes, drop towers, aircraft, sounding rockets, and a wide variety of other ground-based equipment can be used to simulate microgravity. This paper concentrates on the materials processing capabilities available at NASA Lewis Research Center (NASA Lewis), Marshall Space Flight Center (MSFC), and the California Institute of Technology Jet Propulsion Laboratory (JPL). Also included is information on gaining access to these facilities. Author

A88-22186*# Rensselaer Polytechnic Inst., Troy, NY.
DENDRITIC SOLIDIFICATION UNDER MICROGRAVITY CONDITIONS

M. E. GLICKSMAN, R. C. HAHN, T. A. LOGRASSO, S. TIRMIZI (Rensselaer Polytechnic Institute, Troy, NY), E. WINSA (NASA, Lewis Research Center, Cleveland, OH) et al. AIAA, Aerospace Sciences Meeting, 26th, Reno, NV, Jan. 11-14, 1988. 7 p. refs (Contract NAG3-333)

(AIAA PAPER 88-0248)

The Isothermal Dendritic Growth Experiment is undergoing development in cooperation with NASA-Lewis in order to test dendritic growth theory at small supercoolings in low earth orbit. The apparatus encompasses four major subsystems: a temperature-controlled thermostatic bath capable of millikelvin stability, a photographic data collection system, a crystal-growth chamber, and a start-detection system which initiates data collection. Comparisons are made with ground-based study methods for dendritic growth. O.C.

A88-28554* Wisconsin Univ., Madison.

CONTAINERLESS PROCESSING OF UNDERCOOLED MELTS

D. S. SHONG, J. A. GRAVES, Y. UJIE, and J. H. PEREPEZKO (Wisconsin, University, Madison) IN: Materials processing in the reduced gravity environment of space; Proceedings of the Symposium, Boston, MA, Dec. 1-3, 1986. Pittsburgh, PA, Materials Research Society, 1987, p. 17-27. refs (Contract NAG3-436)

Containerless drop tube processing allows for significant levels of liquid undercooling through control of parameters such as sample size, surface coating and cooling rate. A laboratory scale (3 m) drop tube has been developed which allows the undercooling and solidification behavior of powder samples to be evaluated under low gravity free-fall conditions. The level of undercooling obtained in an InSb-Sb eutectic alloy has been evaluated by comparing the eutectic spacing in drop tube samples with a spacing/undercooling relationship established using thermal analysis techniques. Undercoolings of 0.17 and 0.23 T(e) were produced by processing under vacuum and He gas conditions respectively. Alternatively, the formation of an amorphous phase in a Ni-Nb eutectic alloy indicates that undercooling levels of approximately 500 C were obtained by drop tube processing. The influence of droplet size and gas environment on undercooling behavior in the Ni-Nb eutectic was evaluated through their effect on the amorphous/crystalline phase ratio. To supplement the structural analysis, heat flow modeling has been developed to describe the undercooling history during drop tube processing, and the model has been tested experimentally. Author

A88-28556* Rensselaer Polytechnic Inst., Troy, NY.
ISOTHERMAL DENDRITIC GROWTH - A LOW GRAVITY EXPERIMENT

M. E. GLICKSMAN, R. C. HAHN, T. A. LOGRASSO, E. R. RUBINSTEIN (Rensselaer Polytechnic Institute, Troy, NY), and E. WINSA (NASA, Lewis Research center, Cleveland, OH) IN:

Materials processing in the reduced gravity environment of space; Proceedings of the Symposium, Boston, MA, Dec. 1-3, 1986. Pittsburgh, PA, Materials Research Society, 1987, p. 37-46. refs (Contract NAG3-333)

The Isothermal Dendritic Growth Experiment has been designed to test dendritic growth theory at low undercoolings, under microgravity conditions in the Space Shuttle Cargo Bay-borne Material Science Laboratory. The experiment will be essentially autonomous, although limited in-flight interaction through a computer interface is planned. A crystal growth chamber able to yield oriented single-crystal dendritic growth will be incorporated; 'seeding' the chamber with a crystal of the requisite orientation will not in itself meet this requirement. O.C.

A88-28557* Massachusetts Inst. of Tech., Cambridge.
SOLIDIFICATION OF UNDERCOOLED NI-SN EUTECTIC ALLOY UNDER MICROGRAVITY CONDITIONS IN THE SPACE SHUTTLE

T. J. PICCONE, Y. WU, Y. SHIOHARA, M. C. FLEMINGS (MIT, Cambridge, MA), F. H. HART, and E. A. WINSA (NASA, Lewis Research Center, Cleveland, OH) IN: Materials processing in the reduced gravity environment of space; Proceedings of the Symposium, Boston, MA, Dec. 1-3, 1986. Pittsburgh, PA, Materials Research Society, 1987, p. 47-56. refs (Contract NSG-7645; NAG3-597; NAS3-24383; NAS3-24875)

The Space Shuttle Columbia carried an Alloy Undercooling Experiment on its STS 61-C mission in January, 1986. The experiment was performed in an electromagnetic levitator. A sample of Ni-32.5 wt pct Sn eutectic was melted and solidified under microgravity conditions in the Space Shuttle. The specimen achieved only a fairly small undercooling, probably less than 30 K. The specimen was examined by optical and scanning electron microscopy. The surface and cross-sectional microstructures were primarily composed of normal lamellar eutectic, but showed several interesting features, including an apparent surface nucleation site, curved dendrites with nonorthogonal secondary arms, dendrite fragments with extremely fine arm spacing, submicron precipitates, and faceted crystals. The results of the space experiment are presented and compared with ground-based results obtained with the same alloy. Author

A88-28564* Los Alamos National Lab., NM.
CHARACTERISTICS OF FLUID FLOW IN THE COMBUSTION SYNTHESIS OF TiC FROM THE ELEMENTS

S. M. VALONE and R. G. BEHRENS (Los Alamos National Laboratory, NM) IN: Materials processing in the reduced gravity environment of space; Proceedings of the Symposium, Boston, MA, Dec. 1-3, 1986. Pittsburgh, PA, Materials Research Society, 1987, p. 113-120. refs (Contract NASA ORDER C-80011-F)

The results of a numerical investigation of finite reservoir effects on capillary spreading at small reservoir dimensions are presently related to wave propagation phenomena in the combustion synthesis of TiC from its two elemental constituents. It is noted that gravitational forces can affect bubble coalescence by nonbuoyant means under the suitable conditions, although these conditions are expected to be rare in combustion synthesis. Finite-curved reservoirs can drive capillary flow due to surface tension and wall contact forces; these cause the wall and the metal to be completely reconfigured during combustion synthesis. O.C.

A88-35130* Rensselaer Polytechnic Inst., Troy, NY.
SOLIDIFICATION UNDER MICROGRAVITY CONDITIONS - DENDRITIC GROWTH

M. E. GLICKSMAN, R. C. HAHN, T. A. LOGRASSO, E. R. RUBINSTEIN (Rensselaer Polytechnic Institute, Troy, NY), E. WINSA (NASA, Lewis Research Center, Cleveland, OH) et al. IN: Aerospace century XXI: Space sciences, applications, and commercial developments; Proceedings of the Thirty-third Annual AAS International Conference, Boulder, CO, Oct. 26-29, 1986. San Diego, CA, Univelt, Inc., 1987, p. 1259-1273. refs

(Contract NAG3-33)
(AAS PAPER 86-380)

The experimental approach and apparatus of a zero-gravity active crystal growth experiment to test dendritic growth theory at low supercoolings are discussed. The experiment consists of 20 experimental cycles. Estimates have been made as to how low gravitational accelerations would have to be reduced to observe convection-free dendritic growth at supercoolings from 0.01-1.0 K. The experiment requires temperature control of \pm or \pm 2 mK and photographic resolution of a few microns with a depth of field of \pm or \pm 6 mm. The thermostatic bath and temperature control system, photographic system, growth chamber, and dendrite detection system are described in detail. R.R.

A88-37155* Rensselaer Polytechnic Inst., Troy, NY.
GRAVITATIONAL CONTRIBUTIONS TO MICROSTRUCTURAL COARSENING IN LIQUID PHASE SINTERING
C. M. KIPPHUT, T. KISHI, A. BOSE, and R. M. GERMAN (Rensselaer Polytechnic Institute, Troy, NY) IN: 1987 Annual Powder Metallurgy Conference, Dallas, TX, May 17-20, 1987, Proceedings. Princeton, NJ, Metal Powder Industries Federation, 1987, p. 93-106. refs
(Contract NAG3-744)

Preliminary experiments for determining the role of gravity in liquid phase sintering have been carried out. Tungsten heavy alloys were selected for this investigation because of the large density difference between solid and liquid, extensive interest in the alloys and considerable data on these alloys. By identifying and isolating the role that gravity plays in shape distortion and microstructural coarsening, further insight into the mechanisms of coarsening kinetics may be realized. Improvements in mechanical properties, shape complexity, and dimensional stability may be realized in the future from low gravity sintering. Author

A88-37715* Princeton Univ., NJ.
GROWTH OF NEEDLE-SHAPED CRYSTALS IN THE PRESENCE OF CONVECTION
D. A. SAVILLE and P. J. BEAGHTON (Princeton University, NJ) Physical Review A - General Physics, 3rd Series (ISSN 0556-2791), vol. 37, May 1, 1988, p. 3423-3430. refs
(Contract NAG3-447)

The motion of the freezing front between a needle-shaped crystal and a supercooled liquid is analyzed for situations where there is forced convection aligned with the crystal axis. It is shown that in the absence of capillary effects the shape of the crystal-melt interface is a paraboloid of revolution, similar to that found in situations where diffusion is the sole heat-transfer mechanism. A relation between the supercooling, the product of tip velocity and tip radius, and the strength of the flow is derived which reduces to the well-known Ivantsov theory in the absence of convection. Author

A88-41211* Case Western Reserve Univ., Cleveland, OH.
GRAVITATIONAL MACROSEGREGATION IN BINARY PB-SN ALLOY INGOTS
V. LAXMANAN, A. STUDER, L. WANG, J. F. WALLACE (Case Western Reserve University, Cleveland, OH), and E. A. WINSA (NASA, Lewis Research Center, Cleveland, OH) IN: Low-gravity sciences. San Diego, CA, Univelt, Inc., 1987, p. 119-148. Previously announced in STAR as N87-24579. refs

A space shuttle experiment employing the General Purpose (Rocket) Furnace (GPF) in its isothermal mode of operation is manifested on MSL-3, circa 1989. The central aim of this experiment is to investigate the effect of reduced gravity levels on the segregation behavior in a slowly, and isothermally, cooled sample of a binary Pb-15 wt pct Sn alloy. This experiment should be able to simulate, in a small laboratory sample, some aspects of the segregation phenomena occurring in large industrial ingots. Ground-based experiments conducted in the single-cavity simulator of the GPF, in support of the microgravity experiment are described in detail. The results of the MSFC experiments are compared with other related experiments conducted at Case Western Reserve University (CWRU), wherein the isothermal constraints were

relaxed. The isothermally processed samples indicate a small and gradual increase in fraction eutectic, and a corresponding increase in tin content, from the bottom to the top of the ingot. The radial variations are minimal near the ingot bottom, but there are large radial variations in the top half. In the CWRU experiments, more severe segregations, including segregation defects known as freckles. Follow up experiments employing the GPF without the isothermal constraints, or other suitably modified space shuttle hardware are suggested. Author

A88-42908* National Aeronautics and Space Administration. Lewis Research Center, Cleveland, OH.

PREPARATION FOR MICROGRAVITY - THE ROLE OF THE MICROGRAVITY MATERIAL SCIENCE LABORATORY
J. CHRISTOPHER JOHNSTON, BRUCE N. ROSENTHAL, MARYJO B. MEYER, and THOMAS K. GLASGOW (NASA, Lewis Research Center, Cleveland, OH) AIAA, Space Programs and Technologies Conference, Houston, TX, June 21-24, 1988. 5 p. refs
(AIAA PAPER 88-3510)

Experiments at the NASA Lewis Research Center's Microgravity Material Science Laboratory using physical and mathematical models to delineate the effects of gravity on processes of scientific and commercial interest are discussed. Where possible, transparent model systems are used to visually track convection, settling, crystal growth, phase separation, agglomeration, vapor transport, diffusive flow, and polymer reactions. Materials studied include metals, alloys, salts, glasses, ceramics, and polymers. Specific technologies discussed include the General Purpose furnace used in the study of metals and crystal growth, the isothermal dendrite growth apparatus, the electromagnetic levitator/instrumented drop tube, the high temperature directional solidification furnace, the ceramics and polymer laboratories and the center's computing facilities. R.B.

A88-43170* Westinghouse Research and Development Center, Pittsburgh, PA.
CHARACTERIZATION OF DIRECTIONALLY SOLIDIFIED LEAD CHLORIDE

NARSINGH BAHADUR SINGH (Westinghouse Research and Development Center, Pittsburgh, PA), W. M. B. DUVAL, and B. N. ROSENTHAL (NASA, Lewis Research Center, Cleveland, OH) Journal of Crystal Growth (ISSN 0022-0248), vol. 89, no. 1, June 1988, p. 80-85. refs

A directionally solidified PbCl₂ material was prepared and analyzed and subsequently used to grow single crystals. It was found that silicon, halogens, sulfur, magnesium, and phosphorus were the hardest impurities to remove by the single-pass directional freezing. Single crystals grown from the purified material displayed good scattering beam quality and showed no absorption peaks between 0.30 to 20 microns. Direct photographic observations of the solid-liquid interface at several G/V (denoting the temperature gradient and the translation velocity, respectively) ratio values showed that, as the G/V ratio decreased, the interface varied from a smooth convex surface to dendritic. I.S.

A88-43172* Rensselaer Polytechnic Inst., Troy, NY.
PREPARATION OF MULTISTAGE ZONE-REFINED MATERIALS FOR THERMOCHEMICAL STANDARDS

E. RUBINSTEIN, M. E. GLICKSMAN (Rensselaer Polytechnic Institute, Troy, NY), B. W. MANGUM (NBS, Center for Absolute Physical Quantities, Gaithersburg, MD), Q. T. FANG (Alcoa Technical Center, Alcoa Center, PA), and N. B. SINGH (Westinghouse Research and Development Center, Pittsburgh, PA) Journal of Crystal Growth (ISSN 0022-0248), vol. 89, no. 1, June 1988, p. 101-110. refs
(Contract NAG3-333)

This paper describes the steps of a two-step zone purification procedure for completed minicells filled with ultrahigh-purity succinonitrile (SCN) in which the CNS is under its own vapor pressure. The solid-liquid equilibrium, as determined by melting and freezing point measurements, is therefore considered to be a realization of the triple-point. The freezing-point plateaus measured at a variety of bath temperatures demonstrated both the

29 MATERIALS PROCESSING

fundamental reproducibility of the measurement for a given sample and the lack of dependence of that measurement on the bath temperature which controls the freezing rate. The measurement reproducibility and the sample consistency indicate that the method described is indeed suitable for the preparation of pure material which can be used for the purposes of thermistor and thermometer calibration at 58.0796 + or - 0.0015 C. I.S.

A88-49085*# National Aeronautics and Space Administration. Lewis Research Center, Cleveland, OH.

CONTAINMENT OF A SILICONE FLUID FREE SURFACE IN REDUCED GRAVITY

A. PLINE and T. JACOBSON (NASA, Lewis Research Center, Cleveland, OH) Metallurgical Transactions A - Physical Metallurgy and Materials Science (ISSN 0360-2133), vol. 19A, Aug. 1988, p. 1883-1888. refs

In support of the surface tension driven convection experiment planned for flight aboard the Space Shuttle, tests were conducted under reduced gravity in the 2.2-sec drop tower and the 5.0-sec Zero-G facility at the Lewis Research Center. The dynamics of controlling the test fluid, a 10-centistoke viscosity silicone fluid, in a low-gravity environment were investigated using different container designs and barrier coatings. Three container edge designs were tested without a barrier coating: a square edge, a sharp edge with a 45-deg slope, and a saw-tooth edge. All three edge designs were successful in containing the fluid below the edge. Author

A88-49089* Rensselaer Polytechnic Inst., Troy, NY.
GRAVITY AND CONFIGURATIONAL ENERGY INDUCED MICROSTRUCTURAL CHANGES IN LIQUID PHASE SINTERING

C. M. KIPPHUT, A. BOSE, S. FAROOQ, and R. M. GERMAN (Rensselaer Polytechnic Institute, Troy, NY) Metallurgical Transactions A - Physical Metallurgy and Materials Science (ISSN 0360-2133), vol. 19A, Aug. 1988, p. 1905-1913. Army-supported research. refs
(Contract NAG3-744)

Experiments were performed with W-Ni-Fe heavy alloys in order to measure the microstructural changes vs. position that occur in liquid-phase sintering under normal gravity. The experimentally observed segregation is less than the calculated equilibrium segregation due to the retarding effect from the rigid solid skeleton formed during sintering. These results improve understanding of microstructure, mechanical properties, component shape, and dimensional stability benefits that may be realized from low-gravity sintering. Author

A88-49090*# National Aeronautics and Space Administration. Lewis Research Center, Cleveland, OH.

GROUND-BASED MICROGRAVITY MATERIALS SCIENCE RESEARCH AT NASA'S MICROGRAVITY MATERIALS SCIENCE LABORATORY

BRUCE N. ROSENTHAL (NASA, Lewis Research Center, Cleveland, OH) Metallurgical Transactions A - Physical Metallurgy and Materials Science (ISSN 0360-2133), vol. 19A, Aug. 1988, p. 1915-1917.

A88-49093*# National Aeronautics and Space Administration. Lewis Research Center, Cleveland, OH.

MIXING FUEL PARTICLES FOR SPACE COMBUSTION RESEARCH USING ACOUSTICS

ROBERT J. BURNS, JEROME A. JOHNSON, and ROBERT B. KLIMEK (NASA, Lewis Research Center, Cleveland, OH) Metallurgical Transactions A - Physical Metallurgy and Materials Science (ISSN 0360-2133), vol. 19A, Aug. 1988, p. 1931-1937. Previously announced in STAR as N88-21186.

Part of the microgravity science to be conducted aboard the Shuttle (STS) involves combustion using solids, particles, and liquid droplets. The central experimental facts needed for characterization of premixed quiescent particle cloud flames cannot be adequately established by normal gravity studies alone. The experimental results to date of acoustically mixing a prototypical particulate,

lycopodium, in a 5 cm diameter by 75 cm long flame tube aboard a Learjet aircraft flying a 20-sec low-gravity trajectory are described. Photographic and light detector instrumentation combine to measure and characterize particle cloud uniformity. Author

A88-49095* Rensselaer Polytechnic Inst., Troy, NY.
ISOTHERMAL DENDRITIC GROWTH - A PROPOSED MICROGRAVITY EXPERIMENT

M. E. GLICKSMAN, R. C. HAHN, T. A. LOGRASSO, S. H. TIRMIZI (Rensselaer Polytechnic Institute, Troy, NY), E. WINSA (NASA, Lewis Research Center, Cleveland, OH) et al. Metallurgical Transactions A - Physical Metallurgy and Materials Science (ISSN 0360-2133), vol. 19A, Aug. 1988, p. 1945-1953. refs
(Contract NAG3-333)

This paper describes an isothermal dendritic growth experiment (IDGE), a microgravity-oriented spaceborne scientific experiment designed to obtain 'convection-free' dendritic growth and thereby provide a test of dendritic growth theory. The apparatus includes a controlled thermostatic bath capable of providing + or - 2 mK stability, a photographic data collection system, a crystal growth chamber ensuring 'free' dendritic growth, and an optical RAM camera for crystal growth detection. The experiment will be carried on essentially automatically aboard the Materials Science Laboratory in the cargo bay of the Space Shuttle. The results of preliminary ground-based studies are presented. I.S.

N88-12528*# National Aeronautics and Space Administration. Lewis Research Center, Cleveland, OH.

MICROGRAVITY COMBUSTION FUNDAMENTALS

KURT R. SACKSTEDER *In its* Spacecraft Fire Safety p 89-94 1987

Avail: NTIS HC A07/MF A01 CSCL 22A

A brief summary of some of the important physical processes involved in low gravity combustion is given. While the discussion is generally limited to the processes involved in the combustion of continuous, solid, nonmetallic fuels, much of the reasoning presented can be applied to other fuel types and configurations. Author

N88-18739*# Texas Univ., Austin.
INVESTIGATION OF SURFACE TENSION DRIVEN CONVECTION AS A FEASIBILITY STUDY FOR A MICRO-GRAVITY EXPERIMENT Final Report

E. L. KOSCHMIEDER Mar. 1988 64 p

(Contract NAG3-393)

(NASA-CR-182504; NAS 1.26:182504) Avail: NTIS HC A04/MF A01 CSCL 22A

The work performed for the feasibility study of a microgravity surface tension driven convection experiment was reviewed. An experimental investigation of the onset of convection in shallow fluid layers heated uniformly from below and cooled from above by an air layer was made. Results are discussed in relation to the formation of Benard cells. The onset of Rayleigh-Benard convection in thin fluid layers heated uniformly from below were studied experimentally. It was found that in thin fluid layers the onset of Rayleigh-Benard convection is preceded by subcritical convective motions. Secondly, it was found that the onset of Rayleigh-Benard convection in non-Boussinesq fluid layers takes place in the form of hexagonal cells at Rayleigh numbers larger than the critical Rayleigh number $R_{sub C} = 1708$ which determines the onset of convection in Boussinesq fluid layers. B.G.

N88-23899*# Wisconsin Univ., Madison. Dept. of Metallurgical and Mineral Engineering.

NONCONTACT TEMPERATURE MEASUREMENT: REQUIREMENTS AND APPLICATIONS FOR METALS AND ALLOYS RESEARCH

J. H. PEREPEZKO *In* NASA, Washington, D.C. Noncontact Temperature Measurement p 79-106 Mar. 1988

(Contract NAG3-436)

Avail: NTIS HC A19/MF A01 CSCL 22A

Temperature measurement is an essential capability for almost all areas of metals and alloys research. In the microgravity

environment many of the science priorities that have been identified for metals and alloys also require noncontact temperature measurement capability. For example, in order to exploit the full potential of containerless processing, it is critical to have available a suitable noncontact temperature measurement system. This system is needed to track continuously the thermal history, including melt undercooling and rapid recalescence, of relatively small metal spheres during free-fall motion in drop tube systems. During containerless processing with levitation-based equipment, accurate noncontact temperature measurement is required to monitor one or more quasi-static samples with sufficient spatial and thermal resolution to follow the progress of solidification fronts originating in undercooled melts. In crystal growth, thermal migration, coarsening and other experiments high resolution thermal maps would be a valuable asset in the understanding and modeling of solidification processes, fluid flows and microstructure development. The science and applications requirements place several constraints on the spatial resolution, response time and accuracy of suitable instrumentation. Author

N88-23901*# National Aeronautics and Space Administration. Lewis Research Center, Cleveland, OH.

NONCONTACT TEMPERATURE MEASUREMENTS IN THE MICROGRAVITY FLUIDS AND TRANSPORT PHENOMENA DISCIPLINE

JACK SALZMAN /in NASA, Washington, D.C. Noncontact Temperature Measurement p 115-122 Mar. 1988
 Avail: NTIS HC A19/MF A01 CSCL 22A

The program of activities within the Microgravity Fluids and Transport Phenomena Discipline has been structured to enable the systematic pursuit of an increased understanding of low gravity fluid behavior/phenomena in a way which ensures that the results are appropriate to the widest range of applications. This structure is discussed and an overview of some of the activities which are underway is given. Of significance is the fact that in the majority of the current and planned activities, the measurement and, or control of the fluid temperature is a key experiment requirement. In addition, many of the experiments require that the temperature measurement be nonintrusive. A description of these requirements together with the current techniques which are being employed or under study to make these measurements is also discussed. Author

N88-23902*# National Aeronautics and Space Administration. Lewis Research Center, Cleveland, OH.

MICROGRAVITY COMBUSTION DISCIPLINE WORKING GROUP SUMMARY OF REQUIREMENTS FOR NONCONTACT TEMPERATURE MEASUREMENTS

KURT SACKSTEDER /in NASA, Washington, D.C. Noncontact Temperature Measurement p 123-128 Mar. 1988
 Avail: NTIS HC A19/MF A01 CSCL 22A

Current efforts of the Microgravity Combustion Working Group are summarized and the temperature measurement requirements for the combustion studies are defined. Many of the combustion systems that are studied in the low gravity environment are near-limit systems, that is, systems that are acting near the limit of flammability in terms of oxygen concentration or fuel concentration. Systems of this type are normally weak in the sense that there is a delicate balance between the heat released in the flame and the heat required to sustain the flame. Intrusive or perturbative temperature measurement probes can be inaccurate in these situations and in the limiting case extinguish the flame. Noncontact techniques then become the only way to obtain the required measurements. Noncontact measurement requirements for each of the three thermodynamic phases are described in terms of spatial and temporal resolution and temperature range. Author

N88-24464*# Michigan Univ., Ann Arbor. Dept. of Mechanical Engineering and Applied Mechanics.

NUCLEATE POOL BOILING: HIGH GRAVITY TO REDUCED GRAVITY; LIQUID METALS TO CRYOGENS

HERMAN MERTE, JR. /in New Mexico Univ., Transactions of

the Fifth Symposium on Space Nuclear Power Systems p 437-442 1988

(Contract NAS8-20228; NAG3-633; NAG3-589)

Avail: NTIS HC A99/MF A01 CSCL 22A

Requirements for the proper functioning of equipment and personnel in reduced gravity associated with space platforms and future space station modules introduce unique problems in temperature control; power generation; energy dissipation; the storage, transfer, control and conditioning of fluids; and liquid-vapor separation. The phase change of boiling is significant in all of these. Although both pool and flow boiling would be involved, research results to date include only pool boiling because buoyancy effects are maximized for this case. The effective application of forced convection boiling heat transfer in the microgravity of space will require a well grounded and cogent understanding of the mechanisms involved. Experimental results are presented for pool boiling from a single geometrical configuration, a flat surface, covering a wide range of body forces from $a/g = 20$ to 1 to $a/g = 0$ to -1 for a cryogenic liquid, and from $a/g = 20$ to 1 for water and a liquid metal. Similarities in behavior are noted for these three fluids at the higher gravity levels, and may reasonably be expected to continue at reduced gravity levels. Author

N88-24811*# National Aeronautics and Space Administration. Lewis Research Center, Cleveland, OH.

PREPARATION FOR MICROGRAVITY: THE ROLE OF THE MICROGRAVITY MATERIALS SCIENCE LABORATORY

J. CHRISTOPHER JOHNSTON, BRUCE N. ROSENTHAL, MARYJO B. MEYER, and THOMAS K. GLASGOW 1988 11 p Presented at the Space Programs and Technologies Conference, Houston, Tex., 21-24 Jun. 1988; sponsored by the AIAA (NASA-TM-100906; E-4157; NAS 1.15:100906; AIAA-88-2645)
 Avail: NTIS HC A03/MF A01 CSCL 22A

A laboratory dedicated to ground based materials processing in preparation for space flight was established at the NASA Lewis Research Center. Experiments are performed to delineate the effects of gravity on processes of both scientific and commercial interest. Processes are modeled physically and mathematically. Transport model systems are used where possible to visually track convection, settling, crystal growth, phase separation, agglomeration, vapor transport, diffusive flow, and polymers reactions. The laboratory contains apparatus which functionally duplicates apparatus available for flight experiments and other pieces instrumented specifically to allow process characterization. Materials addressed include metals, alloys, salts, glasses, ceramics, and polymers. The Microgravity Materials Science Laboratory is staffed by engineers and technicians from a variety of disciplines and is open to users from industry and academia as well as the government. Examples will be given of the laboratory apparatus typical experiments and results. Author

N88-26498*# Intersonics, Inc., Northbrook, IL.

PROGRAM FOR THE FEASIBILITY OF DEVELOPING A HIGH PRESSURE ACOUSTIC LEVITATOR Final Contractor Report

CHARLES A. REY, DENNIS R. MERKLEY, and GREGORY R. HAMMARLUND Jul. 1988 49 p
 (Contract NAS3-25115)

(NASA-CR-182154; NAS 1.26:182154) Avail: NTIS HC A03/MF A01 CSCL 22A

This is the final report for the program for the feasibility of developing a high-pressure acoustic levitator (HPAL). It includes work performed during the period from February 15, 1987 to October 26, 1987. The program was conducted for NASA under contract number NAS3-25115. The HPAL would be used for containerless processing of materials in the 1-g Earth environment. Results show that the use of increased gas pressure produces higher sound pressure levels. The harmonics produced by the acoustic source are also reduced. This provides an improvement in the capabilities of acoustic levitation in 1-g. The reported processing capabilities are directly limited by the design of the Medium Pressure Acoustic Levitator used for this study. Data show that sufficient acoustic intensities can be obtained to levitate and process a specimen of density 5 g/cu cm at 1500 C. However, it

31 ENGINEERING (GENERAL)

is recommended that a working engineering model of the HPAL be developed. The model would be used to establish the maximum operating parameters of furnace temperature and sample density.

Author

31

ENGINEERING (GENERAL)

Includes vacuum technology; control engineering; display engineering; cryogenics; and fire prevention.

A88-10971* National Aeronautics and Space Administration. Lewis Research Center, Cleveland, OH.

CRITERIA FOR SIGNIFICANCE OF SIMULTANEOUS PRESENCE OF BOTH CONDENSIBLE VAPORS AND AEROSOL PARTICLES ON MASS TRANSFER (DEPOSITION) RATES

S. A. GOKOGLU (NASA, Lewis Research Center, Cleveland, OH) IN: 1987 ASME/JSME Thermal Engineering Joint Conference, Honolulu, HI, Mar. 22-26, 1987, Proceedings. Volume 3. New York, American Society of Mechanical Engineers, 1987, p. 79-84. Previously announced in STAR as N86-24869. refs

The simultaneous presence of aerosol particles and condensible vapors in a saturated boundary layer which may affect deposition rates to subcooled surfaces because of vapor-particle interactions is discussed. Scavenging of condensible vapors by aerosol particles may lead to increased particle size and decreased vapor mass fraction, which alters both vapor and particle deposition rates. Particles, if sufficiently concentrated, may also coagulate. Criteria are provided to assess the significance of such phenomena when particles are already present in the mainstream and are not created inside the boundary layer via homogeneous nucleation. It is determined that there is direct proportionality with: (1) the mass concentration of both condensible vapors and aerosol particles; and (2) the square of the boundary layer thickness to particle diameter ratio (δd sub p) square. Inverse proportionality was found for mainstream to surface temperature difference if thermophoresis dominates particle transport. It is concluded that the square of the boundary layer thickness to particle diameter ratio is the most critical factor to consider in deciding when to neglect vapor-particle interactions. Author

A88-38926* National Aeronautics and Space Administration. Lewis Research Center, Cleveland, OH.

ION NITRIDING; PROCEEDINGS OF THE INTERNATIONAL CONFERENCE, CLEVELAND, OH, SEPT. 15-17, 1986

T. SPALVINS, ED. (NASA, Lewis Research Center, Cleveland, OH) Conference sponsored by ASM International and NASA. Metals Park, OH, ASM International, 1987, 208 p. For individual items see A88-38927 to A88-38938.

The present conference discusses plasma-assisted surface coating/modification processes, the applications to date of ion nitriding, the effects of nitrogen on metal surfaces, ion nitriding mechanisms in Cr, Al and Cr + Al-containing 1040 steel, ion nitriding of Al and its alloys, life enhancement for forging dies, novel anode plasma nitriding developments, and a comparative study of the pulsed and dc ion-nitriding behavior in specimens with blind holes. Also discussed are the influence of heating method on ion nitriding, surface hardening of marage steels by ion nitriding without core hardness reduction, plasma nitriding of nodular cast iron sput gears, NbN composites for superconductors, the carburization of tungsten in a glow discharge methane plasma, economic considerations concerning plasma nitriding, and the corrosion properties obtained by ion nitriding. O.C.

A88-38927* National Aeronautics and Space Administration. Lewis Research Center, Cleveland, OH.

PLASMA ASSISTED SURFACE COATING/MODIFICATION PROCESSES - AN EMERGING TECHNOLOGY

T. SPALVINS (NASA, Lewis Research Center, Cleveland, OH) IN: Ion nitriding; Proceedings of the International Conference, Cleveland, OH, Sept. 15-17, 1986. Metals Park, OH, ASM International, 1987, p. 1-8. Previously announced in STAR as N87-12708. refs

A broad understanding of the numerous ion or plasma assisted surface coating/modification processes is sought. An awareness of the principles of these processes is needed before discussing in detail the ion nitriding technology. On the basis of surface modifications arising from ion or plasma energizing and interactions, it can be broadly classified as deposition of distinct overlay coatings (sputtering-dc, radio frequency, magnetron, reactive; ion plating-diode, triode) and surface property modification without forming a discrete coating (ion implantation, ion beam mixing, laser beam irradiation, ion nitriding, ion carburizing, plasma oxidation. These techniques offer a great flexibility and are capable in tailoring desirable chemical and structural surface properties independent of the bulk properties. Author

N88-21374*# National Aeronautics and Space Administration. Lewis Research Center, Cleveland, OH.

POWER COMPONENTS FOR THE SPACE STATION 20-KHZ POWER DISTRIBUTION SYSTEM

DAVID D. RENZ 1988 10 p Proposed for presentation at the 23rd Intersociety Energy Conversion Engineering Conference, Denver, Colo., 31 Jul. - 5 Aug. 1988; sponsored by ASME, AIAA, ANS, SAE, IEEE, ACS and AIChE (NASA-TM-100866; E-4092; NAS 1.15:100866) Avail: NTIS HC A02/MF A01 CSCL 09C

Since 1984, NASA Lewis Research Center was developing high power, high frequency space power components as part of The Space Station Advanced Development program. The purpose of The Advanced Development program was to accelerate existing component programs to ensure their availability for use on the Space Station. These components include a rotary power transfer device, remote power controllers, remote bus isolators, high power semiconductor, a high power semiconductor package, high frequency-high power cable, high frequency-high power connectors, and high frequency-high power transformers. All the components were developed to the prototype level and will be installed in the Lewis Research Center Space Station power system test bed. Author

N88-21375*# National Aeronautics and Space Administration. Lewis Research Center, Cleveland, OH.

MULTI-HUNDRED KILOWATT ROLL RING ASSEMBLY EVALUATION RESULTS

DAVID D. RENZ 1988 10 p Proposed for presentation at the 23rd Intersociety Energy Conversion Engineering Conference, Denver, Colo., 31 Jul. - 5 Aug. 1988; sponsored by ASME, AIAA, ANS, SAE, IEEE, ACS and AIChE (NASA-TM-100865; E-4091; NAS 1.15:100865) Avail: NTIS HC A02/MF A01 CSCL 13B

NASA Lewis Research Center has been evaluating low loss multi-hundred-kilowatt Roll Ring assemblies (an 8 circuit and a 4 circuit) for use on Space Station as the rotating joint power transfer device. In this device ac or dc power is transferred across the rotating joint through compressed rotating flexures. Results and conclusions of the evaluation program are presented. Author

N88-26539*# National Aeronautics and Space Administration. Lewis Research Center, Cleveland, OH.

REDUCING ADHESION AND AGGLOMERATION WITHIN A CLOUD OF COMBUSTIBLE PARTICLES

HOWARD D. ROSS Jul. 1988 42 p (NASA-TM-100902; E-4082; NAS 1.15:100902) Avail: NTIS HC A03/MF A01 CSCL 21B

The study of combustible particle clouds inside flame tubes is of fundamental scientific interest as well as a practical concern. Only the suspended concentration is important to the combustion process, so that assurances must be provided that a minimum of particles adheres to the tube wall. This paper demonstrates experimentally the ability to minimize adhesion and agglomeration

of acoustically-mixed lycopodium particles within a 5-cm diameter lexan flame tube. The area density of particles (ADP) adhering to the wall of bare lexan tubes was measured at greater than 100 particles/sq mm. The nature of adhesion was found to be clearly electrostatic, with the ADP level aggravated by increased mixing time, vigor, and the concentration of particles. Increases in the conductivity of the air and the tube wall did not affect ADP levels substantially. However, the observed adhesion was reduced to less than 10 p/sq mm when the air was ionized by use of an alpha emitter mounted on the inner walls of the flame tube.

Author

N88-28176*# National Aeronautics and Space Administration. Lewis Research Center, Cleveland, OH.

STATUS AND DIRECTIONS OF MODIFIED TRIBOLOGICAL SURFACES BY ION PROCESSES

TALIVALDIS SPALVINS 1988 22 p Prepared for presentation at the 1st International Conference on Plasma Surface Engineering, Garmisch-Partenkirchen, Fed. Republic of Germany, 19-23 Sep. 1988; sponsored by Deutsche Gesellschaft fuer Metallkunde (NASA-TM-101304; E-4294; NAS 1.15:101304) Avail: NTIS HC A03/MF A01 CSDL 20C

An overview is presented of recent advances in modifying contacting surfaces in motion by the various ion assisted surface coating/modification processes to reduce and control tribological failures. The ion assisted coating processes and the surface modification processes offer the greatest potential to custom tailor and optimize the tribological performance. Hard, wear resistant and low shear coatings deposited by the ion assisted processes are discussed. Primarily the recent advances of sputtered MoS₂ ion plated Au, Ag, Pb lubricating films and sputtered and ion plated hard, wear resistant TiN, HfN, TiC films are described in terms of structural property performance interrelationships which lead to improved adhesion, cohesion, nucleation, morphological growth, density, film thickness as determined by structural and chemical characterization and frictional and wear behavior. Also, the recent tribological advances using the surface modification processes such as ion implantation, ion beam mixing is discussed with emphasis on the development of lubricous high temperature ceramic surfaces.

Author

N88-29997*# National Aeronautics and Space Administration. Lewis Research Center, Cleveland, OH.

OPTICAL MEASUREMENTS OF SOOT AND TEMPERATURE PROFILES IN PREMIXED PROPANE-OXYGEN FLAMES

VALERIE J. LYONS and PATRICK J. PAGNI (California Univ., Berkeley.) 1988 20 p Proposed for presentation at the Winter Annual Meeting of the American Society of Mechanical Engineers, Chicago, Ill., 28 Nov. - 2 Dec. 1988 (NASA-TM-101343; E-4363; NAS 1.15:101343) Avail: NTIS HC A03/MF A01 CSDL 13B

Two laser diagnostic techniques were used to measure soot volume fractions, number densities and soot particle radii in premixed propane/oxygen flat flames. The two techniques used were two wavelength extinction, using 514.5 nm to 632.8 nm and 457.9 nm to 632.8 nm wavelength combinations, and extinction/scattering using 514.5 nm light. The flames were fuel-rich (equivalence ratios from 2.1 to 2.8) and had cold gas velocities varying from 3.4 to 5.5 cm/s. Measurements were made at various heights above the sintered-bronze, water-cooled flat flame burner with the equivalence ratio and cold gas velocity fixed. Also, measurements were made at a fixed height above the burner and fixed cold gas velocity while varying the equivalence ratio. Both laser techniques are based on the same underlying assumptions of particle size distribution and soot optical properties. Full Mie theory was used to determine the extinction coefficients $K_{sub ext}$ and the scattering efficiencies, $Q_{sub vv}$. Temperature measurements in the flames were made using infrared radiometry. Good agreement between the two techniques in terms of soot particle radii, number density and volume fraction was found for intensity ratios ($I/I_{sub 0}$) between 0.1 and 0.8. For intensity ratios higher or lower than this range, the differences in extinction coefficients at the wavelengths chosen for the two-wavelength

method are too small to give accurate results for comparing particle radii and number densities. However, when comparing only soot volume fractions, the agreement between the two techniques continued to be good for intensity ratios up to 0.95. Author

32

COMMUNICATIONS AND RADAR

Includes radar; land and global communications; communications theory; and optical communications.

A88-14091* Virginia Polytechnic Inst. and State Univ., Blacksburg.

VSAT NETWORKS - AN OVERVIEW

MARK MAGGENTI, TRI T. HA, and TIMOTHY PRATT (Virginia Polytechnic Institute and State University, Blacksburg) International Journal of Satellite Communications (ISSN 0737-2884), vol. 5, July-Sept. 1987, p. 219-225. refs (Contract NAS3-24887)

This paper examines the technology and constraints of very small aperture terminals (VSAT) networks, a special type of wide-area thin-route satellite network that represents a recent innovation in the field of satellite communications. VSAT network architectures suitable for both data and voice communications are studied in this paper. Several issues concerning the frequency of operations, that is, C-band versus Ku-band are examined, and trade-offs between nonspread spectrum and spread spectrum techniques, as well as modulation and multiple access schemes, are considered in detail. Link design examples are given to illustrate the performance of various types of VSAT networks. Author

A88-14100* National Aeronautics and Space Administration. Lewis Research Center, Cleveland, OH.

CHARACTERISTICS OF A TWO-LAYER ELECTROMAGNETICALLY COUPLED RECTANGULAR PATCH ANTENNA

R. Q. LEE (NASA, Lewis Research Center, Cleveland, OH), K. F. LEE, and J. BOBINCHAK (Akron, University, OH) Electronics Letters (ISSN 0013-5194), vol. 23, Sept. 24, 1987, p. 1070-1072. refs

Experimental results on the characteristics of a two-layer electromagnetically coupled rectangular patch antenna are presented. The variations of pattern shape, 3 dB beam width, and impedance bandwidth with spacing s between the two layers are studied for s between 0 and 0.37 λ (0). A relatively high-gain region is found for s between 0.31 λ (0) and 0.37 λ (0). Author

A88-24863* Illinois Univ., Urbana.

HOW GOOD IS THE IMPEDANCE BOUNDARY CONDITION?

SHUNG-WU LEE (Illinois, University, Urbana) and W. GEE (Deskin Research Group, Santa Clara, CA) IEEE Transactions on Antennas and Propagation (ISSN 0018-926X), vol. AP-35, Nov. 1987, p. 1313-1315. refs (Contract NAG3-473)

The impedance boundary condition (IBC) is often used in scattering problems involving material-coated conducting bodies. It is shown that for some commonly encountered coating configurations, the value of the impedance varies significantly as functions of the incident angle and polarization. Hence, the use of IBC in a rigorously formulated problem may affect the accuracy of the final solution. I.E.

A88-26672* Virginia Polytechnic Inst. and State Univ., Blacksburg.

SPREAD-SPECTRUM MULTIPLE ACCESS USING WIDEBAND NONCOHERENT MFSK

TRI T. HA, TIMOTHY PRATT (Virginia Polytechnic Institute and State University, Blacksburg), and MARK A. MAGGENTI IEEE

32 COMMUNICATIONS AND RADAR

Transactions on Aerospace and Electronic Systems (ISSN 0018-9251), vol. AES-23, Nov. 1987, p. 767-775.
(Contract NAS3-24887)

Two spread-spectrum multiple access systems which use wideband M-ary frequency shift keying (FSK) (MFSK) as the primary modulation are presented. A bit error rate performance analysis is presented and system throughput is calculated for sample C band and Ku band satellite systems. Sample link analyses are included to illustrate power and adjacent satellite interference considerations in practical multiple access systems. Author

A88-27551* National Aeronautics and Space Administration. Lewis Research Center, Cleveland, OH.

SERVICE OFFERINGS AND INTERFACES FOR THE ACTS NETWORK OF EARTH STATIONS

T. A. CONEY (NASA, Lewis Research Center, Cleveland, OH), T. R. DOBYNS, D. M. CHITRE, and R. LINDSTROM (COMSAT Laboratories, Clarksburg, MD) IN: AIAA International Communication Satellite Systems Conference, 12th, Arlington, VA, Mar. 13-17, 1988, Technical Papers. Washington, DC, American Institute of Aeronautics and Astronautics, 1988, p. 247-258.
(AIAA PAPER 88-0800)

The NASA Advanced Communications Technology Satellite (ACTS) will use a network of about 20 earth stations to operate as a Mode 1 network. This network will support two ACTS program objectives: to verify the technical performance of ACTS Mode 1 operation in GEO and to demonstrate the types and quality of services that can be provided by an ACTS Mode 1 communications system. The terrestrial interface design is a critical element in assuring that these network earth stations will meet the objectives. In this paper, the applicable terrestrial interface design requirements, the resulting interface specifications, and the associated terrestrial input/output hardware are discussed. A functional block diagram of a network earth station is shown.

C.D.

A88-27560* Communications Satellite Corp., Clarksburg, MD.
BANDWIDTH-EFFICIENT HIGH-SPEED CODED TRELLIS MODULATION

R. J. F. FANG (COMSAT Laboratories, Clarksburg, MD) and J. M. BUDINGER (NASA, Lewis Research Center, Cleveland, OH) IN: AIAA International Communication Satellite Systems Conference, 12th, Arlington, VA, Mar. 13-17, 1988, Technical Papers. Washington, DC, American Institute of Aeronautics and Astronautics, 1988, p. 313-321. refs
(Contract NAS3-26480)
(AIAA PAPER 88-0813)

A burst-mode coded trellis modulation system is discussed which is capable of 200-Mbit/s information rate transmission over nonlinear satellite transponders whose center frequencies are separated by 100 MHz. An overall real bandwidth efficiency of 2 bit/s per Hz of the allocated spectrum is projected. Convolutional codec and 8-PSK modulation subsystems together maximize the minimum Euclidean distance between the modulated codeword sequences in the overall coded trellis, resulting in a 4.3-dB asymptotic coding advantage over an uncoded 8-PSK system signalling at the same information rate over the same channel. The system performance has been evaluated by computer simulation.

R.R.

A88-27604* Ford Aerospace and Communications Corp., Palo Alto, CA.

ADVANCED SATELLITE SYSTEM ARCHITECTURE FOR VSATS WITH ISDN COMPATIBILITY

RONALD E. JORASCH and KENT M. PRICE (Ford Aerospace and Communications Corp., Space Systems Div., Palo Alto, CA) IN: AIAA International Communication Satellite Systems Conference, 12th, Arlington, VA, Mar. 13-17, 1988, Technical Papers. Washington, DC, American Institute of Aeronautics and Astronautics, 1988, p. 642-651.
(Contract NAS3-24683)
(AIAA PAPER 88-0870)

This paper describes a future communications satellite system

architecture concept which allows the use of Very Small Aperture Terminals (VSATs) of 1.2 m to 1.8 m diameter and which provides access according to the international Integrated Services Digital Network (ISDN) standard. This satellite system design could make dial-up integrated voice and data service available nationwide and perhaps worldwide. The paper gives a conceptual system design based on the year 1995 technology for the communications satellite, the earth terminal, and the ground-based master control station and interface to the terrestrial ISDN network. Author

A88-36482* National Aeronautics and Space Administration. Lewis Research Center, Cleveland, OH.

AN ALLOTMENT PLANNING CONCEPT AND RELATED COMPUTER SOFTWARE FOR PLANNING THE FIXED SATELLITE SERVICE AT THE 1988 SPACE WARC

EDWARD F. MILLER, ANN O. HEYWARD, DENISE S. PONCHAK, RODNEY L. SPENCE, WAYNE A. WHYTE, JR. (NASA, Lewis Research Center, Cleveland, OH) et al. IN: GLOBECOM '87 - Global Telecommunications Conference, Tokyo, Japan, Nov. 15-18, 1987, Conference Record. Volume 3. New York, Institute of Electrical and Electronics Engineers, Inc., 1987, p. 2170-2174.

The authors describe a two-phase approach to allotment planning suitable for use in planning the fixed satellite service at the 1988 Space World Administrative radio Conference (ORB-88). The two phases are (1) the identification of predetermined geostationary arc segments common to groups of administrations and (2) the use of a synthesis program to identify example scenarios of space station placements. The planning approach is described in detail and is related to the objectives of the conference. Computer software has been developed to implement the concepts, and the logic and rationale for identifying predetermined arc segments is discussed. Example scenarios are evaluated to give guidance in the selection of the technical characteristics of space communications systems to be planned. The allotment planning concept described guarantees equitable access to the geostationary orbit, provides flexibility in implementation, and reduces the need for coordination among administrations. I.E.

A88-36648* Hughes Aircraft Co., El Segundo, CA.

A SIMPLE CIRCULAR-POLARIZED ANTENNA: CIRCULAR WAVEGUIDE HORN COATED WITH LOSSY MAGNETIC MATERIAL

CHOON S. LEE, D. W. JUSTICE (Hughes Aircraft Co., Space and Communications Group, El Segundo, CA), and SHUNG-WU LEE (Illinois, University, Urbana) IEEE Transactions on Antennas and Propagation (ISSN 0018-926X), vol. 36, Feb. 1988, p. 297-300. refs
(Contract NAG3-475)

It is shown that a circular waveguide horn coated with a lossy material in its interior wall can be used as an alternative to a corrugated waveguide for radiating a circularly polarized (CP) field. To achieve good CP radiation, the diameter of the structure must be larger than the free-space wavelength, and the coating material must be sufficiently lossy and magnetic. The device is cheaper and lighter in weight than the corrugated one. I.E.

A88-47424* Illinois Univ., Urbana.

POLARIZATION DETERMINATION UTILIZING TWO ARBITRARILY POLARIZED ANTENNAS

SHUNG-WU LEE (Illinois, University, Urbana), E. K. OKUBO (Lockheed Missiles and Space Co., Inc., Sunnyvale, CA), and HAO LING (Texas, University, Austin) IEEE Transactions on Antennas and Propagation (ISSN 0018-926X), vol. 36, May 1988, p. 720-723.

(Contract NAG3-149; NSF ECS-86-57524)

Microwave polarimeter systems typically consist of two orthogonally polarized receiving antennas. Formulas for extracting the unknown polarization antennas with known polarization states are presented. Numerical results are generated showing the size of the errors made by assuming perfect orthogonal polarizations (either circular or linear). I.E.

A88-47705* Akron Univ., OH.

CROSSPOLARISATION CHARACTERISTICS OF RECTANGULAR PATCH ANTENNAS

T. HUYNH, K. F. LEE (Akron, University, OH), and R. Q. LEE (NASA, Lewis Research Center, Cleveland, OH) Electronics Letters (ISSN 0013-5194), vol. 24, April 14, 1988, p. 463, 464.

Theoretical results describing the crosspolarization characteristics of rectangular patch antennas are presented. Of particular interest is the result that the copolarization radiation is not sensitive to resonant frequency and substrate thickness while the crosspolarization component increases with resonant frequency and/or substrate thickness. Author

A88-47949* National Aeronautics and Space Administration. Lewis Research Center, Cleveland, OH.

ABSOLUTE GAIN MEASUREMENT OF MICROSTRIP ANTENNAS UNDER MISMATCHED CONDITIONS

R. Q. LEE and M. F. BADDOUR (NASA, Lewis Research Center, Cleveland, OH) Electronics Letters (ISSN 0013-5194), vol. 24, April 28, 1988, p. 521, 522.

The gain of a single microstrip patch and a two-layer parasitic array is measured using the image method under mismatched conditions. This method produces accurate results, even in the case of low-gain microstrip antennas. The advantages of this method over the gain comparison technique are discussed. K.K.

A88-48579* Ohio State Univ., Columbus.

A SATELLITE SYSTEM SYNTHESIS MODEL FOR ORBITAL ARC ALLOTMENT OPTIMIZATION

CHARLES H. REILLY (Ohio State University, Columbus) IEEE Transactions on Communications (ISSN 0090-6778), vol. 36, July 1988, p. 845-849. Previously announced in STAR as N87-25341. refs (Contract NAG3-159)

A mixed-integer programming formulation is presented of a satellite system synthesis problem, or geostationary-orbital-planning synthesis problem, which is referred to as the arc allotment problem (AAP). Each satellite administration is to be allotted a weighted-length segment of the geostationary orbital arc within which its satellites may be positioned at any longitude. The objective function maximizes the length of the unweighted arc segment allotted to every administration, subject to single-entry cochannel interference restrictions and constraints imposed by the visible arc for each administration. Useful relationships between special cases of AAP and another satellite synthesis problem are established. Solutions to two example problems are presented. I.E.

A88-48653* National Aeronautics and Space Administration. Lewis Research Center, Cleveland, OH.

GAIN ENHANCEMENT OF MICROSTRIP ANTENNAS WITH OVERLAYING PARASITIC DIRECTORS

R. Q. LEE (NASA, Lewis Research Center, Cleveland, OH) and K. F. LEE (Akron, University, OH) Electronics Letters (ISSN 0013-5194), vol. 24, May 26, 1988, p. 656-658. refs

An experimental study of gain enhancement in microstrip antennas using identical parasitic patch directors is reported. The results indicate that, with two overlying parasitic directors, the gain of a rectangular microstrip antenna is enhanced from 4.7 dB to 10.6 dB, while the 3 dB beamwidth is reduced from 103 deg to 30 deg for the E-plane and from 70 deg to 35 deg for the H-plane. The three-layer electromagnetically coupled patch antenna exhibits similar antenna characteristics to those of the Yagi array, with over 120 dB gain and with about 1 percent bandwidth. C.D.

A88-50305* National Aeronautics and Space Administration. Lewis Research Center, Cleveland, OH.

DETECTION OF RADIO-FREQUENCY MODULATED OPTICAL SIGNALS BY TWO AND THREE TERMINAL MICROWAVE DEVICES

K. B. BHASIN, R. N. SIMONS (NASA, Lewis Research Center, Cleveland, OH), and S. WOJTCZUK (Cornell University, Ithaca, NY) IN: Optical technology for microwave applications III;

Proceedings of the Meeting, Orlando, FL, May 19, 20, 1987. Bellingham, WA, Society of Photo-Optical Instrumentation Engineers, 1987, p. 60-66. Previously announced in STAR as N87-29750. refs

An interdigitated photoconductor (two terminal device) on GaAlAs/GaAs heterostructure was fabricated and tested by an electro-optical sampling technique. Further, the photoresponse of GaAlAs/GaAs HEMT (three terminal device) was obtained by illuminating the device with an optical signal modulated up to 8 GHz. Gain-bandwidth product, response time, and noise properties of photoconductor and HEMT devices were obtained. Monolithic integration of these photodetectors with GaAs microwave devices for optically controlled phased array antenna applications is discussed. Author

N88-11925*# National Aeronautics and Space Administration. Lewis Research Center, Cleveland, OH.

LEWIS INFORMATION NETWORK (LINK): BACKGROUND AND OVERVIEW

ROGER R. SCHULTE Nov. 1987 34 p (NASA-TM-100162; E-3724; NAS 1.15:100162) Avail: NTIS HC A03/MF A01 CSCL 17B

The NASA Lewis Research Center supports many research facilities with many isolated buildings, including wind tunnels, test cells, and research laboratories. These facilities are all located on a 350 acre campus adjacent to the Cleveland Hopkins Airport. The function of NASA-Lewis is to do basic and applied research in all areas of aeronautics, fluid mechanics, materials and structures, space propulsion, and energy systems. These functions require a great variety of remote high speed, high volume data communications for computing and interactive graphic capabilities. In addition, new requirements for local distribution of intercenter video teleconferencing and data communications via satellite have developed. To address these and future communications requirements for the next 15 yrs, a project team was organized to design and implement a new high speed communication system that would handle both data and video information in a common lab-wide Local Area Network. The project team selected cable television broadband coaxial cable technology as the communications medium and first installation of in-ground cable began in the summer of 1980. The Lewis Information Network (LINK) became operational in August 1982 and has become the backbone of all data communications and video. Author

N88-11944*# National Aeronautics and Space Administration. Lewis Research Center, Cleveland, OH.

AN ALLOTMENT PLANNING CONCEPT AND RELATED COMPUTER SOFTWARE FOR PLANNING THE FIXED SATELLITE SERVICE AT THE 1988 SPACE WARC

EDWARD F. MILLER, ANN O. HEYWARD, DENISE S. PONCHAK, RODNEY L. SPENCE, WAYNE A. WHYTE, JR., and JOHN E. ZUZEK Nov. 1987 12 p Presented at the Global Telecommunications Conference, Tokyo, Japan, 15-18 Nov. 1987; sponsored by IEEE

(NASA-TM-100244; E-3777; NAS 1.15:100244) Avail: NTIS HC A03/MF A01 CSCL 17B

Described is a two-phase approach to allotment planning suitable for use in establishing the fixed satellite service at the 1988 Space World Administrative Radio Conference (ORB-88). The two phases are (1) the identification of predetermined geostationary arc segments common to groups of administrations, and (2) the use of a synthesis program to identify example scenarios of space station placements. The planning approach is described in detail and is related to the objectives of the conference. Computer software has been developed to implement the concepts, and a complete discussion on the logic and rationale for identifying predetermined arc segments is given. Example scenarios are evaluated to give guidance in the selection of the technical characteristics of space communications systems to be planned. The allotment planning concept described guarantees in practice equitable access to the geostationary orbit, provides flexibility in implementation, and reduces the need for coordination among administrations. Author

32 COMMUNICATIONS AND RADAR

N88-11945*# National Aeronautics and Space Administration. Lewis Research Center, Cleveland, OH.

A STATISTICAL RAIN ATTENUATION PREDICTION MODEL WITH APPLICATION TO THE ADVANCED COMMUNICATION TECHNOLOGY SATELLITE PROJECT. PART 2: THEORETICAL DEVELOPMENT OF A DYNAMIC MODEL AND APPLICATION TO RAIN FADE DURATIONS AND TOLERABLE CONTROL DELAYS FOR FADE COUNTERMEASURES

ROBERT M. MANNING Dec. 1987 101 p
(NASA-TM-100242; E-3866; NAS 1.15:100242) Avail: NTIS HC A03/MF A01 CSCL 17B

A dynamic rain attenuation prediction model is developed for use in obtaining the temporal characteristics, on time scales of minutes or hours, of satellite communication link availability. Analogous to the associated static rain attenuation model, which yields yearly attenuation predictions, this dynamic model is applicable at any location in the world that is characterized by the static rain attenuation statistics peculiar to the geometry of the satellite link and the rain statistics of the location. Such statistics are calculated by employing the formalism of Part I of this report. In fact, the dynamic model presented here is an extension of the static model and reduces to the static model in the appropriate limit. By assuming that rain attenuation is dynamically described by a first-order stochastic differential equation in time and that this random attenuation process is a Markov process, an expression for the associated transition probability is obtained by solving the related forward Kolmogorov equation. This transition probability is then used to obtain such temporal rain attenuation statistics as attenuation durations and allowable attenuation margins versus control system delay. Author

N88-13513*# National Aeronautics and Space Administration. Lewis Research Center, Cleveland, OH.

COMMUNICATIONS PAYLOAD CONCEPTS FOR GEOSTATIONARY FACILITIES

WILLIAM A. POLEY and JACK LEKAN Dec. 1987 96 p
(NASA-TM-100154; E-3353; NAS 1.15:100154) Avail: NTIS HC A05/MF A01 CSCL 17B

Summarized and compared are the major results of two NASA sponsored studies that defined potential communication payload concepts to meet the satellite traffic forecast for the turn of the century for the continental US and Region 2 of the International Telecommunications Union. The studies were performed by the Ford Aerospace and Communications Corporation and RCA Astro-Electronics (now GE-RCA Astro-Space Division). Future scenarios of aggregations of communications services are presented. Payload concepts are developed and defined in detail for nine of the scenarios. Payload costs and critical technologies per payload are also presented. Finally the payload concepts are compared and the findings of the reports are discussed. Author

N88-13515*# National Aeronautics and Space Administration. Lewis Research Center, Cleveland, OH.

AN EVOLUTIONARY COMMUNICATIONS SCENARIO FOR MARS EXPLORATION

STEVEN M. STEVENSON 1987 31 p Presented at The Case For Mars 3, Boulder, Colo., 18-22 Jul. 1987; sponsored by the American Astronautical Society
(NASA-TM-100263; E-3892; NAS 1.15:100263) Avail: NTIS HC A03/MF A01 CSCL 17B

As Mars exploration grows in complexity with time, the corresponding communication needs will grow in variety and complexity also. From initial Earth/Mars links, further needs will arise for complete surface connectivity for the provision of navigation, position location, and voice, data, and video communications services among multiple Mars bases and remote exploration sites. This paper addresses the likely required communication functions over the first few decades of Martian exploration and postulates systems for providing these services. Required technologies are identified and development requirements indicated. Author

N88-14260*# National Aeronautics and Space Administration. Lewis Research Center, Cleveland, OH.

SATELLITE GROUND-TERMINAL USER SIMULATION

MARY JO W. SHALKHAUSER Jan. 1988 15 p
(NASA-TM-100234; E-3859; NAS 1.15:100234) Avail: NTIS HC A03/MF A01 CSCL 17B

Realistic simulation of satellite communication systems and evaluation of satellite networking schemes require emulation of the systems's users. A laboratory model of a Ka-band satellite-switched time-division multiple-access (SS-TDMA) communication network, referred to as the System Integration, Test, and Evaluation (SITE) project, uses special bit-error-rate (BER) test sets to simulate the transmitting and receiving users of a communication network. The bit-error-rate test sets contain circuit boards that can be modified to create a variety of interfaces to satellite system ground terminals. Author

N88-15130*# Ohio State Univ., Columbus. ElectroScience Lab. **ELECTROMAGNETIC FIELDS BACKSCATTERED FROM AN S-SHAPED INLET CAVITY WITH AN ABSORBER COATING ON ITS INNER WALLS Final Report**

R. J. BURKHOLDER, C. W. CHUANG, and P. H. PATHAK 30 Jul. 1987 127 p

(Contract NAG3-476)
(NASA-CR-182401; NAS 1.26:182401; FR-715723-2) Avail: NTIS HC A07/MF A01 CSCL 20N

The EM backscatter from a two-dimensional S-shaped inlet cavity is analyzed using three different techniques, namely a hybrid combination of asymptotic high frequency and modal methods, an integral equation method, and the geometrical optics ray method, respectively. This inlet has a thin absorber coating on its perfectly conducting inner walls and the planar interior termination is made perfectly conducting. The effect of the absorber on the inner wall is treated via a perturbation scheme in the hybrid approach where it is assumed that the loss is sufficiently small for the method to be valid. The results are compared with the backscatter from a straight inlet cavity to evaluate the effect of offsetting the termination in the S-bend configuration such that it is not visible from the open end of the inlet. The envelope of the backscatter pattern for the straight inlet is always seen to peak around the forward axis due to the large return from the directly visible termination, and the pattern envelope tapers off away from the forward axis. Offsetting the termination causes the envelope of the backscatter pattern to flatten out, thereby reducing the return near the forward axis by several dB. The absorber coating reduces the pattern level of the straight inlet in directions away from the forward axis but has little effect on the peak near the axis; furthermore, the absorber coating is seen to consistently reduce the backscatter from the S-bend inlet for almost all incidence angles. The hybrid method gives excellent agreement with experimental data and with the integral equation solution, whereas, the geometrical optics ray tracing method is able to generally predict the average of the backscatter pattern but not the pattern details. Author

N88-15910*# National Aeronautics and Space Administration. Lewis Research Center, Cleveland, OH.

NUMERICAL ARC SEGMENTATION ALGORITHM FOR A RADIO CONFERENCE-NASARC (VERSION 2.0) TECHNICAL MANUAL

WAYNE A. WHYTE, JR., ANN O. HEYWARD, DENISE S. PONCHAK, RODNEY L. SPENCE, and JOHN E. ZUZAK 16 Oct. 1987 116 p
(NASA-TM-100160; E-3722; NAS 1.15:100160) Avail: NTIS HC A06/MF A01 CSCL 17B

The information contained in the NASARC (Version 2.0) Technical Manual (NASA TM-100160) and NASARC (Version 2.0) User's Manual (NASA TM-100161) relates to the state of NASARC software development through October 16, 1987. The Technical Manual describes the Numerical Arc Segmentation Algorithm for a Radio Conference (NASARC) concept and the algorithms used to implement the concept. The User's Manual provides information on computer system considerations, installation instructions,

description of input files, and program operating instructions. Significant revisions have been incorporated in the Version 2.0 software. These revisions have enhanced the modeling capabilities of the NASARC procedure while greatly reducing the computer run time and memory requirements. Array dimensions within the software have been structured to fit within the currently available 6-megabyte memory capacity of the International Frequency Registration Board (IFRB) computer facility. A piecewise approach to predetermined arc generation in NASARC (Version 2.0) allows worldwide scenarios to be accommodated within these memory constraints while at the same time effecting an overall reduction in computer run time. Author

N88-16928*# National Aeronautics and Space Administration. Lewis Research Center, Cleveland, OH.

NUMERICAL ARC SEGMENTATION ALGORITHM FOR A RADIO CONFERENCE-NASARC, VERSION 2.0: USER'S MANUAL

WAYNE A. WHYTE, JR., ANN O. HEYWARD, DENISE S. PONCHAK, RODNEY L. SPENCE, and JOHN E. ZUZK 16 Oct. 1987 93 p (NASA-TM-100161; E-3723; NAS 1.15:100161) Avail: NTIS HC A05/MF A01 CSCL 17B

The information contained in the NASARC (Version 2.0) Technical Manual (NASA TM-100160) and the NASARC (Version 2.0) User's Manual (NASA TM-100161) relates to the state of the Numerical Arc Segmentation Algorithm for a Radio Conference (NASARC) software development through October 16, 1987. The technical manual describes the NASARC concept and the algorithms which are used to implement it. The User's Manual provides information on computer system considerations, installation instructions, description of input files, and program operation instructions. Significant revisions have been incorporated in the Version 2.0 software over prior versions. These revisions have enhanced the modeling capabilities of the NASARC procedure while greatly reducing the computer run time and memory requirements. Array dimensions within the software have been structured to fit into the currently available 6-megabyte memory capacity of the International Frequency Registration Board (IFRB) computer facility. A piecewise approach to predetermined arc generation in NASARC (Version 2.0) allows worldwide scenarios to be accommodated within these memory constraints while at the same time reducing computer run time. Author

N88-17880*# National Aeronautics and Space Administration. Lewis Research Center, Cleveland, OH.

MODELING OF SOME COPLANAR WAVEGUIDE DISCONTINUITIES

RAINEE N. SIMONS and GEORGE E. PONCHAK 1988 10 p Proposed for presentation at the IEEE MTT-S International Microwave Symposium, New York, N.Y., 25-27 May 1988 (NASA-TM-100808; E-3981; NAS 1.15:100808) Avail: NTIS HC A02/MF A01 CSCL 20N

Presented are lumped equivalent circuit models for several coplanar waveguide discontinuities such as an open circuit, a series gap, and a symmetric step, and their element values as a function of the discontinuity physical dimensions. The model element values are de-embedded from measured S-parameters. The frequency dependence of the effective dielectric constant was measured and compared to computed values. Author

N88-17892*# Arizona Univ., Tucson. Optical Sciences Center. **GUIDED-WAVE APPROACHES TO SPECTRALLY SELECTIVE ENERGY ABSORPTION Final Report, 25 Jan. 1983 - 2 Mar. 1987**

G. I. STEGEMAN and J. J. BURKE Mar. 1987 14 p (Contract NAG3-392) (NASA-CR-182532; NAS 1.26:182532) Avail: NTIS HC A03/MF A01 CSCL 20N

Results of experiments designed to demonstrate spectrally selective absorption in dielectric waveguides on semiconductor substrates are reported. These experiments were conducted with three waveguides formed by sputtering films of PSK2 glass onto

silicon-oxide layers grown on silicon substrates. The three waveguide samples were studied at 633 and 532 nm. The samples differed only in the thickness of the silicon-oxide layer, specifically 256 nm, 506 nm, and 740 nm. Agreement between theoretical predictions and measurements of propagation constants (mode angles) of the six or seven modes supported by these samples was excellent. However, the loss measurements were inconclusive because of high scattering losses in the structures fabricated (in excess of 10 dB/cm). Theoretical calculations indicated that the power distribution among all the modes supported by these structures will reach its steady state value after a propagation length of only 1 mm. Accordingly, the measured loss rates were found to be almost independent of which mode was initially excited. The excellent agreement between theory and experiment leads to the conclusion that low loss waveguides confirm the predicted loss rates. Author

N88-17899*# National Aeronautics and Space Administration. Lewis Research Center, Cleveland, OH.

COMPLEMENTARY SATELLITE SOUND BROADCASTING SYSTEMS: A NASA ASSESSMENT FOR THE VOICE OF AMERICA

GRADY H. STEVENS and RODNEY L. SPENCE Jan. 1988 84 p

(NASA-TM-100300; E-3948; NAS 1.15:100300) Avail: NTIS HC A05/MF A01 CSCL 17B

Satellite concepts are examined which offer potentially significant sound broadcast coverage of audio as a complement to VOA's existing and planned terrestrial sound broadcasting system. HF bands are emphasized but additional discussion is included for systems using higher frequencies. Low altitude satellites, shuttle altitude (275 km) and sun synchronous (about 1600 to 1800 km), would not be practical for international broadcasting since many satellites would be required for reliable and widespread coverage. Two concepts are discussed which would offer significant and practical broadcast coverage at HF. One, an 8-hr posigrade equatorial orbit, would offer about 1 hr of widespread, twice daily, coverage to three areas of the globe. The time of coverage is even greater when confined to densely populated areas only (2 to 3 hrs). Another orbit, the Apogee at Constant Time/Equatorial (ACE), provides the same coverage, but only once daily to each area. The latter orbit is highly elliptical, allowing insertion of a greater payload (more broadcast channels) with the existing launch capability. The ACE and 8-hr orbit concepts led to systems of about equal costs, with the ACE being slightly better. Author

N88-18805*# National Aeronautics and Space Administration. Lewis Research Center, Cleveland, OH.

COMPENSATION OF REFLECTOR ANTENNA SURFACE DISTORTION USING AN ARRAY FEED

A. R. CHERRETTE, R. J. ACOSTA, P. T. LAM, and S. W. LEE (Illinois Univ., Urbana.) Jan. 1988 49 p

(Contract NAG3-419)

(NASA-TM-100286; E-3929; NAS 1.15:100286) Avail: NTIS HC A03/MF A01 CSCL 20N

The dimensional stability of the surface of a large reflector antenna is important when high gain or low sidelobe performance is desired. If the surface is distorted due to thermal or structural reasons, antenna performance can be improved through the use of an array feed. The design of the array feed and its relation to the surface distortion are examined. The sensitivity of antenna performance to changing surface parameters for fixed feed array geometries is also studied. This allows determination of the limits of usefulness for feed array compensation. Author

N88-18809*# National Aeronautics and Space Administration. Lewis Research Center, Cleveland, OH.

OPTICALLY CONTROLLED PHASED-ARRAY ANTENNA TECHNOLOGY FOR SPACE COMMUNICATION SYSTEMS

RICHARD R. KUNATH and KUL B. BHASIN 1988 7 p Presented at Optoelectronics and Laser Applications in Science and Engineering (O-E/LASE '88), Los Angeles, Calif., 10-15 Jan. 1988;

32 COMMUNICATIONS AND RADAR

sponsored by the Society of Photo-Optical Instrumentation Engineers
(NASA-TM-100852; E-4055; NAS 1.15:100852) Avail: NTIS HC A02/MF A01 CSCL 17B

Using MMICs in phased-array applications above 20 GHz requires complex RF and control signal distribution systems. Conventional waveguide, coaxial cable, and microstrip methods are undesirable due to their high weight, high loss, limited mechanical flexibility and large volume. An attractive alternative to these transmission media, for RF and control signal distribution in MMIC phased-array antennas, is optical fiber. Presented are potential system architectures and their associated characteristics. The status of high frequency opto-electronic components needed to realize the potential system architectures is also discussed. It is concluded that an optical fiber network will reduce weight and complexity, and increase reliability and performance, but may require higher power. Author

N88-19698*# National Aeronautics and Space Administration. Lewis Research Center, Cleveland, OH.

ELECTROMAGNETIC PROPAGATION IN PEC AND ABSORBING CURVED S-DUCTS

KENNETH J. BAUMEISTER 1988 27 p Proposed for presentation at the 1988 IEEE AP-S International Symposium and URSI Radio Science Meeting, Syracuse, N.Y., 6-10 Jun. 1988 (NASA-TM-100833; E-3507; NAS 1.15:100833) Avail: NTIS HC A03/MF A01 CSCL 20N

A finite-element Galerkin formulation has been developed to study transverse magnetic (TM) wave propagation in 2-D S-curved ducts with both perfectly conducting and absorbing walls. The reflection and transmission at the entrances and the exits of the curved ducts are determined by coupling the finite-element solutions in the curved ducts to the eigenfunctions of an infinite, uniform, perfectly conducting duct. Example solutions are presented for a double mitred and S-ducts of various lengths. The length of the S-duct is found to significantly effect the reflective characteristics of the duct. Also, the effect of curvature on an absorbing duct is illustrated. Author

N88-21389*# National Aeronautics and Space Administration. Lewis Research Center, Cleveland, OH.

MONOLITHIC MICROWAVE INTEGRATED CIRCUIT TECHNOLOGY FOR ADVANCED SPACE COMMUNICATION

GEORGE E. PONCHAK and ROBERT R. ROMANOFISKY Apr. 1988 14 p
(NASA-TM-100829; E-3848; NAS 1.15:100829) Avail: NTIS HC A03/MF A01 CSCL 09C

Future Space Communications subsystems will utilize GaAs Monolithic Microwave Integrated Circuits (MMIC's) to reduce volume, weight, and cost and to enhance system reliability. Recent advances in GaAs MMIC technology have led to high-performance devices which show promise for insertion into these next generation systems. The status and development of a number of these devices operating from Ku through Ka band will be discussed along with anticipated potential applications. Author

N88-23070*# National Aeronautics and Space Administration. Lewis Research Center, Cleveland, OH.

SPACE COMMUNICATION LINK PROPAGATION DATA FOR SELECTED CITIES WITHIN THE MULTIPLE BEAM AND STEERABLE ANTENNA COVERAGE AREAS OF THE ADVANCED COMMUNICATIONS TECHNOLOGY SATELLITE

ROBERT M. MANNING Apr. 1988 214 p
(NASA-TM-100861; E-4073; NAS 1.15:100861) Avail: NTIS HC A10/MF A01 CSCL 17B

Rain attenuation propagation data for 68 cities within the coverage area of the multiple beam and steerable antennas of the Advanced Communications Technology Satellite (ACTS) are presented. These data provide the necessary data base for purposes of communication link power budgeting and rain attenuation mitigation controller design. These propagation parameters are derived by applying the ACTS Rain Attenuation Prediction Model to these 68 locations. The propagation parameters

enumerated in tabular form for each location are as follows: (1) physical description of the link and location (e.g., latitude, longitude, antenna elevation angle, etc.), link availability versus attenuation margin (also in graphical form), fading time across fade depths of 3, 5, 8, and 15 dB versus fade duration, and required fade control response time for controller availabilities of 99.999, 99.99, 99.9, and 99 percent versus sub-threshold attenuation levels. The data for these specific locations can be taken to be representative of regions near these locations. Author

N88-23073*# National Aeronautics and Space Administration. Lewis Research Center, Cleveland, OH.

CASE STUDY OF ACTIVE ARRAY FEED COMPENSATION WITH SIDELobe CONTROL FOR REFLECTOR SURFACE DISTORTION

R. J. ACOSTA, A. J. M. ZAMAN, E. A. BOBINSKY, A. R. CHERRETTE, and S. W. LEE (Illinois Univ., Urbana-Champaign.) 1988 7 p Presented at the 1988 AP-S/URSI International Symposium, Syracuse, N.Y., 6-10 Jun. 1988; sponsored by IEEE (NASA-TM-100287; E-3932; NAS 1.15:100287) Avail: NTIS HC A02/MF A01 CSCL 20N

The feasibility of electromagnetically compensating for reflector surface distortions has been investigated. The performance characteristics (gain, sidelobe levels, etc.) of large communication antenna systems degrade as the reflector surface distorts mainly due to thermal effects from a varying solar flux. The techniques described in this report can be used to maintain the design performance characteristics independently of thermal effects on the reflector surface. With the advent of monolithic microwave integrated circuits (MMIC), a greater flexibility in array-fed reflector system design can be achieved. MMIC arrays provide independent control of amplitude and phase for each of many radiating elements of the feed array. It is assumed that the surface characteristics (x,y,z, its first and second derivatives) under distorted conditions are known. Author

N88-24847*# National Aeronautics and Space Administration. Lewis Research Center, Cleveland, OH.

CHARACTERIZATION OF A 30-GHZ IMPATT SOLID STATE AMPLIFIER

LAWRENCE W. WALD Jul. 1988 16 p
(NASA-TM-100876; E-4110; NAS 1.15:100876) Avail: NTIS HC A03/MF A01 CSCL 09A

Described are the characterization and testing of a 20 W solid state amplifier operating in the Ka band to be used in low cost experimental ground terminals. The amplifier was developed by the TRW Electronic Systems Group under NASA Contract NAS3-23266 as a proof-of-concept (POC) device in support of the Advanced Communications Technology Satellite (ACTS) program. Additional goals were development of high-power IMPATT devices and circulators, and multistage diode circuits, which are an integral part of the amplifier. The amplifier underwent acceptance testing at the NASA Lewis Research Center, Cleveland, Ohio. Characteristics measured include the output power of 42 dB m, gain of 30 dB, an injection-locking RF bandwidth of 260 MHz, and an overall direct current-to-radiofrequency (dc-to-RF) efficiency of 6.7 percent. Author

N88-25762*# National Aeronautics and Space Administration. Lewis Research Center, Cleveland, OH.

ACTIVE FEED ARRAY COMPENSATION FOR REFLECTOR ANTENNA SURFACE DISTORTIONS Ph.D. Thesis - Akron Univ., Ohio

ROBERTO J. ACOSTA Jun. 1988 177 p
(NASA-TM-100826; E-4015; NAS 1.15:100826) Avail: NTIS HC A09/MF A01 CSCL 20N

The feasibility of electromagnetic compensation for reflector antenna surface distortions is investigated. The performance characteristics of large satellite communication reflector antenna systems degrade as the reflector surface distorts, mainly due to thermal effects from solar radiation. The technique developed can be used to maintain the antenna boresight directivity and sidelobe level independent of thermal effects on the reflector surface. With

the advent of monolithic microwave integrated circuits (MMIC), a greater flexibility in array fed reflector antenna systems can be achieved. MMIC arrays provide independent control of amplitude and phase for each of the many radiating elements in the feed array. By assuming a known surface distortion profile, a simulation study is carried out to examine the antenna performance as a function of feed array size and number of elements. Results indicate that the compensation technique can effectively control boresight directivity and sidelobe level under peak surface distortion in the order of tenth of a wavelength. Author

N88-26566* National Aeronautics and Space Administration. Lewis Research Center, Cleveland, OH.

COSPAS/SARSAT 406-MHZ EMERGENCY BEACON DIGITAL CONTROLLER

WILLIAM D. IVANCIC Jul. 1988 18 p
(NASA-TM-100859; E-4064; NAS 1.15:100859) Avail: NTIS HC A03/MF A01 CSCL 20N

The digital control portion of a low-cost 406-MHz COSPAS/SARSAT emergency beacon has been designed and breadboarded at the NASA Lewis Research Center. This report discusses the requirements and design tradeoffs of the digital controller and describes the hardware and software design, which is available only to United States citizens and companies. Author

N88-27424* National Aeronautics and Space Administration. Lewis Research Center, Cleveland, OH.

ANALYTICAL APPROXIMATION OF A DISTORTED REFLECTOR SURFACE DEFINED BY A DISCRETE SET OF POINTS

ROBERTO J. ACOSTA and AFROZ A. ZAMAN 1988 15 p
Presented at the Antenna Applications Symposium, Monticello, Ill., 21-23 Sep. 1988; sponsored by Illinois Univ. and RADC
(NASA-TM-101323; E-4327; NAS 1.15:101323) Avail: NTIS HC A03/MF A01 CSCL 20N

Reflector antennas on Earth orbiting spacecrafts generally cannot be described analytically. The reflector surface is subjected to a large temperature fluctuation and gradients, and is thus warped from its true geometrical shape. Aside from distortion by thermal stresses, reflector surfaces are often purposely shaped to minimize phase aberrations and scanning losses. To analyze distorted reflector antennas defined by discrete surface points, a numerical technique must be applied to compute an interpolatory surface passing through a grid of discrete points. In this paper, the distorted reflector surface points are approximated by two analytical components: an undistorted surface component and a surface error component. The undistorted surface component is a best fit paraboloid polynomial for the given set of points and the surface error component is a Fourier series expansion of the deviation of the actual surface points, from the best fit paraboloid. By applying the numerical technique to approximate the surface normals of the distorted reflector surface, the induced surface current can be obtained using physical optics technique. These surface currents are integrated to find the far field radiation pattern. Author

N88-28222* National Aeronautics and Space Administration. Lewis Research Center, Cleveland, OH.

ARRAY TRADE-OFF STUDY USING MULTILAYER PARASITIC SUBARRAYS

A. ZAMAN, R. Q. LEE, and R. J. ACOSTA Sep. 1988 13 p
Presented at the Antenna Applications Symposium, Monticello, Ill., 21-23 Sep. 1988; sponsored in part by Illinois Univ., and by Rome Air Development Center
(NASA-TM-101321; E-4325; NAS 1.15:101321) Avail: NTIS HC A03/MF A01 CSCL 20N

The use of multilayer parasitic patch arrays in a microstrip phased array offers many potential advantages. An analytical study of microstrip arrays with high gain multilayer parasitic patch subarrays and conventional patch antennas is presented. It is indicated that a thinned array of half as many multilayer parasitic patch subarrays (per row and column) at twice the spacing will perform as well as the full array of ordinary patch antennas. The

criterion for comparison was array gain, 3 dB beamwidth and sidelobe level. The attendant reduction in the required number of patch antennas and consequently, MMIC phase shifters is very significant in terms of array complexity, cost and power loss.

NASA

N88-29077* Analox Corp., Cleveland, OH.

A STATISTICAL RAIN ATTENUATION PREDICTION MODEL WITH APPLICATION TO THE ADVANCED COMMUNICATION TECHNOLOGY SATELLITE PROJECT. 1: THEORETICAL DEVELOPMENT AND APPLICATION TO YEARLY PREDICTIONS FOR SELECTED CITIES IN THE UNITED STATES Final Report

ROBERT M. MANNING Sep. 1986 206 p

(Contract NAS3-24564)

(NASA-CR-179498; E-3187; NAS 1.26:179498) Avail: NTIS HC A10/MF A01 CSCL 20N

A rain attenuation prediction model is described for use in calculating satellite communication link availability for any specific location in the world that is characterized by an extended record of rainfall. Such a formalism is necessary for the accurate assessment of such availability predictions in the case of the small user-terminal concept of the Advanced Communication Technology Satellite (ACTS) Project. The model employs the theory of extreme value statistics to generate the necessary statistical rainrate parameters from rain data in the form compiled by the National Weather Service. These location dependent rain statistics are then applied to a rain attenuation model to obtain a yearly prediction of the occurrence of attenuation on any satellite link at that location. The predictions of this model are compared to those of the Crane Two-Component Rain Model and some empirical data and found to be very good. The model is then used to calculate rain attenuation statistics at 59 locations in the United States (including Alaska and Hawaii) for the 20 GHz downlinks and 30 GHz uplinks of the proposed ACTS system. The flexibility of this modeling formalism is such that it allows a complete and unified treatment of the temporal aspects of rain attenuation that leads to the design of an optimum stochastic power control algorithm, the purpose of which is to efficiently counter such rain fades on a satellite link. Author

33

ELECTRONICS AND ELECTRICAL ENGINEERING

Includes test equipment and maintainability; components, e.g., tunnel diodes and transistors; microminiaturization; and integrated circuitry.

A88-10481* National Aeronautics and Space Administration. Lewis Research Center, Cleveland, OH.

RADIATION CHARACTERISTICS OF MICROSTRIP ARRAYS WITH PARASITIC ELEMENTS

R. Q. LEE, R. ACOSTA (NASA, Lewis Research Center, Cleveland, OH), and K. F. LEE (Akron, University, OH) Electronics Letters (ISSN 0013-5194), vol. 23, July 30, 1987, p. 835-837. refs

Detailed experimental results on microstrip antennas consisting of one center-fed patch and several identical parasitic patches are presented. The effects of the number of elements and interelement spacing are studied for two configurations: a linear array and a five-element array. It is shown that placing identical parasitic elements adjacent to a fed patch permits broadside radiation patterns with significant enhancement in gain to be obtained without any degradation of the pattern characteristics. C.D.

A88-11865* National Aeronautics and Space Administration. Lewis Research Center, Cleveland, OH.

COAXIAL TUBE ARRAY SPACE TRANSMISSION LINE CHARACTERIZATION

33 ELECTRONICS AND ELECTRICAL ENGINEERING

COLLEEN A. SWITZER and DAVID J. BENTS (NASA, Lewis Research Center, Cleveland, OH) IN: IECEC '87; Proceedings of the Twenty-second Intersociety Energy Conversion Engineering Conference, Philadelphia, PA, Aug. 10-14, 1987. Volume 1. New York, American Institute of Aeronautics and Astronautics, 1987, p. 565-570. Previously announced in STAR as N87-22003.

The coaxial tube array tether/transmission line used to connect an SP-100 nuclear power system to the space station was characterized over the range of reactor-to-platform separation distances of 1 to 10 km. Characterization was done with respect to array performance, physical dimensions and masses. Using a fixed design procedure, a family of designs was generated for the same power level (300 kWe), power loss (1.5 percent), and meteoroid survival probability (99.5 percent over 10 yr). To differentiate between vacuum insulated and gas insulated lines, two different maximum values of the E field were considered: 20 kV/cm (appropriate to vacuum insulation) and 50 kV/cm (compressed SF₆). Core conductor, tube, bumper, standoff, spacer and bumper support dimensions, and masses were also calculated. The results of the characterization show mainly how transmission line size and mass scale with reactor-to-platform separation distance.

Author

A88-11878* Toledo Univ., OH.

FAST SIMULATION TECHNIQUES FOR SWITCHING CONVERTERS

ROGER J. KING (Toledo, University, OH) IN: IECEC '87; Proceedings of the Twenty-second Intersociety Energy Conversion Engineering Conference, Philadelphia, PA, Aug. 10-14, 1987. Volume 2. New York, American Institute of Aeronautics and Astronautics, 1987, p. 646-654. refs (Contract NAG3-708)

Techniques for simulating a switching converter are examined. The state equations for the equivalent circuits, which represent the switching converter, are presented and explained. The uses of the Newton-Raphson iteration, low ripple approximation, half-cycle symmetry, and discrete time equations to compute the interval durations are described. An example is presented in which these methods are illustrated by applying them to a parallel-loaded resonant inverter with three equivalent circuits for its continuous mode of operation.

I.F.

A88-15423* Case Western Reserve Univ., Cleveland, OH.

BEHAVIOR OF ION-IMPLANTED JUNCTION DIODES IN 3C SIC R. E. AVILA, J. J. KOPANSKI, and C. D. FUNG (Case Western Reserve University, Cleveland, OH) Journal of Applied Physics (ISSN 0021-8979), vol. 62, Oct. 15, 1987, p. 3469-3471. Research supported by the Universidad de Puerto Rico. refs (Contract NAG3-490; NAG3-389)

p-n junction diodes have been formed by ion implantation of B or Al in 3C SiC and annealing at 1365 C. The current-voltage characteristics of the Al-implanted structures show little rectification. The B-implanted diodes show rectification, with ideality factors of 2.2 and higher, breakdown voltages between 5 and 10 V, and a series resistance of the order of 20 kohm. The current-voltage characteristics were measured between room temperature and 270 C. The extracted ideality factors increase with temperature.

Author

A88-16133* National Aeronautics and Space Administration. Lewis Research Center, Cleveland, OH.

MONOLITHIC MICROWAVE INTEGRATED CIRCUIT (MMIC) TECHNOLOGY FOR SPACE COMMUNICATIONS APPLICATIONS

DENIS J. CONNOLLY, KUL B. BHASIN, and ROBERT R. ROMANOFKY (NASA, Lewis Research Center, Cleveland, OH) IAF, International Astronautical Congress, 38th, Brighton, England, Oct. 10-17, 1987. 17 p. Previously announced in STAR as N87-27883. refs (IAF PAPER 87-491)

Future communications satellites are likely to use gallium arsenide (GaAs) monolithic microwave integrated-circuit (MMIC) technology in most, if not all, communications payload subsystems.

Multiple-scanning-beam antenna systems are expected to use GaAs MMIC's to increase functional capability, to reduce volume, weight, and cost, and to greatly improve system reliability. RF and IF matrix switch technology based on GaAs MMIC's is also being developed for these reasons. MMIC technology, including gigabit-rate GaAs digital integrated circuits, offers substantial advantages in power consumption and weight over silicon technologies for high-throughput, on-board baseband processor systems. For the more distant future pseudomorphic indium gallium arsenide (InGaAs) and other advanced III-V materials offer the possibility of MMIC subsystems well up into the millimeter wavelength region. All of these technology elements are in NASA's MMIC program. Their status is reviewed.

Author

A88-18633* TRW Space Technology Labs., Redondo Beach, CA.

30-CM ELECTRON CYCLOTRON PLASMA GENERATOR

HANK GOEDE (TRW, Inc., TRW Space and Technology Group, Redondo Beach, CA) Journal of Spacecraft and Rockets (ISSN 0022-4650), vol. 24, Sept.-Oct. 1987, p. 437-443. refs (Contract NAS3-22473)

Experimental results on the development of a 30-cm-diam electron cyclotron resonance plasma generator are presented. This plasma source utilizes samarium-cobalt magnets and microwave power at a frequency of 4.9 GHz to produce a uniform plasma with densities of up to 3×10^{10} to the 11th/cu cm in a continuous fashion. The plasma generator contains no internal structures, and is thus inherently simple in construction and operation and inherently durable. The generator was operated with two different magnetic geometries. One used the rare-earth magnets arranged in an axial line cusp configuration, which directly showed plasma production taking place near the walls of the generator where the electron temperature was highest but with the plasma density peaking in the central low B-field regions. The second configuration had magnets arranged to form azimuthal line cusps with approximately closed electron drift surfaces; this configuration showed an improved electrical efficiency of about 135 eV/ion.

Author

A88-19659* National Aeronautics and Space Administration. Lewis Research Center, Cleveland, OH.

SUBMILLIMETER BACKWARD WAVE OSCILLATORS

J. A. DAYTON, V. O. HEINEN, N. STANKIEWICZ, and T. M. WALLETT (NASA, Lewis Research Center, Cleveland, OH) (NASA and SDIO, Submillimeter /Terahertz/ Receiver Technology Conference, Lake Arrowhead, CA, Apr. 7, 8, 1987) International Journal of Infrared and Millimeter Waves (ISSN 0195-9271), vol. 8, Oct. 1987, p. 1257-1268. refs

A NASA program for the development of backward wave oscillators (BWOs) for the 500-2000 GHz frequency range is discussed. The BWO operation is based on a periodic etched slow wave structure which supports the induced traveling electromagnetic wave. The present submillimeter wave BWOs will employ a variation of the folded wave guide, the interdigital line. The use of a noncompressed electron beam results in less thermal loading of the circuit, smaller magnetic focusing fields, and higher current density of the circuit interaction region. The diamond etching procedure is described. Aluminum will be used for the metallization of the diamonds.

R.R.

A88-19781* National Aeronautics and Space Administration. Lewis Research Center, Cleveland, OH.

BIT-ERROR-RATE TESTING OF HIGH-POWER 30-GHZ TRAVELING-WAVE TUBES FOR GROUND-TERMINAL APPLICATIONS

KURT A. SHALKHAUSER (NASA, Lewis Research Center, Cleveland, OH) IEEE Transactions on Electron Devices (ISSN 0018-9383), vol. ED-34, Dec. 1987, pt. 2, p. 2625-2633. refs

Tests were conducted at NASA Lewis to measure the bit-error-rate performance of two 30-GHz 200-W coupled-cavity traveling-wave tubes (TWTs). The transmission effects of each TWT on a band-limited 220-Mbit/s SMSK signal were investigated. The tests relied on the use of a recently developed digital simulation

and evaluation system constructed at Lewis as part of the 30/20-GHz technology development program. This paper describes the approach taken to test the 30-GHz tubes and discusses the test data. A description of the bit-error-rate measurement system and the adaptations needed to facilitate TWT testing are also presented. Author

A88-21605* National Aeronautics and Space Administration. Lewis Research Center, Cleveland, OH.

SPACE SOLAR CELL RESEARCH - PROBLEMS AND POTENTIAL

DENNIS J. FLOOD (NASA, Lewis Research Center, Cleveland, OH) IN: Photovoltaics for commercial solar power applications; Proceedings of the Meeting, Cambridge, MA, Sept. 18, 19, 1986. Bellingham, WA, Society of Photo-Optical Instrumentation Engineers, 1986, p. 34-39. Previously announced in STAR as N86-31793. refs

The value of a passive, maintenance-free, renewable energy source was immediately recognized in the early days of the space program, and the silicon solar cell, despite its infancy, was quickly pressed into service. Efficiencies of those early space solar arrays were low, and lifetimes shorter than hoped for, but within a decade significant advances had been made in both areas. Better performance was achieved because of a variety of factors, ranging from improvements in silicon single crystal material, to better device designs, to a better understanding of the factors that affect the performance of a solar cell in space. Chief among the latter, particularly for the mid-to-high altitude (HEO) and geosynchronous (GEO) orbits, are the effects of the naturally occurring particulate radiation environment. Although not as broadly important to the photovoltaic community at large as increased efficiency, the topic of radiation damage is critically important to use of solar cells in space, and is a major component of the NASA research program in space photovoltaics. This paper will give a brief overview of some of the opportunities and challenges for space photovoltaic applications, and will discuss some of the current research directed at achieving high efficiency and controlling the effects of radiation damage in space solar cells. Author

A88-22704* Hampden-Sydney Coll., VA.

GIGARAD-TOLERANT POWER SWITCHES AND MEMORY ELEMENTS

W. T. JOYNER, G. F. BECKNELL, and J. M. A. DONELSON (Hampden-Sydney College, VA) IN: Space nuclear power systems 1986; Proceedings of the Third Symposium, Albuquerque, NM, Jan. 13-16, 1986. Malabar, FL, Orbit Book Co., Inc., 1987, p. 333-339. refs (Contract NAG3-605)

A new class of silicon devices operating without p-n junctions has been studied for radiation hardness. The electric field in these devices is uniform over most of the device, thus causing high-voltage breakdown to increase with electrode spacing. Deep acceptor levels are created in the silicon by diffusing gold atoms into the lattice, or by electron radiation. These acceptor levels, near the center of the band gap, trap out electrons so that the low resistivity of the n-type doped wafer can be raised to intrinsic resistivity. Switching between a high-resistivity state at low currents and a low-resistivity state at high currents occurs at a definite threshold voltage, exhibiting characteristics similar to silicon-controlled rectifiers. Compensating 0.1 ohm-meter (10 ohm-cm) silicon wafers requires electron fluxes of 10 to the 23rd electrons per square meter (10 to the 19th electrons per square centimeter). Experiments demonstrating gamma tolerance to 1 Gigarad(Si) are described. Calculations for maximum tolerable neutron fluence are shown, and a phenomenological explanation for these results is presented. Author

A88-24911* National Aeronautics and Space Administration. Lewis Research Center, Cleveland, OH.

MICROWAVE PERFORMANCE OF AN OPTICALLY CONTROLLED ALGAS/GAAS HIGH ELECTRON MOBILITY TRANSISTOR AND GAAS MESFET

RAINEE N. SIMONS (NASA, Lewis Research Center, Cleveland,

OH) IEEE Transactions on Microwave Theory and Techniques (ISSN 0018-9480), vol. MTT-35, Dec. 1987, p. 1444-1455. Previously announced in STAR as N87-17993. refs

Direct current and also the microwave characteristics of optically illuminated AlGaAs/GaAs HEMT are experimentally measured for the first time and compared with that of GaAs MESFET. The results showed that the average increase in the gain is 2.89 dB under 1.7 mW optical intensity at 0.83 microns. Further, the effect of illumination on S-parameters is more pronounced when the devices are biased close to pinch off. Novel applications of optically illuminated HEMT as a variable gain amplifier, high speed high frequency photodetector, and mixer are demonstrated. Author

A88-27558*# Communications Satellite Corp., Clarksburg, MD.

A FLEXIBLE ON-BOARD DEMULTIPLEXER/DEMULATOR

S. JOSEPH CAMPANELLA and SOHEIL SAYEGH (COMSAT Laboratories, Clarksburg, MD) IN: AIAA International Communication Satellite Systems Conference, 12th, Arlington, VA, Mar. 13-17, 1988, Technical Papers. Washington, DC, American Institute of Aeronautics and Astronautics, 1988, p. 299-303. (Contract NAS3-24885)

(AIAA PAPER 88-0811)

Optimization of satellite communications system performance from the point of view of reduced overall system cost per unit of service delivered, requires that economies be exercised at all levels. Introduction of onboard regeneration which necessarily involves on-board demultiplexing and demodulation is an essential ingredient in meeting this goal. To achieve maximum benefit from this approach, the uplink transmission data rate and bandwidth from each earth terminal and consequently uplink EIRP needs to be minimized. This necessarily introduces multiple carriers of different bandwidths on the uplinks and creates an attending need onboard for simultaneous demodulation of many carriers. This paper addresses a digitally implemented bulk demultiplexer/demodulator that processes a large number of carriers having differing carrier bandwidths, bit rates and center frequencies. The device is programmable from the ground to accommodate changes in the complexion of the carriers. Author

A88-27559*# Ford Aerospace and Communications Corp., Palo Alto, CA.

BANDWIDTH AND POWER EFFICIENT SATELLITE TDMA DEMULATOR AND DECODER

STEPHEN A. AMES, PAUL A. MONTE, CHRISTOPHER F. HOEBER, and FRANK CHETHIK (Ford Aerospace and Communications Corp., Western Development Laboratories Div., Palo Alto, CA) IN: AIAA International Communication Satellite Systems Conference, 12th, Arlington, VA, Mar. 13-17, 1988, Technical Papers. Washington, DC, American Institute of Aeronautics and Astronautics, 1988, p. 304-312. Research supported by Ford Aerospace and Communications Corp. refs (Contract NAS3-24678)

(AIAA PAPER 88-0812)

A proof-of-concept demodulator for TDMA applications requiring high total data rates composed of many low data rate users is proposed. High-spectrum efficiency is obtained via a bandwidth efficient combined modulation and coding system, and low TDMA overhead is obtained via a fast acquiring digital phase lock loop. The system employs a data rate of 200 Mb/s with a bit error rate of better than 5×10^{-6} to the -7 th in the presence of adjacent channel interference 20 dB above the weakest user. The 8-PSK modulation combined with the rate 5/6 forward error correction coding results in a bandwidth efficiency of better than 2 bits/second per Hz. R.R.

A88-27572*# National Aeronautics and Space Administration. Lewis Research Center, Cleveland, OH.

THE BIT-ERROR RATE PERFORMANCE OF A SATELLITE MICROWAVE MATRIX SWITCH

ROBERT J. KERCZEWSKI (NASA, Lewis Research Center, Cleveland, OH) IN: AIAA International Communication Satellite Systems Conference, 12th, Arlington, VA, Mar. 13-17, 1988,

33 ELECTRONICS AND ELECTRICAL ENGINEERING

Technical Papers. Washington, DC, American Institute of Aeronautics and Astronautics, 1988, p. 403-414. refs (AIAA PAPER 88-0826)

The matrix switch is a critical element of communications satellites employing multiple beam antennas and on-board switching. Two proof-of-concept models of a microwave matrix switch have been developed under NASA-sponsored contracts. These switches have undergone extensive testing at NASA Lewis Research Center to determine their operating characteristics in a system environment. The results of these tests indicate the effect of the matrix switch on the overall system operation. Author

**A88-27575*# Motorola, Inc., Chandler, AZ.
HARDWARE REALIZATION OF A BASEBAND PROCESSOR
FOR A SS-FDMA/TDMA/DAMA SYSTEM**

RICHARD L. MOAT and DAVID R. CARROLL (Motorola, Inc., Government Electronics Group, Chandler, AZ) IN: AIAA International Communication Satellite Systems Conference, 12th, Arlington, VA, Mar. 13-17, 1988, Technical Papers. Washington, DC, American Institute of Aeronautics and Astronautics, 1988, p. 430-437. Research supported by TRW, Inc. refs (Contract NAS3-23790) (AIAA PAPER 88-0830)

Hardware implementation of the NASA ACTS baseband processor is described which achieves the system message data handling performance required to perform satellite switching of high-rate baseband data. The hardware meets payload specifications for size, weight, and power. Hardware redundancy applied to critical paths in several functional areas insures that the reliability and life expectancy requirements are fulfilled. The remote reprogrammability of the processor message data handling and routing functions provides system flexibility for dynamic reconfiguration during rapidly changing traffic loads. R.R.

**A88-27578*# National Aeronautics and Space Administration.
Lewis Research Center, Cleveland, OH.
HIGH EFFICIENCY, LONG LIFE TRAVELING WAVE TUBES
FOR FUTURE COMMUNICATIONS SATELLITES**

J. A. DAYTON, JR. (NASA, Lewis Research Center, Cleveland, OH) IN: AIAA International Communication Satellite Systems Conference, 12th, Arlington, VA, Mar. 13-17, 1988, Technical Papers. Washington, DC, American Institute of Aeronautics and Astronautics, 1988, p. 452-456. refs (AIAA PAPER 88-0835)

Electron beam devices, primarily traveling wave tubes (TWTs), have been used as the power amplifiers in almost all space communications and data transmission systems. Based on the technology that is presently available and the expected success of current research efforts, it is reasonable to predict the development of a new class of microwave TWTs with efficiencies in excess of 60 percent and lifetimes of at least ten years. Because of this rapid advance of technology, the TWT is expected to remain the dominant device for power amplifiers in space. Author

**A88-28673* National Aeronautics and Space Administration.
Lewis Research Center, Cleveland, OH.**

**A RE-EXAMINATION OF SPENT BEAM REFocusing FOR
HIGH-EFFICIENCY HELIX TWT'S AND SMALL MDC'S**

PETER RAMINS, SHELLY PEET, and DALE A. FORCE (NASA, Lewis Research Center, Cleveland, OH) IEEE Transactions on Electron Devices (ISSN 0018-9383), vol. 35, pt. 2, April 1988, p. 539-548. refs

The usefulness of the concept of spent-beam refocusing in optimizing the performance of low- and medium-power helix TWTs (traveling-wave tubes) equipped with small multistage depressed collectors (MDCs) is examined. Several direct comparisons of the performance of individually optimized TWT-MDC combinations with and without controlled beam expansion and recollimation are presented. The collector efficiency of a number of representative space and airborne TWT-MDCs, which do not use refocusing, is compared to a measure of quality (standard of excellence) established by an examination of irrecoverable MDC losses. The results suggest that the application of the traditional concept of

spent-beam refocusing to most helix TWTs that are equipped with small MDCs in order to obtain maximum efficiency is not required (or even desired). Two effects combine to obviate the need for refocusing: 1) the unexpanded beam more nearly meets the 'point source' ideal at the input to the small MDC, and 2) the larger space-charge spreading and the slightly larger (but manageable) injection angles of the unexpanded beam can reduce the amount of backstreaming current and the attendant loss in efficiency. I.E.

**A88-29821* Honeywell, Inc., Bloomington, MN.
TWO STAGE DUAL GATE MESFET MONOLITHIC GAIN
CONTROL AMPLIFIER FOR KA-BAND**

V. SOKOLOV, J. GEDDES, and A. CONTOLATIS (Honeywell Physical Sciences Center, Bloomington, MN) IN: IEEE, 1987 Microwave and Millimeter-Wave Monolithic Circuits Symposium, Las Vegas, NV, June 8, 9, 1987, Proceedings. New York, Institute of Electrical and Electronics Engineers, 1987, p. 75-79. refs (Contract NAS3-23356)

A monolithic two stage gain control amplifier has been developed using submicron gate length dual gate MESFETs fabricated on ion implanted material. The amplifier has a gain of 12 dB at 30 GHz with a gain control range of over 30 dB. This ion implanted monolithic IC is readily integrable with other phased array receiver functions such as low noise amplifiers and phase shifters. Author

**A88-32836* National Aeronautics and Space Administration.
Lewis Research Center, Cleveland, OH.**

**HIGH-EFFICIENCY HELICAL TRAVELING-WAVE TUBE WITH
DYNAMIC VELOCITY TAPER AND ADVANCED MULTISTAGE
DEPRESSED COLLECTOR**

ARTHUR N. CURREN, RAYMOND W. PALMER, DALE A. FORCE (NASA, Lewis Research Center, Cleveland, OH), LOUIS DOMBO, and JAMES A. LONG (Watkins-Johnson Co., Palo Alto, CA) IN: IEDM - International Electron Devices Meeting, Washington, DC, Dec. 6-9, 1987, Proceedings. New York, Institute of Electrical and Electronics Engineers, 1987, p. 473-476. refs

A NASA-sponsored research and development contract has been established with the Watkins-Johnson Company to fabricate high-efficiency 20-watt helical traveling wave tubes (TWTs) operating at 8.4 to 8.43 GHz. The TWTs employ dynamic velocity tapers (DVTs) and advanced multistage depressed collectors (MDCs) having electrodes with low secondary electron emission characteristics. The TWT designs include two different DVTs; one for maximum efficiency and the other for minimum distortion and phase shift. The MDC designs include electrodes of untreated and ion-textured graphite as well as copper which has been treated for secondary electron emission suppression. Objectives of the program include achieving at least 55 percent overall efficiency. Tests with the first TWTs (with undepressed collectors) indicate good agreement between predicted and measured RF efficiencies with as high as 30 percent improvement in RF efficiency over conventional helix designs. Author

**A88-34249* Cleveland State Univ., OH.
SELF-CONSISTENT CALCULATIONS AND DESIGN
CONSIDERATIONS FOR A GAAS NIPI DOPING
SUPERLATTICE SOLAR CELL**

RALPH O. CLARK, CHANDRA GORADIA (Cleveland State University, OH), and DAVID BRINKER (NASA, Lewis Research Center, Cleveland, OH) IN: IEEE Photovoltaic Specialists Conference, 19th, New Orleans, LA, May 4-8, 1987, Proceedings. New York, Institute of Electrical and Electronics Engineers, Inc., 1987, p. 133-139. NASA-supported research. refs

The authors present design constraints which show that a previously proposed GaAs nipi doping superlattice solar cell structure would not work as an efficient space solar cell. A structure based on the CLEFT process, which shows promise of being an efficient cell with very high radiation tolerance, is proposed. In order to test theoretically its viability and to optimize its design, self-consistent quantum mechanical calculations were made for a number of thicknesses of the n, i, and p layers and the dopings

in the n and p layers. These results show that: 1) an i layer is not necessary; in fact, its presence makes it difficult to satisfy one of the key constraints; 2) a near-optimum design with 750-Å thick n and p layers with dopings of $2.5 \times 10^{18}/\text{cm}^3$ and a selective contact separation of 20 microns would yield both high efficiency and very high radiation tolerance. I.E.

A88-34286* National Aeronautics and Space Administration. Lewis Research Center, Cleveland, OH.

LASER INDUCED OMCVD GROWTH OF ALGAS ON GAAS

DAVID M. WILT, JOSEPH D. WARNER, PAUL R. ARON, JOHN J. POUCH, and RICHARD W. HOFFMAN, JR. (NASA, Lewis Research Center, Cleveland, OH) IN: IEEE Photovoltaic Specialists Conference, 19th, New Orleans, LA, May 4-8, 1987, Proceedings. New York, Institute of Electrical and Electronics Engineers, Inc., 1987, p. 352-355. refs

A major factor limiting the efficiency of the GaAs-GaAlAs solar cell is the rate of recombination at the GaAs-AlGaAs interface. Evidence has been previously reported which indicates that recombination at this interface can be greatly reduced if the AlGaAs layer is grown at lower than normal temperatures. The authors examine the epitaxial growth of AlGaAs on GaAs using a horizontal OMCVD reactor and an excimer laser operating in the UV ($\lambda = 193 \text{ nm}$) region. The growth temperatures were 450 and 500 °C. The laser beam was utilized in two orientations: 75 deg angle of incidence and parallel to the substrate. Film composition and structure were determined by Auger electron spectroscopy (AES) and transmission electron microscopy (TEM). Auger analysis of epilayers grown at 500 °C with the laser impinging show no carbon or oxygen contamination of the epitaxial layers or interfaces. TEM diffraction patterns of these same epilayers exhibit single crystal (100) zone axis patterns. I.E.

A88-34298* National Aeronautics and Space Administration. Lewis Research Center, Cleveland, OH.

PIEZORESISTANCE AND SOLAR CELL EFFICIENCY

VICTOR G. WEIZER (NASA, Lewis Research Center, Cleveland, OH) IN: IEEE Photovoltaic Specialists Conference, 19th, New Orleans, LA, May 4-8, 1987, Proceedings. New York, Institute of Electrical and Electronics Engineers, Inc., 1987, p. 411-416. refs

Diffusion-induced stresses in silicon are shown to result in large localized changes in the minority-carrier mobility which in turn can have a significant effect on cell output. Evidence is given that both compressive and tensile stresses can be generated in either the emitter or the base region. Tensile stresses in the base appear to be much more effective in altering cell performance than do compressive stresses. While most stress-related effects appear to degrade cell efficiency, this is not always the case. Evidence is presented showing that arsenic-induced stresses can result in emitter characteristics comparable to those found in the MINP cell without requiring a high degree of surface passivation. I.E.

A88-34300* National Aeronautics and Space Administration. Lewis Research Center, Cleveland, OH.

A V-GROOVED ALGAS/GAAS PASSIVATED PN JUNCTION

S. G. BAILEY, R. P. LEON, and A. ARRISON (NASA, Lewis Research Center, Cleveland, OH) IN: IEEE Photovoltaic Specialists Conference, 19th, New Orleans, LA, May 4-8, 1987, Proceedings. New York, Institute of Electrical and Electronics Engineers, Inc., 1987, p. 421-426. refs

A passivated, V-grooved GaAs solar cell offers important advantages in terms of improved optical coupling, higher short-circuit current, and increased tolerance to particle radiation when compared to the planar cell configuration. An AlGaAs epilayer has been deposited on a p-type GaAs epilayer grown on an n-type V-grooved GaAs surface using MOCVD. A wet chemical etching process was used to produce a V-pattern with a 7.0-micron periodicity. Reflectivity measurements substantiate the expected decrease in solar reflectance. Scanning electron microscopy techniques were used to confirm the presence of the AlGaAs layer and verify the existence of a pn junction. Author

A88-34321* National Aeronautics and Space Administration. Lewis Research Center, Cleveland, OH.

RADIATION AND TEMPERATURE EFFECTS IN GALLIUM ARSENIDE, INDIUM PHOSPHIDE, AND SILICON SOLAR CELLS

I. WEINBERG, C. K. SWARTZ, R. E. HART, JR. (NASA, Lewis Research Center, Cleveland, OH), and R. L. STATLER (U.S. Navy, Naval Research Laboratory, Washington, DC) IN: IEEE Photovoltaic Specialists Conference, 19th, New Orleans, LA, May 4-8, 1987, Proceedings. New York, Institute of Electrical and Electronics Engineers, Inc., 1987, p. 548-557. Previously announced in STAR as N87-22098. refs

The effects of radiation on performance are determined for both n+p and p+n GaAs and InP cells and for silicon n+p cells. It is found that the radiation resistance of InP is greater than that of both GaAs and Si under 1-MeV electron irradiation. For silicon, the observed decreased radiation resistance with decreased resistivity is attributed to the presence of a radiation-induced boron-oxygen defect. Comparison of radiation damage in both p+n and n+p GaAs yields a decreased radiation resistance for the n+p cell attributable to increased series resistance, decreased shunt resistance, and relatively greater losses in the cell's p-region. For InP, the n+p configuration is found to have greater radiation resistance than the p+n cell. The increased loss in this latter cell is attributed to losses in the cell's emitter region. Temperature dependency results are interpreted using a theoretical relation for dV_{oc}/dT , which predicts that increased V_{oc} should result in decreased numerical values for dP_m/dT . The predicted correlation is observed for GaAs but not for InP, a result which is attributed to variations in cell processing. Author

A88-34340* Cleveland State Univ., OH.

RADIATION DAMAGE AND DEFECT BEHAVIOR IN PROTON IRRADIATED LITHIUM-COUNTERDOPED N+P SILICON SOLAR CELLS

JOHN STUPICA, CHANDRA GORADIA (Cleveland State University, OH), CLIFFORD K. SWARTZ, and IRVING WEINBERG (NASA, Lewis Research Center, Cleveland, OH) IN: IEEE Photovoltaic Specialists Conference, 19th, New Orleans, LA, May 4-8, 1987, Proceedings. New York, Institute of Electrical and Electronics Engineers, Inc., 1987, p. 650-653. refs

Two lithium-counterdoped n+p silicon solar cells with different lithium concentrations were irradiated by 10-MeV protons. Cell performance was measured as a function of fluence, and it was found that the cell with the highest concentration of lithium had the highest radiation resistance. Deep level transient spectroscopy which showed two deep level defects that were lithium related. Relating the defect energy levels obtained from this study with those from earlier work using 1-MeV electron irradiation shows no correlation of the defect energy levels. There is one marked similarity: the absence of the boron-interstitial-oxygen-interstitial defect. This consistency strengthens the belief that lithium interacts with oxygen to prevent the formation of the boron interstitial-oxygen interstitial defect. The results indicate that, in general, addition of lithium in small amounts to the p-base of a boron doped silicon solar cell such that the base remains p-type, tends to increase the radiation resistance of the cell. I.E.

A88-34356* National Aeronautics and Space Administration. Lewis Research Center, Cleveland, OH.

RADIATION PERFORMANCE OF ALGAS AND INGAAS CONCENTRATOR CELLS AND EXPECTED PERFORMANCE OF CASCADE STRUCTURES

H. B. CURTIS, C. K. SWARTZ, and R. E. HART, JR. (NASA, Lewis Research Center, Cleveland, OH) IN: IEEE Photovoltaic Specialists Conference, 19th, New Orleans, LA, May 4-8, 1987, Proceedings. New York, Institute of Electrical and Electronics Engineers, Inc., 1987, p. 727-732. Previously announced in STAR as N88-12878.

Aluminum gallium arsenide, GaAs, silicon and InGaAs cells have been irradiated with 1-MeV electrons and 37-MeV protons. These cells are candidates for individual cells in a cascade structure.

33 ELECTRONICS AND ELECTRICAL ENGINEERING

Data are presented for both electron and proton irradiation studies for one sun and a concentration level of 100X AM0. Results of calculations on the radiation resistance of cascade cell structures based on the individual cell data are also presented. Both series-connected and separately connected structures are investigated. Author

A88-34370* National Aeronautics and Space Administration. Lewis Research Center, Cleveland, OH.
DIFFUSION LENGTH MEASUREMENT IN BULK AND EPITAXIALLY GROWN III-V SEMICONDUCTORS USING CHARGE COLLECTION MICROSCOPY

R. P. LEON (NASA, Lewis Research Center, Cleveland, OH) IN: IEEE Photovoltaic Specialists Conference, 19th, New Orleans, LA, May 4-8, 1987, Proceedings. New York, Institute of Electrical and Electronics Engineers, Inc., 1987, p. 808-812. Previously announced in STAR as N87-27121. refs

Diffusion lengths and surface recombination velocities were measured in GaAs diodes and InP finished solar cells. The basic technique used was charge collection microscopy, also known as electron beam induced current (EBIC). The normalized currents and distances from the pn junction were read directly from the calibrated curves obtained while using the line-scan mode in an SEM. These values were then equated to integral and infinite series expressions resulting from the solution of the diffusion equation with both extended-generation and point-generation functions. This expands previous work by examining both thin and thick samples. The surface recombination velocity was either treated as an unknown in a system of two equations or measured directly using low e^{-} beam accelerating voltages. These techniques give accurate results by accounting for the effects of surface recombination and the finite size of the generation volume. Author

A88-37844* National Aeronautics and Space Administration. Lewis Research Center, Cleveland, OH.
PROGRESS IN MMIC TECHNOLOGY FOR SATELLITE COMMUNICATIONS

EDWARD J. HAUGLAND and REGIS F. LEONARD (NASA, Lewis Research Center, Cleveland, OH) IN: MILCOM '87 - IEEE Military Communications Conference, Washington, DC, Oct. 19-22, 1987, Conference Record. Volume 2. New York, Institute of Electrical and Electronics Engineers, Inc., 1987, p. 666-668.

NASA's Lewis Research Center is actively involved in the development of monolithic microwave and millimeter-wave integrated circuits (MMICs). The approach of the program is to support basic research under grant or in-house, while MMIC development is done under contract, thereby facilitating the transfer of technology to users. Preliminary thrusts of the program have been the extension of technology to higher frequencies (60 GHz), degrees of complexity, and performance (power, efficiency, noise figure) by utilizing novel circuit designs, processes, and materials. A review of the progress made so far is presented. I.E.

A88-38796* Virginia Polytechnic Inst. and State Univ., Blacksburg.

IMPLEMENTATION OF OPTIMAL TRAJECTORY CONTROL OF SERIES RESONANT CONVERTER

RAMESH ORUGANTI, JAMES J. YANG, and FRED C. LEE (Virginia Polytechnic Institute and State University, Blacksburg) IN: PESC '87 - Annual IEEE Power Electronics Specialists Conference, 18th, Blacksburg, VA, June 21-26, 1987, Record. New York, Institute of Electrical and Electronics Engineers, Inc., 1987, p. 451-459. refs (Contract NAG3-551)

Due to the presence of a high-frequency LC tank circuit, the dynamics of a resonant converter are unpredictable. There is often a large surge of tank energy during transients. Using state-plane analysis technique, an optimal trajectory control utilizing the desired solution trajectory as the control law was previously proposed for the series resonant converters. The method predicts the fastest response possible with minimum energy surge in the resonant tank. The principle of the control and its experimental

implementation are described here. The dynamics of the converter are shown to be close to time-optimal. I.E.

A88-38822* National Aeronautics and Space Administration. Lewis Research Center, Cleveland, OH.

A NEW MODEL FOR BROADBAND WAVEGUIDE-TO-MICROSTRIP TRANSITION DESIGN

GEORGE E. PONCHAK and ALAN N. DOWNEY (NASA, Lewis Research Center, Cleveland, OH) Microwave Journal (ISSN 0192-6225), vol. 31, May 1988, p. 333-335, 337 (4 ff.). Previously announced in STAR as N87-16958. refs

A new model is presented which permits the prediction of the resonant frequencies created by antipodal finline waveguide to microstrip transitions. The transition is modeled as a tapered transmission line in series with an infinite set of coupled resonant circuits. The resonant circuits are modeled as simple microwave resonant cavities of which the resonant frequencies are easily determined. The model is developed and the resonant frequencies determined for several different transitions. Experimental results are given to confirm the models. Author

A88-44170* Illinois Univ., Urbana.

SLOTLINE FED MICROSTRIP ANTENNA ARRAY MODULES

Y. T. LO, M. L. OBERHART, J. S. BRENNEMAN, P. AOYAGI, J. MOORE (Illinois, University, Urbana), and R. Q. H. LEE (NASA, Lewis Research Center, Cleveland, OH) Microwave and Optical Technology Letters (ISSN 0895-2477), vol. 1, March 1988, p. 26-29. NASA-USAF-supported research.

A feed network comprised of a combination of coplanar waveguide and slot transmission line is described for use in an array module of four microstrip elements. Examples of the module incorporating such networks are presented as well as experimentally obtained impedance and radiation characteristics. Author

A88-45755* Ohio State Univ., Columbus.
MODAL ATTENUATION IN MULTILAYERED COATED WAVEGUIDES

RI-CHEE CHOU (Ohio State University, Columbus) and SHUNG-WU LEE (Illinois, University, Urbana) IEEE Transactions on Microwave Theory and Techniques (ISSN 0018-9480), vol. 36, July 1988, p. 1167-1176. refs (Contract NAG3-475)

Propagation and attenuation constants of low-order normal modes in a circular waveguide lined with lossy coating layers are calculated using a generalized dispersion equation. It is found that the use of multilayered coating can significantly enhance modal attenuations over a broader frequency range compared to that for a single-layer coated structure. For a cylinder with radius $a = 2\lambda$, the attenuation constants for the dominant modes are shown to increase by 20 dB per a by adding a lossless padding layer to a lossy magnetic coating. Application of this result in radar cross-section (RCS) reduction is discussed. I.E.

A88-47599* Michigan Univ., Ann Arbor.
MICROWAVE AND MILLIMETER-WAVE POWER GENERATION IN SILICON CARBIDE AVALANCHE DEVICES

I. MEHDI, G. I. HADDAD, and R. K. MAINS (Michigan, University, Ann Arbor) Journal of Applied Physics (ISSN 0021-8979), vol. 64, Aug. 1, 1988, p. 1533-1540. refs (Contract NAG3-618)

Numerical simulations were performed to investigate the typical power-generating capabilities of SiC IMPATT diodes. Using available material parameters, SiC double-drift IMPATT diodes were simulated at 10, 35, 60, and 94 GHz, and the operating characteristics of these devices were compared to those of Si and GaAs devices. Compared to the Si and GaAs IMPATT performances in the pulsed mode, the SiC IMPATT performance was found to be far superior. The performance of SiC devices in the CW mode was also superior to that of GaAs devices, especially at lower frequencies. At a high frequency (94 GHz), the performance of the SiC device was found to be comparable to that of Si devices. I.S.

A88-49760* National Aeronautics and Space Administration. Lewis Research Center, Cleveland, OH.

HIGH TC SCREEN-PRINTED YBA₂CU₃O(7-x) FILMS - EFFECT OF THE SUBSTRATE MATERIAL

NAROTTAM P. BANSAL, RAINEE N. SIMONS (NASA, Lewis Research Center, Cleveland, OH), and D. E. FARRELL (Case Western Reserve University, Cleveland, OH) Applied Physics Letters (ISSN 0003-6951), vol. 53, Aug. 15, 1988, p. 603-605. refs

Thick films of YBa₂Cu₃O(7-x) have been deposited on highly polished alumina, magnesia spinel, nickel aluminum titanate (Ni-Al-Ti), and barium tetratitanate (Ba-Ti) substrates by the screen printing technique. Properties of the films were found to be highly sensitive to the choice of the substrate material. The film on Ba-Ti turned green after firing, due to a reaction with the substrate and were insulating. A film on Ni-Al-Ti had a T_c (onset) of about 95 K and lost 90 percent of its resistance by about 75 K. However, even at 4 K it was not fully superconducting, possibly due to a reaction between the film and the substrate and interdiffusion of the reaction products. The film on alumina had T_c (onset) of about 96 K, T_c (zero) of about 66 K, and Delta T_c of about 10 K. The best film was obtained on spinel and had T_c (onset) of about 94 K, zero resistance at 81 K, and a transition width of about 7 K. Author

A88-53396* Pittsburgh Univ., PA.

LOW-TEMPERATURE PHOTOLUMINESCENCE STUDIES OF CHEMICAL-VAPOR-DEPOSITION-GROWN 3C-SIC ON SI

W. J. CHOYKE (Pittsburgh, University; Westinghouse Research and Development Center, Pittsburgh, PA), Z. C. FENG (Pittsburgh, University, PA), and J. A. POWELL (NASA, Lewis Research Center, Cleveland, OH) Journal of Applied Physics (ISSN 0021-8979), vol. 64, Sept. 15, 1988, p. 3163-3175. refs (Contract NAG3-603; NSF DMR-84-03596)

Low-temperature photoluminescence studies of 26 cubic SiC films, ranging in thickness from 600 Å to 25 microns, grown by CVD on (100)Si are presented. It is suggested that the G band near 1.90-1.92 eV and its phonon side bands G1 and G2 are related to dislocations and extended defects. Formulas for the band-gap shift due to an axial stress have been obtained and applied to the CVD 3C-SiC/Si system. The results indicate that a 1-3-micron transition layer greatly reduces the interface misfit strain, and that biaxial stress in the SiC/Si system depresses the intensity of the no-phonon line. R.R.

A88-53397* Pittsburgh Univ., PA.

RAMAN SCATTERING STUDIES OF

CHEMICAL-VAPOR-DEPOSITED CUBIC SIC FILMS OF (100)SI

Z. C. FENG, A. J. MASCARENHAS (Pittsburgh, University, PA), W. J. CHOYKE (Pittsburgh, University; Westinghouse Research and Development Center, Pittsburgh, PA), and J. A. POWELL (NASA, Lewis Research Center, Cleveland, OH) Journal of Applied Physics (ISSN 0021-8979), vol. 64, Sept. 15, 1988, p. 3176-3186. refs (Contract NAG3-603; NSF DMR-84-03596)

Raman scattering studies for a series of CVD-grown cubic SiC single-crystal films with film thickness from 600 Å to 17 microns are discussed. The results suggest that the crystalline orientations of the Si substrate and the 3C-SiC film are the same. It is found that the Si 522/cm phonon from a Si wafer is enhanced in intensity by a factor of 2-3 due to a CVD overlayer of cubic SiC, and that the 3C-SiC longitudinal optical phonon at the Gamma point from SiC/Si samples is enhanced by a factor of two or three following the removal of the Si substrate. The variation of the Raman spectrum with incident power is investigated, and a method for determining the Raman cross section for 3 C-SiC is proposed. R.R.

A88-54711* Wisconsin Univ., Madison.

FIELD ORIENTED CONTROL OF AN INDUCTION MACHINE IN A HIGH FREQUENCY LINK POWER SYSTEM

SEUNG K. SUL and THOMAS A. LIPO (Wisconsin, University, Madison) IN: PESC '88 - Annual IEEE Power Electronics

Specialists Conference, 19th, Kyoto, Japan, Apr. 11-14, 1988, Record. Volume 2. New York, Institute of Electrical and Electronics Engineers, 1988, p. 1084-1090. refs (Contract NAG3-786)

A field-oriented controlled induction machine drive operating with a high-frequency single-phase sinusoidal voltage link is presented. System performance is investigated by computer simulation and is verified by a test on a prototype system. A novel control loop to minimize the link voltage fluctuation is proposed. The capability of rapid demagnetization of the induction machine by current regulation is investigated. A current-modulation technique termed mode control is proposed, and its performance is compared with that of the conventional delta-modulation technique. I.E.

A88-54713* Toledo Univ., OH.

A CASCADED SCHWARZ CONVERTER FOR HIGH FREQUENCY POWER DISTRIBUTION

BISWAJIT RAY and THOMAS A. STUART (Toledo, University, OH) IN: PESC '88 - Annual IEEE Power Electronics Specialists Conference, 19th, Kyoto, Japan, Apr. 11-14, 1988, Record. Volume 2. New York, Institute of Electrical and Electronics Engineers, 1988, p. 1199-1206. USAF-supported research. refs (Contract NAG3-708)

It is shown that two Schwarz converters in cascade provide a very reliable 20-kHz source that features zero current commutation, constant frequency, and fault-tolerant operation, meeting requirements for spacecraft applications. A steady-state analysis of the converter is presented, and equations for the steady-state performance are derived. Fault-current limiting is discussed. Experimental results are presented for a 900-W version, which has been successfully tested under no-load, full-load, and short-circuit conditions. I.E.

N88-10266*# National Aeronautics and Space Administration. Lewis Research Center, Cleveland, OH.

EFFECTS OF ELECTRON AND PROTON IRRADIATIONS ON

N/P AND P/N GAAS CELLS GROWN BY MOCVD

IRVING WEINBERG, CLIFFORD K. SWARTZ, and RUSSELL E. HART, JR. 1987 8 p Presented at the 3rd International Photovoltaic Science and Engineering Conference, Tokyo, Japan, 3-6 Nov. 1987; sponsored by the Japan Society of Applied Physics (NASA-TM-100199; E-3792; NAS 1.15:100199) Avail: NTIS HC A02/MF A01 CSCL 09C

State-of-the-art n/p and p/n heteroface GaAs cells, processed by metal organic chemical vapor deposition, were irradiated by 1 MeV electrons and 37 MeV protons and their performance determined as a function of fluence. It was found that the p/n cells were more radiation resistant than the n/p cells. The increased loss in the n/p cells was attributed to increases in series resistance and losses in the p-region resulting from the irradiation. The greater loss in fill factor observed for the n/p cells introduces the possibility that the presently observed superiority of the p/n cells may not be an intrinsic property of this configuration in GaAs. Author

N88-11948*# General Dynamics Corp., San Diego, CA. Space Systems Div.

THE AC POWER SYSTEM TESTBED Final Report

J. MILDICE and R. SUNDBERG Nov. 1987 138 p (Contract NAS3-24399)

(NASA-CR-175068; NAS 1.26:175068) Avail: NTIS HC A07/MF A01 CSCL 09C

The object of this program was to design, build, test, and deliver a high frequency (20 kHz) Power System Testbed which would electrically approximate a single, separable power channel of an IOC Space Station. That program is described, including the technical background, and the results are discussed showing that the major assumptions about the characteristics of this class of hardware (size, mass, efficiency, control, etc.) were substantially correct. This testbed equipment was completed and delivered and is being operated as part of the Space Station Power System Test Facility. Author

33 ELECTRONICS AND ELECTRICAL ENGINEERING

N88-11966*# National Aeronautics and Space Administration. Lewis Research Center, Cleveland, OH.

RECENT PROGRESS IN SPACE PHOTOVOLTAIC SYSTEMS

HENRY W. BRANDHORST, JR., DENNIS J. FLOOD, and IRVING WEINBERG Oct. 1987 13 p Presented at the 3rd International Photovoltaic Science and Engineering Conference, Tokyo, Japan, 3-6 Nov. 1987; sponsored by the Japan Soc. of Appl. Phys., Inst. of Elec. Engineers of Japan and the Foundation for the Advan. of International Science

(NASA-TM-100208; E-3807; NAS 1.15:100208) Avail: NTIS HC A03/MF A01 CSCL 09C

Key issues and opportunities in space photovoltaic research and technology relative to future NASA mission requirements and drivers are addressed. Examples are given of space missions and/or operational capabilities on NASA's planning horizon presenting major technology challenges to the use of photovoltaic power generation in space. The status of cell R and D and the performance goals to be met by space photovoltaic power systems to remain competitive are described. Author

N88-12727*# National Aeronautics and Space Administration. Lewis Research Center, Cleveland, OH.

AN ANALYTICAL AND EXPERIMENTAL STUDY OF INJECTION-LOCKED TWO-PORT OSCILLATORS

JON C. FREEMAN and ALAN N. DOWNEY Jul. 1987 39 p (NASA-TM-100119; E-3663; NAS 1.15:100119) Avail: NTIS HC A03/MF A01 CSCL 09A

A Ku-band IMPATT oscillator with two distinct output power ports was injection-locked alternately at both ports. The transmission locking bandwidth was nearly the same for either port. The lower free running power port had a reflection locking bandwidth that was narrower than its transmission locking one. Just the opposite was found at the other port. A detailed analytical model for two-port injection-locked oscillators is presented, and its results agree quite well with the experiments. A critique of the literature on this topic is included to clear up misconceptions and errors. It is concluded that two-port injection-locked oscillators may prove useful in certain communication systems. Author

N88-15146*# National Aeronautics and Space Administration. Lewis Research Center, Cleveland, OH.

PERFORMANCE OF A SMALL, GRAPHITE ELECTRODE, MULTISTAGE DEPRESSED COLLECTOR WITH A 500-W, CONTINUOUS WAVE, 4.8- TO 9.6-GHZ TRAVELING WAVE TUBE

PETER RAMINS, GARY G. LESNY, BEN T. EBIHARA, and SHELLY PEET Feb. 1988 15 p (NASA-TP-2788; E-3800; NAS 1.60:2788) Avail: NTIS HC A03/MF A01 CSCL 09A

A small, isotropic graphite multistage depressed collector (MDC) and a short permanent magnet refocuser were designed, fabricated, and evaluated in conjunction with a 500-W, continuous-wave (CW), 4.8 to 9.6 GHz traveling wave tube (TWT). A novel performance optimization system and technique were used to optimize the TWT-MDC performance for saturated broad-band operation. The MDC performance was evaluated in both four- and three-stage configurations. Average TWT overall and four-stage collector efficiencies of 43.8 and 82.6 percent, respectively, were obtained for saturated octave-bandwidth operation. The isotropic graphite electrode material performed well, and shows considerable promise. However, considerably more test experience is required before definitive conclusions on its suitability for space and airborne TWT's can be made. Author

N88-15797*# National Aeronautics and Space Administration. Lewis Research Center, Cleveland, OH.

HIGH-TEMPERATURE ELECTRONICS

GARY T. SENG *In its* Aeropropulsion '87. Session 4: Instrumentation and Controls Research 10 p Nov. 1987 Avail: NTIS HC A05/MF A01 CSCL 20F

In recent years, there was a growing need for electronics capable of sustained high-temperature operation for aerospace propulsion system instrumentation, control and condition

monitoring, and integrated sensors. The desired operating temperature in some applications exceeds 600 C, which is well beyond the capability of currently available semiconductor devices. Silicon carbide displays a number of properties which make it very attractive as a semiconductor material, one of which is the ability to retain its electronic integrity at temperatures well above 600 C. An IR-100 award was presented to NASA Lewis in 1983 for developing a chemical vapor deposition process to grow single crystals of this material on standard silicon wafers. Silicon carbide devices were demonstrated above 400 C, but much work remains in the areas of crystal growth, characterization, and device fabrication before the full potential of silicon carbide can be realized. The presentation will conclude with current and future high-temperature electronics program plans. Although the development of silicon carbide falls into the category of high-risk research, the future looks promising, and the potential payoffs are tremendous. Author

N88-18835*# National Aeronautics and Space Administration. Lewis Research Center, Cleveland, OH.

MICROWAVE RESPONSE OF AN HEMT PHOTOCONDUCTOR

P. C. CLASPY (Case Western Reserve Univ., Cleveland, Ohio.) and K. B. BHASIN Jan. 1988 10 p Presented at the Optoelectronics and Laser Applications in Science and Engineering (O-E/LASE), Los Angeles, Calif., 10-15 Jan. 1988; sponsored in part by The Society of Photo-Optical Instrumentation Engineers (NASA-TM-100819; E-4009; NAS 1.15:100819) Avail: NTIS HC A02/MF A01 CSCL 09A

Interdigitated photodetectors of various geometries have been fabricated on GaAlAs/GaAs heterostructure material. Optical response characteristics of these devices have been examined at both dc and microwave frequencies. The microwave response, at frequencies to 8 GHz, was studied by illuminating the devices with the output of an internally modulated GaAlAs diode laser. Results of these measurements are presented and compared with that of GaAs photoconductors. Author

N88-20555*# National Aeronautics and Space Administration. Lewis Research Center, Cleveland, OH.

OPTICAL RF DISTRIBUTION LINKS FOR MMIC PHASED ARRAY ANTENNAS

RICHARD R. KUNATH, KUL B. BHASIN, and CHARLES A. RAQUET 1987 7 p Presented at the IEEE AP-S International Symposium and URSI Radio Science Meeting, Blacksburg, Va., 15-19 Jun. 1987 (NASA-TM-100841; E-4031; NAS 1.15:100841) Avail: NTIS HC A02/MF A01 CSCL 09C

Conventional methods to distribute RF signals to GaAs Monolithic Microwave Integrated Circuits Phased Array Antennas are inadequate for arrays having large numbers of elements. Optical RF distribution links have been proposed as a lightweight, mechanically flexible, and low volume solution. Three candidate techniques for providing optical RF distribution are discussed along with the electro-optic devices required to configure them. A discussion of the present status of applicable electro-optics devices is also included. Author

N88-21400*# National Aeronautics and Space Administration. Lewis Research Center, Cleveland, OH.

OPTICALLY INTERCONNECTED PHASED ARRAYS

KUL B. BHASIN and RICHARD R. KUNATH 1988 9 p Presented at Advances in Semiconductors and Superconductors: Physics and Device Applications, Newport, Calif., 13-18 Mar. 1988; sponsored by the Society of Photo-Optical Instrumentation Engineers (NASA-TM-100855; E-4058; NAS 1.15:100855) Avail: NTIS HC A02/MF A01 CSCL 09A

Phased-array antennas are required for many future NASA missions. They will provide agile electronic beam forming for communications and tracking in the range of 1 to 100 GHz. Such phased arrays are expected to use several hundred GaAs monolithic integrated circuits (MMICs) as transmitting and receiving elements. However, the interconnections of these elements by conventional coaxial cables and waveguides add weight, reduce

flexibility, and increase electrical interference. Alternative interconnections based on optical fibers, optical processing, and holography are under evaluation as possible solutions. In this paper, the current status of these techniques is described. Since high-frequency optical components such as photodetectors, lasers, and modulators are key elements in these interconnections, their performance and limitations are discussed. Author

N88-23084*# Honeywell, Inc., Bloomington, MN. Sensors and Signal Processing Lab.

A 30 GHZ MONOLITHIC RECEIVE MODULE TECHNOLOGY ASSESSMENT

J. GEDDES, V. SOKOLOV, P. BAUHAHN, and T. CONTOLATIS
Apr. 1988 31 p
(Contract NAS3-23356)
(NASA-CR-180825; NAS 1.26:180825) Avail: NTIS HC A03/MF A01 CSDL 09C

This report is a technology assessment relevant to the 30 GHz Monolithic Receive Module development. It is based on results obtained on the present NASA Contract (NAS3-23356) as well as on information gathered from literature and other industry sources. To date the on-going Honeywell program has concentrated on demonstrating the so-called interconnected receive module which consists of four monolithic chips - the low noise front-end amplifier (LNA), the five bit phase shifter (PS), the gain control amplifier (GC), and the RF to IF downconverter (RF/IF). Results on all four individual chips have been obtained and interconnection of the first three functions has been accomplished. Future work on this contract is aimed at a higher level of integration, i.e., integration of the first three functions (LNA + PS + GC) on a single GaAs chip. The report presents the status of this technology and projections of its future directions. Author

N88-23936*# National Aeronautics and Space Administration. Lewis Research Center, Cleveland, OH.

MINIATURE TRAVELING WAVE TUBE AND METHOD OF MAKING Patent Application

HENRY G. KOSMAHL 8 Dec. 1987 15 p
(NASA-CASE-LEW-14520-1; NAS 1.71:LEW-14520-1;
US-PATENT-APPL-SN-130058) Avail: NTIS H A03/MF A01 CSDL 09A

A miniature traveling wave tube is provided which will have most of the advantages of solid state circuitry but with higher efficiency and without being highly sensitive to temperature and various types of electromagnetic radiation and subatomic particles as are solid state devices. The traveling wave tube is about 2.5 cm in length and includes a slow wave circuit (SWS) comprised of apertured fins with a top cover which is insulated from the fins by strips or rungs of electrically insulating, dielectric material. An extremely small SWS is constructed by employing various grooving and etching methods, and by providing insulating strips or rungs by various deposition and masking techniques. NASA

N88-23939*# Induction General, Inc., Pittsburgh, PA.
HIGH FREQUENCY POWER DISTRIBUTION SYSTEM Final Report

MIKUND R. PATEL Apr. 1986 159 p
(Contract NAS3-23894)
(NASA-CR-175071; NAS 1.26:175071) Avail: NTIS HC A08/MF A01 CSDL 09C

The objective of this project was to provide the technology of high frequency, high power transmission lines to the 100 kW power range at 20 kHz frequency. In addition to the necessary design studies, a 150 m long, 600 V, 60 A transmission line was built, tested and delivered for full vacuum tests. The configuration analysis on five alternative configurations resulted in the final selection of the three parallel Litz straps configuration, which gave a virtually concentric design in the electromagnetic sense. Low inductance, low EMI and flexibility in handling are the key features of this configuration. The final design was made after a parametric study to minimize the losses, weight and inductance. The construction of the cable was completed with no major difficulties.

The R,L,C parameters measured on the cable agreed well with the calculated values. The corona tests on insulation samples showed a safety factor of 3. Author

N88-24256*# National Aeronautics and Space Administration. Lewis Research Center, Cleveland, OH.

BENEFITS OF 20 KHZ PMAD IN A NUCLEAR SPACE STATION GALE R. SUNDBERG In New Mexico Univ., Transactions of the Fourth Symposium on Space Nuclear Power Systems p 7-10 1987

Avail: NTIS HC A22/MF A01 CSDL 09C

Compared to existing systems, high frequency ac power provides higher efficiency, lower cost, and improved safety benefits. The 20 kHz power system has exceptional flexibility, is inherently user friendly, and is compatible with all types of energy sources; photovoltaic, solar dynamic, rotating machines and nuclear. A 25 kW, 20 kHz ac power distribution system testbed was recently (1986) developed. The testbed possesses maximum flexibility, versatility, and transparency to user technology while maintaining high efficiency, low mass, and reduced volume. Several aspects of the 20 kHz power management and distribution (PMAD) system that have particular benefits for a nuclear power Space Station are discussed. Author

N88-24463*# National Aeronautics and Space Administration. Lewis Research Center, Cleveland, OH.

NEUTRON EFFECTS ON THE ELECTRICAL AND SWITCHING CHARACTERISTICS OF NPN BIPOLAR POWER TRANSISTORS

ALBERT J. FRASCA (Wittenberg Univ., Springfield, Ohio.) and GENE E. SCHWARZE In New Mexico Univ., Transactions of the Fifth Symposium on Space Nuclear Power Systems p 431-435 1988

Avail: NTIS HC A99/MF A01 CSDL 09C

The use of nuclear reactors to generate electrical power for future space missions will require the electrical components used in the power conditioning, control, and transmission subsystem to operate in the associated radiation environments. An initial assessment of neutron irradiation on the electrical and switching characteristics of commercial high power NPN bipolar transistors was investigated. The results clearly show the detrimental effects caused by neutron irradiation on the electrical and switching characteristics of the NPN bipolar power transistor. Author

N88-24506*# National Aeronautics and Space Administration. Lewis Research Center, Cleveland, OH.

SPACE POWER RADIATION COOLED DC TRANSMISSION LINE ANALYSIS

GENE E. SCHWARZE In New Mexico Univ., Transactions of the Fifth Symposium on Space Nuclear Power Systems p 649-653 1988

Avail: NTIS HC A99/MF A01 CSDL 09C

The results of this analysis show that both mass and percent power loss reductions result from an increase in source voltage. A decrease in conductor diameter also leads to reduced mass, but this decrease gives higher percent power losses since the operating temperature increases. The results also show that increasing the source voltage beyond a certain limit for a fixed operating temperature only gives minimal decreases in both the mass and the percent power loss; likewise, the results show that decreasing the diameter below a certain point for a fixed voltage causes minimal decreases in the mass but excessive percent power losses and thus high operating temperatures. The plots generated by using the mathematical results derived in this analysis clearly show when these diminishing mass reductions and excessive operating temperatures occur. Depending on the mission objectives, a trade-off between mass, diameter, and percent power loss in terms of voltage, operating temperature, and conductor material will most likely be required when the total power system is considered. Thus, the results of this analysis should aid the system designer in conducting these trade studies with respect to the performance characteristics of a radiation cooled dc transmission line. Author

33 ELECTRONICS AND ELECTRICAL ENGINEERING

N88-24870*# National Aeronautics and Space Administration. Lewis Research Center, Cleveland, OH.

PROGRESS IN INP SOLAR CELL RESEARCH

IRVING WEINBERG and DAVID J. BRINKER 1988 16 p
Presented at the 23rd Intersociety Energy Conversion Engineering Conference, Denver, Colo., 31 Jul. - 5 Aug. 1988; sponsored by ASME, AIAA, ANS, SAE, IEEE, ACS and AIChE (NASA-TM-100914; E-4166; NAS 1.15:100914) Avail: NTIS HC A03/MF A01 CSCL 10A

Progress, in the past year, in InP solar cell research is reviewed. Small area cells with AMO, total area efficiencies of 18.8 percent were produced by OMCVD and Ion Implantation. Larger area cells (2 and 4 sq cm) were processed on a production basis. One thousand of the 2 sq cm cells will be used to supply power to a small piggyback lunar orbiter scheduled for launch in February 1990. Laboratory tests of ITO/InP cells, under 10 MeV proton irradiation, indicate radiation resistance comparable to InP n/p homojunction cells. Computer modeling studies indicate that, for identical geometries and dopant concentrations, InP solar cells are significantly more radiation resistant than GaAs under 1 MeV electron irradiation. Additional computer modeling calculations were used to produce rectangular and circular InP concentrator cell designs for both the low concentration SLATS and higher concentration Cassegrainian Concentrators. Author

N88-25830*# National Aeronautics and Space Administration. Lewis Research Center, Cleveland, OH.

A ROLE FOR HIGH FREQUENCY SUPERCONDUCTING DEVICES IN FREE SPACE POWER TRANSMISSION SYSTEMS

JOSE L. CHRISTIAN, JR. and RONALD C. CULL 1988 11 p
Presented at the 23rd Intersociety Energy Conversion Engineering Conference, Denver, Colo., 31 Jul. - 5 Aug. 1988; sponsored by ASME, AIAA, ANS, SAE, IEEE, ACS and AIChE (NASA-TM-100971; E-4264; NAS 1.15:100971) Avail: NTIS HC A03/MF A01 CSCL 10B

Major advances in space power technology are being made in photovoltaic, solar thermal, and nuclear systems. Despite these advances, the power systems required by the energy and power intensive mission of the future will be massive due to the large collecting surfaces, large thermal management systems, and heavy shielding. Reducing this mass on board the space vehicle can result in significant benefits because of the high cost of transporting and moving mass about in space. An approach to this problem is beaming the power from a point where the massiveness of the power plant is not such a major concern. The viability of such an approach was already investigated. Efficient microwave power beam transmission at 2.45 GHz was demonstrated over short range. Higher frequencies are desired for efficient transmission over several hundred or thousand kilometers in space. Superconducting DC-RF conversion as well as RF-DC conversion offers exciting possibilities. Multivoltage power conditioning for multicavity high power RF tubes could be eliminated since only low voltages are required for Josephson junctions. Small, high efficiency receivers may be possible using the reverse Josephson effects. A conceptual receiving antenna design using superconducting devices to determine possible system operating efficiency is assessed. If realized, these preliminary assessments indicate a role for superconducting devices in millimeter and submillimeter free space power transmission systems. Author

N88-25831*# Sverdrup Technology, Inc., Cleveland, OH.
AGING BEHAVIOR OF AU-BASED OHMIC CONTACTS TO GAAS Final Contractor Report

NAVID S. FATEMI Jul. 1988 15 p
(Contract NAS3-24105)
(NASA-CR-182146; E-4171; NAS 1.26:182146) Avail: NTIS HC A03/MF A01 CSCL 09A

Gold based alloys, commonly used as ohmic contacts for solar cells, are known to react readily with GaAs. It is shown that the contact interaction with the underlying GaAs can continue even at room temperature upon aging, altering both the electrical characteristics of the contacts and the nearby pn junction. Au-Ge-Ni as-deposited (no heat treatment) contacts made to thin emitter

(0.15 micrometer) GaAs diodes have shown severe shunting of the pn junction upon aging for several months at room temperature. The heat-treated contacts, despite showing degradation in contact resistance did not affect the underlying pn junction. Au-Zn-Au contacts to p-GaAs emitter (0.2 micrometer) diodes, however, showed slight improvement in contact resistance upon 200 C isothermal annealing for several months, without degrading the pn junction. The effect of aging on electrical characteristics of the as-deposited and heat-treated contacts and the nearby pn junction, as well as on the surface morphology of the contacts are presented. Author

N88-26239*# Varian Associates, Palo Alto, CA. Microwave Tube Div.

A MILLIMETER-WAVE TUNNELADDER TWT Final Report

A. JACQUEZ, A. KARP, D. WILSON, and A. SCOTT Aug. 1988 73 p
(Contract NAS3-22466; NAS3-21930; NAS3-22445)
(NASA-CR-182184; NAS 1.26:182184) Avail: NTIS HC A04/MF A01 CSCL 09A

A millimeter wave traveling wave tube was developed using a dispersive, high impedance forward interaction structure based on a ladder, with non-space harmonic interaction, for a tube with high gain per unit length and high efficiency. The Tunneladder interaction structure combines ladder properties modified to accommodate Pierce gun beam optics in a radially magnetized permanent magnet focusing structure. The development involved the fabrication of chemically milled, shaped ladders diffusion brazed to diamond cubes which are in turn active-diffusion brazed to each ridge of a doubly ridged waveguide. Cold test data are presented, representing the omega-beta and impedance characteristics of the modified ladder circuit. These results were used in small and large signal computer programs to predict TWT gain and efficiency. Actual data from tested tubes verify the predicted performance while providing broader bandwidth than expected. Author

N88-28240*# National Aeronautics and Space Administration. Lewis Research Center, Cleveland, OH.

A HIGH FREQUENCY GAALAS TRAVELLING WAVE ELECTRO-OPTIC MODULATOR AT 0.82 MICROMETERS

CHRISTOPHER M. CHOREY, ALTAN FERENDECI (Case Western Reserve Univ., Cleveland, Ohio.), and KUL B. BHASIN 1988 8 p
Presented at the 1988 IEEE MTT-S International Symposium, N.Y., N.Y., 25-27 May 1988
(NASA-TM-100970; E-4261; NAS 1.15:100970) Avail: NTIS HC A02/MF A01 CSCL 09A

Experimental GaAlAs modulators operating at 0.82 micrometers using a Mach-Zehnder interferometer configuration were designed and fabricated. Coplanar 50 ohm travelling wave microwave electrodes were used to obtain a bandwidth length product of 11.95 GHz-cm. The design, fabrication and dc performance of the GaAlAs travelling wave modulator is presented. Author

N88-30048*# National Aeronautics and Space Administration. Lewis Research Center, Cleveland, OH.

HIGH FREQUENCY GAALAS MODULATOR AND PHOTODETECTOR FOR PHASED ARRAY ANTENNA APPLICATIONS

P. C. CLASPY, C. M. CHOREY, S. M. HILL (Case Western Reserve Univ., Cleveland, Ohio.), and K. B. BHASIN Sep. 1988 12 p
Presented at the International Symposium and Exhibition on Fiber Optics, Optoelectronics, and Laser Applications, Boston, Mass., 6-9 Sep. 1988; sponsored in part by Society of Photo-Optical Instrumentation Engineers
(NASA-TM-101328; E-4339; NAS 1.15:101328) Avail: NTIS HC A03/MF A01 CSCL 09C

A waveguide Mach-Zehnder electro-optic modulator and an indigitated photoconductive detector designed to operate at 820 nm, fabricated on different GaAlAs/GaAs heterostructure materials, are being investigated for use in optical interconnects in phased array antenna systems. Measured optical attenuation effects in

the modulator are discussed and the observed modulation performance up to 1 GHz is presented. Measurements of detector frequency response are described and results presented. Author

N88-30055*# Case Western Reserve Univ., Cleveland, OH.
OPTOELECTRONIC GAIN CONTROL OF A MICROWAVE SINGLE STAGE GaAs MESFET AMPLIFIER Final Report
 RAINEE N. SIMONS Sep. 1988 12 p
 (Contract NAG3-816)
 (NASA-CR-182201; E-3963; NAS 1.26:182201) Avail: NTIS HC A03/MF A01 CSCL 09A

Gain control of a single stage GaAs MESFET amplifier is demonstrated by the use of optical illumination of photon energy greater than the GaAs bandgap. The optical illumination is supplied by a semiconductor laser diode and is coupled to the Schottky gate of the MESFET by an optical fiber. The increase in gain is observed to be as much as 5.15 dB when the MESFET is biased close to pinchoff, that is, V_{gs} equals -1.5 V and with optical illumination of 1.5 mW. The computed maximum available gain (MAG) and current gain ($h_{sub 21}$) from the de-embedded s-parameters show that MAG is unaffected by optical illumination, however, $h_{sub 21}$ increases by more than 2 dB under optical illumination of 1.5 mW. The maximum frequency of oscillation ($F_{sub max}$) and the unity current gain cut-off frequency ($F_{sub t}$) obtained by extrapolating the MAG and $h_{sub 21}$ curves, respectively, show that the $F_{sub max}$ is insensitive to optical illumination but $F_{sub t}$ increases by 5 GHz. Author

34

FLUID MECHANICS AND HEAT TRANSFER

Includes boundary layers; hydrodynamics; fluidics; mass transfer; and ablation cooling.

A88-11000*# Aerometrics, Inc., Mountain View, CA.
EXPERIMENTS ON SPRAY INTERACTIONS IN THE WAKE OF A BLUFF BODY
 R. C. RUDOFF, M. J. HOUSER, and W. D. BACHALO (Aerometrics, Inc., Mountain View, CA) ASME, International Gas Turbine Conference and Exhibition, 32nd, Anaheim, CA, May 31-June 4, 1987. 9 p. refs
 (Contract NAS3-24844)
 (ASME PAPER 87-GT-48)

The dynamics of spray drop interaction within the turbulent wake of a bluff body were investigated using the Aerometrics Phase Doppler Particle Analyzer that determines both drop size and velocity. Detailed measurements included spray drop size, axial and radial velocity, angle of trajectory, and size-velocity correlations. The gas-phase flow field was also ascertained via the behavior of the smallest drops. Results showed dramatic differences in drop behavior when interacting with turbulence for the various size classes. Small drops were recirculated in a pair of toroidal vortices located behind the bluff body, whereas the larger drops followed the general direction of the spray cone angle. The spray field interaction illustrated by these data casts some doubt on attempts to describe sprays via simple integral quantities such as the Sauter mean diameter. Author

A88-11033*# Texas A&M Univ., College Station.
EFFECT OF RIB ANGLE ON LOCAL HEAT/MASS TRANSFER DISTRIBUTION IN A TWO-PASS RIB-ROUGHENED CHANNEL
 P. R. CHANDRA, J. C. HAN, and S. C. LAU (Texas A & M University, College Station) ASME, International Gas Turbine Conference and Exhibition, 32nd, Anaheim, CA, May 31-June 4, 1987. 9 p. refs
 (Contract NAS3-24227)
 (ASME PAPER 87-GT-94)

The naphthalene sublimation technique is used to investigate the heat transfer characteristics of turbulent air flow in a two-pass

channel. A test section that resembles the internal cooling passages of gas turbine airfoils is employed. The local Sherwood numbers on the ribbed walls were found to be 1.5-6.5 times those for a fully developed flow in a smooth square duct. Depending on the rib angle-of-attack and the Reynolds number, the average ribbed-wall Sherwood numbers were 2.5-3.5 times higher than the fully developed values. R.R.

A88-11089*# City Coll. of the City Univ. of New York.
WALL SHEAR STRESS MEASUREMENT IN BLADE END-WALL CORNER REGION
 R. BHARGAVA, R. RAJ (City College, New York), and D. R. BOLDMAN (NASA, Lewis Research Center, Cleveland, OH) ASME, International Gas Turbine Conference and Exhibition, 32nd, Anaheim, CA, May 31-June 4, 1987. 12 p. refs
 (ASME PAPER 87-GT-181)

The magnitude and the direction of wall shear stress and surface pressure in the blade end-wall corner region were investigated. The measurements were obtained on a specially designed Preston tube, the tip of which could be concentrically rotated about its axis of rotation at the measurement location. The magnitude of wall shear stress in the vicinity of the corner was observed to increase significantly (170 percent) compared to its far-upstream value; the increase was consistently higher on the blade surface compared to the value on the plate surface of the blade end-wall corner. On both surfaces in the blade end-wall corner, the variation of the wall shear stress direction was found to be more predominant in the vicinity of the blade leading-edge location. The trend of the measured wall shear stress direction showed good agreement with the limiting streamline directions obtained from the flow visualization studies. I.S.

A88-11103*# Minnesota Univ., Minneapolis.
MEASUREMENTS OF THE TURBULENT TRANSPORT OF HEAT AND MOMENTUM IN CONVEXLY CURVED BOUNDARY LAYERS - EFFECTS OF CURVATURE, RECOVERY AND FREE-STREAM TURBULENCE
 J. KIM and T. W. SIMON (Minnesota, University, Minneapolis) ASME, International Gas Turbine Conference and Exhibition, 32nd, Anaheim, CA, May 31-June 4, 1987. 9 p. Research supported by the University of Minnesota and AMOCO Foundation. refs
 (Contract F49620-83-C-0062; NAG3-286)
 (ASME PAPER 87-GT-199)

The effects of streamwise convex curvature, recovery, and freestream turbulence intensity on the turbulent transport of heat and momentum in a mature boundary layer are studied using a specially designed three-wire hot-wire probe. Increased freestream turbulence is found to increase the profiles throughout the boundary layer on the flat developing wall. Curvature effects were found to dominate turbulence intensity effects for the present cases considered. For the higher TI (turbulence intensity) case, negative values of the turbulent Prandtl number are found in the outer half of the boundary layer, indicating a breakdown in Reynolds analogy. R.R.

A88-11130*# Pennsylvania State Univ., State College.
THE MEASUREMENT OF BOUNDARY LAYERS ON A COMPRESSOR BLADE IN CASCADE. I - A UNIQUE EXPERIMENTAL FACILITY
 STEVEN DEUTSCH and WILLIAM C. ZIERKE (Pennsylvania State University, State College) ASME, International Gas Turbine Conference and Exhibition, 32nd, Anaheim, CA, May 31-June 4, 1987. 8 p. refs
 (Contract NSG-3264)
 (ASME PAPER 87-GT-248)

A unique cascade facility is described which makes it possible to use LDV for measuring blade boundary layer profiles. Because of the need for a laser access window, the facility cannot rely on continuous blade pack suction to achieve stable flow. Instead, a combination of tailboards and strong suction upstream of the blade pack is used to create a two-dimensional periodic flow field at a chord Reynolds number of 500,000. The distribution of the upstream suction is controlled through a complex baffling system.

34 FLUID MECHANICS AND HEAT TRANSFER

Details of the inlet and outlet flow are documented using five-hole pressure probes, blade static-pressure measurements, and sublimation flow visualization. Experimental data are presented on the flow field on the suction surface of the blade, the pressure surface, and near-wake flow fields. I.S.

A88-11131*# Pennsylvania State Univ., State College.
THE MEASUREMENT OF BOUNDARY LAYERS ON A COMPRESSOR BLADE IN CASCADE. II - SUCTION SURFACE BOUNDARY LAYERS

STEVEN DEUTSCH and WILLIAM C. ZIERKE (Pennsylvania State University, State College) ASME, International Gas Turbine Conference and Exhibition, 32nd, Anaheim, CA, May 31-June 4, 1987. 10 p. refs
(Contract NSG-3264)
(ASME PAPER 87-GT-249)

A one-component laser Doppler velocimeter (LDV) has been used to measure the two-dimensional, periodic flow field about a double circular arc, compressor blade in cascade. Eleven boundary layer profiles were taken on both the pressure and suction surfaces of the blade, and two were taken in the near wake. In this part of the study, the LDV system is described and the suction surface flow field is documented. The suction surface profiles appear to separate both at the leading edge and again somewhat beyond midchord; the leading edge separation apparently reattaches by 2.6 percent chord. C.D.

A88-11132*# Pennsylvania State Univ., State College.
THE MEASUREMENT OF BOUNDARY LAYERS ON A COMPRESSOR BLADE IN CASCADE. III - PRESSURE SURFACE BOUNDARY LAYERS AND THE NEAR WAKE

STEVEN DEUTSCH and WILLIAM C. ZIERKE (Pennsylvania State University, State College) ASME, International Gas Turbine Conference and Exhibition, 32nd, Anaheim, CA, May 31-June 4, 1987. 10 p. refs
(Contract NSG-3264)
(ASME PAPER 87-GT-250)

A one-component laser Doppler velocimeter (LDV) has been used to measure the two-dimensional periodic flow field about a double circular arc, compressor blade in cascade. Eleven boundary layer profiles were taken on both the pressure and suction surfaces of the blade, and two profiles were taken in the near wake. In this part of the study, the detailed LDV studies are described. The measurements indicate that the onset of transition occurs near 60 percent chord. The lack of a logarithmic region in the data measured at 97.9 percent chord indicates that transition is not complete. The thin laminar boundary layers near the leading edge led to some measurement problems, characterized by large turbulence intensities, in using the LDV. C.D.

A88-11133*# Pennsylvania State Univ., University Park.
LASER DOPPLER VELOCIMETER MEASUREMENT OF ANNULUS WALL BOUNDARY LAYER DEVELOPMENT IN A COMPRESSOR ROTOR

B. LAKSHMINARAYANA (Pennsylvania State University, University Park) and K. N. S. MURTHY ASME, International Gas Turbine Conference and Exhibition, 32nd, Anaheim, CA, May 31-June 4, 1987. 11 p. refs
(Contract NSG-3212)
(ASME PAPER 87-GT-251)

Detailed measurement of the flow field in the tip region of a compressor rotor was carried out using LDV. The axial and tangential components of relative velocities were measured upstream, inside the passage, and at the exit of the rotor, up to about 20 percent of the blade span from the blade tip. The annulus-wall boundary layer is well behaved at the leading edge and far downstream of the rotor. But inside the passage, complex interactions between the leakage flow and the annulus-wall boundary layer result in unconventional profiles with wide deviations from models employed for analyses. Author

A88-11803*# Los Alamos National Lab., NM.
INTEGRATED HEAT PIPE-THERMAL STORAGE SYSTEM PERFORMANCE EVALUATION

E. KEDDY, J. T. SENA, M. MERRIGAN (Los Alamos National Laboratory, NM), and GARY HEIDENREICH (Sundstrand Corp., Rockford, IL) IN: IECEC '87; Proceedings of the Twenty-second Intersociety Energy Conversion Engineering Conference, Philadelphia, PA, Aug. 10-14, 1987. Volume 1. New York, American Institute of Aeronautics and Astronautics, 1987, p. 183-187. Research supported by the Sundstrand Corp.
(Contract NAS3-24666)

An integrated thermal energy storage (TES) system, developed as a part of an organic Rankine cycle solar dynamic power system is described, and the results of the performance verification tests of this TES system are presented. The integrated system consists of potassium heat-pipe elements that incorporate TES canisters within the vapor space, along with an organic fluid heater tube used as the condenser region of the heat pipe. The heat pipe assembly was operated through the range of design conditions from the nominal design input of 4.8 kW to a maximum of 5.7 kW. The performance verification tests show that the system meets the functional requirements of absorbing the solar energy reflected by the concentrator, transporting the energy to the organic Rankine heater, providing thermal storage for the eclipse phase, and allowing uniform discharge from the thermal storage to the heater. I.S.

A88-11807*# Grumman Aerospace Corp., Bethpage, NY.
HEAT PIPE RADIATORS FOR SOLAR DYNAMIC SPACE POWER SYSTEM HEAT REJECTION

ERIC GUSTAFSON and ALBERT CARLSON (Grumman Aerospace Corp., Space Systems Div., Bethpage, NY) IN: IECEC '87; Proceedings of the Twenty-second Intersociety Energy Conversion Engineering Conference, Philadelphia, PA, Aug. 10-14, 1987. Volume 1. New York, American Institute of Aeronautics and Astronautics, 1987, p. 214-221. refs
(Contract NAS3-24665)

The paper presents the results of a concept development study of heat rejection systems for Space Station solar dynamic power systems. The thermal performance and weights of each of the heat rejection subsystems have been addressed in detail, and critical technologies which require development tests and evaluation for successful demonstration were assessed and identified. Baseline and several alternate heat rejection system configurations and optimum designs were developed for both Brayton and Rankine cycles. The thermal performance, mass properties, assembly requirements, reliability, maintenance requirements, and life cycle costs were determined for each of the system configurations. Trade studies were performed on each configuration with respect to the heat pipe wall thickness and the amount of redundancy to determine the effects on system reliability, maintenance requirements, and life cycle costs. An optimum design was then selected for each configuration. Author

A88-11808*# Sundstrand Corp., Rockford, IL.
SOLAR DYNAMIC ORGANIC RANKINE CYCLE HEAT REJECTION SYSTEM SIMULATION

V. N. HAVENS, D. R. RAGALLER (Sundstrand Corp., Rockford, IL), and D. NAMKOONG (NASA, Lewis Research Center, Cleveland, OH) IN: IECEC '87; Proceedings of the Twenty-second Intersociety Energy Conversion Engineering Conference, Philadelphia, PA, Aug. 10-14, 1987. Volume 1. New York, American Institute of Aeronautics and Astronautics, 1987, p. 222-226. refs

The use of a rotary fluid management device (RFMD) and shear flow condenser for two-phase fluid management in microgravity organic Rankine cycle (ORC) applications is examined. A prototype of the proposed Space Station ORC heat rejection system was constructed to evaluate the performance of the inventory control method. The design and operation of the RFMD, shear flow condenser, and inventory control fluid accumulator are described. A schematic diagram of the ORC, RFMD, and condenser, and a functional diagram of the heat rejection system for the ORC are presented. I.F.

A88-11963* Minnesota Univ., Minneapolis.

DESCRIPTION OF AN OSCILLATING FLOW TEST PROGRAM

J. R. SEUME, L. F. GOLDBERG, and T. W. SIMON (Minnesota, University, Minneapolis) IN: IECEC '87; Proceedings of the Twenty-second Intersociety Energy Conversion Engineering Conference, Philadelphia, PA, Aug. 10-14, 1987. Volume 4. New York, American Institute of Aeronautics and Astronautics, 1987, p. 1753-1758. refs

(Contract NAG3-693; NAG3-598)

A description of the University of Minnesota Oscillating Flow Test Program is presented. The rationale for isolating the oscillating flow effect for separate study, the objectives of the test program, and the program design criteria are presented along with a description of the test facility and the test plan. The program test domain covers almost the entire operating domain of Stirling engine heat exchangers expressed in terms of the appropriate dimensionless parameters. Phenomena important to Stirling engine performance which are not simulated in the test program are also discussed. Computer analysis results are used to predict apparatus performance. Author

A88-12926* National Aeronautics and Space Administration. Lewis Research Center, Cleveland, OH.

PIEZOVISCOUS EFFECTS IN NONCONFORMAL CONTACTS LUBRICATED HYDRODYNAMICALLY

YEAU-REN JENG, BERNARD J. HAMROCK (NASA, Lewis Research Center, Cleveland, OH), and DAVID E. BREWE (NASA, Lewis Research Center; U.S. Army, Aviation Research and Technology Activity, Cleveland, OH) ASLE Transactions (ISSN 0569-8197), vol. 30, Oct. 1987, p. 452-464. Previously announced in STAR as N86-21797. refs

(Contract NCC3-30)

The analysis is concerned with the piezoviscous-rigid regime of lubrication for the general case of elliptical contacts. In this regime several formulas of the lubricant film thickness have been proposed by Hamrock and Dowson, by Dowson et al., and more recently by Houpert. However, either they do not include the load parameter W , which has a strong effect on film thickness, or they overestimate the film thickness by using the Barus formula for pressure-viscosity characteristics. The Roelands formula was used for the pressure-viscosity relationship. The effects of the dimensionless load, speed, and materials parameters, the radius ratio, and the lubricant entrainment direction were investigated. The dimensionless load parameter was varied over a range of one order of magnitude. The dimensionless speed parameter was varied by 5.6 times the lowest value. Conditions corresponding to the use of solid materials of steel, bronze, and silicon nitride and lubricants of paraffinic and naphthenic mineral oil were considered in obtaining the exponent in the dimensionless materials parameter. The radius ratio was varied from 0.2 to 64 (a configuration approaching a line contact). Forty-one cases were used in obtaining a minimum film thickness formula. Contour plots indicate in detail the pressure developed between the contacting solids. Author

A88-14125* Michigan State Univ., East Lansing.

COHERENT MOTION INDUCED FLUCTUATIONS IN THE PRIMARY TRANSITION REGION OF A PLANE SHEAR LAYER

J. F. FOSS, E. D. DAVIS, R. C. HAW, and S. K. ALI (Michigan State University, East Lansing) IN: Forum on Turbulent Flows - 1987, Cincinnati, OH, June 14-17, 1987, Proceedings. New York, American Society of Mechanical Engineers, 1987, p. 1-11. Research supported by the United Technologies Corp. refs

(Contract NAG3-671)

The naturally occurring large scale motions in a single stream shear layer (that is initiated from a fully turbulent boundary layer) are made evident by the induced velocities in the entrainment region beyond the active shear layer. The distinctive attributes of these induced motions are particularly evident in the Michigan State University Free Shear Flow Facility since the total test section length (3m) is nominally the same as the location of the first, fully formed, coherent motion, $ca/x \theta(0) = 400$ (or 2.5 m). Hence, detailed studies of the induced motions can be executed. Individual coherent motions are identified by the induced velocity signatures

and conditional-ensemble statistics are used to represent the irrotational field properties. Clusters of such motions exist; some of their properties are substantially different from the unconditionally averaged values. Author

A88-14143* National Aeronautics and Space Administration. Lewis Research Center, Cleveland, OH.

CORONA ANEMOMETRY FOR QUALITATIVE MEASUREMENT OF REVERSING SURFACE FLOW WITH APPLICATION TO SEPARATION CONTROL BY EXTERNAL EXCITATION

P. A. DURBIN and D. J. MCKINZIE (NASA, Lewis Research Center, Cleveland, OH) IN: Forum on Unsteady Flow Separation, Cincinnati, OH, June 14-17, 1987, Proceedings. New York, American Society of Mechanical Engineers, 1987, p. 15-18.

An corona anemometer which detects gas flow by the displacement of an ion beam is described, and experiments are performed using the anemometer to investigate the active control of diffuser separation by periodic forcing. The apparatus is applied to the separated flow over a rearward facing ramp. An oscillating vane is attached to the surface near the separation point. It is suggested that the enhancement in turbulent energy produced by the oscillating vane is due to drastic modification of the wake shear flow, and not to vane-produced turbulence. R.R.

A88-14170* Michigan State Univ., East Lansing.

GRAVITATIONALLY DEFINED VELOCITIES FOR A LOW SPEED HOT-WIRE CALIBRATION

R. C. HAW, S. K. ALI, and J. F. FOSS (Michigan State University, East Lansing) IN: Symposium on Thermal Anemometry, Cincinnati, OH, June 14-17, 1987, Proceedings. New York, American Society of Mechanical Engineers, 1987, p. 7-13. refs

(Contract NAG3-671)

A technique to provide the reference velocity for a low speed hot-wire calibration is described. A pivoted arm falls under the action of gravity and the resulting velocity field can be used to define the transfer function coefficients in a modified Collis and Williams (1959) relationship. In nominal agreement with a published result, a deviation from this relationship for a film Reynolds number such that $Re \exp n$ of less than about 0.24 is observed. Author

A88-15124* National Aeronautics and Space Administration. Lewis Research Center, Cleveland, OH.

A MODEL FOR THE INFLUENCE OF PRESSURE ON THE BULK MODULUS AND THE INFLUENCE OF TEMPERATURE ON THE SOLIDIFICATION PRESSURE FOR LIQUID LUBRICANTS

BO O. JACOBSON and PASCAL VINET (NASA, Lewis Research Center, Cleveland, OH) ASME, Transactions, Journal of Tribology (ISSN 0742-4787), vol. 109, Oct. 1987, p. 709-714. Research supported by Jacob Wallenberg's Foundation and NASA. Previously announced in STAR as N86-19555. (ASME PAPER 86-TRIB-63)

Two pressure chambers, for compression experiments with liquids from zero to 2.2 GPa pressure, are described. The experimentally measured compressions are then compared to theoretical values given by an isothermal model of equation of state recently introduced for solids. The model describes the pressure and bulk modulus as a function of compression for different types of lubricants with a very high accuracy up to the pressure limit of the high pressure chamber used (2.2 GPa). In addition the influence of temperature on static solidification pressure was found to be a simple function of the thermal expansion of the fluid. Author

A88-15749* National Aeronautics and Space Administration. Lewis Research Center, Cleveland, OH.

RADIATIVE COOLING OF A SOLIDIFYING DROPLET LAYER INCLUDING ABSORPTION AND SCATTERING

ROBERT SIEGEL (NASA, Lewis Research Center, Cleveland, OH) International Journal of Heat and Mass Transfer (ISSN 0017-9310), vol. 30, Aug. 1987, p. 1762-1765. refs

A simple solution for the transient cooling of a solidifying layer filled with drops that can emit and scatter radiation is discussed,

34 FLUID MECHANICS AND HEAT TRANSFER

with application to a liquid drop radiator proposed for the Space Station (Mattick and Hertzberg, 1981). The layer remains at uniform temperature during solidification, and the outer portions rapidly lose heat, producing a variation along the length of the layer in the distribution of liquid concentration across the layer. The analysis is used to obtain both the amount of energy dissipated by the two-phase system at uniform temperature and the velocity distribution necessary to maintain a uniform liquid fraction across the entire layer at all locations along the layer length. R.R.

A88-15960* # Cleveland State Univ., OH.

MODELLING THE PERFORMANCE OF THE MONOGROOVE WITH SCREEN HEAT PIPE FOR USE IN THE RADIATOR OF THE SOLAR DYNAMIC POWER SYSTEM OF THE NASA SPACE STATION

AUSTIN LEWIS EVANS (Cleveland State University, OH) IAF, International Astronautical Congress, 38th, Brighton, England, Oct. 10-17, 1987. 8 p. refs
(Contract NCC3-50)
(IAF PAPER 87-238)

A computer code to model the steady-state performance of a monogroove heat pipe for the NASA Space Station is presented, including the effects on heat pipe performance of a screen in the evaporator section which deals with transient surges in the heat input. Errors in a previous code have been corrected, and the new code adds additional loss terms in order to model several different working fluids. Good agreement with existing performance curves is obtained. From a preliminary evaluation of several of the radiator design parameters it is found that an optimum fin width could be achieved but that structural considerations limit the thickness of the fin to a value above optimum. R.R.

A88-16055* # Wisconsin Univ., Madison.

DROPLET VAPORIZATION IN A SUPERCRITICAL MICROGRAVITY ENVIRONMENT

E. W. CURTIS and P. V. FARRELL (Wisconsin, University, Madison) IAF, International Astronautical Congress, 38th, Brighton, England, Oct. 10-17, 1987. 6 p. refs
(Contract NAG3-718)
(IAF PAPER 87-384)

A model is presented which describes single liquid droplet vaporization at nearly critical liquid pressures and temperatures. A modified Redlich-Kwong equation of state is used to evaluate the fugacities and liquid and vapor mole fractions at the interface under the assumption of interface equilibrium. Results obtained for different droplet sizes and conditions indicate significant differences in behavior in comparison with low-pressure quasi-steady droplet vaporization. V.L.

A88-16352* National Aeronautics and Space Administration. Lewis Research Center, Cleveland, OH.

HIGHER EIGENMODES IN THE BLASIUS BOUNDARY-LAYER STABILITY PROBLEM

LENNART S. HULTGREN (NASA, Lewis Research Center, Cleveland, OH) Physics of Fluids (ISSN 0031-9171), vol. 30, Oct. 1987, p. 2947-2951. refs

The higher spatial-stability eigenmodes for the Blasius boundary layer are examined by using asymptotic theory, and an infinite number of modes are found. The asymptotic results are shown to be in close agreement with results from a direct numerical solution of the Orr-Sommerfeld problem. The asymptotic theory would therefore provide an efficient tool in exploratory searches for the eigenvalues. Author

A88-16354* National Aeronautics and Space Administration. Lewis Research Center, Cleveland, OH.

INFRARED PROPERTIES OF AN ANISOTROPICALLY STIRRED FLUID

ROBERT RUBINSTEIN and J. MICHAEL BARTON (NASA, Lewis Research Center; Sverdrup Technology, Inc., Cleveland, OH) Physics of Fluids (ISSN 0031-9171), vol. 30, Oct. 1987, p. 2987-2992. refs
(Contract NAS3-24105)

A renormalization group is developed for the Navier-Stokes equations driven by an anisotropically correlated random stirring force. The stirring force generates homogeneous turbulence with a preferred direction. The force correlation is the sum of a small anisotropic perturbation and an isotropic correlation chosen, so that the fixed point of renormalization group has a $k \exp -5/3$ energy spectrum. Fixed points for the anisotropic correlation are found near this isotropic fixed point. Two types of anisotropy are analyzed. When the additional stirring is in the plane perpendicular to the preferred direction, the renormalized viscosity is increased. When it is aligned with the preferred direction, the viscosity is decreased. A possible connection with the inverse energy cascade of two-dimensional turbulence is discussed. Author

A88-16545* # Brown Univ., Providence, RI.

CONTROL OF FREE SHEAR LAYERS

J. T. C. LIU (Brown University, Providence, RI) and H. T. KAPTANOGLU AIAA, Aeroacoustics Conference, 11th, Sunnyvale, CA, Oct. 19-21, 1987. 43 p. DARPA-supported research. refs
(Contract NSF MSM-83-20307; NAG3-673)
(AIAA PAPER 87-2689)

The fundamental aspects of controlled multiple coherent mode presence in turbulent shear flows is first discussed, including the supplementary averaging procedures in addition to the Reynolds average and the nonlinear energy transfer mechanisms coupling the coherent modes, mean flow and fine-grained turbulence. Then the problem of a fundamental mode and its subharmonic in a developing mixing layer, the prototype problem of subharmonic cascade, is examined. An integral method is presented which allows the determination of the coherent wave envelope or amplitude simultaneously with the mean flow growth rate and turbulence energy. This is then generalized to the presence of multiple subharmonics using a binary-frequency interaction argument. Free shear layer control is discussed in terms of initial coherent mode amplitudes, dimensionless initial frequencies, phase angle between the modes and fine-grained turbulence levels, in particular, how these parameters could enhance or suppress the shear layer spreading rate and the levels of fine-grained turbulence. Author

A88-17318* Akron Univ., OH.

STEADY AND TRANSIENT LEAST SQUARE SOLVERS FOR THERMAL PROBLEMS

JOE PADOVAN (Akron, University, OH) Numerical Heat Transfer (ISSN 0149-5720), vol. 12, no. 3, 1987, p. 263-284. refs
(Contract NAG3-54)

This paper develops a hierarchical least square solution algorithm for highly nonlinear heat transfer problems. The methodology's capability is such that both steady and transient implicit formulations can be handled. This includes problems arising from highly nonlinear heat transfer systems modeled by either finite-element or finite-difference schemes. The overall procedure developed enables localized updating, iteration, and convergence checking as well as constraint application. The localized updating can be performed at a variety of hierarchical levels, i.e., degree of freedom, substructural, material-nonlinear groups, and/or boundary groups. The choice of such partitions can be made via energy partitioning or nonlinearity levels as well as by user selection. Overall, this leads to extremely robust computational characteristics. To demonstrate the methodology, problems are drawn from nonlinear heat conduction. These are used to quantify the robust capabilities of the hierarchical least square scheme. Author

A88-18506* # Oxford Univ. (England).

HIGH-RESOLUTION HEAT-TRANSFER-COEFFICIENT MAPS APPLICABLE TO COMPOUND-CURVE SURFACES USING LIQUID CRYSTALS IN A TRANSIENT WIND TUNNEL

T. V. JONES (Oxford University, England) and S. A. HIPPENSTEELE (NASA, Lewis Research Center, Cleveland, OH) IN: Developments in experimental techniques in heat transfer and combustion; Proceedings of the Twenty-fourth National Heat Transfer Conference and Exhibition, Pittsburgh, PA, Aug. 9-12,

1987. New York, American Society of Mechanical Engineers, 1987, p. 1-9. refs

Tests were performed in a transient heat transfer tunnel in which the model under test was preheated prior to allowing room temperature air to be suddenly drawn over the model. The resulting movement of isothermal contours on the model is revealed using a surface coating of thermochromic liquid crystals that display distinctive colors at particular temperatures. A video record is obtained of a temperature and time data pair for all points on the model during a single test. Experiments on a duct model are reported in which the model was preheated using a hot air stream. A manner in which initial model temperature nonuniformities could be taken into account was investigated. The duct model was also tested with a steady-state measurement technique and results were compared with the transient measurements, but recognizing that differences existed between the upstream thermal boundary conditions. The steady-state and transient measurements were shown to be consistent with predicted values. The main advantage of this transient heat transfer technique using liquid crystals is that since the test model need not be actively heated, high-resolution measurements on surfaces with complex shapes may be obtained. Author

A88-18975* Carnegie-Mellon Univ., Pittsburgh, PA.
**NUMERICAL METHODS FOR ONE-DIMENSIONAL
REACTION-DIFFUSION EQUATIONS ARISING IN
COMBUSTION THEORY**

J. I. RAMOS (Carnegie-Mellon University, Pittsburgh, PA) IN: Annual review of numerical fluid mechanics and heat transfer. Volume 1. Washington, DC, Hemisphere Publishing Corp., 1987, p. 150-261. Research supported by U.S. - Spain Committee for Scientific and Technological Cooperation. refs
(Contract NAG3-21; AF-AFOSR-84-0202)

A review of numerical methods for one-dimensional reaction-diffusion equations arising in combustion theory is presented. The methods reviewed include explicit, implicit, quasi-linearization, time linearization, operator-splitting, random walk and finite-element techniques and methods of lines. Adaptive and nonadaptive procedures are also reviewed. These techniques are applied first to solve two model problems which have exact traveling wave solutions with which the numerical results can be compared. This comparison is performed in terms of both the wave profile and computed wave speed. It is shown that the computed wave speed is not a good indicator of the accuracy of a particular method. A fourth-order time-linearized, Hermitian compact operator technique is found to be the most accurate method for a variety of time and space sizes. Author

A88-19194* National Aeronautics and Space Administration.
Lewis Research Center, Cleveland, OH.

**ROLL-UP OF VORTICITY IN ADVERSE-PRESSURE-GRADIENT
BOUNDARY LAYERS**

M. E. GOLDSTEIN, P. A. DURBIN, and S. J. LEIB (NASA, Lewis Research Center, Cleveland, OH) Journal of Fluid Mechanics (ISSN 0022-1120), vol. 183, Oct. 1987, p. 325-342. refs

It is shown how the unsteady, nonlinear critical-layer equation determines the evolution of instability waves in a weak adverse-pressure-gradient boundary layer. Numerical solutions show that the nonlinearity halts the growth of these inviscidly unstable waves. The stabilizing effect of nonlinearity, in the present case, can be described as a consequence of either the increase (toward zero) of the phase jump across the critical layer or the roll-up of the critical-layer disturbance vorticity. Author

A88-20169*# National Aeronautics and Space Administration.
Lewis Research Center, Cleveland, OH.

**TRANSIENT RADIATIVE COOLING OF A LAYER FILLED WITH
SOLIDIFYING DROPS**

R. SIEGEL (NASA, Lewis Research Center, Cleveland, OH) ASME, Transactions, Journal of Heat Transfer (ISSN 0022-1481), vol. 109, Nov. 1987, p. 977-982. refs

An analysis is carried out for radiative cooling of a plane layer initially filled with liquid drops that solidify and then continue to

cool by loss of sensible heat. This is in connection with a proposed lightweight radiator system for heat dissipation in space. Hot liquid drops would be ejected and then cooled by direct exposure in space; they would then pass into a collector for reuse. The cooling analysis contains three transient zones. In the first, the drops cool by losing latent heat until the outermost drops become solid. Then the cooling continues by loss of both latent and sensible heat. A similarity behavior is eventually achieved in which the transient emittance of the layer depends only on the optical thickness. Author

A88-20182*# Lockheed-Georgia Co., Marietta.
**EFFECTS OF NOZZLE-EXIT BOUNDARY-LAYER CONDITIONS
ON EXCITABILITY OF HEATED FREE JETS**

J. LEPICOVSKY and W. H. BROWN (Lockheed Aeronautical Systems Co., Georgia Div., Marietta) AIAA, Aeroacoustics Conference, 11th, Sunnyvale, CA, Oct. 19-21, 1987. 10 p. refs
(Contract NAS3-23708)
(AIAA PAPER 87-2723)

This paper reports an experimental study on the effects of nozzle-exit boundary-layer conditions on the excitability of heated free jets. The results were obtained at a Mach number 0.8 and total temperatures of 300 K and 670 K. External acoustic excitation was used to excite the jet. The excitation frequencies ranged up to 6 KHZ and the excitation levels were up to 150 dB. A level of 147 dB was used for most of the test points. Nozzle-exit boundary-layer characteristics were controlled by boundary layer tripping upstream of the nozzle exit plane. It has been shown that the free jet mixing rate strongly depends on the boundary-layer characteristics at the nozzle exit. Further, it appears that jets with a thin laminar nozzle-exit boundary layer are more selective about the optimum excitation frequency than those with a thick turbulent nozzle-exit boundary layer. Finally, for the jet of Mach number 0.8, it appears that free jet mixing and development may be controlled by flow excitation as well as by nozzle-exit boundary-layer modifications. Author

A88-20459* Pennsylvania State Univ., University Park.
**A SPACE-MARCHING METHOD FOR THE COMPUTATION OF
VISCOUS INTERNAL FLOWS**

T. R. GOVINDAN and B. LAKSHMINARAYANA (Pennsylvania State University, University Park) Computers and Fluids (ISSN 0045-7930), vol. 16, no. 1, 1988, p. 21-39. refs
(Contract NSG-3212)

A space-marching method has been developed to compute 3-D viscous flows in internal geometries. The Navier-Stokes equations have been posed as an initial-value problem by neglecting the effects of streamwise diffusion and treating the streamwise pressure gradient as a known source term. The fully coupled system of equations has been solved by a noniterative algorithm at each streamwise step of the computation. A low Mach number formulation of the equations has been used to compute incompressible flow fields. A computer program has been written to implement all aspects of the space-marching algorithm. The program is modular and is easily adapted to the widely varying geometries of internal flows. The space-marching algorithm has been tested by computing simple flows with known analytical solutions. The method has been used to predict complex 3-D turbulent flows. The algorithm is stable and very economical. A single sweep of the flow field by the space-marching method is approximately equivalent to one time-step of the time-marching method. Author

A88-20748* National Aeronautics and Space Administration.
Lewis Research Center, Cleveland, OH.

**TORSION EFFECT ON FULLY DEVELOPED FLOW IN A
HELICAL PIPE**

HSIAO C. KAO (NASA, Lewis Research Center, Cleveland, OH) Journal of Fluid Mechanics (ISSN 0022-1120), vol. 184, Nov. 1987, p. 335-356. refs

Two techniques, a series expansion method of perturbed Poiseuille flow valid for low Dean numbers and a solution of the complete Navier-Stokes equation applicable to intermediate Dean

34 FLUID MECHANICS AND HEAT TRANSFER

values, are used to investigate the torsion effect on the fully developed laminar flow in a helical pipe of constant circular cross section. For the secondary flow patterns, the results show that the presence of torsion can produce a significant effect if the ratio of the curvature to the torsion is of order unity. The secondary flow is distorted in these cases. It is noted that the torsion effect is, however, usually small, and that the secondary flow has the usual pattern of a pair of counter-rotating vortices of nearly equal strength. R.R.

A88-20842* National Aeronautics and Space Administration. Lewis Research Center, Cleveland, OH.

ABSOLUTE INSTABILITY OF THE GAUSSIAN WAKE PROFILE
LENNART S. HULTGREN (NASA, Lewis Research Center, Cleveland, OH) and ARUN K. AGGARWAL (Illinois Institute of Technology, Chicago) *Physics of Fluids* (ISSN 0031-9171), vol. 30, Nov. 1987, p. 3383-3387. Research supported by the Illinois Institute of Technology. refs

Linear parallel-flow stability theory has been used to investigate the effect of viscosity on the local absolute instability of a family of wake profiles with a Gaussian velocity distribution. The type of local instability, i.e., convective or absolute, is determined by the location of a branch-point singularity with zero group velocity of the complex dispersion relation for the instability waves. The effects of viscosity were found to be weak for values of the wake Reynolds number, based on the center-line velocity defect and the wake half-width, larger than about 400. Absolute instability occurs only for sufficiently large values of the center-line wake defect. The critical value of this parameter increases with decreasing wake Reynolds number, thereby indicating a shrinking region of absolute instability with decreasing wake Reynolds number. If backflow is not allowed, absolute instability does not occur for wake Reynolds numbers smaller than about 38. Author

A88-20871* Sandia National Labs., Livermore, CA.
THE STRUCTURE AND DYNAMICS OF REACTING PLANE MIXING LAYERS

J. O. KELLER (Sandia National Laboratories, Livermore, CA), J. L. ELLZEY (Wisconsin, University, Madison), R. W. PITZ (Vanderbilt University, Nashville, TN), I. G. SHEPHERD, and J. W. DAILY (California, University, Berkeley) *Experiments in Fluids* (ISSN 0723-4864), vol. 6, no. 1, 1988, p. 33-43. USAF-supported research. refs

(Contract NSF ENG-77-02019; NSG-3227)

Experimental studies of the combustor mixing layers formed over a rearward facing step and between two parallel streams are reported. The steady behavior of the mean properties of the reacting flows is similar to that of nonreacting flows except for the global effects of thermodynamic property changes. Vortices form by the two-dimensional K-H instability and grow by subharmonic combination until the layer begins to interact with the walls. Unsteady behavior occurs when there are resonator interactions with the K-H instability or the instability associated with the recirculation vortex in the rearward facing step flow. B.J.

A88-21155* Grumman Aerospace Corp., Bethpage, NY.
HIGH THERMAL-TRANSPORT CAPACITY HEAT PIPES FOR SPACE RADIATORS

ALBERT W. CARLSON, ERIC GUSTAFSON, and SUSAN L. ROUKIS (Grumman Corp., Space Systems Div., Bethpage, NY) *SAE, Intersociety Conference on Environmental Systems*, 17th, Seattle, WA, July 13-15, 1987. 14 p. refs
(Contract NAS3-24665)
(SAE PAPER 871509)

This paper presents the results of performance tests of several dual-slot heat pipe test articles. The dual-slot configuration has a very high thermal transport capability and has been identified as a very promising candidate for the radiator system for the NASA Space Station solar dynamic power modules. Two six-foot long aluminum heat pipes were built and tested with ammonia and acetone. A 20-ft long heat pipe was also built and tested with ammonia. The test results have been compared with performance

predictions. A thermal transport capacity of 2000 W at an adverse tilt of 1 in. and a 1000 W capacity at an adverse tilt of 2 in. were achieved on the 20-ft long heat pipe. These values are in close agreement with the predicted performance limits. Author

A88-21273*# Wisconsin Univ., Milwaukee.
INVESTIGATION OF THIRD-ORDER CLOSURE MODEL OF TURBULENCE FOR THE COMPUTATION OF INCOMPRESSIBLE FLOWS IN A CHANNEL WITH A BACKWARD-FACING STEP

R. S. AMANO (Wisconsin, University, Milwaukee) and P. GOEL *ASME, Transactions, Journal of Fluids Engineering* (ISSN 0098-2202), vol. 109, Dec. 1987, p. 424-428. refs
(Contract NAG3-546)

To predict the diffusion process of the Reynolds stresses in reattaching shear flows, the transport model for the triple-velocity products has been developed and tested for the computation of the flow in a channel with a backward-facing step. Upon comparison of the results of uuv , uvv , and vuv with those obtained by using existing algebraic correlations, it was shown that the present model improved the prediction of the triple-velocity products. Author

A88-21983*# Arizona State Univ., Tempe.
LOW REYNOLDS NUMBER MODELING OF TURBULENT FLOWS WITH AND WITHOUT WALL TRANSPARATION

RONALD M. C. SO and GEUN JONG YOO (Arizona State University, Tempe) *AIAA Journal* (ISSN 0001-1452), vol. 25, Dec. 1987, p. 1556-1564. Research supported by the Oak Ridge National Laboratory. refs
(Contract NAG3-167; N60530-85-C-0191)

A full Reynolds-stress closure that is capable of describing the flow all the way to the wall is formulated. The closure is based on the conventional high Reynolds number form of the redistribution model, the inclusion of molecular diffusion, and a modified dissipation model to account for viscous effects near a wall. Two dissipation models are investigated along with two gradient diffusion and two redistribution models. Their respective effects on the calculated flow properties are assessed by comparing them with the data of fully developed turbulent flows and a developing pipe flow with wall transpiration. The near-wall behavior is very well predicted; however, the wall correction to the redistribution modeling is found to have little effect on the calculated results. The overall behavior of the fully developed turbulent flows is best described by a nonisotropic gradient diffusion model, a return-to-isotropy redistribution model, and a dissipation model that accounts for viscous behavior near a wall. This same closure also gives the best prediction of the axial pressure drop behavior along a pipe with a uniform wall suction. Furthermore, the near-wall behavior of such a flow is very well predicted by this closure. Author

A88-22207*# National Aeronautics and Space Administration. Lewis Research Center, Cleveland, OH.

MEASUREMENT OF LOCAL CONVECTIVE HEAT TRANSFER COEFFICIENTS FROM A SMOOTH AND ROUGHENED NACA-0012 AIRFOIL - FLIGHT TEST DATA

G. JAMES VAN FOSSEN (NASA, Lewis Research Center, Cleveland, OH), KENNETH J. DE WITT (Toledo, University, OH), JAMES E. NEWTON, and PHILLIP E. POINSATTE *AIAA, Aerospace Sciences Meeting*, 26th, Reno, NV, Jan. 11-14, 1988. 16 p. Previously announced in STAR as N88-13552. refs
(AIAA PAPER 88-0287)

Wind tunnels typically have higher free stream turbulence levels than are found in flight. Turbulence intensity was measured to be 0.5 percent in the NASA Lewis Icing Research Tunnel (IRT) with the cloud making sprays off and around 2 percent with cloud making equipment on. Turbulence intensity for flight conditions was found to be too low to make meaningful measurements for smooth air. This difference between free stream and wind tunnel conditions has raised questions as to the validity of results obtained in the IRT. One objective of these tests was to determine the effect of free stream turbulence on convective heat transfer for the NASA Lewis LEWICE ice growth prediction code. These tests

provide in-flight heat transfer data for a NASA-0012 airfoil with a 533 cm chord. Future tests will measure heat transfer data from the same airfoil in the Lewis Icing Research Tunnel. Roughness was obtained by the attachment of small, 2 mm diameter hemispheres of uniform size to the airfoil in three different patterns. Heat transfer measurements were recorded in flight on the NASA Lewis Twin Otter Icing Research Aircraft. Measurements were taken for the smooth and roughened surfaces at various aircraft speeds and angles of attack up to four degrees. Results are presented as Frossling number versus position on the airfoil for various roughnesses and angles of attack. Author

A88-22209*# National Aeronautics and Space Administration. Lewis Research Center, Cleveland, OH.

STABILITY RELATIONSHIP FOR WATER DROPLET CRYSTALLIZATION WITH THE NASA LEWIS ICING SPRAY NOZZLE

C. JOHN MAREK (NASA, Lewis Research Center, Cleveland, OH) and C. SCOTT BARTLETT (Sverdrup Technology, Inc., Arnold Air Force Station, TN) AIAA, Aerospace Sciences Meeting, 26th, Reno, NV, Jan. 11-14, 1988. 15 p. Previously announced in STAR as N88-10790. refs (AIAA PAPER 88-0289)

In order to produce small droplets for icing cloud simulation, high pressure air atomizing nozzles are used. For certain icing testing applications, median drop sizes as small as 5 mm are needed, which require air atomizing pressures greater than 3000 kPa. Isentropic expansion of the ambient temperature atomizing air to atmospheric pressure can result in air stream temperatures of -160 C which results in ice crystals forming in the cloud. To avoid such low temperatures, it is necessary to heat the air and water to high initial temperatures. An icing spray research program was conducted to map the temperatures below which ice crystals form. A soot slide technique was used to determine the presence of crystals in the spray. Author

A88-22210*# Dayton Univ., OH.

NAVIER-STOKES SOLUTIONS OF FLOWFIELD CHARACTERISTICS PRODUCED BY ICE ACCRETION

J. N. SCOTT, T. P. GIELDA, and W. L. HANKEY (Dayton, University, OH) AIAA, Aerospace Sciences Meeting, 26th, Reno, NV, Jan. 11-14, 1988. 12 p. refs (Contract NAG3-665) (AIAA PAPER 88-0290)

The flowfield and resultant heat transfer rates over a series of ice accretion shapes have been obtained through numerical solutions of the Navier-Stokes equations. The influence of roughness is modeled by including blockage, form drag and stagnation heating effects as source terms in the governing equations. Using the flowfield information obtained from the Navier-Stokes equations the droplet impingement efficiencies are computed using a PNS-type solving scheme. Good agreement is achieved between the numerical results and experimental data. Author

A88-22251*# General Motors Corp., Indianapolis, IN.

K-EPSILON TURBULENCE MODEL ASSESSMENT WITH REDUCED NUMERICAL DIFFUSION FOR COAXIAL JETS

M. NIKJOOY, K. C. KARKI, H. C. MONGIA (General Motors Corp., Allison Gas Turbine Div., Indianapolis, IN), V. G. MCDONELL, and G. S. SAMUELSEN (California, University, Irvine) AIAA, Aerospace Sciences Meeting, 26th, Reno, NV, Jan. 11-14, 1988. 11 p. refs (Contract NAS3-24350) (AIAA PAPER 88-0342)

A numerical study has been conducted to evaluate the performance of the k-epsilon turbulence model for axisymmetric, unconfined, swirling, and nonswirling coaxial jet flows. Two lower order schemes, hybrid and power-law, and two higher order schemes, flux-spline and bounded skew upwind differencing, were employed in this investigation. The predicted results indicate that the higher order numerical schemes have greater potential for future model improvements and complex flow calculations in terms

of storage, accuracy, and execution time. For the nonswirling flow, computations using an algebraic stress model have also been presented. Author

A88-22346*# Cleveland State Univ., OH.

SENSITIVITY STUDY OF THE MONOGROOVE WITH SCREEN HEAT PIPE DESIGN

AUSTIN L. EVANS (Cleveland State University, OH) and MARTIN JOYCE AIAA, Aerospace Sciences Meeting, 26th, Reno, NV, Jan. 11-14, 1988. 7 p. (Contract NCC3-50) (AIAA PAPER 88-0470)

The present sensitivity study of design variable effects on the performance of a monogroove-with-screen heat pipe obtains performance curves for maximum heat-transfer rates vs. operating temperatures by means of a computer code; performance projections for both 1-g and zero-g conditions are obtainable. The variables in question were liquid and vapor channel design, wall groove design, and the number of feed lines in the evaporator and condenser. The effect on performance of three different working fluids, namely ammonia, methanol, and water, were also determined. Greatest sensitivity was to changes in liquid and vapor channel diameters. O.C.

A88-22419*# Massachusetts Inst. of Tech., Cambridge.

VAPOR CONDENSATION RATE AT A TURBULENT LIQUID INTERFACE, FOR APPLICATION TO CRYOGENIC HYDROGEN

M. R. HELMICK, B. C. KHOO, J. S. BROWN, and A. A. SONIN (MIT, Cambridge, MA) AIAA, Aerospace Sciences Meeting, 26th, Reno, NV, Jan. 11-14, 1988. 12 p. refs (Contract NAG3-731) (AIAA PAPER 88-0559)

The condensation of hydrogen vapor onto turbulent liquid hydrogen is simulated experimentally using steam and water at elevated pressure, where water has a Prandtl number comparable to that of liquid hydrogen. A correlation is presented for the condensation rate in terms of the intensity and macroscale of the turbulence on the liquid side. The rate correlation should be applicable to low-gravity conditions at the higher turbulence intensities; at the lower turbulence intensities, however, the data are affected by thermal stratification resulting from buoyancy effects. Author

A88-23312*# National Aeronautics and Space Administration. Lewis Research Center, Cleveland, OH.

A NUMERICAL STUDY OF THE EFFECTS OF CURVATURE AND CONVERGENCE ON DILUTION JET MIXING

J. D. HOLDEMAN (NASA, Lewis Research Center, Cleveland, OH), R. REYNOLDS, and C. WHITE (Garrett Turbine Engine Co., Phoenix, AZ) AIAA, SAE, ASME, and ASCE, Joint Propulsion Conference, 23rd, San Diego, CA, June 29-July 2, 1987. 18 p. Previously announced in STAR as N88-13347. refs (AIAA PAPER 87-1953)

An analytical program was conducted to assemble and assess a three-dimensional turbulent viscous flow computer code capable of analyzing the flow field in the transition liners of small gas turbine engines. This code is of the TEACH type with hybrid numerics, and uses the power law and SIMPLER algorithms, an orthogonal curvilinear coordinate system, and an algebraic Reynolds stress turbulence model. The assessments performed in this study, consistent with results in the literature, showed that in its present form this code is capable of predicting trends and qualitative results. The assembled code was used to perform a numerical experiment to investigate the effects of curvature and convergence in the transition liner on the mixing of single and opposed rows of cool dilution jets injected into a hot mainstream flow. Author

A88-25191* National Aeronautics and Space Administration. Lewis Research Center, Cleveland, OH.

FREE-STREAMLINE ANALYSIS OF DEFORMATION AND DISLODGING BY WIND FORCE OF DROPS ON A SURFACE

34 FLUID MECHANICS AND HEAT TRANSFER

P. A. DURBIN (NASA, Lewis Research Center, Cleveland, OH) *Physics of Fluids* (ISSN 0031-9171), vol. 31, Jan. 1988, p. 43-48. refs

Free-streamline theory is used to analyze the deformation and dislodging by wind pressure of drops of liquid adhered by surface tension to a solid surface. The critical Weber number for droplets to be dislodged is determined as a function of advancing and receding contact angle. Graphical results for drop shape are in good agreement with observation. Author

A88-25828* Michigan Univ., Ann Arbor.

MIXING, TRANSPORT AND COMBUSTION IN SPRAYS

G. M. FAETH (Michigan, University, Ann Arbor) *Progress in Energy and Combustion Science* (ISSN 0360-1285), vol. 13, no. 4, 1987, p. 293-345. refs

(Contract NAG3-190; AF-AFOSR-85-0244; DAAL03-86-K-0154; N00014-85-C-0148; N00014-80-C-0517)

The state-of-the-art in analytical methods for sprays and drop/turbulence interactions in combustion processes is presented with reference to dilute sprays, and dilute dispersed flows, that contain well-defined dispersed-phase elements in volume fractions lower than 1 percent. Attention is given to the near-injector dense spray region. The methods tested are those of locally homogeneous flow, deterministic separated flow, and stochastic separated flow; the first of these was ineffective due to its ignoring finite interphase transport rates, and the second failed by ignoring turbulent dispersion. Stochastic separated flow methodology yielded encouraging results through its treatment of both finite interphase transport rates and dispersed-phase/turbulence interactions.

O.C.

A88-26206* National Aeronautics and Space Administration. Lewis Research Center, Cleveland, OH.

COMPUTATION OF THE VELOCITY FIELD OF AN EXCITED SHEAR LAYER

M. NALLASAMY (NASA, Lewis Research Center; Sverdrup Technology, Inc., Cleveland, OH) *Communications in Applied Numerical Methods* (ISSN 0748-8025), vol. 4, Jan.-Feb. 1988, p. 85-89. refs

An infinitely thin shear layer emanating from a semi-infinite flat plate subjected to acoustic excitation is considered. The flow field outside the excited shear layer is computed employing a source distribution approach. Results are given for the region of the velocity field that cannot easily be obtained by analytical approximations.

Author

A88-26338* Deutsche Forschungs- und Versuchsanstalt fuer Luft- und Raumfahrt, Berlin (Germany, F.R.).

EXCITATION OF INSTABILITY WAVES IN FREE SHEAR LAYERS. I - THEORY

D. W. BECHERT (DFVLR, Berlin, Federal Republic of Germany) *Journal of Fluid Mechanics* (ISSN 0022-1120), vol. 186, Jan. 1988, p. 47-62. refs

(Contract NAG3-198; DFG-BE-889/1-1)

The generation of instability waves in free shear layers has been theoretically studied under the assumption of an infinitesimally thin shear layer shed from a semiinfinite plate which is exposed to sound excitation. The shear-layer excitation by a source which is far away from the plate edge in the downstream direction is found to be very weak, while the excitation upstream from the plate edge is found to be relatively efficient. Sources far away from the plate edge are shown to produce a parabolic pressure field near the edge. The present method is extended to the case of two streams (one on each side of the shear layer) with different velocities and densities. Results are also presented for the excitation of a shear layer in a channel.

R.R.

A88-26339* Deutsche Forschungs- und Versuchsanstalt fuer Luft- und Raumfahrt, Berlin (Germany, F.R.).

EXCITATION OF INSTABILITY WAVES IN FREE SHEAR LAYERS. II - EXPERIMENTS

D. W. BECHERT and B. STAHL (DFVLR, Berlin, Federal Republic

of Germany) *Journal of Fluid Mechanics* (ISSN 0022-1120), vol. 186, Jan. 1988, p. 63-84. refs

(Contract NAG3-198; DFG-BE-889/1-1)

The acoustical excitation of shear layers is investigated experimentally. Acoustical excitation causes, for example, the so-called 'orderly structures' in shear layers and jets. The deviations in the spreading rate between different turbulent-shear-layer experiments are due to the same excitation mechanism. The present investigations focus on measurements in the linear interaction region close to the edge from which the shear layer is shed. Two sets of experiments (Houston, 1981, and Berlin, 1983 and 1984) are reported on. The measurements have been carried out with laminar shear layers in air using hot-wire anemometers and microphones. The agreement between these measurements and the theory is good. Details of the fluctuating flow field are found to correspond to theoretical predictions, such as the local occurrence of negative phase speeds.

Author

A88-27716*# National Aeronautics and Space Administration. Lewis Research Center, Cleveland, OH.

TIME-ACCURATE SIMULATIONS OF A SHEAR LAYER FORCED AT A SINGLE FREQUENCY

R. W. CLAUS (NASA, Lewis Research Center, Cleveland, OH), P. G. HUANG (Michigan Technological University, Houghton), and J. MACINNES (Princeton University, NJ) *AIAA, Aerospace Sciences Meeting*, 26th, Reno, NV, Jan. 11-14, 1988. 16 p. refs (AIAA PAPER 88-0061)

This report presents calculations of the forced shear layer studied experimentally by Oster and Wygnanski (1982) and Weisbrot (1984). Two different computational approaches are examined: Direct Numerical Simulation (DNS) and Large Eddy Simulation (LES). The DNS approach solves the full three-dimensional, Navier-Stokes equations for a temporally evolving mixing layer, while the LES approach (as used in this report) solves the two-dimensional, Navier-Stokes equations with a subgrid scale turbulence model. While the comparison between these calculations and experimental data was hampered by a lack of information on the inflow boundary conditions, the calculations are shown to qualitatively agree with several aspects of the experiment. The sensitivity of these calculations to factors such as mesh refinement and Reynolds number is illustrated.

Author

A88-27719*# Toledo Univ., OH.

MASS TRANSPORT PHENOMENA BETWEEN BUBBLES AND DISSOLVED GASES IN LIQUIDS UNDER REDUCED GRAVITY CONDITIONS

KENNETH J. DEWITT (Toledo, University, OH), JONATHAN L. BROCKWELL (Union Carbide Corp., South Charleston, WV), CHAIN-NAN YUNG, AN-TI CHAI, JOHN B. MCQUILLEN, RAYMOND G. SOTOS, and ERIC S. NEUMANN (NASA, Lewis Research Center, Cleveland, OH) *AIAA, Aerospace Sciences Meeting*, 26th, Reno, NV, Jan. 11-14, 1988. 9 p. NASA-supported research. refs (AIAA PAPER 88-0450)

This paper will describe the experimental and analytical work that has been done to establish justification and feasibility for a Shuttle mid-deck experiment involving mass transfer between a gas bubble and a liquid. The experiment involves the observation and measurement of the dissolution of an isolated, immobile gas bubble of specified size and composition in a thermostatted solvent liquid of known concentration in the reduced gravity environment of earth orbit. Methods to generate and deploy the bubble have been successful both in normal gravity using mutually buoyant fluids and under reduced gravity conditions in the NASA Lear Jet. Initialization of the experiment with a bubble of a prescribed size and composition in a liquid of known concentration has been accomplished using the concept of unstable equilibrium. Subsequent bubble dissolution or growth is obtained by a step increase or decrease in the liquid pressure. A numerical model has been developed which simulates the bubble dynamics and can be used to determine molecular parameters by comparison with the experimental data. The primary objective of the experiment

is the elimination of convective effects that occur in normal gravity. The results will yield information on transport under conditions of pure diffusion. Author

A88-27723* National Aeronautics and Space Administration. Lewis Research Center, Cleveland, OH.

CONSISTENT BOUNDARY CONDITIONS FOR REDUCED NAVIER-STOKES (RNS) SCHEME APPLIED TO THREE-DIMENSIONAL INTERNAL VISCOUS FLOWS

D. R. REDDY (NASA, Lewis Research Center; Sverdrup Technology, Inc., Cleveland, OH) and S. G. RUBIN (Cincinnati, University, OH) AIAA, Aerospace Sciences Meeting, 26th, Reno, NV, Jan. 11-14, 1988. 20 p. refs (AIAA PAPER 88-0714)

Three-dimensional internal viscous flow problems are presently addressed by a consistent and efficient set of boundary conditions for the multisweep space-marching, pressure-elliptic Reduced Navier-Stokes scheme. Since continuity is by this means directly satisfied at all points in the flow domain, the first-order momentum equations are directly solvable for pressure without the requirement for a Poisson pressure-correction equation. Incompressible flow solutions are obtained for straight and curved ducts of square cross section, in order to validate the procedure. Usefulness is demonstrated for internal flows with strong interactions, as would be found in turbomachine geometries. O.C.

A88-28516* Texas A&M Univ., College Station. **LOCAL HEAT/MASS TRANSFER DISTRIBUTIONS AROUND SHARP 180 DEG TURNS IN TWO-PASS SMOOTH AND RIB-ROUGHENED CHANNELS**

J. C. HAN, P. R. CHANDRA, and S. C. LAU (Texas A & M University, College Station) ASME, Transactions, Journal of Heat Transfer (ISSN 0022-1481), vol. 110, Feb. 1988, p. 91-98. refs (Contract NAS3-24227; NSF MEA-82-05234) (ASME PAPER 86-GT-114)

The naphthalene sublimation technique was employed to study the detailed mass transfer distributions around the sharp 180 deg turns in a two-pass, square, smooth channel and in an identical channel with two rib-roughened opposite walls. Experiments conducted for Reynolds numbers of 15,000, 30,000, and 60,000 indicate that the Sherwood numbers on the top, outer, and inner walls around the turn in the rib-roughened channel are higher than the corresponding Sherwood numbers around the turn in the smooth channel. Sherwood numbers after the sharp turn are found to be higher than those before the turn for both the smooth and the ribbed channels. R.R.

A88-30469* National Aeronautics and Space Administration. Lewis Research Center, Cleveland, OH.

A FINITE DIFFERENCE SCHEME FOR THREE-DIMENSIONAL STEADY LAMINAR INCOMPRESSIBLE FLOW

DANNY P. HWANG and HUNG T. HUYNH (NASA, Lewis Research Center, Cleveland, OH) IN: Numerical methods in laminar and turbulent flow; Proceedings of the Fifth International Conference, Montreal, Canada, July 6-10, 1987. Volume 5, Part 1. Swansea, Wales, Pineridge Press, 1987, p. 244-260. Previously announced in STAR as N87-20504. refs

A finite difference scheme for three-dimensional steady laminar incompressible flows is presented. The Navier-Stokes equations are expressed conservatively in terms of velocity and pressure increments (delta form). First order upwind differences are used for first order partial derivatives of velocity increments resulting in a diagonally dominant matrix system. Central differences are applied to all other terms for second order accuracy. The SIMPLE pressure correction algorithm is used to satisfy the continuity equation. Numerical results are presented for cubic cavity flow problems for Reynolds numbers up to 2000 and are in good agreement with other numerical results. Author

A88-30517* Virginia Polytechnic Inst. and State Univ., Blacksburg.

EXPLICIT FINITE-VOLUME TIME-MARCHING CALCULATIONS OF TOTAL TEMPERATURE DISTRIBUTIONS IN TURBULENT FLOW

STEPHEN NICHOLSON, JOAN G. MOORE, and JOHN MOORE (Virginia Polytechnic Institute and State University, Blacksburg) IN: Numerical methods in laminar and turbulent flow; Proceedings of the Fifth International Conference, Montreal, Canada, July 6-10, 1987. Volume 5, Part 2. Swansea, Wales, Pineridge Press, 1987, p. 1021-1032. Previously announced in STAR as N87-23929. refs

(Contract NAG3-593)

A method was developed which calculates two-dimensional, transonic, viscous flow in ducts. The finite volume, time-marching formulation is used to obtain steady flow solutions of the Reynolds-averaged form of the Navier-Stokes equations. The entire calculation is performed in the physical domain. This paper investigates the introduction of a new formulation of the energy equation which gives improved transient behavior as the calculation converges. The effect of variable Prandtl number on the temperature distribution through the boundary layer is also investigated. A turbulent boundary layer in an adverse pressure gradient ($M = 0.55$) is used to demonstrate the improved transient temperature distribution obtained when the new formulation of the energy equation is used. A flat plate turbulent boundary layer with a supersonic free-stream Mach number of 2.8 is used to investigate the effect of Prandtl number on the distribution of properties through the boundary layer. The computed total temperature distribution and recovery factor agree well with the measurements when a variable Prandtl number is used through the boundary layer. m.g.

A88-30518* Virginia Polytechnic Inst. and State Univ., Blacksburg.

AN EXPLICIT FINITE-VOLUME TIME-MARCHING PROCEDURE FOR TURBULENT FLOW CALCULATIONS

STEPHEN NICHOLSON, JOAN G. MOORE, and JOHN MOORE (Virginia Polytechnic Institute and State University, Blacksburg) IN: Numerical methods in laminar and turbulent flow; Proceedings of the Fifth International Conference, Montreal, Canada, July 6-10, 1987. Volume 5, Part 2. Swansea, Wales, Pineridge Press, 1987, p. 1033-1044. Previously announced in STAR as N87-23928. refs

(Contract NAG3-593)

A method was developed which calculates two-dimensional, transonic, viscous flow in ducts. The finite-volume, time-marching formulation is used to obtain steady flow solutions of the Reynolds-averaged form of the Navier-Stokes equations. The entire calculation is performed in the physical domain. Control volumes are chosen so that smoothing of flow properties, typically required for stability, is not required. Different time steps are used in the different governing equations. A new pressure interpolation scheme is introduced which improves the shock capturing ability of the method. A multi-volume method for pressure changes in the boundary layer allows calculations which use very long and thin control volumes (length/height - 1000). The method is compared with two test cases. Essentially incompressible turbulent boundary layer flow in an adverse pressure gradient is calculated and the computed distributions of mean velocity and shear are in good agreement with the measurements. Transonic viscous flow in a converging diverging nozzle is calculated; the Mach number upstream of the shock is approximately 1.25. The agreement between the calculated and measured shock strength and total pressure losses is good. m.g.

A88-30957* National Aeronautics and Space Administration. Lewis Research Center, Cleveland, OH.

DEVELOPING FLUID FLOW IN A CURVED DUCT OF SQUARE CROSS-SECTION AND ITS FULLY DEVELOPED DUAL SOLUTIONS

W. Y. SOH (NASA, Lewis Research Center; Sverdrup Technology,

Inc., Cleveland, OH) Journal of Fluid Mechanics (ISSN 0022-1120), vol. 188, March 1988, p. 337-361. refs

Developing fluid flow in a curved duct of square cross-section is studied numerically by a factored ADI finite-difference method on a staggered grid. A central-difference scheme with primitive variables is used inside the computational domain to reduce numerical diffusion. Two Reynolds numbers, 574 and 790, based upon a bulk velocity and hydraulic diameter are chosen for curvature ratios of 1/6.45 and 1/2.3, respectively. It is found that the secondary flow is far more complicated than expected, with the appearance of at least two pairs of vortices. Main-flow separation is also observed for the higher curvature ratio. Furthermore, it is observed that the flow develops into two quite different states downstream, depending upon the inlet conditions. Solutions of the fully developed Navier-Stokes equations is shown to be not unique beyond a certain critical Reynolds number. Developing flow seems to evolve into the fully developed state along a particular branch into which the fully developed solution bifurcates. Author

A88-39010* California Univ., Berkeley.

UNSTEADY MOTION AND TRANSITION TO TURBULENCE IN DEVELOPING CURVED DUCT FLOW

M. ARNAL (California, University, Berkeley), F. FIRMINO (Instituto Superior Tecnico, Lisbon, Portugal), and J. A. C. HUMPHREY (Liverpool, University, England) IN: Symposium on Turbulent Shear Flows, 6th, Toulouse, France, Sept. 7-9, 1987, Proceedings. University Park, PA, Pennsylvania State University, 1987, p. 13-2-1 to 13-2-8. NATO-supported research. refs

(Contract NAG3-735)

An experiment was performed to further the understanding of developing flows in curved ducts of square cross-section. Unlike most earlier works, attention was paid to investigating the time-dependent character of the motion. Mean and unsteady flow characteristics were determined using flow visualization and a laser-Doppler velocimeter. Only one velocity component, that aligned in the longitudinal (streamwise) coordinate direction, was measured. Notwithstanding, the time histories, autocorrelations and spectra derived reveal a time-periodic motion that becomes turbulent with increasing Reynolds number. The results are of intrinsic fundamental value and also illustrate the danger of imposing symmetry of the conservation equations on numerical solutions of this flow. Author

A88-39472* Florida Univ., Gainesville.

MATHEMATICAL MODELS FOR THE NUMERICAL STUDY OF TURBULENT FLOWS

TOM I-PING SHIH (Florida, University, Gainesville) Chinese Institute of Engineers, Journal (ISSN 0253-3839), vol. 11, March 1988, p. 121-136. refs

(Contract NAG3-363)

This paper presents (1) a brief overview of mathematical models used in the numerical study of turbulent flows; (2) a k-epsilon model of turbulence; and (3) extensions of the k-epsilon model. These account for some of the effects of compressibility, low Reynolds number, streamline curvature, and preferential stress dissipation. Author

A88-41409* National Aeronautics and Space Administration. Lewis Research Center, Cleveland, OH.

TRANSIENT RADIATIVE COOLING OF AN ABSORBING AND SCATTERING CYLINDER - A SEPARABLE SOLUTION

ROBERT SIEGEL (NASA, Lewis Research Center, Cleveland, OH) Journal of Thermophysics and Heat Transfer (ISSN 0887-8722), vol. 2, April 1988, p. 110-117. refs

A cylindrical region filled with absorbing-emitting material is cooled by radiation to surroundings at a much lower temperature. A solution is found showing that, for each set of parameters, the transient radial temperature distribution reaches a fixed shape, although the temperatures are decreasing with time. This 'fully developed' transient region is characterized by having a constant emittance based on instantaneous values of the cylinder heat loss and mean temperature. This emittance depends only on the optical radius of the cylinder and the scattering albedo. The emittance is

lower than that for a cylinder at uniform temperature. This arises from the larger local cooling and, hence, reduced temperatures of the outer layers of the cylinder. An examination of this transient emittance provides the ranges of parameters within which the simplification can be made that the cylinder has uniform radial temperature distribution throughout the cooling process. Author

A88-41568*

Kansas Univ. Center for Research, Inc., Lawrence.

CONTROLLED EXCITATION OF A COLD TURBULENT SWIRLING FREE JET

R. TAGHAVI (Kansas University Center for Research, Inc., Lawrence), E. J. RICE (NASA, Lewis Research Center, Cleveland, OH), and S. FAROKHI (Kansas, University, Lawrence) ASME, Transactions, Journal of Vibration, Acoustics, Stress, and Reliability in Design (ISSN 0739-3717), vol. 110, April 1988, p. 234-237. Previously announced in STAR as N87-27997. refs

(Contract NCC3-56)

(ASME PAPER 87-WA/NCA-18)

Experimental results from acoustic excitation of a cold free turbulent jet with and without swirl are presented. A flow with a swirl number of 0.35 (i.e., moderate swirl) is excited internally by plane acoustic waves at a constant sound pressure level and at various frequencies. It is observed that the cold swirling jet is excitable by plane waves, and that the instability waves grow about 50 percent less in peak rms amplitude, and saturate further upstream compared to corresponding waves in a jet without swirl having the same axial mass flux. The preferred Strouhal number based on the mass-averaged axial velocity and nozzle exit diameter for both swirling and nonswirling flows is 0.4. So far no change in the mean velocity components of the swirling jet is observed as a result of excitation. Author

A88-41572* Arizona Univ., Tucson.

ONSET OF FINGER CONVECTION IN A HORIZONTAL POROUS LAYER UNDERLYING A FLUID LAYER

F. CHEN and C. F. CHEN (Arizona, University, Tucson) ASME, Transactions, Journal of Heat Transfer (ISSN 0022-1481), vol. 110, May 1988, p. 403-409. refs

(Contract NSF MEA-82-06087; NAG3-723)

The problem of the onset of finger convection in a porous layer underlying a fluid layer is considered using linear stability analysis. The linear stability equations for the porous layer are formulated for temperature and salinity gradients existing in both layers. The eigenvalue problem is solved by a shooting method. The solution method and associated computer program are validated by comparison with the results of Sun (1973) for the thermal convection case. Results are also presented for the onset of salt-finger convection. C.D.

A88-41574* National Aeronautics and Space Administration. Lewis Research Center, Cleveland, OH.

EXPERIMENTS FOR THE DETERMINATION OF CONVECTIVE DIFFUSION HEAT/MASS TRANSFER TO BURNER RIG TEST TARGETS COMPARABLE IN SIZE TO JET STREAM DIAMETER

G. J. SANTORO and S. A. GOKOGLU (NASA, Lewis Research Center, Cleveland, OH) ASME, Transactions, Journal of Heat Transfer (ISSN 0022-1481), vol. 110, May 1988, p. 442-448. Previously announced in STAR as N86-18646. refs

The application of a recently formulated vapor transport theory to predict deposition rates of corrosive salts from alkali-seeded combustion gases of a small-capacity, high-velocity, atmospheric-pressure burner rig was hampered by the relatively large dimensions of the cylindrical deposit collector compared to the diameter of the combustion gas stream. The relative dimensions lead to a highly nonadiabatic combustion gas flow around the collector and necessitate two series of experiments. In the first series, mass transfer coefficients are determined by utilizing the naphthalene sublimation technique. The second series of experiments determines the dilution effect on the sodium species concentrations due to the entrainment of ambient air. This second series involves the measurement of the temperature variation along

the surface of the collector under steady state conditions. Vapor deposition rates are determined exploiting this information and the results are found to compare favorably with experimentally obtained rates. Author

A88-42839*# Houston Univ., TX.

GAS LIQUID FLOW AT MICROGRAVITY CONDITIONS - FLOW PATTERNS AND THEIR TRANSITIONS

A. E. DUKLER, J. A. FABRE (Houston, University, TX), J. B. MCQUILLEN, and R. VERNON (NASA, Lewis Research Center, Cleveland, OH) IN: International Symposium on Thermal Problems in Space-Based Systems, Boston, MA, Dec. 13-18, 1987, Proceedings. New York, American Society of Mechanical Engineers, 1987, p. 85-97. refs (Contract NAG3-510)

The prediction of flow patterns during gas-liquid flow in conduits is central to the modern approach for modeling two phase flow and heat transfer. The mechanisms of transition are reasonably well understood for flow in pipes on earth where it has been shown that body forces largely control the behavior observed. This work explores the patterns which exist under conditions of microgravity when these body forces are suppressed. Data are presented which were obtained for air-water flow in tubes during drop tower experiments and Learjet trajectories. Preliminary models to explain the observed flow pattern map are evolved. Author

A88-43011*# Wisconsin Univ., Milwaukee.

TURBULENCE ENERGY AND DIFFUSION TRANSPORT OF THIRD-MOMENTS IN A SEPARATING AND REATTACHING FLOW

R. S. AMANO, J. C. CHAI (Wisconsin, University, Milwaukee), and P. GOEL AIAA Journal (ISSN 0001-1452), vol. 26, March 1988, p. 273-282. refs (Contract NAG3-546)

For accurate prediction of turbulent flow in separated and reattaching regions, it is necessary to incorporate second- and third-moments of turbulent fluctuations. The turbulence energy and the energy dissipation rate equations are modified by incorporating second-order closure. Moreover, a transport equation model for the third-order closure with a near-wall correction is developed for the evaluation of the diffusive action of the second-moments. After comparison of the results with experimental data, it is concluded that the models developed here improve the prediction of triple-velocity correlations in both recirculating and redeveloping flow regions. Author

A88-43746*# Los Alamos National Lab., NM.

DEVELOPMENT OF AN INTEGRATED HEAT PIPE-THERMAL STORAGE SYSTEM FOR A SOLAR RECEIVER

E. KEDDY, J. TOM SENA, M. MERRIGAN (Los Alamos National Laboratory, NM), GARY HEIDENREICH (Sundstrand Corp., Rockford, IL), and STEVE JOHNSON (NASA, Lewis Research Center, Cleveland, OH) AIAA, Thermophysics, Plasmadynamics and Lasers Conference, San Antonio, TX, June 27-29, 1988. 6 p. (AIAA PAPER 88-2683)

An integrated heat pipe-thermal storage system was developed as part of the Organic Rankine Cycle Solar Dynamic Power System solar receiver for space station application. The solar receiver incorporates potassium heat pipe elements to absorb and transfer the solar energy within the receiver cavity. The heat pipes contain thermal energy storage (TES) canisters within the vapor space with a toluene heater tube used as the condenser region of the heat pipe. During the insolation period of the earth orbit, solar energy is delivered to the heat pipe. Part of this thermal energy is delivered to the heater tube and the balance is stored in the TES units. During the eclipse period of earth orbit, the stored energy in the TES units is transferred by the potassium vapor to the toluene heater tube. A developmental heat pipe element was constructed that contains axial arteries and a distribution wick connecting the toluene heater and the TES units to the solar insolation surface of the heat pipe. Tests were conducted to demonstrate the heat pipe, TES units, and the heater tube operation. The heat pipe element was operated at design input

power of 4.8 kW. Thermal cycle tests were conducted to demonstrate the successful charge and discharge of the TES units. Axial power flux levels up to 15 watts/sq cm were demonstrated and transient tests were conducted on the heat pipe element. Details of the heat pipe development and test procedures are presented. Author

A88-43871*# National Aeronautics and Space Administration. Lewis Research Center, Cleveland, OH.

TURBULENCE MODELING AND SURFACE HEAT TRANSFER IN A STAGNATION FLOW REGION

C. R. WANG and F. C. YEH (NASA, Lewis Research Center, Cleveland, OH) IN: Heat transfer in gas turbine engines; Proceedings of the Symposium, ASME Winter Annual Meeting, Boston, MA, Dec. 13-18, 1987. New York, American Society of Mechanical Engineers, 1987, p. 35-48. Previously announced in STAR as N87-26302. refs

Analysis for the turbulent flow field and the effect of freestream turbulence on the surface heat transfer rate of a stagnation flow is presented. The emphasis is on modeling and its augmentation of surface heat transfer rate. The flow field considered is the region near the forward stagnation point of a circular cylinder in a uniform turbulent mean flow. Author

A88-44445* National Aeronautics and Space Administration. Lewis Research Center, Cleveland, OH.

NONLINEAR ROLL-UP OF EXTERNALLY EXCITED FREE SHEAR LAYERS

M. E. GOLDSTEIN (NASA, Lewis Research Center, Cleveland, OH) and S. J. LEIB (Case Western Reserve University, Cleveland, OH) Journal of Fluid Mechanics (ISSN 0022-1120), vol. 191, June 1988, p. 481-515. refs

The effects of strong critical-layer nonlinearity on the spatially growing instabilities of a shear layer between two parallel streams are considered. A composite expansion technique is used to obtain a single formula that accounts for both shear-layer spreading and nonlinear critical-layer effects. Nonlinearity causes the instability to saturate well upstream of the linear neutral stability point. It also produces vorticity roll-up that cannot be predicted by linear theory. Author

A88-44783*# Oklahoma State Univ., Stillwater.

LATERAL JET INJECTION INTO SWIRLING COMBUSTOR FLOWFIELDS

DAVID G. LILLEY (Oklahoma State University, Stillwater, OK) AIAA, ASME, SAE, and ASCE, Joint Propulsion Conference, 24th, Boston, MA, July 11-13, 1988. 15 p. refs (Contract NAG3-549) (AIAA PAPER 88-3183)

An experimental program has been conducted to ascertain the effects of the number of lateral jets, the jet velocity ratio, and the crossflow swirl strength, on the isothermal flowfield patterns in jets injected normally to a round-section crossflow. Attention has been given to the trajectory, penetration, and mixing efficiency of the lateral injection, using flow visualization, pitot-probe and hot-wire methods. In addition, such predictive techniques as a simple, explicit, fully three-dimensional turbulent computer code have been employed. O.C.

A88-46222*# United Technologies Research Center, East Hartford, CT.

FORCED MIXER LOBES IN EJECTOR DESIGNS

WALTER M. PRESZ, JR. (United Technologies Research Center, East Hartford, CT; Western New England College, Springfield, MA), BRUCE L. MORIN (United Technologies Research Center, East Hartford, CT), and ROBERT G. GOUSY Journal of Propulsion and Power (ISSN 0748-4658), vol. 4, July-Aug. 1988, p. 350-355. Previously cited in issue 20, p. 2962, Accession no. A86-42752. refs (Contract NAG3-610)

A88-46316* California Univ., Los Angeles.

EXPERIMENTAL STUDIES IN VORTEX PAIR MOTION COINCIDENT WITH A LIQUID REACTION

A. R. KARAGOZIAN, Y. SUGANUMA, and B. D. STROM (California, University, Los Angeles) *Physics of Fluids* (ISSN 0031-9171), vol. 31, July 1988, p. 1862-1871. refs
(Contract NAG3-543; NSF MEA-83-05960)

An experimental examination of the coincidence of a liquid reaction (acid/base) with the formation of a vortex pair structure is described in which emphasis is placed on the evolution of the strained diffusion layer and reacted core structures. Flow visualization of the reaction process is achieved via the technique of chemically sensitive LIF. The observed growth of reacted core structures associated with each vortex is compared with theoretically predicted behavior (Marble, 1983; Karagozian and Marble, 1986). Vortex pair separation is also compared with theoretical correlations, and the relevance of the analogy between a fast liquid reaction and a gaseous reaction is discussed.

Author

A88-46317* National Aeronautics and Space Administration. Lewis Research Center, Cleveland, OH.

STABILITY OF SWIRLING GAS FLOWS

LENNART S. HULTGREN (NASA, Lewis Research Center, Cleveland, OH) *Physics of Fluids* (ISSN 0031-9171), vol. 31, July 1988, p. 1872-1876. refs

The stability of inviscid swirling gas flows to small nonaxisymmetric perturbations is considered. For small Brunt-Vaisala frequencies, the problem reduces to the classical Sturm-Liouville form and the oscillation theorem can be applied. The resulting necessary and sufficient stability condition is compared to various criteria in the literature and a limited numerical study of isothermal rigidly rotating Poiseuille flow. For given azimuthal and axial wavenumbers, it is found numerically that the higher inertial modes become unstable for successively lower Rossby numbers and that this sequence of critical values approaches the theoretical value from above.

Author

A88-47962*# National Aeronautics and Space Administration. Lewis Research Center, Cleveland, OH.

OXYGEN PLASMA EFFECTS ON SEVERAL LIQUID DROPLET RADIATOR FLUIDS

DANIEL A. GULINO and CAROLYN E. COLES (NASA, Lewis Research Center, Cleveland, OH) *Journal of Spacecraft and Rockets* (ISSN 0022-4650), vol. 25, March-Apr. 1988, p. 99-101. Previously cited in issue 08, p. 1059, Accession no. A87-22401.

A88-48757*# National Aeronautics and Space Administration. Lewis Research Center, Cleveland, OH.

PARTICLE-LADEN WEAKLY SWIRLING FREE JETS - MEASUREMENTS AND PREDICTIONS

DANIEL L. BULZAN (NASA, Lewis Research Center, Cleveland, OH), JIAN-SHUN SHUEN (NASA, Lewis Research Center; Sverdrup Technology, Inc., Cleveland, OH), and GERARD M. FAETH (Michigan, University, Ann Arbor) *AIAA, ASME, SAE, and ASEE, Joint Propulsion Conference, 24th, Boston, MA, July 11-13, 1988*. 21 p. Previously announced in STAR as N88-24639. refs
(AIAA PAPER 88-3138)

A theoretical and experimental investigation of particle-laden, weakly swirling, turbulent free jets was conducted. Glass particles, having a Sauter mean diameter of 39 microns with a standard deviation of 15 microns, were used. A single loading ratio of 0.2 was used in the experiments. Measurements are reported for three swirl numbers, ranging from 0.0 to 0.3. The measurements included mean and fluctuating velocities of both phases, and particle mass flux distributions. Measurements were compared with predictions from three types of multiphase flow analysis: locally homogeneous flow (LHF); deterministic separated flow (DSF); and stochastic separated flow (SSF). For the particle-laden jets, the LHF and DSF models did not provide very satisfactory predictions. The LHF model generally overestimated the rate of decay of particle mean axial and angular velocities with streamwise distance, due to the neglect of particle inertia. The LHF model predictions of

particle mass flux also showed poor agreement with measurements due to the assumption of no-slip between phases. The DSF model also performed quite poorly for predictions of particle mass flux, because turbulent dispersion of the particles was neglected. The SSF model, which accounts for both particle inertia and turbulent dispersion of the particles, yielded reasonably good predictions throughout the flow field for the particle-laden jets. Author

A88-48762*# National Aeronautics and Space Administration. Lewis Research Center, Cleveland, OH.

DEVELOPMENT OF A LIQUID-FED WATER RESISTOJET

W. EARL MORREN and JAMES R. STONE (NASA, Lewis Research Center, Cleveland, OH) *AIAA, ASME, SAE, and ASEE, Joint Propulsion Conference, 24th, Boston, MA, July 11-13, 1988*. 19 p. Previously announced in STAR as N88-24968. refs
(AIAA PAPER 88-3288)

A concept for a forced-flow once-through water vaporizer for application to resistojet thrusters was evaluated as an element of a laboratory model thruster and tested to investigate its operating characteristics. The vaporizer design concept employs flow swirling to attach the liquid flow to the boiler chamber wall, providing for separation of the two liquid phases. This vaporizer was modified with a nozzle and a centrally-located heater to facilitate vaporization, superheating, and expansion of the propellant, allowing it to function as a resistojet. Performance was measured at thrust levels ranging from 170 to 360 mN and at power levels ranging from 443 to 192 W. Maximum measured specific impulse was 192 sec.

Author

A88-48779*# National Aeronautics and Space Administration. Lewis Research Center, Cleveland, OH.

NUMERICAL ANALYSIS OF THREE-DIMENSIONAL VISCOUS INTERNAL FLOWS

RODRICK V. CHIMA (NASA, Lewis Research Center, Cleveland, OH) and JEFFREY W. YOKOTA (Sverdrup Technology, Inc., Cleveland, OH) *IN: AIAA, ASME, SIAM, and APS, National Fluid Dynamics Congress, 1st, Cincinnati, OH, July 25-28, 1988, Technical Papers, Part 1, Washington, DC, American Institute of Aeronautics and Astronautics, 1988, p. 17-24*. Previously announced in STAR as N88-21116. refs
(AIAA PAPER 88-3522)

A 3-D Navier-Stokes code has been developed for analysis of turbomachinery blade rows and other internal flows. The Navier-Stokes equations are written in a Cartesian coordinate system rotating about the x-axis, and then mapped to a general body-fitted coordinate system. Streamwise viscous terms are neglected using the thin-layer assumption, and turbulence effects are modeled using the Baldwin-Lomax turbulence model. The equations are discretized using finite differences on stacked C-type grids and are solved using a multistage Runge-Kutta algorithm with a spatially-varying time step and implicit residual smoothing. Calculations have been made of a horseshoe vortex formed in front of a flat plate with a round leading edge standing in a turbulent endwall boundary layer. Comparisons are made with experimental data taken by Eckerle and Langston for a circular cylinder under similar conditions. Computer and measured results are compared in terms of endwall flow visualization pictures and total pressure loss contours and vector plots on the symmetry plane. Calculated details of the primary vortex show excellent agreement with the experimental data. The calculations also show a small secondary vortex not seen experimentally.

Author

A88-48782*# National Aeronautics and Space Administration. Lewis Research Center, Cleveland, OH.

SPLITTING OF INVISCID FLUXES FOR REAL GASES

MENG-SING LIOU (NASA, Lewis Research Center, Cleveland, OH), BRAM VAN LEER (NASA, Lewis Research Center, Cleveland, OH; Michigan, University, Ann Arbor), and JIAN-SHUN SHUEN (NASA, Lewis Research Center, Cleveland; Sverdrup Technology, Inc., Middleburg Heights, OH) *IN: AIAA, ASME, SIAM, and APS, National Fluid Dynamics Congress, 1st, Cincinnati, OH, July 25-28, 1988, Technical Papers, Part 1, Washington, DC, American Institute*

of Aeronautics and Astronautics, 1988, p. 42-49. Previously announced in STAR as N88-21717. refs (AIAA PAPER 88-3526)

Flux-vector and flux-difference splittings for the inviscid terms of the compressible flow equations are derived under the assumption of a general equation of state for a real gas in equilibrium. No necessary assumptions, approximations or auxiliary quantities are introduced. The formulas derived include several particular cases known for ideal gases and readily apply to curvilinear coordinates. Applications of the formulas in a TVD algorithm to one-dimensional shock-tube and nozzle problems show their quality and robustness. Author

A88-48915* # National Aeronautics and Space Administration. Lewis Research Center, Cleveland, OH.

INITIAL CONDITIONAL EFFECT ON PRESSURE WAVES IN AN AXISYMMETRIC JET

JEFFREY H. MILES (NASA, Lewis Research Center, Cleveland, OH) and GANESH RAMAN (NASA, Lewis Research Center; Sverdrup Technology, Inc., Cleveland, OH) IN: AIAA, ASME, SIAM, and APS, National Fluid Dynamics Congress, 1st, Cincinnati, OH, July 25-28, 1988, Technical Papers. Part 2. Washington, DC, American Institute of Aeronautics and Astronautics, 1988, p. 1148-1158. Previously announced in STAR as N88-23184. refs (AIAA PAPER 88-3702)

A pair of microphones (separated axially by 5.08 cm and laterally by 1.3 cm) are placed on either side of the jet centerline to investigate coherent pressure fluctuations in an axisymmetric jet at Strouhal numbers less than unity. Auto-spectra, transfer-function, and coherence measurements are made for a tripped and untripped boundary layer initial condition. It was found that coherent acoustic pressure waves originating in the upstream plenum chamber propagate a greater distance downstream for the tripped initial condition than for the untripped initial condition. In addition, for the untripped initial condition the development of the coherent hydrodynamic pressure waves shifts downstream. Author

A88-48916* # National Aeronautics and Space Administration. Lewis Research Center, Cleveland, OH.

THREE-DIMENSIONAL VISCOUS FLOW COMPUTATIONS OF A CIRCULAR JET IN SUBSONIC AND SUPERSONIC CROSS FLOW

G. J. HARLOFF and J. K. LYTLE (NASA, Lewis Research Center, Cleveland; Sverdrup Technology, Inc., Middleburg Heights, OH) IN: AIAA, ASME, SIAM, and APS, National Fluid Dynamics Congress, 1st, Cincinnati, OH, July 25-28, 1988, Technical Papers. Part 2. Washington, DC, American Institute of Aeronautics and Astronautics, 1988, p. 1159-1165. refs (Contract NAS3-24105) (AIAA PAPER 88-3703)

Three-dimensional viscous flow computations are presented for 90 deg. injection angle jets in subsonic and supersonic crossflow. Comparisons with experimental data include jet centerline and vortex trajectories for the subsonic crossflow, and surface pressure measurement for the supersonic crossflow case. The vortices induced in the jet/freestream interaction are computed and illustrated. The vortices persist in subsonic flow and die out quickly in supersonic flow. The structure of the shocks in the unconfined supersonic flow is illustrated. Author

A88-48946* # National Aeronautics and Space Administration. Lewis Research Center, Cleveland, OH.

ELECTROHYDRODYNAMIC MIGRATION OF CHARGED DROPLETS IN AN INSULATING FLUID

R. BALASUBRAMANIAM and R. A. WILKINSON (NASA, Lewis Research Center, Cleveland, OH) IN: AIAA, ASME, SIAM, and APS, National Fluid Dynamics Congress, 1st, Cincinnati, OH, July 25-28, 1988, Technical Papers. Part 3. Washington, DC, American Institute of Aeronautics and Astronautics, 1988, p. 1422-1429. Previously announced in STAR as N88-21424. refs (AIAA PAPER 88-3557)

The motion of charged, conducting droplets present in an insulating fluid medium is analyzed under the action of an electric

field, in microgravity. Previous analyses of this problem have considered the Maxwell stresses as the only driving force. In the present study, arguments from macroscopic thermodynamics and the molecular theory of surface tension are used to show that the surface tension gradients can be induced due to the variation of the electric potential on the interface. In the limit of Reynolds numbers small compared to unity, the terminal velocity of migration of the droplet is calculated under the combined action of the Maxwell stresses and the surface tension gradients. The results show that there are no surface tension gradients (i.e., no electric potential variation at the interface) in a case that is due to the convection of the surface charges, surface tension gradients do exist and tend to reduce the terminal velocity of the droplet. The shape of the droplet altered by the motion was also calculated, when the deformations from the spherical shape are small. Author

A88-48974* # Maine Univ., Orono.

THREE-DIMENSIONAL FLOW PAST TWO CYLINDERS MOUNTED SIDE BY SIDE ON AN ENDWALL

M. T. BOYLE (Maine, University, Orono) and L. S. LANGSTON (Connecticut, University, Storrs) IN: AIAA, ASME, SIAM, and APS, National Fluid Dynamics Congress, 1st, Cincinnati, OH, July 25-28, 1988, Technical Papers. Part 3. Washington, DC, American Institute of Aeronautics and Astronautics, 1988, p. 1734-1741. refs

(Contract NSG-3238) (AIAA PAPER 88-3718)

This paper reports on the experimental description of flow past two cylinders that stand side by side on an endwall. Flow visualization performed in a water tunnel provides a qualitative understanding of the three-dimensional flow over a range of control variables. Limiting streamline flow visualization shows the location of the three-dimensional separation for a range of cylinder spacings. For a spacing of 1.5 diameters between centers, the flow is described using a five-hole probe and by cylinder and endwall surface static pressure measurements. At a cylinder diameter Reynolds number of 250,000 the measurements show a single primary vortex with a wide flat cross section. The velocity measurements show high shear on the endwall in the primary vortex region. A small counterrotating vortex is found between the primary vortex and the cylinder leading edge. C.D.

A88-48980* # National Aeronautics and Space Administration. Lewis Research Center, Cleveland, OH.

DYNAMICS OF TWO FLUIDS UNDER PERIODIC ACCELERATION

WALTER M. B. DUVAL and DAVID A. JACQMIN (NASA, Lewis Research Center, Cleveland, OH) IN: AIAA, ASME, SIAM, and APS, National Fluid Dynamics Congress, 1st, Cincinnati, OH, July 25-28, 1988, Technical Papers. Part 3. Washington, DC, American Institute of Aeronautics and Astronautics, 1988, p. 1798-1804. refs (AIAA PAPER 88-3728)

The evolution of the interface between two fluids confined in a rectangular cavity is investigated numerically to predict its transient behavior. These computations address mixing characteristics of fluids under microgravity conditions, particularly g-jitter conditions resulting from aircraft vibration or crew motion, and have applications in solution crystal growth. The two-dimensional formulation employs the Boussinesq approximation and treats the mixing of two fluids as an initial value problem with a prescribed concentration field. For fluid mixing of practical applications inside a cavity, it is shown that nonlinear convective transport can dominate over both viscous and molecular diffusion. However, viscous diffusion can become important for low Reynolds number or certain cavity sizes. A stacking phenomenon is shown to occur for aspect ratios (Ar) approximately between 5 to 10. For aspect ratios in the neighborhood of 0.1 to 0.2, inner cells evolve at the interface with increasing time. For a square cavity of $Ar = 1$, chaotic mixing of the fluid appears to occur for a Stokes-Reynolds number greater than about 5. Author

34 FLUID MECHANICS AND HEAT TRANSFER

A88-49000*# National Aeronautics and Space Administration. Lewis Research Center, Cleveland, OH.

FINGERING FLOW PATTERNS OF THERMOSOLUTAL CONVECTION IN RECTANGULAR ENCLOSURES

L. W. WANG (NASA, Lewis Research Center, Cleveland, OH), J. J. CHEN, and C. T. CHEN (National Cheng Kung University, Tainan, Republic of China) IN: AIAA, ASME, SIAM, and APS, National Fluid Dynamics Congress, 1st, Cincinnati, OH, July 25-28, 1988, Technical Papers. Part 3. Washington, DC, American Institute of Aeronautics and Astronautics, 1988, p. 2111-2115. Previously announced in STAR as N88-21417. refs (AIAA PAPER 88-3823)

Convection in rectangular enclosures with combined horizontal temperature and concentration gradients is studied. An electrochemical system is employed to impose the concentration gradients. Due to a large difference between the thermal and solutal diffusion rates the flow possesses double-diffusive characteristics. Very complex fingering flow patterns are observed around the two-phase interfaces. The main objective of the present work is to obtain more information on the flows near the two vertical phase interfaces under various parametric conditions. The fingering flows near the crystal could be one of the most important factors to cause the crystal imperfections. The ranges of the parameters studied are Sc (Schmidt number) = 2200 to 2400, Pr (Prandtl number) = 4.0 to 7.0, Gr sub T (Grashof number) = 2.50×10 to the 6th to 5.10×10 to the 7th power, Ar (aspect ratio) = 0.61 to 3.0, and N (buoyancy ratio) = 0.05 to 54.8.

Author

A88-49087*# National Taiwan Univ., Taipei.

EXPERIMENTAL STUDY OF THERMOCAPILLARY FLOWS IN A THIN LIQUID LAYER WITH HEAT FLUXES IMPOSED ON THE FREE SURFACE

CHUN-LIANG LAI (National Taiwan University, Taipei, Republic of China), PAUL S. GREENBERG, and AN-TI CHAI (NASA, Lewis Research Center, Cleveland, OH) Metallurgical Transactions A - Physical Metallurgy and Materials Science (ISSN 0360-2133), vol. 19A, Aug. 1988, p. 1895-1898. Previously announced in STAR as N88-12763.

To study thermocapillary flows in a two-dimensional thin liquid layer with heat fluxes imposed on the free surface experimentally, a long tray configuration was employed to simulate the infinite layer. The surface temperature distribution due to thermocapillary convection for different flow regimes was measured and compared with theoretical predictions. A short tray configuration was also employed to study the end wall effects (insulating or conducting). The results show that, for a strong convection flow with an insulating wall as the boundary, the surface temperature distribution became quite uniform. Consequently, the thermocapillary driving force was greatly reduced. On the other hand, a strong fluid motion always existed adjacent to the conducting wall because of the large surface temperature gradient near the wall.

Author

A88-50330*# Cincinnati Univ., OH.

SOLUTION OF THE NEUMANN PRESSURE PROBLEM IN GENERAL ORTHOGONAL COORDINATES USING THE MULTIGRID TECHNIQUE

U. GHIA, R. RAMAMURTI, and K. N. GHIA (Cincinnati, University, OH) AIAA Journal (ISSN 0001-1452), vol. 26, May 1988, p. 538-547. refs

(Contract AF-AFOSR-80-0160; NSG-3267)

The multigrid (MG) technique has been advanced for use with Neumann boundary-value problems in clustered curvilinear orthogonal coordinates. This comprises an important step in the analysis of incompressible flow using the velocity-pressure formulation of the Navier-Stokes equations. The finite-difference representation of the problem and the formulation of the restriction and coarse-grid correction operators are examined in detail. Maintaining consistency between these and the integral constraint associated with the Neumann problem is found to be critical for the success of the MG technique. The influence of the smoothing operator is examined by employing Gauss-Seidel, alternating-direction implicit, and strongly implicit techniques. The

MG procedure enhances the efficiency of fine-grid solutions of the Neumann problem by a factor of 3 to 14, depending on the type of smoothing operator employed and the values of the problem parameters.

Author

A88-50344*# National Aeronautics and Space Administration. Lewis Research Center, Cleveland, OH.

SOLUTIONS OF ONE-DIMENSIONAL STEADY NOZZLE FLOW REVISITED

MENG-SING LIOU (NASA, Lewis Research Center, Cleveland, OH) AIAA Journal (ISSN 0001-1452), vol. 26, May 1988, p. 625-628. refs

A formulation is presented by which any iteration process for obtaining the entropy increase in the flow of a one-dimensional steady nozzle is eliminated, and the simple solution of a quadratic equation is obtained. The proper parameters are then explicitly seen in the equation, and their effects on the solution are easily determined. Since only one root of the equation is physically admissible, entropy production, and therefore the shock wave, are uniquely determined by this set of parameters.

O.C.

A88-50786*# National Aeronautics and Space Administration. Lewis Research Center, Cleveland, OH.

BOUNDARY LAYER DEVELOPMENT AS A FUNCTION OF CHAMBER PRESSURE IN THE NASA LEWIS 1030:1 AREA RATIO ROCKET NOZZLE

TAMARA A. SMITH (NASA, Lewis Research Center, Cleveland, OH) AIAA, ASME, SAE, and ASEE, Joint Propulsion Conference, 24th, Boston, MA, July 11-13, 1988. 32 p. Previously announced in STAR as N88-25841. refs (AIAA PAPER 88-3301)

Through the use of theoretical predictions of fluid properties and experimental heat transfer and thrust measurements, the zones of laminar, transitional, and turbulent boundary layer flow were defined for the NASA Lewis 1039:1 area ratio rocket nozzle. Tests were performed on the nozzle at chamber pressures from 350 to 100 psia. For these conditions, the throat diameter Reynolds numbers varied from 300,000 to 1 million. The propellants used were gaseous hydrogen and gaseous oxygen. Thrust measurements and nozzle outer wall temperature measurements were taken during the 3-sec test runs. Comparison of experimental heat transfer and thrust data with the corresponding predictions from the Two-Dimensional Kinetics (TDK) nozzle analysis program indicated laminar flow in the nozzle at a throat diameter Reynolds number of 320,000 or chamber pressure of 360 psia. Comparison of experimental and predicted heat transfer data indicated transitional flow up to and including a chamber pressure of 1000 psia. Predicted values of the axisymmetric acceleration parameter within the convergent and divergent nozzle were consistent with the above results. Based upon an extrapolation of the heat transfer data and predicted distributions of the axisymmetric acceleration parameter, transitional flow was predicted up to a throat diameter Reynolds number of 220,000 or 2600-psia chamber pressure. Above 2600-psia chamber pressure, fully developed turbulent flow was predicted.

Author

A88-51343*# Dayton Univ., OH.

A NUMERICAL INVESTIGATION OF THE INFLUENCE OF HEATING ON THE EXCITATION OF HIGH AND LOW MACH NUMBER JET FLOWS

J. N. SCOTT and E. A. HOO (Dayton, University, OH) ASME, Winter Annual Meeting, Boston, MA, Dec. 13-18, 1987. 8 p. refs (Contract NAG3-526)

(ASME PAPER 87-WA/NCA-13)

The influence of heating and velocity on the unsteady nature of jet mixing layers is investigated by solving the time-dependent compressible Navier-Stokes equations using MacCormack's explicit finite difference algorithm. The computations are performed for jet Mach numbers of 0.3 and 0.8 with flow total temperatures up to 800 K. The Reynolds number ranges from 3×10 to the 5th to 1.3×10 to the 6th. Excitation is accomplished by imposing an acoustic pressure signal inside the jet duct. The objective of this effort is to compare the response of heated and unheated jets

with acoustic excitation at high and low subsonic Mach numbers. The preliminary results indicate that without acoustic excitation the mixing in the heated jet is greater than in the unheated case. It has also been found that for the low speed heated jets ($M = 0.3$, $T_t = 672K$) acoustic excitation causes the production of large scale vortex structures to occur in a regular periodic manner with organized periodic pairing at some Strouhal numbers. These results are in agreement with experimental data. Author

A88-52679* # National Aeronautics and Space Administration. Lewis Research Center, Cleveland, OH.

EXPERIMENTAL AND THEORETICAL EFFECTS OF NITROGEN GAS FLOW RATE ON LIQUID-JET ATOMIZATION

ROBERT D. INGEBO (NASA, Lewis Research Center, Cleveland, OH) Journal of Propulsion and Power (ISSN 0748-4658), vol. 4, Sept.-Oct. 1988, p. 406-411. Previously cited in issue 20, p. 3219, Accession no. A87-45427. refs

A88-54152* # United Technologies Research Center, East Hartford, CT.

THE EFFECTS OF TURBULENCE AND STATOR/ROTOR INTERACTIONS ON TURBINE HEAT TRANSFER. II - EFFECTS OF REYNOLDS NUMBER AND INCIDENCE

M. F. BLAIR, R. P. DRING, and H. D. JOSLYN (United Technologies Research Center, East Hartford, CT) ASME, Gas Turbine and Aeroengine Congress and Exposition, Amsterdam, Netherlands, June 6-9, 1988. 8 p. refs (Contract NAS3-23717) (ASME PAPER 88-GT-5)

Part I of this paper presents airfoil heat transfer data obtained in a rotating turbine model at its design rotor incidence. This portion of the paper presents heat transfer data obtained in the same model for various combinations of Reynolds number and inlet turbulence and for a very wide range of rotor incidence. On the suction surfaces of the first stage airfoils the locations and lengths of transition were influenced by both the inlet turbulence level and the Reynolds number. In addition it was demonstrated that on the first stage pressure surfaces combinations of high Reynolds number and high turbulence can produce heat transfer rates well in excess of two-dimensional turbulent flow. Rotor heat transfer distributions indicate that for relatively small deviations from the design incidence, local changes to the heat transfer distributions were produced on both pressure and suction sides near the stagnation region. For extremely large negative incidence the flow was completely separated from the rotor pressure surface producing very high local heat transfer. Author

A88-54154* # Purdue Univ., West Lafayette, IN.

SPRAY CHARACTERISTICS OF A SPILL-RETURN AIRBLAST ATOMIZER

X. F. DAI, A. H. LEFEBVRE (Purdue University, West Lafayette, IN), and J. ROLLBUHLER (NASA, Lewis Research Center, Cleveland, OH) ASME, Gas Turbine and Aeroengine Congress and Exposition, Amsterdam, Netherlands, June 6-9, 1988. 9 p. refs (ASME PAPER 88-GT-7)

The spray characteristics of a spill-return airblast atomizer are examined using water as the working fluid. Measurements of mean drop size, drop size distribution, spray cone angle, and circumferential liquid distinction, are carried out over wide ranges of liquid injection pressures and atomizing air velocities. Generally, it is found that an increase in nozzle bypass ratio worsens the atomization quality and widens the spray cone angle. Increase in airblast air velocity may improve or impair atomization quality depending on whether it increases or decreases the relative velocity between the liquid and the surrounding air. Airblast air can also be used to modify the change in spray cone angle that normally accompanies a change in bypass ratio. Author

A88-54164* # Sverdrup Technology, Inc., Cleveland, OH.
DEVELOPMENT OF A THERMAL AND STRUCTURAL ANALYSIS PROCEDURE FOR COOLED RADIAL TURBINES
GANESH N. KUMAR (Sverdrup Technology, Inc., Cleveland, OH)

and RUSSELL G. DEANNA (NASA, Lewis Research Center; U.S. Army, Propulsion Directorate, Cleveland, OH) ASME, Gas Turbine and Aeroengine Congress and Exposition, Amsterdam, Netherlands, June 6-9, 1988. 8 p. refs (ASME PAPER 88-GT-18)

A procedure for computing the rotor temperature and stress distributions in a cooled radial turbine is considered. Existing codes for modeling the external mainstream flow and the internal cooling flow are used to compute boundary conditions for the heat transfer and stress analyses. An inviscid, quasi three-dimensional code computes the external free stream velocity. The external velocity is then used in a boundary layer analysis to compute the external heat transfer coefficients. Coolant temperatures are computed by a viscous one-dimensional internal flow code for the momentum and energy equation. These boundary conditions are input to a three-dimensional heat conduction code for calculation of rotor temperatures. The rotor stress distribution may be determined for the given thermal, pressure and centrifugal loading. The procedure is applied to a cooled radial turbine which will be tested at the NASA Lewis Research Center. Representative results from this case are included. Author

A88-54229* # Indian Inst. of Tech., Madras.

EFFECT OF STAGE LOADING ON ENDWALL FLOWS IN AN AXIAL FLOW COMPRESSOR ROTOR

N. SITARAM (Indian Institute of Technology, Madras, India) ASME, Gas Turbine and Aeroengine Congress and Exposition, Amsterdam, Netherlands, June 6-9, 1988. 7 p. refs (Contract NSG-3032) (ASME PAPER 88-GT-111)

This paper reports results from investigations conducted to determine the effect of stage loading on endwall flows in a low speed axial flow compressor. These investigations consisted of two sets of measurements. The first set consisted of radial transverse of flow properties at the rotor inlet and exit, at five flow coefficients. These measurements are used to determine the boundary layer integral parameters. The displacement thicknesses at the rotor hub and tip agree reasonably well with Smith's (1970) correlation for multistage axial compressors. The second set consisted of measurements of static pressures on the rotor blade at four flow coefficients. From these measurements, lift coefficient is determined. Also, loss of lift coefficient near the tip is calculated, and is attributed mainly to the tip leakage flows. Author

A88-54236* # United Technologies Research Center, East Hartford, CT.

THE EFFECTS OF TURBULENCE AND STATOR/ROTOR INTERACTIONS ON TURBINE HEAT TRANSFER. I - DESIGN OPERATING CONDITIONS

M. F. BLAIR, R. P. DRING, and H. D. JOSLYN (United Technologies Research Center, East Hartford, CT) ASME, Gas Turbine and Aeroengine Congress and Exposition, Amsterdam, Netherlands, June 6-9, 1988. 12 p. refs (Contract NAS3-23717) (ASME PAPER 88-GT-125)

A combined experimental and analytical program was conducted to examine the effects of inlet turbulence, stator-rotor axial spacing, and relative circumferential spacing of first and second stators on turbine airfoil heat transfer. The experimental portion of the study was conducted in a large-scale (approximately 5X engine), ambient temperature, stage-and-a-half rotating turbine model. The data indicate that while turbine inlet turbulence can have a very strong impact on the first stator heat transfer, its impact in downstream rows is minimal. The effects on heat transfer produced by relatively large changes in stator/rotor spacing or by changing the relative row-to-row circumferential positions of stators were very small. Analytical results consist of airfoil heat transfer distributions computed with a finite-difference boundary layer code. Author

A88-54267* # Calspan Advanced Technology Center, Buffalo, NY.

PHASE-RESOLVED HEAT-FLUX MEASUREMENTS ON THE BLADE OF A FULL-SCALE ROTATING TURBINE

34 FLUID MECHANICS AND HEAT TRANSFER

M. G. DUNN, P. J. SEYMOUR (Calspan Advanced Technology Center, Buffalo, NY), S. H. WOODWARD, W. K. GEORGE (New York, State University, Buffalo), and R. E. CHUPP (Teledyne CAE, Toledo, OH) ASME, Gas Turbine and Aeroengine Congress and Exposition, Amsterdam, Netherlands, June 6-9, 1988. 13 p. Research supported by the Teledyne CAE Independent Research and Development Funds. refs
(Contract NAG3-581)
(ASME PAPER 88-GT-173)

This paper presents detailed phase-resolved heat-flux data obtained on the blade of a Teledyne 702 HP full-stage rotating turbine. A shock tube is used as a short-duration source of heated air, and platinum thin-film gages are used to obtain the heat-flux measurements. Results are presented along the midspan at several locations on the blade suction and pressure surfaces from the stagnation point to near the trailing edge. For these measurements, the turbine was operating at the design flow function and at 100 percent corrected speed. Results are presented for the design vane/blade spacing (0.19 Cs) and at a wide spacing (0.50 Cs). Data are also presented illustrating the phase-resolved blade heat-flux distribution with upstream cold gas injection from discrete holes on the vane surface. The results illustrate that several successive passages can be superimposed upon each other and that a heat-flux pattern can be determined within the passage.

Author

A88-54320* Aerometrics, Inc., Sunnyvale, CA.
DIAGNOSTICS DEVELOPMENT FOR SPRAY CHARACTERIZATION IN COMPLEX TURBULENT FLOWS
W. D. BACHALO, A. BRENA DE LA ROSA, and R. C. RUDOFF (Aerometrics, Inc., Sunnyvale, CA) ASME, Gas Turbine and Aeroengine Congress and Exposition, Amsterdam, Netherlands, June 6-9, 1988. 11 p. refs
(Contract NAS3-25204; NAS8-37323)
(ASME PAPER 88-GT-241)

The present work reports a detailed investigation of air-liquid interaction in sprays along with particle number density and mass flux measurements in complex turbulent flows such as those present in gas turbines and rocket combustors. Data have been obtained for the characterization of sprays in complex flows which include detailed drop size and drop velocity distributions, size-velocity correlations, mass flux, and particle number density. Key factors affecting the measurement of the sample volume size are discussed in detail since an accurate estimation of it is essential to the particle number density and volume flux determined by the instrument. The discrimination of refraction and reflective scattering components and their influence on the measurements are also discussed. Data comparing the phase Doppler results to alternate methods of measuring number density and volume flux are also presented. These results showed agreement to within 15 percent in most cases for realistic flow configurations.

Author

A88-55245* Akron Univ., OH.
INPUT-OUTPUT-CONTROLLED NONLINEAR EQUATION SOLVERS

JOSEPH PADOVAN (Akron, University, OH) Numerical Heat Transfer (ISSN 0149-5720), vol. 14, no. 2, 1988, p. 127-148. refs
(Contract NAG3-54)

To upgrade the efficiency and stability of the successive substitution (SS) and Newton-Raphson (NR) schemes, the concept of input-output-controlled solvers (IOCS) is introduced. By employing the formal properties of the constrained version of the SS and NR schemes, the IOCS algorithm can handle indefiniteness of the system Jacobian, can maintain iterate monotonicity, and provide for separate control of load incrementation and iterate excursions, as well as having other features. To illustrate the algorithmic properties, the results for several benchmark examples are presented. These define the associated numerical efficiency and stability of the IOCS.

Author

N88-11148* Avco-Everett Research Lab., MA.
IMPROVED NUMERICAL METHODS FOR TURBULENT VISCOUS RECIRCULATING FLOWS Progress Report
A. TURAN /in NASA. Lewis Research Center, Turbine Engine Hot Section Technology, 1985 p 87-88 Oct. 1985
(Contract NAS3-24351)

Avail: NTIS HC A19/MF A01 CSCL 20D

The hybrid-upwind finite difference schemes employed in generally available combustor codes possess excessive numerical diffusion errors which preclude accurate quantitative calculations. The present study has as its primary objective the identification and assessment of an improved solution algorithm as well as discretization schemes applicable to analysis of turbulent viscous recirculating flows. The assessment is carried out primarily in two dimensional/axisymmetric geometries with a view to identifying an appropriate technique to be incorporated in a three-dimensional code.

Author

N88-11149* General Motors Corp., Detroit, MI. Gas Turbine Div.

AEROTHERMAL MODELING PROGRAM, PHASE 2

H. C. MONGIA, S. V. PATANKAR, S. N. B. MURTHY, J. P. SULLIVAN, and G. S. SAMUELSEN (California Univ., Irvine.) /in NASA. Lewis Research Center, Turbine Engine Hot Section Technology, 1985 p 89-108 Oct. 1985
(Contract NAS3-24350)

Avail: NTIS HC A19/MF A01 CSCL 20D

The main objectives of the Aerothermal Modeling Program, Phase 2 are: to develop an improved numerical scheme for incorporation in a 3-D combustor flow model; to conduct a benchmark quality experiment to study the interaction of a primary jet with a confined swirling crossflow and to assess current and advanced turbulence and scalar transport models; and to conduct experimental evaluation of the air swirler interaction with fuel injectors, assessments of current two-phase models, and verification the improved spray evaporation/dispersion models.

Author

N88-11150* United Technologies Research Center, East Hartford, CT.

FUEL-INJECTOR/AIR-SWIRL CHARACTERIZATION

J. B. MCVEY, J. B. KENNEDY, and J. C. BENNETT (Connecticut Univ., Storrs.) /in NASA. Lewis Research Center, Turbine Engine Hot Section Technology, 1985 p 109-117 Oct. 1985
(Contract NAS3-24352)

Avail: NTIS HC A19/MF A01 CSCL 20D

The objectives of this program are to establish an experimental data base documenting the behavior of gas turbine engine fuel injector sprays as the spray interacts with the swirling gas flow existing in the combustor dome, and to conduct an assessment of the validity of current analytical techniques for predicting fuel spray behavior. Emphasis is placed on the acquisition of data using injector/swirler components which closely resemble components currently in use in advanced aircraft gas turbine engines, conducting tests under conditions that closely simulate or closely approximate those developed in actual combustors, and conducting a well-controlled experimental effort which will comprise using a combination of low-risk experiments and experiments requiring the use of state-of-the-art diagnostic instrumentation. Analysis of the data is to be conducted using an existing, TEACH-type code which employs a stochastic analysis of the motion of the dispersed phase in the turbulent continuum flow field.

Author

N88-11151* Minnesota Univ., Minneapolis.
EFFICIENT NUMERICAL TECHNIQUES FOR COMPLEX FLUID FLOWS

SUHAS V. PATANKAR /in NASA. Lewis Research Center, Turbine Engine Hot Section Technology, 1985 p 119-120 Oct. 1985
(Contract NAS3-596)

Avail: NTIS HC A19/MF A01 CSCL 20D

The aim of the present research program is the development of more efficient and reliable calculation schemes for the coupled

momentum and continuity equations. The resulting schemes would significantly reduce the expense of computing complex flows such as those in combustion chambers, gas turbines, and heat exchangers. Author

N88-11153* Garrett Turbine Engine Co., Phoenix, AZ.
DILUTION JET MIXING PROGRAM, PHASE 3
 R. SRINIVASAN, G. MYERS, and C. WHITE *In* NASA. Lewis Research Center, Turbine Engine Hot Section Technology, 1985 p 127-132 Oct. 1985
 (Contract NAS3-22110)
 Avail: NTIS HC A19/MF A01 CSCL 20D

The objectives of the program were: (1) to extend the data base on mixing of a single-sided row of jets with a confined crossflow, (2) to collect a data base on mixing of multiple rows of jets with confined crossflow, (3) to develop empirical jet mixing correlations, and (4) to perform limited three-dimensional calculations for some of these test configurations. The tests were performed with uniform mainstream conditions for several orifice plate configurations. Schematics of the test section and the orifice configurations are given. Temperature and pressure measurements were made in the test section at 4 axial and 11 transverse stations, using a 60-element rake probe. The measured temperature distributions for these tests are reported. Author

N88-11154* National Aeronautics and Space Administration. Lewis Research Center, Cleveland, OH.
ON THE MIXING OF A ROW OF JETS WITH A CONFINED CROSSFLOW
 J. D. HOLDEMAN *In* its Turbine Engine Hot Section Technology, 1985 p 133-138 Oct. 1985
 Avail: NTIS HC A19/MF A01 CSCL 20D

Mean temperature profiles calculated with an interactive microcomputer code which evaluates dilution-zone design alternatives are presented to show the effects of flow and geometric variables on the mixing of a single row of jets injected through sharp-edged orifices into a uniform flow of a different temperature in a constant area duct. In addition, this program is used to calculate profiles for opposed rows of jets with their centerlines in-line, by assuming that the confining effect of an opposite wall is equivalent to that of a plane of symmetry between opposed jets. Author

N88-11155* National Aeronautics and Space Administration. Lewis Research Center, Cleveland, OH.
HEAT TRANSFER IN A REAL ENGINE ENVIRONMENT
 HERBERT J. GLADDEN *In* its Turbine Engine Hot Section Technology, 1985 p 139-150 Oct. 1985
 Avail: NTIS HC A19/MF A01 CSCL 20D

The hot section facility at the Lewis Research Center was used to demonstrate the capability of instruments to make required measurements of boundary conditions of the flow field and heat transfer processes in the hostile environment of the turbine. The results of thermal scaling tests show that low temperature and pressure rig tests give optimistic estimates of the thermal performance of a cooling design for high pressure and temperature application. The results of measuring heat transfer coefficients on turbine vane airfoils through dynamic data analysis show good comparison with measurements from steady state heat flux gauges. In addition, the data trends are predicted by the STAN5 boundary layer code. However, the magnitude of the experimental data was not predicted by the analysis, particularly in laminar and transitional regions near the leading edge. The infrared photography system was shown capable of providing detailed surface thermal gradients and secondary flow features on a turbine vane and endwall. Author

N88-11156* General Motors Corp., Indianapolis, IN. Gas Turbine Div.
FILM COOLING HEAT TRANSFER ON A TURBINE AIRFOIL
 LARRY D. HYLTON *In* NASA. Lewis Research Center, Turbine Engine Hot Section Technology, 1985 p 151-159 Oct. 1985
 (Contract NAS3-24619)
 Avail: NTIS HC A19/MF A01 CSCL 20D

The objectives of the current program are to develop an analytical approach, based on boundary layer theory, for predicting the effects of airfoil cooling on downstream heat transfer rates and to verify the resulting analytical method by comparison of predictions with hot cascade data obtained under this program. Author

N88-11157* Tennessee Univ. Space Inst., Tullahoma.
FLOW FIELD MEASUREMENTS IN A 90 DEGREE TURNING DUCT
 ROGER A. CRAWFORD and CARROLL E. PETERS *In* NASA. Lewis Research Center, Turbine Engine Hot Section Technology, 1985 p 161-164 Oct. 1985
 (Contract NAG3-617)
 Avail: NTIS HC A19/MF A01 CSCL 20D

The objective of this investigation is the experimental evaluation of the influence of inlet turbulence intensity on secondary flow development in a turning duct. The existing 25.4 cm square turning duct (90) facility is being utilized to investigate of bulk turbulence levels on secondary flow development. The large scale duct flow facility allows detailed mean velocity and turbulence quantities to be measured at several streamwise planes in the curved duct. Non-intrusive laser velocimetry is being used to measure the mean and fluctuating components of velocity in all three orthogonal directions. To assure that the turbulence measurements are unbiased by particle lag and other effects, comparison hot wire data will be taken to validate the laser velocimetry system calibration. Author

N88-11158* United Technologies Research Center, East Hartford, CT.
MEASUREMENT OF AIRFOIL HEAT TRANSFER COEFFICIENTS ON A TURBINE STAGE
 ROBERT P. DRING, MICHAEL F. BLAIR, and H. DAVID JOSLYN *In* NASA. Lewis Research Center, Turbine Engine Hot Section Technology, 1985 p 165-173 Oct. 1985
 (Contract NAS3-23717)
 Avail: NTIS HC A19/MF A01 CSCL 20D

A turbulence generating grid was designed and installed in the turbine inlet which produced the target nominal value of 10 percent free stream turbulence. Aerodynamic documentation of the rotor and stator midspan surface pressure distributions were obtained. Midspan heat transfer data were obtained on the rotor and stator for variations in inlet turbulence, rotor-stator axial spacing, and rotor incidence. Author

N88-11159* Arizona State Univ., Tempe. Dept. of Mechanical and Aerospace Engineering.
HEAT TRANSFER IN THE TIP REGION OF A ROTOR BLADE SIMULATOR
 D. E. METZGER, M. K. CHYU, and H. K. MOON *In* NASA. Lewis Research Center, Turbine Engine Hot Section Technology, 1985 p 175-186 Oct. 1985
 (Contract NAG3-623)
 Avail: NTIS HC A19/MF A01 CSCL 20D

The objective of this study of heat transfer in the tip region of a rotor blade simulator is to acquire, through experimental and computational approaches, improved understanding of the nature of the flow and convective heat transfer in the blade tip region. Such information should enable designers to make more accurate predictions of performance and durability, and should support the future development of improved blade tip cooling schemes. Author

N88-11160* Pratt and Whitney Aircraft, East Hartford, CT.
COOLANT PASSAGE HEAT TRANSFER WITH ROTATION
 T. J. HAJEK and A. W. HIGGINS *In* NASA. Lewis Research Center, Turbine Engine Hot Section Technology, 1985 p 187-201 Oct. 1985
 (Contract NAS3-23691)
 Avail: NTIS HC A19/MF A01 CSCL 20D

The objective is to develop a heat transfer and pressure drop data base, computational fluid dynamic techniques, and correlations

34 FLUID MECHANICS AND HEAT TRANSFER

for multi-pass rotating coolant passages with and without flow turbulators. The experimental effort is focused on the simulation of configurations and conditions expected in the blades of advanced aircraft high pressure turbines. With the use of this data base, the effects of Coriolis and buoyancy forces on the coolant side flow can be included in the design of turbine blades. Author

N88-11161*# Stanford Univ., CA. Thermosciences Div.
HEAT TRANSFER WITH VERY HIGH FREE STREAM TURBULENCE

ROBERT J. MOFFAT and PAUL K. MACIEJEWSKI In NASA. Lewis Research Center, Turbine Engine Hot Section Technology, 1985 p 203-215 Oct. 1985 (Contract NAG3-522)

Avail: NTIS HC A19/MF A01 CSCL 20D

Stanton numbers as much as 350 percent above the accepted correlations for flat plate turbulent boundary layer heat transfer have been found in experiments on a low velocity air flow with very high turbulence (up to 50 percent). These effects are far larger than have been previously reported and the data do not correlate as well in boundary layer coordinates (Stanton number and Reynolds number) as they do in simpler coordinates: h vs. X . The very high relative turbulence levels were achieved by placing the test plate in different positions in the margin of a large diameter free jet. The large increases may be due to organized structures of large scale which are present in the marginal flowfield around a free jet. Author

N88-11162*# Minnesota Univ., Minneapolis.
PREDICTION OF TURBINE BLADE HEAT TRANSFER

SUHAS V. PATANKAR In NASA. Lewis Research Center, Turbine Engine Hot Section Technology, 1985 p 217-219 Oct. 1985 (Contract NAG3-579)

Avail: NTIS HC A19/MF A01 CSCL 20D

It is planned to incorporate a number of low Reynolds number turbulence models in a general two-dimensional boundary layer calculation procedure. This will be applied to different flow conditions over turbine blades and the predictions will be compared with experimental data. The prediction activity will lead to a recommendation about a satisfactory turbulence model for turbine blade heat transfer. Author

N88-11163*# Scientific Research Associates, Inc., Glastonbury, CT.

FLOW IN A MODEL TURBINE STATOR

R. C. BUGGELN, S. J. SHAMROTH, and W. R. BRILEY In NASA. Lewis Research Center, Turbine Engine Hot Section Technology, 1985 p 221-226 Oct. 1985 (Contract NAS3-24358)

Avail: NTIS HC A19/MF A01 CSCL 20D

In view of the complex nature of the flowfield in the hot section of gas turbine engines, the need to predict heat transfer and flow losses, the possible appearance of separation and strong secondary flows, etc., the present effort is focusing upon a Navier-Stokes approach to the three dimensional turbine stator problem. The advantages of a full Navier-Stokes approach are clear since when combined with a suitable turbulence model these equations represent the flow and heat transfer physics. In particular, the Navier-Stokes equations accurately represent possible separated regions and regions of significant secondary flow. In addition, the Navier-Stokes approach allows representation of the entire flow field by a single set of equations, thus avoiding problems associated with representing different regions of the flow by different equations and then matching flow regions. Author

N88-12039*# Texas A&M Univ., College Station. Turbomachinery Labs.

LOCAL HEAT/MASS TRANSFER AND PRESSURE DROP IN A TWO-PASS RIB-ROUGHENED CHANNEL FOR TURBINE AIRFOIL COOLING Final Report

J. C. HAN and P. R. CHANDRA Sep. 1987 170 p (Contract NAS3-24227; DA PROJ. 1L1-62209-AH-76)

(NASA-CR-179635; NAS 1.26:179635; AVSCOM-TR-87-C-14; AD-A191003) Avail: NTIS HC A08/MF A01 CSCL 20D

The heat transfer characteristics of turbulent air flow in a multipass channel were studied via the naphthalene sublimation technique. The naphthalene-coated test section, consisting of two straight, square channels joined by a 180 deg turn, resembled the internal cooling passages of gas turbine airfoils. The top and bottom surfaces of the test channel were roughened by rib turbulators. The rib height-to-hydraulic diameter ratio (e/D) were 0.063 and 0.094, and the rib pitch-to-height ratio (P/e) were 10 and 20. The local heat/mass transfer coefficients on the roughened top wall and on the smooth divider and side walls of the test channel were determined for three Reynolds numbers of 15, 30, and 60, thousand, and for three angles of attack (α) of 90, 60, and 45 deg. Results showed that the local Sherwood numbers on the ribbed walls were 1.5 to 6.5 times those for a fully developed flow in a smooth square duct. The average ribbed-wall Sherwood numbers were 2.5 to 3.5 times higher than the fully developed values, depending on the rib angle of attack and the Reynolds number. The results also indicated that, before the turn, the heat/mass transfer coefficients in the cases of $\alpha = 60$ and 45 deg were higher than those in the case of $\alpha = 90$ deg. However, after the turn, the heat/mass transfer coefficients in the oblique-rib cases were lower than those in the transverse rib case. Correlations for the average Sherwood number ratios for individual channel surfaces and for the overall Sherwood number ratios are reported. Correlations for the fully developed friction factors and for the loss coefficients are also provided. Author

N88-12752*# National Aeronautics and Space Administration. Lewis Research Center, Cleveland, OH.

SIMILAR SOLUTIONS FOR VISCOUS HYPERSONIC FLOW OVER A SLENDER THREE-FOURTHS-POWER BODY OF REVOLUTION

CHIN-SHUN LIN Dec. 1987 23 p

(NASA-TM-100205; ICOMP-87-7; E-3803; NAS 1.15:100205)

Avail: NTIS HC A03/MF A01 CSCL 20D

For hypersonic flow with a shock wave, there is a similar solution consistent throughout the viscous and inviscid layers along a very slender three-fourths-power body of revolution. The strong pressure interaction problem can then be treated by the method of similarity. Numerical calculations are performed in the viscous region with the edge pressure distribution known from the inviscid similar solutions. The compressible laminar boundary-layer equations are transformed into a system of ordinary differential equations. The resulting two-point boundary value problem is then solved by the Runge-Kutta method with a modified Newton's method for the corresponding boundary conditions. The effects of wall temperature, mass bleeding, and body transverse curvature are investigated. The induced pressure, displacement thickness, skin friction, and heat transfer due to the previously mentioned parameters are estimated and analyzed. Author

N88-12763*# National Aeronautics and Space Administration. Lewis Research Center, Cleveland, OH.

EXPERIMENTAL STUDY OF THERMOCAPILLARY FLOWS IN A THIN LIQUID LAYER WITH HEAT FLUXES IMPOSED ON THE FREE SURFACE

CHUN-LIANG LAI, PAUL S. GREENBERG, and AN-TI CHAI 1988 13 p Presented at the Second International Symposium on Experimental Methods for Microgravity Material Science Research, Phoenix, Ariz., 25-28 Jan. 1988

(NASA-TM-100252; E-3831; NAS 1.15:100252) Avail: NTIS HC A03/MF A01 CSCL 20D

To study thermocapillary flows in a two-dimensional thin liquid layer with heat fluxes imposed on the free surface experimentally, a long tray configuration was employed to simulate the infinite layer. The surface temperature distribution due to thermocapillary convective for different flow regimes was measured and compared with theoretical predictions. A short tray configuration was also employed to study the end wall effects (insulating or conducting). The results show that for a strong convection flow with an insulating wall as the boundary the surface temperature distribution became

quite uniform. Consequently, the thermocapillary driving force was greatly reduced. On the other hand, a strong fluid motion always existed adjacent to the conducting wall because of the large surface temperature gradient near the wall. Author

N88-13552*# National Aeronautics and Space Administration. Lewis Research Center, Cleveland, OH.

MEASUREMENT OF LOCAL CONVECTIVE HEAT TRANSFER COEFFICIENTS FROM A SMOOTH AND ROUGHENED NACA-0012 AIRFOIL: FLIGHT TEST DATA

JAMES E. NEWTON, G. JAMES VANFOSSEN, PHILLIP E. POINSATTE, and KENNETH J. DEWITT (Toledo Univ., Ohio.) 1988 17 p Presented at the 26th Aerospace Sciences Meeting, Reno, Nev., 11-14 Jan. 1988; sponsored by AIAA (NASA-TM-100284; E-3924; NAS 1.15:100284; AIAA-88-0287) Avail: NTIS HC A03/MF A01 CSCL 20D

Wind tunnels typically have higher free stream turbulence levels than are found in flight. Turbulence intensity was measured to be 0.5 percent in the NASA Lewis Icing Research Tunnel (IRT) with the cloud making sprays off and around 2 percent with cloud making equipment on. Turbulence intensity for flight conditions was found to be too low to make meaningful measurements for smooth air. This difference between free stream and wing tunnel conditions has raised questions as to the validity of results obtained in the IRT. One objective of these tests was to determine the effect of free stream turbulence on convective heat transfer for the NASA Lewis LEWICE ice growth prediction code. These tests provide in-flight heat transfer data for a NASA-0012 airfoil with a 533 cm chord. Future tests will measure heat transfer data from the same airfoil in the Lewis Icing Research Tunnel. Roughness was obtained by the attachment of small, 2 mm diameter hemispheres of uniform size to the airfoil in three different patterns. Heat transfer measurements were recorded in flight on the NASA Lewis Twin Otter Icing Research Aircraft. Measurements were taken for the smooth and roughened surfaces at various aircraft speeds and angles of attack up to four degrees. Results are presented as Frossling number versus position on the airfoil for various roughnesses and angles of attack. Author

N88-14320*# National Aeronautics and Space Administration. Lewis Research Center, Cleveland, OH.

HOST TURBINE HEAT TRANSFER PROGRAM SUMMARY

HERBERT J. GLADDEN and ROBERT J. SIMONEAU 1988 22 p Prepared for presentation at the 33rd International Gas Turbine and Aeroengine Congress and Exposition, Amsterdam, The Netherlands, 5-9 Jun. 1988; sponsored in part by the American Society of Mechanical Engineers (NASA-TM-100280; E-3876; NAS 1.15:100280) Avail: NTIS HC A03/MF A01 CSCL 20D

The objectives of the HOST Turbine Heat Transfer subproject were to obtain a better understanding of the physics of the aerothermodynamic phenomena and to assess and improve the analytical methods used to predict the flow and heat transfer in high temperature gas turbines. At the time the HOST project was initiated, an across-the-board improvement in turbine design technology was needed. A building-block approach was utilized and the research ranged from the study of fundamental phenomena and modeling to experiments in simulated real engine environments. Experimental research accounted for approximately 75 percent of the funding with the remainder going to analytical efforts. A healthy government/industry/university partnership, with industry providing almost half of the research, was created to advance the turbine heat transfer design technology base. Author

N88-15188*# National Aeronautics and Space Administration. Lewis Research Center, Cleveland, OH.

INTERNAL FLUID MECHANICS RESEARCH ON SUPERCOMPUTERS FOR AEROSPACE PROPULSION SYSTEMS

BRENT A. MILLER, BERNHARD H. ANDERSON, and JOHN R. SZUCH Jan. 1988 17 p Prepared for presentation at the 3rd International Conference on Supercomputing (ICS '88), Boston, Mass., 15-20 May 1988; sponsored by International

Supercomputing Inst., Inc.

(NASA-TM-100289; E-3937; NAS 1.15:100289) Avail: NTIS HC A03/MF A01 CSCL 20D

The Internal Fluid Mechanics Division of the NASA Lewis Research Center is combining the key elements of computational fluid dynamics, aerothermodynamic experiments, and advanced computational technology to bring internal computational fluid mechanics (ICFM) to a state of practical application for aerospace propulsion systems. The strategies used to achieve this goal are to: (1) pursue an understanding of flow physics, surface heat transfer, and combustion via analysis and fundamental experiments, (2) incorporate improved understanding of these phenomena into verified 3-D CFD codes, and (3) utilize state-of-the-art computational technology to enhance experimental and CFD research. Presented is an overview of the ICFM program in high-speed propulsion, including work in inlets, turbomachinery, and chemical reacting flows. Ongoing efforts to integrate new computer technologies, such as parallel computing and artificial intelligence, into high-speed aeropropulsion research are described. Author

N88-15791*# National Aeronautics and Space Administration. Lewis Research Center, Cleveland, OH.

INLETS, DUCTS AND NOZZLES

JOHN M. ABBOTT, BERNHARD H. ANDERSON, and EDWARD J. RICE In its Aeropropulsion '87. Session 3: Internal Fluid Mechanics Research 24 p Nov. 1987 Avail: NTIS HC A04/MF A01 CSCL 20D

The internal fluid mechanics research program in inlets, ducts, and nozzles is described. The program consists of a balanced effort between the development of computational tools and the conduct of experimental research. The experiments are designed to better understand the fluid flow physics, to develop new or improved flow models, and to provide benchmark quality data sets for validation of the computational methods. The inlet, duct, and nozzle research program is described according to three major classifications of flow phenomena: highly three-dimensional flow fields; shock-boundary layer interactions; and shear layer control. Specific examples of current and future elements of the research program are described for each of these phenomena. In particular, the highly three-dimensional flow field phenomena is highlighted by describing the computational and experimental research program in transition ducts having a round-to-rectangular area variation. In the case of shock-boundary layer interactions, the specific details of research for normal shock-boundary layer interactions are described. For shear layer control research in vortex generators and the use of aerodynamic excitation for enhancement of the jet mixing process are described. Future research in inlets, ducts, and nozzles will include more emphasis on three-dimensional full Navier-Stokes methods and corresponding experiments designed to concentrate on the appropriate three-dimensional fluid flow physics. Author

N88-15924*# National Aeronautics and Space Administration. Lewis Research Center, Cleveland, OH.

CRYOGENIC FLUID MANAGEMENT TECHNOLOGY WORKSHOP. VOLUME 1: PRESENTATION MATERIAL AND DISCUSSION

JOHN C. AYDELOTT, ed. and WILLIAM DEVOL, ed. (Sverdrup Technology, Inc., Middleburg Heights, Ohio.) Sep. 1987 386 p Workshop held in Cleveland, Ohio, 28-30 Apr. 1987 (NASA-CP-10001; E-3732; NAS 1.55:10001) Avail: NTIS HC A17/MF A01 CSCL 20D

The major objective of the workshop was to identify future NASA needs for technology that will allow the management of subcritical cryogenic fluids in the low gravity space environment. Workshop participants were asked to identify those technologies which will require in-space experimentation and are thus candidates for inclusion in the flight experiment being defined at the Lewis Research Center.

34 FLUID MECHANICS AND HEAT TRANSFER

N88-15928*# National Aeronautics and Space Administration. Lewis Research Center, Cleveland, OH.

LERC CRYOGENIC FLUID MANAGEMENT PROGRAM OVERVIEW

E. P. SYMONS *In its* Cryogenic Fluid Management Technology Workshop. Volume 1: Presentation Material and Discussion p 83-97 Sep. 1987

Avail: NTIS HC A17/MF A01 CSCL 20D

An overview is given of the Lewis Research Center's cryogenic fluid management program in the form of viewgraphs. Objectives, approach, program elements, cost analysis, modeling, and flight experiment development are outlined. R.J.F.

N88-15929*# National Aeronautics and Space Administration. Lewis Research Center, Cleveland, OH.

CRYOGENIC FLUID MANAGEMENT PROGRAM FLIGHT CONCEPT DEFINITION

ERICH KROEGER *In its* Cryogenic Fluid Management Technology Workshop. Volume 1: Presentation Material and Discussion p 99-115 Sep. 1987

Avail: NTIS HC A17/MF A01 CSCL 20D

The Lewis Research Center's cryogenic fluid management program flight concept definition is presented in viewgraph form. Diagrams are given of the cryogenic fluid management subpallet and its configuration with the Delta launch vehicle. Information is given in outline form on feasibility studies, requirements definition, and flight experiments design. R.J.F.

N88-15939*# Massachusetts Inst. of Tech., Cambridge. Dept. of Mechanical Engineering.

VAPOR CONDENSATION ON A TURBULENT LIQUID INTERFACE

M. R. HELMICK, B. C. KHOO, and A. A. SONIN *In* NASA. Lewis Research Center, Cleveland, Ohio. Cryogenic Fluid Management Technology Workshop. Volume 1: Presentation Material and Discussion p 301-315 Sep. 1987 (Contract NAG3-731)

Avail: NTIS HC A17/MF A01 CSCL 20D

An experimental investigation which seeks the fundamental relationship between the interfacial condensation rate and the parameters which control it when the liquid side is turbulent is discussed. The scaling laws for free-surface condensation are discussed for this case. It is argued that the condensation of cryogenic liquids can, in principle, be simulated in experiments using steam and water. Data are presented for the condensation rate in terms of the dimensionless scaling parameters which involve the fluid properties and the liquid-side turbulence velocity and length scales. Author

N88-15983*# National Aeronautics and Space Administration. Lewis Research Center, Cleveland, OH.

ON THE PERFORMANCE OF FINITE JOURNAL BEARINGS LUBRICATED WITH MICROPOLAR FLUIDS

M. M. KHONSARI and D. E. BREWE (Army Aviation Research and Development Command, St. Louis, Mo.) 1988 22 p Proposed for presentation at the 1988 Annual Meeting of Tribologists and Lubrication Engineers, Cleveland, Ohio, 8-12 May 1988

(NASA-TM-100293; E-3939; NAS 1.15:100293; AVSCOM-TR-88-C-001; AD-A192057) Avail: NTIS HC A03/MF A01 CSCL 20D

A study of the performance parameters for a journal bearing of finite length lubricated with micropolar fluids is undertaken. Results indicate that a significantly higher load carrying capacity than the Newtonian fluids may result depending on the size of material characteristic length and the coupling number. It is also shown that although the frictional force associated with micropolar fluid is in general higher than that of a Newtonian fluid, the friction coefficient of micropolar fluids tends to be lower than that of the Newtonian. Author

N88-15984*# National Aeronautics and Space Administration. Lewis Research Center, Cleveland, OH.

THE EFFECT OF EDDY DISTRIBUTION ON MOMENTUM AND HEAT TRANSFER NEAR THE WALL IN TURBULENT PIPE FLOW

ROBERT L. ZURAWSKI, STANLEY P. GRISNIK, TERRY L. HARDY, and BAHMAN GHORASHI (Cleveland State Univ., Ohio.) Dec. 1987 38 p

(NASA-TM-100257; E-3882; NAS 1.15:100257) Avail: NTIS HC A03/MF A01 CSCL 20D

A study was conducted to determine the effect of eddy distribution on momentum and heat transfer near the wall in turbulent pipe flow. The buffer zone was of particular interest in that it is perhaps the most complicated and least understood region in the turbulent flow field. Six eddy diffusivity relationships are directly compared on their ability to predict mean velocity and temperature distributions in turbulent air flow through a cylindrical, smooth-walled pipe with uniform heat transfer. Turbulent flow theory and the development of the eddy diffusivity relationships are briefly reviewed. Velocity and temperature distributions derived from the eddy diffusivity relationships are compared to experimental data for fully-developed pipe flow in turbulent air at a Prandtl number of 0.73 and Reynolds numbers ranging from 8100 to 25 000. Author

N88-16956*# Nebraska Univ., Lincoln. Lab. for Electro-Optical Measurements.

COMPARISON OF UNL LASER IMAGING AND SIZING SYSTEM AND A PHASE/DOPPLER SYSTEM FOR ANALYZING SPRAYS FROM A NASA NOZZLE Final Report, 1 Apr. 1985 - 19 Aug. 1987

DENNIS R. ALEXANDER 14 Feb. 1988 139 p (Contract NAG3-634)

(NASA-CR-182437; NAS 1.26:182437) Avail: NTIS HC A07/MF A01 CSCL 20D

Aerosol spray characterization was done using a P/DPA and a laser imaging/video processing system on a NASA MOD-1 air-assist nozzle being evaluated for use in aircraft icing research. Benchmark tests were performed on monodispersed particles and on the NASA MOD-1 nozzle under identical laboratory operating conditions. The laser imaging/video processing system and the P/DPA showed agreement on calibration tests in monodispersed aerosol sprays of + or - 2.6 microns with a standard deviation of + or - 2.6 microns. Tests were performed on the NASA MOD-1 nozzle on the centerline and radially at one-half inch increments to the outer edge of the spray plume at a distance two feet (0.61 m) downstream from the exit of the nozzle. Comparative results at two operating conditions of the nozzle are presented for the two instruments. For the first case, the deviation in arithmetic mean diameters determined by the two instruments was in a range of 0.1 to 2.8 microns, and the deviation in Sauter mean diameters varied from 0 to 2.2 microns. Operating conditions in the second case were more severe which resulted in the arithmetic mean diameter deviating from 1.4 to 7.1 microns and the deviation in the Sauter mean diameters ranging from 0.4 to 6.7 microns. Author

N88-16988*# National Aeronautics and Space Administration. Lewis Research Center, Cleveland, OH.

NUMERICAL MODELING OF MULTIDIMENSIONAL FLOW IN SEALS AND BEARINGS USED IN ROTATING MACHINERY

R. C. HENDRICKS, L. T. TAM, A. PRZEKAS, A. MUSZYNSKA, M. J. BRAUN, and R. L. MULLEN (Case Western Reserve Univ., Cleveland, Ohio.) 1988 30 p Prepared for presentation at the 2nd International Symposium on Transport Phenomena, Dynamics, and Design of Rotating Machinery, Honolulu, Hawaii, 4-6 Apr. 1988; sponsored in part by ASME and JSME

(NASA-TM-100779; E-3909; NAS 1.15:100779) Avail: NTIS HC A03/MF A01 CSCL 20D

The rotordynamic behavior of turbomachinery is critically dependent on fluid dynamic rotor forces developed by various types of seals and bearings. The occurrence of self-excited vibrations often depends on the rotor speed and load. Misalignment

and rotor wobbling motion associated with differential clearance were often attributed to stability problems. In general, the rotative character of the flowfield is a complex three dimensional system with secondary flow patterns that significantly alter the average fluid circumferential velocity. A multidimensional, nonorthogonal, body-fitted-grid fluid flow model is presented that describes the fluid dynamic forces and the secondary flow pattern development in seals and bearings. Several numerical experiments were carried out to demonstrate the characteristics of this complex flowfield. Analyses were performed by solving a conservation form of the three dimensional Navier-Stokes equations transformed to those for a rotating observer and using the general-purpose computer code PHOENICS with the assumptions that the rotor orbit is circular and that static eccentricity is zero. These assumptions have enabled a precise steady-state analysis to be used. Fluid injection from ports near the seal or bearing center increased fluid-film direct dynamic stiffness and, in some cases, significantly increased quadrature dynamic stiffness. Injection angle and velocity could be used for active rotordynamic control; for example, injection, when compared with no injection, increased direct dynamic stiffness, which is an important factor for hydrostatic bearings.

Author

N88-17954*# Case Western Reserve Univ., Cleveland, OH. Dept. of Mechanical and Aerospace Engineering.

THE USE OF MULTIGRID TECHNIQUES IN THE SOLUTION OF THE ELROD ALGORITHM FOR A DYNAMICALLY LOADED JOURNAL BEARING M.S. Thesis. Final Report

CLAUDIA M. WOODS Feb. 1988 33 p

(Contract NCC3-30)

(NASA-CR-180873; E-3897; NAS 1.26:180873) Avail: NTIS HC A03/MF A01 CSCL 20D

A numerical solution to a theoretical model of vapor cavitation in a dynamically loaded journal bearing is developed, utilizing a multigrid iterative technique. The code is compared with a presently existing direct solution in terms of computational time and accuracy. The model is based on the Elrod algorithm, a control volume approach to the Reynolds equation which mimics the Jakobsson-Floberg and Olsson cavitation theory. Besides accounting for a moving cavitation boundary and conservation of mass at the boundary, it also conserves mass within the cavitated region via liquid striations. The mixed nature of the equations (elliptic in the full film zone and nonelliptic in the cavitated zone) coupled with the dynamic aspects of the problem create interesting difficulties for the present solution approach. Emphasis is placed on the methods found to eliminate solution instabilities. Excellent results are obtained for both accuracy and reduction of computational time.

Author

N88-18867*# National Aeronautics and Space Administration. Lewis Research Center, Cleveland, OH.

NUMERICAL AND ANALYTICAL STUDY OF FLUID DYNAMIC FORCES IN SEALS AND BEARINGS

L. T. TAM, A. J. PRZEKAS, A. MUSZYNSKA, R. C. HENDRICKS, M. J. BRAUN, and R. L. MULLEN (Case Western Reserve Univ., Cleveland, Ohio.) Sep. 1987 38 p Presented at the 11th Biennial Design Engineering Conference on Vibration and Noise, Boston, Mass., 27-30 Sep. 1987; sponsored by ASME (NASA-TM-100268; E-3903; NAS 1.15:100268) Avail: NTIS HC A03/MF A01 CSCL 20D

A numerical model based on a transformed, conservative form of the three dimensional Navier-Stokes equation and an analytical model based on lumped fluid parameters are presented and compared with studies of modeled rotor bearing seal systems. The rotor destabilizing factors are related to the rotative character of the flow field. It is shown that these destabilizing factors can be reduced through a decrease in the fluid average circumferential velocity. However, the rotative character of the flow field is a complex three dimensional system with bifurcated secondary flow patterns that significantly alter the fluid circumferential velocity. By transforming the Navier-Stokes equations to those for a rotating observer and using the numerical code PHOENICS-84 with a nonorthogonal body fitted grid, several numerical experiments were

carried out to demonstrate the character of this complex flow field. In general, fluid injection and/or preswirl of the flow field opposing the shaft rotation significantly intensified these secondary recirculation zones and thus reduced the average circumferential velocity; injection or preswirl in the direction of rotation significantly weakened these zones.

Author

N88-18870*# National Aeronautics and Space Administration. Lewis Research Center, Cleveland, OH.

UNSTEADY HEAT TRANSFER IN TURBINE BLADE DUCTS: FOCUS ON COMBUSTOR SOURCES

KENNETH J. BAUMEISTER and RONALD HUFF (Huff and Associates, Cleveland, Ohio.) 1988 18 p Prepared for presentation at the National Heat Transfer Conference, Houston, Tex., 24-27 Jul. 1988; sponsored by ASME (NASA-TM-100815; E-4000; NAS 1.15:100815) Avail: NTIS HC A03/MF A01 CSCL 20D

Thermal waves generated by either turbine rotor blades cutting through nonuniform combustor temperature fields or unsteady burning could lead to thermal fatigue cracking in the blades. To determine the magnitude of the thermal oscillation in blades with complex shapes and material compositions, a finite element Galerkin formulation has been developed to study combustor generated thermal wave propagation in a model two-dimensional duct with a uniform plug flow profile. The reflection and transmission of the thermal waves at the entrance and exit boundaries are determined by coupling the finite element solutions at the entrance and exit to the eigenfunctions of an infinitely long adiabatic duct. Example solutions are presented. In general, thermal wave propagation from an air passage into a metallic blade wall is small and not a problem. However, if a thermal barrier coating is applied to a metallic surface under conditions of a high heat transfer, a good impedance match is obtained and a significant portion of the thermal wave can pass into the blade material.

Author

N88-18871*# National Aeronautics and Space Administration. Lewis Research Center, Cleveland, OH.

THERMOSOLUTAL CONVECTION IN HIGH-ASPECT-RATIO ENCLOSURES

L. W. WANG and C. T. CHEN (National Cheng Kung Univ., Tainan, Taiwan) 1988 14 p Prepared for presentation at the 25th National Heat Transfer Conference, Houston, Tex., 24-27 Jul. 1988; sponsored by the ASME (NASA-TM-100803; E-3881; NAS 1.15:100803) Avail: NTIS HC A03/MF A01 CSCL 20D

Convection in high-aspect-ratio rectangular enclosures with combined horizontal temperature and concentration gradients is studied experimentally. An electrochemical system is employed to impose the concentration gradients. The solutal buoyancy force either opposes or augments the thermal buoyancy force. Due to a large difference between the thermal and solutal diffusion rates the flow possesses double-diffusive characteristics. Various complex flow patterns are observed with different experimental conditions.

Author

N88-19739*# National Aeronautics and Space Administration. Lewis Research Center, Cleveland, OH.

HIGH RAYLEIGH NUMBER CONVECTION IN RECTANGULAR ENCLOSURES WITH DIFFERENTIALLY HEATED VERTICAL WALLS AND ASPECT RATIOS BETWEEN ZERO AND UNITY

SIYAVASH A. KASSEM Apr. 1988 21 p (NASA-TM-100277; E-3838; NAS 1.15:100277) Avail: NTIS HC A03/MF A01 CSCL 20D

High Rayleigh number convection in a rectangular cavity with insulated horizontal surfaces and differentially heated vertical walls was analyzed for an arbitrary aspect ratio smaller than or equal to unity. Unlike previous analytical studies, a systematic method of solution based on linearization technique and analytical iteration procedure was developed to obtain approximate closed-form solutions for a wide range of aspect ratios. The predicted velocity and temperature fields are shown to be in excellent agreement with available experimental and numerical data.

Author

34 FLUID MECHANICS AND HEAT TRANSFER

N88-19740*# National Aeronautics and Space Administration. Lewis Research Center, Cleveland, OH.

TIME-ACCURATE SIMULATIONS OF A SHEAR LAYER FORCED AT A SINGLE FREQUENCY

R. W. CLAUS, P. G. HUANG, and J. M. MACINNES (Princeton Univ., N. J.) 1988 20 p Presented at the 26th Aerospace Sciences Meeting, Reno, Nev., 11-14 Jan. 1988; sponsored by AIAA Previously announced in IAA as A88-27716

(NASA-TM-100836; E-3868; NAS 1.15:100836; AIAA-88-0061)

Avail: NTIS HC A03/MF A01 CSCL 20D

Calculations are presented for the forced shear layer studied experimentally by Oster and Wygnanski, and Weisbrodt. Two different computational approaches are examined: Direct Numerical Simulation (DNS) and Large Eddy Simulation (LES). The DNS approach solves the full three dimensional Navier-Stokes equations for a temporally evolving mixing layer, while the LES approach solves the two dimensional Navier-Stokes equations with a subgrid scale turbulence model. While the comparison between these calculations and experimental data was hampered by a lack of information on the inflow boundary conditions, the calculations are shown to qualitatively agree with several aspects of the experiment. The sensitivity of these calculations to factors such as mesh refinement and Reynolds number is illustrated. Author

N88-20599*# National Aeronautics and Space Administration. Lewis Research Center, Cleveland, OH.

CRYOGENIC FLUID MANAGEMENT TECHNOLOGY WORKSHOP. VOLUME 2: ROUNDTABLE DISCUSSION OF TECHNOLOGY REQUIREMENTS

Mar. 1988 84 p Workshop held in Cleveland, Ohio, 28-30 Apr. 1987

(NASA-CP-10009; E-3987; NAS 1.55:10009) Avail: NTIS HC A05/MF A01 CSCL 20D

The Cryogenic Fluid Management Technology Workshop was held April 28 to 30, 1987, at the NASA Lewis Research Center in Cleveland, Ohio. The major objective of the workshop was to identify future NASA needs for technology concerning the management of subcritical cryogenic fluids in the low-gravity space environment. In addition, workshop participants were asked to identify those technologies which will require in-space experimentation and thus are candidates for inclusion in the flight experiment being defined at Lewis. The principal application for advanced fluid management technology is the Space-Based Orbit Transfer Vehicle (SBOTV) and its servicing facility, the On-Orbit Cryogenic Fuel Depot (OOCFD). Other potential applications include the replenishment of cryogenic coolants (with the exception of superfluid helium), reactants, and propellants on board a variety of spacecraft including the space station and space-based weapon systems. The last day was devoted to a roundtable discussion of cryogenic fluid management technology requirements by 30 representatives from NASA, industry, and academia. This volume contains a transcript of the discussion of the eight major technology categories. Author

N88-21417*# National Aeronautics and Space Administration. Lewis Research Center, Cleveland, OH.

FINGERING FLOW PATTERNS OF THERMOSOLUTAL CONVECTION IN RECTANGULAR ENCLOSURES

L. W. WANG, J. J. CHEN, and C. T. CHEN (National Cheng Kung Univ., Tainan, Taiwan) 1988 14 p Proposed for presentation at the National Fluid Dynamics Congress, Cincinnati, Ohio, 24-28 Jul. 1988; sponsored by AIAA, ASME, ASCE, SIAM and APS (NASA-TM-100854; E-4057; NAS 1.15:100854) Avail: NTIS HC A03/MF A01 CSCL 20D

Convection in rectangular enclosures with combined horizontal temperature and concentration gradients is studied. An electrochemical system is employed to impose the concentration gradients. Due to a large difference between the thermal and solutal diffusion rates the flow possesses double-diffusive characteristics. Very complex fingering flow patterns are observed around the two-phase interfaces. The main objective of the present work is to obtain more information on the flows near the two vertical phase interfaces under various parametric conditions. The

fingering flows near the crystal could be one of the most important factors to cause the crystal imperfections. The ranges of the parameters studied are Sc (Schmidt number)=2200 to 2400, Pr (Prandtl number)=4.0 to 7.0, $Gr_{sub T}$ (Grashof number)= 2.50×10 to the 6th to 5.10×10 to the 7th power, Ar (aspect ratio)=0.61 to 3.0, and N (buoyancy ratio)=0.05 to 54.8. Author

N88-21424*# National Aeronautics and Space Administration. Lewis Research Center, Cleveland, OH.

ELECTROHYDRODYNAMIC MIGRATION OF CHARGED DROPLETS IN AN INSULATING FLUID

R. BALASUBRAMANIAM and R. A. WILKINSON 1988 20 p Proposed for presentation at the National Fluid Dynamic Congress, Cincinnati, Ohio, 24-28 Jul. 1988; sponsored by AIAA (NASA-TM-100849; E-4046; NAS 1.15:100849) Avail: NTIS HC A03/MF A01 CSCL 20D

The motion of charged, conducting droplets present in an insulating fluid medium is analyzed under the action of an electric field, in microgravity. Previous analyses of this problem have considered the Maxwell stresses as the only driving force. In the present study, arguments from macroscopic thermodynamics and the molecular theory of surface tension are used to show that the surface tension gradients can be induced due to the variation of the electric potential on the interface. In the limit of Reynolds numbers small compared to unity, the terminal velocity of migration of the droplet is calculated under the combined action of the Maxwell stresses and the surface tension gradients. The results show that there are no surface tension gradients (i.e., no electric potential variation at the interface) in a case that is due to the convection of the surface charges, surface tension gradients do exist and tend to reduce the terminal velocity of the droplet. The shape of the droplet altered by the motion was also calculated, when the deformations from the spherical shape are small. Author

N88-22322*# Minnesota Univ., Minneapolis.

A SURVEY OF OSCILLATING FLOW IN STIRLING ENGINE HEAT EXCHANGERS Annual Contractor Report

TERRENCE W. SIMON and JORGE R. SEUME Mar. 1988 133 p

(Contract NAG3-598)

(NASA-CR-182108; NAS 1.26:182108) Avail: NTIS HC A07/MF A01 CSCL 20D

Similarity parameters for characterizing the effect of flow oscillation on wall shear stress, viscous dissipation, pressure drop and heat transfer rates are proposed. They are based on physical arguments and are derived by normalizing the governing equations. The literature on oscillating duct flows, regenerator and porous media flows is surveyed. The operating characteristics of the heat exchanger of eleven Stirling engines are described in terms of the similarity parameters. Previous experimental and analytical results are discussed in terms of these parameters and used to estimate the nature of the oscillating flow under engine operating conditions. The operating points for many of the modern Stirling engines are in or near the laminar to turbulent transition region. In several engines, working fluid does not pass entirely through heat exchangers during a cycle. Questions that need to be addressed by further research are identified. Author

N88-23182*# Grumman Aerospace Corp., Bethpage, NY.

SOLAR DYNAMIC HEAT REJECTION TECHNOLOGY. TASK 2: HEAT PIPE RADIATOR DEVELOPMENT Final Report

MARK LEAGUE and JOE ALARIO May 1988 46 p

(Contract NAS3-24665)

(NASA-CR-182141; NAS 1.26:182141) Avail: NTIS HC A03/MF A01 CSCL 20D

This report covers the design, fabrication, and test of several dual slot heat pipe engineering development units. The following dual-slot heat pipes were fabricated and tested: two 6-ft. aluminum heat pipes; a 20-ft. aluminum heat pipe; and a 20-ft. aluminum heat pipe with a four-leg evaporator section. The test results of all four test articles are presented and compared to the performance predicted by the design software. Test results from

the four-leg article are incomplete. The methodology for fabricating stainless steel dual slot heat pipes was also studied by performing a tool life test with different single point cutters, and these results are also presented. Although the dual-slot heat pipe has demonstrated the potential to meet the requirements for a high capacity radiator system, uncertainties with the design still exist. The startup difficulties with the aluminum test articles must be solved, and a stainless steel/methanol heat pipe should be built and tested. Author

N88-23184*# National Aeronautics and Space Administration. Lewis Research Center, Cleveland, OH.

INITIAL CONDITION EFFECT ON PRESSURE WAVES IN AN AXISYMMETRIC JET

JEFFREY H. MILES and GANESH RAMAN (Sverdrup Technology, Inc., Cleveland, Ohio.) 1988 14 p Proposed for presentation at the 1st National Fluid Dynamics Congress, Cincinnati, Ohio, 24-28 Jul. 1988; sponsored by AIAA, ASME, ASCE, SIAM and APS (NASA-TM-100915; E-4076; NAS 1.15:100915) Avail: NTIS HC A03/MF A01 CSCL 20D

A pair of microphones (separated axially by 5.08 cm and laterally by 1.3 cm) are placed on either side of the jet centerline to investigate coherent pressure fluctuations in an axisymmetric jet at Strouhal numbers less than unity. Auto-spectra, transfer-function, and coherence measurements are made for a tripped and untripped boundary layer initial condition. It was found that coherent acoustic pressure waves originating in the upstream plenum chamber propagate a greater distance downstream for the tripped initial condition than for the untripped initial condition. In addition, for the untripped initial condition the development of the coherent hydrodynamic pressure waves shifts downstream. Author

N88-23185*# Minnesota Univ., Minneapolis. Dept. of Mechanical Engineering.

TWO-EQUATION LOW-REYNOLDS-NUMBER TURBULENCE MODELING OF TRANSITIONAL BOUNDARY LAYER FLOWS CHARACTERISTIC OF GAS TURBINE BLADES Ph.D. Thesis. Final Contractor Report

RODNEY C. SCHMIDT and SUHAS V. PATANKAR May 1988 273 p (Contract NAG3-579) (NASA-CR-4145; E-3960; NAS 1.26:4145) Avail: NTIS HC A12/MF A01 CSCL 20D

The use of low Reynolds number (LRN) forms of the k-epsilon turbulence model in predicting transitional boundary layer flow characteristic of gas turbine blades is developed. The research presented consists of: (1) an evaluation of two existing models; (2) the development of a modification to current LRN models; and (3) the extensive testing of the proposed model against experimental data. The prediction characteristics and capabilities of the Jones-Launder (1972) and Lam-Bremhorst (1981) LRN k-epsilon models are evaluated with respect to the prediction of transition on flat plates. Next, the mechanism by which the models simulate transition is considered and the need for additional constraints is discussed. Finally, the transition predictions of a new model are compared with a wide range of different experiments, including transitional flows with free-stream turbulence under conditions of flat plate constant velocity, flat plate constant acceleration, flat plate but strongly variable acceleration, and flow around turbine blade test cascades. In general, calculational procedure yields good agreement with most of the experiments. Author

N88-23186*# National Aeronautics and Space Administration. Lewis Research Center, Cleveland, OH.

EXPERIMENTAL STUDY OF BYPASS TRANSITION IN A BOUNDARY LAYER M.S. Thesis

KENNETH L. SUDER, JAMES E. OBRIEN, and ELI RESHOTKO (Case Western Reserve Univ., Cleveland, Ohio.) May 1988 199 p (NASA-TM-100913; E-3953; NAS 1.15:100913) Avail: NTIS HC A09/MF A01 CSCL 20D

A detailed investigation to compare the boundary layer transition process in a low intensity disturbance environment to that in an environment in which the disturbances are initially non-linear in amplitude was conducted using a flat plate model. The transition mechanism based on linear growth of Tollmien Schlichting (T-S) waves was associated with a freestream turbulence level of 0.3 percent; however, for a freestream turbulence intensity of 0.65 percent and higher, the bypass transition mechanism prevailed. The results of detailed measurements acquired to study and compare the two transition mechanisms indicate that there exists a critical value for the peak rms of the velocity fluctuations within the boundary layer of approximately 3 to 3.5 percent of the freestream velocity. Once the unsteadiness within the boundary layer reached this critical value, turbulent bursting initiated, regardless of the transition mechanism. The two point correlations and simultaneous time traces within the transition region illustrate the features of a turbulent burst and its effect on the surrounding flowfield. Author

N88-23718*# Massachusetts Inst. of Tech., Cambridge. EXPERIMENTAL MEASUREMENTS OF HEAT TRANSFER FROM AN ICED SURFACE DURING ARTIFICIAL AND NATURAL CLOUD ICING CONDITIONS

MARK S. KIRBY and R. JOHN HANSMAN, JR. /n NASA, Langley Research Center, Joint University Program for Air Transportation Research, 1986 p 17-26 Apr. 1988 Previously announced in IAA as A86-39948 Sponsored in cooperation with FAA (Contract NGL-22-009-640; NAG3-666) (AIAA-86-1352) Avail: NTIS HC A06/MF A01 CSCL 20D

The heat transfer behavior of accreting ice surfaces in natural (flight test) and simulated (wind tunnel) cloud icing conditions were studied. Observations of wet and dry ice growth regimes as measured by ultrasonic pulse echo techniques were made. Observed wet and dry ice growth regimes at the stagnation point of a cylinder were compared with those predicted using a quasi steady state heat balance model. A series of heat transfer coefficients were employed by the model to infer the local heat transfer behavior of the actual ice surfaces. The heat transfer in the stagnation region was generally inferred to be higher in wind tunnel icing tests than in natural flight icing conditions. Author

N88-23956*# United Technologies Research Center, East Hartford, CT.

THE EFFECTS OF INLET TURBULENCE AND ROTOR/STATOR INTERACTIONS ON THE AERODYNAMICS AND HEAT TRANSFER OF A LARGE-SCALE ROTATING TURBINE MODEL. PART 4: AERODYNAMIC DATA TABULATION

R. P. DRING, H. D. JOSLYN, and M. F. BLAIR Nov. 1987 135 p (Contract NAS3-23717) (NASA-CR-179469; NAS 1.26:179469; UTRC/R86-956480-4) Avail: NTIS HC A07/MF A01 CSCL 20D

A combined experimental and analytical program was conducted to examine the effects of inlet turbulence and airfoil heat transfer. The experimental portion of the study was conducted in a large-scale (approx. 5X engine), ambient temperature, rotating turbine model configured in both single-stage and stage-and-a-half arrangements. Heat transfer measurements were obtained using low-conductivity airfoils with miniature thermocouples welded to a thin, electrically heated surface skin. Heat transfer data were acquired for various combinations of low or high inlet turbulence intensity, flow coefficient, first stator-rotor axial spacing, Reynolds number and relative circumferential position of the first and second stators. Aerodynamic measurements obtained include distributions of the mean and fluctuating velocities at the turbine inlet and, for each airfoil row, midspan airfoil surface pressures and circumferential distributions of the downstream steady state pressures and fluctuating velocities. Results include airfoil heat transfer predictions produced using existing 2-D boundary layer computation schemes and an examination of solutions of the unsteady boundary layer equations. Author

34 FLUID MECHANICS AND HEAT TRANSFER

N88-23957* # National Aeronautics and Space Administration. Lewis Research Center, Cleveland, OH.

HEAT TRANSFER IN AEROSPACE PROPULSION

ROBERT J. SIMONEAU, ROBERT C. HENDRICKS, and HERBERT J. GLADDEN 1988 48 p Presented at the National Heat Transfer Conference, Houston, Tex., 24-27 Jul. 1988; sponsored by ASME, AICE and ANS (NASA-TM-100874; E-4105; NAS 1.15:100874) Avail: NTIS HC A03/MF A01 CSCL 20D

Presented is an overview of heat transfer related research in support of aerospace propulsion, particularly as seen from the perspective of the NASA Lewis Research Center. Aerospace propulsion is defined to cover the full spectrum from conventional aircraft power plants through the Aerospace Plane to space propulsion. The conventional subsonic/supersonic aircraft arena, whether commercial or military, relies on the turbine engine. A key characteristic of turbine engines is that they involve fundamentally unsteady flows which must be properly treated. Space propulsion is characterized by very demanding performance requirements which frequently push systems to their limits and demand tailored designs. The hypersonic flight propulsion systems are subject to severe heat loads and the engine and airframe are truly one entity. The impact of the special demands of each of these aerospace propulsion systems on heat transfer is explored.

Author

N88-24917* # Sverdrup Technology, Inc., Arnold Air Force Station, TN.

HYPERSONIC TURBULENT WALL BOUNDARY LAYER

COMPUTATIONS Final Report

S. C. KIM and G. J. HARLOFF May 1988 9 p Presented at the 24th Joint Propulsion Conference, Boston, Mass., 11-13 Jul. 1988; sponsored in part by AIAA, ASEE, ASME, and SAE (Contract NAS3-25266) (NASA-CR-182147; E-4172; NAS 1.26:182147; AIAA-88-2829) Avail: NTIS HC A02/MF A01 CSCL 20D

The Baldwin-Lomax algebraic turbulence model was modified for hypersonic flow conditions. Two coefficients in the outer layer eddy viscosity model were determined as functions of Mach number and temperature ratio. By matching the solutions from the Baldwin-Lomax model to those from the Cebeci-Smith model for a flat plate at hypersonic speed, the new values of the coefficient were obtained. The results show that the values of $C_{sub\ cp}$ and $C_{sub\ kleb}$ are functions of both Mach number and wall temperature ratio. The $C_{sub\ cp}$ and $C_{sub\ kleb}$ variations with Mach number and wall temperature were used for the calculations of both a 4 deg wedge flow at Mach 18 and an axisymmetric Mach 20 nozzle flow. The Navier-Stokes equations with thin layer approximation were solved for the above hypersonic flow conditions and the results were compared with existing experimental data. The agreement between the numerical solutions and the existing experimental data were good. The modified Baldwin-Lomax model thus is useful in the computations of hypersonic flows.

Author

N88-25841* # National Aeronautics and Space Administration. Lewis Research Center, Cleveland, OH.

BOUNDARY LAYER DEVELOPMENT AS A FUNCTION OF CHAMBER PRESSURE IN THE NASA LEWIS 1030:1 AREA RATIO ROCKET NOZZLE

TAMARA A. SMITH 1988 33 p Presented at the 24th Joint Propulsion Conference, Boston, Mass., 11-13 Jul. 1988; sponsored by AIAA, ASEE, ASME and SAE (NASA-TM-100917; E-4078; NAS 1.15:100917) Avail: NTIS HC A03/MF A01 CSCL 20D

Through the use of theoretical predictions of fluid properties and experimental heat transfer and thrust measurements, the zones of laminar, transitional, and turbulent boundary layer flow were defined for the NASA Lewis 1030:1 area ratio rocket nozzle. Tests were performed on the nozzle at chamber pressures from 350 to 100 psia. For these conditions, the throat diameter Reynolds numbers varied from 300,000 to 1 million. The propellants used were gaseous hydrogen and gaseous oxygen. Thrust measurements and nozzle outer wall temperature measurements

were taken during the 3-sec test runs. Comparison of experimental heat transfer and thrust data with the corresponding predictions from the Two-Dimensional Kinetics (TDK) nozzle analysis program indicated laminar flow in the nozzle at a throat diameter Reynolds number of 320,000 or chamber pressure of 360 psia. Comparison of experimental and predicted heat transfer data indicated transitional flow up to and including a chamber pressure of 1000 psia. Predicted values of the axisymmetric acceleration parameter within the convergent and divergent nozzle were consistent with the above results. Based upon an extrapolation of the heat transfer data and predicted distributions of the axisymmetric acceleration parameter, transitional flow was predicted up to a throat diameter Reynolds number of 220,000 or 2600-psia chamber pressure. Above 2600-psia chamber pressure, fully developed turbulent flow was predicted.

Author

N88-25854* # National Aeronautics and Space Administration. Lewis Research Center, Cleveland, OH.

THE SOLUTION OF THE ELROD ALGORITHM FOR A DYNAMICALLY LOADED JOURNAL BEARING USING MULTIGRID TECHNIQUES

CLAUDIA M. WOODS and DAVID E. BREWE (Army Aviation Research and Development Command, Cleveland, Ohio.) 1988 31 p Proposed for presentation at the 1988 Tribology Conference, Baltimore, Md., 16-19 Oct. 1988; sponsored by ASME and STLE (NASA-TM-100941; E-4222; NAS 1.15:100941; AVSCOM-TR-88-C-006; AD-A197535) Avail: NTIS HC A03/MF A01 CSCL 13I

A numerical solution to a theoretical model of vapor cavitation in a dynamically loaded journal bearing is developed utilizing a multigrid iteration technique. The method is compared with a noniterative approach in terms of computational time and accuracy. The computational model is based on the Elrod algorithm, a control volume approach to the Reynolds equation which mimics the Jakobsson-Floberg and Olsson cavitation theory. Besides accounting for a moving cavitation boundary and conservation of mass at the boundary, it also conserves mass within the cavitated region via a smeared mass or striated flow extending to both surfaces in the film gap. The mixed nature of the equations (parabolic in the full film zone and hyperbolic in the cavitated zone) coupled with the dynamic aspects of the problem create interesting difficulties for the present solution approach. Emphasis is placed on the methods found to eliminate solution instabilities. Excellent results are obtained for both accuracy and reduction of computational time.

Author

N88-25857* # Flow Research, Inc., Kent, WA.

DIRECT SIMULATIONS OF CHEMICALLY REACTING TURBULENT MIXING LAYERS, PART 2 Final Report

RALPH W. METCALFE, PATRICK A. MCMURTRY, WEN-HUEI JOU, JAMES J. RILEY, and PEYMAN GIVI Jun. 1988 61 p (Contract NAS3-24229) (NASA-CR-180853; NAS 1.26:180853; FLOW-RR-425) Avail: NTIS HC A04/MF A01 CSCL 20D

The results of direct numerical simulations of chemically reacting turbulent mixing layers are presented. This is an extension of earlier work to a more detailed study of previous three dimensional simulations of cold reacting flows plus the development, validation, and use of codes to simulate chemically reacting shear layers with heat release. Additional analysis of earlier simulations showed good agreement with self similarity theory and laboratory data. Simulations with a two dimensional code including the effects of heat release showed that the rate of chemical product formation, the thickness of the mixing layer, and the amount of mass entrained into the layer all decrease with increasing rates of heat release. Subsequent three dimensional simulations showed similar behavior, in agreement with laboratory observations. Baroclinic torques and thermal expansion in the mixing layer were found to produce changes in the flame vortex structure that act to diffuse the pairing vortices, resulting in a net reduction in vorticity. Previously unexplained anomalies observed in the mean velocity profiles of reacting jets and mixing layers were shown to result from vorticity generation by baroclinic torques.

Author

N88-26616*# Sverdrup Technology, Inc., Cleveland, OH.
THREE-DIMENSIONAL VISCOUS FLOW COMPUTATIONS OF A CIRCULAR JET IN SUBSONIC AND SUPERSONIC CROSS FLOW Final Contractor Report

G. J. HARLOFF and J. K. LYTLE Jul. 1988 14 p Presented at the 1st National Fluid Dynamics Congress, Cincinnati, Ohio, 24-28 Jul. 1988; sponsored by ASME (Contract NAS3-25266) (NASA-CR-182153; E-4223; NAS 1.26:182153) Avail: NTIS HC A03/MF A01 CSCL 20D

Three-dimensional viscous flow computations are presented for 90 deg injection angle jets in subsonic and supersonic cross flow. Comparisons with experimental data include jet centerline and vortex trajectories for the subsonic cross flow, and surface pressure measurement for the supersonic crossflow case. The vortices induced in the jet/freestream interaction are computed and illustrated. The vortices persist in subsonic flow and die out quickly in supersonic flow. The structure of the shocks in the unconfined supersonic flow is illustrated. Author

N88-27520*# Sverdrup Technology, Inc., Cleveland, OH.
THREE-DIMENSIONAL ADAPTIVE GRID GENERATION FOR BODY-FITTED COORDINATE SYSTEM Final Contractor Report

S. C. CHEN Aug. 1988 12 p Proposed for presentation at the 2nd International Conference on Numerical Grid Generation in Computational Fluid Dynamics, Miami Beach, Fla., 5-8 Dec. 1988; sponsored by NASA and AFOSR (Contract NAS3-24105) (NASA-CR-182192; E-4331; NAS 1.26:182192) Avail: NTIS HC A03/MF A01 CSCL 20D

This report describes a numerical method for generating 3-D grids for general configurations. The basic method involves the solution of a set of quasi-linear elliptic partial differential equations via pointwise relaxation with a local relaxation factor. It allows specification of the grid spacing off the boundary surfaces and the grid orthogonality at the boundary surfaces. It includes adaptive mechanisms to improve smoothness, orthogonality, and flow resolution in the grid interior. Author

N88-30063*# United Technologies Research Center, East Hartford, CT.

USER'S MANUAL FOR THREE DIMENSIONAL BOUNDARY LAYER (BL3-D) CODE Final Report

O. L. ANDERSON and B. CAPLIN 29 Aug. 1985 143 p (Contract NAS3-23716) (NASA-CR-174899; NAS 1.26:174899; R85-956834-1) Avail: NTIS HC A07/MF A01 CSCL 20D

An assessment has been made of the applicability of a 3-D boundary layer analysis to the calculation of heat transfer, total pressure losses, and streamline flow patterns on the surface of both stationary and rotating turbine passages. In support of this effort, an analysis has been developed to calculate a general nonorthogonal surface coordinate system for arbitrary 3-D surfaces and also to calculate the boundary layer edge conditions for compressible flow using the surface Euler equations and experimental data to calibrate the method, calculations are presented for the pressure endwall, and suction surfaces of a stationary cascade and for the pressure surface of a rotating turbine blade. The results strongly indicate that the 3-D boundary layer analysis can give good predictions of the flow field, loss, and heat transfer on the pressure, suction, and endwall surface of a gas turbine passage. Author

N88-30066*# United Technologies Research Center, East Hartford, CT.

ASSESSMENT OF A 3-D BOUNDARY LAYER ANALYSIS TO PREDICT HEAT TRANSFER AND FLOW FIELD IN A TURBINE PASSAGE Final Analysis Report

O. L. ANDERSON 29 Aug. 1985 93 p (Contract NAS3-23716) (NASA-CR-174894; NAS 1.26:174894; R85-956834) Avail: NTIS HC A05/MF A01 CSCL 20D

An assessment was made of the applicability of a three dimensional boundary layer analysis of heat transfer, total pressure losses, and streamline flow patterns on the surfaces of both stationary and rotating turbine passages. In support of this effort, an analysis was developed to calculate a general nonorthogonal surface coordinate system for arbitrary three dimensional surfaces and also to calculate the boundary layer edge conditions for compressible flow using the surface Euler equations and experimental pressure distributions. Calculations are presented for the pressure, endwall, and suction surfaces of a stationary cascade and for the pressure surface of a rotating turbine blade. The results strongly indicate that the three dimensional boundary layer analysis can give good predictions of the flow field, loss, and heat transfer on the pressure, suction, and endwall surface of a gas turbine passage. Author

N88-30072*# National Aeronautics and Space Administration. Lewis Research Center, Cleveland, OH.

CONTAINMENT OF A SILICONE FLUID FREE SURFACE IN REDUCED GRAVITY USING BARRIER COATINGS

ALEXANDER D. PLINE (Case Western Reserve Univ., Cleveland, Ohio.) and THOMAS P. JACOBSON 1988 15 p Presented at the 117th TMS-AIME Annual Meeting, Phoenix, Ariz., 25-29 Jan. 1988; sponsored by ASM (NASA-TM-101314; E-4309; NAS 1.15:101314) Avail: NTIS HC A03/MF A01 CSCL 20D

In support of the Surface Tension Driven Convection Experiment planned for flight aboard the Space Shuttle, tests were conducted under reduced gravity in the 2.2-sec Drop Tower and the 5.0-sec Zero-G facility at the NASA Lewis Research Center. The dynamics of controlling the test fluid, a 10-cSt viscosity silicone fluid in a low gravity environment were investigated using different container designs and barrier coatings. Three container edge designs were tested without a barrier coating; a square edge, a sharp edge with a 45-deg slope, and a sawtooth edge. All three edge designs were successful in containing the fluid below the edge. G-jitter experiments were made in scaled down containers subjected to horizontal accelerations. The data showed that a barrier coating is effective in containing silicone fluid under g-levels up to 10 sup -1 sub g sub 0. In addition, a second barrier coating was found which has similar anti-wetting characteristics and is also more durable. Author

N88-30076*# Garrett Engine Co., Phoenix, AZ.
TRANSITION MIXING STUDY EMPIRICAL MODEL REPORT Report, Sep. 1986 - Jan. 1988

R. SRINIVASAN and C. WHITE Feb. 1988 126 p (Contract NAS3-24340) (NASA-CR-182139; NAS 1.26:182139; GARRETT-21-6689) Avail: NTIS HC A07/MF A01 CSCL 20D

The empirical model developed in the NASA Dilution Jet Mixing Program has been extended to include the curvature effects of transition liners. This extension is based on the results of a 3-D numerical model generated under this contract. The empirical model results agree well with the numerical model results for all tests cases evaluated. The empirical model shows faster mixing rates compared to the numerical model. Both models show drift of jets toward the inner wall of a turning duct. The structure of the jets from the inner wall does not exhibit the familiar kidney-shaped structures observed for the outer wall jets or for jets injected in rectangular ducts. Author

N88-30078*# National Aeronautics and Space Administration. Lewis Research Center, Cleveland, OH.

THREE-DIMENSIONAL ELLIPTIC GRID GENERATION TECHNIQUE WITH APPLICATION TO TURBOMACHINERY CASCADES

S. C. CHEN (Sverdrup Technology, Inc., Cleveland, Ohio.) and J. R. SCHWAB Aug. 1988 20 p (NASA-TM-101330; E-4342; NAS 1.15:101330) Avail: NTIS HC A03/MF A01 CSCL 20D

Described is a numerical method for generating 3-D grids for turbomachinery computational fluid dynamic codes. The basic

34 FLUID MECHANICS AND HEAT TRANSFER

method is general and involves the solution of a quasi-linear elliptic partial differential equation via pointwise relaxation with a local relaxation factor. It allows specification of the grid point distribution on the boundary surfaces, the grid spacing off the boundary surfaces, and the grid orthogonality at the boundary surfaces. A geometry preprocessor constructs the grid point distributions on the boundary surfaces for general turbomachinery cascades. Representative results are shown for a C-grid and an H-grid for a turbine rotor. Two appendices serve as user's manuals for the basic solver and the geometry preprocessor. Author

N88-30084* # National Aeronautics and Space Administration. Lewis Research Center, Cleveland, OH.

EXPERIMENTAL AND NUMERICAL INVESTIGATION OF THE EFFECT OF DISTRIBUTED SUCTION ON OBLIQUE SHOCK WAVE/TURBULENT BOUNDARY LAYER INTERACTION Ph.D. Thesis

DRISS BENHACHMI, ISAAC GREBER (Case Western Reserve Univ., Cleveland, Ohio.), and WARREN R. HINGST Aug. 1988 192 p

(Contract NAG3-61)

(NASA-TM-101334; E-4349; NAS 1.15:101334) Avail: NTIS HC A09/MF A01 CSCL 20D

A combined experimental and numerical study of the interaction of an incident oblique shock wave with a turbulent boundary layer on a rough plate and on a porous plate with suction is presented. The experimental phase involved the acquisition of mean data upstream of, within, and downstream of the interaction region at Mach numbers 2.5 and 3.0. Data were taken at unit Reynolds numbers of 1.66 E7 and 1.85 E7 m respectively, and for flow deflection angles of 0, 4, 6 and 8 degs. Measured data include wall static pressure, pitot pressure profiles, and local bleed distributions on the porous plate. On the rough plate, with no suction, the boundary layer profiles were modified near the wall, but not separated for the 4 deg flow deflection angle. For the higher deflection angles of 6 and 8 degs, the boundary layer was separated. Suction increases the strength of the incident shock required to separate the turbulent boundary layer; for all shock strengths tested, separation is completely eliminated. The pitot pressure profiles are affected throughout the whole boundary layer; they are fuller than the ones obtained on the rough plate. It is also found that the combination of suction and roughness introduces spatial perturbations. Author

N88-30090* # National Aeronautics and Space Administration. Lewis Research Center, Cleveland, OH.

OPTICAL MEASUREMENTS OF SOOT IN PREMIXED FLAMES Ph.D. Thesis - California Univ.

VALERIE J. LYONS Aug. 1988 180 p

(NASA-TM-101305; E-4295; NAS 1.15:101305) Avail: NTIS HC A09/MF A01 CSCL 20D

Two laser diagnostic techniques were used to measure soot volume fractions, number densities and soot particle radii in premixed propane/oxygen flat flames. The two techniques were two wavelength extinction, using 514.5 to 632.8 nm and 457.9 to 632.8 nm wavelength combinations, and extinction/scattering using 514.5 nm light. The flames were fuel rich and had cold gas velocities varying from 3.4 to 5.5 cm/s. Measurements were made at various heights above the sintered bronze, water colored flat flame burner with the equivalence ratio and cold gas velocity fixed. Also, measurements were made at a fixed height above the burner and fixed cold gas velocity while varying the equivalence ratio. Both laser techniques are based on the same underlying assumptions of particle size distribution and soot optical properties. Full Mie theory was used to determine the extinction coefficients and the scattering efficiencies. Temperature measurements in the flame were made using infrared radiometry and fine wire thermocouples. Good agreement between the two techniques in terms of soot particle radii, number density and volume fraction was found for intensity ratios between 0.1 and 0.8. Author

N88-30094* # National Aeronautics and Space Administration. Lewis Research Center, Cleveland, OH.

IMPACT OF ETO PROPELLANTS ON THE AEROTHERMODYNAMIC ANALYSES OF PROPULSION COMPONENTS

K. C. CIVINSKAS, R. J. BOYLE, and H. V. MCCONNAUGHEY 1988 26 p Presented at the 24th Joint Propulsion Conference, Boston, Mass., 11-13 Jul. 1988; sponsored in part by AIAA, ASME, SAE and ASEE Prepared in cooperation with NASA, Marshall Space Flight Center, Huntsville, Ala.; and Army Aviation Systems Command, Cleveland, Ohio (NASA-TM-101303; E-4262; NAS 1.15:101303; AIAA-88-3091; AVSCOM-TP-88-C-001) Avail: NTIS HC A03/MF A01 CSCL 20D

The operating conditions and the propellant transport properties used in Earth-to-Orbit (ETO) applications affect the aerothermodynamic design of ETO turbomachinery in a number of ways. Some aerodynamic and heat transfer implications of the low molecular weight fluids and high Reynolds number operating conditions on future ETO turbomachinery are discussed. Using the current SSME high pressure fuel turbine as a baseline, the aerothermodynamic comparisons are made for two alternate fuel turbine geometries. The first is a revised first stage rotor blade designed to reduce peak heat transfer. This alternate design resulted in a 23 percent reduction in peak heat transfer. The second design concept was a single stage rotor to yield the same power output as the baseline two stage rotor. Since the rotor tip speed was held constant, the turbine work factor doubled. In this alternate design, the peak heat transfer remained the same as the baseline. While the efficiency of the single stage design was 3.1 points less than the baseline two stage turbine, the design was aerothermodynamically feasible, and may be structurally desirable. Author

35

INSTRUMENTATION AND PHOTOGRAPHY

Includes remote sensors; measuring instruments and gages; detectors; cameras and photographic supplies; and holography.

A88-10969* # National Aeronautics and Space Administration. Lewis Research Center, Cleveland, OH.

USE OF A LIQUID-CRYSTAL AND HEATER-ELEMENT COMPOSITE FOR QUANTITATIVE, HIGH-RESOLUTION HEAT-TRANSFER COEFFICIENTS ON A TURBINE AIRFOIL INCLUDING TURBULENCE AND SURFACE-ROUGHNESS EFFECTS

S. A. HIPPENSTEELE, L. M. RUSSELL, and F. J. TORRES (NASA, Lewis Research Center, Cleveland, OH) IN: Pressure temperature measurements. New York, American Society of Mechanical Engineers, 1987, p. 105-120. Previously announced in STAR as N87-22181. refs

Local heat transfer coefficients were measured along the midchord of a three-times-size turbine vane airfoil in a static cascade operated at room temperature over a range of Reynolds numbers. The test surface consisted of a composite of commercially available materials: a Mylar sheet with a layer of cholestric liquid crystals, which change color with temperature, and a heater made of a polyester sheet coated with vapor-deposited gold, which produces uniform heat flux. After the initial selection and calibration of the composite sheet, accurate, quantitative, and continuous heat transfer coefficients were mapped over the airfoil surface. Tests were conducted at two free-stream turbulence intensities: 0.6 percent, which is typical of wind tunnels; and 10 percent, which is typical of real engine conditions. In addition to a smooth airfoil, the effects of local leading-edge sand roughness were also examined for a value greater than the critical roughness. The local heat transfer coefficients are presented for both free-stream turbulence intensities for inlet Reynolds numbers from

1.20 to 5.55×10 to the 5th power. Comparisons are also made with analytical values of heat transfer coefficients obtained from the STAN5 boundary layer code. Author

A88-11129* National Aeronautics and Space Administration. Lewis Research Center, Cleveland, OH.

LASER ANEMOMETRY TECHNIQUES FOR TURBINE APPLICATIONS

MARK P. WERNET and LAWRENCE G. OBERLE (NASA, Lewis Research Center, Cleveland, OH) ASME, International Gas Turbine Conference and Exhibition, 32nd, Anaheim, CA, May 31-June 4, 1987. 11 p. Previously announced in STAR as N87-22959. refs (ASME PAPER 87-GT-241)

Laser anemometry offers a nonintrusive means for obtaining flow field information. Current research at NASA Lewis Research Center is focused on instrumenting a warm turbine facility with a laser anemometer system. In an effort to determine the laser anemometer system best qualified for the warm turbine environment, the performance of a conventional laser fringe anemometer and a two spot time of flight system were compared with a new, modified time of flight system, called a Four Spot laser anemometer. The comparison measurements were made in highly turbulent flows near walls. The Four Spot anemometer uses elliptical spots to increase the flow acceptance angle to be comparable to that of a Laser Fringe Anemometer. Also, the Four Spot uses an optical code that vastly simplifies the pulse detection processor. The results of the comparison measurements will exemplify which laser anemometer system is best suited to the hostile environment typically encountered in warm rotating turbomachinery. Author

A88-11743* National Aeronautics and Space Administration. Lewis Research Center, Cleveland, OH.

FIBER-LINKED INTERFEROMETRIC PRESSURE SENSOR

G. BEHEIM (NASA, Lewis Research Center, Cleveland, OH), K. FRITSCH, and R. N. POORMAN (John Carroll University, Cleveland, OH) Review of Scientific Instruments (ISSN 0034-6748), vol. 58, Sept. 1987, p. 1655-1659. refs (Contract NAG3-571)

A fiber-optic pressure sensor is described which uses a diaphragm to modulate the mirror separation of a Fabry-Perot cavity (the sensing cavity). A multimode optical fiber delivers broadband light to the sensing cavity and returns the spectrally modulated light which the cavity reflects. The sensor's output spectrum is analyzed using a tunable Fabry-Perot cavity (the reference cavity) to determine the mismatch in the mirror separations of the two cavities. An electronic servo control uses this result to cause the mirror separation of the reference cavity to equal that of the sensing cavity. The displacement of the pressure-sensing diaphragm is then obtained by measuring the capacitance of the reference cavity's metal-coated mirrors. Relative to other fiber-optic sensors, an important advantage of this instrument is its high immunity to the effects of variations in both the transmissivity of the fiber link and the wavelength of the optical source. Author

A88-18509* Purdue Univ., West Lafayette, IN.
DESIGN, CALIBRATION AND ERROR ANALYSIS OF INSTRUMENTATION FOR HEAT TRANSFER MEASUREMENTS IN INTERNAL COMBUSTION ENGINES

C. R. FERGUSON, D. R. TREE, D. P. DEWITT (Purdue University, West Lafayette, IN), and S. A. H. WAHIDUZZAMAN (Integral Technologies, Inc., Westmont, IL) IN: Developments in experimental techniques in heat transfer and combustion; Proceedings of the Twenty-fourth National Heat Transfer Conference and Exhibition, Pittsburgh, PA, Aug. 9-12, 1987. New York, American Society of Mechanical Engineers, 1987, p. 67-82. DOE-sponsored research. refs (Contract DEN3-342)

The paper reports the methodology and uncertainty analyses of instrumentation for heat transfer measurements in internal combustion engines. Results are presented for determining the local wall heat flux in an internal combustion engine (using a

surface thermocouple-type heat flux gage) and the apparent flame-temperature and soot volume fraction path length product in a diesel engine (using two-color pyrometry). It is shown that a surface thermocouple heat transfer gage suitably constructed and calibrated will have an accuracy of 5 to 10 percent. It is also shown that, when applying two-color pyrometry to measure the apparent flame temperature and soot volume fraction-path length, it is important to choose at least one of the two wavelengths to lie in the range of 1.3 to 2.3 micrometers. Carefully calibrated two-color pyrometer can ensure that random errors in the apparent flame temperature and in the soot volume fraction path length will remain small (within about 1 percent and 10-percent, respectively). I.S.

A88-22211* National Aeronautics and Space Administration. Lewis Research Center, Cleveland, OH.

OPERATING ENVELOPES OF PARTICLE SIZING INSTRUMENTATION USED FOR ICING RESEARCH

EDWARD A. HOVENAC (NASA, Lewis Research Center; Sverdrup Technology, Inc., Cleveland, OH) AIAA, Aerospace Sciences Meeting, 26th, Reno, NV, Jan. 11-14, 1988. 7 p. Previously announced in STAR as N88-13573. refs (AIAA PAPER 88-0291)

The Forward Scattering Spectrometer Probe and the Optical Array Probe are analyzed in terms of their ability to make accurate determinations of water droplet size distributions. Sources of counting and sizing errors are explained. The paper describes ways of identifying these errors and how they can affect measurement. Author

A88-22317* Ohio State Univ., Columbus.

PERFORMANCE OF LASER DOPPLER VELOCIMETER WITH POLYDISPERSE SEED PARTICLES IN HIGH SPEED FLOWS

M. SAMIMY (Ohio State University, Columbus), S. BHATTACHARYYA, and B. A./K. ABU-HIJLEH AIAA, Aerospace Sciences Meeting, 26th, Reno, NV, Jan. 11-14, 1988. 9 p. refs (Contract NAG3-764) (AIAA PAPER 88-0425)

The flowfield behind an oblique shock wave, where the LDV measured velocities are seed particle size dependent, was used to investigate the effects of LDV system parameters on the range of detectable polydisperse seed particles. The parameters included frequency shifting, laser power, scattered signal amplification level, and number of required fringe crossings. The results showed that with polydisperse seed particles ranging from 0.1 to 4.0 microns available in the flow, the average diameter of the detected particles could change from 0.2 to 3.0 microns by changing different LDV system parameters. The effects of this shift in the range of detectable particles on the frequency response of LDV was discussed. Author

A88-22942* Babcock and Wilcox Co., Alliance, OH.

CALIBRATION OF HIGH-TEMPERATURE, FIBER-OPTIC, MICROBEND, PRESSURE TRANSDUCERS

J. W. BERTHOLD, W. L. GHERING (Babcock and Wilcox Co., Research and Development Div., Alliance, OH), and D. VARSHNEYA (Teledyne Ryan Electronics, San Diego, CA) IN: Fiber optic and laser sensors IV; Proceedings of the Meeting, Cambridge, MA, Sept. 22-24, 1986. Bellingham, WA, Society of Photo-Optical Instrumentation Engineers, 1987, p. 153-159. refs (Contract NAS3-23712)

The microbend pressure transducer was evaluated on the basis of a series of specified tests to determine the pressure, temperature, overpressure, and vibration response. The response was found to be approximately linear with a pressure in the range of -690 to + 690 kPa. The transducer exhibited high sensitivity to diaphragm deflection and rapid response to pressure changes and was insensitive to vibration for frequencies of 50 to 2500 Hz. The microbend transducer test data showed acceptable sensitivity and stability as a function of temperature and pressure to be used as the basis for a compensatable transducer. K.K.

35 INSTRUMENTATION AND PHOTOGRAPHY

A88-22943* National Aeronautics and Space Administration. Lewis Research Center, Cleveland, OH.

LOSS-COMPENSATION OF INTENSITY-MODULATING FIBER-OPTIC SENSORS

GLENN BEHEIM (NASA, Lewis Research Center, Cleveland, OH) and DONALD J. ANTHAN (Cleveland State University, OH) IN: Fiber optic and laser sensors IV; Proceedings of the Meeting, Cambridge, MA, Sept. 22-24, 1986. Bellingham, WA, Society of Photo-Optical Instrumentation Engineers, 1987, p. 259-265. Previously announced in STAR as N87-13637. refs

This report describes a new type of intensity-modulating fiber-optic sensor which has high immunity to the effects of variations in the losses of the fiber-link. A variable-splitting-ratio transducer is used to differentially modulate the intensities of the light which it transmits and reflects. Using a four-fiber optical link, light is impinged onto the transducer from either direction, and, in each case, the transmitted and reflected signals are measured. These four signals are then processed to remove the effects of the fiber and connector losses. Loss-compensated sensors of angular position and displacement are described, and their outputs are shown to be highly stable despite considerable variations in the transmissivities of the fiber-link components. Author

A88-27617* National Aeronautics and Space Administration. Ames Research Center, Moffett Field, CA.

MULTIELEMENT MAPPING OF ALPHA-SiC BY SCANNING AUGER MICROSCOPY

RAY BROWNING (NASA, Ames Research Center, Mountain View, CA), JAMES L. SMIALEK, and NATHAN S. JACOBSON (NASA, Lewis Research Center, Cleveland, OH) Advanced Ceramic Materials (ISSN 0883-5551), vol. 2, Oct. 1987, p. 773-779. Previously announced in STAR as N87-70440. refs

Fine second-phase particles, numerous in sintered alpha-SiC, were analyzed by scanning Auger microscopy and conventional techniques. The Auger analysis utilized computer-controlled data acquisition, multielement correlation diagrams, and a high spatial resolution of 100 nm. This procedure enabled construction of false color maps and the detection of fine compositional details within these particles. Carbon, silicon oxide, and boron-rich particles (qualitatively as BN or B₄C) predominated. The BN particles, sometimes having a carbon core, are believed to result from reaction between B₄C additives and nitrogen sintering atmospheres. Author

A88-29817*# Rockwell International Corp., Canoga Park, CA. **REUSABLE ROCKET ENGINE OPTICAL CONDITION MONITORING**

L. WYETT, J. MARAM, S. BARKHOUDARIAN, and J. REINERT (Rockwell International Corp., Rocketdyne Div., Canoga Park, CA) Joint Army-Navy-NASA-Air Force Interagency Propulsion Committee, Propulsion Meeting, San Diego, CA, Dec. 15-17, 1987, Paper. 5 p. (Contract NAS3-23773)

Plume emission spectrometry and optical leak detection are described as two new applications of optical techniques to reusable rocket engine condition monitoring. Plume spectrometry has been used with laboratory flames and reusable rocket engines to characterize both the nominal combustion spectra and anomalous spectra of contaminants burning in these plumes. Holographic interferometry has been used to identify leaks and quantify leak rates from reusable rocket engine joints and welds. Author

A88-29818*# Rockwell International Corp., Canoga Park, CA. **NONCONTACTING MEASUREMENT TECHNOLOGIES FOR SPACE PROPULSION CONDITION MONITORING**

M. R. RANDALL, S. BARKHOUDARIAN, J. J. COLLINS, and A. SCHWARTZBART (Rockwell International Corp., Rocketdyne Div., Canoga Park, CA) Joint Army-Navy-NASA-Air Force Interagency Propulsion Committee, Propulsion Meeting, San Diego, CA, Dec. 15-17, 1987, Paper. 7 p. refs (Contract NAS3-23349)

This paper describes four noncontacting measurement technologies that can be used in a turbopump condition monitoring

system. The isotope wear analyzer, fiberoptic deflectometer, brushless torque-meter, and fiberoptic pyrometer can be used to monitor component wear, bearing degradation, instantaneous shaft torque, and turbine blade cracking, respectively. A complete turbopump condition monitoring system including these four technologies could predict remaining component life, thus reducing engine operating costs and increasing reliability. Author

A88-33003* Maryland Univ., College Park.

CRITICAL FLUID LIGHT SCATTERING

ROBERT W. GAMMON (Maryland, University, College Park) IN: International SAMPE Technical Conference, 19th, Crystal City, VA, Oct. 13-15, 1987, Proceedings. Covina, CA, Society for the Advancement of Material and Process Engineering, 1987, p. 326-331.

(Contract NAG3-727)

Thermal fluctuations give rise to a host of thermodynamic anomalies near critical points. The background for these phenomena is presented, and an experiment design on STS flight experiment called 'Zeno' described. The objective is to measure the decay rates of critical density fluctuations in a simple fluid (xenon) very near its liquid-vapor critical point using laser light-scattering and photon-correlation spectroscopy. Such experiments have been limited on earth by the presence of gravity, which causes large density gradients in the sample. Fluctuation decay rates in xenon will be measured at least 100 times closer to the critical point than is possible on earth. This will require taking data as close as 145 microK to the critical temperature ($T_c = 289.72$ K), after locating it to ± 10 microK. The minimum mission time of 100 hours will allow a complete range of temperature points to be covered, limited by the thermal response of the sample. An essential part of the apparatus is the thermostat. Its design principles and key features are given together with some observed performance characteristics of a prototype: ± 20 microK stability for 18 hours, and one minute programmed step response for steps less than 10 mK. Author

A88-34479* National Aeronautics and Space Administration. Lewis Research Center, Cleveland, OH.

ENGINE FLOW VISUALIZATION USING A COPPER VAPOR LASER

CAROLYN A. REGAN, KUE S. CHUN, and HAROLD J. SCHOCK, JR. (NASA, Lewis Research Center, Cleveland, OH) IN: New developments and applications in gas lasers; Proceedings of the Meeting, Los Angeles, CA, Jan. 13, 14, 1987. Bellingham, WA, Society of Photo-Optical Instrumentation Engineers, 1987, p. 17-27. refs

A flow visualization system has been developed to determine the air flow within the combustion chamber of a motored, axisymmetric engine. The engine has been equipped with a transparent quartz cylinder, allowing complete optical access to the chamber. A 40-Watt copper vapor laser is used as the light source. Its beam is focused down to a sheet approximately 1 mm thick. The light plane is passed through the combustion chamber, and illuminates oil particles which were entrained in the intake air. The light scattered off of the particles is recorded by a high speed rotating prism movie camera. A movie is then made showing the air flow within the combustion chamber for an entire four-stroke engine cycle. The system is synchronized so that a pulse generated by the camera triggers the laser's thyatron. The camera is run at 5,000 frames per second; the trigger drives one laser pulse per frame. This paper describes the optics used in the flow visualization system, the synchronization circuit, and presents results obtained from the movie. This is believed to be the first published study showing a planar observation of airflow in a four-stroke piston-cylinder assembly. These flow visualization results have been used to interpret flow velocity measurements previously obtained with a laser Doppler velocimetry system. Author

A88-35004*# National Aeronautics and Space Administration. Lewis Research Center, Cleveland, OH.

SOURCES OF ERROR IN HETERODYNE MOIRE DEFLECTOMETRY

ARTHUR J. DECKER, KENNETH E. WEILAND (NASA, Lewis Research Center, Cleveland, OH), JOSEF STRICKER (Technion - Israel Institute of Technology, Haifa, Israel), and DAVID WEIMER (Ohio Northern University, Ada) *Applied Optics* (ISSN 0003-6935), vol. 27, April 15, 1988, p. 1381-1383. refs
(Contract NAGW-933)

Alignment problems, and the accompanying errors, in heterodyne moiré deflectometry are considered. A change in the x-directed offset between two states of a phase object causes a constant phase error, and it is noted that the relative x coordinate of the two photographic plates (the two states of the phase object) must be positioned typically within 1 micron to avoid a detectable offset. Possible solutions for assuring the relative alignment of the two deflectograms are considered, including a sandwich technique and a two-color double-exposure implementation. R.R.

A88-36513*# National Aeronautics and Space Administration. Lewis Research Center, Cleveland, OH.

FOUR SPOT LASER ANEMOMETER AND OPTICAL ACCESS TECHNIQUES FOR TURBINE APPLICATIONS

MARK P. WERNET (NASA, Lewis Research Center, Cleveland, OH) IN: ICIASF '87 - International Congress on Instrumentation in Aerospace Simulation Facilities, 12th, Williamsburg, VA, June 22-25, 1987, Record. New York, Institute of Electrical and Electronics Engineers, Inc., 1987, p. 245-254. Previously announced in STAR as N87-18057. refs

A time-of-flight anemometer (TOFA) system utilizing a spatial lead-lag filter for bipolar pulse generation has been constructed and tested. This system, called a four-spot laser anemometer, was specifically designed for use in high-speed, turbulent flows in the presence of walls or surfaces. The TOFA system uses elliptical spots to increase the flow acceptance angle to be comparable with that of a fringe-type anemometer. The tightly focused spots used in the four spot yield excellent flare light rejection capabilities. Good results have been obtained to 75 microns normal to a surface, with an $f/2.5$ collection lens. This system is being evaluated for use in a warm turbine facility. Results from both a particle-lag velocity experiment and boundary layer profiles will be discussed. In addition, an analysis of the use of curved windows in a turbine casing will be presented. Curved windows, matching the inner radius of the turbine casing, preserve the flow conditions, but introduce astigmatic aberrations. A correction optic was designed that virtually eliminates these astigmatic aberrations throughout the intrablade survey region for normal incidence. Author

A88-40700* National Aeronautics and Space Administration. Lewis Research Center, Cleveland, OH.

REAL TIME OPTICAL CORRELATOR USING A MAGNETOOPTIC DEVICE APPLIED TO PARTICLE IMAGING VELOCIMETRY

MARK P. WERNET (NASA, Lewis Research Center, Cleveland, OH) and ROBERT V. EDWARDS (Case Western Reserve University, Cleveland, OH) *Applied Optics* (ISSN 0003-6935), vol. 27, March 1, 1988, p. 813-815. refs

An optical correlator was constructed and tested for use in the data reduction of particle imaging velocimetry photographs. The optical correlator uses a LIGHT MOD, which is a 128 x 128-pixel magnetooptic spatial light modulator array, as the frequency plane filter. Results from both a computer simulation and an experimental optical correlator setup are discussed. K.K.

A88-43917*# Case Western Reserve Univ., Cleveland, OH.
MEASUREMENTS OF NATURAL CIRCULATION FLOW IN A SCALE MODEL PWR REACTOR SYSTEM DURING POSTULATED DEGRADED CORE ACCIDENTS USING LASER ANEMOMETRY

J. R. KADAMBI (Case Western Reserve University, Cleveland, OH), S. J. SCHNEIDER (NASA, Lewis Research Center, Cleveland, OH), and W. A. STEWART (Westinghouse Electric Corp., Pittsburgh, PA) IN: International Symposium on Laser Anemometry, 3rd, ASME Winter Annual Meeting, Boston, MA, Dec. 13-18, 1987, Proceedings. New York, American Society of Mechanical

Engineers, 1987, p. 195-205. Research supported by the Electric Power Research Institute.

The natural circulation of a single-phase fluid in a scale-model pressurized water reactor system was studied during a postulated degraded core accident. A half section of a one-seventh scale model with a plexiglass adiabatic window was employed. Water and SF₆ were used as the fluid. LDA was used to perform velocity measurements along the center plane of the model at five elevations. It was found that the recirculation flow patterns are nearly symmetric except near the hot legs and in the upper head and that the fluid in the upper plenum is well mixed. K.K.

A88-52557* National Aeronautics and Space Administration. Lewis Research Center, Cleveland, OH.

OPTICAL STRAIN MEASUREMENT SYSTEM DEVELOPMENT

CHRISTIAN T. LANT and WALID QAQISH (NASA, Lewis Research Center; Sverdrup Technology, Inc., Cleveland, OH) IN: International Conference on Photomechanics and Speckle Metrology, San Diego, CA, Aug. 17-20, 1987, Proceedings. Part 1. Bellingham, WA, Society of Photo-Optical Instrumentation Engineers, 1988, p. 184-192. Previously announced in STAR as N87-26326.

A laser speckle, differential strain measurement system has been built and tested for future applications in hostile environments. One-dimensional electronic correlation of speckle pattern movement allows a quasi-real time measure of strain. The system has been used successfully to measure uniaxial strain reaching into plastic deformation of a test specimen, at temperatures ranging to 450 C. A resolution of 126 microstrain is given by the photodiode array sensor pitch and the specimen to sensor separation. The strain measurement error is estimated to be ± 18 microstrain ± 3 percent of the strain reading. The upper temperature limit of the gauge is determined by air density perturbations causing decorrelation of the reference and shifted speckle patterns, and may be improved by limiting convective flow in the immediate vicinity of the test specimen. Author

A88-54139*# National Aeronautics and Space Administration. Lewis Research Center, Cleveland, OH.

ADVANCED HIGH TEMPERATURE INSTRUMENTATION FOR HOT SECTION RESEARCH APPLICATIONS

D. R. ENGLUND and R. G. SEASHOLTZ (NASA, Lewis Research Center, Cleveland, OH) IN: Toward improved durability in advanced aircraft engine hot sections; Proceedings of the Thirty-third ASME International Gas Turbine and Aeroengine Congress and Exposition, Amsterdam, Netherlands, June 5-9, 1988. New York, American Society of Mechanical Engineers, 1988, p. 5-21. refs

Programs to develop research instrumentation for use in turbine engine hot sections are described. These programs were initiated to provide improved measurements capability as support for a multidisciplinary effort to establish technology leading to improved hot section durability. Specific measurement systems described here include heat flux sensors, a dynamic gas temperature measuring system, laser anemometry for hot section applications, an optical system for viewing the interior of a combustor during operation, thin film sensors for surface temperature and strain measurements, and high temperature strain measuring systems. The paper will describe the state of development of these sensors and measuring systems and, in some cases, will show examples of measurements made with this instrumentation. The paper covers work done at the NASA Lewis Research Center and at various contract and grant facilities. Author

A88-54159*# United Technologies Research Center, East Hartford, CT.

APPLICATION OF ADVANCED DIAGNOSTICS TO AIRBLAST INJECTOR FLOWS

JOHN B. MCVEY, JAN B. KENNEDY, and SID RUSSELL (United Technologies Research Center, East Hartford, CT) ASME, Gas Turbine and Aeroengine Congress and Exposition, Amsterdam, Netherlands, June 6-9, 1988. 12 p. refs
(Contract NAS3-24352)
(ASME PAPER 88-GT-12)

35 INSTRUMENTATION AND PHOTOGRAPHY

Experimental data on the characteristics of the spray produced by a gas-turbine engine airblast fuel injector are reported. The data acquired include the mass-flux distribution, measured by use of a high-resolution spray patternator; the gas-phase velocity field, measured by use of a two-component laser Doppler velocimeter, and the liquid droplet size and velocity distribution, measured by use of a single-component phase-Doppler anemometer. The data are intended for use in assessments of two-phase flow computational methods as applied to combustor design procedures. Author

A88-55254* National Aeronautics and Space Administration. Lewis Research Center, Cleveland, OH.

REDUCTION OF TEMPERATURE RISE IN HIGH-SPEED PHOTOGRAPHY

HOWARD A. SLATER (NASA, Lewis Research Center, Cleveland, OH) IN: High speed photography, videography, and photonics V; Proceedings of the Meeting, San Diego, CA, Aug. 17-19, 1987. Bellingham, WA, Society of Photo-Optical Instrumentation Engineers, 1988, p. 107-116. Previously announced in STAR as N88-11100.

Information is provided on filtration with glass and infrared absorbing and reflecting filters. Glass and infrared filtration is a simple and effective method to reduce the radiation heat transfer associated with continuous high intensity tungsten lamps. The results of a filtration experiment are explained. The figures provide starting points for quantifying the effectiveness of various filters and associated light intensities. The combination of a spectrally selective reflector (hot or cold mirror) based on multilayer thin film principles and heat absorbing or infrared opaque glass results in the maximum reduction in temperature rise with a minimum of incident light loss. Use is recommended of a voltage regulator to further control temperature rise and incident light values. Author

N88-11100* National Aeronautics and Space Administration. Lewis Research Center, Cleveland, OH.

REDUCTION OF TEMPERATURE RISE IN HIGH-SPEED PHOTOGRAPHY

HOWARD A. SLATER Aug. 1987 18 p Presented at the 31st International Technical Symposium on Optical and Optoelectronic Applied Sciences and Engineering, San Diego, Calif., 16-21 Aug. 1987; sponsored by the Society of Photo-Optical Instrumentation Engineers (NASA-TM-100222; E-3666; NAS 1.15:100222) Avail: NTIS HC A03/MF A01 CSCL 14E

Information is provided on filtration with glass and infrared absorbing and reflecting filters. Glass and infrared filtration is a simple and effective method to reduce the radiation heat transfer associated with continuous high intensity tungsten lamps. The results of a filtration experiment are explained. The figures provide starting points for quantifying the effectiveness of various filters and associated light intensities. The combination of a spectrally selective reflector (hot or cold mirror) based on multilayer thin film principles and heat absorbing or infrared opaque glass results in the maximum reduction in temperature rise with a minimum of incident light loss. Use is recommended of a voltage regulator to further control temperature rise and incident light values. Author

N88-11141* Pratt and Whitney Aircraft, West Palm Beach, FL. Engineering Div.

FURTHER DEVELOPMENT OF THE DYNAMIC GAS TEMPERATURE MEASUREMENT SYSTEM

D. L. ELMORE, W. W. ROBINSON, and W. B. WATKINS IN NASA. Lewis Research Center, Turbine Engine Hot Section Technology, 1985 p 37-43 Oct. 1985 (Contract NAS3-24228)

Avail: NTIS HC A19/MF A01 CSCL 14B

Two experiments for verifying the frequency response of a previously-developed dynamic gas temperature measurement system were performed. In both experiments, fine-wire resistance temperature sensors were used as standards. The compensated dynamic temperature sensor data will be compared with the

standards to verify the compensation method. The experiments are described in detail. Author

N88-11142* United Technologies Research Center, East Hartford, CT.

THE DEVELOPMENT OF A HIGH TEMPERATURE STATIC STRAIN GAGE SYSTEM

CHARLES O. HULSE, RICHARD S. BAILEY, and HOWARD P. GRANT (Pratt and Whitney Aircraft, East Hartford, Conn.) IN NASA. Lewis Research Center, Turbine Engine Hot Section Technology, 1985 p 45-49 Oct. 1985 (Contract NAS3-23722)

Avail: NTIS HC A19/MF A01 CSCL 14B

The objective of this program is to develop electrical resistance strain gages which will permit the measurement of static strains on nickel and cobalt superalloy parts inside gas turbine engines running on a test stand. The specific goal is to develop a complete system able to make strain measurements up to plus or minus 2000 mu strain with a total error of no more than plus or minus 10 percent over a 50 hour period at 1250 K. The initial part of this work consisted of a strain gage alloy development effort in which a variety of alloys were evaluated after being prepared by drop-casting or splat cooling. Author

N88-11143* Pratt and Whitney Aircraft, East Hartford, CT.

DEVELOPMENT OF HEAT FLUX SENSORS FOR TURBINE AIRFOILS

WILLIAM H. ATKINSON, MARCIA A. CYR, and RICHARD R. STRANGE IN NASA. Lewis Research Center, Turbine Engine Hot Section Technology, 1985 p 51-58 Oct. 1985 (Contract NAS3-23529)

Avail: NTIS HC A19/MF A01 CSCL 14B

The objectives of this program are to develop heat flux sensors suitable for installation in hot section airfoils of advanced aircraft turbine engines and to experimentally verify the operation of these heat flux sensors in a cylinder in a cross flow experiment. Embedded thermocouple and Gardon gauge sensors were developed and fabricated into both blades and vanes. These were then calibrated using a quartz lamp bank heat source and finally subjected to thermal cycle and thermal soak testing. These sensors were also fabricated into cylindrical test pieces and tested in a burner exhaust to verify heat flux measurements produced by these sensors. The results of the cylinder in cross flow tests are given. Author

N88-11144* Northwestern Univ., Evanston, IL.

ELEVATED TEMPERATURE STRAIN GAGES

J. O. BRITAIN, D. GESLIN, and J. F. LEI IN NASA. Lewis Research Center, Turbine Engine Hot Section Technology, 1985 p 59-65 Oct. 1985 (Contract NAG3-501)

Avail: NTIS HC A19/MF A01 CSCL 14B

Materials were evaluated that could be used in manufacturing electrical resistance strain gages for static strain measurements at temperatures at or above 1273 K. Strain gage materials must have a characteristic response to strain, temperature and time that is reproducible or that varies in a predictable manner within specified limits. Several metallic alloys were evaluated, as well as a series of transition metal carbides, nitrides and silicides. Author

N88-11146* National Aeronautics and Space Administration. Lewis Research Center, Cleveland, OH.

THE LEWIS STRAIN GAUGE LABORATORY: STATUS AND PLANS

HOWARD F. HOBART and HERBERT A. WILL IN its Turbine Engine Hot Section Technology, 1985 p 77-79 Oct. 1985

Avail: NTIS HC A19/MF A01 CSCL 14B

An in-house lab was established for developing, testing, and evaluating high-temperature strain gauges and to aid in in-house applications of high-temperature strain instrumentation. The lab is automated to provide computer control of oven temperatures, imposed strain, and data sampling. Author

N88-11147*# National Aeronautics and Space Administration. Lewis Research Center, Cleveland, OH.

CORRELATION OF VELOCITY AND VELOCITY-DENSITY TURBULENCE IN THE EXHAUST OF AN ATMOSPHERIC BURNER

GUSTAVE C. FRALICK *In its Turbine Engine Hot Section Technology*, 1985 p 81-85 Oct. 1985
 Avail: NTIS HC A19/MF A01 CSCL 14B

In the experiment described herein, temperature (density) and velocity are measured separately but simultaneously as functions of time so that it is possible to determine the relationships among velocity, density, and the product of density and velocity. An atmospheric burner rig was used to provide the flow for the experiment. Author

N88-12042*# Sverdrup Technology, Inc., Cleveland, OH.

PERFORMANCE AND OPERATING ENVELOPE OF IMAGING AND SCATTERING PARTICLE SIZING INSTRUMENTS

EDWARD A. HOVENAC Nov. 1987 15 p Presented at the International Conference on Optical Methods in Flow and Particle Diagnostics, San Diego, Calif., 8-12 Nov. 1987 (Contract NAS3-24105)
 (NASA-CR-180859; E-3849; NAS 1.26:180859) Avail: NTIS HC A03/MF A01 CSCL 14B

Scattering and imaging type particle sizing instruments are analyzed in terms of their ability to make accurate determinations of particle size distributions, number density, and total mass. Sources of counting and sizing errors are explained. Ways are described of identifying these errors and how these errors can effect the measurements. Author

N88-12043*# National Aeronautics and Space Administration. Lewis Research Center, Cleveland, OH.

ANALYSIS OF COUNTING ERRORS IN THE PHASE/DOPPLER PARTICLE ANALYZER

JOHN R. OLDENBURG Nov. 1987 12 p Presented at the International Congress on Applications of Lasers and Electro-Optics, San Diego, Calif., 11-12 Nov. 1987; sponsored by Laser Inst. of America
 (NASA-TM-100231; E-3854; NAS 1.15:100231) Avail: NTIS HC A03/MF A01 CSCL 14B

NASA is investigating the application of the Phase Doppler measurement technique to provide improved drop sizing and liquid water content measurements in icing research. The magnitude of counting errors were analyzed because these errors contribute to inaccurate liquid water content measurements. The Phase Doppler Particle Analyzer counting errors due to data transfer losses and coincidence losses were analyzed for data input rates from 10 samples/sec to 70,000 samples/sec. Coincidence losses were calculated by determining the Poisson probability of having more than one event occurring during the droplet signal time. The magnitude of the coincidence loss can be determined, and for less than a 15 percent loss, corrections can be made. The data transfer losses were estimated for representative data transfer rates. With direct memory access enabled, data transfer losses are less than 5 percent for input rates below 2000 samples/sec. With direct memory access disabled losses exceeded 20 percent at a rate of 50 samples/sec preventing accurate number density or mass flux measurements. The data transfer losses of a new signal processor were analyzed and found to be less than 1 percent for rates under 65,000 samples/sec. Author

N88-13573*# Sverdrup Technology, Inc., Cleveland, OH.

OPERATING ENVELOPES OF PARTICLE SIZING INSTRUMENTATION USED FOR ICING RESEARCH Final Contractor Report

EDWARD A. HOVENAC Dec. 1987 16 p (Contract NAS3-24105)
 (NASA-CR-180870; E-3886; NAS 1.26:180870; AIAA-88-0291)
 Avail: NTIS HC A03/MF A01 CSCL 14B

The Forward Scattering Spectrometer Probe and the Optical Array Probe are analyzed in terms of their ability to make accurate determinations of water droplet size distributions. Sources of

counting and sizing errors are explained. The paper describes ways of identifying these errors and how they can affect measurement. Author

N88-14339*# National Aeronautics and Space Administration. Lewis Research Center, Cleveland, OH.

RECENT ADVANCES IN HIGH TEMPERATURE INSTRUMENTATION FOR HOT SECTION APPLICATIONS

DAVID R. ENGLUND and RICHARD G. SEASHOLTZ 1988 25 p Prepared for presentation at the 33rd International Gas Turbine and Aeroengine Congress and Exposition, Amsterdam, The Netherlands, 5-9 Jun. 1988; sponsored in part by the American Society of Mechanical Engineers
 (NASA-TM-100282; E-3923; NAS 1.15:100282) Avail: NTIS HC A03/MF A01 CSCL 14B

Programs to develop research instrumentation for use in turbine engine hot sections are described. These programs were initiated to provide improved measurements capability as support for a multidisciplinary effort to establish technology leading to improved hot section durability. Specific measurement systems described here include heat flux sensors, a dynamic gas temperature measuring system, laser anemometry for hot section applications, an optical system for viewing the interior of a combustor during operation, thin film sensors for surface temperature and strain measurements, and high temperature strain measuring systems. The paper describes the state of the development of these sensors and measuring systems and, in some cases, will show examples of measurements made with this instrumentation. The paper covers work done at the NASA Lewis Research Center and at various contract and grant facilities. Author

N88-15795*# National Aeronautics and Space Administration. Lewis Research Center, Cleveland, OH.

RESEARCH SENSORS

DAVID R. ENGLUND *In its Aeropropulsion '87. Session 4: Instrumentation and Controls Research* 12 p Nov. 1987
 Avail: NTIS HC A05/MF A01 CSCL 14B

The program described covers development of sensors and sensing techniques for research applications on aeropropulsion systems. In general, the sensors are used in-situ to measure the environment at a given location within a turbine engine, or to measure the response of an engine component to the imposed environment. Locations of concern are generally in the gas path and, for the most part, are within the hot section. Specific parameters of concern are dynamic gas temperature, heat flux, airfoil surface temperature, and strain on airfoils and combustor liners. In order to minimize the intrusiveness of surface-mounted sensors, a considerable effort was expended to develop thin-film sensors for surface temperature, strain, and heat flux measurements. Most of the work described is sufficiently advanced that sensors were used and useful data were obtained. The notable exception is the work to develop a high-temperature static strain measuring capability; this work is still in progress. Author

N88-15996*# Cleveland State Univ., OH.

HIGH TEMPERATURE TENSILE TESTING OF CERAMIC COMPOSITES Annual Report

JOHN Z. GYEKENYESI and JOHN H. HEMANN Feb. 1988 46 p (Contract NAG3-749)
 (NASA-CR-180888; NAS 1.26:180888) Avail: NTIS HC A03/MF A01 CSCL 14B

The various components of a high temperature tensile testing system are evaluated. The objective is the high temperature tensile testing of SiC fiber reinforced reaction bonded Si3N4 specimens at test temperatures up to 1650 C (3000 F). Testing is to be conducted in inert gases and air. Gripping fixtures, specimen configurations, furnaces, optical strain measuring systems, and temperature measurement techniques are reviewed. Advantages and disadvantages of the various techniques are also noted. Author

35 INSTRUMENTATION AND PHOTOGRAPHY

N88-18892*# National Aeronautics and Space Administration. Lewis Research Center, Cleveland, OH.

PROTOTYPE THIN-FILM THERMOCOUPLE/HEAT-FLUX SENSOR FOR A CERAMIC-INSULATED DIESEL ENGINE Final Report

WALTER S. KIM and RICHARD F. BARROWS Mar. 1988

16 p

(Contract DE-AI01-86CE-50162)

(NASA-TM-100798; E-3976; DOE/NASA/50162-1; NAS

1.15:100798) Avail: NTIS HC A03/MF A01 CSCL 14B

A platinum versus platinum-13 percent rhodium thin-film thermocouple/heat-flux sensor was devised and tested in the harsh, high-temperature environment of a ceramic-insulated, low-heat-rejection diesel engine. The sensor probe assembly was developed to provide experimental validation of heat transfer and thermal analysis methodologies applicable to the insulated diesel engine concept. The thin-film thermocouple configuration was chosen to approximate an uninterrupted chamber surface and provide a 1-D heat-flux path through the probe body. The engine test was conducted by Purdue University for Integral Technologies, Inc., under a DOE-funded contract managed by NASA Lewis Research Center. The thin-film sensor performed reliably during 6 to 10 hr of repeated engine runs at indicated mean surface temperatures up to 950 K. However, the sensor suffered partial loss of adhesion in the thin-film thermocouple junction area following maximum cyclic temperature excursions to greater than 1150 K.

Author

N88-22430*# National Aeronautics and Space Administration. Lewis Research Center, Cleveland, OH.

RESEARCH SENSORS

DAVID R. ENGLUND *In its* Lewis Structures Technology, 1988. Volume 3: Structural Integrity Fatigue and Fracture Wind Turbines HOST p 323-335 May 1988

Avail: NTIS HC A16/MF A01 CSCL 14B

The work described is part of a program (Englund and Seasholtz, 1988) to develop sensors and sensing techniques for research applications on aircraft turbine engines. In general, the sensors are used to measure the environment at a given location within a turbine engine or to measure the response of an engine component to the imposed environment. Locations of concern are generally in the gas path and, for the most part, are within the hot section. Specific parameters of concern are dynamic gas temperature, heat flux, airfoil surface temperature, and strain on airfoils and combustor liners. To minimize the intrusiveness of surface-mounted sensors, a considerable effort was expended to develop thin-film sensors for surface temperature, strain, and heat flux measurements. In addition, an optical system for viewing the interior of an operating combustor was developed. Most of the work described is sufficiently advanced that the sensors were used and useful data were obtained. The notable exception is the work to develop a high-temperature static strain measuring capability; the work is still in progress.

Author

N88-23194*# National Aeronautics and Space Administration. Lewis Research Center, Cleveland, OH.

EFFECT OF MASS-VELOCITY ON LIQUID JET ATOMIZATION IN MACH 1 GASFLOW

ROBERT D. INGEBRO 1988 8 p Proposed for presentation at the 4th International Conference on Liquid Atomization and Spray Systems, Sendai, Japan, 22-24 Aug. 1988; sponsored by the Fuel Society of Japan

(NASA-TM-100813; E-3944-1; NAS 1.15:100813) Avail: NTIS HC A02/MF A01 CSCL 14B

Interacting two-phase flow in four differently sized pneumatic two-fluid atomizers was investigated to determine the effect of gas mass-velocity on the Sauter mean diameter of sprays produced by small diameter liquid jets breaking up in high velocity gas flow. Tests were conducted primarily in the acceleration-wave regime for liquid jet atomization, where it was found that the loss of droplets due to vaporization had a marked effect on drop size measurements. A scattered-light scanner, developed at NASA Lewis Research Center, was used to measure the Sauter mean

diameter, D_{32} , which was correlated with nitrogen gas mass-velocity to give the following expression: $D_{32} = 11.7(\rho_{sub} n)^{1.33} V_{sub}^{1.33}$. The exponent 1.33 for the gas mass-velocity is identical to that predicted by atomization theory for liquid jet breakup in the acceleration-wave regime.

Author

N88-23196*# National Aeronautics and Space Administration. Lewis Research Center, Cleveland, OH.

DEVELOPMENT AND APPLICATIONS OF OPTICAL INTERFEROMETRIC MICROMETROLOGY IN THE ANGSTROM AND SUBANGSTROM RANGE

JAMES L. LAUER (Rensselaer Polytechnic Inst., Troy, N.Y.) and PHILLIP B. ABEL 1988 22 p Presented at the 34th International Instrumentation Symposium, Albuquerque, N. Mex., 2-5 May 1988; sponsored by the Instrument Society of America

(NASA-TM-100299; E-3945; NAS 1.15:100299) Avail: NTIS HC A03/MF A01 CSCL 14B

The recent development of the scanning electron tunneling microscope and the atomic force microscope requires absolute standards for measurements in the angstrom and subangstrom range. Optical interferometry with lasers and multiple mode laser resonances can provide absolute measurements as the laser wavelengths are very accurately known. A key feature of such measurements is the use of piezoelectric crystals as translators of the highest accuracy for very small disturbances. However, the dimensional changes of these crystals resulting from electrical potential changes depend on many variables, among them the method of mounting, so that accurate calibrations are necessary. Starting from advances in optical metrology made by physicists trying to find gravity waves, advances which led to measurements down to 10 to the -5 A, the author designed and built a much simpler system for the angstrom range. The major limiting factors were mechanical vibrations, air currents, thermal changes and laser instabilities.

Author

N88-26641*# National Aeronautics and Space Administration. Lewis Research Center, Cleveland, OH.

ACTIVE PHASE COMPENSATION SYSTEM FOR FIBER OPTIC HOLOGRAPHY

CAROLYN R. MERCER and GLENN BEHEIM 1988 8 p Prepared for presentation at the 32nd Annual International Technical Symposium on Optical and Optoelectronic Applied Science and Engineering, San Diego, Calif., 14-19 Aug., 1988; sponsored by Society of Photo-Optical Instrumentation Engineers (NASA-TM-101295; E-4277; NAS 1.15:101295) Avail: NTIS HC A02/MF A01 CSCL 14B

Fiber optic delivery systems promise to extend the application of holography to severe environments by simplifying test configurations and permitting the laser to be remotely placed in a more benign location. However, the introduction of optical fiber leads to phase stability problems. Environmental effects cause the pathlengths of the fibers to change randomly, preventing the formation of stationary interference patterns which are required for holography. An active phase control system has been designed and used with an all-fiber optical system to stabilize the phase difference between light emitted from two fibers, and to step the phase difference by 90 deg without applying any constraints on the placement of the fibers. The accuracy of the phase steps is shown to be better than 0.02 deg., and a stable phase difference can be maintained for 30 min. This system can be applied to both conventional and electro-optic holography, as well as to any system where the maintenance of an accurate phase difference between two coherent beams is required.

Author

N88-26644*# National Aeronautics and Space Administration. Lewis Research Center, Cleveland, OH.

FIBER OPTIC SENSORS WITH INTERNAL REFERENCING

GRIGORY ADAMOVSKY and DUNCAN J. MAITLAND, IV (Cleveland State Univ., Ohio.) 1988 12 p Prepared for the Conference on Optical Testing and Metrology 2, Dearborn, Mich., 26-30 Jun. 1988; sponsored by the Society of Photo-Optical Instrumentation Engineers

(Contract NCC3-558)

(NASA-TM-100893; E-4134; NAS 1.15:100893) Avail: NTIS HC A03/MF A01 CSCL 14B

The main problem with amplitude modulating type sensors is that any variation in the intensity of the optical signal which occurs throughout the sensing system is interpreted by the photodetector as resulting from the sensor itself and is reflected as an error in the sensed parameter. To account for these errors, a referencing technique with the signal and reference channels separated in the time domain over the same fiber link can be used. Selected sensing and signal processing techniques involving temporally separated signal and referencing channels are described. A transition from the time into the frequency domain is also discussed. Experimental data are presented. Author

N88-26645*# National Aeronautics and Space Administration. Lewis Research Center, Cleveland, OH.

SMALL-DROPLET SPRAY MEASUREMENTS WITH A SCATTERED-LIGHT SCANNER

ROBERT D. INGEBO and DONALD R. BUCHELE 1988 16 p Presented at the 2nd Symposium on Liquid Particle Size Measurement Techniques, Atlanta, Ga., 9-11 Nov. 1988; sponsored by the American Society for Testing and Materials (NASA-TM-100973; E-4236; NAS 1.15:100973) Avail: NTIS HC A03/MF A01 CSCL 14B

Interacting two-phase flow through pneumatic two-fluid nozzles was investigated to determine the effect of nitrogen gas mass-velocity on the Sauter mean diameter of water sprays produced by the breakup of small diameter liquid-jets in high velocity gas streams. Tests were conducted primarily in the aerodynamic-stripping regime of liquid-jet atomization. It was found that the loss of droplets due to vaporization and dispersion had a marked effect on drop size measurements. A scattered-light scanner, developed at NASA Lewis Research Center was used to measure Sauter mean diameters, D_{32} , as small as 5 microns, which were correlated with nitrogen gas mass-velocity to give the following expression: $D_{32} = 11.7(\rho_n)^{1/3} V_n^{1/3}$ where D_{32} and $p_n V_n$ are given in centimeters and g/sq cm-sec, respectively. The exponent 1.33 is the same as that predicted by atomizing theory for liquid-jet breakup in high velocity gas streams. Author

N88-28286*# National Aeronautics and Space Administration. Lewis Research Center, Cleveland, OH.

OPTICAL MEASUREMENT OF PROPELLER BLADE DEFLECTIONS

ANATOLE P. KURKOV Sep. 1988 31 p (NASA-TP-2841; E-4131; NAS 1.60:2841) Avail: NTIS HC A03/MF A01 CSCL 14B

A nonintrusive optical method for measurement of propeller blade deflections is described and evaluated. It does not depend on the reflectivity of the blade surface but only on its opaqueness. Deflection of a point at the leading edge and a point at the trailing edge in a plane nearly perpendicular to the pitch axis is obtained using a single light beam generated by a low-power helium-neon laser. Quantitative analyses are performed from taped signals on a digital computer. Averaging techniques are employed to reduce random errors. Measured deflections from a static and a high-speed test are compared with available predicted deflections which are also used to evaluate systematic errors. Author

N88-28293*# National Aeronautics and Space Administration. Lewis Research Center, Cleveland, OH.

FIBER OPTIC SENSING SYSTEMS USING HIGH FREQUENCY RESONANT SENSING HEADS WITH INTENSITY SENSORS

GRIGORY ADAMOVSKY and DUNCAN J. MAITLAND, IV (Cleveland State Univ., Ohio.) Sep. 1988 9 p Presented at the High Bandwidth Analog Applications of Photonics 2 Conference, Boston, Mass., 8-9 Sep. 1988; sponsored by the Society of Photo-Optical Instrumentation Engineers (NASA-TM-101318; E-4315; NAS 1.15:101318) Avail: NTIS HC A02/MF A01 CSCL 14B

Optical fibers have an inherent capability of transmitting high

bandwidth analog and digital signals. To apply this property of fiber optics to remote sensing, special sensing heads as well as signal processing electronics have to be developed. In systems employing intensity modulating sensors, there is also a need for a referencing technique to compensate for changes in the transmission of the connecting fibers and light source intensity. Fiber optic sensing systems incorporated in sensing heads of a special configuration are discussed. Different modes of operation as well as resonant conditions are explained. Theoretical and experimental analyses are also given. Author

N88-28299*# Pratt and Whitney Aircraft, East Hartford, CT. **DEVELOPMENT OF SENSORS FOR CERAMIC COMPONENTS IN ADVANCED PROPULSION SYSTEMS: SURVEY AND EVALUATION OF MEASUREMENT TECHNIQUES FOR TEMPERATURE, STRAIN AND HEAT FLUX FOR CERAMIC COMPONENTS IN ADVANCED PROPULSION SYSTEMS Final Report**

W. H. ATKINSON, M. A. CYR, and R. R. STRANGE Jun. 1988 128 p

(Contract NAS3-25141)

(NASA-CR-182111; NAS 1.26:182111; PWA-6113-12) Avail: NTIS HC A07/MF A01 CSCL 14B

The report presents the final results of Tasks 1 and 2, Development of Sensors for Ceramic Components in Advanced Propulsion Systems (NASA program NAS3-25141). During Task 1, an extensive survey was conducted of sensor concepts which have the potential for measuring surface temperature, strain and heat flux on ceramic components for advanced propulsion systems. Each sensor concept was analyzed and evaluated under Task 2; sensor concepts were then recommended for further development. For temperature measurement, both pyrometry and thermographic phosphors are recommended for measurements up to and beyond the melting point of ceramic materials. For lower temperature test programs, the thin-film techniques offer advantages in the installation of temperature sensors. Optical strain measurement techniques are recommended because they offer the possibility of being useful at very high temperature levels. Techniques for the measurement of heat flux are recommended for development based on both a surface mounted sensor and the measurement of the temperature differential across a portion of a ceramic component or metallic substrate. Author

N88-29142*# National Aeronautics and Space Administration. Lewis Research Center, Cleveland, OH.

OPTICAL MEASUREMENT OF UNDUCTED FAN BLADE DEFLECTIONS

ANATOLE P. KURKOV 1988 14 p Proposed for presentation at the 34th International Gas Turbine and Aeroengine Congress and Exposition, Toronto, Ontario, 4-8 Jun. 1989 (NASA-TM-100966; E-4131-1; NAS 1.15:100966) Avail: NTIS HC A03/MF A01 CSCL 14B

A nonintrusive optical method for measuring unducted fan (or propeller) blade deflections is described and evaluated. The measurement does not depend on blade surface reflectivity. Deflection of a point at the leading edge and a point at the trailing edge in a plane nearly perpendicular to the pitch axis is obtained with a single light beam generated by a low-power, helium-neon laser. Quantitative analyses are performed from taped signals on a digital computer. Averaging techniques are employed to reduce random errors. Measured static deflections from a series of high-speed wind tunnel tests of a counterrotating unducted fan model are compared with available, predicted deflections, which are also used to evaluate systematic errors. Author

N88-29152*# National Aeronautics and Space Administration. Lewis Research Center, Cleveland, OH.

APPLICATION OF OPTICAL CORRELATION TECHNIQUES TO PARTICLE IMAGING VELOCIMETRY

MARK P. WERNET and ROBERT V. EDWARDS 1988 23 p Presented at the Conference on Sensors and Measurement Techniques for Aeronautical Applications, Atlanta, Ga., 7-9 Sep.

35 INSTRUMENTATION AND PHOTOGRAPHY

1988; sponsored in part by AIAA, NASA and AFWAL (NASA-TM-101306; E-4297; NAS 1.15:101306) Avail: NTIS HC A03/MF A01 CSCL 14B

Pulsed laser sheet velocimetry yields nonintrusive measurements of velocity vectors across an extended 2-dimensional region of the flow field. The application of optical correlation techniques to the analysis of multiple exposure laser light sheet photographs can reduce and/or simplify the data reduction time and hardware. Here, Matched Spatial Filters (MSF) are used in a pattern recognition system. Usually MSFs are used to identify the assembly line parts. In this application, the MSFs are used to identify the iso-velocity vector contours in the flow. The patterns to be recognized are the recorded particle images in a pulsed laser light sheet photograph. Measurement of the direction of the partial image displacements between exposures yields the velocity vector. The particle image exposure sequence is designed such that the velocity vector direction is determined unambiguously. A global analysis technique is used in comparison to the more common particle tracking algorithms and Young's fringe analysis technique. Author

N88-30099*# National Aeronautics and Space Administration. Lewis Research Center, Cleveland, OH.

MEASUREMENT OF LOCAL HIGH-LEVEL, TRANSIENT SURFACE HEAT FLUX

CURT H. LIEBERT Sep. 1988 9 p Sponsored by NASA, Washington, D.C.

(NASA-TP-2840; E-4200; NAS 1.60:2840) Avail: NTIS HC A02/MF A01 CSCL 14B

This study is part of a continuing investigation to develop methods for measuring local transient surface heat flux. A method is presented for simultaneous measurements of dual heat fluxes at a surface location by considering the heat flux as a separate function of heat stored and heat conducted within a heat flux gage. Surface heat flux information is obtained from transient temperature measurements taken at points within the gage. Heat flux was determined over a range of 4 to 22 MW/sq m. It was concluded that the method is feasible. Possible applications are for heat flux measurements on the turbine blade surfaces of space shuttle main engine turbopumps and on the component surfaces of rocket and advanced gas turbine engines and for testing sensors in heat flux gage calibrators. Author

N88-30106*# Northwestern Univ., Evanston, IL. Technological Inst.

ELECTRICAL PROPERTIES OF MATERIALS FOR ELEVATED TEMPERATURE RESISTANCE STRAIN GAGE APPLICATION

Ph.D. Thesis

JIH-FEN LEI Jun. 1987 276 p

(Contract NAG3-501)

(NASA-CR-182214; NAS 1.26:182214) Avail: NTIS HC A13/MF A01 CSCL 14B

The objective was to study the electrical resistances of materials that are potentially useful as resistance strain gages at 1000 C. Transition metal carbides and nitrides, boron carbide and silicon carbide were selected for the experimental phase of this research. Due to their low temperature coefficient of resistance and good stability, TiC, ZrC, B sub 4 C and beta-SiC are suggested as good candidates for high temperature resistance strain gage applications. Author

36

LASERS AND MASERS

Includes parametric amplifiers.

N88-11145*# National Aeronautics and Space Administration. Lewis Research Center, Cleveland, OH.

THE FOUR SPOT TIME-OF-FLIGHT LASER ANEMOMETER

MARK P. WERNET *In its* Turbine Engine Hot Section Technology, 1985 p 67-75 Oct. 1985

Avail: NTIS HC A19/MF A01 CSCL 20E

The newly constructed, four-spot anemometer was shown to perform as predicted. The new anemometer's measurement region has the required characteristics: wide acceptance angle and high spatial selectivity to permit measurements in turbulent, hostile environments. Author

N88-18910*# National Aeronautics and Space Administration. Lewis Research Center, Cleveland, OH.

A LASER COMMUNICATION EXPERIMENT UTILIZING THE ACT SATELLITE AND AN AIRBORNE LASER TRANSCEIVER

CHARLES E. PROVENCHER, JR. and RODNEY L. SPENCE 1988 26 p Presented at the Optoelectronics and Laser Applications in Science and Engineering (O-E LASE 88), Los Angeles, Calif., 10-17 Jan. 1988; sponsored in part by the Society of Photo-Optical Instrumentation Engineers

(NASA-TM-100792; E-3967; NAS 1.15:100792) Avail: NTIS HC A03/MF A01 CSCL 20E

The launch of a laser communication transmitter package into geosynchronous Earth orbit onboard the Advanced Communications Technology Satellite (ACTS) will present an excellent opportunity for the experimental reception of laser communication signals transmitted from a space orbit. The ACTS laser package includes both a heterodyne transmitter (Lincoln Labs design) and a direct detection transmitter (Goddard Space Flight Center design) with both sharing some common optical components. NASA Lewis Research Center's Space Electronics Division is planning to perform a space communication experiment utilizing the GSFC direct detection laser transceiver. The laser receiver will be installed within an aircraft provided with a glass port for the reception of the signal. This paper describes the experiment and the approach to performing such an experiment. Described are the constraints placed on the NASA Lewis experiment by the performance parameters of the laser transmitter and by the ACTS spacecraft operations. The conceptual design of the receiving terminal is given; also included is the anticipated capability of the detector. Author

37

MECHANICAL ENGINEERING

Includes auxiliary systems (nonpower); machine elements and processes; and mechanical equipment.

A88-10938* Dartmouth Coll., Hanover, NH.

PLASTICITY ANALYSIS OF WEAR PHENOMENA AS AN AID IN THE DEVELOPMENT OF ABRADABLE MATERIALS

F. E. KENNEDY, JR. (Dartmouth College, Hanover, NH), K. E. HAUCK, JR., and L. P. GROTELUESCHEN IN: Mechanisms and surface distress. London, Butterworths, 1986, p. 67-73. refs (Contract NSG-3253)

Plastic deformation accompanying the wear process in fully dense and porous metals was studied in order to develop more abrasible gas path seal material systems for turbine engine applications. The finite element method was used to model high-rate viscoplastic deformation in the vicinity of a moving contact. Techniques were developed for studying such deformation in both solid (fully dense) and porous metals. Results of the analysis were verified by comparison with experimental data obtained using a pendulum-type rub test apparatus and a pin-on-disk sliding wear tester. It was found that the near-surface plastic deformation in fully dense solids was different from that for porous materials because of the compressibility of the latter. Both types of materials exhibit deformation features which can be taken advantage of in the design of more abrasible material systems. Author

A88-10973* Illinois Univ., Chicago.

METHOD FOR GENERATION OF SPIRAL BEVEL GEARS WITH CONJUGATE GEAR TOOTH SURFACES

F. L. LITVIN (Illinois, University, Chicago), J. J. COY (NASA, Lewis Research Center; U.S. Army, Propulsion Directorate, Cleveland, OH), C. HEINE (Dana Corp., Fort Wayne, IN), and WEI-JIUNG TSUNG ASME, Transactions, Journal of Mechanisms, Transmission, and Automation in Design, vol. 109, June 1987, p. 163-170. refs
(ASME PAPER 86-DET-3)

A method for generation of spiral bevel gears is proposed that provides conjugate gear tooth surfaces. This method is based on a new principle for the performance of parallel motion of a straight line that slides along two mating ellipses with related dimensions and parameters of orientation. The parallel motion of the straight line, that is, the contact normal, is performed parallel to the line which passes through the foci of symmetry of the related ellipses. The manufacturing of gears can be performed with the existing Gleason's equipment. Author

A88-11083* Ford Motor Co., Dearborn, MI.

DEVELOPMENT OF THE AGT101 REGENERATOR SEALS

C. A. FUCINARI, J. K. VALLANCE, and C. J. RAHNKE (Ford Motor Co., Dearborn, MI) ASME, International Gas Turbine Conference and Exhibition, 32nd, Anaheim, CA, May 31-June 4, 1987. 10 p. DOE-supported research.
(Contract DEN3-167)
(ASME PAPER 87-GT-173)

The design and development of the regenerator seals used in the AGT101 gas turbine engine are described in this paper. The all ceramic AGT101 gas turbine engine was designed for 100 hp at 5:1 pressure ratio with 2500F(1371C) turbine inlet temperature. Six distinct phases of seal design were investigated experimentally and analytically to develop the final design. Static and dynamic test rig results obtained during the seal development program are presented. In addition, analytical techniques are described. The program objectives of reduced seal leakage, without additional diaphragm cooling, to 3.6 percent of total engine airflow and higher seal operating temperature resulting from the 2000F (1093C) inlet exhaust gas temperature were met. Author

A88-11965* National Aeronautics and Space Administration. Lewis Research Center, Cleveland, OH.

AUTOMOTIVE STIRLING ENGINE DEVELOPMENT PROGRAM - A SUCCESS

WILLIAM K. TABATA (NASA, Lewis Research Center, Cleveland, OH) IN: IECEC '87; Proceedings of the Twenty-second Intersociety Energy Conversion Engineering Conference, Philadelphia, PA, Aug. 10-14, 1987. Volume 4. New York, American Institute of Aeronautics and Astronautics, 1987, p. 1765-1768. Previously announced in STAR as N87-22562.

The original 5-year Automotive Stirling Engine Development Program has been extended to 10 years due to reduced annual funding levels. With an estimated completion date of April 1988, the technical achievements and the perspectives of meeting the original program objectives are reviewed. Various other applications of this developed Stirling engine technology are also discussed. Author

A88-11966* National Aeronautics and Space Administration. Lewis Research Center, Cleveland, OH.

COMPARISON OF MEASURED AND CALCULATED FORCES ON THE RE-1000 FREE-PISTON STIRLING ENGINE DISPLACER

JEFFREY G. SCHREIBER (NASA, Lewis Research Center, Cleveland, OH) IN: IECEC '87; Proceedings of the Twenty-second Intersociety Energy Conversion Engineering Conference, Philadelphia, PA, Aug. 10-14, 1987. Volume 4. New York, American Institute of Aeronautics and Astronautics, 1987, p. 1769-1773. refs

The NASA Lewis Research Center has tested a 1 kW free-piston Stirling engine at the NASA Lewis test facilities. The tests performed over the past several years on the RE-1000 single cylinder engine

are known as the sensitivity tests. This report presents an analysis of some of the data published in the sensitivity test report. A basic investigation into the measured forces acting on the unconstrained displacer of the engine is presented. These measured forces are then correlated with the values predicted by the NASA Lewis Stirling engine computer simulation. The results of the investigation are presented in the form of phasor diagrams. Possible future work resulting from this investigation is outlined. Author

A88-11967* National Aeronautics and Space Administration. Lewis Research Center, Cleveland, OH.

CALIBRATION AND COMPARISON OF THE NASA LEWIS FREE-PISTON STIRLING ENGINE MODEL PREDICTIONS WITH RE-1000 TEST DATA

STEVEN M. GENG (NASA, Lewis Research Center, Cleveland, OH) IN: IECEC '87; Proceedings of the Twenty-second Intersociety Energy Conversion Engineering Conference, Philadelphia, PA, Aug. 10-14, 1987. Volume 4. New York, American Institute of Aeronautics and Astronautics, 1987, p. 1774-1785. Previously announced in STAR as N87-22561. refs

A free-piston Stirling engine performance code is being upgraded and validated at the NASA Lewis Research Center under an interagency agreement between the Department of Energy's Oak Ridge National Laboratory and NASA Lewis. Many modifications were made to the free-piston code in an attempt to decrease the calibration effort. A procedure was developed that made the code calibration process more systematic. Engine-specific calibration parameters are often used to bring predictions and experimental data into better agreement. The code was calibrated to a matrix of six experimental data points. Predictions of the calibrated free-piston code are compared with RE-1000 free-piston Stirling engine sensitivity test data taken at NASA Lewis. Reasonable agreement was obtained between the code prediction and the experimental data over a wide range of engine operating conditions. Author

A88-11972* Mechanical Technology, Inc., Latham, NY.

MOD II ENGINE DEVELOPMENT

DAVID W. KARL (Mechanical Technology, Inc., Latham, NY) IN: IECEC '87; Proceedings of the Twenty-second Intersociety Energy Conversion Engineering Conference, Philadelphia, PA, Aug. 10-14, 1987. Volume 4. New York, American Institute of Aeronautics and Astronautics, 1987, p. 1810-1816. DOE-sponsored research.
(Contract DEN3-32)

The Mod II engine, a four-cylinder, automotive Stirling engine utilizing the Siemens-Rinia double-acting concept, was assembled and became operational in January 1986. This paper describes the Mod II engine, its first assembly, and the subsequent development work done on engine components up to the point that engine performance characterization testing took place. Performance data for the engine are included. Author

A88-14115* General Electric Co., Cincinnati, OH.

OIL FILM THICKNESS MEASUREMENT AND ANALYSIS FOR AN ANGULAR CONTACT BALL BEARING OPERATING IN PARTIALLY ELASTOHYDRODYNAMIC LUBRICATION

S. D. HUNTER (General Electric Co., Cincinnati, OH), E. KINGSBURY (Charles Stark Draper Laboratory, Inc., Cambridge, MA), and J. M. PRAHL (Case Western Reserve University, Cleveland, OH) IN: Symposium on Thin Fluid Films, Cincinnati, OH, June 14-17, 1987. Proceedings. New York, American Society of Mechanical Engineers, 1987, p. 43-46. refs
(Contract NCC3-30)

A88-14591* National Aeronautics and Space Administration. Lewis Research Center, Cleveland, OH.

SURFACE FATIGUE AND FAILURE CHARACTERISTICS OF HOT-FORGED POWDER METAL AISI 4620, AISI 4640, AND MACHINED AISI 4340 STEEL SPUR GEARS

DENNIS P. TOWNSEND (NASA, Lewis Research Center, Cleveland, OH) Lubrication Engineering (ISSN 0024-7154), vol.

37 MECHANICAL ENGINEERING

43, Sept. 1987, p. 706-716. Previously announced in STAR as N86-31889. refs

Spur gear surface fatigue endurance tests were conducted to investigate hot forged powder metal AISI 4620 and 4640 steel for use as a gear material, to determine endurance characteristics and to compare the results with machined AISI 4340 and 9310 steel gear materials. The as-forged and unground AISI 4620 gear exhibited a 10 percent fatigue life that was approximately one-fourth of that for AISI 9310 and less than one-half that for the AISI 4340 gears. The forged and finish ground AISI 4620 gears exhibited a 10 percent life, approximately 70 percent that of AISI 9310 and slightly better than that of AISI 4340. The AISI 4640 hot forged gears had less fracture toughness and slightly less fatigue life than the AISI 4620 test gears. Author

A88-23308* # Texas A&M Univ., College Station.
ANALYSIS OF ECCENTRIC ANNULAR INCOMPRESSIBLE SEALS. I - A NEW SOLUTION USING FAST FOURIER TRANSFORMS FOR DETERMINING HYDRODYNAMIC FORCE
C. C. NELSON and D. T. NGUYEN (Texas A & M University, College Station) ASME and ASLE, Tribology Conference, San Antonio, TX, Oct. 5-8, 1987. 6 p. refs
(Contract NAS3-181)
(ASME PAPER 87-TRIB-52)

A new analysis procedure is presented which solves for the flow variables of an incompressible-flow annular pressure seal in which the rotor has a large static displacement from the centered position. The analysis begins with a set of governing equations based on a turbulent bulk-flow model and Moody's friction equation. No simplification of these bulk-flow equations is required for the solution procedure. Perturbation of the flow variables yields a set of zeroth and first-order equations. The zeroth-order equations (which model the large static displacement) are integrated by means of an efficient new method which employs fast Fourier transforms. Further integration of the zeroth-order pressures yields the hydrodynamic reactive force. Predictions for the hydrodynamic forces from this analysis procedure are in excellent agreement with available experimental results. Author

A88-23309* # Texas A&M Univ., College Station.
ANALYSIS OF ECCENTRIC ANNULAR INCOMPRESSIBLE SEALS. II - EFFECTS OF ECCENTRICITY ON ROTORDYNAMIC COEFFICIENTS
C. C. NELSON and D. T. NGUYEN (Texas A & M University, College Station) ASME and ASLE, Tribology Conference, San Antonio, TX, Oct. 5-8, 1987. 6 p.
(Contract NAS3-181)
(ASME PAPER 87-TRIB-53)

A new analysis procedure has been presented which solves for the flow variables of an annular pressure seal in which the rotor has a large static displacement (eccentricity) from the centered position. The present paper incorporates the solutions to investigate the effect of eccentricity on the rotordynamic coefficients. The analysis begins with a set of governing equations based on a turbulent bulk-flow model and Moody's friction factor equation. Perturbations of the flow variables yields a set of zeroth and first-order equations. After integration of the zeroth-order equations, the resulting zeroth-order flow variables are used as input in the solution of the first-order equations. Further integration of the first order pressures yields the eccentric rotordynamic coefficients. The results from this procedure compare well with available experimental and theoretical data, with accuracy just as good or slightly better than the predictions based on a finite-element model. Author

A88-23310* # Mechanical Technology, Inc., Latham, NY.
ANALYSIS AND DESIGN OF A GAS-LUBRICATED, SECTORED, FLOATING RING SEAL
W. SHAPIRO, C. LEE, and H. JONES (Mechanical Technology, Inc., Latham, NY) ASME and ASLE, Tribology Conference, San Antonio, TX, Oct. 5-8, 1987. 7 p.
(Contract NAS3-24645)
(ASME PAPER 87-TRIB-55)

Helium buffered floating-ring seals used in cryogenic turbopumps are subject to large temperature variations, shaft centrifugal growth, and dynamic shaft excursions. To prevent dangerous contact friction over a wide range of operating conditions generally requires liberal clearances with consequent high leakage. Reduction of helium consumption translates into lower space vehicle helium storage requirements and thus increased payload. A hydrostatic sectored floating-ring seal is described with self-adjusting clearance capabilities that enables the seal to operate with small clearances over the operating range to minimize leakage. Author

A88-23313* National Aeronautics and Space Administration.
Lewis Research Center, Cleveland, OH.
PERFORMANCE AND EFFICIENCY EVALUATION AND HEAT RELEASE STUDY OF A DIRECT-INJECTION STRATIFIED-CHARGE ROTARY ENGINE
H. L. NGUYEN, H. E. ADDY, T. H. BOND, C. M. LEE, and K. S. CHUN (NASA, Lewis Research Center, Cleveland, OH) SAE, International Congress and Exposition, Detroit, MI, Feb. 23-27, 1987. 24 p. Previously announced in STAR as N87-20282. refs
(SAE PAPER 870445)

A computer simulation which models engine performance of the Direct Injection Stratified Charge (DISC) rotary engines was used to study the effect of variations in engine design and operating parameters on engine performance and efficiency of an Outboard Marine Corporation (OMC) experimental rotary combustion engine. Engine pressure data were used in a heat release analysis to study the effects of heat transfer, leakage, and crevice flows. Predicted engine data were compared with experimental test data over a range of engine speeds and loads. An examination of methods to improve the performance of the rotary engine using advanced heat engine concepts such as faster combustion, reduced leakage, and turbocharging is also presented. Author

A88-24034* # National Aeronautics and Space Administration.
Lewis Research Center, Cleveland, OH.
STABILITY OF A RIGID ROTOR SUPPORTED ON FLEXIBLE OIL JOURNAL BEARINGS
B. C. MAJUMDAR (NASA, Lewis Research Center, Cleveland, OH), D. E. BREWE (U.S. Army, Propulsion Directorate, Cleveland, OH), and M. M. KHONSARI (Ohio State University, Columbus) ASME, Transactions, Journal of Tribology (ISSN 0742-4787), vol. 110, Jan. 1988, p. 181-187. Previously announced in STAR as N87-24646. refs
(ASME PAPER 87-TRIB-48)

This investigation deals with the stability characteristics of oil journal bearings, including the effect of elastic distortions in the bearing liner. Graphical results are presented for (1) steady-state load, (2) stiffness and damping coefficients, and (3) the stability. These results are given for various slenderness ratios, eccentricity ratios, and elasticity parameters. The lubricant is first assumed to be isoviscous. The analysis is then extended to the case of a pressure-dependent viscosity. It has been found that stability decreases with increase of the elasticity parameter of the bearing liner for heavily loaded bearings. Author

A88-31527* # National Aeronautics and Space Administration.
Lewis Research Center, Cleveland, OH.
EXPERIMENTS ON DYNAMIC STIFFNESS AND DAMPING OF TAPERED BORE SEALS
D. P. FLEMING (NASA, Lewis Research Center, Cleveland, OH) IN: Rotating machinery dynamics; Proceedings of the Eleventh Biennial ASME Conference on Mechanical Vibration and Noise, Boston, MA, Sept. 27-30, 1987. Volume 1. New York, American Society of Mechanical Engineers, 1987, p. 279-285. Previously announced in STAR as N87-23984. refs

Stiffness and damping were measured in tapered bore ring seals with air as the sealed fluid. Excitation was provided by a known unbalance in the shaft which rotated in the test seals. Results were obtained for various seal supply pressures, clearances, unbalance amounts, and shaft speeds. Stiffness and damping varied little with unbalance level, indicating linearity of

the seal. Greater variation was observed with speed and particularly supply pressure. A one-dimensional analysis predicted stiffness fairly well, but considerably overestimated damping. Author

A88-31534*# CHAM of North America, Inc., Huntsville, AL.
NUMERICAL AND ANALYTICAL STUDY OF FLUID DYNAMIC FORCES IN SEALS AND BEARINGS

L. T. TAM, A. J. PRZEKAS (Cham of North America, Inc., Huntsville, AL), A. MUSZYNSKA (Bently Rotor Dynamics Research Corp., Minden, NV), R. C. HENDRICKS (NASA, Lewis Research Center, Cleveland, OH), M. J. BRAUN (Akron, University, OH) et al. IN: Rotating machinery dynamics; Proceedings of the Eleventh Biennial ASME Conference on Mechanical Vibration and Noise, Boston, MA, Sept. 27-30, 1987. Volume 2. New York, American Society of Mechanical Engineers, 1987, p. 359-370. refs

Study results for rotor/bearing/seal system models are compared with both a numerical model based on a transformed, conservative version of the three-dimensional Navier-Stokes equation, and an analytical model based on 'lumped' fluid parameters. Rotor-destabilizing factors are related to flow field rotation; it is shown that these factors can be reduced through a decrease in the fluid average circumferential velocity. A transformation of the Navier-Stokes equations to those for a rotating observer and a numerical code with a nonorthogonal body-fitted grid are used to carry out numerical experiments demonstrating the character of the complex flow field. O.C.

A88-31535*# Texas A&M Univ., College Station.
THEORY VERSUS EXPERIMENT FOR THE ROTORDYNAMIC COEFFICIENTS OF LABYRINTH GAS SEALS. I - A TWO CONTROL VOLUME MODEL

J. K. SCHARRER (Texas A & M University, College Station) IN: Rotating machinery dynamics; Proceedings of the Eleventh Biennial ASME Conference on Mechanical Vibration and Noise, Boston, MA, Sept. 27-30, 1987. Volume 2. New York, American Society of Mechanical Engineers, 1987, p. 411-426. refs
 (Contract NAS3-181; F49620-82-K-0033)

The basic equations are derived for a two-control-volume model for compressible flow in a labyrinth seal. The recirculation velocity in the cavity is incorporated into the model for the first time. The flow is assumed to be completely turbulent and isoenergetic. The wall friction factors are determined using the Blasius formula. Jet flow theory is used for the calculation of the recirculation velocity in the cavity. Linearized zeroth- and first-order perturbation equations are developed for small motion about a centered position by an expansion in the eccentricity ratio. The zeroth-order pressure distribution is found by satisfying the leakage equation while the circumferential velocity distribution is determined by satisfying the momentum equations. The first-order equations are solved by a separation of variable solution. Integration of the resultant pressure distribution along and around the seal defines the reaction force developed by the seal and the corresponding dynamic coefficients. Author

A88-31536*# Texas A&M Univ., College Station.
THEORY VERSUS EXPERIMENT FOR THE ROTORDYNAMIC COEFFICIENTS OF LABYRINTH GAS SEALS. II - A COMPARISON TO EXPERIMENT

D. W. CHILDS and J. K. SCHARRER (Texas A & M University, College Station) IN: Rotating machinery dynamics; Proceedings of the Eleventh Biennial ASME Conference on Mechanical Vibration and Noise, Boston, MA, Sept. 27-30, 1987. Volume 2. New York, American Society of Mechanical Engineers, 1987, p. 427-434. refs
 (Contract NAS3-181; F49620-82-K-0033)

An experimental test facility is used to measure the leakage and rotordynamic coefficients of teeth-on-rotor and teeth-on-stator labyrinth gas seals. The test results are presented along with the theoretically predicted values for the two seal configurations at three different radial clearances and shaft speeds to 16,000 cpm. The test results show that the theory accurately predicts the cross-coupled stiffness for both seal configurations and shows improvement in the prediction of the direct damping for the

teeth-on-rotor seal. The theory fails to predict a decrease in the direct damping coefficient for an increase in the radial clearance for the teeth-on-stator seal. Author

A88-31539*# National Aeronautics and Space Administration.
 Lewis Research Center, Cleveland, OH.
TRANSIENT ROTOR DYNAMIC RUB PHENOMENA - THEORY AND TEST

A. F. KASCAK, G. MONTAQUE (NASA, Lewis Research Center, Cleveland, OH), and A. B. PALAZZOLO (Texas A & M University, College Station) IN: Rotating machinery dynamics; Proceedings of the Eleventh Biennial ASME Conference on Mechanical Vibration and Noise, Boston, MA, Sept. 27-30, 1987. Volume 2. New York, American Society of Mechanical Engineers, 1987, p. 485-494. refs

This paper develops an implicit integration scheme for transient rotor dynamic rub prediction and includes a correlation study with actual test results. A Nordsieck-like numerical integration scheme is applied directly to the second-order equations of motion. The assumption that forces and torques on the rotor are functions of the position and velocity at the point of application and its nearest neighbor is made in order to make the computational time proportional to the number of elements in the rotor dynamics model rather than the cube of the number. The test rig consists of a turbine driven, flexible shaft supported by squeeze film dampers. The blade loss event occurs due to collision of a balance bolt on one of the disks with a high speed plunger. The rotor is seen to spiral outward and contact against a stationary assemblage of seal shoes. Author

A88-31581*# National Aeronautics and Space Administration.
 Lewis Research Center, Cleveland, OH.
THE IMPACT DAMPED HARMONIC OSCILLATOR IN FREE DECAY

G. V. BROWN (NASA, Lewis Research Center, Cleveland, OH) and C. M. NORTH (Rose-Hulman Institute of Technology, Terre Haute, IN) IN: The role of damping in vibration and noise control; Proceedings of the Eleventh Biennial Conference on Mechanical Vibration and Noise, Boston, MA, Sept. 27-30, 1987. New York, American Society of Mechanical Engineers, 1987, p. 53-64. Previously announced in STAR as N87-23978. refs

The impact-damped oscillator in free decay is studied by using time history solutions. A large range of oscillator amplitude is covered. The amount of damping is correlated with the behavior of the impacting mass. There are three behavior regimes: (1) a low amplitude range with less than one impact per cycle and very low damping, (2) a useful middle amplitude range with a finite number of impacts per cycle, and (3) a high amplitude range with an infinite number of impacts per cycle and progressively decreasing damping. For light damping the impact damping in the middle range is: (1) proportional to impactor mass, (2) additive to proportional damping, (3) a unique function of vibration amplitude, (4) proportional to $1-\epsilon$, where ϵ is the coefficient of restitution, and (5) very roughly inversely proportional to amplitude. The system exhibits jump phenomena and period doublings. An impactor with 2 percent of the oscillator's mass can produce a loss factor near 0.1. Author

A88-31598*# Carnegie-Mellon Univ., Pittsburgh, PA.
AN INTEGRATED APPROACH FOR FRICTION DAMPER DESIGN

T. M. CAMERON, J. H. GRIFFIN, T. M. HOOSAC (Carnegie-Mellon University, Pittsburgh, PA), and R. E. KIELB (NASA, Lewis Research Center, Cleveland, OH) IN: The role of damping in vibration and noise control; Proceedings of the Eleventh Biennial Conference on Mechanical Vibration and Noise, Boston, MA, Sept. 27-30, 1987. New York, American Society of Mechanical Engineers, 1987, p. 205-211. refs
 (Contract NAG3-367)

A procedure is outlined for determining the optimal design of friction dampers for high speed turbomachinery blading. The procedure includes: an integration of bench test results with finite element analysis and a single mode blade model to ensure

37 MECHANICAL ENGINEERING

accuracy of the analytical model and improve reliability of the friction damper design; an extension of the single mode blade model to predict the engine behavior of friction dampers; and a new way of viewing analytical and experimental results to determine optimal design parameters when the levels of excitation and damping in the system are unknown. Analysis and experiments are performed on a test disk in order to demonstrate and verify the accuracy of the design procedure. Author

A88-31623*# Cleveland State Univ., OH.

AUTOMATED ACOUSTIC INTENSITY MEASUREMENTS AND THE EFFECT OF GEAR TOOTH PROFILE ON NOISE

W. J. ATHERTON, A. PINTZ (Cleveland State University, OH), and D. G. LEWICKI (U.S. Army, Propulsion Directorate, Cleveland, OH) IN: Mechanical signature analysis - Machinery vibration, flow-induced vibration, and acoustic noise analysis; Proceedings of the Eleventh Biennial Conference on Mechanical Vibration and Noise, Boston, MA, Sept. 27-30, 1987. New York, American Society of Mechanical Engineers, 1987, p. 109-113. Previously announced in STAR as N87-28917. refs
(Contract NAG3-315)

Acoustic intensity measurements were made at NASA Lewis Research Center on a spur gear test apparatus. The measurements were obtained with the Robotic Acoustic Intensity Measurement System developed by Cleveland State University. This system provided dense spatial positioning, and was calibrated against a high quality acoustic intensity system. The measured gear noise compared gearsets having two different tooth profiles. The tests evaluated the sound field of the different gears for two speeds and three loads. The experimental results showed that gear tooth profile had a major effect on measured noise. Load and speed were found to have an effect on noise also. Author

A88-39703* North Carolina State Univ., Raleigh.

TRANSFER MATRIX MODELING OF GEARED SYSTEM VIBRATION

J. W. DAVID and NO-GILL PARK (North Carolina State University, Raleigh) IN: NOISE-CON 87; Proceedings of the National Conference on Noise Control Engineering, State College, PA, June 8-10, 1987. Poughkeepsie, NY, Noise Control Foundation, 1987, p. 41-46. refs
(Contract NAG3-611)

The need for a general technique to predict geared system response is demonstrated. It is believed that an analytical model that is general enough to allow for the analysis of arbitrarily constructed systems would be the most useful. Transfer matrices in geared system analysis are discussed and an example problem is presented. K.K.

A88-44742*# General Motors Corp., Indianapolis, IN.

DESIGN AND DEVELOPMENT OF CERAMIC COMPONENTS

R. L. HOLTMAN (General Motors Corp., Allison Gas Turbine Div., Indianapolis, IN) AIAA, ASME, SAE, and ASEE, Joint Propulsion Conference, 24th, Boston, MA, July 11-13, 1988. 7 p. DOE-supported research.
(Contract DEN3-168; DEN3-336)
(AIAA PAPER 88-3054)

The development of the AGT 100 turbine components in structural ceramic materials is described. Development is defined as the complete and iterative cycle from design, analysis, test, and design refinement culminating in successful demonstration of the design requirements. The components are analyzed by a linear elastic probabilistic approach, which involves finite element (three- and/or two-dimensional) simulation of the component combined with a Weibull characterization of the brittle ceramic material strength distribution to calculate a probability of survival for the component in the operating environment. Component test failure investigation has resulted in design modifications, and an improvement in component reliability has been demonstrated. Engine testing (over 570 h to date) continues to assess design/development of structural ceramic components. Author

A88-48971*# Texas A&M Univ., College Station.

EXPERIMENTAL VERIFICATION OF A SECONDARY RECIRCULATION ZONE IN A LABYRINTH SEAL

G. L. MORRISON, G. B. TATTERSON (Texas A & M University, College Station), and M. C. JOHNSON IN: AIAA, ASME, SIAM, and APS, National Fluid Dynamics Congress, 1st, Cincinnati, OH, July 25-28, 1988, Technical Papers. Part 3. Washington, DC, American Institute of Aeronautics and Astronautics, 1988, p. 1674-1684. refs
(Contract NAG3-181)
(AIAA PAPER 88-3692)

The existence of a secondary recirculation zone inside the cavities of a labyrinth seal operating at a Reynolds number of 15,000 and a Taylor number of 10,300 has been experimentally verified. A three-dimensional laser Doppler anemometer system was used to measure the complete mean velocity and Reynolds stress tensor distributions in the first, third, fifth and seventh cavities of a seven cavity labyrinth seal which had a clearance of 1.27 mm. Author

A88-49183*# Cleveland State Univ., OH.

ANALYSIS OF CRACK PROPAGATION IN ROLLER BEARINGS USING THE BOUNDARY INTEGRAL EQUATION METHOD - A MIXED-MODE LOADING PROBLEM

L. J. GHOSH (Cleveland State University, OH) ASME, Transactions, Journal of Tribology (ISSN 0742-4787), vol. 110, July 1988, p. 408-413. refs
(Contract NCC3-46)

Crack propagation in a rotating inner raceway of a high-speed roller bearing is analyzed using the boundary integral method. The model consists of an edge plate under plane strain condition upon which varying Hertzian stress fields are superimposed. A multidomain boundary integral equation using quadratic elements was written to determine the stress intensity factors KI and KII at the crack tip for various roller positions. The multidomain formulation allows the two faces of the crack to be modeled in two different subregions, making it possible to analyze crack closure when the roller is positioned on or close to the crack line. KI and KII stress intensity factors along any direction were computed. These calculations permit determination of crack growth direction along which the average KI times the alternating KI is maximum. Author

A88-49409*# Bolt, Beranek, and Newman, Inc., Cambridge, MA.

THE GENERALIZED TRANSMISSION ERROR OF SPIRAL BEVEL GEARS

W. D. MARK (BBN Laboratories, Inc., Cambridge, MA) ASME, Transactions, Journal of Mechanisms, Transmission, and Automation in Design (ISSN 0738-0666), vol. 109, June 1987, p. 275-282. refs
(Contract NAS3-23703)

The traditional definition of the transmission error of parallel-axis gear pairs is reviewed and shown to be unsuitable for characterizing the deviation from conjugate action of bevel gear pairs for vibration excitation characterization purposes. This situation is rectified by generalizing the concept of the transmission error of parallel-axis gears to a three-component transmission error for spiral bevel gears of nominal spherical involute design. A general relationship is derived which expresses the contributions to the three-component transmission error from each gear of a meshing spiral bevel pair as a linear transformation of the six coordinates that describe the deviation of the shaft centerline position of each gear of the pair from the position of its rigid perfect involute counterpart. Author

A88-49410*# Bolt, Beranek, and Newman, Inc., Cambridge, MA.

USE OF THE GENERALIZED TRANSMISSION ERROR IN THE EQUATIONS OF MOTION OF GEAR SYSTEMS

W. D. MARK (BBN Laboratories, Inc., Cambridge, MA) ASME, Transactions, Journal of Mechanisms, Transmission, and

Automation in Design (ISSN 0738-0666), vol. 109, June 1987, p. 283-291. refs
(Contract NAS3-23703)

The vibratory excitation arising from a gear pair is widely recognized to be a consequence of the nonuniform transmission of motion by the gear pair. In the preceding paper in this issue, it is shown that a three-component transmission error is required to describe the nonuniform transmission of motion by bevel gears for vibration excitation characterization purposes. The expression for the three-component transmission error derived in that paper is combined in the present paper with an analysis of the mesh forces and mesh elasticity to yield an equation of constraint involving the six degree-of-freedom unknown vibratory displacements of the gear shaft centerliners, the three unknown components of the generalized force transmitted by the mesh, and the geometric deviations of the tooth running surfaces from perfect involute surfaces which are assumed known. This matrix equation can be combined with the equations of motion of a gear system to predict the vibratory response of the system to the generalized transmission error excitation arising from meshing gear pairs within the system. Author

A88-51082* Draper (Charles Stark) Lab., Inc., Cambridge, MA.
PARCHED ELASTO HYDRODYNAMIC LUBRICATION FILM THICKNESS MEASUREMENT IN AN INSTRUMENT BALL BEARING

E. KINGSBURY (Charles Stark Draper Laboratory, Inc., Cambridge, MA), B. SCHRITZ, and J. PRAHL (Case Western Reserve University, Cleveland, OH) STLE, Annual Meeting, 43rd, Cleveland, OH, May 9-12, 1988. 4 p. refs
(Contract NCC3-30)
(STLE PREPRINT 88-AM-6G-1)

Parched Elasto Hydrodynamic Lubricant (PEHL) film thickness in a large instrument ball bearing is measured by electrical capacitance across its ball set. Correlation is shown between changes in film thickness and changes in Basic Speed Ratio (BSR) measured at the same time. BSR is confirmed as a sensitive, non-intrusive measure of transients in film thickness in a real bearing. Author

A88-53581* National Aeronautics and Space Administration.
Lewis Research Center, Cleveland, OH.

COMPOSITE MONOLAYER FABRICATION BY AN ARC-SPRAY PROCESS

LEONARD J. WESTFALL (NASA, Lewis Research Center, Cleveland, OH) IN: Thermal spray: Advances in coatings technology; Proceedings of the National Thermal Spray Conference, Orlando, FL, Sept. 14-17, 1987. Metals Park, OH, ASM International, 1988, p. 417-426. refs

A single layer (monotape) technique for fabricating complex high-temperature tungsten-fiber-reinforced superalloy composites is proposed. The fabrication of sheets of arc-sprayed monotape 38 cm wide and 122 cm long has been demonstrated. Composites fabricated using the method are shown to have equal tensile strength and a cleaner matrix than composites fabricated from powder metal cloth monotapes, and the present technique is less expensive than the powder metal fabrication techniques. R.R.

A88-54195* Texas A&M Univ., College Station.

3-D LASER ANEMOMETER MEASUREMENTS IN A LABYRINTH SEAL

G. L. MORRISON, G. B. TATTERSON (Texas A & M University, College Station), and M. C. JOHNSON ASME, Gas Turbine and Aeroengine Congress and Exposition, Amsterdam, Netherlands, June 6-9, 1988. 13 p. USAF-supported research. refs
(Contract NAG3-181)
(ASME PAPER 88-GT-63)

The flow field inside a seven cavity labyrinth seal with a 0.00127 m clearance was measured using a 3-D laser Doppler anemometer system. Through the use of this system, the mean velocity vector and the entire Reynolds stress tensor distributions were measured for the first, third, fifth, and seventh cavities of the seal. There was one large recirculation region present in the cavity for the

flow condition tested, $Re = 28,000$ and $Ta = 7,000$. The axial and radial mean velocities as well as all of the Reynolds stress term became cavity independent by the third cavity. The azimuthal mean velocity varied from cavity to cavity with its magnitude increasing as the flow progressed downstream. Author

A88-54196* Texas A&M Univ., College Station.
3-D LASER ANEMOMETER MEASUREMENTS IN AN ANNULAR SEAL

G. L. MORRISON, G. B. TATTERSON (Texas A & M University, College Station), and M. C. JOHNSON ASME, Gas Turbine and Aeroengine Congress and Exposition, Amsterdam, Netherlands, June 6-9, 1988. 15 p. USAF-supported research. refs
(Contract NAG3-181)
(ASME PAPER 88-GT-64)

The flow field inside an annular seal with a 0.00127 m clearance was measured using a 3-D laser Doppler anemometer system. Through the use of this system, the mean velocity vector and the entire Reynolds stress tensor distributions were measured for the entire length of the seal (0.0373 m). The seal was operated at a Reynolds number of 27,000 and a Taylor number of 6,600. Author

A88-54313* Cornell Univ., Ithaca, NY.
APPLICATION OF BIFURCATION THEORY TO AXIAL FLOW COMPRESSOR INSTABILITY

F. E. MCCAUGHAN (Cornell University, Ithaca, NY) ASME, Gas Turbine and Aeroengine Congress and Exposition, Amsterdam, Netherlands, June 6-9, 1988. 9 p. refs
(Contract NAG3-349)
(ASME PAPER 88-GT-231)

When a compression system goes unstable, the mode of response depends on the operating and system parameters, such as throttle setting and B parameter. Previous numerical work on the model developed by Moore and Greitzer (1986) has provided a limited picture of the parametric effects. Applying bifurcation theory to a single-harmonic version of the model has supplied much more complete information, defining the boundaries of each mode of response in the parameter space. Specifically, this is shown in a plot of B vs. throttle setting, which compares well with the corresponding map produced experimentally. The importance of the shape of the rotating stall characteristic is emphasized. The analysis shows a qualitative difference between classic surge and deep surge. Author

A88-54328* Cornell Univ., Ithaca, NY.
NUMERICAL RESULTS FOR AXIAL FLOW COMPRESSOR INSTABILITY

F. E. MCCAUGHAN (Cornell University, Ithaca, NY) ASME, Gas Turbine and Aeroengine Congress and Exposition, Amsterdam, Netherlands, June 6-9, 1988. 9 p. refs
(Contract NAG3-349)
(ASME PAPER 88-GT-252)

Using Cornell's supercomputing facilities, an extensive study of the Moore-Greitzer model was carried out, which gives accurate and reliable information about compressor instability. The bifurcation analysis in the companion paper shows the dependence of the mode of compressor response on the shape of the rotating stall characteristic. The numerical results verify and extend this with a more accurate representation of the characteristic. The effect of the parameters on the shape of the rotating stall characteristic is investigated, and it is found that the parameters with the strongest effects are the inlet length, and the shape of the compressor pressure rise vs. mass flow diagram (i.e. tall diagrams vs. shallow diagrams). The effects of inlet guide vane loss on the characteristic are discussed. Author

A88-54355* Pratt and Whitney Aircraft, East Hartford, CT.
CURRENT STATUS AND FUTURE TRENDS IN TURBINE APPLICATION OF THERMAL BARRIER COATINGS

KEITH D. SHEFFLER and DINESH K. GUPTA (Pratt and Whitney, East Hartford, CT) ASME, Gas Turbine and Aeroengine Congress and Exposition, Amsterdam, Netherlands, June 6-9, 1988. 9 p.

37 MECHANICAL ENGINEERING

refs

(Contract NAS3-23944)
(ASME PAPER 88-GT-286)

This paper provides an overview of the current status and future trends in application of thermal barrier coatings (TBC) to turbine components, and in particular to high turbine airfoils. Included are descriptions of the favorable results achieved to date with bill-of-material applications of plasma deposited TBC, and recent experience with developmental coatings applied by electron beam-physical vapor deposition. Author

A88-54964* # Cleveland State Univ., OH.

FOIL BEARING LUBRICATION THEORY INCLUDING COMPRESSIBILITY EFFECTS

RAMA SUBBA REDDY GORLA and DANIEL A. CATALANO (Cleveland State University, OH) IN: Developments in Mechanics. Volume 14(c) - Midwestern Mechanics Conference, 20th, West Lafayette, IN, Aug. 31-Sept. 2, 1987, Proceedings. West Lafayette, IN, Purdue University, 1987, p. 1122-1127. refs
(Contract NCC3-21)

An analysis is presented to determine the film thickness in a foil bearing. Using the Reynolds equation and including the compressibility effects of the gas, an equation was developed applicable to the film thickness in a foil bearing. The bearing was divided into three regions, namely, the entrance region, middle region and exit region. Solutions are obtained for the film thickness in each region. Author

N88-10339* # General Electric Co., Lynn, MA. Aircraft Engine Business Group.

THE DESIGN OF A TURBOSHAFT SPEED GOVERNOR USING MODERN CONTROL TECHNIQUES Final Report, 30 Sep. 1982 - 20 Feb. 1985

G. DELOSREYES and D. R. GOUCHOE Feb. 1986 220 p
(Contract NAS3-22763)
(NASA-CR-175046; NAS 1.26:175046) Avail: NTIS HC A10/MF A01 CSCL 131

The objectives of this program were: to verify the model of off schedule compressor variable geometry in the T700 turboshaft engine nonlinear model; to evaluate the use of the pseudo-random binary noise (PRBN) technique for obtaining engine frequency response data; and to design a high performance power turbine speed governor using modern control methods. Reduction of T700 engine test data generated at NASA-Lewis indicated that the off schedule variable geometry effects were accurate as modeled. Analysis also showed that the PRBN technique combined with the maximum likelihood model identification method produced a Bode frequency response that was as accurate as the response obtained from standard sinewave testing methods. The frequency response verified the accuracy of linear models consisting of engine partial derivatives and used for design. A power turbine governor was designed using the Linear Quadratic Regulator (LQR) method of full state feedback control. A Kalman filter observer was used to estimate helicopter main rotor blade velocity. Compared to the baseline T700 power turbine speed governor, the LQR governor reduced droop up to 25 percent for a 490 shaft horsepower transient in 0.1 sec simulating a wind gust, and up to 85 percent for a 700 shaft horsepower transient in 0.5 sec simulating a large collective pitch angle transient. Author

N88-10355* # Kentucky Univ., Lexington. Dept. of Electrical Engineering.

STUDY OF FREE-PISTON STIRLING ENGINE DRIVEN LINEAR ALTERNATORS Final Report

S. A. NASAR and C. CHEN 31 Jul. 1987 52 p
(Contract NAG3-722)
(NASA-CR-181425; NAS 1.26:181425) Avail: NTIS HC A04/MF A01 CSCL 131

The analysis, design and operation of single phase, single slot tubular permanent magnet linear alternator is presented. Included is the no-load and on-load magnetic field investigation, permanent magnet's leakage field analysis, parameter identification, design guidelines and an optimal design of a permanent magnet linear

alternator. For analysis of the magnetic field, a simplified magnetic circuit is utilized. The analysis accounts for saturation, leakage and armature reaction. Author

N88-11135* # Timken Co., Canton, OH.

IMPROVED OIL-OFF SURVIVABILITY OF TAPERED ROLLER BEARINGS Final Report, 1982 - 1987

GARY E. KREIDER and PETER W. LEE Oct. 1987 86 p
(Contract NAS3-23689; DA PROJ. 1L1-61102-AH-45)
(NASA-CR-180804; NAS 1.26:180804; AVSCOM-TR-87-C-29; AD-A189359) Avail: NTIS HC A05/MF A01 CSCL 131

The aim of this program is to improve the oil-off survivability of a tapered roller bearing when applied to a helicopter transmission, since the tapered bearing has shown a performance advantage in this application. However, the critical roller end-rib conjunction is vulnerable to damage in an oil-off condition. Three powdered metal materials were selected to use as the rib material for oil-off evaluation. These were: M2 steel to a 65% density, CBS 1000M 65% density, and CBS 1000M 75% density. The bearing styles tested were ribbed cone (inner race) and ribbed cup (outer race). Carburized solid CBS 600 was also used as a ribbed material for comparison of oil-off results. The tests were conducted at six speeds from 4000 rpm (0.26 million DN) through 37000 rpm (2.4 million DN). The ribbed cup style bearing achieved longer lives than the ribbed cone style. A standard bearing lasted only 10 minutes at 4000 rpm; however, the 30-min oil-off goal was achieved through 11000 rpm using the survivable ribbed cup bearing. The oil-off lives at 37000 rpm were less than 10 seconds. The grinding of the powder metal materials and surface preparation to achieve an open porosity is extremely critical to the oil-off performance of the powder metal component. Author

N88-11181* # National Aeronautics and Space Administration. Lewis Research Center, Cleveland, OH.

COATING LIFE PREDICTION

JAMES A. NESBITT and MICHAEL A. GEDWILL In its Turbine Engine Hot Section Technology, 1985 p 397-404 Oct. 1985
Avail: NTIS HC A19/MF A01 CSCL 131

The investigation combines both experimental studies and numerical modeling to predict coating life in an oxidizing environment. The experimental work provides both input to and verification of two numerical models. The coatings being examined are an aluminide coating on Udimet 700 (U-700), a low-pressure plasma spray (LPPS) Ni-18Co-17Cr-24Al-0.2Y overlay coating also on U-700, and bulk deposits of the LPPS NiCoCrAlY coating. Author

N88-11182* # National Aeronautics and Space Administration. Lewis Research Center, Cleveland, OH.

THERMAL EXPANSION MISMATCH AND OXIDATION IN THERMAL BARRIER COATINGS

G. C. CHANG, W. PHUCHAROEN (Cleveland State Univ., Ohio.), and R. A. MILLER In its Turbine Engine Hot Section Technology, 1985 p 405-425 Oct. 1985
(Contract NCC3-27)

Avail: NTIS HC A19/MF A01 CSCL 131

Thermal barrier coatings (TBC) for advanced gas turbine blades have been under intensive development during the last several years. This investigation is intended to achieve a clearer understanding of the mechanical behavior of plasma sprayed zirconia-yttria TBCs, involving a nickel-chromium-aluminum bond coat. The near term objectives are to study the stress states in a relatively simple model TBC subjected to steady state thermal loading. The resulting thermal expansion mismatch and oxidation have been primary targets for the study. The finite element approach and the effects of thermal mismatch and oxidation are described. A proposed mechanism for oxidation induced coating failure is also presented. Author

N88-11184* # General Electric Co., Evendale, OH. Aircraft Engine Business Group.

THERMAL BARRIER COATING LIFE PREDICTION MODEL DEVELOPMENT

R. V. HILLERY, B. H. PILSNER, and E. C. DUDERSTADT /in NASA. Lewis Research Center, Turbine Engine Hot Section Technology, 1985 p 433-444 Oct. 1985
(Contract NAS3-23943)
Avail: NTIS HC A19/MF A01 CSCL 131

The objectives are to determine the predominant modes of degradation of a plasma sprayed thermal barrier coating system, and then to develop and verify life prediction models accounting for these degradation modes. Two possible predominant failure mechanisms being evaluated are bond coat oxidation and bond coat creep. Author

N88-11185*# Pratt and Whitney Aircraft, East Hartford, CT.
THERMAL BARRIER COATING LIFE PREDICTION MODEL DEVELOPMENT

J. T. DEMASI and K. D. SHEFFLER /in NASA. Lewis Research Center, Turbine Engine Hot Section Technology, 1985 p 445-455 Oct. 1985
(Contract NAS3-23944)
Avail: NTIS HC A19/MF A01 CSCL 131

The objective is to develop an integrated life prediction model accounting for all potential life-limiting thermal barrier coating (TBC) degradation and failure modes, including spallation resulting from cyclic thermal stress, oxidation degradation, hot corrosion, erosion and foreign object damage. Author

N88-12796*# National Aeronautics and Space Administration. Lewis Research Center, Cleveland, OH.
MEASURED PERFORMANCE OF THE HEAT EXCHANGER IN THE NASA ICING RESEARCH TUNNEL UNDER SEVERE ICING AND DRY-AIR CONDITIONS

W. OLSEN, J. VANFOSSEN, and R. NUSSLE Dec. 1987 29 p
(NASA-TM-100116; E-3661; NAS 1.15:100116) Avail: NTIS HC A03/MF A01 CSCL 131

Measurements were made of the pressure drop and thermal performance of the unique refrigeration heat exchanger in the NASA Lewis Icing Research Tunnel (IRT) under severe icing and frosting conditions and also with dry air. This data will be useful to those planning to use or extend the capability of the IRT and other icing facilities (e.g., the Altitude Wind Tunnel-AWT). The IRT heat exchanger and refrigeration system is able to cool air passing through the test section down to at least a total temperature of -30 C (well below icing requirements), and usually up to -2 C. The system maintains a uniform temperature across the test section at all airspeeds, which is more difficult and time consuming at low airspeeds, at high temperatures, and on hot, humid days when the cooling towers are less efficient. The very small surfaces of the heat exchanger prevent any icing cloud droplets from passing through it and going through the tests section again. The IRT heat exchanger was originally designed not to be adversely affected by severe icing. During a worst-case icing test the heat exchanger iced up enough so that the temperature uniformity was no worse than about ± 1 deg C. The conclusion is that the heat exchanger design performs well. Author

N88-12797*# National Aeronautics and Space Administration. Lewis Research Center, Cleveland, OH.
ON DYNAMIC LOADS IN PARALLEL SHAFT TRANSMISSIONS. 1: MODELLING AND ANALYSIS

EDWARD HSIANG-HSI LIN, RONALD L. HUSTON, and JOHN J. COY (Army Aviation Research and Development Command, Cleveland, Ohio.) Dec. 1987 16 p
(NASA-TM-100180; E-3756; NAS 1.15:100180; AVSCOM-TM-87-C-2; AD-A189108) Avail: NTIS HC A03/MF A01 CSCL 131

A model of a simple parallel-shaft, spur-gear transmission is presented. The model is developed to simulate dynamic loads in power transmissions. Factors affecting these loads are identified. Included are shaft stiffness, local compliance due to contact stress, load sharing, and friction. Governing differential equations are developed and a solution procedure is outlined. A parameter study of the solutions is presented in NASA TM-100181 (AVSCOM TM-87-C-3). Author

N88-12798*# National Aeronautics and Space Administration. Lewis Research Center, Cleveland, OH.

ON DYNAMIC LOADS IN PARALLEL SHAFT TRANSMISSIONS. 2: PARAMETER STUDY

EDWARD HSIANG-HSI LIN, RONALD L. HUSTON, and JOHN J. COY (Army Aviation Research and Development Command, Cleveland, Ohio.) Dec. 1987 13 p
(NASA-TM-100181; E-3756; NAS 1.15:100181; AVSCOM-TM-87-C-3; AD-A189109) Avail: NTIS HC A03/MF A01 CSCL 131

Solutions to the governing equations of a spur gear transmission model, developed in NASA TM-100180 (AVSCOM TM-87-C-2), are presented. Factors affecting the dynamic load are identified. It is found that the dynamic load increases with operating speed up to a system natural frequency. At operating speeds beyond the natural frequency the dynamic load decreases dramatically. Also, it is found that the applied load and shaft inertia have little effect on the dynamic load. Damping and friction decrease the dynamic load. Finally, tooth stiffness has a significant effect on dynamic loading; the higher the stiffness, the lower the dynamic loading. Also, the higher the stiffness the higher the rotating speed required for dynamic response. Author

N88-13603*# Mechanical Technology, Inc., Latham, NY. Research and Development Div.

SEAL TECHNOLOGY FOR LIQUID OXYGEN (LOX) TURBOPUMPS Final Report, Feb. 1982 - Nov. 1985

WILBUR SHAPIRO and ROBERT HAMM Nov. 1985 388 p
(Contract NAS3-23260)
(NASA-CR-174866; NAS 1.26:174866; REPT-85TR20) Avail: NTIS HC A17/MF A01 CSCL 11A

Two types of advanced seals for liquid oxygen (LOX) turbopumps were investigated. One was a spiral-groove face seal whose function is to seal high-pressure LOX at the impeller end of the turbopump. The other was a floating-ring, Rayleigh-step, helium buffered seal used to prevent LOX ingress to the turbine side of the unit. For each seal type, two sizes were investigated (50 and 20 mm). A turbine-driven test rig was designed and manufactured, and a test program was completed on the 50 mm floating-ring, Rayleigh-step, helium buffered seal. Significant results were: vaporization in the flow path could cause failure by overheating; therefore, the spiral-groove pumping portion of the seal that provides the fluid film must circulate fluid without disruption if vaporization occurs in the sealing dam. This is successfully accomplished by a pressure-balanced spiral-groove concept that is described. The spiral-groove configuration is affected by turbulence in the fluid film and pressure drops due to fluid inertia at sudden contractions. The net results of these effects are deep grooves, large operating films, and high power loss when compared against seals operating with laminar films. Turbulence and inertia are induced by the high-density and low-viscosity characteristics of LOX. The program clearly pointed out the need to consider system environmental factors such as thermal and centrifugal distortions and rotor vibrations in the seal design. Author

N88-13604*# National Aeronautics and Space Administration. Lewis Research Center, Cleveland, OH.

FINITE-ELEMENT GRID IMPROVEMENT BY MINIMIZATION OF STIFFNESS MATRIX TRACE

MADAN G. KITTUR, RONALD L. HUSTON (Cincinnati Univ., Ohio.), and FRED B. OSWALD Dec. 1987 17 p Prepared in cooperation with Army Aviation Research and Development Command, St. Louis, Mo.
(NASA-TM-100255; E-3827; NAS 1.15:100255; AD-A190291) Avail: NTIS HC A03/MF A01 CSCL 20K

A new and simple method of finite-element grid improvement is presented. The objective is to improve the accuracy of the analysis. The procedure is based on a minimization of the trace of the stiffness matrix. For a broad class of problems this minimization is seen to be equivalent to minimizing the potential energy. The method is illustrated with the classical tapered bar problem examined earlier by Prager and Masur. Identical results are obtained. Author

37 MECHANICAL ENGINEERING

N88-15224*# National Aeronautics and Space Administration. Lewis Research Center, Cleveland, OH.

EFFICIENCY TESTING OF A HELICOPTER TRANSMISSION PLANETARY REDUCTION STAGE

ROBERT F. HANDSCHUH and DOUGLAS A. ROHN Feb. 1988 18 p Prepared in cooperation with Army Aviation Research and Development Command, Cleveland, Ohio (Contract DA PROJ. 1L1-61102-AH-45) (NASA-TP-2795; E-3770; NAS 1.60:2795; AVSCOM-TR-87-C-28; AD-A191884) Avail: NTIS HC A03/MF A01 CSCL 13I

A parametric study of the efficiency of a 310-kW (420-hp) helicopter transmission planetary test section (four planets) was performed. The purpose was to determine the planetary contribution to the overall transmission power loss. Test parameters varied were oil flow rate, oil inlet temperature, lubricant type, shaft speed, and applied torque. The measured efficiency over all the test variables ranged from 99.44 to 99.75 percent. These experimental results were compared with other experimental and computational results. Author

N88-15802*# National Aeronautics and Space Administration. Lewis Research Center, Cleveland, OH.

ROTORCRAFT TRANSMISSION

JOHN J. COY *In its Aeropropulsion '87. Session 5: Subsonic Propulsion Technology* 9 p Nov. 1987 Avail: NTIS HC A08/MF A01 CSCL 13I

The NASA Lewis Research Center and the U.S. Army Aviation Systems Command share an interest in advancing the technology for helicopter propulsion systems. In particular, this presentation outlines that portion of the program that applies to the drive train and its various mechanical components. The major goals of the program are to increase the life, reliability, and maintainability; reduce the weight, noise, and vibration; and maintain the relatively high mechanical efficiency of the gear train. The current activity emphasizes noise reduction technology and analytical code development followed by experimental verification. Selected significant advances in technology for transmissions are reviewed, including advanced configurations and new analytical tools. Finally, the plan for transmission research in the future is presented. Author

N88-16006*# Texas A&M Univ., College Station. Turbomachinery Labs.

A COMPARISON OF EXPERIMENTAL AND THEORETICAL RESULTS FOR LABYRINTH GAS SEALS WITH HONEYCOMB STATORS M.S. Thesis

LAWRENCE ALLEN HAWKINS May 1988 150 p (Contract NAG3-181) (NASA-CR-182441; NAS 1.26:182441; TL-SEAL-2-88) Avail: NTIS HC A07/MF A01 CSCL 13I

Experimental results for the rotordynamic stiffness and damping coefficients of a labyrinth-rotor honeycomb-stator seal are presented. The coefficients are compared to the coefficients of a labyrinth-rotor smooth-stator seal having the same geometry. The coefficients are compared to analytical results from a two-control-volume compressible flow model. The experimental results show that the honeycomb stator configuration is more stable than the smooth stator configuration at low rotor speeds. At high rotor speeds and low clearance, the smooth stator seal is more stable. The theoretical model predicts the cross-coupled stiffness of the honeycomb stator seal correctly within 25 percent of measured values. The model provides accurate predictions of direct damping for large clearance seals. Overall, the model does not perform as well for low clearance seals as for high clearance seals. Author

N88-16007*# Texas A&M Univ., College Station. Turbomachinery Labs.

EXPERIMENTAL ROTORDYNAMIC COEFFICIENT RESULTS FOR HONEYCOMB SEALS

DAVID A. ELROD and DARA W. CHILDS Jan. 1988 167 p (Contract NAG3-181)

(NASA-CR-182440; NAS 1.26:182440; TRC-SEAL-1-88) Avail: NTIS HC A08/MF A01 CSCL 13I

Test results (leakage and rotordynamic coefficients) are presented for seven honeycomb-stator smooth-rotor seals. Tests were carried out with air at rotor speeds up to 16,000 cpm and supply pressures up to 8.2 bars. Test results for the seven seals are compared, and the most stable configuration is identified based on the whirl frequency ratio. Results from tests of a smooth-rotor/smooth-stator seal, a teeth-on-stator labyrinth seal, and the most stable honeycomb seal are compared. Author

N88-17045*# National Aeronautics and Space Administration. Lewis Research Center, Cleveland, OH.

DYNAMIC ANALYSIS OF MULTIMESH-GEAR HELICOPTER TRANSMISSIONS

FRED K. CHOY, DENNIS P. TOWNSEND, and FRED B. OSWALD Feb. 1988 22 p (NASA-TP-2789; E-3191; NAS 1.60:2789) Avail: NTIS HC A03/MF A01 CSCL 13I

A dynamic analysis of multimesh-gear helicopter transmission systems was performed by correlating analytical simulations with experimental investigations. The two computer programs used in this study, GRDYNMLT and PGT, were developed under NASA/Army sponsorship. Parametric studies of the numerical model with variations on mesh damping ratios, operating speeds, tip-relief tooth modifications, and tooth-spacing errors were performed to investigate the accuracy, application, and limitations of the two computer programs. Although similar levels of dynamic loading were predicted by both programs, the computer code GRDYNMLT was found to be superior and broader in scope. Results from analytical work were also compared with experimental data obtained from the U.S. Army's UH-60A Black Hawk 2240-kW (3000-hp) class, twin-engine helicopter transmission tested at the NASA Lewis Research Center. Good correlation in gear stresses was obtained between the analytical model simulated by GRDYNMLT and the experimental measurements. More realistic mesh damping can be predicted through experimental data correlation. Author

N88-18007*# National Aeronautics and Space Administration. Lewis Research Center, Cleveland, OH.

CERAMIC BEARINGS FOR USE IN GAS TURBINE ENGINES

ERWIN V. ZARETSKY 1988 15 p Proposed for presentation at the 33rd International Gas Turbine and Aeroengine Congress and Exposition, Amsterdam, Netherlands, 5-9 Jun. 1988; sponsored by ASME (NASA-TM-100288; E-3934; NAS 1.15:100288) Avail: NTIS HC A03/MF A01 CSCL 13I

Three decades of research by U.S. industry and government laboratories have produced a vast body of data related to the use of ceramic rolling element bearings and bearing components for aircraft gas turbine engines. Materials such as alumina, silicon carbide, titanium carbide, silicon nitride, and a crystallized glass ceramic have been investigated. Rolling-element endurance tests and analysis of full-complement bearings have been performed. Materials and bearing design methods have continuously improved over the years. This paper reviews a wide range of data and analyses with emphasis on how early NASA contributions as well as more recent data can enable the engineer or metallurgist to determine just where ceramic bearings are most applicable for gas turbines. Author

N88-18933*# National Aeronautics and Space Administration. Lewis Research Center, Cleveland, OH.

COMPUTER-AIDED DESIGN ANALYSIS OF 57-MM, ANGULAR-CONTACT, CRYOGENIC TURBOPUMP BEARINGS

ELIZABETH S. ARMSTRONG and HAROLD H. COE Mar. 1988 15 p (NASA-TP-2816; E-3890; NAS 1.60:2816) Avail: NTIS HC A03/MF A01 CSCL 13K

The Space Shuttle main engine high-pressure oxygen turbopumps have not experienced the service life required of them. This insufficiency has been due in part to the shortened life of

the bearings. To improve the life of the existing turbopump bearings, an effort is under way to investigate bearing modifications that could be retrofitted into the present bearing cavity. Several bearing parameters were optimized using the computer program SHABERTH, which performs a thermomechanical simulation of a load support system. The computer analysis showed that improved bearing performance is feasible if low friction coefficients can be attained. Bearing geometries were optimized considering heat generation, equilibrium temperatures, and relative life. Thermal gradients through the bearings were found to be lower with liquid lubrication than with solid film lubrication, and a liquid oxygen coolant flowrate of approximately 4.0 kg/s was found to be optimal. This paper describes the analytical modeling used to determine these feasible modifications to improve bearing performance.

Author

N88-21454*# National Aeronautics and Space Administration. Lewis Research Center, Cleveland, OH.

ADVANCED TRANSMISSION STUDIES

JOHN J. COY and ROBERT C. BILL (Army Aviation Research and Development Command, Cleveland, Ohio.) 1988 15 p
Proposed for presentation at the 44th Annual Forum of the American Helicopter Society, Washington, D.C., 16-18 Jun. 1988 (Contract DA PROJ. 1L1-62209-AH-76)
(NASA-TM-100867; E-4089; NAS 1.15:100867;
AVSCOM-TR-88-C-002; AD-A197797) Avail: NTIS HC A03/MF A01 CSCL 13I

The NASA Lewis Research Center and the U.S. Army Aviation Systems Command share an interest in advancing the technology for helicopter propulsion systems. In particular, this paper presents highlights from that portion of the program in drive train technology and the related mechanical components. The major goals of the program are to increase the life, reliability, and maintainability; reduce the weight, noise, and vibration; and maintain the relatively high mechanical efficiency of the gear train. The current activity emphasizes noise reduction technology and analytical code development followed by experimental verification. Selected significant advances in technology for transmissions are reviewed, including advanced configurations and new analytical tools. Finally, the plan for future transmission research is presented.

Author

N88-23216*# Illinois Univ., Chicago. Dept. of Mechanical Engineering.

SPUR GEARS: OPTIMAL GEOMETRY, METHODS FOR GENERATION AND TOOTH CONTACT ANALYSIS (TCA) PROGRAM Final Report

FAYDOR L. LITVIN and JIAO ZHANG Apr. 1988 135 p
(Contract NAG3-655)
(NASA-CR-4135; E-3940; NAS 1.26:4135; AVSCOM-TR-88-C-002; AD-A197797) Avail: NTIS HC A07/MF A01 CSCL 13I

The contents of this report include the following: (1) development of optimal geometry for crowned spur gears; (2) methods for their generation; and (3) tooth contact analysis (TCA) computer programs for the analysis of meshing and bearing contact on the crowned spur gears. The method developed for synthesis is used for the determination of the optimal geometry for crowned pinion surface and is directed to reduce the sensitivity of the gears to misalignment, localize the bearing contact, and guarantee the favorable shape and low level of the transmission errors. A new method for the generation of the crowned pinion surface has been proposed. This method is based on application of the tool with a surface of revolution that slightly deviates from a regular cone surface. The tool can be used as a grinding wheel or as a shaver. The crowned pinion surface can also be generated by a generating plane whose motion is provided by an automatic grinding machine controlled by a computer. The TCA program simulates the meshing and bearing contact of the misaligned gears. The transmission errors are also determined.

Author

N88-23219*# National Aeronautics and Space Administration. Lewis Research Center, Cleveland, OH.

MICROGRAVITY ROBOTICS TECHNOLOGY PROGRAM

DOUGLAS A. ROHN, CHARLES LAWRENCE, and ANDREW S.

BRUSH (Sverdrup Technology, Inc., Cleveland, Ohio.) 1988 14 p
Proposed for presentation at the ISA/88 International Conference and Exhibit, Houston, Tex., 16-21 Oct. 1988; sponsored by the Instrument Society of America
(NASA-TM-100898; E-4148; NAS 1.15:100898) Avail: NTIS HC A03/MF A01 CSCL 13I

A research program to develop technology for robots operating in the microgravity environment of the space station laboratory is described. These robots must be capable of manipulating payloads without causing them to experience harmful levels of acceleration, and the motion of these robots must not disturb adjacent experiments and operations by transmitting reactions that translate into damaging effects throughout the laboratory. Solutions to these problems, based on both mechanism technology and control strategies, are discussed. Methods are presented for reduction of robot base reactions through the use of redundant degrees of freedom, and the development of smoothly operating roller-driven robot joints for microgravity manipulators is discussed.

Author

N88-23220*# National Aeronautics and Space Administration. Lewis Research Center, Cleveland, OH.

COMPUTERIZED LIFE AND RELIABILITY MODELLING FOR TURBOPROP TRANSMISSIONS

M. SAVAGE, K. C. RADIL, D. G. LEWICKI (Army Aviation Research and Development Command, St. Louis, Mo.), and J. J. COY 1988 17 p
Presented at the 24th Joint Propulsion Conference, Boston, Mass., 11-13 Jul. 1988; sponsored by AIAA, ASME, ASSE, and SAE
(Contract DA PROJ. 1L1-61102-AH-45)
(NASA-TM-100918; E-4173; NAS 1.15:100918;
AVSCOM-TR-87-C-37; AIAA-88-2979; AD-A195935) Avail: NTIS HC A03/MF A01 CSCL 13I

A generalized life and reliability model is presented for parallel shaft geared prop-fan and turboprop aircraft transmissions. The transmission life and reliability model is a combination of the individual reliability models for all the bearings and gears in the main load paths. The bearing and gear reliability models are based on classical fatigue theory and the two parameter Weibull failure distribution. A computer program was developed to calculate the transmission life and reliability. The program is modular. In its present form, the program can analyze five different transmission arrangements. However, the program can be modified easily to include additional transmission arrangements. An example is included which compares the life of a compound two-stage transmission with the life of a split-torque, parallel compound two-stage transmission, as calculated by the computer program.

Author

N88-23238*# Carnegie-Mellon Univ., Pittsburgh, PA. Dept. of Mechanical Engineering.

BASE REACTION OPTIMIZATION OF MANIPULATORS WITH REDUNDANT KINEMATICS

C. L. CHUNG and S. DESA /in NASA, Lewis Research Center, Lewis Structures Technology, 1988. Volume 1: Structural Dynamics p 157-173 May 1988
(Contract NAG3-811)
Avail: NTIS HC A20/MF A01 CSCL 13I

A trajectory generation method for space manipulators is introduced. The approach developed employs a manipulator with redundant kinematics. The method is implemented in two steps. First, the end-effector trajectory is developed to satisfy motion requirements. Next, the joint trajectories are developed to minimize base reactions. The analytical development of this method is described and an example illustrating the method is presented.

Author

N88-23242*# Army Aviation Systems Command, Cleveland, OH. Structural Dynamics Branch.

MICROGRAVITY MANIPULATOR DEMONSTRATION

ANDREW S. BRUSH (Sverdrup Technology, Inc., Cleveland, Ohio.) /in NASA, Lewis Research Center, Lewis Structures Technology, 1988. Volume 1: Structural Dynamics p 217-227 May

37 MECHANICAL ENGINEERING

1988

(Contract NAS3-24105)

Avail: NTIS HC A20/MF A01 CSCL 13I

A test rig is being developed that will be used to demonstrate and evaluate approaches to limiting manipulator base reactions in microgravity environments. The demonstration will include a 4-degrees-of-freedom arm, control computing facilities, and a base reaction measurement system. Author

N88-23243*# Cellulose Conversion Enterprises, Berkeley, CA.
**ACCURATE POSITIONING OF LONG, FLEXIBLE ARM'S
(ARTICULATED ROBOTIC MANIPULATOR)**

MICHAEL J. MALACHOWSKI /in NASA, Lewis Research Center, Lewis Structures Technology, 1988. Volume 1: Structural Dynamics p 129-244 May 1988

(Contract NAS3-25197)

Avail: NTIS HC A20/MF A01 CSCL 13I

An articulated robotic manipulator (ARM) system is being designed for space applications. Work being done on a concept utilizing an infinitely stiff laser beam for position reference is summarized. The laser beam is projected along the segments of the ARM, and the position is sensed by the beam rider modules (BRM) mounted on the distal ends of the segments. The BRM concept is the heart of the system. It utilizes a combination of lateral displacements and rotational and distance measurement sensors. These determine the relative position of the two ends of the segments with respect to each other in six degrees of freedom. The BRM measurement devices contain microprocessor controlled data acquisition and active positioning components. An indirect adaptive controller is used to accurately control the position of the ARM. Author

N88-23977*# National Aeronautics and Space Administration. Lewis Research Center, Cleveland, OH.

**VIBRATION AND CONTROL OF FLEXIBLE ROTOR
SUPPORTED BY MAGNETIC BEARINGS**

KENZOU NONAMI 1988 23 p Presented at the 1st International Conference on Magnetic Bearings, Zurich, Switzerland, 6-8 Jun. 1988; sponsored in part by the Swiss Federal Inst. of Technology, and the Swiss Society of Microtechnics (NASA-TM-100888; E-4123; NAS 1.15:100888) Avail: NTIS HC A03/MF A01 CSCL 13E

Active vibration control of flexible rotors supported by magnetic bearings is discussed. Using a finite-element method for a mathematical model of the flexible rotor, the eigenvalue problem is formulated taking into account the interaction between a mechanical system of the flexible rotor and an electrical system of the magnetic bearings and the controller. However, for the sake of simplicity, gyroscopic effects are disregarded. It is possible to adapt this formulation to a general flexible rotor-magnetic bearing system. Controllability with and without collocation sensors and actuators located at the same distance along the rotor axis is discussed for the higher order flexible modes of the test rig. In conclusion, it is proposed that it is necessary to add new active control loops for the higher flexible modes even in the case of collocation. Then it is possible to stabilize for the case of uncollocation by means of this method. Author

N88-23978* National Aeronautics and Space Administration. Lewis Research Center, Cleveland, OH.

**THERMAL STRESS MINIMIZED, TWO COMPONENT, TURBINE
SHROUD SEAL Patent**

ROBERT F. HANDSCHUH, inventor (to NASA) 1 Mar. 1988 12 p Filed 18 Jun. 1986 Supersedes N86-32740 (24 - 24, P 3735)

(NASA-CASE-LEW-14212-1; US-PATENT-4,728,257; US-PATENT-APPL-SN-875798; US-PATENT-CLASS-415-136; US-PATENT-CLASS-415-170-R) Avail: US Patent and Trademark Office CSCL 13I

In a turbine machine, a two-component shroud seal which maximizes insulation and sealing around the rotating turbine blades, and is made by independently fabricating each of the two components then joining them together, is disclosed. The two

components may be joined together at room temperature. The resulting shroud seal provides greater engine efficiency and thrust. Official Gazette of the U.S. Patent and Trademark Office

N88-24968*# National Aeronautics and Space Administration. Lewis Research Center, Cleveland, OH.

DEVELOPMENT OF A LIQUID-FED WATER RESISTOJET

W. EARL MORREN and JAMES R. STONE 1988 20 p Presented at the 24th Joint Propulsion Conference, Boston, Mass., 11-13 Jul. 1988; sponsored by AIAA, ASME, SAE and ASEE (NASA-TM-100927; E-4192; NAS 1.15:100927; AIAA-88-3288)

Avail: NTIS HC A03/MF A01 CSCL 13I

A concept for a forced-flow once-through water vaporizer for application to resistojet thrusters was evaluated as an element of a laboratory model thruster and tested to investigate its operating characteristics. The vaporizer design concept employs flow swirling to attach the liquid flow to the boiler chamber wall, providing for separation of the two liquid phases. This vaporizer was modified with a nozzle and a centrally-located heater to facilitate vaporization, superheating, and expansion of the propellant, allowing it to function as a resistojet. Performance was measured at thrust levels ranging from 170 to 360 mN and at power levels ranging from 443 to 192 W. Maximum measured specific impulse was 192 sec. Author

N88-24975*# Transmission Technology Co., Inc., Fairfield, NJ.

**DESIGN, MANUFACTURE AND SPIN TEST OF HIGH
CONTACT RATIO HELICOPTER TRANSMISSION UTILIZING
SELF-ALIGNING BEARINGLESS PLANETARY (SABP) Final
Contractor Report**

DEZI FOLENTA and WILLIAM LEBOW Washington NASA Jun. 1988 112 p

(Contract NAS3-24539; DA PROJ. 1L1-62209-AH-76)

(NASA-CR-4155; E-4049; NAS 1.26:4155; TTC-87-07R;

AVSCOM-TR-88-C-009; AD-A199405) Avail: NTIS HC A06/MF A01 CSCL 13I

A 450 hp high ratio Self-Aligning Bearingless Planetary (SABP) for a helicopter application was designed, manufactured, and spin tested under NASA contract NAS3-24539. The objective of the program was to conduct research and development work on a high contact ratio helical gear SABP to reduce weight and noise and to improve efficiency. The results accomplished include the design, manufacturing, and no-load spin testing of two prototype helicopter transmissions, rated at 450 hp with an input speed of 35,000 rpm and an output speed of 350 rpm. The weight power density ratio of these gear units is 0.33 lb hp. The measured airborne noise at 35,000 rpm input speed and light load is 94 dB at 5 ft. The high speed, high contact ratio SABP transmission appears to be significantly lighter and quieter than contemporary helicopter transmissions. The concept of the SABP is applicable not only to high ratio helicopter type transmissions but also to other rotorcraft and aircraft propulsion systems. Author

N88-24976*# Illinois Univ., Chicago.

**DETERMINATION OF SETTINGS OF A TILTED HEAD-CUTTER
FOR GENERATION OF HYPOID AND SPIRAL BEVEL GEARS
Final Report**

F. L. LITVIN, Y. ZHANG, M. LUNDY, and C. HEINE (Dana Corp., Fort Wayne, Ind.) Jun. 1988 27 p

(Contract NAG3-783)

(NASA-CR-182138; NAS 1.26:182138; AVSCOM-TR-88-C-016;

AD-A196985) Avail: NTIS HC A03/MF A01 CSCL 13I

Kinematics of Gleason mechanisms of hypoid and spiral bevel cutting machines are considered. These mechanisms are designated to install the position and tilt of the head cutter. The tilt of the head cutter with standard blades provides the required pressure angle. The authors have developed the matrix presentation of kinematics of these mechanisms and basic equations for the required settings. An example is presented based on the developed computation procedure. Author

N88-25916*# National Aeronautics and Space Administration. Lewis Research Center, Cleveland, OH.

SURFACE FATIGUE LIFE OF CBN AND VITREOUS GROUND CARBURIZED AND HARDENED AISI 9310 SPUR GEARS

DENNIS P. TOWNSEND and P. R. PATEL (Textron Bell Helicopter, Fort Worth, Tex.) 1988 13 p Proposed for presentation at the International Off Highway and Powerplant Congress and Exposition, Milwaukee, Wis., 12-15 Sep. 1988; sponsored by the Society of Automotive Engineers Prepared in cooperation with Army Aviation Research and Development Command, Cleveland, Ohio

(Contract DA PROJ. 1L1-62209-A-47-A)

(NASA-TM-100960; E-4185; NAS 1.15:100960;

AVSCOM-TR-88-C-019) Avail: NTIS HC A03/MF A01 CSCL 131

Spur gear surface endurance tests were conducted to investigate CBN ground AISI 9310 spur gears for use in aircraft applications, to determine their endurance characteristics and to compare the results with the endurance of standard vitreous ground AISI 9310 spur gears. Tests were conducted with VIM-VAR AISI 9310 carburized and hardened gears that were finish ground with either CBN or vitreous grinding methods. Test conditions were an inlet oil temperature of 320 K (116 F), an outlet oil temperature of 350 K (170 F), a maximum Hertz stress of 1.71 GPa (248 ksi), and a speed of 10,000 rpm. The CBN ground gears exhibited a surface fatigue life that was slightly better than the vitreous ground gears. The subsurface residual stress of the CBN ground gears was approximately the same as that for the standard vitreous ground gears for the CBN grinding method used. Author

N88-25921*# Texas A&M Univ., College Station. Turbomachinery Lab.

ENTRANCE AND EXIT REGION FRICTION FACTOR MODELS FOR ANNULAR SEAL ANALYSIS Ph.D. Thesis

DAVID ALAN ELROD Aug. 1988 81 p

(Contract NAG3-181)

(NASA-CR-183084; NAS 1.26:183084; TL-SEAL-5-88) Avail:

NTIS HC A05/MF A01 CSCL 131

The Mach number definition and boundary conditions in Nelson's nominally-centered, annular gas seal analysis are revised. A method is described for determining the wall shear stress characteristics of an annular gas seal experimentally. Two friction factor models are developed for annular seal analysis; one model is based on flat-plate flow theory; the other uses empirical entrance and exit region friction factors. The friction factor predictions of the models are compared to experimental results. Each friction model is used in an annular gas seal analysis. The seal characteristics predicted by the two seal analyses are compared to experimental results and to the predictions of Nelson's analysis. The comparisons are for smooth-rotor seals with smooth and honeycomb stators. The comparisons show that the analysis which uses empirical entrance and exit region shear stress models predicts the static and stability characteristics of annular gas seals better than the other analyses. The analyses predict direct stiffness poorly. Author

N88-26675*# Ohio State Univ., Columbus. Dept. of Mechanical Engineering.

A REVIEW OF GEAR HOUSING DYNAMICS AND ACOUSTICS LITERATURE Technical Report, Mar. - Dec. 1987

RAJENDRA SINGH and TEIK CHIN LIM Jul. 1988 85 p

(Contract NAG3-773)

(NASA-CR-183110; NAS 1.26:183110) Avail: NTIS HC A05/MF A01 CSCL 131

A review of the available literature on gear housing vibration and noise reduction is presented. Analytical and experimental methodologies used for bearing dynamics, housing vibration and noise, mounts and suspensions, and the overall geared and housing system are discussed. Typical design guidelines as outlined by various investigators are given. Author

N88-26679*# National Aeronautics and Space Administration. Lewis Research Center, Cleveland, OH.

CONTACT FORCE HISTORY AND DYNAMIC RESPONSE DUE TO THE IMPACT OF A SOFT PROJECTILE

J. E. GRADY Aug. 1988 23 p

(NASA-TM-100961; E-4035; NAS 1.15:100961) Avail: NTIS HC A03/MF A01 CSCL 131

A series of ballistic impact tests on several different instrumented targets was performed to characterize the dynamic contact force history resulting from the impact of a compliant projectile. The results show that the variation of contact force history with impact velocity does not follow the trends predicted by classical impact models. An empirical model was therefore developed to describe this behavior. This model was then used in a finite-element analysis to estimate the force history and calculate the resulting dynamic strain response in a transversely impacted composite laminate. Author

N88-28312*# National Aeronautics and Space Administration. Lewis Research Center, Cleveland, OH.

APPLICATIONS OF AN EXPONENTIAL FINITE DIFFERENCE TECHNIQUE

ROBERT F. HANDSCHUH and THEO G. KEITH, JR. (Toledo Univ., Ohio.) Jul. 1988 28 p

(NASA-TM-100939; E-4006; AVSCOM-TM-88-C-004; NAS

1.15:100939; AD-A199197) Avail: NTIS HC A03/MF A01

CSCL 12A

An exponential finite difference scheme first presented by Bhattacharya for one dimensional unsteady heat conduction problems in Cartesian coordinates was extended. The finite difference algorithm developed was used to solve the unsteady diffusion equation in one dimensional cylindrical coordinates and was applied to two and three dimensional conduction problems in Cartesian coordinates. Heat conduction involving variable thermal conductivity was also investigated. The method was used to solve nonlinear partial differential equations in one and two dimensional Cartesian coordinates. Predicted results are compared to exact solutions where available or to results obtained by other numerical methods. Author

N88-28319*# Sikorsky Aircraft, Stratford, CT.

DESIGN AND EVALUATION OF HIGH CONTACT RATIO GEARING Final Report

HAROLD K. FRINT Jul. 1986 44 p

(Contract NAS3-17859)

(NASA-CR-174958; NAS 1.26:174958) Avail: NTIS HC A03/MF A01 CSCL 131

Scoring test and surface fatigue tests were conducted on spur gears of a standard design and spur gears of a high contact ratio design. All testing was conducted in the Sikorsky 6-inch dynamic test facility at a speed of 8000 rpm using 23699 oil. Bulk gear temperatures were also recorded. The surface fatigue tests were run at Hertz stresses of 165 x 10 to the 7th power N/sq m and 145 x 10 to the 7th power N/sq m (240,000 and 210,000 psi), respectively. Author

N88-30128*# National Aeronautics and Space Administration. Lewis Research Center, Cleveland, OH.

HELICOPTER TRANSMISSION RESEARCH AT NASA LEWIS RESEARCH CENTER

JOHN J. COY, DENNIS P. TOWNSEND, DAVID G. LEWICKI (Army Aviation Systems Command, Cleveland, Ohio.), and HAROLD H. COE 1988 19 p Prepared for presentation at the International Conference on Gearing, Zhengzhou, Peoples Republic of China, 5-10 Nov. 1988; sponsored in part by the Chinese Mechanical Engineering Society

(Contract DA PROJ. 1L1-62209-A-47-A)

(NASA-TM-100962; E-4181; AVSCOM-TM-88-C-003; NAS

1.15:100962) Avail: NTIS HC A03/MF A01 CSCL 131

A joint helicopter transmission research program between NASA Lewis Research Center and the U.S. Army Aviation Systems Command has existed since 1970. Program goals are to reduce weight and noise and to increase life and reliability. Reviewed are

38 QUALITY ASSURANCE AND RELIABILITY

significant advances in technology for gears and transmissions and the experimental facilities at NASA Lewis for helicopter transmission testing are described. A description of each of the rigs is presented along with some significant results from the experiments. Author

38

QUALITY ASSURANCE AND RELIABILITY

Includes product sampling procedures and techniques; and quality control.

A88-12581* General Motors Corp., Indianapolis, IN. **CORRELATION BETWEEN ULTRASONIC VELOCITY AND DENSITY OF CERAMIC TURBINE BLADES**

P. K. KHANDELWAL and P. W. HEITMAN (General Motors Corp., Allison Gas Turbine Div., Indianapolis, IN) Ceramic Engineering and Science Proceedings (ISSN 0196-6219), vol. 8, July-Aug. 1987, p. 483-492.
(Contract DEN3-17; DEN3-168)

A computer-aided ultrasonic velocity measurement system to detect small density variations in structural ceramic materials has been developed. Longitudinal wave ultrasonic velocity and density of ceramic turbine blades and bars were measured and statistically correlated. Density variations of 1 to 2 percent were reliably detected. Burst speed of ceramic blades was inversely proportional to the grain size of the material. Author

A88-18158* National Aeronautics and Space Administration. Lewis Research Center, Cleveland, OH.

ULTRASONIC NONDESTRUCTIVE EVALUATION, MICROSTRUCTURE, AND FRACTURE TOUGHNESS INTERRELATIONS

ALEX VARY (NASA, Lewis Research Center, Cleveland, OH) IN: Solid mechanics research for quantitative non-destructive evaluation. Dordrecht, Martinus Nijhoff Publishers, 1987, p. 135-152. Previously announced in STAR as N85-10371. refs

Ultrasonic techniques for mechanical property characterizations are reviewed and conceptual models are advanced for explaining and interpreting the empirically based results. At present, the technology is generally empirically based and is emerging from the research laboratory. Advancement of the technology will require establishment of theoretical foundations for the experimentally observed interrelations among ultrasonic measurements, mechanical properties, and microstructure. Conceptual models are applied to ultrasonic assessment of fracture toughness to illustrate an approach for predicting correlations found among ultrasonic measurements, microstructure, and mechanical properties. Author

A88-21340*# National Aeronautics and Space Administration. Lewis Research Center, Cleveland, OH.

ULTRASONIC EVALUATION OF MECHANICAL PROPERTIES OF THICK, MULTILAYERED, FILAMENT-WOUND COMPOSITES

H. E. KAUTZ (NASA, Lewis Research Center, Cleveland, OH) Materials Evaluation (ISSN 0025-5327), vol. 45, Dec. 1987, p. 1404-1412. Previously announced in STAR as N86-10561. refs

A preliminary investigation is conducted to define capabilities and limitations of ultrasonic and acousto-ultrasonic measurements related to mechanical properties of filament wound graphite/epoxy composite structures. The structures studied are segments of filament wound cylinders formed of multiple layers of hoop and helical windings. The segments consist of 24 to 35 layers and range from 3.02 to 3.34 cm in wall thickness. The resultant structures are anisotropic, heterogeneous, porous, and highly attenuating to ultrasonic frequencies greater than 1 MHz. The segments represent structures to be used for Space Shuttle booster cases. Ultrasonic velocity and acousto-ultrasonic stress wave factor

measurement approaches are discussed. Correlations among velocity, density, and porosity, and between the acousto-ultrasonic stress wave factor and interlaminar shear strength are presented.

Author

A88-30425* National Aeronautics and Space Administration. Lewis Research Center, Cleveland, OH.

DETERMINATION OF GRAIN-SIZE DISTRIBUTION FUNCTION USING TWO-DIMENSIONAL FOURIER TRANSFORMS OF TONE-PULSE-ENCODED IMAGES

E. R. GENERAZIO (NASA, Lewis Research Center, Cleveland, OH) Materials Evaluation (ISSN 0025-5327), vol. 46, March 1988, p. 528-534. Previously announced in STAR as N86-31065. refs

Microstructural images may be tone pulse encoded and subsequently Fourier transformed to determine the two-dimensional density of frequency components. A theory is developed relating the density of frequency components to the density of length components. The density of length components corresponds directly to the actual grain-size distribution function from which the mean grain shape, size, and orientation can be obtained.

Author

A88-44853* National Aeronautics and Space Administration. Lewis Research Center, Cleveland, OH.

MATERIALS ANALYSIS BY ULTRASONICS: METALS, CERAMICS, COMPOSITES

ALEX VARY, ED. (NASA, Lewis Research Center, Cleveland, OH) Park Ridge, NJ, Noyes Data Corp., 1987, 364 p. Previously announced in STAR as N86-22962; No individual items are abstracted in this volume.

Research results in analytical ultrasonics for characterizing structural materials from metals and ceramics to composites are presented. General topics covered by the conference included: status and advances in analytical ultrasonics for characterizing material microstructures and mechanical properties; status and prospects for ultrasonic measurements of microdamage, degradation, and underlying morphological factors; status and problems in precision measurements of frequency-dependent velocity and attenuation for materials analysis; procedures and requirements for automated, digital signal acquisition, processing, analysis, and interpretation; incentives for analytical ultrasonics in materials research and materials processing, testing, and inspection; and examples of progress in ultrasonics for interrelating microstructure, mechanical properties, and dynamic response.

Author

A88-46828* Virginia Polytechnic Inst. and State Univ., Blacksburg.

ACOUSTO-ULTRASONICS AS A MONITOR OF MATERIAL ANISOTROPY

J. C. DUKE, JR. (Virginia Polytechnic and State University, Blacksburg) and M. T. KIERNAN Materials Evaluation (ISSN 0025-5327), vol. 46, July 1988, p. 1105-1113. refs
(Contract NAG3-172)

This paper discusses experimental results obtained by performing the acousto-ultrasonic (AU) method at various azimuthal angles on the surface of fiber-reinforced composite plates. The use of an IBM-PC/data-acquisition board to obtain a digitized AU signal to be analyzed by specially developed software is described. An introduction is given to the use of AU parameters to quantify information evidenced in amplitude/frequency plots. A description of how the parameters are obtained by calculating various spectral moments and the area under particular ranges of the spectral density curve is presented. Results are given from voltage/time plots, amplitude/frequency plots, and plots showing the variation of calculated AU parameters with azimuthal angle. Finally, how the variation of AU parameters with azimuthal angle may be related to variation in material properties with azimuthal angle is discussed. Author

N88-12106*# National Aeronautics and Space Administration. Lewis Research Center, Cleveland, OH.

FLAW IMAGING AND ULTRASONIC TECHNIQUES FOR CHARACTERIZING SINTERED SILICON CARBIDE

GEORGE Y. BAAKLINI (Cleveland State Univ., Ohio.) and PHILLIP B. ABEL Aug. 1987 21 p Presented at the Conference on Nondestructive Testing of High-Performance Ceramics, Boston, Mass., 25-27 Aug. 1987; sponsored in part by American Ceramic Society and the American Society for Nondestructive Testing (NASA-TM-100177; E-3753; NAS 1.15:100177) Avail: NTIS HC A03/MF A01 CSCL 14D

The capabilities were investigated of projection microfocus x-radiography, ultrasonic velocity and attenuation, and reflection scanning acoustic microscopy for characterizing silicon carbide specimens. Silicon carbide batches covered a range of densities and different microstructural characteristics. Room temperature, four point flexural strength tests were conducted. Fractography was used to identify types, sizes, and locations of fracture origins. Fracture toughness values were calculated from fracture strength and flaw characterization data. Detection capabilities of radiography and acoustic microscopy for fracture-causing flaws were evaluated. Applicability of ultrasonics for verifying material strength and toughness was examined. Author

N88-15257*# National Aeronautics and Space Administration. Lewis Research Center, Cleveland, OH.

IMAGING SUBTLE MICROSTRUCTURAL VARIATIONS IN CERAMICS WITH PRECISION ULTRASONIC VELOCITY AND ATTENUATION MEASUREMENTS

EDWARD R. GENERAZIO, DON J. ROTH, and GEORGE Y. BAAKLINI Nov. 1987 11 p Presented at the Review of Progress in Quantitative NDE, Williamsburg, Va., 21-26 Jun. 1987; sponsored by Iowa State Univ. (NASA-TM-100129; E-3710; NAS 1.15:100129) Avail: NTIS HC A03/MF A01 CSCL 14D

Acoustic images of a silicon carbide ceramic disk were obtained using a precision scanning contact pulse echo technique. Phase and cross-correlation velocity, and attenuation maps were used to form color images of microstructural variations. These acoustic images reveal microstructural variations not observable with X-ray radiography. Author

N88-22412*# National Aeronautics and Space Administration. Lewis Research Center, Cleveland, OH.

NONDESTRUCTIVE EVALUATION BY ACOUSTO-ULTRASONICS

HAROLD E. KAUTZ In its Lewis Structures Technology, 1988. Volume 3: Structural Integrity Fatigue and Fracture Wind Turbines HOST p 67-77 May 1988 Avail: NTIS HC A16/MF A01 CSCL 14D

Acousto-ultrasonics is an ultrasonic technique that was originally devised to cope with the particular problems associated with nondestructive evaluation (NDE) of fiber/polymer composite structures. The fiber/polymer composites are more attenuating to ultrasound than any other material presently of interest. This limits the applicability of high-frequency ultrasonics. A common use of ultrasound is the imaging of flaws internal to a structure by scattering from the interface with the flaw. However, structural features of composites can scatter ultrasound internally, thus obscuring the flaws. A need relative to composites is to be able to nondestructively measure the strength of laminar boundaries in order to assess the integrity of a structure. Acousto-ultrasonics has exhibited the ability to use the internal scattering to provide information for determining the strength of laminar boundaries. Analysis of acousto-ultrasonic signals by the wave ray paths that compose it leads to waveform partitioning that enhances the sensitivity to mechanical strength parameters. Author

N88-22413*# National Aeronautics and Space Administration. Lewis Research Center, Cleveland, OH.

CHARACTERIZATION OF SINTERED SIC BY USING NDE

GEORGE Y. BAAKLINI In its Lewis Structures Technology, 1988.

Volume 3: Structural Integrity Fatigue and Fracture Wind Turbines HOST p 79-91 May 1988

Avail: NTIS HC A16/MF A01 CSCL 14D

Capabilities of projection microfocus X-radiography and of ultrasonic velocity and attenuation for characterizing silicon carbide specimens were assessed. Silicon carbide batches covered a range of densities and different microstructural characteristics. Room-temperature, four-point flexural strength tests were conducted. Fractography was used to identify types, sizes, and locations of fracture origins. Fracture toughness values were calculated from fracture strength and flaw characterization data. Detection capabilities of radiography for fracture-causing flaws were evaluated. Applicability of ultrasonics for verifying material strength and toughness was examined. Radiography proved useful in detecting high-density inclusions and isolated voids, but failed in detecting surface and subsurface agglomerates and large grains as fracture origins. Ultrasonic velocity dependency on density was evident. Attenuation dependency on density and mean pore size was clearly demonstrated. Understanding attenuation as a function of toughness was limited by shortcomings in K sub IC determination. Author

N88-22414*# National Aeronautics and Space Administration. Lewis Research Center, Cleveland, OH.

SYSTEMS FOR ULTRASONIC SCANNING, ANALYSIS AND IMAGERY

DAVID B. STANG, EDWARD R. GENERAZIO, and STEVE ABE (Cleveland State Univ., Ohio.) In its Lewis Structures Technology, 1988. Volume 3: Structural Integrity Fatigue and Fracture Wind Turbines HOST p 93-105 May 1988 (Contract NAS3-24105; NCC3-24) Avail: NTIS HC A16/MF A01 CSCL 14D

A variety of ultrasonic scanning and imagery techniques are used to investigate various aspects of materials and microstructures. Two ultrasonic scanning systems are in use by the Lewis Research Center's Structural Integrity Branch: an immersion scanner and a contact scanning system. The basic principles of scanning are reviewed, examples of images are presented, and structural features suggested by these images are discussed. Both of these systems are custom designed; their capabilities, advantages, and disadvantages are highlighted. Author

N88-22415*# National Aeronautics and Space Administration. Lewis Research Center, Cleveland, OH.

FLAW CHARACTERIZATION IN STRUCTURAL CERAMICS USING SCANNING LASER ACOUSTIC MICROSCOPY

DON J. ROTH In its Lewis Structures Technology, 1988. Volume 3: Structural Integrity Fatigue and Fracture Wind Turbines HOST p 107-122 May 1988 Avail: NTIS HC A16/MF A01 CSCL 14D

The ability of scanning laser acoustic microscopy (SLAM) to characterize artificially seeded voids in sintered silicon nitride structural ceramic specimens was investigated. The voids ranged from 20 to 430 microns in diameter and were embedded up to 2 mm beneath the surface of the specimens. Probability of detection was determined as a function of void depth and size. Trigonometric relationships and Airy's diffraction theory were used to obtain predictions of void depth and size from acoustic diffraction patterns produced by the voids. Agreement was observed between actual and predicted void depths. However, predicted void diameters were generally much greater than actual diameters. Precise diameter predictions are difficult to obtain because of measurement uncertainty and the limitations of the 100 MHz SLAM applied to typical ceramic specimens. Author

N88-22416*# National Aeronautics and Space Administration. Lewis Research Center, Cleveland, OH.

NONDESTRUCTIVE EVALUATION OF SINTERED CERAMICS

GEORGE Y. BAAKLINI, STANLEY J. KLIMA, and WILLIAM A. SANDERS In its Lewis Structures Technology, 1988. Volume 3: Structural Integrity Fatigue and Fracture Wind Turbines HOST p

38 QUALITY ASSURANCE AND RELIABILITY

123-133 May 1988

Avail: NTIS HC A16/MF A01 CSCL 14D

Radiography and several acoustic and thermoacoustic microscopy techniques are investigated for application to structural ceramics for advanced heat engines. A comparison is made of the results obtained from the use of scanning acoustic microscopy (SAM), scanning laser acoustic microscopy (SLAM), and thermoacoustic microscopy (TAM). These techniques are evaluated on research samples of green and sintered monolithic silicon nitrides and silicon carbides in the form of modulus-of-rupture (MOR) bars containing deliberately introduced flaws. Strengths and limitations of the techniques are described, with the emphasis being on statistics of detectability of flaws that constitute potential fracture origins. Further, it is shown that radiographic evaluation and guidance helped develop uniform high-density Si₃N₄ MOR bars with improved four-point flexural strength (875, 544, and 462 MPa at room temperature, 1200 C, 1370 C, respectively) and reduced scatter in bend strength. Author

N88-22425*# National Aeronautics and Space Administration. Lewis Research Center, Cleveland, OH.

LIFE PREDICTION MODELING BASED ON STRAINRANGE PARTITIONING

GARY R. HALFORD *In its* Lewis Structures Technology, 1988. Volume 3: Structural Integrity Fatigue and Fracture Wind Turbines HOST p 231-244 May 1988

Avail: NTIS HC A16/MF A01 CSCL 14D

Strainrange partitioning (SRP) is an integrated low-cycle-fatigue life predicting system. It was created specifically for calculating cyclic crack initiation life under severe high-temperature fatigue conditions. The key feature of the SRP system is its recognition of the interacting mechanisms of cyclic inelastic deformation that govern cyclic life at high temperatures. The SRP system bridges the gap between the mechanistic level of understanding that breeds new and better materials and the phenomenological level wherein workable engineering life prediction methods are in great demand. The system was recently expanded to address engineering fatigue problems in the low-strain, long-life, nominally elastic regime. This breakthrough, along with other advances in material behavior and testing technology, has permitted the system to also encompass low-strain thermomechanical loading conditions. Other important refinements of the originally proposed method include procedures for dealing with life-reducing effects of multiaxial loading, ratcheting, mean stresses, nonrepetitive (cumulative loading) loading, and environmental and long-time exposure. Procedure were also developed for partitioning creep and plastic strain and for estimating strainrange versus life relations from tensile and creep rupture properties. Each of the important engineering features of the SRP system are discussed and examples shown of how they help toward predicting high-temperature fatigue life under practical, although complex, loading conditions. Author

N88-22426*# Pratt and Whitney Aircraft, East Hartford, CT.

LIFE PREDICTION MODELING BASED ON CYCLIC DAMAGE ACCUMULATION

RICHARD S. NELSON *In* NASA. Lewis Research Center, Lewis Structures Technology, 1988. Volume 3: Structural Integrity Fatigue and Fracture Wind Turbines HOST p 245-257 May 1988 (Contract NAS3-23288)

Avail: NTIS HC A16/MF A01 CSCL 14D

A high temperature, low cycle fatigue life prediction method was developed. This method, Cyclic Damage Accumulation (CDA), was developed for use in predicting the crack initiation lifetime of gas turbine engine materials, where initiation was defined as a 0.030 inch surface length crack. A principal engineering feature of the CDA method is the minimum data base required for implementation. Model constants can be evaluated through a few simple specimen tests such as monotonic loading and rapid cycle fatigue. The method was expanded to account for the effects on creep-fatigue life of complex loadings such as thermomechanical fatigue, hold periods, waveshapes, mean stresses, multiaxiality, cumulative damage, coatings, and environmental attack. A significant data base was generated on the behavior of the cast

nickel-base superalloy B1900+Hf, including hundreds of specimen tests under such loading conditions. This information is being used to refine and extend the CDA life prediction model, which is now nearing completion. The model is also being verified using additional specimen tests on wrought INCO 718, and the final version of the model is expected to be adaptable to most any high-temperature alloy. The model is currently available in the form of equations and related constants. A proposed contract addition will make the model available in the near future in the form of a computer code to potential users. Author

N88-22428*# National Aeronautics and Space Administration. Lewis Research Center, Cleveland, OH.

LIFE AND RELIABILITY OF ROTATING DISKS

ERWIN V. ZARETSKY, TODD E. SMITH, and RICHARD AUGUST (Sverdrup Technology, Inc., Cleveland, Ohio.) *In its* Lewis Structures Technology, 1988. Volume 3: Structural Integrity Fatigue and Fracture Wind Turbines HOST p 271-284 May 1988 (Contract NAS3-24105)

Avail: NTIS HC A16/MF A01 CSCL 14D

In aerospace applications, an engineer must be especially cognizant of size and weight constraints which affect design decisions. Although designing at or below the material fatigue limit may be desirable in most industrial applications, in aerospace application it is almost mandatory to design certain components for a finite life at an acceptable probability of survival. Zaretsky outlined such a methodology based in part on the work of W. Weibull (1939, 1951) and G. Lundberg and A. Palmgren (1947a, 1947b, 1952). It is the objective of this work to apply the method of Zaretsky (1987) to statistically predict the life of a generic solid disk with and without bolt holes; determine the effect of disk design variables, thermal loads, and speed on relative life; and develop a generalized equation for determining disk life by incorporating only these variables. Author

N88-23224*# Massachusetts Inst. of Tech., Cambridge. Dept. of Mechanical Engineering.

ACOUSTO-ULTRASONIC INPUT-OUTPUT CHARACTERIZATION OF UNIDIRECTIONAL FIBER COMPOSITE PLATE BY SV WAVES Final Contractor Report

PETER LIAO and JAMES H. WILLIAMS, JR. Jun. 1988 89 p (Contract NAG3-328)

(NASA-CR-4152; E-3996; NAS 1.26:4152) Avail: NTIS HC A05/MF A01 CSCL 14D

A unidirectional fiberglass epoxy composite specimen is modelled as a homogeneous transversely isotropic continuum plate medium. Acousto-ultrasonic noncontact input-output characterization is studied theoretically with a transmitting and a receiving transducer located on the same face of the plate. The single reflection problem for an incident SV wave at a plane boundary in transversely isotropic medium is analyzed. An obliquely incident SV wave results in a reflected SV wave and a reflected P wave for an angle of incidence of the incident SV wave less than the critical angle. Otherwise, there exists only an SV wave in the medium as the reflected P wave degenerates into a surface wave travelling parallel to the plane boundary. The amplitude ratio of the reflected SV wave is -1 when the angle of incidence is greater than or = the critical angle. The directional dependence of the phase velocity of the SV wave propagating in the transversely isotropic medium has a significant effect on the delay time, as opposed to the directional independence of the phase velocity of a shear wave propagating in an isotropic medium. The displacements associated with the SV wave in the plate and which may be detected by the noncontact receiving transducer are approximated by an asymptotic solution for an infinite transversely isotropic medium subjected to a harmonic point load. Author

N88-23876*# National Aeronautics and Space Administration. Lewis Research Center, Cleveland, OH.

NONDESTRUCTIVE EVALUATION OF STRUCTURAL CERAMICS

ALEX VARY *In its* Structural Ceramics p 35-46 May 1986
Avail: NTIS HC A11/MF A01 CSCL 14D

Research on nondestructive evaluation (NDE) of structural ceramics for heat engine applications is reviewed. Microfocus radiography and scanning laser acoustic microscopy are the NDE techniques highlighted. The techniques were applied to research samples of sintered silicon nitride and silicon carbide in the form of modulus-of-rupture (MOR) bars. The strength and limitations of the aforementioned techniques are given in terms of probability of detection for voids in green and sintered MOR bars. Voids for this purpose were introduced by seeding green ceramic bars and characterizing each void in terms of its size, shape, location, and nature before and after sintering. The effects of material density, microstructure, surface finish, thickness, void depth, and size characteristics on detectability are summarized. Author

N88-23886*# Garrett Turbine Engine Co., Phoenix, AZ.
THERMAL CYCLIC DURABILITY TESTING OF CERAMIC MATERIALS FOR TURBINE ENGINES

L. J. LINDBERG / In NASA, Lewis Research Center, Structural Ceramics p 163-171 May 1986
 (Contract DEN3-27)
 Avail: NTIS HC A11/MF A01 CSCL 14D

The thermal cyclic durability of commercial ceramic materials for turbine engines was under evaluation since 1978. Ceramic materials are exposed to cyclic diesel-fired burner exhaust at either 1204 or 1371 C (2200 or 2500 F) for up to 3500 hours. The test conditions are selected to simulate the environment experienced by the hot flow path components in an automotive gas turbine engine. The silicon nitride and silicon carbide materials tested are the same ceramic materials currently used on the AGT100 and AGT101 ceramic turbine engine program. Author

N88-23985*# National Aeronautics and Space Administration.
 Lewis Research Center, Cleveland, OH.

HIGH FREQUENCY ULTRASONIC CHARACTERIZATION OF SINTERED SiC

GEORGE Y. BAAKLINI, EDWARD R. GENERAZIO, and JAMES D. KISER 1987 19 p Presented at the 11th Annual Conference on Composite and Advanced Ceramic Materials, Cocoa Beach, Fla., 18-23 Jan. 1987; sponsored by the American Ceramic Society
 (NASA-TM-100825; E-4013; NAS 1.15:100825) Avail: NTIS HC A03/MF A01 CSCL 14D

High frequency (60 to 160 MHz) ultrasonic nondestructive evaluation was used to characterize variations in density and microstructural constituents of sintered SiC bars. Ultrasonic characterization methods included longitudinal velocity, reflection coefficient, and precise attenuation measurements. The SiC bars were tailored to provide bulk densities ranging from 90 to 98 percent of theoretical, average grain sizes ranging from 3.0 to 12.0 microns, and average pore sizes ranging from 1.5 to 4.0 microns. Velocity correlated with specimen bulk density irrespective of specimen average grain size, average pore size, and average pore orientation. Attenuation coefficient was found to be sensitive to both density and average pore size variations, but was not affected by large differences in average grain size. Author

N88-23986*# Massachusetts Inst. of Tech., Cambridge. Dept. of Mechanical Engineering.

INPUT-OUTPUT CHARACTERIZATION OF FIBER COMPOSITES BY SH WAVES Final Contractor Report

JOHN D. RENNEISEN and JAMES H. WILLIAMS, JR. Washington NASA Jun. 1988 44 p
 (Contract NAG3-328)
 (NASA-CR-4153; E-4043; NAS 1.26:4153) Avail: NTIS HC A03/MF A01 CSCL 14D

Input-output characterization of fiber composites is studied theoretically by tracing SH waves in the media. A fiberglass epoxy composite is modeled as a homogeneous transversely isotropic continuum plate. The reflection of an SH wave at a stress-free plane boundary in a semi-infinite transversely isotropic medium is considered first. It is found that an incident SH wave reflects only a similar SH wave back into the medium. It is also established that the angle of reflection of the reflected wave is equal to the

angle of incidence of the incident wave. The phase velocity of the SH waves and the delay time of the SH waves in reaching the receiving transducer are computed as functions of a reflection index, defined as the number of reflections of the SH waves from the bottom face of the continuum plate. The directivity function corresponding to the shear stress associated with the SH waves in the continuum plate is also derived as a function of the reflection index. A theoretical output voltage from the receiving transducer is calculated for a tone burst (a periodic input voltage of finite duration). The output voltage is shown for tone bursts of duration 60 microseconds and center frequencies of 0.75, 1.00, and 1.25 MHz. The study enhances the quantitative and qualitative understanding of the nondestructive evaluation (NDE) of fiber composites which can be modeled as transversely isotropic media. Author

N88-23987*# Massachusetts Inst. of Tech., Cambridge. Dept. of Mechanical Engineering.

CHARACTERIZATION OF NONCONTACT PIEZOELECTRIC TRANSDUCER WITH CONICALLY SHAPED PIEZOELEMENT

JAMES H. WILLIAMS, JR. and SIMEON C. U. OCHI Washington, D.C. NASA Jun. 1988 88 p
 (Contract NAG3-328)
 (NASA-CR-4151; E-3995; NAS 1.26:4151) Avail: NTIS HC A05/MF A01 CSCL 14D

The characterization of a dynamic surface displacement transducer (IQI Model 501) by a noncontact method is presented. The transducer is designed for ultrasonic as well as acoustic emission measurements and, according to the manufacturer, its characteristic features include a flat frequency response range which is from 50 to 1000 kHz and a quality factor Q of less than unity. The characterization is based on the behavior of the transducer as a receiver and involves exciting the transducer directly by transient pulse input stress signals of quasi-electrostatic origin and observing its response in a digital storage oscilloscope. Theoretical models for studying the response of the transducer to pulse input stress signals and for generating pulse stress signals are presented. The characteristic features of the transducer which include the central frequency f , quality factor Q, and flat frequency response range are obtained by this noncontact characterization technique and they compare favorably with those obtained by a tone burst method which are also presented. Author

N88-24491*# National Aeronautics and Space Administration.
 Lewis Research Center, Cleveland, OH.

FATIGUE FAILURE OF REGENERATOR SCREENS IN A HIGH FREQUENCY STIRLING ENGINE

DAVID R. HULL, DONALD L. ALGER, THOMAS J. MOORE, and COULSON M. SCHEUERMANN / In New Mexico Univ., Transactions of the Fifth Symposium on Space Nuclear Power Systems p 575-578 1988 Previously announced as N87-18882
 Avail: NTIS HC A99/MF A01 CSCL 14D

Failure of Stirling Space Power Demonstrator Engine (SPDE) regenerator screens was investigated. After several hours of operation the SPDE was shut down for inspection and on removing the regenerator screens, debris of unknown origin was discovered along with considerable cracking of the screens in localized areas. Metallurgical analysis of the debris determined it to be cracked-off-deformed pieces of the 41 micron thickness Type 304 stainless steel wire screen. Scanning electron microscopy of the cracked screens revealed failures occurring at wire crossovers and fatigue striations on the fracture surface of the wires. Thus, the screen failure can be characterized as a fatigue failure of the wires. The crossovers were determined to contain 30 percent reduction in wire thickness and a highly worked microstructure occurring from the manufacturing process of the wire screens. Later it was found that reduction in wire thickness occurred because the screen fabricator had subjected it to a light cold-roll process after weaving. Installation of this screen left a clearance in the regenerator allowing the screens to move. The combined effects

38 QUALITY ASSURANCE AND RELIABILITY

of the reduction in wire thickness, stress concentration (caused by screen movement), and highly worked microstructure at the wire crossovers led to the fatigue failure of the screens. Author

N88-25923* Massachusetts Inst. of Tech., Cambridge. Dept. of Mechanical Engineering.

ACOUSTO-ULTRASONIC INPUT-OUTPUT CHARACTERIZATION OF UNIDIRECTIONAL FIBER COMPOSITE PLATE BY P WAVES Final Report

PETER LIAO and JAMES H. WILLIAMS, JR. Jul. 1988 78 p
(Contract NAG3-328)
(NASA-CR-4162; E-4208; NAS 1.26:4162) Avail: NTIS HC A05/MF A01 CSCL 14D

The single reflection problem for an incident P wave at a stress free plane boundary in a semi-infinite transversely isotropic medium whose isotropic plane is parallel to the plane boundary is analyzed. It is found that an obliquely incident P wave results in a reflected P wave and a reflected SV wave. The delay time for propagation between the transmitting and the receiving transducers is computed as if the P waves were propagating in an infinite half space. The displacements associated with the P waves in the plate and which may be detected by a noncontact NDE receiving transducer are approximated by an asymptotic solution for an infinite transversely isotropic medium subjected to a harmonic point load. Author

N88-28323* National Aeronautics and Space Administration. Lewis Research Center, Cleveland, OH.

NEW ACOUSTO-ULTRASONIC TECHNIQUES APPLIED TO AEROSPACE MATERIALS

HAROLD E. KAUTZ Aug. 1988 21 p Presented at the Non-Destructive Testing and Evaluation for Manufacturing and Construction, Urbana, Ill., 9-12 Aug. 1988; sponsored in part by Illinois Univ., Urbana-Champaign; and US Army Construction Engineering Research Lab.
(NASA-TM-101299; E-4281; NAS 1.15:101299) Avail: NTIS HC A03/MF A01 CSCL 14D

The use of an NdYAG pulsed laser for generating ultrasonic waves for NDE in resin matrix composites was investigated. A study was conducted of the use of the 1.064 micron wavelength NdYAG pulsed laser with the neat, unreinforced resin as well as graphite fiber/polymer composite specimens. In the case of the neat resins it was found that, at normal incidence, about 25 percent of the laser pulse energy was reflected at the incident surface. An attenuation coefficient for the polyimide resin, PMR-15 was determined to be approximately 5.8 np/cm. It was found in energy balance studies that graphite fiber/polymer specimens attenuate the laser beam more than do neat resins. The increase absorption is in the graphite fibers. The occurrence of laser induced surface damage was also studied. For the polymer neat resin, damage appears as pit formation over a small fraction of the pulse impact area and discoloration over a larger part of the area. A damage threshold was inferred from observed damage as a function of pulse energy. The 600 F cured PMR-15 and PMR-11 exhibit about the same amount of damage for a given laser pulse energy. The damage threshold is between 0.06 and 0.07 J/sq cm. Author

39

STRUCTURAL MECHANICS

Includes structural element design and weight analysis; fatigue; and thermal stress.

A88-14579* Case Western Reserve Univ., Cleveland, OH.

THE EFFECTS OF CRACK SURFACE FRICTION AND ROUGHNESS ON CRACK TIP STRESS FIELDS

ROBERTO BALLARINI (Case Western Reserve University, Cleveland, OH) and MICHAEL E. PLESHA (Wisconsin, University, Madison) International Journal of Fracture (ISSN 0376-9429),

vol. 34, July 1987, p. 195-207. refs
(Contract NCC3-46; DAAL03-86-K-0134)

A model is presented which can be used to incorporate the effects of friction and tortuosity along crack surfaces through a constitutive law applied to the interface between opposing crack surfaces. The problem of a crack with a saw-tooth surface in an infinite medium subjected to a far-field shear stress is solved and the ratios of mode I stress intensity to mode II stress intensity are calculated for various coefficients of friction and material properties. The results show that tortuosity and friction lead to an increase in fracture loads and alter the direction of crack propagation. Author

A88-16933* Southwest Research Inst., San Antonio, TX. **EFFICIENT PROBABILISTIC FRACTURE MECHANICS ANALYSIS**

Y.-T. WU, O. H. BURNSIDE (Southwest Research Institute, San Antonio, TX), and J. DOMINGUEZ (Sevilla, Universidad, Sevilla, Spain) IN: Numerical methods in fracture mechanics; Proceedings of the Fourth International Conference, San Antonio, TX, Mar. 23-27, 1987. Swansea, Wales, Pineridge Press, 1987, p. 85-100. refs
(Contract NAS3-24389)

A systematic and efficient method for probabilistic fracture mechanics analysis is proposed. The method is based on a most-probable-point-locus concept. The locus is obtained iteratively where the initial locus is determined using the linear approximation of the service life $N(X)$ function about the mean values of the random variables X . Linear and quadratic approximations of $N(X)$ are established locally at the most probable points, and the reliability analysis methods are used to compute the cumulative probabilities. By using two examples, the proposed method is demonstrated to be efficient and accurate. One example involved a random loading and $N(X)$ was computed using cycle-by-cycle integration. The method is general and can be applied to other performance functions. It is particularly suitable when the computation of the performance function is time consuming such that Monte Carlo simulation is prohibitively costly. Author

A88-16955* Cornell Univ., Ithaca, NY.

INTERACTIVE COMPUTER SIMULATION OF FRACTURE PROCESSES

ANTHONY R. INGRAFFEA (Cornell University, Ithaca, NY) IN: Numerical methods in fracture mechanics; Proceedings of the Fourth International Conference, San Antonio, TX, Mar. 23-27, 1987. Swansea, Wales, Pineridge Press, 1987, p. 677-699. refs
(Contract NSF CEE-83-51914; NSF CEE-83-16730; NAG3-395)

A88-18380* Toledo Univ., OH.

THERMAL STRESSES OF A WIND TURBINE BLADE MADE OF ORTHOTROPIC MATERIAL

KUAN-CHEN FU and AWAD HARB (Toledo, University, OH) Computers and Structures (ISSN 0045-7949), vol. 27, no. 2, 1987, p. 225-235. refs
(Contract NAG3-373)

This study is to investigate the thermal stress of a wind turbine blade made of wood composite material. First, the governing partial differential equation on heat conduction is stated, then, a finite element procedure using a variational approach is employed for the solution of the governing equation. Thus, the temperature field throughout the blade is determined. Next, based on the temperature field, a finite element procedure using potential energy approach is applied to determine the thermal stress field. A set of results is obtained through the use of a computer, which is considered to be satisfactory. Author

A88-18696* Illinois Univ., Chicago.

A PROBABILISTIC MODEL OF BRITTLE CRACK FORMATION

A. CHUDNOVSKY and B. KUNIN (Illinois, University, Chicago) Journal of Applied Physics (ISSN 0021-8979), vol. 62, Nov. 15, 1987, p. 4124-4129. Navy-supported research. refs
(Contract NAG3-754)

Probability of a brittle crack formation in an elastic solid with

fluctuating strength is considered. A set Ω of all possible crack trajectories reflecting the fluctuation of the strength field is introduced. The probability $P(X)$ that crack penetration depth exceeds X is expressed as a functional integral over Ω of a conditional probability of the same event taking place along a particular path. Various techniques are considered to evaluate the integral. Under rather nonrestrictive assumptions, the integral is reduced to solving a diffusion-type equation. A new characteristic of fracture process, 'crack diffusion coefficient', is introduced. An illustrative example is then considered where the integration is reduced to solving an ordinary differential equation. The effect of the crack diffusion coefficient and of the magnitude of strength fluctuations on probability density of crack penetration depth is presented. Practical implications of the proposed model are discussed. Author

A88-24054* Illinois Univ., Chicago.

ON SELF-SIMILARITY OF CRACK LAYER

J. BOTSIS and B. KUNIN (Illinois, University, Chicago) International Journal of Fracture (ISSN 0376-9429), vol. 35, Nov. 1987, p. R51-R56. refs
(Contract NAG3-754)

The crack layer (CL) theory of Chudnovsky (1986), based on principles of thermodynamics of irreversible processes, employs a crucial hypothesis of self-similarity. The self-similarity hypothesis states that the value of the damage density at a point x of the active zone at a time t coincides with that at the corresponding point in the initial ($t = 0$) configuration of the active zone, the correspondence being given by a time-dependent affine transformation of the space variables. In this paper, the implications of the self-similarity hypothesis for quasi-static CL propagation is investigated using polystyrene as a model material and examining the evolution of damage distribution along the trailing edge which is approximated by a straight segment perpendicular to the crack path. The results support the self-similarity hypothesis adopted by the CL theory. I.S.

A88-26450* National Aeronautics and Space Administration. Lewis Research Center, Cleveland, OH.

CALCULATION OF THERMOMECHANICAL FATIGUE LIFE BASED ON ISOTHERMAL BEHAVIOR

G. R. HALFORD and J. F. SALTSMAN (NASA, Lewis Research Center, Cleveland, OH) IN: Thermal stress, material deformation, and thermo-mechanical fatigue. New York, American Society of Mechanical Engineers, 1987, p. 9-21. Previously announced in STAR as N87-20565. refs

The isothermal and thermomechanical fatigue (TMF) crack initiation response of a hypothetical material was analyzed. Expected thermomechanical behavior was evaluated numerically based on simple, isothermal, cyclic stress-strain-time characteristics and on strainrange versus cyclic life relations that have been assigned to the material. The attempt was made to establish basic minimum requirements for the development of a physically accurate TMF life-prediction model. A worthy method must be able to deal with the simplest of conditions: that is, those for which thermal cycling, per se, introduces no damage mechanisms other than those found in isothermal behavior. Under these assumed conditions, the TMF life should be obtained uniquely from known isothermal behavior. The ramifications of making more complex assumptions will be dealt with in future studies. Although analyses are only in their early stages, considerable insight has been gained in understanding the characteristics of several existing high-temperature life-prediction methods. The present work indicates that the most viable damage parameter is based on the inelastic strainrange. Author

A88-30236* Tulane Univ., New Orleans, LA.

MACROCRACK INTERACTION WITH TRANSVERSE ARRAY OF MICROCRACKS

A. A. RUBINSTEIN (Tulane University, New Orleans, LA) and H. C. CHOI (Illinois, University, Urbana) International Journal of Fracture (ISSN 0376-9429), vol. 36, Jan. 1988, p. 15-26. Previously

announced in STAR as N87-25607. refs
(Contract NAG3-751)

General formulation of a problem involving a macrocrack propagating through an area with microcracks is considered. The analysis is based on the simultaneous solution of a system of singular integral equations. Various methods described in the literature are discussed in detail and compared. The specific problem considered was a macrocrack approaching an infinite transverse array of microcracks. Results illustrate the effects of different loading types and can be used for interpretation of the microcrack toughening mechanisms. Numerical comparisons are made with data recently appearing in literature which demonstrates the importance of numerical accuracy. Reported results differ by a factor in certain cases as compared with data given in other literature. Author

A88-31347* National Aeronautics and Space Administration. Lewis Research Center, Cleveland, OH.

AN IDEAL CLAMPING ANALYSIS FOR A CROSS-PLY LAMINATE

R. R. VALISETTY (NASA, Lewis Research Center, Cleveland, OH), P. L. N. MURTHY (Cleveland State University, OH), and L. W. REHFELD (Georgia Institute of Technology, Atlanta) Journal of Composite Materials (ISSN 0021-9983), vol. 22, Feb. 1988, p. 136-153. refs

Different elementary clamping models are discussed for a three layer crossply laminate to study the sensitivity of clamping to the definition of cross-sectional rotation. All of these models leave a considerable residual warping at the edges. Using a complimentary energy principle and principle of superposition, an analysis is conducted to reduce this residual warping. This led to the identification of exact interior solution corresponding to the ideal clamping. This study also suggests a presence of stress singularities at the corners and between different layers near the fixed edge. Author

A88-31561* Case Western Reserve Univ., Cleveland, OH.

IDENTIFICATION OF STRUCTURAL INTERFACE CHARACTERISTICS USING COMPONENT MODE SYNTHESIS

A. A. HUCKELBRIDGE (Case Western Reserve University, Cleveland, OH) and C. LAWRENCE (NASA, Lewis Research Center, Cleveland, OH) IN: Modal testing and analysis; Proceedings of the Eleventh Biennial Conference on Mechanical Vibration and Noise, Boston, MA, Sept. 27-30, 1987. New York, American Society of Mechanical Engineers, 1987, p. 121-129. Previously announced in STAR as N87-24006. refs

The inability to adequately model connections has limited the ability to predict overall system dynamic response. Connections between structural components are often mechanically complex and difficult to accurately model analytically. Improved analytical models for connections are needed to improve system dynamic predictions. This study explores combining Component Mode synthesis methods for coupling structural components with Parameter Identification procedures for improving the analytical modeling of the connections. Improvements in the connection properties are computed in terms of physical parameters so the physical characteristics of the connections can be better understood, in addition to providing improved input for the system model. Two sample problems, one utilizing simulated data, the other using experimental data from a rotor dynamic test rig, are presented. Author

A88-32219* Cleveland State Univ., OH.

FRACTURE TOUGHNESS COMPUTATIONAL SIMULATION OF GENERAL DELAMINATIONS IN FIBER COMPOSITES

P. L. N. MURTHY (Cleveland State University, OH), C. C. CHAMIS (NASA, Lewis Research Center, Cleveland, OH), and T. E. WILT IN: Structures, Structural Dynamics and Materials Conference, 29th, Williamsburg, VA, Apr. 18-20, 1988, Technical Papers. Part 1. Washington, DC, American Institute of Aeronautics and Astronautics, 1988, p. 391-401. refs
(AIAA PAPER 88-2261)

A procedure is described to computationally simulate composite

39 STRUCTURAL MECHANICS

laminate fracture toughness in terms of strain energy release rate (SERR). It is also used to evaluate the degradation in laminate structural integrity in terms of displacements, loss in stiffness, loss in vibration frequencies and loss in buckling resistance. Specific laminates are selected for detail studies in order to demonstrate the generality of the procedure. These laminates had center delaminations, off-center delaminations, and pocket delaminations (center and off-center) at the free-edge and center delaminations at the interior. The laminates had two different thicknesses and were made from three different materials. The results obtained are presented in graphical form to illustrate the effects of delamination on the laminate structural integrity and on the laminate strain energy release rate (composite fracture toughness).

Author

A88-32289* # Toledo Univ., OH.

THE EFFECTS OF ROTATIONAL FLOW, VISCOSITY, THICKNESS, AND SHAPE ON TRANSONIC FLUTTER DIP PHENOMENA

T. S. R. REDDY (Toledo, University, OH), RAKESH SRIVASTAVA (Georgia Institute of Technology, Atlanta), and KRISHNA RAO V. KAZA (NASA, Lewis Research Center, Cleveland, OH) IN: Structures, Structural Dynamics and Materials Conference, 29th, Williamsburg, VA, Apr. 18-20, 1988, Technical Papers. Part 2. Washington, DC, American Institute of Aeronautics and Astronautics, 1988, p. 1096-1108. Previously announced in STAR as N88-18969. refs

(Contract NSG-3139; NAG3-730)

(AIAA PAPER 88-2348)

The transonic flutter dip phenomena on thin airfoils, which are employed for propfan blades, is investigated using an integrated Euler/Navier-Stokes code and a two degrees of freedom typical section structural model. As a part of the code validation, the flutter characteristics of the NACA 64A010 airfoil are also investigated. In addition, the effects of artificial dissipation models, rotational flow, initial conditions, mean angle of attack, viscosity, airfoil thickness, and shape on flutter are investigated. The results obtained with an Euler code for the NACA 64A010 airfoil are in reasonable agreement with published results obtained by using transonic small disturbance and Euler codes. The two artificial dissipation models, one based on the local pressure gradient scaled by a common factor and the other based on the local pressure gradient scaled by a spectral radius, predicted the same flutter speeds except in the recovery region for the case studied. The effects of rotation flow, initial conditions, mean angle of attack, and viscosity for the Reynolds number studied seem to be negligible or small on the minima of the flutter dip.

Author

A88-32308* # Notre Dame Univ., IN.

AN EXPERT SYSTEM FOR PROBABILISTIC DESCRIPTION OF LOADS ON SPACE PROPULSION SYSTEM STRUCTURAL COMPONENTS

B. F. SPENCER, JR. (Notre Dame, University, IN) and D. A. HOPKINS (NASA, Lewis Research Center, Cleveland, OH) IN: Structures, Structural Dynamics and Materials Conference, 29th, Williamsburg, VA, Apr. 18-20, 1988, Technical Papers. Part 3. Washington, DC, American Institute of Aeronautics and Astronautics, 1988, p. 1262-1266. refs

(AIAA PAPER 88-2371)

LDEXPT, an expert system that generates probabilistic characterizations of the loads spectra borne by spacecraft propulsion systems' structural components, is found by recent experience at NASA-Lewis to be useful in the cases of components representative of the Space Shuttle Main Engine's turbopumps and fluid transfer ducting. LDEXPT is composed of a knowledge base management system and a rule base management system. The ANLOAD load-modeling module of LDEXPT encompasses three independent probabilistic analysis techniques.

O.C.

A88-32310* # Sverdrup Technology, Inc., Middleburg Heights, OH.

PROBABILISTIC STRUCTURAL ANALYSIS OF AEROSPACE COMPONENTS USING NESSUS

MICHAEL C. SHIAO, VINOD K. NAGPAL (Sverdrup Technology, Inc., Middleburg Heights, OH), and CHRISTOS C. CHAMIS (NASA, Lewis Research Center, Cleveland, OH) IN: Structures, Structural Dynamics and Materials Conference, 29th, Williamsburg, VA, Apr. 18-20, 1988, Technical Papers. Part 3. Washington, DC, American Institute of Aeronautics and Astronautics, 1988, p. 1275-1282. refs

(AIAA PAPER 88-2373)

Probabilistic structural analysis of a Space Shuttle main engine turbopump blade is conducted using the computer code NESSUS (numerical evaluation of stochastic structures under stress). The goal of the analysis is to derive probabilistic characteristics of blade response given probabilistic descriptions of uncertainties in blade geometry, material properties, and temperature and pressure distributions. Probability densities are derived for critical blade responses. Risk assessment and failure life analysis is conducted assuming different failure models.

Author

A88-32312* # Cleveland State Univ., OH.

PROBABILISTIC COMPOSITE MICROMECHANICS

T. A. STOCK, P. X. BELLINI, P. L. N. MURTHY (Cleveland State University, OH), and C. C. CHAMIS (NASA, Lewis Research Center, Cleveland, OH) IN: Structures, Structural Dynamics and Materials Conference, 29th, Williamsburg, VA, Apr. 18-20, 1988, Technical Papers. Part 3. Washington, DC, American Institute of Aeronautics and Astronautics, 1988, p. 1289-1298.

(AIAA PAPER 88-2375)

Probabilistic composite micromechanics methods are developed that simulate expected uncertainties in unidirectional fiber composite properties. These methods are in the form of computational procedures using Monte Carlo simulation. A graphite/epoxy unidirectional composite (ply) is studied to demonstrate fiber composite material properties at the micro level. Regression results are presented to show the relative correlation between predicted and response variables in the study.

Author

A88-32313* # Texas Univ., San Antonio.

PROBABILISTIC CONSTITUTIVE RELATIONSHIPS FOR CYCLIC MATERIAL STRENGTH MODELS

L. BOYCE (Texas, University, San Antonio) and C. C. CHAMIS (NASA, Lewis Research Center, Cleveland, OH) IN: Structures, Structural Dynamics and Materials Conference, 29th, Williamsburg, VA, Apr. 18-20, 1988, Technical Papers. Part 3. Washington, DC, American Institute of Aeronautics and Astronautics, 1988, p. 1299-1306. refs

(AIAA PAPER 88-2376)

A methodology is developed that provides a probabilistic treatment for the lifetime of structural components of aerospace propulsion systems subjected to fatigue. Material strength degradation models, based on primitive variables, include both a fatigue strength reduction model and a fatigue crack growth model. Probabilistic analysis is based on simulation, and both maximum entropy and maximum penalized likelihood methods are used for the generation of probability density functions. The resulting constitutive relationships are included in several computer programs.

Author

A88-32322* # National Aeronautics and Space Administration. Lewis Research Center, Cleveland, OH.

SUPERELEMENT METHODS APPLICATIONS TO MICROMECHANICS OF HIGH TEMPERATURE METAL MATRIX COMPOSITES

J. J. CARUSO and C. C. CHAMIS (NASA, Lewis Research Center, Cleveland, OH) IN: Structures, Structural Dynamics and Materials Conference, 29th, Williamsburg, VA, Apr. 18-20, 1988, Technical Papers. Part 3. Washington, DC, American Institute of Aeronautics and Astronautics, 1988, p. 1388-1400.

(AIAA PAPER 88-2390)

Adaptation of the superelement finite-element method for micromechanics of continuous fiber high temperature metal matrix composites (HT-MMC) is described. The method is used to predict the thermomechanical behavior of P100-graphite/copper composites using MSC/NASTRAN and it is also used to validate

those predicted by using an in-house computer program designed to perform micromechanics for HT-MMC. Typical results presented in the paper include unidirectional composite thermal properties, mechanical properties, and microstresses. Author

A88-40121* Akron Univ., OH.
A MIXED FORMULATION OF C(0)-LINEAR TRIANGULAR PLATE/SHELL ELEMENT - THE ROLE OF EDGE SHEAR CONSTRAINTS

A. F. SALEEB, T. Y. CHANG, and S. YINGYEUNYONG (Akron, University, OH) International Journal for Numerical Methods in Engineering (ISSN 0029-5981), vol. 26, May 1988, p. 1101-1128. refs
 (Contract NAG3-307)

A simple and effective linear C(0)-triangular element for plates and shells is developed on the basis of the Hellinger-Reissner mixed variational principle with independently assumed stress and displacement fields. Two main features are emphasized in this development concerning the assumed transverse shear stress field. First, this assumption results in edge-type penalty constraints in the thin plate/shell regimes. Second, the element is used in the form of a four-triangle, cross-diagonal macroelement mesh. As a result, the element is shown to be free from shear locking in thin plate/shell applications, and it satisfies all the appropriate patch tests required for Kirchhoff plate models. In addition, the element exhibits good overall convergence properties in a variety of test problems for plates and shells. Finally, from the computational standpoint, the element is very efficient since all stiffness component matrices are derived in explicit forms. Author

A88-41042* Georgia Inst. of Tech., Atlanta.
THERMO-ELASTO-VISCOPLASTIC ANALYSIS OF PROBLEMS IN EXTENSION AND SHEAR

R. RIFF and G. J. SIMITSES (Georgia Institute of Technology, Atlanta) Computers and Structures (ISSN 0045-7949), vol. 29, no. 2, 1988, p. 293-300. Previously announced in STAR as N87-29896. refs
 (Contract NAG3-534)

The problems of extension and shear behavior of structural elements made of carbon steel and subjected to large thermomechanical loads are investigated. The analysis is based on nonlinear geometric and constitutive relations, and is expressed in a rate form. The material constitutive equations are capable of reproducing all nonisothermal, elasto-viscoplastic characteristics. The results of the test problems show that: (1) the formulation can accommodate very large strains and rotations; (2) the model incorporates the simplification associated with rate-insensitive elastic response without losing the ability to model a rate-temperature dependent yield strength and plasticity; and (3) the formulation does not display oscillatory behavior in the stresses for the simple shear problem. Author

A88-46666* National Aeronautics and Space Administration. Lewis Research Center, Cleveland, OH.

IDENTIFICATION OF DIFFERENCES BETWEEN FINITE ELEMENT ANALYSIS AND EXPERIMENTAL VIBRATION DATA
 CHARLES LAWRENCE (NASA, Lewis Research Center, Cleveland, OH) Society of Environmental Engineers, Journal (ISSN 0374-356X), vol. 27-2, June 1988, p. 13-19, 30. Previously announced in STAR as N86-27617. refs

An important problem that has emerged from combined analytical/experimental investigations is the task of identifying and quantifying the differences between results predicted by F.E. analysis and results obtained from experiment. The objective of this study is to extend and evaluate the procedure developed by Sidhu for correlation of linear F.E. and modal test data to include structures with viscous damping. The desirability of developing this procedure is that the differences are identified in terms of physical mass, damping, and stiffness parameters instead of in terms of frequencies and modes shapes. Since the differences are computed in terms of physical parameters, locations of modeling problems can be directly identified in the F.E. model. From simulated data it was determined that the accuracy of the

computed differences increases as the number of experimentally measured modes included in the calculations is increased. When the number of experimental modes is at least equal to the number of translational degrees of freedom in the F.E. model both the location and magnitude of the differences can be computed very accurately. When the number of modes is less than this amount the location of the differences may be determined even though their magnitudes will be underestimated. Author

A88-47001* General Electric Co., Cincinnati, OH.
A REVIEW OF PATH-INDEPENDENT INTEGRALS IN ELASTIC-PLASTIC FRACTURE MECHANICS

KWANG S. KIM (General Electric Co., Cincinnati, OH) and THOMAS W. ORANGE (NASA, Lewis Research Center, Cleveland, OH) IN: Fracture mechanics. Philadelphia, PA, American Society for Testing and Materials, 1988, p. 713-729. refs
 (Contract NAS3-23940)

The objective of this paper is to review the path-independent (P-I) integrals in elastic plastic fracture mechanics which have been proposed in recent years to overcome the limitations imposed on the J-integral. The P-I integrals considered are the J-integral by Rice (1968), the thermoelastic P-I integrals by Wilson and Yu (1979) and Gurtin (1979), the J-integral by Blackburn (1972), the J(theta)-integral by Ainsworth et al. (1978), the J-integral by Kishimoto et al. (1980), and the Delta-T(p) and Delta T(p)-asterisk integrals by Alturi et al. (1982). The theoretical foundation of the P-I integrals is examined with an emphasis on whether or not the path independence is maintained in the presence of nonproportional loading and unloading in the plastic regime, thermal gradient, and material inhomogeneities. The similarities, difference, salient features, and limitations of the P-I integrals are discussed. Comments are also made with regard to the physical meaning, the possibility of experimental measurement, and computational aspects. Author

A88-47014* National Aeronautics and Space Administration. Lewis Research Center, Cleveland, OH.

CALIBRATION OF A MODE II TEST SPECIMEN
 ROBERT J. BUZZARD and BERNARD GROSS (NASA, Lewis Research Center, Cleveland, OH) IN: Fracture mechanics. Philadelphia, PA, American Society for Testing and Materials, 1988, p. 1083-1088. refs

Mode II and Mode I calibrations of the NASA Lewis Research Center Mode II fatigue specimen were performed experimentally over crack length to specimen width ratios (a/W) of 0.5 to 0.9. Mode II displacements were measured both at the specimen notch mouth and at the intersection of the notch with the centerline of the loading pin holes. Mode I displacements were measured across the span of the specimen at the loading pins' centerline. Analytical stress intensity factor coefficients for both Mode II and Mode I are also presented. Author

A88-47681* Illinois Univ., Chicago.
SEMI-EMPIRICAL CRACK TIP ANALYSIS

A. CHUDNOVSKY (Illinois, University, Chicago) and M. BEN OUEZDON (Case Western Reserve University, Cleveland, OH) International Journal of Fracture (ISSN 0376-9429), vol. 37, May 1988, p. 3-11. refs
 (Contract NAG3-754)

Experimentally observed crack opening displacements are employed as the solution of the multiple crack interaction problem. Then the near and far fields are reconstructed analytically by means of the double layer potential technique. Evaluation of the effective stress intensity factor resulting from the interaction of the main crack and its surrounding crazes in addition to the remotely applied load is presented as an illustrative example. It is shown that crazing (as well as microcracking) may constitute an alternative mechanism to Dugdale-Berenblatt models responsible for the cancellation of the singularity at the crack tip. Author

A88-48638* State Univ. of New York at Buffalo, Amherst.
TIME-DOMAIN TRANSIENT ELASTODYNAMIC ANALYSIS OF 3-D SOLIDS BY BEM

39 STRUCTURAL MECHANICS

S. AHMAD and P. K. BANERJEE (New York, State University, Amherst) International Journal for Numerical Methods in Engineering (ISSN 0029-5981), vol. 26, Aug. 1988, p. 1709-1728. refs
(Contract NAS3-23697)

The BEM algorithm developed by Banerjee and Ahmad (1985) and Banerjee et al. (1986) for the analysis of three-dimensional time-dependent elastodynamics problems is extended and refined to improve the accuracy of the internal stress predictions. A quadratic spatial shape function and a linear temporal shape function are employed, and the complete numerical implementation (as part of BEST3D) is outlined. Applications of the improved BEM to typical problems are presented graphically and briefly characterized. Included are spherical cavities subjected to sudden radial expansion, triangular or rectangular pulses of radial pressure, or ramp loading; a circular loaded area on a half space; and a flexible square plate foundation on an elastic half space. T.K.

A88-49714* Georgia Inst. of Tech., Atlanta.
FREQUENCY DOMAIN SOLUTIONS TO MULTI-DEGREE-OF-FREEDOM, DRY FRICTION DAMPED SYSTEMS

A. A. FERRI (Georgia Institute of Technology, Atlanta) and E. H. DOWELL (Duke University, Durham, NC) Journal of Sound and Vibration (ISSN 0022-460X), vol. 124, July 22, 1988, p. 207-224. refs
(Contract AF-AFOSR-83-0346; NAG3-516)

Dry friction damping has been considered as a means of increasing the passive damping of a variety of systems including large space structures and turbomachinery blades. However, dry friction is highly nonlinear, and hence, analytical investigations are difficult to perform. Here, a multiharmonic, frequency domain solution technique is developed and applied to a multi-degree-of-freedom, dry friction damped system. It is seen that the multiharmonic method is more accurate than traditional, one-harmonic solution methods. The method also compares favorably with time integration. Finally, comparisons are made with experimental results. Author

A88-51328*# Purdue Univ., West Lafayette, IN.
AEROELASTIC EFFECTS OF ALTERNATE BLADE SWEEP ON ADVANCED PROPPAN ROTOR

MARC H. WILLIAMS (Purdue University, West Lafayette, IN) ASME, Winter Annual Meeting, Boston, MA, Dec. 13-18, 1987. 6 p. refs
(Contract NAG3-499)
(ASME PAPER 87-WA/AERO-8)

Recent progress in the development of a general purpose unsteady aerodynamic and aeroelastic analysis capability for Advanced Turboprops will be reviewed. An application to a rotor with alternating forward and backward swept blades is described, which illustrates the general 'mistuning' capability of the method. Author

A88-53088* State Univ. of New York at Buffalo, Amherst.
A NEW BOUNDARY ELEMENT FORMULATION FOR TWO- AND THREE-DIMENSIONAL THERMOELASTICITY USING PARTICULAR INTEGRALS

DONALD P. HENRY, JR. and PRASANTA K. BANERJEE (New York, State University, Amherst) International Journal for Numerical Methods in Engineering (ISSN 0029-5981), vol. 26, Sept. 1988, p. 2061-2077. Research supported by Pratt and Whitney. refs
(Contract NAS3-23697)

New two- and three-dimensional BEM formulations are developed for steady-state and transient uncoupled thermoelasticity. These new procedures differ from previous work in that additional surface of volume integration is not required to incorporate thermal loads in the analysis. Instead, thermal body forces are introduced in the BEM system via particular integrals. The present formulation is implemented in a general-purpose multiregion system, and examples are presented to demonstrate the accuracy and versatility of the method. Author

A88-53089* State Univ. of New York at Buffalo, Amherst.

A NEW BEM FORMULATION FOR TWO- AND THREE-DIMENSIONAL ELASTOPLASTICITY USING PARTICULAR INTEGRALS

DONALD P. HENRY, JR. and PRASANTA K. BANERJEE (New York, State University, Amherst) International Journal for Numerical Methods in Engineering (ISSN 0029-5981), vol. 26, Sept. 1988, p. 2079-2096. Research supported by Pratt and Whitney. refs
(Contract NAS3-23697)

New two- and three-dimensional BEM formulations are developed for elastoplastic stress analysis. These new procedures differ from previous work in that volume integration is not required to incorporate the nonlinear effects in the analysis. Instead, initial stress rates are introduced in the BEM system via particular integrals. The present formulation is implemented in a general-purpose multi-region system, and examples are presented to demonstrate the accuracy and versatility of the method.

Author

A88-54142*# National Aeronautics and Space Administration. Lewis Research Center, Cleveland, OH.

STRUCTURAL ANALYSIS METHODS DEVELOPMENT FOR TURBINE HOT SECTION COMPONENTS

R. L. THOMPSON (NASA, Lewis Research Center, Cleveland, OH) IN: Toward improved durability in advanced aircraft engine hot sections; Proceedings of the Thirty-third ASME International Gas Turbine and Aeroengine Congress and Exposition, Amsterdam, Netherlands, June 5-9, 1988. New York, American Society of Mechanical Engineers, 1988, p. 57-82. Previously announced in STAR as N88-18967. refs

The structural analysis technologies and activities of the NASA Lewis Research Center's gas turbine engine Hot Section Technology (HOST) Program are summarized. The technologies synergistically developed and validated include: time-varying thermal/mechanical load models; component-specific automated geometric modeling and solution strategy capabilities; advanced inelastic analysis methods; inelastic constitutive models; high-temperature experimental techniques and experiments; and nonlinear structural analysis codes. Features of the program that incorporate the new technologies and their application to hot section component analysis and design are described. Improved and, in some cases, first-time 3-D nonlinear structural analyses of hot section components of isotropic and anisotropic nickel-base superalloys are presented. Author

A88-54144*# National Aeronautics and Space Administration. Lewis Research Center, Cleveland, OH.

FATIGUE LIFE PREDICTION MODELING FOR TURBINE HOT SECTION MATERIALS

G. R. HALFORD (NASA, Lewis Research Center, Cleveland, OH), T. G. MEYER, R. S. NELSON, D. M. NISSLEY, and G. A. SWANSON (United Technologies Corp., Pratt and Whitney, East Hartford, CT) IN: Toward improved durability in advanced aircraft engine hot sections; Proceedings of the Thirty-third ASME International Gas Turbine and Aeroengine Congress and Exposition, Amsterdam, Netherlands, June 5-9, 1988. New York, American Society of Mechanical Engineers, 1988, p. 97-107. Previously announced in STAR as N88-14453. refs

A major objective of the fatigue and fracture efforts under the Hot Section Technology (HOST) program was to significantly improve the analytic life prediction tools used by the aeronautical gas turbine engine industry. This was achieved in the areas of high-temperature thermal and mechanical fatigue of bare and coated high-temperature superalloys. The cyclic crack initiation and propagation resistance of nominally isotropic polycrystalline and highly anisotropic single crystal alloys were addressed. Life prediction modeling efforts were devoted to creep-fatigue interaction, oxidation, coatings interactions, multiaxiality of stress-strain states, mean stress effects, cumulative damage, and thermomechanical fatigue. The fatigue crack initiation life models developed to date include the Cyclic Damage Accumulation (CDA) and the Total Strain Version of Strainrange Partitioning (TS-SRP)

for nominally isotropic materials, and the Tensile Hysteretic Energy Model for anisotropic superalloys. A fatigue model is being developed based upon the concepts of Path-Independent Integrals (PII) for describing cyclic crack growth under complex nonlinear response at the crack tip due to thermomechanical loading conditions. A micromechanistic oxidation crack extension model was derived. The models are described and discussed. Author

A88-54276*# Utah Univ., Salt Lake City.
EFFECTS OF SUBCRITICAL CRACK GROWTH ON FRACTURE TOUGHNESS OF CERAMICS ASSESSED IN CHEVRON-NOTCHED THREE-POINT BEND TESTS
 L. Y. CHAO, D. SINGH, and D. K. SHETTY (Utah, University, Salt Lake City) ASME, Gas Turbine and Aeroengine Congress and Exposition, Amsterdam, Netherlands, June 6-9, 1988. 6 p. refs (Contract NAG3-789)
 (ASME PAPER 88-GT-185)

A numerical computational study was carried out to assess the effects of subcritical crack growth on crack stability in the chevron-notched three-point bend specimens. A power-law relationship between the subcritical crack velocity and the applied stress intensity were used along with compliance and stress-intensity relationships for the chevron-notched bend specimen to calculate the load response under fixed deflection rate and a machine compliance. The results indicate that the maximum load during the test occurs at the same crack length for all the deflection rates; the maximum load, however, is dependent on the deflection rate for rates below the critical rate. The resulting dependence of the apparent fracture toughness on the deflection rate is compared to experimental results on soda-lime glass and polycrystalline alumina. Author

A88-54912*# Purdue Univ., West Lafayette, IN.
A NONLINEAR VISCOELASTIC CONSTITUTIVE EQUATION - YIELD PREDICTIONS IN MULTIAXIAL DEFORMATIONS
 R. M. SHAY, JR. and J. M. CARUTHERS (Purdue University, West Lafayette, IN) IN: Developments in Mechanics. Volume 14(b) - Midwestern Mechanics Conference, 20th, West Lafayette, IN, Aug. 31-Sept. 2, 1987, Proceedings. West Lafayette, IN, Purdue University, 1987, p. 493-498. refs
 (Contract NAG3-599)

Yield stress predictions of a nonlinear viscoelastic constitutive equation for amorphous polymer solids have been obtained and are compared with the phenomenological von Mises yield criterion. Linear viscoelasticity theory has been extended to include finite strains and a material timescale that depends on the instantaneous temperature, volume, and pressure. Results are presented for yield and the correct temperature and strain-rate dependence in a variety of multiaxial deformations. The present nonlinear viscoelastic constitutive equation can be formulated in terms of either a Cauchy or second Piola-Kirchhoff stress tensor, and in terms of either atmospheric or hydrostatic pressure. R.R.

N88-10388*# Georgia Inst. of Tech., Atlanta. School of Aerospace Engineering.
ANALYSIS OF SHELL-TYPE STRUCTURES SUBJECTED TO TIME-DEPENDENT MECHANICAL AND THERMAL LOADING
Semiannual Status Report
 G. J. SIMITSES and R. RIFF Oct. 1987 7 p
 (Contract NAG3-534)
 (NASA-CR-181409; NAS 1.26:181409) Avail: NTIS HC A02/MF A01 CSCL 20K

A general mathematical model and solution methodologies for analyzing structural response of thin, metallic shell-type structures under large transient, cyclic, or static thermomechanical loads are developed. Among the system responses, which are associated with these load conditions, are thermal buckling, creep buckling and ratcheting. Thus, geometric as well as material type nonlinearities (of high order) can be anticipated and must be considered in the development of the mathematical model. Furthermore, this must also be accommodated in the solution procedures. Author

N88-11140*# National Aeronautics and Space Administration. Lewis Research Center, Cleveland, OH.
TURBINE ENGINE HOT SECTION TECHNOLOGY, 1985
 Oct. 1985 443 p Conference held in Cleveland, Ohio, 22-23 Oct. 1985
 (NASA-CP-2405; E-2727; NAS 1.55:2405) Avail: NTIS HC A19/MF A01 CSCL 20K

The Turbine Engine Section Technology (HOST) Project Office of the Lewis Research Center sponsored a workshop to discuss current research pertinent to turbine engine hot section durability problems. Presentations were made concerning hot section environment and the behavior of combustion liners, turbine blades, and turbine vanes.

N88-11164*# General Electric Co., Cincinnati, OH. Aircraft Engine Business Group.
3D INELASTIC ANALYSIS METHODS FOR HOT SECTION COMPONENTS
 L. T. DAME, P. C. CHEN, M. S. HARTLE, and H. T. HUANG /in NASA. Lewis Research Center, Turbine Engine Hot Section Technology, 1985 p 227-237 Oct. 1985
 (Contract NAS3-23698)
 Avail: NTIS HC A19/MF A01 CSCL 20K

The objective is to develop analytical tools capable of economically evaluating the cyclic time dependent plasticity which occurs in hot section engine components in areas of strain concentration resulting from the combination of both mechanical and thermal stresses. Three models were developed. A simple model performs time dependent inelastic analysis using the power law creep equation. The second model is the classical model of Professors Walter Haisler and David Allen of Texas A and M University. The third model is the unified model of Bodner, Partom, et al. All models were customized for linear variation of loads and temperatures with all material properties and constitutive models being temperature dependent. Author

N88-11170*# National Aeronautics and Space Administration. Lewis Research Center, Cleveland, OH.
HIGH TEMPERATURE STRESS-STRAIN ANALYSIS
 ROBERT L. THOMPSON /in its Turbine Engine Hot Section Technology, 1985 p 287-301 Oct. 1985
 Avail: NTIS HC A19/MF A01 CSCL 20K

The objectives of the high temperature structures program are threefold: to assist in the development of analytical tools needed to improve design analysis and procedures for the efficient and accurate prediction of the nonlinear structural response of hot-section components; to aid in the calibration, validation, and evaluation of the analytical tools by comparing predictions with experimental data; and to evaluate existing as well as advanced temperature and strain measurement instrumentation. Author

N88-11171*# Southwest Research Inst., San Antonio, TX.
CONSTITUTIVE MODELING FOR ISOTROPIC MATERIALS
 ULRIC S. LINDHOLM /in NASA. Lewis Research Center, Turbine Engine Hot Section Technology, 1985 p 303-306 Oct. 1985
 (Contract NAS3-23925)
 Avail: NTIS HC A19/MF A01 CSCL 20K

The objective is to develop a unified constitutive model for finite element structural analysis of turbine engine hot-section components. This effort constitutes a different approach for non-linear finite-element computer codes which have heretofore been based on classical inelastic methods. The unified constitutive theory to be developed will avoid the simplifying assumptions of classical theory and should more accurately represent the behavior of superalloy materials under cyclic loading conditions and high temperature environments. During the first two years of the program, extensive experimental correlations were made with two representative unified models. The experiments were both uniaxial and biaxial at temperatures up to 1093 C (2000 F). In addition, the unified models were adopted to the MARC finite element code and used for stress analysis of notched bar and turbine blade geometries. Author

39 STRUCTURAL MECHANICS

N88-11172*# General Electric Co., Cincinnati, OH. Aircraft Engine Business Group.

CONSTITUTIVE MODELING FOR ISOTROPIC MATERIALS

V. G. RAMASWAMY, R. H. VANSTONE, L. T. DAME, and J. H. LAFLIN *In* NASA. Lewis Research Center, Turbine Engine Hot Section Technology, 1985 p 307-320 Oct. 1985

(Contract NAS3-23927)

Avail: NTIS HC A19/MF A01 CSCL 20K

Constitutive theories were evaluated against a large uniaxial and multiaxial data base that was generated as part of this work. The experimental approach was to determine the constitutive behavior of Rene 80 under a multitude of conditions that are important in the design of gas turbine blades and vanes. The experimental and analytical goals of this program were successfully accomplished. A new multiaxial constitutive model which can represent the complex nonlinear high temperature behavior of Rene 80 was developed. The model was extensively verified on data at several temperatures. Author

N88-11173*# Pratt and Whitney Aircraft, East Hartford, CT.

CREEP FATIGUE LIFE PREDICTION FOR ENGINE HOT SECTION MATERIALS (ISOTROPIC): THIRD YEAR PROGRESS REVIEW

RICHARD S. NELSON and JOHN F. SCHOENDORF *In* NASA. Lewis Research Center, Turbine Engine Hot Section Technology, 1985 p 321-327 Oct. 1985

(Contract NAS3-23288)

Avail: NTIS HC A19/MF A01 CSCL 20K

This program is designed to investigate fundamental damage processes, identify modeling strategies, and develop practical models which can be used to guide the early design and development of new engines and to increase the durability of existing engines. A review is given of the base program, completed in 1984, which included the comparison and evaluation of several popular high-temperature life prediction approaches as applied to continuously cycled isothermal specimen tests. The option program, of which one year is completed, is designed to develop models which can account for complex cycles and loadings, such as thermomechanical cycling, cumulative damage, multiaxial stress/strain rates, and environmental effects. Author

N88-11174*# General Electric Co., Cincinnati, OH. Aircraft Engine Business Group.

ELEVATED TEMPERATURE CRACK GROWTH

S. N. MALIK, R. H. VANSTONE, K. S. KIM, and J. H. LAFLIN *In* NASA. Lewis Research Center, Turbine Engine Hot Section Technology, 1985 p 329-340 Oct. 1985

(Contract NAS3-23940)

Avail: NTIS HC A19/MF A01 CSCL 20K

The purpose is to determine the ability of currently available P-I integrals to correlate fatigue crack propagation under conditions that simulate the turbojet engine combustor liner environment. The utility of advanced fracture mechanics measurements will also be evaluated during the course of the program. To date, an appropriate specimen design, a crack displacement measurement method, and boundary condition simulation in the computational model of the specimen were achieved. Alloy 718 was selected as an analog material based on its ability to simulate high temperature behavior at lower temperatures. Tensile and cyclic tests were run at several strain rates so that an appropriate constitutive model could be developed. Suitable P-I integrals were programmed into a finite element post-processor for eventual comparison with experimental data. Author

N88-11175*# Pratt and Whitney Aircraft, East Hartford, CT.

LIFE PREDICTION AND CONSTITUTIVE MODELS FOR ENGINE HOT SECTION ANISOTROPIC MATERIALS PROGRAM

G. A. SWANSON *In* NASA. Lewis Research Center, Turbine Engine Hot Section Technology, 1985 p 341-349 Oct. 1985

(Contract NAS3-23939)

Avail: NTIS HC A19/MF A01 CSCL 20K

The purpose is to develop life prediction models for coated

anisotropic materials used in gas temperature airfoils. Two single crystal alloys and two coatings are now being tested. These include PWA 1480; Alloy 185; overlay coating, PWA 286; and aluminide coating, PWA 273. Constitutive models are also being developed for these materials to predict the plastic and creep strain histories of the materials in the lab tests and for actual design conditions. This nonlinear material behavior is particularly important for high temperature gas turbine applications and is basic to any life prediction system. Author

N88-11176*# National Aeronautics and Space Administration. Lewis Research Center, Cleveland, OH.

CREEP-FATIGUE BEHAVIOR OF NICOAL COATED PWA 1480

R. V. MINER, J. GAYDA, and M. G. HESBUR *In* its Turbine Engine Hot Section Technology, 1985 p 351-360 Oct. 1985

Avail: NTIS HC A19/MF A01 CSCL 20E

This study of high-temperature fatigue and creep-fatigue behavior is part of a program to identify the basic features of the effects of temperature, creep, fatigue, and environment on the behavior of a single crystal superalloy, a bulk coating alloy, and a coated alloy system. A system was selected which has had considerable production experience: the Ni-base superalloy, PWA 1480, and the NiCoCrAlY coating, PWA 276. Isothermal behavior was studied first. A series of fatigue and creep fatigue tests of the types commonly designated as pp, cp, pc and cc were conducted. These tests were conducted at various constant total strain ranges. The creep-fatigue cycles employed constant stress dwells at the maximum and/or minimum load. Test results are given. Author

N88-11177*# National Aeronautics and Space Administration. Lewis Research Center, Cleveland, OH.

LEWIS' ENHANCED LABORATORY FOR RESEARCH INTO THE FATIGUE AND CONSTITUTIVE BEHAVIOR OF HIGH TEMPERATURE MATERIALS

MICHAEL A. MCGAW *In* its Turbine Engine Hot Section Technology, 1985 p 361-371 Oct. 1985

Avail: NTIS HC A19/MF A01 CSCL 20K

Lewis Research Center's high temperature fatigue laboratory has undergone significant changes resulting in the addition of several new experimental capabilities. New materials testing systems have been installed enabling research to be conducted in multiaxial fatigue and deformation at high temperature, as well as cumulative creep-fatigue damage wherein the relative failure-life levels are widely separated. A key component of the new high-temperature fatigue and structures laboratory is a local, distributed computer system whose hardware and software architecture emphasizes a high degree of configurability, which in turn, enables the researcher to tailor a solution to the problem at hand. Author

N88-12825*# National Aeronautics and Space Administration. Lewis Research Center, Cleveland, OH.

CREEP LIFE PREDICTION BASED ON STOCHASTIC MODEL OF MICROSTRUCTURALLY SHORT CRACK GROWTH

TAKAYUKI KITAMURA and RYUICHI OHTANI (Kyoto Univ., Japan) 1988 23 p Proposed for presentation to the Summer Annual Meeting of the American Society of Mechanical Engineers, Berkeley, Calif., 20-22 Jun. 1988

(NASA-TM-100245; E-3867; NAS 1.15:100245) Avail: NTIS HC A03/MF A01 CSCL 20K

A nondimensional model of microstructurally short crack growth in creep is developed based on a detailed observation of the creep fracture process of 304 stainless steel. In order to deal with the scatter of small crack growth rate data caused by microstructural inhomogeneity, a random variable technique is used in the model. A cumulative probability of the crack length at an arbitrary time, $G(\bar{a}, \bar{a}, \bar{t})$, and that of the time when a crack reaches an arbitrary length, $F(\bar{t}, \bar{a}, \bar{a})$, are obtained numerically by means of a Monte Carlo method. $G(\bar{a}, \bar{a}, \bar{t})$, and $F(\bar{t}, \bar{a}, \bar{a})$ are the probabilities for a single crack. However, multiple cracks generally initiate on the surface of a smooth specimen

from the early stage of creep life to the final stage. Taking into account the multiple crack initiations, the actual crack length distribution observed on the surface of a specimen is predicted by the combination of probabilities for a single crack. The prediction shows a fairly good agreement with the experimental result for creep of 304 stainless steel at 923 K. The probability of creep life is obtained from an assumption that creep fracture takes place when the longest crack reaches a critical length. The observed and predicted scatter of the life is fairly small for the specimens tested. Author

N88-13732*# Georgia Inst. of Tech., Atlanta. Fracture and Fatigue Research Lab.

DEFORMATION, FATIGUE AND FRACTURE BEHAVIOR OF TWO CAST ANISOTROPIC SUPERALLOYS

WALTER W. MILLIGAN, ERIC S. HURON (Pratt and Whitney Aircraft, East Hartford, Conn.), and STEPHEN D. ANTOLOVICH (Virginia Univ., Fatigue 87, Volume 3 p 1561-1591 1987 (Contract NAG3-503)

Avail: NTIS HC A22/MF A01 CSCL 20K

Tensile and low cycle fatigue (LCF) tests were conducted on two cast anisotropic superalloys. The effects of temperature, strain rate and stress range were investigated. Deformation behavior was extensively characterized and modeled. LCF and fracture behavior were studied and correlated with deformation behavior. Author

N88-13745*# National Aeronautics and Space Administration. Lewis Research Center, Cleveland, OH.

THERMAL FINITE-ELEMENT ANALYSIS OF SPACE SHUTTLE MAIN ENGINE TURBINE BLADE

ALI ABDUL-AZIZ, MICHAEL T. TONG (Sverdrup Technology, Inc., Cleveland, Ohio.), and ALBERT KAUFMAN Oct. 1987 11 p (NASA-TM-100117; E-3535; NAS 1.15:100117) Avail: NTIS HC A03/MF A01 CSCL 20K

Finite-element, transient heat transfer analyses were performed for the first-stage blades of the space shuttle main engine (SSME) high-pressure fuel turbopump. The analyses were based on test engine data provided by Rocketdyne. Heat transfer coefficients were predicted by performing a boundary-layer analysis at steady-state conditions with the STAN5 boundary-layer code. Two different peak-temperature overshoots were evaluated for the startup transient. Cutoff transient conditions were also analyzed. A reduced gas temperature profile based on actual thermocouple data was also considered. Transient heat transfer analyses were conducted with the MARC finite-element computer code. Author

N88-13754*# National Aeronautics and Space Administration. Lewis Research Center, Cleveland, OH.

STAEBL/GENERAL COMPOSITES WITH HYGROTHERMAL EFFECTS (STAEBL/GENCOM)

ROBERT RUBENSTEIN (Sverdrup Technology, Inc., Cleveland, Ohio.) and CHRISTOS C. CHAMIS Dec. 1987 14 p (NASA-TM-100266; E-3896; NAS 1.15:100266) Avail: NTIS HC A03/MF A01 CSCL 11D

A computer code has been developed to perform structural optimization of turbine blades made from angle ply fiber composite laminates. Design variables available for optimization include geometric parameters such as blade thickness distribution and root chord, and composite material parameters such as ply angles and numbers of plies of each constituent material. Design constraints include resonance margins, forced response margins, maximum stress, and maximum ply combined stress. A general description of this code is given. Design optimization studies for typical blades are presented. Author

N88-14453*# National Aeronautics and Space Administration. Lewis Research Center, Cleveland, OH.

FATIGUE LIFE PREDICTION MODELING FOR TURBINE HOT SECTION MATERIALS

G. R. HALFORD, T. G. MEYER, R. S. NELSON, D. M. NISSLEY, and G. A. SWANSON (United Technologies Research Center, East Hartford, Conn.) 1988 17 p Prepared for presentation at the

33rd International Gas Turbine and Aeroengine Congress and Exposition, Amsterdam, The Netherlands, 5-9 Jun. 1988; sponsored in part by American Society of Mechanical Engineers (NASA-TM-100291; E-3927; NAS 1.15:100291) Avail: NTIS HC A03/MF A01 CSCL 20K

A major objective of the fatigue and fracture efforts under the Hot Section Technology (HOST) program was to significantly improve the analytic life prediction tools used by the aeronautical gas turbine engine industry. This was achieved in the areas of high-temperature thermal and mechanical fatigue of bare and coated high-temperature superalloys. The cyclic crack initiation and propagation resistance of nominally isotropic polycrystalline and highly anisotropic single crystal alloys were addressed. Life prediction modeling efforts were devoted to creep-fatigue interaction, oxidation, coatings interactions, multiaxiality of stress-strain states, mean stress effects, cumulative damage, and thermomechanical fatigue. The fatigue crack initiation life models developed to date include the Cyclic Damage Accumulation (CDA) and the Total Strain Version of Strainrange Partitioning (TS-SRP) for nominally isotropic materials, and the Tensile Hysteretic Energy Model for anisotropic superalloys. A fatigue model is being developed based upon the concepts of Path-Independent Integrals (PII) for describing cyclic crack growth under complex nonlinear response at the crack tip due to thermomechanical loading conditions. A micromechanistic oxidation crack extension model was derived. The models are described and discussed. Author

N88-15263*# National Aeronautics and Space Administration. Lewis Research Center, Cleveland, OH.

LIFE PREDICTION OF THERMOMECHANICAL FATIGUE USING TOTAL STRAIN VERSION OF STRAINRANGE PARTITIONING (SRP): A PROPOSAL

JAMES F. SALTSMAN and GARY R. HALFORD Feb. 1988 25 p

(NASA-TP-2779; E-3795; NAS 1.60:2779) Avail: NTIS HC A03/MF A01 CSCL 20K

A method is proposed (without experimental verification) for extending the total strain version of Strainrange Partitioning (TS-SRP) to predict the lives of thermomechanical fatigue (TMF) cycles. The principal feature of TS SRP is the determination of the time-temperature-waveshape dependent elastic strainrange versus life lines that are added subsequently to the classical inelastic strainrange versus life lines to form the total strainrange versus life relations. The procedure is based on a derived relation between failure and flow behavior. Failure behavior is represented by conventional SRP inelastic strainrange versus cyclic life relations, while flow behavior is captured in terms of the cyclic stress-strain response characteristics. Stress-strain response is calculated from simple equations developed from approximations to more complex cyclic constitutive models. For applications to TMF life prediction, a new testing technique, bithermal cycling, is proposed as a means for generating the inelastic strainrange versus life relations. Flow relations for use in predicting TMF lives would normally be obtained from approximations to complex thermomechanical constitutive models. Bithermal flow testing is also proposed as an alternative to thermomechanical flow testing at low strainranges where the hysteresis loop is difficult to analyze. Author

N88-16701*# National Aeronautics and Space Administration. Lewis Research Center, Cleveland, OH.

CREEP AND FATIGUE RESEARCH EFFORTS ON ADVANCED MATERIALS

JOHN GAYDA In its Aeropropulsion '87. Session 1: Aeropropulsion Materials Research 18 p Nov. 1987

Avail: NTIS HC A06/MF A01 CSCL 20K

Two of the more important materials problems encountered in turbine blades of aircraft engines are creep and fatigue. To withstand these high-temperature phenomena modern engines utilize single-crystal, nickel-based superalloys as the material of choice in critical applications. Recent research activities at Lewis on single-crystal blading material as well as future research initiatives on metal matrix composites related to creep and fatigue

39 STRUCTURAL MECHANICS

are discussed. The goal of these research efforts is improving the understanding of microstructure-property relationships and thereby guide material development. Author

N88-17095*# National Aeronautics and Space Administration. Lewis Research Center, Cleveland, OH.

STRESS INTENSITY AND CRACK DISPLACEMENT FOR SMALL EDGE CRACKS

THOMAS W. ORANGE Feb. 1988 11 p
(NASA-TP-2801; E-3744; NAS 1.60:2801) Avail: NTIS HC A03/MF A01 CSCL 20K

The weight function method was used to derive stress intensity factors and crack mouth displacement coefficients for small edge cracks (less than 20 percent of the specimen width) in common fracture specimen configurations. Contact stresses due to point application of loads were found to be small but significant for three-point bending and insignificant for four-point bending. The results are compared with available equations and numerical solutions from the literature and with unpublished boundary collocation results. Author

N88-18036*# National Aeronautics and Space Administration. Lewis Research Center, Cleveland, OH.

VIBRATION AND FLUTTER CHARACTERISTICS OF THE SR7L LARGE-SCALE PROPPAN

RICHARD AUGUST (Sverdrup Technology, Inc., Cleveland, Ohio.) and KRISHNA RAO V. KAZA Jan. 1988 22 p
(NASA-TM-100272; E-3908; NAS 1.15:100272) Avail: NTIS HC A03/MF A01 CSCL 20K

An investigation of the vibration characteristics and aeroelastic stability of the SR7L Large-Scale Advanced Propfan was performed using a finite element blade model and an improved aeroelasticity code. Analyses were conducted for different blade pitch angles, blade support conditions, number of blades, rotational speeds, and freestream Mach numbers. A finite element model of the blade was used to determine the blade's vibration behavior and sensitivity to support stiffness. The calculated frequencies and mode shape obtained with this model agreed well with the published experimental data. A computer code recently developed at NASA Lewis Research Center and based on three-dimensional, unsteady, lifting surface aerodynamic theory was used for the aeroelastic analysis to examine the blade's stability at a cruise condition of Mach 0.8 at 1700 rpm. The results showed that the blade is stable for that operating point. However, a flutter condition was predicted if the cruise Mach number was increased to 0.9. Author

N88-18040*# National Aeronautics and Space Administration. Lewis Research Center, Cleveland, OH.

RELATIONSHIP BETWEEN FATIGUE LIFE IN THE CREEP-FATIGUE REGION AND STRESS-STRAIN RESPONSE

A. BERKOVITS and S. NADIV (Technion - Israel Inst. of Tech., Haifa.) 1988 21 p Proposed for presentation at the 6th International Congress on Experimental Mechanics, Portland, Oreg., 5-10 Jun. 1988; sponsored by the Society of Experimental Mechanics

(NASA-TM-100796; E-3972; NAS 1.15:100796) Avail: NTIS HC A03/MF A01 CSCL 20K

On the basis of mechanical tests and metallographic studies, strainrange partitioned lives were predicted by introducing stress-strain materials parameters into the Universal Slopes Equation. This was the result of correlating fatigue damage mechanisms and deformation mechanisms operating at elevated temperatures on the basis of observed mechanical and microstructural behavior. Correlation between high temperature fatigue and stress strain properties for nickel base superalloys and stainless steel substantiated the method. Parameters which must be evaluated for PP- and CC- life are the maximum stress achievable under entirely plastic and creep conditions respectively and corresponding inelastic strains, and the elastic modulus. For plasticity/creep interaction conditions (PC and CP) two more pairs of stress strain parameters must be ascertained. Author

N88-18967*# National Aeronautics and Space Administration. Lewis Research Center, Cleveland, OH.

STRUCTURAL ANALYSIS METHODS DEVELOPMENT FOR TURBINE HOT SECTION COMPONENTS

ROBERT L. THOMPSON 1988 38 p Prepared for presentation at the International Gas Turbine and Aerospace Congress, Amsterdam, The Netherlands, 5-9 Jun. 1988; sponsored by ASME

(NASA-TM-100298; E-3926; NAS 1.15:100298) Avail: NTIS HC A03/MF A01 CSCL 20K

The structural analysis technologies and activities of the NASA Lewis Research Center's gas turbine engine Hot Section Technology (HOST) program are summarized. The technologies synergistically developed and validated include: time-varying thermal/mechanical load models; component-specific automated geometric modeling and solution strategy capabilities; advanced inelastic analysis methods; inelastic constitutive models; high-temperature experimental techniques and experiments; and nonlinear structural analysis codes. Features of the program that incorporate the new technologies and their application to hot section component analysis and design are described. Improved and, in some cases, first-time 3-D nonlinear structural analyses of hot section components of isotropic and anisotropic nickel-base superalloys are presented. Author

N88-18968*# National Aeronautics and Space Administration. Lewis Research Center, Cleveland, OH.

STRUCTURE OF A VISCOPLASTIC THEORY

ALAN D. FREED 1988 27 p Prepared for presentation at the Summer Annual Meeting Symposium on Constitutive Equations and Life Prediction Models for High Temperature Applications, Berkeley, Calif., 20-22 Jun. 1988; sponsored by ASME
(NASA-TM-100794; E-3969; NAS 1.15:100794) Avail: NTIS HC A03/MF A01 CSCL 20L

The general structure of a viscoplastic theory is developed from physical and thermodynamical considerations. The flow equation is of classical form. The dynamic recovery approach is shown to be superior to the hardening function approach for incorporating nonlinear strain hardening into the material response through the evolutionary equation for back stress. A novel approach for introducing isotropic strain hardening into the theory is presented, which results in a useful simplification. In particular, the limiting stress for the kinematic saturation of state (not the drag stress) is the chosen scalar-valued state variable. The resulting simplification is that there is no coupling between dynamic and thermal recovery terms in each evolutionary equation. The derived theory of viscoplasticity has the structure of a two-surface plasticity theory when the response is plasticlike, and the structure of a Bailey-Orowan creep theory when the response is creeplike. Author

N88-18969*# National Aeronautics and Space Administration. Lewis Research Center, Cleveland, OH.

THE EFFECTS OF ROTATIONAL FLOW, VISCOSITY, THICKNESS, AND SHAPE ON TRANSONIC FLUTTER DIP PHENOMENA

T. S. R. REDDY, RAKESH SRIVASTAVA (Georgia Inst. of Tech., Atlanta.), and KRISHNA RAO V. KAZA 1988 21 p Prepared for presentation at the 29th Structures, Structural Dynamics and Materials Conference, Williamsburg, Va., 18-20 Apr. 1988; sponsored in part by AIAA, ASME, ASCE, and AHS
(Contract NSG-3139; NAG3-370)

(NASA-TM-100811; E-3993; AIAA-88-2348; NAS 1.15:100811) Avail: NTIS HC A03/MF A01 CSCL 20K

The transonic flutter dip phenomena on thin airfoils, which are employed for propfan blades, is investigated using an integrated Euler/Navier-Stokes code and a two degrees of freedom typical section structural model. As a part of the code validation, the flutter characteristics of the NACA 64A010 airfoil are also investigated. In addition, the effects of artificial dissipation models, rotational flow, initial conditions, mean angle of attack, viscosity, airfoil thickness and shape on flutter are investigated. The results obtained with a Euler code for the NACA 64A010 airfoil are in

reasonable agreement with published results obtained by using transonic small disturbance and Euler codes. The two artificial dissipation models, one based on the local pressure gradient scaled by a common factor and the other based on the local pressure gradient scaled by a spectral radius, predicted the same flutter speeds except in the recovery region for the case studied. The effects of rotational flow, initial conditions, mean angle of attack, and viscosity for the Reynold's number studied seem to be negligible or small on the minima of the flutter dip. Author

N88-18974*# National Aeronautics and Space Administration. Lewis Research Center, Cleveland, OH.

CHARACTERIZATION OF DAMPED STRUCTURAL CONNECTIONS FOR MULTI-COMPONENT SYSTEMS
CHARLES LAWRENCE and ARTHUR A. HUCKELBRIDGE (Case Western Reserve Univ., Cleveland, Ohio.) Mar. 1988 19 p (NASA-TM-100801; E-3980; NAS 1.15:100801) Avail: NTIS HC A03/MF A01 CSCL 20K

The inability to model connections adequately has historically limited the ability to predict overall system dynamic response. Connections between structural components are often mechanically complex and difficult to accurately model analytically. Improved analytical models for connections are needed to improve system dynamic predictions. This study explores combining Component Mode Synthesis methods for coupling structural components with Parameter Identification procedures for improving the analytical modeling of the connections. Improvements in the connection stiffness and damping properties are computed in terms of physical parameters so the physical characteristics of the connections can be better understood, in addition to providing improved input for the system model. Author

N88-18975*# Cleveland State Univ., OH.

RELIABILITY BASED ANALYSIS OF CONTACT PROBLEMS
Final Contractor Report

LYNN M. POWERS and LOUIS J. GHOSN Mar. 1988 8 p
Proposed for presentation at the Probabilistic Methods Conference, Blacksburg, Va., 25-27 May 1988; sponsored by the American Society of Civil Engineering
(Contract NCC3-46)
(NASA-CR-182117; E-4007; NAS 1.26:182117) Avail: NTIS HC A02/MF A01 CSCL 20K

The Batdorf model is modified to include the reduction in shear due to the effect of compressive stresses on the crack face. This new formulation was used to obtain the probability of failure of ceramic components under contact stress conditions. The combined effect of the surface and volume flaws are included in the analysis. Due to the nature of the fracture of brittle materials under compressive loading, the component is modeled as a series system in order to establish bounds on the probability of failure. Author

N88-18976*# National Aeronautics and Space Administration. Lewis Research Center, Cleveland, OH.

A SEMIANALYTICAL TECHNIQUE FOR SENSITIVITY ANALYSIS OF UNSTEADY AERODYNAMIC COMPUTATIONS
DURBHA V. MURTHY (Toledo Univ., Ohio.) and KRISHNA RAO V. KAZA 1988 24 p Presented at the 29th Structures, Structural Dynamics and Materials Conference, Williamsburg, Va., 18-20 Apr. 1988; sponsored by AIAA, ASME, ASCE, AHS and ACS
(NASA-TM-100810; E-3990; NAS 1.15:100810; AIAA-88-2377)
Avail: NTIS HC A03/MF A01 CSCL 20K

A semianalytical approach is developed for the sensitivity analysis of linear unsteady aerodynamic loads. The semianalytical approach is easier to implement than the analytical approach. It is also computationally less expensive than the finite difference approach when used with panel methods, which require a large number of panels. The semianalytical approach is applied to an isolated airfoil in a 2-D flow and rotating propfan blades in 3-D flow. Sensitivity coefficients with respect to non-shape-dependent variables are shown for some cases. It is expected that the semianalytical approach will be useful in aeroelastic design

procedures particularly when mistuning is present, and that it is potentially useful for shape sensitivity analysis of linear unsteady aerodynamics. Author

N88-20668*# Georgia Inst. of Tech., Atlanta. School of Aerospace Engineering.

ANALYSIS OF SHELL-TYPE STRUCTURES SUBJECTED TO TIME-DEPENDENT MECHANICAL AND THERMAL LOADING
Semiannual Status Report

G. J. SIMITSES and R. RIFF Apr. 1988 57 p
(Contract NAG3-534)
(NASA-CR-182705; NAS 1.26:182705) Avail: NTIS HC A04/MF A01 CSCL 20K

This research is performed to develop a general mathematical model and solution methodologies for analyzing structural response of thin, metallic shell-type structures under large transient, cyclic or static thermomechanical loads. Among the system responses, which are associated with these load conditions, are thermal buckling, creep buckling, and ratcheting. Thus, geometric as well as material-type nonlinearities (of high order) can be anticipated and must be considered in the development of the mathematical model. Furthermore, this must also be accommodated in the solution procedures. Author

N88-21497*# National Aeronautics and Space Administration. Lewis Research Center, Cleveland, OH.

A VISCOPLASTIC THEORY APPLIED TO COPPER

ALAN D. FREED and MICHAEL J. VERRILLI 1988 15 p
Proposed for presentation at the International Seminar on the Inelastic Behavior of Solids Models and Utilization, Besancon, France, 30 Aug. - 1 Sep. 1988; sponsored by MECAMAT
(NASA-TM-100831; E-4020; NAS 1.15:100831) Avail: NTIS HC A03/MF A01 CSCL 20K

A phenomenologically based viscoplastic model is derived for copper. The model is thermodynamically constrained by the condition of material dissipativity. Two internal state variables are considered. The back stress accounts for strain-induced anisotropy, or kinematic hardening. The drag stress accounts for isotropic hardening. Static and dynamic recovery terms are not coupled in either evolutionary equation. The evolution of drag stress depends on static recovery, while the evolution of back stress depends on dynamic recovery. The material constants are determined from isothermal data. Model predictions are compared with experimental data for thermomechanical test conditions. They are in good agreement at the hot end of the loading cycle, but the model overpredicts the stress response at the cold end of the cycle. Author

N88-21498*# National Aeronautics and Space Administration. Lewis Research Center, Cleveland, OH.

NONLINEAR CONSTITUTIVE RELATIONS FOR HIGH TEMPERATURE APPLICATIONS, 1986

Apr. 1988 482 p Symposium held in Akron, Ohio, 11-13 Jun. 1986; sponsored by NASA, Lewis Research Center, Cleveland, Ohio and Akron Univ., Ohio
(NASA-CP-10010; E-3956; NAS 1.55:10010) Avail: NTIS HC A21/MF A01 CSCL 20K

The purpose of the symposium was to review the state-of-the-art in nonlinear constitutive modeling of high temperature materials for aeronautics applications and to identify the need for future research and development efforts in this area. Through this symposium, it was recognized that considerable research efforts are urgently needed in the development of nonlinear constitutive relations for high temperature applications. In the aerospace industry this need is further prompted by recent advances in high temperature materials technology and new demands on material and component performance.

N88-21505*# Rensselaer Polytechnic Inst., Troy, NY.

A SIMPLIFIED ORTHOTROPIC FORMULATION OF THE VISCOPLASTICITY THEORY BASED ON OVERSTRESS

M. SUTCU and E. KREMPL In NASA. Lewis Research Center, Nonlinear Constitutive Relations for High Temperature Applications,

39 STRUCTURAL MECHANICS

1986 p 89-95 Apr. 1988 Previously announced as N88-70180
Sponsored in part by NSF
(Contract NAG3-262)

Avail: NTIS HC A21/MF A01 CSCL 20K

An orthotropic, small strain viscoplasticity theory based on overstress is presented. In each preferred direction the stress is composed of time (rate) independent (or plastic) and viscous (or rate dependent) contributions. Tension-compression asymmetry can depend on direction and is included in the model. Upon a proper choice of a material constant one preferred direction can exhibit linear elastic response while the other two deform in a viscoplastic manner.

Author

N88-21508*# National Aeronautics and Space Administration. Lewis Research Center, Cleveland, OH.

A THEORY OF VISCOPLASTICITY ACCOUNTING FOR INTERNAL DAMAGE

A. D. FREED and D. N. ROBINSON (Akron Univ., Ohio.) *In its* Nonlinear Constitutive Relations for High Temperature Applications, 1986 p 119-136 Apr. 1988

Avail: NTIS HC A21/MF A01 CSCL 20K

A constitutive theory for use in structural and durability analyses of high temperature isotropic alloys is presented. Constitutive equations based upon a potential function are determined from conditions of stability and physical considerations. The theory is self-consistent; terms are not added in an ad hoc manner. It extends a proven viscoplastic model by introducing the Kachanov-Rabotnov concept of net stress. Material degradation and inelastic deformation are unified; they evolve simultaneously and interactively. Both isotropic hardening and material degradation evolve with dissipated work which is the sum of inelastic work and internal work. Internal work is a continuum measure of the stored free energy resulting from inelastic deformation.

Author

N88-21511*# National Aeronautics and Space Administration. Lewis Research Center, Cleveland, OH.

EVALUATION OF STRUCTURAL ANALYSIS METHODS FOR LIFE PREDICTION

A. KAUFMAN, J. F. SALTSMAN, G. R. HALFORD, and M. TONG (Sverdrup Technology, Inc., Cleveland, Ohio.) *In its* Nonlinear Constitutive Relations for High Temperature Applications, 1986 p 201-216 Apr. 1988

Avail: NTIS HC A21/MF A01 CSCL 20K

The utility of advanced constitutive models and structural analysis methods are evaluated for predicting the cyclic life of an air-cooled turbine blade for a gas turbine aircraft engine. Structural analysis methods of various levels of sophistication were exercised to obtain the cyclic stress-strain response at the critical airfoil location. Calculated strain ranges and mean stresses from the stress-strain cycles were used to predict crack initiation lives by using the total strain version of the strain range partitioning life prediction method. The major results are given and discussed.

Author

N88-21523*# Southwest Research Inst., San Antonio, TX.
UNIFIED CONSTITUTIVE MODELS FOR HIGH-TEMPERATURE STRUCTURAL APPLICATIONS

U. S. LINDHOLM, K. S. CHAN, S. R. BODNER, R. M. WEBER, and K. P. WALKER (Engineering Science Software, Inc., Smithfield, R.I.) *In* NASA. Lewis Research Center, Nonlinear Constitutive Relations for High Temperature Applications, 1986 p 371-394 Apr. 1988

(Contract NAS3-23925)

Avail: NTIS HC A21/MF A01 CSCL 20K

Unified constitutive models are characterized by the use of a single inelastic strain rate term for treating all aspects of inelastic deformation, including plasticity, creep, and stress relaxation under monotonic or cyclic loading. The structure of this class of constitutive theory pertinent for high temperature structural applications is first outlined and discussed. The effectiveness of the unified approach for representing high temperature deformation of Ni-base alloys is then evaluated by extensive comparison of experimental data and predictions of the Bodner-Partom and the

Walker models. The use of the unified approach for hot section structural component analyses is demonstrated by applying the Walker model in finite element analyses of a benchmark notch problem and a turbine blade problem.

Author

N88-21526*# Georgia Inst. of Tech., Atlanta. School of Engineering Science and Mechanics.

NON-ISOTHERMAL ELASTOVISCOPLASTIC ANALYSIS OF PLANAR CURVED BEAMS

G. J. SIMITSES, R. L. CARLSON, and R. RIFF *In* NASA. Lewis Research Center, Nonlinear Constitutive Relations for High Temperature Applications, 1986 p 437-459 Apr. 1988

(Contract NAG3-54)

Avail: NTIS HC A21/MF A01 CSCL 20K

The development of a general mathematical model and solution methodologies, to examine the behavior of thin structural elements such as beams, rings, and arches, subjected to large nonisothermal elastoviscoplastic deformations is presented. Thus, geometric as well as material type nonlinearities of higher order are present in the analysis. For this purpose a complete true abinitio rate theory of kinematics and kinetics for thin bodies, without any restriction on the magnitude of the transformation is presented. A previously formulated elasto-thermo-viscoplastic material constitutive law is employed in the analysis. The methodology is demonstrated through three different straight and curved beams problems.

Author

N88-21534*# National Aeronautics and Space Administration. Lewis Research Center, Cleveland, OH.

TEST FACILITIES OF THE STRUCTURAL DYNAMICS BRANCH OF NASA LEWIS RESEARCH CENTER

GERALD T. MONTAGUE (Sverdrup Technology, Inc., Cleveland, Ohio.) and ROBERT E. KIELB May 1988 26 p

(NASA-TM-100800; E-3978; NAS 1.15:100800) Avail: NTIS HC A03/MF A01 CSCL 20K

The NASA Lewis Research Center Structural Dynamics Branch conducts experimental and analytical research related to the structural dynamics of aerospace propulsion and power systems. The experimental testing facilities of the branch are examined. Presently there are 10 research rigs and 4 laboratories within the branch. These facilities are described along with current and past research work.

Author

N88-21535*# Pratt and Whitney Aircraft, East Hartford, CT. Commercial Engineering Dept.

ON 3-D INELASTIC ANALYSIS METHODS FOR HOT SECTION COMPONENTS. VOLUME 1: SPECIAL FINITE ELEMENT

MODELS Annual Report No. 4, 14 Feb. 1986 - 14 Feb. 1987

S. NAKAZAWA May 1988 81 p Original contains color illustrations

(Contract NAS3-23697)

(NASA-CR-180893; NAS 1.26:180893; PWA-5940-62-VOL-1)

Avail: NTIS HC A05/MF A01 CSCL 20K

This annual status report presents the results of work performed during the fourth year of the 3-D Inelastic Analysis Methods for Hot Section Components program (NASA Contract NAS3-23697). The objective of the program is to produce a series of new computer codes permitting more accurate and efficient 3-D analysis of selected hot section components, i.e., combustor liners, turbine blades and turbine vanes. The computer codes embody a progression of math models and are streamlined to take advantage of geometrical features, loading conditions, and forms of material response that distinguish each group of selected components. Volume 1 of this report discusses the special finite element models developed during the fourth year of the contract.

Author

N88-22382*# National Aeronautics and Space Administration. Lewis Research Center, Cleveland, OH.

LEWIS STRUCTURES TECHNOLOGY, 1988. VOLUME 2: STRUCTURAL MECHANICS

May 1988 307 p Symposium held in Cleveland, Ohio, 24-25 May 1988

(NASA-CP-3003-VOL-2; E-3970-VOL-2; NAS 1.55:3003-VOL-2)
 Avail: NTIS HC A14/MF A01 CSCL 20K

Lewis Structures Div. performs and disseminates results of research conducted in support of aerospace engine structures. These results have a wide range of applicability to practitioners of structural engineering mechanics beyond the aerospace arena. The engineering community was familiarized with the depth and range of research performed by the division and its academic and industrial partners. Sessions covered vibration control, fracture mechanics, ceramic component reliability, parallel computing, nondestructive evaluation, constitutive models and experimental capabilities, dynamic systems, fatigue and damage, wind turbines, hot section technology (HOST), aeroelasticity, structural mechanics codes, computational methods for dynamics, structural optimization, and applications of structural dynamics, and structural mechanics computer codes.

N88-22385*# National Aeronautics and Space Administration. Lewis Research Center, Cleveland, OH.
EXPERIMENTS INVESTIGATING ADVANCED MATERIALS UNDER THERMOMECHANICAL LOADING

PAUL A. BARTOLOTTA *In its* Lewis Structures Technology, 1988. Volume 2: Structural Mechanics p 27-35 May 1988
 Avail: NTIS HC A14/MF A01 CSCL 20K

Many high temperature aircraft and rocket engine components experience large mechanical loads as well as severe thermal gradients and transients. These nonisothermal conditions are often large enough to cause inelastic deformations, which are the ultimate cause for failure in those parts. A way to alleviate this problem is through improved engine designs based on better predictions of thermomechanical material behavior. To address this concern, an experimental effort was recently initiated within the Hot Section Technology (HOST) program at Lewis. As part of this effort, two new test systems were added to the Fatigue and Structures Lab., which allowed thermomechanical tests to be conducted under closely controlled conditions. These systems are now being used for thermomechanical testing for the Space Station Receiver program, and will be used to support development of metal matrix composites. Author

N88-22386*# National Aeronautics and Space Administration. Lewis Research Center, Cleveland, OH.
BIAXIAL EXPERIMENTS SUPPORTING THE DEVELOPMENT OF CONSTITUTIVE THEORIES FOR ADVANCED HIGH-TEMPERATURE MATERIALS

J. R. ELLIS *In its* Lewis Structures Technology, 1988. Volume 2: Structural Mechanics p 37-48 May 1988
 Avail: NTIS HC A14/MF A01 CSCL 20K

Complex states of stress and strain are introduced into components during service in engineering applications. It follows that analysis of such components requires material descriptions, or constitutive theories, which reflect the tensorial nature of stress and strain. For applications involving stress levels above yield, the situation is more complex in that material response is both nonlinear and history dependent. This has led to the development of viscoplastic constitutive theories which introduce time by expressing the flow and evolutionary equation in the form of time derivatives. Models were developed here which can be used to analyze high temperature components manufactured from advanced composite materials. In parallel with these studies, effort was directed at developing multiaxial testing techniques to verify the various theories. Recent progress in the development of constitutive theories from both the theoretical and experimental viewpoints are outlined. One important aspect is that material descriptions for advanced composite materials which can be implemented in general purpose finite element codes and used for practical design are verified. Author

N88-22388*# Engineering Science Software, Inc., Smithfield, RI.

UNIFIED CONSTITUTIVE MODEL FOR SINGLE CRYSTAL DEFORMATION BEHAVIOR WITH APPLICATIONS

K. P. WALKER, T. G. MEYER, and E. H. JORDAN (Connecticut

Univ., Storrs.) *In* NASA. Lewis Research Center, Lewis Structures Technology, 1988. Volume 2: Structural Mechanics p 57-71 May 1988

(Contract NAS3-23939; NAG3-512)

Avail: NTIS HC A14/MF A01 CSCL 20K

Single crystal materials are being used in gas turbine airfoils and are candidates for other hot section components because of their increased temperature capabilities and resistance to thermal fatigue. Development of a constitutive model which assesses the inelastic behavior of these materials has been studied in 2 NASA programs: Life Prediction and Constitutive Models for Engine Hot Section Anisotropic Materials and Biaxial Constitutive Equation Development for Single Crystals. The model has been fit to a large body of constitutive data for single crystal PWA 1480 material. The model uses a unified approach for computing total inelastic strains (creep plus plasticity) on crystallographic slip systems reproducing observed directional and strain rate effects as a natural consequence of the summed slip system quantities. The model includes several of the effects that have been reported to influence deformation in single crystal materials, such as shear stress, latent hardening, and cross slip. The model is operational in a commercial Finite Element code and is being installed in a Boundary Element Method code. Author

N88-22389*# National Aeronautics and Space Administration. Lewis Research Center, Cleveland, OH.

FINITE ELEMENT (MARC) SOLUTION TECHNOLOGIES FOR VISCOPLASTIC ANALYSES

V. K. ARYA (National Academy of Sciences - National Research Council, Washington, D. C.) and ROBERT L. THOMPSON *In its* Lewis Structures Technology, 1988. Volume 2: Structural Mechanics p 73-79 May 1988

Avail: NTIS HC A14/MF A01 CSCL 20K

A need for development of realistic constitutive models for structural components operating at high temperatures, accompanied by appropriate solution technologies for stress/life analyses of these components is studied. Viscoplastic models provide a better description of inelastic behavior of materials, but their mathematical structure is very complex. The highly nonlinear and stiff nature of the constitutive equations makes analytical solutions difficult. Therefore, suitable solution, finite element or other numerical, technologies must be developed to make these models adaptable for better and rational designs of components. NASA-Lewis has developed several solution technologies and successfully applied them to the solution of a number of uniaxial and multiaxial problems. Some of these solution technologies are described along with the models and representative results. The solution technologies developed and presented encompass a wide range of models, such as, isotropic, anisotropic, metal matrix composites, and single crystal models. Author

N88-22397*# Sverdrup Technology, Inc., Cleveland, OH.

PROBABILISTIC STRUCTURAL ANALYSIS COMPUTER CODE (NESSUS)

MICHAEL C. SHIAO *In* NASA. Lewis Research Center, Lewis Structures Technology, 1988. Volume 2: Structural Mechanics p 173-181 May 1988

(Contract NAG3-24105)

Avail: NTIS HC A14/MF A01 CSCL 20K

Probabilistic structural analysis has been developed to analyze the effects of fluctuating loads, variable material properties, and uncertain analytical models especially for high performance structures such as SSME turbopump blades. The computer code NESSUS (Numerical Evaluation of Stochastic Structure Under Stress) was developed to serve as a primary computation tool for the characterization of the probabilistic structural response due to the stochastic environments by statistical description. The code consists of three major modules NESSUS/PRE, NESSUS/FEM, and NESSUS/FPI. NESSUS/PRE is a preprocessor which decomposes the spatially correlated random variables into a set of uncorrelated random variables using a modal analysis method. NESSUS/FEM is a finite element module which provides structural sensitivities to all the random variables considered. NESSUS/FPI

39 STRUCTURAL MECHANICS

is Fast Probability Integration method by which a cumulative distribution function or a probability density function is calculated.

Author

N88-22400*# National Aeronautics and Space Administration. Lewis Research Center, Cleveland, OH.

STRUCTURAL TAILORING OF ADVANCED TURBOPROPS

K. W. BROWN (Pratt and Whitney Aircraft, East Hartford, Conn.) and DALE A. HOPKINS *In its* Lewis Structures Technology, 1988. Volume 2: Structural Mechanics p 205-217 May 1988 (Contract NAS3-23941)

Avail: NTIS HC A14/MF A01 CSCL 20K

The Structural Tailoring of Advanced Turboprops (STAT) computer program was developed to perform numerical optimization on highly swept propfan blades. The optimization procedure seeks to minimize an objective function defined as either: (1) direct operating cost of full scale blade or, (2) aeroelastic differences between a blade and its scaled model, by tuning internal and external geometry variables that must satisfy realistic blade design constraints. The STAT analysis system includes an aerodynamic efficiency evaluation, a finite element stress and vibration analysis, an acoustic analysis, a flutter analysis, and a once-per-revolution forced response life prediction capability. STAT includes all relevant propfan design constraints.

Author

N88-22403*# National Aeronautics and Space Administration. Lewis Research Center, Cleveland, OH.

THERMOSTRUCTURAL ANALYSIS OF SIMULATED COWL LIPS

MATTHEW E. MELIS *In its* Lewis Structures Technology, 1988. Volume 2: Structural Mechanics p 245-254 May 1988

Avail: NTIS HC A14/MF A01 CSCL 20K

Three dimensional finite element analyses using MSC/NASTRAN and MARC are performed to predict the thermal and structural response of various cooling schemes under high heat loads. Steady state heat transfer analyses and elastic stress analyses are performed using MSC/NASTRAN. Elastic/plastic analyses are done using MARC. To help verify these analyses experimentally, a hydrogen-oxygen rocket engine was modified to use the exhaust stream as a high enthalpy, high heat flux source to evaluate various actively cooled, simulated cowl lip (leading edges) segments as well as flat structural segments. Cross flow and parallel flow cooling configurations were tested and analyzed using cooling fluids of water and gaseous hydrogen. In addition, various material types, including high conductivity copper, nickel, and a copper and graphite metal matrix composite were tested and compared.

Author

N88-22406*# National Aeronautics and Space Administration. Lewis Research Center, Cleveland, OH.

STRUCTURAL ASSESSMENT OF A SPACE STATION SOLAR DYNAMIC HEAT RECEIVER THERMAL ENERGY STORAGE CANISTER

R. L. THOMPSON, T. W. KERSLAKE, and M. T. TONG (Sverdrup Technology, Inc., Cleveland, Ohio.) *In its* Lewis Structures Technology, 1988. Volume 2: Structural Mechanics p 281-294 May 1988 Previously announced in IAA as N88-31396

Avail: NTIS HC A14/MF A01 CSCL 20K

The structural performance of a space station thermal energy storage (TES) canister subject to orbital solar flux variation and engine cold start up operating conditions was assessed. The impact of working fluid temperature and salt-void distribution on the canister structure are assessed. Both analytical and experimental studies were conducted to determine the temperature distribution of the canister. Subsequent finite element structural analyses of the canister were performed using both analytically and experimentally obtained temperatures. The Arrhenius creep law was incorporated into the procedure, using secondary creep data for the canister material, Haynes 188 alloy. The predicted cyclic creep strain accumulations at the hot spot were used to assess the structural performance of the canister. In addition, the structural performance of the canister based on the analytically determined

temperature was compared with that based on the experimentally measured temperature data.

Author

N88-22407*# National Aeronautics and Space Administration. Lewis Research Center, Cleveland, OH.

AN EFFICIENT MINDLIN FINITE STRIP PLATE ELEMENT BASED ON ASSUMED STRAIN DISTRIBUTION

ABHISAK CHULYA (Case Western Reserve Univ., Cleveland, Ohio.) and ROBERT L. THOMPSON *In its* Lewis Structures Technology, 1988. Volume 2: Structural Mechanics p 295-306 May 1988

Avail: NTIS HC A14/MF A01 CSCL 20K

A simple two node, linear, finite strip plate bending element based on Mindlin-Reissner plate theory for the analysis of very thin to thick bridges, plates, and axisymmetric shells is presented. The new transverse shear strains are assumed for constant distribution in the two node linear strip. The important aspect is the choice of the points that relate the nodal displacements and rotations through the locking transverse shear strains. The element stiffness matrix is explicitly formulated for efficient computation and ease in computer implementation. Numerical results showing the efficiency and predictive capability of the element for analyzing plates with different supports, loading conditions, and a wide range of thicknesses are given. The results show no sign of the shear locking phenomenon.

Author

N88-22408*# National Aeronautics and Space Administration. Lewis Research Center, Cleveland, OH.

LEWIS STRUCTURES TECHNOLOGY, 1988. VOLUME 3: STRUCTURAL INTEGRITY FATIGUE AND FRACTURE WIND TURBINES HOST

May 1988 366 p Symposium held in Cleveland, Ohio, 24-25 May 1988

(NASA-CP-3003-VOL-3; E-3970-VOL-3; NAS 1.55:3003-VOL-3)

Avail: NTIS HC A16/MF A01 CSCL 20K

The charter of the Structures Division is to perform and disseminate results of research conducted in support of aerospace engine structures. These results have a wide range of applicability to practitioners of structural engineering mechanics beyond the aerospace arena. The specific purpose of the symposium was to familiarize the engineering structures community with the depth and range of research performed by the division and its academic and industrial partners. Sessions covered vibration control, fracture mechanics, ceramic component reliability, parallel computing, nondestructive evaluation, constitutive models and experimental capabilities, dynamic systems, fatigue and damage, wind turbines, hot section technology (HOST), aeroelasticity, structural mechanics codes, computational methods for dynamics, structural optimization, and applications of structural dynamics, and structural mechanics computer codes.

N88-22417*# National Aeronautics and Space Administration. Lewis Research Center, Cleveland, OH.

FRACTURE TECHNOLOGY FOR BRITTLE MATERIALS

JONATHAN A. SALEM *In its* Lewis Structures Technology, 1988. Volume 3: Structural Integrity Fatigue and Fracture Wind Turbines HOST p 141-148 May 1988

Avail: NTIS HC A16/MF A01 CSCL 20K

Ceramics materials have the potential for use in high-temperature, fuel-efficient engines. However, because these materials are brittle, their fracture characteristics must be well documented prior to their application. Thus Lewis is working to understand the fracture and strength properties of brittle ceramic and ceramic matrix materials. An understanding of fracture properties aids both designers who are attempting to design high-temperature structures and materials scientists who seek to design more temperature-resistant materials. Both analytical and experimental approaches to fracture analysis are being taken. Methods for testing fracture toughness, crack growth resistance, and strength are being developed. The failure mechanisms at both room and elevated temperatures are also being investigated. Such investigations aid materials scientists in developing better high-temperature materials. Of concern is the anisotropy of ceramic

materials and the experimental verification of ceramic design codes that will allow brittle material behavior to be accurately predicted at high temperature. Author

N88-22418*# National Aeronautics and Space Administration. Lewis Research Center, Cleveland, OH.

MODE 2 FRACTURE MECHANICS

ROBERT J. BUZZARD and LOUIS GHOSN (Cleveland State Univ., Ohio.) *In its* Lewis Structures Technology, 1988. Volume 3: Structural Integrity Fatigue and Fracture Wind Turbines HOST p 149-159 May 1988 (Contract NCC3-46)

Avail: NTIS HC A16/MF A01 CSCL 20K

Current development of high-performance rolling element bearings for aircraft engines (up to 3 million DN, where DN is the product of shaft diameter in millimeters and speed in revolutions per minute) has aroused concern about fatigue crack growth in the inner bearing race that leads to catastrophic failure of the bearing and the engine. A failure sequence was postulated by Srawley, and an analytical program was undertaken to simulate fatigue crack propagation in the inner raceway of such a bearing. A fatigue specimen was developed at NASA by which fatigue data may be obtained relative to the cracking problems. The specimen may be used to obtain either mode 2 data alone or a combination of mixed-mode (1 and 2) data as well and was calibrated in this regard. Mixed-mode fracture data for M-50 bearing steel are presented, and a method for performing reversed-loading tests is described. Author

N88-22419*# National Aeronautics and Space Administration. Lewis Research Center, Cleveland, OH.

IN SITU FATIGUE LOADING STAGE INSIDE SCANNING ELECTRON MICROSCOPE

JACK TELESMA, PETER KANTZOS, and DAVID BREWER (Army Propulsion Lab., Cleveland, Ohio.) *In its* Lewis Structures Technology, 1988. Volume 3: Structural Integrity Fatigue and Fracture Wind Turbines HOST p 161-172 May 1988

Avail: NTIS HC A16/MF A01 CSCL 20K

A fatigue loading stage inside a scanning electron microscopy (SEM) was developed. The stage allows dynamic and static high-magnification and high-resolution viewing of the fatigue crack initiation and crack propagation processes. The loading stage is controlled by a closed-loop servohydraulic system. Maximum load is 1000 lb (4450 N) with test frequencies ranging up to 30 Hz. The stage accommodates specimens up to 2 inches (50 mm) in length and tolerates substantial specimen translation to view the propagating crack. At room temperature, acceptable working resolution is obtainable for magnifications ranging up to 10,000X. The system is equipped with a high-temperature setup designed for temperatures up to 2000 F (1100 C). The signal can be videotaped for further analysis of the pertinent fatigue damage mechanisms. The design allows for quick and easy interchange and conversion of the SEM from a loading stage configuration to its normal operational configuration and vice versa. Tests are performed entirely in the in-situ mode. In contrast to other designs, the NASA design has greatly extended the life of the loading stage by not exposing the bellows to cyclic loading. The loading stage was used to investigate the fatigue crack growth mechanisms in the (100)-oriented PWA 1480 single-crystal, nickel-based superalloy. The high-magnification observations revealed the details of the crack growth processes. Author

N88-22420*# Syracuse Univ., NY.

GRAIN BOUNDARY OXIDATION AND LOW-CYCLE FATIGUE AT ELEVATED TEMPERATURES

H. W. LIU and Y. OSHIDA *In* NASA. Lewis Research Center, Lewis Structures Technology, 1988. Volume 3: Structural Integrity Fatigue and Fracture Wind Turbines HOST p 173-185 May 1988 (Contract NAG3-348)

Avail: NTIS HC A16/MF A01 CSCL 20K

Fatigue life consists of fatigue crack nucleation and propagation periods. In order to predict fatigue life accurately, a methodology

for the quantitative assessment of these two fatigue damage processes had to be devised. Grain boundary oxidation penetrates faster than does oxidation within a grain. This faster oxidation penetration causes intergranular fatigue failures at elevated temperatures. Grain boundary oxidation accelerates both crack nucleation and propagation. Grain boundary oxidation kinetics and the statistical distribution of grain boundary oxide penetration depth were measured. Quantitative applications of the grain boundary oxidation kinetics to fatigue crack nucleation and propagation were analyzed. A method, based on the Weibull distribution, of extrapolating the laboratory oxidation data measured with small samples to large engineering structures is presented. Author

N88-22421*# General Electric Co., Evendale, OH.

ELEVATED TEMPERATURE CRACK GROWTH

K. S. KIM, R. H. VANSTONE, S. N. MALIK, and J. H. LAFFLEN *In* NASA. Lewis Research Center, Lewis Structures Technology, 1988. Volume 3: Structural Integrity Fatigue and Fracture Wind Turbines HOST p 187-198 May 1988 (Contract NAS3-23940)

Avail: NTIS HC A16/MF A01 CSCL 20K

The problem of crack growth in hot path components such as combustor liners is complicated by several practical and theoretical considerations. The loading environment of such components involves high temperature levels and gradients that lead to considerations such as thermal stresses, crack closure, hold time, inelastic strains (both time dependent and independent), and Thermal Mechanical Fatigue (TMF). In general, a good understanding of the influence of these factors on crack growth was not obtained. At the same time, several nonlinear fracture mechanics parameters were suggested for such applications; however, most of the proposed methods were not tested for broad applications such as required for hot section components. It was the purpose of this program to evaluate proposed nonlinear methods by performing a thorough experimental and analytical study. The results illustrated that much progress was made in developing nonlinear methods. Author

N88-22422*# National Aeronautics and Space Administration. Lewis Research Center, Cleveland, OH.

CUMULATIVE FATIGUE DAMAGE MODELS

MICHAEL A. MCGAW *In its* Lewis Structures Technology, 1988. Volume 3: Structural Integrity Fatigue and Fracture Wind Turbines HOST p 201-212 May 1988

Avail: NTIS HC A16/MF A01 CSCL 20K

The problem of calculating expected component life under fatigue loading conditions is complicated by the fact that component loading histories contain, in many cases, cyclic loads of widely varying amplitudes. In such a case a cumulative damage model is required, in addition to a fatigue damage criterion, or life relationship, in order to compute the expected fatigue life. The traditional cumulative damage model used in design is the linear damage rule. This model, while being simple to use, can yield grossly unconservative results under certain loading conditions. Research at the NASA Lewis Research Center has led to the development of a nonlinear cumulative damage model, named the double damage curve approach (DDCA), that has greatly improved predictive capability. This model, which considers the life (or loading) level dependence of damage evolution, was applied successfully to two polycrystalline materials, 316 stainless steel and Haynes 188. The cumulative fatigue behavior of the PWA 1480 single-crystal material is currently being measured to determine the applicability of the DDCA for this material. Author

N88-22423*# Illinois Univ., Urbana-Champaign. Dept. of Mechanical and Industrial Engineering.

FATIGUE DAMAGE MAPPING

DARRELL SOCIE *In* NASA. Lewis Research Center, Lewis Structures Technology, 1988. Volume 3: Structural Integrity Fatigue and Fracture Wind Turbines HOST p 213-220 May 1988 (Contract NAG3-465)

Avail: NTIS HC A16/MF A01 CSCL 20K

Observations of fatigue crack nucleation and early growth are

39 STRUCTURAL MECHANICS

presented. The state of stress/strain was shown to play a significant role in this process. Early growth occurs on planes experiencing the largest range of shear strain (Mode 2) or normal strain (Mode 1) depending on the stress state, strain amplitude, and microstructure. These observations were summarized in a fatigue map for each material. These maps provide regions where one fatigue failure mode dominates the behavior. Each failure mechanism results in a different failure mode. Once the expected failure mode is identified, bulk deformation models based on the cyclic stresses and strains can be used to obtain reliable estimates of fatigue lives for complex loading situations. Author

N88-22424*# National Aeronautics and Space Administration. Lewis Research Center, Cleveland, OH.

BITHERMAL FATIGUE: A SIMPLIFIED ALTERNATIVE TO THERMOMECHANICAL FATIGUE

MICHAEL J. VERRILLI *In its* Lewis Structures Technology, 1988. Volume 3: Structural Integrity Fatigue and Fracture Wind Turbines HOST p 221-230 May 1988
Avail: NTIS HC A16/MF A01 CSCL 20K

A bithermal fatigue test technique was proposed as a simplified alternative to the thermomechanical fatigue test. Both the thermomechanical cycle and the bithermal technique can be used to study nonisothermal fatigue behavior. The difference between the two cycles is that in a conventional thermomechanical fatigue cycle the temperature is continuously varied concurrently with the applied mechanical strains, but in the bithermal fatigue cycle the specimen is held at zero load during the temperature excursions and all the loads are applied at the two extreme temperatures of the cycle. Experimentally, the bithermal fatigue test technique offers advantages such as ease in synchronizing the temperature and mechanical strain waveforms, in minimizing temperature gradients in the specimen gauge length, and in reducing and interpreting thermal fatigue such as the influence of alternate high and low temperatures on the cyclic stress-strain response characteristics, the effects of thermal state, and the possibility of introducing high- and low-temperature deformation mechanisms within the same cycle. The bithermal technique was used to study nonisothermal fatigue behavior of alloys such as single-crystal PWA 1480, single-crystal Rene N4, cast B1900+Hf, and wrought Haynes 188. Author

N88-22446*# National Aeronautics and Space Administration. Lewis Research Center, Cleveland, OH.

STRUCTURAL DYNAMICS BRANCH RESEARCH AND ACCOMPLISHMENTS FOR FISCAL YEAR 1987

May 1988 34 p
(NASA-TM-100279; E-3920; NAS 1.15:100279) Avail: NTIS HC A03/MF A01 CSCL 20K

This publication contains a collection of fiscal year 1987 research highlights from the Structural Dynamics Branch at NASA Lewis Research Center. Highlights from the branch's four major work areas, Aeroelasticity, Vibration Control, Dynamic Systems, and Computational Structural Methods, are included in the report as well as a complete listing of the FY87 branch publications. Author

N88-23226*# National Aeronautics and Space Administration. Lewis Research Center, Cleveland, OH.

LEWIS STRUCTURES TECHNOLOGY, 1988. VOLUME 1: STRUCTURAL DYNAMICS

May 1988 463 p Symposium held in Cleveland, Ohio, 24-25 May 1988
(NASA-CP-3003-VOL-1; E-3970-VOL-1; NAS 1.55:3003-VOL-1)
Avail: NTIS HC A20/MF A01 CSCL 20K

The specific purpose of the symposium was to familiarize the engineering structures community with the depth and range of research performed by the Structures Division of the Lewis Research Center and its academic and industrial partners. Sessions covered vibration control, fracture mechanics, ceramic component reliability, parallel computing, nondestructive testing, dynamical systems, fatigue and damage, wind turbines, hot section

technology, structural mechanics codes, computational methods for dynamics, structural optimization, and applications of structural dynamics.

N88-23272*# Illinois Univ., Chicago. Dept. of Civil Engineering, Mechanics and Metallurgy.

ON GOVERNING EQUATIONS FOR CRACK LAYER PROPAGATION Final Report

A. CHUDNOVSKY and J. BOTSIS Apr. 1988 27 p
(Contract NAG3-754)
(NASA-CR-182120; NAS 1.26:182120) Avail: NTIS HC A03/MF A01 CSCL 20K

Results of analysis on damage distribution of a crack layer, in a model material, supported the self-similarity hypothesis of damage evolution which has been adopted by the crack layer theory. On the basis of measurements of discontinuity density and the double layer potential technique, a solution to the crack damage interaction problem has been developed. Evaluation of the stress intensity factor illustrated the methodology. Analysis of experimental results showed that Arrhenius type constitutive relationship described very well the expansion of the active zone of a crack layer. Author

N88-23278*# National Aeronautics and Space Administration. Lewis Research Center, Cleveland, OH.

METHOD AND MODELS FOR R-CURVE INSTABILITY CALCULATIONS

THOMAS W. ORANGE 1988 13 p Presented at the 21st National Symposium on Fracture Mechanics, Annapolis, Md., 28-30 Jun. 1988; sponsored by the American Society for Testing and Materials
(NASA-TM-100935; E-4212; NAS 1.15:100935) Avail: NTIS HC A03/MF A01 CSCL 20K

This paper presents a simple method for performing elastic R-curve instability calculations. For a single material-structure combination, the calculations can be done on some pocket calculators. On microcomputers and larger, it permits the development of a comprehensive program having libraries of driving force equations for different configurations and R-curve model equations for different materials. The paper also presents several model equations for fitting to experimental R-curve data, both linear elastic and elastoplastic. The models are fit to data from the literature to demonstrate their viability. Author

N88-23877*# National Aeronautics and Space Administration. Lewis Research Center, Cleveland, OH.

FRACTURE MECHANICS

JOHN L. SHANNON, JR. *In its* Structural Ceramics p 47-57 May 1988
Avail: NTIS HC A11/MF A01 CSCL 20K

The application of fracture mechanics to the design of ceramic structures will require the precise measurement of crack growth and fracture resistance of these materials over their entire range of anticipated service temperatures and standardized test methods for making such measurements. The development of a standard test for measuring the plane strain fracture toughness is sought. Stress intensity factor coefficients were determined for three varieties of chevron-notch specimens, and fracture toughness measurements were made on silicon nitrides, silicon carbides, and aluminum oxides to assess the performance of each specimen variety. It was determined that silicon nitride and silicon carbides have flat crack growth resistance curves, but aluminum oxide does not. Additionally, batch-to-batch differences were noticed for the aluminum oxide. Experiments are continuing to explain the rising crack growth resistance and batch-to-batch variations for the aluminum oxide. Author

N88-23994*# National Aeronautics and Space Administration. Lewis Research Center, Cleveland, OH.

PARAMETER IDENTIFICATION METHODS FOR IMPROVING STRUCTURAL DYNAMIC MODELS Ph.D. Thesis

CHARLES LAWRENCE Jun. 1988 155 p
(NASA-TM-100812; E-3994; NAS 1.15:100812) Avail: NTIS HC A08/MF A01 CSCL 20K

There is an increasing need to develop Parameter Identification methods for improving structural dynamic models, based on the inability of engineers to produce mathematical models which correlate with experimental data. This research explores the efficiency of combining Component Mode Synthesis (substructuring) methods with Parameter Identification procedures in order to improve analytical modeling of structural components and their connections. Improvements are computed in terms of physical stiffness and damping parameters in order that the physical characteristics of the model can be better understood. Connections involving both viscous and friction damping are investigated. Substructuring methods are utilized to reduce the complexity of the identification problem. Component and inter-component structural connection properties are evaluated and identified independently, thus simplifying the identification problem. It is shown that modal test data is effective for identifying modeling problems associated with structural components, and for determining the stiffness and damping properties of intercomponent connections. In general, Parameter Identification is improved when greater quantities of experimental data are available. Author

N88-24002*# National Aeronautics and Space Administration. Lewis Research Center, Cleveland, OH.

ENGINE STRUCTURES: A BIBLIOGRAPHY OF LEWIS RESEARCH CENTER'S RESEARCH FOR 1980-1987

Apr. 1988 212 p Compiled by the Committee for LST 88, the Lewis Structures Technology Symposium and Exposition, Cleveland, Ohio, 24-25 May 1988
(NASA-TM-100842; E-4033; NAS 1.15:100842) Avail: NTIS HC A01/MF A01 CSCL 20K

This compilation of abstracts describes and indexes the technical reporting that resulted from the scientific and engineering work performed and managed by the Structures Division of the NASA Lewis Research Center from 1980 through 1987. All the publications were announced in the 1980 to 1987 issues of STAR (Scientific and Technical Aerospace Reports) and or IAA (International Aerospace Abstracts). Included are research reports, journal articles, conference presentations, patents and patent applications, and theses. Author

N88-24997*# Syracuse Univ., NY. Dept. of Mechanical and Aerospace Engineering.

RESOLVED SHEAR STRESS INTENSITY COEFFICIENT AND FATIGUE CRACK GROWTH IN LARGE CRYSTALS Final Contractor Report

QI CHEN and HAO-WEN LIU Jun. 1988 56 p
(Contract NAG3-348)
(NASA-CR-182137; NAS 1.26:182137) Avail: NTIS HC A04/MF A01 CSCL 20K

Fatigue crack growth in large grain Al alloy was studied. Fatigue crack growth is caused primarily by shear decohesion due to dislocation motion in the crack tip region. The crack paths in the large crystals are very irregular and zigzag. The crack planes are often inclined to the loading axis both in the inplane direction and the thickness direction. The stress intensity factors of such inclined cracks are approximated from the two dimensional finite element calculations. The plastic deformation in a large crystal is highly anisotropic, and dislocation motion in such crystals are driven by the resolved shear stress. The resolved shear stress intensity coefficient in a crack solid, RSSIC, is defined, and the coefficients for the slip systems at a crack tip are evaluated from the calculated stress intensity factors. The orientations of the crack planes are closely related to the slip planes with the high RSSIC values. If a single slip system has a much higher RSSIC than all the others, the crack will follow the slip plane, and the slip plane becomes the crack plane. If two or more slip systems have a high RSSIC, the crack plane is the result of the decohesion processes on these active slip planes. Author

N88-25016*# Illinois Univ., Urbana. Dept. of Mechanical Engineering.

CYCLIC FATIGUE DAMAGE CHARACTERISTICS OBSERVED FOR SIMPLE LOADINGS EXTENDED TO MULTIAXIAL LIFE PREDICTION

DAVID J. JONES and PETER KURATH Jun. 1988 100 p
(Contract NAG3-465)
(NASA-CR-182126; NAS 1.26:182126) Avail: NTIS HC A05/MF A01 CSCL 20K

Fully reversed uniaxial strain controlled fatigue tests were performed on smooth cylindrical specimens made of 304 stainless steel. Fatigue life data and cracking observations for uniaxial tests were compared with life data and cracking behavior observed in fully reversed torsional tests. It was determined that the product of maximum principle strain amplitude and maximum principle stress provided the best correlation of fatigue lives for these two loading conditions. Implementation of this parameter is in agreement with observed physical damage and it accounts for the variation of stress-strain response, which is unique to specific loading conditions. Biaxial fatigue tests were conducted on tubular specimens employing both in-phase and out-of-phase tension torsion cyclic strain paths. Cracking observations indicated that the physical damage which occurred in the biaxial tests was similar to the damage observed in uniaxial and torsional tests. The Smith, Watson, and Topper parameter was then extended to predict the fatigue lives resulting from the more complex loading conditions. Author

N88-25935*# National Aeronautics and Space Administration. Lewis Research Center, Cleveland, OH.

IMPROVED METHOD FOR STRESS AND COMPATIBILITY ANALYSIS OF MULTICOMPONENT ROTATING SYSTEMS

GERALD A. CAREK Jun. 1988 31 p
(NASA-TM-100884; E-4117; NAS 1.15:100884) Avail: NTIS HC A03/MF A01 CSCL 20K

An improved method of analyzing multicomponent rotating assemblies for the determination of operating stresses and component compatibility has been developed. In this method, a single finite element model is developed which contains all of the separate components in the rotating assembly. This is made possible by using gap elements to simulate the contact surfaces between components. The MARC finite element computer program is then used to perform the analysis. This improved method is less time consuming and more reliable than the conventional method of analyzing such systems. Results are presented for two different stress-compatibility analyses of a six-component axial flow compressor rotor. The results for the previously used flexibility analysis method are compared with those for the improved analysis method. The stresses predicted by each method compare quite well with each other. The predictions of the component compatibility, as well as the magnitude of the forces at the contact surfaces, also compare well for these two analysis procedures. It is therefore recommended that the improved analysis method be used to determine the stress-compatibility characteristics of multicomponent rotating systems. Author

N88-25937*# National Aeronautics and Space Administration. Lewis Research Center, Cleveland, OH.

CHARACTERIZATION OF FATIGUE CRACK INITIATION AND PROPAGATION IN Ti-6AL-4V WITH ELECTRICAL POTENTIAL DROP TECHNIQUE

SREERAMESH KALLURI and JACK TELESMAAN Jul. 1988 25 p Prepared in cooperation with Sverdrup Technology, Inc., Cleveland, Ohio
(NASA-TM-100877; E-4111; NAS 1.15:100877) Avail: NTIS HC A03/MF A01 CSCL 20K

Electrical potential methods have been used in the past primarily to monitor crack length in long crack specimens subjected to fatigue loading. An attempt was made to develop test procedures for monitoring the fatigue crack initiation and the growth of short fatigue cracks in a turbine disk alloy with the electrical potential drop technique (EPDT). In addition, the EPDT was also applied to monitor the fatigue crack growth in long crack specimens of the

39 STRUCTURAL MECHANICS

same alloy. The resolution of the EPDT for different specimen geometries was determined. Factors influencing the EPDT are identified and the applicability of EPDT in implementing damage tolerant design concepts for turbine disk materials is discussed. The experimental procedure adopted and the results obtained is discussed. No substantial differences were observed between the fatigue crack growth data of short and long crack specimens.

Author

N88-27611* Illinois Univ., Urbana-Champaign. Dept. of Mechanical and Industrial Engineering.

THE RELATIONSHIP BETWEEN OBSERVED FATIGUE DAMAGE AND LIFE ESTIMATION MODELS Final Contractor Report

PETER KURATH and DARRELL F. SOCIE Aug. 1988 43 p
(Contract NAG3-465)
(NASA-CR-182191; NAS 1.26:182191) Avail: NTIS HC A03/MF A01 CSCL 20K

Observations of the surface of laboratory specimens subjected to axial and torsional fatigue loadings has resulted in the identification of three damage fatigue phenomena: crack nucleation, shear crack growth, and tensile crack growth. Material, microstructure, state of stress/strain, and loading amplitude all influence which of the three types of fatigue damage occurs during a dominant fatigue life fraction. Fatigue damage maps are employed to summarize the experimental observations. Appropriate bulk stress/strain damage parameters are suggested to model fatigue damage for the dominant fatigue life fraction. Extension of the damage map concept to more complex loadings is presented.

Author

N88-28332* National Aeronautics and Space Administration. Lewis Research Center, Cleveland, OH.

A TRANSVERSELY ISOTROPIC THERMOELASTIC THEORY

S. M. ARNOLD Aug. 1988 29 p
(NASA-TM-101302; E-4288; NAS 1.15:101302) Avail: NTIS HC A03/MF A01 CSCL 20K

A continuum theory is presented for representing the thermoelastic behavior of composites that can be idealized as transversely isotropic. This theory is consistent with anisotropic viscoplastic theories being developed presently at NASA Lewis Research Center. A multiaxial statement of the theory is presented, as well as plane stress and plane strain reductions. Experimental determination of the required material parameters and their theoretical constraints are discussed. Simple homogeneously stressed elements are examined to illustrate the effect of fiber orientation on the resulting strain distribution. Finally, the multiaxial stress-strain relations are expressed in matrix form to simplify and accelerate implementation of the theory into structural analysis codes.

Author

N88-28344* National Aeronautics and Space Administration. Lewis Research Center, Cleveland, OH.

EXPERIMENTAL INVESTIGATION OF PROPFAN AEROELASTIC RESPONSE IN OFF-AXIS FLOW WITH MISTUNING

ORAL MEHMED and DURBHA V. MURTHY (Toledo Univ., Ohio.) 1988 29 p Presented at the 24th Joint Propulsion Conference, Boston, Mass., 11-13 Jul. 1988; sponsored by AIAA, ASEE, ASME and SAE
(NASA-TM-101320; E-4321; NAS 1.15:101320; AIAA-88-3153)
Avail: NTIS HC A03/MF A01 CSCL 20K

Measured vibratory strain amplitudes from off-axis flow are compared for the blades of two, 8-bladed propfan model rotors with mistuning. One rotor had inherent mistuning. The other was intentionally mistuned by replacing every other blade of the first rotor with a blade of same geometry but different frequencies and mode shapes. The data shows that the intentional mistuning had a beneficial effect on the aeroelastic response of the propfan motors for a wide range of off-axis flow angles, blade pitch angles, and rotational speeds. Statistical trends of blade strain amplitudes are compared for both the rotors in terms of the ratio of the maximum to the mean and the coefficient of variation. Author

N88-29195* National Aeronautics and Space Administration. Lewis Research Center, Cleveland, OH.

IMPROVED FINITE STRIP MINDLIN PLATE BENDING ELEMENT USING ASSUMED SHEAR STRAIN DISTRIBUTIONS ABHISAK CHULYA and ROBERT L. THOMPSON Jul. 1988 20 p

(Contract NASA ORDER C-99066-G)
(NASA-TM-100928; ICOMP-88-12; E-4194; NAS 1.15:100928)
Avail: NTIS HC A03/MF A01 CSCL 20K

A linear finite strip plate element based on Mindlin/Reissner plate theory is developed. The analysis is suitable for both thin and thick plates. In the formulation new transverse shear strains are introduced and assumed constant in each two-code linear strip. The element stiffness matrix is explicitly formulated for efficient computation and computer implementation. Numerical results showing the efficiency and predictive capability of the element for the analysis of plates are presented for different support and loading conditions and a wide range of thicknesses. No sign of shear locking phenomenon was observed with the newly developed element. Author

N88-30164* Akron Univ., OH. Dept. of Civil Engineering. **AN EXPERIMENTAL STUDY OF BIAXIAL YIELD IN MODIFIED 9Cr-1Mo STEEL AT ROOM TEMPERATURE Final Report**

J. R. ELLIS Nov. 1985 16 p Presented at the 8th International Conference on Structural Mechanics in Reactor Technology, Brussels, Belgium, 19-23 Aug. 1985 Sponsored in cooperation with DOE and Union Carbide Corp.
(Contract NAG3-379)

(NASA-CR-175012; E-2776; NAS 1.26:175012) Avail: NTIS HC A03/MF A01 CSCL 20K

Described are two biaxial experiments which investigated yield, hardening, and flow behavior in modified 9Cr-1Mo steel at room temperature. The aim of these experiments was to determine whether the procedures recommended in NE Standard F9-5T for inelastic design analysis are applicable for this material in normalized and tempered condition. The first experiment investigated small offset yield behavior subsequent to radial preloads ($\sqrt{3}$ sub σ_{12} = sub σ_{11}) in tension-torsion stress space. The second experiment investigated yield behavior subsequent to nonradial preloads and also the time-dependent flow occurring during 0.5 hour periods at constant stress. The results of these experiments were qualitatively similar to those obtained earlier for types 304 and 316 stainless steel. Specifically, the von Mises yield criterion was found to provide a reasonable approximation of initial yield behavior. Although the subsequent yield surfaces suffered considerable distortion from their near-circular form after both radial and nonradial preloads, the hardening behavior was to the first order kinematic in nature. The strain-time data obtained during the 0.5 hr hold periods showed characteristics typical of creep curves. As in the case of earlier experiments, the high initial flow rates diminished more rapidly than would be estimated from elevated temperature data.

Author

44

ENERGY PRODUCTION AND CONVERSION

Includes specific energy conversion systems, e.g., fuel cells; global sources of energy; geophysical conversion; and windpower.

A88-11804* National Aeronautics and Space Administration. Lewis Research Center, Cleveland, OH.

FLUORIDE SALTS AND CONTAINER MATERIALS FOR THERMAL ENERGY STORAGE APPLICATIONS IN THE TEMPERATURE RANGE 973 - 1400 K

AJAY K. MISRA and J. DANIEL WHITTENBERGER (NASA, Lewis Research Center, Cleveland, OH) IN: IECEC '87; Proceedings of the Twenty-second Intersociety Energy Conversion Engineering

Conference, Philadelphia, PA, Aug. 10-14, 1987. Volume 1. New York, American Institute of Aeronautics and Astronautics, 1987, p. 188-201. Previously announced in STAR as N87-24026. refs

Multicomponent fluoride salt mixtures were characterized for use as latent heat of fusion heat storage materials in advanced solar dynamic space power systems with operating temperatures in the range of 973 to 1400 K. The melting points and eutectic composition for many systems with published phase diagrams were verified, and several new eutectic compositions were identified. Additionally, the heats of fusion of several binary and ternary eutectics and congruently melting intermediate compounds were measured by differential scanning calorimetry. The extent of corrosion of various metals by fluoride melts was estimated from thermodynamic considerations, and equilibrium conditions inside a containment vessel were calculated as functions of the initial moisture content of the salt and free volume above the molten salt. Preliminary experimental data on the corrosion of commercial, high-temperature alloys in LiF-19.5CaF_2 and $\text{NaF-27CaF}_2\text{-36MgF}_2$ melts are presented and compared to the thermodynamic predictions. Author

A88-11811*# National Aeronautics and Space Administration. Lewis Research Center, Cleveland, OH.

A NOVEL PHOTOVOLTAIC POWER SYSTEM WHICH USES A LARGE AREA CONCENTRATOR MIRROR

ANNE ARRISON (NASA, Lewis Research Center, Cleveland, OH) and NAVID FATEMI (Cleveland State University, OH) IN: IECEC '87; Proceedings of the Twenty-second Intersociety Energy Conversion Engineering Conference, Philadelphia, PA, Aug. 10-14, 1987. Volume 1. New York, American Institute of Aeronautics and Astronautics, 1987, p. 241-247. refs

A preliminary analysis has been made of a novel photovoltaic power system concept. The system is composed of a small area, dense photovoltaic array, a large area solar concentrator, and a battery system for energy storage. The feasibility of such a system is assessed for space power applications. The orbital efficiency, specific power, mass, and area of the system are calculated under various conditions and compared with those for the organic Rankine cycle solar dynamic system proposed for Space Station. Near term and advanced large area concentrator photovoltaic systems not only compare favorably to solar dynamic systems in terms of performance but offer other benefits as well. Author

A88-11813*# National Aeronautics and Space Administration. Lewis Research Center, Cleveland, OH.

PERFORMANCE CHARACTERISTICS OF A COMBINATION SOLAR PHOTOVOLTAIC HEAT ENGINE ENERGY CONVERTER

DONALD L. CHUBB (NASA, Lewis Research Center, Cleveland, OH) IN: IECEC '87; Proceedings of the Twenty-second Intersociety Energy Conversion Engineering Conference, Philadelphia, PA, Aug. 10-14, 1987. Volume 1. New York, American Institute of Aeronautics and Astronautics, 1987, p. 254-263. Previously announced in STAR as N87-23028. refs

A combination solar photovoltaic heat engine converter is proposed. Such a system is suitable for either terrestrial or space power applications. The combination system has a higher efficiency than either the photovoltaic array or the heat engine alone can attain. Advantages in concentrator and radiator area and receiver mass of the photovoltaic heat engine system over a heat-engine-only system are estimated. A mass and area comparison between the proposed space station organic Rankine power system and a combination PV-heat engine system is made. The critical problem for the proposed converter is the necessity for high temperature photovoltaic array operation. Estimates of the required photovoltaic temperature are presented. Author

A88-11896*# National Aeronautics and Space Administration. Lewis Research Center, Cleveland, OH.

A PREDICTION MODEL OF THE DEPTH-OF-DISCHARGE EFFECT ON THE CYCLE LIFE OF A STORAGE CELL

LAWRENCE H. THALLER (NASA, Lewis Research Center, Cleveland, OH) and HONG S. LIM (Hughes Research Laboratories,

Malibu, CA) IN: IECEC '87; Proceedings of the Twenty-second Intersociety Energy Conversion Engineering Conference, Philadelphia, PA, Aug. 10-14, 1987. Volume 2. New York, American Institute of Aeronautics and Astronautics, 1987, p. 751-757. Previously announced in STAR as N87-22311. refs
(Contract NAS3-22238)

Cycle life requirements are very high for batteries used in aerospace applications in low earth orbit. The data base required to establish confidence in a particular cell design is thus both extensive and expensive. Reliable accelerated cycle life testing and performance decay modeling represent attractive alternatives to real-time tests of cycle life. In light of certain long-term cycle life test results, this paper examines a very simple performance decay model developed earlier. Application of that model to available data demonstrates a rigid relationship between a battery's expected cycle life and the depth of discharge of cycling. Further, modeling analysis of the data suggests that a significantly improved cycle life can be obtained with advanced components, materials, and designs; and that cycle life can be reliably predicted from the results of accelerated testing. Author

A88-11903*# National Aeronautics and Space Administration. Lewis Research Center, Cleveland, OH.

STRESS-LIFE INTERRELATIONSHIPS ASSOCIATED WITH ALKALINE FUEL CELLS

LAWRENCE H. THALLER (NASA, Lewis Research Center, Cleveland, OH), RONALD E. MARTIN, and JAMES K. STEDMAN (International Fuel Cells Corp., South Windsor, CT) IN: IECEC '87; Proceedings of the Twenty-second Intersociety Energy Conversion Engineering Conference, Philadelphia, PA, Aug. 10-14, 1987. Volume 2. New York, American Institute of Aeronautics and Astronautics, 1987, p. 791-796. Previously announced in STAR as N87-22307. refs

A review is presented concerning the interrelationships between applied stress and the expected service life of alkaline fuel cells. Only the physical, chemical, and electrochemical phenomena that take place within the fuel cell stack portion of an overall fuel cell system will be discussed. A brief review will be given covering the significant improvements in performance and life over the past two decades as well as summarizing the more recent advances in understanding which can be used to predict the performance and life characteristics of fuel cell systems that have yet to be built. Author

A88-11905*# National Aeronautics and Space Administration. Lewis Research Center, Cleveland, OH.

HIGH TEMPERATURE SOLID OXIDE REGENERATIVE FUEL CELL FOR SOLAR PHOTOVOLTAIC ENERGY STORAGE

DAVID J. BENTS (NASA, Lewis Research Center, Cleveland, OH) IN: IECEC '87; Proceedings of the Twenty-second Intersociety Energy Conversion Engineering Conference, Philadelphia, PA, Aug. 10-14, 1987. Volume 2. New York, American Institute of Aeronautics and Astronautics, 1987, p. 808-817. refs

A hydrogen-oxygen regenerative fuel cell energy storage system based on high temperature solid oxide fuel cell technology is discussed which has application to darkside energy storage for solar photovoltaics. The forward and reverse operating cycles are described, and heat flow, mass, and energy balance data are presented to characterize the system's performance and the variation of performance with changing reactant storage pressure. The present system weighs less than nickel hydrogen battery systems after 0.7 darkside operation, and it maintains a specific weight advantage over radioisotope generators for discharge periods up to 72 hours. R.R.

A88-11914*# National Aeronautics and Space Administration. Lewis Research Center, Cleveland, OH.

COMPONENT VARIATIONS AND THEIR EFFECTS ON BIPOLAR NICKEL-HYDROGEN CELL PERFORMANCE

MICHELLE A. MANZO, RANDALL F. GAHN, OLGA D. GONZALEZ-SANABRIA, ROBERT L. CATALDO, and RUSSEL P. GEMEINER (NASA, Lewis Research Center, Cleveland, OH) IN: IECEC '87; Proceedings of the Twenty-second Intersociety Energy

44 ENERGY PRODUCTION AND CONVERSION

Conversion Engineering Conference, Philadelphia, PA, Aug. 10-14, 1987. Volume 2. New York, American Institute of Aeronautics and Astronautics, 1987, p. 864-868. Previously announced in STAR as N87-23029. refs

A 50 cell bipolar nickel-hydrogen battery was assembled to demonstrate the feasibility of constructing a high voltage stack of cells. Various component combinations were tested in this battery. The battery had approximately 1 ampere-hour of capacity and was constructed from components with an active area of 2 x 2 inches. The components were parametrically varied to give a comparison of nickel electrodes, hydrogen electrodes, separators, fill procedures and electrolyte reservoir plate thicknesses. Groups of five cells were constructed using the same components; ten combinations were tested in all. The battery was thoroughly characterized at various charge and discharge rates as well as with various pulse patterns and rates. Over a period of 1400 40-percent DOD LEO cycles some of the groups began to exhibit performance differences. In general, only separator variations had a significant effect on cell performance. It also appears that shunt currents may have been operating within the stack, resulting in electrolyte transfer from one cell to another, thus contributing to cell performance variations. Author

A88-11916* National Aeronautics and Space Administration. Lewis Research Center, Cleveland, OH.

TEST RESULTS OF A 60 VOLT BIPOLAR NICKEL-HYDROGEN BATTERY

ROBERT L. CATALDO, OLGA GONZALEZ-SANABRIA, RANDALL F. GAHN, MICHELLE A. MANZO, and RUSSEL P. GEMEINER (NASA, Lewis Research Center, Cleveland, OH) IN: IECEC '87; Proceedings of the Twenty-second Intersociety Energy Conversion Engineering Conference, Philadelphia, PA, Aug. 10-14, 1987. Volume 2. New York, American Institute of Aeronautics and Astronautics, 1987, p. 873-877. Previously announced in STAR as N87-24029.

In July 1986, a high-voltage nickel-hydrogen battery was assembled at the NASA Lewis Research Center. This battery incorporated bipolar construction techniques to build a 50-cell stack with approximately 1.0 A-hr capacity (C) and an open-circuit voltage of 65 V. The battery was characterized at both low and high current rates prior to pulsed and nonpulsed discharges. Pulse discharges at 5 and 10 C were performed before placing the battery on over 1400, 40-percent depth-of-discharge, low-earth-orbit cycles. The successful demonstration of a high-voltage bipolar battery in one containment vessel has advanced the technology to where nickel-hydrogen high-voltage systems can be constructed of several modules instead of hundreds of individual cells. Author

A88-11925* National Aeronautics and Space Administration. Lewis Research Center, Cleveland, OH.

STATUS OF COMMERCIAL FUEL CELL POWERPLANT SYSTEM DEVELOPMENT

MARVIN WARSHAY (NASA, Lewis Research Center, Cleveland, OH) IN: IECEC '87; Proceedings of the Twenty-second Intersociety Energy Conversion Engineering Conference, Philadelphia, PA, Aug. 10-14, 1987. Volume 2. New York, American Institute of Aeronautics and Astronautics, 1987, p. 983-987. Previously announced in STAR as N87-22171. refs

The primary focus is on the development of commercial Phosphoric Acid Fuel Cell (PAFC) powerplant systems because the PAFC, which has undergone extensive development, is currently the closest fuel cell system to commercialization. Shorter discussions are included on the high temperature fuel cell systems which are not as mature in their development, such as the Molten Carbonate Fuel Cell (MCFC) and the Solid Oxide Fuel Cell (SOFC). The alkaline and the Solid Polymer Electrolyte (SPE) fuel cell systems, are also included, but their discussions are limited to their prospects for commercial development. Currently, although the alkaline fuel cell continues to be used for important space applications there are no commercial development programs of significant size in the USA and only small efforts outside. The market place for fuel cells and the status of fuel cell programs in

the USA receive extensive treatment. The fuel cell efforts outside the USA, especially the large Japanese programs, are also discussed. Author

A88-16631* National Aeronautics and Space Administration. Lewis Research Center, Cleveland, OH.

LIGHTWEIGHT NICKEL ELECTRODE FOR NICKEL HYDROGEN CELLS AND BATTERIES

DORIS L. BRITTON (NASA, Lewis Research Center, Cleveland, OH) IN: International Power Sources Symposium, 32nd, Cherry Hill, NJ, June 9-12, 1986, Proceedings. Pennington, NJ, Electrochemical Society, Inc., 1986, p. 420-428. Previously announced in STAR as N86-21978. refs

The nickel electrode was identified as the heaviest component of the nickel hydrogen (NiH₂) battery. The NASA Lewis Research Center is developing nickel electrodes for NiH₂ battery devices which will be lighter in weight and have higher energy densities when cycled under a low Earth orbit regime at deep depths of discharge. Lightweight plaques are first exposed to 31 percent potassium hydroxide for 3 months to determine their suitability for use as electrode substrates from a chemical corrosion standpoint. Pore size distribution and porosity of the plaques are then measured. The lightweight plaques examined are nickel foam, nickel felt, nickel plastic and nickel plated graphite. Plaques are then electrochemically impregnated in an aqueous solution. Initial characterization tests of the impregnated plaques are performed at five discharge levels, C/2, 1.0 C, 1.37 C, 2.0 C, and 2.74 C rates. Electrodes that passed the initial characterization screening test will be life cycle tested. Lightweight electrodes are approximately 30 to 50 percent lighter in weight than the sintered nickel electrode. Author

A88-16632* National Aeronautics and Space Administration. Lewis Research Center, Cleveland, OH.

ASSESSMENT OF COMMERCIALLY AVAILABLE AND EXPERIMENTAL HYDROGEN ELECTRODES

JO ANN CHARLESTON (NASA, Lewis Research Center, Cleveland, OH) IN: International Power Sources Symposium, 32nd, Cherry Hill, NJ, June 9-12, 1986, Proceedings. Pennington, NJ, Electrochemical Society, Inc., 1986, p. 429-438. Previously announced in STAR as N86-23035.

NASA Lewis Research Center is currently involved in advanced cell component development for nickel-hydrogen cells and batteries. Long life, high energy density, improved performance and reliability are required for energy storage systems in future space missions. Commercially available as well as experimental hydrogen electrodes were assessed and compared to the state-of-the-art hydrogen electrode that is currently being used in nickel-hydrogen batteries. These electrodes were evaluated by scanning electron microscopy and standard electrochemical polarization measurements. Production variables such as Teflon content and platinum catalyst loading were considered in order to assess various hydrogen electrodes with regard to the different electrode manufacturing processes. Author

A88-18580* National Aeronautics and Space Administration. Lewis Research Center, Cleveland, OH.

COMPARATIVE RADIATION RESISTANCE, TEMPERATURE DEPENDENCE AND PERFORMANCE OF DIFFUSED JUNCTION INDIUM PHOSPHIDE SOLAR CELLS

I. WEINBERG, C. K. SWARTZ, R. E. HART, JR. (NASA, Lewis Research Center, Cleveland, OH), S. K. GHANDHI, J. M. BORREGO (Rensselaer Polytechnic Institute, Troy, NY) et al. Solar Cells (ISSN 0379-6787), vol. 22, Oct. 1987, p. 113-124. refs

Indium phosphide solar cells whose p-n junctions were processed by the open tube capped diffusion and by the closed tube uncapped diffusion of sulfur into Czochralski-grown p-type substrates are compared. Differences found in radiation resistance were attributed to the effects of increased base dopant concentration. Both sets of cells showed superior radiation resistance to that of gallium arsenide cells, in agreement with previous results. No correlation was, however, found between the

44 ENERGY PRODUCTION AND CONVERSION

open-circuit voltage and the temperature dependence of the maximum power. R.R.

A88-24072* National Aeronautics and Space Administration. Lewis Research Center, Cleveland, OH.
IDENTIFICATION OF SALT-ALLOY COMBINATIONS FOR THERMAL ENERGY STORAGE APPLICATIONS IN ADVANCED SOLAR DYNAMIC POWER SYSTEMS

J. D. WHITTENBERGER (NASA, Lewis Research Center, Cleveland, OH) and A. K. MISRA (Case Western Reserve University, Cleveland, OH) *Journal of Materials Engineering* (ISSN 0931-7058), vol. 9, no. 3, 1987, p. 293-302.

Thermodynamic calculations based on the available data for fluoride salt systems reveal that a number of congruently melting compositions and eutectics exist which have the potential to meet the lightweight, high energy storage requirements imposed for advanced solar dynamic systems operating between about 1000 and 1400 K. Compatibility studies to determine suitable containment alloys to be used with NaF-22CaF₂-13MgF₂, NaF-32CaF₂, and NaF-23MgF₂ have been conducted at the eutectic temperature + 25 K for each system. For these three NaF-based eutectics, none of the common, commercially available high temperature alloys appear to offer adequate corrosion resistance for a long lifetime; however mild steel, pure nickel and Nb-1Zr could prove useful. These latter materials suggest the possibility that a strong, corrosion resistant, nonrefractory, elevated temperature alloy based on the Ni-Ni₃Nb system could be developed. Author

A88-33734* National Aeronautics and Space Administration. Lewis Research Center, Cleveland, OH.

FLUORIDE SALTS AS PHASE CHANGE MATERIALS FOR THERMAL ENERGY STORAGE IN THE TEMPERATURE RANGE 1000-1400 K

AJAY K. MISRA (NASA, Lewis Research Center, Cleveland, OH) *Electrochemical Society, Journal* (ISSN 0013-4651), vol. 135, April 1988, p. 850-854. refs

Eutectic compositions and congruently melting intermediate compounds in binary and ternary fluoride salt systems were characterized for potential use as latent heat of fusion phase change materials to store thermal energy in the temperature range 1000-1400 K. The melting points and eutectic compositions for many systems with published phase diagrams were experimentally verified and new eutectic compositions having melting points between 1000 and 1400 K were identified. Heats of fusion of several binary and ternary eutectics and congruently melting compounds were experimentally measured by differential scanning calorimetry. For a few systems in which heats of mixing in the melts have been measured, heats of fusion of the eutectics were calculated from thermodynamic considerations and good agreement was obtained between the measured and calculated values. Several combinations of salts with high heats of fusion per unit mass (greater than 0.7 kJ/g) have been identified for possible use as phase change materials in advanced solar dynamic space power applications. Author

A88-34230*# National Aeronautics and Space Administration. Lewis Research Center, Cleveland, OH.

ISSUES IN SPACE PHOTOVOLTAIC RESEARCH AND TECHNOLOGY

DENNIS J. FLOOD (NASA, Lewis Research Center, Cleveland, OH) IN: IEEE Photovoltaic Specialists Conference, 19th, New Orleans, LA, May 4-8, 1987, Proceedings. New York, Institute of Electrical and Electronics Engineers, Inc., 1987, p. 34-42. Previously announced in STAR as N87-23901. refs

Key issues and opportunities in space photovoltaic research and technology are addressed relative to future NASA mission requirements and drivers. Examples are given of future space missions and/or operational capabilities that are on NASA's planning horizon, presenting major technology challenges to the use of photovoltaic power generation in space. A brief description of the capabilities ascribed to the competing technologies of nuclear and solar thermal power systems are discussed. The performance

goals that space photovoltaic power systems must meet to remain competitive are described. Author

A88-34250*

INP BASED SOLAR CELLS FOR SPACE APPLICATION: REDUCTION OF EXTERNAL LOSSES

X. WU, T. J. COUTTS, R. G. DHERE, T. A. GESSERT, and N. G. DHERE (Solar Energy Research Institute, Golden, CO) IN: IEEE Photovoltaic Specialists Conference, 19th, New Orleans, LA, May 4-8, 1987, Proceedings. New York, Institute of Electrical and Electronics Engineers, Inc., 1987, p. 140-145. refs
(Contract NASA ORDER C-300020-J; DE-AC02-83CH-10093)

Although InP-based solar cells have considerable potential for space applications, it is necessary to improve efficiencies to around the level of GaAs or Si cells before their excellent radiation resistance can be regarded as a dominant advantage. The authors concentrate on indium-tin-oxide/InP cells, presenting data relating to reduction of the contact resistance of the rear surface metallization, reduction of reflectance losses by choosing indium-tin-oxide deposition conditions to give specific optical properties, and reduction of losses associated with the grid. Simultaneous optimization of all of these has led to improved values of J_{sc}. For devices of approximately 1 cm² in area, the largest J_{sc} achieved to date is 28.1 mA/eq cm (AM1.5, SERI/NASA direct normal spectrum, 25 C, total area, 100 mW/sq cm). For this particular cell, the equivalent AM0 value of J_{sc} was 34.6 mA/sq cm, which appears to be the largest reported for any InP-based cell. I.E.

A88-34270* Rensselaer Polytechnic Inst., Troy, NY.

CHARACTERIZATION AND MODELLING OF OPEN TUBE DIFFUSED N+P BULK INP SOLAR CELLS

S. BOTHRA, H. G. BHIMNATHWALA, K. K. PARAT, S. K. GHANDHI, and J. M. BORREGO (Rensselaer Polytechnic Institute, Troy, NY) IN: IEEE Photovoltaic Specialists Conference, 19th, New Orleans, LA, May 4-8, 1987, Proceedings. New York, Institute of Electrical and Electronics Engineers, Inc., 1987, p. 261-266. refs
(Contract NAG3-604)

The authors describe the photovoltaic characteristics of an n+p junction solar cell fabricated on bulk InP by an open-tube-diffusion technique. Analysis of the forward characteristics shows that the forward current is dominated by recombination in the quasineutral regions, indicating that the fabrication technique produces a clean junction. Spectral response measurements are analyzed and more realistic boundary conditions are used to model the solar cell to determine important material and device parameters. I.E.

A88-34310* ENTECH Corp., Dallas-Fort Worth Airport, TX.

DEVELOPMENT OF A DOME FRESNEL LENS/GALLIUM ARSENIDE PHOTOVOLTAIC CONCENTRATOR FOR SPACE APPLICATIONS

MARK J. O'NEILL (Entech, Inc., Fort Worth, TX) and MICHAEL F. PISZCZOR (NASA, Lewis Research Center, Cleveland, OH) IN: IEEE Photovoltaic Specialists Conference, 19th, New Orleans, LA, May 4-8, 1987, Proceedings. New York, Institute of Electrical and Electronics Engineers, Inc., 1987, p. 479-484. refs

A novel photovoltaic concentrator system is currently being developed. Phase I of the program, completed in late 1986, produced a conceptual design for the concentrator system, including an array weight and performance estimates based on optical, electrical, and thermal analyses. Phase II of the program, just underway, concerns the fabrication and testing of prototype concentrator panels of the design. The concentrator system uses dome Fresnel lenses for optical concentration; gallium arsenide concentrator cells for power generation; prismatic cell covers to eliminate gridline obscuration losses; a backplane radiator for heat rejection; and a honeycomb structure for the deployable panel assembly. The conceptual design of the system, its anticipated performance, and its estimated weight are reported. I.E.

44 ENERGY PRODUCTION AND CONVERSION

A88-34312* Spectrolab, Inc., Sylmar, CA.

DEVELOPMENT OF 8 CM X 8 CM SILICON GRIDDED BACK SOLAR CELL FOR SPACE STATION

D. R. LILLINGTON, J. R. KUKULKA, S. M. BUNYAN, G. F. J. GARLICK (Spectrolab, Inc., Sylmar, CA), and B. SATER (NASA, Lewis Research Center, Cleveland, OH) IN: IEEE Photovoltaic Specialists Conference, 19th, New Orleans, LA, May 4-8, 1987, Proceedings. New York, Institute of Electrical and Electronics Engineers, Inc., 1987, p. 489-493. (Contract NAS3-24672)

The 8-cm x 8-cm gridded back cell being developed for the space station photovoltaic array is described. Modeling studies show that the beginning of life power output of 1.039 W per cell may be met by several different configurations, the most promising being either a fielded or nonfielded 2 ohm-cm planar 8-mil cell. Experimental data are presented which show that a thermal alpha of 0.63 is achievable on a planar cell but at the expense of some Isc. Planar cells are found to possess short-circuit currents which are 9 percent lower than on textured cells due to the loss of near-IR radiation by transmission through the cell. Preliminary modeling shows that the efficiency of the textured cell exceeds the planar cell by approximately 9 percent at 25 C but the situation is reversed in orbit due to the high thermal alpha of textured cells (0.82). Experimental data show that the IR absorption in textured cells can be reduced by about 3 alpha points without loss of efficiency by controlling the doping concentration in the diffused layers, thus increasing the efficiency in orbit. I.E.

A88-34343* National Aeronautics and Space Administration, Lewis Research Center, Cleveland, OH.

PERFORMANCE OF GAAS AND SILICON CONCENTRATOR CELLS UNDER 37 MEV PROTON IRRADIATION

HENRY B. CURTIS and CLIFFORD K. SWARTZ (NASA, Lewis Research Center, Cleveland, OH) IN: IEEE Photovoltaic Specialists Conference, 19th, New Orleans, LA, May 4-8, 1987, Proceedings. New York, Institute of Electrical and Electronics Engineers, Inc., 1987, p. 664-668. Previously announced in STAR as N88-12877.

Gallium arsenide concentrator cells from three sources and silicon concentrator cells from one source were exposed to 37-MeV protons at fluences up to 2.8×10^{10} to the 12th protons/sq cm. Performance data were taken after several fluences, at two temperatures (25 and 80 C), and at concentration levels from 1 to about 150X AM0. Data at one sun and 25 C were taken with an X-25 xenon-lamp solar simulator. Data at concentration were taken using a pulsed solar simulator with the assumption of a linear relationship between short-circuit current and irradiance. The cells are 5 mm x 5 mm with a 4-mm-diameter illuminated area.

Author

A88-34394* Cleveland State Univ., OH.

MODELLING AND DESIGN OF HIGH EFFICIENCY RADIATION TOLERANT INDIUM PHOSPHIDE SPACE SOLAR CELLS

CHANDRA GORADIA, JAMES V. GEIER (Cleveland State University, OH), and IRVING WEINBERG (NASA, Lewis Research Center, Cleveland, OH) IN: IEEE Photovoltaic Specialists Conference, 19th, New Orleans, LA, May 4-8, 1987, Proceedings. New York, Institute of Electrical and Electronics Engineers, Inc., 1987, p. 937-943. refs

Using a fairly comprehensive model, a parametric variation study was performed of the InP shallow homojunction solar cell with a view to determining the maximum realistically achievable efficiency and an optimum design that would yield this efficiency. Calculations show that with good-quality epitaxial material, a beginning-of-life efficiency of about 20.3 percent at 1AM0, 25 C may be possible. The design parameters of the near-optimum cell are given. Also presented are the expected effect on the performance parameters of radiation damage by 1-MeV electrons and a possible explanation of the high radiation tolerance of InP solar cells. I.E.

A88-51289* Midwest Research Inst., Golden, CO.

DIRECT-CURRENT MAGNETRON FABRICATION OF INDIUM TIN OXIDE/INP SOLAR CELLS

T. J. COUTTS, X. WU, T. A. GESSERT, and X. LI (Solar Energy

Research Institute, Golden, CO) Journal of Vacuum Science and Technology A (ISSN 0734-2101), vol. 6, May-June 1988, pt. 2, p. 1722-1726. refs

(Contract DE-AC02-83CH-10093; NASA ORDER C-300020-J)

Efficient solar cells of indium tin oxide (ITO)/InP have been fabricated using dc magnetron deposition of the ITO into single-crystal InP substrates. Efficiencies of over 16.5 percent have been achieved, the highest ever recorded for devices of this construction. The results of studies of the annealing behavior of the cells and observations of interfacial changes using Raman spectroscopy and secondary ion mass spectroscopy, together with measurements of light and dark current/voltage and quantum efficiency characteristics, are used to model the behavior of the cells and explain their lack of sensitivity to fabrication conditions. C.D.

N88-12875*# Hughes Aircraft Co., Long Beach, CA.

DESIGN DESCRIPTION REPORT FOR A PHOTOVOLTAIC POWER SYSTEM FOR A REMOTE SATELLITE EARTH TERMINAL

N. A. MARSHALL and G. J. NAFF Jan. 1987 136 p

(Contract NAS3-23862)

(NASA-CR-179586; NAS 1.26:179586) Avail: NTIS HC A07/MF A01 CSCL 10B

A photovoltaic (PV) power system has been installed as an adjunct to an agricultural school at Wawatobi on the large northern island of the Republic of Indonesia. Its purpose is to provide power for a satellite earth station and a classroom. The renewable energy developed supports the video and audio teleconferencing systems as well as the facility at large. The ground station may later be used to provide telephone service. The installation was made in support of the Agency for International Development's Rural Satellite Program, whose purpose is to demonstrate the use of satellite communications for rural development assistance applications. The objective of this particular PV power system is to demonstrate the suitability of a hybrid PV engine-generator configuration for remote satellite earth stations. F.M.R.

N88-12877*# National Aeronautics and Space Administration, Lewis Research Center, Cleveland, OH.

PERFORMANCE OF GAAS AND SILICON CONCENTRATOR CELLS UNDER 37 MEV PROTON IRRADIATION

HENRY B. CURTIS and CLIFFORD K. SWARTZ 1987 10 p Presented at the 19th Photovoltaic Specialists Conference, New Orleans, La., 4-8 May 1987; sponsored by IEEE

(NASA-TM-100144; E-3696; NAS 1.15:100144) Avail: NTIS HC A02/MF A01 CSCL 10A

Gallium arsenide concentrator cells from three sources and silicon concentrator cells from one source were exposed to 37 MeV protons at fluences up to 2.8×10^{10} to the 12th protons/sq cm. Performance data were taken after several fluences, at two temperatures (25 and 80 C), and at concentration levels from 1 to about 150 x AM0. Data at one sun and 25 C were taken with an X-25 xenon lamp solar simulator. Data at concentration were taken using a pulsed solar simulator with the assumption of a linear relationship between short circuit current and irradiance. The cells are 5 x 5 mm with a 4-mm diameter illuminated area.

Author

N88-12878*# National Aeronautics and Space Administration, Lewis Research Center, Cleveland, OH.

RADIATION PERFORMANCE OF ALGAAS CONCENTRATOR CELLS AND EXPECTED PERFORMANCE OF CASCADE STRUCTURES

HENRY B. CURTIS, CLIFFORD K. SWARTZ, and RUSSELL E. HART, JR. 1987 11 p Presented at the 19th Photovoltaic Specialists Conference, New Orleans, La., 4-8 May 1987; sponsored by IEEE

(NASA-TM-100145; E-3697; NAS 1.15:100145) Avail: NTIS HC A03/MF A01 CSCL 10A

Aluminum gallium arsenide, GaAs, silicon and InGaAs cells have been irradiated with 1 MeV electrons and 37 MeV protons. These cells are candidates for individual cells in a cascade structure.

Data is presented for both electron and proton irradiation studies for one sun and a concentration level of 100X AMO. Results of calculations on the radiation resistance of cascade cell structures based on the individual cell data are also presented. Both series connected and separately connected structures are investigated.

Author

N88-14486*# National Aeronautics and Space Administration. Lewis Research Center, Cleveland, OH.

HOT PISTON RING TESTS Final Report

DAVID J. ALLEN (Sverdrup Technology, Inc., Middleburg Heights, Ohio.) and WILLIAM A. TOMAZIC Dec. 1987 17 p Presented at the 25th Automotive Technology Development Contractors' Coordination Meeting, Dearborn, Mich., 26 Oct. 1987; sponsored by DOE

(Contract DE-AI01-85CE-50112)

(NASA-TM-100256; E-3808; NAS 1.15:100256;

DOE/NASA/50112-72) Avail: NTIS HC A03/MF A01 CSCL 10B

As part of the DOE/NASA Automotive Stirling Engine Project, tests were made at NASA Lewis Research Center to determine whether appendix gap losses could be reduced and Stirling engine performance increased by installing an additional piston ring near the top of each piston dome. An MTI-designed upgraded Mod I Automotive Stirling Engine was used. Unlike the conventional rings at the bottom of the piston, these hot rings operated in a high temperature environment (700 C). They were made of a high temperature alloy (Stellite 6B) and a high temperature solid lubricant coating (NASA Lewis-developed PS-200) was applied to the cylinder walls. Engine tests were run at 5, 10, and 15 MPa operating pressure over a range of operating speeds. Tests were run both with hot rings and without to provide a baseline for comparison. Minimum data to assess the potential of both the hot rings and high temperature low friction coating was obtained. Results indicated a slight increase in power and efficiency, an increase over and above the friction loss introduced by the hot rings. Seal leakage measurements showed a significant reduction. Wear on both rings and coating was low.

Author

N88-18068*# Harris Corp., Melbourne, FL. Government Aerospace Systems Div.

SOLAR CONCENTRATOR ADVANCED DEVELOPMENT PROGRAM, TASK 1 Final Report

Jun. 1986 223 p

(Contract NAS3-24670)

(NASA-CR-179489; NAS 1.26:179489) Avail: NTIS HC A10/MF A01 CSCL 10A

Solar dynamic power generation has been selected by NASA to provide power for the space station. Solar dynamic concentrator technology has been demonstrated for terrestrial applications but has not been developed for space applications. The object of the Solar Concentrator Advanced Development program is to develop the technology of solar concentrators which would be used on the space station. The first task of this program was to develop conceptual concentrator designs and perform trade-off studies and to develop a materials data base and perform material selection. Three unique concentrator concepts; Truss Hex, Spline Radial Panel and Domed Fresnel, were developed and evaluated against weighted trade criteria. The Truss Hex concept was recommended for the space station. Materials data base development demonstrated that several material systems are capable of withstanding extended periods of atomic oxygen exposure without undesirable performance degradation. Descriptions of the conceptual designs and materials test data are included. Author

N88-19000*# Clarkson Univ., Potsdam, NY. Dept. of Electrical and Computer Engineering.

COMPUTER-AIDED MODELING AND PREDICTION OF PERFORMANCE OF THE MODIFIED LUNDELL CLASS OF ALTERNATORS IN SPACE STATION SOLAR DYNAMIC POWER SYSTEMS Semiannual Progress Report, 15 Aug. 1987 - 14 Feb. 1988

NABEEL A. O. DEMERDASH and REN-HONG WANG 15 Mar.

1988 62 p

(Contract NAG3-818)

(NASA-CR-182538; NAS 1.26:182538) Avail: NTIS HC A04/MF A01 CSCL 10B

The main purpose of this project is the development of computer-aided models for purposes of studying the effects of various design changes on the parameters and performance characteristics of the modified Lundell class of alternators (MLA) as components of a solar dynamic power system supplying electric energy needs in the forthcoming space station. Key to this modeling effort is the computation of magnetic field distribution in MLAs. Since the nature of the magnetic field is three-dimensional, the first step in the investigation was to apply the finite element method to discretize volume, using the tetrahedron as the basic 3-D element. Details of the stator 3-D finite element grid are given. A preliminary look at the early stage of a 3-D rotor grid is presented.

J.P.B.

N88-19013*# National Aeronautics and Space Administration. Lewis Research Center, Cleveland, OH.

TEST RESULTS OF A 40-KW STIRLING ENGINE AND COMPARISON WITH THE NASA LEWIS COMPUTER CODE PREDICTIONS Final Report

DAVID J. ALLEN (Sverdrup Technology, Inc., Cleveland, Ohio.) and JAMES E. CAIRELLI Mar. 1988 14 p Presented at the 20th Intersociety Energy Conversion Engineering Conference, Miami Beach, Fla., 18-23 Aug. 1985; sponsored by SAE, ANS, ASME, IEEE, AIAA, ACS and AIChE Previously announced in IAA as A86-24889

(Contract DE-AI01-85CE-50112)

(NASA-TM-87050; DOE/NASA/50112-74; E-2593; NAS 1.15:87050) Avail: NTIS HC A03/MF A01 CSCL 10B

A Stirling engine was tested without auxiliaries at Nasa-Lewis. Three different regenerator configurations were tested with hydrogen. The test objectives were: (1) to obtain steady-state and dynamic engine data, including indicated power, for validation of an existing computer model for this engine; and (2) to evaluate structurally the use of silicon carbide regenerators. This paper presents comparisons of the measured brake performance, indicated mean effective pressure, and cyclic pressure variations from those predicted by the code. The silicon carbide foam generators appear to be structurally suitable, but the foam matrix showed severely reduced performance.

Author

N88-19014*# National Aeronautics and Space Administration. Lewis Research Center, Cleveland, OH.

TESTING OF A ONE-BLADED 30-METER-DIAMETER ROTOR ON THE DOE/NASA MOD-O WIND TURBINE Final Report

C. B. F. ENSWORTH, III, R. D. CORRIGAN, and B. M. BERKOWITZ (Sverdrup Technology, Inc., Cleveland, Ohio.) Mar. 1988 13 p (Contract DE-AI01-76ET-10320)

(NASA-TM-100274; E-3916; DOE/NASA/20320-74; NAS 1.15:100274) Avail: NTIS HC A03/MF A01 CSCL 10B

Tests were conducted on the DOE/NASA Mod-O 200-kW horizontal-axis wind turbine in a one-bladed rotor configuration. The objectives of the test were to evaluate the performance, loads, and dynamic characteristics of a one-bladed rotor, and then to compare these parameters with those of an aerodynamically similar two-bladed rotor configuration. Test operations showed that this intermediate-size (15.2-m radius) one-bladed rotor configuration can be operated successfully. Test results show that the one-bladed rotor had cyclic blade loads comparable to those of a two-bladed rotor. A moderate power penalty equivalent to a reduction in windspeed of 1 m/sec occurred with the one-bladed rotor when operated at a rotor speed 50 percent higher than that of the two-bladed rotor.

Author

N88-21593*# National Aeronautics and Space Administration. Lewis Research Center, Cleveland, OH.

COMPARISON OF PRESSURE DISTRIBUTIONS ON MODEL AND FULL-SCALE NACA 64-621 AIRFOILS WITHAILERONS FOR WIND TURBINE APPLICATION Final Report

G. M. GREGOREK, R. J. KUNIEGA (Ohio State Univ., Columbus.),

44 ENERGY PRODUCTION AND CONVERSION

and T. W. NYLAND Apr. 1988 14 p
(Contract DE-AI01-76ET-20320)

(NASA-TM-100802; DOE/NASA/20320-75; E-3982; NAS
1.15:100802) Avail: NTIS HC A03/MF A01 CSCL 10B

The aerodynamic similarity between a small (4-inch chord) wind tunnel model and a full-scale wind turbine blade (24-foot tip section with a 36-inch chord) was evaluated by comparing selected pressure distributions around the geometrically similar cross sections. The airfoils were NACA 64-621 sections, including trailing-edge ailerons with a width equal to 38 percent of the airfoil chord. The model airfoil was tested in the OSU 6- by 12-inch High Reynolds Number Wind Tunnel; the full-scale blade section was tested in the NASA Langley Research Center 30- by 60-foot Subsonic Wind Tunnel. The model airfoil contained 61 pressure taps connected by embedded tubes to pressure transducers. A belt containing 29 pressure taps was fixed to the full-scale section at midspan to obtain surface pressure data. Lift coefficients were obtained by integrating pressures, and corrections were made for the 3-D effects of blade twist and downwash in the blade tip section. The results of the two different experimental methods correlated well for angles of attack from minus 4 to 36 degrees and aileron reflections from 0 to 90 degrees. Author

N88-22429* # National Aeronautics and Space Administration. Lewis Research Center, Cleveland, OH.

LARGE-SCALE WIND TURBINE STRUCTURES

DAVID A. SPERA *In its* Lewis Structures Technology, 1988. Volume 3: Structural Integrity Fatigue and Fracture Wind Turbines HOST p 285-297 May 1988

Avail: NTIS HC A16/MF A01 CSCL 10A

The purpose of this presentation is to show how structural technology was applied in the design of modern wind turbines, which were recently brought to an advanced stage of development as sources of renewable power. Wind turbine structures present many difficult problems because they are relatively slender and flexible; subject to vibration and aeroelastic instabilities; acted upon by loads which are often nondeterministic; operated continuously with little maintenance in all weather; and dominated by life-cycle cost considerations. Progress in horizontal-axis wind turbines (HAWT) development was paced by progress in the understanding of structural loads, modeling of structural dynamic response, and designing of innovative structural response. During the past 15 years a series of large HAWTs was developed. This has culminated in the recent completion of the world's largest operating wind turbine, the 3.2 MW Mod-5B power plane installed on the island of Oahu, Hawaii. Some of the applications of structures technology to wind turbine will be illustrated by referring to the Mod-5B design. First, a video overview will be presented to provide familiarization with the Mod-5B project and the important components of the wind turbine system. Next, the structural requirements for large-scale wind turbines will be discussed, emphasizing the difficult fatigue-life requirements. Finally, the procedures used to design the structure will be presented, including the use of the fracture mechanics approach for determining allowable fatigue stresses.

Author

N88-22458* # National Aeronautics and Space Administration. Lewis Research Center, Cleveland, OH.

DEVELOPMENT OF AN INTEGRATED HEAT PIPE-THERMAL STORAGE SYSTEM FOR A SOLAR RECEIVER

E. S. KEDDY, J. T. SENA, M. A. MERRIGAN, G. HEIDENREICH (Sundstrand Advanced Technology Group, Rockford, Ill.), and S. JOHNSON 1987 10 p Presented at the Thermophysics Conference, San Antonio, Tex., 27 Jun. 1987 (Contract W-7405-ENG-36)

(NASA-TM-101099; NAS 1.15:101099; DE88-003153; LA-UR-87-3950; CONF-8706254-1) Avail: NTIS HC A02/MF A01 CSCL 10A

The Organic Rankine Cycle (ORC) Solar Dynamic Power System (SDPS) is one of the candidates for Space Station prime power application. In the low Earth orbit of the Space Station approximately 34 minutes of the 94-minute orbital period is spent in eclipse with no solar energy input to the power system. For

this period the SDPS will use thermal energy storage (TES) material to provide a constant power output. An integrated heat-pipe thermal storage receiver system is being developed as part of the ORC-SDPS solar receiver. This system incorporates potassium heat pipe elements to absorb and transfer the solar energy within the receiver cavity. The heat pipes contain the TES canisters within the potassium vapor space with the toluene heater tube used as the condenser region of the heat pipe. During the insolation period of the Earth orbit, solar energy is delivered to the heat pipe in the ORC-SDPS receiver cavity. The heat pipe transforms the non-uniform solar flux incident in the heat pipe surface within the receiver cavity to an essentially uniform flux at the potassium vapor condensation interface in the heat pipe. During solar insolation, part of the thermal energy is delivered to the heater tube and the balance is stored in the TES units. During the eclipse period of the orbit, the balance stored in the TES units is transferred by the potassium vapor to the toluene heater tube. DOE

N88-24255* # National Aeronautics and Space Administration. Lewis Research Center, Cleveland, OH.

OVERVIEW OF NASA LEWIS RESEARCH CENTER FREE-PISTON STIRLING ENGINE TECHNOLOGY ACTIVITIES APPLICABLE TO SPACE POWER SYSTEMS

JACK G. SLABY *In* New Mexico Univ., Transactions of the Fourth Symposium on Space Nuclear Power Systems p 1-6 1987

Avail: NTIS HC A22/MF A01 CSCL 10B

A brief overview is presented of the development and technological activities of the free-piston Stirling engine. The engine started as a small scale fractional horsepower engine which demonstrated basic engine operating principles and the advantages of being hermetically sealed, highly efficient, and simple. It eventually developed into the free piston Stirling engine driven heat pump, and then into the SP-100 Space Reactor Power Program from which came the Space Power Demonstrator Engine (SPDE). The SPDE successfully operated for over 300 hr and delivered 20 kW of PV power to an alternator plunger. The SPDE demonstrated that a dynamic power conversion system can, with proper design, be balanced; and the engine performed well with externally pumped hydrostatic gas bearings. E.R.

N88-24258* # National Aeronautics and Space Administration. Lewis Research Center, Cleveland, OH.

SPECULATIONS ON FUTURE OPPORTUNITIES TO EVOLVE BRAYTON POWERPLANTS ABOARD THE SPACE STATION

ROBERT E. ENGLISH *In* New Mexico Univ., Transactions of the Fourth Symposium on Space Nuclear Power Systems p 15-18 1987 Previously announced as N87-23674

Avail: NTIS HC A22/MF A01 CSCL 10B

The Space Station provides a unique, low risk environment in which to evolve new capabilities. In this way, the Space Station will grow in capacity, in its range of capabilities, and its economy of operation as a laboratory and as a center for space operations. The Brayton cycle using a mixture of He and Xe as its working fluid is examined herein. Using a Brayton powerplant to supply the station's increasing demands for both electric power and heat has the potential to gradually evolve higher and higher performance by exploiting already evolved materials (Ta alloy and molten-Li heat storage), its peak cycle temperature rising ultimately to 1500 K. Adapting the station to exploit long tethers (200 to 300 km) could yield increases in payloads to LEO, to GEO, and to distant destinations in the solar system. Such tethering of the Space Station would not only require additional power for electric propulsion but also would so increase nuclear safety that nuclear powerplants might provide this power. From an 8000 kWt SP-100 reactor, thermoelectric power generation could produce 300 kWe, or adapted solar-Brayton cycle, 2400 to 2800 kWe. Author

N88-25059* # National Aeronautics and Space Administration. Lewis Research Center, Cleveland, OH.

SMALL SCALE BIPOLAR NICKEL-HYDROGEN TESTING

MICHELLE A. MANZO 1988 10 p Presented at the 33rd International Power Sources Symposium, Cherry Hill, N.J., 13-16

Jun. 1988; sponsored by the Department of the Army (NASA-TM-100936; E-4216; NAS 1.15:100936) Avail: NTIS HC A02/MF A01 CSCL 10C

Bipolar nickel-hydrogen batteries, ranging in capacity from 6 to 40 A-hr, have been tested at the NASA Lewis Research Center over the past six years. Small scale tests of 1 A-hr nickel-hydrogen stacks have been initiated as a means of screening design and component variations for bipolar nickel-hydrogen cells and batteries. Four small-scale batteries have been built and tested. Characterization and limited cycle testing were performed to establish the validity of test results in the scaled down hardware. The results show characterization test results to be valid. LEO test results in the small scale hardware have limited value.

Author

N88-25970*# Arkansas Univ., Fayetteville. Dept. of Electrical Engineering.

STUDY OF STAEBLER-WRONSKY DEGRADATION EFFECT IN A Si:H BASED P-I-N SOLAR CELLS Semiannual Report

HAMEED NASEEM and A. M. HERMAN Jul. 1988 23 p

(Contract NAG3-802)

(NASA-CR-182564; NAS 1.26:182564) Avail: NTIS HC A03/MF A01 CSCL 10A

The objective of this study is to improve the stability and efficiency of thin solar cells with emphasis on a-Si:H devices. The research project was broken down into three main phases. The first involves designing and building a UHV glow discharge system; the second involves making good quality films and eventually efficient cells; the final phase will be analytical.

Author

N88-25977*# AiResearch Mfg. Co., Torrance, CA. **ADVANCED HEAT RECEIVER CONCEPTUAL DESIGN STUDY Final Report, Jul. 1986 - Nov. 1987**

HAL J. STRUMPF and MURRAY G. COOMBS Dec. 1987 327 p

(Contract NAS3-24859)

(NASA-CR-180901; NAS 1.26:180901; AIRESEARCH-87-61069)

Avail: NTIS HC A15/MF A01 CSCL 10A

A study was conducted to generate and evaluate advanced solar heat receiver concepts for orbital application with Brayton and Stirling engines approximately 7 kWe in size. The resulting designs have thermal storage capability, and will be lighter, smaller, and/or more efficient than baseline systems such as the configuration used for the Brayton solar receiver currently under development by Garrett AiResearch for the NASA Space Station.

Author

N88-25978*# National Aeronautics and Space Administration. Lewis Research Center, Cleveland, OH.

EFFECT OF LEO CYCLING AT SHALLOW DEPTHS OF DISCHARGE ON MANTECH IPV NICKEL-HYDROGEN CELLS

JOHN J. SMITHRICK 1988 9 p Presented at the 23rd Intersociety Energy Conversion Engineering Conference, Denver, Colo., 31 Jul. - 5 Aug. 1988; sponsored in part by ASME, AIAA, ANS, SAE, IEEE, ACS, and AIChE

(NASA-TM-101300; E-4122; NAS 1.15:101300) Avail: NTIS HC A02/MF A01 CSCL 10A

An individual pressure vessel nickel-hydrogen battery is being considered as an alternate for a nickel-cadmium battery on the Hubble Space Telescope. The space telescope battery will primarily be operating at a shallow depth of discharge (10 percent DOD) with an occasional 40 percent DOD. This shallow DOD raises several issues: (1) What is the cycle life. It is projected to be acceptable; however, there is no reported real time data base for validation. (2) The state of charge of the nickel electrode at the beginning of charge is 90 percent. Will this cause an acceleration of divergence in the battery individual cell voltages. (3) After prolonged cycling at 10 percent DOD, will there be enough capacity remaining to support the 40 percent DOD. (4) Is the state of charge really 90 percent during cycling. There is no reported real time data base at shallow depths of discharge. A data base to address the above issues was initiated.

Author

N88-26732*# National Aeronautics and Space Administration. Lewis Research Center, Cleveland, OH.

THE DESIGN AND FABRICATION OF A STIRLING ENGINE HEAT EXCHANGER MODULE WITH AN INTEGRAL HEAT PIPE

JEFFREY G. SCHREIBER 1988 11 p Presented at the 23rd Intersociety Energy Conversion Engineering Conference, Denver, Colorado, 31 Jul. - 5 Aug. 1988; sponsored in part by ASME, AIAA, ANS, SAE, IEEE, ACS and AIChE

(NASA-TM-101296; E-4101; NAS 1.15:101296) Avail: NTIS HC A03/MF A01 CSCL 10B

The conceptual design of a free-piston Stirling Space Engine (SSE) intended for space power applications has been generated. The engine was designed to produce 25 kW of electric power with heat supplied by a nuclear reactor. A novel heat exchanger module was designed to reduce the number of critical joints in the heat exchanger assembly while also incorporating a heat pipe as the link between the engine and the heat source. Two inexpensive verification tests are proposed. The SSE heat exchanger module is described and the operating conditions for the module are outlined. The design process of the heat exchanger modules, including the sodium heat pipe, is briefly described. Similarities between the proposed SSE heat exchanger modules and the LeRC test modules for two test engines are presented. The benefits and weaknesses of using a sodium heat pipe to transport heat to a Stirling engine are discussed. Similarly, the problems encountered when using a true heat pipe, as opposed to a more simple reflux boiler, are described. The instruments incorporated into the modules and the test program are also outlined.

Author

N88-27621*# Purdue Univ., West Lafayette, IN. School of Electrical Engineering.

SOLAR ENERGY CONVERSION THROUGH THE INTERACTION OF PLASMONS WITH TUNNEL JUNCTIONS. PART A: SOLAR CELL ANALYSIS. PART B: PHOTOCONDUCTOR ANALYSIS Final Report

P. E. WELSH and R. J. SCHWARTZ Jul. 1988 145 p

(Contract NAG3-433)

(NASA-CR-183044; NAS 1.26:183044; TR-EE-88-37) Avail: NTIS HC A07/MF A01 CSCL 10A

A solar cell utilizing guided optical waves and tunnel junctions was analyzed to determine its feasibility. From this analysis, it appears that the limits imposed upon conventional multiple cell systems also limit this solar cell. Due to this limitation, it appears that the relative simplicity of the conventional multiple cell systems over the solar cell make the conventional multiple cell systems the more promising candidate for improvement. It was discovered that some superlattice structures studied could be incorporated into an infrared photodetector. This photoconductor appears to be promising as a high speed, sensitive (high D sup star sub BLIP) detector in the wavelength range from 15 to over 100 micrometers.

Author

N88-27624*# National Aeronautics and Space Administration. Lewis Research Center, Cleveland, OH.

A COMPARISON OF THE RADIATION TOLERANCE CHARACTERISTICS OF MULTI-JUNCTION SOLAR CELLS WITH SERIES AND VOLTAGE-MATCHED CONFIGURATIONS

J. M. GEE (Sandia National Labs., Albuquerque, N. Mex.) and H. B. CURTIS 1988 7 p Presented at the 9th Space Photovoltaic Research and Technology Conference, Cleveland, Ohio, 19 Apr. 1988

(Contract DE-AC04-76DP-00789)

(NASA-TM-101177; NAS 1.15:101177; DE88-009468;

SAND-88-0865C; CONF-8804122-1) Avail: NTIS HC A02/MF A01 CSCL 10A

The effect of series and voltage-matched configurations on the performance of multijunction solar cells in a radiation environment was investigated. It was found that the configuration of the multijunction solar cell can have a significant impact on its radiation tolerance characteristics.

DOE

44 ENERGY PRODUCTION AND CONVERSION

N88-30184*# United Technologies Corp., South Windsor, CT. Power Systems Div.

REGENERATIVE FUEL CELL ENERGY STORAGE SYSTEM FOR A LOW EARTH ORBIT SPACE STATION

R. E. MARTIN, J. GAROW, and K. B. MICHAELS 1988 139 p
(Contract NAS3-22234)
(NASA-CR-174802; FCR-6128; NAS 1.26:174802) Avail: NTIS HC A07/MF A01 CSCL 10C

A study was conducted to define characteristics of a Regenerative Fuel Cell System (RFCS) for low earth orbit Space Station missions. The RFCS's were defined and characterized based on both an alkaline electrolyte fuel cell integrated with an alkaline electrolyte water electrolyzer and an alkaline electrolyte fuel cell integrated with an acid solid polymer electrolyte (SPE) water electrolyzer. The study defined the operating characteristics of the systems including system weight, volume, and efficiency. A maintenance philosophy was defined and the implications of system reliability requirements and modularization were determined. Finally, an Engineering Model System was defined and a program to develop and demonstrate the EMS and pacing technology items that should be developed in parallel with the EMS were identified. The specific weight of an optimized RFCS operating at 140 F was defined as a function of system efficiency for a range of module sizes. An EMS operating at a nominal temperature of 180 F and capable of delivery of 10 kW at an overall efficiency of 55.4 percent is described. A program to develop the EMS is described including a technology development effort for pacing technology items. Author

46

GEOPHYSICS

Includes aeronomy; upper and lower atmosphere studies; ionospheric and magnetospheric physics; and geomagnetism.

A88-35775* National Aeronautics and Space Administration. Marshall Space Flight Center, Huntsville, AL.

COMMENT ON 'RAM ION SCATTERING CAUSED BY SPACE SHUTTLE V X B INDUCED DIFFERENTIAL CHARGING' BY I. KATZ AND V. A. DAVIS

N. H. STONE (NASA, Marshall Space Flight Center, Huntsville, AL), U. SAMIR (Tel Aviv University, Israel; Michigan, University, Ann Arbor), K. H. WRIGHT, JR., and K. S. HWANG (Alabama, University, Huntsville) Journal of Geophysical Research (ISSN 0148-0227), vol. 93, May 1, 1988, p. 4143-4147; Reply, p. 4149, 4150. refs

(Contract NGR-23-005-320; NAG8-058; NAS8-37107; NAS3-23881)

A88-53464* Iowa Univ., Iowa City.

DOUBLE-PROBE POTENTIAL MEASUREMENTS NEAR THE SPACELAB 2 ELECTRON BEAM

J. T. STEINBERG, D. A. GURNETT (Iowa, University, Iowa City), P. M. BANKS (Stanford University, CA), and W. J. RAITT (Utah State University, Logan) Journal of Geophysical Research (ISSN 0148-0227), vol. 93, Sept. 1, 1988, p. 10001-10010. refs
(Contract NAS8-32807; NAG3-449; NGL-16-001-043)

As part of the Spacelab 2 mission the plasma diagnostics package (PDP) was released from the shuttle as a free-flying satellite. The PDP carried a quasi-static electric field instrument which made differential voltage measurements between two floating probes. At various times during the free flight, an electron beam was ejected from the shuttle. Large differential voltages between the double probes were recorded in association with the electron beam. However, analysis indicates that these large signals are probably not caused by ambient electric fields. Instead, they can be explained by considering three effects: shadowing of the probes from streaming electrons by the PDP chassis, crossing of the PDP wake by the probes, and spatial gradients in the fluxes of

energetic electrons reaching the probes. Plasma measurements on the PDP show that energetic electrons exist in a region 20 m wide and up to at least 170 m downstream from the electron beam. At 80 or more meters downstream from the beam, the double probe measurements show that the energetic electron flux is opposite to the injection direction, as would be expected for a secondary returning electron beam produced by scattering of the primary electron beam. Author

54

MAN/SYSTEM TECHNOLOGY AND LIFE SUPPORT

Includes human engineering; biotechnology; and space suits and protective clothing.

A88-50223*# Case Western Reserve Univ., Cleveland, OH.

REDUNDANT MANIPULATORS FOR MOMENTUM COMPENSATION IN A MICRO-GRAVITY ENVIRONMENT

R. D. QUINN, J. L. CHEN (Case Western Reserve University, Cleveland, OH), and C. LAWRENCE (NASA, Lewis Research Center, Cleveland, OH) IN: AIAA Guidance, Navigation and Control Conference, Minneapolis, MN, Aug. 15-17, 1988, Technical Papers. Part 2. Washington, DC, American Institute of Aeronautics and Astronautics, 1988, p. 581-587. refs
(Contract NAG3-797)
(AIAA PAPER 88-4121)

This paper is concerned with the implementation and assessment of joint motion management strategies for kinematically redundant robotic manipulators operating in the micro-gravity environment of Space Station. These robots must be capable of conducting experiments and manufacturing processes without disturbing the micro-gravity environment through base reactions/motions. The redundant degrees of freedom of the manipulator permit the inverse kinematic problem to be solved simultaneously with the minimization of a cost function. The cost function in this case is the weighted sum of the squares of the base forces and moments and is minimized over discrete time segments. The Generalized Inverse Method and Rayleigh Ritz technique are used to solve the combined optimization/inverse kinematics problem. Numerical examples include various robotic configurations and degrees of manipulator redundancy. Author

59

MATHEMATICAL AND COMPUTER SCIENCES (GENERAL)

N88-19102*# National Aeronautics and Space Administration. Lewis Research Center, Cleveland, OH.

APPLICATION OF ADVANCED COMPUTATIONAL TECHNOLOGY TO PROPULSION CFD

JOHN R. SZUCH 1988 21 p Proposed for presentation at the Symposium on Advances and Trends in Computational Structural Mechanics and Fluid Dynamics, Washington, D.C., 17-19 Oct. 1988
(NASA-TM-100843; E-4034; NAS 1.15:100843) Avail: NTIS HC A03/MF A01 CSCL 12A

The Internal Fluid Mechanics Division of the NASA Lewis Research Center is combining the key elements of computational fluid dynamics, aerothermodynamic experiments, and advanced computational technology to bring internal computational fluid dynamics (ICFM) to a state of practical application for aerospace propulsion system design. This paper presents an overview of

COMPUTER PROGRAMMING AND SOFTWARE

Includes computer programs, routines, and algorithms, and specific applications, e.g., CAD/CAM.

A88-15427* Wyoming Univ., Laramie.
A HYPERMATRIX FORMULATION FOR SUBSPACE ITERATION

RICHARD J. SCHMIDT (Wyoming University, Laramie) and ROBERT H. DODDS, JR. (Kansas University, Lawrence) Engineering Computations (ISSN 0264-4401), vol. 4, Sept. 1987, p. 190-198. refs
 (Contract NAG3-32)

The computational efficiency of subspace iteration is addressed relative to the data structures adopted for the very large and generally sparse coefficient matrices. The frequent triangulations and matrix multiplications demand that access to the terms in the coefficient matrices be unbiased. Reliance on virtual memory (paging) operating systems with no special considerations for localized data access is not adequate. Specific data structures must be designed that accommodate the needs of the numerical algorithm yet eliminate unnecessary paging. An implementation of the subspace iteration method using hypermatrix data structures is presented. Use of hypermatrices is shown to provide unbiased and localized data access. The various modifications to the conventional formulation are described and an example problem illustrates the potential benefits of the hypermatrix formulation. Possibilities for adapting hypermatrix data structures to new supercomputer architectures are discussed. Author

A88-27795* Case Western Reserve Univ., Cleveland, OH.
I-BIEM, AN ITERATIVE BOUNDARY INTEGRAL EQUATION METHOD FOR COMPUTER SOLUTIONS OF CURRENT DISTRIBUTION PROBLEMS WITH COMPLEX BOUNDARIES: A NEW ALGORITHM. I - THEORETICAL

B. D. CAHAN, DANIEL SCHERSON (Case Western Reserve University, Cleveland, OH), and MARGARET A. REID (NASA, Lewis Research Center; Case Western Reserve University, Cleveland, OH) Electrochemical Society, Journal (ISSN 0013-4651), vol. 135, Feb. 1988, p. 285-293. Research supported by IBM Instruments, Inc. refs

A new algorithm for an iterative computation of solutions of Laplace's or Poisson's equations in two dimensions, using Green's second identity, is presented. This algorithm converges strongly and geometrically and can be applied to curved, irregular, or moving boundaries with nonlinear and/or discontinuous boundary conditions. It has been implemented in Pascal on a number of micro- and minicomputers and applied to several geometries. Cases with known analytic solutions have been tested. Convergence to within 0.1 percent to 0.01 percent of the theoretical values are obtained in a few minutes on a microcomputer. Author

A88-32309*# Southwest Research Inst., San Antonio, TX.
VALIDATION OF THE NESSUS PROBABILISTIC FINITE ELEMENT ANALYSIS COMPUTER PROGRAM

Y.-T. WU and O. H. BURNSIDE (Southwest Research Institute, San Antonio, TX) IN: Structures, Structural Dynamics and Materials Conference, 29th, Williamsburg, VA, Apr. 18-20, 1988, Technical Papers. Part 3. Washington, DC, American Institute of Aeronautics and Astronautics, 1988, p. 1267-1274. refs
 (Contract NAS3-24389)
 (AIAA PAPER 88-2372)

A computer program, NESSUS, is being developed as part of a NASA-sponsored project to develop probabilistic structural analysis methods for propulsion system components. This paper describes the process of validating the NESSUS code, as it has been developed to date, and presents numerical results comparing NESSUS and exact solutions for a set of selected problems. Author

efforts under way at NASA Lewis to advance and apply computational technology to ICFM. These efforts include the use of modern, software engineering principles for code development, the development of an AI-based user-interface for large codes, the establishment of a high-performance, data communications network to link ICFM researchers and facilities, and the application of parallel processing to speed up computationally intensive and/or time-critical ICFM problems. A multistage compressor flow physics program is cited as an example of efforts to use advanced computational technology to enhance a current NASA Lewis ICFM research program. Author

COMPUTER OPERATIONS AND HARDWARE

Includes hardware for computer graphics, firmware, and data processing.

A88-17223* Bell Communications Research, Inc., Red Bank, NJ.

IMPLEMENTATION OF A FAST DIGITAL OPTICAL MATRIX-VECTOR MULTIPLIER USING A HOLOGRAPHIC LOOK-UP TABLE AND RESIDUE ARITHMETIC

SARRY F. HABIBY (Bell Communications Research, Inc., Red Bank, NJ) and STUART A. COLLINS, JR. (Ohio State University, Columbus) Applied Optics (ISSN 0003-6935), vol. 26, Nov. 1, 1987, p. 4639-4652. refs
 (Contract NSG-3302)

The design and implementation of a digital (numerical) optical matrix-vector multiplier are presented. A Hughes liquid crystal light valve, the residue arithmetic representation, and a holographic optical memory are used to construct position coded optical look-up tables. All operations are performed in effectively one light valve response time with a potential for a high information density. Author

N88-10496*# Ohio State Univ., Columbus. ElectroScience Lab.
IMPLEMENTATION OF A DIGITAL OPTICAL MATRIX-VECTOR MULTIPLIER USING A HOLOGRAPHIC LOOK-UP TABLE AND RESIDUE ARITHMETIC

SARRY F. HABIBY Aug. 1987 163 p
 (Contract NSG-3302)
 (NASA-CR-180431; NAS 1.26:180431; TR-712257-6) Avail: NTIS HC A08/MF A01 CSCL 09B

The design and implementation of a digital (numerical) optical matrix-vector multiplier are presented. The objective is to demonstrate the operation of an optical processor designed to minimize computation time in performing a practical computing application. This is done by using the large array of processing elements in a Hughes liquid crystal light valve, and relying on the residue arithmetic representation, a holographic optical memory, and position coded optical look-up tables. In the design, all operations are performed in effectively one light valve response time regardless of matrix size. The features of the design allowing fast computation include the residue arithmetic representation, the mapping approach to computation, and the holographic memory. In addition, other features of the work include a practical light valve configuration for efficient polarization control, a model for recording multiple exposures in silver halides with equal reconstruction efficiency, and using light from an optical fiber for a reference beam source in constructing the hologram. The design can be extended to implement larger matrix arrays without increasing computation time. Author

61 COMPUTER PROGRAMMING AND SOFTWARE

A88-32311* Southwest Research Inst., San Antonio, TX.

NESSUS/EXPERT - AN EXPERT SYSTEM FOR PROBABILISTIC STRUCTURAL ANALYSIS METHODS

H. MILLWATER, K. PALMER, and P. FINK (Southwest Research Institute, San Antonio, TX) IN: Structures, Structural Dynamics and Materials Conference, 29th, Williamsburg, VA, Apr. 18-20, 1988, Technical Papers. Part 3. Washington, DC, American Institute of Aeronautics and Astronautics, 1988, p. 1283-1288. refs (Contract NAS3-24389) (AIAA PAPER 88-2374)

An expert system (NESSUS/EXPERT) is presented which provides assistance in using probabilistic structural analysis methods. NESSUS/EXPERT is an interactive menu-driven expert system that provides information to assist in the use of the probabilistic finite element code NESSUS/FEM and the fast probability integrator. NESSUS/EXPERT was developed with a combination of FORTRAN and CLIPS, a C language expert system tool, to exploit the strengths of each language. Author

A88-46961* National Aeronautics and Space Administration. Lewis Research Center, Cleveland, OH.

TIME-PARTITIONING SIMULATION MODELS FOR CALCULATION OF PARALLEL COMPUTERS

EDWARD J. MILNER, RICHARD A. BLECH, and RODRICK V. CHIMA (NASA, Lewis Research Center, Cleveland, OH) IN: 1987 Annual Summer Computer Simulation Conference, 19th, Montreal, Canada, July 27-30, 1987, Proceedings. San Diego, CA, Society for Computer Simulation, 1987, p. 196-201. Previously announced in STAR as N87-20766. refs

A technique allowing time-staggered solution of partial differential equations is presented in this report. Using this technique, called time-partitioning, simulation execution speedup is proportional to the number of processors used because all processors operate simultaneously, with each updating of the solution grid at a different time point. The technique is limited by neither the number of processors available nor by the dimension of the solution grid. Time-partitioning was used to obtain the flow pattern through a cascade of airfoils, modeled by the Euler partial differential equations. An execution speedup factor of 1.77 was achieved using a two processor Cray X-MP/24 computer. Author

A88-46963* National Aeronautics and Space Administration. Lewis Research Center, Cleveland, OH.

AUTOMATING THE PARALLEL PROCESSING OF FLUID AND STRUCTURAL DYNAMICS CALCULATIONS

DALE J. ARPASI and GARY L. COLE (NASA, Lewis Research Center, Cleveland, OH) IN: 1987 Annual Summer Computer Simulation Conference, 19th, Montreal, Canada, July 27-30, 1987, Proceedings. San Diego, CA, Society for Computer Simulation, 1987, p. 214-218. Previously announced in STAR as N87-19002. refs

The NASA Lewis Research Center is actively involved in the development of expert system technology to assist users in applying parallel processing to computational fluid and structural dynamic analysis. The goal of this effort is to eliminate the necessity for the physical scientist to become a computer scientist in order to effectively use the computer as a research tool. Programming and operating software utilities have previously been developed to solve systems of ordinary nonlinear differential equations on parallel scalar processors. Current efforts are aimed at extending these capabilities to systems of partial differential equations, that describe the complex behavior of fluids and structures within aerospace propulsion systems. This paper presents some important considerations in the redesign, in particular, the need for algorithms and software utilities that can automatically identify data flow patterns in the application program and partition and allocate calculations to the parallel processors. A library-oriented multiprocessing concept for integrating the hardware and software functions is described. Author

N88-11165* Pratt and Whitney Aircraft, East Hartford, CT.
3-D INELASTIC ANALYSIS METHODS FOR HOT SECTION COMPONENTS

E. S. TODD /in NASA. Lewis Research Center, Turbine Engine Hot Section Technology, 1985 p 239-243 Oct. 1985 (Contract NAS3-23697)

Avail: NTIS HC A19/MF A01 CSCL 09B

The objective is to produce a series of new computer codes that permit more accurate and efficient three dimensional inelastic structural analysis of combustor liners, turbine blades, and turbine vanes. Each code embodies a progression of mathematical models for increasingly comprehensive representation of the geometrical features, loading conditions, and forms of nonlinear material response that distinguish these three groups of hot section components. Author

N88-11166* General Electric Co., Cincinnati, OH. Aircraft Engine Business Group.

COMPONENT SPECIFIC MODELING

R. L. MCKNIGHT and M. T. TIPTON /in NASA. Lewis Research Center, Turbine Engine Hot Section Technology, 1985 p 245-257 Oct. 1985

(Contract NAS3-23687)

Avail: NTIS HC A19/MF A01 CSCL 09B

The objective is to develop and verify a series of interdisciplinary modeling and analysis techniques that have been specialized to address three specific hot section components. These techniques will incorporate data as well as theoretical methods from many diverse areas including cycle and performance analysis, heat transfer analysis, linear and nonlinear stress analysis, and mission analysis. The new methods developed will be integrated to provide an accurate, efficient, and unified approach to analyzing combustor burner liners, hollow air-cooled turbine blades, and air-cooled turbine vanes. For these components, the methods developed will predict temperature, deformation, stress, and strain histories throughout a complete flight mission. Author

N88-12288* National Aeronautics and Space Administration. Lewis Research Center, Cleveland, OH.

A FORTRAN CODE FOR THE CALCULATION OF PROBE VOLUME GEOMETRY CHANGES IN A LASER ANEMOMETRY SYSTEM CAUSED BY WINDOW REFRACTION

ALBERT K. OWEN (Army Aviation Research and Development Command, Cleveland, Ohio.) Nov. 1987 31 p (NASA-TM-100210; E-3820; NAS 1.15:100210; AVSCOM-TR-87-C-27; AD-A188714) Avail: NTIS HC A03/MF A01 CSCL 09B

A computer code was written which utilizes ray tracing techniques to predict the changes in position and geometry of a laser Doppler velocimeter probe volume resulting from refraction effects. The code predicts the position change, changes in beam crossing angle, and the amount of uncrossing that occur when the beams traverse a region with a changed index of refraction, such as a glass window. The code calculates the changes for flat plate, cylinder, general axisymmetric and general surface windows and is currently operational on a VAX 8600 computer system. Author

N88-19147* National Aeronautics and Space Administration. Lewis Research Center, Cleveland, OH.

DISTRIBUTED COMPUTATION OF GRAPHICS PRIMITIVES ON A TRANSPUTER NETWORK

GRAHAM K. ELLIS 1988 7 p Prepared for presentation at the Summer Computer Simulation Conference, Seattle, Wash., 25-28 Jul. 1988; sponsored in part by The Society for Computer Simulation (NASA-TM-100814; ICOMP-88-3; E-3999; NAS 1.15:100814) Avail: NTIS HC A02/MF A01 CSCL 09B

A method is developed for distributing the computation of graphics primitives on a parallel processing network. Off-the-shelf transputer boards are used to perform the graphics transformations and scan-conversion tasks that would normally be assigned to a single transputer based display processor. Each node in the network performs a single graphics primitive computation. Frequently requested tasks can be duplicated on several nodes. The results indicate that the current distribution of commands on

the graphics network shows a performance degradation when compared to the graphics display board alone. A change to more computation per node for every communication (perform more complex tasks on each node) may cause the desired increase in throughput. Author

N88-21682*# Pratt and Whitney Aircraft, East Hartford, CT. Commercial Engine Business.

AERO/STRUCTURAL TAILORING OF ENGINE BLADES (AERO/STAEBL) Interim Report

K. W. BROWN Mar. 1988 60 p

(Contract NAS3-22525)

(NASA-CR-180805; NAS 1.26:180805; PWA-5774-82) Avail: NTIS HC A04/MF A01 CSCL 09B

This report describes the Aero/Structural Tailoring of Engine Blades (AERO/STAEBL) program, which is a computer code used to perform engine fan and compressor blade aero/structural numerical optimizations. These optimizations seek a blade design of minimum operating cost that satisfies realistic blade design constraints. This report documents the overall program (i.e., input, optimization procedures, approximate analyses) and also provides a detailed description of the validation test cases. Author

N88-22591*# National Aeronautics and Space Administration. Lewis Research Center, Cleveland, OH.

TWO-DIMENSIONAL GRAPHICS TOOLS FOR A TRANSPUTER BASED DISPLAY BOARD

GRAHAM K. ELLIS 1988 16 p Presented at the Parallel Computing Workshop/OCCAM User Group Meeting, Portland, Oregon, 11-13 Apr. 1988; sponsored by OSU/OCATE and INMOS

(NASA-TM-100820; E-4010; ICOMP-88-4; NAS 1.15:100820)

Avail: NTIS HC A03/MF A01 CSCL 09B

A package of 2-D graphics routines has been developed in an effort to standardize and simplify the user interface for a transputer based graphics display board. The routines available take advantage of the graphic board's capabilities while also presenting an intuitive approach for generating drawings. The routines allow a user to perform graphics rendering in a 2-D real-coordinate space without regard to the actual screen coordinates. Multiple windows, which can be placed arbitrarily on the screen as well as the ability to use double-buffering techniques for smooth animations are also supported. The routines are designed to be run on a transputer other than the graphics display board. The window and screen parameters are maintained locally. The conversion to device coordinates is also performed locally. The only data sent to the display board are control and device coordinate display commands. The routines available include: rotation translation, and scaling commands; absolute and relative point and line commands; circle, rectangle and polygon commands; and window and viewpoint definition commands. Author

N88-23233*# Army Aviation Systems Command, Cleveland, OH. Dept. of Civil Engineering.

PARALLEL COMPUTER METHODS FOR EIGENVALUE EXTRACTION

FRED AKL (Ohio Univ., Athens.) In NASA, Lewis Research Center, Lewis Structures Technology, 1988. Volume 1: Structural Dynamics p 91-102 May 1988

(Contract NAG3-762)

Avail: NTIS HC A20/MF A01 CSCL 09B

A new numerical algorithm for the solution of large-order eigenproblems typically encountered in linear elastic finite element systems is presented. The architecture of parallel processing is used in the algorithm to achieve increased speed and efficiency of calculations. The algorithm is based on the frontal technique for the solution of linear simultaneous equations and the modified subspace eigenanalysis method for the solution of the eigenproblem. The advantages of this new algorithm in parallel computer architecture are discussed. Author

N88-23234*# Toledo Univ., OH. Dept. of Computer Science and Engineering.

ADAPTING HIGH-LEVEL LANGUAGE PROGRAMS FOR PARALLEL PROCESSING USING DATA FLOW

HILDA M. STANDLEY In NASA, Lewis Research Center, Lewis Structures Technology, 1988. Volume 1: Structural Dynamics p 203-111 May 1988

(Contract NAG3-699)

Avail: NTIS HC A20/MF A01 CSCL 09B

EASY-FLOW, a very high-level data flow language, is introduced for the purpose of adapting programs written in a conventional high-level language to a parallel environment. The level of parallelism provided is of the large-grained variety in which parallel activities take place between subprograms or processes. A program written in EASY-FLOW is a set of subprogram calls as units, structured by iteration, branching, and distribution constructs. A data flow graph may be deduced from an EASY-FLOW program. Author

N88-26127*# National Aeronautics and Space Administration. Lewis Research Center, Cleveland, OH.

THE DEVELOPMENT OF AN INTELLIGENT INTERFACE TO A COMPUTATIONAL FLUID DYNAMICS FLOW-SOLVER CODE

ANTHONY D. WILLIAMS 1988 23 p Prepared for presentation at the Symposium on Advances and Trends in Computational Structural Mechanics and Fluid Dynamics, Washington, D.C., 17-19 Oct. 1988; sponsored in part by George Washington Univ. and Langley Research Center

(NASA-TM-100908; E-4160; NAS 1.15:100908) Avail: NTIS HC A03/MF A01 CSCL 09B

Researchers at NASA Lewis are currently developing an 'intelligent' interface to aid in the development and use of large, computational fluid dynamics flow-solver codes for studying the internal fluid behavior of aerospace propulsion systems. This paper discusses the requirements, design, and implementation of an intelligent interface to Proteus, a general purpose, 3-D, Navier-Stokes flow solver. The interface is called PROTAIS to denote its introduction of artificial intelligence (AI) concepts to the Proteus code. Author

N88-27796*# National Aeronautics and Space Administration. Lewis Research Center, Cleveland, OH.

IMPLEMENTING DIRECT, SPATIALLY ISOLATED PROBLEMS ON TRANSPUTER NETWORKS

GRAHAM K. ELLIS Aug. 1988 57 p

(NASA-TM-101297; ICOMP-88-14; E-4278; NAS 1.15:101297)

Avail: NTIS HC A04/MF A01 CSCL 09B

Parametric studies were performed on transputer networks of up to 40 processors to determine how to implement and maximize the performance of the solution of problems where no processor-to-processor data transfer is required for the problem solution (spatially isolated). Two types of problems are investigated a computationally intensive problem where the solution required the transmission of 160 bytes of data through the parallel network, and a communication intensive example that required the transmission of 3 Mbytes of data through the network. This data consists of solutions being sent back to the host processor and not intermediate results for another processor to work on. Studies were performed on both integer and floating-point transputers. The latter features an on-chip floating-point math unit and offers approximately an order of magnitude performance increase over the integer transputer on real valued computations. The results indicate that a minimum amount of work is required on each node per communication to achieve high network speedups (efficiencies). The floating-point processor requires approximately an order of magnitude more work per communication than the integer processor because of the floating-point unit's increased computing capacity. Author

N88-27799*# National Aeronautics and Space Administration. Lewis Research Center, Cleveland, OH.

USER'S MANUAL FOR THE TWO-DIMENSIONAL TRANSPUTER GRAPHICS TOOLKIT

62 COMPUTER SYSTEMS

GRAHAM K. ELLIS Aug. 1988 105 p
(Contract NASA ORDER C-99066-G)
(NASA-TM-100974; ICOMP-88-13; E-4266; NAS 1.15:100974)
Avail: NTIS HC A06/MF A01 CSCL 09B

The user manual for the 2-D graphics toolkit for a transputer based parallel processor is presented. The toolkit consists of a package of 2-D display routines that can be used for the simulation visualizations. It supports multiple windows, double buffered screens for animations, and simple graphics transformations such as translation, rotation, and scaling. The display routines are written in occam to take advantage of the multiprocessing features available on transputers. The package is designed to run on a transputer separate from the graphics board. Author

62

COMPUTER SYSTEMS

Includes computer networks and special application computer systems.

A88-40458*# National Aeronautics and Space Administration. Lewis Research Center, Cleveland, OH.
HYPERCLUSTER - PARALLEL PROCESSING FOR COMPUTATIONAL MECHANICS
RICHARD A. BLECH (NASA, Lewis Research Center, Cleveland, OH) Mechanical Engineering (ISSN 0025-6501), vol. 110, May 1988, p. 52-56.

An account is given of the development status, performance capabilities and implications for further development of NASA-Lewis' testbed 'hypercluster' parallel computer network, in which multiple processors communicate through a shared memory. Processors have local as well as shared memory; the hypercluster is expanded in the same manner as the hypercube, with processor clusters replacing the normal single processor node. The NASA-Lewis machine has three nodes with a vector personality and one node with a scalar personality. Each of the vector nodes uses four board-level vector processors, while the scalar node uses four general-purpose microcomputer boards. O.C.

A88-49101* Arizona State Univ., Tempe.
PERFORMANCE LIMITATIONS IN PARALLEL PROCESSOR SIMULATIONS
E. PEARSE O'GRADY (Arizona State University, Tempe) and CHUNG-HSIEN WANG (Sierra Semiconductor, Inc., San Jose, CA) Society for Computer Simulation, Transactions (ISSN 0740-6797), vol. 4, Oct. 1987, p. 311-330. refs
(Contract NAG3-113)

A jet-engine model is partitioned and simulated on a parallel processor system consisting of five 8086/8087 floating-point computers. The simulation uses Heun's integration method. A near-optimal parallel simulation (in the sense of minimum execution time) achieves speedup of only 2.13 and efficiency of 42.6 percent, in effect wasting 57.4 percent of the available processing power. A detailed analysis identifies and graphically demonstrates why the system fails to achieve ideal performance (viz., speedup of 5 and efficiency of 100 percent). Inherent characteristics of the problem equations and solution algorithm account for the loss of nearly half of the available processing power. Overheads associated with interprocessor communication and processor synchronization account for only a small fraction of the lost processing power. The effects of these and other factors which limit parallel processor performance are illustrated through real-time timing-analyzer tracers describing the run/idle status of the parallel processors during the simulation. Author

N88-21697*# National Aeronautics and Space Administration. Lewis Research Center, Cleveland, OH.
LABORATORY INFORMATION MANAGEMENT SYSTEM (LIMS): A CASE STUDY

KAREN S. CRANDALL, JUDITH V. AUPING, and ROBERT G. MEGARGLE (Cleveland State Univ., Ohio.) 1987 18 p Presented at the 1st International Laboratory Information Management Systems Meeting, Pittsburgh, Pa., 23-25 Jan. 1987
(NASA-TM-100835; E-4024; NAS 1.15:100835) Avail: NTIS HC A03/MF A01 CSCL 09B

In the late 70's, a refurbishment of the analytical laboratories serving the Materials Division at NASA Lewis Research Center was undertaken. As part of the modernization efforts, a Laboratory Information Management System (LIMS) was to be included. Preliminary studies indicated a custom-designed system as the best choice in order to satisfy all of the requirements. A scaled down version of the original design has been in operation since 1984. The LIMS, a combination of computer hardware, provides the chemical characterization laboratory with an information data base, a report generator, a user interface, and networking capabilities. This paper is an account of the processes involved in designing and implementing that LIMS. Author

63

CYBERNETICS

Includes feedback and control theory, artificial intelligence, robotics and expert systems.

A88-54202*# Texas A&M Univ., College Station.
ACTIVE CONTROL OF TRANSIENT ROTORDYNAMIC VIBRATION BY OPTIMAL CONTROL METHODS

A. B. PALAZZOLO, R. R. LIN, R. M. ALEXANDER (Texas A & M University, College Station), and A. F. KASCAK (NASA, Lewis Research Center, Cleveland, OH) ASME, Gas Turbine and Aeroengine Congress and Exposition, Amsterdam, Netherlands, June 6-9, 1988. 8 p. Research supported by Texas A & M University. refs
(Contract NAG3-763)
(ASME PAPER 88-GT-73)

Although considerable effort has been put into the study of steady state vibration control, there are few methods applicable to transient vibration control of rotorbearing systems. In this paper optimal control theory has been adopted to minimize rotor vibration due to sudden imbalance, e.g., blade loss. The system gain matrix is obtained by choosing the weighting matrices and solving the Riccati equation. Control forces are applied to the system via a feedback loop. A seven mass rotor system is simulated for illustration. A relationship between the number of sensors and the number of modes used in the optimal control model is investigated. Comparisons of responses are made for various configurations of modes, sensors, and actuators. Furthermore, spillover effect is examined by comparing results from collocated and noncollocated sensor configurations. Results show that shaft vibration is significantly attenuated in the closed loop system. Author

A88-54537* Pennsylvania State Univ., University Park.
FINITE-DIMENSIONAL MODELING OF NETWORK-INDUCED DELAYS FOR REAL-TIME CONTROL SYSTEMS
ASOK RAY (Pennsylvania State University, University Park) and YORAM HALEVI (Technion - Israel Institute of Technology, Haifa) IN: 1988 American Control Conference, 7th, Atlanta, GA, June 15-17, 1988, Proceedings. Volume 2. New York, Institute of Electrical and Electronics Engineers, 1988, p. 1077-1082. refs
(Contract NAG3-823; NSF DMC-87-07648)

In integrated control systems (ICS), a feedback loop is closed by the common communication channel, which multiplexes digital data from the sensor to the controller and from the controller to the actuator along with the data traffic from other control loops and management functions. Due to asynchronous time-division multiplexing in the network access protocols, time-varying delays are introduced in the control loop, which degrade the system dynamic performance and are a potential source of instability.

The delayed control system is represented by a finite-dimensional, time-varying, discrete-time model which is less complex than the existing continuous-time models for time-varying delays; this approach allows for simpler schemes for analysis and simulation of the ICS. I.E.

64

NUMERICAL ANALYSIS

Includes iteration, difference equations, and numerical approximation.

A88-22472*# National Aeronautics and Space Administration. Lewis Research Center, Cleveland, OH.

CHOICE OF IMPLICIT AND EXPLICIT OPERATORS FOR THE UPWIND DIFFERENCING METHOD

MENG-SING LIOU (NASA, Lewis Research Center, Cleveland, OH) and BRAM VAN LEER (NASA, Lewis Research Center; Institute for Computational Mechanics in Propulsion, Cleveland, OH; Michigan, University, Ann Arbor) AIAA, Aerospace Sciences Meeting, 26th, Reno, NV, Jan. 11-14, 1988. 26 p. refs (AIAA PAPER 88-0624)

The flux-vector and flux-difference splittings of Steger-Warming, Van Leer and Roe are tested in all possible combinations in the implicit and explicit operators that can be distinguished in implicit relaxation methods for the steady Euler and Navier-Stokes equations. The tests include one-dimensional inviscid nozzle flow, and two-dimensional inviscid and viscous shock reflection. Roe's splitting, as anticipated, is found to uniformly yield the most accurate results. On the other hand, an approximate Roe splitting of the implicit operator (the complete Roe splitting is too complicated for practical use) proves to be the least robust with regard to convergence to the steady state. In this respect, the Steger-Warming splitting is the most robust: it leads to convergence when combined with any of the splittings in the explicit operator, although not necessarily in the most efficient way. Author

A88-29269* National Aeronautics and Space Administration. Lewis Research Center, Cleveland, OH.

DERIVATIVES OF EIGENVALUES AND EIGENVECTORS OF A GENERAL COMPLEX MATRIX

DURBHA V. MURTHY (NASA, Lewis Research Center, Cleveland, OH; Virginia Polytechnic Institute and State University, Blacksburg) and RAPHAEL T. HAFKA (Virginia Polytechnic Institute and State University, Blacksburg) International Journal for Numerical Methods in Engineering (ISSN 0029-5981), vol. 26, Feb. 1988, p. 293-311. refs (Contract NAG3-347; NAG1-224)

A survey of methods for sensitivity analysis of the algebraic eigenvalue problem for non-Hermitian matrices is presented. In addition, a modification of one method based on a better normalizing condition is proposed. Methods are classified as Direct or Adjoint and are evaluated for efficiency. Operation counts are presented in terms of matrix size, number of design variables and number of eigenvalues and eigenvectors of interest. The effect of the sparsity of the matrix and its derivatives is also considered, and typical solution times are given. General guidelines are established for the selection of the most efficient method. Author

A88-32840* National Aeronautics and Space Administration. Lewis Research Center, Cleveland, OH.

AN ALGORITHM FOR A GENERALIZATION OF THE RICHARDSON EXTRAPOLATION PROCESS

WILLIAM F. FORD (NASA, Lewis Research Center, Cleveland, OH) and AVRAM SIDI (Technion - Israel Institute of Technology, Haifa) SIAM Journal on Numerical Analysis (ISSN 0036-1429), vol. 24, Oct. 1987, p. 1212-1232. refs (Contract NAS3-24231)

The paper presents a recursive method, designated the W exp (m)-algorithm, for implementing a generalization of the Richardson extrapolation process. Compared to the direct solution of the linear systems of equations defining the extrapolation procedure, this method requires a small number of arithmetic operations and very little storage. The technique is also applied to solve recursively the coefficient problem associated with the rational approximations obtained by applying a d-transformation to power series. In the course of development a new recursive algorithm for implementing a very general extrapolation procedure is introduced, for solving the same problem. A FORTRAN program for the W exp (m)-algorithm is also appended. Author

A88-37363* Columbia Univ., New York, NY.

ADAPTIVE GRID GENERATION

PETER R. EISEMAN (Columbia University, New York) (University of Texas, NSF, U.S. Navy, et al., World Congress on Computational Mechanics, 1st, Austin, TX, Sept. 22-26, 1986) Computer Methods in Applied Mechanics and Engineering (ISSN 0045-7825), vol. 64, Oct. 1987, p. 321-376. refs (Contract NAG3-715; AF-AFOSR-86-0307)

The fundamental principles of adaptive grid generation for the numerical analysis of physical phenomena described by systems of partial differential equations are examined in an analytical review. Topics addressed include weight functions, equidistribution in one dimension, the specification of coefficients in the linear weight, the attraction to a given grid on a curve, evolutionary forces, and metric notation. Consideration is given to curve-by-curve methods, finite-volume methods, variational methods, and temporal aspects. T.K.

A88-48791*# National Aeronautics and Space Administration. Lewis Research Center, Cleveland, OH.

A DIAGONALLY INVERTED LU IMPLICIT MULTIGRID SCHEME

J. W. YOKOTA (NASA, Lewis Research Center; Sverdrup Technology, Inc., Cleveland, OH), D. A. CAUGHEY (Cornell University, Ithaca, NY), and R. V. CHIMA (NASA, Lewis Research Center, Cleveland, OH) IN: AIAA, ASME, SIAM, and APS, National Fluid Dynamics Congress, 1st, Cincinnati, OH, July 25-28, 1988, Technical Papers. Part 1. Washington, DC, American Institute of Aeronautics and Astronautics, 1988, p. 104-111. refs (AIAA PAPER 88-3565)

A new Diagonally Inverted LU Implicit scheme is developed within the framework of the multigrid method for the three-dimensional unsteady Euler equations. The matrix systems that are to be inverted in the LU scheme are treated by local diagonalizing transformations that decouple them into systems of scalar equations. Unlike the Diagonalized ADI method, the time accuracy of the LU scheme is not reduced since the diagonalizing procedure does not destroy time conservation. Even more importantly, this diagonalization significantly reduces the computational effort required to solve the LU approximation and therefore transforms it into a more efficient method of numerically solving the three-dimensional Euler equations. Author

A88-48806*# National Aeronautics and Space Administration. Lewis Research Center, Cleveland, OH.

THIRD-ORDER MULTI-DIMENSIONAL EULER/NAVIER-STOKES SOLVER

B. P. LEONARD (NASA, Lewis Research Center, Cleveland, OH) IN: AIAA, ASME, SIAM, and APS, National Fluid Dynamics Congress, 1st, Cincinnati, OH, July 25-28, 1988, Technical Papers. Part 1. Washington, DC, American Institute of Aeronautics and Astronautics, 1988, p. 226-231. refs (AIAA PAPER 88-3645)

A nonoscillatory multidimensional advection code is presented which is applicable to the study of very high Reynolds number steady flow, and results are obtained for the oblique advection of a step profile. The scheme is based on an exponential upwinding or linear extrapolation refinement of a previous QUICK scheme, allowing sharp monotonic resolution of the step while retaining third-order accuracy. The resulting simple flux-limiting criteria have

64 NUMERICAL ANALYSIS

been applied to a higher order method and a formally third-order supercompressive algorithm. Results are presented for first-order, second-order, and third-order upwinding. R.R.

A88-48831*# National Aeronautics and Space Administration. Lewis Research Center, Cleveland, OH.

A COMPARISON OF ENO AND TVD SCHEMES

SHIH-HUNG CHANG (NASA, Lewis Research Center; Cleveland State University, OH) and MENG-SING LIOU (NASA, Lewis Research Center, Cleveland, OH) IN: AIAA, ASME, SIAM, and APS, National Fluid Dynamics Congress, 1st, Cincinnati, OH, July 25-28, 1988, Technical Papers. Part 1. Washington, DC, American Institute of Aeronautics and Astronautics, 1988, p. 427-434. refs (AIAA PAPER 88-3707)

The numerical performance of a second-order upwind-based TVD scheme is compared with that of a uniform second-order ENO scheme on shock capturing. The cases considered include flows with Mach numbers of 2.9, 5.0, and 10.0. For cases with Mach numbers of 5.0 and 10.0, the computed ENO results are inferior to the corresponding TVD results. K.K.

A88-54980*# Akron Univ., OH.

HIERARCHICALLY PARTITIONED NONLINEAR EQUATION SOLVERS

JOSEPH PADOVAN (Akron, University, OH) IN: Developments in Mechanics. Volume 14(c) - Midwestern Mechanics Conference, 20th, West Lafayette, IN, Aug. 31-Sept. 2, 1987, Proceedings. West Lafayette, IN, Purdue University, 1987, p. 1384-1389. (Contract NAG3-664)

By partitioning solution space into a number of subspaces, a new multiply constrained partitioned Newton-Raphson nonlinear equation solver is developed. Specifically, for a given iteration, each of the various separate partitions are individually and simultaneously controlled. Due to the generality of the scheme, a hierarchy of partition levels can be employed. For finite-element-type applications, this includes the possibility of degree-of-freedom, nodal, elemental, geometric substructural, material and kinematically nonlinear group controls. It is noted that such partitioning can be continuously updated, depending on solution conditioning. In this context, convergence is ascertained at the individual partition level. Author

N88-10563*# National Aeronautics and Space Administration. Lewis Research Center, Cleveland, OH.

APPROXIMATE POLYNOMIAL PRECONDITIONING APPLIED TO BIHARMONIC EQUATIONS ON VECTOR SUPERCOMPUTERS

YAU SHU WONG and HONG JIANG (Alberta Univ., Edmonton.) Oct. 1987 20 p
(NASA-TM-100217; E-3826; NAS 1.15:100217; ICOMP-87-5)
Avail: NTIS HC A03/MF A01 CSCL 12A

Applying a finite difference approximation to a biharmonic equation results in a very ill-conditioned system of equations. This paper examines the conjugate gradient method used in conjunction with the generalized and approximate polynomial preconditionings for solving such linear systems. An approximate polynomial preconditioning is introduced, and is shown to be more efficient than the generalized polynomial preconditionings. This new technique provides a simple but effective preconditioning polynomial, which is based on another coefficient matrix rather than the original matrix operator as commonly used. Author

N88-12323*# National Aeronautics and Space Administration. Lewis Research Center, Cleveland, OH.

MONTE CARLO SIMULATION OF MODULATED PHASES

D. J. SROLOVITZ, G. N. HASSOLD, and J. GAYDA 1987 11 p
Presented at the Dynamics of Ordering Processes in Condensed Matter, Kyoto, Japan, 27 Aug. 1987 Prepared in cooperation with Los Alamos National Lab., N. Mex. and Michigan Univ., Ann Arbor
(Contract W-7405-ENG-36)
(NASA-TM-89654; NAS 1.15:89654; DE87-014729;

LA-UR-87-2702; CONF-8708122-1) Avail: NTIS HC A03/MF A01 CSCL 12A

This paper presents Monte Carlo simulation results for the formation of modulated phases in the framework of the two dimensional ANNNI model with a nonconserved order parameter. This work complements the earlier studies of Kaski, et al. by examining a different, wider area of parameter space and temperature. Like Kaski, et al., it is found that for certain temperatures and values of the frustration parameter, kappa, ordered domains form quickly and the correlation length grows as the square root of time. However, there exists a range of kappa for which a quench from high to low temperature results in the formation of a metastable glassy phase. In addition to the ANNNI model study, preliminary results are presented on a newly developed model which exhibits phase modulation due to the presence of elastic interactions between the different phase and with an externally applied stress. DOE

N88-12330*# National Aeronautics and Space Administration. Lewis Research Center, Cleveland, OH.

INSTITUTE FOR COMPUTATIONAL MECHANICS IN PROPULSION (ICOMP) FIRST YEAR SUMMARY

Nov. 1987 15 p Sponsored in part by the Space Act Agreement No. C99066G
(NASA-TM-100225; ICOMP-87-8; E-3844; NAS 1.15:100225)
Avail: NTIS HC A03/MF A01 CSCL 12A

The Institute for Computational Mechanics in Propulsion (ICOMP) in Cleveland, Ohio, is operated jointly by Case Western Reserve University and the NASA Lewis Research Center. The purpose of ICOMP is to develop techniques to improve problem-solving capabilities in all aspects of computational mechanics related to propulsion. The Institute began operation in 1985. Described are the events leading to its formation, its organization and method of operation, and the technical activities of the first year. Author

N88-13931*# National Aeronautics and Space Administration. Lewis Research Center, Cleveland, OH.

SHARP SIMULATION OF DISCONTINUITIES IN HIGHLY CONVECTIVE STEADY FLOW

B. P. LEONARD Dec. 1987 35 p Prepared in cooperation with Akron Univ., Ohio.
(NASA-TM-100240; E-3863; ICOMP-87-9; NAS 1.15:100240)
Avail: NTIS HC A03/MF A01 CSCL 20D

For steady multidimensional convection, the Quadratic Upstream Interpolation for Convective Kinematics (QUICK) scheme has several attractive properties. However, for highly convective simulation of step profiles, QUICK produces unphysical overshoots and a few oscillations, and this may cause serious problems in nonlinear flows. Fortunately, it is possible to modify the convective flux by writing the normalized convected control-volume face value as a function of the normalized adjacent upstream node value, developing criteria for monotonic resolution without sacrificing formal accuracy. This results in a nonlinear functional relationship between the normalized variables, whereas standard methods are all linear in this sense. The resulting Simple High Accuracy Resolution Program (SHARP) can be applied to steady multidimensional flows containing thin shear or mixing layers, shock waves, and other frontal phenomena. This represents a significant advance in modeling highly convective flows of engineering and geophysical importance. SHARP is based on an explicit, conservative, control-volume flux formation, equally applicable to one, two, or three dimensional elliptic, parabolic, hyperbolic, or mixed-flow regimes. Results are given for the bench-mark purely convective first-order results and the nonmonotonic predictions of second- and third-order upwinding. Author

N88-19182*# National Aeronautics and Space Administration. Lewis Research Center, Cleveland, OH.

ACCURATE BOUNDARY CONDITIONS FOR EXTERIOR PROBLEMS IN GAS DYNAMICS

THOMAS HAGSTROM and S. I. HARIHARAN (Akron Univ., Ohio.) Mar. 1988 24 p

(Contract NSF DMS-86-04047)
(NASA-TM-100807; ICOMP-88-2; E-3988; NAS 1.15:100807)
Avail: NTIS HC A03/MF A01 CSCL 12A

The numerical solution of exterior problems is typically accomplished by introducing an artificial, far field boundary and solving the equations on a truncated domain. For hyperbolic systems, boundary conditions at this boundary are often derived by imposing a principle of no reflection. However, waves with spherical symmetry in gas dynamics satisfy equations where incoming and outgoing Riemann variables are coupled. This suggests that natural reflections may be important. A reflecting boundary condition is proposed based on an asymptotic solution of the far field equations. Nonlinear energy estimates are obtained for the truncated problem and numerical experiments presented to validate the theory. Author

N88-19202*# National Aeronautics and Space Administration. Lewis Research Center, Cleveland, OH.

**INSTITUTE FOR COMPUTATIONAL MECHANICS IN
PROPULSION (ICOMP) Annual Report No. 2, 1987**

Mar. 1988 49 p
(NASA-TM-100790; ICOMP-88-1; E-3964; NAS 1.15:100790)
Avail: NTIS HC A03/MF A01 CSCL 12A

The Institute for Computational Mechanics in Propulsion (ICOMP) is operated jointly by Case Western Reserve University and the NASA Lewis Research Center in Cleveland, Ohio. The purpose of ICOMP is to develop techniques to improve problem-solving capabilities in all aspects of computational mechanics related to propulsion. Described are the activities of ICOMP during 1987. Author

N88-21717*# National Aeronautics and Space Administration. Lewis Research Center, Cleveland, OH.

SPLITTING OF INVISCID FLUXES FOR REAL GASES

MENG-SING LIOU, BRAM VANLEER, and JIAN-SHUN SHUEN (Sverdrup Technology, Inc., Cleveland, Ohio.) Apr. 1988 31 p
(NASA-TM-100856; ICOMP-88-7; E-4059; NAS 1.15:100856)
Avail: NTIS HC A03/MF A01 CSCL 12A

Flux-vector and flux-difference splittings for the inviscid terms of the compressible flow equations are derived under the assumption of a general equation of state for a real gas in equilibrium. No necessary assumptions, approximations or auxiliary quantities are introduced. The formulas derived include several particular cases known for ideal gases and readily apply to curvilinear coordinates. Applications of the formulas in a TVD algorithm to one-dimensional shock-tube and nozzle problems show their quality and robustness. Author

N88-21718*# National Aeronautics and Space Administration. Lewis Research Center, Cleveland, OH.

**CHOICE OF IMPLICIT AND EXPLICIT OPERATORS FOR THE
UPWIND DIFFERENCING METHOD**

MENG-SING LIOU and BRAM VANLEER 1988 27 p Presented at the 26th Aerospace Sciences Meeting, Reno, Nev., 11-14 Jan. 1988; sponsored by AIAA
(NASA-TM-100857; ICOMP-88-8; E-4061; NAS 1.15:100857)
Avail: NTIS HC A03/MF A01 CSCL 12A

The flux-vector and flux-difference splittings of Steger-Warming, van Leer and Roe are tested in all possible combinations on the implicit and explicit operators that can be distinguished in implicit relaxation methods for the steady Euler and Navier-Stokes equations. The tests include one-dimensional inviscid nozzle flow, and two-dimensional inviscid and viscous shock reflection. Roe's splitting, as anticipated, is found to uniformly yield the most accurate results. On the other hand, an approximate Roe splitting of the implicit operator (the complete Roe splitting is too complicated for practical use) proves to be the least robust with regard to convergence to the steady state. In this respect, the Steger-Warming splitting is the most robust; it leads to convergence when combined with any of the splittings in the explicit operator, although not necessarily in the most efficient way. Author

N88-22652*# National Aeronautics and Space Administration. Lewis Research Center, Cleveland, OH.

**A PHYSICALLY CONSISTENT MODEL FOR ARTIFICIAL
DISSIPATION IN TRANSONIC POTENTIAL FLOW
COMPUTATIONS**

GEORGE S. DULIKRACH, KARL W. MORTARA, and LIONEL MARRAFFA (Office National d'Etudes et de Recherches Aeronautiques, Paris, France) May 1988 14 p
(NASA-TM-100846; E-4040; ICOMP-88-6; NAS 1.15:100846)
Avail: NTIS HC A03/MF A01 CSCL 12A

The effect that artificial dissipation has on numerical solutions of the transonic Full Potential Equation (FPE) are investigated by comparing the artificially dissipative FPE to a Physically Dissipative Potential (PDP) equation. Analytic expressions were derived from the variables C and $M_{sub c}$ that are used in the artificial density formulation. It was shown that these new values generate artificial dissipation which is equivalent to the physical dissipation existing in the PDP equation. The new expression for the variables C and $M_{sub c}$ can easily be incorporated into the existing full potential codes which are based either on the artificial density or on the artificial viscosity formulation. A comparison of Physically Dissipative Potential (PDP), Artificial Density or Viscosity (ADV), Artificial Mass Flux (AMF), and ADV with variable C and $M_{sub c}$ formulation (MCC) is also presented. Author

N88-25239*# National Aeronautics and Space Administration. Lewis Research Center, Cleveland, OH.

**SOLVING TIME-DEPENDENT TWO-DIMENSIONAL EDDY
CURRENT PROBLEMS**

MIN EIG LEE, S. I. HARIHARAN, and NATHAN IDA (Akron Univ., Ohio.) Jun. 1988 32 p
(Contract NSF DMS-86-04047)
(NASA-TM-100875; E-4106; NAS 1.15:100875) Avail: NTIS HC A03/MF A01 CSCL 12A

Results of transient eddy current calculations are reported. For simplicity, a two-dimensional transverse magnetic field which is incident on an infinitely long conductor is considered. The conductor is assumed to be a good but not perfect conductor. The resulting problem is an interface initial boundary value problem with the boundary of the conductor being the interface. A finite difference method is used to march the solution explicitly in time. The method is shown. Treatment of appropriate radiation conditions is given special consideration. Results are validated with approximate analytic solutions. Two stringent test cases of high and low frequency incident waves are considered to validate the results. Author

N88-26885*# National Aeronautics and Space Administration. Lewis Research Center, Cleveland, OH.

EVOLUTION OF HAIRPIN VORTICES IN A SHEAR FLOW

T.-L. HON (Lehigh Univ., Bethlehem, Pa.) and J. D. A. WALKER Jul. 1988 23 p
(Contract NASA ORDER C-99066-G)
(NASA-TM-100858; ICOMP-88-9; E-4062; NAS 1.15:100858)
Avail: NTIS HC A03/MF A01 CSCL 12A

Recent experimental studies suggest that the hairpin vortex plays an important (and perhaps dominant) role in the dynamics of turbulent flows near walls. In this study a numerical procedure is developed to allow the accurate computation of the trajectory of a 3-D vortex having a small core radius. For hairpin vortices which are convected in a shear flow above a wall, the calculated results show that a 2-D vortex containing a small 3-D disturbance distorts into a complex shape with subsidiary hairpin vortices forming outboard of the original hairpin vortex. As the vortex moves above the wall, it induces unsteady motion in the viscous flow near the wall: numerical solutions suggest that the boundary-layer flow near the wall will ultimately erupt in response to the motion of the hairpin vortex and in the process a secondary hairpin vortex will be created. The computer results agree with recent experimental investigations. Author

64 NUMERICAL ANALYSIS

N88-30377*# National Aeronautics and Space Administration. Lewis Research Center, Cleveland, OH.

CONVERGENCE ACCELERATION FOR VECTOR SEQUENCES AND APPLICATIONS TO COMPUTATIONAL FLUID DYNAMICS
AVRAM SIDI and MARK L. CELESTINA (Sverdrup Technology, Inc., Cleveland, Ohio.) Aug. 1988 25 p
(NASA-TM-101327; E-4338; ICOMP-88-17; NAS 1.15:101327)
Avail: NTIS HC A03/MF A01 CSCL 12A

Some recent developments in acceleration of convergence methods for vector sequences are reviewed. The methods considered are the minimal polynomial extrapolation, the reduced rank extrapolation, and the modified minimal polynomial extrapolation. The vector sequences to be accelerated are those that are obtained from the iterative solution of linear or nonlinear systems of equations. The convergence and stability properties of these methods as well as different ways of numerical implementation are discussed in detail. Based on the convergence and stability results, strategies that are useful in practical applications are suggested. Two applications to computational fluid mechanics involving the three dimensional Euler equations for ducted and external flows are considered. The numerical results demonstrate the usefulness of the methods in accelerating the convergence of the time marching techniques in the solution of steady state problems. Author

66

SYSTEMS ANALYSIS

Includes mathematical modeling; network analysis; and operations research.

A88-22696* Apogee Research Corp., San Diego, CA.

EXPERT SYSTEMS FOR SPACE POWER SUPPLY - DESIGN, ANALYSIS, AND EVALUATION

RALPH S. COOPER (Apogee Research Corp, San Diego, CA), M. KEMER THOMSON, and ALAN HOSHOR (Q-Systems, San Diego, CA) IN: Space nuclear power systems 1986; Proceedings of the Third Symposium, Albuquerque, NM, Jan. 13-16, 1986. Malabar, FL, Orbit Book Co., Inc., 1987, p. 259-266. refs
(Contract NAS3-23900)

The feasibility of applying expert systems to the conceptual design, analysis, and evaluation of space power supplies in particular, and complex systems in general is evaluated. To do this, the space power supply design process and its associated knowledge base were analyzed and characterized in a form suitable for computer emulation of a human expert. The existing expert system tools and the results achieved with them were evaluated to assess their applicability to power system design. Some new concepts for combining program architectures (modular expert systems and algorithms) with information about the domain were applied to create a 'deep' system for handling the complex design problem. NOVICE, a code to solve a simplified version of a scoping study of a wide variety of power supply types for a broad range of missions, has been developed, programmed, and tested as a concrete feasibility demonstration. Author

A88-27531*# National Aeronautics and Space Administration. Lewis Research Center, Cleveland, OH.

NUMERICAL ARC SEGMENTATION ALGORITHM FOR A RADIO CONFERENCE - A SOFTWARE TOOL FOR COMMUNICATION SATELLITE SYSTEMS PLANNING

W. A. WHYTE, A. O. HEYWARD, D. S. PONCHAK, R. L. SPENCE, and J. E. ZUZEK (NASA, Lewis Research Center, Cleveland, OH) IN: AIAA International Communication Satellite Systems Conference, 12th, Arlington, VA, Mar. 13-17, 1988, Technical Papers. Washington, DC, American Institute of Aeronautics and Astronautics, 1988, p. 32-45.
(AIAA PAPER 88-0788)

A detailed description of a Numerical Arc Segmentation

Algorithm for a Radio Conference (NASARC) software package for communication satellite systems planning is presented. This software provides a method of generating predetermined arc segments for use in the development of an allotment planning procedure to be carried out at the 1988 World Administrative Radio Conference (WARC - 88) on the use of the GEO and the planning of space services utilizing GEO. The features of the NASARC software package are described, and detailed information is given about the function of each of the four NASARC program modules. The results of a sample world scenario are presented and discussed. C.D.

70

PHYSICS (GENERAL)

A88-10410* Fermi National Accelerator Lab., Batavia, IL.

WILSON-LOOP INSTANTONS

KIMYEONG LEE (Fermi National Accelerator Laboratory, Batavia, IL), RICHARD HOLMAN (Carnegie-Mellon University, Pittsburgh, PA), and EDWARD W. KOLB (NASA/Fermilab Astrophysics Center, Batavia, IL) Physical Review Letters (ISSN 0031-9007), vol. 59, Sept. 7, 1987, p. 1069-1071. DOE-NASA-supported research. refs

Wilson-loop symmetry breaking is considered on a space-time of the form $M^4 \times K$, where M^4 is a four-dimensional space-time and K is an internal space with nontrivial and finite fundamental group. It is shown in a simple model that the different vacua obtained by breaking a non-Abelian gauge group by Wilson loops are separated in the space of gauge potentials by a finite energy barrier. An interpolating gauge configuration is then constructed between these vacua and shown to have minimum energy. Finally some implications of this construction are discussed. Author

A88-16577*# National Aeronautics and Space Administration. Lewis Research Center, Cleveland, OH.

A FINITE ELEMENT MODEL FOR WAVE PROPAGATION IN AN INHOMOGENEOUS MATERIAL INCLUDING EXPERIMENTAL VALIDATION

KENNETH J. BAUMEISTER and MILO D. DAHL (NASA, Lewis Research Center, Cleveland, OH) AIAA, Aeroacoustics Conference, 11th, Sunnyvale, CA, Oct. 19-21, 1987. 11 p. Previously announced in STAR as N87-25821. refs
(AIAA PAPER 87-2741)

A finite element model was developed to solve for the acoustic pressure field in a nonhomogeneous region. The derivations from the governing equations assumed that the material properties could vary with position resulting in a nonhomogeneous variable property two-dimensional wave equation. This eliminated the necessity of finding the boundary conditions between the different materials. For a two media region consisting of part air (in the duct) and part bulk absorber (in the wall), a model was used to describe the bulk absorber properties in two directions. An experiment to verify the numerical theory was conducted in a rectangular duct with no flow and absorbing material mounted on one wall. Changes in the sound field, consisting of planar waves, was measured on the wall opposite the absorbing material. As a function of distance along the duct, fairly good agreement was found in the standing wave pattern upstream of the absorber and in the decay of pressure level opposite the absorber. Author

A88-29060* Northwestern Univ., Evanston, IL.

FINITE ELEMENT METHODS IN PROBABILISTIC MECHANICS

WING KAM LIU, A. MANI, and TED BELYTCHKO (Northwestern University, Evanston, IL) Probabilistic Engineering Mechanics (ISSN 0266-8920), vol. 2, Dec. 1987, p. 201-213. refs
(Contract NAG3-535)

Probabilistic methods, synthesizing the power of finite element

ACOUSTICS

Includes sound generation, transmission, and attenuation.

methods with second-order perturbation techniques, are formulated for linear and nonlinear problems. Random material, geometric properties and loads can be incorporated in these methods, in terms of their fundamental statistics. By construction, these methods are applicable when the scale of randomness is not too large and when the probabilistic density functions have decaying tails. By incorporating certain computational techniques, these methods are shown to be capable of handling large systems with many sources of uncertainties. Applications showing the effects of combined random fields and cyclic loading/stress reversal are studied and compared with Monte Carlo simulation results.

Author

A88-43950* Cleveland State Univ., OH.
**UNIVERSALITY RELATIONSHIPS IN CONDENSED MATTER -
 BULK MODULUS AND SOUND VELOCITY**

HERBERT SCHLOSSER (Cleveland State University, OH) and JOHN FERRANTE (NASA, Lewis Research Center, Cleveland, OH) Physical Review B - Condensed Matter, 3rd Series (ISSN 0163-1829), vol. 37, no. 9, March 15, 1988, p. 4351-4357. refs

New forms for the bulk modulus and sound velocity of solids under compression, based on the universal equation of state of Vinet, Ferrante, Smith, and Rose (1987) are presented. These expressions are compared with a number of bulk modulus formulas previously utilized in high-pressure studies. It is demonstrated that this form yields a superior fit to experimental data to very high compressions, for a very wide range of solids. These solids cover the entire range of values of the pressure derivative of the bulk modulus which has been observed in high-pressure measurements.

Author

N88-20962*# Ohio State Univ., Columbus. ElectroScience Lab.
**MEASUREMENT OF THE PROPERTIES OF LOSSY
 MATERIALS INSIDE A FINITE CONDUCTING CYLINDER**
Semiannual Report

A. DOMINEK, A. PARK, and R. CALDECOTT Mar. 1988 34 p
 (Contract NAG3-784)
 (NASA-CR-182664; NAS 1.26:182664; ESL-719300-1) Avail:
 NTIS HC A03/MF A01 CSCL 20C

Broadband, swept frequency measurement techniques were investigated for the evaluation of the electrical performance of thin, high temperature material coatings. Reflections and transmission measurements using an HP8510B Network Analyzer were developed for an existing high temperature test rig at NASA Lewis Research Center. Reflection measurements will be the initial approach used due to fixture simplicity even though surface wave transmission measurements would be more sensitive. The minimum goal is to monitor the electrical change of the material's performance as a function of temperature. If possible, the materials constitutive parameters, epsilon and muon will be found. Author

N88-25260*# National Aeronautics and Space Administration.
 Lewis Research Center, Cleveland, OH.
**RECENT ADVANCES IN LOW-THRUST PROPULSION
 TECHNOLOGY**

JAMES R. STONE 1988 27 p Presented at the 24th Joint Propulsion Conference, Boston, Mass., 11-13 Jul. 1988; sponsored by AIAA, ASME, SAE, and ASEE
 (NASA-TM-100959; E-4245; NAS 1.15:100959; AIAA-88-3283)
 Avail: NTIS HC A03/MF A01 CSCL 20C

The NASA low-thrust propulsion technology program is aimed at providing high performance options to a broad class of near-term and future missions. Major emphases of the program are on storable and hydrogen/oxygen low-thrust chemical, low-power (auxiliary) electrothermal, and high-power electric propulsion. This paper represents the major accomplishments of the program and discusses their impact.

Author

A88-13963* Houston Univ., TX.
**ROLES OF INITIAL CONDITION AND VORTEX PAIRING IN
 JET NOISE**

J. E. BRIDGES and A. K. M. F. HUSSAIN (Houston, University, TX) Journal of Sound and Vibration (ISSN 0022-460X), vol. 117, Sept. 8, 1987, p. 289-311. refs
 (Contract NAG3-639)

Sound generation by vortex pairing in circular and elliptic cold-air jets at Mach 0.15-0.35 is investigated experimentally, with a focus on the effects of initial conditions. The results are presented in graphs and interpreted using the theory of vortex sound proposed by Moehring (1978) and vortex-filament models of jet coherent structure. Tripping the nozzle boundary layer is shown to (1) preempt formation of shear-layer vortices, (2) remove the sound they produce in later pairing, and (3) increase the diffusion of coherent vorticity in the vortex rings. Hence pairing noise should not be significant in practical jets, which are initially turbulent.

T.K.

A88-16526*# Hamilton Standard Div., United Aircraft Corp., Windsor Locks, CT.
**NOISE CHARACTERISTICS OF MODEL COUNTER-ROTATING
 PROP-FANS**

B. MAGLIOZZI (United Technologies Corp., Hamilton Standard Div., Windsor Locks, CT) AIAA, Aeroacoustics Conference, 11th, Sunnyvale, CA, Oct. 19-21, 1987. 14 p. refs
 (Contract NAS3-24222)
 (AIAA PAPER 87-2656)

Results of acoustics tests of 24.5 in. diameter model counter-rotating propfans are presented. In these tests several configurations were investigated, including tractors and pushers downstream of a pylon, both at zero degrees and at four degrees angle-of-attack. The effects on noise of spacing between rotors and between the pylon and the rotors were also measured. Effects of rotor spacing were found to cause small changes in noise. Increasing blade count from 5-front and 5-rear to 6-front and 6-rear results in about a 1 EPNdB reduction in noise. Increasing only the front rotor blade count to six blades resulted in a noise reduction of about 2 EPNdB. The presence of the pylon resulted in a 1 EPNdB increase in noise. Angle of attack effects showed an increase of 3.5 EPNdB for the tractor configuration and only 1.5 EPNdB for the pusher configuration. Tip speed was found to be the strongest parameter in reducing noise. However, for a given thrust loading, an optimum tip speed is seen. Correlations between measurements and predictions are shown to be in good agreement.

Author

A88-16539*# Arizona Univ., Tucson.
**A PARAMETRIC STUDY OF MEAN LOADING EFFECTS ON
 AIRFOIL GUST INTERACTION NOISE**

E. J. KERSCHEN and M. R. MYERS (Arizona, University, Tucson) AIAA, Aeroacoustics Conference, 11th, Sunnyvale, CA, Oct. 19-21, 1987. 11 p. refs
 (Contract NAG3-357)
 (AIAA PAPER 87-2677)

The influence of airfoil mean loading parameters on the sound generated by interaction with short wavelength vorticity and entropy gusts is examined. It is found that there are two mean flow parameters of importance, the effective leading edge incidence angle and the airfoil lift coefficient. The former controls the total sound power level, while the latter has an important effect on the directivity pattern. For vorticity gusts, positive gust angles result in noise levels which increase with leading edge loading (LEL), while for negative gust angles an increase in LEL may actually reduce

71 ACOUSTICS

the noise level. For low levels of LEL, entropy gusts generate less sound than vorticity gusts, while for larger values of LEL, entropy gusts are at least as important as vorticity gusts. C.D.

A88-16565*# National Aeronautics and Space Administration. Lewis Research Center, Cleveland, OH.

CRUISE NOISE OF THE 2/9 SCALE MODEL OF THE LARGE-SCALE ADVANCED PROPPAN (LAP) PROPELLER, SR-7A

JAMES H. DITTMAR (NASA, Lewis Research Center, Cleveland, OH) and DAVID B. STANG (NASA, Lewis Research Center; Sverdrup Technology, Inc., Cleveland, OH) AIAA, Aeroacoustics Conference, 11th, Sunnyvale, CA, Oct. 19-21, 1987. 18 p. Previously announced in STAR as N87-28398. refs (AIAA PAPER 87-2717)

Noise data on the Large-scale Advanced Propfan (LAP) propeller model SR-7A were taken in the NASA Lewis Research Center 8 x 6 foot Wind Tunnel. The maximum blade passing tone noise first rises with increasing helical tip Mach number to a peak level, then remains the same or decreases from its peak level when going to higher helical tip Mach numbers. This trend was observed for operation at both constant advance ratio and approximately equal thrust. This noise reduction or, leveling out at high helical tip Mach numbers, points to the use of higher propeller tip speeds as a possible method to limit airplane cabin noise while maintaining high flight speed and efficiency. Projections of the tunnel model data are made to the full scale LAP propeller mounted on the test bed aircraft and compared with predictions. The prediction method is found to be somewhat conservative in that it slightly overpredicts the projected model data at the peak.

Author

A88-16571*# National Aeronautics and Space Administration. Lewis Research Center, Cleveland, OH.

AEROAACOUSTICS OF SUBSONIC TURBULENT SHEAR FLOWS

MARVIN E. GOLDSTEIN (NASA, Lewis Research Center, Cleveland, OH) AIAA, Aeroacoustics Conference, 11th, Sunnyvale, CA, Oct. 19-21, 1987. 10 p. Previously announced in STAR as N87-26615. refs (AIAA PAPER 87-2731)

Sound generation in turbulent shear flows is examined. The emphasis is on simultaneous calculation of the turbulent flow along with the resulting sound generation rather than the alternative acoustic analogy approach. The first part of the paper is concerned with solid surface interaction. The second part concentrates on the sound generated by turbulence interacting with itself. Author

A88-16578*# Missouri Univ., Rolla.

A MODEL OF THE WALL BOUNDARY LAYER FOR DUCTED PROPELLERS

WALTER EVERSMAN (Missouri-Rolla, University, Rolla) and WILLI MOEHRING (Max-Planck-Institut fuer Stroemungsforschung, Goettingen, Federal Republic of Germany) AIAA, Aeroacoustics Conference, 11th, Sunnyvale, CA, Oct. 19-21, 1987. 10 p. refs (Contract NAG3-178) (AIAA PAPER 87-2742)

The objective of the present study is to include a representation of a wall boundary layer in an existing finite element model of the propeller in the wind tunnel environment. The major consideration is that the new formulation should introduce only modest alterations in the numerical model and should still be capable of producing economical predictions of the radiated acoustic field. This is accomplished by using a stepped approximation in which the velocity profile is piecewise constant in layers. In the limit of infinitesimally thin layers, the velocity profile of the stepped approximation coincides with that of the continuous profile. The approach described here could also be useful in modeling the boundary layer in other duct applications, particularly in the computation of the radiated acoustic field for sources contained in a duct. V.L.

A88-18541*# Southern Methodist Univ., Dallas, TX.

A MAPPED FINITE DIFFERENCE STUDY OF NOISE PROPAGATION IN NONUNIFORM DUCTS WITH MEAN FLOW

PETER E. RAAD (Southern Methodist University, Dallas, TX) and JAMES W. WHITE (Tennessee, University, Knoxville) ASME, Transactions, Journal of Vibration, Acoustics, Stress, and Reliability in Design (ISSN 0739-3717), vol. 109, Oct. 1987, p. 372-380. refs

(Contract NAG3-18)

The primary objective of this work is to study noise propagation in acoustically lined variable area ducts with mean fluid flow. The method of study is numerical in nature and involves a body-fitted grid mapping procedure in conjunction with a factored-implicit finite difference technique. The mean fluid flow model used is two-dimensional, inviscid, irrotational, incompressible, and nonheat conducting. Fully-coupled solutions of the linearized gasdynamic equations are obtained for both positive and negative Mach numbers as well as for hard and soft wall conditions. The factored-implicit finite difference technique used did give rise to short wavelength perturbations, but these were dampened by the introduction of higher order artificial dissipation terms into the scheme. Results compared favorably with available numerical and experimental data.

Author

A88-20176*# National Aeronautics and Space Administration. Lewis Research Center, Cleveland, OH.

NOISE OF A MODEL HIGH SPEED COUNTERROTATION PROPELLER AT SIMULATED TAKEOFF/APPROACH CONDITIONS (F7/A7)

RICHARD P. WOODWARD (NASA, Lewis Research Center, Cleveland, OH) AIAA, Aeroacoustics Conference, 11th, Sunnyvale, CA, Oct. 19-21, 1987. 25 p. Previously announced in STAR as N88-10592. refs (AIAA PAPER 87-2657)

A high speed advanced counterrotation propeller, was tested in the NASA-Lewis 9 x 15 foot Anechoic Wind Tunnel at simulated takeoff/approach conditions of 0.2 Mach number. Acoustic measurements were taken with fixed floor microphones, an axially translating microphone probe, and with a polar microphone probe which was fixed to the propeller nacelle and could take both sideline and circumferential acoustic surveys. Aerodynamic measurements were also made to establish the propeller operating conditions. The propeller was run over a range of blade setting angles from 36.4/36.5 to 41.1/39.4 deg, tip speeds from 165 to 259 m/sec, rotor spacings from 1.56 to 3.63 based on forward rotor tip chord to aerodynamic separation, and angles of attack to + or - 16 deg. First order rotor alone tones showed highest directivity levels near the propeller plane, while interaction tone showed high levels throughout sideline directivity, especially toward the propeller rotation axis. Interaction tone levels were sensitive to propeller row spacing while rotor alone tones showed little spacing effect. There is a decreased noise level associated with higher propeller blade numbers for the same overall propeller thrust. Author

A88-22192*# National Aeronautics and Space Administration. Lewis Research Center, Cleveland, OH.

NOISE OF A MODEL COUNTERROTATION PROPELLER WITH REDUCED AFT ROTOR DIAMETER AT SIMULATED TAKEOFF/APPROACH CONDITIONS (F7/A3)

RICHARD P. WOODWARD (NASA, Lewis Research Center, Cleveland, OH) and ELIOTT B. GORDON (NASA, Lewis Research Center; Sverdrup Technology, Inc., Cleveland, OH) AIAA, Aerospace Sciences Meeting, 26th, Reno, NV, Jan. 11-14, 1988. 29 p. Previously announced in STAR as N88-13961. refs (AIAA PAPER 88-0263)

A model high-speed advanced counterrotation propeller, F7/A3, was tested in the NASA Lewis Research Center 9 by 15 foot Anechoic Wind Tunnel at simulated takeoff/approach conditions of 0.2 Mach number. Acoustic measurements were taken with an axially translating microphone probe, and with a polar microphone probe which was fixed to the propeller nacelle and could take both sideline and circumferential acoustic surveys. Aerodynamic

measurements were also made to establish propeller operating conditions. The propeller was run at two setting angles (front angle/rear angle) of 36.4/43.5 and 41.1/46.4 degrees, forward rotor tip speeds from 165 to 259 m/sec, rotor spacings from 8.48 to 14.99 cm based on pitch change axis separation, and angles of attack to 16 degrees. The aft rotor diameter was 85 percent of the forward rotor diameter to reduce tip vortex-aft rotor interaction as a major interaction noise source. Results are compared with equal diameter F7/A7 data which was previously obtained under similar operating conditions. The aft rotor-alone tone was 7 dB lower for the reduced diameter aft rotor, due to reduced tip speed at constant rpm. Interaction tone levels for the F7/A3 propeller were higher at minimum row spacing and lower at maximum spacing. Author

A88-22193* National Aeronautics and Space Administration. Lewis Research Center, Cleveland, OH.

HIGH SPEED PROPELLER PERFORMANCE AND NOISE PREDICTIONS AT TAKEOFF/LANDING CONDITIONS

M. NALLASAMY (NASA, Lewis Research Center; Sverdrup Technology, Inc., Cleveland, OH), R. P. WOODWARD, and J. F. GROENEWEG (NASA, Lewis Research Center, Cleveland, OH) AIAA, Aerospace Sciences Meeting, 26th, Reno, NV, Jan. 11-14, 1988. 17 p. Previously announced in STAR as N88-13960. refs (AIAA PAPER 88-0264)

The performance and noise of a high speed SR-7A model propeller under takeoff/landing conditions are considered. The blade loading distributions are obtained by solving the three-dimensional Euler equations and the sound pressure levels are computed using a time domain approach. At the nominal takeoff operating point, the blade sections near the hub are lightly or negatively loaded. The chordwise loading distributions are distinctly different from those of cruise conditions. The noise of the SR-7A model propeller at takeoff is dominated by the loading noise, similar to that at cruise conditions. The waveforms of the acoustic pressure signature are nearly sinusoidal in the plane of the propeller. The computed directivity of the blade passing frequency tone agrees fairly well with the data at nominal takeoff blade angle. Author

A88-30998* Lockheed Aircraft Corp., Marietta, GA.

AERACOUSTICS OF ADVANCED STOVL AIRCRAFT PLUMES

K. K. AHUJA and D. A. SPENCER (Lockheed Aeronautical Systems Co., Marietta, GA) SAE, International Powered Lift Conference and Exposition, Santa Clara, CA, Dec. 7-10, 1987. 12 p. refs (Contract NAS3-23708) (SAE PAPER 872358)

This paper summarizes a basic and well-controlled experimental study involving flow visualization and noise measurements to define the acoustic and flow fields of single plumes impinging on a simulated ground plane. The flow visualization was made by strobing a laser light source at the discrete frequencies generated by the impingement of the jets and measured by a nearfield microphone. This enabled visualization of instability waves generated by the interaction between the plumes and the sound generated during impingement, and also by dynamic coupling between the two plumes. These data were acquired as a function of distance between the ground and the nozzle exit. Nearfield acoustic data were acquired simultaneously. Data for nozzle diameters of 0.265 in. and 0.4 in. are described. For selected nozzles, effects of exit boundary layer characteristics and nozzle protrusion through a simulated aircraft body are also presented. Author

A88-35939* McDonnell-Douglas Corp., Saint Louis, MO.

ACOUSTICS TECHNOLOGIES FOR STOVL AIRCRAFT

DAVID S. GROEN (McDonnell Douglas Corp., Saint Louis, MO) AIAA SDM Issues of the International Space Station, Conference, Williamsburg, VA, Apr. 21, 22, 1988. 17 p. refs (Contract NAS3-24621) (AIAA PAPER 88-2238)

State-of-the-art acoustic fatigue technologies that are relevant to supersonic Short Takeoff/Vertical Landing (STOVL) aircraft are investigated. Data and methods assessments of acoustic fatigue

technologies for acoustic load predictions and stress response predictions are evaluated. Subsonic and supersonic jet noise generation mechanisms, axisymmetric and two-dimensional nozzles, and noise suppression methods are discussed. STOVL far field noise during hover, near field noise, and internal cockpit noise levels are predicted. Stress response prediction methods for acoustic, thermal, and maneuvering loads are addressed and the need for structural analysis methods with all three types of loads applied simultaneously is assessed. Author

A88-36270* Sverdrup Technology, Inc., Cleveland, OH.
HIGH-SPEED PROPELLER NOISE PREDICTIONS - EFFECTS OF BOUNDARY CONDITIONS USED IN BLADE LOADING CALCULATIONS

M. NALLASAMY (Sverdrup Technology, Inc., Cleveland, OH), B. J. CLARK, and J. F. GROENEWEG (NASA, Lewis Research Center, Cleveland, OH) Journal of Aircraft (ISSN 0021-8669), vol. 25, Feb. 1988, p. 154-162. Previously cited in issue 09, p. 1328, Accession no. A87-24978. refs

A88-37219* Lockheed Aeronautical Systems Co., Marietta, GA.
AERACOUSTICS OF ADVANCED STOVL AIRCRAFT PLUMES

K. K. AHUJA and D. A. SPENCER (Lockheed Aeronautical Systems Co., Marietta, GA) IN: International Powered Lift Conference and Exposition, Santa Clara, CA, Dec. 7-10, 1987, Proceedings. Warrendale, PA, Society of Automotive Engineers, Inc., 1988, p. 531-541. refs (Contract NAS3-23708) (SAE PAPER 872358)

This paper summarizes a basic and well-controlled experimental study involving flow visualization and noise measurements to define the acoustic and flow fields of single plumes impinging on a simulated ground plane. The flow visualization was made by strobing a laser light source at the discrete frequencies generated by the impingement of the jets and measured by a nearfield microphone. This enabled visualization of instability waves generated by the interaction between the plumes and the sound generated during impingement, and also by dynamic coupling between the two plumes. These data were acquired as a function of distance between the ground and the nozzle exit. Nearfield acoustic data were acquired simultaneously. Data for nozzle diameters of 0.265 in. and 0.4 in. are described. For selected nozzles, effects of exit boundary layer characteristics and nozzle protrusion through a simulated aircraft body are also presented. Author

A88-37221* McDonnell Aircraft Co., Saint Louis, MO.

STOVL ACOUSTIC FATIGUE TECHNOLOGIES

DAVID S. GROEN (McDonnell Aircraft Co., Saint Louis, MO) IN: International Powered Lift Conference and Exposition, Santa Clara, CA, Dec. 7-10, 1987, Proceedings. Warrendale, PA, Society of Automotive Engineers, Inc., 1988, p. 553-562. refs (Contract NAS3-24621) (SAE PAPER 872360)

This paper assesses the state of the art in acoustic fatigue technologies as applied to an advanced supersonic short takeoff and vertical landing (STOVL) aircraft. The topics covered include advanced materials, fatigue, acoustic loads prediction, and stress response prediction. Advanced materials are compared from the standpoints of fatigue resistance and fatigue data availability. State of the art acoustic load prediction techniques are evaluated. Subsonic and supersonic jet noise generation mechanisms, axisymmetric and two-dimensional nozzles, and noise suppression methods are covered. Stress response prediction methods for acoustic, thermal, and maneuvering loads are addressed and the necessity of structural analysis with all three loading types applied simultaneously is assessed. Author

A88-39708* National Aeronautics and Space Administration. Lewis Research Center, Cleveland, OH.

COMBUSTION NOISE FROM GAS TURBINE AIRCRAFT ENGINES MEASUREMENT OF FAR-FIELD LEVELS

EUGENE A. KREJSA (NASA, Lewis Research Center, Cleveland,

OH) IN: NOISE-CON 87; Proceedings of the National Conference on Noise Control Engineering, State College, PA, June 8-10, 1987. Poughkeepsie, NY, Noise Control Foundation, 1987, p. 129-134. Previously announced in STAR as N87-17480. refs

Combustion noise can be a significant contributor to total aircraft noise. Measurement of combustion noise is made difficult by the fact that both jet noise and combustion noise exhibit broadband spectra and peak in the same frequency range. Since in-flight reduction of jet noise is greater than that of combustion noise, the latter can be a major contributor to the in-flight noise of an aircraft but will be less evident, and more difficult to measure, under static conditions. Several methods for measuring the far-field combustion noise of aircraft engines are discussed in this paper. These methods make it possible to measure combustion noise levels even in situations where other noise sources, such as jet noise, dominate. Measured far-field combustion noise levels for several turbofan engines are presented. These levels were obtained using a method referred to as three-signal coherence, requiring that fluctuating pressures be measured at two locations within the engine core in addition to the far-field noise measurement. Cross-spectra are used to separate the far-field combustion noise from far-field noise due to other sources. Spectra and directivities are presented. Comparisons with existing combustion noise predictions are made. Author

N88-10592*# National Aeronautics and Space Administration. Lewis Research Center, Cleveland, OH.

NOISE OF A MODEL HIGH SPEED COUNTERROTATION PROPELLER AT SIMULATED TAKEOFF/APPROACH CONDITIONS (F7/A7)

RICHARD P. WOODWARD 1987 25 p Presented at the 11th Aeroacoustics Conference, Sunnyvale, Calif., 19-21 Oct. 1987; sponsored by AIAA

(NASA-TM-100206; E-3766; NAS 1.15:100206; AIAA-87-2657)

Avail: NTIS HC A03/MF A01 CSCL 20A

A high speed advanced counterrotation propeller, was tested in the NASA-Lewis 9 x 15 foot Anechoic Wind Tunnel at simulated takeoff/approach conditions of 0.2 Mach number. Acoustic measurements were taken with fixed floor microphones, an axially translating microphone probe, and with a polar microphone probe which was fixed to the propeller nacelle and could take both sideline and circumferential acoustic surveys. Aerodynamic measurements were also made to establish the propeller operating conditions. The propeller was run over a range of blade setting angles from 36.4/36.5 to 41.1/39.4 deg, tip speeds from 165 to 259 m/sec, rotor spacings from 1.56 to 3.63 based on forward rotor tip chord to aerodynamic separation, and angles of attack to + or - 16 deg. First order rotor alone tones showed highest directivity levels near the propeller plane, while interaction tone showed high levels throughout sideline directivity, especially toward the propeller rotation axis. Interaction tone levels were sensitive to propeller row spacing while rotor alone tones showed little spacing effect. There is a decreased noise level associated with higher propeller blade numbers for the same overall propeller thrust. Author

N88-12352*# Calspan Advanced Technology Center, Buffalo, NY. Physical Sciences Dept.

A HYBRID NUMERICAL TECHNIQUE FOR PREDICTING THE AERODYNAMIC AND ACOUSTIC FIELDS OF ADVANCED TURBOPROPS Final Report

G. F. HOMICZ and J. R. MOSELLE Apr. 1985 71 p

(Contract NAS3-23699)

(NASA-CR-174926; NAS 1.26:174926; CALSPAN-7157-A-1)

Avail: NTIS HC A04/MF A01 CSCL 20A

A hybrid numerical procedure is presented for the prediction of the aerodynamic and acoustic performance of advanced turboprops. A hybrid scheme is proposed which in principle leads to a consistent simultaneous prediction of both fields. In the inner flow a finite difference method, the Approximate-Factorization Alternating-Direction-Implicit (ADI) scheme, is used to solve the nonlinear Euler equations. In the outer flow the linearized acoustic equations are solved via a Boundary-Integral Equation (BIE)

method. The two solutions are iteratively matched across a fictitious interface in the flow so as to maintain continuity. At convergence the resulting aerodynamic load prediction will automatically satisfy the appropriate free-field boundary conditions at the edge of the finite difference grid, while the acoustic predictions will reflect the back-reaction of the radiated field on the magnitude of the loading source terms, as well as refractive effects in the inner flow. The equations and logic needed to match the two solutions are developed and the computer program implementing the procedure is described. Unfortunately, no converged solutions were obtained, due to unexpectedly large running times. The reasons for this are discussed and several means to alleviate the situation are suggested. Author

N88-13960*# National Aeronautics and Space Administration. Lewis Research Center, Cleveland, OH.

HIGH SPEED PROPELLER PERFORMANCE AND NOISE PREDICTIONS AT TAKEOFF/LANDING CONDITIONS

M. NALLASAMY (Sverdrup Technology, Inc., Cleveland, Ohio.), R. P. WOODWARD, and J. F. GROENEWEG 1987 17 p Prepared for presentation at the 26th Aerospace Sciences Meeting, Reno, Nev., 11-14, Jan. 1988; sponsored by AIAA

(NASA-TM-100267; E-3898; NAS 1.15:100267) Avail: NTIS HC A03/MF A01 CSCL 20A

The performance and noise of a high speed SR-7A model propeller under takeoff/landing conditions are considered. The blade loading distributions are obtained by solving the three-dimensional Euler equations and the sound pressure levels are computed using a time domain approach. At the nominal takeoff operating point, the blade sections near the hub are lightly or negatively loaded. The chordwise loading distributions are distinctly different from those of cruise conditions. The noise of the SR-7A model propeller at takeoff is dominated by the loading noise, similar to that at cruise conditions. The waveforms of the acoustic pressure signature are nearly sinusoidal in the plane of the propeller. The computed directivity of the blade passing frequency tone agrees fairly well with the data at nominal takeoff blade angle. Author

N88-13961*# National Aeronautics and Space Administration. Lewis Research Center, Cleveland, OH.

NOISE OF A MODEL COUNTERROTATION PROPELLER WITH REDUCED AFT ROTOR DIAMETER AT SIMULATED TAKEOFF/APPROACH CONDITIONS (F7/A3)

RICHARD P. WOODWARD and ELIOTT B. GORDON (Sverdrup Technology, Inc., Cleveland, Ohio.) 1988 31 p Presented at the 26th Aerospace Sciences Meeting, Reno, Nev., 11-14 Jan. 1988; sponsored by AIAA

(NASA-TM-100254; E-3880; NAS 1.15:100254; AIAA-88-0263)

Avail: NTIS HC A03/MF A01 CSCL 20A

A model high-speed advanced counterrotation propeller, F7/A3, was tested in the NASA Lewis Research Center 9 by 15 foot Anechoic Wind Tunnel at simulated takeoff/approach conditions of 0.2 Mach number. Acoustic measurements were taken with an axially translating microphone probe, and with a polar microphone probe which was fixed to the propeller nacelle and could take both sideline and circumferential acoustic surveys. Aerodynamic measurements were also made to establish propeller operating conditions. The propeller was run at two setting angles (front angle/rear angle) of 36.4/43.5 and 41.1/46.4 degrees, forward rotor tip speeds from 165 to 259 m/sec, rotor spacings from 8.48 to 14.99 cm based on pitch change axis separation, and angles of attack to 16 degrees. The aft rotor diameter was 85 percent of the forward rotor diameter to reduce tip vortex-aft rotor interaction as a major interaction noise source. Results are compared with equal diameter F7/A7 data which was previously obtained under similar operating conditions. The aft rotor-alone tone was 7 dB lower for the reduced diameter aft rotor, due to reduced tip speed at constant rpm. Interaction tone levels for the F7/A3 propeller were higher at minimum row spacing and lower at maximum spacing. Author

N88-18379*# National Aeronautics and Space Administration. Lewis Research Center, Cleveland, OH.

AN ESTIMATE OF THE NOISE SHIELDING ON THE FUSELAGE RESULTING FROM INSTALLING A SHORT DUCT AROUND AN ADVANCED PROPELLER

JAMES H. DITTMAR Mar. 1988 14 p
(NASA-TM-100262; E-3891; NAS 1.15:100262) Avail: NTIS HC A03/MF A01 CSCL 20A

A simple barrier shielding model was used to estimate the amount of noise shielding on the fuselage that could result from installing a short duct around a wing-mounted advanced propeller. With the propeller located one-third of the duct length from the inlet, estimates for the maximum blade passing tone attenuation varied from 7 dB for a duct 0.25 propeller diameter long to 16.75 dB for a duct 1 diameter long. Attenuations for the higher harmonics would be even larger because of their shorter wavelengths relative to the duct length. These estimates show that the fuselage noise reduction potential of a ducted compared with an unducted propeller is significant. Even more reduction might occur if acoustic attenuation material were installed in the duct. Author

73

NUCLEAR AND HIGH-ENERGY PHYSICS

Includes elementary and nuclear particles; and reactor theory.

A88-47477* National Aeronautics and Space Administration. Lewis Research Center, Cleveland, OH.

PRIMORDIAL NUCLEOSYNTHESIS WITH DECAYING PARTICLES. I - ENTROPY-PRODUCING DECAYS. II - INERT DECAYS

ROBERT J. SCHERRER (Chicago, University, IL) and MICHAEL S. TURNER (NASA/Fermi National Accelerator Laboratory, Batavia; Chicago, University, IL) Astrophysical Journal, Part 1 (ISSN 0004-637X), vol. 331, Aug. 1, 1988, p. 19-37. refs
(Contract DE-AC02-80ER-10773; NSF PHY-86-04396)

The effect of a nonrelativistic particle X, which decays out of equilibrium, on primordial nucleosynthesis is investigated, including both the energy density of the X particle and the electromagnetic entropy production from its decay. The results are parametrized in terms of the X particle lifetime and the density parameter $rm(X)$, where $m(X)$ is the X particle mass and r is the ratio of X number density to photon number density prior to nucleosynthesis. The results rule out particle lifetimes greater than 1-10 s for large values of $rm(X)$. The question of a decaying particle which produces no electromagnetic entropy in the course of its decay is addressed, and particles which produce both entropy and an inert component in their decay are discussed. C.D.

N88-24409*# Oregon State Univ., Corvallis. Dept. of Nuclear Engineering.

ASSESSMENT OF NUCLEAR REACTOR CONCEPTS FOR LOW POWER SPACE APPLICATIONS

ANDREW C. KLEIN, STEPHEN R. GEDEON, and DENNIS C. MOREY In New Mexico Univ., Transactions of the Fifth Symposium on Space Nuclear Power Systems p 167-170 1988
(Contract NAG3-752)

Avail: NTIS HC A99/MF A01 CSCL 18I

The results of a preliminary small reactor concepts feasibility and safety evaluation designed to provide a first order validation of the nuclear feasibility and safety of six small reactor concepts are given. These small reactor concepts have potential space applications for missions in the 1 to 20 kWe power output range. It was concluded that low power concepts are available from the U.S. nuclear industry that have the potential for meeting both the operational and launch safety space mission requirements. However, each design has its uncertainties, and further work is required. The reactor concepts must be mated to a power

conversion technology that can offer safe and reliable operation.

Author

74

OPTICS

Includes light phenomena and optical devices.

A88-12660* National Aeronautics and Space Administration. Lewis Research Center, Cleveland, OH.

TIME DOMAIN REFERENCING IN INTENSITY MODULATION FIBER OPTIC SENSING SYSTEMS

GRIGORY ADAMOVSKY (NASA, Lewis Research Center, Cleveland; John Carroll University, University Heights, OH) IN: Optical testing and metrology; Proceedings of the Meeting, Quebec, Canada, June 3-6, 1986. Bellingham, WA, Society of Photo-Optical Instrumentation Engineers, 1986, p. 145-151. refs
(Contract NAG3-366)

Intensity modulation sensors are classified by the way in which the reference and signal channels are separated: in space, wavelength, or time domains. To implement the time-domain referencing, different types of fiber-optic loops have been used. A pulse of short duration sent into the loop results in a series of pulses of different amplitudes. The information about the measured parameter is retrieved from the relative amplitudes of pulses in the same train. Author

A88-17221*# National Aeronautics and Space Administration. Lewis Research Center, Cleveland, OH.

ZOOM LENS COMPENSATOR FOR A CYLINDRICAL WINDOW IN LASER ANEMOMETER USES

MARK P. WERNET and RICHARD G. SEASHOLTZ (NASA, Lewis Research Center, Cleveland, OH) Applied Optics (ISSN 0003-6935), vol. 26, Nov. 1, 1987, p. 4603-4611. refs

In laser anemometer systems, the flow fields under study are typically enclosed by a window. Aberration of a flat window can be corrected by a shift of the object distance. A zooming correction lens eliminates the astigmatism caused by a thick cylindrical window and yields diffraction-limited performance for a monochromatic laser anemometer system. The effects of residual anamorphic distortion are discussed, and procedures for correcting these effects are presented. Author

A88-33161*# National Aeronautics and Space Administration. Lewis Research Center, Cleveland, OH.

FIBER-OPTIC DISPLACEMENT SENSOR WITH TEMPORALLY SEPARATED SIGNAL AND REFERENCE CHANNELS

GRIGORY ADAMOVSKY (NASA, Lewis Research Center, Cleveland, OH) Applied Optics (ISSN 0003-6935), vol. 27, April 1, 1988, p. 1313-1315. refs

A fiber-optic displacement sensor with temporally separated signal and reference channels is proposed. The sensing technique used is based on determining the relative amplitude of the signal and reference pulses that together form a double pulse. The relative amplitude of the pulses in the double pulse is a function of the displacement. A setup to generate the double pulse with individual pulses of 5-ns duration and 10-ns delay is described. A novel signal processing technique, used to determine the relative amplitude of such pulses in the double pulse by analyzing different portions of the signal spectrum, is explained. Experimental data are also provided. Author

A88-42604* National Aeronautics and Space Administration. Lewis Research Center, Cleveland, OH.

REFERENCING IN FIBER OPTIC SENSING SYSTEMS

GRIGORY ADAMOVSKY (NASA, Lewis Research Center, Cleveland, OH) IN: Optical techniques for sensing and measurement in hostile environments; Proceedings of the Meeting,

74 OPTICS

Orlando, FL, May 21, 22, 1987. Bellingham, WA, Society of Photo-Optical Instrumentation Engineers, 1987, p. 17-23. Previously announced in STAR as N87-20475. refs

Different techniques to account for losses induced by the environment on signals in intensity modulation fiber optic sensing systems are described and analyzed. Author

N88-15796* # National Aeronautics and Space Administration. Lewis Research Center, Cleveland, OH.

OPTICAL MEASUREMENT SYSTEMS

DANIEL J. LESCO *In its* Aeropropulsion '87. Session 4: Instrumentation and Controls Research 17 p Nov. 1987
Avail: NTIS HC A05/MF A01 CSCL 09C

Some of the areas of research conducted at Lewis on optical measurement techniques are described. Two laser anemometer systems developed at Lewis are used to illustrate the special instrumentation needs encountered in aeropropulsion research. Velocity measurements to be made through small viewing ports, close to surfaces within the propulsion system components, and in turbulent or highly-accelerating flows are some of the significant challenges. The application to research facilities of two advanced optical systems, the rainbow schlieren and the combustor viewing system, is presented. The calibration and verification of commercial optical measuring systems, such as droplet sizing systems, are also discussed. Calibration techniques capable of simulating moving droplets for flight-type sizing systems are being developed at Lewis. The presentation concludes with a brief look at the forces driving future research on optical instrumentation. Author

N88-15798* # National Aeronautics and Space Administration. Lewis Research Center, Cleveland, OH.

FIBER OPTICS FOR CONTROLS

GARY T. SENG *In its* Aeropropulsion '87. Session 4: Instrumentation and Controls Research 14 p Nov. 1987
Avail: NTIS HC A05/MF A01 CSCL 20F

The challenge of those involved in control-system hardware development is to accommodate an ever-increasing complexity in aircraft control, while limiting the size and weight of the components and improving system reliability. A technology that displays promise towards this end is the area of fiber optics for controls. The primary advantages of employing optical fibers, passive optical sensors, and optically controlled actuators are weight and volume reduction, immunity from electromagnetic effects, superior bandwidth capabilities, and freedom from short circuits and sparking contacts. Since 1975, NASA Lewis has performed in-house, contract, and grant research in fiber optic sensors, high-temperature electro-optic switches, and fly-by-light control-system architecture. Passive optical sensor development is an essential yet challenging area of work and has therefore received much attention during this period. A major effort to develop fly-by-light control-system technology, known as the Fiber-Optic Control System Integration (FOCSI) program, was initiated in 1985 as a cooperative effort between NASA and DOD. Phase 1 of FOCSI, completed in 1986, was aimed at the design of a fiber-optic integrated propulsion/flight control system. Phase 2, yet to be initiated, will provide subcomponent and system development, and a system engine test. In addition to a summary of the benefits of fiber optics, the FOCSI program, sensor advances, and future directions in the NASA Lewis program will be discussed. Author

N88-28760* # National Aeronautics and Space Administration. Lewis Research Center, Cleveland, OH.

COMPARISON OF THE BIDIRECTIONAL REFLECTANCE DISTRIBUTION FUNCTION OF VARIOUS SURFACES

RENE FERNANDEZ, RICHARD G. SEASHOLTZ, LAWRENCE G. OBERLE, and JAIKRISHNAN R. KADAMBI (Case Western Reserve Univ., Cleveland, Ohio.) Aug. 1988 13 p Presented at the 32nd Annual International Technical Symposium on Optical and Optoelectronic Applied Science and Engineering, San Diego, Calif., 14-19 Aug. 1988; sponsored by the Society of Photo-Optical Instrumentation Engineers
(NASA-TM-101317; E-4314; NAS 1.15:101317) Avail: NTIS HC A03/MF A01 CSCL 20F

Described is the development and use of a system to measure the Bidirectional Reflectance Distribution Function (BRDF) of various surfaces. The BRDF measurements are used in the analysis and design of optical measurement systems, such as laser anemometers. An argon ion laser (514 nm) is the light source. Preliminary results are presented for eight samples: two glossy black paints, two flat black paints, black glass, sand blasted aluminum, unworked aluminum, and a white paint. A BaSO₄ white reflectance standard was used as the reference sample throughout the tests. The reflectance characteristics of these surfaces are compared. Author

75

PLASMA PHYSICS

Includes magnetohydrodynamics and plasma fusion.

A88-47783* Iowa Univ., Iowa City.

PLASMA WAVE TURBULENCE AROUND THE SHUTTLE - RESULTS FROM THE SPACELAB-2 FLIGHT

D. A. GURNETT, W. S. KURTH, J. T. STEINBERG (Iowa, University, Iowa City), and S. D. SHAWHAN (NASA, Washington, DC) Geophysical Research Letters (ISSN 0094-8276), vol. 15, Aug. 1988, p. 760-763. refs
(Contract NAS8-32807; NGL-16-001-043; NAG3-449)

During the Spacelab-2 flight, which occurred from July 29, to August 6, 1985, a spacecraft called the Plasma Diagnostics Package (PDP) was released from the shuttle to explore the plasma environment around the shuttle. The plasma wave instrument on the PDP detected a region of intense broadband turbulence around the shuttle at frequencies extending from a few Hz to about 10 kHz. The noise has broadband intensities ranging from 1 to 5 mV/m and was observed at distances of up to 400 m from the shuttle. The highest intensities occurred in the region downstream of the shuttle and along magnetic field lines passing near the shuttle. The intensities also tended to increase during periods of high thruster activity, which provides strong evidence that the noise is caused by an interaction of the ionosphere with gaseous emissions from the shuttle, similar in many respects to the interaction of a comet with the solar wind. Antenna interference patterns observed in the wideband data show that the wavelength of the turbulence is very short, a few meters or less. Author

A88-47973* # Maxwell Labs., Inc., San Diego, CA.

HOLLOW CATHODES AS ELECTRON EMITTING PLASMA CONTACTORS - THEORY AND COMPUTER MODELING

V. A. DAVIS, I. KATZ, M. J. MANDELL, and D. E. PARKS (Maxwell Laboratories, Inc., S-Cubed Div., La Jolla, CA) Journal of Spacecraft and Rockets (ISSN 0022-4650), vol. 25, March-Apr. 1988, p. 175-179. Previously cited in issue 08, p. 1159, Accession no. A87-22712. refs
(Contract NAS3-23881)

A88-54992* # Iowa Univ., Iowa City.

EXPOSED HIGH-VOLTAGE SOURCE EFFECT ON THE POTENTIAL OF AN IONOSPHERIC SATELLITE

A. C. TRIBBLE, N. D'ANGELO, G. B. MURPHY, J. S. PICKETT, and J. T. STEINBERG (Iowa, University, Iowa City) Journal of Spacecraft and Rockets (ISSN 0022-4650), vol. 25, Jan.-Feb. 1988, p. 64-69. refs
(Contract NAG3-449; NAS8-32807)

A pulsed, high-voltage source, which is able to draw a current from the surrounding plasma, is seen to induce large changes in the potential of an ionospheric satellite (the Iowa Plasma Diagnostics Package flown on Space Shuttle flight STS-51F). This, in turn, may affect the operation of other instruments that use the chassis of the satellite as a ground for electrical circuits. The magnitude of the change in satellite potential is dependent upon both the orientation of the high-voltage source, relative to the

SOLID-STATE PHYSICS

plasma flow, and the characteristics of the high-voltage source. When the satellite is grounded to the Shuttle Orbiter, this effect is sufficient to change the potential of the Orbiter by a small, but noticeable, amount. Author

A88-54999* # Maxwell Labs., La Jolla, CA.

ELECTRON COLLECTION BY MULTIPLE OBJECTS WITHIN A SINGLE SHEATH

V. A. DAVIS, M. J. MANDELL, and I. KATZ (Maxwell Laboratories, Inc., La Jolla, CA) Journal of Spacecraft and Rockets (ISSN 0022-4650), vol. 25, Jan.-Feb. 1988, p. 94, 95. refs (Contract NAS3-23881)

NASCAP/LEO, a computer program for the three-dimensional simulation of high-voltage surfaces with plasma, has been developed as a tool in the design of reliable, high-power spacecraft. NASCAP/LEO computes the potentials using analytic formulations for space charge, and only uses particle tracking to compute the current to the surfaces. Carruth's (1987) experimental results agree with the NASCAP/LEO simulations for the cases of both individual and overlapping sheaths. O.C.

N88-23649* # Colorado State Univ., Fort Collins. Dept. of Mechanical Engineering.

SPACE PLASMA CONTACTOR RESEARCH, 1987 Annual Report, 1 Jan. 1987 - 1 Jan. 1988

PAUL J. WILBUR Jan. 1988 87 p

(Contract NAG3-776)

(NASA-CR-182148; NAS 1.26:182148) Avail: NTIS HC A05/MF A01 CSCL 201

A simple model describing the process of electron collection from a low pressure ambient plasma in the absence of magnetic field and contactor velocity effects is presented. Experimental measurements of the plasma surrounding the contactor are used to demonstrate that a double-sheath generally develops and separates the ambient plasma from a higher density, anode plasma located adjacent to the contactor. Agreement between the predictions of the model and experimental measurements obtained at the electron collection current levels ranging to 1 A suggests the surface area at the ambient plasma boundary of the double-sheath is equal to the electron current being collected divided by the ambient plasma random electron current density; the surface area of the higher density anode plasma boundary of the double-sheath is equal to the ion current being emitted across this boundary divided by the ion current density required to sustain a stable sheath; and the voltage drop across the sheath is determined by the requirement that the ion and electron currents counterflowing across the boundaries be at space-charge limited levels. The efficiency of contactor operation is shown to improve when significant ionization and excitation is induced by electrons that stream from the ambient plasma through the double-sheath and collide with neutral atoms being supplied through the hollow cathode. Author

N88-26223* # Ohio State Univ., Columbus. Dept. of Aeronautical and Astronautical Engineering.

THE EFFECTS OF MAGNETIC NOZZLE CONFIGURATIONS ON PLASMA THRUSTERS Semiannual Program Report, 5 Dec. 1987 - 4 Dec. 1988

THOMAS M. YORK 21 Jul. 1988 6 p

(Contract NAG3-843)

(NASA-CR-183096; NAS 1.26:183096) Avail: NTIS HC A02/MF A01 CSCL 201

Magnetoplasmodynamics (MPD) arc devices have been operated at power levels from 10 KW to 0.1 MW. When these devices have magnetic fields applied to them, they show marked increases in thrust in direct proportion to the magnitude of the applied field. Electrode erosion may be influenced by applied fields. This proposal will study the application of variable magnetic fields over a range of thruster powers, gas densities, and thruster configurations. It is proposed to examine this behavior with numerical codes and limited but relevant experimental tests. Author

Includes superconductivity.

A88-10431* National Aeronautics and Space Administration. Lewis Research Center, Cleveland, OH.

IMPROVED BETA-SiC HETEROEPITAXIAL FILMS USING OFF-AXIS Si SUBSTRATES

J. A. POWELL, L. G. MATUS, M. A. KUCZMARSKI (NASA, Lewis Research Center, Cleveland, OH), C. M. CHOREY, T. T. CHENG (Case Western Reserve University, Cleveland, OH) et al. Applied Physics Letters (ISSN 0003-6951), vol. 51, Sept. 14, 1987, p. 823-825. refs

All beta-SiC films grown using on-axis (001) Si substrates that have been examined with transmission electron microscopy exhibit a high density of interfacial twins, stacking faults, and antiphase disorder. The antiphase boundaries can be decorated by chemical etching, sputter etching, wet oxidation, and beta-SiC growth in the presence of diborane. All traces of antiphase disorder are eliminated when the heteroepitaxial growth is carried out on vicinal (001) Si substrates that are tilted 2 deg about a 110-line axis. In addition, growth on the off-axis Si produces beta-SiC films that are significantly smoother than on-axis films. The density of stacking faults is apparently unaffected by growth on the off-axis substrates. Author

A88-11150* Cincinnati Univ., OH.

OHMIC CONTACT FORMATION IN SEMI-INSULATING GAAS USING SHALLOW HEAVILY DOPED P-TYPE LAYERS

AMITAVA BOSE and H. T. HENDERSON (Cincinnati, University, OH) Electrochemical Society, Journal (ISSN 0013-4651), vol. 134, Sept. 1987, p. 2372-2374. refs (Contract NAG3-297)

The paper describes a simple, safe, and effective method for forming shallow zinc-doped p-type layers on chromium-doped semiinsulating GaAs, using an open-tube diffusion technique. The resulting peak dopant concentration for the 850-C diffusion was 10 to the 20th/cu cm. The contact resistance of ohmic contacts fabricated on these layers was found to be about 0.00005 ohm/sq cm. The variation of the contact resistance across the wafer reflected the variation of the doping concentration. I.S.

A88-18467* Michigan Technological Univ., Houghton.

LOCAL CONVECTIVE FLOWS IN PARTLY SOLIDIFIED ALLOYS

A. HELLAWELL (Michigan Technological University, Houghton) IN: Structure and dynamics of partially solidified systems; Proceedings of the NATO Advanced Research Workshop, Tahoe, CA, May 12-16, 1986. Dordrecht, Martinus Nijhoff Publishers, 1987, p. 5-22. refs (Contract NAS8-33727; NAG3-560)

Channel formation in a dendritic mushy zone is examined with reference to experimental results obtained for an aqueous system, NH₄Cl-H₂O, and a low-melting metallic system, Pb-Sn. The problems of channel nucleation, propagation, and prevention are considered for a configuration in which heat flow is directed downwards and growth occurs upwards into a positive temperature gradient. It is found that channels nucleate at the growth front by double diffusive perturbations into the quiescent bulk liquid, and not by perturbations within the dendritic framework of the mushy zone. V.L.

A88-18814* Case Western Reserve Univ., Cleveland, OH.

WEAK-FIELD MAGNETIZATION OF SUPERCONDUCTING Y1BA2CU3O(X) - RELATIONSHIP TO MICROSTRUCTURE

D. E. FARRELL, M. R. DEGUIRE, B. S. CHANDRASEKHAR (Case Western Reserve University, Cleveland, OH), S. A. ALTEROVITZ, P. R. ARON (NASA, Lewis Research Center, Cleveland, OH) et al. (Physical Review B, 3rd Series, vol. 35, June 1, 1987, p.

8797-8799) IN: High-temperature superconductivity. New York, American Physical Society, 1987, p. 8797-8799. Research supported by the Ohio Board of Regents. refs

The granular magnetization model of Finnemore et al. (1987) has been tested on a well-characterized sample of $Y_1Ba_2Cu_3O_x$. The temperature dependence of the magnetic susceptibility is in excellent agreement with the model. In addition, the grain size deduced from the magnetization data (1-2 microns) is in reasonable agreement with direct scanning-electron-microscopy measurements of the microstructure. Author

A88-26196* Cincinnati Univ., OH.

RAPID THERMAL ANNEALING OF INDIUM PHOSPHIDE COMPOUND SEMICONDUCTORS

MICHAEL D. BIEDENBENDER, VIK J. KAPOOR (Cincinnati, University, OH), and W. D. WILLIAMS (NASA, Lewis Research Center, Cleveland, OH) Journal of Vacuum Science and Technology A (ISSN 0734-2101), vol. 5, July-Aug. 1987, pt. 2, p. 1437-1441. refs

The rapid thermal annealing (RTA) of indium phosphide (InP) substrates using a proximity contact method and silicon nitride encapsulation is investigated. The surface conditions of the InP substrates following cleaning with procedures A and B are analyzed. Procedure A involves using an iodic acid solution to remove work-damage InP surface layers and B is a degassing process and hydrofluoric acid solution for native oxide removal. AES, XPS, and SIMS data of the proximity contact and silicon nitride encapsulated annealed samples are examined. The data reveal that RTA using proximity contact with silicon wafers does not provide adequate protection; however, the InP sample is successfully annealed when protected by a silicon nitride encapsulant. I.F.

A88-28711* Case Western Reserve Univ., Cleveland, OH.

LATTICE DEFECTS IN BETA-SiC GROWN EPITAXIALLY ON SILICON SUBSTRATES

P. PIROUZ, C. M. CHOREY, T. T. CHENG (Case Western Reserve University, Cleveland, OH), and J. A. POWELL (NASA, Lewis Research Center, Cleveland, OH) IN: Heteroepitaxy on silicon technology; Proceedings of the MRS Spring Meeting, Anaheim, CA, Apr. 21-25, 1987. Pittsburgh, PA, Materials Research Society (MRS Symposia Proceedings. Volume 91), 1987, p. 399-404. refs

(Contract NAG3-758)

Defects generated on beta-SiC grown on a (001) silicon substrate by chemical vapor deposition are characterized and their mechanism of formation discussed. It is argued that nucleation plays a primary role in this heteroepitaxial system where the lattice mismatch is so large. Author

A88-29297* National Aeronautics and Space Administration. Lewis Research Center, Cleveland, OH.

EFFECT OF FLUORIDE DOPING ON THE TRANSITION TEMPERATURE OF $YBa_2Cu_3O_{(6.5+\Delta)}$

NAROTTAM P. BANSAL, ANN L. SANDKUHL (NASA, Lewis Research Center, Cleveland, OH), and D. E. FARRELL (Case Western Reserve University, Cleveland, OH) Applied Physics Letters (ISSN 0003-6951), vol. 52, March 7, 1988, p. 838-840. refs

The effects of F content on the T_c of superconducting $YBa_2Cu_3F(x)O_{(6.5+\Delta-0.5x)}$ ($x = 0.0165-1.65$) prepared by the solid-state reaction method (Bandsahl and Sandkuhl, 1988) are investigated experimentally. The results are presented in tables and graphs and characterized. T_c is found to increase steadily from 90.8 to 93.4 K as x is increased from 0.0165 to 0.066, but to decrease as x is further increased ($T_c = 90.3$ K at $x = 1.65$). The structure of the samples with $x = 0.066$ or lower is found to be single-phase perovskite. T.K.

A88-32862* National Aeronautics and Space Administration. Lewis Research Center, Cleveland, OH.

PLASMA DEPOSITION OF AMORPHOUS HYDROGENATED CARBON FILMS ON III-V SEMICONDUCTORS

JOHN J. POUCH, JOSEPH D. WARNER, DAVID C. LIU, and SAMUEL A. ALTEROVITZ (NASA, Lewis Research Center, Cleveland, OH) Thin Solid Films (ISSN 0040-6090), vol. 157, 1988, p. 97-104. refs

Amorphous hydrogenated carbon films were grown on GaAs, InP and fused silica substrates using plasmas generated from hydrocarbon gases. Methane and n-butane sources were utilized. The effects of flow rate and power density on film growth were investigated. Carbon was the major constituent in the films. The degree of asymmetry at the carbon-semiconductor interface was approximately independent of the power density. Different H-C bonding configurations were detected by the technique of secondary-ion mass spectrometry. Band gaps up to 3 eV were obtained from optical absorption studies. Breakdown strengths as high as 600 MV/m were measured. Author

A88-40139* National Aeronautics and Space Administration. Lewis Research Center, Cleveland, OH.

VARIABLE ANGLE SPECTROSCOPIC ELLIPSOMETRY - APPLICATION TO GaAs-ALGaAs MULTILAYER HOMOGENEITY CHARACTERIZATION

SAMUEL A. ALTEROVITZ (NASA, Lewis Research Center, Cleveland, OH), PAUL G. SNYDER, KENNETH G. MERKEL, JOHN A. WOOLLAM (Nebraska, University, Lincoln), DAVID C. RADULESCU (Cornell University, Ithaca, NY) et al. Journal of Applied Physics (ISSN 0021-8979), vol. 63, May 15, 1988, p. 5081-5084. Research supported by the Joint Services Electronics Program. refs

(Contract NAG3-154)

Variable angle spectroscopic ellipsometry has been applied to a GaAs-AlGaAs multilayer structure to obtain a three-dimensional characterization, using repetitive measurements at several spots on the same sample. The reproducibility of the layer thickness measurements is of order 10 Å, while the lateral dimension is limited by beam diameter, presently of order 1 mm. Thus, the three-dimensional result mainly gives the sample homogeneity. In the present case three spots were used to scan the homogeneity over 1 in of a wafer which had molecular-beam epitaxially grown layers. The thickness of the AlGaAs, GaAs, and oxide layers and the Al concentration varied by 1 percent or less from edge to edge. This result was confirmed by two methods of data analysis. No evidence of an interfacial layer was observed on top of the AlGaAs. Author

A88-40796* Jet Propulsion Lab., California Inst. of Tech., Pasadena.

EFFECT OF HIGH TEMPERATURE ANNEALING ON THE THERMOELECTRIC PROPERTIES OF GAP DOPED SiGe

JAN W. VANDERSANDE, CHARLES WOOD (California Institute of Technology, Jet Propulsion Laboratory, Pasadena), and SUSAN DRAPER (NASA, Lewis Research Center, Cleveland, OH) IN: Novel refractory semiconductors. Pittsburgh, PA, Materials Research Society (MRS Symposium Proceedings. Volume 97), 1987, p. 347-352. refs

Silicon-germanium alloys doped with GaP are used for thermoelectric energy conversion in the temperature range 300-1000 C. The conversion efficiency depends on $Z = S^2/\rho\lambda$, a material's parameter (the figure of merit), where S is the Seebeck coefficient, ρ is the electrical resistivity and λ is the thermal conductivity. The annealing of several samples in the temperature range of 1100-1300 C resulted in the power factor $P (= S^2/\rho)$ increasing with increased annealing temperature. This increase in P was due to a decrease in ρ which was not completely offset by a drop in S^2 suggesting that other changes besides that in the carrier concentration took place. SEM and EDX analysis of the samples indicated the formation of a Ga-P-Ge rich phase as a result of the annealing. It is speculated that this phase is associated with the improved properties. Several reasons which could account for the improvement in the power factor of annealed GaP doped SiGe are given. Author

A88-40797* Jet Propulsion Lab., California Inst. of Tech., Pasadena.

EFFECT OF THE MICROSTRUCTURE ON THE THERMOELECTRIC PROPERTIES OF POLYCRYSTALLINE LANTHANUM CHALCOGENIDES

A. LOCKWOOD, C. WOOD, J. VANDERSANDE, A. ZOLTAN, J. PARKER (California Institute of Technology, Jet Propulsion Laboratory, Pasadena), L. DANIELSON, M. ALEXANDER (Thermal Electron Corp., Waltham, MA), and D. WHITTENBERGER (NASA, Lewis Research Center, Cleveland, OH) IN: Novel refractory semiconductors. Pittsburgh, PA, Materials Research Society (MRS Symposium Proceedings. Volume 97), 1987, p. 385-390. refs

Small amounts of second phase materials can have important effects on the thermoelectric properties of polycrystalline $\gamma\text{-La}(3-x)\text{X}_4$ (X-S, Te; X in the range of 0 to 1/3). Microscopic examination by SEM of hot pressed $\text{La}(3-x)\text{Te}_4$ samples has revealed from 1-5 vol. pct of $\text{La}_2\text{O}_2\text{Te}$, an amount which is not detected by X-ray powder diffraction measurements. This amount of $\text{La}_2\text{O}_2\text{Te}$ resulting from oxygen contamination can reduce the concentration of electrons by as much as 10 to 75 percent below the electron concentration calculated for single phase $\text{La}(3-x)\text{Te}_4$ in the composition range of greatest interest. Small amounts of second phase materials can also lower the lattice thermal conductivity by scattering low frequency phonons. These results indicate that microstructural effects should be considered when electrical and thermal properties of polycrystalline materials are analyzed. Author

A88-41496* National Aeronautics and Space Administration. Lewis Research Center, Cleveland, OH.

ADVANTAGES OF BARIUM PEROXIDE IN THE POWDER SYNTHESIS OF PEROVSKITE SUPERCONDUCTORS

A. F. HEPP, J. R. GAIER, W. H. PHILIPP, J. D. WARNER, R. G. GARLICK, J. J. POUCH (NASA, Lewis Research Center, Cleveland, OH) et al. IN: High-temperature superconductors; Proceedings of the Symposium, Boston, MA, Nov. 30-Dec. 4, 1987. Pittsburgh, PA, Materials Research Society, 1988, p. 615-618. refs (Contract NCC3-19)

This paper compares reaction chemistry, material processing, and material characteristics for the solid state reaction using BaCO_3 or BaO_2 in the synthesis of perovskite superconductors. Results are presented for weight loss and X-ray diffraction, sample morphology and homogeneity as monitored by SEM and EDS, and the superconductivity critical temperature and ac susceptibility. Greater mass density, increased sample homogeneity, lower resistance, and improved reproducibility for material are found when BaO_2 is used. C.D.

A88-43933* # Arizona Univ., Tucson.

DOUBLE-DIFFUSIVE EFFECTS DURING SOLIDIFICATION

C. F. CHEN (Arizona, University, Tucson) IN: Interdisciplinary issues in materials processing and manufacturing; Proceedings of the Symposium, ASME Winter Annual Meeting, Boston, MA, Dec. 13-18, 1987. Volume 2. New York, American Society of Mechanical Engineers, 1987, p. 527-540. refs (Contract NAG3-723; NSF MSM-87-02732)

When a fluid contains two diffusing components with different molecular diffusivities, such as heat and solute concentration, convective motion may be generated when potential energy is released owing to differential diffusion. In the solidification of binary alloys and doped semiconductors, temperature and concentration gradients do exist simultaneously. If these gradients are aligned in a suitable manner, convection may ensue. In the case of the binary alloy, such convection may extend through the mushy zone and may be the cause of macrosegregations. In the case of doped semiconductors, the convective motion may cause the nonuniform distribution of dopant in the product. In this paper, the fundamentals of double-diffusive convection will be reviewed, and its effect on solidification will be discussed. Author

A88-45858* Massachusetts Univ., Amherst.

TEMPERATURE STABILITY OF $\text{Al}(\text{X})\text{Ga}(1-\text{X})\text{AS}$ ($\text{X} = 0-1$) THERMAL OXIDE MASKS FOR SELECTIVE-AREA EPITAXY

STEPHEN H. JONES, KEI MAY LAU (Massachusetts, University, Amherst), and JOHN J. POUCH (NASA, Lewis Research Center, Cleveland, OH) Journal of Applied Physics (ISSN 0021-8979), vol. 64, July 15, 1988, p. 922-925. refs

The use of thermal oxides of $\text{Al}(\text{x})\text{Ga}(1-\text{x})\text{As}$ ($\text{x} = 0-1$) as masking materials for selective-area epitaxy by a organometallic chemical-vapor deposition has been investigated. It was found that the thermal oxide of GaAs is only applicable for low growth temperatures (less than or equal to 600 C), and the addition of aluminum significantly improves the thermal stability of the oxide. The oxide of $\text{Al}(0.4)\text{Ga}(0.6)\text{As}$ is suitable for high-temperature deposition, but there are criteria for the thickness and oxidation temperature. Thin layers of AlAs oxidized at 475 C are excellent masks and allow precise thickness control. Promising results of selective-area deposition using these aluminum oxide masks have been obtained. High-quality single crystal grew in mask openings uniformly surrounded by dense and fine-grain polycrystalline deposits, producing a planar duplication of the original pattern. Author

A88-49376* National Aeronautics and Space Administration. Lewis Research Center, Cleveland, OH.

CHARACTERIZATION OF $\text{Ba}_2\text{YCu}_3\text{O}(7-\text{x})$ PREPARED IN AN INERT ATMOSPHERE

A. F. HEPP, P. R. ARON, J. R. GAIER, D. K. WHEELER, and R. G. GARLICK (NASA, Lewis Research Center, Cleveland, OH) IN: High-temperature superconductors II. Pittsburgh, PA, Materials Research Society, 1988, p. 183-186. refs

Reaction data, X-ray data, and critical temperature measurements have been used to show that superconducting $\text{Ba}_2\text{YCu}_3\text{O}(7-\text{x})$ can be produced in an inert atmosphere using BaO_2 as the barium source. Weight loss data are presented for samples produced in O_2 and N_2 . The use of BaO_2 is found to result in decreased levels of intergrain BaCO_3 . The necessity for total inert atmosphere handling and tighter control of the carbon content of starting materials is pointed out. It is shown that materials made with BaO_2 and handled in inert atmospheres can be used to improve the $J_{\text{sub } c}$ of melt processed materials. R.R.

A88-51286* Illinois Univ., Urbana.

DEPOSITION OF VANADIUM OXIDE FILMS BY DIRECT-CURRENT MAGNETRON REACTIVE SPUTTERING

E. KUSANO, J. A. THEIL, and JOHN A. THORNTON (Illinois, University, Urbana) Journal of Vacuum Science and Technology A (ISSN 0734-2101), vol. 6, May-June 1988, pt. 2, p. 1663-1667. Research supported by the Nippon Sheet Glass Co. refs (Contract NAG3-591)

It is demonstrated here that thin films of vanadium oxide can be deposited at modest substrate temperatures by dc reactive sputtering from a vanadium target in an $\text{O}_2\text{-Ar}$ working gas using a planar magnetron source. Resistivity ratios of about 5000 are found between a semiconductor phase with a resistivity of about 5 Ohm cm and a metallic phase with a resistivity of about 0.001 Ohm cm for films deposited onto borosilicate glass substrates at about 400 C. X-ray diffraction shows the films to be single-phase VO_2 with a monoclinic structure. The VO_2 films are obtained for a narrow range of O_2 injection rates which correspond to conditions where cathode poisoning is just starting to occur. C.D.

N88-17702* # GTE Labs., Inc., Waltham, MA.

A PAYLOAD FOR INVESTIGATING THE INFLUENCE OF CONVECTION ON GAAS CRYSTAL GROWTH

ALFRED H. BELLOWES and GLENN A. DUCHENE IN: NASA. Goddard Space Flight Center, The 1987 Get Away Special Experimenter's Symposium p 77-82 Feb. 1988 (Contract NAS3-24644)

Avail: NTIS HC A08/MF A01 CSCL 20L

A comparative study of the influence of buoyancy driven fluid flow on gallium arsenide (GaAs) crystal growth was undertaken. Crystals will be grown from melts with different degrees of convective flow including growth in the microgravity environment of space. The space growth of GaAs will be performed in a Get Away Special payload. A well insulated growth furnace was

76 SOLID-STATE PHYSICS

designed for both Earth-based and space-based experiments. The self contained payload will carry two such furnaces in addition to a large battery power source and a microprocessor-based control and data acquisition system for regulating the growth process with high precision. The microcomputer will also monitor the growth conditions and measure and record the acceleration in 3 axes.

Author

N88-22805*# National Aeronautics and Space Administration. Lewis Research Center, Cleveland, OH.

SYNTHESIS AND CHARACTERIZATION OF HIGH-T(SUB C) SCREEN-PRINTED Y-BA-CU-O FILMS ON ALUMINA

NAROTTAM P. BANSAL, RAINEE N. SIMONS, and D. E. FARRELL (Case Western Reserve Univ., Cleveland, Ohio.) 1988 11 p Presented at the 90th Annual Meeting of the American Ceramic Society, Cincinnati, Ohio, 1-5 May 1988

(NASA-TM-100860; E-4069; NAS 1.15:100860) Avail: NTIS HC A03/MF A01 CSCL 20L

Thick films of YBa₂Cu₃O(sub 7-x) have been deposited on highly polished alumina substrates by the screen printing technique. To optimize the post-printing heat treatment, the films were baked at various temperatures for different lengths of time and oxygen-annealed at a lower temperature. The resulting films were characterized by electrical resistivity measurements, x-ray diffraction, and optical and scanning electron microscopy. Properties of the films were found to be highly sensitive to the post-printing thermal treatment. Films baked for 15 min at 1000 C in oxygen were hard, adherent, near single phase, and superconducting with T(sub c)(onset) approx 96 K, T(sub c)(zero) approx 66 K and Delta T sub c (10 to 90 percent) approx 10 K.

Author

N88-24316*# Hampden-Sydney Coll., VA. Dept. of Physics.

NEUTRON RADIATION TOLERANCE OF AU-ACTIVATED SILICON

W. T. JOYNER /in New Mexico Univ., Transactions of the Fourth Symposium on Space Nuclear Power Systems p 263-264 1987 (Contract NAG3-605)

Avail: NTIS HC A22/MF A01 CSCL 20L

Double injection devices prepared by the introduction of deep traps, using the Au activation method have been found to tolerate gamma irradiation into the Gigerad (Si) region without significant degradation of operating characteristics. Silicon double injection devices, using deep levels created by Au diffusion, can tolerate fast neutron irradiation up to 10 to the 15th n/sq cm. Significant parameter degradation occurs at 10 to the 16th n/sq cm. However, since the actual doping of the basic material begins to change as a result of the transmutation of silicon into phosphorus for neutron fluences greater than 10 to the 17th/sq cm, the radiation tolerance of these devices is approaching the limit possible for any device based on initially doped silicon.

Author

N88-24539*# Rockwell International Science Center, Thousand Oaks, CA.

DEVELOPMENT OF 20 GHZ MONOLITHIC TRANSMIT MODULES Final Report, 30 Nov. 1981 - 30 Nov. 1987

J. A. HIGGINS May 1988 101 p

(Contract NAS3-23247)

(NASA-CR-182134; NAS 1.26:182134; SC5492.FR) Avail: NTIS HC A06/MF A01 CSCL 20L

The history of the development of a transmit module for the band 17.7 to 20.2 GHz is presented. The module was to monolithically combine, on one chip, five bits of phase shift, a buffer amplifier and a power amplifier to produce 200 mW to the antenna element. The approach taken was MESFET ion implanted device technology. A common pinch-off voltage was decided upon for each application. The beginning of the total integration phases revealed hitherto unencountered hazards of large microwave circuit integration which were successfully overcome. Yield and customer considerations finally led to two separate chips, one containing the power amplifiers and the other containing the complete five bit phase shifter.

Author

N88-25327*# Princeton Univ., NJ. Dept. of Chemical Engineering.

NASA RESEARCH PROGRAM: THE ROLES OF FLUID MOTION AND OTHER TRANSPORT PHENOMENA IN THE MORPHOLOGY OF MATERIALS Final Report, Jul. 1983 - Oct. 1987

D. A. SAVILLE May 1988 208 p

(Contract NAG3-447)

(NASA-CR-182801; NAS 1.26:182801) Avail: NTIS HC A10/MF A01 CSCL 20L

The influence of transport phenomena on the morphology of crystalline materials was investigated. Two problems were studied: the effects of convection on the crystallization of pure materials, and the crystallization of proteins from solution.

N88-25346*# Westinghouse Research and Development Center, Pittsburgh, PA.

ADVANCED DEVELOPMENT OF DOUBLE-INJECTION, DEEP-IMPURITY SEMICONDUCTOR SWITCHES Final Report, 13 Jun. 1985 - 15 Dec. 1987

M. H. HANES 7 Dec. 1987 143 p

(Contract NAS3-24637)

(NASA-CR-182118; NAS 1.26:182118) Avail: NTIS HC A07/MF A01 CSCL 20L

Deep-impurity, double-injection devices, commonly referred to as (DI) squared devices, represent a class of semiconductor switches possessing a very high degree of tolerance to electron and neutron irradiation and to elevated temperature operation. These properties have caused them to be considered as attractive candidates for space power applications. The design, fabrication, and testing of several varieties of (DI) squared devices intended for power switching are described. All of these designs were based upon gold-doped silicon material. Test results, along with results of computer simulations of device operation, other calculations based upon the assumed mode of operation of (DI) squared devices, and empirical information regarding power semiconductor device operation and limitations, have led to the conclusion that these devices are not well suited to high-power applications. When operated in power circuitry configurations, they exhibit high-power losses in both the off-state and on-state modes. These losses are caused by phenomena inherent to the physics and material of the devices and cannot be much reduced by device design optimizations. The (DI) squared technology may, however, find application in low-power functions such as sensing, logic, and memory, when tolerance to radiation and temperature are desirable (especially if device performance is improved by incorporation of deep-level impurities other than gold).

Author

77

THERMODYNAMICS AND STATISTICAL PHYSICS

Includes quantum mechanics; theoretical physics; and Bose and Fermi statistics.

A88-53050* National Bureau of Standards, Gaithersburg, MD.

CRITICAL EXPONENT FOR THE VISCOSITY OF FOUR BINARY LIQUIDS

ROBERT F. BERG and MICHAEL R. MOLDOVER (NBS, Thermophysics Div., Gaithersburg, MD) Journal of Chemical Physics (ISSN 0021-9606), vol. 89, Sept. 15, 1988, p. 3694-3704. refs

(Contract NASA ORDER C-86129-D)

The viscosity of the following binary mixtures was measured near their consolute points: (1) methanol + cyclohexane, (2) isobutyric acid + water, (3) nitroethane + 3-methylpentane, and (4) 2-butoxyethanol + water. It is shown that the multiplicative hypothesis is valid for these mixtures. It is also found that the concentration closest to critical has the largest viscosity enhancement.

K.K.

ADMINISTRATION AND MANAGEMENT

Includes management planning and research.

A88-44003*# National Aeronautics and Space Administration. Lewis Research Center, Cleveland, OH.

SPACE COMMERCIALIZATION AND POWER SYSTEM TECHNOLOGY

H. BRANDHORST, JR. and K. A. FAYMON (NASA, Lewis Research Center, Cleveland, OH) IN: Advanced topics in manufacturing technology: Product design, bioengineering; Proceedings of the Symposium, ASME Winter Annual Meeting, Boston, MA, Dec. 13-18, 1987. New York, American Society of Mechanical Engineers, 1987, p. 61-72.

The development and application of power and energy technologies important to the commercialization of space is discussed, stressing the significance of these technologies to space transportation systems, on-orbit services and on-orbit commercial production and processing ventures. Energy conversion systems examined include solar photovoltaic systems, solar thermal dynamic power systems, and nuclear power systems. Energy storage systems include electrochemical systems, inertial storage systems, and magnetic energy storage systems. In addition, power management and distribution systems used in space commercialization and NASA programs for the commercial development of space are discussed. R.B.

N88-16699*# National Aeronautics and Space Administration. Lewis Research Center, Cleveland, OH.

LEWIS MATERIALS RESEARCH AND TECHNOLOGY: AN OVERVIEW

SALVATORE J. GRISAFFE *In its Aeropropulsion '87*. Session 1: Aeropropulsion Materials Research 8 p Nov. 1987
Avail: NTIS HC A06/MF A01 CSCL 05A

The Materials Division at the Lewis Research Center has a long record of contributions to both materials and process technology as well as to the understanding of key high-temperature phenomena. An overview of the division staff, facilities, past history, recent progress, and future interests is presented. Author

DOCUMENTATION AND INFORMATION SCIENCE

Includes information management; information storage and retrieval technology; technical writing; graphic arts; and micrography.

N88-28832*# National Aeronautics and Space Administration. Lewis Research Center, Cleveland, OH.

BIBLIOGRAPHY OF LEWIS RESEARCH CENTER TECHNICAL PUBLICATIONS ANNOUNCED IN 1987

Jun. 1988 362 p
(NASA-TM-100910; E-4162; NAS 1.15:100910) Avail: NTIS HC A16/MF A01 CSCL 05B

This compilation of abstracts describes and indexes the technical reporting that resulted from the scientific and engineering work performed and managed by the Lewis Research Center in 1987. All the publications were announced in the 1987 issues of STAR (Scientific and Technical Aerospace Reports) and/or IAA (International Aerospace Abstracts). Included are research reports, journal articles, conference presentations, patents and patent applications, and theses. Author

URBAN TECHNOLOGY AND TRANSPORTATION

Includes applications of space technology to urban problems; technology transfer; technology assessment; and surface and mass transportation.

N88-10700*# National Aeronautics and Space Administration. Lewis Research Center, Cleveland, OH.

RE-1000 FREE-PISTON STIRLING ENGINE HYDRAULIC OUTPUT SYSTEM DESCRIPTION

JEFFREY G. SCHREIBER and STEVEN M. GENG Oct. 1987 21 p

(NASA-TM-100185; E-3802; NAS 1.15:100185) Avail: NTIS HC A03/MF A01 CSCL 13I

The NASA Lewis Research Center was involved in free-piston Stirling engine research since 1976. Most of the work performed in-house was related to characterization of the RE-1000 engine. The data collected from the RE-1000 tests were intended to provide a data base for the validation of Stirling cycle simulations. The RE-1000 was originally built with a dashpot load system which did not convert the output of the engine into useful power, but was merely used as a load for the engine to work against during testing. As part of the interagency program between NASA Lewis and the Oak Ridge National Laboratory, (ORNL), the RE-1000 was converted into a configuration that produces useable hydraulic power. A goal of the hydraulic output conversion effort was to retain the same thermodynamic cycle that existed with the dashpot loaded engine. It was required that the design must provide a hermetic seal between the hydraulic fluid and the working gas of the engine. The design was completed and the hardware was fabricated. The RE-1000 was modified in 1985 to the hydraulic output configuration. The early part of the RE-1000 hydraulic output program consisted of modifying hardware and software to allow the engine to run at steady-state conditions. A complete description of the engine is presented in sufficient detail so that the device can be simulated on a computer. Tables are presented showing the masses of the oscillating components and key dimensions needed for modeling purposes. Graphs are used to indicate the spring rate of the diaphragms used to separate the helium of the working and bounce space from the hydraulic fluid. Author

N88-11578*# Mechanical Technology, Inc., Latham, NY.

AUTOMOTIVE STIRLING ENGINE: MOD 2 DESIGN REPORT Final Report

NOEL P. NIGHTINGALE Oct. 1986 56 p
(Contract DEN3-32; DE-AI01-85CE-50112)
(NASA-CR-175106; DOE/NASA/0032-28; NAS 1.26:175106; MT186ASE58SRI) Avail: NTIS HC A04/MF A01 CSCL 13F

The design of an automotive Stirling engine that achieves the superior fuel economy potential of the Stirling cycle is described. As the culmination of a 9-yr development program, this engine, designated the Mod 2, also nullifies arguments that Stirling engines are heavy, expensive, unreliable, demonstrating poor performance. Installed in a General Motors Chevrolet Celebrity car, this engine has a predicted combined fuel economy on unleaded gasoline of 17.5 km/l (41 mpg)- a value 50% above the current vehicle fleet average. The Mod 2 Stirling engine is a four-cylinder V-drive design with a single crankshaft. The engine is also equipped with all the controls and auxiliaries necessary for automotive operation. Author

N88-12427*# National Aeronautics and Space Administration. Lewis Research Center, Cleveland, OH.

OVERVIEW OF FREE-PISTON STIRLING ENGINE TECHNOLOGY FOR SPACE POWER APPLICATION Final Report

JACK G. SLABY 1987 23 p Presented at the Solar Energy Conference, Honolulu, Hawaii, 22-27 Mar. 1987; sponsored by ASME, JSME and JSES

(Contract DE-AI05-82OR-1005)

(NASA-TM-88886; DOE/NASA/1005-12; E-3295; NAS 1.15:88886) Avail: NTIS HC A03/MF A01 CSCL 10B

An overview is presented of free-piston Stirling engine activities, directed toward space power applications. One of the major elements of the program is the development of advanced power conversion. Under this program the status of the 25 kWe opposed-piston Space Power Demonstrator Engine (SPDE) is presented. Initial differences between predicted and experimental power outputs and power output influenced by variations in regenerators are discussed. Technology work was conducted on heat-exchanger concepts to minimize the number of joints as well as to enhance the heat transfer in the heater. Design parameters and conceptual design features are also presented for a 25 kWe, single-cylinder free-piston Stirling space power converter. Projections are made for future space power requirements over the next few decades along with a recommendation to consider the use of dynamic power conversion systems, either solar or nuclear. A cursory comparison is presented showing the mass benefits of a Stirling system over a Brayton system for the same peak temperature and output power. A description of a study to investigate the feasibility of scaling a single-cylinder free-piston Stirling space power module to the 150 kWe power range is presented.

Author

N88-12428*# Detroit Diesel Allison, MI.

ADIABATIC DIESEL ENGINE COMPONENT DEVELOPMENT: REFERENCE ENGINE FOR ON-HIGHWAY APPLICATIONS

Interim Report, 1 May 1985 - 30 Apr. 1986

NABIL S. HAKIM Apr. 1986 470 p

(Contract DEN3-329; DE-AL01-86CE-50162)

(NASA-CR-179531; DOE/NASA/0329-1; NAS 1.26:179531;

DDA-R01-ADECD-NAS) Avail: NTIS HC A20/MF A01 CSCL 13F

The main objectives were to select an advanced low heat rejection diesel reference engine (ADRE) and to carry out systems analysis and design. The ADRE concept selection consisted of: (1) rated point performance optimization; (2) study of various exhaust energy recovery scenarios; (3) components, systems and engine configuration studies; and (4) life cycle cost estimates of the ADRE economic worth. The resulting ADRE design proposed a reciprocator with many advanced features for the 1995 technology demonstration time frame. These included ceramic air gap insulated hot section structural components, high temperature tribology treatments, nonmechanical (camless) valve actuation systems, and elimination of the cylinder head gasket. ADRE system analysis and design resulted in more definition of the engine systems. These systems include: (1) electro-hydraulic valve actuation, (2) electronic common rail injection system; (3) engine electronic control; (4) power transfer for accessory drives and exhaust energy recovery systems; and (5) truck installation. Tribology and performance assessments were also carried out. Finite element and probability of survival analyses were undertaken for the ceramic low heat rejection component.

Author

N88-14046*# National Aeronautics and Space Administration. Lewis Research Center, Cleveland, OH.

PROGRESS TOWARD THE EVOLUTION OF A STIRLING SPACE ENGINE

DONALD L. ALGER 1987 15 p Prepared for presentation at the 1988 International Congress and Exposition, Detroit, Mich., 29-Feb. - 4 Mar. 1988; sponsored by Society of Automotive Engineers, Inc.

(NASA-TM-100221; E-3833; NAS 1.15:100221) Avail: NTIS HC A03/MF A01 CSCL 10B

Following the successful testing of the 25 kWe Space Power Demonstrator (SPD) engine in 1985, a Stirling Space Engine (SSE) technology advancement program was initiated. The program's objective was to advance free-piston Stirling engine/linear alternator technology sufficiently so that a Stirling engine system may become a viable candidate for space power applications. Evolution of the SSE technology is planned to occur at three different engine heater temperature levels: 650, 1050, and 1300

K. These temperatures define three phases of technology development with the first phase involving the 650 K SPD engine. Technology development of the 650 K engine and preliminary design of the 1050 K engine will be discussed.

Author

N88-17561*# National Aeronautics and Space Administration. Lewis Research Center, Cleveland, OH.

OVERVIEW OF HEAT TRANSFER AND FLUID FLOW PROBLEM AREAS ENCOUNTERED IN STIRLING ENGINE MODELING

ROY C. TEW, JR. Feb. 1988 23 p Presented at the 1987 Winter Annual meeting of the American Society of Mechanical Engineers, Boston, Massachusetts, 14-16 Dec. 1987

(NASA-TM-100131; E-3680; NAS 1.15:100131) Avail: NTIS HC A03/MF A01 CSCL 10B

NASA Lewis Research Center has been managing Stirling engine development programs for over a decade. In addition to contractual programs, this work has included in-house engine testing and development of engine computer models. Attempts to validate Stirling engine computer models with test data have demonstrated that engine thermodynamic losses need better characterization. Various Stirling engine thermodynamic losses and efforts that are underway to characterize these losses are discussed.

Author

N88-19377*# Priem Consultants, Inc., Cleveland, OH.

STUDY OF INDUSTRY REQUIREMENTS THAT CAN BE FULFILLED BY COMBUSTION EXPERIMENTATION ABOARD SPACE STATION Final Contractor Report

RICHARD J. PRIEM Mar. 1988 62 p

(Contract NAS3-24105)

(NASA-CR-180854; E-3901; NAS 1.26:180854) Avail: NTIS HC A04/MF A01 CSCL 22A

The purpose of this study is to define the requirements of commercially motivated microgravity combustion experiments and the optimal way for space station to accommodate these requirements. Representatives of commercial organizations, universities and government agencies were contacted. Interest in and needs for microgravity combustion studies are identified for commercial/industrial groups involved in fire safety with terrestrial applications, fire safety with space applications, propulsion and power, industrial burners, or pollution control. From these interests and needs experiments involving: (1) no flow with solid or liquid fuels; (2) homogeneous mixtures of fuel and air; (3) low flow with solid or liquid fuels; (4) low flow with gaseous fuel; (5) high pressure combustion; and (6) special burner systems are described and space station resource requirements for each type of experiment provided. Critical technologies involving the creation of a laboratory environment and methods for combining experimental needs into one experiment in order to obtain effective use of space station are discussed. Diagnostic techniques for monitoring combustion process parameters are identified.

Author

N88-20229*# Standard Oil Engineered Materials Co., Niagara Falls, NY. Structural Ceramics Div.

ADVANCED GAS TURBINE (AGT) TECHNOLOGY DEVELOPMENT PROJECT, CERAMIC COMPONENT DEVELOPMENTS Topical Report, Oct. 1979 - Jul. 1987

M. O. TENYCK, J. W. MACBETH, and T. B. SWEETING 1987 237 p Sponsored in part by DOE, Washington, D.C.

(Contract DEN3-167)

(NASA-CR-180871; DOE/NASA/0167-13; NAS 1.26:180871; GARRETT-31-3725(13)) Avail: NTIS HC A11/MF A01 CSCL 13B

The ceramic component technology development activity conducted by Standard Oil Engineered Materials Company while performing as a principal subcontractor to the Garrett Auxiliary Power Division for the Advanced Gas Turbine (AGT) Technology Development Project (NASA Contract DEN3-167) is summarized. The report covers the period October 1979 through July 1987, and includes information concerning ceramic technology work categorized as common and unique. The former pertains to ceramic development applicable to two parallel AGT projects established

by NASA contracts DEN3-168 (AGT100) and DEN3-167 (AGT101), whereas the unique work solely pertains to Garrett directed activity under the latter contract. The AGT101 Technology Development Project is sponsored by DOE and administered by NASA-Lewis. Standard Oil directed its efforts toward the development of ceramic materials in the silicon-carbide family. Various shape forming and fabrication methods, and nondestructive evaluation techniques were explored to produce the static structural components for the ceramic engine. This permitted engine testing to proceed without program slippage. Author

N88-20230*# Garrett Corp., Phoenix, AZ. Auxiliary Power Div.
**ADVANCED GAS TURBINE (AGT) TECHNOLOGY
 DEVELOPMENT PROJECT Final Report**

Dec. 1987 381 p
 (Contract DEN3-167)
 (NASA-CR-180891; NAS 1.26:180891; REPT-31-3725(12);
 DOE/NASA/0167-12) Avail: NTIS HC A17/MF A01 CSDL 13B

This report is the final in a series of Technical Summary Reports for the Advanced Gas Turbine (AGT) Technology Development Project, authorized under NASA Contract DEN3-167 and sponsored by the DOE. The project was administered by NASA-Lewis Research Center of Cleveland, Ohio. Plans and progress are summarized for the period October 1979 through June 1987. This program aims to provide the US automotive industry the high risk, long range technology necessary to produce gas turbine engines for automobiles that will reduce fuel consumption and reduce environmental impact. The intent is that this technology will reach the marketplace by the 1990s. The Garrett/Ford automotive AGT was designated AGT101. The AGT101 is a 74.5 kW (100 shp) engine, capable of speeds to 100,000 rpm, and operates at turbine inlet temperatures to 1370 C (2500 F) with a specific fuel consumption level of 0.18 kg/kW-hr (0.3 lbs/hp-hr) over most of the operating range. This final report summarizes the powertrain design, power section development and component/ceramic technology development. Author

N88-27980*# National Aeronautics and Space Administration.
 Lewis Research Center, Cleveland, OH.

**PHASE 1 RESULTS FROM THE STIRLING-POWERED
 VEHICLE PROJECT**

RICHARD K. SHALTENS 1988 17 p Proposed for presentation at the 4th International Conference on Stirling Engines, Tokyo, Japan, 7-10 Nov. 1988; sponsored by Japan Society of Mechanical Engineers
 (NASA-TM-100978; DOE/NASA/50112-76; E-4270; NAS 1.15:100978) Avail: NTIS HC A03/MF A01 CSDL 10B

The NASA Technology Utilization (TU) Office is sponsoring a multiyear, multiphase demonstration program to assess the technology developed under the DOE/NASA automotive Stirling engine (ASE) program with engines installed in various Air Force vehicles while being evaluated by independent third parties under realistic conditions. This paper reviews the operational history of Phase 1 with a Mod 1 Stirling engine installed in an Air Force multistop van in a variety of missions. Ten months of operation were with Air Force personnel at Langley Air Force Base, Virginia, where over 1100 hr and 4000 mi were logged on the Langley flight line. The Stirling-powered van operated on unleaded gasoline, JP-4 aircraft fuel, and diesel fuel at Langley Air Force Base. Two months of operation were completed with Deere and Company personnel in the Moline, Illinois area where over 175 hr and 2650 mi were logged on a Deere mail delivery route. Author

N88-30472*# National Aeronautics and Space Administration.
 Lewis Research Center, Cleveland, OH.

**TESTING OF A VARIABLE-STROKE STIRLING ENGINE Final
 Report**

LANNY G. THIEME and DAVID J. ALLEN (Sverdrup Technology, Inc., Cleveland, Ohio.) 1986 31 p Presented at the 21st Intersociety Energy Conversion Engineering Conference (IECEC), San Diego, Calif., 25-29 Aug. 1986; sponsored by ACS, SAE, ANS, ASME, IEEE, AIAA and AIChE Previously announced in IAA as

A87-18036

(NASA-TM-100899; DOE/NASA/50112-75; E-3056; NAS 1.15:100899) Avail: NTIS HC A03/MF A01 CSDL 10B

Testing of a variable-stroke Stirling engine at NASA Lewis has been completed. In support of the DOE Stirling Engine Highway Vehicle Systems Program, the engine was tested for about 70 hours total with both He and H₂ as working fluids over a range of pressures and strokes. A direct comparison was made of part-load efficiencies obtained with variable-stroke (VS) and variable-pressure operation. Two failures with the variable-angle swash-plate drive system limited testing to low power levels. These failures are not thought to be caused by problems inherent with the VS concept but do emphasize the need for careful design in the area of the crossheads. Author

88

SPACE SCIENCES (GENERAL)

N88-12429*# National Aeronautics and Space Administration.
 Lewis Research Center, Cleveland, OH.

**LOW EARTH ORBIT ENVIRONMENTAL EFFECTS ON THE
 SPACE STATION PHOTOVOLTAIC POWER GENERATION
 SYSTEMS**

HENRY K. NAHRA 1987 20 p Proposed for presentation at the 1988 Solar Energy Conference, Golden, Colo., 10-14 Apr. 1988; sponsored by ASME
 (NASA-TM-100230; E-3852; NAS 1.15:100230) Avail: NTIS HC A03/MF A01 CSDL 10A

A summary of the Low Earth Orbital Environment, its impact on the Photovoltaic Power systems of the space station and the solutions implemented to resolve the environmental concerns or issues are described. Low Earth Orbital Environment (LEO) presents several concerns to the Photovoltaic power systems of the space station. These concerns include atomic oxygen interaction with the polymeric substrate of the solar arrays, ionized environment effects on the array operating voltage, the effects of the meteoroids and debris impacts and penetration through the different layers of the solar cells and their circuits, and the high energy particle and radiation effects on the overall solar array performance. Potential solutions to some of the degrading environmental interactions that will provide the photovoltaic power system of the space station with the desired life are also summarized. Author

90

ASTROPHYSICS

Includes cosmology; celestial mechanics; space plasmas; and interstellar and interplanetary gases and dust.

A88-27446* National Aeronautics and Space Administration.
 Lewis Research Center, Cleveland, OH.

STRING-DRIVEN INFLATION

NEIL TUROK (NASA/Fermilab Astrophysics Center, Batavia, IL) Physical Review Letters (ISSN 0031-9007), vol. 60, Feb. 15, 1988, p. 549-552. DOE-NASA-supported research. refs

It is argued that, in fundamental string theories, as one traces the universe back in time a point is reached when the expansion rate is so fast that the rate of string creation due to quantum effects balances the dilution of the string density due to the expansion. One is therefore led into a phase of constant string density and an exponentially expanding universe. Fundamental strings therefore seem to lead naturally to inflation. Author

A88-28762 Chicago Univ., IL.

COSMIC STRING INDUCED PECULIAR VELOCITIES

ANTHONY VAN DALEN and DAVID N. SCHRAMM (Chicago, University; NASA/Fermi National Accelerator Laboratory, Batavia, IL) *Astrophysical Journal*, Part 1 (ISSN 0004-637X), vol. 326, March 1, 1988, p. 70-76. NSF-DOE-NASA-supported research. refs

This paper considers the scenario of a flat universe with a network of heavy cosmic strings as the primordial fluctuation spectrum. The joint probability of finding streaming velocities of at least 600 km/s on large scales and local peculiar velocities of less than 800 km/s is calculated. It is shown how the effects of loops breaking up and being born with a spectrum of sizes can be estimated. It is found that to obtain large-scale streaming velocities of at least 600 km/s, it is necessary that either a large value for β or $G\mu$ exist or the effect of loop fissioning and production details be considerable. C.D.

A88-31145* National Aeronautics and Space Administration. Lewis Research Center, Cleveland, OH.

PRIMORDIAL LITHIUM - NEW REACTION RATES, NEW ABUNDANCES, NEW CONSTRAINTS

LAWRENCE KAWANO, DAVID SCHRAMM (NASA/Fermilab Astrophysics Center, Batavia; Chicago, University, IL), and GARY STEIGMAN (Ohio State University, Columbus) *Astrophysical Journal*, Part 1 (ISSN 0004-637X), vol. 327, April 15, 1988, p. 750-754. NSF-DOE-NASA-supported research. refs

Newly measured nuclear reaction rates for $H-3(\alpha, \gamma)Li-7$ (higher than previous values) and $Li-7(p, \alpha)He-4$ (lower than previous values) are shown to increase the $Li-7$ yield from big band nucleosynthesis for lower baryon-to-photon ratio (less than about 4×10 to the 10th). Recent revisions in the $He-3(\alpha, \gamma)Be-7$ and the $D(p, \gamma)He-3$ rates enhance the high (greater than 4×10 to the 10th) $Li-7(Be)$ production. New, independent determinations of Li abundances in extreme population II stars are in excellent agreement with the work of Spites and give continued confidence in the use of $Li-7$ in big bang baryon density determinations. B.J.

A88-31163* Joint Inst. for Lab. Astrophysics, Boulder, CO.

MAGNETIC FIELDS INTERACTING WITH NONLINEAR COMPRESSIBLE CONVECTION

NEAL E. HULBURT and JURI TOOMRE (Joint Institute for Laboratory Astrophysics, Boulder, CO) *Astrophysical Journal*, Part 1 (ISSN 0004-637X), vol. 327, April 15, 1988, p. 920-932. refs
(Contract NSG-7511; NAGW-91; NSF ATM-83-02729; NAS3-31958)

Two-dimensional numerical simulations are used to study fully compressible convection in the presence of an imposed magnetic field. Highly nonlinear flows are considered that span multiple density scale heights. The convection tends to sweep the initially uniform vertical magnetic field into concentrated flux sheets with significant magnetic pressures. These flux sheets are partially evacuated, and effects of buoyancy and Lorentz forces there can serve to suppress motions. The flux sheets can be surrounded by a sheath of descending flow. If the imposed magnetic field is sufficiently strong, the convection can become oscillatory. The unstably stratified fluid layer has an initial density ratio (bottom to top of layer) of 11. Surveys of solutions at fixed Rayleigh number sample Chandrasekhar numbers from 1 to 1000 and magnetic Prandtl numbers from $1/16$ to 1. These nonlinear simulations utilize a two-dimensional numerical scheme based on a modified two-step Lax-Wendroff method. Author

A88-35586* National Aeronautics and Space Administration. Lewis Research Center, Cleveland, OH.

AXIONS FROM 1987A

MICHAEL S. TURNER (NASA/Fermilab Astrophysics Center, Batavia; Chicago, University, IL) *Physical Review Letters* (ISSN 0031-9007), vol. 60, May 2, 1988, p. 1797-1800. DOE-supported research. refs

The process of axion emission from SN 1987A by

nucleon-nucleon axion bremsstrahlung is investigated based on neutrino observations. The results indicate that the axion luminosity must be less than about 10 to the 53rd erg/s if: (1) axions couple very weakly (with an axion mass of less than about 0.75×10 to the -3rd); or (2) axions couple strongly enough to be trapped and radiated from an axion sphere with T sub a of less than about 8 MeV (with an axion mass of greater than about 2.2 eV). Axion trapping is found to occur for axion masses of greater than about 0.016 eV. R.R.

A88-39313* Stanford Univ., CA.

PRIMORDIAL ORIGIN OF NONTOPOLOGICAL SOLITONS

JOSHUA A. FRIEMAN (Stanford University, CA), GRACIELA B. GELMINI (International Centre for Theoretical Physics; Scuola Internazionale Superiore di Studi Avanzati, Trieste, Italy), MARCELO GLEISER, and EDWARD W. KOLB (NASA/Fermilab Astrophysics Center, Batavia, IL) *Physical Review Letters* (ISSN 0031-9007), vol. 60, May 23, 1988, p. 2101-2104. NASA-supported research. refs

(Contract DE-AC03-76SF-00515)

The formation of nontopological solitons in a second-order phase transition in the early universe is discussed. Ratios of dimensionless coupling constants in the Lagrangian determine their abundance and mass. For a large range of parameters, nontopological solitons can be cosmologically significant, contributing a significant fraction of the present mass density of the universe. Author

A88-39734* National Aeronautics and Space Administration. Lewis Research Center, Cleveland, OH.

COSMOLOGY AND PARTICLE PHYSICS

MICHAEL S. TURNER (NASA/Fermilab Astrophysics Center, Batavia; Chicago, University, IL) IN: The early universe; Proceedings of the NATO Advanced Study Institute, Victoria, Canada, Aug. 17-30, 1986. Dordrecht, D. Reidel Publishing Co., 1988, p. 19-113. DOE-supported research. refs

The interplay between cosmology and elementary particle physics is discussed. The standard cosmology is reviewed, concentrating on primordial nucleosynthesis and discussing how the standard cosmology has been used to place constraints on the properties of various particles. Baryogenesis is discussed, showing how a scenario in which the B-, C-, and CP-violating interactions in GUTs provide a dynamical explanation for the predominance of matter over antimatter and for the present baryon-to-photon ratio. It is shown how the very early dynamical evolution of a very weakly coupled scalar field which is initially displaced from the minimum of its potential may explain a handful of very fundamental cosmological facts which are not explained by the standard cosmology. C.D.

LUNAR AND PLANETARY EXPLORATION

Includes planetology; and manned and unmanned flights.

A88-22879* California Univ., Los Angeles.

VOIDS IN JOVIAN MAGNETOSPHERE REVISITED - EVIDENCE OF SPACECRAFT CHARGING

K. K. KHURANA, M. G. KIVELSON, R. J. WALKER (California, University, Los Angeles), and T. P. ARMSTRONG (Kansas, University, Lawrence) *Journal of Geophysical Research* (ISSN 0148-0227), vol. 92, Dec. 1, 1987, p. 13399-13408. refs
(Contract JPL-955232; NSG-7295; NSG-3290; NSF ATM-83-00523; NSF ATM-86-10858)

The Voyager 2 Plasma Science Instrument (PLS) measuring cold plasma number density observed about a dozen 'voids', lasting from a few minutes to 20 min, in the vicinity of the Ganymede-orbit crossing, when the low-energy ion and electron fluxes recorded fell to very low levels. Original interpretations associated these

'voids' with Ganymede wake effects. In the present study, the PLS data are reexamined, in conjunction with data from the magnetic field experiment and the low-energy charged particle (LECP) experiment. The LECP data showed that the PLS voids were accompanied by large enhancements of the flux of energetic electrons and ions, while the magnetic data exhibited no systematic signatures. It is suggested that increased energetic electron fluxes in the void regions intermittently charged the spacecraft negatively to values between a few kV and a few tens of kV, and that spacecraft charging could have produced dropouts in the measured cold ion and electron fluxes and enhancements in the measured fluxes of hot particles consistent with the observations. I.S.

N88-13209* # National Aeronautics and Space Administration. Lewis Research Center, Cleveland, OH.

SMALL REACTOR POWER SYSTEMS FOR MANNED PLANETARY SURFACE BASES

HARVEY S. BLOOMFIELD Dec. 1987 15 p
(NASA-TM-100223; E-3839; NAS 1.15:100223) Avail: NTIS HC A03/MF A01 CSCL 10B

A preliminary feasibility study of the potential application of small nuclear reactor space power systems to manned planetary surface base missions was conducted. The purpose of the study was to identify and assess the technology, performance, and safety issues associated with integration of reactor power systems with an evolutionary manned planetary surface exploration scenario. The requirements and characteristics of a variety of human-rated modular reactor power system configurations selected for a range of power levels from 25 kWe to hundreds of kilowatts is described. Trade-off analyses for reactor power systems utilizing both man-made and indigenous shielding materials are provided to examine performance, installation and operational safety feasibility issues. The results of this study have confirmed the preliminary feasibility of a wide variety of small reactor power plant configurations for growth oriented manned planetary surface exploration missions. The capability for power level growth with increasing manned presence, while maintaining safe radiation levels, was favorably assessed for nominal 25 to 100 kWe modular configurations. No feasibility limitations or technical barriers were identified and the use of both distance and indigenous planetary soil material for human rated radiation shielding were shown to be viable and attractive options. Author

N88-14054* # National Aeronautics and Space Administration. Lewis Research Center, Cleveland, OH.

SMALL SPACE REACTOR POWER SYSTEMS FOR UNMANNED SOLAR SYSTEM EXPLORATION MISSIONS

HARVEY S. BLOOMFIELD Dec. 1987 117 p
(NASA-TM-100228; E-3847; NAS 1.15:100228) Avail: NTIS HC A06/MF A01 CSCL 03B

A preliminary feasibility study of the application of small nuclear reactor space power systems to the Mariner Mark II Cassini spacecraft/mission was conducted. The purpose of the study was to identify and assess the technology and performance issues associated with the reactor power system/spacecraft/mission integration. The Cassini mission was selected because study of the Saturn system was identified as a high priority outer planet exploration objective. Reactor power systems applied to this mission were evaluated for two different uses. First, a very small 1 kWe reactor power system was used as an RTG replacement for the nominal spacecraft mission science payload power requirements while still retaining the spacecraft's usual bipropellant chemical propulsion system. The second use of reactor power involved the additional replacement of the chemical propulsion system with a small reactor power system and an electric propulsion system. The study also provides an examination of potential applications for the additional power available for scientific data collection. The reactor power system characteristics utilized in the study were based on a parametric mass model that was developed specifically for these low power applications. The model was generated following a neutronic safety and operational feasibility assessment of six small reactor concepts solicited from U.S.

industry. This assessment provided the validation of reactor safety for all mission phases and generated the reactor mass and dimensional data needed for the system mass model. Author

N88-28853* # National Aeronautics and Space Administration. Lewis Research Center, Cleveland, OH.

ENERGY STORAGE CONSIDERATIONS FOR A ROBOTIC MARS SURFACE SAMPLER

PATRICIA M. O'DONNELL, ROBERT L. CATALDO, and OLGA D. GONZALEZ-SANABRIA 1988 10 p Presented at Case for Mars 3, Boulder, Colo., 18-22 Jul. 1988; sponsored by American Astronautical Society, JPL, Los Alamos Lab., NASA, Ames Research Center, NASA, Lyndon B. Johnson Space Center, NASA, George C. Marshall Space Flight Center
(NASA-TM-100969; E-4259; NAS 1.15:100969) Avail: NTIS HC A02/MF A01 CSCL 03B

A Mars Rover capable of obtaining surface samples will need a power system for motive power and to power scientific instrumentation. Several different power systems are considered along with a discussion of the location options. The weight and volume advantages of the different systems are described for a particular power profile. The conclusions are that a Mars Rover Sample Return Mission and Extended Mission can be accomplished utilizing photovoltaics and electrochemical storage. Author

93

SPACE RADIATION

Includes cosmic radiation; and inner and outer earth's radiation belts.

A88-48463* National Aeronautics and Space Administration. Lewis Research Center, Cleveland, OH.

CALCULATIONS OF RATES FOR DIRECT DETECTION OF NEUTRALINO DARK MATTER

KIM GRIEST (NASA/Fermilab Astrophysics Center, Batavia; Chicago, University, IL) Physical Review Letters (ISSN 0031-9007), vol. 61, Aug. 8, 1988, p. 666-669. DOE-supported research. refs

The detection rates in cryogenic detectors of neutralinos, the most well motivated supersymmetric dark-matter candidate, are calculated. These rates can differ greatly from the special case of pure photinos and pure Higgsinos which are usually considered. In addition, a new term is found in the elastic-scattering cross section proportional to the Z-ino component which is 'spin independent', even for these Majorana particles. As a result, substantial detection rates exist for previously disfavored, mostly spinless materials such as germanium and mercury. Author

99

GENERAL

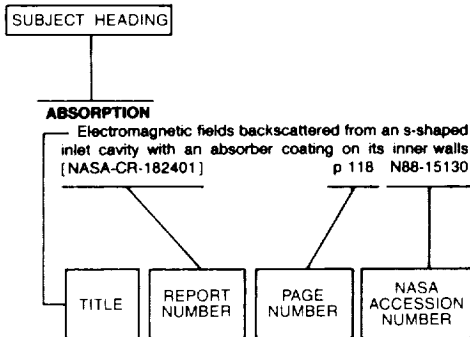
N88-22851* # National Aeronautics and Space Administration. Lewis Research Center, Cleveland, OH.

RESEARCH AND TECHNOLOGY Annual Report, 1987

1987 103 p
(NASA-TM-100172; E-3740; NAS 1.15:100172) Avail: NTIS HC A06/MF A01 CSCL 05A

The NASA Lewis Research Center's research and technology accomplishments for fiscal year 1987 are summarized. It comprises approximately 100 short articles submitted by staff members of the technical directorates and is organized into four sections: aeronautics, aerospace technology (which includes space communications), space station systems, and computational support. A table of contents by subject was developed to assist the reader in finding articles of special interest. Author

Typical Subject Index Listing



The subject heading is a key to the subject content of the document. Titles, report numbers, and accession numbers of pertinent documents are provided under each subject heading. When the title is insufficiently descriptive of the document content, a title extension has been added, separated from the title by three hyphens. The report number helps to indicate the type of document cited (e.g., NASA report, NASA translation, NASA contractor report). The NASA accession number is the number by which the document abstracts are arranged in this journal and by which the document is sold or requested. The titles, with title extensions if present, are arranged under each subject heading in ascending accession number order. The subject headings have been selected from the latest revision of the *NASA Thesaurus* (NASA SP-7064).

A

ABSORPTION

Electromagnetic fields backscattered from an s-shaped inlet cavity with an absorber coating on its inner walls [NASA-CR-182401] p 118 N88-15130

ABSORPTION SPECTRA

Guided-wave approaches to spectrally selective energy absorption [NASA-CR-182532] p 119 N88-17892

ABSTRACTS

Engine structures: A bibliography of Lewis Research Center's research for 1980-1987 [NASA-TM-100842] p 195 N88-24002
Bibliography of Lewis Research Center technical publications announced in 1987 [NASA-TM-100910] p 223 N88-28832

ABUNDANCE

Primordial lithium - New reaction rates, new abundances, new constraints p 226 A88-31145
Primordial origin of nontopological solitons p 226 A88-39313

AC GENERATORS

Study of free-piston Stirling engine driven linear alternators [NASA-CR-181425] p 170 N88-10355
The ac power system testbed [NASA-CR-175068] p 127 N88-11948
Computer-aided modeling and prediction of performance of the modified Lundell class of alternators in space station solar dynamic power systems [NASA-CR-182538] p 201 N88-19000

ACCELERATED LIFE TESTS

Effect of storage and LEO cycling on manufacturing technology IPV nickel-hydrogen cells p 53 A88-11917

ACCUMULATORS

Performance of a small, graphite electrode, multistage depressed collector with a 500-W, continuous wave, 4.8- to 9.6-GHz traveling wave tube [NASA-TP-2788] p 128 N88-15146

ACCURACY

Operating envelopes of particle sizing instrumentation used for icing research [AIAA PAPER 88-0291] p 157 A88-22211
Performance and operating envelope of imaging and scattering particle sizing instruments [NASA-CR-180859] p 161 N88-12042
Operating envelopes of particle sizing instrumentation used for icing research [NASA-CR-180870] p 161 N88-13573

ACEE PROGRAM

SR-7A aeroelastic model design report [NASA-CR-174791] p 36 N88-28928

ACETYLENE

Ethynylated aromatics as high temperature matrix resins [NASA-TM-89829] p 73 N88-18640

ACID BASE EQUILIBRIUM

Experimental studies in vortex pair motion coincident with a liquid reaction p 142 A88-46316

ACIDS

Wear of iron and nickel in corrosive liquid environments p 88 A88-40790
Wear of iron and nickel in corrosive liquid environments [NASA-TM-100246] p 91 N88-11817

ACOUSTIC DUCTS

A mapped finite difference study of noise propagation in nonuniform ducts with mean flow p 214 A88-18541

ACOUSTIC EMISSION

Materials analysis by ultrasonics: Metals, ceramics, composites --- Book p 176 A88-44853
Transply crack density detection by acousto-ultrasonics [NASA-TM-100224] p 72 N88-11758

ACOUSTIC EXCITATION

Effect of acoustic excitation on the flow over a low-Re airfoil p 3 A88-14459
Control of shear flows by artificial excitation [AIAA PAPER 87-2722] p 3 A88-16567
On the correlation of plume centerline velocity decay of turbulent acoustically excited jets p 3 A88-18654
Initial turbulence effect on jet evolution with and without tonal excitation [AIAA PAPER 87-2725] p 4 A88-20184
Computation of the velocity field of an excited shear layer p 138 A88-26206
Excitation of instability waves in free shear layers. I - Theory p 138 A88-26338
Excitation of instability waves in free shear layers. II - Experiments p 138 A88-26339
Controlled excitation of a cold turbulent swirling free jet [ASME PAPER 87-WA/NCA-18] p 140 A88-41568
A numerical investigation of the influence of heating on the excitation of high and low Mach number jet flows [ASME PAPER 87-WA/NCA-13] p 144 A88-51343
On the correlation of plume centerline velocity decay of turbulent acoustically excited jets [NASA-TM-100193] p 11 N88-16661
Acoustically excited heated jets. 1: Internal excitation [NASA-CR-4129-PT-1] p 12 N88-23751
Acoustically excited heated jets. 2: In search of a better understanding [NASA-CR-4129-PT-2] p 12 N88-23752
Acoustically excited heated jets. 3: Mean flow data [NASA-CR-4129-PT-3] p 12 N88-23753

ACOUSTIC FATIGUE

Acoustics technologies for STOVL aircraft [AIAA PAPER 88-2238] p 215 A88-35839
STOVL acoustic fatigue technologies [SAE PAPER 872360] p 215 A88-37221

ACOUSTIC LEVITATION

Program for the feasibility of developing a high pressure acoustic levitator [NASA-CR-182154] p 113 N88-26498

ACOUSTIC MEASUREMENT

Automated acoustic intensity measurements and the effect of gear tooth profile on noise p 168 A88-31623
Scale model acoustic testing of counterrotating fans [AIAA PAPER 88-2057] p 22 A88-37947

Combustion noise from gas turbine aircraft engines measurement of far-field levels p 215 A88-39708

ACOUSTIC MICROSCOPES

Imaging subtle microstructural variations in ceramics with precision ultrasonic velocity and attenuation measurements [NASA-TM-100129] p 177 N88-15257

ACOUSTIC VELOCITY

Universality relationships in condensed matter - Bulk modulus and sound velocity p 213 A88-43950

ACOUSTICS

Mixing fuel particles for space combustion research using acoustics p 112 A88-49093
A hybrid numerical technique for predicting the aerodynamic and acoustic fields of advanced turboprops [NASA-CR-174926] p 216 N88-12352
Mixing fuel particles for space combustion research using acoustics [NASA-TM-100295] p 43 N88-21186
Nondestructive evaluation by acousto-ultrasonics p 177 N88-22412
Flaw characterization in structural ceramics using scanning laser acoustic microscopy p 177 N88-22415
Nondestructive evaluation of sintered ceramics p 177 N88-22416
Acousto-ultrasonic input-output characterization of unidirectional fiber composite plate by P waves [NASA-CR-4162] p 180 N88-25923

ACRYLONITRILES

Differential scanning calorimetric survey of brominated PAN, pitch-based and vapor-grown fibers p 98 A88-32854

ACTIVATION ENERGY

Compressive creep behavior of alloys based on B2 FeAl p 82 A88-10043

ACTIVE CONTROL

Active control of transient rotordynamic vibration by optimal control methods [ASME PAPER 88-GT-73] p 208 A88-54202
Vibration and control of flexible rotor supported by magnetic bearings [NASA-TM-100888] p 174 N88-23977
Active phase compensation system for fiber optic holography [NASA-TM-101295] p 162 N88-26641

ACTS

Service offerings and interfaces for the ACTS network of earth stations [AIAA PAPER 88-0800] p 116 A88-27551
Progress in MMIC technology for satellite communications p 126 A88-37844
A laser communication experiment utilizing the ACT satellite and an airborne laser transceiver [NASA-TM-100792] p 164 N88-18910
Space communication link propagation data for selected cities within the multiple beam and steerable antenna coverage areas of the advanced communications technology satellite [NASA-TM-100861] p 120 N88-23070
Service offerings and interfaces for the ACTS network of Earth stations [NASA-TM-100809] p 46 N88-24663
Experiments applications guide: Advanced Communications Technology Satellite (ACTS) [NASA-TM-100265] p 49 N88-28082
A statistical rain attenuation prediction model with application to the advanced communication technology satellite project. 1: Theoretical development and application to yearly predictions for selected cities in the United States [NASA-CR-179498] p 121 N88-29077

ADAPTIVE CONTROL

An integrated approach to space station power system autonomous control p 52 A88-11853
Accurate positioning of long, flexible ARM's (Articulated Robotic Manipulator) p 174 N88-23243

ADDITIVES

Fatigue crack propagation of nickel-base superalloys at 650 deg C p 86 A88-35908

- Effect of high-temperature annealing on the microstructure and thermoelectric properties of GaP doped SiGe [NASA-TM-100164] p 101 N88-10188
- Slip casting and extruding shapes of rhemium with metal oxide additives. Part 2: Development of grain stabilized rhemium parts for resistojets [NASA-CR-180851] p 57 N88-11749
- ADHESION**
- Thermal desorption study of physical forces at the PTFE surface p 77 A88-10963
- Adherent Al₂O₃ scales produced on undoped NiCrAl alloys p 85 A88-30269
- The effect of sulfur and zirconium Co-doping on the oxidation of NiCrAl [NASA-TM-100209] p 90 N88-10940
- Adhesion, friction and micromechanical properties of ceramics [NASA-TM-100782] p 104 N88-17801
- Interfacial adhesion: Theory and experiment [NASA-TM-100830] p 92 N88-20417
- Development of a torsion balance for adhesion measurements [NASA-TM-100799] p 104 N88-20454
- Reducing adhesion and agglomeration within a cloud of combustible particles [NASA-TM-100902] p 114 N88-26539
- ADHESIVE BONDING**
- Some adhesion/cohesion characteristics of plasma-sprayed ZrO₂-Y₂O₃ under tensile loading p 95 A88-12589
- ADHESIVES**
- High temperature polymer matrix composites p 70 A88-36775
- ADIABATIC CONDITIONS**
- Adiabatic diesel engine component development: Reference engine for on-highway applications [NASA-CR-179531] p 224 N88-12428
- AERATION**
- Modified reaction mechanism of aerated n-dodecane liquid flowing over heated metal tubes p 108 A88-44268
- AEROACOUSTICS**
- Roles of initial condition and vortex pairing in jet noise p 213 A88-13963
- Aeroacoustics of subsonic turbulent shear flows [AIAA PAPER 87-2731] p 214 A88-16571
- A finite element model for wave propagation in an inhomogeneous material including experimental validation [AIAA PAPER 87-2741] p 212 A88-16577
- Noise of a model high speed counterrotation propeller at simulated takeoff/approach conditions (F7/A7) [AIAA PAPER 87-2657] p 214 A88-20176
- Aeroacoustics of advanced STOVL aircraft plumes [SAE PAPER 872358] p 215 A88-30998
- High-speed propeller noise predictions - Effects of boundary conditions used in blade loading calculations p 215 A88-36270
- Aeroacoustics of advanced STOVL aircraft plumes [SAE PAPER 872358] p 215 A88-37219
- Noise of a model high speed counterrotation propeller at simulated takeoff/approach conditions (F7/A7) [NASA-TM-100206] p 216 N88-10592
- AERODYNAMIC CHARACTERISTICS**
- A hybrid numerical technique for predicting the aerodynamic and acoustic fields of advanced turboprops [NASA-CR-174926] p 216 N88-12352
- AERODYNAMIC COEFFICIENTS**
- Experimental rotordynamic coefficient results for honeycomb seals [NASA-CR-182440] p 172 N88-16007
- AERODYNAMIC CONFIGURATIONS**
- Summary of low-speed wind tunnel results of several high-speed counterrotation propeller configurations [AIAA PAPER 88-3149] p 7 A88-48758
- In-flight measurement of airfoil icing using an array of ultrasonic transducers p 15 A88-50910
- Large-Scale Advanced Prop-Fan (LAP) blade design [NASA-CR-174790] p 27 N88-14097
- Summary of low-speed wind tunnel results of several high-speed counterrotation propeller configurations [NASA-TM-100945] p 13 N88-24597
- AERODYNAMIC DRAG**
- A preliminary design study of supersonic through-flow fan inlets [AIAA PAPER 88-3075] p 23 A88-53137
- Comparison of pressure distributions on model and full-scale NACA 64-621 airfoils with ailerons for wind turbine application [NASA-TM-100802] p 201 N88-21593
- AERODYNAMIC FORCES**
- Bladed disk assemblies; Proceedings of the Eleventh Biennial Conference on Mechanical Vibration and Noise, Boston, MA, Sept. 27-30, 1987 p 20 A88-31608
- Aerodynamically forced vibration analysis of turbomachines p 20 A88-31610
- Reduced order models for nonlinear aerodynamics p 11 N88-23248
- AERODYNAMIC HEATING**
- A numerical investigation of the influence of heating on the excitation of high and low Mach number jet flows [ASME PAPER 87-WA/NCA-13] p 144 A88-51343
- AERODYNAMIC INTERFERENCE**
- Porous wind tunnel corrections for counterrotation propeller testing [AIAA PAPER 88-2055] p 6 A88-44490
- Porous wind tunnel corrections for counterrotation propeller testing [NASA-TM-100873] p 11 N88-22019
- AERODYNAMIC LOADS**
- Application of a semi-analytical technique for sensitivity analysis of unsteady aerodynamic computations [AIAA PAPER 88-2377] p 6 A88-32314
- Testing of a one-bladed 30-meter-diameter rotor on the DOE/NASA Mod-O wind turbine [NASA-TM-100274] p 201 N88-19014
- The 2-D and 3-D time marching transonic potential flow method for propfans p 11 N88-23245
- AERODYNAMIC NOISE**
- A parametric study of mean loading effects on airfoil gust interaction noise [AIAA PAPER 87-2677] p 213 A88-16539
- Cruise noise of the 2/9 scale model of the Large-scale Advanced Propfan (LAP) propeller, SR-7A [AIAA PAPER 87-2717] p 214 A88-16565
- AERODYNAMIC STABILITY**
- Analysis and test evaluation of the dynamic response and stability of three advanced turboprop models at low forward speed [NASA-CR-175026] p 27 N88-14096
- AERODYNAMIC STALLING**
- Effect of spatial inlet temperature and pressure distortion on turbofan engine stability [AIAA PAPER 88-3016] p 22 A88-44727
- Effect of spatial inlet temperature and pressure distortion on turbofan engine stability [NASA-TM-100850] p 32 N88-21162
- Application of Navier-Stokes analysis to stall flutter E3 10C compressor test analysis of high-speed post-stall data [NASA-CR-179521] p 36 N88-28929
- AERODYNAMICS**
- Unsteady aerodynamics of an oscillating cascade in a compressible flow field [NASA-TM-100219] p 26 N88-13346
- Reduced order models for nonlinear aerodynamics p 11 N88-23248
- The effects of inlet turbulence and rotor/stator interactions on the aerodynamics and heat transfer of a large-scale rotating turbine model. Part 4: Aerodynamic data tabulation [NASA-CR-179469] p 153 N88-23956
- AEROELASTICITY**
- Application of structural tailoring to spar/shell turboprops [AIAA PAPER 88-2333] p 20 A88-32277
- Recent developments in flutter suppression techniques for turbomachinery rotors p 21 A88-35530
- Aeroelastic effects of alternate blade sweep on advanced propfan rotor [ASME PAPER 87-WA/AERO-8] p 184 A88-51328
- Flutter of a fan blade in supersonic axial flow [ASME PAPER 88-GT-78] p 8 A88-54206
- Vibration and flutter characteristics of the SR7L large-scale propfan [NASA-TM-100272] p 188 N88-18036
- Lewis Structures Technology, 1988. Volume 1: Structural Dynamics [NASA-CP-3003-VOL-1] p 194 N88-23226
- The 2-D and 3-D time marching transonic potential flow method for propfans p 11 N88-23245
- Aeroelastic forced response analysis of turbomachinery p 34 N88-23247
- Experimental investigation of propfan aeroelastic response in off-axis flow with mistuning [NASA-TM-101320] p 196 N88-28344
- SR-7A aeroelastic model design report [NASA-CR-174791] p 36 N88-28928
- Aeroelastic response of metallic and composite propfan models in yawed flow [NASA-TM-100964] p 37 N88-29807
- AERONAUTICAL ENGINEERING**
- A distributed data acquisition system for aeronautics test facilities p 39 A88-33065
- Impact and promise of NASA aeropropulsion technology p 31 N88-16698
- Research and technology [NASA-TM-100172] p 227 N88-22851
- AEROSOLS**
- Criteria for significance of simultaneous presence of both condensable vapors and aerosol particles on mass transfer (deposition) rates p 114 A88-10971
- Comparison of UNL laser imaging and sizing system and a phase/Doppler system for analyzing sprays from a NASA nozzle [NASA-CR-182437] p 150 N88-16956
- AEROSPACE ENGINEERING**
- Internal fluid mechanics research on supercomputers for aerospace propulsion systems [NASA-TM-100289] p 149 N88-15188
- Life and reliability of rotating disks p 178 N88-22428
- AEROSPACE ENVIRONMENTS**
- SP-100 Advanced Technology Program p 52 A88-11846
- Test results of a 60 volt bipolar nickel-hydrogen battery p 198 A88-11916
- Modelling and design of high efficiency radiation tolerant indium phosphide space solar cells p 200 A88-34394
- Tribological properties of polymer films and solid bodies in a vacuum environment p 98 A88-35565
- High temperature metal matrix composites for future aerospace systems [AIAA PAPER 88-3059] p 71 A88-44745
- High temperature metal matrix composites for future aerospace systems [NASA-TM-100212] p 90 N88-10938
- Low Earth orbit environmental effects on the space station photovoltaic power generation systems [NASA-TM-100230] p 225 N88-12429
- Oxidation and protection of fiberglass-epoxy composite nests for photovoltaic arrays in the low Earth orbital environment [NASA-TM-100839] p 104 N88-18734
- Study of industry requirements that can be fulfilled by combustion experimentation aboard space station [NASA-CR-180854] p 224 N88-19377
- Microgravity robotics technology program [NASA-TM-100698] p 173 N88-23219
- AEROSPACE PLANES**
- Heat transfer in aerospace propulsion [NASA-TM-100874] p 154 N88-23957
- AEROTHERMODYNAMICS**
- Hypersonic turbulent wall boundary layer computations [AIAA PAPER 88-2829] p 7 A88-44667
- NASA HOST project overview --- hot section technology p 24 A88-54138
- Assessment, development, and application of combustor aerothermal models p 24 A88-54140
- Review and assessment of the database and numerical modeling for turbine heat transfer p 24 A88-54141
- Aerothermal modeling program, phase 2 p 146 N88-11149
- HOST turbine heat transfer program summary [NASA-TM-100280] p 149 N88-14320
- Assessment, development and application of combustor aerothermal models [NASA-TM-100290] p 32 N88-19469
- Review and assessment of the HOST turbine heat transfer program p 34 N88-22431
- Experimental measurements of heat transfer from an iced surface during artificial and natural cloud icing conditions [AIAA-86-1352] p 153 N88-23718
- Impact of ETO propellants on the aerothermodynamic analyses of propulsion components [NASA-TM-101303] p 156 N88-30094
- AGGLOMERATION**
- Reducing adhesion and agglomeration within a cloud of combustible particles [NASA-TM-100902] p 114 N88-26539
- AGING (MATERIALS)**
- Fracture characteristics of angleplied laminates fabricated from overaged graphite/epoxy prepreg p 69 A88-16965
- Precipitation in a rapidly solidified and aged Ni-Al-Mo alloy p 82 A88-18528
- AGING (METALLURGY)**
- Thermal aging effects in refractory metal alloys p 84 A88-22700
- Lattice parameter variations during aging in nickel-base superalloys p 90 A88-51318
- Aging behavior of Au-based ohmic contacts to GaAs [NASA-CR-182146] p 130 N88-25831
- AILERONS**
- Comparison of pressure distributions on model and full-scale NACA 64-621 airfoils with ailerons for wind turbine application [NASA-TM-100802] p 201 N88-21593
- AIR**
- Fuel-injector/air-swirl characterization p 146 N88-11150
- Dilution jet mixing program, phase 3 p 147 N88-11153

SUBJECT INDEX

- Fuel-injector/air-swirl characterization
[NASA-CR-180864] p 27 N88-14985
- AIR BREATHING ENGINES**
Ground tests confirm the promise of hypersonic propulsion p 2 A88-10369
- AIR COOLING**
The design of an air-cooled metallic high temperature radial turbine
[AIAA PAPER 88-2872] p 22 A88-45011
- AIR FLOW**
Effect of rib angle on local heat/mass transfer distribution in a two-pass rib-roughened channel
[ASME PAPER 87-GT-94] p 131 A88-11033
- AIRCRAFT CARRIERS**
Multiple-Purpose Subsonic Naval Aircraft (MPSNA): Multiple Application Propfan Study (MAPS)
[NASA-CR-175104] p 18 N88-28917
- AIRCRAFT CONFIGURATIONS**
Retooling CFD for hypersonic aircraft p 1 A88-16749
- AIRCRAFT CONSTRUCTION MATERIALS**
Hypersonic structures and materials - A progress report p 17 A88-16748
High temperature polymer matrix composites p 70 A88-36775
STOVL acoustic fatigue technologies
[SAE PAPER 872360] p 215 A88-37221
- AIRCRAFT CONTROL**
Cooperative synthesis of control and display augmentation for a STOL aircraft in the approach and landing task
[AIAA PAPER 88-4182] p 37 A88-50272
Fiber optics for controls p 218 N88-15798
Rotorcraft flight-propulsion control integration: An eclectic design concept
[NASA-TP-2815] p 38 N88-19475
Overview of NASA research in fiber optics for aircraft controls
[NASA-TM-100919] p 35 N88-25458
Propfan test assessment testbed aircraft stability and control/performance 1/9-scale wind tunnel tests
[NASA-CR-182121] p 17 N88-26360
- AIRCRAFT DESIGN**
Ground tests confirm the promise of hypersonic propulsion p 2 A88-10369
Retooling CFD for hypersonic aircraft p 1 A88-16749
Flight propulsion control integration for V/STOL aircraft
[SAE PAPER 872330] p 21 A88-37199
Flight propulsion control integration for V/STOL aircraft
[NASA-TM-100226] p 38 N88-11680
The NASA aircraft icing research program p 15 N88-15803
Overview of NASA PTA propfan flight test program p 29 N88-15805
NASA's rotorcraft icing research program p 15 N88-16641
Rotorcraft flight-propulsion control integration p 38 N88-16643
- AIRCRAFT ENGINES**
Progress toward life modeling of thermal barrier coatings for aircraft gas turbine engines
[ASME PAPER 87-ICE-18] p 96 A88-15120
Results of NASA's Energy Efficient Engine Program p 19 A88-20785
Transient engine performance with water ingestion p 19 A88-27295
Parametric studies of advanced turboprops
[AIAA PAPER 88-2266] p 20 A88-32223
Control of rotor aerodynamically forced vibrations by splitters p 23 A88-52684
Toward improved durability in advanced aircraft engine hot sections: Proceedings of the Thirty-third ASME International Gas Turbine and Aeroengine Congress and Exposition, Amsterdam, Netherlands, June 5-9, 1988 p 24 A88-54137
NASA HOST project overview --- hot section technology p 24 A88-54138
Views on the impact of HOST --- hot section technology p 24 A88-54146
Development of heat flux sensors for turbine airfoils p 160 N88-11143
Technology developments for a compound cycle engine p 30 N88-16637
Small gas turbine engine technology p 30 N88-16638
Creep and fatigue research efforts on advanced materials p 187 N88-16701
Ceramic bearings for use in gas turbine engines
[NASA-TM-100288] p 172 N88-18007
Lewis Structures Technology, 1988. Volume 2: Structural Mechanics p 190 N88-22382

- Engine structures: A bibliography of Lewis Research Center's research for 1980-1987
[NASA-TM-100842] p 195 N88-24002
- AIRCRAFT EQUIPMENT**
Electro-impulse de-icing electrodynamic solution by discrete elements
[AIAA PAPER 88-0018] p 17 A88-22016
- AIRCRAFT FUELS**
Large-Scale Advanced Prop-Fan (LAP)
[NASA-CR-182112] p 32 N88-20306
- AIRCRAFT HAZARDS**
Model helicopter performance degradation with simulated ice shapes p 17 A88-22783
Measurement of ice thickness (icing) in aeronautics p 15 A88-32714
An experimental and theoretical study of the ice accretion process during artificial and natural icing conditions
[NASA-CR-182119] p 16 N88-21143
In-flight measurement of ice growth on an airfoil using an array of ultrasonic transducers
[AIAA-87-0178] p 16 N88-23717
Experimental measurements of heat transfer from an iced surface during artificial and natural cloud icing conditions
[AIAA-86-1352] p 153 N88-23718
- AIRCRAFT INSTRUMENTS**
Measurement of ice thickness (icing) in aeronautics p 15 A88-32714
- AIRCRAFT MANEUVERS**
Rotorcraft flight-propulsion control integration p 38 N88-16643
- AIRCRAFT NOISE**
Cruise noise of the 2/9 scale model of the Large-scale Advanced Propfan (LAP) propeller, SR-7A
[AIAA PAPER 87-2717] p 214 A88-16565
Noise of a model high speed counterrotation propeller at simulated takeoff/approach conditions (F7/A7)
[AIAA PAPER 87-2657] p 214 A88-20176
Aeroacoustics of advanced STOVL aircraft plumes
[SAE PAPER 872358] p 215 A88-30998
Combustion noise from gas turbine aircraft engines
[NASA-CR-180546] p 215 A88-39708
Noise of a model high speed counterrotation propeller at simulated takeoff/approach conditions (F7/A7)
[NASA-TM-100206] p 216 N88-10592
Identification and proposed control of helicopter transmission noise at the source p 38 N88-16647
- AIRCRAFT PARTS**
A heater made from graphite composite material for potential deicing application p 17 A88-15724
Lewis materials research and technology: An overview p 223 N88-16699
High temperature polymer matrix composites p 73 N88-16700
- AIRCRAFT PERFORMANCE**
Analytical determination of propeller performance degradation due to ice accretion p 19 A88-19669
Effects of environmentally imposed roughness on airfoil performance p 15 N88-15778
Directions in propulsion control p 28 N88-15799
Propfan test assessment testbed aircraft stability and control/performance 1/9-scale wind tunnel tests
[NASA-CR-182121] p 17 N88-26360
- AIRCRAFT SAFETY**
Ultrasonic techniques for aircraft ice accretion measurement
[AIAA PAPER 88-4656] p 18 A88-51910
Experimental evidence for modifying the current physical model for ice accretion on aircraft surfaces
[NASA-TM-87184] p 15 N88-12473
Theoretical analysis of the electrical aspects of the basic electro-impulse problem in aircraft de-icing applications
[NASA-CR-180845] p 15 N88-13310
A flow visualization study of the leading edge separation bubble on a NACA 0012 airfoil with simulated glaze ice
[NASA-CR-180846] p 10 N88-14966
- AIRCRAFT STABILITY**
Propfan test assessment testbed aircraft stability and control/performance 1/9-scale wind tunnel tests
[NASA-CR-182121] p 17 N88-26360
- AIRCRAFT STRUCTURES**
Hypersonic structures and materials - A progress report p 17 A88-16748
- AIRFOIL OSCILLATIONS**
A natural low frequency oscillation in the wake of an airfoil near stalling conditions
[AIAA PAPER 88-0131] p 4 A88-22093
A natural low frequency oscillation in the wake of an airfoil near stalling conditions p 9 N88-10779
- AIRFOILS**
Use of a liquid-crystal and heater-element composite for quantitative, high-resolution heat-transfer coefficients on a turbine airfoil including turbulence and surface-roughness effects p 156 A88-10969

ALGORITHMS

- Transition and separation control on a low-Reynolds number airfoil p 2 A88-11186
Effect of acoustic excitation on the flow over a low-Re airfoil p 3 A88-14459
A parametric study of mean loading effects on airfoil gust interaction noise
[AIAA PAPER 87-2677] p 213 A88-16539
The calculation of flow over iced airfoils
[AIAA PAPER 88-0112] p 4 A88-22078
Investigation of surface water behavior during glaze ice accretion p 14 A88-22079
Measurement of local convective heat transfer coefficients from a smooth and roughened NACA-0012 airfoil - Flight test data
[AIAA PAPER 88-0287] p 136 A88-22207
Experimental evaluation of corner vanes - Summary
[SAE PAPER 871784] p 39 A88-30778
In-flight measurement of airfoil icing using an array of ultrasonic transducers p 15 A88-50910
Current status and future trends in turbine application of thermal barrier coatings
[ASME PAPER 88-GT-286] p 169 A88-54355
Development of heat flux sensors for turbine airfoils p 160 N88-11143
Film cooling heat transfer on a turbine airfoil p 147 N88-11156
Measurement of airfoil heat transfer coefficients on a turbine stage p 147 N88-11158
Coolant passage heat transfer with rotation p 147 N88-11160
Thermal barrier coating life prediction model development p 171 N88-11185
Local heat/mass transfer and pressure drop in a two-pass rib-roughened channel for turbine airfoil cooling
[NASA-CR-179635] p 148 N88-12039
Measurement of local convective heat transfer coefficients from a smooth and roughened NACA-0012 airfoil: Flight test data
[NASA-TM-100284] p 149 N88-13552
A flow visualization study of the leading edge separation bubble on a NACA 0012 airfoil with simulated glaze ice
[NASA-CR-180546] p 10 N88-14966
An experimental mapping of the flow field behind a glaze ice shape on a NACA 0012 airfoil
[NASA-CR-180847] p 10 N88-15766
Effects of environmentally imposed roughness on airfoil performance p 15 N88-15778
Comparison of pressure distributions on model and full-scale NACA 64-621 airfoils with ailerons for wind turbine application
[NASA-TM-100802] p 201 N88-21593
Reduced order models for nonlinear aerodynamics p 11 N88-23248
Application of Navier-Stokes analysis to stall flutter p 38 N88-23249
In-flight measurement of ice growth on an airfoil using an array of ultrasonic transducers p 16 N88-23717
Thermal barrier coating life-prediction model development p 107 N88-28142
The effects of inlet turbulence and rotor/stator interactions on the aerodynamics and heat transfer of a large-scale rotating turbine model. Volume 3: Heat transfer data tabulation 65 percent axial spacing
[NASA-CR-179468] p 37 N88-28930
The effects of inlet turbulence and rotor/stator interactions on the aerodynamics and heat transfer of a large-scale rotating turbine model. Volume 2: Heat transfer data tabulation, 15 percent axial spacing
[NASA-CR-179467] p 37 N88-29804
- ALGORITHMS**
I-BIEM, an iterative boundary integral equation method for computer solutions of current distribution problems with complex boundaries: A new algorithm. I - Theoretical p 205 A88-27795
A Navier-Stokes solver using the LU-SSOR TVD algorithm p 6 A88-30560
An algorithm for a generalization of the Richardson extrapolation process p 209 A88-32840
Numerical arc segmentation algorithm for a radio conference-NASARC (version 2.0) technical manual
[NASA-TM-100160] p 118 N88-15910
Numerical arc segmentation algorithm for a radio conference-NASARC, version 2.0: User's manual
[NASA-TM-100161] p 119 N88-16928
Material parameter measurements at high temperatures p 80 N88-20397
Numerical arc segmentation algorithm for a radio conference: A software tool for communication satellite systems planning
[NASA-TM-100789] p 46 N88-22919
Parallel computer methods for eigenvalue extraction p 207 N88-23233

- Microgravity manipulator demonstration
p 173 N88-23242
- The solution of the Elrod algorithm for a dynamically loaded journal bearing using multigrid techniques
[NASA-TM-100941] p 154 N88-25854
- Applications of an exponential finite difference technique
[NASA-TM-100939] p 175 N88-28312
- ALIGNMENT**
- Optical alignment of Centaur's inertial guidance system
[NASA-TM-88844] p 43 N88-12515
- ALKALINE BATTERIES**
- Evaluation studies on carbon supported catalysts for oxygen reduction in alkaline medium p 77 A88-16643
- Alkaline fuel cell performance investigation
[NASA-TM-100937] p 81 N88-27267
- Regenerative fuel cell energy storage system for a low earth orbit space station
[NASA-CR-174802] p 204 N88-30184
- ALKYL COMPOUNDS**
- Surface catalytic degradation study of two linear perfluoropolyalkylethers at 345 C
[NASA-TP-2774] p 68 N88-12543
- Improved perfluoropolyether fluid development
[NASA-CR-180872] p 80 N88-15851
- ALKYLATION**
- Improved perfluoropolyether fluid development
p 68 A88-28624
- ALLOCATIONS**
- An allotment planning concept and related computer software for planning the fixed satellite service at the 1988 space WARC
[NASA-TM-100244] p 117 N88-11944
- Engineering calculations for the Delta S method of solving the orbital allotment problem
[NASA-CR-182372] p 42 N88-14110
- ALLOYING**
- On producing an alloy of uniform composition during rapid solidification processing p 89 A88-41654
- ALLOYS**
- Elevated temperature strain gages
p 160 N88-11144
- Creep fatigue life prediction for engine hot section materials (isotropic): Third year progress review
p 186 N88-11173
- Life prediction and constitutive models for engine hot section anisotropic materials program
p 186 N88-11175
- Effects of surface chemistry on hot corrosion life
p 91 N88-11180
- Bithermal fatigue: A simplified alternative to thermomechanical fatigue p 194 N88-22424
- Noncontact temperature measurement: Requirements and applications for metals and alloys research
p 112 N88-23899
- Solid-state combustion synthesis of ceramics and alloys in reduced gravity
[NASA-CR-4163] p 75 N88-25479
- Refractory metal alloys and composites for space power systems
[NASA-TM-100946] p 95 N88-27310
- ALTERNATING DIRECTION IMPLICIT METHODS**
- Effects of numerical dissipation on finite-volume solutions of compressible flow problems
[AIAA PAPER 88-0621] p 5 A88-22469
- ALTITUDE CONTROL**
- Magnetic emissions testing of the space station engineering model resistojet
[NASA-TM-100788] p 48 N88-17728
- ALTITUDE SIMULATION**
- Experimental evaluation of turning vane designs for high-speed and coupled fan-drive corners of 0.1-scale model of NASA Lewis Research Center's proposed altitude wind tunnel
[NASA-TP-2681] p 40 N88-17686
- Techniques utilized in the simulated altitude testing of a 2D-CD vectoring and reversing nozzle
[NASA-TM-100872] p 40 N88-25464
- ALTITUDE TESTS**
- Measured performance of the heat exchanger in the NASA icing research tunnel under severe icing and dry-air conditions
[NASA-TM-100116] p 171 N88-12796
- Techniques utilized in the simulated altitude testing of a 2D-CD vectoring and reversing nozzle
[NASA-TM-100872] p 40 N88-25464
- ALUMINIDES**
- Preliminary investigation of inertia friction welding B2 aluminides p 82 A88-14567
- B2 aluminides for high temperature applications
p 85 A88-31684
- SiC reinforced aluminide composites
p 70 A88-31687
- Powder processing of nickel and other aluminides by hot consolidation p 87 A88-37158
- ALUMINUM**
- High frequency GaAlAs modulator and photodetector for phased array antenna applications
[NASA-TM-101328] p 130 N88-30048
- ALUMINUM ALLOYS**
- Precipitation in a rapidly solidified and aged Ni-Al-Mo alloy p 82 A88-18528
- A thermodynamic prediction for microporosity formation in aluminum-rich Al-Cu alloys p 82 A88-18886
- Dynamic recrystallization and grain boundary migration in B2 FeAl p 83 A88-20269
- Interdiffusion in Ni-rich, Ni-Cr-Al alloys at 1100 and 1200 C. I - Diffusion paths and microstructures. II - Diffusion coefficients and predicted concentration profiles
p 84 A88-24485
- Predicting diffusion paths and interface motion in gamma/gamma + beta, Ni-Cr-Al diffusion couples
p 84 A88-24486
- Diffusional transport during the cyclic oxidation of gamma + beta, Ni-Cr-Al(Y, Zr) alloys
p 85 A88-28902
- The influence of grain size and composition on 1000 to 1400 K slow plastic flow properties of NiAl
p 85 A88-29098
- The microstructure and tensile properties of extruded melt-spun ribbons of iron-rich B2 FeAl
p 85 A88-31679
- B2 aluminides for high temperature applications
p 85 A88-31684
- Room temperature tensile ductility in powder processed B2 FeAl alloys p 85 A88-31694
- Powder processing of nickel and other aluminides by hot consolidation p 87 A88-37158
- Dispersion strengthened NiAl alloys produced by rapid solidification processing p 88 A88-40588
- Coating life prediction p 170 N88-11181
- Processing, physical metallurgy and creep of NiAl + Ta and NiAl + Nb alloys
[NASA-CR-182113] p 92 N88-21295
- ALUMINUM GALLIUM ARSENIDES**
- Microwave performance of an optically controlled AlGaAs/GaAs high electron mobility transistor and GaAs MESFET p 123 A88-24911
- Laser induced OMCVD growth of AlGaAs on GaAs
p 125 A88-34286
- A V-grooved AlGaAs/GaAs passivated pn junction
p 125 A88-34300
- Variable angle spectroscopic ellipsometry - Application to GaAs-AlGaAs multilayer homogeneity characterization
p 220 A88-40139
- Temperature stability of Al(x)Ga(1-x)As (x = 0-1) thermal oxide masks for selective-area epitaxy
p 221 A88-45858
- A high frequency GaAlAs travelling wave electro-optic modulator at 0.82 micrometers
[NASA-TM-100970] p 130 N88-28240
- ALUMINUM OXIDES**
- Glass properties in the yttria-alumina-silica system
p 96 A88-18361
- Strength characterization of yttria/alumina-doped sintered silicon nitride p 97 A88-26154
- Adherent Al₂O₃ scales produced on undoped NiCrAl alloys p 85 A88-30269
- The effect of texture on the crack growth resistance of alumina
[NASA-TM-100250] p 102 N88-14206
- Synthesis and characterization of high-T(sub c) screen-printed Y-Ba-Cu-O films on alumina
[NASA-TM-100860] p 222 N88-22805
- The high temperature creep deformation of Si₃N₄-6Y₂O₃-2Al₂O₃
[NASA-CR-183204] p 76 N88-28981
- AMMONIUM CHLORIDES**
- Channel formation in Pb-Sn, Pb-Sb, and Pb-Sn-Sb alloy ingots and comparison with the system NH₄Cl-H₂O
p 89 A88-46038
- AMORPHOUS MATERIALS**
- Ion beam deposition of amorphous carbon films with diamond like properties p 97 A88-20300
- Effect of high-temperature hydrogen exposure on sintered alpha-SiC p 97 A88-29714
- Study of Staebler-Wronsky degradation effect in a Si:H based P-I-N solar cells
[NASA-CR-182564] p 203 N88-25970
- AMORPHOUS SEMICONDUCTORS**
- Plasma deposition of amorphous hydrogenated carbon films on III-V semiconductors p 220 A88-32862
- AMPLIFICATION**
- Optoelectronic gain control of a microwave single stage GaAs MESFET amplifier
[NASA-CR-182201] p 131 N88-30055
- AMPLIFIER DESIGN**
- High-efficiency helical traveling-wave tube with dynamic velocity taper and advanced multistage depressed collector p 124 A88-32836
- AMPLIFIERS**
- Characterization of a 30-GHz IMPATT solid state amplifier
[NASA-TM-100876] p 120 N88-24847
- ANALYSIS (MATHEMATICS)**
- Aero/structural tailoring of engine blades (AERO/STAEBL)
[NASA-CR-180805] p 207 N88-21682
- ANEMOMETERS**
- Corona anemometry for qualitative measurement of reversing surface flow with application to separation control by external excitation p 133 A88-14143
- ANISOTROPIC PLATES**
- Acousto-ultrasonics as a monitor of material anisotropy p 176 A88-46828
- ANISOTROPY**
- Life prediction and constitutive models for engine hot section anisotropic materials program
p 186 N88-11175
- Anisotropic constitutive modeling for nickel-base single crystal superalloys
[NASA-CR-182157] p 95 N88-29961
- ANNEALING**
- Electrical resistivity (4K to 2100K) of annealed vapor growth carbon fibers p 96 A88-17214
- Rapid thermal annealing of indium phosphide compound semiconductors p 220 A88-26196
- Effect of high temperature annealing on the thermoelectric properties of GaP doped SiGe
p 220 A88-40796
- Effect of high-temperature annealing on the microstructure and thermoelectric properties of GaP doped SiGe
[NASA-TM-100164] p 101 N88-10188
- ANNULAR DUCTS**
- Entrance and exit region friction factor models for annular seal analysis
[NASA-CR-183084] p 175 N88-25921
- ANNULAR FLOW**
- Laser Doppler velocimeter measurement of annulus wall boundary layer development in a compressor rotor
[ASME PAPER 87-GT-251] p 132 A88-11133
- Theory versus experiment for the rotordynamic coefficients of labyrinth gas seals. II - A comparison to experiment p 167 A88-31536
- 3-D laser anemometer measurements in an annular seal
[ASME PAPER 88-GT-64] p 169 A88-54196
- ANNULI**
- Analysis of eccentric annular incompressible seals. I - A new solution using fast Fourier transforms for determining hydrodynamic force
[ASME PAPER 87-TRIB-52] p 166 A88-23308
- ANTENNA ARRAYS**
- Radiation characteristics of microstrip arrays with parasitic elements p 121 A88-10481
- Slotline fed microstrip antenna array modules
p 126 A88-44170
- Absolute gain measurement of microstrip antennas under mismatched conditions p 117 A88-47949
- Gain enhancement of microstrip antennas with overlaying parasitic directors p 117 A88-48653
- Compensation of reflector antenna surface distortion using an array feed
[NASA-TM-100286] p 119 N88-18805
- Case study of active array feed compensation with sidelobe control for reflector surface distortion
[NASA-TM-100287] p 120 N88-23073
- Active feed array compensation for reflector antenna surface distortions
[NASA-TM-100826] p 120 N88-25762
- Array trade-off study using multilayer parasitic subarrays
[NASA-TM-101321] p 121 N88-28222
- High frequency GaAlAs modulator and photodetector for phased array antenna applications
[NASA-TM-101328] p 130 N88-30048
- ANTENNA COMPONENTS**
- Features and applications of the integrated composites analyzer (ICAN) code p 74 N88-22391
- ANTENNA DESIGN**
- Crosspolarisation characteristics of rectangular patch antennas p 117 A88-47705
- Mechanical properties characterization of composite sandwich materials intended for space antenna applications
[NASA-TM-88893] p 71 N88-10121
- Optically interconnected phased arrays
[NASA-TM-100855] p 128 N88-21400
- A role for high frequency superconducting devices in free space power transmission systems
[NASA-TM-100971] p 130 N88-25830
- Experiments applications guide: Advanced Communications Technology Satellite (ACTS)
[NASA-TM-100265] p 49 N88-28082

ANTENNA FEEDS

- Compensation of reflector antenna surface distortion using an array feed [NASA-TM-100286] p 119 N88-18805
- Development of 20 GHz monolithic transmit modules [NASA-CR-182134] p 222 N88-24539
- Active feed array compensation for reflector antenna surface distortions [NASA-TM-100826] p 120 N88-25762

ANTENNA RADIATION PATTERNS

- Characteristics of a two-layer electromagnetically coupled rectangular patch antenna p 115 A88-14100
- A simple circular-polarized antenna: Circular waveguide horn coated with lossy magnetic material p 116 A88-36648
- Gain enhancement of microstrip antennas with overlying parasitic directors p 117 A88-48653
- Active feed array compensation for reflector antenna surface distortions [NASA-TM-100826] p 120 N88-25762
- Analytical approximation of a distorted reflector surface defined by a discrete set of points [NASA-TM-101323] p 121 N88-27424

ANTENNAS

- System architecture of MMIC-based large aperture arrays for space applications p 45 A88-35274
- Optically controlled phased-array antenna technology for space communication systems [NASA-TM-100852] p 119 N88-18809
- Optical RF distribution links for MMIC phased array antennas [NASA-TM-100841] p 128 N88-20555
- Optically interconnected phased arrays [NASA-TM-100855] p 128 N88-21400

ANTIMISSILE DEFENSE

- Comparative analysis of the space power architecture studies [NASA-TM-100977] p 66 N88-28090

ANTIREFLECTION COATINGS

- Solar dynamic concentrator durability in atomic oxygen and micrometeoroid environments p 68 A88-51393
- Atomic-oxygen durability of impact-damaged solar reflectors p 68 A88-54988

APPLICATIONS PROGRAMS (COMPUTERS)

- Use of a liquid-crystal and heater-element composite for quantitative, high-resolution heat-transfer coefficients on a turbine airfoil including turbulence and surface-roughness effects p 156 A88-10969
- Application of advanced computational codes in the design of an experiment for a supersonic throughflow fan rotor

- [ASME PAPER 87-GT-160] p 2 A88-11072
- Calibration and comparison of the NASA Lewis free-piston Stirling engine model predictions with RE-1000 test data p 165 A88-11967
- A numerical study of the effects of curvature and convergence on dilution jet mixing [AIAA PAPER 87-1953] p 137 A88-23312
- RE-1000 free-piston Stirling engine hydraulic output system description [NASA-TM-100185] p 223 N88-10700

- A hybrid numerical technique for predicting the aerodynamic and acoustic fields of advanced turboprops [NASA-CR-174926] p 216 N88-12352
- A numerical study of the effects of curvature and convergence on dilution jet mixing [NASA-TM-89878] p 26 N88-13347

- Numerical modeling of multidimensional flow in seals and bearings used in rotating machinery [NASA-TM-100779] p 150 N88-16988
- Vibration and flutter characteristics of the SR7L large-scale propfan [NASA-TM-100272] p 188 N88-18036

- Monolithic ceramic analysis using the SCARE program p 105 N88-22409
- Continuous fiber ceramic matrix composites for heat engine components p 106 N88-22411

- Numerical arc segmentation algorithm for a radio conference: A software tool for communication satellite systems planning [NASA-TM-100789] p 46 N88-22919

- Two-equation low-Reynolds-number turbulence modeling of transitional boundary layer flows characteristic of gas turbine blades [NASA-CR-4145] p 153 N88-23185

- Improved method for stress and compatibility analysis of multicomponent rotating systems [NASA-TM-100884] p 195 N88-25935

APPROACH

- Noise of a model high speed counterrotation propeller at simulated takeoff/approach conditions (F7/A7) [AIAA PAPER 87-2657] p 214 A88-20176

- Noise of a model high speed counterrotation propeller at simulated takeoff/approach conditions (F7/A7) [NASA-TM-100206] p 216 N88-10592

APPROACH INDICATORS

- Cooperative synthesis of control and display augmentation for a STOL aircraft in the approach and landing task [AIAA PAPER 88-4182] p 37 A88-50272

APPROXIMATION

- Approximate polynomial preconditioning applied to biharmonic equations on vector supercomputers [NASA-TM-100217] p 210 N88-10563
- Analytical approximation of a distorted reflector surface defined by a discrete set of points [NASA-TM-101323] p 121 N88-27424

AQUEOUS SOLUTIONS

- Chemical durability of high-temperature superconductor YBa₂Cu₃O_{7-x} in aqueous environments p 78 A88-25023

ARC DISCHARGES

- Threshold-determining mechanisms for discharges in high-voltage solar arrays p 50 A88-11738

ARC JET ENGINES

- Evaluation of the communications impact of a low power arcjet thruster [AIAA PAPER 88-3105] p 55 A88-48755
- An extended life and performance test of a low-power arcjet [AIAA PAPER 88-3106] p 55 A88-48756

- A low-power arcjet cyclic lifetest [NASA-TM-100233] p 57 N88-11748
- Arcjet thruster research and technology [NASA-CR-180865] p 59 N88-17732

- An experimental investigation of an arcjet thruster exhaust using Langmuir probes [NASA-TM-100258] p 60 N88-21253
- Arcjet thruster research and technology, phase 1 [NASA-CR-182107] p 62 N88-23830

- Electric propulsion options for the SP-100 reference mission p 62 N88-24296
- Status of high power electric propulsion technology p 63 N88-24443

- Evaluation of the communications impact of a low power arcjet thruster [NASA-TM-100926] p 63 N88-24682

- An extended life and performance test of a low-power arcjet [NASA-TM-100942] p 63 N88-24687
- Arcjet power supply and start circuit [NASA-CASE-LEW-14374-1] p 41 N88-28939

- Performance and lifetime assessment of MPD arc thruster technology [NASA-TM-101293] p 66 N88-29860

ARC SPRAYING

- Composite monolayer fabrication by an arc-spray process p 169 A88-53581

ARCHITECTURE

- System architecture of MMIC-based large aperture arrays for space applications p 45 A88-35274
- Comparative analysis of the space power architecture studies [NASA-TM-100977] p 66 N88-28090

ARCHITECTURE (COMPUTERS)

- Advanced satellite system architecture for VSATs with ISDN compatibility [AIAA PAPER 88-0870] p 116 A88-27604
- Parallel computer methods for eigenvalue extraction p 207 N88-23233

- Microgravity manipulator demonstration p 173 N88-23242

ARCS

- Numerical arc segmentation algorithm for a radio conference: A software tool for communication satellite systems planning [NASA-TM-100789] p 46 N88-22919

ARITHMETIC

- Implementation of a digital optical matrix-vector multiplier using a holographic look-up table and residue arithmetic [NASA-CR-180431] p 205 N88-10496

ARITHMETIC AND LOGIC UNITS

- Implementation of a fast digital optical matrix-vector multiplier using a holographic look-up table and residue arithmetic p 205 A88-17223

AROMATIC COMPOUNDS

- Ethynylated aromatics as high temperature matrix resins [NASA-TM-89829] p 73 N88-18640

ARRAYS

- Performance characteristics of a combination solar photovoltaic heat engine energy converter p 197 A88-11813
- Macrocrack interaction with transverse array of microcracks p 181 A88-30236

ARTIFICIAL INTELLIGENCE

- Directions in propulsion control p 28 N88-15799
- The development of an intelligent interface to a computational fluid dynamics flow-solver code [NASA-TM-100908] p 207 N88-26127

ASPECT RATIO

- High Rayleigh number convection in rectangular enclosures with differentially heated vertical walls and aspect ratios between zero and unity [NASA-TM-100277] p 151 N88-19739

ASSEMBLING

- Space station assembly/servicing capabilities p 48 N88-10100

ASTIGMATISM

- Zoom lens compensator for a cylindrical window in laser anemometer uses p 217 A88-17221

ASYMPTOTIC PROPERTIES

- Nonlinear roll-up of externally excited free shear layers p 141 A88-44445

ATMOSPHERES

- The effects of atmosphere on the tribological properties of a chromium carbide based coating for use to 760 C p 98 A88-32372

ATMOSPHERIC ATTENUATION

- Space communication link propagation data for selected cities within the multiple beam and steerable antenna coverage areas of the advanced communications technology satellite [NASA-TM-100861] p 120 N88-23070

ATMOSPHERIC COMPOSITION

- Spacecraft Fire Safety [NASA-CP-2476] p 45 N88-12520

ATMOSPHERIC PRESSURE

- Direct mass spectrometric identification of silicon oxychloride compounds p 78 A88-44425

ATOMIC WEIGHTS

- Diamond like carbon coatings: Categorization by atomic number density [NASA-CR-174895] p 108 N88-28151

ATOMIZERS

- Spray characteristics of a spill-return airblast atomizer [ASME PAPER 88-GT-7] p 145 A88-54154

ATOMIZING

- Small-droplet spray measurements with a scattered-light scanner [NASA-TM-100973] p 163 N88-26645

ATS 6

- Record charging events from Applied Technology Satellite 6 p 46 A88-11737

ATTACK AIRCRAFT

- NASA supersonic STOVL propulsion technology program [SAE PAPER 872352] p 21 A88-37215
- NASA supersonic STOVL propulsion technology program [NASA-TM-100227] p 26 N88-14093

ATTENUATION

- Ultrasonic evaluation of mechanical properties of thick, multilayered, filament-wound composites p 176 A88-21340

- A statistical rain attenuation prediction model with application to the advanced communication technology satellite project. Part 2: Theoretical development of a dynamic model and application to rain fade durations and tolerable control delays for fade countermeasures [NASA-TM-100242] p 118 N88-11945

- A statistical rain attenuation prediction model with application to the advanced communication technology satellite project. 1: Theoretical development and application to yearly predictions for selected cities in the United States [NASA-CR-179498] p 121 N88-29077

ATTENUATION COEFFICIENTS

- Modal attenuation in multilayered coated waveguides p 126 A88-45755

AUDIO FREQUENCIES

- Complementary satellite sound broadcasting systems: A NASA assessment for the Voice of America [NASA-TM-100300] p 119 N88-17899

AUGMENTATION

- Saturation and the limit of jet mixing enhancement by single frequency plane wave excitation - Experiment and theory [AIAA PAPER 88-3613] p 8 A88-48899

- Saturation and the limit of jet mixing enhancement by single frequency plane wave excitation: Experiment and theory [NASA-TM-100882] p 12 N88-23732

AUTOCULAVES

- The 700 F properties of autoclave cured PMR-2 composites [NASA-TM-100923] p 75 N88-24712

AUTOMATIC CONTROL

- An integrated approach to space station power system autonomous control p 52 A88-11853
- LERC power system autonomy program 1990 demonstration p 52 A88-11861

- Automating the parallel processing of fluid and structural dynamics calculations p 206 A88-46963
- Automated design of controlled diffusion blades [NASA-TM-100251] p 9 N88-13304

- Spray automated balancing of rotors: Methods and materials
[NASA-CR-182151] p 41 N88-29825
- AUTOMATIC GAIN CONTROL**
Two stage dual gate MESFET monolithic gain control amplifier for Ka-band p 124 A88-29821
- AUTOMATION**
A systems engineering approach to automated failure cause diagnosis in space power systems p 52 A88-11870
- AUTOMOBILE ENGINES**
Automotive Stirling engine development program - A success p 185 A88-11965
Alloy chemistry and microstructural control to meet the demands of the automotive Stirling engine p 88 A88-40332
Shear rheological characterization of motor oils p 100 A88-47562
Automotive Stirling engine: Mod 2 design report [NASA-CR-175106] p 223 N88-11578
Hot piston ring tests [NASA-TM-100256] p 201 N88-14486
Advanced Gas Turbine (AGT) Technology Development Project, ceramic component developments [NASA-CR-180871] p 224 N88-20229
Advanced Gas Turbine (AGT) technology development project [NASA-CR-180891] p 225 N88-20230
Phase 1 results from the Stirling-powered vehicle project [NASA-TM-100978] p 225 N88-27980
Testing of a variable-stroke Stirling engine [NASA-TM-100899] p 225 N88-30472
- AUXILIARY PROPULSION**
An 8-cm ion thruster characterization [NASA-CR-180819] p 56 N88-10106
Auxiliary propulsion system flight package [NASA-CR-180828] p 56 N88-10886
Auxiliary propulsion technology for advanced Earth-to-orbit vehicles [NASA-TM-100237] p 58 N88-14127
Component data base for space station resistojet auxiliary propulsion [NASA-CR-180834] p 59 N88-17731
A cyclic ground test of an ion auxiliary propulsion system: Description and operational considerations [NASA-TM-100870] p 62 N88-23829
Successful completion of a cyclic ground test of a mercury ion auxiliary propulsion system [NASA-TM-101351] p 67 N88-29873
- AVALANCHE DIODES**
Microwave and millimeter-wave power generation in silicon carbide avalanche devices p 126 A88-47599
Characterization of a 30-GHz IMPATT solid state amplifier [NASA-TM-100876] p 120 N88-24847
- AVIONICS**
Fiber optics for advanced aircraft [NASA-TM-101294] p 1 N88-26328
- AXIAL FLOW**
Measurements of the unsteady flow field within the stator row of a transonic axial-flow fan. I - Measurement and analysis technique [ASME PAPER 87-GT-226] p 4 A88-18660
Numerical and analytical study of fluid dynamic forces in seals and bearings p 167 A88-31534
Flutter of a fan blade in supersonic axial flow [ASME PAPER 88-GT-78] p 8 A88-54206
Experimental investigation of propan aerelastic response in off-axis flow with mistuning [NASA-TM-101320] p 196 N88-28344
- AXIAL FLOW TURBINES**
Measurements of the unsteady flow field within the stator row of a transonic axial-flow fan. II - Results and discussion [ASME PAPER 87-GT-227] p 4 A88-18661
Experimental vibration damping characteristics of the third-stage rotor of a three-stage transonic axial-flow compressor [AIAA PAPER 88-3229] p 23 A88-48759
Experimental vibration damping characteristics of the third-stage rotor of a three-stage transonic axial-flow compressor [NASA-TM-100948] p 35 N88-24642
- AXISYMMETRIC FLOW**
Initial turbulence effect on jet evolution with and without tonal excitation [AIAA PAPER 87-2725] p 4 A88-20184
Saturation and the limit of jet mixing enhancement by single frequency plane wave excitation - Experiment and theory [AIAA PAPER 88-3613] p 8 A88-48899
Initial conditional effect on pressure waves in an axisymmetric jet [AIAA PAPER 88-3702] p 143 A88-48915

- A computational analysis of under-expanded jets in the hypersonic regime [AIAA PAPER 88-4361] p 8 A88-50604
Numerical simulation of axisymmetric turbulent flow in combustors and diffusers [NASA-CR-4115] p 11 N88-17582
Initial condition effect on pressure waves in an axisymmetric jet [NASA-TM-100915] p 153 N88-23184
Saturation and the limit of jet mixing enhancement by single frequency plane wave excitation: Experiment and theory [NASA-TM-100882] p 12 N88-23732
- AZIMUTH**
Optical alignment of Centaur's inertial guidance system [NASA-TM-88844] p 43 N88-12515

B

- BACKSCATTERING**
Electromagnetic fields backscattered from an s-shaped inlet cavity with an absorber coating on its inner walls [NASA-CR-182401] p 118 N88-15130
- BACKWARD FACING STEPS**
The structure and dynamics of reacting plane mixing layers p 136 A88-20871
Investigation of third-order closure model of turbulence for the computation of incompressible flows in a channel with a backward-facing step p 136 A88-21273
- BACKWARD WAVE TUBES**
Submillimeter backward wave oscillators p 122 A88-19659
- BALANCE**
Development of a torsion balance for adhesion measurements [NASA-TM-100799] p 104 N88-20454
- BALANCING**
Spray automated balancing of rotors: Methods and materials [NASA-CR-182151] p 41 N88-29825
- BALL BEARINGS**
Oil film thickness measurement and analysis for an angular contact ball bearing operating in parched elastohydrodynamic lubrication p 165 A88-14115
Parched elastohydrodynamic lubrication film thickness measurement in an instrument ball bearing [STLE PREPRINT 88-AM-6G-1] p 169 A88-51082
- BALLISTICS**
Contact force history and dynamic response due to the impact of a soft projectile [NASA-TM-100961] p 175 N88-26679
- BARIUM**
Synthesis and characterization of high-T(sub c) screen-printed Y-Ba-Cu-O films on alumina [NASA-TM-100860] p 222 N88-22805
- BARIUM OXIDES**
Weak-field magnetization of superconducting Y1Ba2Cu3O(x) - Relationship to microstructure p 219 A88-18814
Advantages of barium peroxide in the powder synthesis of perovskite superconductors p 221 A88-41496
- BARIUM TITANATES**
High Tc screen-printed YBa2Cu3O(7-x) films - Effect of the substrate material p 127 A88-49760
- BARRIER LAYERS**
Containment of a silicone fluid free surface in reduced gravity using barrier coatings [NASA-TM-101314] p 155 N88-30072
- BEACONS**
COSPAS/SARSAT 406-MHz emergency beacon digital controller [NASA-TM-100859] p 121 N88-26566
- BEAM CURRENTS**
Electron beam experiments at high altitudes p 47 A88-46799
A millimeter-wave tunnel Ladder TWT [NASA-CR-182184] p 130 N88-28239
- BEAM INJECTION**
A re-examination of spent beam refocusing for high-efficiency helix TWT's and small MDC's p 124 A88-28673
- BEAM SPLITTERS**
Modulated-splitting-ratio fiber-optic temperature sensor [NASA-TM-101332] p 18 N88-28062
- BEAM WAVEGUIDES**
A millimeter-wave tunnel Ladder TWT [NASA-CR-182184] p 130 N88-28239
- BEARINGLESS ROTORS**
Design, manufacture and spin test of high contact ratio helicopter transmission utilizing Self-Aligning Bearingless Planetary (SABP) [NASA-CR-4155] p 174 N88-24975

BEARINGS

- Active control of transient rotordynamic vibration by optimal control methods [ASME PAPER 88-GT-73] p 208 A88-54202
Coatings for high-temperature bearings and seals [NASA-TM-100249] p 102 N88-13453
Results of NASA/Army transmission research p 31 N88-16640
Self-lubricating coatings for high-temperature applications p 103 N88-16703
Numerical modeling of multidimensional flow in seals and bearings used in rotating machinery [NASA-TM-100779] p 150 N88-16988
Numerical and analytical study of fluid dynamic forces in seals and bearings [NASA-TM-100268] p 151 N88-18867
Computer-aided design analysis of 57-mm, angular-contact, cryogenic turbopump bearings [NASA-TP-2816] p 172 N88-18933
Mode 2 fracture mechanics p 193 N88-22418
- BEND TESTS**
Effects of subcritical crack growth on fracture toughness of ceramics assessed in chevron-notched three-point bend tests [ASME PAPER 88-GT-185] p 185 A88-54276
- BENDING**
An efficient Mindlin finite strip plate element based on assumed strain distribution p 192 N88-22407
Improved finite strip Mindlin plate bending element using assumed shear strain distributions [NASA-TM-100928] p 196 N88-29195
- BENDING MOMENTS**
Design and development of ceramic components [AIAA PAPER 88-3054] p 168 A88-44742
- BENZENE**
Detailed mechanism of benzene oxidation [NASA-TM-100202] p 79 N88-11775
Detailed mechanism of toluene oxidation and comparison with benzene [NASA-TM-100261] p 79 N88-13428
- BIBLIOGRAPHIES**
Spacecraft fire detection and extinguishment: A bibliography [NASA-CR-180880] p 45 N88-18612
Engine structures: A bibliography of Lewis Research Center's research for 1980-1987 [NASA-TM-100842] p 195 N88-24002
Bibliography of Lewis Research Center technical publications announced in 1987 [NASA-TM-100910] p 223 N88-28832
- BIDIRECTIONAL REFLECTANCE**
Comparison of the bidirectional reflectance distribution function of various surfaces [NASA-TM-101317] p 218 N88-28760
- BIG BANG COSMOLOGY**
Cosmology and particle physics p 226 A88-39734
- BIHARMONIC EQUATIONS**
Approximate polynomial preconditioning applied to biharmonic equations on vector supercomputers [NASA-TM-100217] p 210 N88-10563
- BINARY ALLOYS**
Compressive creep behavior of alloys based on B2 FeAl p 82 A88-10043
Dendritic growth in a supercooled alloy melt p 83 A88-19966
Primary arm spacing in chill block melt spun Ni-Mo alloys p 89 A88-41655
Double-diffusive effects during solidification p 221 A88-43933
Channel formation in Pb-Sn, Pb-Sb, and Pb-Sn-Sb alloy ingots and comparison with the system NH4Cl-H2O p 89 A88-46038
- BINARY FLUIDS**
Critical exponent for the viscosity of four binary liquids p 222 A88-53050
- BIPOLAR TRANSISTORS**
Neutron effects on the electrical and switching characteristics of NPN bipolar power transistors p 129 N88-24463
- BIPOLARITY**
Component variations and their effects on bipolar nickel-hydrogen cell performance p 197 A88-11914
Small scale bipolar nickel-hydrogen testing [NASA-TM-100936] p 202 N88-25059
- BIT ERROR RATE**
Bit-error-rate testing of high-power 30-GHz traveling-wave tubes for ground-terminal applications p 122 A88-19781
Spread-spectrum multiple access using wideband noncoherent MFSK p 115 A88-26672
The bit-error rate performance of a satellite microwave matrix switch [AIAA PAPER 88-0826] p 123 A88-27572
The bit-error rate performance of a satellite microwave matrix switch [NASA-TM-100285] p 46 N88-22920

BLADE TIPS

- Experimental investigation of the performance of a supersonic compressor cascade [ASME PAPER 88-GT-306] p 9 A88-54375
- Heat transfer in the tip region of a rotor blade simulator p 147 N88-11159
- Recent advances in capacitance type of blade tip clearance measurements [NASA-TM-101291] p 35 N88-25460

BLADES

- A multistage mesh generator for solving the average-passage equation system [NASA-CR-179539] p 10 N88-15769
- Vibration and flutter characteristics of the SR7L large-scale propfan [NASA-TM-100272] p 188 N88-18036

BLASIUS FLOW

- Higher eigenmodes in the Blasius boundary-layer stability problem p 134 A88-16352

BLOWDOWN WIND TUNNELS

- An isentropic compression heated Ludwig tube transient wind tunnel [AIAA PAPER 88-2019] p 40 A88-37926

BLUFF BODIES

- Experiments on spray interactions in the wake of a bluff body [ASME PAPER 87-GT-48] p 131 A88-11000

BODIES OF REVOLUTION

- Similar solutions for viscous hypersonic flow over a slender three-fourths-power body of revolution [NASA-TM-100205] p 148 N88-12752

BODY CENTERED CUBIC LATTICES

- Predicting diffusion paths and interface motion in gamma/gamma + beta, Ni-Cr-Al diffusion couples p 84 A88-24486
- Lattice defects in beta-SiC grown epitaxially on silicon substrates p 220 A88-28711
- Microscopy of epitaxially grown beta-SiC on 001-plane silicon p 98 A88-31023

BOLTED JOINTS

- Simplified procedures for designing composite bolted joints [NASA-TM-100281] p 73 N88-15020

BONDING

- Interfacial adhesion: Theory and experiment [NASA-TM-100830] p 92 N88-20417

BORON CARBIDES

- Electrical properties of materials for elevated temperature resistance strain gage application [NASA-CR-182214] p 164 N88-30106

BORON NITRIDES

- Mechanical strength and tribological behavior of ion-beam-deposited boron nitride films on non-metallic substrates p 98 A88-32866
- Boron nitride - Composition, optical properties, and mechanical behavior p 99 A88-40794

BOSONS

- Axions from 1987A p 226 A88-35586

BOUNDARY ELEMENT METHOD

- Time-domain transient elastodynamic analysis of 3-D solids by BEM p 183 A88-48638
- A new boundary element formulation for two- and three-dimensional thermoelasticity using particular integrals p 184 A88-53088
- A new BEM formulation for two- and three-dimensional elastoplasticity using particular integrals p 184 A88-53089

BOUNDARY INTEGRAL METHOD

- I-BIEM, an iterative boundary integral equation method for computer solutions of current distribution problems with complex boundaries: A new algorithm. I - Theoretical p 205 A88-27795
- Analysis of crack propagation in roller bearings using the boundary integral equation method - A mixed-mode loading problem p 168 A88-49183

BOUNDARY LAYER FLOW

- Measurements of the turbulent transport of heat and momentum in convexly curved boundary layers - Effects of curvature, recovery and free-stream turbulence [ASME PAPER 87-GT-199] p 131 A88-11103
- Laser Doppler velocimeter measurement of annulus wall boundary layer development in a compressor rotor [ASME PAPER 87-GT-251] p 132 A88-11133
- Higher eigenmodes in the Blasius boundary-layer stability problem p 134 A88-16352
- A model of the wall boundary layer for ducted propellers [AIAA PAPER 87-2742] p 214 A88-16578
- Roll-up of vorticity in adverse-pressure-gradient boundary layers p 135 A88-19194
- Glancing shock wave-turbulent boundary layer interaction with boundary layer suction [AIAA PAPER 88-0308] p 6 A88-27718

Boundary layer development as a function of chamber pressure in the NASA Lewis 1030:1 area ratio rocket nozzle [AIAA PAPER 88-3301] p 144 A88-50786

- Two-equation low-Reynolds-number turbulence modeling of transitional boundary layer flows characteristic of gas turbine blades [NASA-CR-4145] p 153 N88-23185
- Hypersonic turbulent wall boundary layer computations [NASA-CR-182147] p 154 N88-24917
- Correlations of velocity and temperature fluctuations in the stagnation-point flow of circular cylinder in turbulent flow [NASA-TM-100930] p 13 N88-25435
- Boundary layer development as a function of chamber pressure in the NASA Lewis 1030:1 area ratio rocket nozzle [NASA-TM-100917] p 154 N88-25841

BOUNDARY LAYER SEPARATION

- The measurement of boundary layers on a compressor blade in cascade. II - Suction surface boundary layers [ASME PAPER 87-GT-249] p 132 A88-11131
- Transition and separation control on a low-Reynolds number airfoil p 2 A88-11186
- High-speed inlet research program and supporting analyses p 17 N88-15811

BOUNDARY LAYER STABILITY

- Higher eigenmodes in the Blasius boundary-layer stability problem p 134 A88-16352

BOUNDARY LAYER TRANSITION

- Coherent motion induced fluctuations in the primary transition region of a plane shear layer p 133 A88-14125
- Development of a special-purpose test surface guided by uncertainty analysis - Introduction of a new uncertainty analysis step [AIAA PAPER 88-0169] p 39 A88-22121
- Boundary layer development as a function of chamber pressure in the NASA Lewis 1030:1 area ratio rocket nozzle [AIAA PAPER 88-3301] p 144 A88-50786
- Two-equation low-Reynolds-number turbulence modeling of transitional boundary layer flows characteristic of gas turbine blades [NASA-CR-4145] p 153 N88-23185
- Experimental study of bypass transition in a boundary layer [NASA-TM-100913] p 153 N88-23186
- Boundary layer development as a function of chamber pressure in the NASA Lewis 1030:1 area ratio rocket nozzle [NASA-TM-100917] p 154 N88-25841

BOUNDARY LAYERS

- Criteria for significance of simultaneous presence of both condensable vapors and aerosol particles on mass transfer (deposition) rates p 114 A88-10971
- The measurement of boundary layers on a compressor blade in cascade. I - A unique experimental facility [ASME PAPER 87-GT-248] p 131 A88-11130
- Radiative cooling of a solidifying droplet layer including absorption and scattering p 133 A88-15749
- Experiments for the determination of convective diffusion heat/mass transfer to burner rig test targets comparable in size to jet stream diameter p 140 A88-41574
- Significance of vapor phase chemical reactions on CVD rates predicted by chemically frozen and local thermochemical equilibrium boundary layer theories p 78 A88-44424
- The four spot time-of-flight laser anemometer p 164 N88-11145
- Heat transfer in a real engine environment p 147 N88-11155
- Film cooling heat transfer on a turbine airfoil p 147 N88-11156
- Flow field measurements in a 90 degree turning duct p 147 N88-11157
- Consistent boundary conditions for Reduced Navier-Stokes (RNS) scheme applied to 3-dimensional internal viscous flows [NASA-CR-180874] p 10 N88-15762

BOUNDARY VALUE PROBLEMS

- Effects of nozzle-exit boundary-layer conditions on excitability of heated free jets [AIAA PAPER 87-2723] p 135 A88-20182
- How good is the impedance boundary condition? p 115 A88-24863
- Consistent boundary conditions for reduced Navier-Stokes (RNS) scheme applied to three-dimensional internal viscous flows [AIAA PAPER 88-0714] p 139 A88-27723
- An ideal clamping analysis for a cross-ply laminate p 181 A88-31347
- Diffusion length measurement in bulk and epitaxially grown III-V semiconductors using charge collection microscopy p 126 A88-34370

- Onset of finger convection in a horizontal porous layer underlying a fluid layer p 140 A88-41572
- Accurate boundary conditions for exterior problems in gas dynamics [NASA-TM-100807] p 210 N88-19182
- Solving time-dependent two-dimensional eddy current problems [NASA-TM-100875] p 211 N88-25239

BOX BEAMS

- Design procedures for fiber composite box beams [NASA-TM-100296] p 73 N88-16828

BRANCHING (MATHEMATICS)

- Application of bifurcation theory to axial flow compressor instability [ASME PAPER 88-GT-231] p 169 A88-54313

BRAYTON CYCLE

- Speculations on future opportunities to evolve Brayton powerplants aboard the space station p 202 N88-24258

BREADBOARD MODELS

- Breadboard RL10-2B low-thrust operating mode (second iteration) test report [NASA-CR-182160] p 66 N88-29867
- The dc power control for a liquid-fed resistor [NASA-TM-101326] p 67 N88-29869

BRITTLE MATERIALS

- A probabilistic model of brittle crack formation p 180 A88-18696

BRITTLENESS

- Fracture technology for brittle materials p 192 N88-22417
- Some design considerations for ceramic components in heat engine applications p 106 N88-23875

BROADBAND

- A new model for broadband waveguide-to-microstrip transition design p 126 A88-38822
- Lewis Information Network (LINK): Background and overview [NASA-TM-100162] p 117 N88-11925

BROADCASTING

- Complementary satellite sound broadcasting systems: A NASA assessment for the Voice of America [NASA-TM-100300] p 119 N88-17899

BROMINATION

- Thermal conductivity of pristine and brominated highly graphitized pitch based carbon fibers p 97 A88-20257
- A comparison of the bromination dynamics of various carbon and graphite fibers p 97 A88-20278
- Specific heat of pristine and brominated graphite fibers, composites and HOPG - Highly Oriented Pyrolytic Graphite p 98 A88-32853
- Differential scanning calorimetric survey of brominated PAN, pitch-based and vapor-grown fibers p 98 A88-32854
- The effect of bromination of carbon fibers on the coefficient of thermal expansion of graphite fiber-epoxy composites [NASA-TM-100236] p 72 N88-10899
- Improving the interlaminar shear strength of carbon fiber-epoxy composites through carbon fiber bromination [NASA-TM-100248] p 72 N88-15018
- Brominated graphite fibers and method of producing the same [NASA-CASE-LEW-14698-1] p 76 N88-29888

BUBBLES

- Mass transport phenomena between bubbles and dissolved gases in liquids under reduced gravity conditions [AIAA PAPER 88-0450] p 138 A88-27719
- A flow visualization study of the leading edge separation bubble on a NACA 0012 airfoil with simulated glaze ice [NASA-CR-180846] p 10 N88-14966
- Mass transport phenomena between bubbles and dissolved gases in liquids under reduced gravity conditions [NASA-TM-100273] p 80 N88-18672

BUCKLING

- Measurement of impact-induced delamination buckling in composite laminates p 71 A88-47214

BULK MODULUS

- Universality relationships in condensed matter - Bulk modulus and sound velocity p 213 A88-43950

BUOYANCY

- A payload for investigating the influence of convection on GaAs crystal growth p 221 N88-17702

BURNERS

- Experiments for the determination of convective diffusion heat/mass transfer to burner rig test targets comparable in size to jet stream diameter p 140 A88-41574
- Correlation of velocity and velocity-density turbulence in the exhaust of an atmospheric burner p 161 N88-11147
- Experimental verification of vapor deposition rate theory in high velocity burner rigs p 91 N88-11179

BYPASS RATIO

Effects of surface chemistry on hot corrosion life
p 91 N88-11180

BYPASS RATIO

Experimental study of bypass transition in a boundary layer
[NASA-TM-100913] p 153 N88-23186

C

CADMIUM CHLORIDES

Production and characterization of CdCl₂ intercalated graphite fibers
p 101 A88-51307

CALIBRATING

Calibration and comparison of the NASA Lewis free-piston Stirling engine model predictions with RE-1000 test data
p 165 A88-11967
Gravitationally defined velocities for a low speed hot-wire calibration
p 133 A88-14170
Calibration of high-temperature, fiber-optic, microbend, pressure transducers
p 157 A88-22942
Calibration of a Mode II test specimen
p 183 A88-47014

Research sensors
p 161 N88-15795
Optical measurement systems
p 218 N88-15796
Fiber optic sensors with internal referencing
[NASA-TM-100893] p 162 N88-26644

CALORIMETERS

Differential scanning calorimetric survey of brominated PAN, pitch-based and vapor-grown fibers
p 98 A88-32854

CAPACITANCE

Recent advances in capacitance type of blade tip clearance measurements
[NASA-TM-101291] p 35 N88-25460

CAPACITORS

The application of high temperature superconductors to space electrical power distribution components
[NASA-TM-100901] p 61 N88-22939

CAPILLARY FLOW

Containment of a silicone fluid free surface in reduced gravity
p 112 A88-49085
Experimental study of thermocapillary flows in a thin liquid layer with heat fluxes imposed on the free surface
p 144 A88-49087
Experimental study of thermocapillary flows in a thin liquid layer with heat fluxes imposed on the free surface
[NASA-TM-100252] p 148 N88-12763

CARBON

Ion beam deposition of amorphous carbon films with diamond like properties
p 97 A88-20300
Comparison of the tribological properties of fluorinated cokes and graphites
[STLE PREPRINT 88-AM-7F-1] p 100 A88-51300
Characterization of precipitates in a niobium-zirconium-carbon alloy
[NASA-TM-100848] p 93 N88-22981

CARBON DIOXIDE

The carbon dioxide chaperon efficiency for the reaction $H + O_2 + M \text{ yields } HO_2 + M$ from ignition delay times behind reflected shock waves
[NASA-TM-100125] p 79 N88-15036

CARBON FIBERS

Electrical resistivity (4K to 2100K) of annealed vapor growth carbon fibers
p 96 A88-17214
Electron-spin-resonance studies of vapor-grown carbon fibers
p 96 A88-17368
A comparison of the bromination dynamics of various carbon and graphite fibers
p 97 A88-20278
Synthesis, electrical and thermal conductivities, and potential applications of graphite fluoride fibers
p 97 A88-26963

Specific heat of pristine and brominated graphite fibers, composites and HOPG --- Highly Oriented Pyrolytic Graphite
p 98 A88-32853

Differential scanning calorimetric survey of brominated PAN, pitch-based and vapor-grown fibers
p 98 A88-32854

Stability of the electrical resistivity of bromine, iodine monochloride, copper(II) chloride, and nickel(II) chloride intercalated pitch-based graphite fibers
p 100 A88-49403

Production and characterization of CdCl₂ intercalated graphite fibers
p 101 A88-51307

The effect of bromination of carbon fibers on the coefficient of thermal expansion of graphite fiber-epoxy composites
[NASA-TM-100236] p 72 N88-10899

Improving the interlaminar shear strength of carbon fiber-epoxy composites through carbon fiber bromination
[NASA-TM-100248] p 72 N88-15018

Brominated graphite fibers and method of producing the same
[NASA-CASE-LEW-14698-1] p 76 N88-29888

CARBON-CARBON COMPOSITES

Stress rupture behavior of silicon carbide coated, low modulus carbon/carbon composites
[NASA-CR-180863] p 72 N88-14150

CARBURIZING

Surface fatigue life of CBN and vitreous ground carburized and hardened AISI 9310 spur gears
[NASA-TM-100960] p 175 N88-25916

CARRIER INJECTION

Neutron radiation tolerance of Au-activated silicon
p 222 N88-24316

CARRIER TRANSPORT (SOLID STATE)

Characterization and modelling of open tube diffused n + p bulk InP solar cells
p 199 A88-34270
Piezoresistance and solar cell efficiency
p 125 A88-34298

CASCADE FLOW

Inter and intra blade row laser velocimetry studies of gas turbine compressor flows
[ASME PAPER 87-GT-235] p 2 A88-11126

The measurement of boundary layers on a compressor blade in cascade. I - A unique experimental facility
[ASME PAPER 87-GT-248] p 131 A88-11130

The measurement of boundary layers on a compressor blade in cascade. II - Suction surface boundary layers
[ASME PAPER 87-GT-249] p 132 A88-11131

The measurement of boundary layers on a compressor blade in cascade. III - Pressure surface boundary layers and the near wake
[ASME PAPER 87-GT-250] p 132 A88-11132

Navier-Stokes cascade analysis with a stiff k-epsilon turbulence solver
[AIAA PAPER 88-0594] p 5 A88-22444

Recent developments in flutter suppression techniques for turbomachinery rotors
p 21 A88-35530

Comparison of computational methods for three-dimensional turbulent turbomachinery flows
p 6 A88-42452

Design point variation of 3-D loss and deviation for axial compressor middle stages
[ASME PAPER 88-GT-57] p 8 A88-54189

Experimental investigation of the performance of a supersonic compressor cascade
[ASME PAPER 88-GT-306] p 9 A88-54375

Navier-Stokes cascade analysis with a stiff Kappa-Epsilon turbulence solver
[NASA-TM-100218] p 9 N88-10778

Unsteady aerodynamics of an oscillating cascade in a compressible flow field
[NASA-TM-100219] p 26 N88-13346

Investigation of oscillating cascade aerodynamics by an experimental influence coefficient technique
[NASA-TM-101313] p 14 N88-28041

Three-dimensional elliptic grid generation technique with application to turbomachinery cascades
[NASA-TM-101330] p 155 N88-30078

CAST ALLOYS

Effect of alloy composition on the sodium-sulfate induced hot corrosion attack of cast nickel-base superalloys at 900 C
p 81 A88-10028

Processing, physical metallurgy and creep of NiAl + Ta and NiAl + Nb alloys
[NASA-CR-182113] p 92 N88-21295

CASTING

Cast iron-base alloy for cylinder/regenerator housing
[NASA-CR-182116] p 92 N88-19613

CATALOGS

Component data base for space station resistojet auxiliary propulsion
[NASA-CR-180834] p 59 N88-17731

CATALYSIS

Surface catalytic degradation study of two linear perfluoropolyalkylethers at 345 C
[NASA-TP-2774] p 68 N88-12543

CATALYSTS

Assessment of commercially available and experimental hydrogen electrodes
p 198 A88-16632

Catalytic ignition of hydrogen and oxygen propellants
[AIAA PAPER 88-3300] p 109 A88-48764

A life test of a 22-Newton (5-lbf) hydrazine rocket
[NASA-TM-100232] p 57 N88-11750

Phase purity of NiCo₂O₄, a catalyst candidate for electrolysis of water
[NASA-TM-100239] p 69 N88-13385

Catalytic ignition of hydrogen and oxygen propellants
[NASA-TM-100957] p 63 N88-24669

Alkaline fuel cell performance investigation
[NASA-TM-100937] p 81 N88-27267

CATHODES

Alkaline fuel cell performance investigation
[NASA-TM-100937] p 81 N88-27267

Electrocatalytic reduction of oxygen on modified oxide surfaces
[NASA-TM-101333] p 81 N88-29952

SUBJECT INDEX

CAVITATION FLOW

The use of multigrid techniques in the solution of the Elrod algorithm for a dynamically loaded journal bearing
[NASA-CR-180873] p 151 N88-17954

CAVITIES

Electromagnetic fields backscattered from an s-shaped inlet cavity with an absorber coating on its inner walls
[NASA-CR-182401] p 118 N88-15130

CENTAUR LAUNCH VEHICLE

Modal test/analysis correlation for the Centaur G prime launch vehicle
p 44 A88-18631
Design, development, and test of Shuttle/Centaur G-prime cryogenic tankage thermal protection systems
p 47 A88-53182

Centaur operations at the space station
[NASA-CR-179593] p 49 N88-25473

Centaur operations at the space station: Cost and transportation analysis
[NASA-CR-182128] p 44 N88-29835

CERAMIC BONDING

Preliminary investigation of inertia friction welding B2 aluminides
p 82 A88-14567

CERAMIC COATINGS

Interface roughness effect on stresses in ceramic coatings
p 95 A88-12587

Some adhesion/cohesion characteristics of plasma-sprayed ZrO₂-Y₂O₃ under tensile loading
p 95 A88-12589

Thermal barrier coating life prediction model development
[ASME PAPER 88-GT-284] p 68 A88-54353

Thermal barrier coating life prediction model development
p 171 N88-11185

CERAMIC FIBERS

Silsesquioxanes as precursors to ceramic composites
p 69 A88-12589

SiC fiber analysis
p 107 N88-23891

SiC fiber reinforced reaction-bonded Si₃N₄ composites
p 75 N88-23892

Auger analysis of a fiber/matrix interface in a ceramic matrix composite
[NASA-TM-100892] p 76 N88-25487

CERAMIC MATRIX COMPOSITES

Silsesquioxanes as precursors to ceramic composites
p 69 A88-12599

Ceramic matrix and resin matrix composites - A comparison
p 69 A88-13158

High temperature tensile testing of ceramic composites
[NASA-CR-180888] p 161 N88-15996

Continuous fiber ceramic matrix composites for heat engine components
p 106 N88-22411

Fracture technology for brittle materials
p 192 N88-22417

Ceramic matrix composites
p 75 N88-23888

Auger analysis of a fiber/matrix interface in a ceramic matrix composite
[NASA-TM-100892] p 76 N88-25487

CERAMICS

Correlation between ultrasonic velocity and density of ceramic turbine blades
p 176 A88-12581

Thermomechanical behavior of plasma-sprayed ZrO₂-Y₂O₃ coatings influenced by plasticity, creep, and oxidation
p 95 A88-12588

Design and development of ceramic components
[AIAA PAPER 88-3054] p 168 A88-44742

Elevated temperature durability of ceramic materials
[AIAA PAPER 88-3055] p 100 A88-44743

Effects of subcritical crack growth on fracture toughness of ceramics assessed in chevron-notched three-point bend tests
[ASME PAPER 88-GT-185] p 185 A88-54276

Microstructural effects on fracture toughness of polycrystalline ceramics in combined mode I and mode II loading
[ASME PAPER 88-GT-208] p 101 A88-54294

Acoustic imaging of subtle porosity variations in ceramics
p 101 A88-55044

Structure and grain coarsening during the processing of engineering ceramics
[NASA-TM-100235] p 101 N88-11838

Adiabatic diesel engine component development: Reference engine for on-highway applications
[NASA-CR-179531] p 224 N88-12428

The effect of texture on the crack growth resistance of alumina
[NASA-TM-100250] p 102 N88-14206

Imaging subtle microstructural variations in ceramics with precision ultrasonic velocity and attenuation measurements
[NASA-TM-100129] p 177 N88-15257

Aeropropulsion '87. Session 1: Aeropropulsion Materials Research
[NASA-CP-10003-SESS-1] p 31 N88-16697

Ceramics for engines
p 103 N88-16704

- Nondestructive evaluation of structural ceramics by photoacoustic microscopy
[NASA-CR-180858] p 103 N88-16868
- Friction and wear of monolithic and fiber reinforced silicon-ceramics sliding against IN-718 alloy at 25 to 800 C in atmospheric air at ambient pressure
[NASA-TM-100294] p 103 N88-17796
- Adhesion, friction and micromechanical properties of ceramics
[NASA-TM-100782] p 104 N88-17801
- Ceramic bearings for use in gas turbine engines
[NASA-TM-100288] p 172 N88-18007
- Tribological properties of alumina-boria-silicate fabric from 25 to 850 C
[NASA-TM-100806] p 104 N88-18726
- Prototype thin-film thermocouple/heat-flux sensor for a ceramic-insulated diesel engine
[NASA-TM-100798] p 162 N88-18892
- Reliability based analysis of contact problems
[NASA-CR-182117] p 189 N88-18975
- Advanced Gas Turbine (AGT) Technology Development Project, ceramic component developments
[NASA-CR-180871] p 224 N88-20229
- Development of a torsion balance for adhesion measurements
[NASA-TM-100799] p 104 N88-20454
- Hafnia-rich mixed oxide ceramics of the system $\text{HfO}_2\text{-ZrO}_2\text{-TiO}_2$ for heaters and heat exchangers in electrothermal thrusters: The effects of titania on selected electrical and mechanical properties of Hafnia-rich mixed oxides in the system Hafnia-Zirconia-Titania, volume 1
[NASA-CR-182800-VOL-1] p 105 N88-22197
- Monolithic ceramic analysis using the SCARE program
p 105 N88-22409
- Whisker-reinforced ceramic composites for heat engine components
p 105 N88-22410
- Nondestructive evaluation of sintered ceramics
p 177 N88-22416
- Synthesis and characterization of high-T(sub c) screen-printed Y-Ba-Cu-O films on alumina
[NASA-TM-100860] p 222 N88-22805
- Structural Ceramics
[NASA-CP-2427] p 106 N88-23872
- Ceramics for turbine engines
p 106 N88-23873
- Friction and wear of ceramics
p 106 N88-23874
- Some design considerations for ceramic components in heat engine applications
p 106 N88-23875
- Nondestructive evaluation of structural ceramics
p 178 N88-23876
- Fracture mechanics
p 194 N88-23877
- Molten salt corrosion of SiC and Si₃N₄
p 107 N88-23885
- Thermal cyclic durability testing of ceramic materials for turbine engines
p 179 N88-23886
- Polymer precursors for ceramic composites
p 75 N88-23890
- Thrust chamber thermal barrier coating techniques
[NASA-TM-100933] p 64 N88-24690
- Solid-state combustion synthesis of ceramics and alloys in reduced gravity
[NASA-CR-4163] p 75 N88-25479
- Fracture resistance of a TiB₂ particle/SiC matrix composite at elevated temperature
[NASA-TM-100967] p 107 N88-26482
- Development of sensors for ceramic components in advanced propulsion systems: Survey and evaluation of measurement techniques for temperature, strain and heat flux for ceramic components in advanced propulsion systems
[NASA-CR-182111] p 163 N88-28299
- CERMENTS**
SiC reinforced aluminide composites
p 70 N88-31687
- CHALCOGENIDES**
Effect of the microstructure on the thermoelectric properties of polycrystalline lanthanum chalcogenides
p 221 N88-40797
- CHANNEL FLOW**
Effect of rib angle on local heat/mass transfer distribution in a two-pass rib-roughened channel
[ASME PAPER 87-GT-94] p 131 N88-11033
- A method for calculating turbulent boundary layers and losses in the flow channels of turbomachines
[ASME PAPER 87-GT-225] p 2 N88-11121
- Investigation of third-order closure model of turbulence for the computation of incompressible flows in a channel with a backward-facing step
p 136 N88-21273
- Local heat/mass transfer distributions around sharp 180 deg turns in two-pass smooth and rib-roughened channels
[ASME PAPER 86-GT-114] p 139 N88-28516
- CHARACTERIZATION**
High temperature polymer matrix composites
p 70 N88-36775
- Mechanical properties characterization of composite sandwich materials intended for space antenna applications
[NASA-TM-88893] p 71 N88-10121
- Elevated temperature strain gages
p 160 N88-11144
- Comparison of UNL laser imaging and sizing system and a phase/Doppler system for analyzing sprays from a NASA nozzle
[NASA-CR-182437] p 150 N88-16956
- Synthesis and characterization of high-T(sub c) screen-printed Y-Ba-Cu-O films on alumina
[NASA-TM-100860] p 222 N88-22805
- Characterization of precipitates in a niobium-zirconium-carbon alloy
[NASA-TM-100848] p 93 N88-22981
- High frequency ultrasonic characterization of sintered SiC
[NASA-TM-100825] p 179 N88-23985
- Characterization of a 30-GHz IMPATT solid state amplifier
[NASA-TM-100876] p 120 N88-24847
- CHARGE EFFICIENCY**
Effect of storage and LEO cycling on manufacturing technology IPV nickel-hydrogen cells
p 53 N88-11917
- CHARGED PARTICLES**
Voids in Jovian magnetosphere revisited - Evidence of spacecraft charging
p 226 N88-22879
- CHEMICAL ANALYSIS**
Analysis of plasma nitrided steels
p 88 N88-38936
- Improved silicon nitride for advanced heat engines
[NASA-CR-175006] p 102 N88-15886
- CHEMICAL COMPOSITION**
A comparison of the bromination dynamics of various carbon and graphite fibers
p 97 N88-20278
- Boron nitride - Composition, optical properties, and mechanical behavior
p 99 N88-40794
- CHEMICAL ELEMENTS**
Diamond like carbon coatings: Categorization by atomic number density
[NASA-CR-174895] p 108 N88-28151
- CHEMICAL EQUILIBRIUM**
Numerical simulation of hypersonic inlet flows with equilibrium or finite rate chemistry
[AIAA PAPER 88-0273] p 5 N88-27717
- NNEPEC: Chemical equilibrium version of the Navy/NASA Engine Program
[NASA-TM-100851] p 32 N88-21161
- CHEMICAL EVOLUTION**
Primordial lithium - New reaction rates, new abundances, new constraints
p 226 N88-31145
- CHEMICAL PROPERTIES**
Plasma assisted surface coating/modification processes - An emerging technology
p 114 N88-38927
- Oxygen plasma effects on several liquid droplet radiator fluids
p 142 N88-47962
- CHEMICAL PROPULSION**
Recent advances in low-thrust propulsion technology
[AIAA PAPER 88-3283] p 55 N88-48761
- Space station onboard propulsion system: Technology study
[NASA-CR-179233] p 59 N88-15006
- Recent advances in low-thrust propulsion technology
[NASA-TM-100959] p 213 N88-25260
- CHEMICAL REACTIONS**
Stress-life interrelationships associated with alkaline fuel cells
p 197 N88-11903
- Numerical study of chemically reacting flows using an LU scheme
[AIAA PAPER 88-0436] p 5 N88-24825
- Molten-salt corrosion of silicon nitride. I - Sodium carbonate. II - Sodium sulfate
p 97 N88-26222
- Modified reaction mechanism of aerated n-dodecane liquid flowing over heated metal tubes
p 108 N88-44268
- Significance of vapor phase chemical reactions on CVD rates predicted by chemically frozen and local thermochemical equilibrium boundary layer theories
p 78 N88-44424
- Numerical study of chemically reacting flows using an LU scheme
[NASA-CR-180882] p 26 N88-14094
- Aeropropulsion '87. Session 3: Internal Fluid Mechanics Research
[NASA-CP-10003-SESS-3] p 28 N88-15790
- Chemical reacting flows
p 79 N88-15793
- Direct simulations of chemically reacting turbulent mixing layers, part 2
[NASA-CR-180853] p 154 N88-25857
- CHIPS (ELECTRONICS)**
A 30 GHz monolithic receive module technology assessment
[NASA-CR-180825] p 129 N88-23084
- Development of 20 GHz monolithic transmit modules
[NASA-CR-182134] p 222 N88-24539
- CHROMIUM**
An experimental study of biaxial yield in modified 9Cr-1Mo steel at room temperature
[NASA-CR-175012] p 196 N88-30164
- CHROMIUM ALLOYS**
Interdiffusion in Ni-rich, Ni-Cr-Al alloys at 1100 and 1200 C. I - Diffusion paths and microstructures. II - Diffusion coefficients and predicted concentration profiles
p 84 N88-24485
- Predicting diffusion paths and interface motion in gamma/gamma + beta, Ni-Cr-Al diffusion couples
p 84 N88-24486
- Diffusional transport during the cyclic oxidation of gamma + beta, Ni-Cr-Al(Y, Zr) alloys
p 85 N88-28902
- The effect of sulfur and zirconium Co-doping on the oxidation of NiCrAl
[NASA-TM-100209] p 90 N88-10940
- CHROMIUM CARBIDES**
Sputtered silver films to improve chromium carbide based solid lubricant coatings for use to 900 C
p 100 N88-47563
- Sputtered silver films to improve chromium carbide based solid lubricant coatings for use to 900 C
[NASA-TM-100783] p 102 N88-15885
- CIRCLES (GEOMETRY)**
Numerical arc segmentation algorithm for a radio conference-NASARC (version 2.0) technical manual
[NASA-TM-100160] p 118 N88-15910
- CIRCUITS**
Radiation performance of AlGaAs and InGaAs concentrator cells and expected performance of cascade structures
p 125 N88-34356
- Radiation performance of AlGaAs concentrator cells and expected performance of cascade structures
[NASA-TM-100145] p 200 N88-12878
- A millimeter-wave tunnel Ladder TWT
[NASA-CR-182184] p 130 N88-28239
- Arctjet power supply and start circuit
[NASA-CASE-LEW-14374-1] p 41 N88-28939
- CIRCULAR CYLINDERS**
Three-dimensional flow past two cylinders mounted side by side on an endwall
[AIAA PAPER 88-3718] p 143 N88-48974
- Correlations of velocity and temperature fluctuations in the stagnation-point flow of circular cylinder in turbulent flow
[NASA-TM-100930] p 13 N88-25435
- CIRCULAR POLARIZATION**
A simple circular-polarized antenna: Circular waveguide horn coated with lossy magnetic material
p 116 N88-36648
- Polarization determination utilizing two arbitrarily polarized antennas
p 116 N88-47424
- CIRCULAR WAVEGUIDES**
Modal attenuation in multilayered coated waveguides
p 126 N88-45755
- CIVIL AVIATION**
Electro-impulse de-icing - A status report
[AIAA PAPER 88-0019] p 17 N88-22017
- The challenges and opportunities of supersonic transport propulsion technology
[AIAA PAPER 88-2985] p 23 N88-48032
- Availability and cost estimate of a high naphthene, modified aviation turbine fuel
[NASA-TM-100823] p 104 N88-20455
- The challenges and opportunities of supersonic transport propulsion technology
[NASA-TM-100921] p 34 N88-23806
- CLASSICAL MECHANICS**
Institute for Computational Mechanics in Propulsion (ICOMP) first year summary
[NASA-TM-100225] p 210 N88-12330
- Composite mechanics for engine structures
[NASA-TM-100176] p 72 N88-12552
- Institute for Computational Mechanics in Propulsion (ICOMP)
[NASA-TM-100790] p 211 N88-19202
- CLEARANCES**
Recent advances in capacitance type of blade tip clearance measurements
[NASA-TM-101291] p 35 N88-25460
- CLOSE PACKED LATTICES**
Multielement mapping of alpha-SiC by scanning Auger microscopy
p 158 N88-27617
- Improved processing of alpha-SiC
p 99 N88-38318
- CLOSED CYCLES**
Analysis of closed cycle megawatt class space power systems with nuclear reactor heat sources
p 62 N88-24351
- CLOSURE LAW**
Investigation of third-order closure model of turbulence for the computation of incompressible flows in a channel with a backward-facing step
p 136 N88-21273

CLOUD GLACIATION

CLOUD GLACIATION

Experimental measurements of heat transfer from an iced surface during artificial and natural cloud icing conditions
[AIAA-86-1352] p 153 N88-23718

CLOUDS

Three-dimensional trajectory analyses of two drop sizing instruments: PMS OAP and PMS FSSP
[NASA-CR-4113] p 16 N88-18574

COARSENESS

Structure and grain coarsening during the processing of engineering ceramics
[NASA-TM-100235] p 101 N88-11838

COATINGS

How good is the impedance boundary condition?
p 115 N88-24863

Sputtered silver films to improve chromium carbide based solid lubricant coatings for use to 900 C
p 100 A88-47563

Electromagnetic fields backscattered from an s-shaped inlet cavity with an absorber coating on its inner walls
[NASA-CR-182401] p 118 N88-15130

Sputtered silver films to improve chromium carbide based solid lubricant coatings for use to 900 C
[NASA-TM-100783] p 102 N88-15885

Self-lubricating coatings for high-temperature applications
p 103 N88-16703

Fatigue damage modeling for coated single crystal superalloys
p 93 N88-22427

Design and demonstration of a system for the deposition of atomic-oxygen durable coatings for reflective solar dynamic power system concentrators
[NASA-CR-4158] p 64 N88-25474

Thin film coatings for space electrical power system applications
[NASA-TM-101325] p 69 N88-28966

Iridium-coated rhenium thrusters by CVD
[NASA-TM-101309] p 67 N88-29874

Containment of a silicone fluid free surface in reduced gravity using barrier coatings
[NASA-TM-101314] p 155 N88-30072

COAXIAL CABLES

Coaxial tube array space transmission line characterization
p 121 A88-11865

Power transmission studies for tethered SP-100
[NASA-TM-100864] p 60 N88-21251

COBALT

The effect of variations of cobalt content on the cyclic oxidation resistance of selected Ni-base superalloys
p 82 A88-10031

COBALT OXIDES

Phase purity of NiCo₂O₄, a catalyst candidate for electrolysis of water
[NASA-TM-100239] p 69 N88-13385

CODING

Numerical study of chemically reacting flows using an LU scheme
[AIAA PAPER 88-0436] p 5 A88-24825

Numerical study of chemically reacting flows using an LU scheme
[NASA-CR-180882] p 26 N88-14094

The development of an intelligent interface to a computational fluid dynamics flow-solver code
[NASA-TM-100908] p 207 N88-26127

COEFFICIENT OF FRICTION

Tribological properties of alumina-boria-silicate fabric from 25 to 850 C
[NASA-TM-100806] p 104 N88-18726

COFFIN-MANSON LAW

Thermal cycling of tungsten-fibre-reinforced superalloy composites
p 70 A88-31770

COHESION

Some adhesion/cohesion characteristics of plasma-sprayed ZrO₂-Y₂O₃ under tensile loading
p 95 A88-12589

COKE

Comparison of the tribological properties of fluorinated cokes and graphites
[STLE PREPRINT 88-AM-7F-1] p 100 A88-51300

COLLECTION

Techniques utilized in the simulated altitude testing of a 2D-CD vectored and reversing nozzle
[NASA-TM-100872] p 40 N88-25464

COLLOIDS

Colloidal characterization of silicon nitride and silicon carbide
p 107 N88-23883

COMBINED STRESS

Design procedures for fiber composite box beams
[NASA-TM-100296] p 73 N88-16828

COMBUSTIBLE FLOW

The structure and dynamics of reacting plane mixing layers
p 136 A88-20871

Mixing, transport and combustion in sprays
p 138 A88-25828

COMBUSTION

Combustion noise from gas turbine aircraft engines measurement of far-field levels
p 215 A88-39708

Improved numerical methods for turbulent viscous recirculating flows
p 146 N88-11148

Microgravity combustion fundamentals
p 112 N88-12528

The effect of microgravity on flame spread over a thin fuel
[NASA-TM-100195] p 80 N88-15853

Solid-state combustion synthesis of ceramics and alloys in reduced gravity
[NASA-CR-4163] p 75 N88-25479

Optical measurements of soot and temperature profiles in premixed propane-oxygen flames
[NASA-TM-101343] p 115 N88-29997

COMBUSTION CHAMBERS

Soot loading in a generic gas turbine combustor
p 19 A88-27296

Experiments for the determination of convective diffusion heat/mass transfer to burner rig test targets comparable in size to jet stream diameter
p 140 A88-41574

Lateral jet injection into swirling combustor flowfields
[AIAA PAPER 88-3183] p 141 A88-44783

An empirical model of the effects of curvature and convergence on dilution jet mixing
[AIAA PAPER 88-3180] p 23 A88-50783

Assessment, development, and application of combustor aerothermal models
p 24 A88-54140

Diagnostics development for spray characterization in complex turbulent flows
[ASME PAPER 88-GT-241] p 146 A88-54320

Turbine Engine Hot Section Technology, 1985
[NASA-CP-2405] p 185 N88-11140

Aerothermal modeling program, phase 2
p 146 N88-11149

Fuel-injector/air-swirl characterization
p 146 N88-11150

Dilution jet mixing program, phase 3
p 147 N88-11153

On the mixing of a row of jets with a confined crossflow
p 147 N88-11154

3D inelastic analysis methods for hot section components
p 185 N88-11164

3-D inelastic analysis methods for hot section components
p 206 N88-11165

Recent advances in high temperature instrumentation for hot section applications
[NASA-TM-100282] p 161 N88-14339

Numerical simulation of axisymmetric turbulent flow in combustors and diffusers
[NASA-CR-4115] p 11 N88-17582

Unsteady heat transfer in turbine blade ducts: Focus on combustor sources
[NASA-TM-100815] p 151 N88-18870

Assessment, development and application of combustor aerothermal models
[NASA-TM-100290] p 32 N88-19469

Finite area combustor theoretical rocket performance
[NASA-TM-100785] p 60 N88-21252

High-temperature combustor liner tests in structural component response test facility
p 33 N88-22383

Life assessment of combustor liner using unified constitutive models
p 33 N88-22384

An empirical model of the effects of curvature and convergence on dilution jet mixing
[NASA-TM-100896] p 34 N88-24640

Thrust chamber thermal barrier coating techniques
[NASA-TM-100933] p 64 N88-24690

Transition mixing study empirical model report
[NASA-CR-182139] p 155 N88-30076

COMBUSTION CHEMISTRY

Integrating combustion kinetic rate equations by selective use of stiff and nonstiff methods
p 78 A88-19233

Characteristics of fluid flow in the combustion synthesis of TiC from the elements
p 110 A88-28564

Detailed mechanism of toluene oxidation and comparison with benzene
[NASA-TM-100261] p 79 N88-13428

COMBUSTION CONTROL

Study of industry requirements that can be fulfilled by combustion experimentation aboard space station
[NASA-CR-180854] p 224 N88-19377

COMBUSTION EFFICIENCY

Performance and efficiency evaluation and heat release study of a direct-injection stratified-charge rotary engine
[SAE PAPER 870445] p 166 A88-23313

Performance and combustion characteristics of direct-injection stratified-charge rotary engines
[NASA-TM-100134] p 25 N88-12490

Small engine technology programs
p 29 N88-15801

Finite area combustor theoretical rocket performance
[NASA-TM-100785] p 60 N88-21252

COMBUSTION PHYSICS

Numerical methods for one-dimensional reaction-diffusion equations arising in combustion theory
p 135 A88-18975

Modelling ignition characteristics of rich H₂/O₂ mixture in a monolithic catalytic reactor
[AIAA PAPER 88-3224] p 78 A88-46499

Spacecraft Fire Safety
[NASA-CP-2476] p 45 N88-12520

Microgravity combustion fundamentals
p 112 N88-12528

Combustion characteristics of gas turbine alternative fuels
[NASA-TM-100247] p 25 N88-13338

The carbon dioxide chaperon efficiency for the reaction H + O₂ + M yields HO₂ + M from ignition delay times behind reflected shock waves
[NASA-TM-100125] p 79 N88-15036

Microgravity combustion discipline working group summary of requirements for noncontact temperature measurements
p 113 N88-23902

COMBUSTION PRODUCTS

Experimental verification of vapor deposition rate theory in high velocity burner rigs
p 91 N88-11179

COMBUSTION STABILITY

Velocity-coupled flow oscillations in a simulated solid-propellant rocket environment
[AIAA PAPER 88-0543] p 108 A88-27720

COMMERCIAL AIRCRAFT

NASA advanced turboprop research and concept validation program
[NASA-TM-100891] p 34 N88-22902

COMMERCIAL ENERGY

Status of commercial fuel cell powerplant system development
p 198 A88-11925

COMMERCIAL SPACECRAFT

Economic benefits of the Space Station to commercial communication satellite operators
[IAF PAPER 87-622] p 41 A88-16215

Space commercialization and power system technology
p 223 A88-44003

COMMUNICATION

Evaluation of the communications impact of a low power arcjet thruster
[AIAA PAPER 88-3105] p 55 A88-48755

Research and technology
[NASA-TM-100172] p 227 N88-22851

Evaluation of the communications impact of a low power arcjet thruster
[NASA-TM-100926] p 63 N88-24682

COMMUNICATION NETWORKS

Cost-effective intersatellite link applications to the fixed satellite services
[AIAA PAPER 88-0770] p 45 A88-27544

Service offerings and interfaces for the ACTS network of earth stations
[AIAA PAPER 88-0800] p 116 A88-27551

Advanced satellite system architecture for VSATs with ISDN compatibility
[AIAA PAPER 88-0870] p 116 A88-27604

Optical technologies for space communication systems; Proceedings of the Meeting, Los Angeles, CA, Jan. 15, 16, 1987
[SPIE-756] p 45 A88-35251

Communications payload concepts for geostationary facilities
[NASA-TM-100154] p 118 N88-13513

An evolutionary communications scenario for Mars exploration
[NASA-TM-100263] p 118 N88-13515

COMMUNICATION SATELLITES

New non-geosynchronous orbits for communications satellites to off-load daily peaks in geostationary traffic
[AAS PAPER 87-547] p 42 A88-10957

VSAT networks - An overview --- Very Small Aperture Terminals
p 115 A88-14091

Monolithic Microwave Integrated Circuit (MMIC) technology for space communications applications
[IAF PAPER 87-491] p 122 A88-16133

Economic benefits of the Space Station to commercial communication satellite operators
[IAF PAPER 87-622] p 41 A88-16215

Numerical arc segmentation algorithm for a radio conference - A software tool for communication satellite systems planning
[AIAA PAPER 88-0788] p 212 A88-27531

A flexible on-board demultiplexer/demodulator
[AIAA PAPER 88-0811] p 123 A88-27558

Bandwidth and power efficient satellite TDMA demodulator and decoder
[AIAA PAPER 88-0812] p 123 A88-27559

Bandwidth-efficient high-speed coded trellis modulation
[AIAA PAPER 88-0813] p 116 A88-27560

SUBJECT INDEX

- The bit-error rate performance of a satellite microwave matrix switch
[AIAA PAPER 88-0826] p 123 A88-27572
- Hardware realization of a baseband processor for a SS-FDMA/TDMA/DAMA system --- Demand Assignment Multiple Access
[AIAA PAPER 88-0830] p 124 A88-27575
- High efficiency, long life traveling wave tubes for future communications satellites
[AIAA PAPER 88-0835] p 124 A88-27578
- Communications satellites in non-geostationary orbits
[AIAA PAPER 88-0842] p 46 A88-27583
- Advanced satellite system architecture for VSATs with ISDN compatibility
[AIAA PAPER 88-0870] p 116 A88-27604
- A satellite system synthesis model for orbital arc allotment optimization
p 117 A88-48579
- Engineering calculations for the Delta S method of solving the orbital allotment problem
[NASA-CR-182372] p 42 N88-14110
- Numerical arc segmentation algorithm for a radio conference-NASARC (version 2.0) technical manual
[NASA-TM-100160] p 118 N88-15910
- Communications satellite systems operations with the space station. Volume 3: Supplementary technical report
[NASA-CR-180675] p 48 N88-16794
- High efficiency, long life traveling wave tubes for future communications satellites
[NASA-TM-100837] p 45 N88-19565
- Numerical arc segmentation algorithm for a radio conference: A software tool for communication satellite systems planning
[NASA-TM-100789] p 46 N88-22919
- The bit-error rate performance of a satellite microwave matrix switch
[NASA-TM-100285] p 46 N88-22920
- Experimental radio frequency link for Ka-band communications applications
[NASA-TM-100824] p 43 N88-24659
- COMPARISON**
- Comparison of the tribological properties of fluorinated cokes and graphites
[STLE PREPRINT 88-AM-7F-1] p 100 A88-51300
- A comparison of experimental and theoretical results for labyrinth gas seals with honeycomb stators
[NASA-CR-182441] p 172 N88-16006
- Comparison of pressure distributions on model and full-scale NACA 64-621 airfoils with ailerons for wind turbine application
[NASA-TM-100802] p 201 N88-21593
- Comparison of the bidirectional reflectance distribution function of various surfaces
[NASA-TM-101317] p 218 N88-28760
- COMPATIBILITY**
- Compatibility of dispersion-strengthened platinum with resistojet propellants
[NASA-TP-2765] p 58 N88-12538
- Improved method for stress and compatibility analysis of multicomponent rotating systems
[NASA-TM-100884] p 195 N88-25935
- COMPENSATION**
- Case study of active array feed compensation with sidelobe control for reflector surface distortion
[NASA-TM-100287] p 120 N88-23073
- COMPENSATORS**
- Zoom lens compensator for a cylindrical window in laser anemometer uses
p 217 A88-17221
- COMPONENT RELIABILITY**
- Small space reactor power systems for unmanned solar system exploration missions
[NASA-TM-100228] p 227 N88-14054
- Small engine technology programs
p 29 N88-15801
- Results of NASA/Army transmission research
p 31 N88-16640
- Ceramics for engines
p 103 N88-16704
- Power components for the space station 20-kHz power distribution system
[NASA-TM-100866] p 114 N88-21374
- Monolithic ceramic analysis using the SCARE program
p 105 N88-22409
- Continuous fiber ceramic matrix composites for heat engine components
p 106 N88-22411
- Cumulative fatigue damage models
p 193 N88-22422
- Life and reliability of rotating disks
p 178 N88-22428
- Small scale bipolar nickel-hydrogen testing
[NASA-TM-100936] p 202 N88-25059
- Probabilistic structural analysis to quantify uncertainties associated with turbopump blades
[NASA-TM-100278] p 76 N88-28094

COMPONENTS

- Development of sensors for ceramic components in advanced propulsion systems: Survey and evaluation of measurement techniques for temperature, strain and heat flux for ceramic components in advanced propulsion systems
[NASA-CR-182111] p 163 N88-28299
- COMPOSITE MATERIALS**
- PMR polyimide compositions for improved performance at 371 C
p 96 A88-13172
- High temperature polymer matrix composites
p 70 A88-36775
- Materials analysis by ultrasonics: Metals, ceramics, composites --- Book
p 176 A88-44853
- Measurement of impact-induced delamination buckling in composite laminates
p 71 A88-47214
- Mechanical properties characterization of composite sandwich materials intended for space antenna applications
[NASA-TM-88893] p 71 N88-10121
- Composite mechanics for engine structures
[NASA-TM-100176] p 72 N88-12552
- Simplified procedures for designing composite bolted joints
[NASA-TM-100281] p 73 N88-15020
- Creep behavior of tungsten/nickel and tungsten/nickel-1 percent zirconium composites
[NASA-TM-100804] p 92 N88-18707
- Biaxial experiments supporting the development of constitutive theories for advanced high-temperature materials
p 191 N88-22386
- The 700 F properties of autoclave cured PMR-2 composites
[NASA-TM-100923] p 75 N88-24712
- Status and prognosis for alternative engine materials
[NASA-TM-100903] p 94 N88-24749
- A transversely isotropic thermoelastic theory
[NASA-TM-101302] p 196 N88-28332
- COMPOSITE STRUCTURES**
- Development of composite facets for the surface of a space-based solar dynamic concentrator
p 54 A88-18230
- Thermal stresses of a wind turbine blade made of orthotropic material
p 180 A88-18380
- Advanced composite turboprops - Modeling, structural, and dynamic analyses
[ASME PAPER 87-GT-78] p 21 A88-36745
- Composite mechanics for engine structures
[NASA-TM-100176] p 72 N88-12552
- Hygrothermomechanical fiber composite fatigue: Computational simulation
[NASA-TM-100840] p 74 N88-21257
- Features and applications of the integrated composites analyzer (ICAN) code
p 74 N88-22391
- COMPOSITE WRAPPING**
- An ideal clamping analysis for a cross-ply laminate
p 181 A88-31347
- COMPOSITION (PROPERTY)**
- On producing an alloy of uniform composition during rapid solidification processing
p 89 A88-41654
- COMPRESSIBILITY**
- Compressive creep behavior of alloys based on B2 FeAl
p 82 A88-10043
- A model for the influence of pressure on the bulk modulus and the influence of temperature on the solidification pressure for liquid lubricants
[ASME PAPER 86-TRIB-63] p 133 A88-15124
- COMPRESSIBILITY EFFECTS**
- Foil bearing lubrication theory including compressibility effects
p 170 A88-54964
- COMPRESSIBLE FLOW**
- A parametric study of mean loading effects on airfoil gust interaction noise
[AIAA PAPER 87-2677] p 213 A88-16539
- Effects of numerical dissipation on finite-volume solutions of compressible flow problems
[AIAA PAPER 88-0621] p 5 A88-22469
- Choice of implicit and explicit operators for the upwind differencing method
[AIAA PAPER 88-0624] p 209 A88-22472
- Magnetic fields interacting with nonlinear compressible convection
p 226 A88-31163
- Theory versus experiment for the rotordynamic coefficients of labyrinth gas seals. I - A two control volume model
p 167 A88-31535
- Splitting of inviscid fluxes for real gases
[AIAA PAPER 88-3526] p 142 A88-48782
- Unsteady aerodynamics of an oscillating cascade in a compressible flow field
[NASA-TM-100219] p 26 N88-13346
- Splitting of inviscid fluxes for real gases
[NASA-TM-100856] p 211 N88-21717
- COMPRESSION LOADS**
- Effect of component compression on the initial performance of an IPV nickel-hydrogen cell --- Individual Pressure Vessel
p 53 A88-11913

COMPUTATIONAL FLUID DYNAMICS

- The effect of compression on individual pressure vessel nickel/hydrogen components
[NASA-TM-101312] p 81 N88-28109
- COMPRESSION TESTS**
- The effect of compression on individual pressure vessel nickel/hydrogen components
[NASA-TM-101312] p 81 N88-28109
- COMPRESSION WAVES**
- An isentropic compression heated Ludwig tube transient wind tunnel
[AIAA PAPER 88-2019] p 40 A88-37926
- COMPRESSOR BLADES**
- Inter and intra blade row laser velocimetry studies of gas turbine compressor flows
[ASME PAPER 87-GT-235] p 2 A88-11126
- The measurement of boundary layers on a compressor blade in cascade. I - A unique experimental facility
[ASME PAPER 87-GT-248] p 131 A88-11130
- The measurement of boundary layers on a compressor blade in cascade. II - Suction surface boundary layers
[ASME PAPER 87-GT-249] p 132 A88-11131
- The measurement of boundary layers on a compressor blade in cascade. III - Pressure surface boundary layers and the near wake
[ASME PAPER 87-GT-250] p 132 A88-11132
- Advanced turboprop wing installation effects measured by unsteady blade pressure and noise
[AIAA PAPER 87-2719] p 3 A88-18655
- Experimental investigation of the performance of a supersonic compressor cascade
[ASME PAPER 88-GT-306] p 9 A88-54375
- Advanced turboprop wing installation effects measured by unsteady blade pressure and noise
[NASA-TM-100200] p 9 N88-10008
- Automated design of controlled diffusion blades
[NASA-TM-100251] p 9 N88-13304
- Aero/structural tailoring of engine blades
[NASA-CR-180805] p 207 N88-21682
- COMPRESSOR EFFICIENCY**
- Small engine technology programs
p 29 N88-15801
- COMPRESSOR ROTORS**
- Laser Doppler velocimeter measurement of annulus wall boundary layer development in a compressor rotor
[ASME PAPER 87-GT-251] p 132 A88-11133
- COMPRESSORS**
- Determination of compressor in-stall characteristics from engine surge transients
p 21 A88-35505
- Experimental vibration damping characteristics of the third-stage rotor of a three-stage transonic axial-flow compressor
[AIAA PAPER 88-3229] p 23 A88-48759
- Experimental vibration damping characteristics of the third-stage rotor of a three-stage transonic axial-flow compressor
[NASA-TM-100948] p 35 N88-24642
- E3 10C compressor test analysis of high-speed post-stall data
[NASA-CR-179521] p 36 N88-28929
- COMPUTATION**
- Two-dimensional viscous flow computations of hypersonic scramjet nozzle flowfields at design and off-design conditions
[AIAA PAPER 88-3280] p 23 A88-50785
- Institute for Computational Mechanics in Propulsion (ICOMP) first year summary
[NASA-TM-100225] p 210 N88-12330
- Computational prediction of propellant reorientation
p 109 N88-15940
- A semianalytical technique for sensitivity analysis of unsteady aerodynamic computations
[NASA-TM-100810] p 189 N88-18976
- Institute for Computational Mechanics in Propulsion (ICOMP)
[NASA-TM-100790] p 211 N88-19202
- A physically consistent model for artificial dissipation in transonic potential flow computations
[NASA-TM-100846] p 211 N88-22652
- Two-dimensional viscous flow computations of hypersonic scramjet nozzle flowfields at design and off-design conditions
[NASA-CR-182150] p 35 N88-25459
- High speed inlet calculations with real gas effects
[NASA-CR-182167] p 13 N88-26336
- A computational analysis of under-expanded jets in the hypersonic regime
[NASA-TM-101319] p 13 N88-27174
- COMPUTATIONAL FLUID DYNAMICS**
- Application of advanced computational codes in the design of an experiment for a supersonic throughflow fan rotor
[ASME PAPER 87-GT-160] p 2 A88-11072
- Control of free shear layers
[AIAA PAPER 87-2689] p 134 A88-16545
- Retooling CFD for hypersonic aircraft
p 1 A88-16749

- Steady and transient least square solvers for thermal problems p 134 A88-17318
- Numerical methods for one-dimensional reaction-diffusion equations arising in combustion theory p 135 A88-18975
- Roll-up of vorticity in adverse-pressure-gradient boundary layers p 135 A88-19194
- A space-marching method for the computation of viscous internal flows p 135 A88-20459
- The calculation of flow over iced airfoils [AIAA PAPER 88-0112] p 4 A88-22078
- K-epsilon turbulence model assessment with reduced numerical diffusion for coaxial jets [AIAA PAPER 88-0342] p 137 A88-22251
- Measurement and prediction of propeller flow field on the PTA aircraft at speeds of up to Mach 0.85 --- Propfan Test Assessment [AIAA PAPER 88-0667] p 19 A88-22497
- A numerical study of the effects of curvature and convergence on dilution jet mixing [AIAA PAPER 87-1953] p 137 A88-23312
- Numerical study of chemically reacting flows using an LU scheme [AIAA PAPER 88-0436] p 5 A88-24825
- Time-accurate simulations of a shear layer forced at a single frequency [AIAA PAPER 88-0061] p 138 A88-27716
- Numerical simulation of hypersonic inlet flows with equilibrium or finite rate chemistry [AIAA PAPER 88-0273] p 5 A88-27717
- Velocity-coupled flow oscillations in a simulated solid-propellant rocket environment [AIAA PAPER 88-0543] p 108 A88-27720
- Consistent boundary conditions for reduced Navier-Stokes (RNS) scheme applied to three-dimensional internal viscous flows [AIAA PAPER 88-0714] p 139 A88-27723
- Explicit finite-volume time-marching calculations of total temperature distributions in turbulent flow p 139 A88-30517
- An explicit finite-volume time-marching procedure for turbulent flow calculations p 139 A88-30518
- Developing fluid flow in a curved duct of square cross-section and its fully developed dual solutions p 139 A88-30957
- Numerical and analytical study of fluid dynamic forces in seals and bearings p 167 A88-31534
- Application of a semi-analytical technique for sensitivity analysis of unsteady aerodynamic computations [AIAA PAPER 88-2377] p 6 A88-32314
- Adaptive grid generation p 209 A88-37363
- Mathematical models for the numerical study of turbulent flows p 140 A88-39472
- Hypercluster - Parallel processing for computational mechanics p 208 A88-40458
- Optimizing advanced propeller designs by simultaneously updating flow variables and design parameters [AIAA PAPER 88-2532] p 6 A88-40718
- Comparison of computational methods for three-dimensional turbulent turbomachinery flows p 6 A88-42452
- Automating the parallel processing of fluid and structural dynamics calculations p 206 A88-46963
- Third-order multi-dimensional Euler/Navier-Stokes solver [AIAA PAPER 88-3645] p 209 A88-48806
- A comparison of ENO and TVD schemes [AIAA PAPER 88-3707] p 210 A88-48831
- Three-dimensional viscous flow computations of a circular jet in subsonic and supersonic cross flow [AIAA PAPER 88-3703] p 143 A88-48916
- Dynamics of two fluids under periodic acceleration [AIAA PAPER 88-3728] p 143 A88-48980
- Solution of the Neumann pressure problem in general orthogonal coordinates using the multigrid technique p 144 A88-50330
- Solutions of one-dimensional steady nozzle flow revisited p 144 A88-50344
- Application of bifurcation theory to axial flow compressor instability [ASME PAPER 88-GT-231] p 169 A88-54313
- Diagnostics development for spray characterization in complex turbulent flows [ASME PAPER 88-GT-241] p 146 A88-54320
- Coolant passage heat transfer with rotation p 147 A88-11160
- A numerical study of the effects of curvature and convergence on dilution jet mixing [NASA-TM-89878] p 26 A88-13347
- SHARP simulation of discontinuities in highly convective steady flow [NASA-TM-100240] p 210 A88-13931
- Numerical study of chemically reacting flows using an LU scheme [NASA-CR-180882] p 26 A88-14094
- Consistent boundary conditions for Reduced Navier-Stokes (RNS) scheme applied to 3-dimensional internal viscous flows [NASA-CR-180874] p 10 A88-15762
- Chemical reacting flows p 79 A88-15793
- High-speed inlet research program and supporting analyses p 17 A88-15811
- CFD validation experiments for internal flows [NASA-TM-100797] p 10 A88-16679
- The use of multigrid techniques in the solution of the Elrod algorithm for a dynamically loaded journal bearing [NASA-CR-180873] p 151 A88-17954
- Application of advanced computational technology to propulsion CFD [NASA-TM-100843] p 204 A88-19102
- Time-accurate simulations of a shear layer forced at a single frequency [NASA-TM-100836] p 152 A88-19740
- Utilization of parallel processing in solving the inviscid form of the average-passageway equation system for multistage turbomachinery [NASA-TM-89845] p 32 A88-21160
- Two-equation low-Reynolds-number turbulence modeling of transitional boundary layer flows characteristic of gas turbine blades [NASA-CR-4145] p 153 A88-23185
- Aeroelastic forced response analysis of turbomachinery p 34 A88-23247
- The development of an intelligent interface to a computational fluid dynamics flow-solver code [NASA-TM-100908] p 207 A88-26127
- Three-dimensional viscous flow computations of a circular jet in subsonic and supersonic cross flow [NASA-CR-182153] p 155 A88-26616
- Convergence acceleration for vector sequences and applications to computational fluid dynamics [NASA-TM-101327] p 212 A88-30377
- COMPUTATIONAL GRIDS**
- Adaptive grid generation p 209 A88-37363
- Time-partitioning simulation models for calculation of parallel computers p 206 A88-46961
- A diagonally inverted LU implicit multigrid scheme [AIAA PAPER 88-3565] p 209 A88-48791
- Solution of the Neumann pressure problem in general orthogonal coordinates using the multigrid technique p 144 A88-50330
- Finite-element grid improvement by minimization of stiffness matrix trace [NASA-TM-100255] p 171 A88-13604
- A multistage mesh generator for solving the average-passageway equation system [NASA-CR-179539] p 10 A88-15769
- The use of multigrid techniques in the solution of the Elrod algorithm for a dynamically loaded journal bearing [NASA-CR-180873] p 151 A88-17954
- Computer-aided modeling and prediction of performance of the modified Lundell class of alternators in space station solar dynamic power systems [NASA-CR-182538] p 201 A88-19000
- The solution of the Elrod algorithm for a dynamically loaded journal bearing using multigrid techniques [NASA-TM-100941] p 154 A88-25854
- A diagonally inverted LU implicit multigrid scheme [NASA-TM-100911] p 13 A88-26340
- COMPUTER AIDED DESIGN**
- Retooling CFD for hypersonic aircraft p 1 A88-16749
- Expert systems for space power supply - Design, analysis, and evaluation p 212 A88-22696
- Application of structural tailoring to spar/shell turboprops [AIAA PAPER 88-2333] p 20 A88-32277
- Development of 8 cm x 8 cm silicon gridded back solar cell for space station p 200 A88-34312
- Probabilistic Structural Analysis Methods for select space propulsion system structural components (PSAM) p 56 A88-49659
- Heat transfer in a real engine environment p 147 A88-11155
- Computer-aided design analysis of 57-mm, angular-contact, cryogenic turbopump bearings [NASA-TP-2816] p 172 A88-18933
- Computer-aided modeling and prediction of performance of the modified Lundell class of alternators in space station solar dynamic power systems [NASA-CR-182538] p 201 A88-19000
- Improved method for stress and compatibility analysis of multicomponent rotating systems [NASA-TM-100884] p 195 A88-25935
- COMPUTER GRAPHICS**
- Interactive computer simulation of fracture processes p 180 A88-16955
- Distributed computation of graphics primitives on a transputer network [NASA-TM-100814] p 206 A88-19147
- Two-dimensional graphics tools for a transputer based display board [NASA-TM-100820] p 207 A88-22591
- User's manual for the two-dimensional transputer graphics toolkit [NASA-TM-100874] p 207 A88-27799
- COMPUTER NETWORKS**
- Hypercluster - Parallel processing for computational mechanics p 208 A88-40458
- Distributed computation of graphics primitives on a transputer network [NASA-TM-100814] p 206 A88-19147
- Implementing direct, spatially isolated problems on transputer networks [NASA-TM-101297] p 207 A88-27796
- COMPUTER PROGRAMMING**
- A satellite system synthesis model for orbital arc allotment optimization p 117 A88-48579
- Adapting high-level language programs for parallel processing using data flow p 207 A88-23234
- COMPUTER PROGRAMS**
- Validation of the NESSUS probabilistic finite element analysis computer program [AIAA PAPER 88-2372] p 205 A88-32309
- Computerized life and reliability modelling for turboprop transmissions [AIAA PAPER 88-2979] p 100 A88-48031
- Blade loss transient dynamics analysis, volume 1. Task 2: TETRA 2 theoretical development [NASA-CR-179632] p 25 A88-10791
- Heat transfer in a real engine environment p 147 A88-11155
- A FORTRAN code for the calculation of probe volume geometry changes in a laser anemometry system caused by window refraction [NASA-TM-100210] p 206 A88-12288
- Internal fluid mechanics research on supercomputers for aerospace propulsion systems [NASA-TM-100289] p 149 A88-15188
- Rotorcraft transmission p 172 A88-15802
- Overview of heat transfer and fluid flow problem areas encountered in Stirling engine modeling [NASA-TM-100131] p 224 A88-17561
- NNEPEC: Chemical equilibrium version of the Navy/NASA Engine Program [NASA-TM-100851] p 32 A88-21161
- The composite blade structural analyzer (COBSTAN) p 33 A88-22390
- MHOST: An efficient finite element program for inelastic analysis of solids and structures p 33 A88-22394
- METCAN: The metal matrix composite analyzer p 74 A88-22395
- Probabilistic structural analysis computer code (NESSUS) p 191 A88-22397
- Computational structural mechanics for engine structures p 33 A88-22399
- Structural tailoring of advanced turboprops p 192 A88-22400
- Computerized life and reliability modelling for turboprop transmissions [NASA-TM-100918] p 173 A88-23220
- The development of an intelligent interface to a computational fluid dynamics flow-solver code [NASA-TM-100908] p 207 A88-26127
- High speed inlet calculations with real gas effects [NASA-CR-182167] p 13 A88-26336
- COMPUTER TECHNIQUES**
- I-BIEM, an iterative boundary integral equation method for computer solutions of current distribution problems with complex boundaries: A new algorithm. I - Theoretical p 205 A88-27795
- Lewis Structures Technology, 1988. Volume 1: Structural Dynamics [NASA-CP-3003-VOL-1] p 194 A88-23226
- Parallel computer methods for eigenvalue extraction p 207 A88-23233
- COMPUTERIZED SIMULATION**
- Computer modeling and simulation of a 20kHz ac distribution system for Space Station p 51 A88-11827
- Fast simulation techniques for switching converters p 122 A88-11878
- Description of an oscillating flow test program p 133 A88-11963
- Interactive computer simulation of fracture processes p 180 A88-16955
- A thermodynamic prediction for microporosity formation in aluminum-rich Al-Cu alloys p 82 A88-18886
- A numerical study of the effects of curvature and convergence on dilution jet mixing [AIAA PAPER 87-1953] p 137 A88-23312
- Performance and efficiency evaluation and heat release study of a direct-injection stratified-charge rotary engine [SAE PAPER 870445] p 166 A88-23313
- Probabilistic structural analysis of aerospace components using NESSUS [AIAA PAPER 88-2373] p 182 A88-32310

SUBJECT INDEX

- Probabilistic composite micromechanics
[AIAA PAPER 88-2375] p 182 A88-32312
- Probabilistic constitutive relationships for cyclic material strength models
[AIAA PAPER 88-2376] p 182 A88-32313
- Determination of compressor in-stall characteristics from engine surge transients p 21 A88-35505
- Mathematical models for the numerical study of turbulent flows p 140 A88-39472
- Real time optical correlator using a magnetooptic device applied to particle imaging velocimetry p 159 A88-40700
- Hygrothermomechanical fiber composite fatigue - Computational simulation p 71 A88-42437
- Time-partitioning simulation models for calculation of parallel computers p 206 A88-46961
- Field oriented control of an induction machine in a high frequency link power system p 127 A88-54711
- RE-1000 free-piston Stirling engine hydraulic output system description p 223 A88-10700
- [NASA-TM-100185]
- Monte Carlo simulation of modulated phases p 210 A88-12323
- [NASA-TM-89654]
- A numerical study of the effects of curvature and convergence on dilution jet mixing p 26 A88-13347
- [NASA-TM-89878]
- The NASA aircraft icing research program p 15 A88-15803
- Simulation test beds for the space station electrical power system p 44 A88-17715
- [NASA-TM-100786]
- Test results of a 40-kW Stirling engine and comparison with the NASA Lewis computer code predictions p 201 A88-19013
- [NASA-TM-87050]
- Hygrothermomechanical fiber composite fatigue: Computational simulation p 74 A88-21257
- [NASA-TM-100840]
- An integrated and modular digital modeling approach for the space station electrical power system development p 61 A88-22935
- [NASA-TM-100904]
- Computer simulation of a single pilot flying a modern high-performance helicopter p 39 A88-26376
- [NASA-TM-100182]
- Computer simulation of multiple pilots flying a modern high performance helicopter p 39 A88-26377
- [NASA-TM-100183]
- COMSAT PROGRAM**
- Service offerings and interfaces for the ACTS network of earth stations p 116 A88-27551
- [AIAA PAPER 88-0800]
- CONCENTRATION (COMPOSITION)**
- The effect of variations of cobalt content on the cyclic oxidation resistance of selected Ni-base superalloys p 82 A88-10031
- Criteria for significance of simultaneous presence of both condensable vapors and aerosol particles on mass transfer (deposition) rates p 114 A88-10971
- Feasibility of hydroxyl concentration measurements by laser-saturated fluorescence in high-pressure flames p 77 A88-17218
- CONCENTRATORS**
- A novel photovoltaic power system which uses a large area concentrator mirror p 197 A88-11811
- Development of an advanced photovoltaic concentrator system for space applications p 51 A88-11812
- Development of a dome Fresnel lens/gallium arsenide photovoltaic concentrator for space applications p 199 A88-34310
- Radiation performance of AlGaAs and InGaAs concentrator cells and expected performance of cascade structures p 125 A88-34356
- Radiation performance of AlGaAs concentrator cells and expected performance of cascade structures p 200 A88-12878
- [NASA-TM-100145]
- Solar concentrator advanced development program, task 1 p 201 A88-18068
- [NASA-CR-179489]
- Space station solar concentrator materials research p 60 A88-21250
- [NASA-TM-100862]
- Thermal distortion analysis of the space station solar dynamic concentrator p 64 A88-25475
- [NASA-TM-100868]
- CONDENSATION**
- Vapor condensation on a turbulent liquid interface p 150 A88-15939
- CONDENSED MATTER PHYSICS**
- Universality relationships in condensed matter - Bulk modulus and sound velocity p 213 A88-43950
- CONDENSERS**
- Study of toluene rotary fluid management device and shear flow condenser performance for a space-based organic Rankine power system p 67 A88-29872
- [NASA-CR-180885]

CONDENSING

- Vapor condensation rate at a turbulent liquid interface, for application to cryogenic hydrogen p 137 A88-22419
- [AIAA PAPER 88-0559]
- Turbine airfoil deposition models and their hot corrosion implications p 91 A88-11178

CONDUCTIVE HEAT TRANSFER

- Steady and transient least square solvers for thermal problems p 134 A88-17318
- Input-output-controlled nonlinear equation solvers p 146 A88-55245
- Applications of an exponential finite difference technique p 175 A88-28312
- [NASA-TM-100939]
- CONDUCTORS**
- Measurement of the properties of lossy materials inside a finite conducting cylinder p 213 A88-20962
- [NASA-CR-182664]
- CONFERENCES**
- Bladed disk assemblies; Proceedings of the Eleventh Biennial Conference on Mechanical Vibration and Noise, Boston, MA, Sept. 27-30, 1987 p 20 A88-31608
- Optical technologies for space communication systems; Proceedings of the Meeting, Los Angeles, CA, Jan. 15, 16, 1987 p 45 A88-35251
- [SPIE-756]
- Low cycle fatigue p 86 A88-35901
- [ASTM STP-942]
- Ion nitriding; Proceedings of the International Conference, Cleveland, OH, Sept. 15-17, 1986 p 114 A88-38926
- Materials analysis by ultrasonics: Metals, ceramics, composites --- Book p 176 A88-44853
- Toward improved durability in advanced aircraft engine hot sections; Proceedings of the Thirty-third ASME International Gas Turbine and Aeroengine Congress and Exposition, Amsterdam, Netherlands, June 5-9, 1988 p 24 A88-54137

- Spacecraft 2000 p 48 A88-10084
- [NASA-CP-2473]
- Turbine Engine Hot Section Technology, 1985 p 185 A88-11140
- [NASA-CP-2405]
- Spacecraft Fire Safety p 45 A88-12520
- [NASA-CP-2476]
- Aeropropulsion '87. Session 4: Instrumentation and Controls Research p 28 A88-15794
- [NASA-CP-10003-SESS-4]
- Aeropropulsion '87. Session 5: Subsonic Propulsion Technology p 28 A88-15800
- [NASA-CP-10003-SESS-5]
- Aeropropulsion '87. Session 6: High-Speed Propulsion Technology p 29 A88-15807
- [NASA-CP-10003-SESS-6]
- Cryogenic Fluid Management Technology Workshop. Volume 1: Presentation material and discussion p 149 A88-15924
- [NASA-CP-10001]
- Cryogenic Fluid Management Technology Workshop. Volume 2: Roundtable Discussion of Technology Requirements p 152 A88-20599
- [NASA-CP-10009]
- Lewis Structures Technology, 1988. Volume 3: Structural Integrity Fatigue and Fracture Wind Turbines HOST p 192 A88-22408
- [NASA-CP-3003-VOL-3]
- Lewis Structures Technology, 1988. Volume 1: Structural Dynamics p 194 A88-23226
- [NASA-CP-3003-VOL-1]
- Structural Ceramics p 106 A88-23872
- [NASA-CP-2427]
- CONFIGURATION INTERACTION**
- Gravity and configurational energy induced microstructural changes in liquid phase sintering p 112 A88-49089

CONFORMAL MAPPING

- Solution of the Neumann pressure problem in general orthogonal coordinates using the multigrid technique p 144 A88-50330

CONSOLIDATION

- Powder processing of nickel and other aluminides by hot consolidation p 87 A88-37158

CONSTITUTIVE EQUATIONS

- Probabilistic constitutive relationships for cyclic material strength models p 182 A88-32313
- [AIAA PAPER 88-2376]
- A nonlinear viscoelastic constitutive equation - Yield predictions in multiaxial deformations p 185 A88-54912
- Constitutive modeling of superalloy single crystals with verification testing p 91 A88-11169
- Structure of a viscoplastic theory p 188 A88-18968
- [NASA-TM-100794]
- Nonlinear Constitutive Relations for High Temperature Applications, 1986 p 189 A88-21498
- [NASA-CP-10010]
- A theory of viscoplasticity accounting for internal damage p 190 A88-21508

CONTROL SYSTEMS DESIGN

- A constitutive model with damage for high temperature superalloys p 93 A88-21510
- Evaluation of structural analysis methods for life prediction p 190 A88-21511
- Unified constitutive models for high-temperature structural applications p 190 A88-21523
- A constitutive model for an overlay coating p 105 A88-21525
- Life assessment of combustor liner using unified constitutive models p 33 A88-22384
- Biaxial experiments supporting the development of constitutive theories for advanced high-temperature materials p 191 A88-22386
- Unified constitutive model development for metal matrix composites at high temperature p 74 A88-22387
- Unified constitutive model for single crystal deformation behavior with applications p 191 A88-22388
- Finite element (MARC) solution technologies for viscoplastic analyses p 191 A88-22389
- Constitutive modeling for isotropic materials p 37 A88-29811
- [NASA-CR-182132]
- Anisotropic constitutive modeling for nickel-base single crystal superalloys p 95 A88-29961
- [NASA-CR-182157]
- CONTACT LOADS**
- Reliability based analysis of contact problems p 189 A88-18975
- [NASA-CR-182117]
- Spur gears: Optimal geometry, methods for generation and Tooth Contact Analysis (TCA) program p 173 A88-23216
- [NASA-CR-4135]
- Design and evaluation of high contact ratio gearing p 175 A88-28319
- [NASA-CR-174958]
- CONTACTORS**
- Space plasma contactor research, 1987 p 219 A88-23649
- [NASA-CR-182148]
- CONTAINERLESS MELTS**
- Containerless processing of undercooled melts p 110 A88-28554
- Containment of a silicone fluid free surface in reduced gravity p 112 A88-49085
- Program for the feasibility of developing a high pressure acoustic levitator p 113 A88-26498
- [NASA-CR-182154]
- CONTAMINATION**
- A life test of a 22-Newton (5-lbf) hydrazine rocket p 57 A88-11750
- [NASA-TM-100232]
- Experimental evaluation of resistojel thruster plume shields p 66 A88-29868
- [NASA-TM-101363]
- CONTINUITY EQUATION**
- Efficient numerical techniques for complex fluid flows p 146 A88-11151
- CONTINUOUS RADIATION**
- Performance of a small, graphite electrode, multistage depressed collector with a 500-W, continuous wave, 4.8- to 9.6-GHz traveling wave tube p 128 A88-15146
- [NASA-TP-2788]
- CONTINUUM MECHANICS**
- A transversely isotropic thermoelastic theory p 196 A88-28332
- [NASA-TM-101302]
- CONTRAROTATING PROPELLERS**
- Noise of a model high speed counterrotation propeller at simulated takeoff/approach conditions (F7/A7) p 214 A88-20176
- [AIAA PAPER 87-2657]
- Summary of low-speed wind tunnel results of several high-speed counterrotation propeller configurations p 7 A88-48758
- [AIAA PAPER 88-3149]
- Noise of a model high speed counterrotation propeller at simulated takeoff/approach conditions (F7/A7) p 216 A88-10592
- [NASA-TM-100206]
- Summary of low-speed wind tunnel results of several high-speed counterrotation propeller configurations p 13 A88-24597
- [NASA-TM-100945]
- CONTROL EQUIPMENT**
- Microwave performance of an optically controlled AlGaAs/GaAs high electron mobility transistor and GaAs MESFET p 123 A88-24911
- CONTROL SYSTEMS DESIGN**
- Conceptual design of an optic based engine control system p 18 A88-11079
- [ASME PAPER 87-GT-168]
- An integrated approach to space station power system autonomous control p 52 A88-11853
- Control of shear flows by artificial excitation p 3 A88-16567
- [AIAA PAPER 87-2722]
- The design of a turboshaft speed governor using modern control techniques p 170 A88-10339
- [NASA-CR-175046]
- Space station resistojel system requirements and interface definition study p 58 A88-12541
- [NASA-CR-180832]
- Aeropropulsion '87. Session 2: Aeropropulsion Structures Research p 27 A88-15785
- [NASA-CP-10003-SESS-2]

- Aeropropulsion '87. Session 4: Instrumentation and Controls Research
 [NASA-CP-10003-SESS-4] p 28 N88-15794
 Directions in propulsion control p 28 N88-15799
 Supersonic STOVL propulsion technology program: An overview p 29 N88-15808
 Optically controlled phased-array antenna technology for space communication systems
 [NASA-TM-100852] p 119 N88-18809
 Microgravity robotics technology program
 [NASA-TM-100896] p 173 N88-23219
 Fiber optics for advanced aircraft
 [NASA-TM-101294] p 1 N88-26328
 Computer simulation of multiple pilots flying a modern high performance helicopter
 [NASA-TM-100183] p 39 N88-26377
 A reusable rocket engine intelligent control
 [NASA-TM-100963] p 65 N88-26401
- CONTROL THEORY**
 Directions in propulsion control p 28 N88-15799
- CONTROL VALVES**
 Application of several variable-valve-timing concepts to an LHR engine
 [ASME PAPER 87-ICE-29] p 19 A88-15119
- CONTROLLERS**
 COSPAS/SARSAT 406-MHz emergency beacon digital controller
 [NASA-TM-100859] p 121 N88-26566
- CONVECTION**
 Local convective flows in partly solidified alloys p 219 A88-18467
 Growth of needle-shaped crystals in the presence of convection p 111 A88-37715
 Fingering flow patterns of thermosolutal convection in rectangular enclosures
 [AIAA PAPER 88-3823] p 144 A88-49000
 Fingering flow patterns of thermosolutal convection in rectangular enclosures
 [NASA-TM-100854] p 152 N88-21417
- CONVECTION CURRENTS**
 Double-diffusive effects during solidification p 221 A88-43933
- CONVECTIVE FLOW**
 Isothermal dendritic growth - A low gravity experiment p 110 A88-28556
 Dynamics of two fluids under periodic acceleration
 [AIAA PAPER 88-3728] p 143 A88-48980
 SHARP simulation of discontinuities in highly convective steady flow
 [NASA-TM-100240] p 210 N88-13931
 A payload for investigating the influence of convection on GaAs crystal growth p 221 N88-17702
 High Rayleigh number convection in rectangular enclosures with differentially heated vertical walls and aspect ratios between zero and unity
 [NASA-TM-100277] p 151 N88-19739
- CONVECTIVE HEAT TRANSFER**
 Development of a special-purpose test surface guided by uncertainty analysis - Introduction of a new uncertainty analysis step
 [AIAA PAPER 88-0169] p 39 A88-22121
 Measurement of local convective heat transfer coefficients from a smooth and roughened NACA-0012 airfoil - Flight test data
 [AIAA PAPER 88-0287] p 136 A88-22207
 Magnetic fields interacting with nonlinear compressible convection p 226 A88-31163
 Experiments for the determination of convective diffusion heat/mass transfer to burner rig test targets comparable in size to jet stream diameter p 140 A88-41574
 Heat transfer in the tip region of a rotor blade simulator p 147 N88-11159
 Measurement of local convective heat transfer coefficients from a smooth and roughened NACA-0012 airfoil: Flight test data
 [NASA-TM-100284] p 149 N88-13552
 Experimental measurements of heat transfer from an iced surface during artificial and natural cloud icing conditions
 [AIAA-86-1352] p 153 N88-23718
 Impact of ETO propellants on the aerothermodynamic analyses of propulsion components
 [NASA-TM-101303] p 156 N88-30094
- CONVERGENCE**
 A numerical study of the effects of curvature and convergence on dilution jet mixing
 [AIAA PAPER 87-1953] p 137 A88-23312
 An empirical model of the effects of curvature and convergence on dilution jet mixing
 [AIAA PAPER 88-3180] p 23 A88-50783
 A numerical study of the effects of curvature and convergence on dilution jet mixing
 [NASA-TM-89678] p 26 N88-13347
- An empirical model of the effects of curvature and convergence on dilution jet mixing
 [NASA-TM-100896] p 34 N88-24640
 Convergence acceleration for vector sequences and applications to computational fluid dynamics
 [NASA-TM-101327] p 212 N88-30377
- CONVERGENT-DIVERGENT NOZZLES**
 Techniques utilized in the simulated altitude testing of a 2D-CD vectoring and reversing nozzle
 [NASA-TM-100872] p 40 N88-25464
- CONVERTERS**
 A study of Schwarz converters for nuclear powered spacecraft p 51 A88-11823
- CONVERTIBLE FAN-SHAFT ENGINES**
 Test stand performance of a convertible engine for advanced V/STOL and rotorcraft propulsion
 [NASA-TM-100211] p 25 N88-11679
 The convertible engine: A dual-mode propulsion system p 31 N88-16639
- COOLANTS**
 Oxygen plasma effects on several liquid droplet radiator fluids p 142 A88-47962
- COOLING**
 Heat transfer in the tip region of a rotor blade simulator p 147 N88-11159
 Coolant passage heat transfer with rotation p 147 N88-11160
 Heat transfer with very high free stream turbulence p 148 N88-11161
 Local heat/mass transfer and pressure drop in a two-pass rib-roughened channel for turbine airfoil cooling
 [NASA-CR-179635] p 148 N88-12039
 Space power radiation cooled dc transmission line analysis p 129 N88-24506
 Fraction eutectic measurements in slowly cooled Pb - 15 wt percent Sn alloys
 [NASA-CR-180630] p 94 N88-25531
- COOLING SYSTEMS**
 Development of a thermal and structural analysis procedure for cooled radial turbines
 [ASME PAPER 88-GT-18] p 145 A88-54164
 Aircraft engine hot section technology: An overview of the HOST Project p 29 N88-15804
- COORDINATES**
 Three-dimensional adaptive grid generation for body-fitted coordinate system
 [NASA-CR-182192] p 155 N88-27520
- COPLANARITY**
 Modeling of some coplanar waveguide discontinuities
 [NASA-TM-100808] p 119 N88-17880
- COPPER**
 A viscoplastic theory applied to copper
 [NASA-TM-100831] p 189 N88-21497
- COPPER ALLOYS**
 A thermodynamic prediction for microporosity formation in aluminum-rich Al-Cu alloys p 82 A88-18886
- COPPER CHLORIDES**
 Stability of the electrical resistivity of bromine, iodine monochloride, copper(II) chloride, and nickel(II) chloride intercalated pitch-based graphite fibers p 100 A88-49403
- COPPER OXIDES**
 Weak-field magnetization of superconducting Y1Ba2Cu3O(x) - Relationship to microstructure p 219 A88-18814
 Characterization of Ba2YCu3O(7-x) prepared in an inert atmosphere p 221 A88-49376
 Synthesis and characterization of high-T(sub c) screen-printed Y-Ba-Cu-O films on alumina
 [NASA-TM-100860] p 222 N88-22805
- CORE FLOW**
 High Rayleigh number convection in rectangular enclosures with differentially heated vertical walls and aspect ratios between zero and unity
 [NASA-TM-100277] p 151 N88-19739
- CORNER FLOW**
 Wall shear stress measurement in blade end-wall corner region
 [ASME PAPER 87-GT-181] p 131 A88-11089
 Experimental evaluation of corner vanes - Summary
 [SAE PAPER 871784] p 39 A88-30778
 Experimental evaluation of turning vane designs for high-speed and coupled fan-drive corners of 0.1-scale model of NASA Lewis Research Center's proposed altitude wind tunnel
 [NASA-TP-2681] p 40 N88-17686
- CORRELATION**
 On the correlation of plume centerline velocity decay of turbulent acoustically excited jets
 [AIAA PAPER 87-2692] p 3 A88-18654
 Correlation of velocity and velocity-density turbulence in the exhaust of an atmospheric burner p 161 N88-11147
 Application of optical correlation techniques to particle imaging velocimetry
 [NASA-TM-101306] p 163 N88-29152
- CORROSION**
 Wear of iron and nickel in corrosive liquid environments p 88 A88-40790
 Wear of iron and nickel in corrosive liquid environments
 [NASA-TM-100246] p 91 N88-11817
 Structural Ceramics
 [NASA-CP-2427] p 106 N88-23872
- CORROSION TESTS**
 Sodium sulfate-induced corrosion of pure nickel and superalloy Udimer 700 in a high velocity burner rig at 900 C p 83 A88-20266
- COSMOLOGY**
 String-driven inflation p 225 A88-27446
 Cosmic string induced peculiar velocities p 226 A88-28762
 Calculations of rates for direct detection of neutralino dark matter p 227 A88-48463
- COSPAS**
 COSPAS/SARSAT 406-MHz emergency beacon digital controller
 [NASA-TM-100859] p 121 N88-26566
- COST ANALYSIS**
 Economic benefits of the Space Station to commercial communication satellite operators
 [IAF PAPER 87-622] p 41 A88-16215
 Communications satellite systems operations with the space station. Volume 3: Supplementary technical report
 [NASA-CR-180875] p 48 N88-16794
 Centaur operations at the space station: Cost and transportation analysis
 [NASA-CR-182128] p 44 N88-29835
- COST EFFECTIVENESS**
 Cost-effective intersatellite link applications to the fixed satellite services
 [AIAA PAPER 88-0770] p 45 A88-27544
 Communications satellites in non-geostationary orbits
 [AIAA PAPER 88-0842] p 46 A88-27583
 The economics of satellite retrieval
 [AIAA PAPER 88-0843] p 44 A88-27584
 Automotive Stirling engine: Mod 2 design report
 [NASA-CR-175106] p 223 N88-11578
- COST REDUCTION**
 Ground-based microgravity materials science research at NASA's Microgravity Materials Science Laboratory p 112 A88-49090
 Small gas turbine engine technology p 30 N88-16638
- COUNTER ROTATION**
 Noise characteristics of model counter-rotating Prop-Fans
 [AIAA PAPER 87-2656] p 213 A88-16526
 Noise of a model high speed counterrotation propeller at simulated takeoff/approach conditions (F7/A7)
 [AIAA PAPER 87-2657] p 214 A88-20176
 Noise of a model counterrotation propeller with reduced aft rotor diameter at simulated takeoff/approach conditions (F7/A3)
 [AIAA PAPER 88-0263] p 214 A88-22192
 Scale model acoustic testing of counterrotating fans
 [AIAA PAPER 88-2057] p 22 A88-37947
 Porous wind tunnel corrections for counterrotation propeller testing
 [AIAA PAPER 88-2055] p 6 A88-44490
 Noise of a model high speed counterrotation propeller at simulated takeoff/approach conditions (F7/A7)
 [NASA-TM-100206] p 216 N88-10592
 Noise of a model counterrotation propeller with reduced aft rotor diameter at simulated takeoff/approach conditions (F7/A3)
 [NASA-TM-100254] p 216 N88-13961
 Porous wind tunnel corrections for counterrotation propeller testing
 [NASA-TM-100873] p 11 N88-22019
 The 2-D and 3-D time marching transonic potential flow method for propfans p 11 N88-23245
- COUPLING**
 Experimental evaluation of turning vane designs for high-speed and coupled fan-drive corners of 0.1-scale model of NASA Lewis Research Center's proposed altitude wind tunnel
 [NASA-TP-2681] p 40 N88-17686
- COWLING**
 Thermostructural analysis with experimental verification in a high heat flux facility of a simulated cowl lip
 [AIAA PAPER 88-2222] p 39 A88-32188
 Thermostructural analysis of simulated cowl lips p 192 N88-22403
- CRACK GEOMETRY**
 Calibration of a Mode II test specimen p 183 A88-47014
 Microstructural effects on fracture toughness of polycrystalline ceramics in combined mode I and mode II loading
 [ASME PAPER 88-GT-208] p 101 A88-54294

CRACK INITIATION

- A probabilistic model of brittle crack formation
p 180 A88-18696
- Fatigue crack propagation of nickel-base superalloys at 650 deg C
p 86 A88-35908
- Fatigue life prediction modeling for turbine hot section materials
p 184 A88-54144
- Flaw imaging and ultrasonic techniques for characterizing sintered silicon carbide
[NASA-TM-100177] p 177 N88-12106
- Creep life prediction based on stochastic model of microstructurally short crack growth
[NASA-TM-100245] p 186 N88-12825
- Fatigue life prediction modeling for turbine hot section materials
[NASA-TM-100291] p 187 N88-14453
- Evaluation of structural analysis methods for life prediction
p 190 N88-21511
- In situ fatigue loading stage inside scanning electron microscope
p 193 N88-22419
- Grain boundary oxidation and low-cycle fatigue at elevated temperatures
p 193 N88-22420
- Fatigue damage mapping
p 193 N88-22423
- Life prediction modeling based on strainrange partitioning
p 178 N88-22425
- Life prediction modeling based on cyclic damage accumulation
p 178 N88-22426
- Fatigue damage modeling for coated single crystal superalloys
p 93 N88-22427
- The analysis of fatigue crack growth mechanism and oxidation and fatigue life at elevated temperatures
[NASA-CR-182129] p 94 N88-22987
- Cyclic fatigue damage characteristics observed for simple loadings extended to multiaxial life prediction
[NASA-CR-182126] p 195 N88-25016
- Characterization of fatigue crack initiation and propagation in Ti-6Al-4V with electrical potential drop technique
[NASA-TM-100877] p 195 N88-25937
- CRACK PROPAGATION**
- Curvilinear crack layer propagation
p 96 A88-14568
- The effects of crack surface friction and roughness on crack tip stress fields
p 180 A88-14579
- Interactive computer simulation of fracture processes
p 180 A88-16955
- A probabilistic model of brittle crack formation
p 180 A88-18696
- On self-similarity of crack layer
p 181 A88-24054
- Macrocrack interaction with transverse array of microcracks
p 181 A88-30236
- Fatigue crack propagation of nickel-base superalloys at 650 deg C
p 86 A88-35908
- Creep-fatigue behavior of NiCoCrAlY coated PWA 1480 superalloy single crystals
p 86 A88-35911
- Crack diffusion coefficient - A candidate fracture toughness parameter for short fiber composites
p 70 A88-36945
- Semi-empirical crack tip analysis
p 183 A88-47681
- Accelerated crack growth rate at low Delta K in a single crystal superalloy
p 89 A88-47687
- Analysis of crack propagation in roller bearings using the boundary integral equation method - A mixed-mode loading problem
p 168 A88-49183
- Fatigue life prediction modeling for turbine hot section materials
p 184 A88-54144
- Effects of subcritical crack growth on fracture toughness of ceramics assessed in chevron-notched three-point bend tests
[ASME PAPER 88-GT-185] p 185 A88-54276
- Elevated temperature crack growth
p 186 N88-11174
- Creep life prediction based on stochastic model of microstructurally short crack growth
[NASA-TM-100245] p 186 N88-12825
- The effect of texture on the crack growth resistance of alumina
[NASA-TM-100250] p 102 N88-14206
- Fatigue life prediction modeling for turbine hot section materials
[NASA-TM-100291] p 187 N88-14453
- Mode 2 fracture mechanics
p 193 N88-22418
- In situ fatigue loading stage inside scanning electron microscope
p 193 N88-22419
- Grain boundary oxidation and low-cycle fatigue at elevated temperatures
p 193 N88-22420
- Elevated temperature crack growth
p 193 N88-22421
- Fatigue damage mapping
p 193 N88-22423
- Fatigue crack growth behavior of a single crystal alloy as observed through an in situ fatigue loading stage
[NASA-TM-100863] p 93 N88-22986
- The analysis of fatigue crack growth mechanism and oxidation and fatigue life at elevated temperatures
[NASA-CR-182129] p 94 N88-22987
- On governing equations for crack layer propagation
[NASA-CR-182120] p 194 N88-23272

- Fracture mechanics
p 194 N88-23877
- Resolved shear stress intensity coefficient and fatigue crack growth in large crystals
[NASA-CR-182137] p 195 N88-24997
- Characterization of fatigue crack initiation and propagation in Ti-6Al-4V with electrical potential drop technique
[NASA-TM-100877] p 195 N88-25937
- Accelerated fatigue crack growth behavior of PWA 1480 single crystal alloy and its dependence on the deformation mode
[NASA-TM-100943] p 95 N88-26436
- CRACK TIPS**
- Curvilinear crack layer propagation
p 96 A88-14568
- The effects of crack surface friction and roughness on crack tip stress fields
p 180 A88-14579
- On self-similarity of crack layer
p 181 A88-24054
- A review of path-independent integrals in elastic-plastic fracture mechanics
p 183 A88-47001
- Semi-empirical crack tip analysis
p 183 A88-47681
- CRACKING (FRACTURING)**
- Curvilinear crack layer propagation
p 96 A88-14568
- Reliability based analysis of contact problems
[NASA-CR-182117] p 189 N88-18975
- CRACKS**
- Stress intensity and crack displacement for small edge cracks
[NASA-TP-2801] p 188 N88-17095
- SiC fiber reinforced reaction-bonded Si3N4 composites
p 75 N88-23892
- CREEP ANALYSIS**
- Fatigue crack propagation of nickel-base superalloys at 650 deg C
p 86 A88-35908
- CREEP PROPERTIES**
- Compressive creep behavior of alloys based on B2 FeAl
p 82 A88-10043
- Thermomechanical behavior of plasma-sprayed ZrO2-Y2O3 coatings influenced by plasticity, creep, and oxidation
p 95 A88-12588
- Effect of initial gamma prime size on the elevated temperature creep properties of single crystal nickel base superalloys
p 82 A88-18884
- An update of the total-strain version of SRP
p 86 A88-35910
- Creep-fatigue behavior of NiCoCrAlY coated PWA 1480 superalloy single crystals
p 86 A88-35911
- Creep fatigue life prediction for engine hot section materials (isotropic): Third year progress review
p 186 N88-11173
- Creep life prediction based on stochastic model of microstructurally short crack growth
[NASA-TM-100245] p 186 N88-12825
- Aeropropulsion '87. Session 1: Aeropropulsion Materials Research
[NASA-CP-10003-SESS-1] p 31 N88-16697
- Creep and fatigue research efforts on advanced materials
p 187 N88-16701
- Relationship between fatigue life in the creep-fatigue region and stress-strain response
[NASA-TM-100796] p 188 N88-18040
- Creep behavior of tungsten/nickelium and tungsten/nickelium-1 percent zirconium composites
[NASA-TM-100804] p 92 N88-18707
- Structure of a viscoplastic theory
[NASA-TM-100794] p 188 N88-18968
- Processing, physical metallurgy and creep of NiAl + Ta and NiAl + Nb alloys
[NASA-CR-182113] p 92 N88-21295
- Creep behavior of tungsten/nickelium and tungsten/nickelium-1 percent zirconium composites
p 75 N88-24427
- The high temperature creep deformation of Si3N4-6Y2O3-2Al2O3
[NASA-CR-183204] p 76 N88-28981
- CREEP RUPTURE STRENGTH**
- Elevated temperature durability of ceramic materials
[AIAA PAPER 88-3055] p 100 A88-44743
- Stress rupture behavior of silicon carbide coated, low modulus carbon/carbon composites
[NASA-CR-180863] p 72 N88-14150
- CREEP TESTS**
- Creep-fatigue behavior of NiCoCrAlY coated PWA 1480
p 186 N88-11176
- CRITICAL FLOW**
- Numerical study of multicomponent droplet vaporization at near critical conditions
[AIAA PAPER 88-0637] p 108 A88-27721
- CRITICAL TEMPERATURE**
- Critical fluid light scattering
p 158 A88-33003
- Characterization of Ba2YCu3O(7-x) prepared in an inert atmosphere
p 221 A88-49376
- Critical exponent for the viscosity of four binary liquids
p 222 A88-53050
- CRITICAL VELOCITY**
- Free-streamline analysis of deformation and dislodging by wind force of drops on a surface
p 137 A88-25191

CROSS FLOW

- Three-dimensional viscous flow computations of a circular jet in subsonic and supersonic cross flow
[AIAA PAPER 88-3703] p 143 A88-48916
- Aerothermal modeling program, phase 2
p 146 N88-11149
- Dilution jet mixing program, phase 3
p 147 N88-11153
- On the mixing of a row of jets with a confined crossflow
p 147 N88-11154
- Three-dimensional viscous flow computations of a circular jet in subsonic and supersonic cross flow
[NASA-CR-182153] p 155 N88-26616

CROSS POLARIZATION

- Crosspolarisation characteristics of rectangular patch antennas
p 117 A88-47705

CRUISING FLIGHT

- Propulsion challenges and opportunities for high-speed transport aircraft
p 30 N88-15809

CRYOGENIC COOLING

- Design, development, and test of Shuttle/Centaur G-prime cryogenic tankage thermal protection systems
[NASA-CR-182153] p 47 A88-53182

- Cryogenic Fluid Management Technology Workshop. Volume 1: Presentation material and discussion
[NASA-CP-10001] p 149 N88-15924

CRYOGENIC EQUIPMENT

- Analysis and design of a gas-lubricated, sectorized, floating ring seal
[ASME PAPER 87-TRIB-55] p 166 A88-23310

CRYOGENIC FLUID STORAGE

- Vapor condensation rate at a turbulent liquid interface, for application to cryogenic hydrogen
[AIAA PAPER 88-0559] p 137 A88-22419
- Cryogenic Fluid Management Technology Workshop. Volume 1: Presentation material and discussion
[NASA-CP-10001] p 149 N88-15924
- LeRC cryogenic fluid management program overview
p 150 N88-15928
- Technology requirements for an orbiting fuel depot: A necessary element of a space infrastructure
[NASA-TM-101370] p 49 N88-29845

CRYOGENIC FLUIDS

- Cryogenic Fluid Management Technology Workshop. Volume 1: Presentation material and discussion
[NASA-CP-10001] p 149 N88-15924
- Cryogenic fluid management program flight concept definition
p 150 N88-15929
- Vapor condensation on a turbulent liquid interface
p 150 N88-15939
- Computer-aided design analysis of 57-mm, angular-contact, cryogenic turbopump bearings
[NASA-TP-2816] p 172 N88-18933
- Cryogenic Fluid Management Technology Workshop. Volume 2: Roundtable Discussion of Technology Requirements
[NASA-CP-10009] p 152 N88-20599
- Nucleate pool boiling: High gravity to reduced gravity; liquid metals to cryogenics
p 113 N88-24464

CRYOGENIC ROCKET PROPELLANTS

- Cryogenic Fluid Management Technology Workshop. Volume 1: Presentation material and discussion
[NASA-CP-10001] p 149 N88-15924
- Breadboard RL10-2B low-thrust operating mode (second iteration) test report
[NASA-CR-182160] p 66 N88-29867

CRYOGENICS

- Thermodynamic modeling of the no-vent fill methodology for transferring cryogenics in low gravity
[AIAA PAPER 88-3403] p 55 A88-48765
- Cryogenic Fluid Management Technology Workshop. Volume 1: Presentation material and discussion
[NASA-CP-10001] p 149 N88-15924
- LeRC cryogenic fluid management program overview
p 150 N88-15928
- Cryogenic fluid management program flight concept definition
p 150 N88-15929
- Thermodynamic modeling of the no-vent fill methodology for transferring cryogenics in low gravity
[NASA-TM-100932] p 63 N88-24686

CRYSTAL DEFECTS

- Improved beta-SiC heteroepitaxial films using off-axis Si substrates
p 219 A88-10431
- Lattice defects in beta-SiC grown epitaxially on silicon substrates
p 220 A88-28711
- Gravitational macrosegregation in binary Pb-Sn alloy ingots
p 111 A88-41211
- Fingering flow patterns of thermosolutal convection in rectangular enclosures
[AIAA PAPER 88-3823] p 144 A88-49000
- Fingering flow patterns of thermosolutal convection in rectangular enclosures
[NASA-TM-100854] p 152 N88-21417
- Improved silicon carbide for advanced heat engines
p 106 N88-23879

CRYSTAL GROWTH

- Strength optimization of alpha-SiC by improved processing p 107 N88-23880
Improved processing of Si3N4 p 107 N88-23882

CRYSTAL GROWTH

- Simulation of fluid flows during growth of organic crystals in microgravity p 109 A88-13163
Electrical resistivity (4K to 2100K) of annealed vapor growth carbon fibers p 96 A88-17214
Local convective flows in partly solidified alloys p 219 A88-18467

- Dendritic growth in a supercooled alloy melt p 83 A88-19966
Dendritic solidification under microgravity conditions [AIAA PAPER 88-0248] p 110 A88-22186

- Isothermal dendritic growth - A low gravity experiment p 110 A88-28556
Silicon carbide - Progress in crystal growth p 99 A88-40792

- Preparation for microgravity - The role of the Microgravity Material Science Laboratory [AIAA PAPER 88-3510] p 111 A88-42908

- Characterization of directionally solidified lead chloride p 111 A88-43170
Microwave and millimeter-wave power generation in silicon carbide avalanche devices p 126 A88-47599

- Ground-based microgravity materials science research at NASA's Microgravity Materials Science Laboratory p 112 A88-49090
Ground based materials science experiments p 43 A88-52364

- High-temperature electronics p 128 A88-15797
A payload for investigating the influence of convection on GaAs crystal growth p 221 A88-17702

- High Rayleigh number convection in rectangular enclosures with differentially heated vertical walls and aspect ratios between zero and unity [NASA-TM-100277] p 151 A88-19739

- Preparation for microgravity: The role of the microgravity materials science laboratory [NASA-TM-100906] p 113 A88-24811

- CRYSTAL LATTICES**
Lattice defects in beta-SiC grown epitaxially on silicon substrates p 220 A88-28711

- Lattice parameter variations during aging in nickel-base superalloys p 90 A88-51318

- CRYSTAL STRUCTURE**
Microscopy of epitaxially grown beta-SiC on 001-plane silicon p 98 A88-31023

- Growth of needle-shaped crystals in the presence of convection p 111 A88-37715
Variable angle spectroscopic ellipsometry - Application to GaAs-AlGaAs multilayer homogeneity characterization p 220 A88-40139

- Silicon carbide - Progress in crystal growth p 99 A88-40792
Monte Carlo simulation of modulated phases [NASA-TM-89654] p 210 A88-12323

- CRYSTALLIZATION**
Crystallization behavior of a melt-spun Fe-Ni based steel p 83 A88-19958

- Stability relationship for water droplet crystallization with the NASA Lewis icing spray nozzle [AIAA PAPER 88-0289] p 137 A88-22209

- Stability relationship for water droplet crystallization with the NASA Lewis icing spray [NASA-TM-100220] p 24 A88-10790

- NASA research Program: The roles of fluid motion and other transport phenomena in the morphology of materials [NASA-CR-182801] p 222 A88-25327

- CRYSTALLOGRAPHY**
A crystallographic model for nickel base single crystal alloys p 89 A88-48182

- Constitutive modeling for single crystal superalloys p 90 A88-11168

- CRYSTALS**
NASA research Program: The roles of fluid motion and other transport phenomena in the morphology of materials [NASA-CR-182801] p 222 A88-25327

- CUBIC LATTICES**
Low-temperature photoluminescence studies of chemical-vapor-deposition-grown 3C-SiC on Si p 127 A88-53396

- Raman scattering studies of chemical-vapor-deposited cubic SiC films of (100)Si p 127 A88-53397

- CUMULATIVE DAMAGE**
On self-similarity of crack layer p 181 A88-24054

- A nonlinear history-dependent damage model for low cycle fatigue p 86 A88-35905

- CURING**
The 700 F properties of autoclave cured PMR-2 composites [NASA-TM-100923] p 75 A88-24712

CURRENT DISTRIBUTION

- I-BIEM, an iterative boundary integral equation method for computer solutions of current distribution problems with complex boundaries: A new algorithm. I - Theoretical p 205 A88-27795

CURRENT REGULATORS

- Field oriented control of an induction machine in a high frequency link power system p 127 A88-54711

- A cascaded Schwarz converter for high frequency power distribution p 127 A88-54713

CURVATURE

- Measurements of the turbulent transport of heat and momentum in convexly curved boundary layers - Effects of curvature, recovery and free-stream turbulence [ASME PAPER 87-GT-199] p 131 A88-11103

- Development of a special-purpose test surface guided by uncertainty analysis - Introduction of a new uncertainty analysis step [AIAA PAPER 88-0169] p 39 A88-22121

- A numerical study of the effects of curvature and convergence on dilution jet mixing [AIAA PAPER 87-1953] p 137 A88-23312

- An empirical model of the effects of curvature and convergence on dilution jet mixing [AIAA PAPER 88-3180] p 23 A88-50783

- A numerical study of the effects of curvature and convergence on dilution jet mixing [NASA-TM-89878] p 26 A88-13347

- An empirical model of the effects of curvature and convergence on dilution jet mixing [NASA-TM-100896] p 34 A88-24640

- CURVED BEAMS**
Non-isothermal elastoviscoplastic analysis of planar curved beams p 190 A88-21526

- CURVES**
Method and models for R-curve instability calculations [NASA-TM-100935] p 194 A88-23278

- CURVES (GEOMETRY)**
A satellite system synthesis model for orbital arc allotment optimization p 117 A88-48579

- Numerical arc segmentation algorithm for a radio conference-NASARC, version 2.0: User's manual [NASA-TM-100161] p 119 A88-16928

- CYCLIC LOADS**
Finite element methods in probabilistic mechanics p 212 A88-29060

- Probabilistic constitutive relationships for cyclic material strength models [AIAA PAPER 88-2376] p 182 A88-32313

- Low cycle fatigue [ASTM STP-942] p 86 A88-35901

- A nonlinear history-dependent damage model for low cycle fatigue p 86 A88-35905

- An extended life and performance test of a low-power arcjet [AIAA PAPER 88-3106] p 55 A88-48756

- Bithermal low-cycle fatigue behavior of a NiCoCrAlY-coated single crystal superalloy p 90 A88-51736

- Constitutive modeling for isotropic materials p 185 A88-11171

- A low-power arcjet cyclic lifetest [NASA-TM-100233] p 57 A88-11748

- The cyclic stress-strain behavior of a single crystal nickel-base superalloy [NASA-TM-100269] p 92 A88-19610

- High-temperature combustor liner tests in structural component response test facility p 33 A88-22383

- Life assessment of combustor liner using unified constitutive models p 33 A88-22384

- A cyclic ground test of an ion auxiliary propulsion system: Description and operational considerations [NASA-TM-100870] p 62 A88-23829

- An extended life and performance test of a low-power arcjet [NASA-TM-100942] p 63 A88-24687

- Cyclic fatigue damage characteristics observed for simple loadings extended to multiaxial life prediction [NASA-CR-182126] p 195 A88-25016

- CYCLOTRON RESONANCE DEVICES**
30-cm electron cyclotron plasma generator p 122 A88-18633

- CYLINDERS**
Hot piston ring/cylinder liner materials: Selection and evaluation [NASA-TM-100276] p 102 A88-15872

- Cast iron-base alloy for cylinder/regenerator housing [NASA-CR-182116] p 92 A88-19613

- Measurement of the properties of lossy materials inside a finite conducting cylinder [NASA-CR-182664] p 213 A88-20962

- CYLINDRICAL BODIES**
Transient radiative cooling of an absorbing and scattering cylinder - A separable solution p 140 A88-41409

CYLINDRICAL CHAMBERS

- Overview of free-piston Stirling engine technology for space power application [NASA-TM-88886] p 223 A88-12427

D

DAMAGE

- Curvilinear crack layer propagation p 96 A88-14568
Fiber composite structural durability and damage tolerance: Simplified predictive methods [NASA-TM-100179] p 72 A88-13409

- Relationship between fatigue life in the creep-fatigue region and stress-strain response [NASA-TM-100796] p 188 A88-18040

- The relationship between observed fatigue damage and life estimation models [NASA-CR-182191] p 196 A88-27611

DAMAGE ASSESSMENT

- A nonlinear history-dependent damage model for low cycle fatigue p 86 A88-35905

- A theory of viscoplasticity accounting for internal damage p 190 A88-21508

- A constitutive model with damage for high temperature superalloys p 93 A88-21510

- Impact damage in composite laminates p 74 A88-22402

- Life prediction modeling based on cyclic damage accumulation p 178 A88-22426

- Characterization of fatigue crack initiation and propagation in Ti-6Al-4V with electrical potential drop technique [NASA-TM-100877] p 195 A88-25937

- DAMPERS**
An integrated approach for friction damper design p 167 A88-31598

- DAMPING**
The impact damped harmonic oscillator in free decay p 167 A88-31581

- Characterization of damped structural connections for multi-component systems [NASA-TM-100801] p 189 A88-18974

- Experimental determination of aerodynamic damping in a three-stage transonic axial-flow compressor [NASA-TM-100953] p 35 A88-27200

- DARK MATTER**
Cosmic string induced peculiar velocities p 226 A88-28762

- Calculations of rates for direct detection of neutralino dark matter p 227 A88-48463

- DATA ACQUISITION**
Inter and intra blade row laser velocimetry studies of gas turbine compressor flows [ASME PAPER 87-GT-235] p 2 A88-11126

- A distributed data acquisition system for aeronautics test facilities p 39 A88-33065

- Further development of the dynamic gas temperature measurement system p 160 A88-11141

- Accurate positioning of long, flexible ARM's (Articulated Robotic Manipulator) p 174 A88-23243

- DATA BASE MANAGEMENT SYSTEMS**
Laboratory Information Management System (LIMS): A case study [NASA-TM-100835] p 208 A88-21697

- DATA BASES**
Space communication link propagation data for selected cities within the multiple beam and steerable antenna coverage areas of the advanced communications technology satellite [NASA-TM-100861] p 120 A88-23070

- DATA CORRELATION**
Comparison of measured and calculated forces on the RE-1000 free-piston Stirling engine displacer p 165 A88-11966

- DATA FLOW ANALYSIS**
Adapting high-level language programs for parallel processing using data flow p 207 A88-23234

- DATA REDUCTION**
Real time optical correlator using a magneto-optic device applied to particle imaging velocimetry p 159 A88-40700

- DATA RETRIEVAL**
The economics of satellite retrieval [AIAA PAPER 88-0843] p 44 A88-27584

- DATA STRUCTURES**
A hypermatrix formulation for subspace iteration p 205 A88-15427

- DATA TRANSFER (COMPUTERS)**
Analysis of counting errors in the phase/Doppler particle analyzer [NASA-TM-100231] p 161 A88-12043

- DATA TRANSMISSION**
Lewis Information Network (LINK): Background and overview [NASA-TM-100162] p 117 A88-11925

DECAY RATES

- The impact damped harmonic oscillator in free decay
p 167 A88-31581

DEFECTS

- Nondestructive evaluation of sintered ceramics
p 177 N88-22416

DEFLECTION

- Optical measurement of propeller blade deflections
[NASA-TP-2841] p 163 N88-28286
Optical measurement of unducted fan blade deflections
[NASA-TM-100966] p 163 N88-29142

DEFORMATION

- Free-streamline analysis of deformation and dislodging by wind force of drops on a surface p 137 A88-25191
Deformation, fatigue and fracture behavior of two cast anisotropic superalloys p 187 N88-13732
Unified constitutive model for single crystal deformation behavior with applications p 191 N88-22388
Accelerated fatigue crack growth behavior of PWA 1480 single crystal alloy and its dependence on the deformation mode
[NASA-TM-100943] p 95 N88-26436
The high temperature creep deformation of Si3N4-6Y2O3-2Al2O3
[NASA-CR-183204] p 76 N88-28981

DEGRADATION

- Effect of storage and LEO cycling on manufacturing technology IPV nickel-hydrogen cells p 53 A88-11917
Degradation mechanisms of materials for large space systems in low Earth orbit
[NASA-CR-181472] p 71 N88-10896
Surface catalytic degradation study of two linear perfluoropolyalkylethers at 345 C
[NASA-TP-2774] p 68 N88-12543
Improved perfluoropolyether fluid development
[NASA-CR-180872] p 80 N88-15851

DEGREES OF FREEDOM

- Hierarchically partitioned nonlinear equation solvers
p 210 A88-54980

DEICERS

- Electro-impulse de-icing - A status report
[AIAA PAPER 88-0019] p 17 A88-22017

DEICING

- A heater made from graphite composite material for potential deicing application p 17 A88-15724
Electro-impulse de-icing electrodynamic solution by discrete elements
[AIAA PAPER 88-0018] p 17 A88-22016
Theoretical analysis of the electrical aspects of the basic electro-impulse problem in aircraft de-icing applications
[NASA-CR-180845] p 15 N88-13310
The NASA aircraft icing research program
p 15 N88-15803

DELAMINATING

- Dynamic delamination fracture toughness of a graphite/epoxy laminate under impact
p 70 A88-29455
Fracture toughness computational simulation of general delaminations in fiber composites
[AIAA PAPER 88-2261] p 181 A88-32219
Measurement of impact-induced delamination buckling in composite laminates p 71 A88-47214
Free-edge delamination: Laminate width and loading conditions effects
[NASA-TM-100238] p 72 N88-12551

DEMAND ASSIGNMENT MULTIPLE ACCESS

- Hardware realization of a baseband processor for a SS-FDMA/TDMA/DAMA system --- Demand Assignment Multiple Access
[AIAA PAPER 88-0830] p 124 A88-27575

DEMODULATORS

- A flexible on-board demultiplexer/demodulator
[AIAA PAPER 88-0811] p 123 A88-27558
Bandwidth and power efficient satellite TDMA demodulator and decoder
[AIAA PAPER 88-0812] p 123 A88-27559

DEMULTIPLEXING

- A flexible on-board demultiplexer/demodulator
[AIAA PAPER 88-0811] p 123 A88-27558

DENDRITIC CRYSTALS

- Dendritic growth in a supercooled alloy melt
p 83 A88-19966
Dendritic solidification under microgravity conditions
[AIAA PAPER 88-0248] p 110 A88-22186
Isothermal dendritic growth - A low gravity experiment
p 110 A88-28556
Dendritic growth of undercooled nickel-tin. III
p 86 A88-32887
Solidification under microgravity conditions - Dendritic growth
[AAS PAPER 86-380] p 110 A88-35130
On producing an alloy of uniform composition during rapid solidification processing p 89 A88-41654

- Channel formation in Pb-Sn, Pb-Sb, and Pb-Sn-Sb alloy ingots and comparison with the system NH4Cl-H2O
p 89 A88-46038
Isothermal dendritic growth - A proposed microgravity experiment p 112 A88-49095

DENSITY (MASS/VOLUME)

- Correlation of velocity and velocity-density turbulence in the exhaust of an atmospheric burner
p 161 N88-11147
Diamond like carbon coatings: Categorization by atomic number density
[NASA-CR-174895] p 108 N88-28151

DENSITY MEASUREMENT

- Correlation between ultrasonic velocity and density of ceramic turbine blades
p 176 A88-12581

DEPOLYMERIZATION

- Oxygen plasma effects on several liquid droplet radiator fluids
p 142 A88-47962

DEPOSITION

- Mechanical strength and tribological behavior of ion-beam-deposited boron nitride films on non-metallic substrates p 98 A88-32866
Turbine airfoil deposition models and their hot corrosion implications p 91 N88-11178
An experimental and theoretical study of the ice accretion process during artificial and natural icing conditions
[NASA-CR-182119] p 16 N88-21143

DEPTH MEASUREMENT

- Measurement of ice thickness (icing) in aeronautics
p 15 A88-32714
In-flight measurement of ice growth on an airfoil using an array of ultrasonic transducers
[AIAA-87-0178] p 16 N88-23717

DESIGN ANALYSIS

- Application of advanced computational codes in the design of an experiment for a supersonic throughflow fan rotor
[ASME PAPER 87-GT-160] p 2 A88-11072
Submillimeter backward wave oscillators
p 122 A88-19659
High speed propeller performance and noise predictions at takeoff/landing conditions
[AIAA PAPER 88-0264] p 215 A88-22193
Design and performance of controlled-diffusion stator compared with original double-circular-arc stator
[SAE PAPER 871783] p 20 A88-30777
Evaluation of a turbine blade damper using an integral approach
[AIAA PAPER 88-2400] p 20 A88-32332
High temperature polymer matrix composites
p 70 A88-36775

- Optimizing advanced propeller designs by simultaneously updating flow variables and design parameters
[AIAA PAPER 88-2532] p 6 A88-40718
Two-dimensional viscous flow computations of hypersonic scramjet nozzle flowfields at design and off-design conditions
[AIAA PAPER 88-3280] p 23 A88-50785
Study of free-piston Stirling engine driven linear alternators
[NASA-CR-181425] p 170 N88-10355
On dynamic loads in parallel shaft transmissions. 1: Modelling and analysis
[NASA-TM-100180] p 171 N88-12797
On dynamic loads in parallel shaft transmissions. 2: Parametric study
[NASA-TM-100181] p 171 N88-12798
STAEBL/general composites with hygrothermal effects (STAEBL/GENCOM)
[NASA-TM-100266] p 187 N88-13754

- High speed propeller performance and noise predictions at takeoff/landing conditions
[NASA-TM-100267] p 216 N88-13960
Large-Scale Advanced Prop-Fan (LAP) blade design
[NASA-CR-174790] p 27 N88-14097
Space station onboard propulsion system: Technology study
[NASA-CR-179233] p 59 N88-15006
Simplified procedures for designing composite bolted joints
[NASA-TM-100281] p 73 N88-15020

- Aeropropulsion '87. Session 2: Aeropropulsion Structures Research
[NASA-CP-10003-SESS-2] p 27 N88-15785
Aeropropulsion structures p 27 N88-15786
Determining structural performance
p 27 N88-15787

- Life prediction technologies for aeronautical propulsion systems p 27 N88-15788
Integrated analysis and applications
p 28 N88-15789

- Aircraft engine hot section technology: An overview of the HOST Project p 29 N88-15804

- Design procedures for fiber composite box beams
[NASA-TM-100296] p 73 N88-16828

- Application of advanced computational technology to propulsion CFD
[NASA-TM-100843] p 204 N88-19102

- Rotorcraft flight-propulsion control integration: An eclectic design concept
[NASA-TP-2815] p 38 N88-19475

- Advanced transmission studies
[NASA-TM-100867] p 173 N88-21454

- Aero/structural tailoring of engine blades (AERO/STAEBL)
[NASA-CR-180805] p 207 N88-21682

- Assessment of nuclear reactor concepts for low power space applications
p 217 N88-24409

- Two-dimensional viscous flow computations of hypersonic scramjet nozzle flowfields at design and off-design conditions
[NASA-CR-182150] p 35 N88-25459

- Advanced heat receiver conceptual design study
[NASA-CR-180901] p 203 N88-25977

- Structural Tailoring of Advanced Turboprops (STAT)
[NASA-CR-180861] p 36 N88-28074

- Design and evaluation of high contact ratio gearing
[NASA-CR-174958] p 175 N88-28319

- Euler analysis of a swirl recovery vane design for use with an advanced single-rotation propfan
[NASA-TM-101357] p 14 N88-29771

DESORPTION

- Thermal desorption study of physical forces at the PTFE surface
p 77 A88-10963

DETECTION

- Detection of radio-frequency modulated optical signals by two and three terminal microwave devices
p 117 A88-50305

DIAGNOSIS

- Optical measurements of soot and temperature profiles in premixed propane-oxygen flames
[NASA-TM-101343] p 115 N88-29997

DIAMONDS

- Diamond like carbon coatings: Categorization by atomic number density
[NASA-CR-174895] p 108 N88-28151

DIELECTRICS

- Guided-wave approaches to spectrally selective energy absorption
[NASA-CR-182532] p 119 N88-17892

- Spacecraft dielectric surface charging property determination
[NASA-CR-180879] p 49 N88-21243

DIESEL ENGINES

- Application of several variable-valve-timing concepts to an LHR engine
[ASME PAPER 87-ICE-29] p 19 A88-15119
Porosity determination of thermal barrier coatings
[ASME PAPER 88-GT-278] p 68 A88-54350

- Adiabatic diesel engine component development: Reference engine for on-highway applications
[NASA-CR-179531] p 224 N88-12428

- Liquid sprays and flow studies in the direct-injection diesel engine under motored conditions
[NASA-TM-100135] p 31 N88-18594

- Prototype thin-film thermocouple/heat-flux sensor for a ceramic-insulated diesel engine
[NASA-TM-100798] p 162 N88-18892

- Documentation of the Benson Diesel Engine Simulation Program
[NASA-TM-100940] p 36 N88-27201

DIFFERENTIAL CALCULUS

- Derivatives of eigenvalues and eigenvectors of a general complex matrix
p 209 A88-29269

DIFFERENTIAL EQUATIONS

- Integrating combustion kinetic rate equations by selective use of stiff and nonstiff methods
p 78 A88-19233

DIFFUSERS

- Numerical simulation of axisymmetric turbulent flow in combustors and diffusers
[NASA-CR-4115] p 11 N88-17582

DIFFUSION

- A method for calculating turbulent boundary layers and losses in the flow channels of turbomachines
[ASME PAPER 87-GT-225] p 2 A88-11121

- Simulation of fluid flows during growth of organic crystals in microgravity
p 109 A88-13163

- Design and performance of controlled-diffusion stator compared with original double-circular-arc stator
[SAE PAPER 871783] p 20 A88-30777

- Diffusion length measurement in bulk and epitaxially grown III-V semiconductors using charge collection microscopy
p 126 A88-34370

- Experiments for the determination of convective diffusion heat/mass transfer to burner rig test targets comparable in size to jet stream diameter
p 140 A88-41574

A microstructural lattice model for strain oriented problems: A combined Monte Carlo finite element technique
[NASA-TM-100215] p 90 N88-10939
Automated design of controlled diffusion blades
[NASA-TM-100251] p 9 N88-13304

DIFFUSION COEFFICIENT

A probabilistic model of brittle crack formation
p 180 A88-18696
Interdiffusion in Ni-rich, Ni-Cr-Al alloys at 1100 and 1200 C. I - Diffusion paths and microstructures. II - Diffusion coefficients and predicted concentration profiles
p 84 A88-24485
Predicting diffusion paths and interface motion in gamma/gamma + beta, Ni-Cr-Al diffusion couples
p 84 A88-24486
Turbulence energy and diffusion transport of third-moments in a separating and reattaching flow
p 141 A88-43011

DIFFUSION FLAMES

A theoretical analysis of the extinction limits of a methane-air opposed-jet diffusion flame
p 77 A88-16497
Laminar diffusion flames under micro-gravity conditions
[AIAA PAPER 88-0645] p 78 A88-27722
Temperature and velocity profiles in sooting free convection diffusion flames
p 78 A88-43018

DIFFUSION THEORY

Numerical methods for one-dimensional reaction-diffusion equations arising in combustion theory
p 135 A88-18975

DIFFUSIVITY

Mass transport phenomena between bubbles and dissolved gases in liquids under reduced gravity conditions
[NASA-TM-100273] p 80 N88-18672

DIGITAL SIMULATION

Automating the parallel processing of fluid and structural dynamics calculations
p 206 A88-46963
Direct simulations of chemically reacting turbulent mixing layers, part 2
[NASA-CR-180853] p 154 N88-25857

DIGITAL SYSTEMS

Automating the parallel processing of fluid and structural dynamics calculations
p 206 A88-46963
Implementation of a digital optical matrix-vector multiplier using a holographic look-up table and residue arithmetic
[NASA-CR-180431] p 205 N88-10496
COSPAS/SARSAT 406-MHz emergency beacon digital controller
[NASA-TM-100859] p 121 N88-26566

DILUTION

A numerical study of the effects of curvature and convergence on dilution jet mixing
[AIAA PAPER 87-1953] p 137 A88-23312
An empirical model of the effects of curvature and convergence on dilution jet mixing
[AIAA PAPER 88-3180] p 23 A88-50783
Dilution jet mixing program, phase 3
p 147 N88-11153

A numerical study of the effects of curvature and convergence on dilution jet mixing
[NASA-TM-89878] p 26 N88-13347
An empirical model of the effects of curvature and convergence on dilution jet mixing
[NASA-TM-100896] p 34 N88-24640

DIMENSIONS

A two-dimensional finite difference program for thermal analysis of rocket thrust chambers
[NASA-TM-100191] p 58 N88-12539
Solving time-dependent two-dimensional eddy current problems
[NASA-TM-100875] p 211 N88-25239

DIRECT CURRENT

Arcjet power supply and start circuit
[NASA-CASE-LEW-14374-1] p 41 N88-28939
The dc power control for a liquid-fed resistojet
[NASA-TM-101326] p 67 N88-29869

DIRECTIONAL SOLIDIFICATION (CRYSTALS)

Microstructure-property relationships in directionally solidified single-crystal nickel-base superalloys
p 88 A88-40329
Onset of finger convection in a horizontal porous layer underlying a fluid layer
p 140 A88-41572
Characterization of directionally solidified lead chloride
p 111 A88-43170
Channel formation in Pb-Sn, Pb-Sb, and Pb-Sn-Sb alloy ingots and comparison with the system NH₄Cl-H₂O
p 89 A88-46038
Ground based materials science experiments
p 43 A88-52364

DIRECTORS (ANTENNA ELEMENTS)

Gain enhancement of microstrip antennas with overlaying parasitic directors
p 117 A88-48653

DISCONTINUITY

SHARP simulation of discontinuities in highly convective steady flow
[NASA-TM-100240] p 210 N88-13931
Modeling of some coplanar waveguide discontinuities
[NASA-TM-100808] p 119 N88-17880

DISKS (SHAPES)

Bladed disk assemblies; Proceedings of the Eleventh Biennial Conference on Mechanical Vibration and Noise, Boston, MA, Sept. 27-30, 1987
p 20 A88-31608

DISPERSING

Compatibility of dispersion-strengthened platinum with resistojet propellants
[NASA-TP-2765] p 58 N88-12538

DISPLACEMENT

An ideal clamping analysis for a cross-ply laminate
p 181 A88-31347
Stress intensity and crack displacement for small edge cracks
[NASA-TP-2801] p 188 N88-17095
An efficient Mindlin finite strip plate element based on assumed strain distribution
p 192 N88-22407

DISPLACEMENT MEASUREMENT

Noncontacting measurement technologies for space propulsion condition monitoring
p 158 A88-29818
Optical measurement of propeller blade deflections
[NASA-TP-2841] p 163 N88-28286

DISPLAY DEVICES

Cooperative synthesis of control and display augmentation for a STOL aircraft in the approach and landing task
[AIAA PAPER 88-4182] p 37 A88-50272
Two-dimensional graphics tools for a transputer based display board
[NASA-TM-100820] p 207 N88-22591

DISSIPATION

A physically consistent model for artificial dissipation in transonic potential flow computations
[NASA-TM-100846] p 211 N88-22652

DISSOCIATION

NNEPEC: Chemical equilibrium version of the Navy/NASA Engine Program
[NASA-TM-100851] p 32 N88-21161

DISSOLVED GASES

Mass transport phenomena between bubbles and dissolved gases in liquids under reduced gravity conditions
[AIAA PAPER 88-0450] p 138 A88-27719
Mass transport phenomena between bubbles and dissolved gases in liquids under reduced gravity conditions
[NASA-TM-100273] p 80 N88-18672

DISTORTION

Effect of spatial inlet temperature and pressure distortion on turbofan engine stability
[AIAA PAPER 88-3016] p 22 A88-44727
Effect of spatial inlet temperature and pressure distortion on turbofan engine stability
[NASA-TM-100850] p 32 N88-21162
Analytical approximation of a distorted reflector surface defined by a discrete set of points
[NASA-TM-101323] p 121 N88-27424

DISTRIBUTED PROCESSING

A distributed data acquisition system for aeronautics test facilities
p 39 A88-33065
Distributed computation of graphics primitives on a transputer network
[NASA-TM-100814] p 206 N88-19147

DISTRIBUTION FUNCTIONS

Determination of grain-size distribution function using two-dimensional Fourier transforms of tone-pulse-encoded images
p 176 A88-30425
Comparison of the bidirectional reflectance distribution function of various surfaces
[NASA-TM-101317] p 218 N88-28760

DOCUMENTATION

Documentation of the Benson Diesel Engine Simulation Program
[NASA-TM-100940] p 36 N88-27201
Bibliography of Lewis Research Center technical publications announced in 1987
[NASA-TM-100910] p 223 N88-28832

DOMESTIC SATELLITE COMMUNICATIONS SYSTEMS

Cost-effective intersatellite link applications to the fixed satellite services
[AIAA PAPER 88-0770] p 45 A88-27544

DOPED CRYSTALS

Ohmic contact formation in semi-insulating GaAs using shallow heavily doped p-type layers
p 219 A88-11150
Electrical resistivity (4K to 2100K) of annealed vapor growth carbon fibers
p 96 A88-17214
Strength characterization of yttria/alumina-doped sintered silicon nitride
p 97 A88-26154
Effect of fluoride doping on the transition temperature of YBa₂Cu₃O₇(δ)
p 220 A88-29297

Radiation damage and defect behavior in proton irradiated lithium-counterdoped n + p silicon solar cells
p 125 A88-34340

Effect of high temperature annealing on the thermoelectric properties of GaP doped SiGe
p 220 A88-40796

DOPPLER EFFECT

Analysis of counting errors in the phase/Doppler particle analyzer
[NASA-TM-100231] p 161 N88-12043
Comparison of UNL laser imaging and sizing system and a phase/Doppler system for analyzing sprays from a NASA nozzle
[NASA-CR-182437] p 150 N88-16956

DOUBLE BASE PROPELLANTS

Modelling ignition characteristics of rich H₂/O₂ mixture in a monolithic catalytic reactor
[AIAA PAPER 88-3224] p 78 A88-46499

DOWNLINKING

A statistical rain attenuation prediction model with application to the advanced communication technology satellite project. 1: Theoretical development and application to yearly predictions for selected cities in the United States
[NASA-CR-179498] p 121 N88-29077

DRAG

Effect of acoustic excitation on the flow over a low-Re airfoil
p 3 A88-14459
Propulsion challenges and opportunities for high-speed transport aircraft
p 30 N88-15809

DROP SIZE

Stability relationship for water droplet crystallization with the NASA Lewis icing spray nozzle
[AIAA PAPER 88-0289] p 137 A88-22209
Experimental and theoretical effects of nitrogen gas flow rate on liquid-jet atomization
p 145 A88-52679
Spray characteristics of a spill-return airblast atomizer
[ASME PAPER 88-GT-7] p 145 A88-54154
Stability relationship for water droplet crystallization with the NASA Lewis icing spray
[NASA-TM-100220] p 24 N88-10790
Analysis of counting errors in the phase/Doppler particle analyzer
[NASA-TM-100231] p 161 N88-12043
Three-dimensional trajectory analyses of two drop sizing instruments: PMS OAP and PMS FSSP
[NASA-CR-4113] p 16 N88-18574
Small-droplet spray measurements with a scattered-light scanner
[NASA-TM-100973] p 163 N88-26645

DROP TESTS

Sooting and disruption in spherically symmetrical combustion of decane droplets in air
[IAF PAPER 87-403] p 77 A88-16076

DROP TOWERS

Containment of a silicone fluid free surface in reduced gravity
p 112 A88-49085

DROPS (LIQUIDS)

Radiative cooling of a solidifying droplet layer including absorption and scattering
p 133 A88-15749
Droplet vaporization in a supercritical microgravity environment
[IAF PAPER 87-384] p 134 A88-16055
Sooting and disruption in spherically symmetrical combustion of decane droplets in air
[IAF PAPER 87-403] p 77 A88-16076
Transient radiative cooling of a layer filled with solidifying drops
p 135 A88-20169
Stability relationship for water droplet crystallization with the NASA Lewis icing spray nozzle
[AIAA PAPER 88-0289] p 137 A88-22209
Operating envelopes of particle sizing instrumentation used for icing research
[AIAA PAPER 88-0291] p 157 A88-22211
Free-streamline analysis of deformation and dislodging by wind force of drops on a surface
p 137 A88-25191
Numerical study of multicomponent droplet vaporization at near critical conditions
[AIAA PAPER 88-0637] p 108 A88-27721
Electrohydrodynamic migration of charged droplets in an insulating fluid
[AIAA PAPER 88-3557] p 143 A88-48946
Stability relationship for water droplet crystallization with the NASA Lewis icing spray
[NASA-TM-100220] p 24 N88-10790
Experimental evidence for modifying the current physical model for ice accretion on aircraft surfaces
[NASA-TM-87184] p 15 N88-12473
Operating envelopes of particle sizing instrumentation used for icing research
[NASA-CR-180870] p 161 N88-13573
Three-dimensional trajectory analyses of two drop sizing instruments: PMS OAP and PMS FSSP
[NASA-CR-4113] p 16 N88-18574

- Electrohydrodynamic migration of charged droplets in an insulating fluid
[NASA-TM-100849] p 152 N88-21424
- Small-droplet spray measurements with a scattered-light scanner
[NASA-TM-100973] p 163 N88-26645
- DRUMS (CONTAINERS)**
- Containment of a silicone fluid free surface in reduced gravity using barrier coatings
[NASA-TM-101314] p 155 N88-30072
- DRY FRICTION**
- Frequency domain solutions to multi-degree-of-freedom, dry friction damped systems p 184 A88-49714
- DUCTED FLOW**
- Explicit finite-volume time-marching calculations of total temperature distributions in turbulent flow
p 139 A88-30517
- An explicit finite-volume time-marching procedure for turbulent flow calculations p 139 A88-30518
- Developing fluid flow in a curved duct of square cross-section and its fully developed dual solutions
p 139 A88-30957
- Unsteady motion and transition to turbulence in developing curved duct flow p 140 A88-39010
- Flow field measurements in a 90 degree turning duct p 147 N88-11157
- A survey of oscillating flow in Stirling engine heat exchangers
[NASA-CR-182108] p 152 N88-22322
- DUCTILITY**
- Room temperature tensile ductility in powder processed B2 FeAl alloys p 85 A88-31694
- DUCTS**
- Aeropropulsion '87. Session 3: Internal Fluid Mechanics Research
[NASA-CP-10003-SESS-3] p 28 N88-15790
- Inlets, ducts and nozzles p 149 N88-15791
- An estimate of the noise shielding on the fuselage resulting from installing a short duct around an advanced propeller
[NASA-TM-100262] p 217 N88-18379
- Unsteady heat transfer in turbine blade ducts: Focus on combustor sources
[NASA-TM-100815] p 151 N88-18870
- Electromagnetic propagation in PEC and absorbing curved S-ducts
[NASA-TM-100833] p 120 N88-19698
- Optical measurement of unducted fan blade deflections
[NASA-TM-100966] p 163 N88-29142
- DURABILITY**
- Toward improved durability in advanced aircraft engine hot sections; Proceedings of the Thirty-third ASME International Gas Turbine and Aeroengine Congress and Exposition, Amsterdam, Netherlands, June 5-9, 1988
p 24 A88-54137
- Views on the impact of HOST --- hot section technology p 24 A88-54146
- Computational structural mechanics for engine structures p 33 N88-22399
- DYNAMIC CHARACTERISTICS**
- Dynamic and static fatigue behavior of sintered silicon nitrides p 96 A88-12602
- Modal test/analysis correlation for the Centaur G prime launch vehicle p 44 A88-18631
- Analysis of eccentric annular incompressible seals. II - Effects of eccentricity on rotordynamic coefficients
[ASME PAPER 87-TRIB-53] p 166 A88-23309
- Linear and nonlinear mechanical properties of a series of epoxy resins p 101 A88-54976
- Dynamic analysis of multimesh-gear helicopter transmissions
[NASA-TP-2789] p 172 N88-17045
- DYNAMIC LOADS**
- Free-edge delamination: Laminate width and loading conditions effects
[NASA-TM-100238] p 72 N88-12551
- On dynamic loads in parallel shaft transmissions. 1: Modeling and analysis
[NASA-TM-100180] p 171 N88-12797
- On dynamic loads in parallel shaft transmissions. 2: Parameter study
[NASA-TM-100181] p 171 N88-12798
- The use of multigrid techniques in the solution of the Elrod algorithm for a dynamically loaded journal bearing
[NASA-CR-180873] p 151 N88-17954
- The solution of the Elrod algorithm for a dynamically loaded journal bearing using multigrid techniques
[NASA-TM-100941] p 154 N88-25854
- DYNAMIC MODELS**
- A statistical rain attenuation prediction model with application to the advanced communication technology satellite project. Part 2: Theoretical development of a dynamic model and application to rain fade durations and tolerable control delays for fade countermeasures
[NASA-TM-100242] p 118 N88-11945

DYNAMIC RESPONSE

- Transfer matrix modeling of geared system vibration
p 168 A88-39703
- Blade loss transient dynamics analysis, volume 1. Task 2: TETRA 2 theoretical development
[NASA-CR-179632] p 25 N88-10791
- Blade loss transient dynamics analysis, volume 2. Task 2: TETRA 2 user's manual
[NASA-CR-179633] p 25 N88-10792
- Analysis and test evaluation of the dynamic response and stability of three advanced turboprop models at low forward speed
[NASA-CR-175026] p 27 N88-14096
- Vibration and flutter characteristics of the SR7L large-scale propfan
[NASA-TM-100272] p 188 N88-18036
- Microwave response of an HEMT photoconductor
[NASA-TM-100819] p 128 N88-18835
- Contact force history and dynamic response due to the impact of a soft projectile
[NASA-TM-100961] p 175 N88-26679
- Experimental investigation of propfan aeroelastic response in off-axis flow with mistuning
[NASA-TM-101320] p 196 N88-28344
- DYNAMIC STABILITY**
- Analysis and test evaluation of the dynamic stability of three advanced turboprop models at zero forward speed
[NASA-CR-175025] p 26 N88-14095
- DYNAMIC STRUCTURAL ANALYSIS**
- Theory versus experiment for the rotordynamic coefficients of labyrinth gas seals. I - A two control volume model
p 167 A88-31535
- Theory versus experiment for the rotordynamic coefficients of labyrinth gas seals. II - A comparison to experiment
p 167 A88-31536
- Transient rotor dynamic rub phenomena - Theory and test
p 167 A88-31539
- Identification of structural interface characteristics using component mode synthesis p 181 A88-31561
- Advanced composite turboprops - Modeling, structural, and dynamic analyses
[ASME PAPER 87-GT-78] p 21 A88-36745
- Identification of differences between finite element analysis and experimental vibration data
p 183 A88-46666
- Automating the parallel processing of fluid and structural dynamics calculations p 206 A88-46963
- Analysis and test evaluation of the dynamic response and stability of three advanced turboprop models at low forward speed
[NASA-CR-175026] p 27 N88-14096
- Determining structural performance
p 27 N88-15787
- Characterization of damped structural connections for multi-component systems
[NASA-TM-100801] p 189 N88-18974
- Test facilities of the structural dynamics branch of NASA Lewis Research Center
[NASA-TM-100800] p 190 N88-21534
- Lewis Structures Technology, 1988. Volume 2: Structural Mechanics
[NASA-CP-3003-VOL-2] p 190 N88-22382
- Lewis Structures Technology, 1988. Volume 3: Structural Integrity Fatigue and Fracture Wind Turbines HOST
[NASA-CP-3003-VOL-3] p 192 N88-22408
- Structural dynamics branch research and accomplishments for fiscal year 1987
[NASA-TM-100279] p 194 N88-22446
- Lewis Structures Technology, 1988. Volume 1: Structural Dynamics
[NASA-CP-3003-VOL-1] p 194 N88-23226
- Parameter identification methods for improving structural dynamic models
[NASA-TM-100812] p 194 N88-23994
- Contact force history and dynamic response due to the impact of a soft projectile
[NASA-TM-100961] p 175 N88-26679
- DYNAMICAL SYSTEMS**
- Finite-dimensional modeling of network-induced delays for real-time control systems p 208 A88-54537
- E**
- EARTH GRAVITATION**
- Program for the feasibility of developing a high pressure acoustic levitator
[NASA-CR-182154] p 113 N88-26498
- EARTH IONOSPHERE**
- Exposed high-voltage source effect on the potential of an ionospheric satellite p 218 A88-54992
- EARTH ORBITAL ENVIRONMENTS**
- Oxidation-resistant reflective surfaces for solar dynamic power generation in near earth orbit p 54 A88-18523
- Gaseous environment of the Shuttle early in the Spacelab 2 mission p 47 A88-47972

- Technologies for protection of the Space Station power system surfaces in atomic oxygen environment
p 41 A88-52331
- Effect of NASA advanced designs on thermal behavior of Ni-H2 cells
[NASA-TM-100197] p 79 N88-10132
- EARTH ORBITS**
- Communications satellites in non-geostationary orbits
[AIAA PAPER 88-0842] p 46 A88-27583
- Low Earth orbit environmental effects on the space station photovoltaic power generation systems
[NASA-TM-100230] p 225 N88-12429
- EARTH TERMINALS**
- VSAT networks - An overview --- Very Small Aperture Terminals p 115 A88-14091
- Bit-error-rate testing of high-power 30-GHz traveling-wave tubes for ground-terminal applications
p 122 A88-19781
- ECONOMIC FACTORS**
- The economics of satellite retrieval
[AIAA PAPER 88-0843] p 44 A88-27584
- EDDY CURRENTS**
- Solving time-dependent two-dimensional eddy current problems
[NASA-TM-100875] p 211 N88-25239
- EDGES**
- Free-edge delamination: Laminate width and loading conditions effects
[NASA-TM-100238] p 72 N88-12551
- Stress intensity and crack displacement for small edge cracks
[NASA-TP-2801] p 188 N88-17095
- EFFICIENCY**
- High power ion thruster performance
[NASA-TM-100127] p 58 N88-12542
- Advanced propeller research p 29 N88-15806
- EIGENVALUES**
- Higher eigenmodes in the Blasius boundary-layer stability problem p 134 A88-16352
- Derivatives of eigenvalues and eigenvectors of a general complex matrix p 209 A88-29269
- Parallel computer methods for eigenvalue extraction
p 207 N88-23233
- Reduced order models for nonlinear aerodynamics
p 11 N88-23248
- EIGENVECTORS**
- Derivatives of eigenvalues and eigenvectors of a general complex matrix p 209 A88-29269
- Reduced order models for nonlinear aerodynamics
p 11 N88-23248
- EJECTORS**
- Forced mixer lobes in ejector designs
p 141 A88-46222
- ELASTIC DEFORMATION**
- Thermostructural analysis with experimental verification in a high heat flux facility of a simulated cowl lip
[AIAA PAPER 88-2222] p 39 N88-32188
- Stress intensity and crack displacement for small edge cracks
[NASA-TP-2801] p 188 N88-17095
- Unified constitutive models for high-temperature structural applications p 190 N88-21523
- A constitutive model for an overlay coating
p 105 N88-21525
- Non-isothermal elastoviscoplastic analysis of planar curved beams p 190 N88-21526
- ELASTIC MEDIA**
- A probabilistic model of brittle crack formation
p 180 A88-18696
- ELASTIC PROPERTIES**
- Parallel computer methods for eigenvalue extraction
p 207 N88-23233
- ELASTIC WAVES**
- Initial conditional effect on pressure waves in an axisymmetric jet
[AIAA PAPER 88-3702] p 143 A88-48915
- Initial condition effect on pressure waves in an axisymmetric jet
[NASA-TM-100915] p 153 N88-23184
- ELASTODYNAMICS**
- Time-domain transient elastodynamic analysis of 3-D solids by BEM p 183 A88-48638
- ELASTOHYDRODYNAMICS**
- Oil film thickness measurement and analysis for an angular contact ball bearing operating in parched elastohydrodynamic lubrication p 165 A88-14115
- A model for the influence of pressure on the bulk modulus and the influence of temperature on the solidification pressure for liquid lubricants
[ASME PAPER 86-TRIB-63] p 133 A88-15124
- Shear rheological characterization of motor oils
p 100 A88-47562
- Parched elasto hydrodynamic lubrication film thickness measurement in an instrument ball bearing
[STLE PREPRINT 88-AM-6G-1] p 169 A88-51082

ELASTOPLASTICITY

- A review of path-independent integrals in elastic-plastic fracture mechanics p 183 A88-47001
- A new BEM formulation for two- and three-dimensional elastoplasticity using particular integrals p 184 A88-53089
- Non-isothermal elastoviscoplastic analysis of planar curved beams p 190 N88-21526
- ELECTRIC ARCS**
- Threshold-determining mechanisms for discharges in high-voltage solar arrays p 50 A88-11738
- Arc-textured metal surfaces for high thermal emittance space radiators p 94 N88-24754
- ELECTRIC BATTERIES**
- Advanced photovoltaic power system technology for lunar base applications [NASA-TM-100965] p 65 N88-26402
- ELECTRIC CHARGE**
- Effect of component compression on the initial performance of an IPV nickel-hydrogen cell --- Individual Pressure Vessel p 53 A88-11913
- ELECTRIC CURRENT**
- A heater made from graphite composite material for potential deicing application p 17 A88-15724
- ELECTRIC DISCHARGES**
- A prediction model of the depth-of-discharge effect on the cycle life of a storage cell p 197 A88-11896
- Effect of component compression on the initial performance of an IPV nickel-hydrogen cell --- Individual Pressure Vessel p 53 A88-11913
- ELECTRIC FIELDS**
- Double-probe potential measurements near the Spacelab 2 electron beam p 204 A88-53464
- ELECTRIC FURNACES**
- Low cost Get-Away-Special (GAS) furnace p 41 A88-26583
- ELECTRIC GENERATORS**
- Design description report for a photovoltaic power system for a remote satellite earth terminal [NASA-CR-179586] p 200 N88-12875
- Comparative analysis of the space power architecture studies [NASA-TM-100977] p 66 N88-28090
- ELECTRIC POTENTIAL**
- Effect of component compression on the initial performance of an IPV nickel-hydrogen cell --- Individual Pressure Vessel p 53 A88-11913
- Exposed high-voltage source effect on the potential of an ionospheric satellite p 218 A88-54992
- Characterization of fatigue crack initiation and propagation in Ti-6Al-4V with electrical potential drop technique [NASA-TM-100877] p 195 N88-25937
- ELECTRIC POWER**
- Space commercialization and power system technology p 223 A88-44003
- ELECTRIC POWER SUPPLIES**
- Space Station electric power system requirements and design p 50 A88-11782
- Computer modeling and simulation of a 20kHz ac distribution system for Space Station p 51 A88-11827
- A comparison of Stirling engines for use with a 25 kW dish-electric conversion system p 53 A88-11943
- Recent progress in space photovoltaic systems [NASA-TM-100208] p 128 N88-11966
- High frequency power distribution system [NASA-CR-175071] p 129 N88-23939
- Advanced photovoltaic power system technology for lunar base applications [NASA-TM-100965] p 65 N88-26402
- ELECTRIC POWER TRANSMISSION**
- The ac power system testbed [NASA-CR-175068] p 127 N88-11948
- Power transmission studies for tethered SP-100 [NASA-TM-100864] p 60 N88-21251
- ELECTRIC PROPULSION**
- Auxiliary propulsion system flight package [NASA-CR-180828] p 56 N88-10886
- A low-power arcjet cyclic lifetest [NASA-TM-100233] p 57 N88-11748
- High power ion thruster performance [NASA-TM-100127] p 58 N88-12542
- High power ion thruster performance p 62 N88-24295
- Electric propulsion options for the SP-100 reference mission p 62 N88-24296
- Status of high power electric propulsion technology p 63 N88-24443
- Performance and lifetime assessment of MPD arc thruster technology [NASA-TM-101293] p 66 N88-29860
- The dc power control for a liquid-fed resistojet [NASA-TM-101326] p 67 N88-29869

- Successful completion of a cyclic ground test of a mercury ion auxiliary propulsion system [NASA-TM-101351] p 67 N88-29873
- ELECTRIC PULSES**
- Electro-impulse de-icing - A status report [AIAA PAPER 88-0019] p 17 A88-22017
- ELECTRIC RELAYS**
- Hollow cathodes as electron emitting plasma contactors - Theory and computer modeling p 218 A88-47973
- ELECTRICAL IMPEDANCE**
- How good is the impedance boundary condition? p 115 A88-24863
- ELECTRICAL INSULATION**
- Power transmission studies for tethered SP-100 [NASA-TM-100864] p 60 N88-21251
- ELECTRICAL MEASUREMENT**
- Recent advances in capacitance type of blade tip clearance measurements [NASA-TM-101291] p 35 N88-25460
- ELECTRICAL PROPERTIES**
- Effect of the microstructure on the thermoelectric properties of polycrystalline lanthanum chalcogenides p 221 A88-40797
- Measurement of the properties of lossy materials inside a finite conducting cylinder [NASA-CR-182664] p 213 N88-20962
- ELECTRICAL RESISTANCE**
- A comparison of the bromination dynamics of various carbon and graphite fibers p 97 A88-20278
- The development of a high temperature static strain gage system p 160 N88-11142
- Electrical properties of materials for elevated temperature resistance strain gage application [NASA-CR-182214] p 164 N88-30106
- ELECTRICAL RESISTIVITY**
- Electrical resistivity (4K to 2100K) of annealed vapor growth carbon fibers p 96 A88-17214
- Synthesis, electrical and thermal conductivities, and potential applications of graphite fluoride fibers p 97 A88-26963
- Specific heat of pristine and brominated graphite fibers, composites and HOPG --- Highly Oriented Pyrolytic Graphite p 98 A88-32853
- Stability of the electrical resistivity of bromine, iodine monochloride, copper(II) chloride, and nickel(II) chloride intercalated pitch-based graphite fibers p 100 A88-49403
- Deposition of vanadium oxide films by direct-current magnetron reactive sputtering p 221 A88-51286
- ELECTRO-OPTICS**
- Fiber optics for controls p 218 N88-15798
- A high frequency GaAlAs travelling wave electro-optic modulator at 0.82 micrometers [NASA-TM-100970] p 130 N88-28240
- ELECTROCATALYSTS**
- Evaluation studies on carbon supported catalysts for oxygen reduction in alkaline medium p 77 A88-16643
- Electrocatalytic reduction of oxygen on modified oxide surfaces [NASA-TM-101333] p 81 N88-29952
- ELECTROCHEMICAL CELLS**
- Component variations and their effects on bipolar nickel-hydrogen cell performance p 197 A88-11914
- Effect of NASA advanced designs on thermal behavior of Ni-H₂ cells [NASA-TM-100197] p 79 N88-10132
- ELECTROCHEMISTRY**
- Stress-life interrelationships associated with alkaline fuel cells p 197 A88-11903
- Lightweight nickel electrode for nickel hydrogen cells and batteries p 198 A88-16631
- ELECTRODES**
- Assessment of commercially available and experimental hydrogen electrodes p 198 A88-16632
- Performance of a small, graphite electrode, multistage depressed collector with a 500-W, continuous wave, 4.8- to 9.6-GHz traveling wave tube [NASA-TP-2788] p 128 N88-15146
- Performance of lightweight nickel electrodes [NASA-TM-100958] p 80 N88-26430
- ELECTRODYNAMICS**
- Electro-impulse de-icing electrodynamic solution by discrete elements [AIAA PAPER 88-0018] p 17 A88-22016
- Theoretical analysis of the electrical aspects of the basic electro-impulse problem in aircraft de-icing applications [NASA-CR-180845] p 15 N88-13310
- Space plasma contactor research, 1987 [NASA-CR-182148] p 219 N88-23649
- ELECTROHYDRODYNAMICS**
- Electrohydrodynamic migration of charged droplets in an insulating fluid [AIAA PAPER 88-3557] p 143 A88-48946
- Electrohydrodynamic migration of charged droplets in an insulating fluid [NASA-TM-100849] p 152 N88-21424

ELECTROLYSIS

- Phase purity of NiCo₂O₄, a catalyst candidate for electrolysis of water [NASA-TM-100239] p 69 N88-13385

ELECTROMAGNETIC FIELDS

- Electromagnetic fields backscattered from an s-shaped inlet cavity with an absorber coating on its inner walls [NASA-CR-182401] p 118 N88-15130

ELECTROMAGNETIC INTERFERENCE

- EMC and power quality standards for 20-kHz power distribution p 52 A88-11830

ELECTROMAGNETIC PROPULSION

- Electromagnetic powered vehicles (EMPV) for Mars exploration p 62 N88-24388
- Application of superconducting technology to earth-to-orbit electromagnetic launch systems [NASA-TM-101134] p 43 N88-26385

ELECTROMAGNETIC PULSES

- Theoretical analysis of the electrical aspects of the basic electro-impulse problem in aircraft de-icing applications [NASA-CR-180845] p 15 N88-13310

ELECTROMAGNETIC RADIATION

- Electromagnetic propagation in PEC and absorbing curved S-ducts [NASA-TM-100833] p 120 N88-19698

ELECTROMAGNETIC SCATTERING

- How good is the impedance boundary condition? p 115 A88-24863

ELECTROMAGNETIC WAVE TRANSMISSION

- Development of 20 GHz monolithic transmit modules [NASA-CR-182134] p 222 N88-24539

ELECTRON BEAMS

- A re-examination of spent beam refocusing for high-efficiency helix TWT's and small MDC's p 124 A88-28673
- Double-probe potential measurements near the Spacelab 2 electron beam p 204 A88-53464
- Effects of electron and proton irradiations on n/p and p/n GaAs cells grown by MOCVD [NASA-TM-100199] p 127 N88-10266

ELECTRON CYCLOTRON HEATING

- 30-cm electron cyclotron plasma generator p 122 A88-18633

ELECTRON EMISSION

- Hollow cathodes as electron emitting plasma contactors - Theory and computer modeling p 218 A88-47973

ELECTRON ENERGY

- Voids in Jovian magnetosphere revisited - Evidence of spacecraft charging p 226 A88-28279

ELECTRON GUNS

- Electron beam experiments at high altitudes p 47 A88-46799

ELECTRON IRRADIATION

- Radiation and temperature effects in gallium arsenide, indium phosphide, and silicon solar cells p 125 A88-34321

ELECTRON MICROSCOPES

- In situ fatigue loading stage inside scanning electron microscope p 193 N88-22419

ELECTRON MICROSCOPY

- Multielement mapping of alpha-SiC by scanning Auger microscopy p 158 A88-27617
- Diffusion length measurement in bulk and epitaxially grown III-V semiconductors using charge collection microscopy p 126 A88-34370
- Effect of the microstructure on the thermoelectric properties of polycrystalline lanthanum chalcogenides p 221 A88-40797

ELECTRON PARAMAGNETIC RESONANCE

- Electron-spin-resonance studies of vapor-grown carbon fibers p 96 A88-17368

ELECTRON PLASMA

- Threshold-determining mechanisms for discharges in high-voltage solar arrays p 50 A88-11738

ELECTRON RADIATION

- Gigard-tolerant power switches and memory elements p 123 A88-22704

ELECTRON SCATTERING

- Double-probe potential measurements near the Spacelab 2 electron beam p 204 A88-53464

ELECTRON SPIN

- Electron-spin-resonance studies of vapor-grown carbon fibers p 96 A88-17368

ELECTRON TRAJECTORIES

- A re-examination of spent beam refocusing for high-efficiency helix TWT's and small MDC's p 124 A88-28673

ELECTRON TUNNELING

- Solar energy conversion through the interaction of plasmons with tunnel junctions. Part A: Solar cell analysis. Part B: Photoconductor analysis [NASA-CR-183044] p 203 N88-27621

ELECTROSTATIC PROBES

- An experimental investigation of an arcjet thruster exhaust using Langmuir probes [NASA-TM-100258] p 60 N88-21253

SUBJECT INDEX

ELECTROSTATICS

- Electron beam experiments at high altitudes
p 47 A88-46799

ELECTROTHERMAL ENGINES

- Electrothermal propulsion of spacecraft with millimeter and submillimeter electromagnetic energy
p 54 A88-46220

ELEMENTARY PARTICLES

- Cosmology and particle physics p 226 A88-39734
Primordial nucleosynthesis with decaying particles. I - Entropy-producing decays. II - Inert decays
p 217 A88-47477

ELLIPSOIDAL METERS

- Investigation of PTFE transfer films by infrared emission spectroscopy and phase-locked ellipsometry
p 99 A88-35568

ELLIPTIC FUNCTIONS

- Three-dimensional elliptic grid generation technique with application to turbomachinery cascades
[NASA-TM-101330] p 155 A88-30078

ELLIPTICAL ORBITS

- Low thrust power-limited transfer for a pole squatter
[AIAA PAPER 88-4310] p 42 A88-50435

EMBRITTLMENT

- Thermal aging effects in refractory metal alloys
p 84 A88-22700

EMERGENCY LOCATOR TRANSMITTERS

- COSPAS/SARSAT 406-MHz emergency beacon digital controller
[NASA-TM-100859] p 121 A88-26566

EMULSIONS

- Quantitative characterization of the viscosity of a microemulsion
p 77 A88-11167

ENCLOSURES

- Fingering flow patterns of thermosolutal convection in rectangular enclosures
[AIAA PAPER 88-3823] p 144 A88-49000
Thermosolutal convection in high-aspect-ratio enclosures
[NASA-TM-100803] p 151 A88-18871
Fingering flow patterns of thermosolutal convection in rectangular enclosures
[NASA-TM-100854] p 152 A88-21417

ENERGY ABSORPTION

- Guided-wave approaches to spectrally selective energy absorption
[NASA-CR-182532] p 119 A88-17892

ENERGY CONSERVATION

- Automotive Stirling engine: Mod 2 design report
[NASA-CR-175106] p 223 A88-11578
Large-Scale Advanced Prop-Fan (LAP)
[NASA-CR-182112] p 32 A88-20306
NASA advanced turboprop research and concept validation program
[NASA-TM-100891] p 34 A88-22902
NASA/industry advanced turboprop technology program
[NASA-TM-100929] p 35 A88-24641

ENERGY CONVERSION

- Status of commercial fuel cell powerplant system development
p 198 A88-11925
Multi-hundred kilowatt roll ring assembly evaluation results
[NASA-TM-100865] p 114 A88-21375
Comparative analysis of the space power architecture studies
[NASA-TM-100977] p 66 A88-28090

ENERGY CONVERSION EFFICIENCY

- Impact of thermal energy storage properties on solar dynamic space power conversion system mass
p 51 A88-11805
Mod II engine development
p 165 A88-11972
Space solar cell research - Problems and potential
p 123 A88-21605
Modelling and design of high efficiency radiation tolerant indium phosphide space solar cells
p 200 A88-34394
Overview of NASA Lewis Research Center free-piston Stirling engine technology activities applicable to space power systems
p 202 A88-24255
Benefits of 20 kHz PMAD in a nuclear space station
p 129 A88-24256

- Progress in InP solar cell research
[NASA-TM-100914] p 130 A88-24670

- Study of Staebler-Wronsky degradation effect in a Si:H based P-I-N solar cells
[NASA-CR-182564] p 203 A88-25970

- Solar energy conversion through the interaction of plasmons with tunnel junctions. Part A: Solar cell analysis. Part B: Photoconductor analysis
[NASA-CR-183044] p 203 A88-27621

ENERGY DISSIPATION

- Navier-Stokes cascade analysis with a stiff k-epsilon turbulence solver
[AIAA PAPER 88-0594] p 5 A88-22444

- Navier-Stokes cascade analysis with a stiff Kappa-Epsilon turbulence solver
[NASA-TM-100218] p 9 A88-10778

ENERGY REQUIREMENTS

- Power systems for production, construction, life support and operations in space
[NASA-TM-100838] p 60 A88-21254

ENERGY STORAGE

- Regenerative fuel cell study for satellites in GEO orbit
p 52 A88-11904
High temperature solid oxide regenerative fuel cell for solar photovoltaic energy storage
p 197 A88-11905
Effect of component compression on the initial performance of an IPV nickel-hydrogen cell --- Individual Pressure Vessel
p 53 A88-11913
Fluoride salts as phase change materials for thermal energy storage in the temperature range 1000-1400 K
p 199 A88-33734
Electrical Power Working Group report
p 48 A88-10095

- Power systems for production, construction, life support and operations in space
[NASA-TM-100838] p 60 A88-21254
Effect of LEO cycling at shallow depths of discharge on MANTECH IPV nickel-hydrogen cells
[NASA-TM-101300] p 203 A88-25978

- Energy storage considerations for a robotic Mars surface sampler
[NASA-TM-100969] p 227 A88-28853

- Regenerative fuel cell energy storage system for a low earth orbit space station
[NASA-CR-174802] p 204 A88-30184

ENERGY TECHNOLOGY

- Space commercialization and power system technology
p 223 A88-44003

ENERGY TRANSFER

- A microstructural lattice model for strain oriented problems: A combined Monte Carlo finite element technique
[NASA-TM-100215] p 90 A88-10939

ENGINE CONTROL

- Conceptual design of an optic based engine control system
[ASME PAPER 87-GT-168] p 18 A88-11079

ENGINE DESIGN

- Development of the AGT101 regenerator seals
[ASME PAPER 87-GT-173] p 165 A88-11083
Mod II engine development
p 165 A88-11972
Results of NASA's Energy Efficient Engine Program
p 19 A88-20785
Design and experimental evaluation of a high temperature radial turbine with a moveable sidewall nozzle
[SAE PAPER 871782] p 19 A88-30776

- Design and development of ceramic components
[AIAA PAPER 88-3054] p 168 A88-44742
Lateral jet injection into swirling combustor flowfields
[AIAA PAPER 88-3183] p 141 A88-44783

- The design of an air-cooled metallic high temperature radial turbine
[AIAA PAPER 88-2872] p 22 A88-45011

- A preliminary design study of supersonic through-flow fan inlets
[AIAA PAPER 88-3075] p 23 A88-53137

- Review and assessment of the database and numerical modeling for turbine heat transfer
p 24 A88-54141
Adiabatic diesel engine component development: Reference engine for on-highway applications
[NASA-CR-179531] p 224 A88-12428

- Automated design of controlled diffusion blades
[NASA-TM-100251] p 9 A88-13304
Hot piston ring tests
[NASA-TM-100256] p 201 A88-14486

- Aeropropulsion '87. Session 5: Subsonic Propulsion Technology
[NASA-CP-10003-SESS-5] p 28 A88-15800

- Small engine technology programs
p 29 A88-15801
Aircraft engine hot section technology: An overview of the HOST Project
p 29 A88-15804

- Advanced propeller research
p 29 A88-15806
Propulsion challenges and opportunities for high-speed transport aircraft
p 30 A88-15809

- Technology developments for a compound cycle engine
p 30 A88-16637
Small gas turbine engine technology
p 30 A88-16638

- The convertible engine: A dual-mode propulsion system
p 31 A88-16639
Aeropropulsion '87. Session 1: Aeropropulsion Materials Research
[NASA-CP-10003-SESS-1] p 31 A88-16697

- Impact and promise of NASA aeropropulsion technology
p 31 A88-16698
High temperature polymer matrix composites
p 73 A88-16700

- Ceramics for engines
p 103 A88-16704

- Experimental evaluation of a translating nozzle sidewall radial turbine
p 31 A88-17656

- Continuous fiber ceramic matrix composites for heat engine components
p 106 A88-22411
Status and prognosis for alternative engine materials
[NASA-TM-100903] p 94 A88-24749

- Design, manufacture and spin test of high contact ratio helicopter transmission utilizing Self-Aligning Bearingless Planetary (SABP)
[NASA-CR-4155] p 174 A88-24975

- The design and fabrication of a Stirling engine heat exchanger module with an integral heat pipe
[NASA-TM-101296] p 203 A88-26732

- Documentation of the Benson Diesel Engine Simulation Program
[NASA-TM-100940] p 36 A88-27201

- Impact of ETO propellants on the aerothermodynamic analyses of propulsion components
[NASA-TM-101303] p 156 A88-30094

ENGINE FAILURE

- A natural low frequency oscillation in the wake of an airfoil near stalling conditions
[AIAA PAPER 88-0131] p 4 A88-22093

- Progress toward an advanced condition monitoring system for reusable rocket engines
p 54 A88-32868
A natural low frequency oscillation in the wake of an airfoil near stalling conditions
[NASA-TM-100213] p 9 A88-10779

- ENGINE INLETS
Experimental and analytical evaluation of the effects of simulated engine inlets on the blade vibratory stresses of the SR-3 model prop-fan
[NASA-CR-174959] p 36 A88-28927

ENGINE MONITORING INSTRUMENTS

- Uncertainty of in-flight thrust determination
[SAE AIR 1678] p 16 A88-15228
Reusable rocket engine optical condition monitoring
p 158 A88-29817

- Noncontacting measurement technologies for space propulsion condition monitoring
p 158 A88-29818
Progress toward an advanced condition monitoring system for reusable rocket engines
p 54 A88-32868

- Engine flow visualization using a copper vapor laser
p 158 A88-34479
An expert system approach to turbopump health monitoring
[AIAA PAPER 88-3117] p 42 A88-48038

ENGINE NOISE

- Aeroacoustics of subsonic turbulent shear flows
[AIAA PAPER 87-2731] p 214 A88-16571
Advanced turboprop wing installation effects measured by unsteady blade pressure and noise
[AIAA PAPER 87-2719] p 3 A88-18655

- Turboprop engine core noise source diagnostics
p 22 A88-39707
Advanced turboprop wing installation effects measured by unsteady blade pressure and noise
[NASA-TM-100200] p 9 A88-10008

ENGINE PARTS

- Development of the AGT101 regenerator seals
[ASME PAPER 87-GT-173] p 165 A88-11083
Thermomechanical behavior of plasma-sprayed ZrO₂-Y₂O₃ coatings influenced by plasticity, creep, and oxidation
p 95 A88-12588

- Probabilistic structural analysis methods for space propulsion system components
p 54 A88-16441
Simple processing method for high-strength silicon carbide
p 97 A88-19056

- Small engine components test facility turbine testing cell
[AIAA PAPER 88-2962] p 22 A88-44706
Design and development of ceramic components
[AIAA PAPER 88-3054] p 168 A88-44742

- Structural analysis methods development for turbine hot section components
p 184 A88-54142
Porosity determination of thermal barrier coatings
[ASME PAPER 88-GT-278] p 68 A88-54350

- High temperature stress-strain analysis
p 185 A88-11170
Adiabatic diesel engine component development: Reference engine for on-highway applications
[NASA-CR-179531] p 224 A88-12428

- Composite mechanics for engine structures
[NASA-TM-100176] p 72 A88-12552
Aeropropulsion '87. Session 1: Aeropropulsion Materials Research
[NASA-CP-10003-SESS-1] p 31 A88-16697

- Ceramics for engines
p 103 A88-16704
Ceramic bearings for use in gas turbine engines
[NASA-TM-100288] p 172 A88-18007

- Structural analysis methods development for turbine hot section components
[NASA-TM-100298] p 188 A88-18967

- Advanced Gas Turbine (AGT) Technology Development Project, ceramic component developments
[NASA-CR-180871] p 224 A88-20229

ENGINE TESTS

- Small engine components test facility turbine testing cell
[NASA-TM-100887] p 33 N88-22037
- Computational structural mechanics for engine structures p 33 N88-22399
- Thermal-structural analyses of Space Shuttle Main Engine (SSME) hot section components p 61 N88-22404
- Molten salt corrosion of SiC and Si₃N₄ p 107 N88-23885
- Thermal cyclic durability testing of ceramic materials for turbine engines p 179 N88-23886
- Thermal stress minimized, two component, turbine shroud seal
[NASA-CASE-LEW-14212-1] p 174 N88-23978
- Status and prognosis for alternative engine materials
[NASA-TM-100903] p 94 N88-24749
- Component improvement of free-piston Stirling engine key technology for space power
[NASA-TM-100950] p 64 N88-25476
- ### ENGINE TESTS
- Mod II engine development p 165 A88-11972
- Transient engine performance with water ingestion p 19 A88-27295
- Test stand performance of a convertible engine for advanced V/STOL and rotorcraft propulsion
[SAE PAPER 872355] p 21 A88-37217
- Small engine components test facility turbine testing cell
[AIAA PAPER 88-2962] p 22 A88-44706
- An experimental investigation of the effect of test-cell pressure on the performance of resistojets
[AIAA PAPER 88-3286] p 40 A88-44820
- Advanced high temperature instrumentation for hot section research applications p 159 A88-54139
- Test stand performance of a convertible engine for advanced V/STOL and rotorcraft propulsion
[NASA-TM-100211] p 25 N88-11679
- SPRE 1 free-piston Stirling engine testing at NASA Lewis Research Center
[NASA-TM-100241] p 57 N88-11747
- A life test of a 22-Newton (5-lbf) hydrazine rocket
[NASA-TM-100232] p 57 N88-11750
- Performance and combustion characteristics of direct-injection stratified-charge rotary engines
[NASA-TM-100134] p 25 N88-12490
- Hot piston ring tests
[NASA-TM-100256] p 201 N88-14486
- Efficiency testing of a helicopter transmission planetary reduction stage
[NASA-TP-2795] p 172 N88-15224
- Hot piston ring/cylinder liner materials: Selection and evaluation
[NASA-TM-100276] p 102 N88-15872
- Test results of a 40-kW Stirling engine and comparison with the NASA Lewis computer code predictions
[NASA-TM-87050] p 201 N88-19013
- NNEPEC: Chemical equilibrium version of the Navy/NASA Engine Program
[NASA-TM-100851] p 32 N88-21161
- Small engine components test facility turbine testing cell
[NASA-TM-100887] p 33 N88-22037
- High-temperature combustor liner tests in structural component response test facility p 33 N88-22383
- Description of an oscillating flow pressure drop test rig
[NASA-TM-100905] p 61 N88-22933
- The 1988 overview of free-piston Stirling technology for space power at the NASA Lewis Research Center
[NASA-TM-100795] p 61 N88-22934
- Techniques utilized in the simulated altitude testing of a 2D-CD vectoring and reversing nozzle
[NASA-TM-100872] p 40 N88-25464
- Documentation of the Benson Diesel Engine Simulation Program
[NASA-TM-100940] p 36 N88-27201
- Phase I results from the Stirling-powered vehicle project
[NASA-TM-100978] p 225 N88-27980
- Orbital transfer vehicle 3000 LBF thrust chamber assembly hot fire test program
[NASA-CR-182145] p 66 N88-29858
- Testing of a variable-stroke Stirling engine
[NASA-TM-100899] p 225 N88-30472
- ### ENGINES
- Some design considerations for ceramic components in heat engine applications p 106 N88-23875
- Nondestructive evaluation of structural ceramics p 178 N88-23876
- Improved silicon carbide for advanced heat engines p 106 N88-23879
- ### ENTROPY
- Primordial nucleosynthesis with decaying particles. I - Entropy-producing decays. II - Inert decays p 217 A88-47477

ENVIRONMENT EFFECTS

- High temperature polymer matrix composites p 70 A88-36775
- ### ENVIRONMENT MODELS
- Effects of environmentally imposed roughness on airfoil performance p 15 N88-15778
- ### ENVIRONMENTAL TESTS
- Oxygen plasma effects on several liquid droplet radiator fluids p 142 A88-47962
- ### ENVIRONMENTS
- Wear of iron and nickel in corrosive liquid environments p 88 A88-40790
- Wear of iron and nickel in corrosive liquid environments
[NASA-TM-100246] p 91 N88-11817
- ### EPITAXY
- Improved beta-SiC heteroepitaxial films using off-axis Si substrates p 219 A88-10431
- Temperature stability of Al(x)Ga(1-x)As (x = 0-1) thermal oxide masks for selective-area epitaxy p 221 A88-45858
- ### EPOXY MATRIX COMPOSITES
- Improving the interlaminar shear strength of carbon fiber-epoxy composites through carbon fiber bromination
[NASA-TM-100248] p 72 N88-15018
- Oxidation and protection of fiberglass-epoxy composite masts for photovoltaic arrays in the low Earth orbital environment
[NASA-TM-100839] p 104 N88-18734
- ### EPOXY RESINS
- Linear and nonlinear mechanical properties of a series of epoxy resins p 101 A88-54976
- ### EQUATIONS OF MOTION
- Transient rotor dynamic rub phenomena - Theory and test p 167 A88-31539
- Particle-laden weakly swirling free jets - Measurements and predictions
[AIAA PAPER 88-3138] p 142 A88-48757
- Use of the generalized transmission error in the equations of motion of gear systems p 168 A88-49410
- Application of Navier-Stokes analysis to stall flutter p 38 N88-23249
- Particle-laden weakly swirling free jets: Measurements and predictions
[NASA-TM-100920] p 34 N88-24639
- ### EQUIPMENT SPECIFICATIONS
- Advanced space solar dynamic power systems beyond IOC Space Station p 50 A88-11798
- In situ fatigue loading stage inside scanning electron microscope p 193 N88-22419
- Research sensors p 162 N88-22430
- ### EROSION
- Internal erosion rates of a 10-kW xenon ion thruster
[AIAA PAPER 88-2912] p 55 A88-48753
- Internal erosion rates of a 10-kW xenon ion thruster
[NASA-TM-100954] p 63 N88-24688
- ### ERROR ANALYSIS
- Design, calibration and error analysis of instrumentation for heat transfer measurements in internal combustion engines p 157 A88-18509
- Operating envelopes of particle sizing instrumentation used for icing research
[AIAA PAPER 88-0291] p 157 A88-22211
- The generalized transmission error of spiral bevel gears p 168 A88-49409
- Operating envelopes of particle sizing instrumentation used for icing research
[NASA-CR-180870] p 161 N88-13573
- ### ERRORS
- Optical alignment of Centaur's inertial guidance system
[NASA-TM-88844] p 43 N88-12515
- ### ETHERS
- Surface catalytic degradation study of two linear perfluoropolyalkylethers at 345 C
[NASA-TP-2774] p 68 N88-12543
- Improved perfluoropolyalkylether fluid development
[NASA-CR-180872] p 80 N88-15851
- ### EULER EQUATIONS OF MOTION
- Explicit multigrid algorithm for quasi-three-dimensional viscous flows in turbomachinery p 2 A88-10355
- A diagonally inverted LU implicit multigrid scheme
[AIAA PAPER 88-3565] p 209 A88-48791
- Third-order multi-dimensional Euler/Navier-Stokes solver
[AIAA PAPER 88-3645] p 209 A88-48806
- Application of Runge Kutta time marching scheme for the computation of transonic flows in turbomachines
[NASA-TM-86997] p 9 N88-12461
- SHARP simulation of discontinuities in highly convective steady flow
[NASA-TM-100240] p 210 N88-13931
- Advanced propeller research p 29 N88-15806

SUBJECT INDEX

- Choice of implicit and explicit operators for the upwind differencing method
[NASA-TM-100857] p 211 N88-21718
- A diagonally inverted LU implicit multigrid scheme
[NASA-TM-100911] p 13 N88-26340
- Euler analysis of a swirl recovery vane design for use with an advanced single-rotation propfan
[NASA-TM-101357] p 14 N88-29771
- ### EUTECTIC ALLOYS
- Identification of salt-alloy combinations for thermal energy storage applications in advanced solar dynamic power systems p 199 A88-24072
- Containerless processing of undercooled melts p 110 A88-28554
- Solidification of undercooled Ni-Sn eutectic alloy under microgravity conditions in the Space Shuttle p 110 A88-28557
- Dendritic growth of undercooled nickel-tin. III p 86 A88-32887
- Fluoride salts as phase change materials for thermal energy storage in the temperature range 1000-1400 K p 199 A88-33734
- Fraction eutectic measurements in slowly cooled Pb - 15 wt percent Sn alloys
[NASA-CR-180830] p 94 N88-25531
- ### EVALUATION
- Ultrasonic evaluation of mechanical properties of thick, multilayered, filament-wound composites p 176 A88-21340
- Evaluation of the communications impact of a low power arcjet thruster
[AIAA PAPER 88-3105] p 55 A88-48755
- Analysis and test evaluation of the dynamic stability of three advanced turboprop models at zero forward speed
[NASA-CR-175025] p 26 N88-14095
- Analysis and test evaluation of the dynamic response and stability of three advanced turboprop models at low forward speed
[NASA-CR-175026] p 27 N88-14096
- Multi-hundred kilowatt roll ring assembly evaluation results p 114 N88-21375
- Evaluation of the communications impact of a low power arcjet thruster
[NASA-TM-100926] p 63 N88-24682
- Development of sensors for ceramic components in advanced propulsion systems: Survey and evaluation of measurement techniques for temperature, strain and heat flux for ceramic components in advanced propulsion systems
[NASA-CR-182111] p 163 N88-28299
- Design and evaluation of high contact ratio gearing
[NASA-CR-174958] p 175 N88-28319
- ### EVOLUTION (DEVELOPMENT)
- Evolution of hairpin vortices in a shear flow
[NASA-TM-100858] p 211 N88-26885
- ### EXCITATION
- Saturation and the limit of jet mixing enhancement by single frequency plane wave excitation - Experiment and theory
[AIAA PAPER 88-3613] p 8 A88-48899
- Saturation and the limit of jet mixing enhancement by single frequency plane wave excitation: Experiment and theory
[NASA-TM-100882] p 12 N88-23732
- ### EXHAUST EMISSION
- Adiabatic diesel engine component development: Reference engine for on-highway applications
[NASA-CR-179531] p 224 N88-12428
- ### EXHAUST GASES
- Effects of nozzle-exit boundary-layer conditions on excitability of heated free jets
[AIAA PAPER 87-2723] p 135 A88-20182
- Aeroacoustics of advanced STOVL aircraft plumes
[SAE PAPER 872358] p 215 A88-30998
- An experimental investigation of an arcjet thruster exhaust using Langmuir probes
[NASA-TM-100258] p 60 N88-21253
- Techniques utilized in the simulated altitude testing of a 2D-CD vectoring and reversing nozzle
[NASA-TM-100872] p 40 N88-25464
- ### EXHAUST NOZZLES
- Acoustics technologies for STOVL aircraft
[AIAA PAPER 88-2238] p 215 A88-35939
- Experimental evaluation of a translating nozzle sidewall radial turbine p 31 N88-17656
- ### EXHAUST SYSTEMS
- Adiabatic diesel engine component development: Reference engine for on-highway applications
[NASA-CR-179531] p 224 N88-12428
- ### EXHAUST VELOCITY
- On the correlation of plume centerline velocity decay of turbulent acoustically excited jets
[AIAA PAPER 87-2692] p 3 A88-18654

EXOTHERMIC REACTIONS

The carbon dioxide chaperon efficiency for the reaction $H + O_2 + M$ yields $HO_2 + M$ from ignition delay times behind reflected shock waves
[NASA-TM-100125] p 79 N88-15036

EXPENDABLE STAGES (SPACECRAFT)

Communications satellite systems operations with the space station. Volume 3: Supplementary technical report [NASA-CR-180875] p 48 N88-16794

EXPERIMENT DESIGN

A finite element model for wave propagation in an inhomogeneous material including experimental validation
[AIAA PAPER 87-2741] p 212 A88-16577

Experiments to ensure Space Station fire safety - A challenge
[AIAA PAPER 88-0540] p 41 A88-22405

Model helicopter performance degradation with simulated ice shapes
[NASA-TM-100830] p 92 N88-20417

EXPERIMENTATION

Identification of differences between finite element analysis and experimental vibration data
[NASA-TM-100830] p 92 N88-20417

EXPERT SYSTEMS

Expert systems for space power supply - Design, analysis, and evaluation
[AIAA PAPER 88-2371] p 182 A88-32308

An expert system for probabilistic description of loads on space propulsion system structural components
[AIAA PAPER 88-2371] p 182 A88-32308

NESSUS/EXPERT - An expert system for probabilistic structural analysis methods
[AIAA PAPER 88-2374] p 206 A88-32311

An expert system approach to turbopump health monitoring
[AIAA PAPER 88-3117] p 42 A88-48038

A reusable rocket engine intelligent control
[NASA-TM-100963] p 65 N88-26401

EXPONENTIAL FUNCTIONS

Applications of an exponential finite difference technique
[NASA-TM-100939] p 175 N88-28312

EXPOSURE

The effects of atmosphere on the tribological properties of a chromium carbide based coating for use to 760 C
[NASA-TM-100939] p 175 N88-28312

EXTENSIONS

Thermo-elasto-viscoplastic analysis of problems in extension and shear
[NASA-TM-101305] p 156 N88-30090

EXTINCTION

A theoretical analysis of the extinction limits of a methane-air opposed-jet diffusion flame
[NASA-TM-101305] p 156 N88-30090

EXTINGUISHING

Spacecraft fire detection and extinguishment: A bibliography
[NASA-CR-180880] p 45 N88-18612

EXTRAPOLATION

An algorithm for a generalization of the Richardson extrapolation process
[NASA-TM-101327] p 212 N88-30377

EXTREMELY HIGH FREQUENCIES

Experimental radio frequency link for Ka-band communications applications
[NASA-TM-100824] p 43 N88-24659

EXTRUDING

Powder processing of nickel and other aluminides by hot consolidation
[NASA-CR-180851] p 57 N88-11749

Sip casting and extruding shapes of rhodium with metal oxide additives. Part 2: Development of grain stabilized rhodium parts for resistojets
[NASA-CR-180851] p 57 N88-11749

Processing, physical metallurgy and creep of NiAl + Ta and NiAl + Nb alloys
[NASA-CR-182113] p 92 N88-21295

F**FABRICATION**

Fracture characteristics of angleplied laminates fabricated from overaged graphite/epoxy prepreg
[ASTM STP-942] p 86 A88-35901

High-temperature electronics
[NASA-CASE-LEW-14520-1] p 129 N88-23936

FABRICS

Tribological properties of alumina-boria-silicate fabric from 25 to 850 C
[NASA-TM-100806] p 104 N88-18726

FABRY-PEROT INTERFEROMETERS

Fiber-linked interferometric pressure sensor
p 157 A88-11743

FACE CENTERED CUBIC LATTICES

Effect of initial gamma prime size on the elevated temperature creep properties of single crystal nickel base superalloys
p 82 A88-18884

Predicting diffusion paths and interface motion in gamma/gamma + beta, Ni-Cr-Al diffusion couples
p 84 A88-24486

Lattice parameter variations during aging in nickel-base superalloys
p 90 A88-51318

FACILITIES

Lewis materials research and technology: An overview
p 223 N88-16699

FADING

A statistical rain attenuation prediction model with application to the advanced communication technology satellite project. Part 2: Theoretical development of a dynamic model and application to rain fade durations and tolerable control delays for fade countermeasures
[NASA-TM-100242] p 118 N88-11945

FAILURE ANALYSIS

A systems engineering approach to automated failure cause diagnosis in space power systems
p 52 A88-11870

Effect of storage and LEO cycling on manufacturing technology IPV nickel-hydrogen cells
p 53 A88-11917

Internal erosion rates of a 10-kW xenon ion thruster
[AIAA PAPER 88-2912] p 55 A88-48753

Experiments investigating advanced materials under thermomechanical loading
p 191 N88-22385

Monolithic ceramic analysis using the SCARE program
p 105 N88-22409

Fracture technology for brittle materials
p 192 N88-22417

Internal erosion rates of a 10-kW xenon ion thruster
[NASA-TM-100954] p 63 N88-24688

FAILURE MODES

Stress-life interrelationships associated with alkaline fuel cells
p 197 A88-11903

Thermomechanical behavior of plasma-sprayed ZrO₂-Y₂O₃ coatings influenced by plasticity, creep, and oxidation
p 95 A88-12588

Probabilistic structural analysis of aerospace components using NESSUS
[AIAA PAPER 88-2373] p 182 A88-32310

An expert system approach to turbopump health monitoring
[AIAA PAPER 88-3117] p 42 A88-48038

Mode 2 fracture mechanics
p 183 N88-22418

Some design considerations for ceramic components in heat engine applications
p 106 N88-23875

Fatigue failure of regenerator screens in a high frequency Stirling engine
p 179 N88-24491

FALKNER-SKAN EQUATION

The measurement of boundary layers on a compressor blade in cascade. III - Pressure surface boundary layers and the near wake
[ASME PAPER 87-GT-250] p 132 A88-11132

FAN BLADES

Application of advanced computational codes in the design of an experiment for a supersonic throughflow fan rotor
[ASME PAPER 87-GT-160] p 2 A88-11072

Advanced composite turboprops - Modeling, structural, and dynamic analyses
[ASME PAPER 87-GT-78] p 21 A88-36745

Scale model acoustic testing of counterrotating fans
[AIAA PAPER 88-2057] p 22 A88-37947

The composite blade structural analyzer (COBSTRAN)
p 33 N88-22390

Structural tailoring of advanced turboprops
p 192 N88-22400

Optical measurement of unducted fan blade deflections
[NASA-TM-100966] p 163 N88-29142

FANS

Supersonic throughflow fans for high-speed aircraft
p 30 N88-15810

FAST FOURIER TRANSFORMATIONS

Analysis of eccentric annular incompressible seals. I - A new solution using fast Fourier transforms for determining hydrodynamic force
[ASME PAPER 87-TRIB-52] p 166 A88-23308

FAST NEUTRONS

Neutron radiation tolerance of Au-activated silicon
p 222 N88-24316

FATIGUE (MATERIALS)

Low cycle fatigue
[ASTM STP-942] p 86 A88-35901

Fatigue crack propagation of nickel-base superalloys at 650 deg C
p 86 A88-35908

An update of the total-strain version of SRP
p 86 A88-35910

Creep-fatigue behavior of NiCoCrAlY coated PWA 1480
p 186 N88-11176

Lewis' enhanced laboratory for research into the fatigue and constitutive behavior of high temperature materials
p 186 N88-11177

Aeropropulsion '87. Session 1: Aeropropulsion Materials Research
[NASA-CP-10003-SESS-1] p 31 N88-16697

Lewis Structures Technology, 1988. Volume 2: Structural Mechanics
[NASA-CP-3003-VOL-2] p 190 N88-22382

Mode 2 fracture mechanics
p 193 N88-22418

In situ fatigue loading stage inside scanning electron microscope
p 193 N88-22419

Grain boundary oxidation and low-cycle fatigue at elevated temperatures
p 193 N88-22420

Cumulative fatigue damage models
p 193 N88-22422

Fatigue damage mapping
p 193 N88-22423

Fatigue crack growth behavior of a single crystal alloy as observed through an in situ fatigue loading stage
[NASA-TM-100863] p 93 N88-22986

Fatigue failure of regenerator screens in a high frequency Stirling engine
p 179 N88-24491

Resolved shear stress intensity coefficient and fatigue crack growth in large crystals
[NASA-CR-182137] p 195 N88-24997

FATIGUE LIFE

Calculation of thermomechanical fatigue life based on isothermal behavior
p 181 A88-26450

Probabilistic constitutive relationships for cyclic material strength models
p 182 A88-32313

A model for life predictions of nickel-base superalloys in high-temperature low cycle fatigue
p 87 A88-35913

Grain boundary oxidation and an analysis of the effects of oxidation on fatigue crack nucleation life
p 87 A88-35938

Accelerated crack growth rate at low Delta K in a single crystal superalloy
p 89 A88-47687

Computerized life and reliability modelling for turboprop transmissions
[AIAA PAPER 88-2979] p 100 A88-48031

Bithermal low-cycle fatigue behavior of a NiCoCrAlY-coated single crystal superalloy
p 90 A88-51736

Fatigue life prediction modeling for turbine hot section materials
p 184 A88-54144

Creep fatigue life prediction for engine hot section materials (isotropic): Third year progress review
p 186 N88-11173

Fatigue life prediction modeling for turbine hot section materials
[NASA-TM-100291] p 187 N88-14453

Life prediction of thermomechanical fatigue using total strain version of strainrange partitioning (SRP): A proposal
[NASA-TP-2779] p 187 N88-15263

Life prediction technologies for aeronautical propulsion systems
p 27 N88-15788

Relationship between fatigue life in the creep-fatigue region and stress-strain response
[NASA-TM-100796] p 188 N88-18040

Hygrothermomechanical fiber composite fatigue: Computational simulation
[NASA-TM-100640] p 74 N88-21257

A constitutive model for an overlay coating
p 105 N88-21525

Life assessment of combustor liner using unified constitutive models
p 33 N88-22384

Computational structural mechanics for engine structures
p 33 N88-22399

Large-scale wind turbine structures
p 202 N88-22429

The analysis of fatigue crack growth mechanism and oxidation and fatigue life at elevated temperatures
[NASA-CR-182129] p 94 N88-22987

Computerized life and reliability modelling for turboprop transmissions
[NASA-TM-100918] p 173 N88-23220

Cyclic fatigue damage characteristics observed for simple loadings extended to multiaxial life prediction
[NASA-CR-182126] p 195 N88-25016

Surface fatigue life of CBN and vitreous ground carburized and hardened AISI 9310 spur gears
[NASA-TM-100960] p 175 N88-25916

Accelerated fatigue crack growth behavior of PWA 1480 single crystal alloy and its dependence on the deformation mode
[NASA-TM-100943] p 95 N88-26436

The relationship between observed fatigue damage and life estimation models
[NASA-CR-182191] p 196 N88-27611

Spray automated balancing of rotors: Methods and materials
[NASA-CR-182151] p 41 N88-29825

FATIGUE TESTS

- Dynamic and static fatigue behavior of sintered silicon nitrides p 96 A88-12602
- Electro-impulse de-icing - A status report [AIAA PAPER 88-0019] p 17 A88-22017
- Anisotropic constitutive modeling for nickel base single crystal superalloys using a crystallographic approach [AIAA PAPER 88-2440] p 85 A88-32357
- Creep-fatigue behavior of NiCoCrAlY coated PWA 1480 superalloy single crystals p 86 A88-35911
- Crack diffusion coefficient - A candidate fracture toughness parameter for short fiber composites p 70 A88-36945
- Calibration of a Mode II test specimen p 183 A88-47014
- Creep fatigue life prediction for engine hot section materials (isotropic): Third year progress review p 186 A88-11173
- Creep-fatigue behavior of NiCoCrAlY coated PWA 1480 p 186 A88-11176
- The cyclic stress-strain behavior of a single crystal nickel-base superalloy [NASA-TM-100269] p 92 A88-19610
- Bithermal fatigue of a nickel-base superalloy single crystal [NASA-TM-100885] p 93 A88-22168
- FAULT TOLERANCE**
 - Space Station electric power system requirements and design p 50 A88-11782
 - A cascaded Schwarz converter for high frequency power distribution p 127 A88-54713
- FEASIBILITY ANALYSIS**
 - Feasibility of hydroxyl concentration measurements by laser-saturated fluorescence in high-pressure flames p 77 A88-17218
 - Assessment of nuclear reactor concepts for low power space applications p 217 A88-24409
 - Program for the feasibility of developing a high pressure acoustic levitator [NASA-CR-182154] p 113 A88-26498
- FEEDBACK CONTROL**
 - Finite-dimensional modeling of network-induced delays for real-time control systems p 208 A88-54537
 - The design of a turboshaft speed governor using modern control techniques [NASA-CR-175046] p 170 A88-10339
- FIBER COMPOSITES**
 - A heater made from graphite composite material for potential deicing application p 17 A88-15724
 - Thermal cycling of tungsten-fibre-reinforced superalloy composites p 70 A88-31770
 - Fracture toughness computational simulation of general delaminations in fiber composites [AIAA PAPER 88-2261] p 181 A88-32219
 - Superelement methods applications to micromechanics of high temperature metal matrix composites [AIAA PAPER 88-2390] p 182 A88-32322
 - Advanced composite turboprops - Modeling, structural, and dynamic analyses [ASME PAPER 87-GT-78] p 21 A88-36745
 - Crack diffusion coefficient - A candidate fracture toughness parameter for short fiber composites p 70 A88-36945
 - Hygrothermomechanical fiber composite fatigue - Computational simulation p 71 A88-42437
 - Acousto-ultrasonics as a monitor of material anisotropy p 176 A88-46828
 - Pressure effects on the thermal stability of SiC fibers [NASA-TM-100146] p 71 A88-10120
 - Transply crack density detection by acousto-ultrasonics [NASA-TM-100224] p 72 A88-11758
 - Fiber composite structural durability and damage tolerance: Simplified predictive methods [NASA-TM-100179] p 72 A88-13409
 - Design procedures for fiber composite box beams [NASA-TM-100296] p 73 A88-16828
 - Mechanics of composite materials: Past, present and future [NASA-TM-100793] p 73 A88-17744
 - Finite element substructuring methods for composite mechanics [NASA-TM-100297] p 73 A88-17745
 - Friction and wear of monolithic and fiber reinforced silicon-ceramics sliding against IN-718 alloy at 25 to 800 C in atmospheric air at ambient pressure [NASA-TM-100294] p 103 A88-17796
 - Oxidation and protection of fiberglass-epoxy composite masts for photovoltaic arrays in the low Earth orbital environment [NASA-TM-100839] p 104 A88-18734
 - Hygrothermomechanical fiber composite fatigue: Computational simulation p 74 A88-21257
 - [NASA-TM-100840] p 74 A88-21257
 - The composite blade structural analyzer (COBSTRAN) p 33 A88-22390

- Whisker-reinforced ceramic composites for heat engine components p 105 A88-22410
- Nondestructive evaluation by acousto-ultrasonics p 177 A88-22412
- Acousto-ultrasonic input-output characterization of unidirectional fiber composite plate by SV waves [NASA-CR-4152] p 178 A88-23224
- Ceramics for turbine engines p 106 A88-23873
- Ceramic matrix composites p 75 A88-23888
- Polymer precursors for ceramic composites p 75 A88-23890
- SiC fiber reinforced reaction-bonded Si3N4 composites p 75 A88-23892
- Input-output characterization of fiber composites by SH waves [NASA-CR-4153] p 179 A88-23986
- Creep behavior of tungsten/niobium and tungsten/niobium-1 percent zirconium composites p 75 A88-24427
- Acousto-ultrasonic input-output characterization of unidirectional fiber composite plate by P waves [NASA-CR-4162] p 180 A88-25923
- As-received microstructure of a SiC/Ti-15-3 composite [NASA-TM-100938] p 76 A88-28095
- Investigation of a SiC/Ti-24Al-11Nb composite [NASA-TM-100956] p 76 A88-28980
- FIBER OPTICS**
 - Conceptual design of an optic based engine control system [ASME PAPER 87-GT-168] p 18 A88-11079
 - Fiber-linked interferometric pressure sensor p 157 A88-11743
 - Time domain referencing in intensity modulation fiber optic sensing systems p 217 A88-12660
 - Calibration of high-temperature, fiber-optic, microbend, pressure transducers p 157 A88-22942
 - Loss-compensation of intensity-modulating fiber-optic sensors p 158 A88-22943
 - Fiber-optic displacement sensor with temporally separated signal and reference channels p 217 A88-33161
 - Referencing in fiber optic sensing systems p 217 A88-42604
 - Aeropropulsion '87, Session 4: Instrumentation and Controls Research [NASA-CP-10003-SESS-4] p 28 A88-15794
 - Optical measurement systems p 218 A88-15796
 - Fiber optics for controls p 218 A88-15798
 - Overview of NASA research in fiber optics for aircraft controls [NASA-TM-100919] p 35 A88-25458
 - Fiber optics for advanced aircraft [NASA-TM-101294] p 1 A88-26328
 - Active phase compensation system for fiber optic holography [NASA-TM-101295] p 162 A88-26641
 - Fiber optic sensors with internal referencing [NASA-TM-100893] p 162 A88-26644
 - Modulated-splitting-ratio fiber-optic temperature sensor [NASA-TM-101332] p 18 A88-28062
 - Fiber optic sensing systems using high frequency resonant sensing heads with intensity sensors [NASA-TM-101318] p 163 A88-28293
- FIBER STRENGTH**
 - Composite monolayer fabrication by an arc-spray process p 169 A88-53581
 - Pressure effects on the thermal stability of SiC fibers [NASA-TM-100146] p 71 A88-10120
- FIBERS**
 - Thermal conductivity of pristine and brominated highly graphitized pitch based carbon fibers p 97 A88-20257
- FIELD EFFECT TRANSISTORS**
 - Microwave performance of an optically controlled AlGaAs/GaAs high electron mobility transistor and GaAs MESFET p 123 A88-24911
 - Two stage dual gate MESFET monolithic gain control amplifier for Ka-band p 124 A88-29821
 - Development of 20 GHz monolithic transmit modules [NASA-CR-182134] p 222 A88-24539
 - Optoelectronic gain control of a microwave single stage GaAs MESFET amplifier [NASA-CR-182201] p 131 A88-30055
- FIGHTER AIRCRAFT**
 - Conceptual design of an optic based engine control system [ASME PAPER 87-GT-168] p 18 A88-11079
 - Flight propulsion control integration for V/STOL aircraft [SAE PAPER 872330] p 21 A88-37199
 - NASA supersonic STOVL propulsion technology program [SAE PAPER 872352] p 21 A88-37215
 - Flight propulsion control integration for V/STOL aircraft [NASA-TM-100226] p 38 A88-11680

- NASA supersonic STOVL propulsion technology program [NASA-TM-100227] p 26 A88-14093
- Multiple-Purpose Subsonic Naval Aircraft (MPSNA): Multiple Application Propfan Study (MAPS) [NASA-CR-175104] p 18 A88-28917
- FILAMENT WINDING**
 - Ultrasonic evaluation of mechanical properties of thick, multilayered, filament-wound composites p 176 A88-21340
- FILM COOLING**
 - Film cooling heat transfer on a turbine airfoil p 147 A88-11156
- FILM THICKNESS**
 - Oil film thickness measurement and analysis for an angular contact ball bearing operating in parched elastohydrodynamic lubrication p 165 A88-14115
 - Parched elasto hydrodynamic lubrication film thickness measurement in an instrument ball bearing [STLE PREPRINT 88-AM-6G-1] p 169 A88-51082
 - Low-temperature photoluminescence studies of chemical-vapor-deposition-grown 3C-SiC on Si p 127 A88-53396
 - Raman scattering studies of chemical-vapor-deposited cubic SiC films of (100)Si p 127 A88-53397
 - Foil bearing lubrication theory including compressibility effects p 170 A88-54964
- FILTRATION**
 - Reduction of temperature rise in high-speed photography p 160 A88-55254
 - Reduction of temperature rise in high-speed photography [NASA-TM-100222] p 160 A88-11100
- FINITE DIFFERENCE THEORY**
 - A mapped finite difference study of noise propagation in nonuniform ducts with mean flow p 214 A88-18541
 - A finite difference scheme for three-dimensional steady laminar incompressible flow p 139 A88-30469
 - Hierarchically partitioned nonlinear equation solvers p 210 A88-54980
 - Input-output-controlled nonlinear equation solvers p 146 A88-55245
 - Improved numerical methods for turbulent viscous recirculating flows p 146 A88-11148
 - A two-dimensional finite difference program for thermal analysis of rocket thrust chambers [NASA-TM-100191] p 58 A88-12539
 - Accurate boundary conditions for exterior problems in gas dynamics [NASA-TM-100807] p 210 A88-19182
 - Reduced order models for nonlinear aerodynamics p 11 A88-23248
 - Applications of an exponential finite difference technique [NASA-TM-100939] p 175 A88-28312
- FINITE ELEMENT METHOD**
 - Plasticity analysis of wear phenomena as an aid in the development of abrasable materials p 164 A88-10938
 - A finite element model for wave propagation in an inhomogeneous material including experimental validation [AIAA PAPER 87-2741] p 212 A88-16577
 - Numerical methods for one-dimensional reaction-diffusion equations arising in combustion theory p 135 A88-18975
 - Finite element methods in probabilistic mechanics p 212 A88-29060
 - An integrated approach for friction damper design p 167 A88-31598
 - Validation of the NESSUS probabilistic finite element analysis computer program [AIAA PAPER 88-2372] p 205 A88-32309
 - Superelement methods applications to micromechanics of high temperature metal matrix composites [AIAA PAPER 88-2390] p 182 A88-32322
 - Identification of differences between finite element analysis and experimental vibration data p 183 A88-46666
 - Hierarchically partitioned nonlinear equation solvers p 210 A88-54980
 - Input-output-controlled nonlinear equation solvers p 146 A88-55245
 - A microstructural lattice model for strain oriented problems: A combined Monte Carlo finite element technique [NASA-TM-100215] p 90 A88-10939
 - Component specific modeling p 206 A88-11166
 - Constitutive modeling for single crystal superalloys p 90 A88-11168
 - Constitutive modeling for isotropic materials p 185 A88-11171
 - Constitutive modeling for isotropic materials p 186 A88-11172
 - Thermal expansion mismatch and oxidation in thermal barrier coatings p 170 A88-11182

- Finite-element grid improvement by minimization of stiffness matrix trace
[NASA-TM-100255] p 171 N88-13604
- Thermal finite-element analysis of space shuttle main engine turbine blade
[NASA-TM-100117] p 187 N88-13745
- Finite element substructuring methods for composite mechanics
[NASA-TM-100297] p 73 N88-17745
- Vibration and flutter characteristics of the SR7L large-scale propfan
[NASA-TM-100272] p 188 N88-18036
- Evaluation of structural analysis methods for life prediction
p 190 N88-21511
- On 3-D inelastic analysis methods for hot section components. Volume 1: Special finite element models
[NASA-CR-180893] p 190 N88-21535
- Finite element (MARC) solution technologies for viscoplastic analyses
p 191 N88-22389
- MHOST: An efficient finite element program for inelastic analysis of solids and structures
p 33 N88-22394
- Fatigue damage modeling for coated single crystal superalloys
p 93 N88-22427
- Parallel computer methods for eigenvalue extraction
p 207 N88-23233
- Improved method for stress and compatibility analysis of multicomponent rotating systems
[NASA-TM-100884] p 195 N88-25935
- FINITE VOLUME METHOD**
- Effects of numerical dissipation on finite-volume solutions of compressible flow problems
[AIAA PAPER 88-0621] p 5 A88-22469
- Numerical simulation of hypersonic inlet flows with equilibrium or finite rate chemistry
[AIAA PAPER 88-0273] p 5 A88-27717
- Explicit finite-volume time-marching calculations of total temperature distributions in turbulent flow
p 139 A88-30517
- An explicit finite-volume time-marching procedure for turbulent flow calculations
p 139 A88-30518
- Adaptive grid generation
p 208 A88-37363
- The 2-D and 3-D time marching transonic potential flow method for propfans
p 11 N88-23245
- FIRE EXTINGUISHERS**
- Spacecraft Fire Safety
[NASA-CP-2476] p 45 N88-12520
- FIRE PREVENTION**
- Experiments to ensure Space Station fire safety - A challenge
[AIAA PAPER 88-0540] p 41 A88-22405
- Spacecraft fire detection and extinguishment: A bibliography
[NASA-CR-180880] p 45 N88-18612
- Spacecraft fire-safety experiments for space station: Technology development mission
[NASA-CR-182114] p 48 N88-20353
- FIRES**
- Spacecraft Fire Safety
[NASA-CP-2476] p 45 N88-12520
- Microgravity combustion fundamentals
p 112 N88-12528
- FITNESS**
- Three-dimensional adaptive grid generation for body-fitted coordinate system
[NASA-CR-182192] p 155 N88-27520
- FLAME PROPAGATION**
- Numerical methods for one-dimensional reaction-diffusion equations arising in combustion theory
p 135 A88-18975
- Laminar diffusion flames under micro-gravity conditions
[AIAA PAPER 88-0645] p 78 A88-27722
- The effect of gravity on premixed flame propagation and extinction in a vertical standard flammability tube
p 78 A88-38532
- Microgravity combustion fundamentals
p 112 N88-12528
- The effect of microgravity on flame spread over a thin fuel
[NASA-TM-100195] p 80 N88-15853
- FLAME SPRAYING**
- Mixing, transport and combustion in sprays
p 138 A88-25828
- FLAMEOUT**
- A theoretical analysis of the extinction limits of a methane-air opposed-jet diffusion flame
p 77 A88-16497
- FLAMES**
- Reducing adhesion and agglomeration within a cloud of combustible particles
[NASA-TM-100902] p 114 N88-26539
- FLAMMABILITY**
- The effect of gravity on premixed flame propagation and extinction in a vertical standard flammability tube
p 78 A88-38532
- Spacecraft Fire Safety
[NASA-CP-2476] p 45 N88-12520
- Reducing adhesion and agglomeration within a cloud of combustible particles
[NASA-TM-100902] p 114 N88-26539
- FLAT PLATES**
- Computation of the velocity field of an excited shear layer
p 138 A88-26206
- Heat transfer with very high free stream turbulence
p 148 N88-11161
- Two-equation low-Reynolds-number turbulence modeling of transitional boundary layer flows characteristic of gas turbine blades
[NASA-CR-4145] p 153 N88-23185
- FLEXIBILITY**
- Vibration and control of flexible rotor supported by magnetic bearings
[NASA-TM-100888] p 174 N88-23977
- FLEXIBLE BODIES**
- Hierarchically partitioned nonlinear equation solvers
p 210 A88-54980
- FLEXIBLE SPACECRAFT**
- A flexible on-board demultiplexer/demodulator
[AIAA PAPER 88-0811] p 123 A88-27558
- FLIGHT CONDITIONS**
- In-flight measurement of airfoil icing using an array of ultrasonic transducers
p 15 A88-50910
- FLIGHT CONTROL**
- Fight propulsion control integration for V/STOL aircraft
[SAE PAPER 872330] p 21 A88-37199
- Fight propulsion control integration for V/STOL aircraft
[NASA-TM-100226] p 38 N88-11680
- Rotorcraft flight-propulsion control integration
p 38 N88-16643
- Computer simulation of a single pilot flying a modern high-performance helicopter
[NASA-TM-100182] p 39 N88-26376
- FLIGHT SIMULATION**
- Noise of a model counterrotation propeller with reduced aft rotor diameter at simulated takeoff/approach conditions (F7/A3)
[AIAA PAPER 88-0263] p 214 A88-22192
- Noise of a model counterrotation propeller with reduced aft rotor diameter at simulated takeoff/approach conditions (F7/A3)
[NASA-TM-100254] p 216 N88-13961
- FLIGHT TESTS**
- Auxiliary propulsion system flight package
[NASA-CR-180828] p 56 N88-10886
- Overview of NASA PTA propfan flight test program
p 29 N88-15805
- An experimental and theoretical study of the ice accretion process during artificial and natural icing conditions
[NASA-CR-182119] p 16 N88-21143
- FLOATING POINT ARITHMETIC**
- Performance limitations in parallel processor simulations
p 208 A88-49101
- FLOW CHARACTERISTICS**
- Structure of a reattaching supersonic shear flow
[AIAA PAPER 88-3615] p 8 A88-48901
- Experimental investigation of the subsonic high-altitude operation of the NASA Lewis 10- by 10-foot supersonic wind tunnel
[NASA-TM-100214] p 40 N88-15814
- FLOW DEFLECTION**
- Local heat/mass transfer distributions around sharp 180 deg turns in two-pass smooth and rib-roughened channels
[ASME PAPER 86-GT-114] p 139 A88-28516
- Three-dimensional flow past two cylinders mounted side by side on an endwall
[AIAA PAPER 88-3718] p 143 A88-48974
- FLOW DISTRIBUTION**
- Experiments on spray interactions in the wake of a bluff body
[ASME PAPER 87-GT-48] p 131 A88-11000
- Control of shear flows by artificial excitation
[AIAA PAPER 87-2722] p 3 A88-16567
- Measurements of the unsteady flow field within the stator row of a transonic axial-flow fan. I - Measurement and analysis technique
[ASME PAPER 87-GT-226] p 4 A88-18660
- Measurements of the unsteady flow field within the stator row of a transonic axial-flow fan. II - Results and discussion
[ASME PAPER 87-GT-227] p 4 A88-18661
- A space-marching method for the computation of viscous internal flows
p 135 A88-20459
- The calculation of flow over iced airfoils
[AIAA PAPER 88-0112] p 4 A88-22078
- A natural low frequency oscillation in the wake of an airfoil near stalling conditions
[AIAA PAPER 88-0131] p 4 A88-22093
- Navier-Stokes solutions of flowfield characteristics produced by ice accretion
[AIAA PAPER 88-0290] p 137 A88-22210
- Performance of laser Doppler velocimeter with polydisperse seed particles in high speed flows
[AIAA PAPER 88-0425] p 157 A88-22317
- Navier-Stokes cascade analysis with a stiff k-epsilon turbulence solver
[AIAA PAPER 88-0594] p 5 A88-22444
- Measurement and prediction of propeller flow field on the PTA aircraft at speeds of up to Mach 0.85 --- Propfan Test Assessment
[AIAA PAPER 88-0667] p 19 A88-22497
- A numerical study of the effects of curvature and convergence on dilution jet mixing
[AIAA PAPER 87-1953] p 137 A88-23312
- Numerical study of chemically reacting flows using an LU scheme
[AIAA PAPER 88-0436] p 5 A88-24825
- Computation of the velocity field of an excited shear layer
p 138 A88-26206
- Excitation of instability waves in free shear layers. II - Experiments
p 138 A88-26339
- Numerical and analytical study of fluid dynamic forces in seals and bearings
p 167 A88-31534
- Comparison of computational methods for three-dimensional turbulent turbomachinery flows
p 6 A88-42452
- Gas liquid flow at microgravity conditions - Flow patterns and their transitions
p 141 A88-42839
- Turbulence energy and diffusion transport of third-moments in a separating and reattaching flow
p 141 A88-43011
- Turbulence modeling and surface heat transfer in a stagnation flow region
p 141 A88-43871
- A numerical study of the hot gas environment around a STOVL aircraft in ground proximity
[AIAA PAPER 88-2882] p 23 A88-48752
- Centerline Mach number characteristics of highly heated free jets
[AIAA PAPER 88-3612] p 7 A88-48898
- Experimental verification of a secondary recirculation zone in a labyrinth seal
[AIAA PAPER 88-3692] p 168 A88-48971
- Two-dimensional viscous flow computations of hypersonic scramjet nozzle flowfields at design and off-design conditions
[AIAA PAPER 88-3280] p 23 A88-50785
- 3-D laser anemometer measurements in a labyrinth seal
[ASME PAPER 88-GT-63] p 169 A88-54195
- 3-D laser anemometer measurements in an annular seal
[ASME PAPER 88-GT-64] p 169 A88-54196
- Navier-Stokes cascade analysis with a stiff Kappa-Epsilon turbulence solver
[NASA-TM-100218] p 9 N88-10778
- A natural low frequency oscillation in the wake of an airfoil near stalling conditions
[NASA-TM-100213] p 9 N88-10779
- The four spot time-of-flight laser anemometer
p 164 N88-11145
- Fuel-injector/air-swirl characterization
p 146 N88-11150
- Heat transfer in a real engine environment
p 147 N88-11155
- Flow field measurements in a 90 degree turning duct
p 147 N88-11157
- Heat transfer with very high free stream turbulence
p 148 N88-11161
- Flow in a model turbine stator
p 148 N88-11163
- Unsteady aerodynamics of an oscillating cascade in a compressible flow field
[NASA-TM-100219] p 26 N88-13346
- A numerical study of the effects of curvature and convergence on dilution jet mixing
[NASA-TM-89878] p 26 N88-13347
- Numerical study of chemically reacting flows using an LU scheme
[NASA-CR-180882] p 26 N88-14094
- An experimental mapping of the flow field behind a glaze ice shape on a NACA 0012 airfoil
[NASA-CR-180847] p 10 N88-15766
- CFD validation experiments for internal flows
[NASA-TM-100797] p 10 N88-16679
- Liquid sprays and flow studies in the direct-injection diesel engine under motored conditions
[NASA-TM-100135] p 31 N88-18594
- Description of an oscillating flow pressure drop test rig
[NASA-TM-100905] p 61 N88-22933
- A numerical study of the hot gas environment around a STOVL aircraft in ground proximity
[NASA-TM-100895] p 1 N88-23729

Two-dimensional viscous flow computations of hypersonic scramjet nozzle flowfields at design and off-design conditions

[NASA-CR-182150] p 35 N88-25459

Application of optical correlation techniques to particle imaging velocimetry

[NASA-TM-101306] p 163 N88-29152

User's manual for three dimensional boundary layer (BL3-D) code

[NASA-CR-174899] p 155 N88-30063

Assessment of a 3-D boundary layer analysis to predict heat transfer and flow field in a turbine passage

[NASA-CR-174894] p 155 N88-30066

Experimental and numerical investigation of the effect of distributed suction on oblique shock wave/turbulent boundary layer interaction

[NASA-TM-101334] p 156 N88-30084

FLOW GEOMETRY

Measurements of the turbulent transport of heat and momentum in convexly curved boundary layers - Effects of curvature, recovery and free-stream turbulence

[ASME PAPER 87-GT-199] p 131 A88-11103

Developing fluid flow in a curved duct of square cross-section and its fully developed dual solutions

p 139 A88-30957

Unsteady motion and transition to turbulence in developing curved duct flow

p 140 A88-39010

Lateral jet injection into swirling combustor flowfields

[AIAA PAPER 88-3183] p 141 A88-44783

FLOW MEASUREMENT

Laser Doppler velocimeter measurement of annulus wall boundary layer development in a compressor rotor

[ASME PAPER 87-GT-251] p 132 A88-11133

Corona anemometry for qualitative measurement of reversing surface flow with application to separation control by external excitation

p 133 A88-14143

Four spot laser anemometer and optical access techniques for turbine applications

p 159 A88-36513

Application of advanced diagnostics to airblast injector flows

[ASME PAPER 88-GT-12] p 159 A88-54159

The four spot time-of-flight laser anemometer

p 164 A88-11145

FLOW STABILITY

Control of free shear layers

[AIAA PAPER 87-2689] p 134 A88-16545

Absolute instability of the Gaussian wake profile

p 136 A88-20842

Excitation of instability waves in free shear layers. I - Theory

p 138 A88-26338

Excitation of instability waves in free shear layers. II - Experiments

p 138 A88-26339

Controlled excitation of a cold turbulent swirling free jet

[ASME PAPER 87-WA/NCA-18] p 140 A88-41568

Nonlinear roll-up of externally excited free shear layers

p 141 A88-44445

Effect of spatial inlet temperature and pressure distortion on turbofan engine stability

[AIAA PAPER 88-3016] p 22 A88-44727

Stability of swirling gas flows

p 142 A88-46317

Application of bifurcation theory to axial flow compressor instability

[ASME PAPER 88-GT-231] p 169 A88-54313

Numerical results for axial flow compressor instability

[ASME PAPER 88-GT-252] p 169 A88-54328

Effect of spatial inlet temperature and pressure distortion on turbofan engine stability

[NASA-TM-100850] p 32 N88-21162

FLOW THEORY

Excitation of instability waves in free shear layers. I - Theory

p 138 A88-26338

FLOW VELOCITY

Gravitationally defined velocities for a low speed hot-wire calibration

p 133 A88-14170

Absolute instability of the Gaussian wake profile

p 136 A88-20842

An explicit finite-volume time-marching procedure for turbulent flow calculations

p 139 A88-30518

Experimental and theoretical effects of nitrogen gas flow rate on liquid-jet atomization

p 145 A88-52679

3-D laser anemometer measurements in a labyrinth seal

[ASME PAPER 88-GT-63] p 169 A88-54195

The four spot time-of-flight laser anemometer

p 164 A88-11145

Correlation of velocity and velocity-density turbulence in the exhaust of an atmospheric burner

p 161 N88-11147

Correlations of velocity and temperature fluctuations in the stagnation-point flow of circular cylinder in turbulent flow

[NASA-TM-100930] p 13 N88-25435

FLOW VISUALIZATION

The measurement of boundary layers on a compressor blade in cascade. III - Pressure surface boundary layers and the near wake

[ASME PAPER 87-GT-250] p 132 A88-11132

The structure and dynamics of reacting plane mixing layers

p 136 A88-20871

Engine flow visualization using a copper vapor laser

p 158 A88-34479

Unsteady motion and transition to turbulence in developing curved duct flow

p 140 A88-39010

A flow visualization study of the leading edge separation bubble on a NACA 0012 airfoil with simulated glaze ice

[NASA-CR-180846] p 10 N88-14966

Acoustically excited heated jets. 1: Internal excitation

[NASA-CR-4129-PT-1] p 12 N88-23751

Acoustically excited heated jets. 2: In search of a better understanding

[NASA-CR-4129-PT-2] p 12 N88-23752

Acoustically excited heated jets. 3: Mean flow data

[NASA-CR-4129-PT-3] p 12 N88-23753

FLUCTUATION THEORY

Coherent motion induced fluctuations in the primary transition region of a plane shear layer

p 133 A88-14125

FLUID DYNAMICS

The structure and dynamics of reacting plane mixing layers

p 136 A88-20871

Improved perfluoroalkyl ether fluid development

p 68 A88-28624

Boundary layer development as a function of chamber pressure in the NASA Lewis 1030:1 area ratio rocket nozzle

[AIAA PAPER 88-3301] p 144 A88-50786

Efficient numerical techniques for complex fluid flows

p 146 N88-11151

Computational prediction of propellant reorientation

p 109 N88-15940

Review and assessment of the HOST turbine heat transfer program

p 34 N88-22431

A physically consistent model for artificial dissipation in transonic potential flow computations

[NASA-TM-100846] p 211 N88-22652

Noncontact temperature measurements in the microgravity fluids and transport phenomena discipline

p 113 N88-23901

Correlations of velocity and temperature fluctuations in the stagnation-point flow of circular cylinder in turbulent flow

[NASA-TM-100930] p 13 N88-25435

Boundary layer development as a function of chamber pressure in the NASA Lewis 1030:1 area ratio rocket nozzle

[NASA-TM-100917] p 154 N88-25841

Assessment of a 3-D boundary layer analysis to predict heat transfer and flow field in a turbine passage

[NASA-CR-174894] p 155 N88-30066

FLUID FILMS

Oil film thickness measurement and analysis for an angular contact ball bearing operating in parched elastohydrodynamic lubrication

p 165 A88-14115

Foil bearing lubrication theory including compressibility effects

p 170 A88-54964

FLUID FLOW

Simulation of fluid flows during growth of organic crystals in microgravity

p 109 A88-13163

A mapped finite difference study of noise propagation in nonuniform ducts with mean flow

p 214 A88-18541

Characteristics of fluid flow in the combustion synthesis of TiC from the elements

p 110 A88-28564

Heat transfer in the tip region of a rotor blade simulator

p 147 N88-11159

Turbomachinery

p 28 N88-15792

Chemical reacting flows

p 79 N88-15793

Overview of heat transfer and fluid flow problem areas encountered in Stirling engine modeling

[NASA-TM-100131] p 224 N88-17561

NASA research Program: The roles of fluid motion and other transport phenomena in the morphology of materials

[NASA-CR-182801] p 222 N88-25327

FLUID JETS

Experimental and theoretical effects of nitrogen gas flow rate on liquid-jet atomization

p 145 A88-52679

Effect of mass-velocity on liquid jet atomization in Mach 1 gas flow

[NASA-TM-100813] p 162 N88-23194

Small-droplet spray measurements with a scattered-light scanner

[NASA-TM-100973] p 163 N88-26645

FLUID MANAGEMENT

Space station resistojet system requirements and interface definition study

[NASA-CR-180832] p 58 N88-12541

LeRC cryogenic fluid management program overview

p 150 N88-15928

Cryogenic fluid management program flight concept definition

p 150 N88-15929

Cryogenic Fluid Management Technology Workshop. Volume 2: Roundtable Discussion of Technology Requirements

[NASA-CP-10009] p 152 N88-20599

Study of toluene rotary fluid management device and shear flow condenser performance for a space-based organic Rankine power system

[NASA-CR-180885] p 67 N88-29872

FLUID MECHANICS

The measurement of boundary layers on a compressor blade in cascade. II - Suction surface boundary layers

[ASME PAPER 87-GT-249] p 132 A88-11131

Internal fluid mechanics research on supercomputers for aerospace propulsion systems

[NASA-TM-100289] p 149 N88-15188

Aeropropulsion '87. Session 3: Internal Fluid Mechanics Research

[NASA-CP-10003-SESS-3] p 28 N88-15790

Inlets, ducts and nozzles

p 149 N88-15791

Chemical reacting flows

p 79 N88-15793

Aeropropulsion '87. Session 4: Instrumentation and Controls Research

[NASA-CP-10003-SESS-4] p 28 N88-15794

Aeropropulsion '87. Session 5: Subsonic Propulsion Technology

[NASA-CP-10003-SESS-5] p 28 N88-15800

Aeropropulsion '87. Session 6: High-Speed Propulsion Technology

[NASA-CP-10003-SESS-6] p 29 N88-15807

Investigation of surface tension driven convection as a feasibility study for a micro-gravity experiment

[NASA-CR-182504] p 112 N88-18739

Research and technology

[NASA-TM-100172] p 227 N88-22851

FLUORIDES

Fluoride salts and container materials for thermal energy storage applications in the temperature range 973 - 1400 K

p 196 A88-11804

Fluoride salts as phase change materials for thermal energy storage in the temperature range 1000-1400 K

p 199 A88-33734

FLUORINATION

Synthesis, electrical and thermal conductivities, and potential applications of graphite fluoride fibers

p 97 A88-26963

Comparison of the tribological properties of fluorinated cokes and graphites

[STLE PREPRINT 88-AM-7F-1] p 100 A88-51300

FLUORINE ORGANIC COMPOUNDS

Improved perfluoroalkylether fluid development

[NASA-CR-180872] p 80 N88-15851

FLUOROCARBONS

Synthesis, electrical and thermal conductivities, and potential applications of graphite fluoride fibers

p 97 A88-26963

Substituted 1,1,1-Triaryl-2,2,2-Trifluoroethanes and processes for their synthesis

[NASA-CASE-LEW-14345-1] p 69 N88-26404

FLUOROPOLYMERS

Substituted 1,1,1-Triaryl-2,2,2-Trifluoroethanes and processes for their synthesis

[NASA-CASE-LEW-14345-1] p 69 N88-26404

FLUTTER

A natural low frequency oscillation in the wake of an airfoil near stalling conditions

[AIAA PAPER 88-0131] p 4 A88-22093

The effects of rotational flow, viscosity, thickness, and shape on transonic flutter dip phenomena

[AIAA PAPER 88-2348] p 182 A88-32289

A natural low frequency oscillation in the wake of an airfoil near stalling conditions

[NASA-TM-100213] p 9 N88-10779

The effects of rotational flow, viscosity, thickness, and shape on transonic flutter dip phenomena

[NASA-TM-100811] p 188 N88-18969

A semianalytical technique for sensitivity analysis of unsteady aerodynamic computations

[NASA-TM-100810] p 189 N88-18976

Application of Navier-Stokes analysis to stall flutter

p 38 N88-23249

FLUTTER ANALYSIS

Experimental classical flutter results of a composite advanced turboprop model

p 21 A88-35528

Flutter of a fan blade in supersonic axial flow

[ASME PAPER 88-GT-78] p 8 A88-54206

FLUX VECTOR SPLITTING

Choice of implicit and explicit operators for the upwind differencing method

[AIAA PAPER 88-0624] p 209 A88-22472

Splitting of inviscid fluxes for real gases

[AIAA PAPER 88-3526] p 142 A88-48782

Splitting of inviscid fluxes for real gases

[NASA-TM-100856] p 211 N88-21717

- Choice of implicit and explicit operators for the upwind differencing method
[NASA-TM-100857] p 211 N88-21718
- FOCUSING**
A re-examination of spent beam refocusing for high-efficiency helix TWT's and small MDC's
p 124 A88-28673
- FOIL BEARINGS**
Foil bearing lubrication theory including compressibility effects
p 170 A88-54964
- FORCED CONVECTION**
A theoretical analysis of the extinction limits of a methane-air opposed-jet diffusion flame
p 77 A88-16497
Regressed relations for forced convection heat transfer in a direct injection stratified charge rotary engine
[NASA-TM-100124] p 25 N88-13345
Impact of ETO propellants on the aerothermodynamic analyses of propulsion components
[NASA-TM-101303] p 156 N88-30094
- FORCED VIBRATION**
Aerodynamically forced vibration analysis of turbomachines
p 20 A88-31610
Control of rotor aerodynamically forced vibrations by splitters
p 23 A88-52684
- FOULING**
Experiments for the determination of convective diffusion heat/mass transfer to burner rig test targets comparable in size to jet stream diameter
p 140 A88-41574
- FOURIER TRANSFORMATION**
Determination of grain-size distribution function using two-dimensional Fourier transforms of tone-pulse-encoded images
p 176 A88-30425
- FRACTOGRAPHY**
Nondestructive evaluation of structural ceramics by photoacoustic microscopy
[NASA-CR-180858] p 103 N88-16868
Characterization of sintered SiC by using NDE
p 177 N88-22413
- FRAC TURE MECHANICS**
Efficient probabilistic fracture mechanics analysis
p 180 A88-16933
Interactive computer simulation of fracture processes
p 180 A88-16955
Elevated temperature durability of ceramic materials
[AIAA PAPER 88-3055] p 100 A88-44743
A review of path-independent integrals in elastic-plastic fracture mechanics
p 183 A88-47001
Fatigue life prediction modeling for turbine hot section materials
p 184 A88-54144
Elevated temperature crack growth
p 186 N88-11174
Deformation, fatigue and fracture behavior of two cast anisotropic superalloys
p 187 N88-13732
Fatigue life prediction modeling for turbine hot section materials
[NASA-TM-100291] p 187 N88-14453
Ceramics for engines
p 103 N88-16704
Lewis Structures Technology, 1988. Volume 2: Structural Mechanics
[NASA-CP-3003-VOL-2] p 190 N88-22382
Lewis Structures Technology, 1988. Volume 3: Structural Integrity Fatigue and Fracture Wind Turbines HOST
[NASA-CP-3003-VOL-3] p 192 N88-22408
Monolithic ceramic analysis using the SCARE program
p 105 N88-22409
Fracture technology for brittle materials
p 192 N88-22417
Mode 2 fracture mechanics
p 193 N88-22418
Elevated temperature crack growth
p 193 N88-22421
Large-scale wind turbine structures
p 202 N88-22429
Structural Ceramics
[NASA-CP-2427] p 106 N88-23872
Friction and wear of ceramics
p 106 N88-23874
Some design considerations for ceramic components in heat engine applications
p 106 N88-23875
Nondestructive evaluation of structural ceramics
p 178 N88-23876
Fracture mechanics
p 194 N88-23877
Isothermal and bithermal thermomechanical fatigue behavior of a NiCoCrAlY-coated single crystal superalloy
[NASA-TM-100907] p 94 N88-24766
- FRAC TURE STRENGTH**
Fracture characteristics of angleplied laminates fabricated from overaged graphite/epoxy prepreg
p 69 A88-16965
Dynamic delamination fracture toughness of a graphite/epoxy laminate under impact
p 70 A88-29455
Macrocrack interaction with transverse array of microcracks
p 181 A88-30236
- Fracture toughness computational simulation of general delaminations in fiber composites
[AIAA PAPER 88-2261] p 181 A88-32219
Crack diffusion coefficient - A candidate fracture toughness parameter for short fiber composites
p 70 A88-36945
Effects of subcritical crack growth on fracture toughness of ceramics assessed in chevron-notched three-point bend tests
[ASME PAPER 88-GT-185] p 185 A88-54276
Microstructural effects on fracture toughness of polycrystalline ceramics in combined mode I and mode II loading
[ASME PAPER 88-GT-208] p 101 A88-54294
Improved silicon nitride for advanced heat engines
[NASA-CR-175006] p 102 N88-15886
Finite element substructuring methods for composite mechanics
[NASA-TM-100297] p 73 N88-17745
Ceramic matrix composites
p 75 N88-23888
Polymer precursors for ceramic composites
p 75 N88-23890
Fracture resistance of a TiB₂ particle/SiC matrix composite at elevated temperature
[NASA-TM-100967] p 107 N88-26482
- FREE CONVECTION**
Onset of finger convection in a horizontal porous layer underlying a fluid layer
p 140 A88-41572
Temperature and velocity profiles in sooting free convection diffusion flames
p 78 A88-43018
Measurements of natural circulation flow in a scale model PWR reactor system during postulated degraded core accidents using laser anemometry
p 159 A88-43917
Ground based materials science experiments
p 43 A88-52364
Thermosolutal convection in high-aspect-ratio enclosures
[NASA-TM-100803] p 151 N88-18871
High Rayleigh number convection in rectangular enclosures with differentially heated vertical walls and aspect ratios between zero and unity
[NASA-TM-100277] p 151 N88-19739
- FREE FLOW**
Free-streamline analysis of deformation and dislodging by wind force of drops on a surface
p 137 A88-25191
Measurement of airfoil heat transfer coefficients on a turbine stage
p 147 N88-11158
Experimental study of bypass transition in a boundary layer
[NASA-TM-100913] p 153 N88-23186
Containment of a silicone fluid free surface in reduced gravity using barrier coatings
[NASA-TM-101314] p 155 N88-30072
- FREE JETS**
Effects of nozzle-exit boundary-layer conditions on excitability of heated free jets
[AIAA PAPER 87-2723] p 135 A88-20182
Excitation of instability waves in free shear layers. I - Theory
p 138 A88-26338
Controlled excitation of a cold turbulent swirling free jet
[ASME PAPER 87-WA/NCA-18] p 140 A88-41568
Particle-laden weakly swirling free jets - Measurements and predictions
[AIAA PAPER 88-3138] p 142 A88-48757
Effect of initial tangential velocity distribution on the mean evolution of a swirling turbulent free jet
[AIAA PAPER 88-3592] p 7 A88-48893
Centerline Mach number characteristics of highly heated free jets
[AIAA PAPER 88-3612] p 7 A88-48898
Heat transfer with very high free stream turbulence
p 148 N88-11161
Effect of initial tangential velocity distribution on the mean evolution of a swirling turbulent free jet
[NASA-TM-100934] p 12 N88-24592
Particle-laden weakly swirling free jets: Measurements and predictions
[NASA-TM-100920] p 34 N88-24639
- FREE-PISTON ENGINES**
Comparison of measured and calculated forces on the RE-1000 free-piston Stirling engine displacer
p 165 A88-11966
Study of free-piston Stirling engine driven linear alternators
[NASA-CR-181425] p 170 N88-10355
RE-1000 free-piston Stirling engine hydraulic output system description
[NASA-TM-100185] p 223 N88-10700
SPRE 1 free-piston Stirling engine testing at NASA Lewis Research Center
[NASA-TM-100241] p 57 N88-11747
Description of an oscillating flow pressure drop test rig
[NASA-TM-100905] p 61 N88-22933
- The 1988 overview of free-piston Stirling technology for space power at the NASA Lewis Research Center
[NASA-TM-100795] p 61 N88-22934
Overview of NASA Lewis Research Center free-piston Stirling engine technology activities applicable to space power systems
p 202 N88-24255
Component improvement of free-piston Stirling engine key technology for space power
[NASA-TM-100950] p 64 N88-25476
- FREEZING**
Experimental evidence for modifying the current physical model for ice accretion on aircraft surfaces
[NASA-TM-87184] p 15 N88-12473
- FREQUENCIES**
Investigation of the validity of Reynolds averaged turbulence models at the frequencies that occur in turbomachinery
[NASA-CR-182162] p 65 N88-28087
- FREQUENCY ASSIGNMENT**
An allotment planning concept and related computer software for planning the fixed satellite service at the 1988 space WARC
p 116 A88-36482
Numerical arc segmentation algorithm for a radio conference-NASARC (version 2.0) technical manual
[NASA-TM-100160] p 118 N88-15910
- FREQUENCY CONTROL**
Implementation of optimal trajectory control of series resonant converter
p 126 A88-38796
- FREQUENCY CONVERTERS**
Implementation of optimal trajectory control of series resonant converter
p 126 A88-38796
- FREQUENCY DIVISION MULTIPLE ACCESS**
Hardware realization of a baseband processor for a SS-FDMA/TDMA/DAMA system --- Demand Assignment Multiple Access
[AIAA PAPER 88-0830] p 124 A88-27575
- FREQUENCY MEASUREMENT**
Material parameter measurements at high temperatures
[NASA-CR-182707] p 80 N88-20397
- FREQUENCY MODULATION**
Bandwidth-efficient high-speed coded trellis modulation
[AIAA PAPER 88-0813] p 116 A88-27560
Detection of radio-frequency modulated optical signals by two and three terminal microwave devices
p 117 A88-50305
- FREQUENCY RESPONSE**
Further development of the dynamic gas temperature measurement system
p 160 N88-11141
- FREQUENCY SHIFT KEYING**
Spread-spectrum multiple access using wideband noncoherent MFSK
p 115 A88-26672
- FRESNEL LENSES**
Development of a dome Fresnel lens/gallium arsenide photovoltaic concentrator for space applications
p 199 A88-34310
- FRICTION**
The effects of atmosphere on the tribological properties of a chromium carbide based coating for use to 760 C
p 98 A88-32372
Friction and wear of monolithic and fiber reinforced silicon-ceramics sliding against IN-718 alloy at 25 to 800 C in atmospheric air at ambient pressure
[NASA-TM-100294] p 103 N88-17796
Adhesion, friction and micromechanical properties of ceramics
[NASA-TM-100782] p 104 N88-17801
Friction and wear of ceramics
p 106 N88-23874
Entrance and exit region friction factor models for annular seal analysis
[NASA-CR-183084] p 175 N88-25921
- FRICTION REDUCTION**
An integrated approach for friction damper design
p 167 A88-31598
Frequency domain solutions to multi-degree-of-freedom, dry friction damped systems
p 184 A88-49714
- FRICTION WELDING**
Preliminary investigation of inertia friction welding B2 aluminides
p 82 A88-14567
- FUEL CELL POWER PLANTS**
Status of commercial fuel cell powerplant system development
p 198 A88-11925
- FUEL CELLS**
Stress-life interrelationships associated with alkaline fuel cells
p 197 A88-11903
Phase purity of NiCo₂O₄, a catalyst candidate for electrolysis of water
[NASA-TM-100239] p 69 N88-13385
Electrocatalytic reduction of oxygen on modified oxide surfaces
[NASA-TM-101333] p 81 N88-29952
- FUEL COMBUSTION**
Numerical study of multicomponent droplet vaporization at near critical conditions
[AIAA PAPER 88-0637] p 108 A88-27721

- Modelling ignition characteristics of rich H₂/O₂ mixture in a monolithic catalytic reactor
[AIAA PAPER 88-3224] p 78 A88-46499
- Effect of mass-velocity on liquid jet atomization in Mach 1 gasflow
[NASA-TM-100813] p 162 N88-23194

FUEL CONSUMPTION

- Results of NASA's Energy Efficient Engine Program
p 19 A88-20785
- Optimal cooperative time-fixed impulsive rendezvous
[AIAA PAPER 88-4279] p 42 A88-50406
- Automotive Stirling engine: Mod 2 design report
[NASA-CR-175106] p 223 N88-11578
- Small engine technology programs p 29 N88-15801
- Large-Scale Advanced Prop-Fan (LAP)
[NASA-CR-182112] p 32 N88-20306
- NASA advanced turboprop research and concept validation program
[NASA-TM-100891] p 34 N88-22902
- NASA/industry advanced turboprop technology program
[NASA-TM-100929] p 35 N88-24641
- FUEL CORROSION**
Molten salt corrosion of SiC and Si₃N₄
p 107 N88-23885

FUEL FLOW

- Arjet thruster research and technology, phase 1
[NASA-CR-182107] p 62 N88-23830

FUEL INJECTION

- Application of advanced diagnostics to airblast injector flows
[ASME PAPER 88-GT-12] p 159 A88-54159
- Performance and combustion characteristics of direct-injection stratified-charge rotary engines
[NASA-TM-100134] p 25 N88-12490
- Regressed relations for forced convection heat transfer in a direct injection stratified charge rotary engine
[NASA-TM-100124] p 25 N88-13345
- Fuel-injector/air-swirl characterization
[NASA-CR-180864] p 27 N88-14985
- Liquid sprays and flow studies in the direct-injection diesel engine under motored conditions
[NASA-TM-100135] p 31 N88-18594
- The dc power control for a liquid-fed resistor
[NASA-TM-101326] p 67 N88-29869

FUEL SPRAYS

- Experiments on spray interactions in the wake of a bluff body
[ASME PAPER 87-GT-48] p 131 A88-11000
- Droplet vaporization in a supercritical microgravity environment
[IAF PAPER 87-384] p 134 A88-16055
- Sooting and disruption in spherically symmetrical combustion of decane droplets in air
[IAF PAPER 87-403] p 77 A88-16076
- Numerical study of multicomponent droplet vaporization at near critical conditions
[AIAA PAPER 88-0637] p 108 A88-27721
- Application of advanced diagnostics to airblast injector flows
[ASME PAPER 88-GT-12] p 159 A88-54159
- Diagnostics development for spray characterization in complex turbulent flows
[ASME PAPER 88-GT-241] p 146 A88-54320
- Fuel-injector/air-swirl characterization
p 146 N88-11150
- Liquid sprays and flow studies in the direct-injection diesel engine under motored conditions
[NASA-TM-100135] p 31 N88-18594

FUEL-AIR RATIO

- Sooting and disruption in spherically symmetrical combustion of decane droplets in air
[IAF PAPER 87-403] p 77 A88-16076
- The effect of gravity on premixed flame propagation and extinction in a vertical standard flammability tube
p 78 A88-38532

- Diagnostics development for spray characterization in complex turbulent flows
[ASME PAPER 88-GT-241] p 146 A88-54320

FUELS

- The effect of microgravity on flame spread over a thin fuel
[NASA-TM-100195] p 80 N88-15853

FULL SCALE TESTS

- Phase-resolved heat-flux measurements on the blade of a full-scale rotating turbine
[ASME PAPER 88-GT-173] p 145 A88-54267

FUNCTIONAL DESIGN SPECIFICATIONS

- Research sensors p 161 N88-15795
- Optical measurement systems p 218 N88-15796
- Preparation for microgravity: The role of the microgravity materials science laboratory
[NASA-TM-100906] p 113 N88-24811

FURNACES

- Gravitational macrosegregation in binary Pb-Sn alloy ingots p 111 A88-41211

FUSION (MELTING)

- Fluoride salts as phase change materials for thermal energy storage in the temperature range 1000-1400 K
p 199 A88-33734

G**GALACTIC CLUSTERS**

- String-driven inflation p 225 A88-27446

GALLIUM ARSENIDES

- Ohmic contact formation in semi-insulating GaAs using shallow heavily doped p-type layers p 219 A88-11150
- Microwave performance of an optically controlled AlGaAs/GaAs high electron mobility transistor and GaAs MESFET p 123 A88-24911
- Plasma deposition of amorphous hydrogenated carbon films on III-V semiconductors p 220 A88-32862
- Self-consistent calculations and design considerations for a GaAs nipi doping superlattice solar cell p 124 A88-34249
- Laser induced OMCVD growth of AlGaAs on GaAs p 125 A88-34286
- A V-grooved AlGaAs/GaAs passivated pn junction p 125 A88-34300

- Development of a dome Fresnel lens/gallium arsenide photovoltaic concentrator for space applications
p 199 A88-34310

- Performance of GaAs and silicon concentrator cells under 37 MeV proton irradiation p 200 A88-34343
- Radiation performance of AlGaAs and InGaAs concentrator cells and expected performance of cascade structures p 125 A88-34356
- Variable angle spectroscopic ellipsometry - Application to GaAs-AlGaAs multilayer homogeneity characterization p 220 A88-40139

- Effects of electron and proton irradiations on n/p and p/n GaAs cells grown by MOCVD
[NASA-TM-100199] p 127 N88-10266

- Performance of GaAs and silicon concentrator cells under 37 MeV proton irradiation
[NASA-TM-100144] p 200 N88-12877

- Radiation performance of AlGaAs concentrator cells and expected performance of cascade structures
[NASA-TM-100145] p 200 N88-12878

- A payload for investigating the influence of convection on GaAs crystal growth p 221 N88-17702

- Monolithic microwave integrated circuit technology for advanced space communication
[NASA-TM-100829] p 120 N88-21389

- Aging behavior of Au-based ohmic contacts to GaAs
[NASA-CR-182146] p 130 N88-25831

- High frequency GaAlAs modulator and photodetector for phased array antenna applications
[NASA-TM-101328] p 130 N88-30048

- Optoelectronic gain control of a microwave single stage GaAs MESFET amplifier
[NASA-CR-182201] p 131 N88-30055

GALLIUM PHOSPHIDES

- Effect of high temperature annealing on the thermoelectric properties of GaP doped SiGe
p 220 A88-40796

- Effect of high-temperature annealing on the microstructure and thermoelectric properties of GaP doped SiGe
[NASA-TM-100164] p 101 N88-10188

GANYMEDE

- VOIDS in Jovian magnetosphere revisited - Evidence of spacecraft charging p 226 A88-22879

GAS BEARINGS

- Numerical and analytical study of fluid dynamic forces in seals and bearings p 167 A88-31534
- Theory versus experiment for the rotordynamic coefficients of labyrinth gas seals. II - A companion to experiment p 167 A88-31536

GAS DYNAMICS

- Accurate boundary conditions for exterior problems in gas dynamics
[NASA-TM-100807] p 210 N88-19182

- Research sensors p 162 N88-22430

- Entrance and exit region friction factor models for annular seal analysis
[NASA-CR-183084] p 175 N88-25921

GAS FLOW

- Corona anemometry for qualitative measurement of reversing surface flow with application to separation control by external excitation p 133 A88-14143

- Stability of swirling gas flows p 142 A88-46317

- Experimental and theoretical effects of nitrogen gas flow rate on liquid-jet atomization p 145 A88-52679

- A comparison of experimental and theoretical results for labyrinth gas seals with honeycomb stators
[NASA-CR-182441] p 172 N88-16006

- Effect of mass-velocity on liquid jet atomization in Mach 1 gasflow
[NASA-TM-100813] p 162 N88-23194

GAS GENERATORS

- Experimental evaluation of a translating nozzle sidewall radial turbine p 31 N88-17656

GAS INJECTION

- Three-dimensional viscous flow computations of a circular jet in subsonic and supersonic cross flow
[NASA-CR-182153] p 155 N88-26616

GAS LUBRICANTS

- Analysis and design of a gas-lubricated, sectored, floating ring seal
[ASME PAPER 87-TRIB-55] p 166 A88-23310

GAS MIXTURES

- A theoretical analysis of the extinction limits of a methane-air opposed-jet diffusion flame
p 77 A88-16497

- Modelling ignition characteristics of rich H₂/O₂ mixture in a monolithic catalytic reactor
[AIAA PAPER 88-3224] p 78 A88-46499

- Detailed mechanism of benzene oxidation
[NASA-TM-100202] p 79 N88-11775

- The carbon dioxide chaperon efficiency for the reaction H + O₂ + M yields HO₂ + M from ignition delay times behind reflected shock waves
[NASA-TM-100125] p 79 N88-15036

GAS STREAMS

- Experiments for the determination of convective diffusion heat/mass transfer to burner rig test targets comparable in size to jet stream diameter
p 140 A88-41574

GAS TEMPERATURE

- Further development of the dynamic gas temperature measurement system p 160 N88-11141
- Research sensors p 161 N88-15795
- Research sensors p 162 N88-22430

GAS TRANSPORT

- Preparation for microgravity - The role of the Microgravity Material Science Laboratory
[AIAA PAPER 88-3510] p 111 A88-42908

- Preliminary study of niobium alloy contamination by transport through helium p 94 N88-24279

GAS TURBINE ENGINES

- Development of the AGT101 regenerator seals
[ASME PAPER 87-GT-173] p 165 A88-11083

- Progress toward life modeling of thermal barrier coatings for aircraft gas turbine engines
[ASME PAPER 87-ICE-18] p 96 A88-15120

- A numerical study of the effects of curvature and convergence on dilution jet mixing
[AIAA PAPER 87-1953] p 137 A88-23312

- Soot loading in a generic gas turbine combustor
p 19 A88-27296

- Design and experimental evaluation of a high temperature radial turbine with a moveable sidewall nozzle
[SAE PAPER 871782] p 19 A88-30776

- Combustion noise from gas turbine aircraft engines measurement of far-field levels p 215 A88-39708

- Effect of spatial inlet temperature and pressure distortion on turbofan engine stability
[AIAA PAPER 88-3016] p 22 A88-44727

- Design and development of ceramic components
[AIAA PAPER 88-3054] p 168 A88-44742

- Lateral jet injection into swirling combustor flowfields
[AIAA PAPER 88-3183] p 141 A88-44783

- The design of an air-cooled metallic high temperature radial turbine
[AIAA PAPER 88-2872] p 22 A88-45011

- A crystallographic model for nickel base single crystal alloys p 89 A88-48182

- NASA HOST project overview --- hot section technology p 24 A88-54138

- Life modeling of thermal barrier coatings for aircraft gas turbine engines p 90 A88-54145

- Application of advanced diagnostics to airblast injector flows
[ASME PAPER 88-GT-12] p 159 A88-54159

- Development of a thermal and structural analysis procedure for cooled radial turbines
[ASME PAPER 88-GT-18] p 145 A88-54164

- Current status and future trends in turbine application of thermal barrier coatings
[ASME PAPER 88-GT-286] p 169 A88-54355

- Turbine Engine Hot Section Technology, 1985
[NASA-CF-2405] p 185 N88-11140

- The development of a high temperature static strain gage system p 160 N88-11142

- The Lewis Strain Gauge Laboratory: Status and plans p 160 N88-11146

- Fuel-injector/air-swirl characterization p 146 N88-11150

- Dilution jet mixing program, phase 3 p 147 N88-11153

- On the mixing of a row of jets with a confined crossflow p 147 N88-11154

- Measurement of airfoil heat transfer coefficients on a turbine stage p 147 N88-11158

- Heat transfer in the tip region of a rotor blade simulator p 147 N88-11159
- Coolant passage heat transfer with rotation p 147 N88-11160
- Heat transfer with very high free stream turbulence p 148 N88-11161
- Prediction of turbine blade heat transfer p 148 N88-11162
- Flow in a model turbine stator p 148 N88-11163
- 3D inelastic analysis methods for hot section components p 185 N88-11164
- 3-D inelastic analysis methods for hot section components p 206 N88-11165
- Component specific modeling p 206 N88-11166
- Constitutive modeling of superalloy single crystals with verification testing p 91 N88-11169
- High temperature stress-strain analysis p 185 N88-11170
- Constitutive modeling for isotropic materials p 185 N88-11171
- Constitutive modeling for isotropic materials p 186 N88-11172
- Creep fatigue life prediction for engine hot section materials (isotropic): Third year progress review p 186 N88-11173
- Elevated temperature crack growth p 186 N88-11174
- Life prediction and constitutive models for engine hot section anisotropic materials program p 186 N88-11175
- Turbine airfoil deposition models and their hot corrosion implications p 91 N88-11178
- Experimental verification of vapor deposition rate theory in high velocity burner rigs p 91 N88-11179
- Effects of surface chemistry on hot corrosion life p 91 N88-11180
- Thermal expansion mismatch and oxidation in thermal barrier coatings p 170 N88-11182
- Composite mechanics for engine structures [NASA-TM-100176] p 72 N88-12552
- A numerical study of the effects of curvature and convergence on dilution jet mixing [NASA-TM-89878] p 26 N88-13347
- Fuel-injector/air-swirl characterization [NASA-CR-180864] p 27 N88-14985
- Life modeling of thermal barrier coatings for aircraft gas turbine engines [NASA-TM-100283] p 92 N88-15060
- Small gas turbine engine technology p 30 N88-16638
- Self-lubricating coatings for high-temperature applications p 103 N88-16703
- Experimental evaluation of a translating nozzle sidewall radial turbine p 31 N88-17656
- Ceramic bearings for use in gas turbine engines [NASA-TM-100288] p 172 N88-18007
- Effect of spatial inlet temperature and pressure distortion on turbofan engine stability [NASA-TM-100850] p 32 N88-21162
- Review and assessment of the HOST turbine heat transfer program p 34 N88-22431
- Thermal stress minimized, two component, turbine shroud seal [NASA-CASE-LEW-14212-1] p 174 N88-23978
- Constitutive modeling for isotropic materials [NASA-CR-182132] p 37 N88-29811
- Spray automated balancing of rotors: Methods and materials [NASA-CR-182151] p 41 N88-29825
- Assessment of a 3-D boundary layer analysis to predict heat transfer and flow field in a turbine passage [NASA-CR-174894] p 155 N88-30066
- GAS TURBINES**
- Effect of rib angle on local heat/mass transfer distribution in a two-pass rib-roughened channel [ASME PAPER 87-GT-94] p 131 A88-11033
- Inter and intra blade row laser velocimetry studies of gas turbine compressor flows [ASME PAPER 87-GT-235] p 2 A88-11126
- Laser anemometry techniques for turbine applications [ASME PAPER 87-GT-241] p 157 A88-11129
- Small engine components test facility turbine testing cell [AIAA PAPER 88-2962] p 22 A88-44706
- An empirical model of the effects of curvature and convergence on dilution jet mixing [AIAA PAPER 88-3180] p 23 A88-50783
- Assessment, development, and application of combustor aerothermal models p 24 A88-54140
- Review and assessment of the database and numerical modeling for turbine heat transfer p 24 A88-54141
- Structural analysis methods development for turbine hot section components p 184 A88-54142
- The effects of turbulence and stator/rotor interactions on turbine heat transfer. I - Design operating conditions [ASME PAPER 88-GT-125] p 145 A88-54236
- Combustion characteristics of gas turbine alternative fuels [NASA-TM-100247] p 25 N88-13338
- HOST turbine heat transfer program summary [NASA-TM-100280] p 149 N88-14320
- Recent advances in high temperature instrumentation for hot section applications [NASA-TM-100282] p 161 N88-14339
- Small engine technology programs p 29 N88-15801
- Aircraft engine hot section technology: An overview of the HOST Project p 29 N88-15804
- Structural analysis methods development for turbine hot section components [NASA-TM-100298] p 188 N88-18967
- Assessment, development and application of combustor aerothermal models [NASA-TM-100290] p 32 N88-19469
- Advanced Gas Turbine (AGT) Technology Development Project, ceramic component developments [NASA-CR-180871] p 224 N88-20229
- Advanced Gas Turbine (AGT) technology development project [NASA-CR-180891] p 225 N88-20230
- Small engine components test facility turbine testing cell [NASA-TM-100887] p 33 N88-22037
- Two-equation low-Reynolds-number turbulence modeling of transitional boundary layer flows characteristic of gas turbine blades [NASA-CR-4145] p 153 N88-23185
- The effects of inlet turbulence and rotor/stator interactions on the aerodynamics and heat transfer of a large-scale rotating turbine model. Part 4: Aerodynamic data tabulation [NASA-CR-179469] p 153 N88-23956
- An empirical model of the effects of curvature and convergence on dilution jet mixing [NASA-TM-100896] p 34 N88-24640
- User's manual for three dimensional boundary layer (BL3-D) code [NASA-CR-174899] p 155 N88-30063
- GAS-LIQUID INTERACTIONS**
- Gas liquid flow at microgravity conditions - Flow patterns and their transitions p 141 A88-42839
- GASEOUS ROCKET PROPELLANTS**
- 25-LBF GO2/GH2 space station thruster [AIAA PAPER 88-2793] p 56 A88-53101
- GAUGE THEORY**
- Wilson-loop instantons p 212 A88-10410
- GEAR TEETH**
- Method for generation of spiral bevel gears with conjugate gear tooth surfaces [ASME PAPER 86-DET-3] p 165 A88-10973
- Automated acoustic intensity measurements and the effect of gear tooth profile on noise p 168 A88-31623
- Spur gears: Optimal geometry, methods for generation and Tooth Contact Analysis (TCA) program [NASA-CR-4135] p 173 N88-23216
- GEARS**
- Method for generation of spiral bevel gears with conjugate gear tooth surfaces [ASME PAPER 86-DET-3] p 165 A88-10973
- Surface fatigue and failure characteristics of hot-forged powder metal AISI 4620, AISI 4640, and machined AISI 4340 steel spur gears p 165 A88-14591
- Transfer matrix modeling of geared system vibration p 168 A88-39703
- The generalized transmission error of spiral bevel gears p 168 A88-49409
- Use of the generalized transmission error in the equations of motion of gear systems p 168 A88-49410
- On dynamic loads in parallel shaft transmissions. 1: Modelling and analysis [NASA-TM-100180] p 171 N88-12797
- On dynamic loads in parallel shaft transmissions. 2: Parameter study [NASA-TM-100181] p 171 N88-12798
- Efficiency testing of a helicopter transmission planetary reduction stage [NASA-TP-2795] p 172 N88-15224
- Rotorcraft transmission p 172 N88-15802
- Results of NASA/Army transmission research p 31 N88-16640
- Dynamic analysis of multimesh-gear helicopter transmissions [NASA-TP-2789] p 172 N88-17045
- Advanced transmission studies [NASA-TM-100867] p 173 N88-21454
- Spur gears: Optimal geometry, methods for generation and Tooth Contact Analysis (TCA) program [NASA-CR-4135] p 173 N88-23216
- Design, manufacture and spin test of high contact ratio helicopter transmission utilizing Self-Aligning Bearingless Planetary (SABP) [NASA-CR-4155] p 174 N88-24975
- Determination of settings of a tilted head-cutter for generation of hypoid and spiral bevel gears [NASA-CR-182138] p 174 N88-24976
- Surface fatigue life of CBN and vitreous ground carburized and hardened AISI 9310 spur gears [NASA-TM-100960] p 175 N88-25916
- A review of gear housing dynamics and acoustics literature [NASA-CR-183110] p 175 N88-26675
- Design and evaluation of high contact ratio gearing [NASA-CR-174958] p 175 N88-28319
- GELLED PROPELLANTS**
- Characterization of aluminum/RP-1 gel propellant properties [AIAA PAPER 88-2821] p 109 A88-48751
- Characterization of aluminum/RP-1 gel propellant properties [NASA-TM-100951] p 109 N88-24808
- GELS**
- Sol-gel synthesis of magnesium oxide-silicon dioxide glass compositions p 100 A88-49105
- GENERATORS**
- Cast iron-base alloy for cylinder/regenerator housing [NASA-CR-182116] p 92 N88-19613
- GEOMETRY**
- A multistage mesh generator for solving the average-passage equation system [NASA-CR-179539] p 10 N88-15769
- Spur gears: Optimal geometry, methods for generation and Tooth Contact Analysis (TCA) program [NASA-CR-4135] p 173 N88-23216
- GEOSYNCHRONOUS ORBITS**
- An allotment planning concept and related computer software for planning the fixed satellite service at the 1988 space WARC [NASA-TM-100244] p 117 N88-11944
- A laser communication experiment utilizing the ACT satellite and an airborne laser transceiver [NASA-TM-100792] p 164 N88-18910
- Centaur operations at the space station [NASA-CR-179593] p 49 N88-25473
- GERMANIUM**
- Effect of high-temperature annealing on the microstructure and thermoelectric properties of GaP doped SiGe [NASA-TM-100164] p 101 N88-10188
- GET AWAY SPECIALS (STS)**
- Low cost Get-Away-Special (GAS) furnace p 41 A88-28583
- A payload for investigating the influence of convection on GaAs crystal growth p 221 N88-17702
- GLASS**
- Glass properties in the yttria-alumina-silica system p 96 A88-18361
- Sol-gel synthesis of magnesium oxide-silicon dioxide glass compositions p 100 A88-49105
- GLASS FIBERS**
- Mast material test program (MAMATEP) [NASA-TM-100821] p 74 N88-19592
- GLASS TRANSITION TEMPERATURE**
- Linear and nonlinear mechanical properties of a series of epoxy resins p 101 A88-54976
- Correlations of norbornenyl crosslinked polyimide resin structures with resin thermo-oxidative stability, resin glass transition temperature and composite initial mechanical properties [NASA-TM-100791] p 103 N88-16877
- GLAZES**
- A flow visualization study of the leading edge separation bubble on a NACA 0012 airfoil with simulated glaze ice [NASA-CR-180846] p 10 N88-14966
- An experimental mapping of the flow field behind a glaze ice shape on a NACA 0012 airfoil [NASA-CR-180847] p 10 N88-15766
- GOALS**
- Supersonic STOVl propulsion technology program: An overview p 29 N88-15808
- Advanced development of double-injection, deep-impurity semiconductor switches [NASA-CR-182118] p 222 N88-25346
- GOLD ALLOYS**
- Aging behavior of Au-based ohmic contacts to GaAs [NASA-CR-182146] p 130 N88-25831
- GOVERNMENT/INDUSTRY RELATIONS**
- Advanced space solar dynamic power systems beyond IOC Space Station p 50 A88-11798
- GRAIN BOUNDARIES**
- Dynamic recrystallization and grain boundary migration in B2 FeAl p 83 A88-20269
- Room temperature tensile ductility in powder processed B2 FeAl alloys p 85 A88-31694
- Fatigue crack propagation of nickel-base superalloys at 650 deg C p 86 A88-35908
- Grain boundary oxidation and an analysis of the effects of oxidation on fatigue crack nucleation life p 87 A88-35938

- Slip casting and extruding shapes of rhenium with metal oxide additives. Part 2: Development of grain stabilized rhenium parts for resistors
[NASA-CR-180851] p 57 N88-11749
- Grain boundary oxidation and low-cycle fatigue at elevated temperatures p 193 N88-22420

GRAIN SIZE

- Cyclic hardening mechanisms in Nimonic 80A p 84 A88-24490
- The influence of grain size and composition on 1000 to 1400 K slow plastic flow properties of NiAl p 85 A88-29098
- Determination of grain-size distribution function using two-dimensional Fourier transforms of tone-pulse-encoded images p 176 A88-30425
- Fatigue crack propagation of nickel-base superalloys at 650 deg C p 86 A88-35908
- Effect of melt spinning on grain size and texture in Ni-Mo alloys p 89 A88-46030
- Microstructural effects on fracture toughness of polycrystalline ceramics in combined mode I and mode II loading p 101 A88-54294
- [ASME PAPER 88-GT-208] p 101 A88-54294
- Structure and grain coarsening during the processing of engineering ceramics p 101 N88-11838
- [NASA-TM-100235] p 101 N88-11838

GRAPHITE

- Thermal conductivity of pristine and brominated highly graphitized pitch based carbon fibers p 97 A88-20257
- A comparison of the bromination dynamics of various carbon and graphite fibers p 97 A88-20278
- Synthesis, electrical and thermal conductivities, and potential applications of graphite fluoride fibers p 97 A88-26963
- Comparison of the tribological properties of fluorinated cokes and graphites p 100 A88-51300
- [STLE PREPRINT 88-AM-7F-1] p 100 A88-51300
- Production and characterization of CdCl₂ intercalated graphite fibers p 101 A88-51307
- Transply crack density detection by acousto-ultrasonics p 72 N88-11758
- [NASA-TM-100224] p 72 N88-11758
- Performance of a small, graphite electrode, multistage depressed collector with a 500-W, continuous wave, 4.8- to 9.6-GHz traveling wave tube p 128 N88-15146
- [NASA-TP-2788] p 128 N88-15146

GRAPHITE-EPOXY COMPOSITES

- A heater made from graphite composite material for potential deicing application p 17 A88-15724
- Fracture characteristics of angleplated laminates fabricated from overaged graphite/epoxy prepreg p 69 A88-16965
- Ultrasonic evaluation of mechanical properties of thick, multilayered, filament-wound composites p 176 A88-21340
- Dynamic delamination fracture toughness of a graphite/epoxy laminate under impact p 70 A88-29455

- Probabilistic composite micromechanics [AIAA PAPER 88-2375] p 182 A88-32312
- Measurement of impact-induced delamination buckling in composite laminates p 71 A88-47214
- The effect of bromination of carbon fibers on the coefficient of thermal expansion of graphite fiber-epoxy composites p 72 N88-10899
- [NASA-TM-100236] p 72 N88-10899

GRAPHITE-POLYIMIDE COMPOSITES

- The 700 F properties of autoclave cured PMR-2 composites p 75 N88-24712
- [NASA-TM-100923] p 75 N88-24712
- A thermally modified polymer matrix composite material with structural integrity to 371 C p 76 N88-25483
- [NASA-TM-100922] p 76 N88-25483

GRAPHITIZATION

- Brominated graphite fibers and method of producing the same [NASA-CASE-LEW-14698-1] p 76 N88-29888

GRAVITATION

- Low thrust power-limited transfer for a pole squatter [AIAA PAPER 88-4310] p 42 A88-50435

GRAVITATIONAL EFFECTS

- Characteristics of fluid flow in the combustion synthesis of TiC from the elements p 110 A88-28564
- Gravitational contributions to microstructural coarsening in liquid phase sintering p 111 A88-37155
- Gravitational macrosegregation in binary Pb-Sn alloy ingots p 111 A88-41211
- Dynamics of two fluids under periodic acceleration [AIAA PAPER 88-3728] p 143 A88-48980
- Ground-based microgravity materials science research at NASA's Microgravity Materials Science Laboratory p 112 A88-49090
- Nucleate pool boiling: High gravity to reduced gravity; liquid metals to cryogenics p 113 N88-24464

- Fraction eutectic measurements in slowly cooled Pb - 15 wt percent Sn alloys [NASA-CR-180830] p 94 N88-25531

GRAVITATIONAL FIELDS

- Gravitationally defined velocities for a low speed hot-wire calibration p 133 A88-14170

GREASES

- Improved perfluoroalkylether fluid development [NASA-CR-180872] p 80 N88-15851

GRID GENERATION (MATHEMATICS)

- Adaptive grid generation p 209 A88-37363
- A multistage mesh generator for solving the average-passage equation system [NASA-CR-179539] p 10 N88-15769
- Three-dimensional adaptive grid generation for body-fitted coordinate system [NASA-CR-182192] p 155 N88-27520
- Three-dimensional elliptic grid generation technique with application to turbomachinery cascades [NASA-TM-101330] p 155 N88-30078

GRINDING

- Surface fatigue life of CBN and vitreous ground carburized and hardened AISI 9310 spur gears [NASA-TM-100960] p 175 N88-25916

GROOVES

- Sensitivity study of the monogroove with screen heat pipe design [AIAA PAPER 88-0470] p 137 A88-22346
- A V-grooved AlGaAs/GaAs passivated pn junction p 125 A88-34300

GROUND EFFECT (AERODYNAMICS)

- A numerical study of the hot gas environment around a STOVL aircraft in ground proximity [AIAA PAPER 88-2882] p 23 A88-48752
- A numerical study of the hot gas environment around a STOVL aircraft in ground proximity [NASA-TM-100895] p 1 N88-23729

GROUND STATIONS

- VSAT networks - An overview --- Very Small Aperture Terminals p 115 A88-14091
- Service offerings and interfaces for the ACTS network of earth stations [AIAA PAPER 88-0800] p 116 A88-27551
- Design description report for a photovoltaic power system for a remote satellite earth terminal [NASA-CR-179586] p 200 N88-12875
- Satellite ground-terminal user simulation [NASA-TM-100234] p 118 N88-14260
- Service offerings and interfaces for the ACTS network of Earth stations [NASA-TM-100809] p 46 N88-24663

GROUND TESTS

- Ground tests confirm the promise of hypersonic propulsion p 2 A88-10369
- Research opportunities in microgravity science and applications during Shuttle hiatus p 109 A88-13164
- Ground based materials science experiments p 43 A88-52364
- A cyclic ground test of an ion auxiliary propulsion system: Description and operational considerations [NASA-TM-100870] p 62 N88-23829
- Successful completion of a cyclic ground test of a mercury ion auxiliary propulsion system [NASA-TM-101351] p 67 N88-29873

GUIDE VANES

- Test stand performance of a convertible engine for advanced V/STOL and rotorcraft propulsion [SAE PAPER 87-2355] p 21 A88-37217
- Test stand performance of a convertible engine for advanced V/STOL and rotorcraft propulsion [NASA-TM-100211] p 25 N88-11679
- Experimental evaluation of turning vane designs for high-speed and coupled fan-drive corners of 0.1-scale model of NASA Lewis Research Center's proposed altitude wind tunnel [NASA-TP-2681] p 40 N88-17686

GUST LOADS

- A parametric study of mean loading effects on airfoil gust interaction noise [AIAA PAPER 87-2677] p 213 A88-16539

H**H WAVES**

- Input-output characterization of fiber composites by SH waves [NASA-CR-4153] p 179 N88-23986

HAFNIUM

- Hafnia-rich mixed oxide ceramics of the system HfO₂-ZrO₂-TiO₂ for heaters and heat exchangers in electrothermal thrusters: The effects of titania on selected electrical and mechanical properties of Hafnia-rich mixed oxides in the system Hafnia-Zirconia-Titania, volume 1 [NASA-CR-182800-VOL-1] p 105 N88-22197

HAFNIUM ALLOYS

- Thermal-mechanical cyclic stress-strain responses of cast B-1900 + Hf p 87 A88-35919

HARDENING (MATERIALS)

- Cyclic hardening mechanisms in Nimonic 80A p 84 A88-24490
- Surface fatigue life of CBN and vitreous ground carburized and hardened AISI 9310 spur gears [NASA-TM-100960] p 175 N88-25916

HARMONIC OSCILLATION

- The impact damped harmonic oscillator in free decay p 167 A88-31581

HEAD DOWN TILT

- Determination of settings of a tilted head-cutter for generation of hypoid and spiral bevel gears [NASA-CR-182138] p 174 N88-24976

HEAD-UP DISPLAYS

- Cooperative synthesis of control and display augmentation for a STOL aircraft in the approach and landing task [AIAA PAPER 88-4182] p 37 A88-50272

HEAT EXCHANGERS

- Description of an oscillating flow test program p 133 A88-11963
- Overview of free-piston Stirling engine technology for space power application p 223 N88-12427
- [NASA-TM-88886] p 223 N88-12427
- Measured performance of the heat exchanger in the NASA icing research tunnel under severe icing and dry-air conditions [NASA-TM-100116] p 171 N88-12796
- Hafnia-rich mixed oxide ceramics of the system HfO₂-ZrO₂-TiO₂ for heaters and heat exchangers in electrothermal thrusters: The effects of titania on selected electrical and mechanical properties of Hafnia-rich mixed oxides in the system Hafnia-Zirconia-Titania, volume 1 [NASA-CR-182800-VOL-1] p 105 N88-22197
- A survey of oscillating flow in Stirling engine heat exchangers [NASA-CR-182108] p 152 N88-22322
- Moving belt radiator development status [NASA-TM-100909] p 64 N88-25477
- The design and fabrication of a Stirling engine heat exchanger module with an integral heat pipe [NASA-TM-101296] p 203 N88-26732
- Oxidizer heat exchanger component test [NASA-CR-182159] p 67 N88-29876

HEAT FLUX

- Design, calibration and error analysis of instrumentation for heat transfer measurements in internal combustion engines p 157 A88-18509
- Navier-Stokes solutions of flowfield characteristics produced by ice accretion [AIAA PAPER 88-0290] p 137 A88-22210
- Experimental study of thermocapillary flows in a thin liquid layer with heat fluxes imposed on the free surface p 144 A88-49087
- Phase-resolved heat-flux measurements on the blade of a full-scale rotating turbine [ASME PAPER 88-GT-173] p 145 A88-54267
- Effect of NASA advanced designs on thermal behavior of Ni-H₂ cells [NASA-TM-100197] p 79 N88-10132
- Development of heat flux sensors for turbine airfoils p 160 N88-11143
- Experimental study of thermocapillary flows in a thin liquid layer with heat fluxes imposed on the free surface [NASA-TM-100252] p 148 N88-12763
- Prototype thin-film thermocouple/heat-flux sensor for a ceramic-insulated diesel engine [NASA-TM-100798] p 162 N88-18892
- Thermostructural analysis of simulated cowl lips p 192 N88-22403
- Research sensors p 162 N88-22430
- Development of sensors for ceramic components in advanced propulsion systems: Survey and evaluation of measurement techniques for temperature, strain and heat flux for ceramic components in advanced propulsion systems [NASA-CR-182111] p 163 N88-28299
- Measurement of local high-level, transient surface heat flux [NASA-TP-2840] p 164 N88-30099

HEAT PIPES

- Integrated heat pipe-thermal storage system performance evaluation p 132 A88-11803
- Heat pipe radiators for solar dynamic space power system heat rejection p 132 A88-11807
- Modelling the performance of the monogroove with screen heat pipe for use in the radiator of the solar dynamic power system of the NASA Space Station [IAF PAPER 87-238] p 134 A88-15960
- High thermal-transport capacity heat pipes for space radiators [SAE PAPER 871509] p 136 A88-21155

- Sensitivity study of the monogroove with screen heat pipe design
[AIAA PAPER 88-0470] p 137 A88-22346
- Development of an integrated heat pipe-thermal storage system for a solar receiver
[AIAA PAPER 88-2683] p 141 A88-43746
- Modelling the performance of the tapered artery heat pipe design for use in the radiator of the solar dynamic power system of the NASA Space Station
[IAF PAPER 88-213] p 56 A88-55361
- Overview of free-piston Stirling engine technology for space power application
[NASA-TM-88886] p 223 A88-12427
- Development of an integrated heat pipe-thermal storage system for a solar receiver
[NASA-TM-101099] p 202 A88-22458
- Solar dynamic heat rejection technology. Task 2: Heat pipe radiator development
[NASA-CR-182141] p 152 A88-23182
- Moving belt radiator development status
[NASA-TM-100909] p 64 A88-25477
- The design and fabrication of a Stirling engine heat exchanger module with an integral heat pipe
[NASA-TM-101296] p 203 A88-26732
- HEAT RADIATORS**
- Solar dynamic organic Rankine cycle heat rejection system simulation p 132 A88-11808
- Adiabatic diesel engine component development: Reference engine for on-highway applications
[NASA-CR-179531] p 224 A88-12428
- Solar dynamic heat rejection technology. Task 2: Heat pipe radiator development
[NASA-CR-182141] p 152 A88-23182
- HEAT RESISTANT ALLOYS**
- Effect of alloy composition on the sodium-sulfate induced hot corrosion attack of cast nickel-base superalloys at 900 C p 81 A88-10028
- High-temperature oxidation/corrosion of iron-based superalloys p 81 A88-10029
- Role of molybdenum in the Na₂SO₄ induced corrosion of superalloys at high temperature p 81 A88-10030
- The effect of variations of cobalt content on the cyclic oxidation resistance of selected Ni-base superalloys p 82 A88-10031
- Preliminary investigation of inertia friction welding B2 aluminides p 82 A88-14567
- Effect of initial gamma prime size on the elevated temperature creep properties of single crystal nickel base superalloys p 82 A88-18884
- Phenomenological modeling of hardening and thermal recovery in metals p 84 A88-24037
- Cyclic hardening mechanisms in Nimonic 80A p 84 A88-24490
- On the cyclic stress-strain behaviour of a Ni-base superalloy at room temperature p 84 A88-24521
- B2 aluminides for high temperature applications p 85 A88-31684
- Thermal cycling of tungsten-fibre-reinforced superalloy composites p 70 A88-31770
- Anisotropic constitutive modeling for nickel base single crystal superalloys using a crystallographic approach [AIAA PAPER 88-2440] p 85 A88-32357
- Fatigue crack propagation of nickel-base superalloys at 650 deg C p 86 A88-35908
- Thermal-mechanical cyclic stress-strain responses of cast B-1900 + Hf p 87 A88-35919
- Effect of temperature, microstructure, and stress state on the low cycle fatigue behavior of Waspaloy p 87 A88-35922
- Grain boundary oxidation and an analysis of the effects of oxidation on fatigue crack nucleation life p 87 A88-35938
- Microstructure-property relationships in directionally solidified single-crystal nickel-base superalloys p 88 A88-40329
- Accelerated crack growth rate at low Delta K in a single crystal superalloy p 89 A88-47687
- Lattice parameter variations during aging in nickel-base superalloys p 90 A88-51318
- Bithermal low-cycle fatigue behavior of a NiCoCrAlY-coated single crystal superalloy p 90 A88-51736
- Composite monolayer fabrication by an arc-spray process p 169 A88-53581
- The development of a high temperature static strain gage system p 160 A88-11142
- Constitutive modeling for single crystal superalloys p 90 A88-11168
- Constitutive modeling of superalloy single crystals with verification testing p 91 A88-11169
- Constitutive modeling for isotropic materials p 185 A88-11171
- Constitutive modeling for isotropic materials p 186 A88-11172
- Creep-fatigue behavior of NiCoCrAlY coated PWA 1480 p 186 A88-11176
- Deformation, fatigue and fracture behavior of two cast anisotropic superalloys p 187 A88-13732
- Development of a new generation of high-temperature composite materials p 73 A88-16702
- The cyclic stress-strain behavior of a single crystal nickel-base superalloy [NASA-TM-100269] p 92 A88-19610
- A theory of viscoplasticity accounting for internal damage p 190 A88-21508
- A constitutive model with damage for high temperature superalloys p 93 A88-21510
- Bithermal fatigue of a nickel-base superalloy single crystal [NASA-TM-100885] p 93 A88-22168
- Life prediction modeling based on cyclic damage accumulation p 178 A88-22426
- Fatigue damage modeling for coated single crystal superalloys p 93 A88-22427
- Fatigue crack growth behavior of a single crystal alloy as observed through an in situ fatigue loading stage [NASA-TM-100863] p 93 A88-22986
- Isothermal and bithermal thermomechanical fatigue behavior of a NiCoCrAlY-coated single crystal superalloy [NASA-TM-100907] p 94 A88-24766
- Accelerated fatigue crack growth behavior of PWA 1480 single crystal alloy and its dependence on the deformation mode [NASA-TM-100943] p 95 A88-26436
- Anisotropic constitutive modeling for nickel-base single crystal superalloys [NASA-CR-182157] p 95 A88-29961
- HEAT STORAGE**
- Selection of high temperature thermal energy storage materials for advanced solar dynamic space power systems p 68 A88-11801
- Integrated heat pipe-thermal storage system performance evaluation p 132 A88-11803
- Fluoride salts and container materials for thermal energy storage applications in the temperature range 973 - 1400 K p 196 A88-11804
- Impact of thermal energy storage properties on solar dynamic space power conversion system mass p 51 A88-11805
- Identification of salt-alloy combinations for thermal energy storage applications in advanced solar dynamic power systems p 199 A88-24072
- Structural assessment of a Space Station solar dynamic heat receiver thermal energy storage canister [AIAA PAPER 88-2487] p 47 A88-31396
- Development of an integrated heat pipe-thermal storage system for a solar receiver [AIAA PAPER 88-2683] p 141 A88-43746
- Structural assessment of a space station solar dynamic heat receiver thermal energy storage canister p 192 A88-22406
- Development of an integrated heat pipe-thermal storage system for a solar receiver [NASA-TM-101099] p 202 A88-22458
- Advanced heat receiver conceptual design study [NASA-CR-180901] p 203 A88-25977
- HEAT TRANSFER**
- Use of a liquid-crystal and heater-element composite for quantitative, high-resolution heat-transfer coefficients on a turbine airfoil including turbulence and surface-roughness effects p 156 A88-10969
- Effect of rib angle on local heat/mass transfer distribution in a two-pass rib-roughened channel [ASME PAPER 87-GT-94] p 131 A88-11033
- Regenerative fuel cell study for satellites in GEO orbit p 52 A88-11904
- Performance and efficiency evaluation and heat release study of a direct-injection stratified-charge rotary engine [SAE PAPER 870445] p 166 A88-23313
- Thermostructural analysis with experimental verification in a high heat flux facility of a simulated cowl lip [AIAA PAPER 88-2222] p 39 A88-32188
- Specific heat of pristine and brominated graphite fibers, composites and HOPG --- Highly Oriented Pyrolytic Graphite p 98 A88-32853
- Review and assessment of the database and numerical modeling for turbine heat transfer p 24 A88-54141
- The effects of turbulence and stator/rotor interactions on turbine heat transfer. I - Design operating conditions [ASME PAPER 88-GT-125] p 145 A88-54236
- Heat transfer in a real engine environment p 147 A88-11155
- Film cooling heat transfer on a turbine airfoil p 147 A88-11156
- Coolant passage heat transfer with rotation p 147 A88-11160
- Prediction of turbine blade heat transfer p 148 A88-11162
- Flow in a model turbine stator p 148 A88-11163
- Component specific modeling p 206 A88-11166
- Local heat/mass transfer and pressure drop in a two-pass rib-roughened channel for turbine airfoil cooling [NASA-CR-179635] p 148 A88-12039
- HOST turbine heat transfer program summary [NASA-TM-100280] p 149 A88-14320
- Turbomachinery p 28 A88-15792
- The effect of eddy distribution on momentum and heat transfer near the wall in turbulent pipe flow [NASA-TM-100257] p 150 A88-15984
- Overview of heat transfer and fluid flow problem areas encountered in Stirling engine modeling [NASA-TM-100131] p 224 A88-17561
- Investigation of surface tension driven convection as a feasibility study for a micro-gravity experiment [NASA-CR-182504] p 112 A88-18739
- Unsteady heat transfer in turbine blade ducts: Focus on combustor sources [NASA-TM-100815] p 151 A88-18870
- Thermosolutal convection in high-aspect-ratio enclosures [NASA-TM-100803] p 151 A88-18871
- Thermal-structural analyses of Space Shuttle Main Engine (SME) hot section components p 61 A88-22404
- Review and assessment of the HOST turbine heat transfer program p 34 A88-22431
- The effects of inlet turbulence and rotor/stator interactions on the aerodynamics and heat transfer of a large-scale rotating turbine model. Part 4: Aerodynamic data tabulation [NASA-CR-179469] p 153 A88-23956
- Heat transfer in aerospace propulsion [NASA-TM-100874] p 154 A88-23957
- Nucleate pool boiling: High gravity to reduced gravity; liquid metals to cryogenics p 113 A88-24464
- Correlations of velocity and temperature fluctuations in the stagnation-point flow of circular cylinder in turbulent flow [NASA-TM-100930] p 13 A88-25435
- The effects of inlet turbulence and rotor/stator interactions on the aerodynamics and heat transfer of a large-scale rotating turbine model. Volume 3: Heat transfer data tabulation 65 percent axial spacing [NASA-CR-179468] p 37 A88-28930
- The effects of inlet turbulence and rotor/stator interactions on the aerodynamics and heat transfer of a large-scale rotating turbine model. Volume 2: Heat transfer data tabulation. 15 percent axial spacing [NASA-CR-179467] p 37 A88-29804
- Assessment of a 3-D boundary layer analysis to predict heat transfer and flow field in a turbine passage [NASA-CR-174894] p 155 A88-30066
- HEAT TRANSFER COEFFICIENTS**
- Use of a liquid-crystal and heater-element composite for quantitative, high-resolution heat-transfer coefficients on a turbine airfoil including turbulence and surface-roughness effects p 156 A88-10969
- Steady and transient least square solvers for thermal problems p 134 A88-17318
- High-resolution heat-transfer-coefficient maps applicable to compound-curve surfaces using liquid crystals in a transient wind tunnel p 134 A88-18506
- Sensitivity study of the monogroove with screen heat pipe design [AIAA PAPER 88-0470] p 137 A88-22346
- Local heat/mass transfer distributions around sharp 180 deg turns in two-pass smooth and rib-roughened channels [ASME PAPER 86-GT-114] p 139 A88-28516
- Ultrasonic techniques for aircraft ice accretion measurement [AIAA PAPER 88-4656] p 18 A88-51910
- Measurement of airfoil heat transfer coefficients on a turbine stage p 147 A88-11158
- Heat transfer with very high free stream turbulence p 148 A88-11161
- Regressed relations for forced convection heat transfer in a direct injection stratified charge rotary engine [NASA-TM-100124] p 25 A88-13345
- HEAT TRANSMISSION**
- High thermal-transport capacity heat pipes for space radiators [SAE PAPER 871509] p 136 A88-21155
- HEAT TREATMENT**
- On the cyclic stress-strain behaviour of a Ni-base superalloy at room temperature p 84 A88-24521
- Solidification under microgravity conditions - Dendritic growth [AAS PAPER 86-380] p 110 A88-35130
- HEATERS**
- A heater made from graphite composite material for potential deicing application p 17 A88-15724
- HEATING**
- Overview of free-piston Stirling engine technology for space power application [NASA-TM-88886] p 223 A88-12427

HELICAL FLOW

HELICAL FLOW

Torsion effect on fully developed flow in a helical pipe p 135 A88-20748

HELICOPTER DESIGN

Rotorcraft transmission p 172 N88-15802

HELICOPTER ENGINES

An overview of rotorcraft propulsion research at Lewis Research Center p 22 A88-40554

Efficiency testing of a helicopter transmission planetary reduction stage p 172 N88-15224

Dynamic analysis of multimesh-gear helicopter transmissions [NASA-TP-2789] p 172 N88-17045

HELICOPTER PERFORMANCE

Model helicopter performance degradation with simulated ice shapes p 17 A88-22783

HELICOPTERS

Improved oil-off survivability of tapered roller bearings [NASA-CR-180804] p 170 N88-11135

Results of NASA/Army transmission research p 31 N88-16640

NASA's rotorcraft icing research program p 15 N88-16641

Rotorcraft flight-propulsion control integration p 38 N88-16643

Advanced transmission studies [NASA-TM-100867] p 173 N88-21454

Design, manufacture and spin test of high contact ratio helicopter transmission utilizing Self-Aligning Bearingless Planetary (SABP) [NASA-CR-4155] p 174 N88-24975

Computer simulation of a single pilot flying a modern high-performance helicopter [NASA-TM-100182] p 39 N88-26376

Computer simulation of multiple pilots flying a modern high performance helicopter [NASA-TM-100183] p 39 N88-26377

HEXAGONAL CELLS

Multielement mapping of alpha-SiC by scanning Auger microscopy p 158 A88-27617

Improved processing of alpha-SiC p 99 A88-38318

HIGH ASPECT RATIO

Thermosolubility convection in high-aspect-ratio enclosures [NASA-TM-100803] p 151 N88-18871

A detailed description of the uncertainty analysis for high area ratio rocket nozzle tests at the NASA Lewis Research Center p 65 N88-25580

HIGH ELECTRON MOBILITY TRANSISTORS

Microwave performance of an optically controlled AlGaAs/GaAs high electron mobility transistor and GaAs MESFET p 123 A88-24911

Microwave response of an HEMT photoconductor [NASA-TM-100819] p 128 N88-18835

HIGH FREQUENCIES

Control considerations for high frequency, resonant, power processing equipment used in large systems p 51 A88-11829

Field oriented control of an induction machine in a high frequency link power system p 127 A88-54711

High frequency power distribution system [NASA-CR-175071] p 129 N88-23939

High frequency ultrasonic characterization of sintered SiC [NASA-TM-100825] p 179 N88-23985

High frequency GaAlAs modulator and photodetector for phased array antenna applications [NASA-TM-101328] p 130 N88-30048

HIGH LEVEL LANGUAGES

Adapting high-level language programs for parallel processing using data flow p 207 N88-23234

HIGH PRESSURE

Parched elastohydrodynamic lubrication film thickness measurement in an instrument ball bearing [STLE PREPRINT 88-AM-6G-1] p 169 A88-51082

E3 10C compressor test analysis of high-speed post-stall data [NASA-CR-179521] p 36 N88-28929

HIGH RESOLUTION

High-resolution heat-transfer-coefficient maps applicable to compound-curve surfaces using liquid crystals in a transient wind tunnel p 134 A88-18506

HIGH SPEED

High-speed inlet research program and supporting analyses p 17 N88-15811

Experimental evaluation of turning vane designs for high-speed and coupled fan-drive corners of 0.1-scale model of NASA Lewis Research Center's proposed altitude wind tunnel [NASA-TP-2681] p 40 N88-17686

High speed inlet calculations with real gas effects [NASA-CR-182167] p 13 N88-26336

E3 10C compressor test analysis of high-speed post-stall data [NASA-CR-179521] p 36 N88-28929

HIGH SPEED PHOTOGRAPHY

Reduction of temperature rise in high-speed photography p 160 A88-55254

Reduction of temperature rise in high-speed photography [NASA-TM-100222] p 160 N88-11100

HIGH STRENGTH ALLOYS

Dispersion strengthened NiAl alloys produced by rapid solidification processing p 88 A88-40588

HIGH TEMPERATURE

Selection of high temperature thermal energy storage materials for advanced solar dynamic space power systems p 68 A88-11801

High temperature solid oxide regenerative fuel cell for solar photovoltaic energy storage p 197 A88-11905

Thermal aging effects in refractory metal alloys p 84 A88-22700

Calibration of high-temperature, fiber-optic, microbend, pressure transducers p 157 A88-22942

High temperature metal matrix composites for future aerospace systems [AIAA PAPER 88-3059] p 71 A88-44, 45

Sputtered silver films to improve chromium carbide based solid lubricant coatings for use to 900 C p 100 A88-47563

Effect of high-temperature annealing on the microstructure and thermoelectric properties of GaP doped SiGe [NASA-TM-100164] p 101 N88-10188

High temperature metal matrix composites for future aerospace systems [NASA-TM-100212] p 90 N88-10938

High temperature stress-strain analysis p 185 N88-11170

Elevated temperature crack growth p 186 N88-11174

Lewis' enhanced laboratory for research into the fatigue and constitutive behavior of high temperature materials p 186 N88-11177

Adiabatic diesel engine component development: Reference engine for on-highway applications [NASA-CR-179531] p 224 N88-12428

Coatings for high-temperature bearings and seals [NASA-TM-100249] p 102 N88-13453

Recent advances in high temperature instrumentation for hot section applications [NASA-TM-100282] p 161 N88-14339

Hot piston ring tests [NASA-TM-100256] p 201 N88-14486

High-temperature electronics p 128 N88-15797

Aircraft engine hot section technology: An overview of the HOST Project p 29 N88-15804

Hot piston ring/cylinder liner materials: Selection and evaluation [NASA-TM-100276] p 102 N88-15872

Sputtered silver films to improve chromium carbide based solid lubricant coatings for use to 900 C [NASA-TM-100783] p 102 N88-15885

High temperature polymer matrix composites p 73 N88-16700

Development of a new generation of high-temperature composite materials p 73 N88-16702

Material parameter measurements at high temperatures [NASA-CR-182707] p 80 N88-20397

On 3-D inelastic analysis methods for hot section components. Volume 1: Special finite element models [NASA-CR-180893] p 190 N88-21535

Fracture technology for brittle materials p 192 N88-22417

Elevated temperature crack growth p 193 N88-22421

The analysis of fatigue crack growth mechanism and oxidation and fatigue life at elevated temperatures [NASA-CR-182129] p 94 N88-22987

Creep behavior of tungsten/nitrogen and tungsten/nitrogen-1 percent zirconium composites p 75 N88-24427

A thermally modified polymer matrix composite material with structural integrity to 371 C [NASA-TM-100922] p 76 N88-25483

Fracture resistance of a TiB₂ particle/SiC matrix composite at elevated temperature [NASA-TM-100967] p 107 N88-26482

The high temperature creep deformation of Si₃N₄-6Y₂O₃-2Al₂O₃ [NASA-CR-183204] p 76 N88-28981

Electrical properties of materials for elevated temperature resistance strain gage application [NASA-CR-182214] p 164 N88-30106

HIGH TEMPERATURE ENVIRONMENTS

Effect of high-temperature hydrogen exposure on sintered alpha-SiC p 97 A88-29714

Review and assessment of the database and numerical modeling for turbine heat transfer p 24 A88-54141

Views on the impact of HOST --- hot section technology p 24 A88-54146

High speed inlet calculations with real gas effects [NASA-CR-182167] p 13 N88-26336

HIGH TEMPERATURE GASES

Design and experimental evaluation of a high temperature radial turbine with a moveable sidewall nozzle [SAE PAPER 871782] p 19 A88-30776

The design of an air-cooled metallic high temperature radial turbine [AIAA PAPER 88-2872] p 22 A88-45011

A numerical study of the hot gas environment around a STOVL aircraft in ground proximity [AIAA PAPER 88-2882] p 23 A88-48752

Centerline Mach number characteristics of highly heated free jets [AIAA PAPER 88-3612] p 7 A88-48898

HOST turbine heat transfer program summary [NASA-TM-100280] p 149 N88-14320

A numerical study of the hot gas environment around a STOVL aircraft in ground proximity [NASA-TM-100895] p 1 N88-23729

HIGH TEMPERATURE RESEARCH

Toward improved durability in advanced aircraft engine hot sections: Proceedings of the Thirty-third ASME International Gas Turbine and Aeroengine Congress and Exposition, Amsterdam, Netherlands, June 5-9, 1988 p 24 A88-54137

Advanced high temperature instrumentation for hot section research applications p 159 A88-54139

HIGH TEMPERATURE SUPERCONDUCTORS

Weak-field magnetization of superconducting YBa₂Cu₃O(x) - Relationship to microstructure p 219 A88-18814

Chemical durability of high-temperature superconductor YBa₂Cu₃O(7-x) in aqueous environments p 78 A88-25023

Effect of fluoride doping on the transition temperature of YBa₂Cu₃O(6.5 + delta) p 220 A88-29297

Advantages of barium peroxide in the powder synthesis of perovskite superconductors p 221 A88-41496

Characterization of Ba₂YCu₃O(7-x) prepared in an inert atmosphere p 221 A88-49376

High T_c screen-printed YBa₂Cu₃O(7-x) films - Effect of the substrate material p 127 A88-49760

The application of high temperature superconductors to space electrical power distribution components [NASA-TM-100901] p 61 N88-22939

HIGH TEMPERATURE TESTS

Effect of initial gamma prime size on the elevated temperature creep properties of single crystal nickel base superalloys p 82 A88-18884

Sodium sulfate-induced corrosion of pure nickel and superalloy Udimet 700 in a high velocity burner rig at 900 C p 83 A88-20266

A model for life predictions of nickel-base superalloys in high-temperature low cycle fatigue p 87 A88-35913

Dispersion strengthened NiAl alloys produced by rapid solidification processing p 88 A88-40588

Effect of high temperature annealing on the thermoelectric properties of GaP doped SiGe p 220 A88-40796

Elevated temperature durability of ceramic materials [AIAA PAPER 88-3055] p 100 A88-44743

High temperature tensile testing of ceramic composites [NASA-CR-180888] p 161 N88-15996

Unified constitutive model development for metal matrix composites at high temperature p 74 N88-22387

HIGH VOLTAGES

A study of Schwarz converters for nuclear powered spacecraft p 51 A88-11823

Coaxial tube array space transmission line characterization p 121 A88-11865

Exposed high-voltage source effect on the potential of an ionospheric satellite p 218 A88-54992

High frequency power distribution system [NASA-CR-175071] p 129 N88-23939

HISTORIES

Lewis materials research and technology: An overview p 223 N88-16689

Spacecraft fire detection and extinguishment: A bibliography [NASA-CR-180880] p 45 N88-18612

HOLE GEOMETRY (MECHANICS)

Life and reliability of rotating disks p 178 N88-22428

HOLLOW CATHODES

Hollow cathodes as electron emitting plasma contactors - Theory and computer modeling p 218 A88-47973

Space plasma contactor research, 1987 [NASA-CR-182148] p 219 N88-23649

HOLOGRAPHIC INTERFEROMETRY

Reusable rocket engine optical condition monitoring p 158 A88-29817

HOLOGRAPHY

Implementation of a fast digital optical matrix-vector multiplier using a holographic look-up table and residue arithmetic p 205 N88-17223

Implementation of a digital optical matrix-vector multiplier using a holographic look-up table and residue arithmetic [NASA-CR-180431] p 205 N88-10496

Active phase compensation system for fiber optic holography [NASA-TM-101295] p 162 N88-26641

HOMOJUNCTIONS

Recent developments in indium phosphide space solar cell research p 50 A88-11785

HONEYCOMB STRUCTURES

A comparison of experimental and theoretical results for labyrinth gas seals with honeycomb stators [NASA-CR-182441] p 172 N88-16006

Experimental rotordynamic coefficient results for honeycomb seals [NASA-CR-182440] p 172 N88-16007

HOT CORROSION

Effect of alloy composition on the sodium-sulfate induced hot corrosion attack of cast nickel-base superalloys at 900 C p 81 A88-10028

High-temperature oxidation/corrosion of iron-based superalloys p 81 A88-10029

Role of molybdenum in the Na₂SO₄ induced corrosion of superalloys at high temperature p 81 A88-10030

Molten-salt corrosion of silicon nitride. I - Sodium carbonate. II - Sodium sulfate p 97 A88-26222

Adherent Al₂O₃ scales produced on undoped NiCrAl alloys p 85 A88-30269

Experiments for the determination of convective diffusion heat/mass transfer to burner rig test targets comparable in size to jet stream diameter p 140 A88-41574

Turbine airfoil deposition models and their hot corrosion implications p 91 N88-11178

Experimental verification of vapor deposition rate theory in high velocity burner rigs p 91 N88-11179

Effects of surface chemistry on hot corrosion life p 91 N88-11180

Molten salt corrosion of SiC and Si₃N₄ p 107 N88-23885

HOT ISOSTATIC PRESSING

Improved processing of alpha-SiC p 99 A88-38318

HOT PRESSING

Processing, physical metallurgy and creep of NiAl + Ta and NiAl + Nb alloys [NASA-CR-182113] p 92 N88-21295

Strength optimization of alpha-SiC by improved processing p 107 N88-23880

HOT SURFACES

Structural analysis methods development for turbine hot section components p 184 A88-54142

Recent advances in high temperature instrumentation for hot section applications p 161 N88-14339

Structural analysis methods development for turbine hot section components [NASA-TM-100298] p 188 N88-18967

On 3-D inelastic analysis methods for hot section components. Volume 1: Special finite element models [NASA-CR-180893] p 190 N88-21535

Constitutive modeling for isotropic materials [NASA-CR-182132] p 37 N88-29811

HOT-WIRE ANEMOMETERS

Gravitationally defined velocities for a low speed hot-wire calibration p 133 A88-14170

Excitation of instability waves in free shear layers. II - Experiments p 138 A88-26339

HOT-WIRE FLOWMETERS

Measurements of the turbulent transport of heat and momentum in convexly curved boundary layers - Effects of curvature, recovery and free-stream turbulence (ASME PAPER 87-GT-199) p 131 A88-11103

HOUSINGS

Cast iron-base alloy for cylinder/regenerator housing [NASA-CR-182116] p 92 N88-19613

A review of gear housing dynamics and acoustics literature [NASA-CR-183110] p 175 N88-26675

HUMAN FACTORS ENGINEERING

Spacecraft fire detection and extinguishment: A bibliography [NASA-CR-180880] p 45 N88-18612

Computer simulation of multiple pilots flying a modern high performance helicopter [NASA-TM-100183] p 39 N88-26377

HUMAN REACTIONS

Computer simulation of a single pilot flying a modern high-performance helicopter [NASA-TM-100182] p 39 N88-26376

HYBRID PROPULSION

The convertible engine: A dual-mode propulsion system p 31 N88-16639

HYBRID STRUCTURES

Design description report for a photovoltaic power system for a remote satellite earth terminal [NASA-CR-179586] p 200 N88-12875

HYDRAULIC EQUIPMENT

RE-1000 free-piston Stirling engine hydraulic output system description [NASA-TM-100185] p 223 N88-10700

HYDRAZINES

A life test of a 22-Newton (5-lbf) hydrazine rocket [NASA-TM-100232] p 57 N88-11750

HYDROCARBON COMBUSTION

The effect of gravity on premixed flame propagation and extinction in a vertical standard flammability tube p 78 A88-38532

HYDROCARBON FUELS

Sooting and disruption in spherically symmetrical combustion of decane droplets in air [IAF PAPER 87-403] p 77 A88-16076

Modified reaction mechanism of aerated n-dodecane liquid flowing over heated metal tubes p 108 A88-44268

HYDROCARBONS

Diamond like carbon coatings: Categorization by atomic number density [NASA-CR-174895] p 108 N88-28151

HYDRODYNAMIC COEFFICIENTS

Analysis of eccentric annular incompressible seals. I - A new solution using fast Fourier transforms for determining hydrodynamic force [ASME PAPER 87-TRIB-52] p 166 A88-23308

HYDRODYNAMICS

Piezoviscous effects in nonconformal contacts lubricated hydrodynamically p 133 A88-12926

Higher eigenmodes in the Blasius boundary-layer stability problem p 134 A88-16352

Initial conditional effect on pressure waves in an axisymmetric jet [AIAA PAPER 88-3702] p 143 A88-48915

Initial condition effect on pressure waves in an axisymmetric jet [NASA-TM-100915] p 153 N88-23184

HYDROGEN

The carbon dioxide chaperon efficiency for the reaction H + O₂ + M yields HO₂ + M from ignition delay times behind reflected shock waves [NASA-TM-100125] p 79 N88-15036

HYDROGEN EMBRITTLEMENT

Thermal aging effects in refractory metal alloys p 84 A88-22700

Effect of high-temperature hydrogen exposure on sintered alpha-SiC p 97 A88-29714

HYDROGEN FUELS

Catalytic ignition of hydrogen and oxygen propellants [AIAA PAPER 88-3300] p 109 A88-48764

Catalytic ignition of hydrogen and oxygen propellants [NASA-TM-100957] p 63 N88-24689

HYDROGEN ISOTOPES

Primordial lithium - New reaction rates, new abundances, new constraints p 226 A88-31145

HYDROGEN OXYGEN ENGINES

Space Station propulsion system technology p 54 A88-21255

Recent advances in low-thrust propulsion technology [AIAA PAPER 88-3283] p 55 A88-48761

25-LBF GO₂/GH₂ space station thruster [AIAA PAPER 88-2793] p 56 A88-53101

Space station propulsion [NASA-TM-100216] p 57 N88-11746

Auxiliary propulsion technology for advanced Earth-to-orbit vehicles [NASA-TM-100237] p 58 N88-14127

Recent advances in low-thrust propulsion technology [NASA-TM-100959] p 213 N88-25260

HYDROGEN OXYGEN FUEL CELLS

Regenerative fuel cell study for satellites in GEO orbit p 52 A88-11904

High temperature solid oxide regenerative fuel cell for solar photovoltaic energy storage p 197 A88-11905

Regenerative fuel cell energy storage system for a low earth orbit space station [NASA-CR-174802] p 204 N88-30184

HYDROGEN-BASED ENERGY

High temperature solid oxide regenerative fuel cell for solar photovoltaic energy storage p 197 A88-11905

HYDROTHERMAL STRESS ANALYSIS

STAEBL/general composites with hygrothermal effects (STAEBL/GENCOM) [NASA-TM-100266] p 187 N88-13754

HYDROXYL RADICALS

Feasibility of hydroxyl concentration measurements by laser-saturated fluorescence in high-pressure flames p 77 A88-17218

HYGRAL PROPERTIES

STAEBL/general composites with hygrothermal effects (STAEBL/GENCOM) [NASA-TM-100266] p 187 N88-13754

HYPERBOLIC DIFFERENTIAL EQUATIONS

Accurate boundary conditions for exterior problems in gas dynamics [NASA-TM-100807] p 210 N88-19182

HYPERCUBE MULTIPROCESSORS

Hypercluster - Parallel processing for computational mechanics p 208 A88-40458

HYPERSONIC AIRCRAFT

Hypersonic structures and materials - A progress report p 17 A88-16748

Retooling CFD for hypersonic aircraft p 1 A88-16749

Aerpropulsion '87. Session 6: High-Speed Propulsion Technology [NASA-CP-10003-SESS-6] p 29 N88-15807

HYPERSONIC BOUNDARY LAYER

Hypersonic turbulent wall boundary layer computations [AIAA PAPER 88-2829] p 7 A88-44667

Hypersonic turbulent wall boundary layer computations [NASA-CR-182147] p 154 N88-24917

HYPERSONIC FLIGHT

Ground tests confirm the promise of hypersonic propulsion p 2 A88-10369

HYPERSONIC FLOW

Numerical simulation of hypersonic inlet flows with equilibrium or finite rate chemistry [AIAA PAPER 88-0273] p 5 A88-27717

An isentropic compression heated Ludwieg tube transient wind tunnel [AIAA PAPER 88-2019] p 40 A88-37926

Turbulence modeling in hypersonic inlets [AIAA PAPER 88-2957] p 7 A88-44705

A computational analysis of under-expanded jets in the hypersonic regime [AIAA PAPER 88-4361] p 8 A88-50604

Two-dimensional viscous flow computations of hypersonic scramjet nozzle flowfields at design and off-design conditions p 23 A88-50785

Similar solutions for viscous hypersonic flow over a slender three-fourths-power body of revolution [NASA-TM-100205] p 148 A88-12752

Hypersonic turbulent wall boundary layer computations [NASA-CR-182147] p 154 N88-24917

Two-dimensional viscous flow computations of hypersonic scramjet nozzle flowfields at design and off-design conditions [NASA-CR-182150] p 35 N88-25459

HYPERSONIC INLETS

Thermostructural analysis with experimental verification in a high heat flux facility of a simulated cowl lip [AIAA PAPER 88-2222] p 39 A88-32188

Turbulence modeling in hypersonic inlets [AIAA PAPER 88-2957] p 7 A88-44705

HYPERSONIC SPEED

A computational analysis of under-expanded jets in the hypersonic regime [NASA-TM-101319] p 13 N88-27174

HYPERVELOCITY IMPACT

The effect of the near earth micrometeoroid environment on a highly reflective mirror surface [NASA-TM-101307] p 44 N88-29833

HYPERVELOCITY LAUNCHERS

Application of superconducting technology to earth-to-orbit electromagnetic launch systems [NASA-TM-101134] p 43 N88-26385

ICE FORMATION

Analytical determination of propeller performance degradation due to ice accretion p 19 A88-19669

The calculation of flow over iced airfoils [AIAA PAPER 88-0112] p 4 A88-22078

Investigation of surface water behavior during glaze ice accretion [AIAA PAPER 88-0115] p 14 A88-22079

Measurement of local convective heat transfer coefficients from a smooth and roughened NACA-0012 airfoil - Flight test data [AIAA PAPER 88-0287] p 136 A88-22207

Stability relationship for water droplet crystallization with the NASA Lewis icing spray nozzle [AIAA PAPER 88-0289] p 137 A88-22209

Navier-Stokes solutions of flowfield characteristics produced by ice accretion [AIAA PAPER 88-0290] p 137 A88-22210

Operating envelopes of particle sizing instrumentation used for icing research [AIAA PAPER 88-0291] p 157 A88-22211

- Model helicopter performance degradation with simulated ice shapes p 17 A88-22783
- Measurement of ice thickness (icing) in aeronautics p 15 A88-32714
- In-flight measurement of airfoil icing using an array of ultrasonic transducers p 15 A88-50910
- Ultrasonic techniques for aircraft ice accretion measurement [AIAA PAPER 88-4656] p 18 A88-51910
- Stability relationship for water droplet crystallization with the NASA Lewis icing spray [NASA-TM-100220] p 24 A88-10790
- Analysis of counting errors in the phase/Doppler particle analyzer [NASA-TM-100231] p 161 A88-12043
- Experimental evidence for modifying the current physical model for ice accretion on aircraft surfaces [NASA-TM-87184] p 15 A88-12473
- Measured performance of the heat exchanger in the NASA icing research tunnel under severe icing and dry-air conditions [NASA-TM-100116] p 171 A88-12796
- Measurement of local convective heat transfer coefficients from a smooth and roughened NACA-0012 airfoil: Flight test data [NASA-TM-100284] p 149 A88-13552
- Operating envelopes of particle sizing instrumentation used for icing research [NASA-CR-180870] p 161 A88-13573
- A flow visualization study of the leading edge separation bubble on a NACA 0012 airfoil with simulated glaze ice [NASA-CR-180846] p 10 A88-14966
- An experimental mapping of the flow field behind a glaze ice shape on a NACA 0012 airfoil [NASA-CR-180847] p 10 A88-15766
- The NASA aircraft icing research program p 15 A88-15803
- NASA's rotorcraft icing research program p 15 A88-16641
- Three-dimensional trajectory analyses of two drop sizing instruments: PMS OAP and PMS FSSP [NASA-CR-4113] p 16 A88-18574
- An experimental and theoretical study of the ice accretion process during artificial and natural icing conditions [NASA-CR-182119] p 16 A88-21143
- In-flight measurement of ice growth on an airfoil using an array of ultrasonic transducers [AIAA-87-0178] p 16 A88-23717
- Experimental measurements of heat transfer from an iced surface during artificial and natural cloud icing conditions [AIAA-86-1352] p 153 A88-23718
- ICE PREVENTION**
- Theoretical analysis of the electrical aspects of the basic electro-impulse problem in aircraft de-icing applications [NASA-CR-180845] p 15 A88-13310
- NASA's rotorcraft icing research program p 15 A88-16641
- IGNITERS**
- Catalytic ignition of hydrogen and oxygen propellants [AIAA PAPER 88-3300] p 109 A88-48764
- Catalytic ignition of hydrogen and oxygen propellants [NASA-TM-100957] p 63 A88-24689
- IGNITION**
- Modelling ignition characteristics of rich H₂/O₂ mixture in a monolithic catalytic reactor [AIAA PAPER 88-3224] p 78 A88-46499
- Catalytic ignition of hydrogen and oxygen propellants [AIAA PAPER 88-3300] p 109 A88-48764
- Detailed mechanism of benzene oxidation [NASA-TM-100202] p 79 A88-11775
- Detailed mechanism of toluene oxidation and comparison with benzene [NASA-TM-100261] p 79 A88-13428
- The carbon dioxide chaperon efficiency for the reaction H + O₂ + M yields HO₂ + M from ignition delay times behind reflected shock waves [NASA-TM-100125] p 79 A88-15036
- Catalytic ignition of hydrogen and oxygen propellants [NASA-TM-100957] p 63 A88-24689
- IMAGE ANALYSIS**
- Determination of grain-size distribution function using two-dimensional Fourier transforms of tone-pulse-encoded images p 176 A88-30425
- IMAGE CORRELATORS**
- Real time optical correlator using a magneto-optic device applied to particle imaging velocimetry p 159 A88-40700
- IMAGE PROCESSING**
- Systems for ultrasonic scanning, analysis and imagery p 177 A88-22414
- IMAGERY**
- Imaging subtle microstructural variations in ceramics with precision ultrasonic velocity and attenuation measurements [NASA-TM-100129] p 177 A88-15257
- Comparison of UNL laser imaging and sizing system and a phase/Doppler system for analyzing sprays from a NASA nozzle [NASA-CR-182437] p 150 A88-16956
- IMAGING TECHNIQUES**
- Systems for ultrasonic scanning, analysis and imagery p 177 A88-22414
- IMPACT**
- The impact damped harmonic oscillator in free decay p 167 A88-31581
- IMPACT DAMAGE**
- Measurement of impact-induced delamination buckling in composite laminates p 71 A88-47214
- Atomic-oxygen durability of impact-damaged solar reflectors p 68 A88-54988
- Impact damage in composite laminates p 74 A88-22402
- Assessment of the effects of space debris and meteoroids environment on the space station solar array assembly [NASA-TM-101315] p 49 A88-28959
- IMPACT LOADS**
- Dynamic delamination fracture toughness of a graphite/epoxy laminate under impact p 70 A88-29455
- Impact damage in composite laminates p 74 A88-22402
- Contact force history and dynamic response due to the impact of a soft projectile [NASA-TM-100961] p 175 A88-26679
- IMPACT TESTS**
- Measurement of impact-induced delamination buckling in composite laminates p 71 A88-47214
- Contact force history and dynamic response due to the impact of a soft projectile [NASA-TM-100961] p 175 A88-26679
- IMPROVEMENT**
- Parameter identification methods for improving structural dynamic models [NASA-TM-100812] p 194 A88-23994
- IMPURITIES**
- Characterization of directionally solidified lead chloride p 111 A88-43170
- Preparation of multistage zone-refined materials for thermochemical standards p 111 A88-43172
- Advanced development of double-injection, deep-impurity semiconductor switches [NASA-CR-182118] p 222 A88-25346
- IN-FLIGHT MONITORING**
- In-flight thrust determination [SAE AIR 1703] p 16 A88-15227
- Uncertainty of in-flight thrust determination [SAE AIR 1678] p 16 A88-15228
- In-flight measurement of airfoil icing using an array of ultrasonic transducers p 15 A88-50910
- INCOMPRESSIBLE FLOW**
- A space-marching method for the computation of viscous internal flows p 135 A88-20459
- Investigation of third-order closure model of turbulence for the computation of incompressible flows in a channel with a backward-facing step p 136 A88-21273
- Analysis of eccentric annular incompressible seals. I - A new solution using fast Fourier transforms for determining hydrodynamic force [ASME PAPER 87-TRIB-52] p 166 A88-23308
- A finite difference scheme for three-dimensional steady laminar incompressible flow p 139 A88-30469
- INDEXES (DOCUMENTATION)**
- Engine structures: A bibliography of Lewis Research Center's research for 1980-1987 [NASA-TM-100842] p 195 A88-24002
- INDIUM ALLOYS**
- Containerless processing of undercooled melts p 110 A88-28554
- INDIUM COMPOUNDS**
- Direct-current magnetron fabrication of indium tin oxide/InP solar cells p 200 A88-51289
- INDIUM PHOSPHIDES**
- Recent developments in indium phosphide space solar cell research p 50 A88-11785
- Comparative radiation resistance, temperature dependence and performance of diffused junction indium phosphide solar cells p 198 A88-18580
- Rapid thermal annealing of indium phosphide compound semiconductors p 220 A88-26196
- Plasma deposition of amorphous hydrogenated carbon films on III-V semiconductors p 220 A88-32862
- InP based solar cells for space application: Reduction of external losses p 199 A88-34250
- Characterization and modelling of open tube diffused n + p bulk InP solar cells p 199 A88-34270
- Modelling and design of high efficiency radiation tolerant indium phosphide space solar cells p 200 A88-34394
- Direct-current magnetron fabrication of indium tin oxide/InP solar cells p 200 A88-51289
- Progress in InP solar cell research [NASA-TM-100914] p 130 A88-24870
- INELASTIC STRESS**
- Constitutive modeling of superalloy single crystals with verification testing p 91 A88-11169
- Unified constitutive models for high-temperature structural applications p 190 A88-21523
- A constitutive model for an overlay coating p 105 A88-21525
- On 3-D inelastic analysis methods for hot section components. Volume 1: Special finite element models [NASA-CR-180893] p 190 A88-21535
- Experiments investigating advanced materials under thermomechanical loading p 191 A88-22385
- MHOST: An efficient finite element program for inelastic analysis of solids and structures p 33 A88-22394
- An experimental study of biaxial yield in modified 9Cr-1Mo steel at room temperature [NASA-CR-175012] p 196 A88-30164
- INERT ATMOSPHERE**
- Characterization of Ba₂YCu₃O(7-x) prepared in an inert atmosphere p 221 A88-49376
- Spacecraft Fire Safety [NASA-CP-2476] p 45 A88-12520
- INERTIAL GUIDANCE**
- Optical alignment of Centaur's inertial guidance system [NASA-TM-88844] p 43 A88-12515
- INFLUENCE COEFFICIENT**
- Investigation of oscillating cascade aerodynamics by an experimental influence coefficient technique [NASA-TM-101313] p 14 A88-28041
- INFORMATION DISSEMINATION**
- Spacecraft 2000 program overview p 48 A88-10085
- INFORMATION MANAGEMENT**
- Laboratory Information Management System (LIMS): A case study [NASA-TM-100835] p 208 A88-21697
- INFORMATION SYSTEMS**
- Lewis Information Network (LINK): Background and overview [NASA-TM-100162] p 117 A88-11925
- INFRARED ABSORPTION**
- Reduction of temperature rise in high-speed photography p 160 A88-55254
- Reduction of temperature rise in high-speed photography [NASA-TM-100222] p 160 A88-11100
- INFRARED REFLECTION**
- Reduction of temperature rise in high-speed photography p 160 A88-55254
- Reduction of temperature rise in high-speed photography [NASA-TM-100222] p 160 A88-11100
- INFRARED SPECTROMETERS**
- Investigation of PTFE transfer films by infrared emission spectroscopy and phase-locked ellipsometry p 99 A88-35568
- INGESTION (ENGINES)**
- Transient engine performance with water ingestion p 19 A88-27295
- A numerical study of the hot gas environment around a STOVL aircraft in ground proximity [AIAA PAPER 88-2682] p 23 A88-48752
- A numerical study of the hot gas environment around a STOVL aircraft in ground proximity [NASA-TM-100895] p 1 A88-23729
- INHOMOGENEITY**
- A finite element model for wave propagation in an inhomogeneous material including experimental validation [AIAA PAPER 87-2741] p 212 A88-16577
- INJECTION LOCKING**
- An analytical and experimental study of injection-locked two-port oscillators [NASA-TM-100119] p 128 A88-12727
- INJECTION MOLDING**
- Improved silicon nitride for advanced heat engines [NASA-CR-175006] p 102 A88-15886
- Improved silicon carbide for advanced heat engines p 106 A88-23879
- INJECTORS**
- Application of advanced diagnostics to airblast injector flows [ASME PAPER 88-GT-12] p 159 A88-54159
- Aerothermal modeling program, phase 2 p 146 A88-11149
- Fuel-injector/air-swirl characterization p 146 A88-11150

INLET FLOW

- Numerical simulation of hypersonic inlet flows with equilibrium or finite rate chemistry
[AIAA PAPER 88-0273] p 5 A88-27717
- Lateral jet injection into swirling combustor flowfields
[AIAA PAPER 88-3183] p 141 A88-44783
- A preliminary design study of supersonic through-flow fan inlets
[AIAA PAPER 88-3075] p 23 A88-53137
- The effects of turbulence and stator/rotor interactions on turbine heat transfer. II - Effects of Reynolds number and incidence
[ASME PAPER 88-GT-5] p 145 A88-54152
- Measurement of airfoil heat transfer coefficients on a turbine stage
p 147 A88-11158
- Aeropropulsion '87. Session 3: Internal Fluid Mechanics Research
[NASA-CP-10003-SESS-3] p 28 A88-15790
- Propulsion challenges and opportunities for high-speed transport aircraft
p 30 A88-15809
- Supersonic throughflow fans for high-speed aircraft
p 30 A88-15810
- High-speed inlet research program and supporting analyses
p 17 A88-15811
- High speed inlet calculations with real gas effects
[NASA-CR-182167] p 13 A88-26336
- The effects of inlet turbulence and rotor/stator interactions on the aerodynamics and heat transfer of a large-scale rotating turbine model. Volume 3: Heat transfer data tabulation 65 percent axial spacing
[NASA-CR-179468] p 37 A88-28930
- The effects of inlet turbulence and rotor/stator interactions on the aerodynamics and heat transfer of a large-scale rotating turbine model. Volume 2: Heat transfer data tabulation. 15 percent axial spacing
[NASA-CR-179467] p 37 A88-29804
- INLET NOZZLES**
- Test stand performance of a convertible engine for advanced V/STOL and rotorcraft propulsion
[SAE PAPER 872355] p 21 A88-37217
- Test stand performance of a convertible engine for advanced V/STOL and rotorcraft propulsion
[NASA-TM-100211] p 25 A88-11679
- Electromagnetic fields backscattered from an s-shaped inlet cavity with an absorber coating on its inner walls
[NASA-CR-182401] p 118 A88-15130
- The effects of inlet turbulence and rotor/stator interactions on the aerodynamics and heat transfer of a large-scale rotating turbine model. Part 4: Aerodynamic data tabulation
[NASA-CR-179469] p 153 A88-23956
- INLET TEMPERATURE**
- Effect of spatial inlet temperature and pressure distortion on turbofan engine stability
[AIAA PAPER 88-3016] p 22 A88-44727
- Effect of spatial inlet temperature and pressure distortion on turbofan engine stability
[NASA-TM-100850] p 32 A88-21162
- INSTALLING**
- Advanced turboprop wing installation effects measured by unsteady blade pressure and noise
[AIAA PAPER 87-2719] p 3 A88-18655
- Advanced turboprop wing installation effects measured by unsteady blade pressure and noise
[NASA-TM-100200] p 9 A88-10008
- INSTRUMENT ERRORS**
- Sources of error in heterodyne moire deflectometry
p 158 A88-35004
- INSULATION**
- Prototype thin-film thermocouple/heat-flux sensor for a ceramic-insulated diesel engine
[NASA-TM-100798] p 162 A88-18892
- INTAKE SYSTEMS**
- A numerical study of the hot gas environment around a STOVL aircraft in ground proximity
[AIAA PAPER 88-2882] p 23 A88-48752
- Inlets, ducts and nozzles
p 149 A88-15791
- A numerical study of the hot gas environment around a STOVL aircraft in ground proximity
[NASA-TM-100895] p 1 A88-23729
- INTEGRALS**
- Elevated temperature crack growth
p 186 A88-11174
- INTEGRATED CIRCUITS**
- Monolithic Microwave Integrated Circuit (MMIC) technology for space communications applications
[IAF PAPER 87-491] p 122 A88-16133
- Two stage dual gate MESFET monolithic gain control amplifier for Ka-band
p 124 A88-29821
- System architecture of MMIC-based large aperture arrays for space applications
p 45 A88-35274
- Progress in MMIC technology for satellite communications
p 126 A88-37844
- Optical RF distribution links for MMIC phased array antennas
[NASA-TM-100841] p 128 A88-20555

- Monolithic microwave integrated circuit technology for advanced space communication
[NASA-TM-100829] p 120 A88-21389
- A 30 GHz monolithic receive module technology assessment
[NASA-CR-180825] p 129 A88-23084
- Array trade-off study using multilayer parasitic subarrays
[NASA-TM-101321] p 121 A88-28222
- INTEGRATED ENERGY SYSTEMS**
- Status of commercial fuel cell powerplant system development
p 198 A88-11925
- Integrated analysis and applications
p 28 A88-15789
- INTEGRATORS**
- Rotorcraft flight-propulsion control integration: An eclectic design concept
[NASA-TP-2815] p 38 A88-19475
- INTERACTIONAL AERODYNAMICS**
- Aerodynamic interaction between propellers and wings
[AIAA PAPER 88-0665] p 5 A88-22495
- Glancing shock wave-turbulent boundary layer interaction with boundary layer suction
[AIAA PAPER 88-0306] p 6 A88-27718
- The effects of turbulence and stator/rotor interactions on turbine heat transfer. II - Effects of Reynolds number and incidence
[ASME PAPER 88-GT-5] p 145 A88-54152
- The effects of turbulence and stator/rotor interactions on turbine heat transfer. I - Design operating conditions
[ASME PAPER 88-GT-125] p 145 A88-54236
- Experimental and numerical investigation of the effect of distributed suction on oblique shock wave/turbulent boundary layer interaction
[NASA-TM-101334] p 156 A88-30084
- INTERCALATION**
- Production and characterization of CdCl₂ intercalated graphite fibers
p 101 A88-51307
- INTERFACES**
- Identification of structural interface characteristics using component mode synthesis
p 181 A88-31561
- Interfacial adhesion: Theory and experiment
[NASA-TM-100830] p 92 A88-20417
- Service offerings and interfaces for the ACTS network of Earth stations
[NASA-TM-100809] p 46 A88-24663
- Auger analysis of a fiber/matrix interface in a ceramic matrix composite
[NASA-TM-100892] p 76 A88-25487
- The development of an intelligent interface to a computational fluid dynamics flow-solver code
[NASA-TM-100908] p 207 A88-26127
- INTERFACIAL TENSION**
- Electrohydrodynamic migration of charged droplets in an insulating fluid
[AIAA PAPER 88-3557] p 143 A88-48946
- Investigation of surface tension driven convection as a feasibility study for a micro-gravity experiment
[NASA-CR-182504] p 112 A88-18739
- Electrohydrodynamic migration of charged droplets in an insulating fluid
[NASA-TM-100849] p 152 A88-21424
- INTERFEROMETRY**
- Development and applications of optical interferometric micrometry in the angstrom and subangstrom range
[NASA-TM-100299] p 162 A88-23196
- INTERLAYERS**
- Improving the interlaminar shear strength of carbon fiber-epoxy composites through carbon fiber bromination
[NASA-TM-100248] p 72 A88-15018
- INTERMETALLICS**
- The influence of grain size and composition on 1000 to 1400 K slow plastic flow properties of NiAl
p 85 A88-29098
- High temperature metal matrix composites for future aerospace systems
[AIAA PAPER 88-3059] p 71 A88-44745
- High temperature metal matrix composites for future aerospace systems
[NASA-TM-100212] p 90 A88-10938
- Processing, physical metallurgy and creep of NiAl + Ta and NiAl + Nb alloys
[NASA-CR-182113] p 92 A88-21295
- INTERNAL COMBUSTION ENGINES**
- Design, calibration and error analysis of instrumentation for heat transfer measurements in internal combustion engines
p 157 A88-18509
- INTERNATIONAL SUN EARTH EXPLORER 1**
- An unusual charging event on ISEE 1
p 47 A88-40013
- INTERPROCESSOR COMMUNICATION**
- Performance limitations in parallel processor simulations
p 208 A88-49101
- INVERSIONS**
- A diagonally inverted LU implicit multigrid scheme
[NASA-TM-100911] p 13 A88-26340

INVISCID FLOW

- Explicit multigrid algorithm for quasi-three-dimensional viscous flows in turbomachinery
p 2 A88-10355
- A mapped finite difference study of noise propagation in nonuniform ducts with mean flow
p 214 A88-18541
- Choice of implicit and explicit operators for the upwind differencing method
[AIAA PAPER 88-0624] p 209 A88-22472
- Splitting of inviscid fluxes for real gases
[AIAA PAPER 88-3526] p 142 A88-48782
- Utilization of parallel processing in solving the inviscid form of the average-passage equation system for multistage turbomachinery
[NASA-TM-89845] p 32 A88-21160
- Splitting of inviscid fluxes for real gases
[NASA-TM-100856] p 211 A88-21717
- ION BEAMS**
- Ion beam deposition of amorphous carbon films with diamond like properties
p 97 A88-20300
- Comment on 'Ram ion scattering caused by Space Shuttle v x B induced differential charging' by I. Katz and V. A. Davis
p 204 A88-35775
- Degradation mechanisms of materials for large space systems in low Earth orbit
[NASA-CR-181472] p 71 A88-10896
- Ion-beam nitriding of steels
[NASA-CASE-LEW-14104-2] p 91 A88-14179
- ION CURRENTS**
- Internal erosion rates of a 10-kW xenon ion thruster
[AIAA PAPER 88-2912] p 55 A88-48753
- Internal erosion rates of a 10-kW xenon ion thruster
[NASA-TM-100954] p 63 A88-24688
- ION ENGINES**
- Internal erosion rates of a 10-kW xenon ion thruster
[AIAA PAPER 88-2912] p 55 A88-48753
- An 8-cm ion thruster characterization
[NASA-CR-180819] p 56 A88-10106
- Electric propulsion options for the SP-100 reference mission
p 62 A88-24296
- Internal erosion rates of a 10-kW xenon ion thruster
[NASA-TM-100954] p 63 A88-24688
- Performance of 10-kW class xenon ion thrusters
[NASA-TM-101292] p 65 A88-28088
- ION IMPLANTATION**
- Behavior of ion-implanted junction diodes in 3C SiC
p 122 A88-15423
- Rapid thermal annealing of indium phosphide compound semiconductors
p 220 A88-26196
- ION IRRADIATION**
- Ion-beam nitriding of steels
[NASA-CASE-LEW-14104-2] p 91 A88-14179
- ION PLATING**
- Status and directions of modified tribological surfaces by ion processes
[NASA-TM-101304] p 115 A88-28176
- ION PROPULSION**
- An 8-cm ion thruster characterization
[NASA-CR-180819] p 56 A88-10106
- Auxiliary propulsion system flight package
[NASA-CR-180828] p 56 A88-10886
- High power ion thruster performance
[NASA-TM-100127] p 58 A88-12542
- A cyclic ground test of an ion auxiliary propulsion system: Description and operational considerations
[NASA-TM-100870] p 62 A88-23829
- High power ion thruster performance
p 62 A88-24295
- ION SCATTERING**
- Comment on 'Ram ion scattering caused by Space Shuttle v x B induced differential charging' by I. Katz and V. A. Davis
p 204 A88-35775
- IONOSPHERIC ION DENSITY**
- Comment on 'Ram ion scattering caused by Space Shuttle v x B induced differential charging' by I. Katz and V. A. Davis
p 204 A88-35775
- IRIDIUM**
- Iridium-coated rhenium thrusters by CVD
[NASA-TM-101309] p 67 A88-29874
- IRON**
- Wear of iron and nickel in corrosive liquid environments
p 88 A88-40790
- Wear of iron and nickel in corrosive liquid environments
[NASA-TM-100246] p 91 A88-11817
- IRON ALLOYS**
- High-temperature oxidation/corrosion of iron-based superalloys
p 81 A88-10029
- Crystallization behavior of a melt-spun Fe-Ni based steel
p 83 A88-19958
- Dynamic recrystallization and grain boundary migration in B2 FeAl
p 83 A88-20269
- The microstructure and tensile properties of extruded melt-spun ribbons of iron-rich B2 FeAl
p 85 A88-31679
- Room temperature tensile ductility in powder processed B2 FeAl alloys
p 85 A88-31694

Alloy chemistry and microstructural control to meet the demands of the automotive Stirling engine

Cast iron-base alloy for cylinder/regenerator housing
[NASA-CR-182116] p 88 A88-40332
p 92 N88-19613

IRON COMPOUNDS

Preliminary investigation of inertia friction welding B2 aluminides p 82 A88-14567

IRRADIATION

Performance of GaAs and silicon concentrator cells under 37 MeV proton irradiation p 200 A88-34343
Effects of electron and proton irradiations on n/p and p/n GaAs cells grown by MOCVD
[NASA-TM-100199] p 127 N88-10266
Degradation mechanisms of materials for large space systems in low Earth orbit
[NASA-CR-181472] p 71 N88-10896
Performance of GaAs and silicon concentrator cells under 37 MeV proton irradiation
[NASA-TM-100144] p 200 N88-12877

ISENTROPIC PROCESSES

An isentropic compression heated Ludwig tube transient wind tunnel
[AIAA PAPER 88-2019] p 40 A88-37926

ISOSTATIC PRESSURE

Strength optimization of alpha-SiC by improved processing p 107 N88-23880

ISOTHERMAL PROCESSES

Calculation of thermomechanical fatigue life based on isothermal behavior p 181 A88-26450
Bithermal fatigue - A link between isothermal and thermomechanical fatigue p 87 A88-35918
Thermal-mechanical cyclic stress-strain responses of cast B-1900 + Hf p 87 A88-35919
Isothermal dendritic growth - A proposed microgravity experiment p 112 A88-49095
Isothermal and bithermal thermomechanical fatigue behavior of a NiCoCrAlY-coated single crystal superalloy
[NASA-TM-100907] p 94 N88-24766

ISOTROPIC MEDIA

Acousto-ultrasonic input-output characterization of unidirectional fiber composite plate by SV waves
[NASA-CR-4152] p 178 N88-23224
A transversely isotropic thermoelastic theory
[NASA-TM-101302] p 196 N88-28332
Constitutive modeling for isotropic materials
[NASA-CR-182132] p 37 N88-29811

ITERATIVE SOLUTION

A hypermatrix formulation for subspace iteration p 205 A88-15427
I-BIEM, an iterative boundary integral equation method for computer solutions of current distribution problems with complex boundaries: A new algorithm. I - Theoretical p 205 A88-27795
Hierarchically partitioned nonlinear equation solvers p 210 A88-54980
Convergence acceleration for vector sequences and applications to computational fluid dynamics
[NASA-TM-101327] p 212 N88-30377

J**J INTEGRAL**

A review of path-independent integrals in elastic-plastic fracture mechanics p 183 A88-47001
Method and models for R-curve instability calculations
[NASA-TM-100935] p 194 N88-23278

JET AIRCRAFT NOISE

Application of structural tailoring to spar/shell turboprops p 20 A88-32277
Acoustics technologies for STOVL aircraft
[AIAA PAPER 88-2238] p 215 A88-35939
Turbofan engine core noise source diagnostics p 22 A88-39707

JET ENGINE FUELS

Availability and cost estimate of a high naphthene, modified aviation turbine fuel
[NASA-TM-100823] p 104 N88-20455

JET ENGINES

Transient engine performance with water ingestion p 19 A88-27295
Performance limitations in parallel processor simulations p 208 A88-49101

JET EXHAUST

Centerline Mach number characteristics of highly heated free jets
[AIAA PAPER 88-3612] p 7 A88-48898
Techniques utilized in the simulated altitude testing of a 2D-CD vectored and reversing nozzle
[NASA-TM-100872] p 40 N88-25464

JET FLOW

Roles of initial condition and vortex pairing in jet noise p 213 A88-13963

K-epsilon turbulence model assessment with reduced numerical diffusion for coaxial jets

[AIAA PAPER 88-0342] p 137 A88-22251
Unsteady features of jets in lift and cruise modes for VTOL aircraft

[SAE PAPER 872359] p 6 A88-37220
Initial conditional effect on pressure waves in an axisymmetric jet

[AIAA PAPER 88-3702] p 143 A88-48915
A computational analysis of under-expanded jets in the hypersonic regime
[AIAA PAPER 88-4361] p 8 A88-50604

A numerical investigation of the influence of heating on the excitation of high and low Mach number jet flows
[ASME PAPER 87-WA/NCA-13] p 144 A88-51343

On the correlation of plume centerline velocity decay of turbulent acoustically excited jets
[NASA-TM-100193] p 11 N88-16681

Initial condition effect on pressure waves in an axisymmetric jet
[NASA-TM-100915] p 153 N88-23184

Acoustically excited heated jets. 1: Internal excitation
[NASA-CR-4129-PT-1] p 12 N88-23751

Acoustically excited heated jets. 2: In search of a better understanding
[NASA-CR-4129-PT-2] p 12 N88-23752

Three-dimensional viscous flow computations of a circular jet in subsonic and supersonic cross flow
[NASA-CR-182153] p 155 N88-26616

A computational analysis of under-expanded jets in the hypersonic regime
[NASA-TM-101319] p 13 N88-27174

JET MIXING FLOW

Numerical simulation of self-sustained and forced oscillations in jet shear layers p 3 A88-14155
Effects of nozzle-exit boundary-layer conditions on excitability of heated free jets

[AIAA PAPER 87-2723] p 135 A88-20182
A numerical study of the effects of curvature and convergence on dilution jet mixing

[AIAA PAPER 87-1953] p 137 A88-23312
Mixing, transport and combustion in sprays p 138 A88-25828

Forced mixer lobes in ejector designs p 141 A88-46222
Effect of initial tangential velocity distribution on the mean evolution of a swirling turbulent free jet

[AIAA PAPER 88-3592] p 7 A88-48893
Saturation and the limit of jet mixing enhancement by single frequency plane wave excitation - Experiment and theory

[AIAA PAPER 88-3613] p 8 A88-48899
An empirical model of the effects of curvature and convergence on dilution jet mixing

[AIAA PAPER 88-3180] p 23 A88-50783
Dilution jet mixing program, phase 3 p 147 N88-11153

On the mixing of a row of jets with a confined crossflow p 147 N88-11154
A numerical study of the effects of curvature and convergence on dilution jet mixing

[NASA-TM-89878] p 26 N88-13347
Saturation and the limit of jet mixing enhancement by single frequency plane wave excitation: Experiment and theory

[NASA-TM-100882] p 12 N88-23732
Acoustically excited heated jets. 1: Internal excitation
[NASA-CR-4129-PT-1] p 12 N88-23751

Acoustically excited heated jets. 2: In search of a better understanding
[NASA-CR-4129-PT-2] p 12 N88-23752

Acoustically excited heated jets. 3: Mean flow data
[NASA-CR-4129-PT-3] p 12 N88-23753

Effect of initial tangential velocity distribution on the mean evolution of a swirling turbulent free jet
[NASA-TM-100934] p 12 N88-24592

An empirical model of the effects of curvature and convergence on dilution jet mixing
[NASA-TM-100896] p 34 N88-24640

JOINING

Optically interconnected phased arrays
[NASA-TM-100855] p 128 N88-21400

JOINTS (JUNCTIONS)

Identification of structural interface characteristics using component mode synthesis p 181 A88-31561
Overview of free-piston Stirling engine technology for space power application

[NASA-TM-88886] p 223 N88-12427
Characterization of damped structural connections for multi-component systems

[NASA-TM-100801] p 189 N88-18974
JOURNAL BEARINGS

Stability of a rigid rotor supported on flexible oil journal bearings
[ASME PAPER 87-TRIB-48] p 166 A88-24034

On the performance of finite journal bearings lubricated with micropolar fluids

[NASA-TM-100293] p 150 N88-15983
The use of multigrid techniques in the solution of the Elrod algorithm for a dynamically loaded journal bearing

[NASA-CR-180873] p 151 N88-17954
The solution of the Elrod algorithm for a dynamically loaded journal bearing using multigrid techniques

[NASA-TM-100941] p 154 N88-25854

JUNCTION DIODES

Behavior of ion-implanted junction diodes in 3C SiC p 122 A88-15423

JUNCTION TRANSISTORS

Comparative radiation resistance, temperature dependence and performance of diffused junction indium phosphide solar cells p 198 A88-18580

JUPITER ATMOSPHERE

Voeds in Jovian magnetosphere revisited - Evidence of spacecraft charging p 226 A88-22879

K**K-EPSILON TURBULENCE MODEL**

K-epsilon turbulence model assessment with reduced numerical diffusion for coaxial jets
[AIAA PAPER 88-0342] p 137 A88-22251

Navier-Stokes cascade analysis with a stiff k-epsilon turbulence solver
[AIAA PAPER 88-0594] p 5 A88-22444

Navier-Stokes cascade analysis with a stiff Kappa-Epsilon turbulence solver
[NASA-TM-100218] p 9 N88-10778

KEROSENE

Availability and cost estimate of a high naphthene, modified aviation turbine fuel
[NASA-TM-100823] p 104 N88-20455

KINEMATICS

SHARP simulation of discontinuities in highly convective steady flow
[NASA-TM-100240] p 210 N88-13931

Base reaction optimization of manipulators with redundant kinematics p 173 N88-23238
Determination of settings of a tilted head-cutter for generation of hypoid and spiral bevel gears

[NASA-CR-182138] p 174 N88-24976

KINETIC ENERGY

Navier-Stokes cascade analysis with a stiff k-epsilon turbulence solver
[AIAA PAPER 88-0594] p 5 A88-22444

Turbulence modeling in hypersonic inlets
[AIAA PAPER 88-2957] p 7 A88-44705

Navier-Stokes cascade analysis with a stiff Kappa-Epsilon turbulence solver
[NASA-TM-100218] p 9 N88-10778

KUTTA-JOUKOWSKI CONDITION

Excitation of instability waves in free shear layers. I - Theory p 138 A88-26338

L**LABORATORIES**

Research opportunities in microgravity science and applications during Shuttle hiatus p 109 A88-13164
The Lewis Strain Gauge Laboratory: Status and plans p 160 N88-11146

Lewis' enhanced laboratory for research into the fatigue and constitutive behavior of high temperature materials p 186 N88-11177

Laboratory Information Management System (LIMS): A case study
[NASA-TM-100835] p 208 N88-21697

LABYRINTH SEALS

Theory versus experiment for the rotordynamic coefficients of labyrinth gas seals. I - A two control volume model p 167 A88-31535

Theory versus experiment for the rotordynamic coefficients of labyrinth gas seals. II - A comparison to experiment p 167 A88-31536

Experimental verification of a secondary recirculation zone in a labyrinth seal
[AIAA PAPER 88-3692] p 168 A88-48971

3-D laser anemometer measurements in a labyrinth seal
[ASME PAPER 88-GT-63] p 169 A88-54195

A comparison of experimental and theoretical results for labyrinth gas seals with honeycomb stators
[NASA-CR-182441] p 172 N88-18006

Experimental rotordynamic coefficient results for honeycomb seals
[NASA-CR-182440] p 172 N88-18007

LAMINAR BOUNDARY LAYER

The measurement of boundary layers on a compressor blade in cascade. III - Pressure surface boundary layers and the near wake

[ASME PAPER 87-GT-250] p 132 A88-11132

Transition and separation control on a low-Reynolds number airfoil p 2 A88-11186

Roles of initial condition and vortex pairing in jet noise p 213 A88-13963

Boundary layer development as a function of chamber pressure in the NASA Lewis 1030:1 area ratio rocket nozzle

[AIAA PAPER 88-3301] p 144 A88-50786

Boundary layer development as a function of chamber pressure in the NASA Lewis 1030:1 area ratio rocket nozzle

[NASA-TM-100917] p 154 N88-25841

LAMINAR FLOW

Torsion effect on fully developed flow in a helical pipe p 135 A88-20748

Laminar diffusion flames under micro-gravity conditions

[AIAA PAPER 88-0645] p 78 A88-27722

A finite difference scheme for three-dimensional steady laminar incompressible flow p 139 A88-30469

Developing fluid flow in a curved duct of square cross-section and its fully developed dual solutions

p 139 A88-30957

Stability of swirling gas flows p 142 A88-46317

Boundary layer development as a function of chamber pressure in the NASA Lewis 1030:1 area ratio rocket nozzle

[AIAA PAPER 88-3301] p 144 A88-50786

Boundary layer development as a function of chamber pressure in the NASA Lewis 1030:1 area ratio rocket nozzle

[NASA-TM-100917] p 154 N88-25841

LAMINATES

Fracture characteristics of angleplied laminates fabricated from overaged graphite/epoxy prepreg

p 69 A88-16965

Ultrasonic evaluation of mechanical properties of thick, multilayered, filament-wound composites

p 176 A88-21340

Dynamic delamination fracture toughness of a graphite/epoxy laminate under impact

p 70 A88-29455

Modal attenuation in multilayered coated waveguides

p 126 A88-45755

Impact damage in composite laminates

p 74 N88-22402

Array trade-off study using multilayer parasitic subarrays

[NASA-TM-101321] p 121 N88-28222

LANDING

High speed propeller performance and noise predictions at takeoff/landing conditions

[AIAA PAPER 88-0264] p 215 A88-22193

High speed propeller performance and noise predictions at takeoff/landing conditions

[NASA-TM-100267] p 216 N88-13960

LANDING INSTRUMENTS

Cooperative synthesis of control and display augmentation for a STOL aircraft in the approach and landing task

[AIAA PAPER 88-4182] p 37 A88-50272

LANTHANUM COMPOUNDS

Effect of the microstructure on the thermoelectric properties of polycrystalline lanthanum chalcogenides

p 221 A88-40797

LAPLACE EQUATION

I-BIEM, an iterative boundary integral equation method for computer solutions of current distribution problems with complex boundaries: A new algorithm. I - Theoretical

p 205 A88-27795

LARGE SPACE STRUCTURES

Control considerations for high frequency, resonant, power processing equipment used in large systems

p 51 A88-11829

System architecture of MMIC-based large aperture arrays for space applications

p 45 A88-35274

LASER ANEMOMETERS

Laser anemometry techniques for turbine applications

[ASME PAPER 87-GT-241] p 157 A88-11129

Zoom lens compensator for a cylindrical window in laser anemometer uses

p 217 A88-17221

Four spot laser anemometer and optical access techniques for turbine applications

p 159 A88-36513

Measurements of natural circulation flow in a scale model PWR reactor system during postulated degraded core accidents using laser anemometry

p 159 A88-43917

3-D laser anemometer measurements in a labyrinth seal

[ASME PAPER 88-GT-63] p 169 A88-54195

3-D laser anemometer measurements in an annular seal

[ASME PAPER 88-GT-64] p 169 A88-54196

The four spot time-of-flight laser anemometer

p 164 N88-11145

A FORTRAN code for the calculation of probe volume geometry changes in a laser anemometry system caused by window refraction

[NASA-TM-100210] p 206 N88-12288

Optical measurement systems

p 218 N88-15796

LASER APPLICATIONS

Performance and operating envelope of imaging and scattering particle sizing instruments

[NASA-CR-180859] p 161 N88-12042

A laser communication experiment utilizing the ACT satellite and an airborne laser transceiver

[NASA-TM-100792] p 164 N88-18910

Optical measurements of soot and temperature profiles in premixed propane-oxygen flames

[NASA-TM-101343] p 115 N88-29997

Optical measurements of soot in premixed flames

[NASA-TM-101305] p 156 N88-30090

LASER BEAMS

Application of optical correlation techniques to particle imaging velocimetry

[NASA-TM-101306] p 163 N88-29152

LASER DAMAGE

New acousto-ultrasonic techniques applied to aerospace materials

[NASA-TM-101299] p 180 N88-28323

LASER DOPPLER VELOCIMETERS

Inter and intra blade row laser velocimetry studies of gas turbine compressor flows

[ASME PAPER 87-GT-235] p 2 A88-11126

The measurement of boundary layers on a compressor blade in cascade. I - A unique experimental facility

[ASME PAPER 87-GT-248] p 131 A88-11130

The measurement of boundary layers on a compressor blade in cascade. III - Pressure surface boundary layers and the near wake

[ASME PAPER 87-GT-250] p 132 A88-11132

Laser Doppler velocimeter measurement of annulus wall boundary layer development in a compressor rotor

[ASME PAPER 87-GT-251] p 132 A88-11133

Performance of laser Doppler velocimeter with polydisperse seed particles in high speed flows

[AIAA PAPER 88-0425] p 157 A88-22317

Unsteady motion and transition to turbulence in developing curved duct flow

p 140 A88-39010

Experimental verification of a secondary recirculation zone in a labyrinth seal

[AIAA PAPER 88-3692] p 168 A88-48971

A FORTRAN code for the calculation of probe volume geometry changes in a laser anemometry system caused by window refraction

[NASA-TM-100210] p 206 N88-12288

LASER INDUCED FLUORESCENCE

Feasibility of hydroxyl concentration measurements by laser-saturated fluorescence in high-pressure flames

p 77 A88-17218

LASER INTERFEROMETRY

Skin friction measurements by laser interferometry in swept shock wave/turbulent boundary-layer interactions

[AIAA PAPER 88-0497] p 5 A88-22364

LASER MICROSCOPY

Flaw characterization in structural ceramics using scanning laser acoustic microscopy

p 177 N88-22415

Nondestructive evaluation of sintered ceramics

p 177 N88-22416

LASER OUTPUTS

Comparison of UNL laser imaging and sizing system and a phase/Doppler system for analyzing sprays from a NASA nozzle

[NASA-CR-182437] p 150 N88-16956

LASER WINDOWS

The measurement of boundary layers on a compressor blade in cascade. I - A unique experimental facility

[ASME PAPER 87-GT-248] p 131 A88-11130

LATENT HEAT

Transient radiative cooling of a layer filled with solidifying drops

p 135 A88-20169

LATTICE PARAMETERS

Lattice parameter variations during aging in nickel-base superalloys

p 90 A88-51318

LATTICES (MATHEMATICS)

A microstructural lattice model for strain oriented problems: A combined Monte Carlo finite element technique

[NASA-TM-100215] p 90 N88-10939

LC CIRCUITS

Implementation of optimal trajectory control of series resonant converter

p 126 A88-38796

LEAD ALLOYS

Local convective flows in partly solidified alloys

p 219 A88-18467

Simulating the cooling of an immiscible alloy

p 83 A88-20199

Low cost Get-Away-Special (GAS) furnace

p 41 A88-28583

Channel formation in Pb-Sn, Pb-Sb, and Pb-Sn-Sb alloy ingots and comparison with the system NH₄Cl-H₂O

p 89 A88-46038

Fraction eutectic measurements in slowly cooled Pb - 15 wt percent Sn alloys

[NASA-CR-180830] p 94 N88-25531

LEAD CHLORIDES

Characterization of directionally solidified lead chloride

p 111 A88-43170

LEADING EDGE SWEEP

Large-Scale Advanced Prop-Fan (LAP)

[NASA-CR-182112] p 32 N88-20306

LEADING EDGES

The measurement of boundary layers on a compressor blade in cascade. II - Suction surface boundary layers

[ASME PAPER 87-GT-249] p 132 A88-11131

Electro-impulse de-icing electrodynamic solution by discrete elements

[AIAA PAPER 88-0018] p 17 A88-22016

A flow visualization study of the leading edge separation bubble on a NACA 0012 airfoil with simulated glaze ice

[NASA-CR-180846] p 10 N88-14966

Thermostructural analysis of simulated cowl lips

p 192 N88-22403

LEAKAGE

Reusable rocket engine optical condition monitoring

p 158 A88-29817

Theory versus experiment for the rotordynamic coefficients of labyrinth gas seals. II - A comparison to experiment

p 167 A88-31536

Experimental rotordynamic coefficient results for honeycomb seals

[NASA-CR-182440] p 172 N88-16007

LEAST SQUARES METHOD

Steady and transient least square solvers for thermal problems

p 134 A88-17318

LEVITATION MELTING

Ground based materials science experiments

p 43 A88-52364

LIFE (DURABILITY)

Progress toward life modeling of thermal barrier coatings for aircraft gas turbine engines

[ASME PAPER 87-ICE-18] p 96 A88-15120

Lightweight nickel electrode for nickel hydrogen cells and batteries

p 198 A88-16631

Assessment of commercially available and experimental hydrogen electrodes

p 198 A88-16632

Internal erosion rates of a 10-kW xenon ion thruster

[AIAA PAPER 88-2912] p 55 A88-48753

Solar dynamic concentrator durability in atomic oxygen and micrometeoroid environments

p 68 A88-51393

Life modeling of thermal barrier coatings for aircraft gas turbine engines

p 90 A88-54145

Life prediction and constitutive models for engine hot section anisotropic materials program

p 186 N88-11175

Lewis' enhanced laboratory for research into the fatigue and constitutive behavior of high temperature materials

p 186 N88-11177

Turbine airfoil deposition models and their hot corrosion implications

p 91 N88-11178

Effects of surface chemistry on hot corrosion life

p 91 N88-11180

Coating life prediction

p 170 N88-11181

Thermal barrier coating life prediction model

p 170 N88-11184

Thermal barrier coating life prediction model

p 171 N88-11185

A low-power arcjet cyclic lifetest

[NASA-TM-100233] p 57 N88-11748

A life test of a 22-Newton (5-lbf) hydrazine rocket

[NASA-TM-100232] p 57 N88-11750

Fiber composite structural durability and damage tolerance: Simplified predictive methods

[NASA-TM-100179] p 72 N88-13409

Life modeling of thermal barrier coatings for aircraft gas turbine engines

[NASA-TM-100283] p 92 N88-15060

Life prediction of thermomechanical fatigue using total strain version of strainrange partitioning (SRP): A proposal

[NASA-TP-2779] p 187 N88-15263

Life prediction technologies for aeronautical propulsion systems

p 27 N88-15788

Rotorcraft transmission

p 172 N88-15802

Aircraft engine hot section technology: An overview of the HOST Project

p 29 N88-15804

Creep and fatigue research efforts on advanced materials

p 187 N88-16701

Ceramics for engines

p 103 N88-16704

- Mechanics of composite materials: Past, present and future**
 [NASA-TM-100793] p 73 N88-17744
 In situ fatigue loading stage inside scanning electron microscope p 193 N88-22419
 Cumulative fatigue damage models p 193 N88-22422
 Life prediction modeling based on strainrange partitioning p 178 N88-22425
 Life prediction modeling based on cyclic damage accumulation p 178 N88-22426
 Fatigue damage modeling for coated single crystal superalloys p 93 N88-22427
 Life and reliability of rotating disks p 178 N88-22428
 Ceramics for turbine engines p 106 N88-23873
 Thermal cyclic durability testing of ceramic materials for turbine engines p 179 N88-23886
 Internal erosion rates of a 10-kW xenon ion thruster [NASA-TM-100954] p 63 N88-24688
 The relationship between observed fatigue damage and life estimation models p 196 N88-27611
 [NASA-CR-182191] p 107 N88-28142
 Thermal barrier coating life-prediction model development p 107 N88-28142
 Performance and lifetime assessment of MPD arc thruster technology [NASA-TM-101293] p 66 N88-29860
 Successful completion of a cyclic ground test of a mercury ion auxiliary propulsion system [NASA-TM-101351] p 67 N88-29873
- LIFT**
 Effect of acoustic excitation on the flow over a low-Re airfoil p 3 A88-14459
- LIGHT EMISSION**
 Loss-compensation of intensity-modulating fiber-optic sensors p 158 A88-22943
 Detection of radio-frequency modulated optical signals by two and three terminal microwave devices p 117 A88-50305
- LIGHT SCATTERING**
 Critical fluid light scattering p 158 A88-33003
- LIGHT SOURCES**
 Fiber optic sensing systems using high frequency resonant sensing heads with intensity sensors [NASA-TM-101318] p 163 N88-28293
- LINE SPECTRA**
 Low-temperature photoluminescence studies of chemical-vapor-deposition-grown 3C-SiC on Si p 127 A88-53396
- LINEAR ARRAYS**
 Radiation characteristics of microstrip arrays with parasitic elements p 121 A88-10481
- LINEAR QUADRATIC REGULATOR**
 The design of a turboshaft speed governor using modern control techniques [NASA-CR-175046] p 170 N88-10339
- LINEAR SYSTEMS**
 A semianalytical technique for sensitivity analysis of unsteady aerodynamic computations [NASA-TM-100810] p 189 N88-18976
 Improved finite strip Mindlin plate bending element using assumed shear strain distributions [NASA-TM-100928] p 196 N88-29195
- LINEARITY**
 Identification of differences between finite element analysis and experimental vibration data p 183 A88-46666
- LININGS**
 Turbine Engine Hot Section Technology, 1985 [NASA-CP-2405] p 185 N88-11140
 High-temperature combustor liner tests in structural component response test facility p 33 N88-22383
 Life assessment of combustor liner using unified constitutive models p 33 N88-22384
- LIQUID AIR CYCLE ENGINES**
 Auxiliary propulsion technology for advanced Earth-to-orbit vehicles [NASA-TM-100237] p 58 N88-14127
- LIQUID ATOMIZATION**
 Stability relationship for water droplet crystallization with the NASA Lewis icing spray nozzle [AIAA PAPER 88-0289] p 137 A88-22209
 Experimental and theoretical effects of nitrogen gas flow rate on liquid-jet atomization p 145 A88-52679
 Spray characteristics of a spill-return airblast atomizer [ASME PAPER 88-GT-7] p 145 A88-54154
 Stability relationship for water droplet crystallization with the NASA Lewis icing spray [NASA-TM-100220] p 24 N88-10790
 Effect of mass-velocity on liquid jet atomization in Mach 1 gasflow [NASA-TM-100813] p 162 N88-23194

LIQUID CRYSTALS

- Use of a liquid-crystal and heater-element composite for quantitative, high-resolution heat-transfer coefficients on a turbine airfoil including turbulence and surface-roughness effects p 156 A88-10969

LIQUID FLOW

- Development of a liquid-fed water resistojel [AIAA PAPER 88-3288] p 142 A88-48762
 Development of a liquid-fed water resistojel [NASA-TM-100927] p 174 N88-24968

LIQUID FUELS

- Modified reaction mechanism of aerated n-dodecane liquid flowing over heated metal tubes p 108 A88-44268

LIQUID HELIUM

- Preliminary study of niobium alloy contamination by transport through helium p 94 N88-24279

LIQUID HYDROGEN

- Vapor condensation rate at a turbulent liquid interface, for application to cryogenic hydrogen [AIAA PAPER 88-0559] p 137 A88-22419
 Design, development, and test of Shuttle/Centaur G-prime cryogenic tankage thermal protection systems p 47 A88-53182

LIQUID METALS

- Gravity and configurational energy induced microstructural changes in liquid phase sintering p 112 A88-49089
 Nucleate pool boiling: High gravity to reduced gravity; liquid metals to cryogenics p 113 N88-24464

LIQUID OXYGEN

- Design, development, and test of Shuttle/Centaur G-prime cryogenic tankage thermal protection systems p 47 A88-53182
 Seal technology for liquid oxygen (LOX) turbopumps [NASA-CR-174866] p 171 N88-13603

LIQUID PHASES

- A thermodynamic prediction for microporosity formation in aluminum-rich Al-Cu alloys p 82 A88-18886
 Simulating the cooling of an immiscible alloy p 83 A88-20199
 Gravitational contributions to microstructural coarsening in liquid phase sintering p 111 A88-37155
 Rapid solidification of highly undercooled liquids p 88 A88-41653
 Isothermal dendritic growth - A proposed microgravity experiment p 112 A88-49095

LIQUID PROPELLANT ROCKET ENGINES

- Space station resistojel system requirements and interface definition study [NASA-CR-180832] p 58 N88-12541
 Breadboard RL10-2B low-thrust operating mode (second iteration) test report [NASA-CR-182160] p 66 N88-29867
 Oxidizer heat exchanger component test [NASA-CR-182159] p 67 N88-29876

LIQUID ROCKET PROPELLANTS

- Space station resistojel system requirements and interface definition study [NASA-CR-180832] p 58 N88-12541
 Computational prediction of propellant reorientation p 109 N88-15940

LIQUID SLOSHING

- Computational prediction of propellant reorientation p 109 N88-15940

LIQUID WASTES

- Space station resistojel system requirements and interface definition study [NASA-CR-180832] p 58 N88-12541

LIQUID-SOLID INTERFACES

- Characterization of directionally solidified lead chloride p 111 A88-43170
 Effect of melt spinning on grain size and texture in Ni-Mo alloys p 89 A88-46030

LIQUID-VAPOR INTERFACES

- Vapor condensation rate at a turbulent liquid interface, for application to cryogenic hydrogen [AIAA PAPER 88-0559] p 137 A88-22419
 Vapor condensation on a turbulent liquid interface p 150 N88-15939

LIQUIDS

- Wear of iron and nickel in corrosive liquid environments p 88 A88-40790
 Experimental study of thermocapillary flows in a thin liquid layer with heat fluxes imposed on the free surface p 144 A88-49087
 Wear of iron and nickel in corrosive liquid environments [NASA-TM-100246] p 91 N88-11817
 Experimental study of thermocapillary flows in a thin liquid layer with heat fluxes imposed on the free surface [NASA-TM-100252] p 148 N88-12763
 The dc power control for a liquid-fed resistojel [NASA-TM-101326] p 67 N88-29869

LITHIUM

- Primordial lithium - New reaction rates, new abundances, new constraints p 226 A88-31145
 Radiation damage and defect behavior in proton irradiated lithium-counterdoped n+p silicon solar cells p 125 A88-34340

LOAD DISTRIBUTION (FORCES)

- An expert system for probabilistic description of loads on space propulsion system structural components [AIAA PAPER 88-2371] p 182 A88-32308
 Use of the generalized transmission error in the equations of motion of gear systems p 168 A88-49410
 Effect of stage loading on endwall flows in an axial flow compressor rotor [ASME PAPER 88-GT-111] p 145 A88-54229

LOAD TESTS

- Deformation, fatigue and fracture behavior of two cast anisotropic superalloys p 187 N88-13732
 Experiments investigating advanced materials under thermomechanical loading p 191 N88-22385
 MHOST: An efficient finite element program for inelastic analysis of solids and structures p 33 N88-22394

LOADING RATE

- Hygrothermomechanical fiber composite fatigue - Computational simulation p 71 A88-42437
 Analysis of crack propagation in roller bearings using the boundary integral equation method - A mixed-mode loading problem p 168 A88-49183

LOADS (FORCES)

- Analysis of shell-type structures subjected to time-dependent mechanical and thermal loading [NASA-CR-181409] p 185 N88-10388
 Design procedures for fiber composite box beams [NASA-TM-100296] p 73 N88-16828
 Analysis of shell-type structures subjected to time-dependent mechanical and thermal loading [NASA-CR-182705] p 189 N88-20668
 Fatigue crack growth behavior of a single crystal alloy as observed through an in situ fatigue loading stage [NASA-TM-100863] p 93 N88-22986

LOCAL AREA NETWORKS

- Lewis Information Network (LINK): Background and overview [NASA-TM-100162] p 117 N88-11925

LONGERONS

- Master material test program (MAMATEP) --- for Solar Array Assembly of Space Station Photovoltaic Power Module [AIAA PAPER 88-2475] p 70 A88-35945

LONGITUDE

- A satellite system synthesis model for orbital arc allotment optimization p 117 A88-48579

LOSS OF COOLANT

- Measurements of natural circulation flow in a scale model PWR reactor system during postulated degraded core accidents using laser anemometry p 159 A88-43917

LOSSES

- Blade loss transient dynamics analysis, volume 1. Task 2: TETRA 2 theoretical development [NASA-CR-179632] p 25 N88-10791
 Blade loss transient dynamics analysis, volume 2. Task 2: TETRA 2 user's manual [NASA-CR-179633] p 25 N88-10792

LOSSY MEDIA

- A simple circular-polarized antenna: Circular waveguide horn coated with lossy magnetic material p 116 A88-36648
 Measurement of the properties of lossy materials inside a finite conducting cylinder [NASA-CR-182664] p 213 N88-20962

LOW GRAVITY MANUFACTURING

- Gravitational macrosegregation in binary Pb-Sn alloy ingots p 111 A88-41211
 Gravity and configurational energy induced microstructural changes in liquid phase sintering p 112 A88-49089
 Preparation for microgravity: The role of the microgravity materials science laboratory [NASA-TM-100906] p 113 N88-24811

LOW REYNOLDS NUMBER

- Transition and separation control on a low-Reynolds number airfoil p 2 A88-11186
 Effect of acoustic excitation on the flow over a low-Re airfoil p 3 A88-14459
 Low Reynolds number modeling of turbulent flows with and without wall transpiration p 136 A88-21983
 Two-equation low-Reynolds-number turbulence modeling of transitional boundary layer flows characteristic of gas turbine blades [NASA-CR-4145] p 153 N88-23185

LOW SPEED

- Gravitationally defined velocities for a low speed hot-wire calibration p 133 A88-14170

LOW SPEED WIND TUNNELS

Summary of low-speed wind tunnel results of several high-speed counterrotation propeller configurations [AIAA PAPER 88-3149] p 7 A88-48758

Summary of low-speed wind tunnel results of several high-speed counterrotation propeller configurations [NASA-TM-100945] p 13 N88-24597

LOW THRUST

Breadboard RL10-2B low-thrust operating mode (second iteration) test report [NASA-CR-182160] p 66 N88-29867

LOW THRUST PROPULSION

Recent advances in low-thrust propulsion technology [AIAA PAPER 88-3283] p 55 A88-48761

Low thrust power-limited transfer for a pole squatter [AIAA PAPER 88-4310] p 42 A88-50435

Recent advances in low-thrust propulsion technology [NASA-TM-100959] p 213 N88-25260

LUBRICANTS

A model for the influence of pressure on the bulk modulus and the influence of temperature on the solidification pressure for liquid lubricants [ASME PAPER 86-TRIB-63] p 133 A88-15124

Improved perfluoroalkylether fluid development [NASA-CR-180872] p 80 N88-15851

On the performance of finite journal bearings lubricated with micropolar fluids [NASA-TM-100293] p 150 N88-15983

Technology developments for a compound cycle engine p 30 N88-16637

Tribological properties of alumina-boria-silicate fabric from 25 to 850 C [NASA-TM-100806] p 104 N88-18726

LUBRICATING OILS

Oil film thickness measurement and analysis for an angular contact ball bearing operating in parched elastohydrodynamic lubrication p 165 A88-14115

Shear rheological characterization of motor oils p 100 A88-47562

Parched elasto hydrodynamic lubrication film thickness measurement in an instrument ball bearing [STLE PREPRINT 88-AM-6G-1] p 169 A88-51082

Foil bearing lubrication theory including compressibility effects p 170 A88-54964

LUBRICATION

Piezoviscous effects in nonconformal contacts lubricated hydrodynamically p 133 A88-12926

Stability of a rigid rotor supported on flexible oil journal bearings [ASME PAPER 87-TRIB-48] p 166 A88-24034

Improved oil-off survivability of tapered roller bearings [NASA-CR-180804] p 170 N88-11135

Status and directions of modified tribological surfaces by ion processes [NASA-TM-101304] p 115 N88-28176

LUMINOUS INTENSITY

Fiber optic sensing systems using high frequency resonant sensing heads with intensity sensors [NASA-TM-101318] p 163 N88-28293

LUNAR BASES

Electromagnetic powered vehicles (EMPV) for Mars exploration p 62 N88-24388

Advanced photovoltaic power system technology for lunar base applications [NASA-TM-100965] p 65 N88-26402

M

MACH NUMBER

Centerline Mach number characteristics of highly heated free jets [AIAA PAPER 88-3612] p 7 A88-48898

A numerical investigation of the influence of heating on the excitation of high and low Mach number jet flows [ASME PAPER 87-WA/NCA-13] p 144 A88-51343

A preliminary design study of supersonic through-flow fan inlets [AIAA PAPER 88-3075] p 23 A88-53137

MACHINE TOOLS

Determination of settings of a tilted head-cutter for generation of hypoid and spiral bevel gears [NASA-CR-182138] p 174 N88-24976

MACHINING

Spur gears: Optimal geometry, methods for generation and Tooth Contact Analysis (TCA) program [NASA-CR-4135] p 173 N88-23216

MAGNESIUM OXIDES

Sol-gel synthesis of magnesium oxide-silicon dioxide glass compositions p 100 A88-49105

MAGNETIC BEARINGS

Vibration and control of flexible rotor supported by magnetic bearings [NASA-TM-100888] p 174 N88-23977

MAGNETIC FIELDS

Computer-aided modeling and prediction of performance of the modified Lundell class of alternators in space station solar dynamic power systems [NASA-CR-182538] p 201 N88-19000

Solving time-dependent two-dimensional eddy current problems [NASA-TM-100875] p 211 N88-25239

The effects of magnetic nozzle configurations on plasma thrusters [NASA-CR-183096] p 219 N88-26223

Application of superconducting technology to earth-to-orbit electromagnetic launch systems [NASA-TM-101134] p 43 N88-26385

MAGNETIC FLUX

Magnetic emissions testing of the space station engineering model resistojet [NASA-TM-100788] p 48 N88-17728

MAGNETIC MATERIALS

A simple circular-polarized antenna: Circular waveguide horn coated with lossy magnetic material p 116 A88-36648

MAGNETIC PROPERTIES

A simple circular-polarized antenna: Circular waveguide horn coated with lossy magnetic material p 116 A88-36648

MAGNETO-OPTICS

Real time optical correlator using a magneto optic device applied to particle imaging velocimetry p 159 A88-40700

MAGNETOHYDRODYNAMIC FLOW

Magnetic fields interacting with nonlinear compressible convection p 226 A88-31163

MAGNETOPLASMA DYNAMICS

The effects of magnetic nozzle configurations on plasma thrusters [NASA-CR-183096] p 219 N88-26223

Performance and lifetime assessment of MPD arc thruster technology [NASA-TM-101293] p 66 N88-29860

MAGNETRON SPUTTERING

Deposition of vanadium oxide films by direct-current magnetron reactive sputtering p 221 A88-51286

MAINTAINABILITY

Improved maintainability of space-based reusable rocket engines [AIAA PAPER 88-3113] p 55 A88-48037

MAINTENANCE

Space station assembly/servicing capabilities p 48 N88-10100

Rotorcraft transmission p 172 N88-15802

MAN-COMPUTER INTERFACE

Interactive computer simulation of fracture processes p 180 A88-16955

MANAGEMENT METHODS

Weight savings in aerospace vehicles through propellant scavenging [NASA-TM-100900] p 44 N88-25470

MANAGEMENT PLANNING

The challenges and opportunities of supersonic transport propulsion technology [AIAA PAPER 88-2985] p 23 A88-48032

An allotment planning concept and related computer software for planning the fixed satellite service at the 1988 space WARC [NASA-TM-100244] p 117 N88-11944

The challenges and opportunities of supersonic transport propulsion technology [NASA-TM-100921] p 34 N88-23806

MANIPULATORS

Redundant manipulators for momentum compensation in a micro-gravity environment [AIAA PAPER 88-4121] p 204 A88-50223

Base reaction optimization of manipulators with redundant kinematics p 173 N88-23238

Microgravity manipulator demonstration p 173 N88-23242

Accurate positioning of long, flexible ARM's (Articulated Robotic Manipulator) p 174 N88-23243

MANUFACTURING

Elevated temperature strain gages p 160 N88-11144

MAPPING

An experimental mapping of the flow field behind a glaze ice shape on a NACA 0012 airfoil [NASA-CR-180847] p 10 N88-15766

Fatigue damage mapping p 193 N88-22423

MARS (PLANET)

An evolutionary communications scenario for Mars exploration [NASA-TM-100263] p 118 N88-13515

Electromagnetic powered vehicles (EMPV) for Mars exploration p 62 N88-24388

MARS LANDING

Energy storage considerations for a robotic Mars surface sampler [NASA-TM-100969] p 227 N88-28853

MARS SURFACE

An evolutionary communications scenario for Mars exploration [NASA-TM-100263] p 118 N88-13515

MASKING

Temperature stability of Al(x)Ga(1-x)As (x = 0-1) thermal oxide masks for selective-area epitaxy p 221 A88-45858

MASS

Impact of thermal energy storage properties on solar dynamic space power conversion system mass p 51 A88-11805

Effect of mass-velocity on liquid jet atomization in Mach 1 gasflow [NASA-TM-100813] p 162 N88-23194

MASS FLOW

Combustion characteristics of gas turbine alternative fuels [NASA-TM-100247] p 25 N88-13338

MASS TRANSFER

Effect of rib angle on local heat/mass transfer distribution in a two-pass rib-roughened channel [ASME PAPER 87-GT-94] p 131 A88-11033

Mass transport phenomena between bubbles and dissolved gases in liquids under reduced gravity conditions [AIAA PAPER 88-0450] p 138 A88-27719

Local heat/mass transfer distributions around sharp 180 deg turns in two-pass smooth and rib-roughened channels [ASME PAPER 86-GT-114] p 139 A88-28516

Experiments for the determination of convective diffusion heat/mass transfer to burner rig test targets comparable in size to jet stream diameter p 140 A88-41574

Local heat/mass transfer and pressure drop in a two-pass rib-roughened channel for turbine airfoil cooling [NASA-CR-179635] p 148 N88-12039

Mass transport phenomena between bubbles and dissolved gases in liquids under reduced gravity conditions [NASA-TM-100273] p 80 N88-18672

MATERIALS SCIENCE

Preparation for microgravity - The role of the Microgravity Material Science Laboratory [AIAA PAPER 88-3510] p 111 A88-42908

Ground-based microgravity materials science research at NASA's Microgravity Materials Science Laboratory p 112 A88-49090

Ground based materials science experiments p 43 A88-52364

MATERIALS TESTS

Thermostructural analysis with experimental verification in a high heat flux facility of a simulated cowl lip [AIAA PAPER 88-2222] p 39 A88-32188

MATHEMATICAL MODELS

Turbulence modeling and surface heat transfer in a stagnation flow region p 141 A88-43871

Particle-laden weakly swirling free jets - Measurements and predictions [AIAA PAPER 88-3138] p 142 A88-48757

Thermodynamic modeling of the no-vent fill methodology for transferring cryogenics in low gravity [AIAA PAPER 88-3403] p 55 A88-48765

Fatigue life prediction modeling for turbine hot section materials p 184 A88-54144

Analysis of shell-type structures subjected to time-dependent mechanical and thermal loading [NASA-CR-181409] p 185 N88-10388

Turbine Engine Hot Section Technology, 1985 [NASA-CR-2405] p 185 N88-11140

Aerothermal modeling program, phase 2 p 146 N88-11149

Constitutive modeling for single crystal superalloys p 90 N88-11168

Life prediction and constitutive models for engine hot section anisotropic materials program p 186 N88-11175

Coating life prediction p 170 N88-11181

Thermal barrier coating life prediction model development p 170 N88-11184

Thermal barrier coating life prediction model development p 171 N88-11185

A hybrid numerical technique for predicting the aerodynamic and acoustic fields of advanced turboprops [NASA-CR-174926] p 216 N88-12352

An analytical and experimental study of injection-locked two-port oscillators [NASA-TM-100119] p 128 N88-12727

Creep life prediction based on stochastic model of microstructurally short crack growth [NASA-TM-100245] p 186 N88-12825

SHARP simulation of discontinuities in highly convective steady flow
[NASA-TM-100240] p 210 N88-13931

Fatigue life prediction modeling for turbine hot section materials
[NASA-TM-100291] p 187 N88-14453

Rotorcraft transmission
[NASA-TM-100291] p 172 N88-15802

Communications satellite systems operations with the space station. Volume 3: Supplementary technical report
[NASA-CR-180875] p 48 N88-16794

Numerical modeling of multidimensional flow in seals and bearings used in rotating machinery
[NASA-TM-100779] p 150 N88-16988

Numerical and analytical study of fluid dynamic forces in seals and bearings
[NASA-TM-100268] p 151 N88-18867

Computer-aided modeling and prediction of performance of the modified Lundell class of alternators in space station solar dynamic power systems
[NASA-CR-182538] p 201 N88-19000

Spacecraft dielectric surface charging property determination
[NASA-CR-180879] p 49 N88-21243

Finite area combustor theoretical rocket performance
[NASA-TM-100785] p 60 N88-21252

Nonlinear Constitutive Relations for High Temperature Applications, 1986
[NASA-CP-10010] p 189 N88-21498

A theory of viscoplasticity accounting for internal damage
p 190 N88-21508

A constitutive model with damage for high temperature superalloys
p 93 N88-21510

Unified constitutive models for high-temperature structural applications
p 190 N88-21523

A constitutive model for an overlay coating
p 105 N88-21525

Non-isothermal elastoviscoplastic analysis of planar curved beams
p 190 N88-21526

Life assessment of combustor liner using unified constitutive models
p 33 N88-22384

Biaxial experiments supporting the development of constitutive theories for advanced high-temperature materials
p 191 N88-22386

Unified constitutive model development for metal matrix composites at high temperature
p 74 N88-22387

Unified constitutive model for single crystal deformation behavior with applications
p 191 N88-22388

Finite element (MARC) solution technologies for viscoplastic analyses
p 191 N88-22389

Continuous fiber ceramic matrix composites for heat engine components
p 106 N88-22411

Cumulative fatigue damage models
p 193 N88-22422

Life prediction modeling based on strainrange partitioning
p 178 N88-22425

Fatigue damage modeling for coated single crystal superalloys
p 93 N88-22427

Review and assessment of the HOST turbine heat transfer program
p 34 N88-22431

Two-equation low-Reynolds-number turbulence modeling of transitional boundary layer flows characteristic of gas turbine blades
[NASA-CR-4145] p 153 N88-23185

Aeroelastic forced response analysis of turbomachinery
p 34 N88-23247

Method and models for R-curve instability calculations
[NASA-TM-100935] p 194 N88-23278

Parameter identification methods for improving structural dynamic models
[NASA-TM-100812] p 194 N88-23994

Particle-laden weakly swirling free jets: Measurements and predictions
[NASA-TM-100920] p 34 N88-24639

Thermodynamic modeling of the no-vent fill methodology for transferring cryogens in low gravity
[NASA-TM-100932] p 63 N88-24686

Thermal barrier coating life-prediction model development
[NASA-CR-179507] p 107 N88-28142

Transition mixing study empirical model report
[NASA-CR-182139] p 155 N88-30076

MATHEMATICAL TABLES

Implementation of a fast digital optical matrix-vector multiplier using a holographic look-up table and residue arithmetic
p 205 N88-17223

MATRICES (MATHEMATICS)

A hypermatrix formulation for subspace iteration
p 205 N88-15427

Implementation of a digital optical matrix-vector multiplier using a holographic look-up table and residue arithmetic
[NASA-CR-180431] p 205 N88-10496

A diagonally inverted LU implicit multigrid scheme
[NASA-TM-100911] p 13 N88-26340

MATRIX MATERIALS

High temperature polymer matrix composites
p 70 A88-36775

MATRIX THEORY

Derivatives of eigenvalues and eigenvectors of a general complex matrix
p 209 A88-29269

MEASURING INSTRUMENTS

Advanced high temperature instrumentation for hot section research applications
p 159 A88-54139

Further development of the dynamic gas temperature measurement system
p 160 N88-11141

Recent advances in high temperature instrumentation for hot section applications
[NASA-TM-100282] p 161 N88-14339

Aeropropulsion '87. Session 4: Instrumentation and Controls Research
[NASA-CP-10003-SESS-4] p 28 N88-15794

Research sensors
p 161 N88-15795

Development of a torsion balance for adhesion measurements
[NASA-TM-100799] p 104 N88-20454

Research sensors
p 162 N88-22430

MECHANICAL DRIVES

Advanced transmission studies
[NASA-TM-100867] p 173 N88-21454

MECHANICAL ENGINEERING

Finite element methods in probabilistic mechanics
p 212 A88-29060

MECHANICAL PROPERTIES

Ceramic matrix and resin matrix composites - A comparison
p 69 A88-13158

PMR polyimide compositions for improved performance at 371 C
p 96 A88-13172

Ultrasonic nondestructive evaluation, microstructure, and fracture toughness interrelations
p 176 A88-18158

Ion beam deposition of amorphous carbon films with diamond like properties
p 97 A88-20300

Ultrasonic evaluation of mechanical properties of thick, multilayered, filament-wound composites
p 176 A88-21340

Strength characterization of yttria/alumina-doped sintered silicon nitride
p 97 A88-26154

Mechanical strength and tribological behavior of ion-beam-deposited boron nitride films on non-metallic substrates
p 98 A88-32866

Microstructure-property relationships in directionally solidified single-crystal nickel-base superalloys
p 88 A88-40329

Boron nitride - Composition, optical properties, and mechanical behavior
p 99 A88-40794

Characterization of aluminum/RP-1 gel propellant properties
[AIAA PAPER 88-2821] p 109 A88-48751

Linear and nonlinear mechanical properties of a series of epoxy resins
p 101 A88-54976

Mechanical properties characterization of composite sandwich materials intended for space antenna applications
[NASA-TM-88893] p 71 N88-10121

Elevated temperature strain gages
p 160 N88-11144

High temperature polymer matrix composites
p 73 N88-16700

Correlations of norbornenyl crosslinked polyimide resin structures with resin thermo-oxidative stability, resin glass transition temperature and composite initial mechanical properties
[NASA-TM-100791] p 103 N88-16877

Mechanics of composite materials: Past, present and future
[NASA-TM-100793] p 73 N88-17744

Adhesion, friction and micromechanical properties of ceramics
[NASA-TM-100782] p 104 N88-17801

Analysis of shell-type structures subjected to time-dependent mechanical and thermal loading
[NASA-CR-182705] p 189 N88-20668

Hafnia-rich mixed oxide ceramics of the system HfO₂-ZrO₂-TiO₂ for heaters and heat exchangers in electrothermal thrusters: The effects of titania on selected electrical and mechanical properties of Hafnia-rich mixed oxides in the system Hafnia-Zirconia-Titania, volume 1
[NASA-CR-182800-VOL-1] p 105 N88-22197

Features and applications of the integrated composites analyzer (ICAN) code
p 74 N88-22391

Improved silicon carbide for advanced heat engines
p 106 N88-23879

Improved processing of Si₃N₄
p 107 N88-23882

Colloidal characterization of silicon nitride and silicon carbide
p 107 N88-23883

SiC fiber analysis
p 107 N88-23891

Characterization of aluminum/RP-1 gel propellant properties
[NASA-TM-100951] p 109 N88-24808

MELT SPINNING

Crystallization behavior of a melt-spun Fe-Ni based steel
p 83 A88-19958

Undercooled and rapidly quenched Ni-Mo alloys
p 83 A88-19960

The microstructure and tensile properties of extruded melt-spun ribbons of iron-rich B2 FeAl
p 85 A88-31679

On producing an alloy of uniform composition during rapid solidification processing
p 89 A88-41654

Primary arm spacing in chill block melt spun Ni-Mo alloys
p 89 A88-41655

Effect of melt spinning on grain size and texture in Ni-Mo alloys
p 89 A88-46030

MELTING POINTS

Preparation of multistage zone-refined materials for thermochemical standards
p 111 A88-43172

MELTS (CRYSTAL GROWTH)

Dendritic growth in a supercooled alloy melt
p 83 A88-19966

Solidification under microgravity conditions - Dendritic growth
[AAS PAPER 86-380] p 110 A88-35130

Growth of needle-shaped crystals in the presence of convection
p 111 A88-37715

Rapid solidification of highly undercooled liquids
p 88 A88-41653

Isothermal dendritic growth - A proposed microgravity experiment
p 112 A88-49095

MEMORY (COMPUTERS)

Gigard-tolerant power switches and memory elements
p 123 A88-22704

Hypercluster - Parallel processing for computational mechanics
p 208 A88-40458

MERCURY ION ENGINES

Auxiliary propulsion system flight package
[NASA-CR-180828] p 56 N88-10886

Successful completion of a cyclic ground test of a mercury ion auxiliary propulsion system
[NASA-TM-101351] p 67 N88-29873

MESH

Fatigue failure of regenerator screens in a high frequency Stirling engine
p 179 N88-24491

METAL COATINGS

The effects of atmosphere on the tribological properties of a chromium carbide based coating for use to 760 C
p 98 A88-32372

METAL CRYSTALS

Crystallization behavior of a melt-spun Fe-Ni based steel
p 83 A88-19958

Dendritic solidification under microgravity conditions
[AIAA PAPER 88-0248] p 110 A88-22186

Solidification under microgravity conditions - Dendritic growth
[AAS PAPER 86-380] p 110 A88-35130

A crystallographic model for nickel base single crystal alloys
p 89 A88-48182

Isothermal dendritic growth - A proposed microgravity experiment
p 112 A88-49095

METAL FATIGUE

Surface fatigue and failure characteristics of hot-forged powder metal AISI 4620, AISI 4640, and machined AISI 4340 steel spur gears
p 165 A88-14591

Transient rotor dynamic rub phenomena - Theory and test
p 167 A88-31539

Low cycle fatigue
[ASTM STP-942] p 86 A88-35901

A nonlinear history-dependent damage model for low cycle fatigue
p 86 A88-35905

Bithermal fatigue - A link between isothermal and thermomechanical fatigue
p 87 A88-35918

Effect of temperature, microstructure, and stress state on the low cycle fatigue behavior of Waspaloy
p 87 A88-35922

Accelerated crack growth rate at low Delta K in a single crystal superalloy
p 89 A88-47687

Fatigue life prediction modeling for turbine hot section materials
p 184 A88-54144

Turbine Engine Hot Section Technology, 1985
[NASA-CP-2405] p 185 N88-11140

Constitutive modeling for single crystal superalloys
p 90 N88-11168

Deformation, fatigue and fracture behavior of two cast anisotropic superalloys
p 187 N88-13732

Fatigue life prediction modeling for turbine hot section materials
[NASA-TM-100291] p 187 N88-14453

Lewis Structures Technology, 1988. Volume 3: Structural Integrity Fatigue and Fracture Wind Turbines HOST
[NASA-CP-3003-VOL-3] p 192 N88-22408

Life prediction modeling based on cyclic damage accumulation
p 178 N88-22426

Fatigue damage modeling for coated single crystal superalloys
p 93 N88-22427

- Isothermal and bithermal thermomechanical fatigue behavior of a NiCoCrAlY-coated single crystal superalloy [NASA-TM-100907] p 94 N88-24766
- Cyclic fatigue damage characteristics observed for simple loadings extended to multiaxial life prediction [NASA-CR-182126] p 195 N88-25016
- Characterization of fatigue crack initiation and propagation in Ti-6Al-4V with electrical potential drop technique [NASA-TM-100877] p 195 N88-25937
- METAL FIBERS**
- Thermal cycling of tungsten-fibre-reinforced superalloy composites p 70 A88-31770
- Composite monolayer fabrication by an arc-spray process p 169 A88-53581
- METAL FILMS**
- Thermal desorption study of physical forces at the PTFE surface p 77 A88-10963
- Composite monolayer fabrication by an arc-spray process p 169 A88-53581
- Status and directions of modified tribological surfaces by ion processes [NASA-TM-101304] p 115 N88-28176
- METAL FLUORIDES**
- Identification of salt-alloy combinations for thermal energy storage applications in advanced solar dynamic power systems p 199 A88-24072
- Effect of fluoride doping on the transition temperature of $\text{YBa}_2\text{Cu}_3\text{O}_{7-x}$ (6.5 + delta) p 220 A88-29297
- METAL FOILS**
- A heater made from graphite composite material for potential deicing application p 17 A88-15724
- METAL MATRIX COMPOSITES**
- SiC reinforced aluminide composites p 70 A88-31687
- Superelement methods applications to micromechanics of high temperature metal matrix composites [AIAA PAPER 88-2390] p 182 A88-32322
- High temperature metal matrix composites for future aerospace systems p 71 A88-44745
- [AIAA PAPER 88-3059] p 71 A88-44745
- Composite monolayer fabrication by an arc-spray process p 169 A88-53581
- High temperature metal matrix composites for future aerospace systems p 90 N88-10938
- [NASA-TM-100212] p 90 N88-10938
- Aeropropulsion '87. Session 1: Aeropropulsion Materials Research [NASA-CP-10003-SESS-1] p 31 N88-16697
- Development of a new generation of high-temperature composite materials p 73 N88-16702
- Creep behavior of tungsten/niobium and tungsten/niobium-1 percent zirconium composites [NASA-TM-100804] p 92 N88-18707
- Unified constitutive model development for metal matrix composites at high temperature p 74 N88-22387
- METCAN: The metal matrix composite analyzer p 74 N88-22395
- Fracture resistance of a TiB₂ particle/SiC matrix composite at elevated temperature [NASA-TM-100967] p 107 N88-26482
- Refractory metal alloys and composites for space power systems [NASA-TM-100946] p 95 N88-27310
- Investigation of a SiC/Ti-24Al-11Nb composite [NASA-TM-100956] p 76 N88-28980
- METAL OXIDES**
- The microstructure and tensile properties of extruded melt-spun ribbons of iron-rich B2 FeAl p 85 A88-31679
- Slip casting and extruding shapes of rhenium with metal oxide additives. Part 2: Development of grain stabilized rhenium parts for resistojets [NASA-CR-180851] p 57 N88-11749
- METAL POLISHING**
- Adherent Al₂O₃ scales produced on undoped NiCrAl alloys p 85 A88-30269
- METAL POWDER**
- Improved silicon nitride for advanced heat engines [NASA-CR-175006] p 102 N88-15886
- METAL PROPELLANTS**
- Characterization of aluminum/RP-1 gel propellant properties [AIAA PAPER 88-2821] p 109 A88-48751
- Characterization of aluminum/RP-1 gel propellant properties [NASA-TM-100951] p 109 N88-24808
- METAL SURFACES**
- Modified reaction mechanism of aerated n-dodecane liquid flowing over heated metal tubes p 108 A88-44268
- Ion-beam nitriding of steels [NASA-CASE-LEW-14104-2] p 91 N88-14179
- METAL VAPOR LASERS**
- Engine flow visualization using a copper vapor laser p 158 A88-34479
- METALLOGRAPHY**
- Determination of grain-size distribution function using two-dimensional Fourier transforms of tone-pulse-encoded images p 176 A88-30425
- As-received microstructure of a SiC/Ti-15-3 composite [NASA-TM-100938] p 76 N88-28095
- METALS**
- Calculation of thermomechanical fatigue life based on isothermal behavior p 181 A88-26450
- Universality relationships in condensed matter - Bulk modulus and sound velocity p 213 A88-43950
- Analysis of shell-type structures subjected to time-dependent mechanical and thermal loading [NASA-CR-181409] p 185 N88-10388
- Life prediction of thermomechanical fatigue using total strain version of strainrange partitioning (SRP): A proposal [NASA-TP-2779] p 187 N88-15263
- Friction and wear of ceramics p 106 N88-23874
- Noncontact temperature measurement: Requirements and applications for metals and alloys research p 112 N88-23899
- Arc-textured metal surfaces for high thermal emittance space radiators [NASA-TM-100894] p 94 N88-24754
- METEORITIC DAMAGE**
- The effect of the near earth micrometeoroid environment on a highly reflective mirror surface [NASA-TM-101307] p 44 N88-29833
- METEOROID HAZARDS**
- Assessment of the effects of space debris and meteoroids environment on the space station solar array assembly [NASA-TM-101315] p 49 N88-28959
- METEOROID PROTECTION**
- Solar dynamic concentrator durability in atomic oxygen and micrometeoroid environments p 68 A88-51393
- METHOD OF CHARACTERISTICS**
- Analysis and optimization of truncated scarf nozzles subject to external flow conditions [NASA-TM-100955] p 14 N88-29746
- METHODOLOGY**
- Structural analysis methods development for turbine hot section components p 184 A88-54142
- Structural analysis methods development for turbine hot section components [NASA-TM-100298] p 188 N88-18967
- METHYL POLYSILOXANE**
- Silsesquioxanes as precursors to ceramic composites p 69 A88-12599
- METROLOGY**
- Development and applications of optical interferometric micrometrology in the angstrom and subangstrom range [NASA-TM-100299] p 162 N88-23196
- MICROCRACKS**
- Macrocrack interaction with transverse array of microcracks p 181 A88-30236
- Semi-empirical crack tip analysis p 183 A88-47681
- Transply crack density detection by acousto-ultrasonics [NASA-TM-100224] p 72 N88-11758
- MICROGRAVITY APPLICATIONS**
- Droplet vaporization in a supercritical microgravity environment [IAF PAPER 87-384] p 134 A88-16055
- Isothermal dendritic growth - A low gravity experiment p 110 A88-28556
- Solidification of undercooled Ni-Sn eutectic alloy under microgravity conditions in the Space Shuttle p 110 A88-28557
- Gas liquid flow at microgravity conditions - Flow patterns and their transitions p 141 A88-42839
- Preparation for microgravity - The role of the Microgravity Material Science Laboratory [AIAA PAPER 88-3510] p 111 A88-42908
- Containment of a silicone fluid free surface in reduced gravity p 112 A88-49085
- Ground-based microgravity materials science research at NASA's Microgravity Materials Science Laboratory p 112 A88-49090
- Redundant manipulators for momentum compensation in a micro-gravity environment [AIAA PAPER 88-4121] p 204 A88-50223
- Ground based materials science experiments p 43 A88-52364
- MICROMECHANICS**
- Probabilistic composite micromechanics [AIAA PAPER 88-2375] p 182 A88-32312
- Superelement methods applications to micromechanics of high temperature metal matrix composites [AIAA PAPER 88-2390] p 182 A88-32322
- Anisotropic constitutive modeling for nickel base single crystal superalloys using a crystallographic approach [AIAA PAPER 88-2440] p 85 A88-32357
- Mechanics of composite materials: Past, present and future [NASA-TM-100793] p 73 N88-17744
- Adhesion, friction and micromechanical properties of ceramics [NASA-TM-100782] p 104 N88-17801
- Whisker-reinforced ceramic composites for heat engine components p 105 N88-22410
- MICROMETEORIODS**
- Assessment of the effects of space debris and meteoroids environment on the space station solar array assembly [NASA-TM-101315] p 49 N88-28959
- The effect of the near earth micrometeoroid environment on a highly reflective mirror surface [NASA-TM-101307] p 44 N88-29833
- MICROPOLAR FLUIDS**
- On the performance of finite journal bearings lubricated with micropolar fluids [NASA-TM-100293] p 150 N88-15983
- MICROPOROSITY**
- A thermodynamic prediction for microporosity formation in aluminum-rich Al-Cu alloys p 82 A88-18886
- MICROPROCESSORS**
- A microprocessor-based real-time simulator of a turbofan engine [NASA-TM-100889] p 32 N88-21163
- MICROSCOPY**
- Microscopy of epitaxially grown beta-SiC on 001-plane silicon p 98 A88-31023
- MICROSTRIP ANTENNAS**
- Radiation characteristics of microstrip arrays with parasitic elements p 121 A88-10481
- Characteristics of a two-layer electromagnetically coupled rectangular patch antenna p 115 A88-14100
- Slotline fed microstrip antenna array modules p 126 A88-44170
- Crosspolarisation characteristics of rectangular patch antennas p 117 A88-47705
- Absolute gain measurement of microstrip antennas under mismatched conditions p 117 A88-47949
- Gain enhancement of microstrip antennas with overlaying parasitic directors p 117 A88-46653
- Array trade-off study using multilayer parasitic subarrays [NASA-TM-101321] p 121 N88-28222
- MICROSTRIP TRANSMISSION LINES**
- Radiation characteristics of microstrip arrays with parasitic elements p 121 A88-10481
- A new model for broadband waveguide-to-microstrip transition design p 126 A88-38822
- Slotline fed microstrip antenna array modules p 126 A88-44170
- MICROSTRUCTURE**
- Ultrasonic nondestructive evaluation, microstructure, and fracture toughness interrelations p 176 A88-18158
- Weak-field magnetization of superconducting $\text{YBa}_2\text{Cu}_3\text{O}_{7-x}$ - Relationship to microstructure p 219 A88-18814
- Thermal aging effects in refractory metal alloys p 84 A88-22700
- Interdiffusion in Ni-rich, Ni-Cr-Al alloys at 1100 and 1200 C. I - Diffusion paths and microstructures. II - Diffusion coefficients and predicted concentration profiles p 84 A88-24485
- Determination of grain-size distribution function using two-dimensional Fourier transforms of tone-pulse-encoded images p 176 A88-30425
- The microstructure and tensile properties of extruded melt-spun ribbons of iron-rich B2 FeAl p 85 A88-31679
- Effect of temperature, microstructure, and stress state on the low cycle fatigue behavior of Waspaloy p 87 A88-35922
- Gravitational contributions to microstructural coarsening in liquid phase sintering p 111 A88-37155
- Microstructure-property relationships in directionally solidified single-crystal nickel-base superalloys p 88 A88-40329
- Alloy chemistry and microstructural control to meet the demands of the automotive Stirling engine p 88 A88-40332
- Boron nitride - Composition, optical properties, and mechanical behavior p 99 A88-40794
- Effect of the microstructure on the thermoelectric properties of polycrystalline lanthanum chalcogenides p 221 A88-40797
- Gravity and configurational energy induced microstructural changes in liquid phase sintering p 112 A88-49089
- Microstructural effects on fracture toughness of polycrystalline ceramics in combined mode I and mode II loading [ASME PAPER 88-GT-208] p 101 A88-54294

Effect of high-temperature annealing on the microstructure and thermoelectric properties of GaP doped SiGe

[NASA-TM-100164] p 101 N88-10188

A microstructural lattice model for strain oriented problems: A combined Monte Carlo finite element technique

[NASA-TM-100215] p 90 N88-10939

Flaw imaging and ultrasonic techniques for characterizing sintered silicon carbide

[NASA-TM-100177] p 177 N88-12106

Monte Carlo simulation of modulated phases

[NASA-TM-89654] p 210 N88-12323

Imaging subtle microstructural variations in ceramics with precision ultrasonic velocity and attenuation measurements

[NASA-TM-100129] p 177 N88-15257

Relationship between fatigue life in the creep-fatigue region and stress-strain response

[NASA-TM-100796] p 188 N88-18040

Characterization of sintered SiC by using NDE

p 177 N88-22413

Improved processing of Si₃N₄

p 107 N88-23882

As-received microstructure of a SiC/Ti-15-3 composite

[NASA-TM-100938] p 76 N88-28095

MICROWAVE AMPLIFIERS

Two stage dual gate MESFET monolithic gain control amplifier for Ka-band

p 124 A88-29821

High-efficiency helical traveling-wave tube with dynamic velocity taper and advanced multistage depressed collector

p 124 A88-32836

MICROWAVE ANTENNAS

Polarization determination utilizing two arbitrarily polarized antennas

p 116 A88-47424

MICROWAVE CIRCUITS

Monolithic Microwave Integrated Circuit (MMIC) technology for space communications applications

[IAA PAPER 87-491] p 122 A88-16133

Optical RF distribution links for MMIC phased array antennas

[NASA-TM-100841] p 128 N88-20555

Monolithic microwave integrated circuit technology for advanced space communication

[NASA-TM-100829] p 120 N88-21389

A 30 GHz monolithic receive module technology assessment

[NASA-CR-180825] p 129 N88-23084

Active feed array compensation for reflector antenna surface distortions

[NASA-TM-100826] p 120 N88-25762

Array trade-off study using multilayer parasitic subarrays

[NASA-TM-101321] p 121 N88-28222

MICROWAVE COUPLING

Characteristics of a two-layer electromagnetically coupled rectangular patch antenna

p 115 A88-14100

MICROWAVE EQUIPMENT

The bit-error rate performance of a satellite microwave matrix switch

[AIAA PAPER 88-0826] p 123 A88-27572

Microwave and millimeter-wave power generation in silicon carbide avalanche devices

p 126 A88-47599

Detection of radio-frequency modulated optical signals by two and three terminal microwave devices

p 117 A88-50305

The bit-error rate performance of a satellite microwave matrix switch

[NASA-TM-100285] p 46 N88-22920

MICROWAVE FREQUENCIES

Microwave response of an HEMT photoconductor

[NASA-TM-100819] p 128 N88-18835

MICROWAVE PHOTOGRAPHY

Investigation of surface water behavior during glaze ice accretion

[AIAA PAPER 88-0115] p 14 A88-22079

MICROWAVE SENSORS

Loss-compensation of intensity-modulating fiber-optic sensors

p 158 A88-22943

MICROWAVE SWITCHING

Future switching satellites

[AIAA PAPER 88-0802] p 46 A88-27553

MICROWAVE TRANSMISSION

A new model for broadband waveguide-to-microstrip transition design

p 126 A88-38822

MICROWAVES

Microwave performance of an optically controlled AlGaAs/GaAs high electron mobility transistor and GaAs MESFET

p 123 A88-24911

Experiments applications guide: Advanced Communications Technology Satellite (ACTS)

[NASA-TM-100265] p 49 N88-28082

MIGRATION

Electrohydrodynamic migration of charged droplets in an insulating fluid

[AIAA PAPER 88-3557] p 143 A88-48946

Electrohydrodynamic migration of charged droplets in an insulating fluid

[NASA-TM-100849] p 152 N88-21424

MILITARY HELICOPTERS

Helicopter transmission research at NASA Lewis Research Center

[NASA-TM-100962] p 175 N88-30128

MILLIMETER WAVES

System architecture of MMIC-based large aperture arrays for space applications

p 45 A88-35274

Electrothermal propulsion of spacecraft with millimeter and submillimeter electromagnetic energy

p 54 A88-46220

Microwave and millimeter-wave power generation in silicon carbide avalanche devices

p 126 A88-47599

A millimeter-wave tunnel Ladder TWT

[NASA-CR-182184] p 130 N88-28239

MINIATURIZATION

Miniature traveling wave tube and method of making

[NASA-CASE-LEW-14520-1] p 129 N88-23936

MIRRORS

A novel photovoltaic power system which uses a large area concentrator mirror

p 197 A88-11811

Chemical vapor deposited silica coatings for solar mirror protection

[AIAA PAPER 88-0027] p 99 A88-41796

Solar dynamic concentrator durability in atomic oxygen and micrometeoroid environments

p 68 A88-51393

Atomic-oxygen durability of impact-damaged solar reflectors

p 68 A88-54988

Chemical vapor deposited silica coatings for solar mirror protection

[NASA-TM-100834] p 105 N88-21306

The effect of the near earth micrometeoroid environment on a highly reflective mirror surface

[NASA-TM-101307] p 44 N88-29833

MISMATCH (ELECTRICAL)

Absolute gain measurement of microstrip antennas under mismatched conditions

p 117 A88-47949

MISSION PLANNING

High power ion thruster performance

[NASA-TM-100127] p 58 N88-12542

Numerical arc segmentation algorithm for a radio conference-NASARC, version 2.0: User's manual

[NASA-TM-100161] p 119 N88-16928

MIXED OXIDES

Weak-field magnetization of superconducting YBa₂Cu₃O_x - Relationship to microstructure

p 219 A88-18814

Chemical durability of high-temperature superconductor YBa₂Cu₃O_{7-x} in aqueous environments

p 78 A88-25023

Effect of fluoride doping on the transition temperature of YBa₂Cu₃O_{7-x}

p 220 A88-29297

Advantages of barium peroxide in the powder synthesis of perovskite superconductors

p 221 A88-41496

Characterization of Ba₂YCu₃O_{7-x} prepared in an inert atmosphere

p 221 A88-49376

High T_c screen-printed YBa₂Cu₃O_{7-x} films - Effect of the substrate material

p 127 A88-49760

MIXING

The structure and dynamics of reacting plane mixing layers

p 136 A88-20871

Dynamics of two fluids under periodic acceleration

[AIAA PAPER 88-3728] p 143 A88-48980

MIXING LAYERS (FLUIDS)

The structure and dynamics of reacting plane mixing layers

p 136 A88-20871

Direct simulations of chemically reacting turbulent mixing layers, part 2

[NASA-CR-180853] p 154 N88-25857

MODAL RESPONSE

Modal test/analysis correlation for the Centaur G prime launch vehicle

p 44 A88-18631

Evaluation of a turbine blade damper using an integral approach

[AIAA PAPER 88-2400] p 20 A88-32332

Identification of differences between finite element analysis and experimental vibration data

p 183 A88-46666

MODELS

A finite element model for wave propagation in an inhomogeneous material including experimental validation

[AIAA PAPER 87-2741] p 212 A88-16577

Experimental classical flutter results of a composite advanced turboprop model

p 21 A88-35528

Computerized life and reliability modelling for turboprop transmissions

[AIAA PAPER 88-2979] p 100 A88-48031

Experimental evidence for modifying the current physical model for ice accretion on aircraft surfaces

[NASA-TM-87184] p 15 N88-12473

On dynamic loads in parallel shaft transmissions. 1: Modelling and analysis

[NASA-TM-100180] p 171 N88-12797

On dynamic loads in parallel shaft transmissions. 2:

Parameter study

[NASA-TM-100181] p 171 N88-12798

Overview of heat transfer and fluid flow problem areas encountered in Stirling engine modeling

[NASA-TM-100131] p 224 N88-17561

Modeling of some coplanar waveguide discontinuities

[NASA-TM-100808] p 119 N88-17880

Characterization of damped structural connections for multi-component systems

[NASA-TM-100801] p 189 N88-18974

Aero/structural tailoring of engine blades

(AERO/STAEBL)

[NASA-CR-180805] p 207 N88-21682

Computerized life and reliability modelling for turboprop transmissions

[NASA-TM-100918] p 173 N88-23220

Entrance and exit region friction factor models for annular seal analysis

[NASA-CR-183084] p 175 N88-25921

The relationship between observed fatigue damage and life estimation models

[NASA-CR-182191] p 196 N88-27611

A statistical rain attenuation prediction model with application to the advanced communication technology satellite project. 1: Theoretical development and application to yearly predictions for selected cities in the United States

[NASA-CR-179498] p 121 N88-29077

Constitutive modeling for isotropic materials

[NASA-CR-182132] p 37 N88-29811

MODFETS

Variable angle spectroscopic ellipsometry - Application to GaAs-AlGaAs multilayer homogeneity characterization

p 220 A88-40139

MODULATION

Modulated-splitting-ratio fiber-optic temperature sensor

[NASA-TM-101332] p 18 N88-28062

MODULATORS

A high frequency GaAlAs travelling wave electro-optic modulator at 0.82 micrometers

[NASA-TM-100970] p 130 N88-28240

High frequency GaAlAs modulator and photodetector for phased array antenna applications

[NASA-TM-101328] p 130 N88-30048

MODULES

A 30 GHz monolithic receive module technology assessment

[NASA-CR-180825] p 129 N88-23084

MOIRE FRINGES

Sources of error in heterodyne moire deflectometry

p 158 A88-35004

MOISTURE

Chemical durability of high-temperature superconductor YBa₂Cu₃O_{7-x} in aqueous environments

p 78 A88-25023

MOISTURE RESISTANCE

Hygrothermomechanical fiber composite fatigue - Computational simulation

p 71 A88-42437

Stability of the electrical resistivity of bromine, iodine monochloride, copper(II) chloride, and nickel(II) chloride intercalated pitch-based graphite fibers

p 100 A88-49403

MOLECULAR CHAINS

Novel ladder polymers for use as high temperature stable resins or coatings

[NASA-CASE-LEW-14203-1] p 108 N88-29984

MOLECULAR STRUCTURE

Linear and nonlinear mechanical properties of a series of epoxy resins

p 101 A88-54976

MOLTEN SALTS

Fluoride salts and container materials for thermal energy storage applications in the temperature range 973 - 1400 K

p 196 A88-11804

Molten-salt corrosion of silicon nitride, I - Sodium carbonate, II - Sodium sulfate

p 97 A88-26222

MOLYBDENUM

Role of molybdenum in the Na₂SO₄ induced corrosion of superalloys at high temperature

p 81 A88-10030

Primary arm spacing in chill block melt spun Ni-Mo alloys

p 89 A88-41655

An experimental study of biaxial yield in modified 9Cr-1Mo steel at room temperature

[NASA-CR-175012] p 196 N88-30164

MOLYBDENUM ALLOYS

Precipitation in a rapidly solidified and aged Ni-Al-Mo alloy

p 82 A88-18528

Undercooled and rapidly quenched Ni-Mo alloys

p 83 A88-19960

MOMENTUM

Determination of compressor in-stall characteristics from engine surge transients

p 21 A88-35505

Redundant manipulators for momentum compensation in a micro-gravity environment

[AIAA PAPER 88-4121] p 204 A88-50223

- Efficient numerical techniques for complex fluid flows
p 146 N88-11151
- MOMENTUM TRANSFER**
Measurements of the turbulent transport of heat and momentum in convexly curved boundary layers - Effects of curvature, recovery and free-stream turbulence
[ASME PAPER 87-GT-199] p 131 A88-11103
The effect of eddy distribution on momentum and heat transfer near the wall in turbulent pipe flow
[NASA-TM-100257] p 150 N88-15984
- MONATOMIC GASES**
Design and demonstration of a system for the deposition of atomic-oxygen durable coatings for reflective solar dynamic power system concentrators
[NASA-CR-4158] p 64 N88-25474
- MONOMERS**
Substituted 1,1,1-Triaryl-2,2,2-Trifluoroethanes and processes for their synthesis
[NASA-CASE-LEW-14345-1] p 69 N88-26404
- MONTE CARLO METHOD**
Efficient probabilistic fracture mechanics analysis
p 180 A88-16933
Finite element methods in probabilistic mechanics
p 212 A88-29060
A microstructural lattice model for strain oriented problems: A combined Monte Carlo finite element technique
[NASA-TM-100215] p 90 N88-10939
Monte Carlo simulation of modulated phases
[NASA-TM-89654] p 210 N88-12323
Creep life prediction based on stochastic model of microstructurally short crack growth
[NASA-TM-100245] p 186 N88-12825
- MORPHOLOGY**
NASA research Program: The roles of fluid motion and other transport phenomena in the morphology of materials
[NASA-CR-182801] p 222 N88-25327
- MULTIPLE ACCESS**
Spread-spectrum multiple access using wideband noncoherent MFSK
p 115 A88-26672
Future switching satellites
[AIAA PAPER 88-0802] p 46 A88-27553
- MULTIPLIERS**
Implementation of a fast digital optical matrix-vector multiplier using a holographic look-up table and residue arithmetic
p 205 A88-17223
Implementation of a digital optical matrix-vector multiplier using a holographic look-up table and residue arithmetic
[NASA-CR-180431] p 205 N88-10496
- MUSHY ZONES**
Local convective flows in partly solidified alloys
p 219 A88-18467
Onset of finger convection in a horizontal porous layer underlying a fluid layer
p 140 A88-41572
- N**
- N-P-N JUNCTIONS**
Neutron effects on the electrical and switching characteristics of NPN bipolar power transistors
p 129 N88-24463
- N-TYPE SEMICONDUCTORS**
Characterization and modelling of open tube diffused n-p bulk InP solar cells
p 199 A88-34270
- NAPHTHENES**
Availability and cost estimate of a high naphthene, modified aviation turbine fuel
[NASA-TM-100823] p 104 N88-20455
- NASA PROGRAMS**
Results of NASA's Energy Efficient Engine Program
p 19 A88-20785
NASA HOST project overview --- hot section technology
p 24 A88-54138
Views on the impact of HOST --- hot section technology
p 24 A88-54146
NASA advanced turboprop research and concept validation program
[NASA-TM-100891] p 34 N88-22902
Overview of NASA research in fiber optics for aircraft controls
[NASA-TM-100919] p 35 N88-25458
Bibliography of Lewis Research Center technical publications announced in 1987
[NASA-TM-100910] p 223 N88-28832
SR-7A aerelastic model design report
[NASA-CR-174791] p 36 N88-28928
- NASA SPACE PROGRAMS**
Research opportunities in microgravity science and applications during Shuttle hiatus
p 109 A88-13164
- NASTRAN**
Aerodynamically forced vibration analysis of turbomachines
p 20 A88-31610

- Thermostructural analysis of simulated cowl lips
p 192 N88-22403
Lewis Structures Technology, 1988. Volume 1: Structural Dynamics
[NASA-CP-3003-VOL-1] p 194 N88-23226
- NAVIER-STOKES EQUATION**
Explicit multigrid algorithm for quasi-three-dimensional viscous flows in turbomachinery
p 2 A88-10355
Application of advanced computational codes in the design of an experiment for a supersonic throughflow fan rotor
[ASME PAPER 87-GT-160] p 2 A88-11072
Infrared properties of an anisotropically stirred fluid
p 134 A88-16354
Torsion effect on fully developed flow in a helical pipe
p 135 A88-20748
Navier-Stokes solutions of flowfield characteristics produced by ice accretion
[AIAA PAPER 88-0290] p 137 A88-22210
Navier-Stokes cascade analysis with a stiff k-epsilon turbulence solver
[AIAA PAPER 88-0594] p 5 A88-22444
Time-accurate simulations of a shear layer forced at a single frequency
[AIAA PAPER 88-0061] p 138 A88-27716
Consistent boundary conditions for reduced Navier-Stokes (RNS) scheme applied to three-dimensional internal viscous flows
[AIAA PAPER 88-0714] p 139 A88-27723
A finite difference scheme for three-dimensional steady laminar incompressible flow
p 139 A88-30469
Explicit finite-volume time-marching calculations of total temperature distributions in turbulent flow
p 139 A88-30517
An explicit finite-volume time-marching procedure for turbulent flow calculations
p 139 A88-30518
A Navier-Stokes solver using the LU-SSOR TVD algorithm
p 6 A88-30560
Numerical and analytical study of fluid dynamic forces in seals and bearings
p 167 A88-31534
Mathematical models for the numerical study of turbulent flows
p 140 A88-39472
Numerical analysis of three-dimensional viscous internal flows
[AIAA PAPER 88-3522] p 142 A88-48779
Third-order multi-dimensional Euler/Navier-Stokes solver
[AIAA PAPER 88-3645] p 209 A88-48806
A numerical investigation of the influence of heating on the excitation of high and low Mach number jet flows
[ASME PAPER 87-WA/NCA-13] p 144 A88-51343
Navier-Stokes cascade analysis with a stiff Kappa-Epsilon turbulence solver
[NASA-TM-100218] p 9 N88-10778
Flow in a model turbine stator
p 148 N88-11163
Consistent boundary conditions for Reduced Navier-Stokes (RNS) scheme applied to 3-dimensional internal viscous flows
[NASA-CR-180874] p 10 N88-15762
Inlets, ducts and nozzles
p 149 N88-15791
Turbomachinery
p 28 N88-15792
Numerical modeling of multidimensional flow in seals and bearings used in rotating machinery
[NASA-TM-100779] p 150 N88-16988
Numerical and analytical study of fluid dynamic forces in seals and bearings
[NASA-TM-100268] p 151 N88-18867
Time-accurate simulations of a shear layer forced at a single frequency
[NASA-TM-100836] p 152 N88-19740
Numerical analysis of three-dimensional viscous internal flows
[NASA-TM-100878] p 1 N88-21116
Choice of implicit and explicit operators for the upwind differencing method
[NASA-TM-100857] p 211 N88-21718
Review and assessment of the HOST turbine heat transfer program
p 34 N88-22431
Reduced order models for nonlinear aerodynamics
p 11 N88-23248
Application of Navier-Stokes analysis to stall flutter
p 38 N88-23249
- NAVY**
Multiple-Purpose Subsonic Naval Aircraft (MPSNA): Multiple Application Propfan Study (MAPS)
[NASA-CR-175104] p 18 N88-28917
- NETWORK CONTROL**
Finite-dimensional modeling of network-induced delays for real-time control systems
p 208 A88-54537
Experiments applications guide: Advanced Communications Technology Satellite (ACTS)
[NASA-TM-100265] p 49 N88-28082
- NETWORK SYNTHESIS**
Two stage dual gate MESFET monolithic gain control amplifier for Ka-band
p 124 A88-29821

- A satellite system synthesis model for orbital arc allotment optimization
p 117 A88-48579
- NEUMANN PROBLEM**
Solution of the Neumann pressure problem in general orthogonal coordinates using the multigrid technique
p 144 A88-50330
- NEUTRINOS**
Axions from 1987A
p 226 A88-35586
- NEUTRON IRRADIATION**
Neutron radiation tolerance of Au-activated silicon
p 222 N88-24316
Neutron effects on the electrical and switching characteristics of NPN bipolar power transistors
p 129 N88-24463
- NEWTON-RAPHSON METHOD**
Efficient numerical techniques for complex fluid flows
p 146 N88-11151
- NICKEL**
Sodium sulfate-induced corrosion of pure nickel and superalloy Udimet 700 in a high velocity burner rig at 900 C
p 83 A88-20266
An update of the total-strain version of SRP
p 86 A88-35910
Wear of iron and nickel in corrosive liquid environments
p 88 A88-40790
Primary arm spacing in chill block melt spun Ni-Mo alloys
p 89 A88-41655
Constitutive modeling for isotropic materials
p 185 N88-11171
Wear of iron and nickel in corrosive liquid environments
[NASA-TM-100246] p 91 N88-11817
Bithermal fatigue of a nickel-base superalloy single crystal
[NASA-TM-100885] p 93 N88-22168
Performance of lightweight nickel electrodes
[NASA-TM-100958] p 80 N88-26430
- NICKEL ALLOYS**
Effect of alloy composition on the sodium-sulfate induced hot corrosion attack of cast nickel-base superalloys at 900 C
p 81 A88-10028
The effect of variations of cobalt content on the cyclic oxidation resistance of selected Ni-base superalloys
p 82 A88-10031
Precipitation in a rapidly solidified and aged Ni-Al-Mo alloy
p 82 A88-18528
Effect of initial gamma prime size on the elevated temperature creep properties of single crystal nickel base superalloys
p 82 A88-18884
Undercooled and rapidly quenched Ni-Mo alloys
p 83 A88-19960
Phenomenological modeling of hardening and thermal recovery in metals
p 84 A88-24037
Interdiffusion in Ni-rich, Ni-Cr-Al alloys at 1100 and 1200 C. I - Diffusion paths and microstructures. II - Diffusion coefficients and predicted concentration profiles
p 84 A88-24485
Predicting diffusion paths and interface motion in gamma/gamma + beta, Ni-Cr-Al diffusion couples
p 84 A88-24486
Cyclic hardening mechanisms in Nimonic 80A
p 84 A88-24490
Containerless processing of undercooled melts
p 110 A88-28554
Solidification of undercooled Ni-Sn eutectic alloy under microgravity conditions in the Space Shuttle
p 110 A88-28557
Diffusional transport during the cyclic oxidation of gamma + beta, Ni-Cr-Al(Y, Zr) alloys
p 85 A88-28902
The influence of grain size and composition on 1000 to 1400 K slow plastic flow properties of NiAl
p 85 A88-29098
Adherent Al₂O₃ scales produced on undoped NiCrAl alloys
p 85 A88-30269
Anisotropic constitutive modeling for nickel base single crystal superalloys using a crystallographic approach
[AIAA PAPER 88-2440] p 85 A88-32357
Dendritic growth of undercooled nickel-tin. III
p 86 A88-32887
Fatigue crack propagation of nickel-base superalloys at 650 deg C
p 86 A88-35908
A model for life predictions of nickel-base superalloys in high-temperature low cycle fatigue
p 87 A88-35913
Bithermal fatigue - A link between isothermal and thermomechanical fatigue
p 87 A88-35918
Powder processing of nickel and other aluminides by hot consolidation
p 87 A88-37158
Microstructure-property relationships in directionally solidified single-crystal nickel-base superalloys
p 88 A88-40329
Dispersion strengthened NiAl alloys produced by rapid solidification processing
p 88 A88-40588
Effect of melt spinning on grain size and texture in Ni-Mo alloys
p 89 A88-46030

- Accelerated crack growth rate at low Delta K in a single crystal superalloy p 89 A88-47887
- A crystallographic model for nickel base single crystal alloys p 89 A88-48182
- Lattice parameter variations during aging in nickel-base superalloys p 90 A88-51318
- Bithermal low-cycle fatigue behavior of a NiCoCrAlY-coated single crystal superalloy p 90 A88-51736
- The effect of sulfur and zirconium Co-doping on the oxidation of NiCrAl p 90 A88-10940
- [NASA-TM-100209] p 90 A88-10940
- Friction and wear of monolithic and fiber reinforced silicon-ceramics sliding against IN-718 alloy at 25 to 800 C in atmospheric air at ambient pressure p 103 A88-17796
- [NASA-TM-100294] p 103 A88-17796
- The cyclic stress-strain behavior of a single crystal nickel-base superalloy p 92 A88-19610
- [NASA-TM-100269] p 92 A88-19610
- Processing, physical metallurgy and creep of NiAl + Ta and NiAl + Nb alloys p 92 A88-21295
- [NASA-CR-182113] p 92 A88-21295
- Anisotropic constitutive modeling for nickel-base single crystal superalloys p 95 A88-29961
- [NASA-CR-182157] p 95 A88-29961
- NICKEL CADMIUM BATTERIES**
- A prediction model of the depth-of-discharge effect on the cycle life of a storage cell p 197 A88-11896
- NICKEL COMPOUNDS**
- Preliminary investigation of inertia friction welding B2 aluminides p 82 A88-14567
- Stability of the electrical resistivity of bromine, iodine monochloride, copper(II) chloride, and nickel(II) chloride intercalated pitch-based graphite fibers p 100 A88-49403
- Phase purity of NiCo₂O₄, a catalyst candidate for electrolysis of water p 69 A88-13385
- [NASA-TM-100239] p 69 A88-13385
- NICKEL HYDROGEN BATTERIES**
- Effect of component compression on the initial performance of an IPV nickel-hydrogen cell — Individual Pressure Vessel p 53 A88-11913
- Component variations and their effects on bipolar nickel-hydrogen cell performance p 197 A88-11914
- Test results of a 60 volt bipolar nickel-hydrogen battery p 198 A88-11916
- Effect of storage and LEO cycling on manufacturing technology IPV nickel-hydrogen cells p 53 A88-11917
- Lightweight nickel electrode for nickel hydrogen cells and batteries p 198 A88-16631
- Assessment of commercially available and experimental hydrogen electrodes p 198 A88-16632
- Effect of NASA advanced designs on thermal behavior of Ni-H₂ cells p 79 A88-10132
- [NASA-TM-100197] p 79 A88-10132
- Small scale bipolar nickel-hydrogen testing p 202 A88-25059
- [NASA-TM-100936] p 202 A88-25059
- Effect of LEO cycling at shallow depths of discharge on MANTech IPV nickel-hydrogen cells p 203 A88-25978
- [NASA-TM-101300] p 203 A88-25978
- Performance of lightweight nickel electrodes p 80 A88-26430
- [NASA-TM-100958] p 80 A88-26430
- The effect of compression on individual pressure vessel nickel/hydrogen components p 81 A88-28109
- [NASA-TM-101312] p 81 A88-28109
- NIMONIC ALLOYS**
- Cyclic hardening mechanisms in Nimonic 80A p 84 A88-24490
- On the cyclic stress-strain behaviour of a Ni-base superalloy at room temperature p 84 A88-24521
- NIObIUM**
- Creep behavior of tungsten/niobium and tungsten/niobium-1 percent zirconium composites p 92 A88-18707
- [NASA-TM-100804] p 92 A88-18707
- Creep behavior of tungsten/niobium and tungsten/niobium-1 percent zirconium composites p 75 A88-24427
- Investigation of a SiC/Ti-24Al-11Nb composite p 76 A88-28980
- [NASA-TM-100956] p 76 A88-28980
- NIObIUM ALLOYS**
- Thermal aging effects in refractory metal alloys p 84 A88-22700
- Characterization of precipitates in a niobium-zirconium-carbon alloy p 93 A88-22981
- [NASA-TM-100848] p 93 A88-22981
- Preliminary study of niobium alloy contamination by transport through helium p 94 A88-24279
- NITRIDING**
- Ion nitriding; Proceedings of the International Conference, Cleveland, OH, Sept. 15-17, 1986 p 114 A88-38926
- Analysis of plasma nitrided steels p 88 A88-38936
- Ion-beam nitriding of steels p 91 A88-14179
- [NASA-CASE-LEW-14104-2] p 91 A88-14179
- SiC fiber reinforced reaction-bonded Si₃N₄ composites p 75 A88-23892

NITROGEN

- Experimental and theoretical effects of nitrogen gas flow rate on liquid-jet atomization p 145 A88-52679

NITROGEN IONS

- Ion nitriding; Proceedings of the International Conference, Cleveland, OH, Sept. 15-17, 1986 p 114 A88-38926

NOISE

- Automated acoustic intensity measurements and the effect of gear tooth profile on noise p 168 A88-31623

NOISE MEASUREMENT

- Overview of NASA PTA proplan flight test program p 29 A88-15805
- Advanced propeller research p 29 A88-15806
- Identification and proposed control of helicopter transmission noise at the source p 38 A88-16647

NOISE PREDICTION

- High speed propeller performance and noise predictions at takeoff/landing conditions [AIAA PAPER 88-0264] p 215 A88-22193
- High speed propeller performance and noise predictions at takeoff/landing conditions [NASA-TM-100267] p 216 A88-13960

NOISE PREDICTION (AIRCRAFT)

- Noise characteristics of model counter-rotating Prop-Fans p 213 A88-16526
- [AIAA PAPER 87-2656] p 213 A88-16526
- High-speed propeller noise predictions - Effects of boundary conditions used in blade loading calculations p 215 A88-36270

NOISE PROPAGATION

- A mapped finite difference study of noise propagation in nonuniform ducts with mean flow p 214 A88-18541

NOISE REDUCTION

- Noise of a model counterrotation propeller with reduced aft rotor diameter at simulated takeoff/approach conditions (F7/A3) p 214 A88-22192
- [AIAA PAPER 88-0263] p 214 A88-22192
- Noise of a model counterrotation propeller with reduced aft rotor diameter at simulated takeoff/approach conditions (F7/A3) p 216 A88-13961
- [NASA-TM-100254] p 216 A88-13961
- Propulsion challenges and opportunities for high-speed transport aircraft p 30 A88-15809
- Identification and proposed control of helicopter transmission noise at the source p 38 A88-16647
- A review of gear housing dynamics and acoustics literature p 175 A88-26675
- [NASA-CR-183110] p 175 A88-26675

NOISE SPECTRA

- Combustion noise from gas turbine aircraft engines measurement of far-field levels p 215 A88-39708

NONDESTRUCTIVE TESTS

- Laser anemometry techniques for turbine applications [ASME PAPER 87-GT-241] p 157 A88-11129
- Ultrasonic nondestructive evaluation, microstructure, and fracture toughness interrelations p 176 A88-18158
- Materials analysis by ultrasonics: Metals, ceramics, composites — Book p 176 A88-44853
- Transply crack density detection by acousto-ultrasonics [NASA-TM-100224] p 72 A88-11758
- Flaw imaging and ultrasonic techniques for characterizing sintered silicon carbide [NASA-TM-100177] p 177 A88-12106
- Determining structural performance p 27 A88-15787
- Nondestructive evaluation of structural ceramics by photoacoustic microscopy [NASA-CR-180858] p 103 A88-16868
- Impact damage in composite laminates p 74 A88-22402
- Lewis Structures Technology, 1988. Volume 3: Structural Integrity Fatigue and Fracture Wind Turbines HOST [NASA-CP-3003-VOL-3] p 192 A88-22408
- Nondestructive evaluation by acousto-ultrasonics p 177 A88-22412
- Characterization of sintered SiC by using NDE p 177 A88-22413
- Nondestructive evaluation of sintered ceramics p 177 A88-22416
- Acousto-ultrasonic input-output characterization of unidirectional fiber composite plate by SV waves [NASA-CR-4152] p 178 A88-23224
- Structural Ceramics [NASA-CP-2427] p 106 A88-23872
- Nondestructive evaluation of structural ceramics p 178 A88-23876
- Input-output characterization of fiber composites by SH waves [NASA-CR-4153] p 179 A88-23986
- Characterization of noncontact piezoelectric transducer with conically shaped piezoelement [NASA-CR-4151] p 179 A88-23987

- New acousto-ultrasonic techniques applied to aerospace materials [NASA-TM-101299] p 180 A88-28323

NONISOTHERMAL PROCESSES

- Bithermal fatigue: A simplified alternative to thermomechanical fatigue p 194 A88-22424

NONLINEAR EQUATIONS

- Input-output-controlled nonlinear equation solvers p 146 A88-55245
- Convergence acceleration for vector sequences and applications to computational fluid dynamics [NASA-TM-101327] p 212 A88-30377

NONLINEARITY

- Reduced order models for nonlinear aerodynamics p 11 A88-23248

NORMAL DENSITY FUNCTIONS

- Absolute instability of the Gaussian wake profile p 136 A88-20842

NOZZLE DESIGN

- Design and experimental evaluation of a high temperature radial turbine with a moveable sidewall nozzle [SAE PAPER 871782] p 19 A88-30776
- Forced mixer lobes in ejector designs p 141 A88-46222
- The effects of magnetic nozzle configurations on plasma thrusters p 219 A88-26223
- [NASA-CR-183096] p 219 A88-26223
- Analysis and optimization of truncated scarf nozzles subject to external flow conditions [NASA-TM-100955] p 14 A88-29746

NOZZLE EFFICIENCY

- Analysis and optimization of truncated scarf nozzles subject to external flow conditions [NASA-TM-100955] p 14 A88-29746

NOZZLE FLOW

- Effects of nozzle-exit boundary-layer conditions on excitability of heated free jets [AIAA PAPER 87-2723] p 135 A88-20182
- Solutions of one-dimensional steady nozzle flow revisited p 144 A88-50344
- Spray characteristics of a spill-return airblast atomizer [ASME PAPER 88-GT-7] p 145 A88-54154
- Experimental evaluation of a translating nozzle sidewall radial turbine p 31 A88-17656

NOZZLE GEOMETRY

- Experimental evaluation of a translating nozzle sidewall radial turbine p 31 A88-17656
- A detailed description of the uncertainty analysis for high area ratio rocket nozzle tests at the NASA Lewis Research Center p 65 A88-25580

NOZZLE WALLS

- Experimental evaluation of a translating nozzle sidewall radial turbine p 31 A88-17656

NOZZLES

- Aeropropulsion '87. Session 3: Internal Fluid Mechanics Research [NASA-CP-10003-SESS-3] p 28 A88-15790
- Inlets, ducts and nozzles p 149 A88-15791
- Comparison of UNL laser imaging and sizing system and a phase/Doppler system for analyzing sprays from a NASA nozzle [NASA-CR-182437] p 150 A88-16956

NUCLEAR ASTROPHYSICS

- Calculations of rates for direct detection of neutralino dark matter p 227 A88-48463

NUCLEAR AUXILIARY POWER UNITS

- Creep behavior of tungsten/niobium and tungsten/niobium-1 percent zirconium composites [NASA-TM-100804] p 92 A88-18707

NUCLEAR ELECTRIC POWER GENERATION

- Benefits of 20 kHz PMAD in a nuclear space station p 129 A88-24256

NUCLEAR ENERGY

- Power systems for production, construction, life support and operations in space [NASA-TM-100838] p 60 A88-21254

NUCLEAR FUSION

- Primordial lithium - New reaction rates, new abundances, new constraints p 226 A88-31145
- Cosmology and particle physics p 226 A88-39734
- Primordial nucleosynthesis with decaying particles. I - Entropy-producing decays. II - Inert decays p 217 A88-47477

NUCLEAR POWER REACTORS

- Coaxial tube array space transmission line characterization p 121 A88-11865
- Small reactor power systems for manned planetary surface bases [NASA-TM-100223] p 227 A88-13209

NUCLEAR REACTIONS

- Primordial lithium - New reaction rates, new abundances, new constraints p 226 A88-31145

NUCLEAR REACTORS

- A study of Schwarz converters for nuclear powered spacecraft p 51 A88-11823

- NUCLEATE BOILING**
Nucleate pool boiling: High gravity to reduced gravity; liquid metals to cryogenics p 113 N88-24464
- NUCLEONS**
Axions from 1987A p 226 A88-35586
- NUMERICAL ANALYSIS**
Numerical study of multicomponent droplet vaporization at near critical conditions [AIAA PAPER 88-0637] p 108 A88-27721
A Navier-Stokes solver using the LU-SSOR TVD algorithm p 6 A88-30560
Numerical analysis of three-dimensional viscous internal flows [AIAA PAPER 88-3522] p 142 A88-48779
Institute for Computational Mechanics in Propulsion (ICOMP) first year summary [NASA-TM-100225] p 210 N88-12330
An analytical and experimental study of injection-locked two-port oscillators [NASA-TM-100119] p 128 N88-12727
A multistage mesh generator for solving the average-passage equation system [NASA-CR-179539] p 10 N88-15769
Numerical simulation of axisymmetric turbulent flow in combustors and diffusers [NASA-CR-4115] p 11 N88-17582
Numerical simulation of subsonic and transonic propeller flow [NASA-TM-100163] p 11 N88-20262
Numerical analysis of three-dimensional viscous internal flows [NASA-TM-100878] p 1 N88-21116
Mode 2 fracture mechanics p 193 N88-22418
Improved numerical methods for turbulent viscous recirculating flows [NASA-CR-180852] p 13 N88-25445
A computational analysis of under-expanded jets in the hypersonic regime [NASA-TM-101319] p 13 N88-27174
Analytical approximation of a distorted reflector surface defined by a discrete set of points [NASA-TM-101323] p 121 N88-27424
Transition mixing study empirical model report [NASA-CR-182139] p 155 N88-30076
- NUMERICAL FLOW VISUALIZATION**
Numerical simulation of self-sustained and forced oscillations in jet shear layers p 3 A88-14155
Roll-up of vorticity in adverse-pressure-gradient boundary layers p 135 A88-19194
- NUMERICAL INTEGRATION**
Integrating combustion kinetic rate equations by selective use of stiff and nonstiff methods p 78 A88-19233
Computation of the velocity field of an excited shear layer p 138 A88-26206
- O**
- O RING SEALS**
Analysis of eccentric annular incompressible seals. II - Effects of eccentricity on rotordynamic coefficients [ASME PAPER 87-TRIB-53] p 166 A88-23309
Analysis and design of a gas-lubricated, sectored, floating ring seal [ASME PAPER 87-TRIB-55] p 166 A88-23310
- OBlique SHOCK WAVES**
Experimental and numerical investigation of the effect of distributed suction on oblique shock wave/turbulent boundary layer interaction [NASA-TM-101334] p 156 N88-30084
- OH-58 HELICOPTER**
Identification and proposed control of helicopter transmission noise at the source p 38 N88-16647
- OHMS LAW**
Aging behavior of Au-based ohmic contacts to GaAs [NASA-CR-182146] p 130 N88-25831
- ONE DIMENSIONAL FLOW**
Solutions of one-dimensional steady nozzle flow revisited p 144 A88-50344
- OPERATING COSTS**
LERC power system autonomy program 1990 demonstration p 52 A88-11861
- OPERATORS (MATHEMATICS)**
Choice of implicit and explicit operators for the upwind differencing method [AIAA PAPER 88-0624] p 209 A88-22472
Choice of implicit and explicit operators for the upwind differencing method [NASA-TM-100857] p 211 N88-21718
- OPTICAL COMMUNICATION**
Optical technologies for space communication systems: Proceedings of the Meeting, Los Angeles, CA, Jan. 15, 16, 1987 [SPIE-756] p 45 A88-35251
- A laser communication experiment utilizing the ACT satellite and an airborne laser transceiver [NASA-TM-100792] p 164 N88-18910
Fiber optics for advanced aircraft [NASA-TM-101294] p 1 N88-26328
- OPTICAL COMPUTERS**
Implementation of a fast digital optical matrix-vector multiplier using a holographic look-up table and residue arithmetic p 205 A88-17223
- OPTICAL CORRECTION PROCEDURE**
Zoom lens compensator for a cylindrical window in laser anemometer uses p 217 A88-17221
- OPTICAL DATA PROCESSING**
Implementation of a digital optical matrix-vector multiplier using a holographic look-up table and residue arithmetic [NASA-CR-180431] p 205 N88-10496
- OPTICAL EMISSION SPECTROSCOPY**
Reusable rocket engine optical condition monitoring p 158 A88-29817
- OPTICAL EQUIPMENT**
Microwave performance of an optically controlled AlGaAs/GaAs high electron mobility transistor and GaAs MESFET p 123 A88-24911
Referencing in fiber optic sensing systems p 217 A88-42604
Detection of radio-frequency modulated optical signals by two and three terminal microwave devices p 117 A88-50305
Optoelectronic gain control of a microwave single stage GaAs MESFET amplifier [NASA-CR-182201] p 131 N88-30055
- OPTICAL FIBERS**
Optically controlled phased-array antenna technology for space communication systems [NASA-TM-100852] p 119 N88-18809
Fiber optic sensing systems using high frequency resonant sensing heads with intensity sensors [NASA-TM-101318] p 163 N88-28293
- OPTICAL FILTERS**
Reduction of temperature rise in high-speed photography p 160 A88-55254
Reduction of temperature rise in high-speed photography [NASA-TM-100222] p 160 N88-11100
- OPTICAL HETERODYNING**
Sources of error in heterodyne moire deflectometry p 158 A88-35004
- OPTICAL MEASUREMENT**
Optical measurements pertaining to Space Station solar dynamic power systems [IAF PAPER 87-229] p 42 A88-15954
Optical strain measurement system development p 159 A88-52557
Optical measurement systems p 218 N88-15796
Ray tracing optical analysis of offset solar collector for space station solar dynamic system [NASA-TM-100853] p 60 N88-22080
Development and applications of optical interferometric micrometry in the angstrom and subangstrom range [NASA-TM-100299] p 162 N88-23196
Optical measurement of propeller blade deflections [NASA-TP-2841] p 163 N88-28286
Optical measurement of unducted fan blade deflections [NASA-TM-100966] p 163 N88-29142
Optical measurements of soot in premixed flames [NASA-TM-101305] p 156 N88-30090
- OPTICAL MEASURING INSTRUMENTS**
Time domain referencing in intensity modulation fiber optic sensing systems p 217 A88-12660
Fiber optics for advanced aircraft [NASA-TM-101294] p 1 N88-26328
- OPTICAL PROPERTIES**
Boron nitride - Composition, optical properties, and mechanical behavior p 99 A88-40794
- OPTICAL WAVEGUIDES**
A high frequency GaAlAs travelling wave electro-optic modulator at 0.82 micrometers [NASA-TM-100970] p 130 N88-28240
- OPTICS**
Optically interconnected phased arrays [NASA-TM-100855] p 128 N88-21400
- OPTIMAL CONTROL**
Implementation of optimal trajectory control of series resonant converter p 126 A88-38796
Active control of transient rotordynamic vibration by optimal control methods [ASME PAPER 88-GT-73] p 208 A88-54202
- OPTIMIZATION**
Derivatives of eigenvalues and eigenvectors of a general complex matrix p 209 A88-29269
Optimizing advanced propeller designs by simultaneously updating flow variables and design parameters [AIAA PAPER 88-2532] p 6 A88-40718
- Finite-element grid improvement by minimization of stiffness matrix trace [NASA-TM-100255] p 171 N88-13604
STAEBL/general composites with hygrothermal effects (STAEBL/GENCOM) [NASA-TM-100266] p 187 N88-13754
Integrated analysis and applications p 28 N88-15789
Aero/structural tailoring of engine blades (AERO/STAEBL) [NASA-CR-180805] p 207 N88-21682
Structural tailoring of advanced turboprops p 192 N88-22400
Spur gears: Optimal geometry, methods for generation and Tooth Contact Analysis (TCA) program [NASA-CR-4135] p 173 N88-23216
Analysis and optimization of truncated scarf nozzles subject to external flow conditions [NASA-TM-100955] p 14 N88-29746
- OPTOELECTRONIC DEVICES**
Implementation of a fast digital optical matrix-vector multiplier using a holographic look-up table and residue arithmetic p 205 A88-17223
A laser communication experiment utilizing the ACT satellite and an airborne laser transceiver [NASA-TM-100792] p 164 N88-18910
Optoelectronic gain control of a microwave single stage GaAs MESFET amplifier [NASA-CR-182201] p 131 N88-30055
- ORBIT SPECTRUM UTILIZATION**
Numerical arc segmentation algorithm for a radio conference - A software tool for communication satellite systems planning [AIAA PAPER 88-0788] p 212 A88-27531
Cost-effective intersatellite link applications to the fixed satellite services [AIAA PAPER 88-0770] p 45 A88-27544
An allotment planning concept and related computer software for planning the fixed satellite service at the 1988 space WARC p 116 A88-36482
- ORBIT TRANSFER VEHICLES**
Centaur operations at the space station [NASA-CR-179593] p 49 N88-25473
Centaur operations at the space station: Cost and transportation analysis [NASA-CR-182128] p 44 N88-29835
Orbital transfer vehicle 3000 LBF thrust chamber assembly hot fire test program [NASA-CR-182145] p 66 N88-29858
- ORBITAL ASSEMBLY**
Centaur operations at the space station: Cost and transportation analysis [NASA-CR-182128] p 44 N88-29835
- ORBITAL ELEMENTS**
Numerical arc segmentation algorithm for a radio conference-NASARC (version 2.0) technical manual [NASA-TM-100160] p 118 N88-15910
Numerical arc segmentation algorithm for a radio conference-NASARC, version 2.0: User's manual [NASA-TM-100161] p 119 N88-16928
- ORBITAL LAUNCHING**
Centaur operations at the space station [NASA-CR-179593] p 49 N88-25473
- ORBITAL LIFETIME**
An extended life and performance test of a low-power arcjet [AIAA PAPER 88-3106] p 55 A88-48756
An extended life and performance test of a low-power arcjet [NASA-TM-100942] p 63 N88-24687
- ORBITAL MECHANICS**
Engineering calculations for the Delta S method of solving the orbital allotment problem [NASA-CR-182372] p 42 N88-14110
Numerical arc segmentation algorithm for a radio conference-NASARC, version 2.0: User's manual [NASA-TM-100161] p 119 N88-16928
- ORBITAL SERVICING**
Space station resistojet system requirements and interface definition study [NASA-CR-180832] p 58 N88-12541
Centaur operations at the space station: Cost and transportation analysis [NASA-CR-182128] p 44 N88-29835
Technology requirements for an orbiting fuel depot: A necessary element of a space infrastructure [NASA-TM-101370] p 49 N88-29845
- ORBITS**
A satellite system synthesis model for orbital arc allotment optimization p 117 A88-48579
- ORGANIC COMPOUNDS**
Simulation of fluid flows during growth of organic crystals in microgravity p 109 A88-13163
- ORGANIC COOLANTS**
Toluene stability Space Station Rankine power system p 50 A88-11794

ORGANIC LIQUIDS

ORGANIC LIQUIDS

- Solar dynamic organic Rankine cycle heat rejection system simulation p 132 A88-11808
Critical exponent for the viscosity of four binary liquids p 222 A88-53050

ORGANOMETALLIC COMPOUNDS

- Laser induced OMCVD growth of AlGaAs on GaAs p 125 A88-34286

ORIFICES

- Dilution jet mixing program, phase 3 p 147 N88-11153

ORTHOGONALITY

- Modal test/analysis correlation for the Centaur G prime launch vehicle p 44 A88-18631

ORTHOTROPISM

- A simplified orthotropic formulation of the viscoplasticity theory based on overstress p 189 N88-21505

OSCILLATING FLOW

- Description of an oscillating flow test program p 133 A88-11963
Numerical simulation of self-sustained and forced oscillations in jet shear layers p 3 A88-14155
Analysis of eccentric annular incompressible seals. II - Effects of eccentricity on rotordynamic coefficients [ASME PAPER 87-TRIB-53] p 166 A88-23309
Velocity-coupled flow oscillations in a simulated solid-propellant rocket environment [AIAA PAPER 88-0543] p 108 A88-27720
Unsteady aerodynamics of an oscillating cascade in a compressible flow field [NASA-TM-100219] p 26 N88-13346
A survey of oscillating flow in Stirling engine heat exchangers [NASA-CR-182108] p 152 N88-22322
Description of an oscillating flow pressure drop test rig [NASA-TM-100905] p 61 N88-22933

OSCILLATIONS

- Investigation of oscillating cascade aerodynamics by an experimental influence coefficient technique [NASA-TM-101313] p 14 N88-28041

OSCILLATORS

- An analytical and experimental study of injection-locked two-port oscillators [NASA-TM-100119] p 128 N88-12727

OXIDATION

- High-temperature oxidation/corrosion of iron-based superalloys p 81 A88-10029
Improved perfluoroalkyl ether fluid development p 68 A88-28624
Grain boundary oxidation and an analysis of the effects of oxidation on fatigue crack nucleation life p 87 A88-35938
The effect of sulfur and zirconium Co-doping on the oxidation of NiCrAl [NASA-TM-100209] p 90 N88-10940
Thermal expansion mismatch and oxidation in thermal barrier coatings p 170 N88-11182
Detailed mechanism of benzene oxidation [NASA-TM-100202] p 79 N88-11775
Detailed mechanism of toluene oxidation and comparison with benzene p 79 N88-13428
Oxidation and protection of fiberglass-epoxy composite masts for photovoltaic arrays in the low Earth orbital environment [NASA-TM-100839] p 104 N88-18734
The analysis of fatigue crack growth mechanism and oxidation and fatigue life at elevated temperatures [NASA-CR-182129] p 94 N88-22987

OXIDATION RESISTANCE

- The effect of variations of cobalt content on the cyclic oxidation resistance of selected Ni-base superalloys p 82 A88-10031
PMR polyimide compositions for improved performance at 371 C p 96 A88-13172
Oxidation-resistant reflective surfaces for solar dynamic power generation in near earth orbit p 54 A88-18523
Diffusional transport during the cyclic oxidation of gamma + beta, Ni-Cr-Al(Y, Zr) alloys p 85 A88-28902
Stability of the electrical resistivity of bromine, iodine monochloride, copper(II) chloride, and nickel(II) chloride intercalated pitch-based graphite fibers p 100 A88-49403
Improved perfluoroalkylether fluid development [NASA-CR-180872] p 80 N88-15851
Correlations of norbornenyl crosslinked polyimide resin structures with resin thermo-oxidative stability, resin glass transition temperature and composite initial mechanical properties [NASA-TM-100791] p 103 N88-16877
Design and demonstration of a system for the deposition of atomic-oxygen durable coatings for reflective solar dynamic power system concentrators [NASA-CR-4158] p 64 N88-25474

- A thermally modified polymer matrix composite material with structural integrity to 371 C [NASA-TM-100922] p 76 N88-25483

OXIDATION-REDUCTION REACTIONS

- Experimental studies in vortex pair motion coincident with a liquid reaction p 142 A88-46316
Electrocatalytic reduction of oxygen on modified oxide surfaces [NASA-TM-101333] p 81 N88-29952

OXIDE FILMS

- Temperature stability of Al(x)Ga(1-x)As (x = 0-1) thermal oxide masks for selective-area epitaxy p 221 A88-45858
Deposition of vanadium oxide films by direct-current magnetron reactive sputtering p 221 A88-51286
Direct-current magnetron fabrication of indium tin oxide/InP solar cells p 200 A88-51289

OXIDIZERS

- Oxidizer heat exchanger component test [NASA-CR-182159] p 67 N88-29876

OXYGEN

- Catalytic ignition of hydrogen and oxygen propellants [AIAA PAPER 88-3300] p 109 A88-48764
The carbon dioxide chaperon efficiency for the reaction $H + O_2 + M$ yields $HO_2 + M$ from ignition delay times behind reflected shock waves [NASA-TM-100125] p 79 N88-15036
Catalytic ignition of hydrogen and oxygen propellants [NASA-TM-100957] p 63 N88-24689
Design and demonstration of a system for the deposition of atomic-oxygen durable coatings for reflective solar dynamic power system concentrators [NASA-CR-4158] p 64 N88-25474

OXYGEN ATOMS

- Oxygen plasma effects on several liquid droplet radiator fluids p 142 A88-47962
Technologies for protection of the Space Station power system surfaces in atomic oxygen environment p 41 A88-52331
Degradation mechanisms of materials for large space systems in low Earth orbit [NASA-CR-181472] p 71 N88-10896
Mast material test program (MAMATEP) [NASA-TM-100821] p 74 N88-19592

OXYHALIDES

- Direct mass spectrometric identification of silicon oxychloride compounds p 78 A88-44425

P

P WAVES

- Acousto-ultrasonic input-output characterization of unidirectional fiber composite plate by P waves [NASA-CR-4162] p 180 N88-25923

P-I-N JUNCTIONS

- Study of Staebler-Wronsky degradation effect in a Si:H based P-I-N solar cells [NASA-CR-182564] p 203 N88-25970

P-N JUNCTIONS

- Behavior of ion-implanted junction diodes in 3C SiC p 122 A88-15423
Gigard-tolerant power switches and memory elements p 123 A88-22704
A V-grooved AlGaAs/GaAs passivated pn junction p 125 A88-34300

P-TYPE SEMICONDUCTORS

- Ohmic contact formation in semi-insulating GaAs using shallow heavily doped p-type layers p 219 A88-11150
Characterization and modelling of open tube diffused n+p bulk InP solar cells p 199 A88-34270

PACKET SWITCHING

- Future switching satellites [AIAA PAPER 88-0802] p 46 A88-27553

PARALLEL COMPUTERS

- Time-partitioning simulation models for calculation of parallel computers p 206 A88-46961

PARALLEL FLOW

- Nonlinear roll-up of externally excited free shear layers p 141 A88-44445

PARALLEL PROCESSING (COMPUTERS)

- Hypercluster - Parallel processing for computational mechanics p 208 A88-40458
Time-partitioning simulation models for calculation of parallel computers p 206 A88-46961
Automating the parallel processing of fluid and structural dynamics calculations p 206 A88-46963
Performance limitations in parallel processor simulations p 208 A88-49101
Distributed computation of graphics primitives on a transputer network [NASA-TM-100814] p 206 N88-19147
Utilization of parallel processing in solving the inviscid form of the average-passage equation system for multistage turbomachinery [NASA-TM-89845] p 32 N88-21160

- Lewis Structures Technology, 1988. Volume 3: Structural Integrity Fatigue and Fracture Wind Turbines HOST [NASA-CP-3003-VOL-3] p 192 N88-22408

- Two-dimensional graphics tools for a transputer based display board [NASA-TM-100820] p 207 N88-22591

- Lewis Structures Technology, 1988. Volume 1: Structural Dynamics [NASA-CP-3003-VOL-1] p 194 N88-23226

- Parallel computer methods for eigenvalue extraction p 207 N88-23233

- Adapting high-level language programs for parallel processing using data flow p 207 N88-23234

- Implementing direct, spatially isolated problems on transputer networks [NASA-TM-101297] p 207 N88-27796

- User's manual for the two-dimensional transputer graphics toolkit [NASA-TM-100974] p 207 N88-27799

PARAMETER IDENTIFICATION

- Material parameter measurements at high temperatures [NASA-CR-182707] p 80 N88-20397

- A survey of oscillating flow in Stirling engine heat exchangers [NASA-CR-182108] p 152 N88-22322

- Parameter identification methods for improving structural dynamic models [NASA-TM-100612] p 194 N88-23994

PARTIAL DIFFERENTIAL EQUATIONS

- Adaptive grid generation p 209 A88-37363

PARTICLE DENSITY (CONCENTRATION)

- Performance and operating envelope of imaging and scattering particle sizing instruments [NASA-CR-180859] p 161 N88-12042

- Optical measurements of soot in premixed flames [NASA-TM-101305] p 156 N88-30090

PARTICLE EMISSION

- Axions from 1987A p 226 A88-35586

PARTICLE MASS

- Performance and operating envelope of imaging and scattering particle sizing instruments [NASA-CR-180859] p 161 N88-12042

PARTICLE MOTION

- Application of optical correlation techniques to particle imaging velocimetry [NASA-TM-101306] p 163 N88-29152

PARTICLE SIZE DISTRIBUTION

- Criteria for significance of simultaneous presence of both condensable vapors and aerosol particles on mass transfer (deposition) rates p 114 A88-10971

- Operating envelopes of particle sizing instrumentation used for icing research [AIAA PAPER 88-0291] p 157 A88-22211

- Performance of laser Doppler velocimeter with polydisperse seed particles in high speed flows [AIAA PAPER 88-0425] p 157 A88-22317

- Characteristics of fluid flow in the combustion synthesis of TiC from the elements p 110 A88-28564

- Performance and operating envelope of imaging and scattering particle sizing instruments [NASA-CR-180859] p 161 N88-12042

- Operating envelopes of particle sizing instrumentation used for icing research [NASA-CR-180870] p 161 N88-13573

- Optical measurements of soot and temperature profiles in premixed propane-oxygen flames [NASA-TM-101343] p 115 N88-29997

- Optical measurements of soot in premixed flames [NASA-TM-101305] p 156 N88-30090

PARTICLE SPIN

- Calculations of rates for direct detection of neutralino dark matter p 227 A88-48463

PARTICLE THEORY

- Cosmology and particle physics p 226 A88-39734

PARTICLE TRACKS

- Application of optical correlation techniques to particle imaging velocimetry [NASA-TM-101306] p 163 N88-29152

PARTICLES

- Criteria for significance of simultaneous presence of both condensable vapors and aerosol particles on mass transfer (deposition) rates p 114 A88-10971

- Four spot laser anemometer and optical access techniques for turbine applications p 159 A88-36513

- Particle-laden weakly swirling free jets - Measurements and predictions [AIAA PAPER 88-3138] p 142 A88-48757

- Particle-laden weakly swirling free jets: Measurements and predictions [NASA-TM-100920] p 34 N88-24639

- Reducing adhesion and agglomeration within a cloud of combustible particles [NASA-TM-100902] p 114 N88-26539

PARTITIONS (MATHEMATICS)

- Time-partitioning simulation models for calculation of parallel computers p 206 A88-46961
- Life prediction modeling based on strainrange partitioning p 178 N88-22425

PASSIVITY

- A V-grooved AlGaAs/GaAs passivated pn junction p 125 A88-34300

PAYLOADS

- Modal test/analysis correlation for the Centaur G prime launch vehicle p 44 A88-18631

PERFLUORO COMPOUNDS

- Surface catalytic degradation study of two linear perfluoropolyalkylethers at 345 C [NASA-TP-2774] p 68 N88-12543
- Improved perfluoroalkylether fluid development [NASA-CR-180872] p 80 N88-15851

PERFLUOROALKANE

- Improved perfluoroalkyl ether fluid development p 68 A88-28624

PERFORMANCE PREDICTION

- Real gas properties and Space Shuttle Main Engine fuel turbine performance prediction [ASME PAPER 87-GT-106] p 50 A88-11038
- Calibration and comparison of the NASA Lewis free-piston Stirling engine model predictions with RE-1000 test data p 165 A88-11967
- Sensitivity study of the monogroove with screen heat pipe design [AIAA PAPER 88-0470] p 137 A88-22346
- Model helicopter performance degradation with simulated ice shapes p 17 A88-22783
- Performance and efficiency evaluation and heat release study of a direct-injection stratified-charge rotary engine [SAE PAPER 870445] p 166 A88-23313
- Performance limitations in parallel processor simulations p 208 A88-49101
- Modelling the performance of the tapered artery heat pipe design for use in the radiator of the solar dynamic power system of the NASA Space Station [IAF PAPER 88-213] p 56 A88-55361
- A hybrid numerical technique for predicting the aerodynamic and acoustic fields of advanced turboprops [NASA-CR-174926] p 216 N88-12352
- Overview of NASA PTA propfan flight test program p 29 N88-15805
- Test results of a 40-kW Stirling engine and comparison with the NASA Lewis computer code predictions [NASA-TM-87050] p 201 N88-19013

PERFORMANCE TESTS

- Integrated heat pipe-thermal storage system performance evaluation p 132 A88-11803
- Regenerative fuel cell study for satellites in GEO orbit p 52 A88-11904
- Component variations and their effects on bipolar nickel-hydrogen cell performance p 197 A88-11914
- Test results of a 60 volt bipolar nickel-hydrogen battery p 198 A88-11916
- Description of an oscillating flow test program p 133 A88-11963
- Bit-error-rate testing of high-power 30-GHz traveling-wave tubes for ground-terminal applications p 122 A88-19781
- High thermal-transport capacity heat pipes for space radiators [SAE PAPER 871509] p 136 A88-21155
- High speed propeller performance and noise predictions at takeoff/landing conditions p 215 A88-22193
- Performance and efficiency evaluation and heat release study of a direct-injection stratified-charge rotary engine [SAE PAPER 870445] p 166 A88-23313
- Design and performance of controlled-diffusion stator compared with original double-circular-arc stator [SAE PAPER 871783] p 20 A88-30777
- Radiation and temperature effects in gallium arsenide, indium phosphide, and silicon solar cells p 125 A88-34321
- An extended life and performance test of a low-power arcjet [AIAA PAPER 88-3106] p 55 A88-48756
- The four spot time-of-flight laser anemometer p 164 N88-11145
- Constitutive modeling for isotropic materials p 186 N88-11172
- Lewis' enhanced laboratory for research into the fatigue and constitutive behavior of high temperature materials p 186 N88-11177
- Performance and combustion characteristics of direct-injection stratified-charge rotary engines [NASA-TM-100134] p 25 N88-12490
- Seal technology for liquid oxygen (LOX) turbopumps [NASA-CR-174866] p 171 N88-13603
- High speed propeller performance and noise predictions at takeoff/landing conditions p 216 N88-13960

Determining structural performance

- Simulation test beds for the space station electrical power system p 27 N88-15787
- [NASA-TM-100786] p 44 N88-17715
- Testing of a one-bladed 30-meter-diameter rotor on the DOE/NASA Mod-O wind turbine [NASA-TM-100274] p 201 N88-19014
- Microgravity manipulator demonstration p 173 N88-23242
- An extended life and performance test of a low-power arcjet [NASA-TM-100942] p 63 N88-24687
- Small scale bipolar nickel-hydrogen testing [NASA-TM-100936] p 202 N88-25059
- Alkaline fuel cell performance investigation [NASA-TM-100937] p 81 N88-27267
- Performance of 10-kW class xenon ion thrusters [NASA-TM-101292] p 65 N88-28088
- Performance and lifetime assessment of MPD arc thruster technology [NASA-TM-101293] p 66 N88-29860

PERMANENT MAGNETS

- Study of free-piston Stirling engine driven linear alternators [NASA-CR-181425] p 170 N88-10355

PEROVSKITES

- Advantages of barium peroxide in the powder synthesis of perovskite superconductors p 221 A88-41496

PEROXIDES

- Electrocatalytic reduction of oxygen on modified oxide surfaces [NASA-TM-101333] p 81 N88-29952

PERSONNEL

- Lewis materials research and technology: An overview p 223 N88-16699

PERTURBATION THEORY

- Finite element methods in probabilistic mechanics p 212 A88-29060
- Theory versus experiment for the rotordynamic coefficients of labyrinth gas seals. I - A two control volume model p 167 A88-31535

PHASE CHANGE MATERIALS

- Fluoride salts as phase change materials for thermal energy storage in the temperature range 1000-1400 K p 199 A88-33734

PHASE CONTROL

- Active phase compensation system for fiber optic holography [NASA-TM-101295] p 162 N88-26641

PHASE DIAGRAMS

- Simulating the cooling of an immiscible alloy p 83 A88-20199
- Interdiffusion in Ni-rich, Ni-Cr-Al alloys at 1100 and 1200 C. I - Diffusion paths and microstructures. II - Diffusion coefficients and predicted concentration profiles p 84 A88-24485

PHASE SHIFT CIRCUITS

- Development of 20 GHz monolithic transmit modules [NASA-CR-182134] p 222 N88-24539

PHASED ARRAYS

- Optically controlled phased-array antenna technology for space communication systems [NASA-TM-100852] p 119 N88-18809
- Optical RF distribution links for MMIC phased array antennas [NASA-TM-100841] p 128 N88-20555
- Optically interconnected phased arrays [NASA-TM-100855] p 128 N88-21400
- High frequency GaAlAs modulator and photodetector for phased array antenna applications [NASA-TM-101328] p 130 N88-30048

PHENOMENOLOGY

- A viscoplastic theory applied to copper [NASA-TM-100831] p 189 N88-21497

PHENYLS

- Silsesquioxanes as precursors to ceramic composites p 69 A88-12599

PHOSPHORIC ACID FUEL CELLS

- Status of commercial fuel cell powerplant system development p 198 A88-11925

PHOTOACOUSTIC MICROSCOPY

- Nondestructive evaluation of structural ceramics by photoacoustic microscopy [NASA-CR-180858] p 103 N88-16868

PHOTOCONDUCTORS

- Microwave response of an HEMT photoconductor [NASA-TM-100819] p 128 N88-18835

PHOTOELECTRON SPECTROSCOPY

- Rapid thermal annealing of indium phosphide compound semiconductors p 220 A88-26196

PHOTOLUMINESCENCE

- Low-temperature photoluminescence studies of chemical-vapor-deposition-grown 3C-SiC on Si p 127 A88-53396

PHOTOMETERS

- High frequency GaAlAs modulator and photodetector for phased array antenna applications [NASA-TM-101328] p 130 N88-30048

PHOTOMICROGRAPHY

- Multielement mapping of alpha-SiC by scanning Auger microscopy p 158 A88-27617

PHOTOVOLTAIC CELLS

- Recent developments in indium phosphide space solar cell research p 50 A88-11785
- A novel photovoltaic power system which uses a large area concentrator mirror p 197 A88-11811
- Performance characteristics of a combination solar photovoltaic heat engine energy converter p 197 A88-11813
- High temperature solid oxide regenerative fuel cell for solar photovoltaic energy storage p 197 A88-11905
- Optical measurements pertaining to Space Station solar dynamic power systems [IAF PAPER 87-229] p 42 A88-15954
- Radiation performance of AlGaAs and InGaAs concentrator cells and expected performance of cascade structures p 125 A88-34356
- Space Station Photovoltaic power modules p 56 A88-52333

- Photovoltaic power modules for NASA's manned space station [NASA-TM-100229] p 57 N88-11745

- Recent progress in space photovoltaic systems [NASA-TM-100208] p 128 N88-11966

- Low Earth orbit environmental effects on the space station photovoltaic power generation systems [NASA-TM-100230] p 225 N88-12429

- Design description report for a photovoltaic power system for a remote satellite earth terminal [NASA-CR-179586] p 200 N88-12875

- Radiation performance of AlGaAs concentrator cells and expected performance of cascade structures [NASA-TM-100145] p 200 N88-12878

- Oxidation and protection of fiberglass-epoxy composite masts for photovoltaic arrays in the low Earth orbital environment [NASA-TM-100839] p 104 N88-18734

- Mast material test program (MAMATEP) [NASA-TM-100821] p 74 N88-19592

- Power systems for production, construction, life support and operations in space [NASA-TM-100838] p 60 N88-21254

- An integrated and modular digital modeling approach for the space station electrical power system development [NASA-TM-100904] p 61 N88-22935

- Advanced photovoltaic power system technology for lunar base applications [NASA-TM-100965] p 65 N88-26402

- Photovoltaic conversion [NASA-TM-100965] p 65 N88-26402

- Solar concentrator advanced development project p 50 A88-11799

- Space solar cell research - Problems and potential p 123 A88-21605

- Issues in space photovoltaic research and technology p 199 A88-34230

- Development of a dome Fresnel lens/gallium arsenide photovoltaic concentrator for space applications p 199 A88-34310

- Mast material test program (MAMATEP) --- for Solar Array Assembly of Space Station Photovoltaic Power Module [AIAA PAPER 88-2475] p 70 A88-35945

- Photovoltaic effect [AIAA PAPER 88-2475] p 70 A88-35945

- Photovoltaic effect [AIAA PAPER 88-2475] p 70 A88-35945

- Photovoltaic effect [AIAA PAPER 88-2475] p 70 A88-35945

- Photovoltaic effect [AIAA PAPER 88-2475] p 70 A88-35945

- Photovoltaic effect [AIAA PAPER 88-2475] p 70 A88-35945

- Photovoltaic effect [AIAA PAPER 88-2475] p 70 A88-35945

- Photovoltaic effect [AIAA PAPER 88-2475] p 70 A88-35945

- Photovoltaic effect [AIAA PAPER 88-2475] p 70 A88-35945

- Photovoltaic effect [AIAA PAPER 88-2475] p 70 A88-35945

- Photovoltaic effect [AIAA PAPER 88-2475] p 70 A88-35945

- Photovoltaic effect [AIAA PAPER 88-2475] p 70 A88-35945

- Photovoltaic effect [AIAA PAPER 88-2475] p 70 A88-35945

- Photovoltaic effect [AIAA PAPER 88-2475] p 70 A88-35945

- Photovoltaic effect [AIAA PAPER 88-2475] p 70 A88-35945

- Photovoltaic effect [AIAA PAPER 88-2475] p 70 A88-35945

- Photovoltaic effect [AIAA PAPER 88-2475] p 70 A88-35945

- Photovoltaic effect [AIAA PAPER 88-2475] p 70 A88-35945

- Photovoltaic effect [AIAA PAPER 88-2475] p 70 A88-35945

- Photovoltaic effect [AIAA PAPER 88-2475] p 70 A88-35945

- Photovoltaic effect [AIAA PAPER 88-2475] p 70 A88-35945

The effect of eddy distribution on momentum and heat transfer near the wall in turbulent pipe flow
[NASA-TM-100257] p 150 N88-15984

PISTON ENGINES

1987 overview of free-piston Stirling technology for space power application p 53 A88-11942
A comparison of Stirling engines for use with a 25 kW dish-electric conversion system p 53 A88-11943

PISTONS

Overview of free-piston Stirling engine technology for space power application
[NASA-TM-88886] p 223 N88-12427
Hot piston ring tests
[NASA-TM-100256] p 201 N88-14486
Hot piston ring/cylinder liner materials: Selection and evaluation
[NASA-TM-100276] p 102 N88-15872

PITCH (MATERIAL)

Differential scanning calorimetric survey of brominated PAN, pitch-based and vapor-grown fibers p 98 A88-32854

PLANE STRAIN

Analysis of crack propagation in roller bearings using the boundary integral equation method - A mixed-mode loading problem p 168 A88-49183
Fracture mechanics p 194 N88-23877

PLANE WAVES

Polarization determination utilizing two arbitrarily polarized antennas p 116 A88-47424
Saturation and the limit of jet mixing enhancement by single frequency plane wave excitation - Experiment and theory
[AIAA PAPER 88-3613] p 8 A88-48899
Saturation and the limit of jet mixing enhancement by single frequency plane wave excitation: Experiment and theory
[NASA-TM-100882] p 12 N88-23732

PLANETARY MAGNETOSPHERES

Voids in Jovian magnetosphere revisited - Evidence of spacecraft charging p 226 A88-22879

PLANETARY SURFACES

Small reactor power systems for manned planetary surface bases
[NASA-TM-100223] p 227 N88-13209
Electromagnetic powered vehicles (EMPV) for Mars exploration p 62 N88-24388

PLASMA DENSITY

Threshold-determining mechanisms for discharges in high-voltage solar arrays p 50 A88-11738
Voids in Jovian magnetosphere revisited - Evidence of spacecraft charging p 226 A88-22879

PLASMA DIAGNOSTICS

Plasma wave turbulence around the shuttle - Results from the Spacelab-2 flight p 218 A88-47783
Double-probe potential measurements near the Spacelab 2 electron beam p 204 A88-53464

PLASMA GENERATORS

30-cm electron cyclotron plasma generator p 122 A88-18633

PLASMA INTERACTIONS

Electron beam experiments at high altitudes p 47 A88-46799
Oxygen plasma effects on several liquid droplet radiator fluids p 142 A88-47962

PLASMA POTENTIALS

Hollow cathodes as electron emitting plasma contactors - Theory and computer modeling p 218 A88-47973

PLASMA PROBES

Comment on 'Ram ion scattering caused by Space Shuttle v x B induced differential charging' by I. Katz and V. A. Davis p 204 A88-35775

PLASMA PROPULSION

The effects of magnetic nozzle configurations on plasma thrusters
[NASA-CR-183096] p 219 N88-26223
Performance and lifetime assessment of MPD arc thruster technology
[NASA-TM-101293] p 66 N88-29860

PLASMA SPRAYING

Some adhesion/cohesion characteristics of plasma-sprayed ZrO₂-Y₂O₃ under tensile loading p 95 A88-12589
The effects of atmosphere on the tribological properties of a chromium carbide based coating for use to 760 C p 98 A88-32372

Plasma deposition of amorphous hydrogenated carbon films on III-V semiconductors p 220 A88-32862
Creep-fatigue behavior of NiCoCrAlY coated PWA 1480 superalloy single crystals p 86 A88-35911
Thermal expansion mismatch and oxidation in thermal barrier coatings p 170 N88-11182
Thermal barrier coating life prediction model development p 170 N88-11184
Self-lubricating coatings for high-temperature applications p 103 N88-16703

Thermal barrier coating life-prediction model development
[NASA-CR-179507] p 107 N88-28142

PLASMA TURBULENCE

Plasma wave turbulence around the shuttle - Results from the Spacelab-2 flight p 218 A88-47783

PLASMA-ELECTROMAGNETIC INTERACTION

Electron collection by multiple objects within a single sheath p 219 A88-54999

PLASMAS (PHYSICS)

Plasma assisted surface coating/modification processes - An emerging technology p 114 A88-38927
Space plasma contactor research, 1987
[NASA-CR-182148] p 219 N88-23649

PLASMONS

Solar energy conversion through the interaction of plasmons with tunnel junctions. Part A: Solar cell analysis. Part B: Photoconductor analysis
[NASA-CR-183044] p 203 N88-27621

PLASTIC DEFORMATION

Plasticity analysis of wear phenomena as an aid in the development of abrasible materials p 164 A88-10938
On the cyclic stress-strain behaviour of a Ni-base superalloy at room temperature p 84 A88-24521
A nonlinear viscoelastic constitutive equation - Yield predictions in multiaxial deformations p 185 A88-54912

Finite element (MARC) solution technologies for viscoplastic analyses p 191 N88-22389
Anisotropic constitutive modeling for nickel-base single crystal superalloys
[NASA-CR-182157] p 95 N88-29961

PLASTIC FLOW

Phenomenological modeling of hardening and thermal recovery in metals p 84 A88-24037
The influence of grain size and composition on 1000 to 1400 K slow plastic flow properties of NiAl p 85 A88-29098

PLASTIC PROPERTIES

Plasticity analysis of wear phenomena as an aid in the development of abrasible materials p 164 A88-10938
Thermomechanical behavior of plasma-sprayed ZrO₂-Y₂O₃ coatings influenced by plasticity, creep, and oxidation p 95 A88-12588
3D inelastic analysis methods for hot section components p 185 N88-11164

PLATE THEORY

An efficient Mindlin finite strip plate element based on assumed strain distribution p 192 N88-22407
Improved finite strip Mindlin plate bending element using assumed shear strain distributions
[NASA-TM-100928] p 196 N88-29195

PLATINUM

Compatibility of dispersion-strengthened platinum with resistojet propellants
[NASA-TP-2765] p 58 N88-12538

PLUMES

Aeroacoustics of advanced STOVL aircraft plumes
[SAE PAPER 872358] p 215 A88-30998
Unsteady features of jets in lift and cruise modes for VTOL aircraft
[SAE PAPER 872359] p 6 A88-37220

Evaluation of the communications impact of a low power arcjet thruster
[AIAA PAPER 88-3105] p 55 A88-48755

A computational analysis of under-expanded jets in the hypersonic regime
[AIAA PAPER 88-4361] p 8 A88-50604

On the correlation of plume centerline velocity decay of turbulent acoustically excited jets
[NASA-TM-100193] p 11 N88-16681

Evaluation of the communications impact of a low power arcjet thruster
[NASA-TM-100926] p 63 N88-24682

A computational analysis of under-expanded jets in the hypersonic regime
[NASA-TM-101319] p 13 N88-27174

Experimental evaluation of resistojet thruster plume shields
[NASA-TM-101363] p 66 N88-29868

PLY ORIENTATION

An ideal clamping analysis for a cross-ply laminate p 181 A88-31347

PNEUMATIC CONTROL

Space station resistojet system requirements and interface definition study
[NASA-CR-180832] p 58 N88-12541

POISSON EQUATION

I-BIEM, an iterative boundary integral equation method for computer solutions of current distribution problems with complex boundaries: A new algorithm. I - Theoretical p 205 A88-27795

POLAR ORBITS

Low thrust power-limited transfer for a pole squatter
[AIAA PAPER 88-4310] p 42 A88-50435

POLARIMETERS

Polarization determination utilizing two arbitrarily polarized antennas p 116 A88-47424

POLARIZATION (WAVES)

Polarization determination utilizing two arbitrarily polarized antennas p 116 A88-47424

POLLUTION TRANSPORT

Criteria for significance of simultaneous presence of both condensable vapors and aerosol particles on mass transfer (deposition) rates p 114 A88-10971

POLYCRYSTALS

Effect of the microstructure on the thermoelectric properties of polycrystalline lanthanum chalcogenides p 221 A88-40797
Microstructural effects on fracture toughness of polycrystalline ceramics in combined mode I and mode II loading
[ASME PAPER 88-GT-208] p 101 A88-54294

POLYIMIDE RESINS

PMR polyimide compositions for improved performance at 371 C p 96 A88-13172
Correlations of norbornenyl crosslinked polyimide resin structures with resin thermo-oxidative stability, resin glass transition temperature and composite initial mechanical properties
[NASA-TM-100791] p 103 N88-16877

POLYIMIDES

Substituted 1,1,1-Triaryl-2,2,2-Trifluoroethanes and processes for their synthesis
[NASA-CASE-LEW-14345-1] p 69 N88-26404

POLYMER CHEMISTRY

Structural Ceramics
[NASA-CP-2427] p 106 N88-23872
Substituted 1,1,1-Triaryl-2,2,2-Trifluoroethanes and processes for their synthesis
[NASA-CASE-LEW-14345-1] p 69 N88-26404
Novel ladder polymers for use as high temperature stable resins or coatings
[NASA-CASE-LEW-14203-1] p 108 N88-29984

POLYMER MATRIX COMPOSITES

PMR polyimide compositions for improved performance at 371 C p 96 A88-13172
Crack diffusion coefficient - A candidate fracture toughness parameter for short fiber composites p 70 A88-36945
Aeropropulsion '87. Session 1: Aeropropulsion Materials Research
[NASA-CP-10003-SESS-1] p 31 N88-16697
High temperature polymer matrix composites p 73 N88-16700
Nondestructive evaluation by acousto-ultrasonics p 177 N88-22412
A thermally modified polymer matrix composite material with structural integrity to 371 C
[NASA-TM-100922] p 76 N88-25483

POLYMER PHYSICS

A nonlinear viscoelastic constitutive equation - Yield predictions in multiaxial deformations p 185 A88-54912

POLYMERIC FILMS

Tribological properties of polymer films and solid bodies in a vacuum environment p 98 A88-35565

POLYMERIZATION

Polymer precursors for ceramic composites p 75 N88-23890
Novel ladder polymers for use as high temperature stable resins or coatings
[NASA-CASE-LEW-14203-1] p 108 N88-29984

POLYNOMIALS

Approximate polynomial preconditioning applied to biharmonic equations on vector supercomputers
[NASA-TM-100217] p 210 N88-10563

POLYSTYRENE

Curvilinear crack layer propagation p 96 A88-14568

POLYTETRAFLUOROETHYLENE

Thermal desorption study of physical forces at the PTFE surface p 77 A88-10963
Investigation of PTFE transfer films by infrared emission spectroscopy and phase-locked ellipsometry p 99 A88-35568

POROSITY

Porosity determination of thermal barrier coatings
[ASME PAPER 88-GT-278] p 68 A88-54350
Acoustic imaging of subtle porosity variations in ceramics p 101 A88-55044

POROUS BOUNDARY LAYER CONTROL

Onset of finger convection in a horizontal porous layer underlying a fluid layer p 140 A88-41572

POROUS MATERIALS

Plasticity analysis of wear phenomena as an aid in the development of abrasible materials p 164 A88-10938

PORTS (OPENINGS)

An analytical and experimental study of injection-locked two-port oscillators
[NASA-TM-100119] p 128 N88-12727

SUBJECT INDEX

PRESSURE GRADIENTS

POSITION INDICATORS

Accurate positioning of long, flexible ARM's (Articulated Robotic Manipulator) p 174 N88-23243

POSITION SENSING

Accurate positioning of long, flexible ARM's (Articulated Robotic Manipulator) p 174 N88-23243

POTENTIAL FLOW

A physically consistent model for artificial dissipation in transonic potential flow computations [NASA-TM-100846] p 211 N88-22652

The 2-D and 3-D time marching transonic potential flow method for propfans p 11 N88-23245
Reduced order models for nonlinear aerodynamics p 11 N88-23248

POWDER (PARTICLES)

Simple processing method for high-strength silicon carbide p 97 A88-19056
Colloidal characterization of silicon nitride and silicon carbide p 107 N88-23883

POWDER METALLURGY

Surface fatigue and failure characteristics of hot-forged powder metal AISI 4620, AISI 4640, and machined AISI 4340 steel spur gears p 165 A88-14591
Room temperature tensile ductility in powder processed B2 FeAl alloys p 85 A88-31694
Powder processing of nickel and other aluminides by hot consolidation p 87 A88-37158
Rapid solidification of highly undercooled liquids p 88 A88-41653
Processing, physical metallurgy and creep of NiAl + Ta and NiAl + Nb alloys [NASA-CR-182113] p 92 N88-21295

POWDERED ALUMINUM

Rapid solidification of highly undercooled liquids p 88 A88-41653

POWER AMPLIFIERS

Progress in MMIC technology for satellite communications p 126 A88-37844
Development of 20 GHz monolithic transmit modules [NASA-CR-182134] p 222 N88-24539

POWER CONDITIONING

Solar concentrator advanced development project p 50 A88-11799
A study of Schwarz converters for nuclear powered spacecraft p 51 A88-11823
Control considerations for high frequency, resonant, power processing equipment used in large systems p 51 A88-11829
SP-100 Advanced Technology Program p 52 A88-11846

Power systems for production, construction, life support and operations in space p 60 N88-21254

A role for high frequency superconducting devices in free space power transmission systems [NASA-TM-100971] p 130 N88-25830

The dc power control for a liquid-fed resistor [NASA-TM-101326] p 107 N88-29869

POWER CONVERTERS

Fast simulation techniques for switching converters p 122 A88-11878
Implementation of optimal trajectory control of series resonant converter p 126 A88-38796
Field oriented control of an induction machine in a high frequency link power system p 127 A88-54711
A cascaded Schwarz converter for high frequency power distribution p 127 A88-54713
Overview of free-piston Stirling engine technology for space power application [NASA-TM-88886] p 223 N88-12427

POWER EFFICIENCY

Adiabatic diesel engine component development: Reference engine for on-highway applications [NASA-CR-179531] p 224 N88-12428
Efficiency testing of a helicopter transmission planetary reduction stage [NASA-TP-2795] p 172 N88-15224

POWER FACTOR CONTROLLERS

An integrated approach to space station power system autonomous control p 52 A88-11853

POWER GAIN

Gain enhancement of microstrip antennas with overlying parasitic directors p 117 A88-48653

POWER MODULES (STS)

Photovoltaic power modules for NASA's manned space station [NASA-TM-100229] p 57 N88-11745

POWER SUPPLY CIRCUITS

Multi-hundred kilowatt roll ring assembly evaluation results [NASA-TM-100865] p 114 N88-21375

POWER TRANSMISSION

Power systems for production, construction, life support and operations in space [NASA-TM-100838] p 60 N88-21254

Power components for the space station 20-kHz power distribution system [NASA-TM-100866] p 114 N88-21374

A role for high frequency superconducting devices in free space power transmission systems [NASA-TM-100971] p 130 N88-25830

PRANDTL NUMBER

Explicit finite-volume time-marching calculations of total temperature distributions in turbulent flow p 139 A88-30517

PRECIPITATES

Characterization of precipitates in a niobium-zirconium-carbon alloy [NASA-TM-100848] p 93 N88-22981

PRECIPITATION HARDENING

Precipitation in a rapidly solidified and aged Ni-Al-Mo alloy p 82 A88-18528
Phenomenological modeling of hardening and thermal recovery in metals p 84 A88-24037
Dispersion strengthened NiAl alloys produced by rapid solidification processing p 88 A88-40588
Compatibility of dispersion-strengthened platinum with resistojel propellants [NASA-TP-2765] p 58 N88-12538

PRECONDITIONING

Approximate polynomial preconditioning applied to biharmonic equations on vector supercomputers [NASA-TM-100217] p 210 N88-10563

PREDICTION ANALYSIS TECHNIQUES

A prediction model of the depth-of-discharge effect on the cycle life of a storage cell p 197 A88-11896
An update of the total-strain version of SRP p 86 A88-35910

A model for life predictions of nickel-base superalloys in high-temperature low cycle fatigue p 87 A88-35913
Particle-laden weakly swirling free jets - Measurements and predictions [AIAA PAPER 88-3138] p 142 A88-48757
Fatigue life prediction modeling for turbine hot section materials p 184 A88-54144
Thermal barrier coating life prediction model development [ASME PAPER 88-GT-284] p 68 A88-54353

Component specific modeling p 206 N88-11166
Creep life prediction based on stochastic model of microstructurally short crack growth [NASA-TM-100245] p 186 N88-12825

Fatigue life prediction modeling for turbine hot section materials [NASA-TM-100291] p 187 N88-14453
Aeropropulsion '87. Session 3: Internal Fluid Mechanics Research [NASA-CP-10003-SESS-3] p 28 N88-15790

Evaluation of structural analysis methods for life prediction p 190 N88-21511
Whisker-reinforced ceramic composites for heat engine components p 105 N88-22410
Fracture technology for brittle materials p 192 N88-22417

Grain boundary oxidation and low-cycle fatigue at elevated temperatures p 193 N88-22420
Cumulative fatigue damage models p 193 N88-22422

Life prediction modeling based on strainrange partitioning p 178 N88-22425
Life prediction modeling based on cyclic damage accumulation p 178 N88-22426

Fatigue damage modeling for coated single crystal superalloys p 93 N88-22427
Life and reliability of rotating disks p 178 N88-22428

Review and assessment of the HOST turbine heat transfer program p 34 N88-22431
Space plasma contactor research, 1987 [NASA-CR-182148] p 219 N88-23649

Ceramics for turbine engines p 106 N88-23873
Some design considerations for ceramic components in heat engine applications p 106 N88-23875

Particle-laden weakly swirling free jets: Measurements and predictions [NASA-TM-100920] p 34 N88-24639
Thermal barrier coating life-prediction model development [NASA-CR-179507] p 107 N88-28142

PREDICTIONS
Calculation of thermomechanical fatigue life based on isothermal behavior p 181 A88-26450
Life prediction and constitutive models for engine hot section anisotropic materials program p 186 N88-11175

Coating life prediction p 170 N88-11181
Thermal barrier coating life prediction model p 170 N88-11184

Thermal barrier coating life prediction model p 171 N88-11185

A statistical rain attenuation prediction model with application to the advanced communication technology satellite project. Part 2: Theoretical development of a dynamic model and application to rain fade durations and tolerable control delays for fade countermeasures [NASA-TM-100242] p 118 N88-11945

Fiber composite structural durability and damage tolerance: Simplified predictive methods [NASA-TM-100179] p 72 N88-13409

Life prediction of thermomechanical fatigue using total strain version of strainrange partitioning (SRP): A proposal [NASA-TP-2779] p 187 N88-15263
Computational prediction of propellant reorientation p 109 N88-15940

A comparison of experimental and theoretical results for labyrinth gas seals with honeycomb stators [NASA-CR-182441] p 172 N88-16006

The analysis of fatigue crack growth mechanism and oxidation and fatigue life at elevated temperatures [NASA-CR-182129] p 94 N88-22987

The 2-D and 3-D time marching transonic potential flow method for propfans p 11 N88-23245

Aeroelastic forced response analysis of turbomachinery p 34 N88-23247

A statistical rain attenuation prediction model with application to the advanced communication technology satellite project. 1: Theoretical development and application to yearly predictions for selected cities in the United States [NASA-CR-179498] p 121 N88-29077

PRELAUNCH TESTS

Modal test/analysis correlation for the Centaur G prime launch vehicle p 44 A88-18631

PREMIXED FLAMES

Feasibility of hydroxyl concentration measurements by laser-saturated fluorescence in high-pressure flames p 77 A88-17218

The effect of gravity on premixed flame propagation and extinction in a vertical standard flammability tube p 78 A88-38532

Optical measurements of soot and temperature profiles in premixed propane-oxygen flames [NASA-TM-101343] p 115 N88-29997

Optical measurements of soot in premixed flames [NASA-TM-101305] p 156 N88-30090

PREMIXING

Mixing fuel particles for space combustion research using acoustics p 112 A88-49093
Mixing fuel particles for space combustion research using acoustics [NASA-TM-100295] p 43 N88-21186

PREPREGS

Fracture characteristics of angleplied laminates fabricated from overaged graphite/epoxy prepreg p 69 A88-16965

PRESSURE

Piezoviscous effects in nonconformal contacts lubricated hydrodynamically p 133 A88-12926

PRESSURE DEPENDENCE

Feasibility of hydroxyl concentration measurements by laser-saturated fluorescence in high-pressure flames p 77 A88-17218

PRESSURE DISTRIBUTION

Advanced turboprop wing installation effects measured by unsteady blade pressure and noise [AIAA PAPER 87-2719] p 3 A88-18655

Theory versus experiment for the rotordynamic coefficients of labyrinth gas seals. I - A two control volume model p 167 A88-31535
Gaseous environment of the Shuttle early in the Spacelab 2 mission p 47 A88-47972

Time-domain transient elastodynamic analysis of 3-D solids by BEM p 183 A88-48638
Solution of the Neumann pressure problem in general orthogonal coordinates using the multigrad technique p 144 A88-50330

Advanced turboprop wing installation effects measured by unsteady blade pressure and noise [NASA-TM-100200] p 9 N88-10008

Comparison of pressure distributions on model and full-scale NACA 64-621 airfoils with ailerons for wind turbine application [NASA-TM-100802] p 201 N88-21593

PRESSURE EFFECTS

An experimental investigation of the effect of test-cell pressure on the performance of resistojets [AIAA PAPER 88-3286] p 40 A88-44820

Pressure effects on the thermal stability of SiC fibers [NASA-TM-100146] p 71 N88-10120

PRESSURE GRADIENTS

The measurement of boundary layers on a compressor blade in cascade. III - Pressure surface boundary layers and the near wake [ASME PAPER 87-GT-250] p 132 A88-11132

PRESSURE MEASUREMENT

- Roll-up of vorticity in adverse-pressure-gradient boundary layers p 135 A88-19194
- Design point variation of 3-D loss and deviation for axial compressor middle stages p 8 A88-54189
- [ASME PAPER 88-GT-57]
- Local heat/mass transfer and pressure drop in a two-pass rib-roughened channel for turbine airfoil cooling [NASA-CR-179635] p 148 N88-12039

PRESSURE MEASUREMENT

- Chordwise pressure measurements on a blade of Mod-2 Wind Turbine p 2 A88-10970
- Wall shear stress measurement in blade end-wall corner region [ASME PAPER 87-GT-181] p 131 A88-11089
- Initial conditional effect on pressure waves in an axisymmetric jet [AIAA PAPER 88-3702] p 143 A88-48915
- Initial condition effect on pressure waves in an axisymmetric jet [NASA-TM-100915] p 153 N88-23184

PRESSURE SENSORS

- Fiber-linked interferometric pressure sensor p 157 A88-11743
- Calibration of high-temperature, fiber-optic, microbend, pressure transducers p 157 A88-22942

PRESSURE VESSELS

- The effect of compression on individual pressure vessel nickel/hydrogen components [NASA-TM-101312] p 81 N88-28109

PRESSURIZED WATER REACTORS

- Measurements of natural circulation flow in a scale model PWR reactor system during postulated degraded core accidents using laser anemometry p 159 A88-43917

PRETREATMENT

- Colloidal characterization of silicon nitride and silicon carbide p 107 N88-23883

PRINTING

- Synthesis and characterization of high-T(sub c) screen-printed Y-Ba-Cu-O films on alumina [NASA-TM-100860] p 222 N88-22805

PRISMS

- Optical alignment of Centaur's inertial guidance system [NASA-TM-88844] p 43 N88-12515

PROBABILITY DENSITY FUNCTIONS

- Efficient probabilistic fracture mechanics analysis p 180 A88-16933
- A probabilistic model of brittle crack formation p 180 A88-18696
- Finite element methods in probabilistic mechanics p 212 A88-29060

PROBABILITY THEORY

- Probabilistic structural analysis methods for space propulsion system components p 54 A88-16441
- An expert system for probabilistic description of loads on space propulsion system structural components [AIAA PAPER 88-2371] p 182 A88-32308
- Validation of the NESSUS probabilistic finite element analysis computer program [AIAA PAPER 88-2372] p 205 A88-32309
- Probabilistic structural analysis of aerospace components using NESSUS [AIAA PAPER 88-2373] p 182 A88-32310
- NESSUS/EXPERT - An expert system for probabilistic structural analysis methods [AIAA PAPER 88-2374] p 206 A88-32311
- Probabilistic composite micromechanics [AIAA PAPER 88-2375] p 182 A88-32312
- Probabilistic constitutive relationships for cyclic material strength models [AIAA PAPER 88-2376] p 182 A88-32313
- Probabilistic Structural Analysis Methods for select space propulsion system structural components (PSAM) p 56 A88-49659
- Probabilistic structural analysis computer code (NESSUS) p 191 N88-22397
- Probabilistic structural analysis to quantify uncertainties associated with turbopump blades [NASA-TM-100278] p 76 N88-28094

PROBLEM SOLVING

- A Navier-Stokes solver using the LU-SSOR TVD algorithm p 6 A88-30560
- Thermo-elasto-viscoplastic analysis of problems in extension and shear p 183 A88-41042
- Implementing direct, spatially isolated problems on transputer networks [NASA-TM-101297] p 207 N88-27796

PROCESS CONTROL (INDUSTRY)

- Method for generation of spiral bevel gears with conjugate gear tooth surfaces [ASME PAPER 86-DET-3] p 165 A88-10973
- Improved silicon nitride for advanced heat engines [NASA-CR-175006] p 102 N88-15886

PRODUCT DEVELOPMENT

- Mod II engine development p 165 A88-11972

- Assessment, development, and application of combustor aerothermal models p 24 A88-54140
- Assessment, development and application of combustor aerothermal models [NASA-TM-100290] p 32 N88-19469
- Advanced Gas Turbine (AGT) technology development project [NASA-CR-180891] p 225 N88-20230

PROGRAM VERIFICATION (COMPUTERS)

- The NASA aircraft icing research program p 15 N88-15803

PROJECT MANAGEMENT

- Aeropropulsion structures p 27 N88-15786

PROJECT PLANNING

- Supersonic STOVL propulsion technology program: An overview p 29 N88-15808

PROJECTILES

- Contact force history and dynamic response due to the impact of a soft projectile [NASA-TM-100961] p 175 N88-26679

PROP-FAN TECHNOLOGY

- Noise characteristics of model counter-rotating Prop-Fans [AIAA PAPER 87-2656] p 213 A88-16526
- Measurement and prediction of propeller flow field on the PTA aircraft at speeds of up to Mach 0.85 --- Propfan Test Assessment [AIAA PAPER 88-0667] p 19 A88-22497
- Experimental classical flutter results of a composite advanced turboprop model p 21 A88-35528
- High-speed propeller noise predictions - Effects of boundary conditions used in blade loading calculations p 215 A88-36270
- Advanced composite turboprops - Modeling, structural, and dynamic analyses [ASME PAPER 87-GT-78] p 21 A88-36745
- Aeroelastic effects of alternate blade sweep on advanced propfan rotor [ASME PAPER 87-WA/AERO-8] p 184 A88-51328
- Analysis and test evaluation of the dynamic stability of three advanced turboprop models at zero forward speed [NASA-CR-175025] p 26 N88-14095
- Analysis and test evaluation of the dynamic response and stability of three advanced turboprop models at low forward speed [NASA-CR-175026] p 27 N88-14096
- Large-Scale Advanced Prop-Fan (LAP) blade design [NASA-CR-174790] p 27 N88-14097
- Aeropropulsion '87. Session 5: Subsonic Propulsion Technology [NASA-CP-10003-SESS-5] p 28 N88-15800
- Overview of NASA PTA propfan flight test program p 29 N88-15805
- Vibration and flutter characteristics of the SR7L large-scale propfan [NASA-TM-100272] p 188 N88-18036
- Large-Scale Advanced Prop-Fan (LAP) [NASA-CR-182112] p 32 N88-20306
- The 2-D and 3-D time marching transonic potential flow method for propfans p 11 N88-23245
- Propfan test assessment testbed aircraft stability and control/performance 1/9-scale wind tunnel tests [NASA-CR-182121] p 17 N88-26360
- Structural Tailoring of Advanced Turboprops (STAT) [NASA-CR-180861] p 36 N88-28074
- Experimental investigation of propfan aeroelastic response in off-axis flow with mistuning [NASA-TM-101320] p 196 N88-28344
- Multiple-Purpose Subsonic Naval Aircraft (MPSNA): Multiple Application Propfan Study (MAPS) [NASA-CR-175104] p 18 N88-28917
- SR-7A aeroelastic model design report [NASA-CR-174791] p 36 N88-28928
- Optical measurement of unducted fan blade deflections [NASA-TM-100966] p 163 N88-29142
- Euler analysis of a swirl recovery vane design for use with an advanced single-rotation propfan [NASA-TM-101357] p 14 N88-29771

PROPAGATION

- Space communication link propagation data for selected cities within the multiple beam and steerable antenna coverage areas of the advanced communications technology satellite [NASA-TM-100861] p 120 N88-23070

PROPELLANT MODES

- Modal attenuation in multilayered coated waveguides p 126 A88-45755

PROPELLANT COMBUSTION

- Catalytic ignition of hydrogen and oxygen propellants [AIAA PAPER 88-3300] p 109 A88-48764
- Mixing fuel particles for space combustion research using acoustics p 112 A88-49093
- Mixing fuel particles for space combustion research using acoustics [NASA-TM-100295] p 43 N88-21186

- Finite area combustor theoretical rocket performance [NASA-TM-100785] p 60 N88-21252
- Catalytic ignition of hydrogen and oxygen propellants [NASA-TM-100957] p 63 N88-24689

PROPELLANT GRAINS

- Mixing fuel particles for space combustion research using acoustics p 112 A88-49093
- Mixing fuel particles for space combustion research using acoustics [NASA-TM-100295] p 43 N88-21186

PROPELLANT STORAGE

- Weight savings in aerospace vehicles through propellant scavenging [NASA-TM-100900] p 44 N88-25470

PROPELLANT TANKS

- Design, development, and test of Shuttle/Centaur G-prime cryogenic tankage thermal protection systems p 47 A88-53182
- Computational prediction of propellant reorientation p 109 N88-15940

PROPELLANT TRANSFER

- Low thrust power-limited transfer for a pole squatter [AIAA PAPER 88-4310] p 42 A88-50435

PROPELLANTS

- Water-propellant resistojets for man-tended platforms [IAF PAPER 87-259] p 54 A88-15975

PROPELLER BLADES

- High speed propeller performance and noise predictions at takeoff/landing conditions [AIAA PAPER 88-0264] p 215 A88-22193
- Parametric studies of advanced turboprops [AIAA PAPER 88-2266] p 20 A88-32223
- Experimental classical flutter results of a composite advanced turboprop model p 21 A88-35528
- Optimizing advanced propeller designs by simultaneously updating flow variables and design parameters [AIAA PAPER 88-2532] p 6 A88-40718
- High speed propeller performance and noise predictions at takeoff/landing conditions [NASA-TM-100267] p 216 N88-13960
- Large-Scale Advanced Prop-Fan (LAP) blade design [NASA-CR-174790] p 27 N88-14097
- Numerical simulation of subsonic and transonic propeller flow [NASA-TM-100163] p 11 N88-20262
- Large-Scale Advanced Prop-Fan (LAP) [NASA-CR-182112] p 32 N88-20306
- Optical measurement of propeller blade deflections [NASA-TP-2841] p 163 N88-28286

PROPELLER EFFICIENCY

- Analytical determination of propeller performance degradation due to ice accretion p 19 A88-19669
- Aerodynamic interaction between propellers and wings [AIAA PAPER 88-0665] p 5 A88-22495
- Summary of low-speed wind tunnel results of several high-speed counterrotation propeller configurations [AIAA PAPER 88-3149] p 7 A88-48758
- Summary of low-speed wind tunnel results of several high-speed counterrotation propeller configurations [NASA-TM-100945] p 13 N88-24597

PROPELLER FANS

- Cruise noise of the 2/9 scale model of the Large-scale Advanced Propfan (LAP) propeller, SR-7A [AIAA PAPER 87-2717] p 214 A88-16565
- The effects of rotational flow, viscosity, thickness, and shape on transonic flutter dip phenomena [AIAA PAPER 88-2348] p 182 A88-32289
- The effects of rotational flow, viscosity, thickness, and shape on transonic flutter dip phenomena [NASA-TM-100811] p 188 N88-18969
- Aeroelastic response of metallic and composite propfan models in yawed flow [NASA-TM-100964] p 37 N88-29807

PROPELLER SLIPSTREAMS

- Aerodynamic interaction between propellers and wings [AIAA PAPER 88-0665] p 5 A88-22495
- Numerical simulation of subsonic and transonic propeller flow [NASA-TM-100163] p 11 N88-20262

PROPELLERS

- Advanced turboprop wing installation effects measured by unsteady blade pressure and noise [AIAA PAPER 87-2719] p 3 A88-18655
- Analytical determination of propeller performance degradation due to ice accretion p 19 A88-19669
- High-speed propeller noise predictions - Effects of boundary conditions used in blade loading calculations p 215 A88-36270
- Porous wind tunnel corrections for counterrotation propeller testing [AIAA PAPER 88-2055] p 6 A88-44490
- Advanced turboprop wing installation effects measured by unsteady blade pressure and noise [NASA-TM-100200] p 9 N88-10008
- Advanced propeller research p 29 N88-15806

SUBJECT INDEX

Porous wind tunnel corrections for counterrotation propeller testing
[NASA-TM-100873] p 11 N88-22019

NASA advanced turboprop research and concept validation program
[NASA-TM-100891] p 34 N88-22902

NASA/industry advanced turboprop technology program
[NASA-TM-100929] p 35 N88-24641

Optical measurement of unducted fan blade deflections
[NASA-TM-100966] p 163 N88-29142

Euler analysis of a swirl recovery vane design for use with an advanced single-rotation propfan
[NASA-TM-101357] p 14 N88-29771

PROPULSION

Recent advances in high temperature instrumentation for hot section applications
[NASA-TM-100282] p 161 N88-14339

Aeropropulsion '87. Session 3: Internal Fluid Mechanics Research
[NASA-CP-10003-SESS-3] p 28 N88-15790

Chemical reacting flows
[NASA-CP-10003-SESS-4] p 28 N88-15794

Aeropropulsion '87. Session 4: Instrumentation and Controls Research
[NASA-CP-10003-SESS-5] p 28 N88-15799

Directions in propulsion control
[NASA-CP-10003-SESS-6] p 28 N88-15799

Aeropropulsion '87. Session 5: Subsonic Propulsion Technology
[NASA-CP-10003-SESS-7] p 28 N88-15800

Rotorcraft transmission
[NASA-CP-10003-SESS-8] p 172 N88-15802

Rotorcraft flight-propulsion control integration
[NASA-CP-10003-SESS-9] p 38 N88-16643

Impact and promise of NASA aeropropulsion technology
[NASA-CP-10003-SESS-10] p 31 N88-16698

Institute for Computational Mechanics in Propulsion (ICOMP)
[NASA-TM-100790] p 211 N88-19202

PROPULSION SYSTEM CONFIGURATIONS

Ground tests confirm the promise of hypersonic propulsion
[NASA-TM-100225] p 2 A88-10369

Space Station propulsion system technology
[NASA-TM-100226] p 54 A88-21255

Flight propulsion control integration for V/STOL aircraft
[SAE PAPER 872330] p 21 A88-37199

Scale model acoustic testing of counterrotating fans
[AIAA PAPER 88-2057] p 22 A88-37947

The challenges and opportunities of supersonic transport propulsion technology
[AIAA PAPER 88-2985] p 23 A88-48032

Recent advances in low-thrust propulsion technology
[AIAA PAPER 88-3283] p 55 A88-48761

An 8-cm ion thruster characterization
[NASA-CR-180819] p 56 N88-10106

Flight propulsion control integration for V/STOL aircraft
[NASA-TM-100226] p 38 N88-11680

Institute for Computational Mechanics in Propulsion (ICOMP) first year summary
[NASA-TM-100225] p 210 N88-12330

Space station onboard propulsion system: Technology study
[NASA-CR-179233] p 59 N88-15006

Internal fluid mechanics research on supercomputers for aerospace propulsion systems
[NASA-TM-100289] p 149 N88-15188

Aeropropulsion '87. Session 2: Aeropropulsion Structures Research
[NASA-CP-10003-SESS-2] p 27 N88-15785

Aeropropulsion structures
[NASA-CP-10003-SESS-3] p 27 N88-15786

Determining structural performance
[NASA-CP-10003-SESS-4] p 27 N88-15787

Life prediction technologies for aeronautical propulsion systems
[NASA-CP-10003-SESS-5] p 27 N88-15788

Integrated analysis and applications
[NASA-CP-10003-SESS-6] p 28 N88-15789

Aeropropulsion '87. Session 6: High-Speed Propulsion Technology
[NASA-CP-10003-SESS-7] p 29 N88-15807

Supersonic STOVL propulsion technology program: An overview
[NASA-CP-10003-SESS-8] p 29 N88-15808

Propulsion challenges and opportunities for high-speed transport aircraft
[NASA-CP-10003-SESS-9] p 30 N88-15809

Supersonic throughflow fans for high-speed aircraft
[NASA-CP-10003-SESS-10] p 30 N88-15810

High-speed inlet research program and supporting analyses
[NASA-TM-100797] p 17 N88-15811

CFD validation experiments for internal flows
[NASA-TM-100797] p 10 N88-16679

Lewis materials research and technology: An overview
[NASA-TM-100843] p 223 N88-16699

Application of advanced computational technology to propulsion CFD
[NASA-TM-100843] p 204 N88-19102

Electromagnetic propagation in PEC and absorbing curved S-ducts
[NASA-TM-100833] p 120 N88-19698

Advanced transmission studies
[NASA-TM-100867] p 173 N88-21454

Research and technology
[NASA-TM-100172] p 227 N88-22851

The challenges and opportunities of supersonic transport propulsion technology
[NASA-TM-100921] p 34 N88-23806

Heat transfer in aerospace propulsion
[NASA-TM-100874] p 154 N88-23957

Recent advances in low-thrust propulsion technology
[NASA-TM-100959] p 213 N88-25260

A reusable rocket engine intelligent control
[NASA-TM-100963] p 65 N88-26401

Development of sensors for ceramic components in advanced propulsion systems: Survey and evaluation of measurement techniques for temperature, strain and heat flux for ceramic components in advanced propulsion systems
[NASA-CR-182111] p 163 N88-28299

Experimental and analytical evaluation of the effects of simulated engine inlets on the blade vibratory stresses of the SR-3 model prop-fan
[NASA-CR-174959] p 36 N88-28927

PROPULSION SYSTEM PERFORMANCE

Real gas properties and Space Shuttle Main Engine fuel turbine performance prediction
[ASME PAPER 87-GT-106] p 50 A88-11038

An expert system for probabilistic description of loads on space propulsion system structural components
[AIAA PAPER 88-2371] p 182 A88-32308

NESSUS/EXPERT - An expert system for probabilistic structural analysis methods
[AIAA PAPER 88-2374] p 206 A88-32311

Flight propulsion control integration for V/STOL aircraft
[SAE PAPER 872330] p 21 A88-37199

NASA supersonic STOVL propulsion technology program
[SAE PAPER 872352] p 21 A88-37215

An overview of rotorcraft propulsion research at Lewis Research Center
[NASA-CR-180819] p 22 A88-40554

An 8-cm ion thruster characterization
[NASA-CR-180819] p 56 N88-10106

Flight propulsion control integration for V/STOL aircraft
[NASA-TM-100226] p 38 N88-11680

Space station propulsion
[NASA-TM-100216] p 57 N88-11746

NASA supersonic STOVL propulsion technology program
[NASA-TM-100227] p 26 N88-14093

High power ion thruster performance
[NASA-TM-100227] p 62 N88-24295

Status of high power electric propulsion technology
[NASA-TM-100227] p 63 N88-24443

PROPULSION EFFICIENCY

Parametric studies of advanced turboprops
[AIAA PAPER 88-2266] p 20 A88-32223

Propulsion challenges and opportunities for high-speed transport aircraft
[NASA-CP-10003-SESS-1] p 30 N88-15809

Rotorcraft flight-propulsion control integration: An eclectic design concept
[NASA-TP-2815] p 38 N88-19475

The 1988 overview of free-piston Stirling technology for space power at the NASA Lewis Research Center
[NASA-TM-100795] p 61 N88-22934

Benefits of 20 kHz PMAD in a nuclear space station
[NASA-CP-10003-SESS-1] p 129 N88-24256

High power ion thruster performance
[NASA-TM-100227] p 62 N88-24295

PROPYL COMPOUNDS

Silsesquioxanes as precursors to ceramic composites
[AIAA PAPER 87-2741] p 69 A88-12599

PROTECTIVE COATINGS

Thermomechanical behavior of plasma-sprayed ZrO₂-Y₂O₃ coatings influenced by plasticity, creep, and oxidation
[AIAA PAPER 88-0027] p 95 A88-12588

Oxidation-resistant reflective surfaces for solar dynamic power generation in near earth orbit
[NASA-TM-100795] p 54 A88-18523

Diffusional transport during the cyclic oxidation of gamma + beta, Ni-Cr-Al(Y, Zr) alloys
[NASA-TM-100795] p 85 A88-28902

Plasma assisted surface coating/modification processes - An emerging technology
[NASA-TM-100795] p 114 A88-38927

Chemical vapor deposited silica coatings for solar mirror protection
[AIAA PAPER 88-0027] p 99 A88-41796

Solar dynamic concentrator durability in atomic oxygen and micrometeoroid environments
[NASA-TM-100795] p 68 A88-51393

Bithermal low-cycle fatigue behavior of a NiCoCrAlY-coated single crystal superalloy
[NASA-TM-100795] p 90 A88-51736

PULSE COMMUNICATION

Technologies for protection of the Space Station power system surfaces in atomic oxygen environment
[NASA-TM-100873] p 41 A88-52331

Life modeling of thermal barrier coatings for aircraft gas turbine engines
[NASA-TM-100891] p 90 A88-54145

Atomic-oxygen durability of impact-damaged solar reflectors
[NASA-TM-100929] p 68 A88-54988

Life prediction and constitutive models for engine hot section anisotropic materials program
[NASA-TM-100966] p 186 N88-11175

Creep-fatigue behavior of NiCoCrAlY coated PWA 1480
[NASA-TM-100966] p 186 N88-11176

Coating life prediction
[NASA-TM-100966] p 170 N88-11181

Coatings for high-temperature bearings and seals
[NASA-TM-100249] p 102 N88-13453

Stress rupture behavior of silicon carbide coated, low modulus carbon/carbon composites
[NASA-CR-180863] p 72 N88-14150

Life modeling of thermal barrier coatings for aircraft gas turbine engines
[NASA-TM-100283] p 92 N88-15060

Hot piston ring/cylinder liner materials: Selection and evaluation
[NASA-TM-100276] p 102 N88-15872

Oxidation and protection of fiberglass-epoxy composite masts for photovoltaic arrays in the low Earth orbital environment
[NASA-TM-100839] p 104 N88-18734

Mast material test program (MAMATEP)
[NASA-TM-100821] p 74 N88-19592

Measurement of the properties of lossy materials inside a finite conducting cylinder
[NASA-CR-182664] p 213 N88-20962

Chemical vapor deposited silica coatings for solar mirror protection
[NASA-TM-100834] p 105 N88-21306

A constitutive model for an overlay coating
[NASA-TM-100834] p 105 N88-21525

Thrust chamber thermal barrier coating techniques
[NASA-TM-100933] p 64 N88-24690

Isothermal and bithermal thermomechanical fatigue behavior of a NiCoCrAlY-coated single crystal superalloy
[NASA-TM-100907] p 94 N88-24766

A thermally modified polymer matrix composite material with structural integrity to 371 C
[NASA-TM-100922] p 76 N88-25483

Thermal barrier coating life-prediction model development
[NASA-CR-179507] p 107 N88-28142

PROTON BEAMS

Performance of GaAs and silicon concentrator cells under 37 MeV proton irradiation
[NASA-TM-100144] p 200 N88-12877

PROTON DAMAGE

Performance of GaAs and silicon concentrator cells under 37 MeV proton irradiation
[NASA-TM-100144] p 200 A88-34343

PROTON IRRADIATION

Radiation damage and defect behavior in proton irradiated lithium-counterdoped n+p silicon solar cells
[NASA-TM-100144] p 125 A88-34340

PROTONS

Effects of electron and proton irradiations on n/p and p/n GaAs cells grown by MOCVD
[NASA-TM-100199] p 127 N88-10266

PROTOTYPES

Prototype thin-film thermocouple/heat-flux sensor for a ceramic-insulated diesel engine
[NASA-TM-100798] p 162 N88-18892

PROVING

A finite element model for wave propagation in an inhomogeneous material including experimental validation
[AIAA PAPER 87-2741] p 212 A88-16577

A flow visualization study of the leading edge separation bubble on a NACA 0012 airfoil with simulated glaze ice
[NASA-CR-180846] p 10 N88-14966

CFD validation experiments for internal flows
[NASA-TM-100797] p 10 N88-16679

Simulation test beds for the space station electrical power system
[NASA-TM-100786] p 44 N88-17715

PSEUDONOISE

Spread-spectrum multiple access using wideband noncoherent MFSK
[AIAA PAPER 87-2741] p 115 A88-26672

PULSE AMPLITUDE

Time domain referencing in intensity modulation fiber optic sensing systems
[AIAA PAPER 87-2741] p 217 A88-12660

PULSE COMMUNICATION

Bandwidth-efficient high-speed coded trellis modulation
[AIAA PAPER 88-0813] p 116 A88-27560

Advanced satellite system architecture for VSATs with ISDN compatibility
[AIAA PAPER 88-0870] p 116 A88-27604

PULSE DURATION

PULSE DURATION

Time domain referencing in intensity modulation fiber optic sensing systems p 217 A88-12660

PULSE HEATING

Electro-impulse de-icing - A status report [AIAA PAPER 88-0019] p 17 A88-22017

PULSE MODULATION

Fiber-optic displacement sensor with temporally separated signal and reference channels p 217 A88-33161

PUMP SEALS

Analysis of eccentric annular incompressible seals. I - A new solution using fast Fourier transforms for determining hydrodynamic force [ASME PAPER 87-TRIB-52] p 166 A88-23308
Analysis and design of a gas-lubricated, sectored, floating ring seal [ASME PAPER 87-TRIB-55] p 166 A88-23310

PUMPING

Determination of compressor in-stall characteristics from engine surge transients p 21 A88-35505

PYROLYSIS

Detailed mechanism of toluene oxidation and comparison with benzene [NASA-TM-100261] p 79 A88-13428

PYROMETERS

Noncontacting measurement technologies for space propulsion condition monitoring p 158 A88-29818

Q

QUALITY CONTROL

EMC and power quality standards for 20-kHz power distribution p 52 A88-11830
High temperature polymer matrix composites p 70 A88-36775
Study of Staebler-Wronsky degradation effect in a Si:H based P-I-N solar cells [NASA-CR-182564] p 203 A88-25970

QUANTITATIVE ANALYSIS

Quantitative characterization of the viscosity of a microemulsion p 77 A88-11167

QUANTUM WELLS

Solar energy conversion through the interaction of plasmons with tunnel junctions. Part A: Solar cell analysis. Part B: Photoconductor analysis [NASA-CR-183044] p 203 A88-27621

QUENCHING (COOLING)

Effect of melt spinning on grain size and texture in Ni-Mo alloys p 89 A88-46030

R

RADAR CROSS SECTIONS

Modal attenuation in multilayered coated waveguides p 126 A88-45755

RADIAL FLOW

The design of an air-cooled metallic high temperature radial turbine [AIAA PAPER 88-2872] p 22 A88-45011

RADIANT COOLING

Radiative cooling of a solidifying droplet layer including absorption and scattering p 133 A88-15749
Transient radiative cooling of a layer filled with solidifying drops p 135 A88-20169
Transient radiative cooling of an absorbing and scattering cylinder - A separable solution p 140 A88-41409

RADIATION DAMAGE

Radiation damage and defect behavior in proton irradiated lithium-counterdoped n+p silicon solar cells p 125 A88-34340
Radiation performance of AlGaAs and InGaAs concentrator cells and expected performance of cascade structures p 125 A88-34356
Effects of electron and proton irradiations on n/p and p/n GaAs cells grown by MOCVD [NASA-TM-100199] p 127 A88-10266
Performance of GaAs and silicon concentrator cells under 37 MeV proton irradiation [NASA-TM-100144] p 200 A88-12877
Radiation performance of AlGaAs concentrator cells and expected performance of cascade structures [NASA-TM-100145] p 200 A88-12878

RADIATION EFFECTS

Recent developments in indium phosphide space solar cell research p 50 A88-11785
Radiation and temperature effects in gallium arsenide, indium phosphide, and silicon solar cells p 125 A88-34321
Degradation mechanisms of materials for large space systems in low Earth orbit [NASA-CR-181472] p 71 A88-10896

Low Earth orbit environmental effects on the space station photovoltaic power generation systems [NASA-TM-100230] p 225 A88-12429

Neutron effects on the electrical and switching characteristics of NPN bipolar power transistors p 129 A88-24463

RADIATION SHIELDING

Neutron effects on the electrical and switching characteristics of NPN bipolar power transistors p 129 A88-24463

RADIATION TOLERANCE

Comparative radiation resistance, temperature dependence and performance of diffused junction indium phosphide solar cells p 198 A88-18580
InP based solar cells for space application: Reduction of external losses p 199 A88-34250
Modelling and design of high efficiency radiation tolerant indium phosphide space solar cells p 200 A88-34394
Direct-current magnetron fabrication of indium tin oxide/InP solar cells p 200 A88-51289
Neutron radiation tolerance of Au-activated silicon p 222 A88-24316

A comparison of the radiation tolerance characteristics of multijunction solar cells with series and voltage-matched configurations [NASA-TM-101177] p 203 A88-27624

RADIATIVE HEAT TRANSFER

Radiative cooling of a solidifying droplet layer including absorption and scattering p 133 A88-15749
Transient radiative cooling of a layer filled with solidifying drops p 135 A88-20169
Transient radiative cooling of an absorbing and scattering cylinder - A separable solution p 140 A88-41409
Moving belt radiator development status [NASA-TM-100909] p 64 A88-25477

RADIO FREQUENCIES

Detection of radio-frequency modulated optical signals by two and three terminal microwave devices p 117 A88-50305
Optical RF distribution links for MMIC phased array antennas [NASA-TM-100841] p 128 A88-20555

Experimental radio frequency link for Ka-band communications applications [NASA-TM-100824] p 43 A88-24659

RADIO FREQUENCY INTERFERENCE

Evaluation of the communications impact of a low power arcjet thruster [AIAA PAPER 88-3105] p 55 A88-48755
Evaluation of the communications impact of a low power arcjet thruster [NASA-TM-100926] p 63 A88-24682

RADIOACTIVE DECAY

Primordial nucleosynthesis with decaying particles. I - Entropy-producing decays. II - Inert decays p 217 A88-47477

RADIOGRAPHY

Flaw imaging and ultrasonic techniques for characterizing sintered silicon carbide [NASA-TM-100177] p 177 A88-12106
Characterization of sintered SiC by using NDE p 177 A88-22413

RAIN

A statistical rain attenuation prediction model with application to the advanced communication technology satellite project. Part 2: Theoretical development of a dynamic model and application to rain fade durations and tolerable control delays for fade countermeasures [NASA-TM-100242] p 118 A88-11945
Space communication link propagation data for selected cities within the multiple beam and steerable antenna coverage areas of the advanced communications technology satellite [NASA-TM-100861] p 120 A88-23070
A statistical rain attenuation prediction model with application to the advanced communication technology satellite project. 1: Theoretical development and application to yearly predictions for selected cities in the United States [NASA-CR-179498] p 121 A88-29077

RAMAN SPECTRA

Raman scattering studies of chemical-vapor-deposited cubic SiC films of (100)Si p 127 A88-53397

RAMJET ENGINES

High-speed inlet research program and supporting analyses p 17 A88-15811

RANDOM PROCESSES

Infrared properties of an anisotropically stirred fluid p 134 A88-16354

RANDOM VARIABLES

Efficient probabilistic fracture mechanics analysis p 180 A88-16933
Finite element methods in probabilistic mechanics p 212 A88-29060

SUBJECT INDEX

RANDOM WALK

Numerical methods for one-dimensional reaction-diffusion equations arising in combustion theory p 135 A88-18975

RANKINE CYCLE

Toluene stability Space Station Rankine power system p 50 A88-11794
Solar dynamic organic Rankine cycle heat rejection system simulation p 132 A88-11808
Development of an integrated heat pipe-thermal storage system for a solar receiver [NASA-TM-101099] p 202 A88-22458
Study of toluene stability for an Organic Rankine Cycle (ORC) space-based power system [NASA-CR-180884] p 66 A88-29863
Study of toluene rotary fluid management device and shear flow condenser performance for a space-based organic Rankine power system [NASA-CR-180885] p 67 A88-29872

RAPID QUENCHING (METALLURGY)

Precipitation in a rapidly solidified and aged Ni-Al-Mo alloy p 82 A88-18528
Undercooled and rapidly quenched Ni-Mo alloys p 83 A88-19960
Solidification of undercooled Ni-Sn eutectic alloy under microgravity conditions in the Space Shuttle p 110 A88-28557
Dendritic growth of undercooled nickel-tin. III p 86 A88-32887
Dispersion strengthened NiAl alloys produced by rapid solidification processing p 88 A88-40588
Rapid solidification of highly undercooled liquids p 88 A88-41653
On producing an alloy of uniform composition during rapid solidification processing p 89 A88-41654
Primary arm spacing in chill block melt spun Ni-Mo alloys p 89 A88-41655

RATES (PER TIME)

Vapor condensation on a turbulent liquid interface p 150 A88-15939

RAY TRACING

A FORTRAN code for the calculation of probe volume geometry changes in a laser anemometry system caused by window refraction [NASA-TM-100210] p 206 A88-12288
Ray tracing optical analysis of offset solar collector for space station solar dynamic system [NASA-TM-100853] p 60 A88-22080

RAYLEIGH NUMBER

High Rayleigh number convection in rectangular enclosures with differentially heated vertical walls and aspect ratios between zero and unity [NASA-TM-100277] p 151 A88-19739

RAYLEIGH-BENARD CONVECTION

Investigation of surface tension driven convection as a feasibility study for a micro-gravity experiment [NASA-CR-182504] p 112 A88-18739

REACTION KINETICS

Integrating combustion kinetic rate equations by selective use of stiff and nonstiff methods p 78 A88-19233

A comparison of the bromination dynamics of various carbon and graphite fibers p 97 A88-20278
Numerical simulation of hypersonic inlet flows with equilibrium or finite rate chemistry [AIAA PAPER 88-0273] p 5 A88-27717
Experimental studies in vortex pair motion coincident with a liquid reaction p 142 A88-46316
Detailed mechanism of benzene oxidation [NASA-TM-100202] p 79 A88-11775
Detailed mechanism of toluene oxidation and comparison with benzene [NASA-TM-100261] p 79 A88-13428
The carbon dioxide chaperon efficiency for the reaction H + O₂ + M yields HO₂ + M from ignition delay times behind reflected shock waves [NASA-TM-100125] p 79 A88-15036

REACTOR MATERIALS

Creep behavior of tungsten/niobium and tungsten/niobium-1 percent zirconium composites p 75 A88-24427

REACTOR SAFETY

Measurements of natural circulation flow in a scale model PWR reactor system during postulated degraded core accidents using laser anemometry p 159 A88-43917

REAL GASES

Real gas properties and Space Shuttle Main Engine fuel turbine performance prediction [ASME PAPER 87-GT-106] p 50 A88-11038
Splitting of inviscid fluxes for real gases [AIAA PAPER 88-3526] p 142 A88-48782
Splitting of inviscid fluxes for real gases [NASA-TM-100856] p 211 A88-21717
High speed inlet calculations with real gas effects [NASA-CR-182167] p 13 A88-26336

REAL TIME OPERATION

Real time optical correlator using a magneto-optic device applied to particle imaging velocimetry

p 159 A88-40700

Finite-dimensional modeling of network-induced delays for real-time control systems

p 208 A88-54537

A microprocessor-based real-time simulator of a turbofan engine

[NASA-TM-100889] p 32 N88-21163

REATTACHED FLOW

Turbulence energy and diffusion transport of third-moments in a separating and reattaching flow

p 141 A88-43011

Structure of a reattaching supersonic shear flow

[AIAA PAPER 88-3615] p 8 A88-48901

RECEIVERS

A 30 GHz monolithic receive module technology assessment

[NASA-CR-180825] p 129 N88-23084

RECIRCULATIVE FLUID FLOW

Turbulence energy and diffusion transport of third-moments in a separating and reattaching flow

p 141 A88-43011

Experimental verification of a secondary recirculation zone in a labyrinth seal

[AIAA PAPER 88-3692] p 168 A88-48971

Improved numerical methods for turbulent viscous recirculating flows

p 146 N88-11148

Aerothermal modeling program, phase 2

p 146 N88-11149

Efficient numerical techniques for complex fluid flows

p 146 N88-11151

Improved numerical methods for turbulent viscous recirculating flows

[NASA-CR-180852] p 13 N88-25445

RECOMBINATION REACTIONS

Diffusion length measurement in bulk and epitaxially grown III-V semiconductors using charge collection microscopy

p 126 A88-34370

RECOVERABILITY

Communications satellite systems operations with the space station. Volume 3: Supplementary technical report

[NASA-CR-180875] p 48 N88-16794

RECRYSTALLIZATION

Dynamic recrystallization and grain boundary migration in B2 FeAl

p 83 A88-20269

RECTANGLES

Crosspolarisation characteristics of rectangular patch antennas

p 117 A88-47705

Fingering flow patterns of thermosolutal convection in rectangular enclosures

[AIAA PAPER 88-3823] p 144 A88-49000

Thermosolutal convection in high-aspect-ratio enclosures

[NASA-TM-100803] p 151 N88-18871

Fingering flow patterns of thermosolutal convection in rectangular enclosures

[NASA-TM-100854] p 152 N88-21417

RECTANGULAR WAVEGUIDES

Characteristics of a two-layer electromagnetically coupled rectangular patch antenna

p 115 A88-14100

RECURSIVE FUNCTIONS

An algorithm for a generalization of the Richardson extrapolation process

p 209 A88-32840

REDUCED GRAVITY

Research opportunities in microgravity science and applications during Shuttle hiatus

p 109 A88-13164

Dendritic solidification under microgravity conditions

[AIAA PAPER 88-0248] p 110 A88-22186

Mass transport phenomena between bubbles and dissolved gases in liquids under reduced gravity conditions

[AIAA PAPER 88-0450] p 138 A88-27719

Laminar diffusion flames under micro-gravity conditions

[AIAA PAPER 88-0645] p 78 A88-27722

Solidification under microgravity conditions - Dendritic growth

[AAS PAPER 86-380] p 110 A88-35130

Gas liquid flow at microgravity conditions - Flow patterns and their transitions

p 141 A88-42839

Preparation for microgravity - The role of the Microgravity Material Science Laboratory

[AIAA PAPER 88-3510] p 111 A88-42908

Thermodynamic modeling of the no-vent fill methodology for transferring cryogens in low gravity

[AIAA PAPER 88-3403] p 55 A88-48765

Dynamics of two fluids under periodic acceleration

[AIAA PAPER 88-3728] p 143 A88-48980

Containment of a silicone fluid free surface in reduced gravity

p 112 A88-49085

Ground-based microgravity materials science research at NASA's Microgravity Materials Science Laboratory

p 112 A88-49090

Mixing fuel particles for space combustion research using acoustics

p 112 A88-49093

Isothermal dendritic growth - A proposed microgravity experiment

p 112 A88-49095

Redundant manipulators for momentum compensation in a micro-gravity environment

[AIAA PAPER 88-4121] p 204 A88-50223

Microgravity combustion fundamentals

p 112 N88-12528

The effect of microgravity on flame spread over a thin fuel

[NASA-TM-100195] p 80 N88-15853

Cryogenic Fluid Management Technology Workshop. Volume 1: Presentation material and discussion

[NASA-CP-10001] p 149 N88-15924

A payload for investigating the influence of convection on GaAs crystal growth

p 221 N88-17702

Mass transport phenomena between bubbles and dissolved gases in liquids under reduced gravity conditions

[NASA-TM-100273] p 80 N88-18672

Investigation of surface tension driven convection as a feasibility study for a micro-gravity experiment

[NASA-CR-182504] p 112 N88-18739

Study of industry requirements that can be fulfilled by combustion experimentation aboard space station

[NASA-CR-180854] p 224 N88-19377

Mixing fuel particles for space combustion research using acoustics

[NASA-TM-100295] p 43 N88-21186

Microgravity robotics technology program

[NASA-TM-100898] p 173 N88-23219

Base reaction optimization of manipulators with redundant kinematics

p 173 N88-23238

Microgravity manipulator demonstration

p 173 N88-23242

Noncontact temperature measurements in the microgravity fluids and transport phenomena discipline

p 113 N88-23901

Microgravity combustion discipline working group summary of requirements for noncontact temperature measurements

p 113 N88-23902

Thermodynamic modeling of the no-vent fill methodology for transferring cryogens in low gravity

[NASA-TM-100932] p 63 N88-24686

Moving belt radiator development status

[NASA-TM-100909] p 64 N88-25477

Solid-state combustion synthesis of ceramics and alloys in reduced gravity

[NASA-CR-4163] p 75 N88-25479

Containment of a silicone fluid free surface in reduced gravity using barrier coatings

[NASA-TM-101314] p 155 N88-30072

REDUCTION

Reducing adhesion and agglomeration within a cloud of combustible particles

[NASA-TM-100902] p 114 N88-26539

REDUCTION (CHEMISTRY)

Evaluation studies on carbon supported catalysts for oxygen reduction in alkaline medium

p 77 A88-16643

REDUNDANCY

Redundant manipulators for momentum compensation in a micro-gravity environment

[AIAA PAPER 88-4121] p 204 A88-50223

Directions in propulsion control

p 28 N88-15799

REFLECTANCE

Design and demonstration of a system for the deposition of atomic-oxygen durable coatings for reflective solar dynamic power system concentrators

[NASA-CR-4158] p 64 N88-25474

The effect of the near earth micrometeoroid environment on a highly reflective mirror surface

[NASA-TM-101307] p 44 N88-29833

REFLECTED WAVES

The carbon dioxide chaperon efficiency for the reaction $H + O_2 + M$ yields $HO_2 + M$ from ignition delay times behind reflected shock waves

[NASA-TM-100125] p 79 N88-15036

REFLECTION

Accurate boundary conditions for exterior problems in gas dynamics

[NASA-TM-100807] p 210 N88-19182

REFLECTOR ANTENNAS

Compensation of reflector antenna surface distortion using an array feed

[NASA-TM-100286] p 119 N88-18805

Case study of active array feed compensation with sidelobe control for reflector surface distortion

[NASA-TM-100287] p 120 N88-23073

Active feed array compensation for reflector antenna surface distortions

[NASA-TM-100826] p 120 N88-25762

Analytical approximation of a distorted reflector surface defined by a discrete set of points

[NASA-TM-101323] p 121 N88-27424

REFLECTORS

Oxidation-resistant reflective surfaces for solar dynamic power generation in near earth orbit

p 54 A88-18523

Features and applications of the integrated composites analyzer (ICAN) code

p 74 N88-22391

REFRACTION

A FORTRAN code for the calculation of probe volume geometry changes in a laser anemometry system caused by window refraction

[NASA-TM-100210] p 206 N88-12288

REFRACTORY COATINGS

Thermal barrier coating life prediction model development

p 170 N88-11184

Thermal barrier coating life prediction model development

p 171 N88-11185

REFRACTORY MATERIALS

High temperature metal matrix composites for future aerospace systems

[AIAA PAPER 88-3059] p 71 A88-44745

High temperature metal matrix composites for future aerospace systems

[NASA-TM-100212] p 90 N88-10938

Ethynylated aromatics as high temperature matrix resins

[NASA-TM-89829] p 73 N88-18640

Nonlinear Constitutive Relations for High Temperature Applications, 1986

[NASA-CP-10010] p 189 N88-21498

Biaxial experiments supporting the development of constitutive theories for advanced high-temperature materials

p 191 N88-22386

REFRACTORY METAL ALLOYS

Thermal aging effects in refractory metal alloys

p 84 A88-22700

Characterization of precipitates in a niobium-zirconium-carbon alloy

[NASA-TM-100848] p 93 N88-22981

REFRACTORY METALS

Refractory metal alloys and composites for space power systems

[NASA-TM-100946] p 95 N88-27310

REFUELING

Thermodynamic modeling of the no-vent fill methodology for transferring cryogens in low gravity

[AIAA PAPER 88-3403] p 55 A88-48765

Thermodynamic modeling of the no-vent fill methodology for transferring cryogens in low gravity

[NASA-TM-100932] p 63 N88-24686

Technology requirements for an orbiting fuel depot: A necessary element of a space infrastructure

[NASA-TM-101370] p 49 N88-29845

REGENERATIVE FUEL CELLS

Regenerative fuel cell study for satellites in GEO orbit

p 52 A88-11904

High temperature solid oxide regenerative fuel cell for solar photovoltaic energy storage

p 197 A88-11905

Regenerative fuel cell energy storage system for a low earth orbit space station

[NASA-CR-174802] p 204 N88-30184

REGENERATORS

Development of the AGT101 regenerator seals

[ASME PAPER 87-GT-173] p 165 A88-11083

Fatigue failure of regenerator screens in a high frequency Stirling engine

p 179 N88-24491

REGRESSION ANALYSIS

Regressed relations for forced convection heat transfer in a direct injection stratified charge rotary engine

[NASA-TM-100124] p 25 N88-13345

REINFORCED PLATES

Acousto-ultrasonics as a monitor of material anisotropy

p 176 A88-46828

REINFORCING FIBERS

Ceramic matrix and resin matrix composites - A comparison

p 69 A88-13158

Pressure effects on the thermal stability of SiC fibers

[NASA-TM-100146] p 71 N88-10120

Creep behavior of tungsten/niobium and tungsten/niobium-1 percent zirconium composites

p 75 N88-24427

REISSNER THEORY

A mixed formulation of C(0)-linear triangular plate/shell element - The role of edge shear constraints

p 183 A88-40121

RELAXATION METHOD (MATHEMATICS)

Choice of implicit and explicit operators for the upwind differencing method

[AIAA PAPER 88-0624] p 209 A88-22472

Choice of implicit and explicit operators for the upwind differencing method

[NASA-TM-100857] p 211 N88-21718

RELIABILITY

Assessment of commercially available and experimental hydrogen electrodes

p 198 A88-16632

Computerized life and reliability modelling for turboprop transmissions

[AIAA PAPER 88-2979] p 100 A88-48031

An extended life and performance test of a low-power arcjet

[AIAA PAPER 88-3106] p 55 A88-48756

- Computerized life and reliability modelling for turboprop transmissions
[NASA-TM-100918] p 173 N88-23220
- An extended life and performance test of a low-power aircraft
[NASA-TM-100942] p 63 N88-24687
- RELIABILITY ANALYSIS**
Integrated analysis and applications p 28 N88-15789
- Reliability based analysis of contact problems
[NASA-CR-182117] p 189 N88-18975
- Whisker-reinforced ceramic composites for heat engine components p 105 N88-22410
- RELIABILITY ENGINEERING**
Toward improved durability in advanced aircraft engine hot sections; Proceedings of the Thirty-third ASME International Gas Turbine and Aeroengine Congress and Exposition, Amsterdam, Netherlands, June 5-9, 1988 p 24 A88-54137
- REMOTE SENSING**
Fiber optic sensing systems using high frequency resonant sensing heads with intensity sensors
[NASA-TM-101318] p 163 N88-28293
- REQUIREMENTS**
System Development Working Group report p 48 N88-10092
- Space station power system requirements
[NASA-TM-100886] p 49 N88-21245
- Large-scale wind turbine structures p 202 N88-22429
- RESEARCH AND DEVELOPMENT**
An overview of rotorcraft propulsion research at Lewis Research Center p 22 A88-40554
- Life prediction technologies for aeronautical propulsion systems p 27 N88-15788
- Supersonic STOVL propulsion technology program: An overview p 29 N88-15808
- Impact and promise of NASA aeropropulsion technology p 31 N88-16698
- Lewis materials research and technology: An overview p 223 N88-16699
- RESEARCH FACILITIES**
Research opportunities in microgravity science and applications during Shuttle hiatus p 109 A88-13164
- Lewis' enhanced laboratory for research into the fatigue and constitutive behavior of high temperature materials p 186 N88-11177
- Life prediction technologies for aeronautical propulsion systems p 27 N88-15788
- Institute for Computational Mechanics in Propulsion (ICOMP)
[NASA-TM-100790] p 211 N88-19202
- Test facilities of the structural dynamics branch of NASA Lewis Research Center
[NASA-TM-100800] p 190 N88-21534
- Laboratory Information Management System (LIMS): A case study
[NASA-TM-100835] p 208 N88-21697
- Structural dynamics branch research and accomplishments for fiscal year 1987
[NASA-TM-100279] p 194 N88-22446
- Preparation for microgravity: The role of the microgravity materials science laboratory
[NASA-TM-100906] p 113 N88-24811
- A detailed description of the uncertainty analysis for high area ratio rocket nozzle tests at the NASA Lewis Research Center p 65 N88-25580
- Bibliography of Lewis Research Center technical publications announced in 1987
[NASA-TM-100910] p 223 N88-28832
- Helicopter transmission research at NASA Lewis Research Center
[NASA-TM-100962] p 175 N88-30128
- RESEARCH MANAGEMENT**
Research opportunities in microgravity science and applications during Shuttle hiatus p 109 A88-13164
- Issues in space photovoltaic research and technology p 199 A88-34230
- HOST turbine heat transfer program summary
[NASA-TM-100280] p 149 N88-14320
- Institute for Computational Mechanics in Propulsion (ICOMP)
[NASA-TM-100790] p 211 N88-19202
- Study of industry requirements that can be fulfilled by combustion experimentation aboard space station
[NASA-CR-180854] p 224 N88-19377
- Advanced Gas Turbine (AGT) technology development project
[NASA-CR-180891] p 225 N88-20230
- Structural dynamics branch research and accomplishments for fiscal year 1987
[NASA-TM-100279] p 194 N88-22446
- Helicopter transmission research at NASA Lewis Research Center
[NASA-TM-100962] p 175 N88-30128

RESIDUAL STRENGTH

- Fiber composite structural durability and damage tolerance: Simplified predictive methods
[NASA-TM-100179] p 72 N88-13409

RESIDUES

- Implementation of a digital optical matrix-vector multiplier using a holographic look-up table and residue arithmetic
[NASA-CR-180431] p 205 N88-10496

RESIN MATRIX COMPOSITES

- Ceramic matrix and resin matrix composites - A comparison p 69 A88-13158
- Mechanics of composite materials: Past, present and future
[NASA-TM-100793] p 73 N88-17744
- Ethynylated aromatics as high temperature matrix resins
[NASA-TM-89829] p 73 N88-18640
- The 700 F properties of autoclave cured PMR-2 composites
[NASA-TM-100923] p 75 N88-24712
- New acousto-ultrasonic techniques applied to aerospace materials
[NASA-TM-101299] p 180 N88-28323
- Novel ladder polymers for use as high temperature stable resins or coatings
[NASA-CASE-LEW-14203-1] p 108 N88-29984

RESISTOJET ENGINES

- Water-propellant resistojets for man-tended platforms
[IAF PAPER 87-259] p 54 A88-15975
- Space station propulsion system technology p 54 A88-21255
- An experimental investigation of the effect of test-cell pressure on the performance of resistojets
[AIAA PAPER 88-3286] p 40 A88-44820
- Development of a liquid-fed water resistojets
[AIAA PAPER 88-3288] p 142 A88-48762
- Space station propulsion
[NASA-TM-100216] p 57 N88-11746
- Slip casting and extruding shapes of rhenium with metal oxide additives. Part 2: Development of grain stabilized rhenium parts for resistojets
[NASA-CR-180851] p 57 N88-11749
- Compatibility of dispersion-strengthened platinum with resistojets propellants
[NASA-TP-2765] p 58 N88-12538
- Space station resistojets system requirements and interface definition study
[NASA-CR-180832] p 58 N88-12541
- Magnetic emissions testing of the space station engineering model resistojets
[NASA-TM-100788] p 48 N88-17728
- Component data base for space station resistojets auxiliary propulsion
[NASA-CR-180834] p 59 N88-17731
- Electric propulsion options for the SP-100 reference mission
[NASA-TM-100927] p 174 N88-24968
- Development of a liquid-fed water resistojets
[NASA-TM-100927] p 174 N88-24968
- Experimental evaluation of resistojets thruster plume shields
[NASA-TM-101363] p 66 N88-29868
- The dc power control for a liquid-fed resistojets
[NASA-TM-101326] p 67 N88-29869

RESONANCE

- Control considerations for high frequency, resonant, power processing equipment used in large systems p 51 A88-11829

RESONANT FREQUENCIES

- Implementation of optimal trajectory control of series resonant converter p 126 A88-38796
- Field oriented control of an induction machine in a high frequency link power system p 127 A88-54711

RESONANT VIBRATION

- Localization of natural modes of vibration in bladed disks
[ASME PAPER 87-GT-46] p 18 A88-10998

RESOURCE ALLOCATION

- Numerical arc segmentation algorithm for a radio conference - A software tool for communication satellite systems planning
[AIAA PAPER 88-0788] p 212 A88-27531

RETROFITTING

- Computer-aided design analysis of 57-mm, angular-contact, cryogenic turbopump bearings
[NASA-TP-2816] p 172 N88-18933

REUSABLE ROCKET ENGINES

- Reusable rocket engine optical condition monitoring p 158 A88-29817
- Progress toward an advanced condition monitoring system for reusable rocket engines p 54 A88-32868
- Improved maintainability of space-based reusable rocket engines
[AIAA PAPER 88-3113] p 55 A88-48037
- A reusable rocket engine intelligent control
[NASA-TM-100963] p 65 N88-26401

REUSABLE SPACECRAFT

- The economics of satellite retrieval
[AIAA PAPER 88-0843] p 44 A88-27584

REVISIONS

- Computer-aided design analysis of 57-mm, angular-contact, cryogenic turbopump bearings
[NASA-TP-2816] p 172 N88-18933

REYNOLDS EQUATION

- Foil bearing lubrication theory including compressibility effects p 170 A88-54964

REYNOLDS NUMBER

- The measurement of boundary layers on a compressor blade in cascade. II - Suction surface boundary layers
[ASME PAPER 87-GT-249] p 132 A88-11131
- Experimental verification of a secondary recirculation zone in a labyrinth seal
[AIAA PAPER 88-3692] p 168 A88-48971
- The effects of turbulence and stator/rotor interactions on turbine heat transfer. II - Effects of Reynolds number and incidence
[ASME PAPER 88-GT-5] p 145 A88-54152
- Regressed relations for forced convection heat transfer in a direct injection stratified charge rotary engine
[NASA-TM-100124] p 25 N88-13345
- Investigation of the validity of Reynolds averaged turbulence models at the frequencies that occur in turbomachinery
[NASA-CR-182162] p 65 N88-28087

REYNOLDS STRESS

- Low Reynolds number modeling of turbulent flows with and without wall transpiration p 136 A88-21983
- Experimental verification of a secondary recirculation zone in a labyrinth seal
[AIAA PAPER 88-3692] p 168 A88-48971
- 3-D laser anemometer measurements in a labyrinth seal
[ASME PAPER 88-GT-63] p 169 A88-54195
- 3-D laser anemometer measurements in an annular seal
[ASME PAPER 88-GT-64] p 169 A88-54196

RHENIUM

- Slip casting and extruding shapes of rhenium with metal oxide additives. Part 2: Development of grain stabilized rhenium parts for resistojets
[NASA-CR-180851] p 57 N88-11749
- Iridium-coated rhenium thrusters by CVD
[NASA-TM-101309] p 67 N88-29874

RHEOLOGY

- Shear rheological characterization of motor oils p 100 A88-47562
- Characterization of aluminum/RP-1 gel propellant properties
[AIAA PAPER 88-2821] p 109 A88-48751
- Characterization of aluminum/RP-1 gel propellant properties
[NASA-TM-100951] p 109 N88-24808

RIBS (SUPPORTS)

- Local heat/mass transfer and pressure drop in a two-pass rib-roughened channel for turbine airfoil cooling
[NASA-CR-179635] p 148 N88-12039

RIGID ROTORS

- Stability of a rigid rotor supported on flexible oil journal bearings
[ASME PAPER 87-TRIB-48] p 166 A88-24034

RINGS

- Hot piston ring tests
[NASA-TM-100256] p 201 N88-14486
- Hot piston ring/cylinder liner materials: Selection and evaluation
[NASA-TM-100276] p 102 N88-15872
- Multi-hundred kilowatt roll ring assembly evaluation results
[NASA-TM-100865] p 114 N88-21375

ROBOTICS

- Redundant manipulators for momentum compensation in a micro-gravity environment
[AIAA PAPER 88-4121] p 204 A88-50223

ROBOTS

- Microgravity robotics technology program
[NASA-TM-100898] p 173 N88-23219
- Accurate positioning of long, flexible ARM's (Articulated Robotic Manipulator) p 174 N88-23243
- Energy storage considerations for a robotic Mars surface sampler
[NASA-TM-100969] p 227 N88-28853

ROBUSTNESS (MATHEMATICS)

- Choice of implicit and explicit operators for the upwind differencing method
[NASA-TM-100857] p 211 N88-21718

ROCKET ENGINE CASES

- Ultrasonic evaluation of mechanical properties of thick, multilayered, filament-wound composites p 176 A88-21340

- Slip casting and extruding shapes of rhemium with metal oxide additives. Part 2: Development of grain stabilized rhemium parts for resistojets
[NASA-CR-180651] p 57 N88-11749
- ROCKET ENGINE DESIGN**
25-LBF GO2/GH2 space station thruster
[AIAA PAPER 88-2793] p 56 A88-53101
Arcjet thruster research and technology
[NASA-CR-180865] p 59 N88-17732
Arcjet thruster research and technology, phase 1
[NASA-CR-182107] p 62 N88-23830
- ROCKET ENGINES**
Three dimensional thermal analysis of rocket thrust chambers
[AIAA PAPER 88-2643] p 54 A88-43721
A life test of a 22-Newton (5-lbf) hydrazine rocket
[NASA-TM-100232] p 57 N88-11750
A two-dimensional finite difference program for thermal analysis of rocket thrust chambers
[NASA-TM-100191] p 58 N88-12539
Thrust chamber thermal barrier coating techniques
[NASA-TM-100933] p 64 N88-24690
Indium-coated rhemium thrusters by CVD
[NASA-TM-101309] p 67 N88-29874
- ROCKET EXHAUST**
On the correlation of plume centerline velocity decay of turbulent acoustically excited jets
[AIAA PAPER 87-2692] p 3 A88-18654
Reusable rocket engine optical condition monitoring
p 158 A88-29817
- ROCKET FIRING**
Orbital transfer vehicle 3000 LBF thrust chamber assembly hot fire test program
[NASA-CR-182145] p 66 N88-29858
- ROCKET NOZZLES**
Three dimensional thermal analysis of rocket thrust chambers
[AIAA PAPER 88-2643] p 54 A88-43721
Boundary layer development as a function of chamber pressure in the NASA Lewis 1030:1 area ratio rocket nozzle
[AIAA PAPER 88-3301] p 144 A88-50786
Arcjet thruster research and technology, phase 1
[NASA-CR-182107] p 62 N88-23830
A detailed description of the uncertainty analysis for high area ratio rocket nozzle tests at the NASA Lewis Research Center
p 65 N88-25580
Boundary layer development as a function of chamber pressure in the NASA Lewis 1030:1 area ratio rocket nozzle
[NASA-TM-100917] p 154 N88-25841
- ROCKET PROPELLANTS**
A life test of a 22-Newton (5-lbf) hydrazine rocket
[NASA-TM-100232] p 57 N88-11750
Compatibility of dispersion-strengthened platinum with resistojet propellants
[NASA-TP-2765] p 58 N88-12538
Space station onboard propulsion system: Technology study
[NASA-CR-179233] p 59 N88-15006
- ROCKET THRUST**
A two-dimensional finite difference program for thermal analysis of rocket thrust chambers
[NASA-TM-100191] p 58 N88-12539
- ROLL**
Multi-hundred kilowatt roll ring assembly evaluation results
[NASA-TM-100865] p 114 N88-21375
- ROLLER BEARINGS**
Analysis of crack propagation in roller bearings using the boundary integral equation method - A mixed-mode loading problem
p 168 A88-49183
Improved oil-off survivability of tapered roller bearings
[NASA-CR-180804] p 170 N88-11135
Ceramic bearings for use in gas turbine engines
[NASA-TM-100288] p 172 N88-18007
- ROLLING**
Mode 2 fracture mechanics
p 193 N88-22418
- ROTARY ENGINES**
Performance and efficiency evaluation and heat release study of a direct-injection stratified-charge rotary engine
[SAE PAPER 870445] p 166 A88-23313
Performance and combustion characteristics of direct-injection stratified-charge rotary engines
[NASA-TM-100134] p 25 N88-12490
Regressed relations for forced convection heat transfer in a direct injection stratified charge rotary engine
[NASA-TM-100124] p 25 N88-13345
- ROTARY STABILITY**
Numerical and analytical study of fluid dynamic forces in seals and bearings
[NASA-TM-100268] p 151 N88-18867
- ROTARY WING AIRCRAFT**
Test stand performance of a convertible engine for advanced V/STOL and rotorcraft propulsion
[SAE PAPER 872355] p 21 A88-37217
- Test stand performance of a convertible engine for advanced V/STOL and rotorcraft propulsion
[NASA-TM-100211] p 25 N88-11679
Rotorcraft flight-propulsion control integration: An eclectic design concept
[NASA-TP-2815] p 38 N88-19475
- ROTATING CYLINDERS**
Moving belt radiator development status
[NASA-TM-100909] p 64 N88-25477
- ROTATING DISKS**
Life and reliability of rotating disks
p 178 N88-22428
- ROTATING FLUIDS**
Study of toluene rotary fluid management device and shear flow condenser performance for a space-based organic Rankine power system
[NASA-CR-180885] p 67 N88-29872
- ROTATING SHAFTS**
Theory versus experiment for the rotordynamic coefficients of labyrinth gas seals. II - A comparison to experiment
p 167 A88-31536
- ROTATING STALLS**
Numerical results for axial flow compressor instability
[ASME PAPER 88-GT-252] p 169 A88-54328
- ROTATION**
Use of the generalized transmission error in the equations of motion of gear systems
p 168 A88-49410
Coolant passage heat transfer with rotation
p 147 N88-11160
The effects of inlet turbulence and rotor/stator interactions on the aerodynamics and heat transfer of a large-scale rotating turbine model. Part 4: Aerodynamic data tabulation
[NASA-CR-179469] p 153 N88-23956
- ROTOR AERODYNAMICS**
Recent developments in flutter suppression techniques for turbomachinery rotors
p 21 A88-35530
High-speed propeller noise predictions - Effects of boundary conditions used in blade loading calculations
p 215 A88-36270
Control of rotor aerodynamically forced vibrations by splitters
p 23 A88-52684
A comparison of experimental and theoretical results for labyrinth gas seals with honeycomb stators
[NASA-CR-182441] p 172 N88-16006
Experimental rotordynamic coefficient results for honeycomb seals
[NASA-CR-182440] p 172 N88-16007
Numerical modeling of multidimensional flow in seals and bearings used in rotating machinery
[NASA-TM-100779] p 150 N88-16988
A review of gear housing dynamics and acoustics literature
[NASA-CR-183110] p 175 N88-26675
- ROTOR BLADES**
Application of structural tailoring to spar/shell turboprops
[AIAA PAPER 88-2333] p 20 A88-32277
Aeroelastic effects of alternate blade sweep on advanced propfan rotor
[ASME PAPER 87-WA/AERO-8] p 184 A88-51328
- ROTOR BLADES (TURBOMACHINERY)**
Localization of natural modes of vibration in bladed disks
[ASME PAPER 87-GT-46] p 18 A88-10998
Application of advanced computational codes in the design of an experiment for a supersonic throughflow fan rotor
[ASME PAPER 87-GT-160] p 2 A88-11072
Noise of a model counterrotation propeller with reduced aft rotor diameter at simulated takeoff/approach conditions (F7/A3)
[AIAA PAPER 88-0263] p 214 A88-22192
An explicit Runge-Kutta method for unsteady rotor/stator interaction
[AIAA PAPER 88-0049] p 5 A88-27715
Bladed disk assemblies; Proceedings of the Eleventh Biennial Conference on Mechanical Vibration and Noise, Boston, MA, Sept. 27-30, 1987
p 20 A88-31608
Experimental vibration damping characteristics of the third-stage rotor of a three-stage transonic axial-flow compressor
[AIAA PAPER 88-3229] p 23 A88-48759
Control of rotor aerodynamically forced vibrations by splitters
p 23 A88-52684
Phase-resolved heat-flux measurements on the blade of a full-scale rotating turbine
[ASME PAPER 88-GT-173] p 145 A88-54267
Noise of a model counterrotation propeller with reduced aft rotor diameter at simulated takeoff/approach conditions (F7/A3)
[NASA-TM-100254] p 216 N88-13961
An explicit Runge-Kutta method for unsteady rotor/stator interaction
[NASA-TM-100787] p 10 N88-14967
- NASA's rotorcraft icing research program
p 15 N88-16641
Experimental vibration damping characteristics of the third-stage rotor of a three-stage transonic axial-flow compressor
[NASA-TM-100948] p 35 N88-24642
SR-7A aeroelastic model design report
[NASA-CR-174791] p 36 N88-28928
- ROTOR BODY INTERACTIONS**
Theory versus experiment for the rotordynamic coefficients of labyrinth gas seals. I - A two control volume model
p 167 A88-31535
Theory versus experiment for the rotordynamic coefficients of labyrinth gas seals. II - A comparison to experiment
p 167 A88-31536
Transient rotor dynamic rub phenomena - Theory and test
p 167 A88-31539
- ROTOR SPEED**
Transient rotor dynamic rub phenomena - Theory and test
p 167 A88-31539
Effect of stage loading on endwall flows in an axial flow compressor rotor
[ASME PAPER 88-GT-111] p 145 A88-54229
- ROTORCRAFT AIRCRAFT**
An overview of rotorcraft propulsion research at Lewis Research Center
p 22 A88-40554
- ROTORS**
Analysis of eccentric annular incompressible seals. II - Effects of eccentricity on rotordynamic coefficients
[ASME PAPER 87-TRIB-53] p 166 A88-23309
The effects of turbulence and stator/rotor interactions on turbine heat transfer. II - Effects of Reynolds number and incidence
[ASME PAPER 88-GT-5] p 145 A88-54152
Active control of transient rotordynamic vibration by optimal control methods
[ASME PAPER 88-GT-73] p 208 A88-54202
Measurement of airfoil heat transfer coefficients on a turbine stage
p 147 N88-11158
Testing of a one-bladed 30-meter-diameter rotor on the DOE/NASA Mod-O wind turbine
[NASA-TM-100274] p 201 N88-19014
The 2-D and 3-D time marching transonic potential flow method for propfans
p 11 N88-23245
Vibration and control of flexible rotor supported by magnetic bearings
[NASA-TM-100888] p 174 N88-23977
Entrance and exit region friction factor models for annular seal analysis
[NASA-CR-183084] p 175 N88-25921
Improved method for stress and compatibility analysis of multicomponent rotating systems
[NASA-TM-100884] p 195 N88-25935
The effects of inlet turbulence and rotor/stator interactions on the aerodynamics and heat transfer of a large-scale rotating turbine model. Volume 3: Heat transfer data tabulation 65 percent axial spacing
[NASA-CR-179468] p 37 N88-28930
An unconditionally stable Runge-Kutta method for unsteady flows
[NASA-TM-101347] p 14 N88-29780
The effects of inlet turbulence and rotor/stator interactions on the aerodynamics and heat transfer of a large-scale rotating turbine model. Volume 2: Heat transfer data tabulation. 15 percent axial spacing
[NASA-CR-179467] p 37 N88-29804
Spray automated balancing of rotors: Methods and materials
[NASA-CR-182151] p 41 N88-29825
- ROVING VEHICLES**
Electromagnetic powered vehicles (EMPV) for Mars exploration
p 62 N88-24388
Energy storage considerations for a robotic Mars surface sampler
[NASA-TM-100969] p 227 N88-28853
- RP-1 ROCKET PROPELLANTS**
Characterization of aluminum/RP-1 gel propellant properties
[AIAA PAPER 88-2821] p 109 A88-48751
Characterization of aluminum/RP-1 gel propellant properties
[NASA-TM-100951] p 109 N88-24808
- RUNGE-KUTTA METHOD**
Navier-Stokes cascade analysis with a stiff k-epsilon turbulence solver
[AIAA PAPER 88-0594] p 5 A88-22444
An explicit Runge-Kutta method for unsteady rotor/stator interaction
[AIAA PAPER 88-0049] p 5 A88-27715
Navier-Stokes cascade analysis with a stiff Kappa-Epsilon turbulence solver
[NASA-TM-100218] p 9 N88-10778
Application of Runge Kutta time marching scheme for the computation of transonic flows in turbomachines
[NASA-TM-86997] p 9 N88-12461

- An explicit Runge-Kutta method for unsteady rotor/stator interaction
[NASA-TM-100787] p 10 N88-14967
- An unconditionally stable Runge-Kutta method for unsteady flows
[NASA-TM-101347] p 14 N88-29780
- RUPTURING**
- Stress rupture behavior of silicon carbide coated, low modulus carbon/carbon composites
[NASA-CR-180863] p 72 N88-14150

S

S CURVES

- Electromagnetic fields backscattered from an s-shaped inlet cavity with an absorber coating on its inner walls
[NASA-CR-182401] p 118 N88-15130
- Electromagnetic propagation in PEC and absorbing curved S-ducts
[NASA-TM-100833] p 120 N88-19698

S WAVES

- Input-output characterization of fiber composites by SH waves
[NASA-CR-4153] p 179 N88-23986

S-N DIAGRAMS

- Cyclic fatigue damage characteristics observed for simple loadings extended to multiaxial life prediction
[NASA-CR-182126] p 195 N88-25016

SAFETY FACTORS

- Small space reactor power systems for unmanned solar system exploration missions
[NASA-TM-100228] p 227 N88-14054

SAFETY MANAGEMENT

- Experiments to ensure Space Station fire safety - A challenge
[AIAA PAPER 88-0540] p 41 A88-22405
- Spacecraft fire-safety experiments for space station: Technology development mission
[NASA-CR-182114] p 48 N88-20353

SALTS

- Turbine airfoil deposition models and their hot corrosion implications
p 91 N88-11178

SANDWICH STRUCTURES

- Mechanical properties characterization of composite sandwich materials intended for space antenna applications
[NASA-TM-88893] p 71 N88-10121

SARSAT

- COSPAS/SARSAT 406-MHz emergency beacon digital controller
[NASA-TM-100859] p 121 N88-26566

SATELLITE COMMUNICATION

- Bit-error-rate testing of high-power 30-GHz traveling-wave tubes for ground-terminal applications
p 122 A88-19781
- Spread-spectrum multiple access using wideband noncoherent MFSK
p 115 A88-26672
- Future switching satellites
[AIAA PAPER 88-0802] p 46 A88-27553
- Progress in MMIC technology for satellite communications
p 126 A88-37844
- An allotment planning concept and related computer software for planning the fixed satellite service at the 1988 space WARC
[NASA-TM-100244] p 117 N88-11944
- A statistical rain attenuation prediction model with application to the advanced communication technology satellite project. Part 2: Theoretical development of a dynamic model and application to rain fade durations and tolerable control delays for fade countermeasures
[NASA-TM-100242] p 118 N88-11945
- Design description report for a photovoltaic power system for a remote satellite earth terminal
[NASA-CR-179586] p 200 N88-12875
- Complementary satellite sound broadcasting systems: A NASA assessment for the Voice of America
[NASA-TM-100300] p 119 N88-17899
- Experiments applications guide: Advanced Communications Technology Satellite (ACTS)
[NASA-TM-100265] p 49 N88-28082
- A statistical rain attenuation prediction model with application to the advanced communication technology satellite project. 1: Theoretical development and application to yearly predictions for selected cities in the United States
[NASA-CR-179498] p 121 N88-29077

SATELLITE DESIGN

- Economic benefits of the Space Station to commercial communication satellite operators
[IAF PAPER 87-622] p 41 A88-16215

SATELLITE INSTRUMENTS

- Exposed high-voltage source effect on the potential of an ionospheric satellite
p 218 A88-54992

SATELLITE NETWORKS

- VSAT networks - An overview --- Very Small Aperture Terminals
p 115 A88-14091
- Cost-effective intersatellite link applications to the fixed satellite services
[AIAA PAPER 88-0770] p 45 A88-27544
- Advanced satellite system architecture for VSATs with ISDN compatibility
[AIAA PAPER 88-0870] p 116 A88-27604

SATELLITE ORBITS

- New non-geosynchronous orbits for communications satellites to off-load daily peaks in geostationary traffic
[AAS PAPER 87-547] p 42 A88-10957
- Communications satellites in non-geostationary orbits
[AIAA PAPER 88-0842] p 46 A88-27583
- Low thrust power-limited transfer for a pole squatter
[AIAA PAPER 88-4310] p 42 A88-50435

SATELLITE SOLAR POWER STATIONS

- Space solar cell research - Problems and potential
p 123 A88-21605

SATELLITE TRACKING

- New non-geosynchronous orbits for communications satellites to off-load daily peaks in geostationary traffic
[AAS PAPER 87-547] p 42 A88-10957

SATELLITE-BORNE INSTRUMENTS

- A flexible on-board demultiplexer/demodulator
[AIAA PAPER 88-0811] p 123 A88-27558
- Bandwidth and power efficient satellite TDMA demodulator and decoder
[AIAA PAPER 88-0812] p 123 A88-27559
- The bit-error rate performance of a satellite microwave matrix switch
[AIAA PAPER 88-0826] p 123 A88-27572
- High efficiency, long life traveling wave tubes for future communications satellites
[AIAA PAPER 88-0835] p 124 A88-27578
- High efficiency, long life traveling wave tubes for future communications satellites
[NASA-TM-100837] p 45 N88-19565
- The bit-error rate performance of a satellite microwave matrix switch
[NASA-TM-100285] p 46 N88-22920

SATURATION

- Saturation and the limit of jet mixing enhancement by single frequency plane wave excitation - Experiment and theory
[AIAA PAPER 88-3613] p 8 A88-48899
- Saturation and the limit of jet mixing enhancement by single frequency plane wave excitation: Experiment and theory
[NASA-TM-100882] p 12 N88-23732

SCALE (CORROSION)

- Adherent Al₂O₃ scales produced on undoped NiCrAl alloys
p 85 A88-30269

SCALE MODELS

- Cruise noise of the 2/9 scale model of the Large-scale Advanced Propfan (LAP) propeller, SR-7A
[AIAA PAPER 87-2717] p 214 A88-16565
- Measurements of natural circulation flow in a scale model PWR reactor system during postulated degraded core accidents using laser anemometry
p 159 A88-43917

SCANNING

- Systems for ultrasonic scanning, analysis and imagery
p 177 N88-22414
- Flaw characterization in structural ceramics using scanning laser acoustic microscopy
p 177 N88-22415
- Nondestructive evaluation of sintered ceramics
p 177 N88-22416

SCATTERING

- Ultrasonic evaluation of mechanical properties of thick, multilayered, filament-wound composites
p 176 A88-21340

SCAVENGING

- Auxiliary propulsion technology for advanced Earth-to-orbit vehicles
[NASA-TM-100237] p 58 N88-14127
- Weight savings in aerospace vehicles through propellant scavenging
[NASA-TM-100900] p 44 N88-25470

SCHOTTKY DIODES

- Two stage dual gate MESFET monolithic gain control amplifier for Ka-band
p 124 A88-29821

SCREEN EFFECT

- Sensitivity study of the monogroove with screen heat pipe design
[AIAA PAPER 88-0470] p 137 A88-22346

SEALS (STOPPERS)

- Development of the AGT101 regenerator seals
[ASME PAPER 87-GT-173] p 165 A88-11083
- Thermomechanical behavior of plasma-sprayed ZrO₂-Y₂O₃ coatings influenced by plasticity, creep, and oxidation
p 95 A88-12588
- Analysis of eccentric annular incompressible seals. II - Effects of eccentricity on rotordynamic coefficients
[ASME PAPER 87-TRIB-53] p 166 A88-23309

- Experiments on dynamic stiffness and damping of tapered bore seals
p 166 A88-31527
- Numerical and analytical study of fluid dynamic forces in seals and bearings
p 167 A88-31534
- 3-D laser anemometer measurements in an annular seal
[ASME PAPER 88-GT-64] p 169 A88-54196
- Coatings for high-temperature bearings and seals
[NASA-TM-100249] p 102 N88-13453
- Seal technology for liquid oxygen (LOX) turbopumps
[NASA-CR-174866] p 171 N88-13603
- Numerical modeling of multidimensional flow in seals and bearings used in rotating machinery
[NASA-TM-100779] p 150 N88-16988
- Tribological properties of alumina-boria-silicate fabric from 25 to 850 C
[NASA-TM-100806] p 104 N88-18726
- Numerical and analytical study of fluid dynamic forces in seals and bearings
[NASA-TM-100268] p 151 N88-18867
- Thermal stress minimized, two component, turbine shroud seal
[NASA-CASE-LEW-14212-1] p 174 N88-23978
- Entrance and exit region friction factor models for annular seal analysis
[NASA-CR-183084] p 175 N88-25921

SECONDARY FLOW

- Torsion effect on fully developed flow in a helical pipe
p 135 A88-20748
- Design point variation of 3-D loss and deviation for axial compressor middle stages
[ASME PAPER 88-GT-57] p 8 A88-54189
- Flow field measurements in a 90 degree turning duct
p 147 N88-11157

SEEDS

- Performance of laser Doppler velocimeter with polydisperse seed particles in high speed flows
[AIAA PAPER 88-0425] p 157 A88-22317

SEGMENTS

- Numerical arc segmentation algorithm for a radio conference-NASARC (version 2.0) technical manual
[NASA-TM-100180] p 118 N88-15910

SELF ALIGNMENT

- Design, manufacture and spin test of high contact ratio helicopter transmission utilizing Self-Aligning Bearingless Planetary (SABP)
[NASA-CR-4155] p 174 N88-24975

SELF CONSISTENT FIELDS

- Self-consistent calculations and design considerations for a GaAs nipi doping superlattice solar cell
p 124 A88-34249

SELF LUBRICATION

- Coatings for high-temperature bearings and seals
[NASA-TM-100249] p 102 N88-13453
- Self-lubricating coatings for high-temperature applications
p 103 N88-16703

SEMICONDUCTING FILMS

- Plasma deposition of amorphous hydrogenated carbon films on III-V semiconductors
p 220 A88-32862

SEMICONDUCTOR DEVICES

- High-temperature electronics
p 128 N88-15797
- Development of 20 GHz monolithic transmit modules
[NASA-CR-182134] p 222 N88-24539
- Advanced development of double-injection, deep-impurity semiconductor switches
[NASA-CR-182118] p 222 N88-25346

SEMICONDUCTOR JUNCTIONS

- A comparison of the radiation tolerance characteristics of multijunction solar cells with series and voltage-matched configurations
[NASA-TM-101177] p 203 N88-27624

SEMIEMPIRICAL EQUATIONS

- Semi-empirical crack tip analysis
p 183 A88-47681

SENSITIVITY

- A semianalytical technique for sensitivity analysis of unsteady aerodynamic computations
[NASA-TM-100810] p 189 N88-18976

SENSORS

- Fiber-optic displacement sensor with temporally separated signal and reference channels
p 217 A88-33161
- Referencing in fiber optic sensing systems
p 217 A88-42604
- Prototype thin-film thermocouple/heat-flux sensor for a ceramic-insulated diesel engine
[NASA-TM-100798] p 162 N88-18892
- Fiber optic sensors with internal referencing
[NASA-TM-100893] p 162 N88-26644

SEPARATED FLOW

- Corona anemometry for qualitative measurement of reversing surface flow with application to separation control by external excitation
p 133 A88-14143
- Mixing, transport and combustion in sprays
p 138 A88-25828

- Turbulence energy and diffusion transport of third-moments in a separating and reattaching flow p 141 A88-43011
- A flow visualization study of the leading edge separation bubble on a NACA 0012 airfoil with simulated glaze ice [NASA-CR-180846] p 10 N88-14966
- SERVICE LIFE**
- A prediction model of the depth-of-discharge effect on the cycle life of a storage cell p 197 A88-11896
- Stress-life interrelationships associated with alkaline fuel cells p 197 A88-11903
- A model for life predictions of nickel-base superalloys in high-temperature low cycle fatigue p 87 A88-35913
- An extended life and performance test of a low-power arcjet [AIAA PAPER 88-3106] p 55 A88-48756
- Space station propulsion [NASA-TM-100216] p 57 N88-11746
- Computer-aided design analysis of 57-mm, angular-contact, cryogenic turbopump bearings [NASA-TP-2816] p 172 N88-18933
- Evaluation of structural analysis methods for life prediction p 190 N88-21511
- Analysis of closed cycle megawatt class space power systems with nuclear reactor heat sources p 62 N88-24351
- An extended life and performance test of a low-power arcjet [NASA-TM-100942] p 63 N88-24687
- Effect of LEO cycling at shallow depths of discharge on MANTECH IPV nickel-hydrogen cells [NASA-TM-101300] p 203 N88-25978
- SH WAVES**
- Input-output characterization of fiber composites by SH waves [NASA-CR-4153] p 179 N88-23986
- SHAPES**
- Electrohydrodynamic migration of charged droplets in an insulating fluid [AIAA PAPER 88-3557] p 143 A88-48946
- Electromagnetic fields backscattered from an s-shaped inlet cavity with an absorber coating on its inner walls [NASA-CR-182401] p 118 N88-15130
- An experimental mapping of the flow field behind a glaze ice shape on a NACA 0012 airfoil [NASA-CR-180847] p 10 N88-15766
- Electrohydrodynamic migration of charged droplets in an insulating fluid [NASA-TM-100849] p 152 N88-21424
- SHEAR FLOW**
- Control of shear flows by artificial excitation [AIAA PAPER 87-2722] p 3 A88-16567
- Aeroacoustics of subsonic turbulent shear flows [AIAA PAPER 87-2731] p 214 A88-16571
- Structure of a reattaching supersonic shear flow [AIAA PAPER 88-3615] p 8 A88-48901
- Evolution of hairpin vortices in a shear flow [NASA-TM-100858] p 211 N88-26885
- Study of toluene rotary fluid management device and shear flow condenser performance for a space-based organic Rankine power system [NASA-CR-180885] p 67 N88-29872
- SHEAR LAYERS**
- Coherent motion induced fluctuations in the primary transition region of a plane shear layer p 133 A88-14125
- Numerical simulation of self-sustained and forced oscillations in jet shear layers p 3 A88-14155
- Control of free shear layers [AIAA PAPER 87-2689] p 134 A88-16545
- Computation of the velocity field of an excited shear layer p 138 A88-26206
- Excitation of instability waves in free shear layers. I - Theory p 138 A88-26338
- Excitation of instability waves in free shear layers. II - Experiments p 138 A88-26339
- Time-accurate simulations of a shear layer forced at a single frequency [AIAA PAPER 88-0061] p 138 A88-27716
- Nonlinear roll-up of externally excited free shear layers p 141 A88-44445
- Time-accurate simulations of a shear layer forced at a single frequency [NASA-TM-100836] p 152 N88-19740
- SHEAR PROPERTIES**
- Thermo-elasto-viscoplastic analysis of problems in extension and shear p 183 A88-41042
- SHEAR STRAIN**
- An efficient Mindlin finite strip plate element based on assumed strain distribution p 192 N88-22407
- Improved finite strip Mindlin plate bending element using assumed shear strain distributions [NASA-TM-100928] p 196 N88-29195

- SHEAR STRENGTH**
- Ultrasonic evaluation of mechanical properties of thick, multilayered, filament-wound composites p 176 A88-21340
- Improving the interlaminar shear strength of carbon fiber-epoxy composites through carbon fiber bromination [NASA-TM-100248] p 72 N88-15018
- SHEAR STRESS**
- Wall shear stress measurement in blade end-wall corner region [ASME PAPER 87-GT-181] p 131 A88-11089
- A mixed formulation of C(0)-linear triangular plate/shell element - The role of edge shear constraints p 183 A88-40121
- Shear rheological characterization of motor oils p 100 A88-47562
- Free-edge delamination: Laminate width and loading conditions effects [NASA-TM-100238] p 72 N88-12551
- The NASA aircraft icing research program p 15 N88-15803
- Ethynylated aromatics as high temperature matrix resins [NASA-TM-89829] p 73 N88-18640
- Resolved shear stress intensity coefficient and fatigue crack growth in large crystals [NASA-CR-182137] p 195 N88-24997
- SHELLS (STRUCTURAL FORMS)**
- A mixed formulation of C(0)-linear triangular plate/shell element - The role of edge shear constraints p 183 A88-40121
- Analysis of shell-type structures subjected to time-dependent mechanical and thermal loading [NASA-CR-181409] p 185 N88-10388
- SHIELDING**
- An estimate of the noise shielding on the fuselage resulting from installing a short duct around an advanced propeller [NASA-TM-100262] p 217 N88-18379
- Experimental evaluation of resistojet thruster plume shields [NASA-TM-101363] p 66 N88-29868
- SHOCK HEATING**
- High-resolution heat-transfer-coefficient maps applicable to compound-curve surfaces using liquid crystals in a transient wind tunnel p 134 A88-18506
- SHOCK WAVE INTERACTION**
- Skin friction measurements by laser interferometry in swept shock wave/turbulent boundary-layer interactions [AIAA PAPER 88-0497] p 5 A88-22364
- Glancing shock wave-turbulent boundary layer interaction with boundary layer suction [AIAA PAPER 88-0308] p 6 A88-27718
- Experimental and numerical investigation of the effect of distributed suction on oblique shock wave/turbulent boundary layer interaction [NASA-TM-101334] p 156 N88-30084
- SHOCK WAVES**
- Performance of laser Doppler velocimeter with polydisperse seed particles in high speed flows [AIAA PAPER 88-0425] p 157 A88-22317
- A comparison of ENO and TVD schemes [AIAA PAPER 88-3707] p 210 A88-48831
- The carbon dioxide chaperon efficiency for the reaction $H + O_2 + M$ yields $HO_2 + M$ from ignition delay times behind reflected shock waves [NASA-TM-100125] p 79 N88-15036
- SHORT TAKEOFF AIRCRAFT**
- Aeroacoustics of advanced STOVL aircraft plumes [SAE PAPER 872358] p 215 A88-30998
- Acoustics technologies for STOVL aircraft [AIAA PAPER 88-2238] p 215 A88-35939
- Aeroacoustics of advanced STOVL aircraft plumes [SAE PAPER 872358] p 215 A88-37219
- STOVL acoustic fatigue technologies [SAE PAPER 872360] p 215 A88-37221
- A numerical study of the hot gas environment around a STOVL aircraft in ground proximity [AIAA PAPER 88-2882] p 23 A88-48752
- Cooperative synthesis of control and display augmentation for a STOL aircraft in the approach and landing task [AIAA PAPER 88-4182] p 37 A88-50272
- A numerical study of the hot gas environment around a STOVL aircraft in ground proximity [NASA-TM-100895] p 1 N88-23729
- SHROUDED PROPELLERS**
- A model of the wall boundary layer for ducted propellers [AIAA PAPER 87-2742] p 214 A88-16578
- An estimate of the noise shielding on the fuselage resulting from installing a short duct around an advanced propeller [NASA-TM-100262] p 217 N88-18379

- SHROUDED TURBINES**
- Localization of natural modes of vibration in bladed disks [ASME PAPER 87-GT-46] p 18 A88-10998
- Thermal stress minimized, two component, turbine shroud seal [NASA-CASE-LEW-14212-1] p 174 N88-23978
- SIDELOBES**
- Compensation of reflector antenna surface distortion using an array feed [NASA-TM-100286] p 119 N88-18805
- Case study of active array feed compensation with sidelobe control for reflector surface distortion [NASA-TM-100287] p 120 N88-23073
- SIGNAL ANALYSIS**
- Evaluation of the communications impact of a low power arcjet thruster [AIAA PAPER 88-3105] p 55 A88-48755
- Evaluation of the communications impact of a low power arcjet thruster [NASA-TM-100926] p 63 N88-24682
- SIGNAL ANALYZERS**
- Analysis of counting errors in the phase/Doppler particle analyzer [NASA-TM-100231] p 161 N88-12043
- SIGNAL PROCESSING**
- Fiber-optic displacement sensor with temporally separated signal and reference channels p 217 A88-33161
- Optical alignment of Centaur's inertial guidance system [NASA-TM-88844] p 43 N88-12515
- Experiments applications guide: Advanced Communications Technology Satellite (ACTS) [NASA-TM-100265] p 49 N88-28082
- SILANES**
- Sol-gel synthesis of magnesium oxide-silicon dioxide glass compositions p 100 A88-49105
- Polymer precursors for ceramic composites p 75 N88-23890
- SILICA GLASS**
- Sol-gel synthesis of magnesium oxide-silicon dioxide glass compositions p 100 A88-49105
- SILICON**
- Improved beta-SiC heteroepitaxial films using off-axis Si substrates p 219 A88-10431
- Gigard-tolerant power switches and memory elements p 123 A88-22704
- Development of 8 cm x 8 cm silicon gridded back solar cell for space station p 200 A88-34312
- Radiation damage and defect behavior in proton irradiated lithium-counterdoped n+p silicon solar cells p 125 A88-34340
- Performance of GaAs and silicon concentrator cells under 37 MeV proton irradiation p 200 A88-34343
- Effect of high-temperature annealing on the microstructure and thermoelectric properties of GaP doped SiGe [NASA-TM-100164] p 101 N88-10188
- Performance of GaAs and silicon concentrator cells under 37 MeV proton irradiation [NASA-TM-100144] p 200 N88-12877
- Neutron radiation tolerance of Au-activated silicon p 222 N88-24316
- SILICON ALLOYS**
- Effect of high temperature annealing on the thermoelectric properties of GaP doped SiGe p 220 A88-40796
- SILICON CARBIDES**
- Improved beta-SiC heteroepitaxial films using off-axis Si substrates p 219 A88-10431
- Behavior of ion-implanted junction diodes in 3C SiC p 122 A88-15423
- Simple processing method for high-strength silicon carbide p 97 A88-19056
- Molten-salt corrosion of silicon nitride. I - Sodium carbonate. II - Sodium sulfate p 97 A88-26222
- Multielement mapping of alpha-SiC by scanning Auger microscopy p 158 A88-27617
- Lattice defects in beta-SiC grown epitaxially on silicon substrates p 220 A88-28711
- Effect of high-temperature hydrogen exposure on sintered alpha-SiC p 97 A88-29714
- Microscopy of epitaxially grown beta-SiC on 001-plane silicon p 98 A88-31023
- SiC reinforced aluminide composites p 70 A88-31687
- Improved processing of alpha-SiC p 99 A88-38318
- Silicon carbide - Progress in crystal growth p 99 A88-40792
- Direct mass spectrometric identification of silicon oxychloride compounds p 78 A88-44425
- Elevated temperature durability of ceramic materials [AIAA PAPER 88-3055] p 100 A88-44743
- Microwave and millimeter-wave power generation in silicon carbide avalanche devices p 126 A88-47599

Low-temperature photoluminescence studies of chemical-vapor-deposition-grown 3C-SiC on Si

p 127 A88-53396

Raman scattering studies of chemical-vapor-deposited cubic SiC films of (100)Si

p 127 A88-53397

Acoustic imaging of subtle porosity variations in ceramics

p 101 A88-55044

Pressure effects on the thermal stability of SiC fibers [NASA-TM-100146]

p 71 N88-10120

Flaw imaging and ultrasonic techniques for characterizing sintered silicon carbide [NASA-TM-100177]

p 177 N88-12106

Stress rupture behavior of silicon carbide coated, low modulus carbon/carbon composites [NASA-CR-180863]

p 72 N88-14150

Friction and wear of monolithic and fiber reinforced silicon-ceramics sliding against IN-718 alloy at 25 to 800 C in atmospheric air at ambient pressure

p 103 N88-17796

Characterization of sintered SiC by using NDE [NASA-TM-100294]

p 177 N88-22413

Nondestructive evaluation of structural ceramics

p 178 N88-23876

Improved silicon carbide for advanced heat engines

p 106 N88-23879

Strength optimization of alpha-SiC by improved processing

p 107 N88-23880

Colloidal characterization of silicon nitride and silicon carbide

p 107 N88-23883

Molten salt corrosion of SiC and Si3N4

p 107 N88-23885

Thermal cyclic durability testing of ceramic materials for turbine engines

p 179 N88-23886

Ceramic matrix composites

p 75 N88-23888

SiC fiber analysis

p 107 N88-23891

SiC fiber reinforced reaction-bonded Si3N4 composites

p 75 N88-23892

High frequency ultrasonic characterization of sintered SiC

p 179 N88-23985

Auger analysis of a fiber/matrix interface in a ceramic matrix composite [NASA-TM-100825]

p 179 N88-23985

As-received microstructure of a SiC/Ti-15-3 composite [NASA-TM-100938]

p 76 N88-25487

Investigation of a SiC/Ti-24Al-11Nb composite [NASA-TM-100956]

p 76 N88-28980

Electrical properties of materials for elevated temperature resistance strain gage application [NASA-CR-182214]

p 164 N88-30106

SILICON DIOXIDE

Chemical vapor deposited silica coatings for solar mirror protection [AIAA PAPER 88-0027]

p 99 A88-41796

Chemical vapor deposited silica coatings for solar mirror protection [NASA-TM-100834]

p 105 N88-21306

SILICON NITRIDES

Dynamic and static fatigue behavior of sintered silicon nitrides

p 96 A88-12602

Strength characterization of yttria/alumina-doped sintered silicon nitride

p 97 A88-26154

Molten-salt corrosion of silicon nitride. I - Sodium carbonate. II - Sodium sulfate

p 97 A88-26222

Direct mass spectrometric identification of silicon oxychloride compounds

p 78 A88-44425

Elevated temperature durability of ceramic materials [AIAA PAPER 88-3055]

p 100 A88-44743

Improved silicon nitride for advanced heat engines [NASA-CR-175006]

p 102 N88-15886

Flaw characterization in structural ceramics using scanning laser acoustic microscopy

p 177 N88-22415

Nondestructive evaluation of structural ceramics

p 178 N88-23876

Improved processing of Si3N4

p 107 N88-23882

Colloidal characterization of silicon nitride and silicon carbide

p 107 N88-23883

Molten salt corrosion of SiC and Si3N4

p 107 N88-23885

Thermal cyclic durability testing of ceramic materials for turbine engines

p 179 N88-23886

SiC fiber reinforced reaction-bonded Si3N4 composites

p 75 N88-23892

Auger analysis of a fiber/matrix interface in a ceramic matrix composite [NASA-TM-100892]

p 76 N88-25487

The high temperature creep deformation of Si3N4-6Y2O3-2Al2O3 [NASA-CR-183204]

p 76 N88-28981

SILICON OXIDES

Glass properties in the yttria-alumina-silica system

p 96 A88-18361

SILICONES

Containment of a silicone fluid free surface in reduced gravity using barrier coatings [NASA-TM-101314]

p 155 N88-30072

SILOXANES

Silasesquioxanes as precursors to ceramic composites

p 69 A88-12599

SILVER

Sputtered silver films to improve chromium carbide based solid lubricant coatings for use to 900 C

p 100 A88-47563

Sputtered silver films to improve chromium carbide based solid lubricant coatings for use to 900 C [NASA-TM-100783]

p 102 N88-15885

SIMILARITY THEOREM

On self-similarity of crack layer

p 181 A88-24054

Similar solutions for viscous hypersonic flow over a slender three-fourths-power body of revolution [NASA-TM-100205]

p 148 N88-12752

SIMULATION

Experimental evaluation of corner vanes - Summary [SAE PAPER 871784]

p 39 A88-30778

Satellite ground-terminal user simulation [NASA-TM-100234]

p 118 N88-14260

An experimental mapping of the flow field behind a glaze ice shape on a NACA 0012 airfoil [NASA-CR-180847]

p 10 N88-15766

A multistage mesh generator for solving the average-passage equation system [NASA-CR-179539]

p 10 N88-15769

Vapor condensation on a turbulent liquid interface

p 150 N88-15939

Numerical simulation of axisymmetric turbulent flow in combustors and diffusers [NASA-CR-4115]

p 11 N88-17582

Numerical simulation of subsonic and transonic propeller flow [NASA-TM-100163]

p 11 N88-20262

Documentation of the Benson Diesel Engine Simulation Program [NASA-TM-100940]

p 36 N88-27201

SIMULATORS

A microprocessor-based real-time simulator of a turbofan engine [NASA-TM-100889]

p 32 N88-21163

SINGLE CRYSTALS

Effect of initial gamma prime size on the elevated temperature creep properties of single crystal nickel base superalloys

p 82 A88-18884

Cyclic hardening mechanisms in Nimonic 80A

p 84 A88-24490

On the cyclic stress-strain behaviour of a Ni-base superalloy at room temperature

p 84 A88-24521

Anisotropic constitutive modeling for nickel base single crystal superalloys using a crystallographic approach [AIAA PAPER 88-2440]

p 85 A88-32357

Creep-fatigue behavior of NiCoCrAlY coated PWA 1480 superalloy single crystals

p 86 A88-35911

Microstructure-property relationships in directionally solidified single-crystal nickel-base superalloys

p 88 A88-40329

Characterization of directionally solidified lead chloride

p 111 A88-43170

Accelerated crack growth rate at low Delta K in a single crystal superalloy

p 89 A88-47687

A crystallographic model for nickel base single crystal alloys

p 89 A88-48182

Deposition of vanadium oxide films by direct-current magnetron reactive sputtering

p 221 A88-51286

Bithermal low-cycle fatigue behavior of a NiCoCrAlY-coated single crystal superalloy

p 90 A88-51736

Raman scattering studies of chemical-vapor-deposited cubic SiC films of (100)Si

p 127 A88-53397

Constitutive modeling for single crystal superalloys

p 90 N88-11168

Constitutive modeling of superalloy single crystals with verification testing

p 91 N88-11169

Creep-fatigue behavior of NiCoCrAlY coated PWA 1480

p 186 N88-11176

The cyclic stress-strain behavior of a single crystal nickel-base superalloy [NASA-TM-100269]

p 92 N88-19610

Bithermal fatigue of a nickel-base superalloy single crystal [NASA-TM-100885]

p 93 N88-22168

Unified constitutive model for single crystal deformation behavior with applications

p 191 N88-22388

Fatigue crack growth behavior of a single crystal alloy as observed through an in situ fatigue loading stage [NASA-TM-100863]

p 93 N88-22986

Isothermal and bithermal thermomechanical fatigue behavior of a NiCoCrAlY-coated single crystal superalloy [NASA-TM-100907]

p 94 N88-24766

Resolved shear stress intensity coefficient and fatigue crack growth in large crystals [NASA-CR-182137]

p 195 N88-24997

Accelerated fatigue crack growth behavior of PWA 1480 single crystal alloy and its dependence on the deformation mode [NASA-TM-100943]

p 95 N88-26436

Anisotropic constitutive modeling for nickel-base single crystal superalloys [NASA-CR-182157]

p 95 N88-29961

SINGLE STAGE TO ORBIT VEHICLES

Ground tests confirm the promise of hypersonic propulsion

p 2 A88-10369

Hypersonic structures and materials - A progress report

p 17 A88-16748

SINTERING

Strength characterization of yttria/alumina-doped sintered silicon nitride

p 97 A88-26154

Characteristics of fluid flow in the combustion synthesis of TiC from the elements

p 110 A88-28564

Effect of high-temperature hydrogen exposure on sintered alpha-SiC

p 97 A88-29714

Gravitational contributions to microstructural coarsening in liquid phase sintering

p 111 A88-37155

Improved processing of alpha-SiC

p 99 A88-38318

Advantages of barium peroxide in the powder synthesis of perovskite superconductors

p 221 A88-41496

Gravity and configurational energy induced microstructural changes in liquid phase sintering

p 112 A88-49089

Structure and grain coarsening during the processing of engineering ceramics [NASA-TM-100235]

p 101 N88-11838

Improved silicon nitride for advanced heat engines [NASA-CR-175006]

p 102 N88-15886

Improved silicon carbide for advanced heat engines

p 106 N88-23879

Strength optimization of alpha-SiC by improved processing

p 107 N88-23880

Improved processing of Si3N4

p 107 N88-23882

High frequency ultrasonic characterization of sintered SiC [NASA-TM-100825]

p 179 N88-23985

SIZE DETERMINATION

Electrohydrodynamic migration of charged droplets in an insulating fluid [AIAA PAPER 88-3557]

p 143 A88-48946

Electrohydrodynamic migration of charged droplets in an insulating fluid [NASA-TM-100849]

p 152 N88-21424

SIZE DISTRIBUTION

Determination of grain-size distribution function using two-dimensional Fourier transforms of tone-pulse-encoded images

p 176 A88-30425

Small-droplet spray measurements with a scattered-light scanner [NASA-TM-100973]

p 163 N88-26645

SKIN FRICTION

Skin friction measurements by laser interferometry in swept shock wave/turbulent boundary-layer interactions [AIAA PAPER 88-0497]

p 5 A88-22364

SKIN TEMPERATURE (NON-BIOLOGICAL)

Correlations of velocity and temperature fluctuations in the stagnation-point flow of circular cylinder in turbulent flow [NASA-TM-100930]

p 13 N88-25435

SLIDING

Friction and wear of monolithic and fiber reinforced silicon-ceramics sliding against IN-718 alloy at 25 to 800 C in atmospheric air at ambient pressure [NASA-TM-100294]

p 103 N88-17796

SLIP CASTING

Slip casting and extruding shapes of rhemium with metal oxide additives. Part 2: Development of grain stabilized rhemium parts for resistojets [NASA-CR-180851]

p 57 N88-11749

SLOT ANTENNAS

Slotline fed microstrip antenna array modules

p 126 A88-44170

SMALL PERTURBATION FLOW

Stability of swirling gas flows

p 142 A88-46317

SODIUM CARBONATES

Molten-salt corrosion of silicon nitride. I - Sodium carbonate. II - Sodium sulfate

p 97 A88-26222

SODIUM CHLORIDES

Experimental verification of vapor deposition rate theory in high velocity burner rigs

p 91 N88-11179

SODIUM SULFATES

Effect of alloy composition on the sodium-sulfate induced hot corrosion attack of cast nickel-base superalloys at 900 C

p 81 A88-10028

Sodium sulfate-induced corrosion of pure nickel and superalloy Udmet 700 in a high velocity burner rig at 900 C

p 83 A88-20266

SOFTWARE TOOLS

Numerical arc segmentation algorithm for a radio conference - A software tool for communication satellite systems planning
[AIAA PAPER 88-0788] p 212 A88-27531

An allotment planning concept and related computer software for planning the fixed satellite service at the 1988 space WARC p 116 A88-36482

Two-dimensional graphics tools for a transputer based display board
[NASA-TM-100820] p 207 N88-22591

An integrated and modular digital modeling approach for the space station electrical power system development
[NASA-TM-100904] p 61 N88-22935

User's manual for the two-dimensional transputer graphics toolkit
[NASA-TM-100974] p 207 N88-27799

SOL-GEL PROCESSES

Sol-gel synthesis of magnesium oxide-silicon dioxide glass compositions p 100 A88-49105

SOLAR ARRAYS

Threshold-determining mechanisms for discharges in high-voltage solar arrays p 50 A88-11738

Mast material test program (MAMATEP) --- for Solar Array Assembly of Space Station Photovoltaic Power Module
[AIAA PAPER 88-2475] p 70 A88-35945

Oxidation and protection of fiberglass-epoxy composite masts for photovoltaic arrays in the low Earth orbital environment
[NASA-TM-100839] p 104 N88-18734

Mast material test program (MAMATEP)
[NASA-TM-100821] p 74 N88-19592

Assessment of the effects of space debris and meteoroids environment on the space station solar array assembly
[NASA-TM-101315] p 49 N88-28959

SOLAR CELLS

High temperature solid oxide regenerative fuel cell for solar photovoltaic energy storage p 197 A88-11905

Comparative radiation resistance, temperature dependence and performance of diffused junction indium phosphide solar cells p 198 A88-18580

Space solar cell research - Problems and potential
p 123 A88-21605

Issues in space photovoltaic research and technology
p 199 A88-34230

Self-consistent calculations and design considerations for a GaAs nipi doping superlattice solar cell
p 124 A88-34249

InP based solar cells for space application: Reduction of external losses p 199 A88-34250

Characterization and modelling of open tube diffused n+p bulk InP solar cells p 199 A88-34270

Laser induced OMCD growth of AlGaAs on GaAs
p 125 A88-34286

Piezoresistance and solar cell efficiency
p 125 A88-34298

Development of 8 cm x 8 cm silicon gridded back solar cell for space station p 200 A88-34312

Radiation and temperature effects in gallium arsenide, indium phosphide, and silicon solar cells
p 125 A88-34321

Radiation damage and defect behavior in proton irradiated lithium-counterdoped n+p silicon solar cells
p 125 A88-34340

Performance of GaAs and silicon concentrator cells under 37 MeV proton irradiation p 200 A88-34343

Radiation performance of AlGaAs and InGaAs concentrator cells and expected performance of cascade structures p 125 A88-34356

Modelling and design of high efficiency radiation tolerant indium phosphide space solar cells p 200 A88-34394

Direct-current magnetron fabrication of indium tin oxide/InP solar cells p 200 A88-51289

Effects of electron and proton irradiations on n/p and p/n GaAs cells grown by MOCVD
[NASA-TM-100199] p 127 N88-10266

Recent progress in space photovoltaic systems
[NASA-TM-100208] p 128 N88-11966

Performance of GaAs and silicon concentrator cells under 37 MeV proton irradiation
[NASA-TM-100144] p 200 N88-12877

Radiation performance of AlGaAs concentrator cells and expected performance of cascade structures
[NASA-TM-100145] p 200 N88-12878

Progress in InP solar cell research
[NASA-TM-100914] p 130 N88-24870

Aging behavior of Au-based ohmic contacts to GaAs
[NASA-CR-182146] p 130 N88-25831

Study of Staebler-Wronsky degradation effect in a Si:H based P-I-N solar cells
[NASA-CR-182564] p 203 N88-25970

Solar energy conversion through the interaction of plasmons with tunnel junctions. Part A: Solar cell analysis. Part B: Photoconductor analysis
[NASA-CR-183044] p 203 N88-27621

A comparison of the radiation tolerance characteristics of multijunction solar cells with series and voltage-matched configurations
[NASA-TM-101177] p 203 N88-27624

SOLAR COLLECTORS

Solar concentrator advanced development project
p 50 A88-11799

Advanced solar receiver conceptual design study
p 51 A88-11800

Development of an advanced photovoltaic concentrator system for space applications p 51 A88-11812

Development of composite facets for the surface of a space-based solar dynamic concentrator
p 54 A88-18230

Performance of GaAs and silicon concentrator cells under 37 MeV proton irradiation p 200 A88-34343

Atomic-oxygen durability of impact-damaged solar reflectors p 68 A88-54988

Performance of GaAs and silicon concentrator cells under 37 MeV proton irradiation
[NASA-TM-100144] p 200 N88-12877

Advanced sensible heat solar receiver for space power
[NASA-TM-100847] p 59 N88-21249

Space station solar concentrator materials research
[NASA-TM-100862] p 60 N88-21250

Ray tracing optical analysis of offset solar collector for space station solar dynamic system
[NASA-TM-100853] p 60 N88-22080

Development of an integrated heat pipe-thermal storage system for a solar receiver
[NASA-TM-101099] p 202 N88-22458

Progress in InP solar cell research
[NASA-TM-100914] p 130 N88-24870

Design and demonstration of a system for the deposition of atomic-oxygen durable coatings for reflective solar dynamic power system concentrators
[NASA-CR-4158] p 64 N88-25474

Thermal distortion analysis of the space station solar dynamic concentrator
[NASA-TM-100868] p 64 N88-25475

Advanced heat receiver conceptual design study
[NASA-CR-180901] p 203 N88-25977

Lewis Research Center space station electric power system test facilities
[NASA-TM-100924] p 43 N88-28942

The effect of the near earth micrometeoroid environment on a highly reflective mirror surface
[NASA-TM-101307] p 44 N88-29833

SOLAR DYNAMIC POWER SYSTEMS

Toluene stability Space Station Rankine power system
p 50 A88-11794

Advanced space solar dynamic power systems beyond IOC Space Station p 50 A88-11798

Solar concentrator advanced development project
p 50 A88-11799

Advanced solar receiver conceptual design study
p 51 A88-11800

Selection of high temperature thermal energy storage materials for advanced solar dynamic space power systems p 68 A88-11801

Integrated heat pipe-thermal storage system performance evaluation p 132 A88-11803

Fluoride salts and container materials for thermal energy storage applications in the temperature range 973 - 1400 K p 196 A88-11804

Impact of thermal energy storage properties on solar dynamic space power conversion system mass
p 51 A88-11805

Heat pipe radiators for solar dynamic space power system heat rejection p 132 A88-11807

Solar dynamic organic Rankine cycle heat rejection system simulation p 132 A88-11808

Optical measurements pertaining to Space Station solar dynamic power systems
[IAF PAPER 87-229] p 42 A88-15954

Space Station Electrical Power System
[IAF PAPER 87-234] p 53 A88-15958

Modelling the performance of the monogroove with screen heat pipe for use in the radiator of the solar dynamic power system of the NASA Space Station
[IAF PAPER 87-238] p 134 A88-15960

Development of composite facets for the surface of a space-based solar dynamic concentrator
p 54 A88-18230

Oxidation-resistant reflective surfaces for solar dynamic power generation in near earth orbit p 54 A88-18523

Identification of salt-alloy combinations for thermal energy storage applications in advanced solar dynamic power systems p 199 A88-24072

Structural assessment of a Space Station solar dynamic heat receiver thermal energy storage canister
[AIAA PAPER 88-2487] p 47 A88-31396

Issues in space photovoltaic research and technology
p 199 A88-34230

Development of an integrated heat pipe-thermal storage system for a solar receiver
[AIAA PAPER 88-2683] p 141 A88-43746

Solar dynamic concentrator durability in atomic oxygen and micrometeoroid environments p 68 A88-51393

Space Station Photovoltaic power modules
p 56 A88-52333

Modelling the performance of the tapered artery heat pipe design for use in the radiator of the solar dynamic power system of the NASA Space Station
[IAF PAPER 88-213] p 56 A88-55361

Electrical Power Working Group report
p 48 N88-10095

Photovoltaic power modules for NASA's manned space station
[NASA-TM-100229] p 57 N88-11745

Status of 20 kHz space station power distribution technology
[NASA-TM-100781] p 59 N88-15838

Solar concentrator advanced development program, task 1
[NASA-CR-179489] p 201 N88-18068

Computer-aided modeling and prediction of performance of the modified Lundell class of alternators in space station solar dynamic power systems
[NASA-CR-182538] p 201 N88-19000

Solar dynamic power system definition study
[NASA-CR-180877] p 59 N88-20361

Space station power system requirements
[NASA-TM-100886] p 49 N88-21245

Advanced sensible heat solar receiver for space power
[NASA-TM-100847] p 59 N88-21249

Space station solar concentrator materials research
[NASA-TM-100862] p 60 N88-21250

Power systems for production, construction, life support and operations in space
[NASA-TM-100838] p 60 N88-21254

Ray tracing optical analysis of offset solar collector for space station solar dynamic system
[NASA-TM-100853] p 60 N88-22080

Structural assessment of a space station solar dynamic heat receiver thermal energy storage canister
p 192 N88-22406

Solar dynamic heat rejection technology. Task 2: Heat pipe radiator development
[NASA-CR-182141] p 152 N88-23182

Speculations on future opportunities to evolve Brayton powerplants aboard the space station
p 202 N88-24258

Design and demonstration of a system for the deposition of atomic-oxygen durable coatings for reflective solar dynamic power system concentrators
[NASA-CR-4158] p 64 N88-25474

Thermal distortion analysis of the space station solar dynamic concentrator
[NASA-TM-100868] p 64 N88-25475

Advanced heat receiver conceptual design study
[NASA-CR-180901] p 203 N88-25977

Study of toluene stability for an Organic Rankine Cycle (ORC) space-based power system
[NASA-CR-180884] p 66 N88-29863

Study of toluene rotary fluid management device and shear flow condenser performance for a space-based organic Rankine power system
[NASA-CR-180885] p 67 N88-29872

SOLAR ENERGY

Impact of thermal energy storage properties on solar dynamic space power conversion system mass
p 51 A88-11805

SOLAR ENERGY ABSORBERS

Identification of salt-alloy combinations for thermal energy storage applications in advanced solar dynamic power systems p 199 A88-24072

SOLAR GENERATORS

Performance characteristics of a combination solar photovoltaic heat engine energy converter
p 197 A88-11813

High thermal-transport capacity heat pipes for space radiators
[SAE PAPER 871509] p 136 A88-21155

Recent progress in space photovoltaic systems
[NASA-TM-100208] p 128 N88-11966

Design description report for a photovoltaic power system for a remote satellite earth terminal
[NASA-CR-179586] p 200 N88-12875

SOLAR MAGNETIC FIELD

Magnetic fields interacting with nonlinear compressible convection p 226 A88-31163

SOLAR REFLECTORS

SOLAR REFLECTORS

- Chemical vapor deposited silica coatings for solar mirror protection [AIAA PAPER 88-0027] p 99 A88-41796
- Chemical vapor deposited silica coatings for solar mirror protection [NASA-TM-100834] p 105 N88-21306
- SOLID LUBRICANTS**
 - Tribological properties of polymer films and solid bodies in a vacuum environment p 98 A88-35565
 - Investigation of PTFE transfer films by infrared emission spectroscopy and phase-locked ellipsometry p 99 A88-35568
 - Sputtered silver films to improve chromium carbide based solid lubricant coatings for use to 900 C p 100 A88-47563
 - Coatings for high-temperature bearings and seals [NASA-TM-100249] p 102 N88-13453
 - Sputtered silver films to improve chromium carbide based solid lubricant coatings for use to 900 C [NASA-TM-100783] p 102 N88-15885
 - Tribological properties of alumina-boria-silicate fabric from 25 to 850 C [NASA-TM-100806] p 104 N88-18726
 - Status and directions of modified tribological surfaces by ion processes [NASA-TM-101304] p 115 N88-28176
- SOLID PROPELLANT COMBUSTION**
 - Velocity-coupled flow oscillations in a simulated solid-propellant rocket environment [AIAA PAPER 88-0543] p 108 A88-27720
- SOLID ROCKET PROPELLANTS**
 - Velocity-coupled flow oscillations in a simulated solid-propellant rocket environment [AIAA PAPER 88-0543] p 108 A88-27720
- SOLID SOLUTIONS**
 - On producing an alloy of uniform composition during rapid solidification processing p 89 A88-41654
- SOLID STATE**
 - Solid-state combustion synthesis of ceramics and alloys in reduced gravity [NASA-CR-4163] p 75 N88-25479
- SOLID STATE DEVICES**
 - Characterization of a 30-GHz IMPATT solid state amplifier [NASA-TM-100876] p 120 N88-24847
- SOLID SURFACES**
 - Free-streamline analysis of deformation and dislodging by wind force of drops on a surface p 137 A88-25191
- SOLID-SOLID INTERFACES**
 - Interface roughness effect on stresses in ceramic coatings p 95 A88-12587
 - Friction and wear of ceramics p 106 N88-23874
- SOLIDIFICATION**
 - A model for the influence of pressure on the bulk modulus and the influence of temperature on the solidification pressure for liquid lubricants [ASME PAPER 86-TR1B-63] p 133 A88-15124
 - Radiative cooling of a solidifying droplet layer including absorption and scattering p 133 A88-15749
 - Local convective flows in partly solidified alloys p 219 A88-18467
 - Simulating the cooling of an immiscible alloy p 83 A88-20199
 - Dendritic solidification under microgravity conditions [AIAA PAPER 88-0248] p 110 A88-22186
 - Containerless processing of undercooled melts p 110 A88-28554
 - Solidification of undercooled Ni-Sn eutectic alloy under microgravity conditions in the Space Shuttle p 110 A88-28557
 - Low cost Get-Away-Special (GAS) furnace p 41 A88-28583
 - Dendritic growth of undercooled nickel-tin. III p 86 A88-32887
 - Solidification under microgravity conditions - Dendritic growth [AAS PAPER 86-380] p 110 A88-35130
 - Gravitational macrosegregation in binary Pb-Sn alloy ingots p 111 A88-41211
 - Primary arm spacing in chill block melt spun Ni-Mo alloys p 89 A88-41655
 - Double-diffusive effects during solidification p 221 A88-43933
- SOLITARY WAVES**
 - Primordial origin of nontopological solitons p 226 A88-39313
- SOLUBILITY**
 - Simulating the cooling of an immiscible alloy p 83 A88-20199
 - Sol-gel synthesis of magnesium oxide-silicon dioxide glass compositions p 100 A88-49105
- SOLUTES**
 - Thermosolutal convection in high-aspect-ratio enclosures [NASA-TM-100803] p 151 N88-18871

SOLUTIONS

- Fingering flow patterns of thermosolutal convection in rectangular enclosures [AIAA PAPER 88-3823] p 144 A88-49000
- Fingering flow patterns of thermosolutal convection in rectangular enclosures [NASA-TM-100854] p 152 N88-21417
- SOOT**
 - Soot loading in a generic gas turbine combustor p 19 A88-27296
 - Temperature and velocity profiles in sooting free convection diffusion flames p 78 A88-43018
 - Optical measurements of soot and temperature profiles in premixed propane-oxygen flames [NASA-TM-101343] p 115 N88-29997
 - Optical measurements of soot in premixed flames [NASA-TM-101305] p 156 N88-30090
- SOUND FIELDS**
 - Automated acoustic intensity measurements and the effect of gear tooth profile on noise p 168 A88-31623
- SOUND TRANSMISSION**
 - Identification and proposed control of helicopter transmission noise at the source p 38 N88-16647
- SPACE BASES**
 - Small reactor power systems for manned planetary surface bases [NASA-TM-100223] p 227 N88-13209
- SPACE COMMERCIALIZATION**
 - Space commercialization and power system technology p 223 A88-44003
 - Preparation for microgravity: The role of the microgravity materials science laboratory [NASA-TM-100906] p 113 N88-24811
- SPACE COMMUNICATION**
 - Monolithic Microwave Integrated Circuit (MMIC) technology for space communications applications [IAF PAPER 87-491] p 122 A88-18133
 - Optical technologies for space communication systems; Proceedings of the Meeting, Los Angeles, CA, Jan. 15, 16, 1987 p 45 A88-35251
 - [SPIE-756] p 45 A88-35251
 - An evolutionary communications scenario for Mars exploration [NASA-TM-100263] p 118 N88-13515
 - Optically controlled phased-array antenna technology for space communication systems [NASA-TM-100852] p 119 N88-18809
 - Monolithic microwave integrated circuit technology for advanced space communication [NASA-TM-100829] p 120 N88-21389
 - Service offerings and interfaces for the ACTS network of Earth stations [NASA-TM-100809] p 46 N88-24663
- SPACE DEBRIS**
 - Assessment of the effects of space debris and meteoroids environment on the space station solar array assembly [NASA-TM-101315] p 49 N88-28959
- SPACE DENSITY**
 - Primordial origin of nontopological solitons p 226 A88-39313
- SPACE ENVIRONMENT SIMULATION**
 - An experimental investigation of the effect of test-cell pressure on the performance of resistojets [AIAA PAPER 88-3286] p 40 A88-44820
- SPACE EXPLORATION**
 - Small reactor power systems for manned planetary surface bases [NASA-TM-100223] p 227 N88-13209
 - An evolutionary communications scenario for Mars exploration [NASA-TM-100263] p 118 N88-13515
 - Small space reactor power systems for unmanned solar system exploration missions [NASA-TM-100228] p 227 N88-14054
 - Electromagnetic powered vehicles (EMPV) for Mars exploration p 62 N88-24388
- SPACE FLIGHT**
 - Preparation for microgravity - The role of the Microgravity Material Science Laboratory [AIAA PAPER 88-3510] p 111 A88-42908
- SPACE MISSIONS**
 - Economic benefits of the Space Station to commercial communication satellite operators [IAF PAPER 87-622] p 41 A88-16215
 - Recent progress in space photovoltaic systems [NASA-TM-100208] p 128 N88-11966
 - Electric propulsion options for the SP-100 reference mission p 62 N88-24296
- SPACE PLASMAS**
 - Record charging events from Applied Technology Satellite 6 p 46 A88-11737
 - An unusual charging event on ISEE 1 p 47 A88-40013
 - Electron beam experiments at high altitudes p 47 A88-46799

- Plasma wave turbulence around the shuttle - Results from the Spacelab-2 flight p 218 A88-47783
- Electron collection by multiple objects within a single sheath p 219 A88-54999
- SPACE PLATFORMS**
 - Communications payload concepts for geostationary facilities [NASA-TM-100154] p 118 N88-13513
 - Technology requirements for an orbiting fuel depot: A necessary element of a space infrastructure [NASA-TM-101370] p 49 N88-29845
- SPACE POWER REACTORS**
 - SP-100 Advanced Technology Program p 52 A88-11846
 - Coaxial tube array space transmission line characterization p 121 A88-11865
 - Thermal aging effects in refractory metal alloys p 84 A88-22700
 - Small space reactor power systems for unmanned solar system exploration missions [NASA-TM-100228] p 227 N88-14054
 - Power transmission studies for tethered SP-100 [NASA-TM-100864] p 60 N88-21251
 - Overview of NASA Lewis Research Center free-piston Stirling engine technology activities applicable to space power systems p 202 N88-24255
 - Speculations on future opportunities to evolve Brayton powerplants aboard the space station p 202 N88-24258
 - Preliminary study of niobium alloy contamination by transport through helium p 94 N88-24279
 - Electric propulsion options for the SP-100 reference mission p 62 N88-24296
 - Analysis of closed cycle megawatt class space power systems with nuclear reactor heat sources p 62 N88-24351
 - Assessment of nuclear reactor concepts for low power space applications p 217 N88-24409
 - Creep behavior of tungsten/niobium and tungsten/niobium-1 percent zirconium composites p 75 N88-24427
 - Comparative analysis of the space power architecture studies [NASA-TM-100977] p 66 N88-28090
 - Lewis Research Center space station electric power system test facilities [NASA-TM-100924] p 43 N88-28942
- SPACE PROCESSING**
 - Simulation of fluid flows during growth of organic crystals in microgravity p 109 A88-13163
 - Dendritic solidification under microgravity conditions [AIAA PAPER 88-0248] p 110 A88-22186
 - Mass transport phenomena between bubbles and dissolved gases in liquids under reduced gravity conditions [AIAA PAPER 88-0450] p 138 A88-27719
 - Containerless processing of undercooled melts p 110 A88-28554
 - Low cost Get-Away-Special (GAS) furnace p 41 A88-28583
 - Gravitational contributions to microstructural coarsening in liquid phase sintering p 111 A88-37155
 - Growth of needle-shaped crystals in the presence of convection p 111 A88-37715
 - Noncontact temperature measurement: Requirements and applications for metals and alloys research p 112 N88-23899
 - Preparation for microgravity: The role of the microgravity materials science laboratory [NASA-TM-100906] p 113 N88-24811
- SPACE PROCESSING APPLICATIONS ROCKET**
 - Application of structural tailoring to spar/shell turboprops [AIAA PAPER 88-2333] p 20 A88-32277
- SPACE RENDEZVOUS**
 - Optimal cooperative time-fixed impulsive rendezvous [AIAA PAPER 88-4279] p 42 A88-50406
- SPACE SHUTTLE MAIN ENGINE**
 - Real gas properties and Space Shuttle Main Engine fuel turbine performance prediction [ASME PAPER 87-GT-106] p 50 A88-11038
 - Probabilistic structural analysis methods for space propulsion system components p 54 A88-16441
 - Probabilistic Structural Analysis Methods for select space propulsion system structural components (PSAM) p 56 A88-49659
 - Thermal finite-element analysis of space shuttle main engine turbine blade [NASA-TM-100117] p 187 N88-13745
 - Computer-aided design analysis of 57-mm, angular-contact, cryogenic turbopump bearings [NASA-TP-2816] p 172 N88-18933
 - Thermal-structural analyses of Space Shuttle Main Engine (SSME) hot section components p 61 N88-22404

SUBJECT INDEX

SPACE SHUTTLE MISSION 51-F

Gaseous environment of the Shuttle early in the Spacelab 2 mission p 47 A88-47972

SPACE SHUTTLE PAYLOADS

Solidification of undercooled Ni-Sn eutectic alloy under microgravity conditions in the Space Shuttle p 110 A88-28557

Low cost Get-Away-Special (GAS) furnace p 41 A88-28583

Gravitational macrosegregation in binary Pb-Sn alloy ingots p 111 A88-41211

High power ion thruster performance [NASA-TM-100127] p 58 N88-12542

High power ion thruster performance p 62 N88-24295

Containment of a silicone fluid free surface in reduced gravity using barrier coatings [NASA-TM-101314] p 155 N88-30072

SPACE SHUTTLES

Comment on 'Ram ion scattering caused by Space Shuttle v x B induced differential charging' by I. Katz and V. A. Davis p 204 A88-35775

Plasma wave turbulence around the shuttle - Results from the Spacelab-2 flight p 218 A88-47783

SPACE STATION PAYLOADS

Communications payload concepts for geostationary facilities [NASA-TM-100154] p 118 N88-13513

SPACE STATION POWER SUPPLIES

Space Station electric power system requirements and design p 50 A88-11782

Toluene stability Space Station Rankine power system p 50 A88-11794

Advanced space solar dynamic power systems beyond IOC Space Station p 50 A88-11798

Solar concentrator advanced development project p 50 A88-11799

Computer modeling and simulation of a 20kHz ac distribution system for Space Station p 51 A88-11827

An integrated approach to space station power system autonomous control p 52 A88-11853

LERC power system autonomy program 1990 demonstration p 52 A88-11861

A systems engineering approach to automated failure cause diagnosis in space power systems p 52 A88-11870

Modelling the performance of the monogroove with screen heat pipe for use in the radiator of the solar dynamic power system of the NASA Space Station [IAF PAPER 87-238] p 134 A88-15960

Development of composite facets for the surface of a space-based solar dynamic concentrator p 54 A88-18230

Structural assessment of a Space Station solar dynamic heat receiver thermal energy storage canister [AIAA PAPER 88-2487] p 47 A88-31396

Development of 8 cm x 8 cm silicon gridded back solar cell for space station p 200 A88-34312

Mast material test program (MAMATEP) --- for Solar Array Assembly of Space Station Photovoltaic Power Module [AIAA PAPER 88-2475] p 70 A88-35945

Development of an integrated heat pipe-thermal storage system for a solar receiver p 141 A88-43746

Space Station Photovoltaic power modules p 56 A88-52333

Space station assembly/servicing capabilities p 48 N88-10100

Power components for the space station 20-kHz power distribution system [NASA-TM-100866] p 114 N88-21374

Structural assessment of a space station solar dynamic heat receiver thermal energy storage canister p 192 N88-22406

Benefits of 20 kHz PMAD in a nuclear space station p 129 N88-24256

Speculations on future opportunities to evolve Brayton powerplants aboard the space station p 202 N88-24258

Lewis Research Center space station electric power system test facilities [NASA-TM-100924] p 43 N88-28942

Regenerative fuel cell energy storage system for a low earth orbit space station [NASA-CR-174802] p 204 N88-30184

SPACE STATION PROPULSION

25-LBF GO2/GH2 space station thruster [AIAA PAPER 88-2793] p 56 A88-53101

SPACE STATION STRUCTURES

Technologies for protection of the Space Station power system surfaces in atomic oxygen environment p 41 A88-52331

Space station resistojel system requirements and interface definition study [NASA-CR-180832] p 58 N88-12541

Solar concentrator advanced development program, task 1 [NASA-CR-179489] p 201 N88-18068

SPACE STATIONS

Space Station electric power system requirements and design p 50 A88-11782

Heat pipe radiators for solar dynamic space power system heat rejection p 132 A88-11807

Performance characteristics of a combination solar photovoltaic heat engine energy converter p 197 A88-11813

Control considerations for high frequency, resonant, power processing equipment used in large systems p 51 A88-11829

EMC and power quality standards for 20-kHz power distribution p 52 A88-11830

Coaxial tube array space transmission line characterization p 121 A88-11865

Optical measurements pertaining to Space Station solar dynamic power systems [IAF PAPER 87-229] p 42 A88-15954

Space Station Electrical Power System [IAF PAPER 87-234] p 53 A88-15958

Water-propellant resistojets for man-tended platforms [IAF PAPER 87-259] p 54 A88-15975

Economic benefits of the Space Station to commercial communication satellite operators [IAF PAPER 87-622] p 41 A88-16215

Space Station propulsion system technology p 54 A88-21255

Modelling the performance of the tapered artery heat pipe design for use in the radiator of the solar dynamic power system of the NASA Space Station [IAF PAPER 88-213] p 56 A88-55361

Spacecraft 2000 [NASA-CP-2473] p 48 N88-10084

Space station assembly/servicing capabilities p 48 N88-10100

Photovoltaic power modules for NASA's manned space station [NASA-TM-100229] p 57 N88-11745

Space station propulsion [NASA-TM-100216] p 57 N88-11746

An allotment planning concept and related computer software for planning the fixed satellite service at the 1988 space WARC [NASA-TM-100244] p 117 N88-11944

Spacecraft Fire Safety [NASA-CP-2476] p 45 N88-12520

Space station onboard propulsion system: Technology study [NASA-CR-179233] p 59 N88-15006

Status of 20 kHz space station power distribution technology [NASA-TM-100781] p 59 N88-15838

Communications satellite systems operations with the space station. Volume 3: Supplementary technical report [NASA-CR-180875] p 48 N88-16794

Simulation test beds for the space station electrical power system [NASA-TM-100786] p 44 N88-17715

Magnetic emissions testing of the space station engineering model resistojel [NASA-TM-100788] p 48 N88-17728

Component data base for space station resistojel auxiliary propulsion [NASA-CR-180834] p 59 N88-17731

Computer-aided modeling and prediction of performance of the modified Lundell class of alternators in space station solar dynamic power systems [NASA-CR-182538] p 201 N88-19000

Study of industry requirements that can be fulfilled by combustion experimentation aboard space station [NASA-CR-180854] p 224 N88-19377

Spacecraft fire-safety experiments for space station: Technology development mission [NASA-CR-182114] p 48 N88-20353

Solar dynamic power system definition study [NASA-CR-180877] p 59 N88-20361

Space station power system requirements [NASA-TM-100866] p 49 N88-21245

Multi-hundred kilowatt roll ring assembly evaluation results [NASA-TM-100865] p 114 N88-21375

Ray tracing optical analysis of offset solar collector for space station solar dynamic system [NASA-TM-100853] p 60 N88-22080

Research and technology [NASA-TM-100172] p 227 N88-22851

An integrated and modular digital modeling approach for the space station electrical power system development [NASA-TM-100904] p 61 N88-22935

Base reaction optimization of manipulators with redundant kinematics p 173 N88-23238

SPACECRAFT ENVIRONMENTS

Centaur operations at the space station [NASA-CR-179593] p 49 N88-25473

Assessment of the effects of space debris and meteoroids environment on the space station solar array assembly [NASA-TM-101315] p 49 N88-28959

Study of toluene rotary fluid management device and shear flow condenser performance for a space-based organic Rankine power system [NASA-CR-180885] p 67 N88-29872

SPACE WEAPONS

Analysis of closed cycle megawatt class space power systems with nuclear reactor heat sources p 62 N88-24351

SPACEBORNE EXPERIMENTS

Critical fluid light scattering p 158 A88-33003

LeRC cryogenic fluid management program overview p 150 N88-15928

Cryogenic fluid management program flight concept definition p 150 N88-15929

Noncontact temperature measurements in the microgravity fluids and transport phenomena discipline p 113 N88-23901

Microgravity combustion discipline working group summary of requirements for noncontact temperature measurements p 113 N88-23902

SPACECRAFT ANTENNAS

System architecture of MMIC-based large aperture arrays for space applications p 45 A88-35274

Mechanical properties characterization of composite sandwich materials intended for space antenna applications [NASA-TM-88893] p 71 N88-10121

Features and applications of the integrated composites analyzer (ICAN) code p 74 N88-22391

SPACECRAFT CHARGING

Record charging events from Applied Technology Satellite 6 p 46 A88-11737

Comment on 'Ram ion scattering caused by Space Shuttle v x B induced differential charging' by I. Katz and V. A. Davis p 204 A88-35775

An unusual charging event on ISEE 1 p 47 A88-40013

Hollow cathodes as electron emitting plasma contactors - Theory and computer modeling p 218 A88-47973

Double-probe potential measurements near the Spacelab 2 electron beam p 204 A88-53464

Exposed high-voltage source effect on the potential of an ionospheric satellite p 218 A88-54992

Electron collection by multiple objects within a single sheath p 219 A88-54999

Spacecraft dielectric surface charging property determination [NASA-CR-180879] p 49 N88-21243

SPACECRAFT COMMUNICATION

Bandwidth-efficient high-speed coded trellis modulation [AIAA PAPER 88-0813] p 116 A88-27560

Satellite ground-terminal user simulation [NASA-TM-100234] p 118 N88-14260

SPACECRAFT COMPONENTS

Identification of structural interface characteristics using component mode synthesis p 181 A88-31561

SPACECRAFT CONSTRUCTION MATERIALS

Experiments to ensure Space Station fire safety - A challenge [AIAA PAPER 88-0540] p 41 A88-22405

Mast material test program (MAMATEP) --- for Solar Array Assembly of Space Station Photovoltaic Power Module [AIAA PAPER 88-2475] p 70 A88-35945

SPACECRAFT CONTAMINATION

Technologies for protection of the Space Station power system surfaces in atomic oxygen environment p 41 A88-52331

SPACECRAFT DESIGN

Spacecraft 2000 program overview p 48 N88-10085

System Development Working Group report p 48 N88-10092

Auxiliary propulsion technology for advanced Earth-to-orbit vehicles [NASA-TM-100237] p 58 N88-14127

Weight savings in aerospace vehicles through propellant scavenging [NASA-TM-100900] p 44 N88-25470

SPACECRAFT ELECTRONIC EQUIPMENT

Spacecraft 2000 [NASA-CP-2473] p 48 N88-10084

SPACECRAFT ENVIRONMENTS

Spacecraft Fire Safety [NASA-CP-2476] p 45 N88-12520

Microgravity combustion fundamentals p 112 N88-12528

- Spacecraft fire detection and extinguishment: A bibliography [NASA-CR-180880] p 45 N88-18612
- SPACECRAFT EQUIPMENT**
- High efficiency, long life traveling wave tubes for future communications satellites [AIAA PAPER 88-0835] p 124 A88-27578
- High efficiency, long life traveling wave tubes for future communications satellites [NASA-TM-100837] p 45 N88-19565
- Accurate positioning of long, flexible ARM's (Articulated Robotic Manipulator) p 174 N88-23243
- SPACECRAFT LAUNCHING**
- Economic benefits of the Space Station to commercial communication satellite operators [IAF PAPER 87-622] p 41 A88-16215
- SPACECRAFT LUBRICATION**
- Tribological properties of polymer films and solid bodies in a vacuum environment p 98 A88-35565
- SPACECRAFT MAINTENANCE**
- Progress toward an advanced condition monitoring system for reusable rocket engines p 54 A88-32668
- Improved maintainability of space-based reusable rocket engines [AIAA PAPER 88-3113] p 55 A88-48037
- SPACECRAFT POWER SUPPLIES**
- Recent developments in indium phosphide space solar cell research p 50 A88-11785
- Advanced solar receiver conceptual design study p 51 A88-11800
- Selection of high temperature thermal energy storage materials for advanced solar dynamic space power systems p 68 A88-11801
- Fluoride salts and container materials for thermal energy storage applications in the temperature range 973 - 1400 K p 196 A88-11804
- A novel photovoltaic power system which uses a large area concentrator mirror p 197 A88-11811
- Development of an advanced photovoltaic concentrator system for space applications p 51 A88-11812
- A study of Schwarz converters for nuclear powered spacecraft p 51 A88-11823
- Control considerations for high frequency, resonant, power processing equipment used in large systems p 51 A88-11829
- EMC and power quality standards for 20-kHz power distribution p 52 A88-11830
- Coaxial tube array space transmission line characterization p 121 A88-11865
- A prediction model of the depth-of-discharge effect on the cycle life of a storage cell p 197 A88-11896
- Test results of a 60 volt bipolar nickel-hydrogen battery p 198 A88-11916
- 1987 overview of free-piston Stirling technology for space power application p 53 A88-11942
- Space Station Electrical Power System [IAF PAPER 87-234] p 53 A88-15958
- Assessment of commercially available and experimental hydrogen electrodes p 198 A88-16632
- Space solar cell research - Problems and potential p 123 A88-21605
- Expert systems for space power supply - Design, analysis, and evaluation p 212 A88-22696
- Issues in space photovoltaic research and technology p 199 A88-34230
- InP based solar cells for space application: Reduction of external losses p 199 A88-34250
- Development of a dome Fresnel lens/gallium arsenide photovoltaic concentrator for space applications p 199 A88-34310
- Technologies for protection of the Space Station power system surfaces in atomic oxygen environment p 41 A88-52331
- Electron collection by multiple objects within a single sheath p 219 A88-54999
- Electrical Power Working Group report p 48 N88-10095
- Photovoltaic power modules for NASA's manned space station [NASA-TM-100229] p 57 N88-11745
- SPRE 1 free-piston Stirling engine testing at NASA Lewis Research Center [NASA-TM-100241] p 57 N88-11747
- The ac power system testbed [NASA-CR-175068] p 127 N88-11948
- Recent progress in space photovoltaic systems [NASA-TM-100208] p 128 N88-11966
- Overview of free-piston Stirling engine technology for space power application p 223 N88-12427
- Low Earth orbit environmental effects on the space station photovoltaic power generation systems [NASA-TM-100230] p 225 N88-12429
- Space station resistojet system requirements and interface definition study [NASA-CR-180832] p 58 N88-12541
- Progress toward the evolution of a Stirling space engine [NASA-TM-100221] p 224 N88-14046
- Status of 20 kHz space station power distribution technology [NASA-TM-100781] p 59 N88-15838
- Simulation test beds for the space station electrical power system [NASA-TM-100786] p 44 N88-17715
- Creep behavior of tungsten/niobium and tungsten/niobium-1 percent zirconium composites [NASA-TM-100804] p 92 N88-18707
- Computer-aided modeling and prediction of performance of the modified Lundell class of alternators in space station solar dynamic power systems [NASA-CR-182538] p 201 N88-19000
- Solar dynamic power system definition study [NASA-CR-180877] p 59 N88-20361
- Advanced sensible heat solar receiver for space power [NASA-TM-100847] p 59 N88-21249
- Power systems for production, construction, life support and operations in space [NASA-TM-100838] p 60 N88-21254
- Test facilities of the structural dynamics branch of NASA Lewis Research Center [NASA-TM-100800] p 190 N88-21534
- Development of an integrated heat pipe-thermal storage system for a solar receiver [NASA-TM-101099] p 202 N88-22458
- The 1988 overview of free-piston Stirling technology for space power at the NASA Lewis Research Center [NASA-TM-100795] p 61 N88-22934
- An integrated and modular digital modeling approach for the space station electrical power system development [NASA-TM-100904] p 61 N88-22935
- The application of high temperature superconductors to space electrical power distribution components [NASA-TM-100901] p 61 N88-22939
- Component improvement of free-piston Stirling engine key technology for space power [NASA-TM-100950] p 64 N88-25476
- Effect of LEO cycling at shallow depths of discharge on MANTECH IPV nickel-hydrogen cells [NASA-TM-101300] p 203 N88-25978
- The design and fabrication of a Stirling engine heat exchanger module with an integral heat pipe [NASA-TM-101296] p 203 N88-26732
- Refractory metal alloys and composites for space power systems [NASA-TM-100946] p 95 N88-27310
- Arcjet power supply and start circuit [NASA-CASE-LEW-14374-1] p 41 N88-28939
- Thin film coatings for space electrical power system applications [NASA-TM-101325] p 69 N88-28966
- SPACECRAFT PROPULSION**
- Water-propellant resistojets for man-tended platforms [IAF PAPER 87-259] p 54 A88-15975
- Noncontacting measurement technologies for space propulsion condition monitoring p 158 A88-29818
- An expert system for probabilistic description of loads on space propulsion system structural components [AIAA PAPER 88-2371] p 182 A88-32308
- High temperature metal matrix composites for future aerospace systems [AIAA PAPER 88-3059] p 71 A88-44745
- Electrothermal propulsion of spacecraft with millimeter and submillimeter electromagnetic energy p 54 A88-46220
- Development of a liquid-fed water resistojet [AIAA PAPER 88-3288] p 142 A88-48762
- Probabilistic Structural Analysis Methods for select space propulsion system structural components (PSAM) p 56 A88-49659
- Spacecraft 2000 [NASA-CP-2473] p 48 N88-10084
- Auxiliary propulsion system flight package [NASA-CR-180828] p 56 N88-10886
- High temperature metal matrix composites for future aerospace systems [NASA-TM-100212] p 90 N88-10938
- Space station propulsion [NASA-TM-100216] p 57 N88-11746
- A low-power arcjet cyclic lifetest [NASA-TM-100233] p 57 N88-11748
- Space station onboard propulsion system: Technology study [NASA-CR-179233] p 59 N88-15006
- Test facilities of the structural dynamics branch of NASA Lewis Research Center [NASA-TM-100800] p 190 N88-21534
- Heat transfer in aerospace propulsion [NASA-TM-100874] p 154 N88-23957
- Status of high power electric propulsion technology p 63 N88-24443
- Development of a liquid-fed water resistojet [NASA-TM-100927] p 174 N88-24968
- Performance of 10-kW class xenon ion thrusters [NASA-TM-101292] p 65 N88-28088
- SPACECRAFT RADIATORS**
- Heat pipe radiators for solar dynamic space power system heat rejection p 132 A88-11807
- Radiative cooling of a solidifying droplet layer including absorption and scattering p 133 A88-15749
- Modelling the performance of the monogroove with screen heat pipe for use in the radiator of the solar dynamic power system of the NASA Space Station [IAF PAPER 87-238] p 134 A88-15960
- High thermal-transport capacity heat pipes for space radiators [SAE PAPER 871509] p 136 A88-21155
- Transient radiative cooling of an absorbing and scattering cylinder - A separable solution p 140 A88-41409
- Oxygen plasma effects on several liquid droplet radiator fluids p 142 A88-47962
- Modelling the performance of the tapered artery heat pipe design for use in the radiator of the solar dynamic power system of the NASA Space Station [IAF PAPER 88-213] p 56 A88-55361
- Space power radiation cooled dc transmission line analysis p 129 N88-24506
- Arc-textured metal surfaces for high thermal emittance space radiators [NASA-TM-100894] p 94 N88-24754
- Moving belt radiator development status [NASA-TM-100909] p 64 N88-25477
- SPACECRAFT STRUCTURES**
- Lewis Structures Technology, 1988. Volume 1: Structural Dynamics [NASA-CP-3003-VOL-1] p 194 N88-23226
- Base reaction optimization of manipulators with redundant kinematics p 173 N88-23238
- SPACECRAFT SURVIVABILITY**
- Spacecraft fire detection and extinguishment: A bibliography [NASA-CR-180880] p 45 N88-18612
- SPACECRAFT TRACKING**
- Spacecraft 2000 [NASA-CP-2473] p 48 N88-10084
- SPACECRAFT TRAJECTORIES**
- Optimal cooperative time-fixed impulsive rendezvous [AIAA PAPER 88-4279] p 42 A88-50406
- SPACELAB**
- Gaseous environment of the Shuttle early in the Spacelab 2 mission p 47 A88-47972
- Double-probe potential measurements near the Spacelab 2 electron beam p 204 A88-53464
- SPACELAB PAYLOADS**
- Plasma wave turbulence around the shuttle - Results from the Spacelab-2 flight p 218 A88-47783
- SPALLATION**
- Thermal barrier coating life prediction model development [ASME PAPER 88-GT-284] p 68 A88-54353
- SPATIAL MARCHING**
- A space-marching method for the computation of viscous internal flows p 135 A88-20459
- Consistent boundary conditions for reduced Navier-Stokes (RNS) scheme applied to three-dimensional internal viscous flows [AIAA PAPER 88-0714] p 139 A88-27723
- SPECIFIC HEAT**
- Specific heat of pristine and brominated graphite fibers, composites and HOPG --- Highly Oriented Pyrolytic Graphite p 98 A88-32853
- SPECIFIC IMPULSE**
- High power ion thruster performance p 62 N88-24295
- SPECIMEN GEOMETRY**
- Calibration of a Mode II test specimen p 183 A88-47014
- SPECKLE PATTERNS**
- Optical strain measurement system development p 159 A88-52557
- SPECTRAL REFLECTANCE**
- Space station solar concentrator materials research [NASA-TM-100862] p 60 N88-21250
- SPECTROSCOPIC ANALYSIS**
- Thermal desorption study of physical forces at the PTFE surface p 77 A88-10963
- SPECTRUM ANALYSIS**
- Variable angle spectroscopic ellipsometry - Application to GaAs-AlGaAs multilayer homogeneity characterization p 220 A88-40139
- Direct mass spectrometric identification of silicon oxychloride compounds p 78 A88-44425

SPEED REGULATORS

The design of a turboshaft speed governor using modern control techniques
[NASA-CR-175046] p 170 N88-10339

SPINEL

High Tc screen-printed YBa₂Cu₃O_{7-x} films - Effect of the substrate material p 127 A88-49760

SPRAY CHARACTERISTICS

Experiments on spray interactions in the wake of a bluff body
[ASME PAPER 87-GT-48] p 131 A88-11000
Spray characteristics of a spill-return airblast atomizer
[ASME PAPER 88-GT-7] p 145 A88-54154
Fuel-injector/air-swirl characterization
[NASA-CR-180864] p 27 N88-14985
Liquid sprays and flow studies in the direct-injection diesel engine under motored conditions
[NASA-TM-100135] p 31 N88-18594

SPRAYED COATINGS

Some adhesion/cohesion characteristics of plasma-sprayed ZrO₂-Y₂O₃ under tensile loading
p 95 A88-12589
Spray automated balancing of rotors: Methods and materials
[NASA-CR-182151] p 41 N88-29825

SPRAYING

Comparison of UNL laser imaging and sizing system and a phase/Doppler system for analyzing sprays from a NASA nozzle
[NASA-CR-182437] p 150 N88-16956
Small-droplet spray measurements with a scattered-light scanner
[NASA-TM-100973] p 163 N88-26645

SPREAD SPECTRUM TRANSMISSION

Spread-spectrum multiple access using wideband noncoherent MFSK p 115 A88-26672

SPUTTERING

Plasma assisted surface coating/modification processes - An emerging technology p 114 A88-38927
Sputtered silver films to improve chromium carbide based solid lubricant coatings for use to 900 C p 100 A88-47563
Sputtered silver films to improve chromium carbide based solid lubricant coatings for use to 900 C
[NASA-TM-100783] p 102 N88-15885
Status and directions of modified tribological surfaces by ion processes
[NASA-TM-101304] p 115 N88-28176

SQUEEZE FILMS

Transient rotor dynamic rub phenomena - Theory and test p 167 A88-31539

STABILITY

Stability of a rigid rotor supported on flexible oil journal bearings
[ASME PAPER 87-TRIB-48] p 166 A88-24034
Method and models for R-curve instability calculations
[NASA-TM-100935] p 194 N88-23278
Study of toluene stability for an Organic Rankine Cycle (ORC) space-based power system
[NASA-CR-180884] p 66 N88-29863

STABILIZATION

Slip casting and extruding shapes of rhemium with metal oxide additives. Part 2: Development of grain stabilized rhemium parts for resistojets
[NASA-CR-180851] p 57 N88-11749

STACKS

Component variations and their effects on bipolar nickel-hydrogen cell performance p 197 A88-11914

STAGNATION FLOW

Turbulence modeling and surface heat transfer in a stagnation flow region p 141 A88-43871
Correlations of velocity and temperature fluctuations in the stagnation-point flow of circular cylinder in turbulent flow
[NASA-TM-100930] p 13 N88-25435

STAGNATION POINT

Turbulence modeling and surface heat transfer in a stagnation flow region p 141 A88-43871
Correlations of velocity and temperature fluctuations in the stagnation-point flow of circular cylinder in turbulent flow
[NASA-TM-100930] p 13 N88-25435

STAINLESS STEELS

Creep life prediction based on stochastic model of microstructurally short crack growth
[NASA-TM-100245] p 186 N88-12825
An experimental study of biaxial yield in modified 9Cr-1Mo steel at room temperature
[NASA-CR-175012] p 196 N88-30164

STANDARDS

Gravitationally defined velocities for a low speed hot-wire calibration p 133 A88-14170
Fiber optic sensors with internal referencing
[NASA-TM-100893] p 162 N88-26644

STARTING

Arctjet power supply and start circuit
[NASA-CASE-LEW-14374-1] p 41 N88-28939

STATIC CHARACTERISTICS

Dynamic and static fatigue behavior of sintered silicon nitrides p 96 A88-12602
The Lewis Strain Gauge Laboratory: Status and plans p 160 N88-11146

STATIONARY ORBITS

Numerical arc segmentation algorithm for a radio conference: A software tool for communication satellite systems planning
[NASA-TM-100789] p 46 N88-22919

STATISTICAL ANALYSIS

A semianalytical technique for sensitivity analysis of unsteady aerodynamic computations
[NASA-TM-100810] p 189 N88-18976

STATISTICAL DISTRIBUTIONS

Grain boundary oxidation and low-cycle fatigue at elevated temperatures p 193 N88-22420

STATORS

Measurements of the unsteady flow field within the stator row of a transonic axial-flow fan. I - Measurement and analysis technique
[ASME PAPER 87-GT-226] p 4 A88-18660

Measurements of the unsteady flow field within the stator row of a transonic axial-flow fan. II - Results and discussion
[ASME PAPER 87-GT-227] p 4 A88-18661

An explicit Runge-Kutta method for unsteady rotor/stator interaction
[AIAA PAPER 88-0049] p 5 A88-27715

Design and performance of controlled-diffusion stator compared with original double-circular-arc stator
[SAE PAPER 871783] p 20 A88-30777

The effects of turbulence and stator/rotor interactions on turbine heat transfer. II - Effects of Reynolds number and incidence
[ASME PAPER 88-GT-5] p 145 A88-54152

Measurement of airfoil heat transfer coefficients on a turbine stage p 147 N88-11158
Flow in a model turbine stator p 148 N88-11163

Turbine airfoil deposition models and their hot corrosion implications p 91 N88-11178
An explicit Runge-Kutta method for unsteady rotor/stator interaction
[NASA-TM-100787] p 10 N88-14967

A comparison of experimental and theoretical results for labyrinth gas seals with honeycomb stators
[NASA-CR-182441] p 172 N88-16006

Experimental rotordynamic coefficient results for honeycomb seals
[NASA-CR-182440] p 172 N88-16007

Computer-aided modeling and prediction of performance of the modified Lundell class of alternators in space station solar dynamic power systems
[NASA-CR-182538] p 201 N88-19000

The effects of inlet turbulence and rotor/stator interactions on the aerodynamics and heat transfer of a large-scale rotating turbine model. Volume 3: Heat transfer data tabulation 65 percent axial spacing
[NASA-CR-179468] p 37 N88-28930

An unconditionally stable Runge-Kutta method for unsteady flows
[NASA-TM-101347] p 14 N88-29780

The effects of inlet turbulence and rotor/stator interactions on the aerodynamics and heat transfer of a large-scale rotating turbine model. Volume 2: Heat transfer data tabulation. 15 percent axial spacing
[NASA-CR-179467] p 37 N88-29804

STEADY FLOW

A parametric study of mean loading effects on airfoil gust interaction noise
[AIAA PAPER 87-2677] p 213 A88-16539

Steady and transient least square solvers for thermal problems p 134 A88-17318
Choice of implicit and explicit operators for the upwind differencing method
[AIAA PAPER 88-0624] p 209 A88-22472

Solutions of one-dimensional steady nozzle flow revisited p 144 A88-50344
SHARP simulation of discontinuities in highly convective steady flow
[NASA-TM-100240] p 210 N88-13931

STEADY STATE

A finite difference scheme for three-dimensional steady laminar incompressible flow p 139 A88-30469
Blade loss transient dynamics analysis, volume 1. Task 2: TETRA 2 theoretical development
[NASA-CR-179632] p 25 N88-10791

Blade loss transient dynamics analysis, volume 2. Task 2: TETRA 2 user's manual p 25 N88-10792
Analysis of closed cycle megawatt class space power systems with nuclear reactor heat sources p 62 N88-24351

STEELS

Surface fatigue and failure characteristics of hot-forged powder metal AISI 4620, AISI 4640, and machined AISI 4340 steel spur gears p 165 A88-14591

Crystallization behavior of a melt-spun Fe-Ni based steel p 83 A88-19958
Analysis of plasma nitrided steels p 88 A88-38936

Ion-beam nitriding of steels
[NASA-CASE-LEW-14104-2] p 91 N88-14179

STIFFNESS

Experiments on dynamic stiffness and damping of tapered bore seals p 166 A88-31527
A comparison of experimental and theoretical results for labyrinth gas seals with honeycomb stators
[NASA-CR-182441] p 172 N88-16006

Development of a new generation of high-temperature composite materials p 73 N88-16702

STIFFNESS MATRIX

A mixed formulation of C(0)-linear triangular plate/shell element - The role of edge shear constraints p 183 A88-40121

An efficient Mindlin finite strip plate element based on assumed strain distribution p 192 N88-22407
Improved finite strip Mindlin plate bending element using assumed shear strain distributions p 196 N88-29195

STIRLING CYCLE

Advanced space solar dynamic power systems beyond IOC Space Station p 50 A88-11798
1987 overview of free-piston Stirling technology for space power application p 53 A88-11942

A comparison of Stirling engines for use with a 25 kW dish-electric conversion system p 53 A88-11943
Alloy chemistry and microstructural control to meet the demands of the automotive Stirling engine p 88 A88-40332

RE-1000 free-piston Stirling engine hydraulic output system description
[NASA-TM-100185] p 223 N88-10700

Overview of free-piston Stirling engine technology for space power application
[NASA-TM-88886] p 223 N88-12427

Test results of a 40-kW Stirling engine and comparison with the NASA Lewis computer code predictions
[NASA-TM-87050] p 201 N88-19013

STIRLING ENGINES

Description of an oscillating flow test program p 133 A88-11963
Automotive Stirling engine development program - A success p 165 A88-11965

Comparison of measured and calculated forces on the RE-1000 free-piston Stirling engine displacer p 165 A88-11966
Calibration and comparison of the NASA Lewis free-piston Stirling engine model predictions with RE-1000 test data p 165 A88-11967

Mod II engine development p 165 A88-11972
Alloy chemistry and microstructural control to meet the demands of the automotive Stirling engine p 88 A88-40332

Study of free-piston Stirling engine driven linear alternators
[NASA-CR-181425] p 170 N88-10355

RE-1000 free-piston Stirling engine hydraulic output system description
[NASA-TM-100185] p 223 N88-10700

Automotive Stirling engine: Mod 2 design report
[NASA-CR-175106] p 223 N88-11578

SPRE 1 free-piston Stirling engine testing at NASA Lewis Research Center
[NASA-TM-100241] p 57 N88-11747

Overview of free-piston Stirling engine technology for space power application
[NASA-TM-88886] p 223 N88-12427

Progress toward the evolution of a Stirling space engine
[NASA-TM-100221] p 224 N88-14046

Hot piston ring tests
[NASA-TM-100256] p 201 N88-14486

Hot piston ring/cylinder liner materials: Selection and evaluation
[NASA-TM-100276] p 102 N88-15872

Overview of heat transfer and fluid flow problem areas encountered in Stirling engine modeling
[NASA-TM-100131] p 224 N88-17561

Test results of a 40-kW Stirling engine and comparison with the NASA Lewis computer code predictions
[NASA-TM-87050] p 201 N88-19013

Cast iron-base alloy for cylinder/regenerator housing
[NASA-CR-182116] p 92 N88-19613

A survey of oscillating flow in Stirling engine heat exchangers
[NASA-CR-182108] p 152 N88-22322

Description of an oscillating flow pressure drop test rig
[NASA-TM-100905] p 61 N88-22933

The 1988 overview of free-piston Stirling technology for space power at the NASA Lewis Research Center
[NASA-TM-100795] p 61 N88-22934

Overview of NASA Lewis Research Center free-piston Stirling engine technology activities applicable to space power systems p 202 N88-24255

Fatigue failure of regenerator screens in a high frequency Stirling engine p 179 N88-24491

Component improvement of free-piston Stirling engine key technology for space power
[NASA-TM-100950] p 64 N88-25476

The design and fabrication of a Stirling engine heat exchanger module with an integral heat pipe
[NASA-TM-101296] p 203 N88-26732

Phase 1 results from the Stirling-powered vehicle project
[NASA-TM-100978] p 225 N88-27980

Testing of a variable-stroke Stirling engine
[NASA-TM-100899] p 225 N88-30472

STOCHASTIC PROCESSES

Probabilistic structural analysis computer code (NESSUS) p 191 N88-22397

STORAGE BATTERIES

A prediction model of the depth-of-discharge effect on the cycle life of a storage cell p 197 A88-11896

Test results of a 60 volt bipolar nickel-hydrogen battery p 198 A88-11916

Small scale bipolar nickel-hydrogen testing
[NASA-TM-100936] p 202 N88-25059

STRAIN ENERGY RELEASE RATE

Fracture toughness computational simulation of general delaminations in fiber composites
[AIAA PAPER 88-2261] p 181 A88-32219

STRAIN GAGES

The development of a high temperature static strain gage system p 160 N88-11142

Elevated temperature strain gages p 160 N88-11144

The Lewis Strain Gauge Laboratory: Status and plans p 160 N88-11146

Electrical properties of materials for elevated temperature resistance strain gage application
[NASA-CR-182214] p 164 N88-30106

STRAIN HARDENING

Thermal-mechanical cyclic stress-strain responses of cast B-1900 + Hf p 87 A88-35919

STRAIN MEASUREMENT

Optical strain measurement system development p 159 A88-52557

The development of a high temperature static strain gage system p 160 N88-11142

The Lewis Strain Gauge Laboratory: Status and plans p 160 N88-11146

High temperature stress-strain analysis p 185 N88-11170

Research sensors p 162 N88-22430

STRAIN RATE

Phenomenological modeling of hardening and thermal recovery in metals p 84 A88-24037

An update of the total-strain version of SRP p 86 A88-35910

Unified constitutive models for high-temperature structural applications p 190 N88-21523

Unified constitutive model development for metal matrix composites at high temperature p 74 N88-22387

Unified constitutive model for single crystal deformation behavior with applications p 191 N88-22388

Development of sensors for ceramic components in advanced propulsion systems: Survey and evaluation of measurement techniques for temperature, strain and heat flux for ceramic components in advanced propulsion systems

[NASA-CR-182111] p 163 N88-28299

A transversely isotropic thermoelastic theory
[NASA-TM-101302] p 196 N88-28332

STRATIFIED FLOW

Regressed relations for forced convection heat transfer in a direct injection stratified charge rotary engine
[NASA-TM-100124] p 25 N88-13345

STRESS ANALYSIS

Interface roughness effect on stresses in ceramic coatings p 95 A88-12587

Thermostructural analysis with experimental verification in a high heat flux facility of a simulated cowl lip
[AIAA PAPER 88-2222] p 39 A88-32188

Validation of the NESSUS probabilistic finite element analysis computer program
[AIAA PAPER 88-2372] p 205 A88-32309

Piezoresistance and solar cell efficiency p 125 A88-34298

A nonlinear history-dependent damage model for low cycle fatigue p 86 A88-35905

A nonlinear viscoelastic constitutive equation - Yield predictions in multiaxial deformations p 185 A88-54912

3D inelastic analysis methods for hot section components p 185 N88-11164

Component specific modeling p 206 N88-11166

Constitutive modeling of superalloy single crystals with verification testing p 91 N88-11169

Constitutive modeling for isotropic materials p 185 N88-11171

Finite element substructuring methods for composite mechanics
[NASA-TM-100297] p 73 N88-17745

Nonlinear Constitutive Relations for High Temperature Applications, 1986 p 189 N88-21498

[NASA-CP-10010] p 189 N88-21498

A constitutive model with damage for high temperature superalloys p 93 N88-21510

On 3-D inelastic analysis methods for hot section components. Volume 1: Special finite element models
[NASA-CR-180693] p 190 N88-21535

Lewis Structures Technology, 1988. Volume 2: Structural Mechanics
[NASA-CP-3003-VOL-2] p 190 N88-22382

Finite element (MARC) solution technologies for viscoplastic analyses p 191 N88-22389

Probabilistic structural analysis computer code (NESSUS) p 191 N88-22397

Structural tailoring of advanced turboprops p 192 N88-22400

Thermal-structural analyses of Space Shuttle Main Engine (SSME) hot section components p 61 N88-22404

Structural assessment of a space station solar dynamic heat receiver thermal energy storage canister p 192 N88-22406

Whisker-reinforced ceramic composites for heat engine components p 105 N88-22410

Improved method for stress and compatibility analysis of multicomponent rotating systems
[NASA-TM-100884] p 195 N88-25935

Aeroelastic response of metallic and composite propfan models in yawed flow
[NASA-TM-100964] p 37 N88-29807

STRESS DISTRIBUTION

Curvilinear crack layer propagation p 96 A88-14568

The effects of crack surface friction and roughness on crack tip stress fields p 180 A88-14579

On self-similarity of crack layer p 181 A88-24054

Free-edge delamination: Laminate width and loading conditions effects p 72 N88-12551

[NASA-TM-100238] p 72 N88-12551

STRESS INTENSITY FACTORS

The effects of crack surface friction and roughness on crack tip stress fields p 180 A88-14579

Semi-empirical crack tip analysis p 183 A88-47681

Analysis of crack propagation in roller bearings using the boundary integral equation method - A mixed-mode loading problem p 168 A88-49183

Stress intensity and crack displacement for small edge cracks
[NASA-TP-2801] p 188 N88-17095

Fracture mechanics p 194 N88-23877

Resolved shear stress intensity coefficient and fatigue crack growth in large crystals
[NASA-CR-182137] p 195 N88-24997

STRESS TENSORS

A simplified orthotropic formulation of the viscoplasticity theory based on overstress p 189 N88-21505

STRESS WAVES

Ultrasonic evaluation of mechanical properties of thick, multilayered, filament-wound composites p 176 A88-21340

Acousto-ultrasonics as a monitor of material anisotropy p 176 A88-46828

Acousto-ultrasonic input-output characterization of unidirectional fiber composite plate by SV waves
[NASA-CR-4152] p 178 N88-23224

STRESS-STRAIN DIAGRAMS

Anisotropic constitutive modeling for nickel base single crystal superalloys using a crystallographic approach
[AIAA PAPER 88-2440] p 85 A88-32357

STRESS-STRAIN RELATIONSHIPS

On the cyclic stress-strain behaviour of a Ni-base superalloy at room temperature p 84 A88-24521

A nonlinear history-dependent damage model for low cycle fatigue p 86 A88-35905

Thermal-mechanical cyclic stress-strain responses of cast B-1900 + Hf p 87 A88-35919

Constitutive modeling of superalloy single crystals with verification testing p 91 N88-11169

High temperature stress-strain analysis p 185 N88-11170

Constitutive modeling for isotropic materials p 186 N88-11172

Relationship between fatigue life in the creep-fatigue region and stress-strain response
[NASA-TM-100796] p 188 N88-18040

The cyclic stress-strain behavior of a single crystal nickel-base superalloy p 92 N88-19610

A simplified orthotropic formulation of the viscoplasticity theory based on overstress p 189 N88-21505

Biaxial experiments supporting the development of constitutive theories for advanced high-temperature materials p 191 N88-22386

Fatigue damage mapping p 193 N88-22423

Bithermal fatigue: A simplified alternative to thermomechanical fatigue p 194 N88-22424

A transversely isotropic thermoelastic theory
[NASA-TM-101302] p 196 N88-28332

Anisotropic constitutive modeling for nickel-base single crystal superalloys
[NASA-CR-182157] p 95 N88-29961

STRESSES

Stress-life interrelationships associated with alkaline fuel cells p 197 A88-11903

Component specific modeling p 206 N88-11166

Creep and fatigue research efforts on advanced materials p 187 N88-16701

STRING THEORY

String-driven inflation p 225 A88-27446

Cosmic string induced peculiar velocities p 226 A88-28762

STRUCTURAL ANALYSIS

Localization of natural modes of vibration in bladed disks
[ASME PAPER 87-GT-46] p 18 A88-10998

Probabilistic structural analysis methods for space propulsion system components p 54 A88-16441

Structural assessment of a Space Station solar dynamic heat receiver thermal energy storage canister
[AIAA PAPER 88-2487] p 47 A88-31396

Probabilistic structural analysis of aerospace components using NESSUS
[AIAA PAPER 88-2373] p 182 A88-32310

NESSUS/EXPERT - An expert system for probabilistic structural analysis methods p 206 A88-32311

[AIAA PAPER 88-2374] p 206 A88-32311

Analysis of plasma nitrided steels p 88 A88-38936

Probabilistic Structural Analysis Methods for select space propulsion system structural components (PSAM) p 56 A88-49659

A new boundary element formulation for two- and three-dimensional thermoelasticity using particular integrals p 184 A88-53088

A new BEM formulation for two- and three-dimensional elastoplasticity using particular integrals p 184 A88-53089

Structural analysis methods development for turbine hot section components p 184 A88-54142

Development of a thermal and structural analysis procedure for cooled radial turbines
[ASME PAPER 88-GT-18] p 145 A88-54164

Analysis of shell-type structures subjected to time-dependent mechanical and thermal loading
[NASA-CR-181409] p 185 N88-10388

Turbine Engine Hot Section Technology, 1985
[NASA-CP-2405] p 185 N88-11140

3D inelastic analysis methods for hot section components p 185 N88-11164

3-D inelastic analysis methods for hot section components p 206 N88-11165

High temperature stress-strain analysis p 185 N88-11170

Constitutive modeling for isotropic materials p 185 N88-11171

Fiber composite structural durability and damage tolerance: Simplified predictive methods
[NASA-TM-100179] p 72 N88-13409

Aeropropulsion '87. Session 2: Aeropropulsion Structures Research
[NASA-CP-10003-SESS-2] p 27 N88-15785

Integrated analysis and applications p 28 N88-15789

Overview of NASA PTA propfan flight test program p 29 N88-15805

Structural analysis methods development for turbine hot section components
[NASA-TM-100298] p 188 N88-18967

Analysis of shell-type structures subjected to time-dependent mechanical and thermal loading
[NASA-CR-182705] p 189 N88-20668

Spacecraft dielectric surface charging property determination
[NASA-CR-180879] p 49 N88-21243

Nonlinear Constitutive Relations for High Temperature Applications, 1986
[NASA-CP-10010] p 189 N88-21498

Evaluation of structural analysis methods for life prediction p 190 N88-21511

Aero/structural tailoring of engine blades (AERO/STAEBL)
[NASA-CR-180805] p 207 N88-21682

SUBJECT INDEX

- The composite blade structural analyzer (COBSTRAN)
p 33 N88-22390
- METCAN: The metal matrix composite analyzer
p 74 N88-22395
- Probabilistic structural analysis computer code (NESSUS)
p 191 N88-22397
- Computational structural mechanics for engine structures
p 33 N88-22399
- Structural tailoring of advanced turboprops
p 192 N88-22400
- Thermostructural analysis of simulated cowl lips
p 192 N88-22403
- Thermal-structural analyses of Space Shuttle Main Engine (SSME) hot section components
p 61 N88-22404
- Structural assessment of a space station solar dynamic heat receiver thermal energy storage canister
p 192 N88-22406
- Whisker-reinforced ceramic composites for heat engine components
p 105 N88-22410
- Continuous fiber ceramic matrix composites for heat engine components
p 106 N88-22411
- Flaw characterization in structural ceramics using scanning laser acoustic microscopy
p 177 N88-22415
- Research and technology
p 227 N88-22851
- [NASA-TM-100172]
p 227 N88-22851
- Structural Tailoring of Advanced Turboprops (STAT)
[NASA-CR-180861]
p 36 N88-28074
- Constitutive modeling for isotropic materials
[NASA-CR-182132]
p 37 N88-29811
- STRUCTURAL DESIGN**
- Space Station electric power system requirements and design
p 50 A88-11782
- Regenerative fuel cell study for satellites in GEO orbit
p 52 A88-11904
- An integrated approach for friction damper design
p 167 A88-31598
- Application of structural tailoring to spar/shell turboprops
[AIAA PAPER 88-2333]
p 20 A88-32277
- Internal erosion rates of a 10-kW xenon ion thruster
[AIAA PAPER 88-2912]
p 55 A88-48753
- Experimental vibration damping characteristics of the third-stage rotor of a three-stage transonic axial-flow compressor
p 23 A88-48759
- [AIAA PAPER 88-3229]
p 23 A88-48759
- Probabilistic Structural Analysis Methods for select space propulsion system structural components (PSAM)
p 56 A88-49659
- Small space reactor power systems for unmanned solar system exploration missions
[NASA-TM-100228]
p 227 N88-14054
- Aircraft engine hot section technology: An overview of the HOST Project
p 29 N88-15804
- Large-scale wind turbine structures
p 202 N88-22429
- Ceramics for turbine engines
p 106 N88-23873
- Experimental vibration damping characteristics of the third-stage rotor of a three-stage transonic axial-flow compressor
[NASA-TM-100948]
p 35 N88-24642
- Internal erosion rates of a 10-kW xenon ion thruster
[NASA-TM-100954]
p 63 N88-24688
- Probabilistic structural analysis to quantify uncertainties associated with turbopump blades
[NASA-TM-100278]
p 76 N88-28094
- STRUCTURAL DESIGN CRITERIA**
- Some design considerations for ceramic components in heat engine applications
p 106 N88-23875
- SR-7A aeroelastic model design report
[NASA-CR-174791]
p 36 N88-28928
- STRUCTURAL ENGINEERING**
- Aeropropulsion structures
p 27 N88-15786
- STRUCTURAL FAILURE**
- Surface fatigue and failure characteristics of hot-forged powder metal AISI 4620, AISI 4640, and machined AISI 4340 steel spur gears
p 165 A88-14591
- STRUCTURAL MEMBERS**
- Identification of structural interface characteristics using component mode synthesis
p 181 A88-31561
- Characterization of damped structural connections for multi-component systems
[NASA-TM-100801]
p 189 N88-18974
- STRUCTURAL RELIABILITY**
- Probabilistic Structural Analysis Methods for select space propulsion system structural components (PSAM)
p 56 A88-49659
- STRUCTURAL STABILITY**
- Chemical durability of high-temperature superconductor YBa₂Cu₃O_{7-x} in aqueous environments
p 78 A88-25023
- A thermally modified polymer matrix composite material with structural integrity to 371 C
[NASA-TM-100922]
p 76 N88-25483

STRUCTURAL VIBRATION

- Bladed disk assemblies; Proceedings of the Eleventh Biennial Conference on Mechanical Vibration and Noise, Boston, MA, Sept. 27-30, 1987
p 20 A88-31608
- Transfer matrix modeling of geared system vibration
p 168 A88-39703
- The generalized transmission error of spiral bevel gears
p 168 A88-49409
- Use of the generalized transmission error in the equations of motion of gear systems
p 168 A88-49410
- Lewis Structures Technology, 1988. Volume 1: Structural Dynamics
[NASA-CP-3003-VOL-1]
p 194 N88-23226
- STRUCTURES**
- Engine structures: A bibliography of Lewis Research Center's research for 1980-1987
[NASA-TM-100842]
p 195 N88-24002
- SUBMILLIMETER WAVES**
- Submillimeter backward wave oscillators
p 122 A88-19659
- Electrothermal propulsion of spacecraft with millimeter and submillimeter electromagnetic energy
p 54 A88-46220
- Development and applications of optical interferometric micrometrology in the angstrom and subangstrom range
[NASA-TM-100299]
p 162 N88-23196
- SUBROUTINES**
- Finite area combustor theoretical rocket performance
[NASA-TM-100785]
p 60 N88-21252
- SUBSONIC AIRCRAFT**
- Measurement and prediction of propeller flow field on the PTA aircraft at speeds of up to Mach 0.85 --- Proplan Test Assessment
[AIAA PAPER 88-0667]
p 19 A88-22497
- SUBSONIC FLOW**
- Aeroacoustics of subsonic turbulent shear flows
[AIAA PAPER 87-2731]
p 214 A88-16571
- Three-dimensional viscous flow computations of a circular jet in subsonic and supersonic cross flow
[AIAA PAPER 88-3703]
p 143 A88-48916
- Experimental investigation of the subsonic high-altitude operation of the NASA Lewis 10- by 10-foot supersonic wind tunnel
[NASA-TM-100214]
p 40 N88-15814
- Numerical simulation of subsonic and transonic propeller flow
[NASA-TM-100163]
p 11 N88-20262
- Three-dimensional viscous flow computations of a circular jet in subsonic and supersonic cross flow
[NASA-CR-182153]
p 155 N88-26616
- SUBSONIC WIND TUNNELS**
- Wall shear stress measurement in blade end-wall corner region
[ASME PAPER 87-GT-181]
p 131 A88-11089
- SUBSTRATES**
- Improved beta-SiC heteroepitaxial films using off-axis Si substrates
p 219 A88-10431
- High Tc screen-printed YBa₂Cu₃O_{7-x} films - Effect of the substrate material
p 127 A88-49760
- Synthesis and characterization of high-T(sub c) screen-printed Y-Ba-Cu-O films on alumina
[NASA-TM-100860]
p 222 N88-22805
- SUBSTRUCTURES**
- Finite element substructuring methods for composite mechanics
[NASA-TM-100297]
p 73 N88-17745
- SUCTION**
- Glancing shock wave-turbulent boundary layer interaction with boundary layer suction
[AIAA PAPER 88-0308]
p 6 A88-27718
- Experimental and numerical investigation of the effect of distributed suction on oblique shock wave/turbulent boundary layer interaction
[NASA-TM-101334]
p 156 N88-30084
- SULFIDATION**
- High-temperature oxidation/corrosion of iron-based superalloys
p 81 A88-10029
- SULFUR**
- The effect of sulfur and zirconium Co-doping on the oxidation of NiCrAl
[NASA-TM-100209]
p 90 N88-10940
- SUPERCARGERS**
- Technology developments for a compound cycle engine
p 30 N88-16637
- SUPERCOMPUTERS**
- Approximate polynomial preconditioning applied to biharmonic equations on vector supercomputers
[NASA-TM-100217]
p 210 N88-10563
- Internal fluid mechanics research on supercomputers for aerospace propulsion systems
[NASA-TM-100289]
p 149 N88-15188
- SUPERCONDUCTIVITY**
- Synthesis and characterization of high-T(sub c) screen-printed Y-Ba-Cu-O films on alumina
[NASA-TM-100860]
p 222 N88-22805

SUPERSONIC FLUTTER

- A role for high frequency superconducting devices in free space power transmission systems
[NASA-TM-100971]
p 130 N88-25830
- Application of superconducting technology to earth-to-orbit electromagnetic launch systems
[NASA-TM-101134]
p 43 N88-26385
- SUPERCOOLING**
- Dendritic growth in a supercooled alloy melt
p 83 A88-19966
- Isothermal dendritic growth - A low gravity experiment
p 110 A88-28556
- Rapid solidification of highly undercooled liquids
p 88 A88-41653
- SUPERLATTICES**
- Self-consistent calculations and design considerations for a GaAs nipi doping superlattice solar cell
p 124 A88-34249
- Solar energy conversion through the interaction of plasmons with tunnel junctions. Part A: Solar cell analysis. Part B: Photoconductor analysis
[NASA-CR-183044]
p 203 N88-27621
- SUPERNOVA 1987A**
- Axions from 1987A
p 226 A88-35586
- SUPERSONIC AIRCRAFT**
- Acoustics technologies for STOVL aircraft
[AIAA PAPER 88-2238]
p 215 A88-35939
- STOVL acoustic fatigue technologies
[SAE PAPER 872360]
p 215 A88-37221
- The challenges and opportunities of supersonic transport propulsion technology
[AIAA PAPER 88-2985]
p 23 A88-48032
- Aeropropulsion '87. Session 6: High-Speed Propulsion Technology
[NASA-CP-10003-SESS-6]
p 29 N88-15807
- The challenges and opportunities of supersonic transport propulsion technology
[NASA-TM-100921]
p 34 N88-23806
- SUPERSONIC COMBUSTION RAMJET ENGINES**
- Two-dimensional viscous flow computations of hypersonic scramjet nozzle flowfields at design and off-design conditions
[AIAA PAPER 88-3280]
p 23 A88-50785
- Aeropropulsion '87. Session 6: High-Speed Propulsion Technology
[NASA-CP-10003-SESS-6]
p 29 N88-15807
- Two-dimensional viscous flow computations of hypersonic scramjet nozzle flowfields at design and off-design conditions
[NASA-CR-182150]
p 35 N88-25459
- SUPERSONIC COMPRESSORS**
- Experimental investigation of the performance of a supersonic compressor cascade
[ASME PAPER 88-GT-306]
p 9 A88-54375
- SUPERSONIC FLOW**
- Application of advanced computational codes in the design of an experiment for a supersonic throughflow fan rotor
[ASME PAPER 87-GT-160]
p 2 A88-11072
- Numerical study of chemically reacting flows using an LU scheme
[AIAA PAPER 88-0436]
p 5 A88-24825
- NASA supersonic STOVL propulsion technology program
[SAE PAPER 872352]
p 21 A88-37215
- An isentropic compression heated Ludwig tube transient wind tunnel
[AIAA PAPER 88-2019]
p 40 A88-37926
- Structure of a reattaching supersonic shear flow
[AIAA PAPER 88-3615]
p 8 A88-48901
- Three-dimensional viscous flow computations of a circular jet in subsonic and supersonic cross flow
[AIAA PAPER 88-3703]
p 143 A88-48916
- A preliminary design study of supersonic through-flow fan inlets
[AIAA PAPER 88-3075]
p 23 A88-53137
- Flutter of a fan blade in supersonic axial flow
[ASME PAPER 88-GT-78]
p 8 A88-54206
- A hybrid numerical technique for predicting the aerodynamic and acoustic fields of advanced turboprops
[NASA-CR-174926]
p 216 N88-12352
- NASA supersonic STOVL propulsion technology program
[NASA-TM-100227]
p 26 N88-14093
- Numerical study of chemically reacting flows using an LU scheme
[NASA-CR-180882]
p 26 N88-14094
- Supersonic throughflow fans for high-speed aircraft
p 30 N88-15810
- Three-dimensional viscous flow computations of a circular jet in subsonic and supersonic cross flow
[NASA-CR-182153]
p 155 N88-26616
- SUPERSONIC FLUTTER**
- Recent developments in flutter suppression techniques for turbomachinery rotors
p 21 A88-35530

SUPERSONIC TRANSPORTS

The challenges and opportunities of supersonic transport propulsion technology
[AIAA PAPER 88-2985] p 23 A88-48032
Propulsion challenges and opportunities for high-speed transport aircraft p 30 N88-15809
The challenges and opportunities of supersonic transport propulsion technology
[NASA-TM-100921] p 34 N88-23806

SUPERSONIC TURBINES

Measurements of the unsteady flow field within the stator row of a transonic axial-flow fan. II - Results and discussion
[ASME PAPER 87-GT-227] p 4 A88-18661

SUPERSONIC WIND TUNNELS

Measurement and prediction of propeller flow field on the PTA aircraft at speeds of up to Mach 0.85 --- Propfan Test Assessment
[AIAA PAPER 88-0667] p 19 A88-22497
Experimental investigation of the subsonic high-altitude operation of the NASA Lewis 10- by 10-foot supersonic wind tunnel
[NASA-TM-100214] p 40 N88-15814

SURFACE CRACKS

The effects of crack surface friction and roughness on crack tip stress fields p 180 A88-14579
On governing equations for crack layer propagation
[NASA-CR-182120] p 194 N88-23272

SURFACE DIFFUSION

Diffusional transport during the cyclic oxidation of gamma + beta, Ni-Cr-Al(Y, Zr) alloys p 85 A88-28902

SURFACE DISTORTION

Compensation of reflector antenna surface distortion using an array feed
[NASA-TM-100286] p 119 N88-18805
Case study of active array feed compensation with sidelobe control for reflector surface distortion
[NASA-TM-100287] p 120 N88-23073
Thermal distortion analysis of the space station solar dynamic concentrator
[NASA-TM-100868] p 64 N88-25475
Active feed array compensation for reflector antenna surface distortions
[NASA-TM-100826] p 120 N88-25762

SURFACE ENERGY

Containment of a silicone fluid free surface in reduced gravity p 112 A88-49085

SURFACE FINISHING

Plasma assisted surface coating/modification processes - An emerging technology p 114 A88-38927
Ion-beam nitriding of steels
[NASA-CASE-LEW-14104-2] p 91 N88-14179

SURFACE LAYERS

Rapid thermal annealing of indium phosphide compound semiconductors p 220 A88-26196
On governing equations for crack layer propagation
[NASA-CR-182120] p 194 N88-23272

SURFACE PROPERTIES

Arc-textured metal surfaces for high thermal emittance space radiators
[NASA-TM-100894] p 94 N88-24754
Surface fatigue life of CBN and vitreous ground carburized and hardened AISI 9310 spur gears
[NASA-TM-100960] p 175 N88-25916
Analytical approximation of a distorted reflector surface defined by a discrete set of points
[NASA-TM-101323] p 121 N88-27424
Comparison of the bidirectional reflectance distribution function of various surfaces
[NASA-TM-101317] p 218 N88-28760

SURFACE REACTIONS

Diffusion length measurement in bulk and epitaxially grown III-V semiconductors using charge collection microscopy p 126 A88-34370
Surface catalytic degradation study of two linear perfluoropolyalkylethers at 345 C
[NASA-TP-2774] p 68 N88-12543

SURFACE ROUGHNESS

Use of a liquid-crystal and heater-element composite for quantitative, high-resolution heat-transfer coefficients on a turbine airfoil including turbulence and surface-roughness effects p 156 A88-10969
The effects of crack surface friction and roughness on crack tip stress fields p 180 A88-14579
Structure and grain coarsening during the processing of engineering ceramics
[NASA-TM-100235] p 101 N88-11838

SURFACE ROUGHNESS EFFECTS

Interface roughness effect on stresses in ceramic coatings p 95 A88-12587
Local heat/mass transfer distributions around sharp 180 deg turns in two-pass smooth and rib-roughened channels
[ASME PAPER 86-GT-114] p 139 A88-28516

Effects of environmentally imposed roughness on airfoil performance p 15 N88-15778

SURFACE TEMPERATURE

Research sensors p 162 N88-22430
Measurement of local high-level, transient surface heat flux
[NASA-TP-2840] p 164 N88-30099

SURFACE WATER

Investigation of surface water behavior during glaze ice accretion
[AIAA PAPER 88-0115] p 14 A88-22079

SURVEYS

Development of sensors for ceramic components in advanced propulsion systems: Survey and evaluation of measurement techniques for temperature, strain and heat flux for ceramic components in advanced propulsion systems
[NASA-CR-182111] p 163 N88-28299

SURVIVAL

Improved oil-off survivability of tapered roller bearings
[AIAA-CR-180804] p 170 N88-11135

SUSPENSION SYSTEMS (VEHICLES)

A review of gear housing dynamics and acoustics literature
[NASA-CR-183110] p 175 N88-26675

SWEEP ANGLE

Aeroelastic effects of alternate blade sweep on advanced propfan rotor
[ASME PAPER 87-WA/AERO-8] p 184 A88-51328

SWEEP EFFECT

Parametric studies of advanced turboprops
[AIAA PAPER 88-2266] p 20 A88-32223

SWEEP FREQUENCY

Material parameter measurements at high temperatures
[NASA-CR-182707] p 80 N88-20397

SWEEPBACK

Structural Tailoring of Advanced Turboprops (STAT)
[NASA-CR-180861] p 36 N88-28074

SWIRLING

Controlled excitation of a cold turbulent swirling free jet
[ASME PAPER 87-WA/NCA-18] p 140 A88-41568
Lateral jet injection into swirling combustor flowfields
[AIAA PAPER 88-3183] p 141 A88-44783
Stability of swirling gas flows p 142 A88-46317
Development of a liquid-fed water resistojet
[AIAA PAPER 88-3288] p 142 A88-48762
Effect of initial tangential velocity distribution on the mean evolution of a swirling turbulent free jet
[AIAA PAPER 88-3592] p 7 A88-48893
Fuel-injector/air-swirl characterization
[NASA-CR-180864] p 27 N88-14985
Effect of initial tangential velocity distribution on the mean evolution of a swirling turbulent free jet
[NASA-TM-100934] p 12 N88-24592
Development of a liquid-fed water resistojet
[NASA-TM-100927] p 174 N88-24968
Euler analysis of a swirl recovery vane design for use with an advanced single-rotation propfan
[NASA-TM-101357] p 14 N88-29771

SWITCHING

Experiments applications guide: Advanced Communications Technology Satellite (ACTS)
[NASA-TM-100265] p 49 N88-28082

SWITCHING CIRCUITS

Fast simulation techniques for switching converters p 122 A88-11878
Gigard-tolerant power switches and memory elements p 123 A88-22704
The bit-error rate performance of a satellite microwave matrix switch
[AIAA PAPER 88-0826] p 123 A88-27572
The bit-error rate performance of a satellite microwave matrix switch
[NASA-TM-100285] p 46 N88-22920
Neutron effects on the electrical and switching characteristics of NPN bipolar power transistors p 129 N88-24463

SWITCHING THEORY

Fast simulation techniques for switching converters p 122 A88-11878

SYMMETRY

Wilson-loop instantons p 212 A88-10410

SYNCHRONOUS PLATFORMS

Communications payload concepts for geostationary facilities
[NASA-TM-100154] p 118 N88-13513

SYNCHRONOUS SATELLITES

New non-geosynchronous orbits for communications satellites to off-load daily peaks in geostationary traffic
[AAS PAPER 87-547] p 42 A88-10957
Record charging events from Applied Technology Satellite 6 p 46 A88-11737

Cost-effective intersatellite link applications to the fixed satellite services
[AIAA PAPER 88-0770] p 45 A88-27544

SYNTHESIS (CHEMISTRY)

Synthesis and characterization of high-T(sub c) screen-printed Y-Ba-Cu-O films on alumina
[NASA-TM-100860] p 222 N88-22805
Solid-state combustion synthesis of ceramics and alloys in reduced gravity
[NASA-CR-4163] p 75 N88-25479
Substituted 1,1,1-Triaryl-2,2,2-Trifluoroethanes and processes for their synthesis
[NASA-CASE-LEW-14345-1] p 69 N88-26404
Novel ladder polymers for use as high temperature stable resins or coatings
[NASA-CASE-LEW-14203-1] p 108 N88-29984

SYNTHETIC FUELS

Combustion characteristics of gas turbine alternative fuels
[NASA-TM-100247] p 25 N88-13338

SYSTEMS ANALYSIS

Spacecraft 2000
[NASA-CP-2473] p 48 N88-10084
System Development Working Group report p 48 N88-10092
Institute for Computational Mechanics in Propulsion (ICOMP) first year summary
[NASA-TM-100225] p 210 N88-12330
On dynamic loads in parallel shaft transmissions. 1: Modelling and analysis
[NASA-TM-100180] p 171 N88-12797
Dynamic analysis of multimesh-gear helicopter transmissions
[NASA-TP-2789] p 172 N88-17045
Solar dynamic power system definition study
[NASA-CR-180877] p 59 N88-20361

SYSTEMS ENGINEERING

A systems engineering approach to automated failure cause diagnosis in space power systems p 52 A88-11870
Expert systems for space power supply - Design, analysis, and evaluation p 212 A88-26966
System architecture of MMIC-based large aperture arrays for space applications p 45 A88-35274
Probabilistic Structural Analysis Methods for select space propulsion system structural components (PSAM) p 56 A88-49659

SYSTEMS INTEGRATION

Integrated heat pipe-thermal storage system performance evaluation p 132 A88-11803
An integrated approach to space station power system autonomous control p 52 A88-11853
Development of an integrated heat pipe-thermal storage system for a solar receiver
[AIAA PAPER 88-2683] p 141 A88-43746
Space Station Photovoltaic power modules p 56 A88-52333
Finite-dimensional modeling of network-induced delays for real-time control systems p 208 A88-54537
Small space reactor power systems for unmanned solar system exploration missions
[NASA-TM-100228] p 227 N88-14054
Fiber optics for controls p 218 N88-15798
Rotorcraft flight-propulsion control integration p 38 N88-16643

SYSTEMS SIMULATION

Solar dynamic organic Rankine cycle heat rejection system simulation p 132 A88-11808
Computer modeling and simulation of a 20kHz ac distribution system for Space Station p 51 A88-11827
Scale model acoustic testing of counterrotating fans
[AIAA PAPER 88-2057] p 22 A88-37947
Performance limitations in parallel processor simulations p 208 A88-49101

T

TABLES (DATA)

Implementation of a digital optical matrix-vector multiplier using a holographic look-up table and residue arithmetic
[NASA-CR-180431] p 205 N88-10496
The effects of inlet turbulence and rotor/stator interactions on the aerodynamics and heat transfer of a large-scale rotating turbine model. Part 4: Aerodynamic data tabulation
[NASA-CR-179469] p 153 N88-23956

TAKEOFF

Noise of a model high speed counterrotation propeller at simulated takeoff/approach conditions (F7/A7)
[AIAA PAPER 87-2657] p 214 A88-20176
High speed propeller performance and noise predictions at takeoff/landing conditions
[AIAA PAPER 88-0264] p 215 A88-22193

- Noise of a model high speed counterrotation propeller at simulated takeoff/approach conditions (F7/A7) [NASA-TM-100206] p 216 N88-10592
- High speed propeller performance and noise predictions at takeoff/landing conditions [NASA-TM-100267] p 216 N88-13960
- TANTALUM ALLOYS**
- Thermal aging effects in refractory metal alloys p 84 A88-22700
- TAPERING**
- Experiments on dynamic stiffness and damping of tapered bore seals p 166 A88-31527
- Improved oil-off survivability of tapered roller bearings [NASA-CR-180804] p 170 N88-11135
- TECHNOLOGICAL FORECASTING**
- Spacecraft 2000 program overview p 48 N88-10085
- Speculations on future opportunities to evolve Brayton powerplants aboard the space station p 202 N88-24258
- TECHNOLOGY ASSESSMENT**
- Automotive Stirling engine development program - A success p 165 A88-11965
- Recent advances in low-thrust propulsion technology [AIAA PAPER 88-3283] p 55 A88-48761
- Assessment, development, and application of combustor aerothermal models p 24 A88-54140
- Current status and future trends in turbine application of thermal barrier coatings [ASME PAPER 88-GT-286] p 169 A88-54355
- Spacecraft 2000 program overview p 48 N88-10085
- System Development Working Group report p 48 N88-10092
- Electrical Power Working Group report p 48 N88-10095
- Progress toward the evolution of a Stirling space engine [NASA-TM-100221] p 224 N88-14046
- Supersonic throughflow fans for high-speed aircraft p 30 N88-15810
- Assessment, development and application of combustor aerothermal models [NASA-TM-100290] p 32 N88-19469
- Advanced Gas Turbine (AGT) technology development project [NASA-CR-180891] p 225 N88-20230
- Spacecraft fire-safety experiments for space station: Technology development mission [NASA-CR-182114] p 48 N88-20353
- Cryogenic Fluid Management Technology Workshop. Volume 2: Roundtable Discussion of Technology Requirements [NASA-CP-10009] p 152 N88-20599
- Power systems for production, construction, life support and operations in space [NASA-TM-100838] p 60 N88-21254
- Monolithic microwave integrated circuit technology for advanced space communication [NASA-TM-100829] p 120 N88-21389
- A 30 GHz monolithic receive module technology assessment [NASA-CR-180825] p 129 N88-23084
- Microgravity robotics technology program [NASA-TM-100898] p 173 N88-23219
- Assessment of nuclear reactor concepts for low power space applications p 217 N88-24409
- Recent advances in low-thrust propulsion technology [NASA-TM-100959] p 213 N88-25260
- Phase 1 results from the Stirling-powered vehicle project [NASA-TM-100978] p 225 N88-27980
- Constitutive modeling for isotropic materials [NASA-CR-182132] p 37 N88-29811
- TECHNOLOGY UTILIZATION**
- Identification of salt-alloy combinations for thermal energy storage applications in advanced solar dynamic power systems p 199 A88-24072
- Spacecraft 2000 program overview p 48 N88-10085
- System Development Working Group report p 48 N88-10092
- Electrical Power Working Group report p 48 N88-10095
- TELECOMMUNICATION**
- Experiments applications guide: Advanced Communications Technology Satellite (ACTS) [NASA-TM-100265] p 49 N88-28082
- TELEMETRY**
- Spacecraft 2000 [NASA-CP-2473] p 48 N88-10084
- TELEVISION SYSTEMS**
- Lewis Information Network (LINK): Background and overview [NASA-TM-100162] p 117 N88-11925
- TEMPERATURE DEPENDENCE**
- Comparative radiation resistance, temperature dependence and performance of diffused junction indium phosphide solar cells p 198 A88-18580
- TEMPERATURE DISTRIBUTION**
- Explicit finite-volume time-marching calculations of total temperature distributions in turbulent flow p 139 A88-30517
- On the mixing of a row of jets with a confined crossflow p 147 N88-11154
- Thermal distortion analysis of the space station solar dynamic concentrator [NASA-TM-100868] p 64 N88-25475
- TEMPERATURE EFFECTS**
- A model for the influence of pressure on the bulk modulus and the influence of temperature on the solidification pressure for liquid lubricants [ASME PAPER 86-TRIB-63] p 133 A88-15124
- Stability relationship for water droplet crystallization with the NASA Lewis icing spray nozzle [AIAA PAPER 88-0289] p 137 A88-22209
- Radiation and temperature effects in gallium arsenide, indium phosphide, and silicon solar cells p 125 A88-34321
- Reduction of temperature rise in high-speed photography p 160 A88-55254
- Stability relationship for water droplet crystallization with the NASA Lewis icing spray [NASA-TM-100220] p 24 N88-10790
- Reduction of temperature rise in high-speed photography [NASA-TM-100222] p 160 N88-11100
- Creep-fatigue behavior of NiCoCrAlY coated PWA 1480 p 186 N88-11176
- Combustion characteristics of gas turbine alternative fuels [NASA-TM-100247] p 25 N88-13338
- Grain boundary oxidation and low-cycle fatigue at elevated temperatures p 193 N88-22420
- Polymer precursors for ceramic composites p 75 N88-23890
- SiC fiber analysis p 107 N88-23891
- Thermal distortion analysis of the space station solar dynamic concentrator [NASA-TM-100868] p 64 N88-25475
- TEMPERATURE GRADIENTS**
- Calibration of high-temperature, fiber-optic, microbend, pressure transducers p 157 A88-22942
- Experiments investigating advanced materials under thermomechanical loading p 191 N88-22385
- TEMPERATURE MEASUREMENT**
- Preparation of multistage zone-refined materials for thermochemical standards p 111 A88-43172
- Further development of the dynamic gas temperature measurement system p 160 N88-11141
- Correlation of velocity and velocity-density turbulence in the exhaust of an atmospheric burner p 161 N88-11147
- Noncontact temperature measurement: Requirements and applications for metals and alloys research p 112 N88-23899
- Noncontact temperature measurements in the microgravity fluids and transport phenomena discipline p 113 N88-23901
- Microgravity combustion discipline working group summary of requirements for noncontact temperature measurements p 113 N88-23902
- Measurement of local high-level, transient surface heat flux [NASA-TP-2840] p 164 N88-30099
- TEMPERATURE MEASURING INSTRUMENTS**
- Measurement of local high-level, transient surface heat flux [NASA-TP-2840] p 164 N88-30099
- TEMPERATURE PROFILES**
- Temperature and velocity profiles in sooting free convection diffusion flames p 78 A88-43018
- Effect of NASA advanced designs on thermal behavior of Ni-H2 cells [NASA-TM-100197] p 79 N88-10132
- TEMPERATURE SENSORS**
- Development of heat flux sensors for turbine airfoils p 160 N88-11143
- Modulated-splitting-ratio fiber-optic temperature sensor [NASA-TM-101332] p 18 N88-28062
- Development of sensors for ceramic components in advanced propulsion systems: Survey and evaluation of measurement techniques for temperature, strain and heat flux for ceramic components in advanced propulsion systems [NASA-CR-182111] p 163 N88-28299
- TENSILE PROPERTIES**
- The microstructure and tensile properties of extruded melt-spun ribbons of iron-rich B2 FeAl p 85 A88-31679
- SiC reinforced aluminide composites p 70 A88-31687
- Room temperature tensile ductility in powder processed B2 FeAl alloys p 85 A88-31694
- Creep behavior of tungsten/niobium and tungsten/niobium-1 percent zirconium composites p 75 N88-24427
- TENSILE STRENGTH**
- Deformation, fatigue and fracture behavior of two cast anisotropic superalloys p 187 N88-13732
- TENSILE STRESS**
- Constitutive modeling of superalloy single crystals with verification testing p 91 N88-11169
- TENSILE TESTS**
- Some adhesion/cohesion characteristics of plasma-sprayed ZrO₂-Y₂O₃ under tensile loading p 95 A88-12589
- Dynamic recrystallization and grain boundary migration in B2 FeAl p 83 A88-20269
- Creep fatigue life prediction for engine hot section materials (isotropic): Third year progress review p 186 N88-11173
- Elevated temperature crack growth p 186 N88-11174
- High temperature tensile testing of ceramic composites [NASA-CR-180888] p 161 N88-15996
- Ethynylated aromatics as high temperature matrix resins [NASA-TM-89829] p 73 N88-18640
- TERNARY ALLOYS**
- Channel formation in Pb-Sn, Pb-Sb, and Pb-Sn-Sb alloy ingots and comparison with the system NH₄Cl-H₂O p 89 A88-46038
- TEST EQUIPMENT**
- Simulation test beds for the space station electrical power system [NASA-TM-100786] p 44 N88-17715
- Techniques utilized in the simulated altitude testing of a 2D-CD vectoring and reversing nozzle [NASA-TM-100872] p 40 N88-25464
- TEST FACILITIES**
- Research opportunities in microgravity science and applications during Shuttle hiatus p 109 A88-13164
- A distributed data acquisition system for aeronautics test facilities p 39 A88-33065
- Small engine components test facility turbine testing cell [AIAA PAPER 88-2962] p 22 A88-44706
- The ac power system testbed [NASA-CR-175068] p 127 N88-11948
- Measured performance of the heat exchanger in the NASA icing research tunnel under severe icing and dry-air conditions [NASA-TM-100116] p 171 N88-12796
- Test facilities of the structural dynamics branch of NASA Lewis Research Center [NASA-TM-100800] p 190 N88-21534
- Small engine components test facility turbine testing cell [NASA-TM-100887] p 33 N88-22037
- Benefits of 20 kHz PMAD in a nuclear space station p 129 N88-24256
- Lewis Research Center space station electric power system test facilities [NASA-TM-100924] p 43 N88-28942
- TEST FIRING**
- Orbital transfer vehicle 3000 LBF thrust chamber assembly hot fire test program [NASA-CR-182145] p 66 N88-29858
- TEST STANDS**
- Description of an oscillating flow pressure drop test rig [NASA-TM-100905] p 61 N88-22933
- TESTS**
- The design and fabrication of a Stirling engine heat exchanger module with an integral heat pipe [NASA-TM-101296] p 203 N88-26732
- TETHERING**
- Coaxial tube array space transmission line characterization p 121 A88-11865
- Space plasma contactor research, 1987 [NASA-CR-182148] p 219 N88-23649
- TETHERLINES**
- Power transmission studies for tethered SP-100 [NASA-TM-100864] p 60 N88-21251
- TEXTURES**
- The effect of texture on the crack growth resistance of alumina [NASA-TM-100250] p 102 N88-14206
- THEODOLITES**
- Optical alignment of Centaur's inertial guidance system [NASA-TM-88844] p 43 N88-12515

THERMAL ANALYSIS

- Three dimensional thermal analysis of rocket thrust chambers
[AIAA PAPER 88-2643] p 54 A88-43721
- Development of a thermal and structural analysis procedure for cooled radial turbines
[ASME PAPER 88-GT-18] p 145 A88-54164
- A two-dimensional finite difference program for thermal analysis of rocket thrust chambers
[NASA-TM-100191] p 58 N88-12539
- Thermal finite-element analysis of space shuttle main engine turbine blade
[NASA-TM-100117] p 187 N88-13745
- Analysis of shell-type structures subjected to time-dependent mechanical and thermal loading
[NASA-CR-182705] p 189 N88-20668
- THERMAL BARRIERS (PLASMA CONTROL)**
- Thrust chamber thermal barrier coating techniques
[NASA-TM-100933] p 64 N88-24690
- THERMAL CONDUCTIVITY**
- Thermal conductivity of pristine and brominated highly graphitized pitch based carbon fibers p 97 A88-20257
- Synthesis, electrical and thermal conductivities, and potential applications of graphite fluoride fibers p 97 A88-26963
- Specific heat of pristine and brominated graphite fibers, composites and HOPG --- Highly Oriented Pyrolytic Graphite p 98 A88-32853
- THERMAL CONTROL COATINGS**
- Progress toward life modeling of thermal barrier coatings for aircraft gas turbine engines
[ASME PAPER 87-ICE-18] p 96 A88-15120
- Porosity determination of thermal barrier coatings
[ASME PAPER 88-GT-278] p 68 A88-54350
- Thermal barrier coating life prediction model development
[ASME PAPER 88-GT-284] p 68 A88-54353
- Current status and future trends in turbine application of thermal barrier coatings
[ASME PAPER 88-GT-286] p 169 A88-54355
- Thermal expansion mismatch and oxidation in thermal barrier coatings p 170 N88-11182
- Low Earth orbit environmental effects on the space station photovoltaic power generation systems
[NASA-TM-100230] p 225 N88-12429
- THERMAL CYCLING TESTS**
- High-temperature oxidation/corrosion of iron-based superalloys p 81 A88-10029
- Thermal cycling of tungsten-fibre-reinforced superalloy composites p 70 A88-31770
- A model for life predictions of nickel-base superalloys in high-temperature low cycle fatigue p 87 A88-35913
- Bithermal fatigue - A link between isothermal and thermomechanical fatigue p 87 A88-35918
- Effect of temperature, microstructure, and stress state on the low cycle fatigue behavior of Waspaloy p 87 A88-35922
- Hygrothermomechanical fiber composite fatigue - Computational simulation p 71 A88-42437
- Elevated temperature durability of ceramic materials
[AIAA PAPER 88-3055] p 100 A88-44743
- Thermal barrier coating life prediction model development
[ASME PAPER 88-GT-284] p 68 A88-54353
- THERMAL DEGRADATION**
- Thermal aging effects in refractory metal alloys p 84 A88-22700
- Modified reaction mechanism of aerated n-dodecane liquid flowing over heated metal tubes p 108 A88-44268
- THERMAL DIFFUSIVITY**
- Improved perfluoroalkyl ether fluid development p 68 A88-28624
- Double-diffusive effects during solidification p 221 A88-43933
- THERMAL EMISSION**
- Unsteady heat transfer in turbine blade ducts: Focus on combustor sources
[NASA-TM-100815] p 151 N88-18870
- Arc-textured metal surfaces for high thermal emittance space radiators
[NASA-TM-100894] p 94 N88-24754
- THERMAL ENERGY**
- Selection of high temperature thermal energy storage materials for advanced solar dynamic space power systems p 68 A88-11801
- Fluoride salts as phase change materials for thermal energy storage in the temperature range 1000-1400 K p 199 A88-33734
- THERMAL ENVIRONMENTS**
- Optical strain measurement system development p 159 A88-52557
- THERMAL EXPANSION**
- Thermal cycling of tungsten-fibre-reinforced superalloy composites p 70 A88-31770

- The effect of bromination of carbon fibers on the coefficient of thermal expansion of graphite fiber-epoxy composites
[NASA-TM-100236] p 72 N88-10899
- Features and applications of the integrated composites analyzer (ICAN) code p 74 N88-22391
- THERMAL FATIGUE**
- Bithermal fatigue - A link between isothermal and thermomechanical fatigue p 87 A88-35918
- Effect of temperature, microstructure, and stress state on the low cycle fatigue behavior of Waspaloy p 87 A88-35922
- Hygrothermomechanical fiber composite fatigue - Computational simulation p 71 A88-42437
- Creep and fatigue research efforts on advanced materials p 187 N88-16701
- Bithermal fatigue of a nickel-base superalloy single crystal
[NASA-TM-100885] p 93 N88-22168
- Unified constitutive model for single crystal deformation behavior with applications p 191 N88-22388
- Elevated temperature crack growth p 193 N88-22421
- Bithermal fatigue: A simplified alternative to thermomechanical fatigue p 194 N88-22424
- THERMAL PROTECTION**
- Design, development, and test of Shuttle/Centaur G-prime cryogenic tankage thermal protection systems p 47 A88-53182
- Life modeling of thermal barrier coatings for aircraft gas turbine engines p 90 A88-54145
- Thermal barrier coating life prediction model development p 170 N88-11184
- Thermal barrier coating life prediction model development p 171 N88-11185
- Life modeling of thermal barrier coatings for aircraft gas turbine engines p 92 N88-15060
- [NASA-TM-100283] p 92 N88-15060
- Thermal stress minimized, two component, turbine shroud seal
[NASA-CASE-LEW-14212-1] p 174 N88-23978
- THERMAL RESISTANCE**
- Superelement methods applications to micromechanics of high temperature metal matrix composites
[AIAA PAPER 88-2390] p 182 A88-32322
- THERMAL SHOCK**
- Fracture mechanics p 194 N88-23877
- Strength optimization of alpha-SiC by improved processing p 107 N88-23880
- Ceramic matrix composites p 75 N88-23888
- THERMAL STABILITY**
- PMR polyimide compositions for improved performance at 371 C p 96 A88-13172
- Temperature stability of Al(x)Ga(1-x)As (x = 0-1) thermal oxide masks for selective-area epitaxy p 221 A88-45858
- Pressure effects on the thermal stability of SiC fibers
[NASA-TM-100146] p 71 N88-10120
- Improved perfluoroalkylether fluid development
[NASA-CR-180872] p 80 N88-15851
- Self-lubricating coatings for high-temperature applications p 103 N88-16703
- Correlations of norbornenyl crosslinked polyimide resin structures with resin thermo-oxidative stability, resin glass transition temperature and composite initial mechanical properties
[NASA-TM-100791] p 103 N88-16877
- SiC fiber analysis p 107 N88-23891
- A thermally modified polymer matrix composite material with structural integrity to 371 C
[NASA-TM-100922] p 76 N88-25483
- THERMAL STRESSES**
- Thermal stresses of a wind turbine blade made of orthotropic material p 180 A88-18380
- Dynamic recrystallization and grain boundary migration in B2 FeAl p 83 A88-20269
- B2 aluminides for high temperature applications p 85 A88-31684
- Oxidation and protection of fiberglass-epoxy composite masts for photovoltaic arrays in the low Earth orbital environment
[NASA-TM-100839] p 104 N88-18734
- High-temperature combustor liner tests in structural component response test facility p 33 N88-22383
- MHOST: An efficient finite element program for inelastic analysis of solids and structures p 33 N88-22394
- METCAN: The metal matrix composite analyzer p 74 N88-22395
- Thermostructural analysis of simulated cow lips p 192 N88-22403
- Thermal-structural analyses of Space Shuttle Main Engine (SSME) hot section components p 61 N88-22404
- Elevated temperature crack growth p 193 N88-22421

- Thermal stress minimized, two component, turbine shroud seal
[NASA-CASE-LEW-14212-1] p 174 N88-23978
- THERMOCHEMICAL PROPERTIES**
- Preparation of multistage zone-refined materials for thermochemical standards p 111 A88-43172
- Significance of vapor phase chemical reactions on CVD rates predicted by chemically frozen and local thermochemical equilibrium boundary layer theories p 78 A88-44424
- THERMOCHEMISTRY**
- Plasma assisted surface coating/modification processes - An emerging technology p 114 A88-38927
- THERMOCOUPLE PYROMETERS**
- Design, calibration and error analysis of instrumentation for heat transfer measurements in internal combustion engines p 157 A88-18509
- THERMOCOUPLES**
- Prototype thin-film thermocouple/heat-flux sensor for a ceramic-insulated diesel engine
[NASA-TM-100798] p 162 N88-18892
- THERMODYNAMIC CYCLES**
- Analysis of shell-type structures subjected to time-dependent mechanical and thermal loading
[NASA-CR-181409] p 185 N88-10388
- THERMODYNAMIC EFFICIENCY**
- Application of several variable-valve-timing concepts to an LHR engine
[ASME PAPER 87-ICE-29] p 19 A88-15119
- THERMODYNAMIC EQUILIBRIUM**
- Critical fluid light scattering p 158 A88-33003
- Significance of vapor phase chemical reactions on CVD rates predicted by chemically frozen and local thermochemical equilibrium boundary layer theories p 78 A88-44424
- THERMODYNAMIC PROPERTIES**
- Thermal desorption study of physical forces at the PTFE surface p 77 A88-10963
- Dispersion strengthened NiAl alloys produced by rapid solidification processing p 88 A88-40588
- Experimental study of thermocapillary flows in a thin liquid layer with heat fluxes imposed on the free surface p 144 A88-49087
- Experimental study of thermocapillary flows in a thin liquid layer with heat fluxes imposed on the free surface
[NASA-TM-100252] p 148 N88-12763
- THERMODYNAMICS**
- Calculation of thermomechanical fatigue life based on isothermal behavior p 181 A88-26450
- Improved perfluoroalkyl ether fluid development p 68 A88-28624
- Thermodynamic modeling of the no-vent fill methodology for transferring cryogens in low gravity
[AIAA PAPER 88-3403] p 55 A88-48765
- Electrohydrodynamic migration of charged droplets in an insulating fluid
[AIAA PAPER 88-3557] p 143 A88-48946
- Electrohydrodynamic migration of charged droplets in an insulating fluid
[NASA-TM-100849] p 152 N88-21424
- A viscoplastic theory applied to copper
[NASA-TM-100831] p 189 N88-21497
- Nondestructive evaluation of sintered ceramics p 177 N88-22416
- Thermodynamic modeling of the no-vent fill methodology for transferring cryogens in low gravity
[NASA-TM-100932] p 63 N88-24686
- Isothermal and bithermal thermomechanical fatigue behavior of a NiCoCrAlY-coated single crystal superalloy
[NASA-TM-100907] p 94 N88-24766
- Advanced development of double-injection, deep-impurity semiconductor switches
[NASA-CR-182118] p 222 N88-25346
- THERMOELASTICITY**
- Thermo-elasto-viscoplastic analysis of problems in extension and shear p 183 A88-41042
- A review of path-independent integrals in elastic-plastic fracture mechanics p 183 A88-47001
- A new boundary element formulation for two- and three-dimensional thermoelasticity using particular integrals p 184 A88-53088
- A transversely isotropic thermoelastic theory
[NASA-TM-101302] p 196 N88-28332
- THERMOELECTRIC GENERATORS**
- Speculations on future opportunities to evolve Brayton powerplants aboard the space station p 202 N88-24258
- THERMOELECTRIC MATERIALS**
- Effect of high temperature annealing on the thermoelectric properties of GaP doped SiGe p 220 A88-40796
- THERMOELECTRICITY**
- Effect of the microstructure on the thermoelectric properties of polycrystalline lanthanum chalcogenides p 221 A88-40797

- Effect of high-temperature annealing on the microstructure and thermoelectric properties of GaP doped SiGe
[NASA-TM-100164] p 101 N88-10188
- THERMOMECHANICAL TREATMENT**
Bithermal fatigue - A link between isothermal and thermomechanical fatigue p 87 A88-35918
Thermal-mechanical cyclic stress-strain responses of cast B-1900 + Hf p 87 A88-35919
Experiments investigating advanced materials under thermomechanical loading p 191 N88-22385
METCAN: The metal matrix composite analyzer p 74 N88-22395
- THICK FILMS**
Improved beta-SiC heteroepitaxial films using off-axis Si substrates p 219 A88-10431
High Tc screen-printed YBa₂Cu₃O_{7-x} films - Effect of the substrate material p 127 A88-49760
Synthesis and characterization of high-T_c (sub c) screen-printed Y-Ba-Cu-O films on alumina [NASA-TM-100860] p 222 N88-22805
- THIN AIRFOILS**
The effects of rotational flow, viscosity, thickness, and shape on transonic flutter dip phenomena [AIAA PAPER 88-2348] p 182 A88-32289
The effects of rotational flow, viscosity, thickness, and shape on transonic flutter dip phenomena [NASA-TM-100811] p 188 N88-18969
- THIN FILMS**
Ion beam deposition of amorphous carbon films with diamond like properties p 97 A88-20300
Mechanical strength and tribological behavior of ion-beam-deposited boron nitride films on non-metallic substrates p 98 A88-32866
Investigation of PTFE transfer films by infrared emission spectroscopy and phase-locked ellipsometry p 99 A88-35568
Sputtered silver films to improve chromium carbide based solid lubricant coatings for use to 900 C p 100 A88-47563
Experimental study of thermocapillary flows in a thin liquid layer with heat fluxes imposed on the free surface p 144 A88-49087
Deposition of vanadium oxide films by direct-current magnetron reactive sputtering p 221 A88-51286
Experimental study of thermocapillary flows in a thin liquid layer with heat fluxes imposed on the free surface [NASA-TM-100252] p 148 N88-12763
Research sensors p 161 N88-15795
Sputtered silver films to improve chromium carbide based solid lubricant coatings for use to 900 C [NASA-TM-100783] p 102 N88-15885
Prototype thin-film thermocouple/heat-flux sensor for a ceramic-insulated diesel engine [NASA-TM-100798] p 162 N88-18892
Measurement of the properties of lossy materials inside a finite conducting cylinder [NASA-CR-182664] p 213 N88-20962
Space station solar concentrator materials research [NASA-TM-100862] p 60 N88-21250
Study of Staebler-Wronsky degradation effect in a Si:H based P-I-N solar cells [NASA-CR-182564] p 203 N88-25970
Thin film coatings for space electrical power system applications [NASA-TM-101325] p 69 N88-28966
- THIN PLATES**
A mixed formulation of C(0)-linear triangular plate/shell element - The role of edge shear constraints p 183 A88-40121
- THIN WALLED SHELLS**
Analysis of shell-type structures subjected to time-dependent mechanical and thermal loading [NASA-CR-181409] p 185 N88-10388
Analysis of shell-type structures subjected to time-dependent mechanical and thermal loading [NASA-CR-182705] p 189 N88-20668
- THREE DIMENSIONAL BODIES**
Time-domain transient elastodynamic analysis of 3-D solids by BEM p 183 A88-48638
- THREE DIMENSIONAL BOUNDARY LAYER**
User's manual for three dimensional boundary layer (BL3-D) code [NASA-CR-174899] p 155 N88-30063
Assessment of a 3-D boundary layer analysis to predict heat transfer and flow field in a turbine passage [NASA-CR-174894] p 155 N88-30066
- THREE DIMENSIONAL FLOW**
Application of advanced computational codes in the design of an experiment for a supersonic throughflow fan rotor [ASME PAPER 87-GT-160] p 2 A88-11072
A space-marching method for the computation of viscous internal flows p 135 A88-20459
- A numerical study of the effects of curvature and convergence on dilution jet mixing [AIAA PAPER 87-1953] p 137 A88-23312
Consistent boundary conditions for reduced Navier-Stokes (RNS) scheme applied to three-dimensional internal viscous flows [AIAA PAPER 88-0714] p 139 A88-27723
A finite difference scheme for three-dimensional steady laminar incompressible flow p 139 A88-30469
Comparison of computational methods for three-dimensional turbulent turbomachinery flows p 6 A88-42452
Numerical analysis of three-dimensional viscous internal flows [AIAA PAPER 88-3522] p 142 A88-48779
A diagonally inverted LU implicit multigrid scheme [AIAA PAPER 88-3565] p 209 A88-48791
Three-dimensional viscous flow computations of a circular jet in subsonic and supersonic cross flow [AIAA PAPER 88-3703] p 143 A88-48916
Three-dimensional flow past two cylinders mounted side by side on an endwall [AIAA PAPER 88-3718] p 143 A88-48974
Flow in a model turbine stator p 148 N88-11163
A numerical study of the effects of curvature and convergence on dilution jet mixing [NASA-TM-89878] p 26 N88-13347
Consistent boundary conditions for Reduced Navier-Stokes (RNS) scheme applied to 3-dimensional internal viscous flows [NASA-CR-180874] p 10 N88-15762
Turbomachinery p 28 N88-15792
Numerical modeling of multidimensional flow in seals and bearings used in rotating machinery [NASA-TM-100779] p 150 N88-16988
Numerical simulation of subsonic and transonic propeller flow [NASA-TM-100163] p 11 N88-20262
Numerical analysis of three-dimensional viscous internal flows [NASA-TM-100878] p 1 N88-21116
Three-dimensional viscous flow computations of a circular jet in subsonic and supersonic cross flow [NASA-CR-182153] p 155 N88-26616
- THREE DIMENSIONAL MODELS**
Design point variation of 3-D loss and deviation for axial compressor middle stages [ASME PAPER 88-GT-57] p 8 A88-54189
Three-dimensional adaptive grid generation for body-fitted coordinate system [NASA-CR-182192] p 155 N88-27520
Three-dimensional elliptic grid generation technique with application to turbomachinery cascades [NASA-TM-101330] p 155 N88-30078
- THRESHOLD VOLTAGE**
Threshold-determining mechanisms for discharges in high-voltage solar arrays p 50 A88-11738
- THRUST**
Development of a liquid-fed water resistojet [AIAA PAPER 88-3288] p 142 A88-48762
High power ion thruster performance [NASA-TM-100127] p 58 N88-12542
An experimental investigation of an arcjet thruster exhaust using Langmuir probes [NASA-TM-100258] p 60 N88-21253
Development of a liquid-fed water resistojet [NASA-TM-100927] p 174 N88-24968
Iridium-coated rhenium thrusters by CVD [NASA-TM-101309] p 67 N88-29874
- THRUST CHAMBER PRESSURE**
Boundary layer development as a function of chamber pressure in the NASA Lewis 1030:1 area ratio rocket nozzle [AIAA PAPER 88-3301] p 144 A88-50786
Boundary layer development as a function of chamber pressure in the NASA Lewis 1030:1 area ratio rocket nozzle [NASA-TM-100917] p 154 N88-25841
- THRUST CHAMBERS**
Three dimensional thermal analysis of rocket thrust chambers [AIAA PAPER 88-2643] p 54 A88-43721
A two-dimensional finite difference program for thermal analysis of rocket thrust chambers [NASA-TM-100191] p 58 N88-12539
Orbital transfer vehicle 3000 LBF thrust chamber assembly hot fire test program [NASA-CR-182145] p 66 N88-29858
- THRUST MEASUREMENT**
In-flight thrust determination [SAE AIR 1703] p 16 A88-15227
Uncertainty of in-flight thrust determination [SAE AIR 1678] p 16 A88-15228
- TIME**
Time-partitioning simulation models for calculation of parallel computers p 206 A88-46961
- TIME DEPENDENCE**
Oil film thickness measurement and analysis for an angular contact ball bearing operating in parched elastohydrodynamic lubrication p 165 A88-14115
Analysis of shell-type structures subjected to time-dependent mechanical and thermal loading [NASA-CR-181409] p 185 N88-10388
3D inelastic analysis methods for hot section components p 185 N88-11164
Analysis of shell-type structures subjected to time-dependent mechanical and thermal loading [NASA-CR-182705] p 189 N88-20668
Solving time-dependent two-dimensional eddy current problems [NASA-TM-100875] p 211 N88-25239
- TIME DIVISION MULTIPLE ACCESS**
Bandwidth and power efficient satellite TDMA demodulator and decoder [AIAA PAPER 88-0812] p 123 A88-27559
Hardware realization of a baseband processor for a SS-FDMA/TDMA/DAMA system --- Demand Assignment Multiple Access [AIAA PAPER 88-0830] p 124 A88-27575
Satellite ground-terminal user simulation [NASA-TM-100234] p 118 N88-14260
- TIME LAG**
Finite-dimensional modeling of network-induced delays for real-time control systems p 208 A88-54537
The carbon dioxide chaperon efficiency for the reaction H + O₂ + M yields HO₂ + M from ignition delay times behind reflected shock waves [NASA-TM-100125] p 79 N88-15036
- TIME MARCHING**
Explicit finite-volume time-marching calculations of total temperature distributions in turbulent flow p 139 A88-30517
An explicit finite-volume time-marching procedure for turbulent flow calculations p 139 A88-30518
Time-domain transient elastodynamic analysis of 3-D solids by BEM p 183 A88-48638
Application of Runge Kutta time marching scheme for the computation of transonic flows in turbomachines [NASA-TM-86997] p 9 N88-12461
The 2-D and 3-D time marching transonic potential flow method for propfans p 11 N88-23245
Reduced order models for nonlinear aerodynamics p 11 N88-23248
- TIN ALLOYS**
Fraction eutectic measurements in slowly cooled Pb - 15 wt percent Sn alloys [NASA-CR-180830] p 94 N88-25531
- TIN OXIDES**
Direct-current magnetron fabrication of indium tin oxide/InP solar cells p 200 A88-51289
- TIP SPEED**
Cruise noise of the 2/9 scale model of the Large-scale Advanced Propfan (LAP) propeller, SR-7A [AIAA PAPER 87-2717] p 214 A88-16565
- TITANIA**
Hafnia-rich mixed oxide ceramics of the system HfO₂-ZrO₂-TiO₂ for heaters and heat exchangers in electrothermal thrusters: The effects of titania on selected electrical and mechanical properties of Hafnia-rich mixed oxides in the system Hafnia-Zirconia-Titania, volume 1 [NASA-CR-182800-VOL-1] p 105 N88-22197
- TITANIUM**
Electrical properties of materials for elevated temperature resistance strain gage application [NASA-CR-182214] p 164 N88-30106
- TITANIUM ALLOYS**
As-received microstructure of a SiC/Ti-15-3 composite [NASA-TM-100938] p 76 N88-28095
Investigation of a SiC/Ti-24Al-11Nb composite [NASA-TM-100956] p 76 N88-28980
- TITANIUM CARBIDES**
Characteristics of fluid flow in the combustion synthesis of TiC from the elements p 110 A88-28564
- TOLUENE**
Toluene stability Space Station Rankine power system p 50 A88-11794
Detailed mechanism of toluene oxidation and comparison with benzene [NASA-TM-100261] p 79 N88-13428
Study of toluene stability for an Organic Rankine Cycle (ORC) space-based power system [NASA-CR-180884] p 66 N88-29863
Study of toluene rotary fluid management device and shear flow condenser performance for a space-based organic Rankine power system [NASA-CR-180885] p 67 N88-29872
- TORQUEMETERS**
Noncontacting measurement technologies for space propulsion condition monitoring p 158 A88-29818
- TORSION**
Torsion effect on fully developed flow in a helical pipe p 135 A88-20748

Development of a torsion balance for adhesion measurements
[NASA-TM-100799] p 104 N88-20454

TOUGHNESS

Finite element substructuring methods for composite mechanics
[NASA-TM-100297] p 73 N88-17745

TRACE CONTAMINANTS

Preliminary study of niobium alloy contamination by transport through helium p 94 N88-24279

TRADEOFFS

Array trade-off study using multilayer parasitic subarrays
[NASA-TM-101321] p 121 N88-28222

TRAILING EDGES

A parametric study of mean loading effects on airfoil gust interaction noise
[AIAA PAPER 87-2677] p 213 A88-16539

TRAJECTORIES

Base reaction optimization of manipulators with redundant kinematics p 173 N88-23238
Microgravity manipulator demonstration p 173 N88-23242

TRAJECTORY ANALYSIS

Three-dimensional trajectory analyses of two drop sizing instruments: PMS OAP and PMS FSSP
[NASA-CR-41113] p 16 N88-18574

TRAJECTORY OPTIMIZATION

Optimal cooperative time-fixed impulsive rendezvous
[AIAA PAPER 88-4279] p 42 A88-50406

TRANSDUCERS

Characterization of noncontact piezoelectric transducer with conically shaped piezoelement
[NASA-CR-4151] p 179 N88-23987

TRANSFER ORBITS

Impact of ETO propellants on the aerothermodynamic analyses of propulsion components
[NASA-TM-101303] p 156 N88-30094

TRANSFERRING

Investigation of PTFE transfer films by infrared emission spectroscopy and phase-locked ellipsometry p 99 A88-35568

TRANSFORMATIONS (MATHEMATICS)

Reduced order models for nonlinear aerodynamics p 11 N88-23248

TRANSFORMERS

The application of high temperature superconductors to space electrical power distribution components
[NASA-TM-100901] p 61 N88-22939

TRANSIENT HEATING

Transient radiative cooling of an absorbing and scattering cylinder - A separable solution p 140 A88-41409

Measurement of local high-level, transient surface heat flux
[NASA-TP-2840] p 164 N88-30099

TRANSIENT OSCILLATIONS

Active control of transient rotordynamic vibration by optimal control methods
[ASME PAPER 88-GT-73] p 208 A88-54202

TRANSIENT RESPONSE

Steady and transient least square solvers for thermal problems p 134 A88-17318

TRANSITION FLOW

A numerical study of the effects of curvature and convergence on dilution jet mixing
[AIAA PAPER 87-1953] p 137 A88-23312

Unsteady motion and transition to turbulence in developing curved duct flow p 140 A88-39010
Gas liquid flow at microgravity conditions - Flow patterns and their transitions p 141 A88-42839

A numerical study of the effects of curvature and convergence on dilution jet mixing p 26 N88-13347
Transition mixing study empirical model report
[NASA-CR-182139] p 155 N88-30076

TRANSITION TEMPERATURE

Effect of fluoride doping on the transition temperature of YBa₂Cu₃O₇(δ) p 220 A88-29297

TRANSMISSION

A study of Schwarz converters for nuclear powered spacecraft p 51 A88-11823

TRANSMISSION LINES

Coaxial tube array space transmission line characterization p 121 A88-11865

The application of high temperature superconductors to space electrical power distribution components
[NASA-TM-100901] p 61 N88-22939

High frequency power distribution system
[NASA-CR-175071] p 129 N88-23939

Space power radiation cooled dc transmission line analysis p 129 N88-24506

TRANSMISSION LOSS

Analysis of counting errors in the phase/Doppler particle analyzer
[NASA-TM-100231] p 161 N88-12043

TRANSMISSIONS (MACHINE ELEMENTS)

Method for generation of spiral bevel gears with conjugate gear tooth surfaces
[ASME PAPER 86-DET-3] p 165 A88-10973

Computerized life and reliability modelling for turboprop transmissions
[AIAA PAPER 88-2979] p 100 A88-48031

The generalized transmission error of spiral bevel gears p 168 A88-49409

Improved oil-off survivability of tapered roller bearings
[NASA-CR-180804] p 170 N88-11135

On dynamic loads in parallel shaft transmissions. 1: Modelling and analysis
[NASA-TM-100180] p 171 N88-12797

On dynamic loads in parallel shaft transmissions. 2: Parameter study
[NASA-TM-100181] p 171 N88-12798

Efficiency testing of a helicopter transmission planetary reduction stage
[NASA-TP-2795] p 172 N88-15224

Results of NASA/Army transmission research p 31 N88-16640

Dynamic analysis of multimesh-gear helicopter transmissions
[NASA-TP-2789] p 172 N88-17045

Advanced transmission studies
[NASA-TM-100867] p 173 N88-21454

Computerized life and reliability modelling for turboprop transmissions
[NASA-TM-100918] p 173 N88-23220

Design, manufacture and spin test of high contact ratio helicopter transmission utilizing Self-Aligning Bearingless Planetary (SABP)
[NASA-CR-4155] p 174 N88-24975

Helicopter transmission research at NASA Lewis Research Center
[NASA-TM-100962] p 175 N88-30128

TRANSMITTER RECEIVERS

A laser communication experiment utilizing the ACT satellite and an airborne laser transceiver
[NASA-TM-100792] p 164 N88-18910

TRANSMITTERS

Development of 20 GHz monolithic transmit modules
[NASA-CR-182134] p 222 N88-24539

TRANSONIC COMPRESSORS

Measurements of the unsteady flow field within the stator row of a transonic axial-flow fan. I - Measurement and analysis technique
[ASME PAPER 87-GT-226] p 4 A88-18660

TRANSONIC FLOW

Effects of numerical dissipation on finite-volume solutions of compressible flow problems
[AIAA PAPER 88-0621] p 5 A88-22469

The effects of rotational flow, viscosity, thickness, and shape on transonic flutter dip phenomena
[AIAA PAPER 88-2348] p 182 A88-32289

Application of Runge Kutta time marching scheme for the computation of transonic flows in turbomachines
[NASA-TM-86997] p 9 N88-12461

The effects of rotational flow, viscosity, thickness, and shape on transonic flutter dip phenomena
[NASA-TM-100811] p 188 N88-18969

Numerical simulation of subsonic and transonic propeller flow
[NASA-TM-100163] p 11 N88-20262

A physically consistent model for artificial dissipation in transonic potential flow computations
[NASA-TM-100846] p 211 N88-22652

The 2-D and 3-D time marching transonic potential flow method for propfans p 11 N88-23245

Experimental determination of aerodynamic damping in a three-stage transonic axial-flow compressor
[NASA-TM-100953] p 35 N88-27200

TRANSPARATION

Low Reynolds number modeling of turbulent flows with and without wall transpiration p 136 A88-21983

TRANSPORT AIRCRAFT

Results of NASA's Energy Efficient Engine Program p 19 A88-20785

Aeropropulsion '87. Session 6: High-Speed Propulsion Technology
[NASA-CP-10003-SESS-6] p 29 N88-15807

TRANSPORT PROPERTIES

Experiments for the determination of convective diffusion heat/mass transfer to burner rig test targets comparable in size to jet stream diameter p 140 A88-41574

Noncontact temperature measurements in the microgravity fluids and transport phenomena discipline p 113 N88-23901

NASA research Program: The roles of fluid motion and other transport phenomena in the morphology of materials
[NASA-CR-182801] p 222 N88-25327

TRAPPED PARTICLES

Axions from 1987A p 226 A88-35586

TRAVELING WAVE MODULATION

A high frequency GaAs travelling wave electro-optic modulator at 0.82 micrometers p 130 N88-28240

TRAVELING WAVE TUBES

Bit-error-rate testing of high-power 30-GHz traveling-wave tubes for ground-terminal applications p 122 A88-19781

High efficiency, long life traveling wave tubes for future communications satellites
[AIAA PAPER 88-0835] p 124 A88-27578

A re-examination of spent beam refocusing for high-efficiency helix TWT's and small MDC's p 124 A88-28673

High-efficiency helical traveling-wave tube with dynamic velocity taper and advanced multistage depressed collector p 124 A88-32836

Performance of a small, graphite electrode, multistage depressed collector with a 500-W, continuous wave, 4.8- to 9.6-GHz traveling wave tube
[NASA-TP-2788] p 128 N88-15146

High efficiency, long life traveling wave tubes for future communications satellites
[NASA-TM-100837] p 45 N88-19565

Miniature traveling wave tube and method of making
[NASA-CASE-LEW-14520-1] p 129 N88-23936

A millimeter-wave tunable Ladder TWT
[NASA-CR-182184] p 130 N88-28239

TRENDS

Lewis materials research and technology: An overview p 223 N88-16699

TRIBOLOGY

Stability of a rigid rotor supported on flexible oil journal bearings
[ASME PAPER 87-TRIB-48] p 166 A88-24034

The effects of atmosphere on the tribological properties of a chromium carbide based coating for use to 760 C p 98 A88-32372

Mechanical strength and tribological behavior of ion-beam-deposited boron nitride films on non-metallic substrates p 98 A88-32866

Tribological properties of polymer films and solid bodies in a vacuum environment p 98 A88-35565

Comparison of the tribological properties of fluorinated cokes and graphites
[STLE PREPRINT 88-AM-7F-1] p 100 A88-51300

Adiabatic diesel engine component development: Reference engine for on-highway applications
[NASA-CR-179531] p 224 N88-12428

Adhesion, friction and micromechanical properties of ceramics
[NASA-TM-100782] p 104 N88-17801

Tribological properties of alumina-boria-silicate fabric from 25 to 850 C p 104 N88-18726

Structural Ceramics
[NASA-CP-2427] p 106 N88-23872

Ceramics for turbine engines p 106 N88-23873

TRUCKS

Adiabatic diesel engine component development: Reference engine for on-highway applications
[NASA-CR-179531] p 224 N88-12428

TRUSSES

Solar concentrator advanced development program, task 1
[NASA-CR-179489] p 201 N88-18068

TUNGSTEN

Thermal cycling of tungsten-fibre-reinforced superalloy composites p 70 A88-31770

Composite monolayer fabrication by an arc-spray process p 169 A88-53581

Creep behavior of tungsten/niobium and tungsten/niobium-1 percent zirconium composites
[NASA-TM-100804] p 92 N88-18707

Creep behavior of tungsten/niobium and tungsten/niobium-1 percent zirconium composites p 75 N88-24427

TUNGSTEN ALLOYS

Gravitational contributions to microstructural coarsening in liquid phase sintering p 111 A88-37155

Gravity and configurational energy induced microstructural changes in liquid phase sintering p 112 A88-49089

TUNING

Experimental investigation of propfan aeroelastic response in off-axis flow with mistuning
[NASA-TM-101320] p 196 N88-28344

TURBINE BLADES

Correlation between ultrasonic velocity and density of ceramic turbine blades p 176 A88-12581

Thermal stresses of a wind turbine blade made of orthotropic material p 180 A88-18380

An integrated approach for friction damper design p 167 A88-31598

- Probabilistic structural analysis of aerospace components using NESSUS
[AIAA PAPER 88-2373] p 182 A88-32310
- Evaluation of a turbine blade damper using an integral approach
[AIAA PAPER 88-2400] p 20 A88-32332
- Probabilistic Structural Analysis Methods for select space propulsion system structural components (PSAM)
p 56 A88-49659
- Phase-resolved heat-flux measurements on the blade of a full-scale rotating turbine
[ASME PAPER 88-GT-173] p 145 A88-54267
- Blade loss transient dynamics analysis, volume 1. Task 2: TETRA 2 theoretical development
[NASA-CR-179632] p 25 N88-10791
- Blade loss transient dynamics analysis, volume 2. Task 2: TETRA 2 user's manual
[NASA-CR-179633] p 25 N88-10792
- Turbine Engine Hot Section Technology, 1985
[NASA-CP-2405] p 185 N88-11140
- Development of heat flux sensors for turbine airfoils
p 160 N88-11143
- Prediction of turbine blade heat transfer
p 148 N88-11162
- 3D inelastic analysis methods for hot section components
p 185 N88-11164
- 3-D inelastic analysis methods for hot section components
p 206 N88-11165
- Component specific modeling
p 206 N88-11166
- Constitutive modeling of superalloy single crystals with verification testing
p 91 N88-11169
- Constitutive modeling for isotropic materials
p 185 N88-11171
- Constitutive modeling for isotropic materials
p 186 N88-11172
- Turbine airfoil deposition models and their hot corrosion implications
p 91 N88-11178
- Experimental verification of vapor deposition rate theory in high velocity burner rigs
p 91 N88-11179
- Thermal expansion mismatch and oxidation in thermal barrier coatings
p 170 N88-11182
- Local heat/mass transfer and pressure drop in a two-pass rib-roughened channel for turbine airfoil cooling
[NASA-CR-179635] p 148 N88-12039
- Thermal finite-element analysis of space shuttle main engine turbine blade
[NASA-TM-100117] p 187 N88-13745
- STAEBL/general composites with hygrothermal effects (STAEBL/GENCOM)
[NASA-TM-100266] p 187 N88-13754
- Creep and fatigue research efforts on advanced materials
p 187 N88-16701
- Unsteady heat transfer in turbine blade ducts: Focus on combustor sources
[NASA-TM-100815] p 151 N88-18870
- Testing of a one-bladed 30-meter-diameter rotor on the DOE/NASA Mod-O wind turbine
[NASA-TM-100274] p 201 N88-19014
- Aero/structural tailoring of engine blades (AERO/STAEBL)
[NASA-CR-180805] p 207 N88-21682
- Two-equation low-Reynolds-number turbulence modeling of transitional boundary layer flows characteristic of gas turbine blades
[NASA-CR-4145] p 153 N88-23185
- Lewis Structures Technology, 1988. Volume 1: Structural Dynamics
[NASA-CP-3003-VOL-1] p 194 N88-23226
- Recent advances in capacitance type of blade tip clearance measurements
[NASA-TM-101291] p 35 N88-25460
- Structural Tailoring of Advanced Turboprops (STAT)
[NASA-CR-180861] p 36 N88-28074
- Probabilistic structural analysis to quantify uncertainties associated with turbopump blades
[NASA-TM-100278] p 76 N88-28094
- Thermal barrier coating life-prediction model development
[NASA-CR-179507] p 107 N88-28142
- User's manual for three dimensional boundary layer (BL3-D) code
[NASA-CR-174899] p 155 N88-30063
- Impact of ETO propellants on the aerothermodynamic analyses of propulsion components
[NASA-TM-101303] p 156 N88-30094
- TURBINE ENGINES**
- Four spot laser anemometer and optical access techniques for turbine applications
p 159 A88-36513
- Advanced high temperature instrumentation for hot section research applications
p 159 A88-54139
- Blade loss transient dynamics analysis, volume 1. Task 2: TETRA 2 theoretical development
[NASA-CR-179632] p 25 N88-10791
- Blade loss transient dynamics analysis, volume 2. Task 2: TETRA 2 user's manual
[NASA-CR-179633] p 25 N88-10792
- Development of heat flux sensors for turbine airfoils
p 160 N88-11143
- Film cooling heat transfer on a turbine airfoil
p 147 N88-11156
- Thermal barrier coating life prediction model development
p 171 N88-11185
- Thermal finite-element analysis of space shuttle main engine turbine blade
[NASA-TM-100117] p 187 N88-13745
- Recent advances in high temperature instrumentation for hot section applications
[NASA-TM-100282] p 161 N88-14339
- Directions in propulsion control
p 28 N88-15799
- Improved silicon nitride for advanced heat engines
[NASA-CR-175006] p 102 N88-15886
- Utilization of parallel processing in solving the inviscid form of the average-passage equation system for multistage turbomachinery
[NASA-TM-89845] p 32 N88-21160
- NNPEQ: Chemical equilibrium version of the Navy/NASA Engine Program
[NASA-TM-100851] p 32 N88-21161
- Ceramics for turbine engines
p 106 N88-23873
- Thermal cyclic durability testing of ceramic materials for turbine engines
p 179 N88-23886
- TURBINE PUMPS**
- Real gas properties and Space Shuttle Main Engine fuel turbine performance prediction
[ASME PAPER 87-GT-106] p 50 A88-11038
- Analysis and design of a gas-lubricated, sectored, floating ring seal
[ASME PAPER 87-TRIB-55] p 166 A88-23310
- Noncontacting measurement technologies for space propulsion condition monitoring
p 158 N88-29818
- An expert system approach to turbopump health monitoring
[AIAA PAPER 88-3117] p 42 A88-48038
- Seal technology for liquid oxygen (LOX) turbopumps
[NASA-CR-174866] p 171 N88-13603
- Thermal finite-element analysis of space shuttle main engine turbine blade
[NASA-TM-100117] p 187 N88-13745
- STAEBL/general composites with hygrothermal effects (STAEBL/GENCOM)
[NASA-TM-100266] p 187 N88-13754
- Computer-aided design analysis of 57-mm, angular-contact, cryogenic turbopump bearings
[NASA-TP-2816] p 172 N88-18933
- Probabilistic structural analysis to quantify uncertainties associated with turbopump blades
[NASA-TM-100278] p 76 N88-28094
- TURBINE WHEELS**
- Localization of natural modes of vibration in bladed disks
[ASME PAPER 87-GT-46] p 18 A88-10998
- TURBINES**
- The effects of inlet turbulence and rotor/stator interactions on the aerodynamics and heat transfer of a large-scale rotating turbine model. Volume 3: Heat transfer data tabulation 65 percent axial spacing
[NASA-CR-179468] p 37 N88-28930
- The effects of inlet turbulence and rotor/stator interactions on the aerodynamics and heat transfer of a large-scale rotating turbine model. Volume 2: Heat transfer data tabulation 15 percent axial spacing
[NASA-CR-179467] p 37 N88-29804
- TURBOCOMPRESSORS**
- Inter and intra blade row laser velocimetry studies of gas turbine compressor flows
[ASME PAPER 87-GT-235] p 2 A88-11126
- Small engine components test facility turbine testing cell
[AIAA PAPER 88-2962] p 22 A88-44706
- Design point variation of 3-D loss and deviation for axial compressor middle stages
[ASME PAPER 88-GT-57] p 8 A88-54189
- Flutter of a fan blade in supersonic axial flow
[ASME PAPER 88-GT-78] p 8 A88-54206
- Effect of stage loading on endwall flows in an axial flow compressor rotor
[ASME PAPER 88-GT-111] p 145 A88-54229
- Application of bifurcation theory to axial flow compressor instability
[ASME PAPER 88-GT-231] p 169 A88-54313
- Numerical results for axial flow compressor instability
[ASME PAPER 88-GT-252] p 169 A88-54328
- Experimental investigation of the performance of a supersonic compressor cascade
[ASME PAPER 88-GT-306] p 9 A88-54375
- Automated design of controlled diffusion blades
[NASA-TM-100251] p 9 N88-13304
- Technology developments for a compound cycle engine
p 30 N88-16637
- Small engine components test facility turbine testing cell
[NASA-TM-100887] p 33 N88-22037
- Experimental determination of aerodynamic damping in a three-stage transonic axial-flow compressor
[NASA-TM-100953] p 35 N88-27200
- TURBOFAN AIRCRAFT**
- Multiple-Purpose Subsonic Naval Aircraft (MPSNA): Multiple Application Propfan Study (MAPS)
[NASA-CR-175104] p 18 N88-28917
- TURBOFAN ENGINES**
- Measurements of the unsteady flow field within the stator row of a transonic axial-flow fan. II - Results and discussion
[ASME PAPER 87-GT-227] p 4 A88-18661
- Test stand performance of a convertible engine for advanced V/STOL and rotorcraft propulsion
[SAE PAPER 872355] p 21 A88-37217
- Turbofan engine core noise source diagnostics
p 22 A88-39707
- A preliminary design study of supersonic through-flow fan inlets
[AIAA PAPER 88-3075] p 23 A88-53137
- Impact and promise of NASA aeropropulsion technology
p 31 N88-16698
- A microprocessor-based real-time simulator of a turbopump engine
[NASA-TM-100889] p 32 N88-21163
- Euler analysis of a swirl recovery vane design for use with an advanced single-rotation propfan
[NASA-TM-101357] p 14 N88-29771
- TURBOFANS**
- Measurements of the unsteady flow field within the stator row of a transonic axial-flow fan. I - Measurement and analysis technique
[ASME PAPER 87-GT-226] p 4 A88-18660
- TURBOJET ENGINES**
- High-speed inlet research program and supporting analyses
p 17 N88-15811
- TURBOMACHINERY**
- Explicit multigrid algorithm for quasi-three-dimensional viscous flows in turbomachinery
p 2 A88-10355
- A method for calculating turbulent boundary layers and losses in the flow channels of turbomachines
[ASME PAPER 87-GT-225] p 2 A88-11121
- Navier-Stokes cascade analysis with a stiff k-epsilon turbulence solver
[AIAA PAPER 88-0594] p 5 A88-22444
- Analysis of eccentric annular incompressible seals. I - A new solution using fast Fourier transforms for determining hydrodynamic force
[ASME PAPER 87-TRIB-52] p 166 A88-23308
- Design and performance of controlled-diffusion stator compared with original double-circular-arc stator
[SAE PAPER 871783] p 20 A88-30777
- Aerodynamically forced vibration analysis of turbomachines
p 20 A88-31610
- Determination of compressor in-stall characteristics from engine surge transients
p 21 A88-35505
- Recent developments in flutter suppression techniques for turbomachinery rotors
p 21 A88-35530
- Comparison of computational methods for three-dimensional turbulent turbomachinery flows
p 6 A88-42452
- Numerical analysis of three-dimensional viscous internal flows
[AIAA PAPER 88-3522] p 142 A88-48779
- Navier-Stokes cascade analysis with a stiff Kappa-Epsilon turbulence solver
[NASA-TM-100218] p 9 N88-10778
- Application of Runge Kutta time marching scheme for the computation of transonic flows in turbomachines
[NASA-TM-86997] p 9 N88-12461
- A multistage mesh generator for solving the average-passage equation system
[NASA-CR-179539] p 10 N88-15769
- Aeropropulsion '87. Session 3: Internal Fluid Mechanics Research
[NASA-CP-10003-SESS-3] p 28 N88-15790
- Turbomachinery
p 28 N88-15792
- Numerical modeling of multidimensional flow in seals and bearings used in rotating machinery
[NASA-TM-100779] p 150 N88-16988
- Numerical analysis of three-dimensional viscous internal flows
[NASA-TM-100878] p 1 N88-21116
- Utilization of parallel processing in solving the inviscid form of the average-passage equation system for multistage turbomachinery
[NASA-TM-89845] p 32 N88-21160
- Aeroelastic forced response analysis of turbomachinery
p 34 N88-23247
- Improved method for stress and compatibility analysis of multicomponent rotating systems
[NASA-TM-100884] p 195 N88-25935
- A diagonally inverted LU implicit multigrid scheme
[NASA-TM-100911] p 13 N88-26340

TURBOPROP AIRCRAFT

- Investigation of the validity of Reynolds averaged turbulence models at the frequencies that occur in turbomachinery p 65 N88-28087
 [NASA-CR-182162]
 An unconditionally stable Runge-Kutta method for unsteady flows p 14 N88-29780
 [NASA-TM-101347]
 Three-dimensional elliptic grid generation technique with application to turbomachinery cascades p 155 N88-30078
 [NASA-TM-101330]
- TURBOPROP AIRCRAFT**
- Noise of a model high speed counterrotation propeller at simulated takeoff/approach conditions (F7/A7) p 214 A88-20176
 [AIAA PAPER 87-2657]
 Noise of a model counterrotation propeller with reduced aft rotor diameter at simulated takeoff/approach conditions (F7/A3) p 214 A88-22192
 [AIAA PAPER 88-0263]
 Aerodynamically forced vibration analysis of turbomachines p 20 A88-31610
 Scale model acoustic testing of counterrotating fans p 22 A88-37947
 [AIAA PAPER 88-2057]
 Noise of a model high speed counterrotation propeller at simulated takeoff/approach conditions (F7/A7) p 216 N88-10592
 [NASA-TM-100206]
 A hybrid numerical technique for predicting the aerodynamic and acoustic fields of advanced turboprops p 216 N88-12352
 [NASA-CR-174926]
 Noise of a model counterrotation propeller with reduced aft rotor diameter at simulated takeoff/approach conditions (F7/A3) p 216 N88-13961
 [NASA-TM-100254]
 NASA advanced turboprop research and concept validation program p 34 N88-22902
 [NASA-TM-100891]
 NASA/industry advanced turboprop technology program p 35 N88-24641
 [NASA-TM-100929]
 Multiple-Purpose Subsonic Naval Aircraft (MPSNA): Multiple Application Propfan Study (MAPS) p 18 N88-28917
 [NASA-CR-175104]
- TURBOPROP ENGINES**
- Advanced turboprop wing installation effects measured by unsteady blade pressure and noise p 3 A88-18655
 [AIAA PAPER 87-2719]
 Parametric studies of advanced turboprops p 20 A88-32223
 [AIAA PAPER 88-2266]
 Application of structural tailoring to spar/shell turboprops p 20 A88-32277
 [AIAA PAPER 88-2333]
 Experimental classical flutter results of a composite advanced turboprop model p 21 A88-35528
 Advanced composite turboprops - Modeling, structural, and dynamic analyses p 21 A88-36745
 [ASME PAPER 87-GT-78]
 Computerized life and reliability modelling for turboprop transmissions p 100 A88-48031
 [AIAA PAPER 88-2979]
 Advanced turboprop wing installation effects measured by unsteady blade pressure and noise p 9 N88-10008
 [NASA-TM-100200]
 Analysis and test evaluation of the dynamic stability of three advanced turboprop models at zero forward speed p 26 N88-14095
 [NASA-CR-175025]
 Analysis and test evaluation of the dynamic response and stability of three advanced turboprop models at low forward speed p 27 N88-14096
 [NASA-CR-175026]
 Impact and promise of NASA aeropropulsion technology p 31 N88-16698
 Computerized life and reliability modelling for turboprop transmissions p 173 N88-23220
 [NASA-TM-100918]
 Experimental and analytical evaluation of the effects of simulated engine inlets on the blade vibratory stresses of the SR-3 model prop-fan p 36 N88-28927
 [NASA-CR-174959]
- TURBOSHAFTS**
- Test stand performance of a convertible engine for advanced V/STOL and rotorcraft propulsion p 21 A88-37217
 [SAE PAPER 872355]
 The design of a turboshaft speed governor using modern control techniques p 170 N88-10339
 [NASA-CR-175046]
 Test stand performance of a convertible engine for advanced V/STOL and rotorcraft propulsion p 25 N88-11679
 [NASA-TM-100211]
 The convertible engine: A dual-mode propulsion system p 31 N88-16639
- TURBULENCE**
- Measurement of local convective heat transfer coefficients from a smooth and roughened NACA-0012 airfoil - Flight test data p 136 A88-22207
 [AIAA PAPER 88-0287]

- K-epsilon turbulence model assessment with reduced numerical diffusion for coaxial jets p 137 A88-22251
 [AIAA PAPER 88-0342]
 Prediction of turbine blade heat transfer p 148 N88-11162
 Flow in a model turbine stator p 148 N88-11163
 Measurement of local convective heat transfer coefficients from a smooth and roughened NACA-0012 airfoil: Flight test data p 149 N88-13552
 [NASA-TM-100284]
 On the correlation of plume centerline velocity decay of turbulent acoustically excited jets p 11 N88-16681
 [NASA-TM-100193]
 Two-equation low-Reynolds-number turbulence modeling of transitional boundary layer flows characteristic of gas turbine blades p 153 N88-23185
 [NASA-CR-4145]
 Experimental study of bypass transition in a boundary layer p 153 N88-23186
 [NASA-TM-100913]
 The effects of inlet turbulence and rotor/stator interactions on the aerodynamics and heat transfer of a large-scale rotating turbine model. Part 4: Aerodynamic data tabulation p 153 N88-23956
 [NASA-CR-179469]
 Correlations of velocity and temperature fluctuations in the stagnation-point flow of circular cylinder in turbulent flow p 13 N88-25435
 [NASA-TM-100930]
 The effects of inlet turbulence and rotor/stator interactions on the aerodynamics and heat transfer of a large-scale rotating turbine model. Volume 3: Heat transfer data tabulation 65 percent axial spacing p 37 N88-28930
 [NASA-CR-179468]
 The effects of inlet turbulence and rotor/stator interactions on the aerodynamics and heat transfer of a large-scale rotating turbine model. Volume 2: Heat transfer data tabulation, 15 percent axial spacing p 37 N88-29804
 [NASA-CR-179467]
- TURBULENCE EFFECTS**
- Initial turbulence effect on jet evolution with and without tonal excitation p 4 A88-20184
 [AIAA PAPER 87-2725]
 The effects of turbulence and stator/rotor interactions on turbine heat transfer. I - Design operating conditions p 145 A88-54236
 [ASME PAPER 88-GT-125]
- TURBULENCE METERS**
- Measurements of the turbulent transport of heat and momentum in convexly curved boundary layers - Effects of curvature, recovery and free-stream turbulence p 131 A88-11103
 [ASME PAPER 87-GT-199]
- TURBULENCE MODELS**
- Investigation of third-order closure model of turbulence for the computation of incompressible flows in a channel with a backward-facing step p 136 A88-21273
 Mathematical models for the numerical study of turbulent flows p 140 A88-39472
 Investigation of the validity of Reynolds averaged turbulence models at the frequencies that occur in turbomachinery p 65 N88-28087
 [NASA-CR-182162]
- TURBULENCE BOUNDARY LAYER**
- A method for calculating turbulent boundary layers and losses in the flow channels of turbomachines p 2 A88-11121
 [ASME PAPER 87-GT-225]
 The measurement of boundary layers on a compressor blade in cascade. II - Suction surface boundary layers p 132 A88-11131
 [ASME PAPER 87-GT-249]
 Effects of nozzle-exit boundary-layer conditions on excitability of heated free jets p 135 A88-20182
 [AIAA PAPER 87-2723]
 Skin friction measurements by laser interferometry in swept shock wave/turbulent boundary-layer interactions p 5 A88-22364
 [AIAA PAPER 88-0497]
 Glancing shock wave-turbulent boundary layer interaction with boundary layer suction p 6 A88-27718
 [AIAA PAPER 88-0308]
 Turbulence modeling and surface heat transfer in a stagnation flow region p 141 A88-43871
 Hypersonic turbulent wall boundary layer computations p 7 A88-44667
 [AIAA PAPER 88-2829]
 Structure of a reattaching supersonic shear flow p 8 A88-48901
 [AIAA PAPER 88-3615]
 Boundary layer development as a function of chamber pressure in the NASA Lewis 1030:1 area ratio rocket nozzle p 144 A88-50786
 [AIAA PAPER 88-3301]
 Heat transfer with very high free stream turbulence p 148 N88-11161
 Hypersonic turbulent wall boundary layer computations p 154 N88-24917
 [NASA-CR-182147]
 Correlations of velocity and temperature fluctuations in the stagnation-point flow of circular cylinder in turbulent flow p 13 N88-25435
 [NASA-TM-100930]

- Boundary layer development as a function of chamber pressure in the NASA Lewis 1030:1 area ratio rocket nozzle p 154 N88-25841
 [NASA-TM-100917]
 Experimental and numerical investigation of the effect of distributed suction on oblique shock wave/turbulent boundary layer interaction p 156 N88-30084
 [NASA-TM-101334]
- TURBULENCE FLOW**
- Effect of rib angle on local heat/mass transfer distribution in a two-pass rib-roughened channel p 131 A88-11033
 [ASME PAPER 87-GT-94]
 A method for calculating turbulent boundary layers and losses in the flow channels of turbomachines p 2 A88-11121
 [ASME PAPER 87-GT-225]
 Infrared properties of an anisotropically stirred fluid p 134 A88-16354
- Control of free shear layers p 134 A88-16545
 [AIAA PAPER 87-2689]
 Aeroacoustics of subsonic turbulent shear flows p 214 A88-16571
 [AIAA PAPER 87-2731]
 Investigation of third-order closure model of turbulence for the computation of incompressible flows in a channel with a backward-facing step p 136 A88-21273
 Low Reynolds number modeling of turbulent flows with and without wall transpiration p 136 A88-21983
 Vapor condensation rate at a turbulent liquid interface, for application to cryogenic hydrogen p 137 A88-22419
 [AIAA PAPER 88-0559]
 Navier-Stokes cascade analysis with a stiff k-epsilon turbulence solver p 5 A88-22444
 [AIAA PAPER 88-0594]
 A numerical study of the effects of curvature and convergence on dilution jet mixing p 137 A88-23312
 [AIAA PAPER 87-1953]
 Mixing, transport and combustion in sprays p 138 A88-25828
 Excitation of instability waves in free shear layers. II - Experiments p 138 A88-26339
 Time-accurate simulations of a shear layer forced at a single frequency p 138 A88-27716
 [AIAA PAPER 88-0061]
 Explicit finite-volume time-marching calculations of total temperature distributions in turbulent flow p 139 A88-30517
 An explicit finite-volume time-marching procedure for turbulent flow calculations p 139 A88-30518
 Four spot laser anemometer and optical access techniques for turbine applications p 159 A88-36513
 Mathematical models for the numerical study of turbulent flows p 140 A88-39472
 Turbulence energy and diffusion transport of third-moments in a separating and reattaching flow p 141 A88-43011
 Turbulence modeling in hypersonic inlets p 7 A88-44705
 [AIAA PAPER 88-2957]
 Experimental verification of a secondary recirculation zone in a labyrinth seal p 168 A88-48971
 [AIAA PAPER 88-3692]
 Diagnostics development for spray characterization in complex turbulent flows p 146 A88-54320
 [ASME PAPER 88-GT-241]
 Navier-Stokes cascade analysis with a stiff Kappa-Epsilon turbulence solver p 9 N88-10778
 [NASA-TM-100218]
 The four spot time-of-flight laser anemometer p 164 N88-11145
 Correlation of velocity and velocity-density turbulence in the exhaust of an atmospheric burner p 161 N88-11147
 Improved numerical methods for turbulent viscous recirculating flows p 146 N88-11148
 Aerothermal modeling program, phase 2 p 146 N88-11149
 Fuel-injector/air-swirl characterization p 146 N88-11150
 Measurement of airfoil heat transfer coefficients on a turbine stage p 147 N88-11158
 A numerical study of the effects of curvature and convergence on dilution jet mixing p 26 N88-13347
 [NASA-TM-89878]
 Chemical reacting flows p 79 N88-15793
 Optical measurement systems p 218 N88-15796
 The effect of eddy distribution on momentum and heat transfer near the wall in turbulent pipe flow p 150 N88-15984
 [NASA-TM-100257]
 Numerical simulation of axisymmetric turbulent flow in combustors and diffusers p 11 N88-17582
 [NASA-CR-4115]
 Time-accurate simulations of a shear layer forced at a single frequency p 152 N88-19740
 [NASA-TM-100836]
 Improved numerical methods for turbulent viscous recirculating flows p 13 N88-25445
 [NASA-CR-180852]

- Direct simulations of chemically reacting turbulent mixing layers, part 2
[NASA-CR-180853] p 154 N88-25857
- Evolution of hairpin vortices in a shear flow
[NASA-TM-100858] p 211 N88-26885
- TURBULENT HEAT TRANSFER**
Measurements of the turbulent transport of heat and momentum in convexly curved boundary layers - Effects of curvature, recovery and free-stream turbulence
[ASME PAPER 87-GT-199] p 131 A88-11103
- Turbulence modeling and surface heat transfer in a stagnation flow region
p 141 A88-43871
- The effects of turbulence and stator/rotor interactions on turbine heat transfer. II - Effects of Reynolds number and incidence
[ASME PAPER 88-GT-5] p 145 A88-54152
- TURBULENT JETS**
On the correlation of plume centerline velocity decay of turbulent acoustically excited jets
[AIAA PAPER 87-2692] p 3 A88-18654
- Initial turbulence effect on jet evolution with and without tonal excitation
[AIAA PAPER 87-2725] p 4 A88-20184
- K-epsilon turbulence model assessment with reduced numerical diffusion for coaxial jets
[AIAA PAPER 88-0342] p 137 A88-22251
- Controlled excitation of a cold turbulent swirling free jet
[ASME PAPER 87-WA/NCA-18] p 140 A88-41568
- Particle-laden weakly swirling free jets - Measurements and predictions
[AIAA PAPER 88-3138] p 142 A88-48757
- Effect of initial tangential velocity distribution on the mean evolution of a swirling turbulent free jet
[AIAA PAPER 88-3592] p 7 A88-48893
- Effect of initial tangential velocity distribution on the mean evolution of a swirling turbulent free jet
[NASA-TM-100934] p 12 N88-24592
- Particle-laden weakly swirling free jets: Measurements and predictions
[NASA-TM-100920] p 34 N88-24639
- TURBULENT MIXING**
Direct simulations of chemically reacting turbulent mixing layers, part 2
[NASA-CR-180853] p 154 N88-25857
- TURBULENT WAKES**
Experiments on spray interactions in the wake of a bluff body
[ASME PAPER 87-GT-48] p 131 A88-11000
- A natural low frequency oscillation in the wake of an airfoil near stalling conditions
[AIAA PAPER 88-0131] p 4 A88-22093
- A natural low frequency oscillation in the wake of an airfoil near stalling conditions
[NASA-TM-100213] p 9 N88-10779
- TWISTING**
Parametric studies of advanced turboprops
[AIAA PAPER 88-2266] p 20 A88-32223
- TWO DIMENSIONAL BODIES**
Electromagnetic propagation in PEC and absorbing curved S-ducts
[NASA-TM-100833] p 120 N88-19698
- Two-dimensional graphics tools for a transputer based display board
[NASA-TM-100820] p 207 N88-22591
- TWO DIMENSIONAL BOUNDARY LAYER**
Prediction of turbine blade heat transfer
p 148 N88-11162
- TWO DIMENSIONAL FLOW**
The measurement of boundary layers on a compressor blade in cascade. I - A unique experimental facility
[ASME PAPER 87-GT-248] p 131 A88-11130
- Coherent motion induced fluctuations in the primary transition region of a plane shear layer
p 133 A88-14125
- A mapped finite difference study of noise propagation in nonuniform ducts with mean flow
p 214 A88-18541
- The structure and dynamics of reacting plane mixing layers
p 136 A88-20871
- An explicit finite-volume time-marching procedure for turbulent flow calculations
p 139 A88-30518
- Third-order multi-dimensional Euler/Navier-Stokes solver
[AIAA PAPER 88-3645] p 209 A88-48806
- Two-dimensional viscous flow computations of hypersonic scramjet nozzle flowfields at design and off-design conditions
[AIAA PAPER 88-3280] p 23 A88-50785
- Two-dimensional viscous flow computations of hypersonic scramjet nozzle flowfields at design and off-design conditions
[NASA-CR-182150] p 35 N88-25459
- Analysis and optimization of truncated scarf nozzles subject to external flow conditions
[NASA-TM-100955] p 14 N88-29746
- TWO DIMENSIONAL JETS**
Techniques utilized in the simulated altitude testing of a 2D-CD vectoring and reversing nozzle
[NASA-TM-100872] p 40 N88-25464
- TWO FLUID MODELS**
Dynamics of two fluids under periodic acceleration
[AIAA PAPER 88-3728] p 143 A88-48980
- TWO PHASE FLOW**
Local convective flows in partly solidified alloys
p 219 A88-18467
- Performance of laser Doppler velocimeter with polydisperse seed particles in high speed flows
[AIAA PAPER 88-0425] p 157 A88-22317
- Gas liquid flow at microgravity conditions - Flow patterns and their transitions
p 141 A88-42839
- U**
- UDIMET ALLOYS**
Sodium sulfate-induced corrosion of pure nickel and superalloy Udimet 700 in a high velocity burner rig at 900 C
p 83 A88-20266
- ULTRASONIC FLAW DETECTION**
Acoustic imaging of subtle porosity variations in ceramics
p 101 A88-55044
- Nondestructive evaluation by acousto-ultrasonics
p 177 N88-22412
- Characterization of sintered SiC by using NDE
p 177 N88-22413
- Systems for ultrasonic scanning, analysis and imagery
p 177 N88-22414
- ULTRASONIC RADIATION**
Materials analysis by ultrasonics: Metals, ceramics, composites --- Book
p 176 A88-44853
- Imaging subtle microstructural variations in ceramics with precision ultrasonic velocity and attenuation measurements
[NASA-TM-100129] p 177 N88-15257
- ULTRASONIC SCANNERS**
Measurement of ice thickness (icing) in aeronautics
p 15 A88-32714
- ULTRASONIC TESTS**
Ultrasonic nondestructive evaluation, microstructure, and fracture toughness interrelations
p 176 A88-18158
- Ultrasonic evaluation of mechanical properties of thick, multilayered, filament-wound composites
p 176 A88-21340
- Improved maintainability of space-based reusable rocket engines
[AIAA PAPER 88-3113] p 55 A88-48037
- Transply crack density detection by acousto-ultrasonics
[NASA-TM-100224] p 72 N88-11758
- Flaw imaging and ultrasonic techniques for characterizing sintered silicon carbide
[NASA-TM-100177] p 177 N88-12106
- Acousto-ultrasonic input-output characterization of unidirectional fiber composite plate by SV waves
[NASA-CR-4152] p 178 N88-23224
- High frequency ultrasonic characterization of sintered SiC
[NASA-TM-100825] p 179 N88-23985
- Input-output characterization of fiber composites by SH waves
[NASA-CR-4153] p 179 N88-23986
- Characterization of noncontact piezoelectric transducer with conically shaped piezoelement
[NASA-CR-4151] p 179 N88-23987
- ULTRASONIC WAVE TRANSDUCERS**
Ultrasonic evaluation of mechanical properties of thick, multilayered, filament-wound composites
p 176 A88-21340
- Acousto-ultrasonics as a monitor of material anisotropy
p 176 A88-46828
- In-flight measurement of airfoil icing using an array of ultrasonic transducers
p 15 A88-50910
- Ultrasonic techniques for aircraft ice accretion measurement
[AIAA PAPER 88-4656] p 18 A88-51910
- In-flight measurement of ice growth on an airfoil using an array of ultrasonic transducers
[AIAA-87-0178] p 16 N88-23717
- UNIVERSE**
Primordial origin of nontopological solitons
p 226 A88-39313
- Primordial nucleosynthesis with decaying particles. I - Entropy-producing decays. II - Inert decays
p 217 A88-47477
- UNIVERSITIES**
Institute for Computational Mechanics in Propulsion (ICOMP)
[NASA-TM-100790] p 211 N88-19202
- UNSTEADY AERODYNAMICS**
Application of a semianalytical technique for sensitivity analysis of unsteady aerodynamic computations
[AIAA PAPER 88-2377] p 6 A88-32314
- Unsteady features of jets in lift and cruise modes for VTOL aircraft
[SAE PAPER 872359] p 6 A88-37220
- Unsteady aerodynamics of an oscillating cascade in a compressible flow field
[NASA-TM-100219] p 26 N88-13346
- A semianalytical technique for sensitivity analysis of unsteady aerodynamic computations
[NASA-TM-100810] p 189 N88-18976
- Experimental determination of aerodynamic damping in a three-stage transonic axial-flow compressor
[NASA-TM-100953] p 35 N88-27200
- Investigation of oscillating cascade aerodynamics by an experimental influence coefficient technique
[NASA-TM-101313] p 14 N88-28041
- Aeroelastic response of metallic and composite propfan models in yawed flow
[NASA-TM-100964] p 37 N88-29807
- UNSTEADY FLOW**
Chordwise pressure measurements on a blade of Mod-2 Wind Turbine
p 2 A88-10970
- Advanced turboprop wing installation effects measured by unsteady blade pressure and noise
[AIAA PAPER 87-2719] p 3 A88-18655
- Measurements of the unsteady flow field within the stator row of a transonic axial-flow fan. I - Measurement and analysis technique
[ASME PAPER 87-GT-226] p 4 A88-18660
- Measurements of the unsteady flow field within the stator row of a transonic axial-flow fan. II - Results and discussion
[ASME PAPER 87-GT-227] p 4 A88-18661
- An explicit Runge-Kutta method for unsteady rotor/stator interaction
[AIAA PAPER 88-0049] p 5 A88-27715
- Unsteady features of jets in lift and cruise modes for VTOL aircraft
[SAE PAPER 872359] p 6 A88-37220
- Unsteady motion and transition to turbulence in developing curved duct flow
p 140 A88-39010
- Nonlinear roll-up of externally excited free shear layers
p 141 A88-44445
- A diagonally inverted LU implicit multigrid scheme
[AIAA PAPER 88-3565] p 209 A88-48791
- Advanced turboprop wing installation effects measured by unsteady blade pressure and noise
[NASA-TM-100200] p 9 N88-10008
- Application of Runge Kutta time marching scheme for the computation of transonic flows in turbomachines
[NASA-TM-86997] p 9 N88-12461
- Unsteady aerodynamics of an oscillating cascade in a compressible flow field
[NASA-TM-100219] p 26 N88-13346
- An explicit Runge-Kutta method for unsteady rotor/stator interaction
[NASA-TM-100787] p 10 N88-14967
- Advanced propeller research
p 29 N88-15806
- Unsteady heat transfer in turbine blade ducts: Focus on combustor sources
p 151 N88-18870
- [NASA-TM-100815] p 118 N88-18870
- An unconditionally stable Runge-Kutta method for unsteady flows
[NASA-TM-101347] p 14 N88-29780
- UPLINKING**
A statistical rain attenuation prediction model with application to the advanced communication technology satellite project. Part 2: Theoretical development of a dynamic model and application to rain fade durations and tolerable control delays for fade countermeasures
[NASA-TM-100242] p 118 N88-11945
- Experimental radio frequency link for Ka-band communications applications
[NASA-TM-100824] p 43 N88-24659
- A statistical rain attenuation prediction model with application to the advanced communication technology satellite project. 1: Theoretical development and application to yearly predictions for selected cities in the United States
[NASA-CR-179498] p 121 N88-29077

URBAN TRANSPORTATION

- Adiabatic diesel engine component development:
Reference engine for on-highway applications
[NASA-CR-179531] p 224 N88-12428
- USER MANUALS (COMPUTER PROGRAMS)**
- Blade loss transient dynamics analysis, volume 2. Task 2: TETRA 2 user's manual
[NASA-CR-179633] p 25 N88-10792
- Numerical arc segmentation algorithm for a radio conference-NASARC, version 2.0: User's manual
[NASA-TM-100161] p 119 N88-16928
- User's manual for the two-dimensional transputer graphics toolkit
[NASA-TM-100974] p 207 N88-27799
- User's manual for three dimensional boundary layer (BL3-D) code
[NASA-CR-174899] p 155 N88-30063
- USER REQUIREMENTS**
- Electrical Power Working Group report
p 48 N88-10095
- Small reactor power systems for manned planetary surface bases
[NASA-TM-100223] p 227 N88-13209
- Advanced development of double-injection, deep-impurity semiconductor switches
[NASA-CR-182118] p 222 N88-25346

V

V/STOL AIRCRAFT

- Flight propulsion control integration for V/STOL aircraft
[SAE PAPER 872330] p 21 A88-37199
- NASA supersonic STOVL propulsion technology program
[SAE PAPER 872352] p 21 A88-37215
- Test stand performance of a convertible engine for advanced V/STOL and rotorcraft propulsion
[SAE PAPER 872355] p 21 A88-37217
- A numerical study of the hot gas environment around a STOVL aircraft in ground proximity
[AIAA PAPER 88-2882] p 23 A88-48752
- Test stand performance of a convertible engine for advanced V/STOL and rotorcraft propulsion
[NASA-TM-100211] p 25 N88-11679
- Flight propulsion control integration for V/STOL aircraft
[NASA-TM-100226] p 38 N88-11680
- NASA supersonic STOVL propulsion technology program
[NASA-TM-100227] p 26 N88-14093
- A numerical study of the hot gas environment around a STOVL aircraft in ground proximity
[NASA-TM-100895] p 1 N88-23729

VACUUM

- High frequency power distribution system
[NASA-CR-175071] p 129 N88-23939

VACUUM DEPOSITION

- Design and demonstration of a system for the deposition of atomic-oxygen durable coatings for reflective solar dynamic power system concentrators
[NASA-CR-4158] p 64 N88-25474

VANADIUM OXIDES

- Deposition of vanadium oxide films by direct-current magnetron reactive sputtering
p 221 A88-51286

VANES

- Use of a liquid-crystal and heater-element composite for quantitative, high-resolution heat-transfer coefficients on a turbine airfoil including turbulence and surface-roughness effects
p 156 A88-10969
- Experimental evaluation of corner vanes - Summary
[SAE PAPER 871784] p 39 A88-30778
- Turbine Engine Hot Section Technology, 1985
[NASA-CP-2405] p 185 N88-11140
- Development of heat flux sensors for turbine airfoils
p 160 N88-11143
- Component specific modeling
p 206 N88-11166
- Constitutive modeling for isotropic materials
p 186 N88-11172
- Turbine airfoil deposition models and their hot corrosion implications
p 91 N88-11178
- Experimental evaluation of a translating nozzle sidewall radial turbine
p 31 N88-17656
- Euler analysis of a swirl recovery vane design for use with an advanced single-rotation propfan
[NASA-TM-101357] p 14 N88-29771

VAPOR DEPOSITION

- Behavior of ion-implanted junction diodes in 3C SiC
p 122 A88-15423
- Electrical resistivity (4K to 2100K) of annealed vapor growth carbon fibers
p 96 A88-17214
- Electron-spin-resonance studies of vapor-grown carbon fibers
p 96 A88-17368
- Lattice defects in beta-SiC grown epitaxially on silicon substrates
p 220 A88-28711

- Microscopy of epitaxially grown beta-SiC on 001-plane silicon
p 98 A88-31023
- Laser induced OMCVD growth of AlGaAs on GaAs
p 125 A88-34286
- Chemical vapor deposited silica coatings for solar mirror protection
[AIAA PAPER 88-0027] p 99 A88-41796
- Significance of vapor phase chemical reactions on CVD rates predicted by chemically frozen and local thermochemical equilibrium boundary layer theories
p 78 A88-44424
- Temperature stability of Al(x)Ga(1-x)As (x = 0-1) thermal oxide masks for selective-area epitaxy
p 221 A88-45858
- Low-temperature photoluminescence studies of chemical-vapor-deposition-grown 3C-SiC on Si
p 127 A88-53396
- Raman scattering studies of chemical-vapor-deposited cubic SiC films of (100)Si
p 127 A88-53397
- Experimental verification of vapor deposition rate theory in high velocity burner rigs
p 91 N88-11179
- High-temperature electronics
p 128 N88-15797
- Chemical vapor deposited silica coatings for solar mirror protection
[NASA-TM-100834] p 105 N88-21306
- SiC fiber reinforced reaction-bonded Si3N4 composites
p 75 N88-23892
- Indium-coated rhenium thrusters by CVD
[NASA-TM-101309] p 67 N88-29874

VAPOR PHASE EPITAXY

- Lattice defects in beta-SiC grown epitaxially on silicon substrates
p 220 A88-28711
- Microscopy of epitaxially grown beta-SiC on 001-plane silicon
p 98 A88-31023

VAPOR PHASES

- A thermodynamic prediction for microporosity formation in aluminum-rich Al-Cu alloys
p 82 A88-18886
- Significance of vapor phase chemical reactions on CVD rates predicted by chemically frozen and local thermochemical equilibrium boundary layer theories
p 78 A88-44424
- Direct mass spectrometric identification of silicon oxychloride compounds
p 78 A88-44425

VAPORIZERS

- Development of a liquid-fed water resistojet
[AIAA PAPER 88-3288] p 142 A88-48762
- Development of a liquid-fed water resistojet
[NASA-TM-100927] p 174 N88-24968

VAPORIZING

- Droplet vaporization in a supercritical microgravity environment
[IAF PAPER 87-384] p 134 A88-16055
- Numerical study of multicomponent droplet vaporization at near critical conditions
[AIAA PAPER 88-0637] p 108 A88-27721
- Liquid sprays and flow studies in the direct-injection diesel engine under motored conditions
[NASA-TM-100135] p 31 N88-18594

VAPORS

- Criteria for significance of simultaneous presence of both condensable vapors and aerosol particles on mass transfer (deposition) rates
p 114 A88-10971

VARIABILITY

- Component variations and their effects on bipolar nickel-hydrogen cell performance
p 197 A88-11914

VARIABLE GEOMETRY STRUCTURES

- Test stand performance of a convertible engine for advanced V/STOL and rotorcraft propulsion
[SAE PAPER 872355] p 21 A88-37217
- Test stand performance of a convertible engine for advanced V/STOL and rotorcraft propulsion
[NASA-TM-100211] p 25 N88-11679

VARIATIONAL PRINCIPLES

- A mixed formulation of C(0)-linear triangular plate/shell element - The role of edge shear constraints
p 183 A88-40121

VARIATIONS

- Correlations of velocity and temperature fluctuations in the stagnation-point flow of circular cylinder in turbulent flow
[NASA-TM-100930] p 13 N88-25435

VECTOR ANALYSIS

- Approximate polynomial preconditioning applied to biharmonic equations on vector supercomputers
[NASA-TM-100217] p 210 N88-10563

VECTORS (MATHEMATICS)

- Implementation of a digital optical matrix-vector multiplier using a holographic look-up table and residue arithmetic
[NASA-CR-180431] p 205 N88-10496

VELOCITY

- Ultrasonic evaluation of mechanical properties of thick, multilayered, filament-wound composites
p 176 A88-21340

- Imaging subtle microstructural variations in ceramics with precision ultrasonic velocity and attenuation measurements
[NASA-TM-100129] p 177 N88-15257
- Effect of mass-velocity on liquid jet atomization in Mach 1 gasflow
[NASA-TM-100813] p 162 N88-23194

VELOCITY DISTRIBUTION

- On the correlation of plume centerline velocity decay of turbulent acoustically excited jets
[AIAA PAPER 87-2692] p 3 A88-18654
- Absolute instability of the Gaussian wake profile
p 136 A88-20842
- Computation of the velocity field of an excited shear layer
p 138 A88-26206
- Cosmic string induced peculiar velocities
p 226 A88-28762
- Temperature and velocity profiles in sooting free convection diffusion flames
p 78 A88-43018
- Effect of initial tangential velocity distribution on the mean evolution of a swirling turbulent free jet
[AIAA PAPER 88-3592] p 7 A88-48893
- Effect of initial tangential velocity distribution on the mean evolution of a swirling turbulent free jet
[NASA-TM-100934] p 12 N88-24592

VELOCITY MEASUREMENT

- Real time optical correlator using a magneto-optic device applied to particle imaging velocimetry
p 159 A88-40700
- Application of optical correlation techniques to particle imaging velocimetry
[NASA-TM-101306] p 163 N88-29152

VERTICAL LANDING

- Aeroacoustics of advanced STOVL aircraft plumes
[SAE PAPER 872358] p 215 A88-30998
- Acoustics technologies for STOVL aircraft
[AIAA PAPER 88-2238] p 215 A88-35939
- Aeroacoustics of advanced STOVL aircraft plumes
[SAE PAPER 872358] p 215 A88-37219
- STOVL acoustic fatigue technologies
[SAE PAPER 872360] p 215 A88-37221
- A numerical study of the hot gas environment around a STOVL aircraft in ground proximity
[AIAA PAPER 88-2882] p 23 A88-48752
- A numerical study of the hot gas environment around a STOVL aircraft in ground proximity
[NASA-TM-100895] p 1 N88-23729

VERTICAL TAKEOFF AIRCRAFT

- Unsteady features of jets in lift and cruise modes for VTOL aircraft
[SAE PAPER 872359] p 6 A88-37220

VIBRATION

- Vibration and flutter characteristics of the SR7L large-scale propfan
[NASA-TM-100272] p 188 N88-18036
- A review of gear housing dynamics and acoustics literature
[NASA-CR-183110] p 175 N88-26675
- Containment of a silicone fluid free surface in reduced gravity using barrier coatings
[NASA-TM-101314] p 155 N88-30072

VIBRATION DAMPING

- Experiments on dynamic stiffness and damping of tapered bore seals
p 166 A88-31527
- Evaluation of a turbine blade damper using an integral approach
[AIAA PAPER 88-2400] p 20 A88-32332
- Recent developments in flutter suppression techniques for turbomachinery rotors
p 21 A88-35530
- Experimental vibration damping characteristics of the third-stage rotor of a three-stage transonic axial-flow compressor
[AIAA PAPER 88-3229] p 23 A88-48759
- Frequency domain solutions to multi-degree-of-freedom, dry friction damped systems
p 184 A88-49714
- Control of rotor aerodynamically forced vibrations by splitters
p 23 A88-52684
- Active control of transient rotordynamic vibration by optimal control methods
[ASME PAPER 88-GT-73] p 208 A88-54202
- Lewis Structures Technology, 1988. Volume 1: Structural Dynamics
[NASA-CP-3003-VOL-1] p 194 N88-23226
- Vibration and control of flexible rotor supported by magnetic bearings
[NASA-TM-100888] p 174 N88-23977
- Experimental vibration damping characteristics of the third-stage rotor of a three-stage transonic axial-flow compressor
[NASA-TM-100948] p 35 N88-24642
- VIBRATION EFFECTS**
- Dynamics of two fluids under periodic acceleration
[AIAA PAPER 88-3728] p 143 A88-48980

VIBRATION MEASUREMENT

Identification of differences between finite element analysis and experimental vibration data p 183 A88-46666

VISCOELASTICITY

A nonlinear viscoelastic constitutive equation - Yield predictions in multiaxial deformations p 185 A88-54912
Linear and nonlinear mechanical properties of a series of epoxy resins p 101 A88-54976

VISCOPLASTICITY

Plasticity analysis of wear phenomena as an aid in the development of abrasible materials p 164 A88-10938
Thermo-elasto-viscoplastic analysis of problems in extension and shear p 183 A88-41042
Structure of a viscoplastic theory [NASA-TM-100794] p 188 A88-18968
A viscoplastic theory applied to copper [NASA-TM-100831] p 189 A88-21497
Nonlinear Constitutive Relations for High Temperature Applications, 1986 [NASA-CP-10010] p 189 A88-21498
A simplified orthotropic formulation of the viscoplasticity theory based on overstress p 189 A88-21505
A theory of viscoplasticity accounting for internal damage p 190 A88-21508
Non-isothermal elastoviscoplastic analysis of planar curved beams p 190 A88-21526
Biaxial experiments supporting the development of constitutive theories for advanced high-temperature materials p 191 A88-22386
Finite element (MARC) solution technologies for viscoplastic analyses p 191 A88-22389

VISCOSITY

Quantitative characterization of the viscosity of a microemulsion p 77 A88-11167
Piezoviscous effects in nonconformal contacts lubricated hydrodynamically p 133 A88-12926
The effects of rotational flow, viscosity, thickness, and shape on transonic flutter dip phenomena [AIAA PAPER 88-2348] p 182 A88-32289
Critical exponent for the viscosity of four binary liquids p 222 A88-53050
The effects of rotational flow, viscosity, thickness, and shape on transonic flutter dip phenomena [NASA-TM-100811] p 188 A88-18969

VISCOUS DAMPING

Identification of differences between finite element analysis and experimental vibration data p 183 A88-46666

VISCOUS FLOW

Explicit multigrid algorithm for quasi-three-dimensional viscous flows in turbomachinery p 2 A88-10355
A space-marching method for the computation of viscous internal flows p 135 A88-20459
Absolute instability of the Gaussian wake profile p 136 A88-20842
A numerical study of the effects of curvature and convergence on dilution jet mixing [AIAA PAPER 87-1953] p 137 A88-23312
Consistent boundary conditions for reduced Navier-Stokes (RNS) scheme applied to three-dimensional internal viscous flows [AIAA PAPER 88-0714] p 139 A88-27723
Explicit finite-volume time-marching calculations of total temperature distributions in turbulent flow p 139 A88-30517
An explicit finite-volume time-marching procedure for turbulent flow calculations p 139 A88-30518
Numerical analysis of three-dimensional viscous internal flows [AIAA PAPER 88-3522] p 142 A88-48779
Three-dimensional viscous flow computations of a circular jet in subsonic and supersonic cross flow [AIAA PAPER 88-3703] p 143 A88-48916
Three-dimensional flow past two cylinders mounted side by side on an endwall [AIAA PAPER 88-3718] p 143 A88-48974
Two-dimensional viscous flow computations of hypersonic scramjet nozzle flowfields at design and off-design conditions [AIAA PAPER 88-3280] p 23 A88-50785
Improved numerical methods for turbulent viscous recirculating flows p 146 A88-11148
Similar solutions for viscous hypersonic flow over a slender three-fourths-power body of revolution [NASA-TM-100205] p 148 A88-12752
A numerical study of the effects of curvature and convergence on dilution jet mixing [NASA-TM-89878] p 26 A88-13347
Consistent boundary conditions for Reduced Navier-Stokes (RNS) scheme applied to 3-dimensional internal viscous flows [NASA-CR-180874] p 10 A88-15762

Numerical analysis of three-dimensional viscous internal flows [NASA-TM-100878] p 1 A88-21116
Improved numerical methods for turbulent viscous recirculating flows [NASA-CR-180852] p 13 A88-25445
Two-dimensional viscous flow computations of hypersonic scramjet nozzle flowfields at design and off-design conditions [NASA-CR-182150] p 35 A88-25459
Three-dimensional viscous flow computations of a circular jet in subsonic and supersonic cross flow [NASA-CR-182153] p 155 A88-26616

VISCOUS FLUIDS

Containment of a silicone fluid free surface in reduced gravity p 112 A88-49085

VOICE OF AMERICA

Complementary satellite sound broadcasting systems: A NASA assessment for the Voice of America [NASA-TM-100300] p 119 A88-17899

VOIDS

Flow characterization in structural ceramics using scanning laser acoustic microscopy p 177 A88-22415

VOLT-AMPERE CHARACTERISTICS

Evaluation studies on carbon supported catalysts for oxygen reduction in alkaline medium p 77 A88-16643

VOLTAGE CONVERTERS (AC TO AC)

A cascaded Schwarz converter for high frequency power distribution p 127 A88-54713

VOLTAGE REGULATORS

Field oriented control of an induction machine in a high frequency link power system p 127 A88-54711
A cascaded Schwarz converter for high frequency power distribution p 127 A88-54713

VORTEX SHEDDING

A numerical investigation of the influence of heating on the excitation of high and low Mach number jet flows [ASME PAPER 87-WA/NCA-13] p 144 A88-51343

VORTICES

Roles of initial condition and vortex pairing in jet noise p 213 A88-13963
The effects of rotational flow, viscosity, thickness, and shape on transonic flutter dip phenomena [AIAA PAPER 88-2348] p 182 A88-32289
Experimental studies in vortex pair motion coincident with a liquid reaction p 142 A88-46316
The effect of eddy distribution on momentum and heat transfer near the wall in turbulent pipe flow [NASA-TM-100257] p 150 A88-15984
The effects of rotational flow, viscosity, thickness, and shape on transonic flutter dip phenomena [NASA-TM-100811] p 188 A88-18969
Evolution of hairpin vortices in a shear flow [NASA-TM-100858] p 211 A88-26885

VORTICITY

Roll-up of vorticity in adverse-pressure-gradient boundary layers p 135 A88-19194
Time-accurate simulations of a shear layer forced at a single frequency [AIAA PAPER 88-0061] p 138 A88-27716
Time-accurate simulations of a shear layer forced at a single frequency [NASA-TM-100836] p 152 A88-19740

W

WAKES

Absolute instability of the Gaussian wake profile p 136 A88-20842

WALL FLOW

Wall shear stress measurement in blade end-wall corner region [ASME PAPER 87-GT-181] p 131 A88-11089
Laser Doppler velocimeter measurement of annulus wall boundary layer development in a compressor rotor [ASME PAPER 87-GT-251] p 132 A88-11133
A model of the wall boundary layer for ducted propellers [AIAA PAPER 87-2742] p 214 A88-16578
Low Reynolds number modeling of turbulent flows with and without wall transpiration p 136 A88-21983
Local heat/mass transfer distributions around sharp 180 deg turns in two-pass smooth and rib-roughened channels [ASME PAPER 86-GT-114] p 139 A88-28516
Hypersonic turbulent wall boundary layer computations [AIAA PAPER 88-2829] p 7 A88-44667
Effect of stage loading on endwall flows in an axial flow compressor rotor [ASME PAPER 88-GT-111] p 145 A88-54229
The effect of eddy distribution on momentum and heat transfer near the wall in turbulent pipe flow [NASA-TM-100257] p 150 A88-15984
Hypersonic turbulent wall boundary layer computations [NASA-CR-182147] p 154 A88-24917

Evolution of hairpin vortices in a shear flow [NASA-TM-100858] p 211 A88-26885

WALL JETS

Transition mixing study empirical model report [NASA-CR-182139] p 155 A88-30076

WALLS

Electromagnetic fields backscattered from an s-shaped inlet cavity with an absorber coating on its inner walls [NASA-CR-182401] p 118 A88-15130

WANKEL ENGINES

Performance and combustion characteristics of direct-injection stratified-charge rotary engines [NASA-TM-100134] p 25 A88-12490

WASPALLOY

Effect of temperature, microstructure, and stress state on the low cycle fatigue behavior of Waspalloy p 87 A88-35922

WATER

Water-propellant resistojets for man-tended platforms [IAF PAPER 87-259] p 54 A88-15975
Operating envelopes of particle sizing instrumentation used for icing research [AIAA PAPER 88-0291] p 157 A88-22211
Development of a liquid-fed water resistojets [AIAA PAPER 88-3288] p 142 A88-48762
Phase purity of NiCo₂O₄, a catalyst candidate for electrolysis of water [NASA-TM-100239] p 69 A88-13385
Operating envelopes of particle sizing instrumentation used for icing research [NASA-CR-180870] p 161 A88-13573
Vapor condensation on a turbulent liquid interface p 150 A88-15939
Development of a liquid-fed water resistojets [NASA-TM-100927] p 174 A88-24968

WATER FLOW

Experimental evidence for modifying the current physical model for ice accretion on aircraft surfaces [NASA-TM-87184] p 15 A88-12473

WATER INJECTION

Transient engine performance with water ingestion p 19 A88-27295

WATER VAPOR

An experimental and theoretical study of the ice accretion process during artificial and natural icing conditions [NASA-CR-182119] p 16 A88-21143

WAVE ATTENUATION

Imaging subtle microstructural variations in ceramics with precision ultrasonic velocity and attenuation measurements [NASA-TM-100129] p 177 A88-15257

WAVE PROPAGATION

A finite element model for wave propagation in an inhomogeneous material including experimental validation [AIAA PAPER 87-2741] p 212 A88-16577
Materials analysis by ultrasonics: Metals, ceramics, composites --- Book p 176 A88-44853
Unsteady heat transfer in turbine blade ducts: Focus on combustor sources [NASA-TM-100815] p 151 A88-18870
Electromagnetic propagation in PEC and absorbing curved S-ducts [NASA-TM-100833] p 120 A88-19698
Acousto-ultrasonic input-output characterization of unidirectional fiber composite plate by SV waves [NASA-CR-4152] p 178 A88-23224
Acousto-ultrasonic input-output characterization of unidirectional fiber composite plate by P waves [NASA-CR-4162] p 180 A88-25923

WAVE REFLECTION

Input-output characterization of fiber composites by SH waves [NASA-CR-4153] p 179 A88-23986

WAVEGUIDE ANTENNAS

A simple circular-polarized antenna: Circular waveguide horn coated with lossy magnetic material p 116 A88-36648
Absolute gain measurement of microstrip antennas under mismatched conditions p 117 A88-47949

WAVEGUIDES

A new model for broadband waveguide-to-microstrip transition design p 126 A88-38822
Slotline fed microstrip antenna array modules p 126 A88-44170
Modeling of some coplanar waveguide discontinuities [NASA-TM-100808] p 119 A88-17880
Guided-wave approaches to spectrally selective energy absorption [NASA-CR-182532] p 119 A88-17892

WEAR

Noncontacting measurement technologies for space propulsion condition monitoring p 158 A88-29818

WEAR TESTS

- The effects of atmosphere on the tribological properties of a chromium carbide based coating for use to 760 C p 98 A88-32372
- Tribological properties of polymer films and solid bodies in a vacuum environment p 98 A88-35565
- Wear of iron and nickel in corrosive liquid environments p 88 A88-40790
- Wear of iron and nickel in corrosive liquid environments [NASA-TM-100246] p 91 N88-11817
- Technology developments for a compound cycle engine p 30 N88-16637
- Friction and wear of monolithic and fiber reinforced silicon-ceramics sliding against IN-718 alloy at 25 to 800 C in atmospheric air at ambient pressure [NASA-TM-100294] p 103 N88-17796
- Friction and wear of ceramics p 106 N88-23874
- WEAR TESTS**
- Plasticity analysis of wear phenomena as an aid in the development of abrasible materials p 164 A88-10938
- Hot piston ring/cylinder liner materials: Selection and evaluation [NASA-TM-100276] p 102 N88-15872
- WEIBULL DENSITY FUNCTIONS**
- Improved processing of alpha-SiC p 99 A88-38318
- WEIGHT (MASS)**
- Spray automated balancing of rotors: Methods and materials [NASA-CR-182151] p 41 N88-29825
- WEIGHT REDUCTION**
- Lightweight nickel electrode for nickel hydrogen cells and batteries p 198 A88-16631
- The application of high temperature superconductors to space electrical power distribution components [NASA-TM-100901] p 61 N88-22939
- Weight savings in aerospace vehicles through propellant scavenging [NASA-TM-100900] p 44 N88-25470
- Performance of lightweight nickel electrodes [NASA-TM-100958] p 80 N88-26430
- WEIGHTLESSNESS**
- The effect of microgravity on flame spread over a thin fuel [NASA-TM-100195] p 80 N88-15853
- WEIGHTLESSNESS SIMULATION**
- Simulation of fluid flows during growth of organic crystals in microgravity p 109 A88-13163
- WHISKER COMPOSITES**
- Whisker-reinforced ceramic composites for heat engine components p 105 N88-22410
- WIND EFFECTS**
- Free-streamline analysis of deformation and dislodging by wind force of drops on a surface p 137 A88-25191
- WIND TUNNEL APPARATUS**
- Experimental evaluation of turning vane designs for high-speed and coupled fan-drive corners of 0.1-scale model of NASA Lewis Research Center's proposed altitude wind tunnel [NASA-TP-2681] p 40 N88-17686
- WIND TUNNEL DRIVES**
- Experimental evaluation of turning vane designs for high-speed and coupled fan-drive corners of 0.1-scale model of NASA Lewis Research Center's proposed altitude wind tunnel [NASA-TP-2681] p 40 N88-17686
- WIND TUNNEL TESTS**
- Chordwise pressure measurements on a blade of Mod-2 Wind Turbine p 2 A88-10970
- Wall shear stress measurement in blade end-wall corner region [ASME PAPER 87-GT-181] p 131 A88-11089
- Transition and separation control on a low-Reynolds number airfoil p 2 A88-11186
- Effect of acoustic excitation on the flow over a low-Re airfoil p 3 A88-14459
- Noise characteristics of model counter-rotating Prop-Fans [AIAA PAPER 87-2656] p 213 A88-16526
- Cruise noise of the 2/9 scale model of the Large-scale Advanced Propfan (LAP) propeller, SR-7A [AIAA PAPER 87-2717] p 214 A88-16565
- High-resolution heat-transfer-coefficient maps applicable to compound-curve surfaces using liquid crystals in a transient wind tunnel p 134 A88-18506
- Investigation of surface water behavior during glaze ice accretion [AIAA PAPER 88-0115] p 14 A88-22079
- Measurement of local convective heat transfer coefficients from a smooth and roughened NACA-0012 airfoil - Flight test data [AIAA PAPER 88-0287] p 136 A88-22207
- Porous wind tunnel corrections for counterrotation propeller testing [AIAA PAPER 88-2055] p 6 A88-44490

- Summary of low-speed wind tunnel results of several high-speed counterrotation propeller configurations [AIAA PAPER 88-3149] p 7 A88-48758
- Structure of a reattaching supersonic shear flow [AIAA PAPER 88-3615] p 8 A88-48901
- Ultrasonic techniques for aircraft ice accretion measurement [AIAA PAPER 88-4656] p 18 A88-51910
- Experimental investigation of the performance of a supersonic compressor cascade [ASME PAPER 88-GT-306] p 9 A88-54375
- Measurement of local convective heat transfer coefficients from a smooth and roughened NACA-0012 airfoil: Flight test data [NASA-TM-100284] p 149 N88-13552
- Analysis and test evaluation of the dynamic stability of three advanced turboprop models at zero forward speed [NASA-CR-175025] p 26 N88-14095
- Supersonic STOVL propulsion technology program: An overview p 29 N88-15808
- An experimental and theoretical study of the ice accretion process during artificial and natural icing conditions [NASA-CR-182119] p 16 N88-21143
- Porous wind tunnel corrections for counterrotation propeller testing [NASA-TM-100873] p 11 N88-22019
- Summary of low-speed wind tunnel results of several high-speed counterrotation propeller configurations [NASA-TM-100945] p 13 N88-24597
- Propan test assessment testbed aircraft stability and control/performance 1/9-scale wind tunnel tests [NASA-CR-182121] p 17 N88-26360
- Experimental and analytical evaluation of the effects of simulated engine inlets on the blade vibratory stresses of the SR-3 model prop-fan [NASA-CR-174959] p 36 N88-28927
- WIND TUNNEL WALLS**
- Porous wind tunnel corrections for counterrotation propeller testing [AIAA PAPER 88-2055] p 6 A88-44490
- Porous wind tunnel corrections for counterrotation propeller testing [NASA-TM-100873] p 11 N88-22019
- WIND TUNNELS**
- Experimental evaluation of corner vanes - Summary [SAE PAPER 871784] p 39 A88-30778
- Measured performance of the heat exchanger in the NASA icing research tunnel under severe icing and dry-air conditions [NASA-TM-100116] p 171 N88-12796
- WIND TURBINES**
- Chordwise pressure measurements on a blade of Mod-2 Wind Turbine p 2 A88-10970
- Thermal stresses of a wind turbine blade made of orthotropic material p 180 A88-18380
- Testing of a one-bladed 30-meter-diameter rotor on the DOE/NASA Mod-O wind turbine [NASA-TM-100274] p 201 N88-19014
- Comparison of pressure distributions on model and full-scale NACA 64-621 airfoils with ailerons for wind turbine application [NASA-TM-100802] p 201 N88-21593
- Lewis Structures Technology, 1988. Volume 3: Structural Integrity Fatigue and Fracture Wind Turbines HOST [NASA-CP-3003-VOL-3] p 192 N88-22408
- Large-scale wind turbine structures p 202 N88-22429
- Lewis Structures Technology, 1988. Volume 1: Structural Dynamics [NASA-CP-3003-VOL-1] p 194 N88-23226
- WIND VELOCITY**
- Chordwise pressure measurements on a blade of Mod-2 Wind Turbine p 2 A88-10970
- WINDOWS (APERTURES)**
- Zoom lens compensator for a cylindrical window in laser anemometer uses p 217 A88-17221
- WINGS**
- Advanced turboprop wing installation effects measured by unsteady blade pressure and noise [AIAA PAPER 87-2719] p 3 A88-18655
- Navier-Stokes solutions of flowfield characteristics produced by ice accretion [AIAA PAPER 88-0290] p 137 A88-22210
- Aerodynamic interaction between propellers and wings [AIAA PAPER 88-0665] p 5 A88-22495
- Advanced turboprop wing installation effects measured by unsteady blade pressure and noise [NASA-TM-100200] p 9 N88-10008
- WIRE CLOTH**
- Fatigue failure of regenerator screens in a high frequency Stirling engine p 179 N88-24491
- WORKING FLUIDS**
- Oxygen plasma effects on several liquid droplet radiator fluids p 142 A88-47962

WORKLOADS (PSYCHOPHYSIOLOGY)

- Identification and proposed control of helicopter transmission noise at the source p 38 N88-16647

X

X RAY ANALYSIS

- Flaw imaging and ultrasonic techniques for characterizing sintered silicon carbide [NASA-TM-100177] p 177 N88-12106

XENON

- Critical fluid light scattering p 158 A88-33003
- Performance of 10-kW class xenon ion thrusters [NASA-TM-101292] p 65 N88-28088

Y

YAGI ANTENNAS

- Gain enhancement of microstrip antennas with overlaying parasitic directors p 117 A88-48653

YAW

- Aeroelastic response of metallic and composite propfan models in yawed flow [NASA-TM-100964] p 37 N88-29807

YIELD POINT

- Fiber composite structural durability and damage tolerance: Simplified predictive methods [NASA-TM-100179] p 72 N88-13409
- An experimental study of biaxial yield in modified 9Cr-1Mo steel at room temperature [NASA-CR-175012] p 196 N88-30164

YIELD STRENGTH

- A nonlinear viscoelastic constitutive equation - Yield predictions in multiaxial deformations p 185 A88-54912

YTTRIUM

- Synthesis and characterization of high-T(sub c) screen-printed Y-Ba-Cu-O films on alumina [NASA-TM-100860] p 222 N88-22805
- The high temperature creep deformation of Si3N4-6Y2O3-2Al2O3 [NASA-CR-183204] p 76 N88-28981

YTTRIUM OXIDES

- Glass properties in the yttria-alumina-silica system p 96 A88-18361
- Weak-field magnetization of superconducting Y1Ba2Cu3O(x) - Relationship to microstructure p 219 A88-18814
- Chemical durability of high-temperature superconductor YBa2Cu3O(7-x) in aqueous environments p 78 A88-25023
- Strength characterization of yttria/alumina-doped sintered silicon nitride p 97 A88-26154

Z

ZINC

- Ohmic contact formation in semi-insulating GaAs using shallow heavily doped p-type layers p 219 A88-11150

ZINC ALLOYS

- Simulating the cooling of an immiscible alloy p 83 A88-20199

ZIRCONIUM

- The effect of sulfur and zirconium Co-doping on the oxidation of NiCrAl [NASA-TM-100209] p 90 N88-10940
- Creep behavior of tungsten/niobium and tungsten/niobium-1 percent zirconium composites [NASA-TM-100804] p 92 N88-18707
- Characterization of precipitates in a niobium-zirconium-carbon alloy [NASA-TM-100848] p 93 N88-22981
- Creep behavior of tungsten/niobium and tungsten/niobium-1 percent zirconium composites p 75 N88-24427
- Electrical properties of materials for elevated temperature resistance strain gage application [NASA-CR-182214] p 164 N88-30106

ZONE MELTING

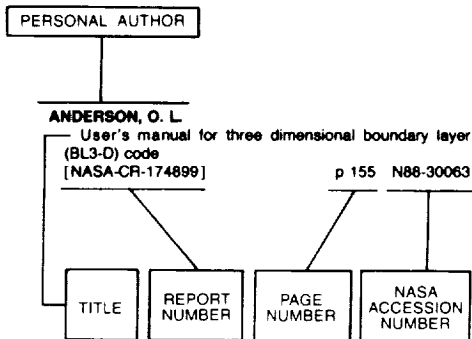
- Preparation of multistage zone-refined materials for thermochemical standards p 111 A88-43172

ZOOM LENSES

- Zoom lens compensator for a cylindrical window in laser anemometer uses p 217 A88-17221

PERSONAL AUTHOR INDEX

Typical Personal Author Index Listing



Listings in this index are arranged alphabetically by personal author. The NASA accession number denotes the number by which the citation is identified.

A

- ABBOTT, JOHN M.**
Inlets, ducts and nozzles p 149 N88-15791
- ABDUL-AZIZ, ALI**
Thermal finite-element analysis of space shuttle main engine turbine blade p 187 N88-13745
[NASA-TM-100117]
Thermal-structural analyses of Space Shuttle Main Engine (SSME) hot section components p 61 N88-22404
- ABE, STEVE**
Systems for ultrasonic scanning, analysis and imagery p 177 N88-22414
- ABEL, PHILLIP B.**
Flaw imaging and ultrasonic techniques for characterizing sintered silicon carbide [NASA-TM-100177] p 177 N88-12106
Development and applications of optical interferometric micrometrology in the angstrom and subangstrom range [NASA-TM-100299] p 162 N88-23196
- ABERNETHY, ROBERT B.**
In-flight thrust determination [SAE AIR 1703] p 16 A88-15227
Uncertainty of in-flight thrust determination [SAE AIR 1678] p 16 A88-15228
- ABU-HIJLEH, B. A. K.**
Structure of a reattaching supersonic shear flow [AIAA PAPER 88-3615] p 8 A88-48901
- ABU-HIJLEH, B. A./K.**
Performance of laser Doppler velocimeter with polydisperse seed particles in high speed flows [AIAA PAPER 88-0425] p 157 A88-22317
- ACOSTA, R.**
Radiation characteristics of microstrip arrays with parasitic elements p 121 A88-10481
- ACOSTA, R. J.**
Compensation of reflector antenna surface distortion using an array feed [NASA-TM-100286] p 119 N88-18805
Case study of active array feed compensation with sidelobe control for reflector surface distortion [NASA-TM-100287] p 120 N88-23073
Array trade-off study using multilayer parasitic subarrays [NASA-TM-101321] p 121 N88-28222

- ACOSTA, ROBERTO J.**
Active feed array compensation for reflector antenna surface distortions [NASA-TM-100826] p 120 N88-25762
Analytical approximation of a distorted reflector surface defined by a discrete set of points [NASA-TM-101323] p 121 N88-27424
- ADAMCZYK, J. J.**
Measurements of the unsteady flow field within the stator row of a transonic axial-flow fan. I - Measurement and analysis technique [ASME PAPER 87-GT-226] p 4 A88-18660
Measurements of the unsteady flow field within the stator row of a transonic axial-flow fan. II - Results and discussion [ASME PAPER 87-GT-227] p 4 A88-18661
- ADAMCZYK, JOHN J.**
Turbomachinery p 28 N88-15792
Utilization of parallel processing in solving the inviscid form of the average-passage equation system for multistage turbomachinery [NASA-TM-89845] p 32 N88-21160
- ADAMOVSKEY, GRIGORY**
Time domain referencing in intensity modulation fiber optic sensing systems p 217 A88-12660
Fiber-optic displacement sensor with temporally separated signal and reference channels p 217 A88-33161
Referencing in fiber optic sensing systems p 217 A88-42604
Fiber optic sensors with internal referencing [NASA-TM-100893] p 162 N88-26644
Fiber optic sensing systems using high frequency resonant sensing heads with intensity sensors [NASA-TM-101318] p 163 N88-28293
- ADAMS, GARY R.**
In-flight thrust determination [SAE AIR 1703] p 16 A88-15227
Uncertainty of in-flight thrust determination [SAE AIR 1678] p 16 A88-15228
- ADDY, H. E.**
Performance and efficiency evaluation and heat release study of a direct-injection stratified-charge rotary engine [SAE PAPER 870445] p 166 A88-23313
- AGGARWAL, ARUN K.**
Absolute instability of the Gaussian wake profile p 136 A88-20842
- AHMAD, S.**
Time-domain transient elastodynamic analysis of 3-D solids by BEM p 183 A88-48638
- AHMED, AKHTER U.**
Electrical resistivity (4K to 2100K) of annealed vapor growth carbon fibers p 96 A88-17214
- AHUJA, K. K.**
Aeroacoustics of advanced STOVL aircraft plumes [SAE PAPER 872358] p 215 A88-30998
Aeroacoustics of advanced STOVL aircraft plumes [SAE PAPER 872358] p 215 A88-37219
Acoustically excited heated jets. 1: Internal excitation [NASA-CR-4129-PT-1] p 12 N88-23751
Acoustically excited heated jets. 2: In search of a better understanding [NASA-CR-4129-PT-2] p 12 N88-23752
Acoustically excited heated jets. 3: Mean flow data [NASA-CR-4129-PT-3] p 12 N88-23753
- AIELLO, R. A.**
Parametric studies of advanced turboprops [AIAA PAPER 88-2266] p 20 A88-32223
Advanced composite turboprops - Modeling, structural, and dynamic analyses [ASME PAPER 87-GT-78] p 21 A88-36745
- AIELLO, ROBERT A.**
The composite blade structural analyzer (COBSTRAN) p 33 N88-22390
- AJMANI, K.**
Turbulence modeling in hypersonic inlets [AIAA PAPER 88-2957] p 7 A88-44705
- AKL, FRED**
Parallel computer methods for eigenvalue extraction p 207 N88-23233

- ALARIO, JOE**
Solar dynamic heat rejection technology. Task 2: Heat pipe radiator development [NASA-CR-182141] p 152 N88-23182
- ALEXANDER, DENNIS R.**
Comparison of UNL laser imaging and sizing system and a phase/Doppler system for analyzing sprays from a NASA nozzle [NASA-CR-182437] p 150 N88-16956
- ALEXANDER, M.**
Effect of the microstructure on the thermoelectric properties of polycrystalline lanthanum chalcogenides p 221 A88-40797
- ALEXANDER, R. M.**
Active control of transient rotordynamic vibration by optimal control methods [ASME PAPER 88-GT-73] p 208 A88-54202
- ALGER, DONALD L.**
1987 overview of free-piston Stirling technology for space power application p 53 A88-11942
Progress toward the evolution of a Stirling space engine [NASA-TM-100221] p 224 N88-14046
Fatigue failure of regenerator screens in a high frequency Stirling engine p 179 N88-24491
Component improvement of free-piston Stirling engine key technology for space power [NASA-TM-100950] p 64 N88-25476
- ALI, S. K.**
Coherent motion induced fluctuations in the primary transition region of a plane shear layer p 133 A88-14125
Gravitationally defined velocities for a low speed hot-wire calibration p 133 A88-14170
- ALJABRI, A. S.**
Propan test assessment testbed aircraft stability and control/performance 1/9-scale wind tunnel tests [NASA-CR-182121] p 17 N88-26360
- ALJABRI, ABDULLAH S.**
Measurement and prediction of propeller flow field on the PTA aircraft at speeds of up to Mach 0.85 [AIAA PAPER 88-0667] p 19 A88-22497
- ALLEN, DAVID J.**
Hot piston ring tests [NASA-TM-100256] p 201 N88-14486
Test results of a 40-kW Stirling engine and comparison with the NASA Lewis computer code predictions [NASA-TM-87050] p 201 N88-19013
Testing of a variable-stroke Stirling engine [NASA-TM-100899] p 225 N88-30472
- ALSTON, WILLIAM B.**
Correlations of norbornenyl crosslinked polyimide resin structures with resin thermo-oxidative stability, resin glass transition temperature and composite initial mechanical properties [NASA-TM-100791] p 103 N88-16877
Substituted 1,1,1-Triaryl-2,2,2-Trifluoroethanes and processes for their synthesis [NASA-CASE-LEW-14345-1] p 69 N88-26404
- ALTEROVITZ, S. A.**
Weak-field magnetization of superconducting Y1Ba2Cu3O(x) - Relationship to microstructure p 219 A88-18814
- ALTEROVITZ, SAMUEL A.**
Plasma deposition of amorphous hydrogenated carbon films on III-V semiconductors p 220 A88-32862
Mechanical strength and tribological behavior of ion-beam-deposited boron nitride films on non-metallic substrates p 98 A88-32866
Variable angle spectroscopic ellipsometry - Application to GaAs-AlGaAs multilayer homogeneity characterization p 220 A88-40139
Boron nitride - Composition, optical properties, and mechanical behavior p 99 A88-40794
- AMANO, R. S.**
Investigation of third-order closure model of turbulence for the computation of incompressible flows in a channel with a backward-facing step p 136 A88-21273
Turbulence energy and diffusion transport of third-moments in a separating and reattaching flow p 141 A88-43011

- AMES, STEPHEN A.**
Bandwidth and power efficient satellite TDMA demodulator and decoder
[AIAA PAPER 88-0812] p 123 A88-27559
- ANDERSON, BERNHARD H.**
Internal fluid mechanics research on supercomputers for aerospace propulsion systems
[NASA-TM-100289] p 149 N88-15188
Inlets, ducts and nozzles p 149 N88-15791
- ANDERSON, GRIFFIN Y.**
Ground tests confirm the promise of hypersonic propulsion p 2 A88-10369
- ANDERSON, O. L.**
User's manual for three dimensional boundary layer (BL3-D) code
[NASA-CR-174899] p 155 N88-30063
Assessment of a 3-D boundary layer analysis to predict heat transfer and flow field in a turbine passage
[NASA-CR-174894] p 155 N88-30066
- ANG, JAMES A.**
Temperature and velocity profiles in sooting free convection diffusion flames p 78 A88-43018
- ANGUS, JOHN C.**
Ion beam deposition of amorphous carbon films with diamond like properties p 97 A88-20300
Diamond like carbon coatings: Categorization by atomic number density
[NASA-CR-174895] p 108 N88-28151
- ANTHAN, DONALD J.**
Loss-compensation of intensity-modulating fiber-optic sensors p 158 A88-22943
Modulated-splitting-ratio fiber-optic temperature sensor
[NASA-TM-101332] p 18 N88-28062
- ANTOLOVICH, S. D.**
Effect of temperature, microstructure, and stress state on the low cycle fatigue behavior of Waspaloy p 87 A88-35922
- ANTOLOVICH, STEPHEN D.**
A model for life predictions of nickel-base superalloys in high-temperature low cycle fatigue p 87 A88-35913
Deformation, fatigue and fracture behavior of two cast anisotropic superalloys p 187 N88-13732
- ANTOON, FRED A.**
Low cost Get-Away-Special (GAS) furnace p 41 A88-28583
- AOYAGI, P.**
Slotline fed microstrip antenna array modules p 126 A88-44170
- APPEL, MARSHALL A.**
Indium-coated rhenium thrusters by CVD
[NASA-TM-101309] p 67 N88-29874
- APPLE, T.**
Electron-spin-resonance studies of vapor-grown carbon fibers p 96 A88-17368
- ARMSTRONG, E. S.**
Three dimensional thermal analysis of rocket thrust chambers
[AIAA PAPER 88-2643] p 54 A88-43721
- ARMSTRONG, ELIZABETH S.**
Computer-aided design analysis of 57-mm, angular-contact, cryogenic turbopump bearings
[NASA-TP-2816] p 172 N88-18933
- ARMSTRONG, T. P.**
Voids in Jovian magnetosphere revisited - Evidence of spacecraft charging p 226 A88-22879
- ARNAL, M.**
Unsteady motion and transition to turbulence in developing curved duct flow p 140 A88-39010
- ARNOLD, S. M.**
A transversely isotropic thermoelastic theory
[NASA-TM-101302] p 196 N88-28332
- ARON, P. R.**
Weak-field magnetization of superconducting YBa₂Cu₃O(x) - Relationship to microstructure p 219 A88-18814
Characterization of Ba₂YC₃O(7-x) prepared in an inert atmosphere p 221 A88-49376
- ARON, PAUL R.**
Laser induced OMCVD growth of AlGaAs on GaAs p 125 A88-34286
The application of high temperature superconductors to space electrical power distribution components
[NASA-TM-100901] p 61 N88-22939
- ARPASI, DALE J.**
Automating the parallel processing of fluid and structural dynamics calculations p 206 A88-46963
- ARRISON, A.**
A V-grooved AlGaAs/GaAs passivated pn junction p 125 A88-34300
- ARRISON, ANNE**
A novel photovoltaic power system which uses a large area concentrator mirror p 197 A88-11811
- ARYA, V. K.**
Finite element (MARC) solution technologies for viscoplastic analyses p 191 N88-22389

- ASCOUGH, JOHN C.**
In-flight thrust determination
[SAE AIR 1703] p 16 A88-15227
Uncertainty of in-flight thrust determination
[SAE AIR 1678] p 16 A88-15228
- ASMUSSEN, J.**
Electrothermal propulsion of spacecraft with millimeter and submillimeter electromagnetic energy p 54 A88-46220
- ATHERTON, W. J.**
Automated acoustic intensity measurements and the effect of gear tooth profile on noise p 168 A88-31623
- ATKINSON, W. H.**
Development of sensors for ceramic components in advanced propulsion systems: Survey and evaluation of measurement techniques for temperature, strain and heat flux for ceramic components in advanced propulsion systems
[NASA-CR-182111] p 163 N88-28299
- ATKINSON, WILLIAM H.**
Development of heat flux sensors for turbine airfoils p 160 N88-11143
- AUGUST, RICHARD**
Vibration and flutter characteristics of the SR7L large-scale propfan
[NASA-TM-100272] p 188 N88-18036
Life and reliability of rotating disks p 178 N88-22428
- AUPING, JUDITH V.**
Laboratory Information Management System (LIMS): A case study
[NASA-TM-100835] p 208 N88-21697
- AUYEUNG, S.**
SR-7A aeroelastic model design report
[NASA-CR-174791] p 36 N88-28928
- AVILA, R. E.**
Behavior of ion-implanted junction diodes in 3C SiC p 122 A88-15423
- AYDELOTT, JOHN C.**
Cryogenic Fluid Management Technology Workshop. Volume 1: Presentation material and discussion
[NASA-CP-10001] p 149 N88-15924
- AYERS, SCHUYLER R.**
Development of composite facets for the surface of a space-based solar dynamic concentrator p 54 A88-18230

B

- BAAKLINI, G. Y.**
Acoustic imaging of subtle porosity variations in ceramics p 101 A88-55044
- BAAKLINI, GEORGE Y.**
Flaw imaging and ultrasonic techniques for characterizing sintered silicon carbide
[NASA-TM-100177] p 177 N88-12106
Imaging subtle microstructural variations in ceramics with precision ultrasonic velocity and attenuation measurements
[NASA-TM-100129] p 177 N88-15257
Characterization of sintered SiC by using NDE p 177 N88-22413
Nondestructive evaluation of sintered ceramics p 177 N88-22416
Improved processing of Si₃N₄ p 107 N88-23882
High frequency ultrasonic characterization of sintered SiC
[NASA-TM-100825] p 179 N88-23985
- BACHALO, W. D.**
Experiments on spray interactions in the wake of a bluff body
[ASME PAPER 87-GT-48] p 131 A88-11000
Diagnostics development for spray characterization in complex turbulent flows
[ASME PAPER 88-GT-241] p 146 A88-54320
- BADDOUR, M. F.**
Absolute gain measurement of microstrip antennas under mismatched conditions p 117 A88-47949
- BADER, CLAYTON H.**
Component data base for space station resistojel auxiliary propulsion
[NASA-CR-180834] p 59 N88-17731
- BAER-RIEDHART, JENNIFER L.**
In-flight thrust determination
[SAE AIR 1703] p 16 A88-15227
Uncertainty of in-flight thrust determination
[SAE AIR 1678] p 16 A88-15228
- BAHADORI, YOUSEF**
Laminar diffusion flames under micro-gravity conditions
[AIAA PAPER 88-0645] p 78 A88-27722
- BAILEY, ALLAN B.**
Experimental evaluation of resistojel thruster plume shields
[NASA-TM-101363] p 66 N88-29868
- BAILEY, R. S.**
High-temperature oxidation/corrosion of iron-based superalloys p 81 A88-10029
- BAILEY, RICHARD S.**
The development of a high temperature static strain gage system p 160 N88-11142
- BAILEY, S. G.**
A V-grooved AlGaAs/GaAs passivated pn junction p 125 A88-34300
- BAIR, SCOTT**
Shear rheological characterization of motor oils p 100 A88-47562
- BAKER, I.**
Dynamic recrystallization and grain boundary migration in B2 FeAl p 83 A88-20269
The microstructure and tensile properties of extruded melt-spun ribbons of iron-rich B2 FeAl p 85 A88-31679
- BALASUBRAMANIAM, R.**
Simulation of fluid flows during growth of organic crystals in microgravity p 109 A88-13163
Electrohydrodynamic migration of charged droplets in an insulating fluid
[AIAA PAPER 88-3557] p 143 A88-48946
Electrohydrodynamic migration of charged droplets in an insulating fluid
[NASA-TM-100849] p 152 N88-21424
- BALDWIN, RICHARD M.**
Spray automated balancing of rotors: Methods and materials
[NASA-CR-182151] p 41 N88-29825
- BALKCOM, GEORGE H.**
In-flight thrust determination
[SAE AIR 1703] p 16 A88-15227
Uncertainty of in-flight thrust determination
[SAE AIR 1678] p 16 A88-15228
- BALL, CALVIN L.**
Supersonic throughflow fans for high-speed aircraft p 30 N88-15810
- BALLARINI, ROBERTO**
The effects of crack surface friction and roughness on crack tip stress fields p 180 A88-14579
- BALLIN, MARK G.**
Rotorcraft flight-propulsion control integration p 38 N88-16643
Rotorcraft flight-propulsion control integration: An eclectic design concept
[NASA-TP-2815] p 38 N88-19475
- BANERJEE, AMITAVA**
Interfacial adhesion: Theory and experiment
[NASA-TM-100830] p 92 N88-20417
- BANERJEE, P. K.**
Time-domain transient elastodynamic analysis of 3-D solids by BEM p 183 A88-48638
- BANERJEE, PRASANTA K.**
A new boundary element formulation for two- and three-dimensional thermoelasticity using particular integrals p 184 A88-53088
A new BEM formulation for two- and three-dimensional elastoplasticity using particular integrals p 184 A88-53089
- BANHOLZER, WILLIAM F.**
Oxidation-resistant reflective surfaces for solar dynamic power generation in near earth orbit p 54 A88-18523
Chemical vapor deposited silica coatings for solar mirror protection
[AIAA PAPER 88-0027] p 99 A88-41796
Chemical vapor deposited silica coatings for solar mirror protection
[NASA-TM-100834] p 105 N88-21306
- BANKS, BRUCE A.**
Arc-textured metal surfaces for high thermal emittance space radiators
[NASA-TM-100894] p 94 N88-24754
- BANKS, P. M.**
Double-probe potential measurements near the Spacelab 2 electron beam p 204 A88-53464
- BANSAL, NAROTTAM P.**
Chemical durability of high-temperature superconductor YBa₂Cu₃O(7-x) in aqueous environments p 78 A88-25023
Effect of fluoride doping on the transition temperature of YBa₂Cu₃O(6.5 + delta) p 220 A88-29297
Sol-gel synthesis of magnesium oxide-silicon dioxide glass compositions p 100 A88-49105
High Tc screen-printed YBa₂Cu₃O(7-x) films - Effect of the substrate material p 127 A88-49760
Synthesis and characterization of high-T(sub c) screen-printed Y-Ba-Cu-O films on alumina
[NASA-TM-100860] p 222 N88-22805

- BANSAL, PREM N.**
Experimental and analytical evaluation of the effects of simulated engine inlets on the blade vibratory stresses of the SR-3 model prop-fan
[NASA-CR-174959] p 36 N88-28927
- BAR-SEVER, A.**
Transition and separation control on a low-Reynolds number airfoil p 2 A88-11186
Effect of acoustic excitation on the flow over a low-Re airfoil p 3 A88-14459
- BARKHOUDARIAN, S.**
Reusable rocket engine optical condition monitoring p 158 A88-29817
Noncontacting measurement technologies for space propulsion condition monitoring p 158 A88-29818
Progress toward an advanced condition monitoring system for reusable rocket engines p 54 A88-32868
Improved maintainability of space-based reusable rocket engines
[AIAA PAPER 88-3113] p 55 A88-48037
- BARNHART, P. J.**
Glancing shock wave-turbulent boundary layer interaction with boundary layer suction
[AIAA PAPER 88-0308] p 6 A88-27718
- BARNHART, PAUL J.**
A preliminary design study of supersonic through-flow fan inlets
[AIAA PAPER 88-3075] p 23 A88-53137
- BARR, FRANCIS A.**
Slip casting and extruding shapes of rhenium with metal oxide additives. Part 2: Development of grain stabilized rhenium parts for resistojets
[NASA-CR-180851] p 57 N88-11749
- BARRANGER, JOHN P.**
Recent advances in capacitance type of blade tip clearance measurements
[NASA-TM-101291] p 35 N88-25460
- BARRETT, C. A.**
Effect of alloy composition on the sodium-sulfate induced hot corrosion attack of cast nickel-base superalloys at 900 C p 81 A88-10028
- BARRETT, CHARLES A.**
The effect of variations of cobalt content on the cyclic oxidation resistance of selected Ni-base superalloys p 82 A88-10031
- BARROWS, RICHARD F.**
Prototype thin-film thermocouple/heat-flux sensor for a ceramic-insulated diesel engine
[NASA-TM-100798] p 162 N88-18892
- BARRY, JENNIFER**
Arc-textured metal surfaces for high thermal emittance space radiators
[NASA-TM-100894] p 94 N88-24754
- BARTLETT, C. SCOTT**
Stability relationship for water droplet crystallization with the NASA Lewis icing spray nozzle
[AIAA PAPER 88-0289] p 137 A88-22209
Stability relationship for water droplet crystallization with the NASA Lewis icing spray
[NASA-TM-100220] p 24 N88-10790
- BARTOLOTTA, P. A.**
Investigation of a SiC/Ti-24Al-11Nb composite
[NASA-TM-100956] p 76 N88-28980
- BARTOLOTTA, PAUL A.**
Experiments investigating advanced materials under thermomechanical loading p 191 N88-22385
- BARTON, J. MICHAEL**
Infrared properties of an anisotropically stirred fluid p 134 A88-16354
- BATTERTON, PETER G.**
NASA supersonic STOVL propulsion technology program
[SAE PAPER 872352] p 21 A88-37215
NASA supersonic STOVL propulsion technology program
[NASA-TM-100227] p 26 N88-14093
Supersonic STOVL propulsion technology program: An overview p 29 N88-15808
- BAUHAHN, P.**
A 30 GHz monolithic receive module technology assessment
[NASA-CR-180825] p 129 N88-23084
- BAUMBICK, R. J.**
Conceptual design of an optic based engine control system
[ASME PAPER 87-GT-168] p 18 A88-11079
- BAUMBICK, ROBERT J.**
Fiber optics for advanced aircraft
[NASA-TM-101294] p 1 N88-26328
- BAUMEISTER, JOSEPH F.**
Thermal distortion analysis of the space station solar dynamic concentrator
[NASA-TM-100868] p 64 N88-25475
- BAUMEISTER, KENNETH J.**
A finite element model for wave propagation in an inhomogeneous material including experimental validation
[AIAA PAPER 87-2741] p 212 A88-16577
Unsteady heat transfer in turbine blade ducts: Focus on combustor sources
[NASA-TM-100815] p 151 N88-18870
Electromagnetic propagation in PEC and absorbing curved S-ducts
[NASA-TM-100833] p 120 N88-19698
- BEAGHTON, P. J.**
Growth of needle-shaped crystals in the presence of convection p 111 A88-37715
- BEARDSLEY, BRAD**
Porosity determination of thermal barrier coatings
[ASME PAPER 88-GT-278] p 68 A88-54350
- BECHERT, D. W.**
Excitation of instability waves in free shear layers. I - Theory p 138 A88-26338
Excitation of instability waves in free shear layers. II - Experiments p 138 A88-26339
- BECKNELL, G. F.**
Gigawatt-tolerant power switches and memory elements p 123 A88-22704
- BECKMAN, D. H.**
Space station onboard propulsion system: Technology study
[NASA-CR-179233] p 59 N88-15006
- BEER, C. M.**
Space station onboard propulsion system: Technology study
[NASA-CR-179233] p 59 N88-15006
- BEHEIM, G.**
Fiber-linked interferometric pressure sensor p 157 A88-11743
- BEHEIM, GLENN**
Loss-compensation of intensity-modulating fiber-optic sensors p 158 A88-22943
Active phase compensation system for fiber optic holography
[NASA-TM-101295] p 162 N88-26641
Modulated-splitting-ratio fiber-optic temperature sensor
[NASA-TM-101332] p 18 N88-28062
- BEHREND, TRACY**
Arc-textured metal surfaces for high thermal emittance space radiators
[NASA-TM-100894] p 94 N88-24754
- BEHRENS, R. G.**
Characteristics of fluid flow in the combustion synthesis of TiC from the elements p 110 A88-28564
Solid-state combustion synthesis of ceramics and alloys in reduced gravity
[NASA-CR-4163] p 75 N88-25479
- BELLINI, P. X.**
Probabilistic composite micromechanics
[AIAA PAPER 88-2375] p 182 A88-32312
- BELLOWS, ALFRED H.**
A payload for investigating the influence of convection on GaAs crystal growth p 221 N88-17702
- BELYTSCHKO, TED**
Finite element methods in probabilistic mechanics p 212 A88-29060
- BEN OUEZDON, M.**
Semi-empirical crack tip analysis p 183 A88-47681
- BENCZE, DANIEL P.**
Ground tests confirm the promise of hypersonic propulsion p 2 A88-10369
- BENDIKSEN, O. O.**
Localization of natural modes of vibration in bladed disks
[ASME PAPER 87-GT-46] p 18 A88-10998
Recent developments in flutter suppression techniques for turbomachinery rotors p 21 A88-35530
- BENHACHMI, DRISS**
Experimental and numerical investigation of the effect of distributed suction on oblique shock wave/turbulent boundary layer interaction
[NASA-TM-101334] p 156 N88-30084
- BENNETT, F.**
Centaur operations at the space station
[NASA-CR-179593] p 49 N88-25473
- BENNETT, J. C.**
Fuel-injector/air-swirl characterization p 146 N88-11150
- BENNETT, TIMOTHY J.**
Advanced sensible heat solar receiver for space power
[NASA-TM-100847] p 59 N88-21249
- BENTS, DAVID J.**
Coaxial tube array space transmission line characterization p 121 A88-11865
High temperature solid oxide regenerative fuel cell for solar photovoltaic energy storage p 197 A88-11905
Power transmission studies for tethered SP-100
[NASA-TM-100864] p 60 N88-21251
- BERCAW, ROBERT R.**
LERC power system autonomy program 1990 demonstration p 52 A88-11861
- BERCAW, ROBERT W.**
Spacecraft 2000 program overview p 48 N88-10085
- BERG, M.**
Hafnia-rich mixed oxide ceramics of the system HfO₂-ZrO₂-TiO₂ for heaters and heat exchangers in electrothermal thrusters: The effects of titania on selected electrical and mechanical properties of Hafnia-rich mixed oxides in the system Hafnia-Zirconia-Titania, volume 1
[NASA-CR-182800-VOL-1] p 105 N88-22197
- BERG, ROBERT F.**
Quantitative characterization of the viscosity of a microemulsion p 77 A88-11167
Critical exponent for the viscosity of four binary liquids p 222 A88-53050
- BERKOVITS, A.**
Relationship between fatigue life in the creep-fatigue region and stress-strain response
[NASA-TM-100796] p 188 N88-18040
- BERKOWITZ, B. M.**
Testing of a one-bladed 30-meter-diameter rotor on the DOE/NASA Mod-O wind turbine
[NASA-TM-100274] p 201 N88-19014
- BERNHART, W. D.**
Electro-impulse de-icing electrodynamic solution by discrete elements
[AIAA PAPER 88-0018] p 17 A88-22016
- BERTHOLD, J. W.**
Calibration of high-temperature, fiber-optic, microbend, pressure transducers p 157 A88-22942
- BHARGAVA, R.**
Wall shear stress measurement in blade end-wall corner region
[ASME PAPER 87-GT-181] p 131 A88-11089
- BHASIN, K. B.**
System architecture of MMIC-based large aperture arrays for space applications p 45 A88-35274
Detection of radio-frequency modulated optical signals by two and three terminal microwave devices p 117 A88-50305
Microwave response of an HEMT photoconductor
[NASA-TM-100819] p 128 N88-18835
High frequency GaAlAs modulator and photodetector for phased array antenna applications
[NASA-TM-101328] p 130 N88-30048
- BHASIN, KUL**
Optical technologies for space communication systems; Proceedings of the Meeting, Los Angeles, CA, Jan. 15, 16, 1987
[SPIE-756] p 45 A88-35251
- BHASIN, KUL B.**
Monolithic Microwave Integrated Circuit (MMIC) technology for space communications applications
[IAF PAPER 87-491] p 122 A88-16133
Optically controlled phased-array antenna technology for space communication systems p 119 N88-18809
Optical RF distribution links for MMIC phased array antennas
[NASA-TM-100841] p 128 N88-20555
Optically interconnected phased arrays
[NASA-TM-100855] p 128 N88-21400
A high frequency GaAlAs travelling wave electro-optic modulator at 0.82 micrometers
[NASA-TM-100970] p 130 N88-28240
- BHATT, RAMAKRISHNA T.**
SiC fiber reinforced reaction-bonded Si₃N₄ composites p 75 N88-23892
- BHATTACHARYYA, S.**
Performance of laser Doppler velocimeter with polydisperse seed particles in high speed flows
[AIAA PAPER 88-0425] p 157 A88-22317
- BHIMNATHWALA, H. G.**
Characterization and modelling of open tube diffused n+p bulk InP solar cells p 199 A88-34270
- BIEDENBENDER, MICHAEL D.**
Rapid thermal annealing of indium phosphide compound semiconductors p 220 A88-26196
- BIESIADNY, THOMAS**
In-flight thrust determination
[SAE AIR 1703] p 16 A88-15227
Uncertainty of in-flight thrust determination
[SAE AIR 1678] p 16 A88-15228
- BIFANO, WILLIAM J.**
System Development Working Group report p 48 N88-10092
- BILL, ROBERT C.**
Bithermal fatigue - A link between isothermal and thermomechanical fatigue p 87 A88-35918
An overview of rotorcraft propulsion research at Lewis Research Center p 22 A88-40554
Advanced transmission studies
[NASA-TM-100867] p 173 N88-21454

- BIRCHENOUGH, ARTHUR G.**
Lewis Research Center space station electric power system test facilities
[NASA-TM-100824] p 43 N88-28942
- BITTKER, DAVID A.**
Detailed mechanism of benzene oxidation
[NASA-TM-100202] p 79 N88-11775
Detailed mechanism of toluene oxidation and comparison with benzene
[NASA-TM-100261] p 79 N88-13428
- BLACK, GERALD**
Blade loss transient dynamics analysis, volume 1. Task 2: TETRA 2 theoretical development
[NASA-CR-179632] p 25 N88-10791
Blade loss transient dynamics analysis, volume 2. Task 2: TETRA 2 user's manual
[NASA-CR-179633] p 25 N88-10792
- BLACK, RICHARD E.**
Research opportunities in microgravity science and applications during Shuttle hiatus p 109 A88-13164
- BLAHA, BERNARD J.**
NASA supersonic STOVL propulsion technology program
[SAE PAPER 872352] p 21 A88-37215
NASA supersonic STOVL propulsion technology program
[NASA-TM-100227] p 26 N88-14093
Supersonic STOVL propulsion technology program: An overview p 29 N88-15808
- BLAIR, M. F.**
The effects of turbulence and stator/rotor interactions on turbine heat transfer. II - Effects of Reynolds number and incidence
[ASME PAPER 88-GT-5] p 145 A88-54152
The effects of turbulence and stator/rotor interactions on turbine heat transfer. I - Design operating conditions
[ASME PAPER 88-GT-125] p 145 A88-54236
The effects of inlet turbulence and rotor/stator interactions on the aerodynamics and heat transfer of a large-scale rotating turbine model. Part 4: Aerodynamic data tabulation
[NASA-CR-179468] p 153 N88-23956
The effects of inlet turbulence and rotor/stator interactions on the aerodynamics and heat transfer of a large-scale rotating turbine model. Volume 3: Heat transfer data tabulation 65 percent axial spacing
[NASA-CR-179468] p 37 N88-28930
The effects of inlet turbulence and rotor/stator interactions on the aerodynamics and heat transfer of a large-scale rotating turbine model. Volume 2: Heat transfer data tabulation. 15 percent axial spacing
[NASA-CR-179467] p 37 N88-29804
- BLAIR, MICHAEL F.**
Measurement of airfoil heat transfer coefficients on a turbine stage p 147 N88-11158
- BLECH, RICHARD A.**
Hypercluster - Parallel processing for computational mechanics p 208 A88-40458
Time-partitioning simulation models for calculation of parallel computers p 206 A88-46961
- BLISS, DONALD B.**
Reduced order models for nonlinear aerodynamics p 11 N88-23248
- BLOCK, H. BRUCE**
Techniques utilized in the simulated altitude testing of a 2D-CD vectoring and reversing nozzle
[NASA-TM-100872] p 40 N88-25464
- BLOOMFIELD, HARVEY S.**
Small reactor power systems for manned planetary surface bases
[NASA-TM-100223] p 227 N88-13209
Small space reactor power systems for unmanned solar system exploration missions
[NASA-TM-100228] p 227 N88-14054
- BLUMENTHAL, PHILIP Z.**
A distributed data acquisition system for aeronautics test facilities p 39 A88-33065
- BOBER, LAWRENCE J.**
Advanced propeller research p 29 N88-15806
- BOBINCHAK, J.**
Characteristics of a two-layer electromagnetically coupled rectangular patch antenna p 115 A88-14100
- BOBINSKY, E. A.**
Case study of active array feed compensation with sidelobe control for reflector surface distortion
[NASA-TM-100287] p 120 N88-23073
- BOBULA, GEORGE A.**
Technology developments for a compound cycle engine p 30 N88-16637
- BODNER, S. R.**
Phenomenological modeling of hardening and thermal recovery in metals p 84 A88-24037
Unified constitutive models for high-temperature structural applications p 190 N88-21523
Constitutive modeling for isotropic materials
[NASA-CR-182132] p 37 N88-29811
- BOLDMAN, D. R.**
Wall shear stress measurement in blade end-wall corner region
[ASME PAPER 87-GT-181] p 131 A88-11089
- BOLDMAN, DONALD**
Experimental evaluation of corner vanes - Summary
[SAE PAPER 871784] p 39 A88-30778
- BOLDMAN, DONALD R.**
Unsteady aerodynamics of an oscillating cascade in a compressible flow field
[NASA-TM-100219] p 26 N88-13346
Experimental evaluation of turning vane designs for high-speed and coupled fan-drive corners of 0.1-scale model of NASA Lewis Research Center's proposed altitude wind tunnel
[NASA-TP-2681] p 40 N88-17686
- BOND, T. H.**
Performance and efficiency evaluation and heat release study of a direct-injection stratified-charge rotary engine
[SAE PAPER 870445] p 166 A88-23313
- BORRERO, J. M.**
Comparative radiation resistance, temperature dependence and performance of diffused junction indium phosphide solar cells p 198 A88-18580
Characterization and modelling of open tube diffused n+p bulk InP solar cells p 199 A88-34270
- BOSE, A.**
Gravitational contributions to microstructural coarsening in liquid phase sintering p 111 A88-37155
Gravity and configurational energy induced microstructural changes in liquid phase sintering p 112 A88-49089
- BOSE, AMITAVA**
Ohmic contact formation in semi-insulating GaAs using shallow heavily doped p-type layers p 219 A88-11150
- BOTHRA, S.**
Characterization and modelling of open tube diffused n+p bulk InP solar cells p 199 A88-34270
- BOTSIS, J.**
On self-similarity of crack layer p 181 A88-24054
On governing equations for crack layer propagation
[NASA-CR-182120] p 194 N88-23272
- BOWDITCH, DAVID N.**
Impact and promise of NASA aeropropulsion technology p 31 N88-16698
- BOWLES, KENNETH J.**
Mechanical properties characterization of composite sandwich materials intended for space antenna applications
[NASA-TM-88893] p 71 N88-10121
Transply crack density detection by acousto-ultrasonics
[NASA-TM-100224] p 72 N88-11758
A thermally modified polymer matrix composite material with structural integrity to 371 C
[NASA-TM-100922] p 76 N88-25483
- BOYCE, L.**
Probabilistic constitutive relationships for cyclic material strength models
[AIAA PAPER 88-2376] p 182 A88-32313
- BOYLE, M. T.**
Three-dimensional flow past two cylinders mounted side by side on an endwall
[AIAA PAPER 88-3718] p 143 A88-48974
- BOYLE, R. J.**
Impact of ETO propellants on the aerothermodynamic analyses of propulsion components
[NASA-TM-101303] p 156 N88-30094
- BOZZOLA, R.**
Application of Runge Kutta time marching scheme for the computation of transonic flows in turbomachines
[NASA-TM-86997] p 9 N88-12461
- BOZZOLO, GUILLERMO H.**
Interfacial adhesion: Theory and experiment
[NASA-TM-100830] p 92 N88-20417
- BRABBS, THEODORE A.**
The carbon dioxide chaperon efficiency for the reaction $H + O_2 + M$ yields $HO_2 + M$ from ignition delay times behind reflected shock waves
[NASA-TM-100125] p 79 N88-15036
- BRADT, RICHARD C.**
The effect of texture on the crack growth resistance of alumina
[NASA-TM-100250] p 102 N88-14206
- BRADY, JOYCE A.**
Oxidation and protection of fiberglass-epoxy composite masts for photovoltaic arrays in the low Earth orbital environment
[NASA-TM-100839] p 104 N88-18734
- BRANDHORST, H. JR.**
Space commercialization and power system technology p 223 A88-44003
- BRANDHORST, HENRY W., JR.**
Recent progress in space photovoltaic systems
[NASA-TM-100208] p 128 N88-11966
- BRAUN, M. J.**
Numerical and analytical study of fluid dynamic forces in seals and bearings p 167 A88-31534
Numerical modeling of multidimensional flow in seals and bearings used in rotating machinery
[NASA-TM-100779] p 150 N88-16988
Numerical and analytical study of fluid dynamic forces in seals and bearings
[NASA-TM-100268] p 151 N88-18867
- BREAKWELL, J. V.**
Low thrust power-limited transfer for a pole squatter
[AIAA PAPER 88-4310] p 42 A88-50435
- BRENA DE LA ROSA, A.**
Diagnostics development for spray characterization in complex turbulent flows
[ASME PAPER 88-GT-241] p 146 A88-54320
- BRENNEMAN, J. S.**
Slotline fed microstrip antenna array modules p 126 A88-44170
- BREWE, D. E.**
Stability of a rigid rotor supported on flexible oil journal bearings
[ASME PAPER 87-TRIB-48] p 166 A88-24034
On the performance of finite journal bearings lubricated with micropolar fluids
[NASA-TM-100293] p 150 N88-15983
- BREWE, DAVID E.**
Piezoviscous effects in nonconformal contacts lubricated hydrodynamically p 133 A88-12926
The solution of the Eirod algorithm for a dynamically loaded journal bearing using multigrid techniques
[NASA-TM-100941] p 154 N88-25854
- BREWER, DAVID**
In situ fatigue loading stage inside scanning electron microscope p 193 N88-22419
- BRIDGES, J. E.**
Roles of initial condition and vortex pairing in jet noise p 213 A88-13963
- BRIEHL, DANIEL**
Magnetic emissions testing of the space station engineering model resistojet
[NASA-TM-100788] p 48 N88-17728
- BRILEY, G. L.**
25-LBF GO2/GH2 space station thruster
[AIAA PAPER 88-2793] p 56 A88-53101
- BRILEY, W. R.**
Flow in a model turbine stator p 148 N88-11163
- BRINDLEY, P. K.**
Investigation of a SiC/Ti-24Al-11Nb composite
[NASA-TM-100956] p 76 N88-28980
- BRINDLEY, PAMELA K.**
SiC reinforced aluminide composites p 70 A88-31687
Development of a new generation of high-temperature composite materials p 73 N88-16702
- BRINKER, DAVID**
Self-consistent calculations and design considerations for a GaAs nipi doping superlattice solar cell p 124 A88-34249
- BRINKER, DAVID J.**
Recent developments in indium phosphide space solar cell research p 50 A88-11785
Progress in InP solar cell research
[NASA-TM-100914] p 130 N88-24870
Advanced photovoltaic power system technology for lunar base applications
[NASA-TM-100965] p 65 N88-26402
- BRITTAIN, J. O.**
Elevated temperature strain gages p 160 N88-11144
- BRITTON, DORIS L.**
Lightweight nickel electrode for nickel hydrogen cells and batteries p 198 A88-16631
Performance of lightweight nickel electrodes
[NASA-TM-100958] p 80 N88-26430
- BROCKWELL, JONATHAN L.**
Mass transport phenomena between bubbles and dissolved gases in liquids under reduced gravity conditions
[AIAA PAPER 88-0450] p 138 A88-27719
Mass transport phenomena between bubbles and dissolved gases in liquids under reduced gravity conditions
[NASA-TM-100273] p 80 N88-18672
- BROWN, G. V.**
The impact damped harmonic oscillator in free decay p 167 A88-31581
- BROWN, J. S.**
Vapor condensation rate at a turbulent liquid interface, for application to cryogenic hydrogen
[AIAA PAPER 88-0559] p 137 A88-22419
- BROWN, K. W.**
Aero/structural tailoring of engine blades (AERO/STAEBL)
[NASA-CR-180805] p 207 N88-21682

- Structural tailoring of advanced turboprops
p 192 N88-22400
- BROWN, KENNETH W.**
Structural Tailoring of Advanced Turboprops (STAT)
[NASA-CR-180861] p 36 N88-28074
- BROWN, S. D.**
Hafnia-rich mixed oxide ceramics of the system
HfO₂-ZrO₂-TiO₂ for heaters and heat exchangers in
electrothermal thrusters: The effects of titania on selected
electrical and mechanical properties of Hafnia-rich mixed
oxides in the system Hafnia-Zirconia-Titania, volume 1
[NASA-CR-182800-VOL-1] p 105 N88-22197
- BROWN, W. H.**
Effects of nozzle-exit boundary-layer conditions on
excitability of heated free jets
[AIAA PAPER 87-2723] p 135 A88-20182
Acoustically excited heated jets. 1: Internal excitation
[NASA-CR-4129-PT-1] p 12 N88-23751
Acoustically excited heated jets. 2: In search of a better
understanding p 12 N88-23752
Acoustically excited heated jets. 3: Mean flow data
[NASA-CR-4129-PT-3] p 12 N88-23753
- BROWNING, RAY**
Multielement mapping of alpha-SiC by scanning Auger
microscopy p 158 A88-27617
- BRUSH, ANDREW S.**
Microgravity robotics technology program
[NASA-TM-100898] p 173 N88-23219
Microgravity manipulator demonstration p 173 N88-23242
- BRYANT, LIVELY**
Techniques utilized in the simulated altitude testing of
a 2D-CD vectoring and reversing nozzle
[NASA-TM-100872] p 40 N88-25464
- BUCHHE, DONALD R.**
Small-droplet spray measurements with a scattered-light
scanner p 163 N88-26645
- BUCKLEY, DONALD H.**
Mechanical strength and tribological behavior of
ion-beam-deposited boron nitride films on non-metallic
substrates p 98 A88-32866
Friction and wear of ceramics p 106 N88-23874
- BUDINGER, J. M.**
Bandwidth-efficient high-speed coded trellis
modulation p 116 A88-27560
- BUFFUM, DANIEL H.**
Unsteady aerodynamics of an oscillating cascade in a
compressible flow field p 26 N88-13346
Investigation of oscillating cascade aerodynamics by an
experimental influence coefficient technique
[NASA-TM-101313] p 14 N88-28041
- BUGGELN, R. C.**
Flow in a model turbine stator p 148 N88-11163
- BULZAN, DANIEL L.**
Particle-laden weakly swirling free jets - Measurements
and predictions p 142 A88-48757
Particle-laden weakly swirling free jets: Measurements
and predictions p 34 N88-24639
- BUNTING, BRUCE G.**
Investigation of PTFE transfer films by infrared emission
spectroscopy and phase-locked ellipsometry p 99 A88-35568
- BUNYAN, S. M.**
Development of 8 cm x 8 cm silicon gridded back solar
cell for space station p 200 A88-34312
- BURKE, J. J.**
Guided-wave approaches to spectrally selective energy
absorption p 119 N88-17892
- BURKHOLDER, R. J.**
Electromagnetic fields backscattered from an s-shaped
inlet cavity with an absorber coating on its inner walls
[NASA-CR-182401] p 118 N88-15130
- BURNS, MAUREEN E.**
Techniques utilized in the simulated altitude testing of
a 2D-CD vectoring and reversing nozzle
[NASA-TM-100872] p 40 N88-25464
- BURNS, ROBERT J.**
Mixing fuel particles for space combustion research
using acoustics p 112 A88-49093
Mixing fuel particles for space combustion research
using acoustics p 43 N88-21186
- BURNSIDE, O. H.**
Efficient probabilistic fracture mechanics analysis
p 180 A88-16933
Validation of the NESSUS probabilistic finite element
analysis computer program p 205 A88-32309
Probabilistic Structural Analysis Methods for select
- space propulsion system structural components (PSAM)
p 56 A88-49659
- BUZZARD, ROBERT J.**
Calibration of a Mode II test specimen p 183 A88-47014
Mode II fracture mechanics p 193 N88-22418
- BYERS, DAVID C.**
Status of high power electric propulsion technology
p 63 N88-24443
- C**
- CAHAN, B. D.**
I-BIEM, an iterative boundary integral equation method
for computer solutions of current distribution problems with
complex boundaries: A new algorithm. I - Theoretical
p 205 A88-27795
- CAIRELLI, JAMES E.**
SPRE 1 free-piston Stirling engine testing at NASA Lewis
Research Center p 57 N88-11747
[NASA-TM-100241] p 57 N88-11747
Test results of a 40-kW Stirling engine and comparison
with the NASA Lewis computer code predictions
[NASA-TM-87050] p 201 N88-19013
- CALDECOTT, R.**
Measurement of the properties of lossy materials inside
a finite conducting cylinder p 213 N88-20962
[NASA-CR-182664]
- CAMERON, T. M.**
An integrated approach for friction damper design
p 167 A88-31598
- CAMPANELLA, S. JOSEPH**
Future switching satellites p 46 A88-27553
[AIAA PAPER 88-0802] p 46 A88-27553
A flexible on-board demultiplexer/demodulator
[AIAA PAPER 88-0811] p 123 A88-27558
- CANN, GORDON L.**
Arcjet thruster research and technology
[NASA-CR-180865] p 59 N88-17732
- CAPLIN, B.**
User's manual for three dimensional boundary layer
(BL3-D) code p 155 N88-30063
[NASA-CR-174899]
- CAREK, GERALD A.**
Improved method for stress and compatibility analysis
of multicomponent rotating systems p 195 N88-25935
[NASA-TM-100884]
- CARLSON, ALBERT**
Heat pipe radiators for solar dynamic space power
system heat rejection p 132 A88-11807
- CARLSON, ALBERT W.**
High thermal-transport capacity heat pipes for space
radiators p 136 A88-21155
[SAE PAPER 871509]
- CARLSON, R. L.**
Non-isothermal elastoviscoplastic analysis of planar
curved beams p 190 N88-21526
- CARNEY, L. M.**
Application of superconducting technology to
earth-to-orbit electromagnetic launch systems
[NASA-TM-101134] p 43 N88-26385
- CARNEY, LYNNETTE M.**
Evaluation of the communications impact of a low power
arcjet thruster p 55 A88-48755
[AIAA PAPER 88-3105] p 55 A88-48755
An experimental investigation of an arcjet thruster
exhaust using Langmuir probes p 60 N88-21253
[NASA-TM-100258] p 60 N88-21253
Evaluation of the communications impact of a low power
arcjet thruster p 63 N88-24682
[NASA-TM-100926] p 63 N88-24682
Experimental evaluation of resistojet thruster plume
shields p 66 N88-29868
[NASA-TM-101363] p 66 N88-29868
- CARPENTER, MARK H.**
Liquid sprays and flow studies in the direct-injection
diesel engine under motored conditions p 31 N88-18594
[NASA-TM-100135]
- CARROLL, DAVID R.**
Hardware realization of a baseband processor for a
SS-FDMA/TDMA/DAMA system p 124 A88-27575
[AIAA PAPER 88-0830] p 124 A88-27575
- CARTER, ALAN L.**
Hypersonic structures and materials - A progress
report p 17 A88-16748
- CARTER, CAMPBELL D.**
Feasibility of hydroxyl concentration measurements by
laser-saturated fluorescence in high-pressure flames
p 77 A88-17218
- CARUSO, J. J.**
Superelement methods applications to micromechanics
of high temperature metal matrix composites
[AIAA PAPER 88-2390] p 182 A88-32322
- CARUTHERS, J. M.**
A nonlinear viscoelastic constitutive equation - Yield
predictions in multiaxial deformations p 185 A88-54912
- Linear and nonlinear mechanical properties of a series
of epoxy resins p 101 A88-54976
- CASTOR, J. G.**
Technology developments for a compound cycle
engine p 30 N88-16637
- CATALANO, DANIEL A.**
Foil bearing lubrication theory including compressibility
effects p 170 A88-54964
- CATALDO, ROBERT L.**
Component variations and their effects on bipolar
nickel-hydrogen cell performance p 197 A88-11914
Test results of a 60 volt bipolar nickel-hydrogen
battery p 198 A88-11916
Energy storage considerations for a robotic Mars surface
sampler p 227 N88-28853
[NASA-TM-100969] p 227 N88-28853
- CAUGHEY, D. A.**
A diagonally inverted LU implicit multigrid scheme
[AIAA PAPER 88-3565] p 209 A88-48791
- CAUGHEY, DAVID A.**
Effects of numerical dissipation on finite-volume
solutions of compressible flow problems p 5 A88-22469
[AIAA PAPER 88-0621] p 5 A88-22469
A diagonally inverted LU implicit multigrid scheme
[NASA-TM-100911] p 13 N88-26340
- CAVANO, PAUL**
Transply crack density detection by
acousto-ultrasonics p 72 N88-11758
[NASA-TM-100224] p 72 N88-11758
- CEBECI, TUNCER**
The calculation of flow over iced airfoils p 4 A88-22078
[AIAA PAPER 88-0112] p 4 A88-22078
Effects of environmentally imposed roughness on airfoil
performance p 15 N88-15778
- CELESTINA, MARK L.**
Utilization of parallel processing in solving the inviscid
form of the average-passage equation system for
multistage turbomachinery p 32 N88-21160
[NASA-TM-89845] p 32 N88-21160
Convergence acceleration for vector sequences and
applications to computational fluid dynamics
[NASA-TM-101327] p 212 N88-30377
- CERNANSKY, N. P.**
Modified reaction mechanism of aerated n-dodecane
liquid flowing over heated metal tubes p 108 A88-44268
- CHAFFINS, SCOTT A.**
Electrocatalytic reduction of oxygen on modified oxide
surfaces p 81 N88-29952
[NASA-TM-101333] p 81 N88-29952
- CHAI, AN-TI**
Mass transport phenomena between bubbles and
dissolved gases in liquids under reduced gravity
conditions p 138 A88-27719
[AIAA PAPER 88-0450] p 138 A88-27719
Experimental study of thermocapillary flows in a thin
liquid layer with heat fluxes imposed on the free surface
p 144 A88-49087
Experimental study of thermocapillary flows in a thin
liquid layer with heat fluxes imposed on the free surface
[NASA-TM-100252] p 148 N88-12763
Mass transport phenomena between bubbles and
dissolved gases in liquids under reduced gravity
conditions p 80 N88-18672
[NASA-TM-100273] p 80 N88-18672
- CHAI, J. C.**
Turbulence energy and diffusion transport of
third-moments in a separating and reattaching flow
p 141 A88-43011
- CHALMERS, HARVEY**
Future switching satellites p 46 A88-27553
[AIAA PAPER 88-0802] p 46 A88-27553
- CHAMIS, C. C.**
Fracture toughness computational simulation of general
delaminations in fiber composites p 181 A88-32219
[AIAA PAPER 88-2261] p 181 A88-32219
Parametric studies of advanced turboprops
[AIAA PAPER 88-2266] p 20 A88-32223
Probabilistic composite micromechanics p 182 A88-32312
[AIAA PAPER 88-2375] p 182 A88-32312
Probabilistic constitutive relationships for cyclic material
strength models p 182 A88-32313
[AIAA PAPER 88-2376] p 182 A88-32313
Superelement methods applications to micromechanics
of high temperature metal matrix composites
[AIAA PAPER 88-2390] p 182 A88-32322
Hygrothermomechanical fiber composite fatigue -
Computational simulation p 71 A88-42437
Free-edge delamination: Laminate width and loading
conditions effects p 72 N88-12551
[NASA-TM-100238] p 72 N88-12551
- CHAMIS, CHRISTOS C.**
Probabilistic structural analysis methods for space
propulsion system components p 54 A88-16441

- Fracture characteristics of angleplied laminates fabricated from overaged graphite/epoxy prepreg p 69 A88-16965
- Application of structural tailoring to spar/shell turboprops [AIAA PAPER 88-2333] p 20 A88-32277
- Probabilistic structural analysis of aerospace components using NESSUS [AIAA PAPER 88-2373] p 182 A88-32310
- Composite mechanics for engine structures [NASA-TM-100176] p 72 N88-12552
- Fiber composite structural durability and damage tolerance: Simplified predictive methods [NASA-TM-100179] p 72 N88-13409
- STAEBL/general composites with hygrothermal effects (STAEBL/GENCOM) [NASA-TM-100266] p 187 N88-13754
- Simplified procedures for designing composite bolted joints [NASA-TM-100281] p 73 N88-15020
- Design procedures for fiber composite box beams [NASA-TM-100296] p 73 N88-16828
- Mechanics of composite materials: Past, present and future [NASA-TM-100793] p 73 N88-17744
- Finite element substructuring methods for composite mechanics [NASA-TM-100297] p 73 N88-17745
- Hygrothermomechanical fiber composite fatigue: Computational simulation [NASA-TM-100840] p 74 N88-21257
- Computational structural mechanics for engine structures p 33 N88-22399
- Probabilistic structural analysis to quantify uncertainties associated with turbopump blades [NASA-TM-100278] p 76 N88-28094
- CHAN, K. S.**
- Phenomenological modeling of hardening and thermal recovery in metals p 84 A88-24037
- Unified constitutive models for high-temperature structural applications p 190 N88-21523
- Constitutive modeling for isotropic materials [NASA-CR-182132] p 37 N88-29811
- CHANDRA, P. R.**
- Effect of rib angle on local heat/mass transfer distribution in a two-pass rib-roughened channel [ASME PAPER 87-GT-94] p 131 A88-11033
- Local heat/mass transfer distributions around sharp 180 deg turns in two-pass smooth and rib-roughened channels [ASME PAPER 86-GT-114] p 139 A88-28516
- Local heat/mass transfer and pressure drop in a two-pass rib-roughened channel for turbine airfoil cooling [NASA-CR-179635] p 148 N88-12039
- CHANDRASEKHAR, B. S.**
- Weak-field magnetization of superconducting Y1Ba2Cu3O(x) - Relationship to microstructure p 219 A88-18814
- CHANG, G. C.**
- Thermal expansion mismatch and oxidation in thermal barrier coatings p 170 N88-11182
- CHANG, J.**
- Dynamic and static fatigue behavior of sintered silicon nitrides p 96 A88-12602
- CHANG, SHIH-HUNG**
- A comparison of ENO and TVD schemes [AIAA PAPER 88-3707] p 210 A88-48831
- CHANG, T. Y.**
- A mixed formulation of C(0)-linear triangular plate/shell element - The role of edge shear constraints p 183 A88-40121
- CHAO, L. Y.**
- Effects of subcritical crack growth on fracture toughness of ceramics assessed in chevron-notched three-point bend tests [ASME PAPER 88-GT-185] p 185 A88-54276
- CHAOUI, KAMEL**
- Curvilinear crack layer propagation p 96 A88-14568
- CHARLESTON, JO ANN**
- Assessment of commercially available and experimental hydrogen electrodes p 198 A88-16632
- CHATO, DAVID J.**
- Thermodynamic modeling of the no-vent fill methodology for transferring cryogenics in low gravity [AIAA PAPER 88-3403] p 55 A88-48765
- Thermodynamic modeling of the no-vent fill methodology for transferring cryogenics in low gravity [NASA-TM-100932] p 63 N88-24686
- CHEN, C.**
- Study of free-piston Stirling engine driven linear alternators [NASA-CR-181425] p 170 N88-10355
- CHEN, C. F.**
- Onset of finger convection in a horizontal porous layer underlying a fluid layer p 140 A88-41572
- Double-diffusive effects during solidification p 221 A88-43933
- CHEN, C. T.**
- Fingering flow patterns of thermosolutal convection in rectangular enclosures [AIAA PAPER 88-3823] p 144 A88-49000
- Thermosolutal convection in high-aspect-ratio enclosures [NASA-TM-100803] p 151 N88-18871
- Fingering flow patterns of thermosolutal convection in rectangular enclosures [NASA-TM-100854] p 152 N88-21417
- CHEN, F.**
- Onset of finger convection in a horizontal porous layer underlying a fluid layer p 140 A88-41572
- CHEN, J.**
- Modal test/analysis correlation for the Centaur G prime launch vehicle p 44 A88-18631
- CHEN, J. J.**
- Fingering flow patterns of thermosolutal convection in rectangular enclosures [AIAA PAPER 88-3823] p 144 A88-49000
- Fingering flow patterns of thermosolutal convection in rectangular enclosures [NASA-TM-100854] p 152 N88-21417
- CHEN, J. L.**
- Redundant manipulators for momentum compensation in a micro-gravity environment [AIAA PAPER 88-4121] p 204 A88-50223
- CHEN, P. C.**
- 3D inelastic analysis methods for hot section components p 185 N88-11164
- CHEN, QI**
- Resolved shear stress intensity coefficient and fatigue crack growth in large crystals [NASA-CR-182137] p 195 N88-24997
- CHEN, S. C.**
- Three-dimensional adaptive grid generation for body-fitted coordinate system [NASA-CR-182192] p 155 N88-27520
- Three-dimensional elliptic grid generation technique with application to turbomachinery cascades [NASA-TM-101330] p 155 N88-30078
- CHEN, W.**
- On the cyclic stress-strain behaviour of a Ni-base superalloy at room temperature p 84 A88-24521
- CHENG, T. T.**
- Improved beta-SiC heteroepitaxial films using off-axis Si substrates p 219 A88-10431
- Lattice defects in beta-SiC grown epitaxially on silicon substrates p 220 A88-28711
- Microscopy of epitaxially grown beta-SiC on 001-plane silicon p 98 A88-31023
- CHERRETTE, A. R.**
- Compensation of reflector antenna surface distortion using an array feed [NASA-TM-100286] p 119 N88-18805
- Case study of active array feed compensation with sidelobe control for reflector surface distortion [NASA-TM-100287] p 120 N88-23073
- CHETHIK, FRANK**
- Bandwidth and power efficient satellite TDMA demodulator and decoder [AIAA PAPER 88-0812] p 123 A88-27559
- CHI, S.**
- Advanced composite turboprops - Modeling, structural, and dynamic analyses [ASME PAPER 87-GT-78] p 21 A88-36745
- CHIARAMONTE, FRANCIS P.**
- Determination of compressor in-stall characteristics from engine surge transients p 21 A88-35505
- CHILDS, D. W.**
- Theory versus experiment for the rotordynamic coefficients of labyrinth gas seals. II - A companion to experiment p 167 A88-31536
- CHILDS, DARA W.**
- Experimental rotordynamic coefficient results for honeycomb seals [NASA-CR-182440] p 172 N88-16007
- CHIMA, R. V.**
- A diagonally inverted LU implicit multigrid scheme [AIAA PAPER 88-3565] p 209 A88-48791
- CHIMA, RODRICK V.**
- Explicit multigrid algorithm for quasi-three-dimensional viscous flows in turbomachinery p 2 A88-10355
- Application of advanced computational codes in the design of an experiment for a supersonic throughflow fan rotor [ASME PAPER 87-GT-160] p 2 A88-11072
- An explicit Runge-Kutta method for unsteady rotor/stator interaction [AIAA PAPER 88-0049] p 5 A88-27715
- Time-partitioning simulation models for calculation of parallel computers p 206 A88-46961
- Numerical analysis of three-dimensional viscous internal flows [AIAA PAPER 88-3522] p 142 A88-48779
- An explicit Runge-Kutta method for unsteady rotor/stator interaction [NASA-TM-100787] p 10 N88-14967
- Numerical analysis of three-dimensional viscous internal flows [NASA-TM-100878] p 1 N88-21116
- A diagonally inverted LU implicit multigrid scheme [NASA-TM-100911] p 13 N88-26340
- An unconditionally stable Runge-Kutta method for unsteady flows [NASA-TM-101347] p 14 N88-29780
- CHITRE, D. M.**
- Service offerings and interfaces for the ACTS network of earth stations [AIAA PAPER 88-0800] p 116 A88-27551
- CHOI, H. C.**
- Macrocrack interaction with transverse array of microcracks p 181 A88-30236
- CHOREY, C. M.**
- Improved beta-SiC heteroepitaxial films using off-axis Si substrates p 219 A88-10431
- Lattice defects in beta-SiC grown epitaxially on silicon substrates p 220 A88-28711
- Microscopy of epitaxially grown beta-SiC on 001-plane silicon p 98 A88-31023
- High frequency GaAlAs modulator and photodetector for phased array antenna applications [NASA-TM-101328] p 130 N88-30048
- CHOREY, CHRISTOPHER M.**
- A high frequency GaAlAs travelling wave electro-optic modulator at 0.82 micrometers [NASA-TM-100970] p 130 N88-28240
- CHOU, RI-CHEE**
- Modal attenuation in multilayered coated waveguides p 126 A88-45755
- CHOY, FRED K.**
- Dynamic analysis of multimesh-gear helicopter transmissions [NASA-TP-2789] p 172 N88-17045
- CHOYKE, W. J.**
- Low-temperature photoluminescence studies of chemical-vapor-deposition-grown 3C-SiC on Si p 127 A88-53396
- Raman scattering studies of chemical-vapor-deposited cubic SiC films of (100)Si p 127 A88-53397
- CHRISTIAN, JOSE L., JR.**
- Electromagnetic powered vehicles (EMPV) for Mars exploration p 62 N88-24388
- A role for high frequency superconducting devices in free space power transmission systems [NASA-TM-100971] p 130 N88-25830
- CHUANG, C. W.**
- Electromagnetic fields backscattered from an s-shaped inlet cavity with an absorber coating on its inner walls [NASA-CR-182401] p 118 N88-15130
- CHUANG, ISAAC**
- A detailed description of the uncertainty analysis for high area ratio rocket nozzle tests at the NASA Lewis Research Center p 65 N88-25580
- CHUANG, S.**
- Scale model acoustic testing of counterrotating fans [AIAA PAPER 88-2057] p 22 A88-37947
- CHUBB, DONALD L.**
- Performance characteristics of a combination solar photovoltaic heat engine energy converter [NASA-TM-100928] p 197 A88-11813
- CHUDNOVSKY, A.**
- A probabilistic model of brittle crack formation p 180 A88-18696
- Crack diffusion coefficient - A candidate fracture toughness parameter for short fiber composites p 70 A88-36945
- Semi-empirical crack tip analysis p 183 A88-47681
- On governing equations for crack layer propagation [NASA-CR-182120] p 194 N88-23272
- CHUDNOVSKY, ALEXANDER**
- Curvilinear crack layer propagation p 96 A88-14568
- CHULYA, ABHISAK**
- An efficient Mindlin finite strip plate element based on assumed strain distribution p 192 N88-22407
- Improved finite strip Mindlin plate bending element using assumed shear strain distributions [NASA-TM-100928] p 196 N88-29195
- CHUN, K. S.**
- Performance and efficiency evaluation and heat release study of a direct-injection stratified-charge rotary engine [SAE PAPER 870445] p 166 A88-23313
- CHUN, KUE S.**
- Engine flow visualization using a copper vapor laser p 158 A88-34479

- CHUNG, B. T. F.**
Thermomechanical behavior of plasma-sprayed ZrO₂-Y₂O₃ coatings influenced by plasticity, creep, and oxidation p 95 A88-12588
- CHUNG, C. L.**
Base reaction optimization of manipulators with redundant kinematics p 173 N88-23238
- CHUPP, R. E.**
Phase-resolved heat-flux measurements on the blade of a full-scale rotating turbine [ASME PAPER 88-GT-173] p 145 A88-54267
- CHYU, M. K.**
Heat transfer in the tip region of a rotor blade simulator p 147 N88-11159
- CIANCONE, MICHAEL L.**
Mast material test program (MAMATEP) [AIAA PAPER 88-2475] p 70 A88-35945
Oxidation and protection of fiberglass-epoxy composite masts for photovoltaic arrays in the low Earth orbital environment [NASA-TM-100839] p 104 N88-18734
Mast material test program (MAMATEP) [NASA-TM-100821] p 74 N88-19592
- CIEMPLUCH, CARL C.**
Results of NASA's Energy Efficient Engine Program p 19 A88-20785
- CIFANI, DIANE**
The 700 F properties of autoclave cured PMR-2 composites [NASA-TM-100923] p 75 N88-24712
- CIVINSKAS, K. C.**
Impact of ETO propellants on the aerothermodynamic analyses of propulsion components [NASA-TM-101303] p 156 N88-30094
- CLARK, B. J.**
High-speed propeller noise predictions - Effects of boundary conditions used in blade loading calculations p 215 A88-36270
- CLARK, RALPH O.**
Self-consistent calculations and design considerations for a GaAs nipi doping superlattice solar cell p 124 A88-34249
- CLASPY, P. C.**
Microwave response of an HEMT photoconductor [NASA-TM-100819] p 128 N88-18835
High frequency GaAlAs modulator and photodetector for phased array antenna applications [NASA-TM-101328] p 130 N88-30048
- CLAUS, R. W.**
Time-accurate simulations of a shear layer forced at a single frequency [AIAA PAPER 88-0061] p 138 A88-27716
Time-accurate simulations of a shear layer forced at a single frequency [NASA-TM-100836] p 152 N88-19740
- COCHRAN, THOMAS H.**
Space Station Electrical Power System [IAF PAPER 87-234] p 53 A88-15958
- COE, HAROLD H.**
Results of NASA/Army transmission research p 31 N88-16640
Computer-aided design analysis of 57-mm, angular-contact, cryogenic turbopump bearings [NASA-TP-2816] p 172 N88-18933
Helicopter transmission research at NASA Lewis Research Center [NASA-TM-100962] p 175 N88-30128
- COHEN, H. A.**
Electron beam experiments at high altitudes p 47 A88-46799
- COHEN, R. S.**
Modified reaction mechanism of aerated n-dodecane liquid flowing over heated metal tubes p 108 A88-44268
- COIRIER, WILLIAM J.**
High speed inlet calculations with real gas effects [NASA-CR-182167] p 13 N88-26336
- COLE, GARY L.**
Automating the parallel processing of fluid and structural dynamics calculations p 206 A88-46963
- COLES-HAMILTON, CAROLYN**
Selection of high temperature thermal energy storage materials for advanced solar dynamic space power systems p 68 A88-11801
- COLES-HAMILTON, CAROLYN E.**
Impact of thermal energy storage properties on solar dynamic space power conversion system mass p 51 A88-11805
- COLES, CAROLYN E.**
Oxygen plasma effects on several liquid droplet radiator fluids p 142 A88-47962
- COLLETT, C. R.**
Auxiliary propulsion system flight package [NASA-CR-180828] p 56 N88-10886
- COLLINS, J. J.**
Noncontacting measurement technologies for space propulsion condition monitoring p 158 A88-29818
- COLLINS, STUART A., JR.**
Implementation of a fast digital optical matrix-vector multiplier using a holographic look-up table and residue arithmetic p 205 A88-17223
- COLTRIN, ROBERT E.**
High-speed inlet research program and supporting analyses p 17 N88-15811
- CONLEY, T. A.**
Service offerings and interfaces for the ACTS network of earth stations [AIAA PAPER 88-0800] p 116 A88-27551
- CONLEY, THOM A.**
Service offerings and interfaces for the ACTS network of Earth stations [NASA-TM-100809] p 46 N88-24663
- CONNOLLY, DENIS J.**
Monolithic Microwave Integrated Circuit (MMIC) technology for space communications applications [IAF PAPER 87-491] p 122 A88-16133
- CONRAY, MARTIN J.**
Experimental radio frequency link for Ka-band communications applications [NASA-TM-100824] p 43 N88-24659
- CONTOLATIS, A.**
Two stage dual gate MESFET monolithic gain control amplifier for Ka-band p 124 A88-29821
- CONTOLATIS, T.**
A 30 GHz monolithic receive module technology assessment [NASA-CR-180825] p 129 N88-23084
- CONWAY, BRUCE A.**
Optimal cooperative time-fixed impulsive rendezvous [AIAA PAPER 88-4279] p 42 A88-50406
- COOMBS, MURRAY G.**
Advanced heat receiver conceptual design study [NASA-CR-180901] p 203 N88-25977
- COOPER, RALPH S.**
Expert systems for space power supply - Design, analysis, and evaluation p 212 A88-22696
- CORBAN, R. R.**
Technology requirements for an orbiting fuel depot: A necessary element of a space infrastructure [NASA-TM-101370] p 49 N88-29845
- CORRIGAN, R. D.**
Testing of a one-bladed 30-meter-diameter rotor on the DOE/NASA Mod-O wind turbine [NASA-TM-100274] p 201 N88-19014
- CORRIGAN, ROBERT D.**
Solar concentrator advanced development project p 50 A88-11799
- COUTTS, T. J.**
InP based solar cells for space application: Reduction of external losses p 199 A88-34250
Direct-current magnetron fabrication of indium tin oxide/InP solar cells p 200 A88-51289
- COY, J. J.**
Method for generation of spiral bevel gears with conjugate gear tooth surfaces [ASME PAPER 88-DET-3] p 165 A88-10973
Computerized life and reliability modelling for turboprop transmissions [AIAA PAPER 88-2979] p 100 A88-48031
Computerized life and reliability modelling for turboprop transmissions [NASA-TM-100918] p 173 N88-23220
- COY, JOHN J.**
An overview of rotorcraft propulsion research at Lewis Research Center p 22 A88-40554
On dynamic loads in parallel shaft transmissions. 1: Modelling and analysis [NASA-TM-100180] p 171 N88-12797
On dynamic loads in parallel shaft transmissions. 2: Parameter study [NASA-TM-100181] p 171 N88-12798
Rotorcraft transmission p 172 N88-15802
Results of NASA/Army transmission research p 31 N88-16640
Identification and proposed control of helicopter transmission noise at the source p 38 N88-16647
Advanced transmission studies [NASA-TM-100867] p 173 N88-21454
Helicopter transmission research at NASA Lewis Research Center [NASA-TM-100962] p 175 N88-30128
- CRANDALL, KAREN S.**
Laboratory Information Management System (LIMS): A case study [NASA-TM-100835] p 208 N88-21697
- CRAWFORD, ROGER A.**
Flow field measurements in a 90 degree turning duct p 147 N88-11157
- CRAWLEY, E.**
Bladed disk assemblies; Proceedings of the Eleventh Biennial Conference on Mechanical Vibration and Noise, Boston, MA, Sept. 27-30, 1987 p 20 A88-31608
- CRIMP, M. A.**
Room temperature tensile ductility in powder processed B2 FeAl alloys p 85 A88-31694
- CRUSE, T. A.**
Probabilistic Structural Analysis Methods for select space propulsion system structural components (PSAM) p 56 A88-49659
Thermal barrier coating life prediction model development [ASME PAPER 88-GT-284] p 68 A88-54353
- CUFFIN, S. M.**
Space station onboard propulsion system: Technology study [NASA-CR-179233] p 59 N88-15006
- CULL, RONALD C.**
A role for high frequency superconducting devices in free space power transmission systems [NASA-TM-100971] p 130 N88-25830
- CURLISS, D. B.**
Linear and nonlinear mechanical properties of a series of epoxy resins p 101 A88-54976
- CURRAN, FRANCIS M.**
An extended life and performance test of a low-power arcjet [AIAA PAPER 88-3106] p 55 A88-48756
A low-power arcjet cyclic lifetest [NASA-TM-100233] p 57 N88-11748
An extended life and performance test of a low-power arcjet [NASA-TM-100942] p 63 N88-24687
- CURREN, ARTHUR N.**
High-efficiency helical traveling-wave tube with dynamic velocity taper and advanced multistage depressed collector p 124 A88-32836
- CURTIS, E. W.**
Droplet vaporization in a supercritical microgravity environment [IAF PAPER 87-384] p 134 A88-16055
- CURTIS, H. B.**
Radiation performance of AlGaAs and InGaAs concentrator cells and expected performance of cascade structures p 125 A88-34356
A comparison of the radiation tolerance characteristics of multijunction solar cells with series and voltage-matched configurations [NASA-TM-101177] p 203 N88-27624
- CURTIS, HENRY B.**
Performance of GaAs and silicon concentrator cells under 37 MeV proton irradiation p 200 A88-34343
Performance of GaAs and silicon concentrator cells under 37 MeV proton irradiation [NASA-TM-100144] p 200 N88-12877
Radiation performance of AlGaAs concentrator cells and expected performance of cascade structures [NASA-TM-100145] p 200 N88-12878
- CYR, M. A.**
Development of sensors for ceramic components in advanced propulsion systems: Survey and evaluation of measurement techniques for temperature, strain and heat flux for ceramic components in advanced propulsion systems [NASA-CR-182111] p 163 N88-28299
- CYR, MARCIA A.**
Development of heat flux sensors for turbine airfoils p 160 N88-11143

D

- D'AMORE, L.**
Silsesquioxanes as precursors to ceramic composites p 69 A88-12599
- D'ANGELO, N.**
Exposed high-voltage source effect on the potential of an ionospheric satellite p 218 A88-54992
- DAHL, MILO D.**
A finite element model for wave propagation in an inhomogeneous material including experimental validation [AIAA PAPER 87-2741] p 212 A88-16577
- DAI, X. F.**
Spray characteristics of a spill-return airblast atomizer [ASME PAPER 88-GT-7] p 145 A88-54154
- DAILY, J. W.**
The structure and dynamics of reacting plane mixing layers p 136 A88-20871
- DALSANIA, VITHAL**
Thermal distortion analysis of the space station solar dynamic concentrator [NASA-TM-100868] p 64 A88-25475

DAME, L. T.

DAME, L. T.

- A crystallographic model for nickel base single crystal alloys p 89 A88-48182
3D inelastic analysis methods for hot section components p 185 N88-11164
Constitutive modeling for isotropic materials p 186 N88-11172

DAME, L. THOMAS

- Constitutive modeling for single crystal superalloys p 90 N88-11168

DANIELSON, L.

- Effect of the microstructure on the thermoelectric properties of polycrystalline lanthanum chalcogenides p 221 A88-40797

DAVID, J. W.

- Transfer matrix modeling of geared system vibration p 168 A88-39703

DAVIDIAN, KENNETH J.

- A detailed description of the uncertainty analysis for high area ratio rocket nozzle tests at the NASA Lewis Research Center p 65 N88-25580

DAVIES, W. J.

- Conceptual design of an optic based engine control system [ASME PAPER 87-GT-168] p 18 A88-11079

DAVIS, DONALD Y.

- Results of NASA's Energy Efficient Engine Program p 19 A88-20785

DAVIS, E. D.

- Coherent motion induced fluctuations in the primary transition region of a plane shear layer p 133 A88-14125

DAVIS, V. A.

- Threshold-determining mechanisms for discharges in high-voltage solar arrays p 50 A88-11738
Hollow cathodes as electron emitting plasma contactors - Theory and computer modeling p 218 A88-47973
Electron collection by multiple objects within a single sheath p 219 A88-54999

DAWSON, JEF M.

- Utilization of parallel processing in solving the inviscid form of the average-passage equation system for multistage turbomachinery [NASA-TM-89845] p 32 N88-21160

DAY, D. E.

- Glass properties in the yttria-alumina-silica system p 96 A88-18361

DAYTON, J. A.

- Submillimeter backward wave oscillators p 122 A88-19659

DAYTON, J. A., JR.

- High efficiency, long life traveling wave tubes for future communications satellites [AIAA PAPER 88-0835] p 124 A88-27578

DAYTON, JAMES A., JR.

- High efficiency, long life traveling wave tubes for future communications satellites [NASA-TM-100837] p 45 N88-19565

DE WITT, K. J.

- An experimental investigation of the effect of test-cell pressure on the performance of resistojets [AIAA PAPER 88-3286] p 40 A88-44820

DE WITT, KENNETH J.

- Measurement of local convective heat transfer coefficients from a smooth and roughened NACA-0012 airfoil - Flight test data [AIAA PAPER 88-0287] p 136 A88-22207

DEADMORE, D. L.

- Effect of alloy composition on the sodium-sulfate induced hot corrosion attack of cast nickel-base superalloys at 900 C p 81 A88-10028

DEADMORE, DANIEL L.

- Sputtered silver films to improve chromium carbide based solid lubricant coatings for use to 900 C p 100 A88-47563

- Sputtered silver films to improve chromium carbide based solid lubricant coatings for use to 900 C [NASA-TM-100783] p 102 N88-15885

- Friction and wear of monolithic and fiber reinforced silicon-ceramics sliding against IN-718 alloy at 25 to 800 C in atmospheric air at ambient pressure [NASA-TM-100294] p 103 N88-17796

DEANNA, RUSSELL G.

- Development of a thermal and structural analysis procedure for cooled radial turbines [ASME PAPER 88-GT-18] p 145 A88-54164

DECKER, ARTHUR J.

- Sources of error in heterodyne moire deflectometry p 158 A88-35004

DEGEORGE, C. L.

- Large-Scale Advanced Prop-Fan (LAP) [NASA-CR-182112] p 32 N88-20306

DEGROH, HENRY C.

- Low cost Get-Away-Special (GAS) furnace p 41 A88-28583

DEQUIRE, M. R.

- Weak-field magnetization of superconducting $YBa_2Cu_3O_{7-x}$ - Relationship to microstructure p 219 A88-18814

DELAAT, JOHN C.

- A microprocessor-based real-time simulator of a turbofan engine [NASA-TM-100889] p 32 N88-21163

DELLACORTE, CHRISTOPHER

- The effects of atmosphere on the tribological properties of a chromium carbide based coating for use to 760 C p 98 A88-32372

- Sputtered silver films to improve chromium carbide based solid lubricant coatings for use to 900 C p 100 A88-47563

- Sputtered silver films to improve chromium carbide based solid lubricant coatings for use to 900 C [NASA-TM-100783] p 102 N88-15885

- Tribological properties of alumina-boria-silicate fabric from 25 to 850 C [NASA-TM-100806] p 104 N88-18726

DELOSREYES, G.

- The design of a turboshaft speed governor using modern control techniques [NASA-CR-175046] p 170 N88-10339

DEMASI, J. T.

- Thermal barrier coating life prediction model development p 171 N88-11185

DEMERDASH, NABEEL A. O.

- Computer-aided modeling and prediction of performance of the modified Lundell class of alternators in space station solar dynamic power systems [NASA-CR-182538] p 201 N88-19000

DEPAOLA, K. J.

- Measurement of impact-induced delamination buckling in composite laminates p 71 A88-47214

DESA, S.

- Base reaction optimization of manipulators with redundant kinematics p 173 N88-23238

DEUTSCH, STEVEN

- The measurement of boundary layers on a compressor blade in cascade. I - A unique experimental facility [ASME PAPER 87-GT-248] p 131 A88-11130

- The measurement of boundary layers on a compressor blade in cascade. II - Surface pressure boundary layers [ASME PAPER 87-GT-249] p 132 A88-11131

- The measurement of boundary layers on a compressor blade in cascade. III - Pressure surface boundary layers and the near wake [ASME PAPER 87-GT-250] p 132 A88-11132

DEVER, THERESE M.

- Chemical vapor deposited silica coatings for solar mirror protection [AIAA PAPER 88-0027] p 99 A88-41796

- Chemical vapor deposited silica coatings for solar mirror protection [NASA-TM-100834] p 105 N88-21306

DEVOL, WILLIAM

- Cryogenic Fluid Management Technology Workshop. Volume 1: Presentation material and discussion [NASA-CP-10001] p 149 N88-15924

DEWITT, D. P.

- Design, calibration and error analysis of instrumentation for heat transfer measurements in internal combustion engines p 157 A88-18509

DEWITT, KENNETH J.

- Mass transport phenomena between bubbles and dissolved gases in liquids under reduced gravity conditions [AIAA PAPER 88-0450] p 138 A88-27719

- Measurement of local convective heat transfer coefficients from a smooth and roughened NACA-0012 airfoil: Flight test data [NASA-TM-100284] p 149 N88-13552

- Mass transport phenomena between bubbles and dissolved gases in liquids under reduced gravity conditions [NASA-TM-100273] p 80 N88-18672

DHERR, N. G.

- INP based solar cells for space application: Reduction of external losses p 199 A88-34250

DHERR, R. G.

- INP based solar cells for space application: Reduction of external losses p 199 A88-34250

DIAS, J. B.

- Probabilistic Structural Analysis Methods for select space propulsion system structural components (PSAM) p 56 A88-49659

DICARLO, JAMES A.

- Pressure effects on the thermal stability of SiC fibers [NASA-TM-100146] p 71 N88-10120

- Ceramics for engines p 103 N88-16704

- Ceramic matrix composites p 75 N88-23888

DICUS, JOHN H.

- Techniques utilized in the simulated altitude testing of a 2D-CD vectoring and reversing nozzle [NASA-TM-100872] p 40 N88-25464

DIECK, RONALD H.

- A detailed description of the uncertainty analysis for high area ratio rocket nozzle tests at the NASA Lewis Research Center p 65 N88-25580

DIFILIPPO, FRANK

- Arc-textured metal surfaces for high thermal emittance space radiators [NASA-TM-100894] p 94 N88-24754

DILLEHAY, MICHAEL E.

- A heater made from graphite composite material for potential deicing application p 17 A88-15724

DILLON, RODNEY O.

- Electrical resistivity (4K to 2100K) of annealed vapor growth carbon fibers p 96 A88-17214

DITTMAR, JAMES H.

- Cruise noise of the 2/9 scale model of the Large-scale Advanced Propfan (LAP) propeller, SR-7A [AIAA PAPER 87-2717] p 214 A88-16565

- An estimate of the noise shielding on the fuselage resulting from installing a short duct around an advanced propeller [NASA-TM-100262] p 217 N88-18379

DIXON, SIDNEY C.

- Hypersonic structures and materials - A progress report p 17 A88-16748

DIXSON, JOHN E.

- Economic benefits of the Space Station to commercial communication satellite operators [IAF PAPER 87-622] p 41 A88-16215

DOBYNS, T. R.

- Service offerings and interfaces for the ACTS network of earth stations [AIAA PAPER 88-0800] p 116 A88-27551

DODDS, ROBERT H., JR.

- A hypermatrix formulation for subspace iteration p 205 A88-15427

DOLCE, JAMES L.

- An integrated approach to space station power system autonomous control p 52 A88-11853

- A systems engineering approach to automated failure cause diagnosis in space power systems p 52 A88-11870

DOMBRO, LOUIS

- High-efficiency helical traveling-wave tube with dynamic velocity taper and advanced multistage depressed collector p 124 A88-32836

DOMINEK, A.

- Material parameter measurements at high temperatures [NASA-CR-182707] p 80 N88-20397

- Measurement of the properties of lossy materials inside a finite conducting cylinder [NASA-CR-182664] p 213 N88-20962

DOMINGUEZ, J.

- Efficient probabilistic fracture mechanics analysis p 180 A88-16933

DONELSON, J. M. A.

- Gigard-tolerant power switches and memory elements p 123 A88-22704

DOONG, WEN

- Communications satellites in non-geostationary orbits [AIAA PAPER 88-0842] p 46 A88-27583

DOWELL, E. H.

- Frequency domain solutions to multi-degree-of-freedom, dry friction damped systems p 184 A88-49714

DOWELL, EARL H.

- Reduced order models for nonlinear aerodynamics p 11 N88-23248

DOWNEY, ALAN N.

- A new model for broadband waveguide-to-microstrip transition design p 126 A88-38822

- An analytical and experimental study of injection-locked two-port oscillators [NASA-TM-100119] p 128 N88-12727

DRAPER, SUSAN

- Effect of high temperature annealing on the thermoelectric properties of GaP doped SiGe p 220 A88-40796

DRAPER, SUSAN L.

- Effect of high-temperature annealing on the microstructure and thermoelectric properties of GaP doped SiGe [NASA-TM-100164] p 101 N88-10188

DRAVID, NARAYAN

- An integrated and modular digital modeling approach for the space station electrical power system development [NASA-TM-100904] p 61 N88-22935

E

DRING, R. P.

The effects of turbulence and stator/rotor interactions on turbine heat transfer. II - Effects of Reynolds number and incidence
[ASME PAPER 88-GT-5] p 145 A88-54152

The effects of turbulence and stator/rotor interactions on turbine heat transfer. I - Design operating conditions
[ASME PAPER 88-GT-125] p 145 A88-54236

The effects of inlet turbulence and rotor/stator interactions on the aerodynamics and heat transfer of a large-scale rotating turbine model. Part 4: Aerodynamic data tabulation
[NASA-CR-179469] p 153 N88-23956

The effects of inlet turbulence and rotor/stator interactions on the aerodynamics and heat transfer of a large-scale rotating turbine model. Volume 3: Heat transfer data tabulation 65 percent axial spacing
[NASA-CR-179468] p 37 N88-28930

The effects of inlet turbulence and rotor/stator interactions on the aerodynamics and heat transfer of a large-scale rotating turbine model. Volume 2: Heat transfer data tabulation. 15 percent axial spacing
[NASA-CR-179467] p 37 N88-29804

DRING, ROBERT P.

Measurement of airfoil heat transfer coefficients on a turbine stage p 147 N88-11158

DRYER, F. L.

Sooting and disruption in spherically symmetrical combustion of decane droplets in air
[IAF PAPER 87-403] p 77 A88-16076

DUCHENE, GLENN A.

A payload for investigating the influence of convection on GaAs crystal growth p 221 N88-17702

DUDESTADT, E. C.

Thermal barrier coating life prediction model development p 170 N88-11184

DUFFY, STEPHEN F.

Whisker-reinforced ceramic composites for heat engine components p 105 N88-22410

DUKE, J. C., JR.

Acousto-ultrasonics as a monitor of material anisotropy p 176 A88-46828

DUKLER, A. E.

Gas liquid flow at microgravity conditions - Flow patterns and their transitions p 141 A88-42839

DULGEROFF, C. R.

An 8-cm ion thruster characterization
[NASA-CR-180819] p 56 N88-10106

DULIKRACH, GEORGE S.

A physically consistent model for artificial dissipation in transonic potential flow computations
[NASA-TM-100846] p 211 N88-22652

DUNN, M. G.

Phase-resolved heat-flux measurements on the blade of a full-scale rotating turbine
[ASME PAPER 88-GT-173] p 145 A88-54267

DUNNING, JOHN W., JR.

Space station power system requirements
[NASA-TM-100886] p 49 N88-21245

DURBIN, P. A.

Corona anemometry for qualitative measurement of reversing surface flow with application to separation control by external excitation p 133 A88-14143

Roll-up of vorticity in adverse-pressure-gradient boundary layers p 135 A88-19194

Free-streamline analysis of deformation and dislodging by wind force of drops on a surface p 137 A88-25191

DUSTIN, MILES O.

Advanced space solar dynamic power systems beyond IOC Space Station p 50 A88-11798

DUTTA, SUNIL

Simple processing method for high-strength silicon carbide p 97 A88-19056

Improved processing of alpha-SiC p 99 A88-38318

Strength optimization of alpha-SiC by improved processing p 107 N88-23880

DUVAL, W. M. B.

Characterization of directionally solidified lead chloride p 111 A88-43170

DUVAL, WALTER M. B.

Dynamics of two fluids under periodic acceleration
[AIAA PAPER 88-3728] p 143 A88-48980

DVORAK, S. D.

E3 10C compressor test analysis of high-speed post-stall data
[NASA-CR-179521] p 36 N88-28929

DWOYER, DOUGLAS L.

Retooling CFD for hypersonic aircraft p 1 A88-16749

EBIHARA, BEN T.

Performance of a small, graphite electrode, multistage depressed collector with a 500-W, continuous wave, 4.8- to 9.6-GHz traveling wave tube
[NASA-TP-2788] p 128 N88-15146

ECKERLE, W. A.

Soot loading in a generic gas turbine combustor p 19 A88-27296

EDELMAN, RAYMOND B.

Laminar diffusion flames under micro-gravity conditions
[AIAA PAPER 88-0645] p 78 A88-27722

EDWARDS, ROBERT V.

Real time optical correlator using a magneto-optic device applied to particle imaging velocimetry p 159 A88-40700

Application of optical correlation techniques to particle imaging velocimetry
[NASA-TM-101306] p 163 N88-29152

EGGER, ROBERT A.

Oxidation-resistant reflective surfaces for solar dynamic power generation in near earth orbit p 54 A88-18523

EHRESMAN, DERIK T.

Solar concentrator advanced development project p 50 A88-11799

EISEMAN, PETER R.

Adaptive grid generation p 209 A88-37363

ELCHURI, V.

Aerodynamically forced vibration analysis of turbomachines p 20 A88-31610

ELLEMAN, DANIEL E.

Research opportunities in microgravity science and applications during Shuttle hiatus p 109 A88-13164

ELLIS, GRAHAM K.

Distributed computation of graphics primitives on a transputer network
[NASA-TM-100814] p 206 N88-19147

Two-dimensional graphics tools for a transputer based display board
[NASA-TM-100820] p 207 N88-22591

Implementing direct, spatially isolated problems on transputer networks
[NASA-TM-101297] p 207 N88-27796

User's manual for the two-dimensional transputer graphics toolkit
[NASA-TM-100974] p 207 N88-27799

ELLIS, J. R.

Biaxial experiments supporting the development of constitutive theories for advanced high-temperature materials p 191 N88-22386

An experimental study of biaxial yield in modified 9Cr-1Mo steel at room temperature
[NASA-CR-175012] p 196 N88-30164

ELLZEY, J. L.

The structure and dynamics of reacting plane mixing layers p 136 A88-20871

ELMORE, D. L.

Further development of the dynamic gas temperature measurement system p 160 N88-11141

ELROD, DAVID A.

Experimental rotordynamic coefficient results for honeycomb seals
[NASA-CR-182440] p 172 N88-16007

ELROD, DAVID ALAN

Entrance and exit region friction factor models for annular seal analysis
[NASA-CR-183084] p 175 N88-25921

ENGELBECK, R. M.

Multiple-Purpose Subsonic Naval Aircraft (MPSNA): Multiple Application Propan Study (MAPS)
[NASA-CR-175104] p 18 N88-28917

ENGLAND, JAMES E.

Design, development, and test of Shuttle/Centaur G-prime cryogenic tankage thermal protection systems p 47 A88-53182

ENGLISH, ROBERT E.

Speculations on future opportunities to evolve Brayton powerplants aboard the space station p 202 N88-24258

ENGLUND, D. R.

Advanced high temperature instrumentation for hot section research applications p 159 A88-54139

ENGLUND, DAVID R.

Recent advances in high temperature instrumentation for hot section applications
[NASA-TM-100282] p 161 N88-14339

Research sensors p 161 N88-15795

Research sensors p 162 N88-22430

ENSWORTH, C. B. F., III

Testing of a one-bladed 30-meter-diameter rotor on the DOE/NASA Mod-O wind turbine
[NASA-TM-100274] p 201 N88-19014

ERNST, MICHAEL A.

Determining structural performance p 27 N88-15787

ESGAR, J. B.

Views on the impact of HOST p 24 A88-54146

EVANS, AUSTIN L.

Sensitivity study of the monogroove with screen heat pipe design
[AIAA PAPER 88-0470] p 137 A88-22346

EVANS, AUSTIN LEWIS

Modelling the performance of the monogroove with screen heat pipe for use in the radiator of the solar dynamic power system of the NASA Space Station
[IAF PAPER 87-238] p 134 A88-15960

Modelling the performance of the tapered artery heat pipe design for use in the radiator of the solar dynamic power system of the NASA Space Station
[IAF PAPER 88-213] p 56 A88-55361

EVERSMAN, WALTER

A model of the wall boundary layer for ducted propellers
[AIAA PAPER 87-2742] p 214 A88-16578

F

FABRE, J. A.

Gas liquid flow at microgravity conditions - Flow patterns and their transitions p 141 A88-42839

FAETH, G. M.

Mixing, transport and combustion in sprays p 138 A88-25828

FAETH, GERARD M.

Particle-laden weakly swirling free jets - Measurements and predictions
[AIAA PAPER 88-3138] p 142 A88-48757

Particle-laden weakly swirling free jets: Measurements and predictions
[NASA-TM-100920] p 34 N88-24639

FANG, Q. T.

Preparation of multistage zone-refined materials for thermochemical standards p 111 A88-43172

FANG, R. J. F.

Bandwidth-efficient high-speed coded trellis modulation
[AIAA PAPER 88-0813] p 116 A88-27560

FANTI, PAOLO D.

Bithermal fatigue - A link between isothermal and thermomechanical fatigue p 87 A88-35918

FAROKHI, S.

Controlled excitation of a cold turbulent swirling free jet
[ASME PAPER 87-WA/NCA-18] p 140 A88-41568

Effect of initial tangential velocity distribution on the mean evolution of a swirling turbulent free jet
[AIAA PAPER 88-3592] p 7 A88-48893

Effect of initial tangential velocity distribution on the mean evolution of a swirling turbulent free jet
[NASA-TM-100934] p 12 N88-24592

FAROOQ, S.

Gravity and configurational energy induced microstructural changes in liquid phase sintering p 112 A88-49089

FARRELL, D. E.

Weak-field magnetization of superconducting Y1Ba2Cu3O(x) - Relationship to microstructure p 219 A88-18814

Effect of fluoride doping on the transition temperature of YBa2Cu3O(6.5+delta) p 220 A88-29297

High Tc screen-printed YBa2Cu3O(7-x) films - Effect of the substrate material p 127 A88-49760

Synthesis and characterization of high-T(sub c) screen-printed Y-Ba-Cu-O films on alumina
[NASA-TM-100860] p 222 N88-22805

FARRELL, P. V.

Droplet vaporization in a supercritical microgravity environment
[IAF PAPER 87-384] p 134 A88-16055

FATEMI, NAVID

A novel photovoltaic power system which uses a large area concentrator mirror p 197 A88-11811

FATEMI, NAVID S.

Aging behavior of Au-based ohmic contacts to GaAs
[NASA-CR-182146] p 130 N88-25831

FAYMON, K. A.

Space commercialization and power system technology p 223 A88-44003

FAYMON, KARL A.

LERC power system autonomy program 1990 demonstration p 52 A88-11861

A systems engineering approach to automated failure cause diagnosis in space power systems p 52 A88-11870

FEKE, DONALD L.

Colloidal characterization of silicon nitride and silicon carbide p 107 N88-23883

G

FENG, Z. C.

- Low-temperature photoluminescence studies of chemical-vapor-deposition-grown 3C-SiC on Si p 127 A88-53396
- Raman scattering studies of chemical-vapor-deposited cubic SiC films of (100)Si p 127 A88-53397

FERENDECI, ALTAN

- A high frequency GaAlAs travelling wave electro-optic modulator at 0.82 micrometers [NASA-TM-100970] p 130 N88-28240

FERGUSON, C. R.

- Design, calibration and error analysis of instrumentation for heat transfer measurements in internal combustion engines p 157 A88-18509

FERNANDEZ, RENE

- Comparison of the bidirectional reflectance distribution function of various surfaces [NASA-TM-101317] p 218 N88-28760

FERRANTE, J.

- Analysis of plasma nitrided steels p 88 A88-38936

FERRANTE, JOHN

- Universality relationships in condensed matter - Bulk modulus and sound velocity p 213 A88-43950
- Interfacial adhesion: Theory and experiment [NASA-TM-100830] p 92 N88-20417

FERRI, A. A.

- Frequency domain solutions to multi-degree-of-freedom, dry friction damped systems p 184 A88-49714

FERTIS, D. G.

- Parametric studies of advanced turboprops [AIAA PAPER 88-2266] p 20 A88-32223

FIELDER, W. L.

- Phase purity of NiCo₂O₄, a catalyst candidate for electrolysis of water [NASA-TM-100239] p 69 N88-13385

FINDEN, L. E.

- 25-LBF GO2/GH2 space station thruster [AIAA PAPER 88-2793] p 56 A88-53101
- Space station resistojet system requirements and interface definition study [NASA-CR-180832] p 58 N88-12541

FINK, P.

- NESSUS/EXPERT - An expert system for probabilistic structural analysis methods [AIAA PAPER 88-2374] p 206 A88-32311

FINLEY, CLARENCE W.

- Interfacial adhesion: Theory and experiment [NASA-TM-100830] p 92 N88-20417

FIRMINO, F.

- Unsteady motion and transition to turbulence in developing curved duct flow p 140 A88-39010

FISHBACH, LAURENCE H.

- NNEPEQ: Chemical equilibrium version of the Navy/NASA Engine Program [NASA-TM-100851] p 32 N88-21161

FLEETER, SANFORD

- Control of rotor aerodynamically forced vibrations by splitters p 23 A88-52684
- Unsteady aerodynamics of an oscillating cascade in a compressible flow field [NASA-TM-100219] p 26 N88-13346
- Investigation of oscillating cascade aerodynamics by an experimental influence coefficient technique [NASA-TM-101313] p 14 N88-28041

FLEMING, D. P.

- Experiments on dynamic stiffness and damping of tapered bore seals p 166 A88-31527

FLEMINGS, M. C.

- Solidification of undercooled Ni-Sn eutectic alloy under microgravity conditions in the Space Shuttle p 110 A88-28557
- Dendritic growth of undercooled nickel-tin. III p 86 A88-32887

FLOOD, DENNIS J.

- Space solar cell research - Problems and potential p 123 A88-21605
- Issues in space photovoltaic research and technology p 199 A88-34230
- Recent progress in space photovoltaic systems [NASA-TM-100208] p 128 N88-11966
- Advanced photovoltaic power system technology for lunar base applications [NASA-TM-100965] p 65 N88-26402

FOLENTA, DEZI

- Design, manufacture and spin test of high contact ratio helicopter transmission utilizing Self-Aligning Bearingless Planetary (SABP) [NASA-CR-4155] p 174 N88-24975

FORCE, DALE A.

- A re-examination of spent beam refocusing for high-efficiency helix TWT's and small MDC's p 124 A88-28673
- High-efficiency helical traveling-wave tube with dynamic velocity taper and advanced multistage depressed collector p 124 A88-32836

FORD, WILLIAM F.

- An algorithm for a generalization of the Richardson extrapolation process p 209 A88-32840

FOSS, J. F.

- Coherent motion induced fluctuations in the primary transition region of a plane shear layer p 133 A88-14125
- Gravitationally defined velocities for a low speed hot-wire calibration p 133 A88-14170

FOWLIS, WILLIAM

- Simulation of fluid flows during growth of organic crystals in microgravity p 109 A88-13163

FOX, D. S.

- Molten salt corrosion of SiC and Si₃N₄ p 107 N88-23885

FOX, DENNIS S.

- Molten-salt corrosion of silicon nitride. I - Sodium carbonate. II - Sodium sulfate p 97 A88-26222
- Direct mass spectrometric identification of silicon oxychloride compounds p 78 A88-44425

FRALICK, GUSTAVE C.

- Correlation of velocity and velocity-density turbulence in the exhaust of an atmospheric burner p 161 N88-11147

FRANCISCO, DAVID R.

- Successful completion of a cyclic ground test of a mercury ion auxiliary propulsion system [NASA-TM-101351] p 67 N88-29873

FRASCA, ALBERT J.

- Neutron effects on the electrical and switching characteristics of NPN bipolar power transistors p 129 N88-24463

FRASCH, L. L.

- Electrothermal propulsion of spacecraft with millimeter and submillimeter electromagnetic energy p 54 A88-46220

FREED, A. D.

- A theory of viscoplasticity accounting for internal damage p 190 N88-21508

FREED, ALAN D.

- Structure of a viscoplastic theory [NASA-TM-100794] p 188 N88-18968
- A viscoplastic theory applied to copper [NASA-TM-100831] p 189 N88-21497

FREEMAN, JON C.

- An analytical and experimental study of injection-locked two-port oscillators [NASA-TM-100119] p 128 N88-12727

FRIEFELD, JERRY M.

- Solar dynamic power system definition study [NASA-CR-180877] p 59 N88-20361

FRIEMAN, JOSHUA A.

- Primordial origin of nontopological solitons p 226 A88-39313

FRINT, HAROLD K.

- Design and evaluation of high contact ratio gearing [NASA-CR-174958] p 175 N88-28319

FRITSCH, K.

- Fiber-linked interferometric pressure sensor p 157 A88-11743

FRITSCH, KLAUS

- Modulated-splitting-ratio fiber-optic temperature sensor [NASA-TM-101332] p 18 N88-28062

FRITZ, R.

- Electrothermal propulsion of spacecraft with millimeter and submillimeter electromagnetic energy p 54 A88-46220

FRONEK, DENNIS L.

- A distributed data acquisition system for aeronautics test facilities p 39 A88-33065

FRYXELL, R. E.

- Effects of surface chemistry on hot corrosion life p 91 N88-11180

FU, KUAN-CHEN

- Thermal stresses of a wind turbine blade made of orthotropic material p 180 A88-18380

FUCINARI, C. A.

- Development of the AGT101 regenerator seals [ASME PAPER 87-GT-173] p 165 A88-11083

FUJIKAWA, GENE

- Experimental radio frequency link for Ka-band communications applications [NASA-TM-100824] p 43 N88-24659

FUNG, C. D.

- Behavior of ion-implanted junction diodes in 3C SiC p 122 A88-15423

FUSARO, ROBERT L.

- Tribological properties of polymer films and solid bodies in a vacuum environment p 98 A88-35565
- Comparison of the tribological properties of fluorinated cokes and graphites [STLE PREPRINT 88-AM-7F-1] p 100 A88-51300

GABB, T. P.

- Fatigue crack propagation of nickel-base superalloys at 650 deg C p 86 A88-35908
- Bithermal low-cycle fatigue behavior of a NiCoCrAlY-coated single crystal superalloy p 90 A88-51736
- Isothermal and bithermal thermomechanical fatigue behavior of a NiCoCrAlY-coated single crystal superalloy [NASA-TM-100907] p 94 N88-24766

GABB, TIMOTHY P.

- The cyclic stress-strain behavior of a single crystal nickel-base superalloy [NASA-TM-100269] p 92 N88-19610

GAHN, RANDALL F.

- Effect of component compression on the initial performance of an IPV nickel-hydrogen cell p 53 A88-11913
- Component variations and their effects on bipolar nickel-hydrogen cell performance p 197 A88-11914
- Test results of a 60 volt bipolar nickel-hydrogen battery p 198 A88-11916

GAIER, J. R.

- Differential scanning calorimetric survey of brominated PAN, pitch-based and vapor-grown fibers p 98 A88-32854
- Advantages of barium peroxide in the powder synthesis of perovskite superconductors p 221 A88-41496
- Characterization of Ba₂YCu₃O(7-x) prepared in an inert atmosphere p 221 A88-49376

GAIER, JAMES R.

- A comparison of the bromination dynamics of various carbon and graphite fibers p 97 A88-20278
- Stability of the electrical resistivity of bromine, iodine monochloride, copper(II) chloride, and nickel(II) chloride intercalated pitch-based graphite fibers p 100 A88-49403
- Production and characterization of CdCl₂ intercalated graphite fibers p 101 A88-51307

GALLARDO, VINCENTE C.

- Blade loss transient dynamics analysis, volume 1. Task 2: TETRA 2 theoretical development [NASA-CR-179632] p 25 N88-10791
- Blade loss transient dynamics analysis, volume 2. Task 2: TETRA 2 user's manual [NASA-CR-179633] p 25 N88-10792

GAMMON, ROBERT W.

- Critical field light scattering p 158 A88-33003

GARG, SANJAY

- Cooperative synthesis of control and display augmentation for a STOL aircraft in the approach and landing task [AIAA PAPER 88-4182] p 37 A88-50272

GARLICK, G. F. J.

- Development of 8 cm x 8 cm silicon gridded back solar cell for space station p 200 A88-34312

GARLICK, R. G.

- Advantages of barium peroxide in the powder synthesis of perovskite superconductors p 221 A88-41496
- Characterization of Ba₂YCu₃O(7-x) prepared in an inert atmosphere p 221 A88-49376
- Lattice parameter variations during aging in nickel-base superalloys p 90 A88-51318
- Phase purity of NiCo₂O₄, a catalyst candidate for electrolysis of water [NASA-TM-100239] p 69 N88-13385

GAROW, J.

- Regenerative fuel cell energy storage system for a low earth orbit space station [NASA-CR-174802] p 204 N88-30184

GAYDA, J.

- Fatigue crack propagation of nickel-base superalloys at 650 deg C p 86 A88-35908
- Creep-fatigue behavior of NiCoCrAlY coated PWA 1480 superalloy single crystals p 86 A88-35911
- Bithermal low-cycle fatigue behavior of a NiCoCrAlY-coated single crystal superalloy p 90 A88-51736

- A microstructural lattice model for strain oriented problems: A combined Monte Carlo finite element technique [NASA-TM-100215] p 90 N88-10939

- Creep-fatigue behavior of NiCoCrAlY coated PWA 1480 p 186 N88-11176
- Monte Carlo simulation of modulated phases [NASA-TM-89654] p 210 N88-12323

- Isothermal and bithermal thermomechanical fatigue behavior of a NiCoCrAlY-coated single crystal superalloy [NASA-TM-100907] p 94 N88-24766

GAYDA, JOHN

- Creep and fatigue research efforts on advanced materials p 187 N88-16701

GAYDOSHI, D.

- Compressive creep behavior of alloys based on B2 FeAl p 82 A88-10043

- GAYDOS, D. J.**
Dynamic recrystallization and grain boundary migration in B2 FeAl p 83 A88-20269
The microstructure and tensile properties of extruded melt-spun ribbons of iron-rich B2 FeAl p 85 A88-31679
Room temperature tensile ductility in powder processed B2 FeAl alloys p 85 A88-31694
- GAZZANIGA, JOHN A.**
Summary of low-speed wind tunnel results of several high-speed counterrotation propeller configurations [AIAA PAPER 88-3149] p 7 A88-48758
Summary of low-speed wind tunnel results of several high-speed counterrotation propeller configurations [NASA-TM-100945] p 13 N88-24597
- GEDDES, J.**
Two stage dual gate MESFET monolithic gain control amplifier for Ka-band p 124 A88-29821
A 30 GHz monolithic receive module technology assessment [NASA-CR-180825] p 129 N88-23084
- GEDEON, DAVID R.**
Description of an oscillating flow pressure drop test rig [NASA-TM-100905] p 61 N88-22933
- GEDEON, STEPHEN R.**
Assessment of nuclear reactor concepts for low power space applications p 217 N88-24409
- GEDWILL, MICHAEL A.**
Coating life prediction p 170 N88-11181
- GEE, J. M.**
A comparison of the radiation tolerance characteristics of multijunction solar cells with series and voltage-matched configurations [NASA-TM-101177] p 203 N88-27624
- GEE, W.**
How good is the impedance boundary condition? p 115 A88-24863
- GEIER, JAMES V.**
Modelling and design of high efficiency radiation tolerant indium phosphide space solar cells p 200 A88-34394
- GELDER, THOMAS**
Experimental evaluation of corner vanes - Summary [SAE PAPER 871784] p 39 A88-30778
- GELDER, THOMAS F.**
Design and performance of controlled-diffusion stator compared with original double-circular-arc stator [SAE PAPER 871783] p 20 A88-30777
Experimental evaluation of turning vane designs for high-speed and coupled fan-drive corners of 0.1-scale model of NASA Lewis Research Center's proposed altitude wind tunnel [NASA-TP-2681] p 40 N88-17686
- GELMINI, GRACIELA B.**
Primordial origin of nontopological solitons p 226 A88-39313
- GEMEINER, RUSSEL P.**
Component variations and their effects on bipolar nickel-hydrogen cell performance p 197 A88-11914
Test results of a 60 volt bipolar nickel-hydrogen battery p 198 A88-11916
- GENERAZIO, E. R.**
Determination of grain-size distribution function using two-dimensional Fourier transforms of tone-pulse-encoded images p 176 A88-30425
Acoustic imaging of subtle porosity variations in ceramics p 101 A88-55044
- GENERAZIO, EDWARD R.**
Imaging subtle microstructural variations in ceramics with precision ultrasonic velocity and attenuation measurements [NASA-TM-100129] p 177 N88-15257
Systems for ultrasonic scanning, analysis and imagery p 177 N88-22414
High frequency ultrasonic characterization of sintered SiC [NASA-TM-100825] p 179 N88-23985
- GENG, STEVEN M.**
Calibration and comparison of the NASA Lewis free-piston Stirling engine model predictions with RE-1000 test data p 165 A88-11967
RE-1000 free-piston Stirling engine hydraulic output system description [NASA-TM-100185] p 223 N88-10700
- GEORGE, W. K.**
Phase-resolved heat-flux measurements on the blade of a full-scale rotating turbine [ASME PAPER 88-GT-173] p 145 A88-54267
- GERMAN, R. M.**
Gravitational contributions to microstructural coarsening in liquid phase sintering p 111 A88-37155
Gravity and configurational energy induced microstructural changes in liquid phase sintering p 112 A88-49089
- GEROLD, V.**
Cyclic hardening mechanisms in Nimonic 80A p 84 A88-24490
- GESLIN, D.**
Elevated temperature strain gages p 160 N88-11144
- GESSERT, T. A.**
InP based solar cells for space application: Reduction of external losses p 199 A88-34250
Direct-current magnetron fabrication of indium tin oxide/InP solar cells p 200 A88-51289
- GHANDHI, S. K.**
Comparative radiation resistance, temperature dependence and performance of diffused junction indium phosphide solar cells p 198 A88-18580
Characterization and modelling of open tube diffused n+p bulk InP solar cells p 199 A88-34270
- GHIERING, W. L.**
Calibration of high-temperature, fiber-optic, microbend, pressure transducers p 157 A88-22942
- GHIA, K. N.**
Solution of the Neumann pressure problem in general orthogonal coordinates using the multigrid technique p 144 A88-50330
- GHIA, U.**
Solution of the Neumann pressure problem in general orthogonal coordinates using the multigrid technique p 144 A88-50330
- GHORASHI, BAHMAN**
The effect of eddy distribution on momentum and heat transfer near the wall in turbulent pipe flow [NASA-TM-100257] p 150 N88-15984
- GHOSH, L. J.**
Analysis of crack propagation in roller bearings using the boundary integral equation method - A mixed-mode loading problem p 168 A88-49183
- GHOSH, LOUIS**
Accelerated crack growth rate at low Delta K in a single crystal superalloy p 89 A88-47687
Mode 2 fracture mechanics p 193 N88-22418
- GHOSH, LOUIS J.**
Reliability based analysis of contact problems [NASA-CR-182117] p 189 N88-18975
Accelerated fatigue crack growth behavior of PWA 1480 single crystal alloy and its dependence on the deformation mode [NASA-TM-100943] p 95 N88-26436
- GIELDA, T. P.**
Navier-Stokes solutions of flowfield characteristics produced by ice accretion [AIAA PAPER 88-0290] p 137 A88-22210
- GINTY, C. A.**
Hygrothermomechanical fiber composite fatigue - Computational simulation p 71 A88-42437
- GINTY, CAROL A.**
Fracture characteristics of angleplied laminates fabricated from overaged graphite/epoxy prepreg p 69 A88-16965
Fiber composite structural durability and damage tolerance: Simplified predictive methods [NASA-TM-100179] p 72 N88-13409
Hygrothermomechanical fiber composite fatigue: Computational simulation [NASA-TM-100840] p 74 N88-21257
Features and applications of the integrated composites analyzer (ICAN) code p 74 N88-22391
- GIVI, PEYMAN**
Direct simulations of chemically reacting turbulent mixing layers, part 2 [NASA-CR-180853] p 154 N88-25857
- GLADDEN, H. J.**
Review and assessment of the database and numerical modeling for turbine heat transfer p 24 A88-54141
- GLADDEN, HERBERT J.**
Thermostructural analysis with experimental verification in a high heat flux facility of a simulated cowl lip [AIAA PAPER 88-2222] p 39 A88-32188
Heat transfer in a real engine environment p 147 N88-11155
HOST turbine heat transfer program summary [NASA-TM-100280] p 149 N88-14320
Review and assessment of the HOST turbine heat transfer program p 34 N88-22431
Heat transfer in aerospace propulsion [NASA-TM-100874] p 154 N88-23957
- GLASGOW, T. K.**
Precipitation in a rapidly solidified and aged Ni-Al-Mo alloy p 82 A88-18528
Crystallization behavior of a melt-spun Fe-Ni based steel p 83 A88-19958
Undercooled and rapidly quenched Ni-Mo alloys p 83 A88-19960
Primary arm spacing in chill block melt spun Ni-Mo alloys p 89 A88-41655
Ground based materials science experiments p 43 A88-52364
- GLASGOW, THOMAS**
Research opportunities in microgravity science and applications during Shuttle hiatus p 109 A88-13164
- GLASGOW, THOMAS K.**
Preparation for microgravity - The role of the Microgravity Material Science Laboratory [AIAA PAPER 88-3510] p 111 A88-42908
Preparation for microgravity: The role of the microgravity materials science laboratory [NASA-TM-100906] p 113 N88-24811
- GLEISER, MARCELO**
Primordial origin of nontopological solitons p 226 A88-39313
- GLICKSMAN, M. E.**
Dendritic solidification under microgravity conditions [AIAA PAPER 88-0248] p 110 A88-22186
Isothermal dendritic growth - A low gravity experiment p 110 A88-28556
Solidification under microgravity conditions - Dendritic growth [AAS PAPER 86-380] p 110 A88-35130
Preparation of multistage zone-refined materials for thermochemical standards p 111 A88-43172
Isothermal dendritic growth - A proposed microgravity experiment p 112 A88-49095
- GOEDE, HANK**
30-cm electron cyclotron plasma generator p 122 A88-18633
- GOEL, P.**
Investigation of third-order closure model of turbulence for the computation of incompressible flows in a channel with a backward-facing step p 136 A88-21273
Turbulence energy and diffusion transport of third-moments in a separating and reattaching flow p 141 A88-43011
- GOKOGLU, S. A.**
Criteria for significance of simultaneous presence of both condensable vapors and aerosol particles on mass transfer (deposition) rates p 114 A88-10971
Experiments for the determination of convective diffusion heat/mass transfer to burner rig test targets comparable in size to jet stream diameter p 140 A88-41574
- GOKOGLU, SULEYMAN A.**
Significance of vapor phase chemical reactions on CVD rates predicted by chemically frozen and local thermochemical equilibrium boundary layer theories p 78 A88-44424
Experimental verification of vapor deposition rate theory in high velocity burner rigs p 91 N88-11179
- GOLAN, O. M.**
Low thrust power-limited transfer for a pole squatter [AIAA PAPER 88-4310] p 42 A88-50435
- GOLDBERG, L. F.**
Description of an oscillating flow test program p 133 A88-11963
- GOLDSTEIN, M. E.**
Roll-up of vorticity in adverse-pressure-gradient boundary layers p 135 A88-19194
Nonlinear roll-up of externally excited free shear layers p 141 A88-44445
- GOLDSTEIN, MARVIN E.**
Aeroacoustics of subsonic turbulent shear flows [AIAA PAPER 87-2731] p 214 A88-16571
- GOMBOS, FRANK J.**
An integrated and modular digital modeling approach for the space station electrical power system development [NASA-TM-100904] p 61 N88-22935
- GONZALEZ-SANABRIA, OLGA**
Regenerative fuel cell study for satellites in GEO orbit p 52 A88-11904
Test results of a 60 volt bipolar nickel-hydrogen battery p 198 A88-11916
- GONZALEZ-SANABRIA, OLGA D.**
Component variations and their effects on bipolar nickel-hydrogen cell performance p 197 A88-11914
Effect of NASA advanced designs on thermal behavior of Ni-H₂ cells [NASA-TM-100197] p 79 N88-10132
Energy storage considerations for a robotic Mars surface sampler [NASA-TM-100969] p 227 N88-28853
- GOODEN, CLARENCE E.**
Production and characterization of CdCl₂ intercalated graphite fibers p 101 A88-51307
- GORADIA, CHANDRA**
Self-consistent calculations and design considerations for a GaAs nipi doping superlattice solar cell p 124 A88-34249
Radiation damage and defect behavior in proton irradiated lithium-counterdoped n+p silicon solar cells p 125 A88-34340
Modelling and design of high efficiency radiation tolerant indium phosphide space solar cells p 200 A88-34394
- GORDAN, ANDREW L.**
Optical alignment of Centaur's inertial guidance system [NASA-TM-88844] p 43 N88-12515

GORDON, ELIOTT B.

- GORDON, ELIOTT B.**
Noise of a model counterrotation propeller with reduced aft rotor diameter at simulated takeoff/approach conditions [F7/A3] p 214 A88-22192
[AIAA PAPER 88-0263]
- Noise of a model counterrotation propeller with reduced aft rotor diameter at simulated takeoff/approach conditions (F7/A3) p 216 N88-13961
[NASA-TM-100254]
- GORDON, SANFORD**
NNEPEC: Chemical equilibrium version of the Navy/NASA Engine Program p 32 N88-21161
[NASA-TM-100851]
Finite area combustor theoretical rocket performance [NASA-TM-100785] p 60 N88-21252
- GORDON, WILLIAM L.**
Degradation mechanisms of materials for large space systems in low Earth orbit p 71 N88-10896
[NASA-CR-181472]
- GORECKI, J.**
Silsesquioxanes as precursors to ceramic composites p 69 A88-12599
- GORLA, RAMA SUBBA REDDY**
Foil bearing lubrication theory including compressibility effects p 170 A88-54964
- GOUCHOE, D. R.**
The design of a turboshaft speed governor using modern control techniques p 170 N88-10339
[NASA-CR-175046]
- GOUSY, ROBERT G.**
Forced mixer lobes in ejector designs p 141 A88-46222
- GOVILA, R. K.**
Strength characterization of yttria/alumina-doped sintered silicon nitride p 97 A88-26154
- GOVINDAN, T. R.**
A space-marching method for the computation of viscous internal flows p 135 A88-20459
- GRABER, EDWIN J.**
Overview of NASA PTA proplan flight test program p 29 N88-15805
- GRADY, J. E.**
Dynamic delamination fracture toughness of a graphite/epoxy laminate under impact p 70 A88-29455
Measurement of impact-induced delamination buckling in composite laminates p 71 A88-47214
Contact force history and dynamic response due to the impact of a soft projectile p 175 N88-26679
[NASA-TM-100961]
- GRADY, JOSEPH E.**
Impact damage in composite laminates p 74 N88-22402
- GRANT, HOWARD P.**
The development of a high temperature static strain gage system p 160 N88-11142
- GRATZ, ROY F.**
Substituted 1,1,1-Triaryl-2,2,2-Trifluoroethanes and processes for their synthesis p 69 N88-26404
[NASA-CASE-LEW-14345-1]
- GRAVES, J. A.**
Containerless processing of undercooled melts p 110 A88-28554
Rapid solidification of highly undercooled liquids p 88 A88-41653
- GRAY, DAVID E.**
Results of NASA's Energy Efficient Engine Program p 19 A88-20785
- GREBER, I.**
Glancing shock wave-turbulent boundary layer interaction with boundary layer suction p 6 A88-27718
[AIAA PAPER 88-0308]
- GREBER, ISAAC**
Experimental and numerical investigation of the effect of distributed suction on oblique shock wave/turbulent boundary layer interaction p 156 N88-30084
[NASA-TM-101334]
- GREEN, JAMES M.**
Catalytic ignition of hydrogen and oxygen propellants [AIAA PAPER 88-3300] p 109 A88-48764
Catalytic ignition of hydrogen and oxygen propellants [NASA-TM-100957] p 63 N88-24689
- GREENBERG, JOEL S.**
The economics of satellite retrieval p 44 A88-27584
[AIAA PAPER 88-0843]
- GREENBERG, PAUL S.**
Experimental study of thermocapillary flows in a thin liquid layer with heat fluxes imposed on the free surface p 144 A88-49087
Experimental study of thermocapillary flows in a thin liquid layer with heat fluxes imposed on the free surface [NASA-TM-100252] p 148 N88-12763

- GREGOREK, G. M.**
Comparison of pressure distributions on model and full-scale NACA 64-621 airfoils with ailerons for wind turbine application p 201 N88-21593
[NASA-TM-100802]
- GRIEST, KIM**
Calculations of rates for direct detection of neutralino dark matter p 227 A88-48463
- GRIFFIN, J. H.**
An integrated approach for friction damper design p 167 A88-31598
- GRIFFIN, JERRY H.**
Evaluation of a turbine blade damper using an integral approach p 20 A88-32332
[AIAA PAPER 88-2400]
- GRISAFFE, SALVATORE J.**
Lewis materials research and technology: An overview p 223 N88-16699
- GRISNIK, STANLEY P.**
The effect of eddy distribution on momentum and heat transfer near the wall in turbulent pipe flow p 150 N88-15984
[NASA-TM-100257]
- GROBSTEIN, T. L.**
Characterization of precipitates in a niobium-zirconium-carbon alloy p 93 N88-22981
[NASA-TM-100848]
- GROEN, DAVID S.**
Acoustics technologies for STOVL aircraft p 215 A88-35939
[AIAA PAPER 88-2238]
STOVL acoustic fatigue technologies p 215 A88-37221
[SAE PAPER 872360]
- GROENEWEG, J. F.**
High speed propeller performance and noise predictions at takeoff/landing conditions p 215 A88-22193
[AIAA PAPER 88-0264]
High-speed propeller noise predictions - Effects of boundary conditions used in blade loading calculations p 215 A88-36270
High speed propeller performance and noise predictions at takeoff/landing conditions p 216 N88-13960
[NASA-TM-100267]
- GROENEWEG, JOHN F.**
Advanced propeller research p 29 N88-15806
- GROSS, BERNARD**
Calibration of a Mode II test specimen p 183 A88-47014
- GROTELUESCHEN, L. P.**
Plasticity analysis of wear phenomena as an aid in the development of abrasible materials p 164 A88-10938
- GRUBER, ROBERT P.**
Arcjet power supply and start circuit p 41 N88-28939
[NASA-CASE-LEW-14374-1]
The dc power control for a liquid-fed resistojet p 67 N88-29869
[NASA-TM-101326]
- GULINO, DANIEL A.**
Oxidation-resistant reflective surfaces for solar dynamic power generation in near earth orbit p 54 A88-18523
Chemical vapor deposited silica coatings for solar mirror protection p 99 A88-41796
[AIAA PAPER 88-0027]
Oxygen plasma effects on several liquid droplet radiator fluids p 142 A88-47962
Solar dynamic concentrator durability in atomic oxygen and micrometeoroid environments p 68 A88-51393
Atomic-oxygen durability of impact-damaged solar reflectors p 68 A88-54988
Space station solar concentrator materials research [NASA-TM-100862] p 60 N88-21250
Chemical vapor deposited silica coatings for solar mirror protection p 105 N88-21306
[NASA-TM-100834]
Thin film coatings for space electrical power system applications p 69 N88-28966
[NASA-TM-101325]
- GUPTA, DINESH K.**
Current status and future trends in turbine application of thermal barrier coatings p 169 A88-54355
[ASME PAPER 88-GT-286]
- GURNETT, D. A.**
Plasma wave turbulence around the shuttle - Results from the Spacelab-2 flight p 218 A88-47783
Double-probe potential measurements near the Spacelab 2 electron beam p 204 A88-53464
- GUSTAFSON, ERIC**
Heat pipe radiators for solar dynamic space power system heat rejection p 132 A88-11807
High thermal-transport capacity heat pipes for space radiators p 136 A88-21155
[SAE PAPER 871509]
- GYEKENYESI, JOHN P.**
Some design considerations for ceramic components in heat engine applications p 106 N88-23875
- GYEKENYESI, JOHN Z.**
High temperature tensile testing of ceramic composites p 161 N88-15996
[NASA-CR-180888]

PERSONAL AUTHOR INDEX

H

- HA, TRI T.**
VSAT networks - An overview p 115 A88-14091
Spread-spectrum multiple access using wideband noncoherent MFSK p 115 A88-26672
- HAAG, THOMAS W.**
An extended life and performance test of a low-power arcjet p 55 A88-48756
[AIAA PAPER 88-3106]
A low-power arcjet cyclic lifetest p 57 N88-11748
[NASA-TM-100233]
An extended life and performance test of a low-power arcjet p 63 N88-24687
[NASA-TM-100942]
- HABIBY, SARRY F.**
Implementation of a fast digital optical matrix-vector multiplier using a holographic look-up table and residue arithmetic p 205 A88-17223
Implementation of a digital optical matrix-vector multiplier using a holographic look-up table and residue arithmetic p 205 N88-10496
[NASA-CR-180431]
- HADDAD, G. I.**
Microwave and millimeter-wave power generation in silicon carbide avalanche devices p 126 A88-47599
- HAFTKA, RAPHAEL E.**
Derivatives of eigenvalues and eigenvectors of a general complex matrix p 209 A88-29269
- HAGGARD, J. B., JR.**
Sooting and disruption in spherically symmetrical combustion of decane droplets in air p 77 A88-16076
[IAF PAPER 87-403]
- HAGSTROM, THOMAS**
Accurate boundary conditions for extenor problems in gas dynamics p 210 N88-19182
[NASA-TM-100807]
- HAHN, R. C.**
Dendritic solidification under microgravity conditions [AIAA PAPER 88-0248] p 110 A88-22186
Isothermal dendritic growth - A low gravity experiment p 110 A88-28556
Solidification under microgravity conditions - Dendritic growth p 110 A88-35130
[AAS PAPER 86-380]
Isothermal dendritic growth - A proposed microgravity experiment p 112 A88-49095
- HAJEK, T. J.**
Coolant passage heat transfer with rotation p 147 N88-11160
- HAKIM, N.**
Application of several variable-valve-timing concepts to an LHR engine p 19 A88-15119
[ASME PAPER 87-ICE-29]
- HAKIM, NABIL S.**
Adiabatic diesel engine component development: Reference engine for on-highway applications p 224 N88-12428
[NASA-CR-179531]
- HALEVI, YORAM**
Finite-dimensional modeling of network-induced delays for real-time control systems p 208 A88-54537
- HALFORD, G. R.**
Calculation of thermomechanical fatigue life based on isothermal behavior p 181 A88-26450
Low cycle fatigue p 86 A88-35901
[ASTM STP-942]
Bithermal low-cycle fatigue behavior of a NiCoCrAlY-coated single crystal superalloy p 90 A88-51736
Fatigue life prediction modeling for turbine hot section materials p 184 A88-54144
Fatigue life prediction modeling for turbine hot section materials p 187 N88-14453
[NASA-TM-100291]
Evaluation of structural analysis methods for life prediction p 190 N88-21511
- HALFORD, GARY R.**
An update of the total-strain version of SRP p 86 A88-35910
Bithermal fatigue - A link between isothermal and thermomechanical fatigue p 87 A88-35918
Life prediction of thermomechanical fatigue using total strain version of strainrange partitioning (SRP): A proposal p 187 N88-15263
[NASA-TP-2779]
Life prediction modeling based on strainrange partitioning p 178 N88-22425
- HALLUM, GARY W.**
Effect of high-temperature hydrogen exposure on sintered alpha-SiC p 97 A88-29714
- HAMM, ROBERT**
Seal technology for liquid oxygen (LOX) turbopumps [NASA-CR-174866] p 171 N88-13603

- HAMMARLUND, GREGORY R.**
Program for the feasibility of developing a high pressure acoustic levitator
[NASA-CR-182154] p 113 N88-26498
- HAMROCK, BERNARD J.**
Piezoviscous effects in nonconformal contacts lubricated hydrodynamically p 133 A88-12926
- HAN, J. C.**
Effect of rib angle on local heat/mass transfer distribution in a two-pass rib-roughened channel
[ASME PAPER 87-GT-94] p 131 A88-11033
Local heat/mass transfer distributions around sharp 180 deg turns in two-pass smooth and rib-roughened channels
[ASME PAPER 86-GT-114] p 139 A88-28516
Local heat/mass transfer and pressure drop in a two-pass rib-roughened channel for turbine airfoil cooling
[NASA-CR-179635] p 148 N88-12039
- HANCOCK, D. J.**
An 8-cm ion thruster characterization
[NASA-CR-180819] p 56 N88-10106
- HANDSCHUH, ROBERT F.**
Efficiency testing of a helicopter transmission planetary reduction stage
[NASA-TP-2795] p 172 N88-15224
Identification and proposed control of helicopter transmission noise at the source p 38 N88-16647
Thermal stress minimized, two component, turbine shroud seal
[NASA-CASE-LEW-14212-1] p 174 N88-23978
Applications of an exponential finite difference technique
[NASA-TM-100939] p 175 N88-28312
- HANES, M. H.**
Advanced development of double-injection, deep-impurity semiconductor switches
[NASA-CR-182118] p 222 N88-25346
- HANKEY, W. L.**
Navier-Stokes solutions of flowfield characteristics produced by ice accretion
[AIAA PAPER 88-0290] p 137 A88-22210
- HANSEN, IRVING G.**
EMC and power quality standards for 20-kHz power distribution p 52 A88-11830
Status of 20 kHz space station power distribution technology
[NASA-TM-100781] p 59 N88-15838
- HANSMAN, R. JOHN**
Measurement of ice thickness (icing) in aeronautics p 15 A88-32714
An experimental and theoretical study of the ice accretion process during artificial and natural icing conditions
[NASA-CR-182119] p 16 N88-21143
- HANSMAN, R. JOHN, JR.**
Investigation of surface water behavior during glaze ice accretion
[AIAA PAPER 88-0115] p 14 A88-22079
In-flight measurement of airfoil icing using an array of ultrasonic transducers p 15 A88-50910
Ultrasonic techniques for aircraft ice accretion measurement
[AIAA PAPER 88-4656] p 18 A88-51910
In-flight measurement of ice growth on an airfoil using an array of ultrasonic transducers
[AIAA-87-0178] p 16 N88-23717
Experimental measurements of heat transfer from an iced surface during artificial and natural cloud icing conditions
[AIAA-86-1352] p 153 N88-23718
- HARB, AWAD**
Thermal stresses of a wind turbine blade made of orthotropic material p 180 A88-18380
- HARDING, JOHN T.**
Iridium-coated rhenium thrusters by CVD
[NASA-TM-101309] p 67 N88-29874
- HARDY, TERRY L.**
A low-power arcjet cyclic lifetest
[NASA-TM-100233] p 57 N88-11748
The effect of eddy distribution on momentum and heat transfer near the wall in turbulent pipe flow
[NASA-TM-100257] p 150 N88-15984
Electric propulsion options for the SP-100 reference mission p 62 N88-24296
- HARF, F. H.**
Solidification of undercooled Ni-Sn eutectic alloy under microgravity conditions in the Space Shuttle p 110 A88-28557
- HARIHARAN, S. I.**
Accurate boundary conditions for exterior problems in gas dynamics
[NASA-TM-100807] p 210 N88-19182
Solving time-dependent two-dimensional eddy current problems
[NASA-TM-100875] p 211 N88-25239
- HARLOFF, G. J.**
Real gas properties and Space Shuttle Main Engine fuel turbine performance prediction
[ASME PAPER 87-GT-106] p 50 A88-11038
Hypersonic turbulent wall boundary layer computations
[AIAA PAPER 88-2829] p 7 A88-44667
Three-dimensional viscous flow computations of a circular jet in subsonic and supersonic cross flow
[AIAA PAPER 88-3703] p 143 A88-48916
Two-dimensional viscous flow computations of hypersonic scramjet nozzle flowfields at design and off-design conditions
[AIAA PAPER 88-3280] p 23 A88-50785
Hypersonic turbulent wall boundary layer computations
[NASA-CR-182147] p 154 N88-24917
Two-dimensional viscous flow computations of hypersonic scramjet nozzle flowfields at design and off-design conditions
[NASA-CR-182150] p 35 N88-25459
Three-dimensional viscous flow computations of a circular jet in subsonic and supersonic cross flow
[NASA-CR-182153] p 155 N88-26616
- HARMON, T.**
Improved maintainability of space-based reusable rocket engines
[AIAA PAPER 88-3113] p 55 A88-48037
- HART, R. E., JR.**
Comparative radiation resistance, temperature dependence and performance of diffused junction indium phosphide solar cells p 198 A88-18580
Radiation and temperature effects in gallium arsenide, indium phosphide, and silicon solar cells p 125 A88-34321
Radiation performance of AlGaAs and InGaAs concentrator cells and expected performance of cascade structures p 125 A88-34356
- HART, RUSSELL E., JR.**
Effects of electron and proton irradiations on n/p and p/n GaAs cells grown by MOCVD
[NASA-TM-100199] p 127 N88-10266
Radiation performance of AlGaAs concentrator cells and expected performance of cascade structures
[NASA-TM-100145] p 200 N88-12878
- HARTLE, M. S.**
3D inelastic analysis methods for hot section components p 185 N88-11164
- HARVEY, W. D.**
Transition and separation control on a low-Reynolds number airfoil p 2 A88-11186
- HASSOLD, G. N.**
Monte Carlo simulation of modulated phases
[NASA-TM-89654] p 210 N88-12323
- HATHAWAY, M. D.**
Measurements of the unsteady flow field within the stator row of a transonic axial-flow fan. I - Measurement and analysis technique
[ASME PAPER 87-GT-226] p 4 A88-18660
Measurements of the unsteady flow field within the stator row of a transonic axial-flow fan. II - Results and discussion
[ASME PAPER 87-GT-227] p 4 A88-18661
- HATHAWAY, MICHAEL D.**
Design and performance of controlled-diffusion stator compared with original double-circular-arc stator
[SAE PAPER 871783] p 20 A88-30777
- HAUCK, K. E., JR.**
Plasticity analysis of wear phenomena as an aid in the development of abrasible materials p 164 A88-10938
- HAUGLAND, EDWARD J.**
Progress in MMIC technology for satellite communications p 126 A88-37844
- HAVENS, V. N.**
Toluene stability Space Station Rankine power system p 50 A88-11794
Solar dynamic organic Rankine cycle heat rejection system simulation p 132 A88-11808
- HAVENS, VANCE**
Study of toluene stability for an Organic Rankine Cycle (ORC) space-based power system
[NASA-CR-180884] p 66 N88-29863
Study of toluene rotary fluid management device and shear flow condenser performance for a space-based organic Rankine power system
[NASA-CR-180885] p 67 N88-29872
- HAVEY, C. T.**
Multiple-Purpose Subsonic Naval Aircraft (MPSNA): Multiple Application Propan Study (MAPS)
[NASA-CR-175104] p 18 N88-28917
- HAW, R. C.**
Coherent motion induced fluctuations in the primary transition region of a plane shear layer p 133 A88-14125
Gravitationally defined velocities for a low speed hot-wire calibration p 133 A88-14170
- HAWKINS, LAWRENCE ALLEN**
A comparison of experimental and theoretical results for labyrinth gas seals with honeycomb stators
[NASA-CR-182441] p 172 N88-16006
- HAYDEN, WARREN R.**
Orbital transfer vehicle 3000 LBF thrust chamber assembly hot fire test program
[NASA-CR-182145] p 66 N88-29858
- HAYKIN, T.**
Transient engine performance with water ingestion p 19 A88-27295
- HEBSUR, M. G.**
Creep-fatigue behavior of NiCoCrAlY coated PWA 1480 superalloy single crystals p 86 A88-35911
Creep-fatigue behavior of NiCoCrAlY coated PWA 1480 p 186 N88-11176
- HECKEL, R. W.**
Interdiffusion in Ni-rich, Ni-Cr-Al alloys at 1100 and 1200 C. I - Diffusion paths and microstructures. II - Diffusion coefficients and predicted concentration profiles p 84 A88-24485
Predicting diffusion paths and interface motion in gamma/gamma + beta, Ni-Cr-Al diffusion couples p 84 A88-24486
Diffusional transport during the cyclic oxidation of gamma + beta, Ni-Cr-Al(Y, Zr) alloys p 85 A88-28902
- HEIDELBERG, LAURENCE J.**
Advanced turboprop wing installation effects measured by unsteady blade pressure and noise
[AIAA PAPER 87-2719] p 3 A88-18655
Advanced turboprop wing installation effects measured by unsteady blade pressure and noise
[NASA-TM-100200] p 9 N88-10008
- HEIDENREICH, G.**
Development of an integrated heat pipe-thermal storage system for a solar receiver
[NASA-TM-101099] p 202 N88-22458
- HEIDENREICH, GARY**
Integrated heat pipe-thermal storage system performance evaluation p 132 A88-11803
Development of an integrated heat pipe-thermal storage system for a solar receiver
[AIAA PAPER 88-2683] p 141 A88-43746
- HEINE, C.**
Method for generation of spiral bevel gears with conjugate gear tooth surfaces
[ASME PAPER 86-DET-3] p 165 A88-10973
Determination of settings of a tilted head-cutter for generation of hypoid and spiral bevel gears
[NASA-CR-182138] p 174 N88-24976
- HEINEN, V. O.**
Submillimeter backward wave oscillators p 122 A88-19659
- HEITMAN, P. W.**
Correlation between ultrasonic velocity and density of ceramic turbine blades p 176 A88-12581
Dynamic and static fatigue behavior of sintered silicon nitrides p 96 A88-12602
- HELLAWELL, A.**
Local convective flows in partly solidified alloys p 219 A88-18467
Channel formation in Pb-Sn, Pb-Sb, and Pb-Sn-Sb alloy ingots and comparison with the system NH₄Cl-H₂O p 89 A88-46038
- HELMICK, M. R.**
Vapor condensation rate at a turbulent liquid interface, for application to cryogenic hydrogen
[AIAA PAPER 88-0559] p 137 A88-22419
Vapor condensation on a turbulent liquid interface p 150 N88-15939
- HEMANN, JOHN H.**
Transply crack density detection by acousto-ultrasonics
[NASA-TM-100224] p 72 N88-11758
High temperature tensile testing of ceramic composites
[NASA-CR-180888] p 161 N88-15996
- HENDERSON, H. T.**
Ohmic contact formation in semi-insulating GaAs using shallow heavily doped p-type layers p 219 A88-11150
- HENDERSON, ROBERT A.**
Theoretical analysis of the electrical aspects of the basic electro-impulse problem in aircraft de-icing applications
[NASA-CR-180845] p 15 N88-13310
- HENDRICKS, R. C.**
Numerical and analytical study of fluid dynamic forces in seals and bearings p 167 A88-31534
Numerical modeling of multidimensional flow in seals and bearings used in rotating machinery
[NASA-TM-100779] p 150 N88-16988
Numerical and analytical study of fluid dynamic forces in seals and bearings
[NASA-TM-100268] p 151 N88-18867

HENDRICKS, ROBERT C.

- Interface roughness effect on stresses in ceramic coatings p 95 A88-12587
- Thermomechanical behavior of plasma-sprayed ZrO₂-Y₂O₃ coatings influenced by plasticity, creep, and oxidation p 95 A88-12588
- Some adhesion/cohesion characteristics of plasma-sprayed ZrO₂-Y₂O₃ under tensile loading p 95 A88-12589

Heat transfer in aerospace propulsion [NASA-TM-100874] p 154 N88-23957

HENRY, DONALD P., JR.

- A new boundary element formulation for two- and three-dimensional thermoelasticity using particular integrals p 184 A88-53088
- A new BEM formulation for two- and three-dimensional elastoplasticity using particular integrals p 184 A88-53089

HEPP, A. F.

- Advantages of barium peroxide in the powder synthesis of perovskite superconductors p 221 A88-41496
- Characterization of Ba₂YCu₃O(7-x) prepared in an inert atmosphere p 221 A88-49376

HERBELL, THOMAS P.

- Effect of high-temperature hydrogen exposure on sintered alpha-SiC p 97 A88-29714

HERCZFELD, P. R.

- System architecture of MMIC-based large aperture arrays for space applications p 45 A88-35274

HERMAN, A. M.

- Study of Staebler-Wronsky degradation effect in a Si:H based P-I-N solar cells [NASA-CR-182564] p 203 N88-25970

HEYWARD, A. O.

- Numerical arc segmentation algorithm for a radio conference - A software tool for communication satellite systems planning [AIAA PAPER 88-0788] p 212 A88-27531
- Numerical arc segmentation algorithm for a radio conference: A software tool for communication satellite systems planning [NASA-TM-100789] p 46 N88-22919

HEYWARD, ANN O.

- An allotment planning concept and related computer software for planning the fixed satellite service at the 1988 space WARC p 116 A88-36482
- An allotment planning concept and related computer software for planning the fixed satellite service at the 1988 space WARC [NASA-TM-100244] p 117 N88-11944
- Numerical arc segmentation algorithm for a radio conference-NASARC (version 2.0) technical manual [NASA-TM-100160] p 118 N88-15910
- Numerical arc segmentation algorithm for a radio conference-NASARC, version 2.0: User's manual [NASA-TM-100161] p 119 N88-16928

HIGGINS, A. W.

- Coolant passage heat transfer with rotation p 147 N88-11160

HIGGINS, J. A.

- Development of 20 GHz monolithic transmit modules [NASA-CR-182134] p 222 N88-24539

HILL, S. M.

- High frequency GaAlAs modulator and photodetector for phased array antenna applications [NASA-TM-101328] p 130 N88-30048

HILLERY, R. V.

- Thermal barrier coating life prediction model development p 170 N88-11184

HINGST, W. R.

- Glancing shock wave-turbulent boundary layer interaction with boundary layer suction [AIAA PAPER 88-0308] p 6 A88-27718

HINGST, WARREN R.

- Experimental and numerical investigation of the effect of distributed suction on oblique shock wave/turbulent boundary layer interaction [NASA-TM-101334] p 156 N88-30084

HIPPENSTEELE, S. A.

- Use of a liquid-crystal and heater-element composite for quantitative, high-resolution heat-transfer coefficients on a turbine airfoil including turbulence and surface-roughness effects p 156 A88-10969
- High-resolution heat-transfer-coefficient maps applicable to compound-curve surfaces using liquid crystals in a transient wind tunnel p 134 A88-18506

HIRSCHBERG, MARVIN H.

- Aircraft engine hot section technology: An overview of the HOST Project p 29 N88-15804

HO, P. Y.

- Scale model acoustic testing of counterrotating fans [AIAA PAPER 88-2057] p 22 A88-37947

HOBBART, HOWARD F.

- The Lewis Strain Gauge Laboratory: Status and plans p 160 N88-11146

HOCHSTEIN, JOHN I.

- Computational prediction of propellant reorientation p 109 N88-15940

HOEBER, CHRISTOPHER F.

- Bandwidth and power efficient satellite TDMA demodulator and decoder [AIAA PAPER 88-0812] p 123 A88-27559

HOELZEMAN, RONALD G.

- Computer simulation of a single pilot flying a modern high-performance helicopter [NASA-TM-100182] p 39 N88-26376
- Computer simulation of multiple pilots flying a modern high performance helicopter [NASA-TM-100183] p 39 N88-26377

HOFFMAN, R. W.

- Degradation mechanisms of materials for large space systems in low Earth orbit [NASA-CR-181472] p 71 N88-10896

HOFFMAN, R., JR.

- Analysis of plasma nitrided steels p 88 A88-38936

HOFFMAN, RICHARD W., JR.

- Laser induced OMCVD growth of AlGaAs on GaAs p 125 A88-34286

HOLDEMAN, J. D.

- A numerical study of the effects of curvature and convergence on dilution jet mixing [AIAA PAPER 87-1953] p 137 A88-23312
- Assessment, development, and application of combustor aerothermal models p 24 A88-54140
- On the mixing of a row of jets with a confined crossflow p 147 N88-11154

- A numerical study of the effects of curvature and convergence on dilution jet mixing [NASA-TM-89878] p 26 N88-13347

- Assessment, development and application of combustor aerothermal models [NASA-TM-100290] p 32 N88-19469

HOLDEMAN, JAMES D.

- A numerical study of the hot gas environment around a STOVL aircraft in ground proximity [AIAA PAPER 88-2882] p 23 A88-48752

- An empirical model of the effects of curvature and convergence on dilution jet mixing [AIAA PAPER 88-3180] p 23 A88-50783

- A numerical study of the hot gas environment around a STOVL aircraft in ground proximity [NASA-TM-100895] p 1 N88-23729

- An empirical model of the effects of curvature and convergence on dilution jet mixing [NASA-TM-100896] p 34 N88-24640

HOLDRIDGE, J.

- Centaur operations at the space station [NASA-CR-179593] p 49 N88-25473

HOLLY, S.

- Optical measurements pertaining to Space Station solar dynamic power systems [IAF PAPER 87-229] p 42 A88-15954

HOLMAN, RICHARD

- Wilson-loop instantons p 212 A88-10410

HOLTMAN, R. L.

- Design and development of ceramic components [AIAA PAPER 88-3054] p 168 A88-44742

HOMICZ, G. F.

- A hybrid numerical technique for predicting the aerodynamic and acoustic fields of advanced turboprops [NASA-CR-174926] p 216 N88-12352

HON, T.-L.

- Evolution of hairpin vortices in a shear flow [NASA-TM-100858] p 211 N88-26885

HONEY, F.

- Analysis of plasma nitrided steels p 88 A88-38936

HONEY, FRANK S.

- Auger analysis of a fiber/matrix interface in a ceramic matrix composite [NASA-TM-100892] p 76 N88-25487

HO, E. A.

- A numerical investigation of the influence of heating on the excitation of high and low Mach number jet flows [ASME PAPER 87-WA/NCA-13] p 144 A88-51343

HOOSAC, T. M.

- An integrated approach for friction damper design p 167 A88-31598

HOPKINS, D. A.

- An expert system for probabilistic description of loads on space propulsion system structural components [AIAA PAPER 88-2371] p 182 A88-32308

HOPKINS, DALE A.

- Integrated analysis and applications p 28 N88-15789

- METCAN: The metal matrix composite analyzer p 74 N88-22395

- Structural tailoring of advanced turboprops p 192 N88-22400

HOSHOR, ALAN

- Expert systems for space power supply - Design, analysis, and evaluation p 212 A88-22696

HOSNY, W. M.

- E3 10C compressor test analysis of high-speed post-stall data [NASA-CR-179521] p 36 N88-28929

HOTES, DEBORAH

- Arc-textured metal surfaces for high thermal emittance space radiators [NASA-TM-100894] p 94 N88-24754

HOUSER, M. J.

- Experiments on spray interactions in the wake of a bluff body [ASME PAPER 87-GT-48] p 131 A88-11000

HOVENAC, EDWARD A.

- Operating envelopes of particle sizing instrumentation used for icing research [AIAA PAPER 88-0291] p 157 A88-22211

- Performance and operating envelope of imaging and scattering particle sizing instruments [NASA-CR-180859] p 161 N88-12042

- Operating envelopes of particle sizing instrumentation used for icing research [NASA-CR-180870] p 161 N88-13573

HOYNIK, DANIEL

- Control of rotor aerodynamically forced vibrations by splitters p 23 A88-52684

HSIEH, KWANG-CHUNG

- Numerical simulation of hypersonic inlet flows with equilibrium or finite rate chemistry [AIAA PAPER 88-0273] p 5 A88-27717

- Velocity-coupled flow oscillations in a simulated solid-propellant rocket environment [AIAA PAPER 88-0543] p 108 A88-27720

- Numerical study of multicomponent droplet vaporization at near critical conditions [AIAA PAPER 88-0637] p 108 A88-27721

HSU, ANDREW T.

- A computational analysis of under-expanded jets in the hypersonic regime [AIAA PAPER 88-4361] p 8 A88-50604

- A computational analysis of under-expanded jets in the hypersonic regime [NASA-TM-101319] p 13 N88-27174

HUANG, H. H.

- Improved silicon nitride for advanced heat engines [NASA-CR-175006] p 102 N88-15886

HUANG, H. T.

- 3D inelastic analysis methods for hot section components p 185 N88-11164

HUANG, JOHN S.

- Quantitative characterization of the viscosity of a microemulsion p 77 A88-11167

HUANG, P. G.

- Time-accurate simulations of a shear layer forced at a single frequency [AIAA PAPER 88-0061] p 138 A88-27716

- Time-accurate simulations of a shear layer forced at a single frequency [NASA-TM-100836] p 152 N88-19740

HUBBELL, THEODORE E.

- Ion-beam nitriding of steels [NASA-CASE-LEW-14104-2] p 91 N88-14179

HUCKELBRIDGE, A. A.

- Identification of structural interface characteristics using component mode synthesis p 181 A88-31561

HUCKELBRIDGE, ARTHUR A.

- Characterization of damped structural connections for multi-component systems [NASA-TM-100801] p 189 N88-18974

HUFF, RONALD

- Unsteady heat transfer in turbine blade ducts: Focus on combustor sources [NASA-TM-100815] p 151 N88-18870

HUFF, RONALD G.

- Identification and proposed control of helicopter transmission noise at the source p 38 N88-16647

HUGHES, CHRISTOPHER E.

- Summary of low-speed wind tunnel results of several high-speed counterrotation propeller configurations [AIAA PAPER 88-3149] p 7 A88-48758

- Experimental investigation of the subsonic high-altitude operation of the NASA Lewis 10- by 10-foot supersonic wind tunnel [NASA-TM-100214] p 40 N88-15814

- Summary of low-speed wind tunnel results of several high-speed counterrotation propeller configurations [NASA-TM-100945] p 13 N88-24597

HULBURT, NEAL E.

- Magnetic fields interacting with nonlinear compressible convection p 226 A88-31163

HULL, DAVID R.

- Fatigue failure of regenerator screens in a high frequency Stirling engine p 179 N88-24491

- As-received microstructure of a SiC/Ti-15-3 composite [NASA-TM-100938] p 76 N88-28095

- HULL, J. R.**
Application of superconducting technology to earth-to-orbit electromagnetic launch systems [NASA-TM-101134] p 43 N88-26385
- HULSE, CHARLES O.**
The development of a high temperature static strain gage system p 160 N88-11142
- HULTGREN, LENNART S.**
Higher eigenmodes in the Blasius boundary-layer stability problem p 134 A88-16352
Absolute instability of the Gaussian wake profile p 136 A88-20842
Stability of swirling gas flows p 142 A88-46317
- HUMES, ROBERT L.**
In-flight measurement of airfoil icing using an array of ultrasonic transducers p 15 A88-50910
In-flight measurement of ice growth on an airfoil using an array of ultrasonic transducers [AIAA-87-0178] p 16 N88-23717
- HUMPHREY, J. A. C.**
Unsteady motion and transition to turbulence in developing curved duct flow p 140 A88-39010
- HUNG, CHING-CHEH**
A heater made from graphite composite material for potential deicing application p 17 A88-15724
Thermal conductivity of pristine and brominated highly graphitized pitch based carbon fibers p 97 A88-20257
Synthesis, electrical and thermal conductivities, and potential applications of graphite fluoride fibers p 97 A88-26963
Brominated graphite fibers and method of producing the same [NASA-CASE-LEW-14698-1] p 76 N88-29888
- HUNG, CHING-CHEN**
Specific heat of pristine and brominated graphite fibers, composites and HOPG p 98 A88-32853
- HUNTER, S. D.**
Oil film thickness measurement and analysis for an angular contact ball bearing operating in parched elastohydrodynamic lubrication p 165 A88-14115
- HURON, ERIC S.**
Deformation, fatigue and fracture behavior of two cast anisotropic superalloys p 187 N88-13732
- HURST, JANET B.**
Simple processing method for high-strength silicon carbide p 97 A88-19056
- HURWITZ, F. I.**
Silsesquioxanes as precursors to ceramic composites p 69 A88-12599
- HURWITZ, FRANCES I.**
Ceramic matrix and resin matrix composites - A comparison p 69 A88-13158
Ethynylated aromatics as high temperature matrix resins [NASA-TM-89829] p 73 N88-18640
Polymer precursors for ceramic composites p 75 N88-23890
- HUSSAIN, A. K. M. F.**
Roles of initial condition and vortex pairing in jet noise p 213 A88-13963
- HUSTON, RONALD L.**
On dynamic loads in parallel shaft transmissions. 1: Modelling and analysis [NASA-TM-100180] p 171 N88-12797
On dynamic loads in parallel shaft transmissions. 2: Parameter study [NASA-TM-100181] p 171 N88-12798
Finite-element grid improvement by minimization of stiffness matrix trace [NASA-TM-100255] p 171 N88-13604
- HUYNH, HUNG T.**
A finite difference scheme for three-dimensional steady laminar incompressible flow p 139 A88-30469
- HUYNH, T.**
Crosspolarisation characteristics of rectangular patch antennas p 117 A88-47705
- HWANG, DANNY P.**
A finite difference scheme for three-dimensional steady laminar incompressible flow p 139 A88-30469
- HWANG, K. S.**
Comment on 'Ram ion scattering caused by Space Shuttle v x B induced differential charging' by I. Katz and V. A. Davis p 204 A88-35775
- HYATT, L.**
Silsesquioxanes as precursors to ceramic composites p 69 A88-12599
- HYATT, M. J.**
Glass properties in the yttria-alumina-silica system p 96 A88-18361
- HYLTON, LARRY D.**
Film cooling heat transfer on a turbine airfoil p 147 N88-11156
- IACABUCCI, R. S.**
25-LBF GO2/GH2 space station thruster [AIAA PAPER 88-2793] p 56 A88-53101
- IDA, NATHAN**
Solving time-dependent two-dimensional eddy current problems [NASA-TM-100875] p 211 N88-25239
- INGEBO, ROBERT D.**
Experimental and theoretical effects of nitrogen gas flow rate on liquid-jet atomization p 145 A88-52679
Effect of mass-velocity on liquid jet atomization in Mach 1 gasflow [NASA-TM-100813] p 162 N88-23194
Small-droplet spray measurements with a scattered-light scanner [NASA-TM-100973] p 163 N88-26645
- INGRAFFEA, ANTHONY R.**
Interactive computer simulation of fracture processes p 180 A88-16955
- IVANCIC, WILLIAM D.**
COSPAS/SARSAT 406-MHz emergency beacon digital controller [NASA-TM-100859] p 121 N88-26566
- JACKSON, L. ROBERT**
Hypersonic structures and materials - A progress report p 17 A88-16748
- JACOBSON, BO O.**
A model for the influence of pressure on the bulk modulus and the influence of temperature on the solidification pressure for liquid lubricants [ASME PAPER 86-TRIB-63] p 133 A88-15124
- JACOBSON, N. S.**
Molten salt corrosion of SiC and Si3N4 p 107 N88-23885
- JACOBSON, NATHAN S.**
Molten-salt corrosion of silicon nitride. I - Sodium carbonate. II - Sodium sulfate p 97 A88-26222
Multielement mapping of alpha-SiC by scanning Auger microscopy p 158 A88-27617
Direct mass spectrometric identification of silicon oxychloride compounds p 78 A88-44425
- JACOBSON, T.**
Containment of a silicone fluid free surface in reduced gravity p 112 A88-49085
- JACOBSON, THOMAS P.**
Containment of a silicone fluid free surface in reduced gravity using barrier coatings [NASA-TM-101314] p 155 N88-30072
- JACQMIN, DAVID A.**
Dynamics of two fluids under periodic acceleration [AIAA PAPER 88-3728] p 143 A88-48980
- JACQUEZ, A.**
A millimeter-wave tunnel Ladder TWT [NASA-CR-182184] p 130 N88-28239
- JANARDAN, B. A.**
Scale model acoustic testing of counterrotating fans [AIAA PAPER 88-2057] p 22 A88-37947
- JASKOWIAK, MARTHA H.**
Pressure effects on the thermal stability of SiC fibers [NASA-TM-100146] p 71 N88-10120
SiC fiber analysis p 107 N88-23891
- JASON, NORA H.**
Spacecraft fire detection and extinguishment: A bibliography [NASA-CR-180880] p 45 N88-18612
- JAWORSKE, D. A.**
Differential scanning calorimetric survey of brominated PAN, pitch-based and vapor-grown fibers p 98 A88-32854
The effect of bromination of carbon fibers on the coefficient of thermal expansion of graphite fiber-epoxy composites [NASA-TM-100236] p 72 N88-10899
- JAWORSKE, DONALD A.**
Improving the interlaminar shear strength of carbon fiber-epoxy composites through carbon fiber bromination [NASA-TM-100248] p 72 N88-15018
- JAYARAMAN, N.**
Constitutive modeling for single crystal superalloys p 90 N88-11168
- JEFFERIES, K. S.**
Optical measurements pertaining to Space Station solar dynamic power systems [IAF PAPER 87-229] p 42 A88-15954
- JEFFERIES, KENT S.**
Ray tracing optical analysis of offset solar collector for space station solar dynamic system [NASA-TM-100853] p 60 N88-22080
- Thermal distortion analysis of the space station solar dynamic concentrator [NASA-TM-100868] p 64 N88-25475
- JENG, YEAU-REN**
Piezoviscous effects in nonconformal contacts lubricated hydrodynamically p 133 A88-12926
- JENKINS, MICHAEL G.**
Fracture resistance of a TiB2 particle/SiC matrix composite at elevated temperature [NASA-TM-100967] p 107 N88-26482
- JERACKI, ROBERT J.**
Porous wind tunnel corrections for counterrotation propeller testing [AIAA PAPER 88-2055] p 6 A88-44490
Experimental investigation of the subsonic high-altitude operation of the NASA Lewis 10- by 10-foot supersonic wind tunnel [NASA-TM-100214] p 40 N88-15814
Porous wind tunnel corrections for counterrotation propeller testing [NASA-TM-100873] p 11 N88-22019
- JHA, S. C.**
Dispersion strengthened NiAl alloys produced by rapid solidification processing p 88 A88-40588
- JIANG, HONG**
Approximate polynomial preconditioning applied to biharmonic equations on vector supercomputers [NASA-TM-100217] p 210 N88-10563
- JOHNSON, JEROME A.**
Mixing fuel particles for space combustion research using acoustics p 112 A88-49093
Mixing fuel particles for space combustion research using acoustics [NASA-TM-100295] p 43 N88-21186
- JOHNSON, M. C.**
Experimental verification of a secondary recirculation zone in a labyrinth seal [AIAA PAPER 88-3692] p 168 A88-48971
3-D laser anemometer measurements in a labyrinth seal [ASME PAPER 88-GT-63] p 169 A88-54195
3-D laser anemometer measurements in an annular seal [ASME PAPER 88-GT-64] p 169 A88-54196
- JOHNSON, S.**
Development of an integrated heat pipe-thermal storage system for a solar receiver [NASA-TM-101099] p 202 N88-22458
- JOHNSON, STEVE**
Development of an integrated heat pipe-thermal storage system for a solar receiver [AIAA PAPER 88-2683] p 141 A88-43746
- JOHNSTON, J. C.**
Ground based materials science experiments p 43 A88-52364
- JOHNSTON, J. CHRISTOPHER**
Preparation for microgravity - The role of the Microgravity Material Science Laboratory [AIAA PAPER 88-3510] p 111 A88-42908
Preparation for microgravity: The role of the microgravity materials science laboratory [NASA-TM-100906] p 113 N88-24811
- JONES, B. I.**
Analysis of closed cycle megawatt class space power systems with nuclear reactor heat sources p 62 N88-24351
- JONES, DAVID J.**
Cyclic fatigue damage characteristics observed for simple loadings extended to multiaxial life prediction [NASA-CR-182126] p 195 N88-25016
- JONES, H.**
Analysis and design of a gas-lubricated, sectored, floating ring seal [ASME PAPER 87-TRIB-55] p 166 A88-23310
- JONES, R. E.**
A life test of a 22-Newton (5-lbf) hydrazine rocket [NASA-TM-100232] p 57 N88-11750
- JONES, ROBERT E.**
Water-propellant resistojets for man-tended platforms [IAF PAPER 87-259] p 54 A88-15975
Space Station propulsion system technology p 54 A88-21255
Space station propulsion [NASA-TM-100216] p 57 N88-11746
- JONES, STEPHEN H.**
Temperature stability of Al(x)Ga(1-x)As (x = 0-1) thermal oxide masks for selective-area epitaxy p 221 A88-45858
- JONES, T. V.**
High-resolution heat-transfer-coefficient maps applicable to compound-curve surfaces using liquid crystals in a transient wind tunnel p 134 A88-18506
- JONES, WILLIAM R., JR.**
Improved perfluoroalkyl ether fluid development p 68 A88-28624

- Investigation of PTFE transfer films by infrared emission spectroscopy and phase-locked ellipsometry
p 99 A88-35568
- JONGEWARD, G. A.**
Threshold-determining mechanisms for discharges in high-voltage solar arrays p 50 A88-11738
- JORASCH, RONALD E.**
Advanced satellite system architecture for VSATs with ISDN compatibility
[AIAA PAPER 88-0870] p 116 A88-27604
- JORDAN, E. H.**
Unified constitutive model for single crystal deformation behavior with applications p 191 N88-22388
- JORDAN, ERIC**
Constitutive modeling of superalloy single crystals with verification testing p 91 N88-11169
- JORGENSEN, PHILIP C. E.**
An explicit Runge-Kutta method for unsteady rotor/stator interaction
[AIAA PAPER 88-0049] p 5 A88-27715
An explicit Runge-Kutta method for unsteady rotor/stator interaction
[NASA-TM-100787] p 10 N88-14967
An unconditionally stable Runge-Kutta method for unsteady flows
[NASA-TM-101347] p 14 N88-29780
- JOSLYN, H. D.**
The effects of turbulence and stator/rotor interactions on turbine heat transfer. II - Effects of Reynolds number and incidence
[ASME PAPER 88-GT-5] p 145 A88-54152
The effects of turbulence and stator/rotor interactions on turbine heat transfer. I - Design operating conditions
[ASME PAPER 88-GT-125] p 145 A88-54236
The effects of inlet turbulence and rotor/stator interactions on the aerodynamics and heat transfer of a large-scale rotating turbine model. Part 4: Aerodynamic data tabulation
[NASA-CR-179469] p 153 N88-23956
The effects of inlet turbulence and rotor/stator interactions on the aerodynamics and heat transfer of a large-scale rotating turbine model. Volume 3: Heat transfer data tabulation 65 percent axial spacing
[NASA-CR-179468] p 37 N88-28930
The effects of inlet turbulence and rotor/stator interactions on the aerodynamics and heat transfer of a large-scale rotating turbine model. Volume 2: Heat transfer data tabulation. 15 percent axial spacing
[NASA-CR-179467] p 37 N88-29804
- JOSLYN, H. DAVID**
Measurement of airfoil heat transfer coefficients on a turbine stage p 147 N88-11158
- JOU, WEN-HUEI**
Direct simulations of chemically reacting turbulent mixing layers, part 2
[NASA-CR-180853] p 154 N88-25857
- JOYCE, JOSEPH**
Space station assembly/servicing capabilities p 48 N88-10100
- JOYCE, MARTIN**
Sensitivity study of the monogroove with screen heat pipe design
[AIAA PAPER 88-0470] p 137 A88-22346
- JOYNER, W. T.**
Gigard-tolerant power switches and memory elements p 123 A88-22704
Neutron radiation tolerance of Au-activated silicon p 222 N88-24316
- JUHASZ, A. J.**
Analysis of closed cycle megawatt class space power systems with nuclear reactor heat sources p 62 N88-24351
- JUHASZ, ALBERT**
Selection of high temperature thermal energy storage materials for advanced solar dynamic space power systems p 68 A88-11801
- JUHASZ, ALBERT J.**
Impact of thermal energy storage properties on solar dynamic space power conversion system mass p 51 A88-11805
- JUSTICE, D. W.**
A simple circular-polarized antenna: Circular waveguide horn coated with lossy magnetic material p 116 A88-36648
- K**
- KADAMBI, J. R.**
Measurements of natural circulation flow in a scale model PWR reactor system during postulated degraded core accidents using laser anemometry p 159 A88-43917
- KADAMBI, JAIRISHNAN R.**
Comparison of the bidirectional reflectance distribution function of various surfaces
[NASA-TM-101317] p 218 N88-28760
- KAI, FEI**
Computer simulation of a single pilot flying a modern high-performance helicopter
[NASA-TM-100182] p 39 N88-26376
Computer simulation of multiple pilots flying a modern high performance helicopter
[NASA-TM-100183] p 39 N88-26377
- KAISAND, L. R.**
Low cycle fatigue
[ASTM STP-942] p 86 A88-35901
- KALDOR, RAYMOND B.**
Breadboard RL10-2B low-thrust operating mode (second iteration) test report
[NASA-CR-182160] p 66 N88-29867
- KALLURI, SREERAMESH**
Characterization of fatigue crack initiation and propagation in Ti-6Al-4V with electrical potential drop technique
[NASA-TM-100877] p 195 N88-25937
- KAM, M.**
System architecture of MMIC-based large aperture arrays for space applications p 45 A88-35274
- KANIC, P. G.**
Oxidizer heat exchanger component test
[NASA-CR-182159] p 67 N88-29876
- KANIC, PAUL G.**
Breadboard RL10-2B low-thrust operating mode (second iteration) test report
[NASA-CR-182160] p 66 N88-29867
- KANTZOS, PETER**
In situ fatigue loading stage inside scanning electron microscope p 193 N88-22419
Fatigue crack growth behavior of a single crystal alloy as observed through an in situ fatigue loading stage
[NASA-TM-100863] p 93 N88-22966
- KAO, HSIAO C.**
Torsion effect on fully developed flow in a helical pipe p 135 A88-20748
- KAPOOR, VIK J.**
Rapid thermal annealing of indium phosphide compound semiconductors p 220 A88-26196
- KAPTANOGLU, H. T.**
Control of free shear layers
[AIAA PAPER 87-2689] p 134 A88-16545
- KARAGOZIAN, A. R.**
Experimental studies in vortex pair motion coincident with a liquid reaction p 142 A88-46316
- KARCHMER, ALLAN M.**
Identification and proposed control of helicopter transmission noise at the source p 38 N88-16647
- KARCHMER, ALLEN M.**
Turbofan engine core noise source diagnostics p 22 A88-39707
- KARKI, K. C.**
K-epsilon turbulence model assessment with reduced numerical diffusion for coaxial jets
[AIAA PAPER 88-0342] p 137 A88-22251
- KARL, DAVID W.**
Mod II engine development p 165 A88-11972
- KARP, A.**
A millimeter-wave tunnel Ladder TWT
[NASA-CR-182184] p 130 N88-28239
- KASCAK, A. F.**
Transient rotor dynamic rub phenomena - Theory and test p 167 A88-31539
Active control of transient rotordynamic vibration by optimal control methods
[ASME PAPER 88-GT-73] p 208 A88-54202
- KASSEMI, SIAVASH A.**
High Rayleigh number convection in rectangular enclosures with differentially heated vertical walls and aspect ratios between zero and unity
[NASA-TM-100277] p 151 N88-19739
- KATZ, I.**
Threshold-determining mechanisms for discharges in high-voltage solar arrays p 50 A88-11738
Hollow cathodes as electron emitting plasma contactors - Theory and computer modeling p 218 A88-47973
Electron collection by multiple objects within a single sheath p 219 A88-54999
- KAUFFMAN, A.**
Evaluation of structural analysis methods for life prediction p 190 N88-21511
- KAUFFMAN, ALBERT**
Thermal finite-element analysis of space shuttle main engine turbine blade
[NASA-TM-100117] p 187 N88-13745
- KAUTZ, H. E.**
Ultrasonic evaluation of mechanical properties of thick, multilayered, filament-wound composites p 176 A88-21340
- KAUTZ, HAROLD**
Transply crack density detection by acousto-ultrasonics
[NASA-TM-100224] p 72 N88-11758
- KAUTZ, HAROLD E.**
Nondestructive evaluation by acousto-ultrasonics p 177 N88-22412
New acousto-ultrasonic techniques applied to aerospace materials
[NASA-TM-101299] p 180 N88-28323
- KAWANO, LAWRENCE**
Primordial lithium - New reaction rates, new abundances, new constraints p 226 A88-31145
- KAZA, K. R. V.**
Experimental classical flutter results of a composite advanced turboprop model p 21 A88-35528
- KAZA, KRISHNA RAO V.**
The effects of rotational flow, viscosity, thickness, and shape on transonic flutter dip phenomena
[AIAA PAPER 88-2348] p 182 A88-32289
Application of a semi-analytical technique for sensitivity analysis of unsteady aerodynamic computations
[AIAA PAPER 88-2377] p 6 A88-32314
Vibration and flutter characteristics of the SR7L large-scale propfan
[NASA-TM-100272] p 188 N88-18036
The effects of rotational flow, viscosity, thickness, and shape on transonic flutter dip phenomena
[NASA-TM-100811] p 188 N88-18969
A semi-analytical technique for sensitivity analysis of unsteady aerodynamic computations
[NASA-TM-100810] p 189 N88-18976
Aeroelastic response of metallic and composite propfan models in yawed flow
[NASA-TM-100964] p 37 N88-29807
- KAZAROFF, JOHN M.**
Iridium-coated rhenium thrusters by CVD
[NASA-TM-101309] p 67 N88-29874
- KEDDY, E.**
Integrated heat pipe-thermal storage system performance evaluation p 132 A88-11803
Development of an integrated heat pipe-thermal storage system for a solar receiver
[AIAA PAPER 88-2683] p 141 A88-43746
- KEDDY, E. S.**
Development of an integrated heat pipe-thermal storage system for a solar receiver
[NASA-TM-101099] p 202 N88-22458
- KEGELMAN, J. T.**
Unsteady features of jets in lift and cruise modes for VTOL aircraft
[SAE PAPER 872359] p 6 A88-37220
- KEITH, T. G., JR.**
An experimental investigation of the effect of test-cell pressure on the performance of resistojets
[AIAA PAPER 88-3286] p 40 A88-44820
- KEITH, THEO G., JR.**
Applications of an exponential finite difference technique
[NASA-TM-100939] p 175 N88-28312
- KELLER, J. O.**
The structure and dynamics of reacting plane mixing layers p 136 A88-20871
- KENNEDY, F. E., JR.**
Plasticity analysis of wear phenomena as an aid in the development of abradable materials p 164 A88-10938
- KENNEDY, J. B.**
Fuel-injector/air-swirl characterization p 146 N88-11150
Fuel-injector/air-swirl characterization
[NASA-CR-180864] p 27 N88-14985
- KENNEDY, JAN B.**
Application of advanced diagnostics to airblast injector flows
[ASME PAPER 88-GT-12] p 159 A88-54159
- KERCZEWSKI, ROBERT J.**
The bit-error rate performance of a satellite microwave matrix switch
[AIAA PAPER 88-0826] p 123 A88-27572
The bit-error rate performance of a satellite microwave matrix switch
[NASA-TM-100285] p 46 N88-22920
- KERIBAR, R.**
Application of several variable-valve-timing concepts to an LHR engine
[ASME PAPER 87-ICE-29] p 19 A88-15119
- KERSCHEN, E. J.**
A parametric study of mean loading effects on airfoil gust interaction noise
[AIAA PAPER 87-2677] p 213 A88-16539
- KERSLAKE, T. W.**
Structural assessment of a Space Station solar dynamic heat receiver thermal energy storage canister
[AIAA PAPER 88-2487] p 47 A88-31396

- Structural assessment of a space station solar dynamic heat receiver thermal energy storage canister p 192 N88-22406
- KERSLAKE, WILLIAM R.**
The effect of the near earth micrometeoroid environment on a highly reflective mirror surface [NASA-TM-101307] p 44 N88-29833
- KESSELI, J. B.**
Advanced solar receiver conceptual design study p 51 A88-11800
- KHANDELWAL, P.**
Dynamic and static fatigue behavior of sintered silicon nitrides p 96 A88-12602
- KHANDELWAL, P. K.**
Correlation between ultrasonic velocity and density of ceramic turbine blades p 176 A88-12581
- KHANDELWAL, PRAMOD K.**
Nondestructive evaluation of structural ceramics by photoacoustic microscopy [NASA-CR-180858] p 103 N88-16868
- KHODADOUST, ABDOLLAH**
A flow visualization study of the leading edge separation bubble on a NACA 0012 airfoil with simulated glaze ice [NASA-CR-180846] p 10 N88-14966
- KHONSARI, M. M.**
Stability of a rigid rotor supported on flexible oil journal bearings [ASME PAPER 87-TRIB-48] p 166 A88-24034
On the performance of finite journal bearings lubricated with micropolar fluids [NASA-TM-100293] p 150 N88-15983
- KHO, B. C.**
Vapor condensation rate at a turbulent liquid interface, for application to cryogenic hydrogen [AIAA PAPER 88-0559] p 137 A88-22419
Vapor condensation on a turbulent liquid interface p 150 N88-15939
- KHURANA, K. K.**
Voids in Jovian magnetosphere revisited - Evidence of spacecraft charging p 226 A88-22879
- KIBENS, V.**
Unsteady features of jets in lift and cruise modes for VTOL aircraft [SAE PAPER 872359] p 6 A88-37220
- KIELB, R.**
Bladed disk assemblies; Proceedings of the Eleventh Biennial Conference on Mechanical Vibration and Noise, Boston, MA, Sept. 27-30, 1987 p 20 A88-31608
- KIELB, R. E.**
An integrated approach for friction damper design p 167 A88-31598
- KIELB, ROBERT E.**
Evaluation of a turbine blade damper using an integral approach [AIAA PAPER 88-2400] p 20 A88-32332
Flutter of a fan blade in supersonic axial flow [ASME PAPER 88-GT-78] p 8 A88-54206
Test facilities of the structural dynamics branch of NASA Lewis Research Center [NASA-TM-100800] p 190 N88-21534
- KIERNAN, M. T.**
Acousto-ultrasonics as a monitor of material anisotropy p 176 A88-46828
- KIM, J.**
Measurements of the turbulent transport of heat and momentum in convexly curved boundary layers - Effects of curvature, recovery and free-stream turbulence [ASME PAPER 87-GT-199] p 131 A88-11103
- KIM, K. S.**
Elevated temperature crack growth p 186 N88-11174
Elevated temperature crack growth p 193 N88-22421
- KIM, KWANG S.**
A review of path-independent integrals in elastic-plastic fracture mechanics p 183 A88-47001
- KIM, KWANG-SOO**
Skin friction measurements by laser interferometry in swept shock wave/turbulent boundary-layer interactions [AIAA PAPER 88-0497] p 5 A88-22364
- KIM, S. C.**
Hypersonic turbulent wall boundary layer computations [AIAA PAPER 88-2829] p 7 A88-44667
Hypersonic turbulent wall boundary layer computations [NASA-CR-182147] p 154 N88-24917
- KIM, WALTER S.**
Prototype thin-film thermocouple/heat-flux sensor for a ceramic-insulated diesel engine [NASA-TM-100798] p 162 N88-18892
- KING, GALEN B.**
Feasibility of hydroxyl concentration measurements by laser-saturated fluorescence in high-pressure flames p 77 A88-17218
- KING, ROGER J.**
Fast simulation techniques for switching converters p 122 A88-11878
- KINGSBURY, E.**
Oil film thickness measurement and analysis for an angular contact ball bearing operating in parched elastohydrodynamic lubrication p 165 A88-14115
Parched elastohydrodynamic lubrication film thickness measurement in an instrument ball bearing [STLE PREPRINT 88-AM-6G-1] p 169 A88-51082
- KIPP, C. M.**
Gravitational contributions to microstructural coarsening in liquid phase sintering p 111 A88-37155
Gravity and configurational energy induced microstructural changes in liquid phase sintering p 112 A88-49089
- KIRALY, LOUIS J.**
Determining structural performance p 27 N88-15787
- KIRBY, MARK S.**
In-flight measurement of airfoil icing using an array of ultrasonic transducers p 15 A88-50910
Ultrasonic techniques for aircraft ice accretion measurement [AIAA PAPER 88-4656] p 18 A88-51910
An experimental and theoretical study of the ice accretion process during artificial and natural icing conditions [NASA-CR-182119] p 16 N88-21143
In-flight measurement of ice growth on an airfoil using an array of ultrasonic transducers [AIAA-87-0178] p 16 N88-23717
Experimental measurements of heat transfer from an iced surface during artificial and natural cloud icing conditions [AIAA-86-1352] p 153 N88-23718
- KIRBY, MARK S. JR.**
Measurement of ice thickness (icing) in aeronautics p 15 A88-32714
- KIRTLEY, K. R.**
Comparison of computational methods for three-dimensional turbulent turbomachinery flows p 6 A88-42452
- KISER, JAMES D.**
Ceramics for engines p 103 N88-16704
High frequency ultrasonic characterization of sintered SiC [NASA-TM-100825] p 179 N88-23985
- KISHI, T.**
Gravitational contributions to microstructural coarsening in liquid phase sintering p 111 A88-37155
- KITAMURA, TAKAYUKI**
Creep life prediction based on stochastic model of microstructurally short crack growth [NASA-TM-100245] p 186 N88-12825
- KITTUR, MADAN G.**
Finite-element grid improvement by minimization of stiffness matrix trace [NASA-TM-100255] p 171 N88-13604
- KIVELSON, M. G.**
Voids in Jovian magnetosphere revisited - Evidence of spacecraft charging p 226 A88-22879
- KLAMKA, A.**
Multiple-Purpose Subsonic Naval Aircraft (MPSNA): Multiple Application Propfan Study (MAPS) [NASA-CR-175104] p 18 N88-28917
- KLEIN, ANDREW C.**
Assessment of nuclear reactor concepts for low power space applications p 217 N88-24409
- KLIMA, S. J.**
Investigation of a SiC/Ti-24Al-11Nb composite [NASA-TM-100956] p 76 N88-28980
- KLIMA, STANLEY J.**
Nondestructive evaluation of sintered ceramics p 177 N88-22416
- KLIMEK, ROBERT B.**
Mixing fuel particles for space combustion research using acoustics p 112 A88-49093
Mixing fuel particles for space combustion research using acoustics [NASA-TM-100295] p 43 N88-21186
- KNOLL, RICHARD H.**
Design, development, and test of Shuttle/Centaur G-prime cryogenic tankage thermal protection systems p 47 A88-53182
- KNOWLES, STEVEN C.**
Arcjet thruster research and technology, phase 1 [NASA-CR-182107] p 62 N88-23830
- KOEPE, GERHARD A.**
Optical technologies for space communication systems; Proceedings of the Meeting, Los Angeles, CA, Jan. 15, 16, 1987 [SPIE-756] p 45 A88-35251
- KOESTER, GARY E.**
Description of an oscillating flow pressure drop test rig [NASA-TM-100905] p 61 N88-22933
- KOHNHORST, P. A.**
Engineering calculations for the Delta S method of solving the orbital allotment problem [NASA-CR-182372] p 42 N88-14110
- KOLB, EDWARD W.**
Wilson-loop instantons p 212 A88-10410
Primordial origin of nontopological solitons p 226 A88-39313
- KOPANSKI, J. J.**
Behavior of ion-implanted junction diodes in 3C SiC p 122 A88-15423
- KORKAN, K. D.**
Analytical determination of propeller performance degradation due to ice accretion p 19 A88-19669
- KORKAN, KENNETH D.**
Model helicopter performance degradation with simulated ice shapes p 17 A88-22783
- KOSCHMIEDER, E. L.**
Investigation of surface tension driven convection as a feasibility study for a micro-gravity experiment [NASA-CR-182504] p 112 N88-18739
- KOSMAHL, HENRY G.**
Miniature traveling wave tube and method of making [NASA-CASE-LEW-14520-1] p 129 N88-23936
- KRAMER, EDWARD H.**
A cyclic ground test of an ion auxiliary propulsion system: Description and operational considerations [NASA-TM-100870] p 62 N88-23829
- KRATZER, R. H.**
Improved perfluoroalkylether fluid development [NASA-CR-180872] p 80 N88-15851
- KRATZER, REINHOLD H.**
Improved perfluoroalkyl ether fluid development p 68 A88-28624
- KREIDER, GARY E.**
Improved oil-off survivability of tapered roller bearings [NASA-CR-180804] p 170 N88-11135
- KREIDLER, ERIC R.**
Direct mass spectrometric identification of silicon oxychloride compounds p 78 A88-44425
- KREJSA, EUGENE A.**
Combustion noise from gas turbine aircraft engines measurement of far-field levels p 215 A88-39708
Identification and proposed control of helicopter transmission noise at the source p 38 N88-16647
- KREMPL, E.**
A simplified orthotropic formulation of the viscoplasticity theory based on overstress p 189 N88-21505
- KROEGER, ERICH**
Cryogenic fluid management program flight concept definition p 150 N88-15929
- KUCZMARSKI, M. A.**
Improved beta-SiC heteroepitaxial films using off-axis Si substrates p 219 A88-10431
- KUHN, GARY D.**
Investigation of the validity of Reynolds averaged turbulence models at the frequencies that occur in turbomachinery [NASA-CR-182162] p 65 N88-28087
- KUKULKA, J. R.**
Development of 8 cm x 8 cm silicon gridded back solar cell for space station p 200 A88-34312
- KUMAR, GANESH N.**
Development of a thermal and structural analysis procedure for cooled radial turbines [ASME PAPER 88-GT-18] p 145 A88-54164
- KUNATH, R. R.**
System architecture of MMIC-based large aperture arrays for space applications p 45 A88-35274
- KUNATH, RICHARD R.**
Optically controlled phased-array antenna technology for space communication systems [NASA-TM-100852] p 119 N88-18809
Optical RF distribution links for MMIC phased array antennas [NASA-TM-100841] p 128 N88-20555
Optically interconnected phased arrays [NASA-TM-100855] p 128 N88-21400
- KUNIEGA, R. J.**
Comparison of pressure distributions on model and full-scale NACA 64-621 airfoils with ailerons for wind turbine application [NASA-TM-100802] p 201 N88-21593
- KUNIK, WILLIAM G.**
Application of advanced computational codes in the design of an experiment for a supersonic throughflow fan rotor [ASME PAPER 87-GT-160] p 2 A88-11072
- KUNIN, B.**
A probabilistic model of brittle crack formation p 180 A88-18696
On self-similarity of crack layer p 181 A88-24054
- KURATH, PETER**
Cyclic fatigue damage characteristics observed for simple loadings extended to multiaxial life prediction [NASA-CR-182126] p 195 N88-25016

- The relationship between observed fatigue damage and life estimation models
[NASA-CR-182191] p 196 N88-27611
- KURKOV, ANATOLE P.**
Optical measurement of propeller blade deflections
[NASA-TP-2841] p 163 N88-28286
Optical measurement of unducted fan blade deflections
[NASA-TM-100966] p 163 N88-29142
- KURTH, W. S.**
Plasma wave turbulence around the shuttle - Results from the Spacelab-2 flight p 218 A88-47783
- KURTH, WILLIAM S.**
Gaseous environment of the Shuttle early in the Spacelab 2 mission p 47 A88-47972
- KURUZAR, DANIEL L.**
Preliminary investigation of inertia friction welding B2 aluminides p 82 A88-14567
- KUSANO, E.**
Deposition of vanadium oxide films by direct-current magnetron reactive sputtering p 221 A88-51286
- KUSSMAUL, MICHAEL**
Arc-textured metal surfaces for high thermal emittance space radiators
[NASA-TM-100894] p 94 N88-24754
- KUTLER, PAUL**
Retooling CFD for hypersonic aircraft p 1 A88-16749

L

- L'ESPERANCE, G.**
Thermal-mechanical cyclic stress-strain responses of cast B-1900 + Hf p 87 A88-35919
- LA PRADE, NICK**
System architecture of MMIC-based large aperture arrays for space applications p 45 A88-35274
- LABUS, THOMAS L.**
Space Station Electrical Power System
[IAF PAPER 87-234] p 53 A88-15958
- LACY, D. E.**
Advanced solar receiver conceptual design study p 51 A88-11800
- LACY, DOVIE E.**
Selection of high temperature thermal energy storage materials for advanced solar dynamic space power systems p 68 A88-11801
Impact of thermal energy storage properties on solar dynamic space power conversion system mass p 51 A88-11805
Advanced sensible heat solar receiver for space power
[NASA-TM-100847] p 59 N88-21249
- LAFLEN, J. H.**
Constitutive modeling for isotropic materials p 186 N88-11172
Elevated temperature crack growth p 186 N88-11174
Elevated temperature crack growth p 193 N88-22421
- LAGRAFF, JOHN E.**
An isentropic compression heated Ludwig tube transient wind tunnel
[AIAA PAPER 88-2019] p 40 A88-37926
- LAI, CHUN-LIANG**
Experimental study of thermocapillary flows in a thin liquid layer with heat fluxes imposed on the free surface p 144 A88-49087
Experimental study of thermocapillary flows in a thin liquid layer with heat fluxes imposed on the free surface
[NASA-TM-100252] p 148 N88-12763
- LAI, H. T.**
Two-dimensional viscous flow computations of hypersonic scramjet nozzle flowfields at design and off-design conditions
[AIAA PAPER 88-3280] p 23 A88-50785
Two-dimensional viscous flow computations of hypersonic scramjet nozzle flowfields at design and off-design conditions
[NASA-CR-182150] p 35 N88-25459
- LAKSHMINARAYANA, B.**
Laser Doppler velocimeter measurement of annulus wall boundary layer development in a compressor rotor
[ASME PAPER 87-GT-251] p 132 A88-11133
A space-marching method for the computation of viscous internal flows p 135 A88-20459
Comparison of computational methods for three-dimensional turbulent turbomachinery flows p 6 A88-42452
- LAM, P. T.**
Compensation of reflector antenna surface distortion using an array feed
[NASA-TM-100286] p 119 N88-18805
- LANGSTON, L. S.**
Three-dimensional flow past two cylinders mounted side by side on an endwall
[AIAA PAPER 88-3718] p 143 A88-48974
- LANT, CHRISTIAN T.**
Optical strain measurement system development p 159 A88-52557
- LAU, KEI MAY**
Temperature stability of Al(x)Ga(1-x)As (x = 0-1) thermal oxide masks for selective-area epitaxy p 221 A88-45858
- LAU, S. C.**
Effect of rib angle on local heat/mass transfer distribution in a two-pass rib-roughened channel
[ASME PAPER 87-GT-94] p 131 A88-11033
Local heat/mass transfer distributions around sharp 180 deg turns in two-pass smooth and rib-roughened channels
[ASME PAPER 86-GT-114] p 139 A88-28516
- LAUER, JAMES L.**
Investigation of PTFE transfer films by infrared emission spectroscopy and phase-locked ellipsometry p 99 A88-35568
Development and applications of optical interferometric micrometrology in the angstrom and subangstrom range
[NASA-TM-100289] p 162 N88-23196
- LAURENDEAU, NORMAND M.**
Feasibility of hydroxyl concentration measurements by laser-saturated fluorescence in high-pressure flames p 77 A88-17218
- LAWRENCE, C.**
Identification of structural interface characteristics using component mode synthesis p 181 A88-31561
Redundant manipulators for momentum compensation in a micro-gravity environment
[AIAA PAPER 88-4121] p 204 A88-50223
- LAWRENCE, CHARLES**
Identification of differences between finite element analysis and experimental vibration data p 183 A88-46666
Characterization of damped structural connections for multi-component systems
[NASA-TM-100801] p 189 N88-18974
Microgravity robotics technology program
[NASA-TM-100898] p 173 N88-23219
Parameter identification methods for improving structural dynamic models
[NASA-TM-100612] p 194 N88-23994
- LAXMANAN, V.**
Crystallization behavior of a melt-spun Fe-Ni based steel p 83 A88-19958
Dendritic growth in a supercooled alloy melt p 83 A88-19966
Gravitational macrosegregation in binary Pb-Sn alloy ingots p 111 A88-41211
On producing an alloy of uniform composition during rapid solidification processing p 89 A88-41654
Fraction eutectic measurements in slowly cooled Pb - 15 wt percent Sn alloys
[NASA-CR-180830] p 94 N88-25531
- LEAGUE, MARK**
Solar dynamic heat rejection technology. Task 2: Heat pipe radiator development
[NASA-CR-182141] p 152 N88-23182
- LEBO, WILLIAM**
Design, manufacture and spin test of high contact ratio helicopter transmission utilizing Self-Aligning Bearingless Planetary (SABP)
[NASA-CR-4155] p 174 N88-24975
- LEE, ALEX K. H.**
Aerodynamic interaction between propellers and wings
[AIAA PAPER 88-0665] p 5 A88-22495
- LEE, C.**
Analysis and design of a gas-lubricated, sectored, floating ring seal
[ASME PAPER 87-TRIB-55] p 166 A88-23310
- LEE, C. M.**
Performance and efficiency evaluation and heat release study of a direct-injection stratified-charge rotary engine
[SAE PAPER 870445] p 166 A88-23313
- LEE, CHI M.**
Regressed relations for forced convection heat transfer in a direct injection stratified charge rotary engine
[NASA-TM-100124] p 25 N88-13345
- LEE, CHOON S.**
A simple circular-polarized antenna: Circular waveguide horn coated with lossy magnetic material p 116 A88-36648
- LEE, FRED C.**
Computer modeling and simulation of a 20kHz ac distribution system for Space Station p 51 A88-11827
Implementation of optimal trajectory control of series resonant converter p 126 A88-38796
- LEE, K. F.**
Radiation characteristics of microstrip arrays with parasitic elements p 121 A88-10481
- Characteristics of a two-layer electromagnetically coupled rectangular patch antenna p 115 A88-14100
Crosspolarisation characteristics of rectangular patch antennas p 117 A88-47705
Gain enhancement of microstrip antennas with overlying parasitic directors p 117 A88-48653
- LEE, KIMYEONG**
Wilson-loop instants p 212 A88-10410
- LEE, MIN EIG**
Solving time-dependent two-dimensional eddy current problems
[NASA-TM-100875] p 211 N88-25239
- LEE, PETER W.**
Improved oil-off survivability of tapered roller bearings
[NASA-CR-180804] p 170 N88-11135
- LEE, R.**
Scale model acoustic testing of counterrotating fans
[AIAA PAPER 88-2057] p 22 A88-37947
- LEE, R. Q.**
Radiation characteristics of microstrip arrays with parasitic elements p 121 A88-10481
Characteristics of a two-layer electromagnetically coupled rectangular patch antenna p 115 A88-14100
Crosspolarisation characteristics of rectangular patch antennas p 117 A88-47705
Absolute gain measurement of microstrip antennas under mismatched conditions p 117 A88-47949
Gain enhancement of microstrip antennas with overlying parasitic directors p 117 A88-48653
Array trade-off study using multilayer parasitic subarrays
[NASA-TM-101321] p 121 N88-28222
- LEE, R. Q. H.**
Slotline fed microstrip antenna array modules p 126 A88-44170
- LEE, S. W.**
Compensation of reflector antenna surface distortion using an array feed
[NASA-TM-100286] p 119 N88-18805
Case study of active array feed compensation with sidelobe control for reflector surface distortion
[NASA-TM-100287] p 120 N88-23073
- LEE, SHUNG-WU**
How good is the impedance boundary condition? p 115 A88-24863
A simple circular-polarized antenna: Circular waveguide horn coated with lossy magnetic material p 116 A88-36648
Modal attenuation in multilayered coated waveguides p 126 A88-45755
Polarization determination utilizing two arbitrarily polarized antennas p 116 A88-47424
- LEE, Y. S.**
Cost-effective intersatellite link applications to the fixed satellite services
[AIAA PAPER 88-0770] p 45 A88-27544
- LEESE, G. E.**
Effects of surface chemistry on hot corrosion life p 91 N88-11180
- LEFEBVRE, A. H.**
Spray characteristics of a spill-return airblast atomizer
[ASME PAPER 88-GT-7] p 145 A88-54154
- LEI, J. F.**
Elevated temperature strain gages p 160 N88-11144
- LEI, JIH-FEN**
Electrical properties of materials for elevated temperature resistance strain gage application
[NASA-CR-182214] p 164 N88-30106
- LEIB, S. J.**
Roll-up of vorticity in adverse-pressure-gradient boundary layers p 135 A88-19194
Nonlinear roll-up of externally excited free shear layers p 141 A88-44445
- LEIS, B. N.**
Low cycle fatigue
[ASTM STP-942] p 86 A88-35901
A nonlinear history-dependent damage model for low cycle fatigue p 86 A88-35905
- LEKAN, JACK**
Communications payload concepts for geostationary facilities
[NASA-TM-100154] p 118 N88-13513
- LEMKEY, F. D.**
High-temperature oxidation/corrosion of iron-based superalloys p 81 A88-10029
- LEON, R. P.**
A V-grooved AlGaAs/GaAs passivated pn junction p 125 A88-34300
Diffusion length measurement in bulk and epitaxially grown III-V semiconductors using charge collection microscopy p 126 A88-34370
- LEONARD, B. P.**
Third-order multi-dimensional Euler/Navier-Stokes solver
[AIAA PAPER 88-3645] p 209 A88-48806

- SHARP simulation of discontinuities in highly convective steady flow
[NASA-TM-100240] p 210 N88-13931
- LEONARD, REGIS F.**
Progress in MMIC technology for satellite communications p 126 A88-37844
- LEONHARDT, TODD A.**
As-received microstructure of a SiC/Ti-15-3 composite [NASA-TM-100938] p 76 N88-28095
- LEPICOVSKY, J.**
Effects of nozzle-exit boundary-layer conditions on excitability of heated free jets
[AIAA PAPER 87-2723] p 135 A88-20182
Acoustically excited heated jets. 1: Internal excitation [NASA-CR-4129-PT-1] p 12 N88-23751
Acoustically excited heated jets. 2: In search of a better understanding [NASA-CR-4129-PT-2] p 12 N88-23752
Acoustically excited heated jets. 3: Mean flow data [NASA-CR-4129-PT-3] p 12 N88-23753
- LEPICOVSKY, JAN**
Centerline Mach number characteristics of highly heated free jets
[AIAA PAPER 88-3612] p 7 A88-48898
- LERCH, B. A.**
Cyclic hardening mechanisms in Nimonic 80A p 84 A88-24490
- LERCH, BRADLEY A.**
As-received microstructure of a SiC/Ti-15-3 composite [NASA-TM-100938] p 76 N88-28095
- LESCO, DANIEL J.**
Optical measurement systems p 218 N88-15796
- LESNY, GARY G.**
Performance of a small, graphite electrode, multistage depressed collector with a 500-W, continuous wave, 4.8- to 9.6-GHz traveling wave tube
[NASA-TP-2788] p 128 N88-15146
- LEVINE, STANLEY R.**
Ceramics for engines p 103 N88-16704
Ceramics for turbine engines p 106 N88-23873
- LEVIS, C. A.**
Engineering calculations for the Delta S method of solving the orbital allotment problem
[NASA-CR-182372] p 42 N88-14110
- LEVY, ALEXANDER**
Regenerative fuel cell study for satellites in GEO orbit p 52 A88-11904
- LEWICKI, D. G.**
Automated acoustic intensity measurements and the effect of gear tooth profile on noise p 168 A88-31623
Computerized life and reliability modelling for turboprop transmissions
[AIAA PAPER 88-2979] p 100 A88-48031
Computerized life and reliability modelling for turboprop transmissions
[NASA-TM-100918] p 173 N88-23220
- LEWICKI, DAVID G.**
Identification and proposed control of helicopter transmission noise at the source p 38 N88-16647
Helicopter transmission research at NASA Lewis Research Center
[NASA-TM-100962] p 175 N88-30128
- LI, X.**
Direct-current magnetron fabrication of indium tin oxide/InP solar cells p 200 A88-51289
- LIAO, PETER**
Acousto-ultrasonic input-output characterization of unidirectional fiber composite plate by SV waves
[NASA-CR-4152] p 178 N88-23224
Acousto-ultrasonic input-output characterization of unidirectional fiber composite plate by P waves
[NASA-CR-4162] p 180 N88-25923
- LICHTENFELTS, FRED**
Ultrasonic techniques for aircraft ice accretion measurement
[AIAA PAPER 88-4656] p 18 A88-51910
- LIEBERT, CURT H.**
Measurement of local high-level, transient surface heat flux
[NASA-TP-2840] p 164 N88-30099
- LILLEY, DAVID G.**
Lateral jet injection into swirling combustor flowfields
[AIAA PAPER 88-3183] p 141 A88-44783
- LILLINGTON, D. R.**
Development of 8 cm x 8 cm silicon gridded back solar cell for space station p 200 A88-34312
- LIM, HONG S.**
A prediction model of the depth-of-discharge effect on the cycle life of a storage cell p 197 A88-11896
- LIM, TEIK CHIN**
A review of gear housing dynamics and acoustics literature
[NASA-CR-183110] p 175 N88-26675
- LIN, CHIN-SHUN**
Similar solutions for viscous hypersonic flow over a slender three-fourths-power body of revolution
[NASA-TM-100205] p 148 N88-12752
- LIN, EDWARD HSIANG-HSI**
On dynamic loads in parallel shaft transmissions. 1: Modelling and analysis
[NASA-TM-100180] p 171 N88-12797
On dynamic loads in parallel shaft transmissions. 2: Parameter study
[NASA-TM-100181] p 171 N88-12798
- LIN, R. R.**
Active control of transient rotordynamic vibration by optimal control methods
[ASME PAPER 88-GT-73] p 208 A88-54202
- LINDBERG, L. J.**
Thermal cyclic durability testing of ceramic materials for turbine engines p 179 N88-23886
- LINDBERG, LAURA J.**
Elevated temperature durability of ceramic materials
[AIAA PAPER 88-3055] p 100 A88-44743
- LINDHOLM, U. S.**
Phenomenological modeling of hardening and thermal recovery in metals p 84 A88-24037
Unified constitutive models for high-temperature structural applications p 190 N88-21523
Constitutive modeling for isotropic materials
[NASA-CR-182132] p 37 N88-29811
- LINDHOLM, ULRIC S.**
Constitutive modeling for isotropic materials p 185 N88-11171
- LINDSTROM, R.**
Service offerings and interfaces for the ACTS network of earth stations
[AIAA PAPER 88-0800] p 116 A88-27551
- LING, HAO**
Polarization determination utilizing two arbitrarily polarized antennas p 116 A88-47424
- LING, JERRI S.**
A cyclic ground test of an ion auxiliary propulsion system: Description and operational considerations
[NASA-TM-100870] p 62 N88-23829
- LIU, MENG-SING**
Choice of implicit and explicit operators for the upwind differencing method
[AIAA PAPER 88-0624] p 209 A88-22472
Splitting of inviscid fluxes for real gases
[AIAA PAPER 88-3526] p 142 A88-48782
A comparison of ENO and TVD schemes
[AIAA PAPER 88-3707] p 210 A88-48831
Solutions of one-dimensional steady nozzle flow revisited p 144 A88-50344
A computational analysis of under-expanded jets in the hypersonic regime
[AIAA PAPER 88-4361] p 8 A88-50604
Splitting of inviscid fluxes for real gases
[NASA-TM-100856] p 211 N88-21717
Choice of implicit and explicit operators for the upwind differencing method
[NASA-TM-100857] p 211 N88-21718
A computational analysis of under-expanded jets in the hypersonic regime
[NASA-TM-101319] p 13 N88-27174
- LIPO, THOMAS A.**
Field oriented control of an induction machine in a high frequency link power system p 127 A88-54711
- LITT, JONATHAN S.**
A microprocessor-based real-time simulator of a turboprop engine
[NASA-TM-100889] p 32 N88-21163
- LITTLE, B. H., JR.**
Propfan test assessment testbed aircraft stability and control/performance 1/9-scale wind tunnel tests
[NASA-CR-182121] p 17 N88-26360
- LITVIN, F. L.**
Method for generation of spiral bevel gears with conjugate gear tooth surfaces
[ASME PAPER 86-DET-3] p 165 A88-10973
Determination of settings of a tilted head-cutter for generation of hypoid and spiral bevel gears
[NASA-CR-182138] p 174 N88-24976
- LITVIN, FAYDOR L.**
Spur gears: Optimal geometry, methods for generation and Tooth Contact Analysis (TCA) program
[NASA-CR-4135] p 173 N88-23216
- LIU, A.**
Thermal barrier coating life-prediction model development
[NASA-CR-179507] p 107 N88-28142
- LIU, DAVID C.**
Plasma deposition of amorphous hydrogenated carbon films on III-V semiconductors p 220 A88-32862
- LIU, H. W.**
Grain boundary oxidation and an analysis of the effects of oxidation on fatigue crack nucleation life p 87 A88-35938
- Grain boundary oxidation and low-cycle fatigue at elevated temperatures p 193 N88-22420
The analysis of fatigue crack growth mechanism and oxidation and fatigue life at elevated temperatures
[NASA-CR-182129] p 94 N88-22987
- LIU, HAO-WEN**
Resolved shear stress intensity coefficient and fatigue crack growth in large crystals
[NASA-CR-182137] p 195 N88-24997
- LIU, J. T. C.**
Control of free shear layers
[AIAA PAPER 87-2689] p 134 A88-16545
- LIU, JONG-SHANG**
Navier-Stokes cascade analysis with a stiff k-epsilon turbulence solver
[AIAA PAPER 88-0594] p 5 A88-22444
Navier-Stokes cascade analysis with a stiff Kappa-Epsilon turbulence solver
[NASA-TM-100218] p 9 N88-10778
- LIU, WING KAM**
Finite element methods in probabilistic mechanics p 212 A88-29060
- LO, Y. T.**
Slotline fed microstrip antenna array modules p 126 A88-44170
- LOCKWOOD, A.**
Effect of the microstructure on the thermoelectric properties of polycrystalline lanthanum chalcogenides p 221 A88-40797
- LOGRASSO, T. A.**
Dendritic solidification under microgravity conditions
[AIAA PAPER 88-0248] p 110 A88-22186
Isothermal dendritic growth - A low gravity experiment p 110 A88-28556
Solidification under microgravity conditions - Dendritic growth
[AAS PAPER 86-380] p 110 A88-35130
Isothermal dendritic growth - A proposed microgravity experiment p 112 A88-49095
- LONG, JAMES A.**
High-efficiency helical traveling-wave tube with dynamic velocity taper and advanced multistage depressed collector p 124 A88-32836
- LONG, MARTIN**
Synthesis, electrical and thermal conductivities, and potential applications of graphite fluoride fibers p 97 A88-26963
- LORENZO, CARL F.**
Determination of compressor in-stall characteristics from engine surge transients p 21 A88-35505
Directions in propulsion control p 28 N88-15799
A reusable rocket engine intelligent control
[NASA-TM-100963] p 65 N88-26401
- LOUVIERE, ALLEN J.**
Water-propellant resistojets for man-tended platforms
[IAF PAPER 87-259] p 54 A88-15975
- LOW, CHARLES A., JR.**
Successful completion of a cyclic ground test of a mercury ion auxiliary propulsion system
[NASA-TM-101351] p 67 N88-29873
- LUNDY, M.**
Determination of settings of a tilted head-cutter for generation of hypoid and spiral bevel gears
[NASA-CR-182138] p 174 N88-24976
- LYONS, VALERIE J.**
Temperature and velocity profiles in sooting free convection diffusion flames p 78 A88-43018
Optical measurements of soot and temperature profiles in premixed propane-oxygen flames
[NASA-TM-101343] p 115 N88-29997
Optical measurements of soot in premixed flames
[NASA-TM-101305] p 156 N88-30090
- LYTLE, J. K.**
Three-dimensional viscous flow computations of a circular jet in subsonic and supersonic cross flow
[AIAA PAPER 88-3703] p 143 A88-48916
Three-dimensional viscous flow computations of a circular jet in subsonic and supersonic cross flow
[NASA-CR-182153] p 155 N88-26616

M

- MACBETH, J. W.**
Advanced Gas Turbine (AGT) Technology Development Project, ceramic component developments
[NASA-CR-180871] p 224 N88-20229
- MACIAG, C.**
Differential scanning calorimetric survey of brominated PAN, pitch-based and vapor-grown fibers p 98 A88-32854
The effect of bromination of carbon fibers on the coefficient of thermal expansion of graphite fiber-epoxy composites
[NASA-TM-100236] p 72 N88-10899

MACIAG, CAROLYN

MACIAG, CAROLYN

- Specific heat of pristine and brominated graphite fibers, composites and HOPG p 98 A88-32853
Improving the interlaminar shear strength of carbon fiber-epoxy composites through carbon fiber bromination [NASA-TM-100248] p 72 N88-15018

MACIEJEWSKI, PAUL K.

- Heat transfer with very high free stream turbulence p 148 N88-11161

MACINNES, J.

- Time-accurate simulations of a shear layer forced at a single frequency [AIAA PAPER 88-0061] p 138 A88-27716

MACINNES, J. M.

- Time-accurate simulations of a shear layer forced at a single frequency [NASA-TM-100836] p 152 N88-19740

MACKAY, R. A.

- Lattice parameter variations during aging in nickel-base superalloys p 90 A88-51318

MACKAY, REBECCA A.

- Microstructure-property relationships in directionally solidified single-crystal nickel-base superalloys p 88 A88-40329

MACNEIL, PETER N.

- Design, development, and test of Shuttle/Centaur G-prime cryogenic tankage thermal protection systems p 47 A88-53182

MADSZAR, GEORGE

- An expert system approach to turbopump health monitoring [AIAA PAPER 88-3117] p 42 A88-48038

MAEDA, CHIKAYOSHI

- Development of a torsion balance for adhesion measurements [NASA-TM-100799] p 104 N88-20454

MAGARI, PATRICK J.

- An isentropic compression heated Ludwig tube transient wind tunnel [AIAA PAPER 88-2019] p 40 A88-37926

MAGGENTI, MARK

- VSAT networks - An overview p 115 A88-14091

MAGGENTI, MARK A.

- Spread-spectrum multiple access using wideband noncoherent MFSK p 115 A88-26672

MAGLIOZZI, B.

- Noise characteristics of model counter-rotating Prop-Fans [AIAA PAPER 87-2656] p 213 A88-16526

MAHAJAN, APARAJIT J.

- Reduced order models for nonlinear aerodynamics p 11 N88-23248

MAINS, R. K.

- Microwave and millimeter-wave power generation in silicon carbide avalanche devices p 126 A88-47599

MAITLAND, DUNCAN J., IV

- Fiber optic sensors with internal referencing [NASA-TM-100893] p 162 N88-26644
Fiber optic sensing systems using high frequency resonant sensing heads with intensity sensors [NASA-TM-101318] p 163 N88-28293

MAJUMDAR, B. C.

- Stability of a rigid rotor supported on flexible oil journal bearings [ASME PAPER 87-TRIB-48] p 166 A88-24034

MAKEL, DARBY B.

- Arjet thruster research and technology [NASA-CR-180865] p 59 N88-17732

MALACHOWSKI, MICHAEL J.

- Accurate positioning of long, flexible ARM's (Articulated Robotic Manipulator) p 174 N88-23243

MALIK, S. N.

- Elevated temperature crack growth p 186 N88-11174
Elevated temperature crack growth p 193 N88-22421

MANDELL, M. J.

- Hollow cathodes as electron emitting plasma contactors - Theory and computer modeling p 218 A88-47973
Electron collection by multiple objects within a single sheath p 219 A88-54999

MANDERSCHIED, JANE M.

- Monolithic ceramic analysis using the SCARE program p 105 N88-22409

MANGALAM, S. M.

- Transition and separation control on a low-Reynolds number airfoil p 2 A88-11186
Effect of acoustic excitation on the flow over a low-Re airfoil p 3 A88-14459

MANGELS, J. A.

- Improved silicon carbide for advanced heat engines p 106 N88-23879

MANGUM, B. W.

- Preparation of multistage zone-refined materials for thermochemical standards p 111 A88-43172

MANI, A.

- Finite element methods in probabilistic mechanics p 212 A88-29060

MANKBADI, REDA R.

- Saturation and the limit of jet mixing enhancement by single frequency plane wave excitation - Experiment and theory [AIAA PAPER 88-3613] p 8 A88-48899
Saturation and the limit of jet mixing enhancement by single frequency plane wave excitation: Experiment and theory [NASA-TM-100882] p 12 N88-23732

MANNING, ROBERT M.

- A statistical rain attenuation prediction model with application to the advanced communication technology satellite project. Part 2: Theoretical development of a dynamic model and application to rain fade durations and tolerable control delays for fade countermeasures [NASA-TM-100242] p 118 N88-11945
Space communication link propagation data for selected cities within the multiple beam and steerable antenna coverage areas of the advanced communications technology satellite [NASA-TM-100861] p 120 N88-23070
A statistical rain attenuation prediction model with application to the advanced communication technology satellite project. 1: Theoretical development and application to yearly predictions for selected cities in the United States [NASA-CR-179498] p 121 N88-29077

MANTENIEKS, MARIS A.

- Performance and lifetime assessment of MPD arc thruster technology [NASA-TM-101293] p 66 N88-29860

MANTRAVADI, N.

- Compressive creep behavior of alloys based on B2 FeAl p 82 A88-10043

MANZELLA, D. H.

- An experimental investigation of the effect of test-cell pressure on the performance of resistojets [AIAA PAPER 88-3286] p 40 A88-44820

MANZO, M. A.

- Alkaline fuel cell performance investigation [NASA-TM-100937] p 81 N88-27267

MANZO, MICHELLE A.

- Component variations and their effects on bipolar nickel-hydrogen cell performance p 197 A88-11914
Test results of a 60 volt bipolar nickel-hydrogen battery p 198 A88-11916
Small scale bipolar nickel-hydrogen testing [NASA-TM-100936] p 202 N88-25059
The effect of compression on individual pressure vessel nickel/hydrogen components [NASA-TM-101312] p 81 N88-28109

MAPLES, A. L.

- A thermodynamic prediction for microporosity formation in aluminum-rich Al-Cu alloys p 82 A88-18886

MARAM, J.

- Reusable rocket engine optical condition monitoring p 158 A88-29817
Progress toward an advanced condition monitoring system for reusable rocket engines p 54 A88-32868

MARCHAND, N.

- Thermal-mechanical cyclic stress-strain responses of cast B-1900 + Hf p 87 A88-35919

MAREK, C. JOHN

- Stability relationship for water droplet crystallization with the NASA Lewis icing spray nozzle [AIAA PAPER 88-0289] p 137 A88-22209
Stability relationship for water droplet crystallization with the NASA Lewis icing spray [NASA-TM-100220] p 24 N88-10790

MARGLE, JANICE M.

- Temperature and velocity profiles in sooting free convection diffusion flames p 78 A88-43018
Spacecraft Fire Safety [NASA-CP-2476] p 45 N88-12520

MARK, HERMAN

- The effect of the near earth micrometeoroid environment on a highly reflective mirror surface [NASA-TM-101307] p 44 N88-29833

MARK, W. D.

- The generalized transmission error of spiral bevel gears p 168 A88-49409
Use of the generalized transmission error in the equations of motion of gear systems p 168 A88-49410

MARRA, JOHN E.

- Direct mass spectrometric identification of silicon oxychloride compounds p 78 A88-44425

MARRAFFA, LIONEL

- A physically consistent model for artificial dissipation in transonic potential flow computations [NASA-TM-100846] p 211 N88-22652

PERSONAL AUTHOR INDEX

MARSHALL, N. A.

- Design description report for a photovoltaic power system for a remote satellite earth terminal [NASA-CR-179586] p 200 N88-12875

MARSHIK, B.

- Electron-spin-resonance studies of vapor-grown carbon fibers p 96 A88-17368

MARTIN, DONALD F.

- Lewis Research Center space station electric power system test facilities [NASA-TM-100924] p 43 N88-28942

MARTIN, R. E.

- Alkaline fuel cell performance investigation [NASA-TM-100937] p 81 N88-27267
Regenerative fuel cell energy storage system for a low earth orbit space station [NASA-CR-174802] p 204 N88-30184

MARTIN, RONALD E.

- Stress-life interrelationships associated with alkaline fuel cells p 197 A88-11903

MASCARENHAS, A. J.

- Raman scattering studies of chemical-vapor-deposited cubic SiC films of (100)Si p 127 A88-53397

MASER, J. G.

- Parametric studies of advanced turboprops [AIAA PAPER 88-2266] p 20 A88-32223

MASON, C. A.

- Propan test assessment testbed aircraft stability and control/performance 1/9-scale wind tunnel tests [NASA-CR-182121] p 17 N88-26360

MASUDA, S. R.

- Improved perfluoroalkylether fluid development [NASA-CR-180872] p 80 N88-15851

MASUO, RYUICHI

- Development of a torsion balance for adhesion measurements [NASA-TM-100799] p 104 N88-20454

MATAGA, THOMAS G.

- Temperature and velocity profiles in sooting free convection diffusion flames p 78 A88-43018

MATUS, L. G.

- Improved beta-SiC heteroepitaxial films using off-axis Si substrates p 219 A88-10431

MCALLISTER, J. G.

- Space station onboard propulsion system: Technology study [NASA-CR-179233] p 59 N88-15006

MCARDLE, JACK G.

- Test stand performance of a convertible engine for advanced V/STOL and rotorcraft propulsion [SAE PAPER 872355] p 21 A88-37217
Test stand performance of a convertible engine for advanced V/STOL and rotorcraft propulsion [NASA-TM-100211] p 25 N88-11679
The convertible engine: A dual-mode propulsion system p 31 N88-16639

MCBRIDE, BONNIE J.

- Numerical simulation of hypersonic inlet flows with equilibrium or finite rate chemistry [AIAA PAPER 88-0273] p 5 A88-27717
Finite area combustor theoretical rocket performance [NASA-TM-100785] p 60 N88-21252

MCCARTHY, K. K.

- Space station onboard propulsion system: Technology study [NASA-CR-179233] p 59 N88-15006

MCCAUGHAN, F. E.

- Application of bifurcation theory to axial flow compressor instability [ASME PAPER 88-GT-231] p 169 A88-54313
Numerical results for axial flow compressor instability [ASME PAPER 88-GT-252] p 169 A88-54328

MCCLURE, DONALD J.

- Design and demonstration of a system for the deposition of atomic-oxygen durable coatings for reflective solar dynamic power system concentrators [NASA-CR-4158] p 64 N88-25474

MCCONNAUGHEY, H. V.

- Impact of ETO propellants on the aerothermodynamic analyses of propulsion components [NASA-TM-101303] p 156 N88-30094

MCDONALD, GLEN

- Interface roughness effect on stresses in ceramic coatings p 95 A88-12587
Some adhesion/cohesion characteristics of plasma-sprayed ZrO₂-Y₂O₃ under tensile loading p 95 A88-12589

MCDONALD, GLEN E.

- Thermomechanical behavior of plasma-sprayed ZrO₂-Y₂O₃ coatings influenced by plasticity, creep, and oxidation p 95 A88-12588

MCDONELL, V. G.

- K-epsilon turbulence model assessment with reduced numerical diffusion for coaxial jets [AIAA PAPER 88-0342] p 137 A88-22251

- MC GAW, MICHAEL A.**
Bithermal fatigue - A link between isothermal and thermomechanical fatigue p 87 A88-35918
Lewis' enhanced laboratory for research into the fatigue and constitutive behavior of high temperature materials p 186 N88-11177
Life prediction technologies for aeronautical propulsion systems p 27 N88-15788
Cumulative fatigue damage models p 193 N88-22422
- MCKINZIE, D. J.**
Corona anemometry for qualitative measurement of reversing surface flow with application to separation control by external excitation p 133 A88-14143
A natural low frequency oscillation in the wake of an airfoil near stalling conditions [AIAA PAPER 88-0131] p 4 A88-22093
A natural low frequency oscillation in the wake of an airfoil near stalling conditions [NASA-TM-100213] p 9 N88-10779
- MCKNIGHT, R. L.**
Component specific modeling p 206 N88-11166
- MCKNIGHT, ROBERT C.**
In-flight measurement of airfoil icing using an array of ultrasonic transducers p 15 A88-50910
In-flight measurement of ice growth on an airfoil using an array of ultrasonic transducers [AIAA-87-0178] p 16 N88-23717
- MC MURTRY, PATRICK A.**
Direct simulations of chemically reacting turbulent mixing layers, part 2 [NASA-CR-180853] p 154 N88-25857
- MC NEIL, C. L.**
Multiple-Purpose Subsonic Naval Aircraft (MPSNA): Multiple Application Propan Study (MAPS) [NASA-CR-175104] p 18 N88-28917
- MCQUILLEN, J. B.**
Gas liquid flow at microgravity conditions - Flow patterns and their transitions p 141 A88-42839
- MCQUILLEN, JOHN B.**
Mass transport phenomena between bubbles and dissolved gases in liquids under reduced gravity conditions [AIAA PAPER 88-0450] p 138 A88-27719
Mass transport phenomena between bubbles and dissolved gases in liquids under reduced gravity conditions [NASA-TM-100273] p 80 N88-18672
- MCVEY, J. B.**
Fuel-injector/air-swirl characterization p 146 N88-11150
Fuel-injector/air-swirl characterization [NASA-CR-180864] p 27 N88-14985
- MCVEY, JOHN B.**
Application of advanced diagnostics to airblast injector flows [ASME PAPER 88-GT-12] p 159 A88-54159
- MEADOR, MARY ANN**
Novel ladder polymers for use as high temperature stable resins or coatings [NASA-CASE-LEW-14203-1] p 108 N88-29984
- MEADOR, MICHAEL A.**
High temperature polymer matrix composites p 73 N88-16700
- MEGARGLE, ROBERT G.**
Laboratory Information Management System (LIMS): A case study [NASA-TM-100835] p 208 N88-21697
- MEHALIC, CHARLES M.**
Determination of compressor in-stall characteristics from engine surge transients p 21 A88-35505
Effect of spatial inlet temperature and pressure distortion on turbofan engine stability [AIAA PAPER 88-3016] p 22 A88-44727
Effect of spatial inlet temperature and pressure distortion on turbofan engine stability [NASA-TM-100850] p 32 N88-21162
- MEHDI, I.**
Microwave and millimeter-wave power generation in silicon carbide avalanche devices p 126 A88-47599
- MEHMED, O.**
Experimental classical flutter results of a composite advanced turboprop model p 21 A88-35528
- MEHMED, ORAL**
Experimental investigation of propan aeroelastic response in off-axis flow with mistuning [NASA-TM-101320] p 196 N88-28344
Aeroelastic response of metallic and composite propan models in yawed flow [NASA-TM-100964] p 37 N88-29807
- MEITNER, PETER L.**
Small gas turbine engine technology p 30 N88-16638
- MELIS, MATTHEW E.**
Thermostructural analysis with experimental verification in a high heat flux facility of a simulated cowl lip [AIAA PAPER 88-2222] p 39 A88-32188
Thermostructural analysis of simulated cowl lips p 192 N88-22403
- MENG, P. R.**
A life test of a 22-Newton (5-lbf) hydrazine rocket [NASA-TM-100232] p 57 N88-11750
- MENG, PHILLIP R.**
Space Station propulsion system technology p 54 A88-21255
- MENG, CHAI-HSIANG**
Evaluation of a turbine blade damper using an integral approach [AIAA PAPER 88-2400] p 20 A88-32332
- MERCER, CAROLYN R.**
Active phase compensation system for fiber optic holography [NASA-TM-101295] p 162 N88-26641
- MERKEL, KENNETH G.**
Variable angle spectroscopic ellipsometry - Application to GaAs-AlGaAs multilayer homogeneity characterization p 220 A88-40139
- MERKLEY, DENNIS R.**
Program for the feasibility of developing a high pressure acoustic levitator [NASA-CR-182154] p 113 N88-26498
- MERRIGAN, M.**
Integrated heat pipe-thermal storage system performance evaluation p 132 A88-11803
Development of an integrated heat pipe-thermal storage system for a solar receiver [AIAA PAPER 88-2683] p 141 A88-43746
- MERRIGAN, M. A.**
Development of an integrated heat pipe-thermal storage system for a solar receiver [NASA-TM-101099] p 202 N88-22458
- MERRILL, WALTER C.**
A microprocessor-based real-time simulator of a turbofan engine [NASA-TM-100889] p 32 N88-21163
A reusable rocket engine intelligent control [NASA-TM-100963] p 65 N88-26401
- MERTE, HERMAN, JR.**
Nucleate pool boiling: High gravity to reduced gravity; liquid metals to cryogenics p 113 N88-24464
- METCALFE, RALPH W.**
Direct simulations of chemically reacting turbulent mixing layers, part 2 [NASA-CR-180853] p 154 N88-25857
- METZGER, D. E.**
Heat transfer in the tip region of a rotor blade simulator p 147 N88-11159
- MEYER, D.**
Electron-spin-resonance studies of vapor-grown carbon fibers p 96 A88-17368
- MEYER, DUANE**
Electrical resistivity (4K to 2100K) of annealed vapor growth carbon fibers p 96 A88-17214
- MEYER, M. B.**
Ground based materials science experiments p 43 A88-52364
- MEYER, MARYJO B.**
Preparation for microgravity - The role of the Microgravity Material Science Laboratory [AIAA PAPER 88-3510] p 111 A88-42908
Preparation for microgravity: The role of the microgravity materials science laboratory [NASA-TM-100906] p 113 N88-24811
- MEYER, T. G.**
Fatigue life prediction modeling for turbine hot section materials p 164 A88-54144
Fatigue life prediction modeling for turbine hot section materials [NASA-TM-100291] p 187 N88-14453
Unified constitutive model for single crystal deformation behavior with applications p 191 N88-22388
- MICHAELS, K. B.**
Regenerative fuel cell energy storage system for a low earth orbit space station [NASA-CR-174802] p 204 N88-30184
- MICHAL, G. M.**
Crystallization behavior of a melt-spun Fe-Ni based steel p 83 A88-19958
- MICKLE, MARLIN H.**
Computer simulation of a single pilot flying a modern high-performance helicopter [NASA-TM-100182] p 39 N88-26376
Computer simulation of multiple pilots flying a modern high performance helicopter [NASA-TM-100183] p 39 N88-26377
- MIHALOEWS, JAMES R.**
Flight propulsion control integration for V/STOL aircraft [SAE PAPER 872330] p 21 A88-37199
- Flight propulsion control integration for V/STOL aircraft [NASA-TM-100226] p 38 N88-11680
Rotorcraft flight-propulsion control integration p 38 N88-16643
Rotorcraft flight-propulsion control integration: An eclectic design concept [NASA-TP-2815] p 38 N88-19475
Computer simulation of a single pilot flying a modern high-performance helicopter [NASA-TM-100182] p 39 N88-26376
Computer simulation of multiple pilots flying a modern high performance helicopter [NASA-TM-100183] p 39 N88-26377
- MILDICE, J.**
The ac power system testbed [NASA-CR-175068] p 127 N88-11948
- MILDICE, J. W.**
Control considerations for high frequency, resonant, power processing equipment used in large systems p 51 A88-11829
- MILES, JEFFREY H.**
Initial conditional effect on pressure waves in an axisymmetric jet [AIAA PAPER 88-3702] p 143 A88-48915
Initial condition effect on pressure waves in an axisymmetric jet [NASA-TM-100915] p 153 N88-23184
- MILLER, BRENT A.**
Internal fluid mechanics research on supercomputers for aerospace propulsion systems [NASA-TM-100289] p 149 N88-15188
- MILLER, CHRISTOPHER J.**
Euler analysis of a swirl recovery vane design for use with an advanced single-rotation propan [NASA-TM-101357] p 14 N88-29771
- MILLER, D.**
Toluene stability Space Station Rankine power system p 50 A88-11794
- MILLER, EDWARD F.**
An allotment planning concept and related computer software for planning the fixed satellite service at the 1988 space WARC p 116 A88-36482
An allotment planning concept and related computer software for planning the fixed satellite service at the 1988 space WARC [NASA-TM-100244] p 117 N88-11944
- MILLER, ERIC L.**
Description of an oscillating flow pressure drop test rig [NASA-TM-100905] p 61 N88-22933
- MILLER, JOHN**
Thermal conductivity of pristine and brominated highly graphitized pitch based carbon fibers p 97 A88-20257
- MILLER, R. A.**
Progress toward life modeling of thermal barrier coatings for aircraft gas turbine engines [ASME PAPER 87-ICE-18] p 96 A88-15120
Life modeling of thermal barrier coatings for aircraft gas turbine engines p 90 A88-54145
Thermal expansion mismatch and oxidation in thermal barrier coatings p 170 N88-11182
- MILLER, ROBERT A.**
Life modeling of thermal barrier coatings for aircraft gas turbine engines [NASA-TM-100283] p 92 N88-15060
- MILLER, T. L.**
Analytical determination of propeller performance degradation due to ice accretion p 19 A88-19669
- MILLER, THOMAS L.**
NASA's rotorcraft icing research program p 15 N88-16641
- MILLIGAN, WALTER W.**
Deformation, fatigue and fracture behavior of two cast anisotropic superalloys p 187 N88-13732
- MILLWATER, H.**
NESSUS/EXPERT - An expert system for probabilistic structural analysis methods [AIAA PAPER 88-2374] p 206 A88-32311
- MILNER, EDWARD J.**
Time-partitioning simulation models for calculation of parallel computers p 206 A88-46961
- MINER, R. V.**
Fatigue crack propagation of nickel-base superalloys at 650 deg C p 86 A88-35908
Creep-fatigue behavior of NiCoCrAlY coated PWA 1480 superalloy single crystals p 86 A88-35911
Bithermal low-cycle fatigue behavior of a NiCoCrAlY-coated single crystal superalloy p 90 A88-51736
Creep-fatigue behavior of NiCoCrAlY coated PWA 1480 p 86 A88-11176
Isothermal and bithermal thermomechanical fatigue behavior of a NiCoCrAlY-coated single crystal superalloy [NASA-TM-100907] p 94 N88-24766

MIRDAMADI, M.

Effect of temperature, microstructure, and stress state on the low cycle fatigue behavior of Waspaloy
p 87 A88-35922

MIRFAKHRAIE, KOOROSH

Optimal cooperative time-fixed impulsive rendezvous
[AIAA PAPER 88-4279] p 42 A88-50406

MIRTICH, MICHAEL J.

Ion beam deposition of amorphous carbon films with diamond like properties p 97 A88-20300

Arc-textured metal surfaces for high thermal emittance space radiators
[NASA-TM-100894] p 94 A88-24754

The effect of the near earth micrometeoroid environment on a highly reflective mirror surface
[NASA-TM-101307] p 44 A88-29833

MISEGADES, KENT P.

Utilization of parallel processing in solving the inviscid form of the average-passage equation system for multistage turbomachinery
[NASA-TM-89845] p 32 A88-21160

MISRA, A. K.

Role of molybdenum in the Na₂SO₄ induced corrosion of superalloys at high temperature p 81 A88-10030

Sodium sulfate-induced corrosion of pure nickel and superalloy Udimet 700 in a high velocity burner rig at 900 C p 83 A88-20266

Identification of salt-alloy combinations for thermal energy storage applications in advanced solar dynamic power systems p 199 A88-24072

MISRA, AJAY K.

Fluoride salts and container materials for thermal energy storage applications in the temperature range 973 - 1400 K p 196 A88-11804

Fluoride salts as phase change materials for thermal energy storage in the temperature range 1000-1400 K p 199 A88-33734

MIYOSHI, KAZUHISA

Mechanical strength and tribological behavior of ion-beam-deposited boron nitride films on non-metallic substrates p 98 A88-32866

Wear of iron and nickel in corrosive liquid environments p 88 A88-40790

Boron nitride - Composition, optical properties, and mechanical behavior p 99 A88-40794

Wear of iron and nickel in corrosive liquid environments
[NASA-TM-100246] p 91 A88-11817

Adhesion, friction and micromechanical properties of ceramics
[NASA-TM-100782] p 104 A88-17801

Development of a torsion balance for adhesion measurements
[NASA-TM-100799] p 104 A88-20454

MOAT, RICHARD L.

Hardware realization of a baseband processor for a SS-FDMA/TDMA/DAMA system
[AIAA PAPER 88-0830] p 124 A88-27575

MOEHRING, WILLI

A model of the wall boundary layer for ducted propellers
[AIAA PAPER 87-2742] p 214 A88-16578

MOET, A.

Crack diffusion coefficient - A candidate fracture toughness parameter for short fiber composites p 70 A88-36945

MOET, ABDELSAMIE

Curvilinear crack layer propagation p 96 A88-14568

MOFFAT, ROBERT J.

Heat transfer with very high free stream turbulence p 148 A88-11161

MOLDOVER, MICHAEL R.

Quantitative characterization of the viscosity of a microemulsion p 77 A88-11167

Critical exponent for the viscosity of four binary liquids p 222 A88-53050

MONGIA, H. C.

K-epsilon turbulence model assessment with reduced numerical diffusion for coaxial jets
[AIAA PAPER 88-0342] p 137 A88-22251

Assessment, development, and application of combustor aerothermal models p 24 A88-54140

Aerothermal modeling program, phase 2 p 146 A88-11149

Assessment, development and application of combustor aerothermal models
[NASA-TM-100290] p 32 A88-19469

MONTAGUE, GERALD T.

Test facilities of the structural dynamics branch of NASA Lewis Research Center
[NASA-TM-100800] p 190 A88-21534

MONTAGUE, G.

Transient rotor dynamic rub phenomena - Theory and test p 167 A88-31539

MONTE, PAUL A.

Bandwidth and power efficient satellite TDMA demodulator and decoder
[AIAA PAPER 88-0812] p 123 A88-27559

MOON, H. K.

Heat transfer in the tip region of a rotor blade simulator p 147 A88-11159

MOORE, ALLAN S.

Techniques utilized in the simulated altitude testing of a 2D-CD vectoring and reversing nozzle
[NASA-TM-100872] p 40 A88-25464

MOORE, J.

Slotline fed microstrip antenna array modules p 126 A88-44170

MOORE, JOAN G.

Explicit finite-volume time-marching calculations of total temperature distributions in turbulent flow p 139 A88-30517

An explicit finite-volume time-marching procedure for turbulent flow calculations p 139 A88-30518

MOORE, JOHN

Explicit finite-volume time-marching calculations of total temperature distributions in turbulent flow p 139 A88-30517

An explicit finite-volume time-marching procedure for turbulent flow calculations p 139 A88-30518

MOORE, ROYCE

Experimental evaluation of corner vanes - Summary
[SAE PAPER 871784] p 39 A88-30778

MOORE, ROYCE D.

Experimental evaluation of turning vane designs for high-speed and coupled fan-drive corners of 0.1-scale model of NASA Lewis Research Center's proposed altitude wind tunnel
[NASA-TP-2681] p 40 A88-17686

MOORE, T. J.

Preliminary study of niobium alloy contamination by transport through helium p 94 A88-24279

MOORE, THOMAS J.

Preliminary investigation of inertia friction welding B2 aluminides p 82 A88-14567

Fatigue failure of regenerator screens in a high frequency Stirling engine p 179 A88-24491

MOORHEAD, PAUL E.

High-temperature combustor liner tests in structural component response test facility p 33 A88-22383

MORALES, WILFREDO

Surface catalytic degradation study of two linear perfluoropolyalkylethers at 345 C
[NASA-TP-2774] p 68 A88-12543

MOREL, DONALD E.

Development of composite facets for the surface of a space-based solar dynamic concentrator p 54 A88-18230

MOREL, T.

Application of several variable-valve-timing concepts to an LHR engine
[ASME PAPER 87-ICE-29] p 19 A88-15119

MOREY, DENNIS C.

Assessment of nuclear reactor concepts for low power space applications p 217 A88-24409

MORGAN, C. J.

A life test of a 22-Newton (5-lbf) hydrazine rocket
[NASA-TM-100232] p 57 A88-11750

MORIN, BRUCE L.

Forced mixer lobes in ejector designs p 141 A88-46222

MORREN, W. EARL

Water-propellant resistojets for man-tended platforms
[IAF PAPER 87-259] p 54 A88-15975

Development of a liquid-fed water resistojel
[AIAA PAPER 88-3288] p 142 A88-48762

Space station propulsion
[NASA-TM-100216] p 57 A88-11746

Development of a liquid-fed water resistojel
[NASA-TM-100927] p 174 A88-24968

MORRIS, P. J.

Acoustically excited heated jets. 1: Internal excitation
[NASA-CR-4129-PT-1] p 12 A88-23751

Acoustically excited heated jets. 2: In search of a better understanding
[NASA-CR-4129-PT-2] p 12 A88-23752

Acoustically excited heated jets. 3: Mean flow data
[NASA-CR-4129-PT-3] p 12 A88-23753

MORRIS, SHELBY J., JR.

The challenges and opportunities of supersonic transport propulsion technology
[AIAA PAPER 88-2985] p 23 A88-48032

The challenges and opportunities of supersonic transport propulsion technology
[NASA-TM-100921] p 34 A88-23806

MORRISON, G. L.

Experimental verification of a secondary recirculation zone in a labyrinth seal
[AIAA PAPER 88-3692] p 168 A88-48971

3-D laser anemometer measurements in a labyrinth seal

[ASME PAPER 88-GT-63] p 169 A88-54195

3-D laser anemometer measurements in an annular seal
[ASME PAPER 88-GT-64] p 169 A88-54196

MORTARA, KARL W.

A physically consistent model for artificial dissipation in transonic potential flow computations
[NASA-TM-100846] p 211 A88-22652

MOSELLE, J. R.

A hybrid numerical technique for predicting the aerodynamic and acoustic fields of advanced turboprops
[NASA-CR-174926] p 216 A88-12352

MUELLER, B. A.

Rapid solidification of highly undercooled liquids p 88 A88-41653

MULAC, RICHARD A.

A multistage mesh generator for solving the average-passage equation system
[NASA-CR-179539] p 10 A88-15769

Utilization of parallel processing in solving the inviscid form of the average-passage equation system for multistage turbomachinery
[NASA-TM-89845] p 32 A88-21160

MULARZ, E. J.

Assessment, development, and application of combustor aerothermal models p 24 A88-54140

Assessment, development and application of combustor aerothermal models
[NASA-TM-100290] p 32 A88-19469

MULARZ, EDWARD J.

Chemical reacting flows p 79 A88-15793

MULL, M. A.

Crack diffusion coefficient - A candidate fracture toughness parameter for short fiber composites p 70 A88-36945

MULLEN, R. L.

Numerical modeling of multidimensional flow in seals and bearings used in rotating machinery
[NASA-TM-100779] p 150 A88-16988

Numerical and analytical study of fluid dynamic forces in seals and bearings
[NASA-TM-100268] p 151 A88-18867

MULLEN, ROBERT L.

Interface roughness effect on stresses in ceramic coatings p 95 A88-12587

Some adhesion/cohesion characteristics of plasma-sprayed ZrO₂-Y₂O₃ under tensile loading p 95 A88-12589

MURPHY, G. B.

Exposed high-voltage source effect on the potential of an ionospheric satellite p 218 A88-54992

MURPHY, GERALD B.

Gaseous environment of the Shuttle early in the Spacelab 2 mission p 47 A88-47972

MURTHY, DURBHA V.

Derivatives of eigenvalues and eigenvectors of a general complex matrix p 209 A88-29269

Application of a semianalytical technique for sensitivity analysis of unsteady aerodynamic computations
[AIAA PAPER 88-2377] p 6 A88-32314

A semianalytical technique for sensitivity analysis of unsteady aerodynamic computations
[NASA-TM-100810] p 189 A88-18976

Experimental investigation of propfan aeroelastic response in off-axis flow with mistuning
[NASA-TM-101320] p 196 A88-28344

MURTHY, K. N. S.

Laser Doppler velocimeter measurement of annulus wall boundary layer development in a compressor rotor
[ASME PAPER 87-GT-251] p 132 A88-11133

MURTHY, P. L. N.

An ideal clamping analysis for a cross-ply laminate p 181 A88-31347

Fracture toughness computational simulation of general delaminations in fiber composites p 181 A88-32219

Probabilistic composite micromechanics
[AIAA PAPER 88-2375] p 182 A88-32312

Free-edge delamination: Laminate width and loading conditions effects
[NASA-TM-100238] p 72 A88-12551

MURTHY, PAPPU L. N.

Design procedures for fiber composite box beams
[NASA-TM-100296] p 73 A88-16828

Finite element substructuring methods for composite mechanics
[NASA-TM-100297] p 73 A88-17745

METCAN: The metal matrix composite analyzer p 74 A88-22395

MURTHY, S. N. B.

Transient engine performance with water ingestion p 19 A88-27295

Aerothermal modeling program, phase 2 p 146 A88-11149

MUSZYNSKA, A.

- Numerical and analytical study of fluid dynamic forces in seals and bearings p 167 A88-31534
 Numerical modeling of multidimensional flow in seals and bearings used in rotating machinery [NASA-TM-100779] p 150 N88-16988
 Numerical and analytical study of fluid dynamic forces in seals and bearings [NASA-TM-100268] p 151 N88-18867

MYERS, G.

- Dilution jet mixing program, phase 3 p 147 N88-11153

MYERS, IRA T.

- Electrical Power Working Group report p 48 N88-10095
 The application of high temperature superconductors to space electrical power distribution components [NASA-TM-100901] p 61 N88-22939
 Electromagnetic powered vehicles (EMPV) for Mars exploration p 62 N88-24388

MYERS, M. R.

- A parametric study of mean loading effects on airfoil gust interaction noise [AIAA PAPER 87-2677] p 213 A88-16539

N**NADI, S.**

- Relationship between fatigue life in the creep-fatigue region and stress-strain response [NASA-TM-100796] p 188 N88-18040

NAFF, G. J.

- Design description report for a photovoltaic power system for a remote satellite earth terminal [NASA-CR-179586] p 200 N88-12875

NAGARAJAN, R.

- Turbine airfoil deposition models and their hot corrosion implications p 91 N88-11178

NAGLE, D.

- SR-7A aeroelastic model design report [NASA-CR-174791] p 36 N88-28928

NAGPAL, VINOD K.

- Probabilistic structural analysis of aerospace components using NESSUS [AIAA PAPER 88-2373] p 182 A88-32310
 Probabilistic structural analysis to quantify uncertainties associated with turbopump blades [NASA-TM-100278] p 76 N88-28094

NAHRA, HENRY K.

- Technologies for protection of the Space Station power system surfaces in atomic oxygen environment p 41 A88-52331
 Low Earth orbit environmental effects on the space station photovoltaic power generation systems [NASA-TM-100230] p 225 N88-12429
 Assessment of the effects of space debris and meteoroids environment on the space station solar array assembly [NASA-TM-101315] p 49 N88-28959

NAKAGAWA, J. H.

- Improved perfluoroalkylether fluid development [NASA-CR-180872] p 80 N88-15851

NAKAGAWA, JAMES H.

- Improved perfluoroalkyl ether fluid development p 68 A88-28624

NAKAZAWA, S.

- On 3-D inelastic analysis methods for hot section components. Volume 1: Special finite element models [NASA-CR-180893] p 190 N88-21535
 MHOST: An efficient finite element program for inelastic analysis of solids and structures p 33 N88-22394

NALLASAMY, M.

- High speed propeller performance and noise predictions at takeoff/landing conditions [AIAA PAPER 88-0264] p 215 A88-22193
 Computation of the velocity field of an excited shear layer p 138 A88-26206
 High-speed propeller noise predictions - Effects of boundary conditions used in blade loading calculations p 215 A88-36270

- High speed propeller performance and noise predictions at takeoff/landing conditions [NASA-TM-100267] p 216 N88-13960

NAMKOONG, D.

- Solar dynamic organic Rankine cycle heat rejection system simulation p 132 A88-11808

NARAGHI, M. H. N.

- Three dimensional thermal analysis of rocket thrust chambers [AIAA PAPER 88-2643] p 54 A88-43721

NARAGHI, MOHAMMAD H.

- A two-dimensional finite difference program for thermal analysis of rocket thrust chambers [NASA-TM-100191] p 58 N88-12539

NASAR, S. A.

- Study of free-piston Stirling engine driven linear alternators [NASA-CR-181425] p 170 N88-10355

NASEEM, HAMEED

- Study of Staebler-Wronsky degradation effect in a Si:H based P-I-N solar cells [NASA-CR-182564] p 203 N88-25970

NASH, P.

- Precipitation in a rapidly solidified and aged Ni-Al-Mo alloy p 82 A88-18528

NATHAL, M. V.

- Effect of initial gamma prime size on the elevated temperature creep properties of single crystal nickel base superalloys p 82 A88-18884
 Lattice parameter variations during aging in nickel-base superalloys p 90 A88-51318

NATHAL, MICHAEL V.

- Microstructure-property relationships in directionally solidified single-crystal nickel-base superalloys p 88 A88-40329

- Compatibility of dispersion-strengthened platinum with resistojet propellants [NASA-TP-2765] p 58 N88-12538

- Status and prognosis for alternative engine materials [NASA-TM-100903] p 94 N88-24749

NAUD, STEVE

- Production and characterization of CdCl₂ intercalated graphite fibers p 101 A88-51307

NEGAS, T.

- Phase purity of NiCo₂O₄, a catalyst candidate for electrolysis of water [NASA-TM-100239] p 69 N88-13385

NELSON, C. C.

- Analysis of eccentric annular incompressible seals. I - A new solution using fast Fourier transforms for determining hydrodynamic force [ASME PAPER 87-TRIB-52] p 166 A88-23308
 Analysis of eccentric annular incompressible seals. II - Effects of eccentricity on rotordynamic coefficients [ASME PAPER 87-TRIB-53] p 166 A88-23309

NELSON, E. S.

- Two-dimensional viscous flow computations of hypersonic scramjet nozzle flowfields at design and off-design conditions [AIAA PAPER 88-3280] p 23 A88-50785
 Two-dimensional viscous flow computations of hypersonic scramjet nozzle flowfields at design and off-design conditions [NASA-CR-182150] p 35 N88-25459

NELSON, R. S.

- Improved maintainability of space-based reusable rocket engines [AIAA PAPER 88-3113] p 55 A88-48037

- Fatigue life prediction modeling for turbine hot section materials p 184 A88-54144

- Fatigue life prediction modeling for turbine hot section materials [NASA-TM-100291] p 187 N88-14453

NELSON, RICHARD S.

- Creep fatigue life prediction for engine hot section materials (isotropic): Third year progress review p 186 N88-11173
 Life prediction modeling based on cyclic damage accumulation p 178 N88-22426

NERAYANAN, G. V.

- Aeroelastic response of metallic and composite propfan models in yawed flow [NASA-TM-100964] p 37 N88-29807

NESBITT, J. A.

- Interdiffusion in Ni-rich, Ni-Cr-Al alloys at 1100 and 1200 C. I - Diffusion paths and microstructures. II - Diffusion coefficients and predicted concentration profiles p 84 A88-24485

- Predicting diffusion paths and interface motion in gamma/gamma + beta, Ni-Cr-Al diffusion couples p 84 A88-24486

- Diffusional transport during the cyclic oxidation of gamma + beta, Ni-Cr-Al(Y, Zr) alloys p 85 A88-28902

NESBITT, JAMES A.

- Coating life prediction p 170 N88-11181

NEUMANN, ERIC S.

- Mass transport phenomena between bubbles and dissolved gases in liquids under reduced gravity conditions [AIAA PAPER 88-0450] p 138 A88-27719

- Mass transport phenomena between bubbles and dissolved gases in liquids under reduced gravity conditions [NASA-TM-100273] p 80 N88-18672

NEUMANN, J.

- Thermal barrier coating life-prediction model development [NASA-CR-179507] p 107 N88-28142

NEWMAN, FREDERICK A.

- Experimental vibration damping characteristics of the third-stage rotor of a three-stage transonic axial-flow compressor [AIAA PAPER 88-3229] p 23 A88-48759

- Experimental vibration damping characteristics of the third-stage rotor of a three-stage transonic axial-flow compressor [NASA-TM-100948] p 35 N88-24642

- Experimental determination of aerodynamic damping in a three-stage transonic axial-flow compressor [NASA-TM-100953] p 35 N88-27200

NEWTON, JAMES E.

- Measurement of local convective heat transfer coefficients from a smooth and roughened NACA-0012 airfoil - Flight test data [AIAA PAPER 88-0287] p 136 A88-22207

- Measurement of local convective heat transfer coefficients from a smooth and roughened NACA-0012 airfoil: Flight test data [NASA-TM-100284] p 149 N88-13552

NG, W. F.

- Turbulence modeling in hypersonic inlets [AIAA PAPER 88-2957] p 7 A88-44705

NGUYEN, D. T.

- Analysis of eccentric annular incompressible seals. I - A new solution using fast Fourier transforms for determining hydrodynamic force [ASME PAPER 87-TRIB-52] p 166 A88-23308

- Analysis of eccentric annular incompressible seals. II - Effects of eccentricity on rotordynamic coefficients [ASME PAPER 87-TRIB-53] p 166 A88-23309

NGUYEN, H. L.

- Performance and efficiency evaluation and heat release study of a direct-injection stratified-charge rotary engine [SAE PAPER 870445] p 166 A88-23313

NGUYEN, HUNG LEE

- Performance and combustion characteristics of direct-injection stratified-charge rotary engines [NASA-TM-100134] p 25 N88-12490

- Liquid sprays and flow studies in the direct-injection diesel engine under motored conditions [NASA-TM-100135] p 31 N88-18594

NGUYEN, TUAN Q.

- Communications satellites in non-geostationary orbits [AIAA PAPER 88-0842] p 46 A88-27583

NICHOLS, LESTER D.

- Aeropropulsion structures p 27 N88-15786

NICHOLSON, STEPHEN

- Explicit finite-volume time-marching calculations of total temperature distributions in turbulent flow p 139 A88-30517

- An explicit finite-volume time-marching procedure for turbulent flow calculations p 139 A88-30518

NIEDZWIECKI, RICHARD W.

- Small engine technology programs p 29 N88-15801

- Small gas turbine engine technology p 30 N88-16638

NIGHTINGALE, NOEL P.

- Automotive Stirling engine: Mod 2 design report [NASA-CR-175106] p 223 N88-11578

NIKJOOY, M.

- K-epsilon turbulence model assessment with reduced numerical diffusion for coaxial jets [AIAA PAPER 88-0342] p 137 A88-22251

NISSLEY, D. M.

- Fatigue life prediction modeling for turbine hot section materials p 184 A88-54144

- Fatigue life prediction modeling for turbine hot section materials [NASA-TM-100291] p 187 N88-14453

- A constitutive model for an overlay coating p 105 N88-21525

NISSLEY, DAVID M.

- Fatigue damage modeling for coated single crystal superalloys p 93 N88-22427

NOE, KURT A.

- The effect of gravity on premixed flame propagation and extinction in a vertical standard flammability tube p 78 A88-38532

NONAMI, KENZOU

- Vibration and control of flexible rotor supported by magnetic bearings [NASA-TM-100888] p 174 N88-23977

NORMAN, ARNIE M.

- An expert system approach to turbopump health monitoring [AIAA PAPER 88-3117] p 42 A88-48038

NORMENT, HILLIER G.

- Three-dimensional trajectory analyses of two drop sizing instruments: PMS OAP and PMS FSSP [NASA-CR-4113] p 16 N88-18574

NORTH, C. M.

- The impact damped harmonic oscillator in free decay p 167 A88-31581

NOWLIN, BRENT C.

- Small engine components test facility turbine testing cell
[AIAA PAPER 88-2962] p 22 A88-44706
- Small engine components test facility turbine testing cell
[NASA-TM-100887] p 33 N88-22037

NOWOTNY, H.

- High-temperature oxidation/corrosion of iron-based superalloys p 81 A88-10029

NUSSLE, R.

- Measured performance of the heat exchanger in the NASA icing research tunnel under severe icing and dry-air conditions
[NASA-TM-100116] p 171 N88-12796

NYLAND, T. W.

- Chordwise pressure measurements on a blade of Mod-2 Wind Turbine p 2 A88-10970
- Comparison of pressure distributions on model and full-scale NACA 64-621 airfoils with ailerons for wind turbine application
[NASA-TM-100802] p 201 N88-21593

O

O'GRADY, E. PEARSE

- Performance limitations in parallel processor simulations p 208 A88-49101

O'NEILL, MARK J.

- Development of an advanced photovoltaic concentrator system for space applications p 51 A88-11812
- Development of a dome Fresnel lens/gallium arsenide photovoltaic concentrator for space applications p 199 A88-34310

OBERHART, M. L.

- Slotline fed microstrip antenna array modules p 126 A88-44170

OBERLE, LAWRENCE G.

- Laser anemometry techniques for turbine applications [ASME PAPER 87-GT-241] p 157 A88-11129
- Comparison of the bidirectional reflectance distribution function of various surfaces p 218 N88-28760

OBRIEN, JAMES E.

- Experimental study of bypass transition in a boundary layer [NASA-TM-100913] p 153 N88-23186

OCHI, SIMEON C. U.

- Characterization of noncontact piezoelectric transducer with conically shaped piezoelement [NASA-CR-4151] p 179 N88-23987

ODONNELL, PATRICIA M.

- Energy storage considerations for a robotic Mars surface sampler [NASA-TM-100969] p 227 N88-28853

OHTANI, RYUICHI

- Creep life prediction based on stochastic model of microstructurally short crack growth [NASA-TM-100245] p 186 N88-12825

OKIISHI, T. H.

- Measurements of the unsteady flow field within the stator row of a transonic axial-flow fan. I - Measurement and analysis technique [ASME PAPER 87-GT-226] p 4 A88-18660
- Measurements of the unsteady flow field within the stator row of a transonic axial-flow fan. II - Results and discussion [ASME PAPER 87-GT-227] p 4 A88-18661

OKUBO, E. K.

- Polarization determination utilizing two arbitrarily polarized antennas p 116 A88-47424

OLDENBURG, JOHN R.

- Analysis of counting errors in the phase/Doppler particle analyzer [NASA-TM-100231] p 161 N88-12043

OLSEN, R. C.

- Record charging events from Applied Technology Satellite 6 p 46 A88-11737
- An unusual charging event on ISEE 1 p 47 A88-40013
- Electron beam experiments at high altitudes p 47 A88-46799

OLSEN, W.

- Experimental evidence for modifying the current physical model for ice accretion on aircraft surfaces [NASA-TM-87184] p 15 N88-12473
- Measured performance of the heat exchanger in the NASA icing research tunnel under severe icing and dry-air conditions [NASA-TM-100116] p 171 N88-12796

OLSON, S. L.

- A theoretical analysis of the extinction limits of a methane-air opposed-jet diffusion flame p 77 A88-16497

OLSON, SANDRA L.

- Laminar diffusion flames under micro-gravity conditions [AIAA PAPER 88-0645] p 78 A88-27722
- The effect of microgravity on flame spread over a thin fuel [NASA-TM-100195] p 80 N88-15853

ORANGE, THOMAS W.

- A review of path-independent integrals in elastic-plastic fracture mechanics p 183 A88-47001
- Stress intensity and crack displacement for small edge cracks [NASA-TP-2801] p 188 N88-17095
- Method and models for R-curve instability calculations [NASA-TM-100935] p 194 N88-23278

ORTIZ, M.

- Thermal barrier coating life prediction model development [ASME PAPER 88-GT-284] p 68 A88-54353

ORUGANTI, RAMESH

- Implementation of optimal trajectory control of series resonant converter p 126 A88-38796

OSHIDA, Y.

- Grain boundary oxidation and an analysis of the effects of oxidation on fatigue crack nucleation life p 87 A88-35938
- Grain boundary oxidation and low-cycle fatigue at elevated temperatures p 193 N88-22420

OSWALD, FRED B.

- Finite-element grid improvement by minimization of stiffness matrix trace [NASA-TM-100255] p 171 N88-13604
- Dynamic analysis of multimesh-gear helicopter transmissions [NASA-TP-2789] p 172 N88-17045

OWEN, ALBERT K.

- A FORTRAN code for the calculation of probe volume geometry changes in a laser anemometry system caused by window refraction [NASA-TM-100210] p 206 N88-12288

P

PACIOREK, K. L.

- Improved perfluoroalkylether fluid development [NASA-CR-180872] p 80 N88-15851

PACIOREK, KAZIMIERA J. L.

- Improved perfluoroalkyl ether fluid development p 68 A88-28624

PADOVAN, J.

- Thermomechanical behavior of plasma-sprayed ZrO₂-Y₂O₃ coatings influenced by plasticity, creep, and oxidation p 95 A88-12588

PADOVAN, JOE

- Steady and transient least square solvers for thermal problems p 134 A88-17318

PADOVAN, JOSEPH

- Hierarchically partitioned nonlinear equation solvers p 210 A88-54980
- Input-output-controlled nonlinear equation solvers p 146 A88-55245

PAGE, RUSSELL J.

- Slip casting and extruding shapes of rhemium with metal oxide additives. Part 2: Development of grain stabilized rhemium parts for resistojets [NASA-CR-180851] p 57 N88-11749

PAGNI, PATRICK J.

- Temperature and velocity profiles in sooting free convection diffusion flames p 78 A88-43018
- Optical measurements of soot and temperature profiles in premixed propane-oxygen flames [NASA-TM-101343] p 115 N88-29997

PAHL, D. A.

- A life test of a 22-Newton (5-lbf) hydrazine rocket [NASA-TM-100232] p 57 N88-11750

PAIGE, M. A.

- Multiple-Purpose Subsonic Naval Aircraft (MPSNA): Multiple Application Proptan Study (MAPS) [NASA-CR-175104] p 18 N88-28917

PALAZZOLO, A. B.

- Transient rotor dynamic rub phenomena - Theory and test p 167 A88-31539

- Active control of transient rotordynamic vibration by optimal control methods [ASME PAPER 88-GT-73] p 208 A88-54202

PALMER, K.

- NESSUS/EXPERT - An expert system for probabilistic structural analysis methods [AIAA PAPER 88-2374] p 206 A88-32311

PALMER, RAYMOND W.

- High-efficiency helical traveling-wave tube with dynamic velocity taper and advanced multistage depressed collector p 124 A88-32836

PAMIDI, P. R.

- Aerodynamically forced vibration analysis of turbomachines p 20 A88-31610

PARAT, K. K.

- Characterization and modelling of open tube diffused n+p bulk InP solar cells p 199 A88-34270

PARK, A.

- Material parameter measurements at high temperatures [NASA-CR-182707] p 80 N88-20397
- Measurement of the properties of lossy materials inside a finite conducting cylinder [NASA-CR-182664] p 213 N88-20962

PARK, NO-GILL

- Transfer matrix modeling of geared system vibration p 168 A88-39703

PARKER, J.

- Effect of the microstructure on the thermoelectric properties of polycrystalline lanthanum chalcogenides p 221 A88-40797

PARKS, D. E.

- Threshold-determining mechanisms for discharges in high-voltage solar arrays p 50 A88-11738
- Hollow cathodes as electron emitting plasma contactors - Theory and computer modeling p 218 A88-47973

PATANKAR, S. V.

- Aerothermal modeling program, phase 2 p 146 A88-11149

PATANKAR, SUHAS V.

- Efficient numerical techniques for complex fluid flows p 146 A88-11151

Prediction of turbine blade heat transfer

- p 148 N88-11162

- Two-equation low-Reynolds-number turbulence modeling of transitional boundary layer flows characteristic of gas turbine blades [NASA-CR-4145] p 153 N88-23185

PATEL, MIKUND R.

- High frequency power distribution system [NASA-CR-175071] p 129 N88-23939

PATEL, P. R.

- Surface fatigue life of CBN and vitreous ground carburized and hardened AISI 9310 spur gears [NASA-TM-100960] p 175 N88-25916

PATHAK, P. H.

- Electromagnetic fields backscattered from an s-shaped inlet cavity with an absorber coating on its inner walls [NASA-CR-182401] p 118 N88-15130

PATHARE, VIREN M.

- Processing, physical metallurgy and creep of NiAl + Ta and NiAl + Nb alloys [NASA-CR-182113] p 92 N88-21295

PATTERSON, MICHAEL J.

- High power ion thruster performance [NASA-TM-100127] p 58 N88-12542
- High power ion thruster performance p 62 N88-24295

- Electric propulsion options for the SP-100 reference mission p 62 N88-24296
- Performance of 10-kW class xenon ion thrusters [NASA-TM-101292] p 65 N88-28088

PAUCKERT, R.

- Improved maintainability of space-based reusable rocket engines [AIAA PAPER 88-3113] p 55 A88-48037

PAULSEN, PHILLIP E.

- Oxidation and protection of fiberglass-epoxy composite masts for photovoltaic arrays in the low Earth orbital environment [NASA-TM-100839] p 104 N88-18734

PEET, SHELLEY

- A re-examination of spent beam refocusing for high-efficiency helix TWT's and small MDC's p 124 A88-28673

- Performance of a small, graphite electrode, multistage depressed collector with a 500-W, continuous wave, 4.8- to 9.6-GHz traveling wave tube [NASA-TP-2788] p 128 N88-15146

PELLOUX, R. M.

- Thermal-mechanical cyclic stress-strain responses of cast B-1900 + Hf p 87 A88-35919

PELLOUX, REGIS M.

- A model for life predictions of nickel-base superalloys in high-temperature low cycle fatigue p 87 A88-35913

PENKO, P. F.

- An experimental investigation of the effect of test-cell pressure on the performance of resistojets [AIAA PAPER 88-3286] p 40 A88-44820

PEPPER, S. V.

- Thermal desorption study of physical forces at the PTFE surface p 77 A88-10963

PEPPER, STEPHEN V.

- Auger analysis of a fiber/matrix interface in a ceramic matrix composite [NASA-TM-100892] p 76 N88-25487

PERSONAL AUTHOR INDEX

- PEREPEZKO, J. H.**
Containerless processing of undercooled melts p 110 A88-28554
Rapid solidification of highly undercooled liquids p 88 A88-1653
Noncontact temperature measurement: Requirements and applications for metals and alloys research p 112 N88-23899
- PEREZ-DAVIS, MARLA E.**
The effect of compression on individual pressure vessel nickel/hydrogen components [NASA-TM-101312] p 81 N88-28109
- PERRY, JOHN G.**
An expert system approach to turbopump health monitoring [AIAA PAPER 88-3117] p 42 A88-48038
- PETERS, CARROLL E.**
Flow field measurements in a 90 degree turning duct p 147 N88-11157
- PETERS, L. JR.**
Material parameter measurements at high temperatures [NASA-CR-182707] p 80 N88-20397
- PETRASEK, D. W.**
Creep behavior of tungsten/niobium and tungsten/niobium-1 percent zirconium composites p 75 N88-24427
- PETRASEK, DONALD W.**
Creep behavior of tungsten/niobium and tungsten/niobium-1 percent zirconium composites [NASA-TM-100804] p 92 N88-18707
Refractory metal alloys and composites for space power systems [NASA-TM-100946] p 95 N88-27310
- PHAM, CHUONG**
Production and characterization of CdCl₂ intercalated graphite fibers p 101 A88-51307
- PHILIPP, W. H.**
Advantages of barium peroxide in the powder synthesis of perovskite superconductors p 221 A88-41496
- PHUCHAROEN, W.**
Thermal expansion mismatch and oxidation in thermal barrier coatings p 170 N88-11182
- PICCONI, T. J.**
Solidification of undercooled Ni-Sn eutectic alloy under microgravity conditions in the Space Shuttle p 110 A88-28557
Dendritic growth of undercooled nickel-tin. III p 86 A88-32887
- PICKETT, J. S.**
Exposed high-voltage source effect on the potential of an ionospheric satellite p 218 A88-54992
- PICKETT, JOLENE S.**
Gaseous environment of the Shuttle early in the Spacelab 2 mission p 47 A88-47972
- PILSNER, B. H.**
Thermal barrier coating life prediction model development p 170 N88-11184
- PINTZ, A.**
Automated acoustic intensity measurements and the effect of gear tooth profile on noise p 168 A88-31623
- PIROUZ, P.**
Lattice defects in beta-SiC grown epitaxially on silicon substrates p 220 A88-28711
Microscopy of epitaxially grown beta-SiC on 001-plane silicon p 98 A88-31023
- PISZCZOR, MICHAEL F.**
Development of a dome Fresnel lens/gallium arsenide photovoltaic concentrator for space applications p 199 A88-34310
- PISZCZOR, MICHAEL F., JR.**
Development of an advanced photovoltaic concentrator system for space applications p 51 A88-11812
- PITZ, R. W.**
The structure and dynamics of reacting plane mixing layers p 136 A88-20871
- PLESNA, MICHAEL E.**
The effects of crack surface friction and roughness on crack tip stress fields p 180 A88-14579
- PLINE, A.**
Containment of a silicone fluid free surface in reduced gravity p 112 A88-49085
- PLINE, ALEXANDER D.**
Containment of a silicone fluid free surface in reduced gravity using barrier coatings [NASA-TM-101314] p 155 N88-30072
- POINSATTE, PHILLIP E.**
Measurement of local convective heat transfer coefficients from a smooth and roughened NACA-0012 airfoil - Flight test data [AIAA PAPER 88-0287] p 136 A88-22207
Measurement of local convective heat transfer coefficients from a smooth and roughened NACA-0012 airfoil: Flight test data [NASA-TM-100284] p 149 N88-13552

- POIRIER, D. R.**
A thermodynamic prediction for microporosity formation in aluminum-rich Al-Cu alloys p 82 A88-18886
- POLCH, E. Z.**
Probabilistic Structural Analysis Methods for select space propulsion system structural components (PSAM) p 56 A88-49659
- POLEY, WILLIAM A.**
Communications payload concepts for geostationary facilities [NASA-TM-100154] p 118 N88-13513
- PONCHAK, D. S.**
Numerical arc segmentation algorithm for a radio conference - A software tool for communication satellite systems planning [AIAA PAPER 88-0788] p 212 A88-27531
Numerical arc segmentation algorithm for a radio conference: A software tool for communication satellite systems planning [NASA-TM-100789] p 46 N88-22919
- PONCHAK, DENISE S.**
An allotment planning concept and related computer software for planning the fixed satellite service at the 1988 space WARC p 116 A88-36482
An allotment planning concept and related computer software for planning the fixed satellite service at the 1988 space WARC [NASA-TM-100244] p 117 N88-11944
Numerical arc segmentation algorithm for a radio conference-NASARC (version 2.0) technical manual [NASA-TM-100160] p 118 N88-15910
Numerical arc segmentation algorithm for a radio conference-NASARC, version 2.0: User's manual [NASA-TM-100161] p 119 N88-16928
- PONCHAK, GEORGE E.**
A new model for broadband waveguide-to-microstrip transition design p 126 A88-38822
Modeling of some coplanar waveguide discontinuities [NASA-TM-100808] p 119 N88-17880
Monolithic microwave integrated circuit technology for advanced space communication [NASA-TM-100829] p 120 N88-21389
- PONTANO, BENJAMIN A.**
Future switching satellites [AIAA PAPER 88-0802] p 46 A88-27553
- POORMAN, R. N.**
Fiber-linked interferometric pressure sensor p 157 A88-11743
- POPE, DALE E.**
Experimental radio frequency link for Ka-band communications applications [NASA-TM-100824] p 43 N88-24659
- PORTER, J.**
Centaur operations at the space station [NASA-CR-179593] p 49 N88-25473
- POUCH, J. J.**
Advantages of barium peroxide in the powder synthesis of perovskite superconductors p 221 A88-41496
- POUCH, JOHN J.**
Plasma deposition of amorphous hydrogenated carbon films on III-V semiconductors p 220 A88-32862
Mechanical strength and tribological behavior of ion-beam-deposited boron nitride films on non-metallic substrates p 98 A88-32866
Laser induced OMCVD growth of AlGaAs on GaAs p 125 A88-34286
Boron nitride - Composition, optical properties, and mechanical behavior p 99 A88-40794
Temperature stability of Al(x)Ga(1-x)As (x = 0-1) thermal oxide masks for selective-area epitaxy p 221 A88-45858
- POVINELLI, LOUIS A.**
Retooling CFD for hypersonic aircraft p 1 A88-16749
CFD validation experiments for internal flows [NASA-TM-100797] p 10 N88-16679
- POWELL, J. A.**
Improved beta-SiC heteroepitaxial films using off-axis Si substrates p 219 A88-10431
Lattice defects in beta-SiC grown epitaxially on silicon substrates p 220 A88-28711
Microscopy of epitaxially grown beta-SiC on 001-plane silicon p 98 A88-31023
Low-temperature photoluminescence studies of chemical-vapor-deposition-grown 3C-SiC on Si p 127 A88-53396
Raman scattering studies of chemical-vapor-deposited cubic SiC films of (100)Si p 127 A88-53397
- POWELL, J. ANTHONY**
Silicon carbide - Progress in crystal growth p 99 A88-40792
- POWER, JOHN L.**
Successful completion of a cyclic ground test of a mercury ion auxiliary propulsion system [NASA-TM-101351] p 67 N88-29873

RADHAKRISHNAN, KRISHNAN

- POWERS, LYNN M.**
Reliability based analysis of contact problems [NASA-CR-182117] p 189 N88-18975
- PRAHL, J.**
Parched elasto hydrodynamic lubrication film thickness measurement in an instrument ball bearing [STLE PREPRINT 88-AM-6G-1] p 169 A88-51082
- PRAHL, J. M.**
Oil film thickness measurement and analysis for an angular contact ball bearing operating in parched elasto hydrodynamic lubrication p 165 A88-14115
- PRAHL, JOSEPH M.**
Navier-Stokes cascade analysis with a stiff k-epsilon turbulence solver [AIAA PAPER 88-0594] p 5 A88-22444
Navier-Stokes cascade analysis with a stiff Kappa-Epsilon turbulence solver [NASA-TM-100218] p 9 N88-10778
- PRATT, TIMOTHY**
VSAT networks - An overview p 115 A88-14091
Spread-spectrum multiple access using wideband noncoherent MFSK p 115 A88-26672
- PRESZ, WALTER M., JR.**
Forced mixer lobes in ejector designs p 141 A88-46222
- PRICE, K. M.**
Communications satellite systems operations with the space station. Volume 3: Supplementary technical report [NASA-CR-180875] p 48 N88-16794
- PRICE, KENT M.**
Economic benefits of the Space Station to commercial communication satellite operators [IAF PAPER 87-622] p 41 A88-16215
Communications satellites in non-geostationary orbits [AIAA PAPER 88-0842] p 46 A88-27583
The economics of satellite retrieval [AIAA PAPER 88-0843] p 44 A88-27584
Advanced satellite system architecture for VSATs with ISDN compatibility [AIAA PAPER 88-0870] p 116 A88-27604
- PRIEM, RICHARD J.**
Study of industry requirements that can be fulfilled by combustion experimentation aboard space station [NASA-CR-180854] p 224 N88-19377
- PROBST, H. B.**
Simulating the cooling of an immiscible alloy p 83 A88-20199
- PROK, GEORGE M.**
Availability and cost estimate of a high naphthene, modified aviation turbine fuel [NASA-TM-100823] p 104 N88-20455
- PROVENCER, CHARLES E., JR.**
A laser communication experiment utilizing the ACT satellite and an airborne laser transceiver [NASA-TM-100792] p 164 N88-18910
- PRUSSING, JOHN E.**
Optimal cooperative time-fixed impulsive rendezvous [AIAA PAPER 88-4279] p 42 A88-50406
- PRZEKAS, A.**
Numerical modeling of multidimensional flow in seals and bearings used in rotating machinery [NASA-TM-100779] p 150 N88-16988
- PRZEKAS, A. J.**
Numerical and analytical study of fluid dynamic forces in seals and bearings p 167 A88-31534
Numerical and analytical study of fluid dynamic forces in seals and bearings [NASA-TM-100268] p 151 N88-18867
- Q**
- QAQISH, WALID**
Optical strain measurement system development p 159 A88-52557
- QUENTMEYER, RICHARD J.**
Thrust chamber thermal barrier coating techniques [NASA-TM-100933] p 64 N88-24690
- QUINN, R. D.**
Redundant manipulators for momentum compensation in a micro-gravity environment [AIAA PAPER 88-4121] p 204 A88-50223
- R**
- RAAD, PETER E.**
A mapped finite difference study of noise propagation in nonuniform ducts with mean flow p 214 A88-18541
- RADCLIFFE, M. D.**
Simulation of fluid flows during growth of organic crystals in microgravity p 109 A88-13163
- RADHAKRISHNAN, KRISHNAN**
Integrating combustion kinetic rate equations by selective use of stiff and nonstiff methods p 78 A88-19233

- RADIL, K. C.**
Computerized life and reliability modelling for turboprop transmissions
[AIAA PAPER 88-2979] p 100 A88-48031
Computerized life and reliability modelling for turboprop transmissions
[NASA-TM-100918] p 173 N88-23220
- RADULESCU, DAVID C.**
Variable angle spectroscopic ellipsometry - Application to GaAs-AlGaAs multilayer homogeneity characterization
p 220 A88-40139
- RAGALLER, D. R.**
Toluene stability Space Station Rankine power system
p 50 A88-11794
Solar dynamic organic Rankine cycle heat rejection system simulation
p 132 A88-11808
- RAGALLER, DANA**
Study of toluene stability for an Organic Rankine Cycle (ORC) space-based power system
[NASA-CR-180884] p 66 N88-29863
Study of toluene rotary fluid management device and shear flow condenser performance for a space-based organic Rankine power system
[NASA-CR-180885] p 67 N88-29872
- RAHNKE, C. J.**
Development of the AGT101 regenerator seals
[ASME PAPER 87-GT-173] p 165 A88-11083
- RAITT, W. J.**
Double-probe potential measurements near the Spacelab 2 electron beam
p 204 A88-53464
- RAJ, R.**
Wall shear stress measurement in blade end-wall corner region
[ASME PAPER 87-GT-181] p 131 A88-11089
- RAMAMURTI, R.**
Solution of the Neumann pressure problem in general orthogonal coordinates using the multigrad technique
p 144 A88-50330
- RAMAN, G.**
Initial turbulence effect on jet evolution with and without tonal excitation
[AIAA PAPER 87-2725] p 4 A88-20184
- RAMAN, GANESH**
Saturation and the limit of jet mixing enhancement by single frequency plane wave excitation - Experiment and theory
[AIAA PAPER 88-3613] p 8 A88-48899
Initial conditional effect on pressure waves in an axisymmetric jet
[AIAA PAPER 88-3702] p 143 A88-48915
Initial condition effect on pressure waves in an axisymmetric jet
[NASA-TM-100915] p 153 N88-23184
Saturation and the limit of jet mixing enhancement by single frequency plane wave excitation: Experiment and theory
[NASA-TM-100882] p 12 N88-23732
- RAMASWAMY, V. G.**
Constitutive modeling for isotropic materials
p 186 N88-11172
- RAMINS, PETER**
A re-examination of spent beam refocusing for high-efficiency helix TWT's and small MDC's
p 124 A88-28673
Performance of a small, graphite electrode, multistage depressed collector with a 500-W, continuous wave, 4.8- to 9.6-GHz traveling wave tube
[NASA-TP-2788] p 128 N88-15146
- RAMOS, J. I.**
Numerical methods for one-dimensional reaction-diffusion equations arising in combustion theory
p 135 A88-18975
- RAMOS, JUAN I.**
Liquid sprays and flow studies in the direct-injection diesel engine under motored conditions
[NASA-TM-100135] p 31 N88-18594
- RAMSEY, JOHN K.**
Flutter of a fan blade in supersonic axial flow
[ASME PAPER 88-GT-78] p 8 A88-54206
- RANDALL, M. R.**
Noncontacting measurement technologies for space propulsion condition monitoring
p 158 A88-29818
- RAPP, DOUGLAS C.**
Characterization of aluminum/RP-1 gel propellant properties
[AIAA PAPER 88-2821] p 109 A88-48751
Characterization of aluminum/RP-1 gel propellant properties
[NASA-TM-100951] p 109 N88-24808
- RAQUET, CHARLES A.**
Optical RF distribution links for MMIC phased array antennas
[NASA-TM-100841] p 128 N88-20555
- RAWLIN, VINCENT K.**
Internal erosion rates of a 10-kW xenon ion thruster
[AIAA PAPER 88-2912] p 55 A88-48753
- High power ion thruster performance
[NASA-TM-100127] p 58 N88-12542
High power ion thruster performance
p 62 N88-24295
Electric propulsion options for the SP-100 reference mission
p 62 N88-24296
Internal erosion rates of a 10-kW xenon ion thruster
[NASA-TM-100954] p 63 N88-24688
Performance of 10-kW class xenon ion thrusters
[NASA-TM-101292] p 65 N88-28088
- RAY, ASOK**
Finite-dimensional modeling of network-induced delays for real-time control systems
p 208 A88-54537
- RAY, BISWAJIT**
A cascaded Schwarz converter for high frequency power distribution
p 127 A88-54713
- RAY, R.**
Dispersion strengthened NiAl alloys produced by rapid solidification processing
p 88 A88-40588
- REDDO, L. R.**
Space station onboard propulsion system: Technology study
[NASA-CR-179233] p 59 N88-15006
- REDDY, D. R.**
Consistent boundary conditions for reduced Navier-Stokes (RNS) scheme applied to three-dimensional internal viscous flows
[AIAA PAPER 88-0714] p 139 A88-27723
Consistent boundary conditions for Reduced Navier-Stokes (RNS) scheme applied to 3-dimensional internal viscous flows
[NASA-CR-180874] p 10 N88-15762
- REDDY, K. T.**
Modified reaction mechanism of aerated n-dodecane liquid flowing over heated metal tubes
p 108 A88-44268
- REDDY, T. S. R.**
The effects of rotational flow, viscosity, thickness, and shape on transonic flutter dip phenomena
[AIAA PAPER 88-2348] p 182 A88-32289
The effects of rotational flow, viscosity, thickness, and shape on transonic flutter dip phenomena
[NASA-TM-100811] p 188 N88-18969
- REED, BRIAN D.**
Weight savings in aerospace vehicles through propellant scavenging
[NASA-TM-100900] p 44 N88-25470
- REGAN, CAROLYN A.**
Engine flow visualization using a copper vapor laser
p 158 A88-34479
- REHFELD, L. W.**
An ideal clamping analysis for a cross-ply laminate
p 181 A88-31347
- REID, LONNIE**
Turbomachinery
p 28 N88-15792
- REID, MARGARET A.**
I-BIEM, an iterative boundary integral equation method for computer solutions of current distribution problems with complex boundaries: A new algorithm. I - Theoretical
p 205 A88-27795
- REILLY, CHARLES H.**
A satellite system synthesis model for orbital arc allotment optimization
p 117 A88-48579
- REINERT, J.**
Reusable rocket engine optical condition monitoring
p 158 A88-29817
- REINMANN, JOHN J.**
The NASA aircraft icing research program
p 15 N88-15803
NASA's rotorcraft icing research program
p 15 N88-16641
- RENGSTORFF, GEORGE W. P.**
Wear of iron and nickel in corrosive liquid environments
p 88 A88-40790
Wear of iron and nickel in corrosive liquid environments
[NASA-TM-100246] p 91 N88-11817
- RENNEISEN, JOHN D.**
Input-output characterization of fiber composites by SH waves
[NASA-CR-4153] p 179 N88-23986
- RENZ, DAVID D.**
Power components for the space station 20-kHz power distribution system
[NASA-TM-100866] p 114 N88-21374
Multi-hundred kilowatt roll ring assembly evaluation results
[NASA-TM-100865] p 114 N88-21375
- RESHOTKO, ELI**
Experimental study of bypass transition in a boundary layer
[NASA-TM-100913] p 153 N88-23186
- REY, CHARLES A.**
Program for the feasibility of developing a high pressure acoustic levitator
[NASA-CR-182154] p 113 N88-26498
- REYNOLDS, R.**
A numerical study of the effects of curvature and convergence on dilution jet mixing
[AIAA PAPER 87-1953] p 137 A88-23312
A numerical study of the effects of curvature and convergence on dilution jet mixing
[NASA-TM-88878] p 26 N88-13347
- RICE, E. J.**
Control of shear flows by artificial excitation
[AIAA PAPER 87-2722] p 3 A88-16567
Initial turbulence effect on jet evolution with and without tonal excitation
[AIAA PAPER 87-2725] p 4 A88-20184
Controlled excitation of a cold turbulent swirling free jet
[ASME PAPER 87-WA/NCA-18] p 140 A88-41568
Effect of initial tangential velocity distribution on the mean evolution of a swirling turbulent free jet
[AIAA PAPER 88-3592] p 7 A88-48893
Effect of initial tangential velocity distribution on the mean evolution of a swirling turbulent free jet
[NASA-TM-100934] p 12 N88-24592
- RICE, EDWARD J.**
Saturation and the limit of jet mixing enhancement by single frequency plane wave excitation - Experiment and theory
[AIAA PAPER 88-3613] p 8 A88-48899
Inlets, ducts and nozzles
p 149 N88-15791
Saturation and the limit of jet mixing enhancement by single frequency plane wave excitation: Experiment and theory
[NASA-TM-100882] p 12 N88-23732
- RIEHEL, JAY P.**
An expert system approach to turbopump health monitoring
[AIAA PAPER 88-3117] p 42 A88-48038
- RIFF, R.**
Thermo-elasto-viscoplastic analysis of problems in extension and shear
p 183 A88-41042
Analysis of shell-type structures subjected to time-dependent mechanical and thermal loading
[NASA-CR-181409] p 185 N88-10388
Analysis of shell-type structures subjected to time-dependent mechanical and thermal loading
[NASA-CR-182705] p 189 N88-20668
Non-isothermal elastoviscoplastic analysis of planar curved beams
p 190 N88-21526
- RILEY, JAMES J.**
Direct simulations of chemically reacting turbulent mixing layers, part 2
[NASA-CR-180853] p 154 N88-25857
- RIZK, MAGDI H.**
Optimizing advanced propeller designs by simultaneously updating flow variables and design parameters
[AIAA PAPER 88-2532] p 6 A88-40718
- ROBERTS, GARY D.**
Simulation of fluid flows during growth of organic crystals in microgravity
p 109 A88-13163
- ROBERTS, WILLIAM B.**
Design point variation of 3-D loss and deviation for axial compressor middle stages
[ASME PAPER 88-GT-57] p 8 A88-54189
- ROBERTSON, THOMAS F.**
The carbon dioxide chaperon efficiency for the reaction $H + O_2 + M$ yields $HO_2 + M$ from ignition delay times behind reflected shock waves
[NASA-TM-100125] p 79 N88-15036
- ROBINSON, D. N.**
A theory of viscoplasticity accounting for internal damage
p 190 N88-21508
Unified constitutive model development for metal matrix composites at high temperature
p 74 N88-22387
- ROBINSON, W. W.**
Further development of the dynamic gas temperature measurement system
p 160 N88-11141
- ROELKE, RICHARD J.**
Design and experimental evaluation of a high temperature radial turbine with a moveable sidewall nozzle
[SAE PAPER 871782] p 19 A88-30776
The design of an air-cooled metallic high temperature radial turbine
[AIAA PAPER 88-2872] p 22 A88-45011
Experimental evaluation of a translating nozzle sidewall radial turbine
p 31 N88-17656
- ROGO, CASIMIR**
Design and experimental evaluation of a high temperature radial turbine with a moveable sidewall nozzle
[SAE PAPER 871782] p 19 A88-30776
Experimental evaluation of a translating nozzle sidewall radial turbine
p 31 N88-17656

- ROHN, DOUGLAS A.**
Efficiency testing of a helicopter transmission planetary reduction stage
[NASA-TP-2795] p 172 N88-15224
Microgravity robotics technology program
[NASA-TM-100898] p 173 N88-23219
- ROLLBUHLER, J.**
Spray characteristics of a spill-return airblast atomizer
[ASME PAPER 88-GT-7] p 145 A88-54154
- ROLLBUHLER, R. JAMES**
Combustion characteristics of gas turbine alternative fuels
[NASA-TM-100247] p 25 N88-13338
- ROMANOFSKY, ROBERT R.**
Monolithic Microwave Integrated Circuit (MMIC) technology for space communications applications
[IAF PAPER 87-491] p 122 A88-16133
Monolithic microwave integrated circuit technology for advanced space communication
[NASA-TM-100829] p 120 N88-21389
- ROMANOSKI, GLENN R.**
A model for life predictions of nickel-base superalloys in high-temperature low cycle fatigue p 87 A88-35913
- RORABAUGH, M. E.**
Improved silicon nitride for advanced heat engines
[NASA-CR-175006] p 102 N88-15886
- ROSE, T. M.**
Modal test/analysis correlation for the Centaur G prime launch vehicle p 44 A88-18631
- ROSENTHAL, B. N.**
Characterization of directionally solidified lead chloride p 111 A88-43170
- ROSENTHAL, BRUCE N.**
Research opportunities in microgravity science and applications during Shuttle hiatus p 109 A88-13164
Preparation for microgravity - The role of the Microgravity Material Science Laboratory
[AIAA PAPER 88-3510] p 111 A88-42908
Ground-based microgravity materials science research at NASA's Microgravity Materials Science Laboratory
p 112 A88-49090
Preparation for microgravity: The role of the microgravity materials science laboratory
[NASA-TM-100906] p 113 N88-24811
- ROSEFJORD, T. J.**
Soot loading in a generic gas turbine combustor p 19 A88-27296
- ROSNER, D. E.**
Turbine airfoil deposition models and their hot corrosion implications p 91 N88-11178
- ROSS, HOWARD D.**
Reducing adhesion and agglomeration within a cloud of combustible particles
[NASA-TM-100902] p 114 N88-26539
- ROST, MARTIN C.**
Electrical resistivity (4K to 2100K) of annealed vapor growth carbon fibers p 96 A88-17214
- ROTH, D. J.**
Acoustic imaging of subtle porosity variations in ceramics p 101 A88-55044
- ROTH, DON J.**
Imaging subtle microstructural variations in ceramics with precision ultrasonic velocity and attenuation measurements
[NASA-TM-100129] p 177 N88-15257
Flaw characterization in structural ceramics using scanning laser acoustic microscopy p 177 N88-22415
- ROUKIS, SUSAN L.**
High thermal-transport capacity heat pipes for space radiators
[SAE PAPER 871509] p 136 A88-21155
- ROZAK, GARY A.**
Stress rupture behavior of silicon carbide coated, low modulus carbon/carbon composites
[NASA-CR-180863] p 72 N88-14150
- RUBENSTEIN, ROBERT**
STAEBL/general composites with hygrothermal effects (STAEBL/GENCOM)
[NASA-TM-100266] p 187 N88-13754
- RUBIN, S. G.**
Consistent boundary conditions for reduced Navier-Stokes (RNS) scheme applied to three-dimensional internal viscous flows
[AIAA PAPER 88-0714] p 139 A88-27723
Consistent boundary conditions for Reduced Navier-Stokes (RNS) scheme applied to 3-dimensional internal viscous flows
[NASA-CR-180874] p 10 N88-15762
- RUBINSTEIN, A. A.**
Macrocrack interaction with transverse array of microcracks p 181 A88-30236
- RUBINSTEIN, E.**
Preparation of multistage zone-refined materials for thermochanical standards p 111 A88-43172
- RUBINSTEIN, E. R.**
Isothermal dendritic growth - A low gravity experiment p 110 A88-28556
Solidification under microgravity conditions - Dendritic growth
[AAS PAPER 86-380] p 110 A88-35130
- RUBINSTEIN, ROBERT**
Infrared properties of an anisotropically stirred fluid p 134 A88-16354
Application of structural tailoring to spar/shell turboprops
[AIAA PAPER 88-2333] p 20 A88-32277
Probabilistic structural analysis to quantify uncertainties associated with turbopump blades
[NASA-TM-100278] p 76 N88-28094
- RUDLAND, R. S.**
Space station onboard propulsion system: Technology study
[NASA-CR-179233] p 59 N88-15006
- RUDOFF, R. C.**
Experiments on spray interactions in the wake of a bluff body
[ASME PAPER 87-GT-48] p 131 A88-11000
Diagnostics development for spray characterization in complex turbulent flows
[ASME PAPER 88-GT-241] p 146 A88-54320
- RUPPE, WALTER A.**
Modulated-splitting-ratio fiber-optic temperature sensor
[NASA-TM-101332] p 18 N88-28062
- RUSSELL, L. M.**
Use of a liquid-crystal and heater-element composite for quantitative, high-resolution heat-transfer coefficients on a turbine airfoil including turbulence and surface-roughness effects p 156 A88-10969
- RUSSELL, P.**
Communications satellite systems operations with the space station. Volume 3: Supplementary technical report
[NASA-CR-180875] p 48 N88-16794
- RUSSELL, S.**
Fuel-injector/air-swirl characterization
[NASA-CR-180864] p 27 N88-14985
- RUSSELL, SID**
Application of advanced diagnostics to airblast injector flows
[ASME PAPER 88-GT-12] p 159 A88-54159
- RUTLEDGE, SHARON K.**
Mast material test program (MAMATEP)
[AIAA PAPER 88-2475] p 70 A88-35945
Technologies for protection of the Space Station power system surfaces in atomic oxygen environment p 41 A88-52331
Oxidation and protection of fiberglass-epoxy composite masts for photovoltaic arrays in the low Earth orbital environment
[NASA-TM-100839] p 104 N88-18734
Mast material test program (MAMATEP)
[NASA-TM-100821] p 74 N88-19592
Arc-textured metal surfaces for high thermal emittance space radiators
[NASA-TM-100894] p 94 N88-24754
- RUTLEDGE, D. C. G.**
Rotorcraft flight-propulsion control integration: An eclectic design concept
[NASA-TP-2815] p 38 N88-19475
- RUTLEDGE, D. G. C.**
Rotorcraft flight-propulsion control integration p 38 N88-16643
- RYN, JOHN R.**
Modulated-splitting-ratio fiber-optic temperature sensor
[NASA-TM-101332] p 18 N88-28062
- S**
- SACKSTEDER, KURT**
Microgravity combustion discipline working group summary of requirements for noncontact temperature measurements p 113 N88-23902
- SACKSTEDER, KURT R.**
Microgravity combustion fundamentals p 112 N88-12528
- SADLER, GERALD G.**
Simulation test beds for the space station electrical power system
[NASA-TM-100786] p 44 N88-17715
- SALEEB, A. F.**
A mixed formulation of C(0)-linear triangular plate/shell element - The role of edge shear constraints p 183 A88-40121
- SALEM, JONATHAN A.**
The effect of texture on the crack growth resistance of alumina
[NASA-TM-100250] p 102 N88-14206
Fracture technology for brittle materials p 192 N88-22417
- Fracture resistance of a TiB₂ particle/SiC matrix composite at elevated temperature
[NASA-TM-100967] p 107 N88-26482
- SALIK, J.**
Analysis of plasma nitrided steels p 88 A88-38936
- SALIK, JOSHUA**
Ion-beam nitriding of steels
[NASA-CASE-LEW-14104-2] p 91 N88-14179
- SALIKUDDIN, M.**
Acoustically excited heated jets. 1: Internal excitation
[NASA-CR-4129-PT-1] p 12 N88-23751
Acoustically excited heated jets. 2: In search of a better understanding
[NASA-CR-4129-PT-2] p 12 N88-23752
Acoustically excited heated jets. 3: Mean flow data
[NASA-CR-4129-PT-3] p 12 N88-23753
- SALMON, J. THADDEUS**
Feasibility of hydroxyl concentration measurements by laser-saturated fluorescence in high-pressure flames p 77 A88-17218
- SALTSMAN, J. F.**
Calculation of thermomechanical fatigue life based on isothermal behavior p 181 A88-26450
Evaluation of structural analysis methods for life prediction p 190 N88-21511
- SALTSMAN, JAMES F.**
An update of the total-strain version of SRP p 86 A88-35910
Life prediction of thermomechanical fatigue using total strain version of strainrange partitioning (SRP): A proposal
[NASA-TP-2779] p 187 N88-15263
- SALZMAN, JACK**
Noncontact temperature measurements in the microgravity fluids and transport phenomena discipline p 113 N88-23901
- SAMIMY, M.**
Performance of laser Doppler velocimeter with polydisperse seed particles in high speed flows
[AIAA PAPER 88-0425] p 157 A88-22317
Structure of a reattaching supersonic shear flow
[AIAA PAPER 88-3615] p 8 A88-48901
- SAMIR, U.**
Comment on 'Ram ion scattering caused by Space Shuttle v x B induced differential charging' by I. Katz and V. A. Davis p 204 A88-35775
- SAMUELSEN, G. S.**
K-epsilon turbulence model assessment with reduced numerical diffusion for coaxial jets
[AIAA PAPER 88-0342] p 137 A88-22251
Aerothermal modeling program, phase 2 p 146 N88-11149
- SANBORN, JAMES A.**
Development of composite facets for the surface of a space-based solar dynamic concentrator p 54 A88-18230
- SANDERCOCK, DONALD M.**
Design point variation of 3-D loss and deviation for axial compressor middle stages
[ASME PAPER 88-GT-57] p 8 A88-54189
- SANDERS, BOBBY W.**
Ground tests confirm the promise of hypersonic propulsion p 2 A88-10369
- SANDERS, WILLIAM A.**
Nondestructive evaluation of sintered ceramics p 177 N88-22416
Improved processing of Si₃N₄ p 107 N88-23882
- SANDKUHL, ANN L.**
Chemical durability of high-temperature superconductor YBa₂Cu₃O_{7-x} in aqueous environments p 78 A88-25023
Effect of fluoride doping on the transition temperature of YBa₂Cu₃O_{7-x} (6.5 + delta) p 220 A88-29297
- SANKAR, L. N.**
Application of Navier-Stokes analysis to stall flutter p 38 N88-23249
- SANTORO, G. J.**
Experiments for the determination of convective diffusion heat/mass transfer to burner rig test targets comparable in size to jet stream diameter p 140 A88-41574
- SANTORO, GILBERT J.**
Experimental verification of vapor deposition rate theory in high velocity burner rigs p 91 N88-11179
- SANZ, JOSE M.**
Automated design of controlled diffusion blades
[NASA-TM-100251] p 9 N88-13304
- SARAZIN, J. R.**
Channel formation in Pb-Sn, Pb-Sb, and Pb-Sn-Sb alloy ingots and comparison with the system NH₄Cl-H₂O p 89 A88-46038
- SARIPALLI, K. R.**
Unsteady features of jets in lift and cruise modes for VTOL aircraft
[SAE PAPER 872359] p 6 A88-37220

- SATER, B.**
Development of 8 cm x 8 cm silicon gridded back solar cell for space station p 200 A88-34312
- SAUNDERS, ALAN L.**
Experimental radio frequency link for Ka-band communications applications [NASA-TM-100824] p 43 N88-24659
- SAUNDERS, NEAL T.**
Impact and promise of NASA aeropropulsion technology p 31 N88-16698
- SAVAGE, M.**
Computerized life and reliability modelling for turboprop transmissions [AIAA PAPER 88-2979] p 100 A88-48031
Computerized life and reliability modelling for turboprop transmissions [NASA-TM-100918] p 173 N88-23220
- SAVILLE, D. A.**
Growth of needle-shaped crystals in the presence of convection p 111 A88-37715
NASA research Program: The roles of fluid motion and other transport phenomena in the morphology of materials [NASA-CR-182801] p 222 N88-25327
- SAWLIVALA, M.**
Application of several variable-valve-timing concepts to an LHR engine [ASME PAPER 87-ICE-29] p 19 A88-15119
- SAYEGH, SOHEIL**
A flexible on-board demultiplexer/demodulator [AIAA PAPER 88-0811] p 123 A88-27558
- SCHARRER, J. K.**
Theory versus experiment for the rotordynamic coefficients of labyrinth gas seals. I - A two control volume model p 167 A88-31535
Theory versus experiment for the rotordynamic coefficients of labyrinth gas seals. II - A comparison to experiment p 167 A88-31536
- SCHERRER, ROBERT J.**
Primordial nucleosynthesis with decaying particles. I - Entropy-producing decays. II - Inert decays p 217 A88-47477
- SCHERSON, DANIEL**
I-BIEM, an iterative boundary integral equation method for computer solutions of current distribution problems with complex boundaries: A new algorithm. I - Theoretical p 205 A88-27795
- SCHUEERMANN, C. M.**
Preliminary study of niobium alloy contamination by transport through helium p 94 N88-24279
- SCHUEERMANN, COULSON M.**
Fatigue failure of regenerator screens in a high frequency Stirling engine p 179 N88-24491
- SCHICK, WILBUR R.**
Spray automated balancing of rotors: Methods and materials [NASA-CR-182151] p 41 N88-29825
- SCHIEBLE, J.**
Improved silicon nitride for advanced heat engines [NASA-CR-175006] p 102 N88-15886
- SCHLOSSER, HERBERT**
Universality relationships in condensed matter - Bulk modulus and sound velocity p 213 A88-43950
- SCHMIDT, DAVID K.**
Cooperative synthesis of control and display augmentation for a STOL aircraft in the approach and landing task [AIAA PAPER 88-4182] p 37 A88-50272
- SCHMIDT, JAMES F.**
Application of advanced computational codes in the design of an experiment for a supersonic throughflow fan rotor [ASME PAPER 87-GT-160] p 2 A88-11072
Design and performance of controlled-diffusion stator compared with original double-circular-arc stator [SAE PAPER 871783] p 20 A88-30777
- SCHMIDT, RICHARD J.**
A hypermatrix formulation for subspace iteration p 205 A88-15427
- SCHMIDT, RODNEY C.**
Two-equation low-Reynolds-number turbulence modeling of transitional boundary layer flows characteristic of gas turbine blades [NASA-CR-4145] p 153 N88-23185
- SCHNEIDER, JUDY**
Orbital transfer vehicle 3000 LBF thrust chamber assembly hot fire test program [NASA-CR-182145] p 66 N88-29858
- SCHNEIDER, S. J.**
Measurements of natural circulation flow in a scale model PWR reactor system during postulated degraded core accidents using laser anemometry p 159 A88-43917
A life test of a 22-Newton (5-lbf) hydrazine rocket [NASA-TM-100232] p 57 N88-11750
- SCHNEIDER, STEVEN J.**
Space Station propulsion system technology p 54 A88-21255
Auxiliary propulsion technology for advanced Earth-to-orbit vehicles [NASA-TM-100237] p 58 N88-14127
Weight savings in aerospace vehicles through propellant scavenging [NASA-TM-100900] p 44 N88-25470
- SCHOCK, HAROLD J.**
Regressed relations for forced convection heat transfer in a direct injection stratified charge rotary engine [NASA-TM-100124] p 25 N88-13345
Liquid sprays and flow studies in the direct-injection diesel engine under motored conditions [NASA-TM-100135] p 31 N88-18594
- SCHOCK, HAROLD J., JR.**
Engine flow visualization using a copper vapor laser p 158 A88-34479
- SCHOENDORF, JOHN F.**
Creep fatigue life prediction for engine hot section materials (isotropic): Third year progress review p 186 N88-11173
- SCHRAG, R. L.**
Electro-impulse de-icing electrodynamic solution by discrete elements [AIAA PAPER 88-0018] p 17 A88-22016
- SCHRAG, ROBERT L.**
Theoretical analysis of the electrical aspects of the basic electro-impulse problem in aircraft de-icing applications [NASA-CR-180845] p 15 N88-13310
- SCHRAMM, DAVID**
Primordial lithium - New reaction rates, new abundances, new constraints p 226 A88-31145
- SCHRAMM, DAVID N.**
Cosmic string induced peculiar velocities p 226 A88-28762
- SCHREIBER, H. A.**
Experimental investigation of the performance of a supersonic compressor cascade [ASME PAPER 88-GT-306] p 9 A88-54375
- SCHREIBER, JEFFREY G.**
Comparison of measured and calculated forces on the RE-1000 free-piston Stirling engine displacer p 185 A88-11966
RE-1000 free-piston Stirling engine hydraulic output system description [NASA-TM-100185] p 223 N88-10700
The design and fabrication of a Stirling engine heat exchanger module with an integral heat pipe [NASA-TM-101296] p 203 N88-26732
- SCHREINER, K. E.**
Control considerations for high frequency, resonant, power processing equipment used in large systems p 51 A88-11829
- SCHRITZ, B.**
Parched elasto hydrodynamic lubrication film thickness measurement in an instrument ball bearing [STLE PREPRINT 88-AM-6G-1] p 169 A88-51082
- SCHULTE, ROGER R.**
Lewis Information Network (LINK): Background and overview [NASA-TM-100162] p 117 N88-11925
- SCHUMANN, LAWRENCE F.**
A method for calculating turbulent boundary layers and losses in the flow channels of turbomachines [ASME PAPER 87-GT-225] p 2 A88-11121
- SCHUSTER, J. C.**
High-temperature oxidation/corrosion of iron-based superalloys p 81 A88-10029
- SCHWAB, J. R.**
Three-dimensional elliptic grid generation technique with application to turbomachinery cascades [NASA-TM-101330] p 155 N88-30078
- SCHWARTZ, R. J.**
Solar energy conversion through the interaction of plasmons with tunnel junctions. Part A: Solar cell analysis. Part B: Photoconductor analysis [NASA-CR-183044] p 203 N88-27621
- SCHWARTZBART, A.**
Noncontacting measurement technologies for space propulsion condition monitoring p 158 A88-29818
- SCHWARZE, GENE E.**
A study of Schwarz converters for nuclear powered spacecraft p 51 A88-11823
Neutron effects on the electrical and switching characteristics of NPN bipolar power transistors p 129 N88-24463
Space power radiation cooled dc transmission line analysis p 129 N88-24506
- SCOTT, A.**
A millimeter-wave tunnel Ladder TWT [NASA-CR-182184] p 130 N88-28239
- SCOTT, J. N.**
Numerical simulation of self-sustained and forced oscillations in jet shear layers p 3 A88-14155
- Navier-Stokes solutions of flowfield characteristics produced by ice accretion [AIAA PAPER 88-0290] p 137 A88-22210
A numerical investigation of the influence of heating on the excitation of high and low Mach number jet flows [ASME PAPER 87-WA/NCA-13] p 144 A88-51343
- SEASHOLTZ, R. G.**
Advanced high temperature instrumentation for hot section research applications p 159 A88-54139
- SEASHOLTZ, RICHARD G.**
Zoom lens compensator for a cylindrical window in laser anemometer uses p 217 A88-17221
Recent advances in high temperature instrumentation for hot section applications [NASA-TM-100282] p 161 N88-14339
Comparison of the bidirectional reflectance distribution function of various surfaces [NASA-TM-101317] p 218 N88-28760
- SEISER, K. M.**
Experiments to ensure Space Station fire safety - A challenge [AIAA PAPER 88-0540] p 41 A88-22405
- SENA, J. T.**
Integrated heat pipe-thermal storage system performance evaluation p 132 A88-11803
Development of an integrated heat pipe-thermal storage system for a solar receiver [NASA-TM-101099] p 202 N88-22458
- SENA, J. TOM**
Development of an integrated heat pipe-thermal storage system for a solar receiver [AIAA PAPER 88-2683] p 141 A88-43746
- SENG, GARY T.**
High-temperature electronics p 128 N88-15797
Fiber optics for controls p 218 N88-15798
Overview of NASA research in fiber optics for aircraft controls [NASA-TM-100919] p 35 N88-25458
- SERAFINI, TITO T.**
High temperature polymer matrix composites p 70 A88-36775
- SEROVY, GEORGE K.**
Design point variation of 3-D loss and deviation for axial compressor middle stages [ASME PAPER 88-GT-57] p 8 A88-54189
- SESHADRI, SRINIVASA G.**
Fracture resistance of a TiB₂ particle/SiC matrix composite at elevated temperature [NASA-TM-100967] p 107 N88-26482
- SETTER, ROBERT N.**
A distributed data acquisition system for aeronautics test facilities p 39 A88-33065
- SETTLES, GARY S.**
Skin friction measurements by laser interferometry in swept shock wave/turbulent boundary-layer interactions [AIAA PAPER 88-0497] p 5 A88-22364
- SEUME, J. R.**
Description of an oscillating flow test program p 133 A88-11963
- SEUME, JORGE R.**
A survey of oscillating flow in Stirling engine heat exchangers [NASA-CR-182108] p 152 N88-22322
- SEYMOUR, P. J.**
Phase-resolved heat-flux measurements on the blade of a full-scale rotating turbine [ASME PAPER 88-GT-173] p 145 A88-54267
- SHAFFER, NANETTE**
Stability of the electrical resistivity of bromine, iodine monochloride, copper(II) chloride, and nickel(II) chloride intercalated pitch-based graphite fibers p 100 A88-49403
- SHAKER, F.**
Modal test/analysis correlation for the Centaur G prime launch vehicle p 44 A88-18631
- SHALKHAUSER, KURT A.**
Bit-error-rate testing of high-power 30-GHz traveling-wave tubes for ground-terminal applications p 122 A88-19781
- SHALKHAUSER, MARY JO W.**
Satellite ground-terminal user simulation [NASA-TM-100234] p 118 N88-14260
- SHALTENS, RICHARD K.**
A comparison of Stirling engines for use with a 25 kW dish-electric conversion system p 53 A88-11943
Phase 1 results from the Stirling-powered vehicle project [NASA-TM-100978] p 225 N88-27980
- SHAMROTH, S. J.**
Flow in a model turbine stator p 148 N88-11163
- SHANNON, JOHN L., JR.**
The effect of texture on the crack growth resistance of alumina [NASA-TM-100250] p 102 N88-14206
Fracture mechanics p 194 N88-23877

- SHAPIRO, W.**
Analysis and design of a gas-lubricated, sectored, floating ring seal
[ASME PAPER 87-TRIB-55] p 166 A88-23310
- SHAPIRO, WILBUR**
Seal technology for liquid oxygen (LOX) turbopumps
[NASA-CR-174866] p 171 N88-13603
- SHAW, B. D.**
Sooting and disruption in spherically symmetrical combustion of decane droplets in air
[IAF PAPER 87-403] p 77 A88-16076
- SHAW, NANCY J.**
Structure and grain coarsening during the processing of engineering ceramics
[NASA-TM-100235] p 101 N88-11838
- SHAW, R. J.**
Analytical determination of propeller performance degradation due to ice accretion p 19 A88-19669
- SHAW, ROBERT J.**
The NASA aircraft icing research program p 15 N88-15803
NASA's rotorcraft icing research program p 15 N88-16641
- SHAWHAN, S. D.**
Plasma wave turbulence around the shuttle - Results from the Spacelab-2 flight p 218 A88-47783
- SHAY, R. M., JR.**
A nonlinear viscoelastic constitutive equation - Yield predictions in multiaxial deformations p 185 A88-54912
- SHEER, IRVING**
Techniques utilized in the simulated altitude testing of a 2D-CD vectoring and reversing nozzle
[NASA-TM-100872] p 40 N88-25464
- SHEFFLER, K. D.**
Thermal barrier coating life prediction model development p 171 N88-11185
- SHEFFLER, KEITH D.**
Current status and future trends in turbine application of thermal barrier coatings
[ASME PAPER 88-GT-286] p 169 A88-54355
- SHEH, M. Y.**
Anisotropic constitutive modeling for nickel base single crystal superalloys using a crystallographic approach
[AIAA PAPER 88-2440] p 85 A88-32357
- SHEH, MICHAEL Y.**
Anisotropic constitutive modeling for nickel-base single crystal superalloys
[NASA-CR-182157] p 95 N88-29961
- SHEPHERD, I. G.**
The structure and dynamics of reacting plane mixing layers p 136 A88-20871
- SHERWOOD, J. A.**
A constitutive model with damage for high temperature superalloys p 93 N88-21510
- SHETTY, D. K.**
Effects of subcritical crack growth on fracture toughness of ceramics assessed in chevron-notched three-point bend tests
[ASME PAPER 88-GT-185] p 185 A88-54276
Microstructural effects on fracture toughness of polycrystalline ceramics in combined mode I and mode II loading
[ASME PAPER 88-GT-208] p 101 A88-54294
- SHIAO, MICHAEL C.**
Probabilistic structural analysis of aerospace components using NESSUS
[AIAA PAPER 88-2373] p 182 A88-32310
Probabilistic structural analysis computer code (NESSUS) p 191 N88-22397
- SHIH, TOM I-PING**
Mathematical models for the numerical study of turbulent flows p 140 A88-39472
- SHIOHARA, Y.**
Solidification of undercooled Ni-Sn eutectic alloy under microgravity conditions in the Space Shuttle p 110 A88-28557
Dendritic growth of undercooled nickel-tin. III p 86 A88-32887
- SHONG, D. S.**
Containerless processing of undercooled melts p 110 A88-28554
- SHUEN, JIAN SHUN**
Numerical study of chemically reacting flows using an LU scheme
[AIAA PAPER 88-0436] p 5 A88-24825
Numerical study of chemically reacting flows using an LU scheme
[NASA-CR-180882] p 26 N88-14094
- SHUEN, JIAN-SHUN**
Numerical simulation of hypersonic inlet flows with equilibrium or finite rate chemistry
[AIAA PAPER 88-0273] p 5 A88-27717
Numerical study of multicomponent droplet vaporization at near critical conditions
[AIAA PAPER 88-0637] p 108 A88-27721
- Particle-laden weakly swirling free jets - Measurements and predictions
[AIAA PAPER 88-3138] p 142 A88-48757
Splitting of inviscid fluxes for real gases
[AIAA PAPER 88-3526] p 142 A88-48782
Splitting of inviscid fluxes for real gases
[NASA-TM-100856] p 211 N88-21717
Particle-laden weakly swirling free jets: Measurements and predictions
[NASA-TM-100920] p 34 N88-24639
- SHYNE, RICKEY J.**
Experimental evaluation of turning vane designs for high-speed and coupled fan-drive corners of 0.1-scale model of NASA Lewis Research Center's proposed altitude wind tunnel
[NASA-TP-2681] p 40 N88-17686
Analysis and optimization of truncated scarf nozzles subject to external flow conditions
[NASA-TM-100955] p 14 N88-29746
- SHYNE, RYCKEY**
Experimental evaluation of corner vanes - Summary
[SAE PAPER 871784] p 39 A88-30778
- SIBERT, L.**
Toluene stability Space Station Rankine power system p 50 A88-11794
- SIDI, AVRAM**
An algorithm for a generalization of the Richardson extrapolation process p 209 A88-32840
Convergence acceleration for vector sequences and applications to computational fluid dynamics
[NASA-TM-101327] p 212 N88-30377
- SIEGEL, R.**
Transient radiative cooling of a layer filled with solidifying drops p 135 A88-20169
- SIEGEL, ROBERT**
Radiative cooling of a solidifying droplet layer including absorption and scattering p 133 A88-15749
Transient radiative cooling of an absorbing and scattering cylinder - A separable solution p 140 A88-41409
- SIEVERS, G. KEITH**
NASA advanced turboprop research and concept validation program
[NASA-TM-100891] p 34 N88-22902
- SIMITSES, G. J.**
Thermo-elasto-viscoplastic analysis of problems in extension and shear p 183 A88-41042
Analysis of shell-type structures subjected to time-dependent mechanical and thermal loading
[NASA-CR-181409] p 185 N88-10388
Analysis of shell-type structures subjected to time-dependent mechanical and thermal loading
[NASA-CR-182705] p 189 N88-20668
Non-isothermal elastoviscoplastic analysis of planar curved beams p 190 N88-21526
- SIMMONS, HAROLD E.**
Cast iron-base alloy for cylinder/regenerator housing
[NASA-CR-182116] p 92 N88-19613
- SIMON, T. W.**
Measurements of the turbulent transport of heat and momentum in convexly curved boundary layers - Effects of curvature, recovery and free-stream turbulence
[ASME PAPER 87-GT-199] p 131 A88-11103
Description of an oscillating flow test program p 133 A88-11963
Development of a special-purpose test surface guided by uncertainty analysis - Introduction of a new uncertainty analysis step
[AIAA PAPER 88-0169] p 39 A88-22121
- SIMON, TERENCE W.**
A survey of oscillating flow in Stirling engine heat exchangers
[NASA-CR-182108] p 152 N88-22322
- SIMONEAU, R. J.**
Review and assessment of the database and numerical modeling for turbine heat transfer p 24 A88-54141
- SIMONEAU, ROBERT J.**
HOST turbine heat transfer program summary
[NASA-TM-100280] p 149 N88-14320
Turbomachinery p 28 N88-15792
Heat transfer in aerospace propulsion
[NASA-TM-100874] p 154 N88-23957
- SIMONIS, J. C.**
Bladed disk assemblies; Proceedings of the Eleventh Biennial Conference on Mechanical Vibration and Noise, Boston, MA, Sept. 27-30, 1987 p 20 A88-31608
- SIMONS, R. N.**
Detection of radio-frequency modulated optical signals by two and three terminal microwave devices p 117 A88-50305
- SIMONS, RAINEE N.**
Microwave performance of an optically controlled AlGaAs/GaAs high electron mobility transistor and GaAs MESFET p 123 A88-24911
High Tc screen-printed YBa₂Cu₃O_{7-x} films - Effect of the substrate material p 127 A88-49760
- Modeling of some coplanar waveguide discontinuities
[NASA-TM-100808] p 119 N88-17880
Synthesis and characterization of high-T(sub c) screen-printed Y-Ba-Cu-O films on alumina
[NASA-TM-100860] p 222 N88-22805
Optoelectronic gain control of a microwave single stage GaAs MESFET amplifier
[NASA-CR-182201] p 131 N88-30055
- SINGER, J.**
Phase purity of NiCo₂O₄, a catalyst candidate for electrolysis of water
[NASA-TM-100239] p 69 N88-13385
- SINGER, JOSEPH**
Evaluation studies on carbon supported catalysts for oxygen reduction in alkaline medium p 77 A88-16643
Electrocatalytic reduction of oxygen on modified oxide surfaces
[NASA-TM-101333] p 81 N88-29952
- SINGH, D.**
Effects of subcritical crack growth on fracture toughness of ceramics assessed in chevron-notched three-point bend tests
[ASME PAPER 88-GT-185] p 185 A88-54276
Microstructural effects on fracture toughness of polycrystalline ceramics in combined mode I and mode II loading
[ASME PAPER 88-GT-208] p 101 A88-54294
- SINGH, N. B.**
Preparation of multistage zone-refined materials for thermochemical standards p 111 A88-43172
- SINGH, NARSINGH BAHADUR**
Characterization of directionally solidified lead chloride p 111 A88-43170
- SINGH, RAJENDRA**
A review of gear housing dynamics and acoustics literature
[NASA-CR-183110] p 175 N88-26675
- SINGH, VAKIL**
On the cyclic stress-strain behaviour of a Ni-base superalloy at room temperature p 84 A88-24521
- SITARAM, N.**
Effect of stage loading on endwall flows in an axial flow compressor rotor
[ASME PAPER 88-GT-111] p 145 A88-54229
- SLABE, M. E.**
Differential scanning calorimetric survey of brominated PAN, pitch-based and vapor-grown fibers p 98 A88-32854
- SLABE, MELISSA E.**
Stability of the electrical resistivity of bromine, iodine monochloride, copper(II) chloride, and nickel(II) chloride intercalated pitch-based graphite fibers p 100 A88-49403
- SLABY, JACK G.**
1987 overview of free-piston Stirling technology for space power application p 53 A88-11942
Overview of free-piston Stirling engine technology for space power application
[NASA-TM-88886] p 223 N88-12427
The 1988 overview of free-piston Stirling technology for space power at the NASA Lewis Research Center
[NASA-TM-100795] p 61 N88-22934
Overview of NASA Lewis Research Center free-piston Stirling engine technology activities applicable to space power systems p 202 N88-24255
- SLATER, HOWARD A.**
Reduction of temperature rise in high-speed photography p 160 A88-55254
Reduction of temperature rise in high-speed photography
[NASA-TM-100222] p 160 N88-11100
- SLINEY, HAROLD E.**
The effects of atmosphere on the tribological properties of a chromium carbide based coating for use to 760 C p 98 A88-32372
Mechanical strength and tribological behavior of ion-beam-deposited boron nitride films on non-metallic substrates p 98 A88-32866
Sputtered silver films to improve chromium carbide based solid lubricant coatings for use to 900 C p 100 A88-47563
Coatings for high-temperature bearings and seals
[NASA-TM-100249] p 102 N88-13453
Hot piston ring/cylinder liner materials: Selection and evaluation
[NASA-TM-100276] p 102 N88-15872
Sputtered silver films to improve chromium carbide based solid lubricant coatings for use to 900 C
[NASA-TM-100783] p 102 N88-15885
Self-lubricating coatings for high-temperature applications p 103 N88-16703
Friction and wear of monolithic and fiber reinforced silicon-ceramics sliding against IN-718 alloy at 25 to 800 C in atmospheric air at ambient pressure
[NASA-TM-100294] p 103 N88-17796

- SMALLEY, ANTHONY J.**
Spray automated balancing of rotors: Methods and materials
[NASA-CR-182151] p 41 N88-29825
- SMALLEY, ROBERT R.**
A distributed data acquisition system for aeronautics test facilities p 39 A88-33065
- SMEGGILL, J. G.**
High-temperature oxidation/corrosion of iron-based superalloys p 81 A88-10029
- SMIALEK, J. L.**
Molten salt corrosion of SiC and Si₃N₄ p 107 N88-23885
- SMIALEK, JAMES L.**
Multielement mapping of alpha-SiC by scanning Auger microscopy p 158 A88-27617
Adherent Al₂O₃ scales produced on undoped NiCrAl alloys p 85 A88-30269
The effect of sulfur and zirconium Co-doping on the oxidation of NiCrAl [NASA-TM-100209] p 90 N88-10940
- SMITH, ARTHUR F.**
Analysis and test evaluation of the dynamic stability of three advanced turboprop models at zero forward speed [NASA-CR-175025] p 26 N88-14095
Analysis and test evaluation of the dynamic response and stability of three advanced turboprop models at low forward speed [NASA-CR-175026] p 27 N88-14096
- SMITH, TAMARA A.**
Boundary layer development as a function of chamber pressure in the NASA Lewis 1030:1 area ratio rocket nozzle [AIAA PAPER 88-3301] p 144 A88-50786
Boundary layer development as a function of chamber pressure in the NASA Lewis 1030:1 area ratio rocket nozzle [NASA-TM-100917] p 154 N88-25841
- SMITH, TODD E.**
Life and reliability of rotating disks p 178 N88-22428
Aeroelastic forced response analysis of turbomachinery p 34 N88-23247
- SMITH, WILLIAM L.**
System Development Working Group report p 48 N88-10092
- SMITHRICK, JOHN J.**
Effect of storage and LEO cycling on manufacturing technology IPV nickel-hydrogen cells p 53 A88-11917
Effect of LEO cycling at shallow depths of discharge on MANTECH IPV nickel-hydrogen cells [NASA-TM-101300] p 203 N88-25978
- SMYTHE, MARK E.**
Improved perfluoroalkyl ether fluid development p 68 A88-28624
- SNYDER, AARON**
Numerical simulation of subsonic and transonic propeller flow [NASA-TM-100163] p 11 N88-20262
- SNYDER, PAUL G.**
Variable angle spectroscopic ellipsometry - Application to GaAs-AlGaAs multilayer homogeneity characterization p 220 A88-40139
- SNYDER, PHILIP H.**
The design of an air-cooled metallic high temperature radial turbine [AIAA PAPER 88-2872] p 22 A88-45011
- SO, RONALD M. C.**
Low Reynolds number modeling of turbulent flows with and without wall transpiration p 136 A88-21983
- SOCIE, DARRELL**
Fatigue damage mapping p 193 N88-22423
- SOCIE, DARRELL F.**
The relationship between observed fatigue damage and life estimation models [NASA-CR-182191] p 196 N88-27611
- SOCKOL, PETER M.**
Navier-Stokes cascade analysis with a stiff k-epsilon turbulence solver [AIAA PAPER 88-0594] p 5 A88-22444
Navier-Stokes cascade analysis with a stiff Kappa-Epsilon turbulence solver [NASA-TM-100218] p 9 N88-10778
Turbomachinery p 28 N88-15792
Chemical reacting flows p 79 N88-15793
- SOH, W. Y.**
Developing fluid flow in a curved duct of square cross-section and its fully developed dual solutions p 139 A88-30957
- SOKOLOV, V.**
Two stage dual gate MESFET monolithic gain control amplifier for Ka-band p 124 A88-29821
A 30 GHz monolithic receive module technology assessment [NASA-CR-180825] p 129 N88-23084
- SOKOLOWSKI, D. E.**
NASA HOST project overview p 24 A88-54138
Views on the impact of HOST p 24 A88-54146
- SOKOLOWSKI, DANIEL E.**
Toward improved durability in advanced aircraft engine hot sections; Proceedings of the Thirty-third ASME International Gas Turbine and Aeroengine Congress and Exposition, Amsterdam, Netherlands, June 5-9, 1988 p 24 A88-54137
Aircraft engine hot section technology: An overview of the HOST Project p 29 N88-15804
- SOLOMON, H. D.**
Low cycle fatigue [ASTM STP-942] p 86 A88-35901
- SOLOMON, ROBERT F.**
Techniques utilized in the simulated altitude testing of a 2D-CD vectoring and reversing nozzle [NASA-TM-100872] p 40 N88-25464
- SONIN, A. A.**
Vapor condensation rate at a turbulent liquid interface, for application to cryogenic hydrogen [AIAA PAPER 88-0559] p 137 A88-22419
Vapor condensation on a turbulent liquid interface p 150 N88-15939
- SOTOS, RAYMOND G.**
Mass transport phenomena between bubbles and dissolved gases in liquids under reduced gravity conditions [AIAA PAPER 88-0450] p 138 A88-27719
Mass transport phenomena between bubbles and dissolved gases in liquids under reduced gravity conditions [NASA-TM-100273] p 80 N88-18672
- SOVEY, JAMES S.**
Water-propellant resistojets for man-tended platforms [IAF PAPER 87-259] p 54 A88-15975
Space Station propulsion system technology p 54 A88-21255
Space station propulsion [NASA-TM-100216] p 57 N88-11746
Performance and lifetime assessment of MPD arc thruster technology [NASA-TM-101293] p 66 N88-29860
- SOVIE, RONALD J.**
SP-100 Advanced Technology Program p 52 A88-11846
Power systems for production, construction, life support and operations in space [NASA-TM-100838] p 60 N88-21254
Comparative analysis of the space power architecture studies [NASA-TM-100977] p 66 N88-28090
- SPALVINS, T.**
Ion nitriding; Proceedings of the International Conference, Cleveland, OH, Sept. 15-17, 1986 p 114 A88-38926
Plasma assisted surface coating/modification processes - An emerging technology p 114 A88-38927
- SPALVINS, TALIVALDIS**
Status and directions of modified tribological surfaces by ion processes [NASA-TM-101304] p 115 N88-28176
- SPENCE, R. L.**
Numerical arc segmentation algorithm for a radio conference - A software tool for communication satellite systems planning [AIAA PAPER 88-0788] p 212 A88-27531
Numerical arc segmentation algorithm for a radio conference: A software tool for communication satellite systems planning [NASA-TM-100789] p 46 N88-22919
- SPENCE, RODNEY L.**
An allotment planning concept and related computer software for planning the fixed satellite service at the 1988 space WARC p 116 A88-36482
An allotment planning concept and related computer software for planning the fixed satellite service at the 1988 space WARC [NASA-TM-100244] p 117 N88-11944
Numerical arc segmentation algorithm for a radio conference-NASARC (version 2.0) technical manual [NASA-TM-100160] p 118 N88-15910
Numerical arc segmentation algorithm for a radio conference-NASARC, version 2.0: User's manual [NASA-TM-100161] p 119 N88-16928
Complementary satellite sound broadcasting systems: A NASA assessment for the Voice of America [NASA-TM-100300] p 119 N88-17899
A laser communication experiment utilizing the ACT satellite and an airborne laser transceiver [NASA-TM-100792] p 164 N88-18910
- SPENCER, B. F., JR.**
An expert system for probabilistic description of loads on space propulsion system structural components [AIAA PAPER 88-2371] p 182 A88-32308
- SPENCER, D. A.**
Aeroacoustics of advanced STOVL aircraft plumes [SAE PAPER 872358] p 215 A88-30998
Aeroacoustics of advanced STOVL aircraft plumes [SAE PAPER 872358] p 215 A88-37219
- SPERA, DAVID A.**
Large-scale wind turbine structures p 202 N88-22429
- SPRING, SAMUEL A.**
An experimental mapping of the flow field behind a glaze ice shape on a NACA 0012 airfoil [NASA-CR-180847] p 10 N88-15766
- SPRINGER, T.**
Optical measurements pertaining to Space Station solar dynamic power systems [IAF PAPER 87-229] p 42 A88-15954
- SRINIVASAN, R.**
Dilution jet mixing program, phase 3 p 147 N88-11153
Transition mixing study empirical model report [NASA-CR-182139] p 155 N88-30076
- SRINIVASAN, RAM**
An empirical model of the effects of curvature and convergence on dilution jet mixing [NASA-TM-100896] p 34 N88-24640
- SRINIVASAN, YAKULA S.**
Evaluation studies on carbon supported catalysts for oxygen reduction in alkaline medium p 77 A88-16643
Electrocatalytic reduction of oxygen on modified oxide surfaces [NASA-TM-101333] p 81 N88-29952
- SRINIVASEN, RAM**
An empirical model of the effects of curvature and convergence on dilution jet mixing [AIAA PAPER 88-3180] p 23 A88-50783
- SRIVASTAVA, R.**
Application of Navier-Stokes analysis to stall flutter p 38 N88-23249
- SRIVASTAVA, RAKESH**
The effects of rotational flow, viscosity, thickness, and shape on transonic flutter dip phenomena [AIAA PAPER 88-2348] p 182 A88-32289
The effects of rotational flow, viscosity, thickness, and shape on transonic flutter dip phenomena [NASA-TM-100811] p 188 N88-18969
- SROLOVITZ, D. J.**
A microstructural lattice model for strain oriented problems: A combined Monte Carlo finite element technique [NASA-TM-100215] p 90 N88-10939
Monte Carlo simulation of modulated phases [NASA-TM-89654] p 210 N88-12323
- STAHL, B.**
Excitation of instability waves in free shear layers. II - Experiments p 138 A88-26339
- STAHL, D. R.**
Effect of temperature, microstructure, and stress state on the low cycle fatigue behavior of Waspaloy p 87 A88-35922
- STAHL, MARK**
A heater made from graphite composite material for potential deicing application p 17 A88-15724
Synthesis, electrical and thermal conductivities, and potential applications of graphite fluoride fibers p 97 A88-26963
- STANDLEY, HILDA M.**
Adapting high-level language programs for parallel processing using data flow p 207 N88-23234
- STANG, DAVID B.**
Cruise noise of the 2/9 scale model of the Large-scale Advanced Propan (LAP) propeller, SR-7A [AIAA PAPER 87-2717] p 214 A88-16565
Systems for ultrasonic scanning, analysis and imagery p 177 N88-22414
- STANKIEWICZ, N.**
Submillimeter backward wave oscillators p 122 A88-19659
- STARKEN, H.**
Experimental investigation of the performance of a supersonic compressor cascade [ASME PAPER 88-GT-306] p 9 A88-54375
- STASZAK, PAUL RUSSELL**
Hafnia-rich mixed oxide ceramics of the system HfO₂-ZrO₂-TiO₂ for heaters and heat exchangers in electrothermal thrusters: The effects of titania on selected electrical and mechanical properties of Hafnia-rich mixed oxides in the system Hafnia-Zirconia-Titania, volume 1 [NASA-CR-182800-VOL-1] p 105 N88-22197
- STATLER, R. L.**
Radiation and temperature effects in gallium arsenide, indium phosphide, and silicon solar cells p 125 A88-34321
- STEARNS, C. A.**
Effect of alloy composition on the sodium-sulfate induced hot corrosion attack of cast nickel-base superalloys at 900 C p 81 A88-10028

- STEDMAN, JAMES K.**
Stress-life interrelationships associated with alkaline fuel cells p 197 A88-11903
- STEENKEN, W. G.**
E3 10C compressor test analysis of high-speed post-stall data [NASA-CR-179521] p 36 N88-28929
- STEFKO, GEORGE L.**
Porous wind tunnel corrections for counterrotation propeller testing [AIAA PAPER 88-2055] p 6 A88-44490
Porous wind tunnel corrections for counterrotation propeller testing [NASA-TM-100873] p 11 N88-22019
- STEGEMAN, G. I.**
Guided-wave approaches to spectrally selective energy absorption [NASA-CR-182532] p 119 N88-17892
- STEGEMAN, JAMES D.**
Liquid sprays and flow studies in the direct-injection diesel engine under motored conditions [NASA-TM-100135] p 31 N88-18594
- STEIGMAN, GARY**
Primordial lithium - New reaction rates, new abundances, new constraints p 226 A88-31145
- STEINBERG, J. T.**
Plasma wave turbulence around the shuttle - Results from the Spacelab-2 flight p 218 A88-47783
Double-probe potential measurements near the Spacelab 2 electron beam p 204 A88-53464
Exposed high-voltage source effect on the potential of an ionospheric satellite p 218 A88-54992
- STEINKE, RONALD J.**
Application of advanced computational codes in the design of an experiment for a supersonic throughflow fan rotor [ASME PAPER 87-GT-160] p 2 A88-11072
- STEPHENS, J. R.**
B2 aluminides for high temperature applications p 85 A88-31684
Powder processing of nickel and other aluminides by hot consolidation p 87 A88-37158
- STEPHENS, JOSEPH R.**
Hypersonic structures and materials - A progress report p 17 A88-16748
Thermal aging effects in refractory metal alloys p 84 A88-22700
Alloy chemistry and microstructural control to meet the demands of the automotive Stirling engine p 88 A88-40332
High temperature metal matrix composites for future aerospace systems [AIAA PAPER 88-3059] p 71 A88-44745
High temperature metal matrix composites for future aerospace systems [NASA-TM-100212] p 90 N88-10938
Status and prognosis for alternative engine materials [NASA-TM-100903] p 94 N88-24749
Refractory metal alloys and composites for space power systems [NASA-TM-100946] p 95 N88-27310
- STEURER, JOHN W.**
Uncertainty of in-flight thrust determination [SAE AIR 1678] p 16 A88-15228
- STEVENS, GRADY H.**
Complementary satellite sound broadcasting systems: A NASA assessment for the Voice of America [NASA-TM-100300] p 119 N88-17899
- STEVENSON, STEVEN M.**
An evolutionary communications scenario for Mars exploration [NASA-TM-100263] p 118 N88-13515
- STEWART, S. E.**
Thermal barrier coating life prediction model development [ASME PAPER 88-GT-284] p 68 A88-54353
- STEWART, W. A.**
Measurements of natural circulation flow in a scale model PWR reactor system during postulated degraded core accidents using laser anemometry p 159 A88-43917
- STIDHAM, CURTIS**
Arc-textured metal surfaces for high thermal emittance space radiators [NASA-TM-100894] p 94 N88-24754
- STOCK, T. A.**
Probabilistic composite micromechanics [AIAA PAPER 88-2375] p 182 A88-32312
- STOCKER, DENNIS P.**
Laminar diffusion flames under micro-gravity conditions [AIAA PAPER 88-0645] p 78 A88-27722
- STONE, JAMES R.**
Recent advances in low-thrust propulsion technology [AIAA PAPER 88-3283] p 55 A88-48761
- Development of a liquid-fed water resistojet [AIAA PAPER 88-3288] p 142 A88-48762
Status of high power electric propulsion technology p 63 N88-24443
- Development of a liquid-fed water resistojet [NASA-TM-100927] p 174 N88-24968
Recent advances in low-thrust propulsion technology [NASA-TM-100959] p 213 N88-25260
- STONE, N. H.**
Comment on 'Ram ion scattering caused by Space Shuttle v x B induced differential charging' by I. Katz and V. A. Davis p 204 A88-35775
- STOUFFER, D. C.**
Anisotropic constitutive modeling for nickel base single crystal superalloys using a crystallographic approach [AIAA PAPER 88-2440] p 85 A88-32357
A crystallographic model for nickel base single crystal alloys p 89 A88-48182
A constitutive model with damage for high temperature superalloys p 93 N88-21510
- STOUFFER, DONALD C.**
Constitutive modeling for single crystal superalloys p 90 N88-11168
- STRACK, WILLIAM C.**
The challenges and opportunities of supersonic transport propulsion technology [AIAA PAPER 88-2985] p 23 A88-48032
Propulsion challenges and opportunities for high-speed transport aircraft p 30 N88-15809
The challenges and opportunities of supersonic transport propulsion technology [NASA-TM-100921] p 34 N88-23806
- STRANGE, R. R.**
Development of sensors for ceramic components in advanced propulsion systems: Survey and evaluation of measurement techniques for temperature, strain and heat flux for ceramic components in advanced propulsion systems [NASA-CR-182111] p 163 N88-28299
- STRANGE, RICHARD R.**
Development of heat flux sensors for turbine airfoils p 160 N88-11143
- STRANGMAN, T. E.**
Thermal barrier coating life-prediction model development [NASA-CR-179507] p 107 N88-28142
- STRAZISAR, A. J.**
Measurements of the unsteady flow field within the stator row of a transonic axial-flow fan. I - Measurement and analysis technique [ASME PAPER 87-GT-226] p 4 A88-18660
Measurements of the unsteady flow field within the stator row of a transonic axial-flow fan. II - Results and discussion [ASME PAPER 87-GT-227] p 4 A88-18661
- STRAZISAR, ANTHONY J.**
Turbomachinery p 28 N88-15792
- STREHLOW, ROGER A.**
The effect of gravity on premixed flame propagation and extinction in a vertical standard flammability tube p 78 A88-38532
- STRICKER, JOSEF**
Sources of error in heterodyne moire deflectometry p 158 A88-35004
- STROM, B. D.**
Experimental studies in vortex pair motion coincident with a liquid reaction p 142 A88-46316
- STRUMPF, HAL J.**
Advanced heat receiver conceptual design study [NASA-CR-180901] p 203 N88-25977
- STUART, THOMAS A.**
A study of Schwarz converters for nuclear powered spacecraft p 51 A88-11823
A cascaded Schwarz converter for high frequency power distribution p 127 A88-54713
- STUBBS, R. M.**
Technology requirements for an orbiting fuel depot: A necessary element of a space infrastructure [NASA-TM-101370] p 49 N88-29845
- STUDER, A.**
Gravitational macrosegregation in binary Pb-Sn alloy ingots p 111 A88-41211
- STUDER, ANTHONY C.**
Fraction eutectic measurements in slowly cooled Pb - 15 wt percent Sn alloys [NASA-CR-180830] p 94 N88-25531
- STUEBER, THOMAS**
Arc-textured metal surfaces for high thermal emittance space radiators [NASA-TM-100894] p 94 N88-24754
- STUPICA, JOHN**
Radiation damage and defect behavior in proton irradiated lithium-counterdoped n+p silicon solar cells p 125 A88-34340
- STYHR, K. H.**
Improved silicon nitride for advanced heat engines [NASA-CR-175006] p 102 N88-15886
- SUBRAMANIAN, S. V.**
Application of Runge Kutta time marching scheme for the computation of transonic flows in turbomachines [NASA-TM-86997] p 9 N88-12461
- SUDER, K. L.**
Measurements of the unsteady flow field within the stator row of a transonic axial-flow fan. I - Measurement and analysis technique [ASME PAPER 87-GT-226] p 4 A88-18660
Measurements of the unsteady flow field within the stator row of a transonic axial-flow fan. II - Results and discussion [ASME PAPER 87-GT-227] p 4 A88-18661
- SUDER, KENNETH L.**
Design and performance of controlled-diffusion stator compared with original double-circular-arc stator [SAE PAPER 871783] p 20 A88-30777
Experimental study of bypass transition in a boundary layer [NASA-TM-100913] p 153 N88-23186
- SUGANUMA, Y.**
Experimental studies in vortex pair motion coincident with a liquid reaction p 142 A88-46316
- SUL, SEUNG K.**
Field oriented control of an induction machine in a high frequency link power system p 127 A88-54711
- SULLIVAN, J. P.**
Aerothermal modeling program, phase 2 p 146 N88-11149
- SULLIVAN, JOHN P.**
Aerodynamic interaction between propellers and wings [AIAA PAPER 88-0665] p 5 A88-22495
- SULLIVAN, WILLIAM E.**
Large-Scale Advanced Prop-Fan (LAP) blade design [NASA-CR-174790] p 27 N88-14097
- SUN, C. T.**
Dynamic delamination fracture toughness of a graphite/epoxy laminate under impact p 70 A88-29455
- SUNDBERG, GALE R.**
LERC power system autonomy program 1990 demonstration p 52 A88-11861
Benefits of 20 kHz PMAD in a nuclear space station p 129 N88-24256
- SUNDBERG, R.**
The ac power system testbed [NASA-CR-175068] p 127 N88-11948
- SUTCU, M.**
A simplified orthotropic formulation of the viscoplasticity theory based on overstress p 189 N88-21505
- SUTTER, JAMES K.**
Simulation of fluid flows during growth of organic crystals in microgravity p 109 A88-13163
- SWANSON, G. A.**
Fatigue life prediction modeling for turbine hot section materials p 184 A88-54144
Life prediction and constitutive models for engine hot section anisotropic materials program p 186 N88-11175
Fatigue life prediction modeling for turbine hot section materials [NASA-TM-100291] p 187 N88-14453
A constitutive model for an overlay coating p 105 N88-21525
- SWARTZ, C. K.**
Comparative radiation resistance, temperature dependence and performance of diffused junction indium phosphide solar cells p 198 A88-18580
Radiation and temperature effects in gallium arsenide, indium phosphide, and silicon solar cells p 125 A88-34321
Radiation performance of AlGaAs and InGaAs concentrator cells and expected performance of cascade structures p 125 A88-34356
- SWARTZ, CLIFFORD K.**
Radiation damage and defect behavior in proton irradiated lithium-counterdoped n+p silicon solar cells p 125 A88-34340
Performance of GaAs and silicon concentrator cells under 37 MeV proton irradiation p 200 A88-34343
Effects of electron and proton irradiations on n/p and p/n GaAs cells grown by MOCVD [NASA-TM-100199] p 127 N88-10266
Performance of GaAs and silicon concentrator cells under 37 MeV proton irradiation [NASA-TM-100144] p 200 N88-12877
Radiation performance of AlGaAs concentrator cells and expected performance of cascade structures [NASA-TM-100145] p 200 N88-12878
- SWEETING, T. B.**
Advanced Gas Turbine (AGT) Technology Development Project, ceramic component developments [NASA-CR-180871] p 224 N88-20229

SWITZER, COLLEEN A.

Coaxial tube array space transmission line
characterization p 121 A88-11865

SYMONS, E. P.

LeRC cryogenic fluid management program overview
p 150 A88-15928

SZEMENYEI, B.

Improved maintainability of space-based reusable rocket
engines [AIAA PAPER 88-3113] p 55 A88-48037

SZUCH, JOHN R.

Internal fluid mechanics research on supercomputers
for aerospace propulsion systems [NASA-TM-100289] p 149 A88-15188
Application of advanced computational technology to
propulsion CFD [NASA-TM-100843] p 204 A88-19102

T

T'EN, J. S.

A theoretical analysis of the extinction limits of a
methane-air opposed-jet diffusion flame p 77 A88-16497

T'EN, JAMES S.

Modelling ignition characteristics of rich H₂/O₂ mixture
in a monolithic catalytic reactor [AIAA PAPER 88-3224] p 78 A88-46499

TABATA, WILLIAM K.

Automotive Stirling engine development program - A
success p 165 A88-11965

TACINA, ROBERT R.

Space Station propulsion system technology
p 54 A88-21255

TAGHAVI, R.

Space station propulsion [NASA-TM-100216] p 57 A88-11746

TAGHAVI, R.

Controlled excitation of a cold turbulent swirling free
jet [ASME PAPER 87-WA/NCA-18] p 140 A88-41568
Effect of initial tangential velocity distribution on the
mean evolution of a swirling turbulent free jet
[AIAA PAPER 88-3592] p 7 A88-48893
Effect of initial tangential velocity distribution on the
mean evolution of a swirling turbulent free jet
[NASA-TM-100934] p 12 A88-24592

TAM, L. T.

Numerical and analytical study of fluid dynamic forces
in seals and bearings p 167 A88-31534
Numerical modeling of multidimensional flow in seals
and bearings used in rotating machinery [NASA-TM-100779] p 150 A88-16988
Numerical and analytical study of fluid dynamic forces
in seals and bearings [NASA-TM-100268] p 151 A88-18867

TATRO, CHARLES A.

Space Station Photovoltaic power modules
p 56 A88-52333
Photovoltaic power modules for NASA's manned space
station [NASA-TM-100229] p 57 A88-11745

TATTERSON, G. B.

Experimental verification of a secondary recirculation
zone in a labyrinth seal [AIAA PAPER 88-3692] p 168 A88-48971
3-D laser anemometer measurements in a labyrinth
seal [ASME PAPER 88-GT-63] p 169 A88-54195
3-D laser anemometer measurements in an annular
seal [ASME PAPER 88-GT-64] p 169 A88-54196

TAYLOR, A. C., III

Turbulence modeling in hypersonic inlets
[AIAA PAPER 88-2957] p 7 A88-44705

TELESMA, JACK

Accelerated crack growth rate at low Delta K in a single
crystal superalloy p 89 A88-47687
In situ fatigue loading stage inside scanning electron
microscope p 193 A88-22419
Fatigue crack growth behavior of a single crystal alloy
as observed through an in situ fatigue loading stage
[NASA-TM-100863] p 93 A88-22986
Characterization of fatigue crack initiation and
propagation in Ti-6Al-4V with electrical potential drop
technique [NASA-TM-100877] p 195 A88-25937
Accelerated fatigue crack growth behavior of PWA 1480
single crystal alloy and its dependence on the deformation
mode [NASA-TM-100943] p 95 A88-26436

TENEYCK, M. O.

Advanced Gas Turbine (AGT) Technology Development
Project, ceramic component developments
[NASA-CR-180871] p 224 A88-20229

TENNEY, DARREL R.

Hypersonic structures and materials - A progress
report p 17 A88-16748

TEREN, FRED

Space Station electric power system requirements and
design p 50 A88-11782

TEW, ROY C., JR.

Overview of heat transfer and fluid flow problem areas
encountered in Stirling engine modeling
[NASA-TM-100131] p 224 A88-17561

TEWARI, S. N.

Undercooled and rapidly quenched Ni-Mo alloys
p 83 A88-19960
Primary arm spacing in chill block melt spun Ni-Mo
alloys p 89 A88-41655
Effect of melt spinning on grain size and texture in Ni-Mo
alloys p 89 A88-46030

THALLER, LAWRENCE H.

A prediction model of the depth-of-discharge effect on
the cycle life of a storage cell p 197 A88-11896
Stress-life interrelationships associated with alkaline fuel
cells p 197 A88-11903

THEIL, J. A.

Deposition of vanadium oxide films by direct-current
magnetron reactive sputtering p 221 A88-51286

THIEME, LANNY G.

Testing of a variable-stroke Stirling engine
[NASA-TM-100899] p 225 A88-30472

THOMPSON, R. L.

Structural assessment of a Space Station solar dynamic
heat receiver thermal energy storage canister
[AIAA PAPER 88-2487] p 47 A88-31396
Structural analysis methods development for turbine hot
section components p 184 A88-54142
Life assessment of combustor liner using unified
constitutive models p 33 A88-22384
Structural assessment of a space station solar dynamic
heat receiver thermal energy storage canister
p 192 A88-22406

THOMPSON, ROBERT L.

High temperature stress-strain analysis p 185 A88-11170
Structural analysis methods development for turbine hot
section components [NASA-TM-100298] p 188 A88-18967
Finite element (MARC) solution technologies for
viscoplastic analyses p 191 A88-22389
Thermal-structural analyses of Space Shuttle Main
Engine (SSME) hot section components p 61 A88-22404

An efficient Mindlin finite strip plate element based on
assumed strain distribution p 192 A88-22407
Improved finite strip Mindlin plate bending element using
assumed shear strain distributions [NASA-TM-100928] p 196 A88-29195

THOMPSON, W.

Centaur operations at the space station
[NASA-CR-179593] p 49 A88-25473

THOMSON, M. KEMER

Expert systems for space power supply - Design,
analysis, and evaluation p 212 A88-22696

THORNTON, JOHN A.

Deposition of vanadium oxide films by direct-current
magnetron reactive sputtering p 221 A88-51286

TIEN, TA-CHING

Modelling ignition characteristics of rich H₂/O₂ mixture
in a monolithic catalytic reactor [AIAA PAPER 88-3224] p 78 A88-46499

TINETTI, ANA F.

Model helicopter performance degradation with
simulated ice shapes p 17 A88-22783

TIPTON, M. T.

Component specific modeling p 206 A88-11166

TIRMIZI, S.

Dendritic solidification under microgravity conditions
[AIAA PAPER 88-0248] p 110 A88-22186

TIRMIZI, S. H.

Isothermal dendritic growth - A proposed microgravity
experiment p 112 A88-49095

TITRAN, R. H.

Compressive creep behavior of alloys based on 82
FeAl p 82 A88-10043
Characterization of precipitates in a
niobium-zirconium-carbon alloy [NASA-TM-100848] p 93 A88-22981
Creep behavior of tungsten/niobium and
tungsten/niobium-1 percent zirconium composites
p 75 A88-24427

TITRAN, ROBERT H.

Creep behavior of tungsten/niobium and
tungsten/niobium-1 percent zirconium composites
[NASA-TM-100804] p 92 A88-18707
Refractory metal alloys and composites for space power
systems [NASA-TM-100946] p 95 A88-27310

TODD, E. S.

3-D inelastic analysis methods for hot section
components p 206 A88-11165

TODD, J. A.

The high temperature creep deformation of
Si₃N₄-6Y₂O₃-2Al₂O₃ [NASA-CR-183204] p 76 A88-28981

TOMAZIC, WILLIAM A.

Hot piston ring tests [NASA-TM-100256] p 201 A88-14486

TOMLIN, K. H.

Propan test assessment testbed aircraft stability and
control/performance 1/9-scale wind tunnel tests
[NASA-CR-182121] p 17 A88-26360

TONG, M.

Evaluation of structural analysis methods for life
prediction p 190 A88-21511

TONG, M. T.

Structural assessment of a Space Station solar dynamic
heat receiver thermal energy storage canister
[AIAA PAPER 88-2487] p 47 A88-31396
Life assessment of combustor liner using unified
constitutive models p 33 A88-22384
Structural assessment of a space station solar dynamic
heat receiver thermal energy storage canister
p 192 A88-22406

TONG, MICHAEL T.

Thermal finite-element analysis of space shuttle main
engine turbine blade [NASA-TM-100117] p 187 A88-13745

TOOMRE, JURI

Magnetic fields interacting with nonlinear compressible
convection p 226 A88-31163

TOPP, DAVID A.

Control of rotor aerodynamically forced vibrations by
splitters p 23 A88-52684

TORRES, F. J.

Use of a liquid-crystal and heater-element composite
for quantitative, high-resolution heat-transfer coefficients
on a turbine airfoil including turbulence and
surface-roughness effects p 156 A88-10969

TOWNSEND, DENNIS P.

Surface fatigue and failure characteristics of hot-forged
powder metal AISI 4620, AISI 4640, and machined AISI
4340 steel spur gears p 165 A88-14591
Results of NASA/Army transmission research
p 31 A88-16640

Dynamic analysis of multimesh-gear helicopter
transmissions [NASA-TP-2789] p 172 A88-17045

Surface fatigue life of CBN and vitreous ground
carburized and hardened AISI 9310 spur gears
[NASA-TM-100960] p 175 A88-25916

Helicopter transmission research at NASA Lewis
Research Center [NASA-TM-100962] p 175 A88-30128

TREE, D. R.

Design, calibration and error analysis of instrumentation
for heat transfer measurements in internal combustion
engines p 157 A88-18509

TRIBBLE, A. C.

Exposed high-voltage source effect on the potential of
an ionospheric satellite p 218 A88-54992

TRIPP, DAVID E.

Continuous fiber ceramic matrix composites for heat
engine components p 106 A88-22411

TRUBERT, M.

Modal test/analysis correlation for the Centaur G prime
launch vehicle p 44 A88-18631

TRUDELL, JEFFREY J.

Thermal distortion analysis of the space station solar
dynamic concentrator [NASA-TM-100868] p 64 A88-25475

TSAI, FU-SHENG

Computer modeling and simulation of a 20kHz ac
distribution system for Space Station p 51 A88-11827

TSENG, JESSE I. S.

Velocity-coupled flow oscillations in a simulated
solid-propellant rocket environment [AIAA PAPER 88-0543] p 108 A88-27720

TSUNG, WEI-JIUNG

Method for generation of spiral bevel gears with
conjugate gear tooth surfaces [ASME PAPER 86-DET-3] p 165 A88-10973

TURAN, A.

Improved numerical methods for turbulent viscous
recirculating flows p 146 A88-11148
Improved numerical methods for turbulent viscous
recirculating flows [NASA-CR-180852] p 13 A88-25445

TURKEL, ELI

Effects of numerical dissipation on finite-volume
solutions of compressible flow problems
[AIAA PAPER 88-0621] p 5 A88-22469

- TURNBERG, J.**
SR-7A aeroelastic model design report
[NASA-CR-174791] p 36 N88-28928
- TURNBERG, JAY E.**
Large-Scale Advanced Prop-Fan (LAP) blade design
[NASA-CR-174790] p 27 N88-14097
- TURNER, A. E.**
New non-geosynchronous orbits for communications satellites to off-load daily peaks in geostationary traffic
[AAS PAPER 87-547] p 42 A88-10957
- TURNER, ANDREW E.**
Communications satellites in non-geostationary orbits
[AIAA PAPER 88-0842] p 46 A88-27583
- TURNER, GLEN D.**
Low cost Get-Away-Special (GAS) furnace
p 41 A88-28583
- TURNER, MICHAEL S.**
Axions from 1987A p 226 A88-35586
Cosmology and particle physics p 226 A88-39734
Primordial nucleosynthesis with decaying particles. I - Entropy-producing decays. II - Inert decays p 217 A88-47477
- TURNOCK, STEPHEN R.**
Investigation of surface water behavior during glaze ice accretion
[AIAA PAPER 88-0115] p 14 A88-22079
- TUOK, NEIL**
String-driven inflation p 225 A88-27446
- TWEEDT, T. L.**
Experimental investigation of the performance of a supersonic compressor cascade
[ASME PAPER 88-GT-306] p 9 A88-54375
- ## U
- UJIE, Y.**
Containerless processing of undercooled melts
p 110 A88-28554
- ## V
- VALERO, N. A.**
Localization of natural modes of vibration in bladed disks
[ASME PAPER 87-GT-46] p 18 A88-10998
- VALISETTY, R. R.**
An ideal clamping analysis for a cross-ply laminate
p 181 A88-31347
- VALLANCE, J. K.**
Development of the AGT101 regenerator seals
[ASME PAPER 87-GT-173] p 165 A88-11083
- VALONE, S. M.**
Characteristics of fluid flow in the combustion synthesis of TiC from the elements p 110 A88-28564
Solid-state combustion synthesis of ceramics and alloys in reduced gravity p 75 N88-25479
[NASA-CR-4163]
- VAN DALEN, ANTHONY**
Cosmic string induced peculiar velocities p 226 A88-28762
- VAN DINE, LESLIE**
Regenerative fuel cell study for satellites in GEO orbit
p 52 A88-11904
- VAN FOSSEN, G. JAMES**
Measurement of local convective heat transfer coefficients from a smooth and roughened NACA-0012 airfoil - Flight test data
[AIAA PAPER 88-0287] p 136 A88-22207
- VAN LEER, BRAM**
Choice of implicit and explicit operators for the upwind differencing method
[AIAA PAPER 88-0624] p 209 A88-22472
Splitting of inviscid fluxes for real gases
[AIAA PAPER 88-3526] p 142 A88-48782
- VAN ROODE, MARK**
Porosity determination of thermal barrier coatings
[ASME PAPER 88-GT-278] p 68 A88-54350
- VANDERSANDE, J.**
Effect of the microstructure on the thermoelectric properties of polycrystalline lanthanum chalcogenides
p 221 A88-40797
- VANDERSANDE, JAN W.**
Effect of high temperature annealing on the thermoelectric properties of GaP doped SiGe
p 220 A88-40796
- VANDOORMAAL, J. P.**
Improved numerical methods for turbulent viscous recirculating flows
[NASA-CR-180852] p 13 N88-25445
- VANFOSSEN, G. JAMES**
Measurement of local convective heat transfer coefficients from a smooth and roughened NACA-0012 airfoil: Flight test data
[NASA-TM-100284] p 149 N88-13552
- VANFOSSEN, J.**
Measured performance of the heat exchanger in the NASA icing research tunnel under severe icing and dry-air conditions
[NASA-TM-100116] p 171 N88-12796
- VANGERPEN, JON**
Documentation of the Benson Diesel Engine Simulation Program
[NASA-TM-100940] p 36 N88-27201
- VANLEER, BRAM**
Splitting of inviscid fluxes for real gases
[NASA-TM-100856] p 211 N88-21717
Choice of implicit and explicit operators for the upwind differencing method
[NASA-TM-100857] p 211 N88-21718
- VANNUCCI, RAYMOND D.**
PMR polyimide compositions for improved performance at 371 C p 96 A88-13172
Mechanical properties characterization of composite sandwich materials intended for space antenna applications
[NASA-TM-88893] p 71 N88-10121
The 700 F properties of autoclave cured PMR-2 composites
[NASA-TM-100923] p 75 N88-24712
- VANOMMERING, GERRIT**
Electrical Power Working Group report p 48 N88-10095
- VANOVERBEKE, THOMAS J.**
A numerical study of the hot gas environment around a STOVL aircraft in ground proximity
[AIAA PAPER 88-2882] p 23 A88-48752
A numerical study of the hot gas environment around a STOVL aircraft in ground proximity
[NASA-TM-100895] p 1 N88-23729
- VANSTONE, R. H.**
Constitutive modeling for isotropic materials p 186 N88-11172
Elevated temperature crack growth p 186 N88-11174
Elevated temperature crack growth p 193 N88-22421
- VARSHNEYA, D.**
Calibration of high-temperature, fiber-optic, microbend, pressure transducers p 157 A88-22942
- VARY, ALEX**
Ultrasonic nondestructive evaluation, microstructure, and fracture toughness interrelations p 176 A88-18158
Materials analysis by ultrasonics: Metals, ceramics, composites p 176 A88-44853
Nondestructive evaluation of structural ceramics p 178 N88-23876
- VEDULA, K.**
Compressive creep behavior of alloys based on B2 FeAl p 82 A88-10043
B2 aluminides for high temperature applications p 85 A88-31684
Powder processing of nickel and other aluminides by hot consolidation p 87 A88-37158
- VEDULA, K. M.**
Room temperature tensile ductility in powder processed B2 FeAl alloys p 85 A88-31694
- VERHOFF, VINCENT G.**
Small engine components test facility turbine testing cell
[AIAA PAPER 88-2962] p 22 A88-44706
Small engine components test facility turbine testing cell
[NASA-TM-100887] p 33 N88-22037
- VERNON, R.**
Gas liquid flow at microgravity conditions - Flow patterns and their transitions p 141 A88-42839
- VERRILLI, MICHAEL J.**
A viscoplastic theory applied to copper
[NASA-TM-100831] p 189 N88-21497
Bithermal fatigue of a nickel-base superalloy single crystal
[NASA-TM-100885] p 93 N88-22168
Bithermal fatigue: A simplified alternative to thermomechanical fatigue p 194 N88-22424
- VINET, PASCAL**
A model for the influence of pressure on the bulk modulus and the influence of temperature on the solidification pressure for liquid lubricants
[ASME PAPER 88-TRIB-63] p 133 A88-15124
- VIOLETTE, JOHN A.**
Large-Scale Advanced Prop-Fan (LAP) blade design
[NASA-CR-174790] p 27 N88-14097
- VIZZINI, R. W.**
Conceptual design of an optic based engine control system
[ASME PAPER 87-GT-168] p 18 A88-11079
- VLCEK, BRIAN L.**
Some adhesion/cohesion characteristics of plasma-sprayed ZrO₂-Y₂O₃ under tensile loading p 95 A88-12589
- VOGT, WILLIAM G.**
Computer simulation of a single pilot flying a modern high-performance helicopter
[NASA-TM-100182] p 39 N88-26376
Computer simulation of multiple pilots flying a modern high performance helicopter
[NASA-TM-100183] p 39 N88-26377
- VON GLAHN, UWE H.**
On the correlation of plume centerline velocity decay of turbulent acoustically excited jets
[AIAA PAPER 87-2692] p 3 A88-18654
- VONGLAHN, UWE H.**
On the correlation of plume centerline velocity decay of turbulent acoustically excited jets
[NASA-TM-100193] p 11 N88-16681
- ## W
- WADA, B.**
Modal test/analysis correlation for the Centaur G prime launch vehicle p 44 A88-18631
- WAHI, R. P.**
On the cyclic stress-strain behaviour of a Ni-base superalloy at room temperature p 84 A88-24521
- WAHIDUZZAMAN, S. A. H.**
Design, calibration and error analysis of instrumentation for heat transfer measurements in internal combustion engines p 157 A88-18509
- WALD, LAWRENCE W.**
Characterization of a 30-GHz IMPATT solid state amplifier
[NASA-TM-100876] p 120 N88-24847
- WALKER, E.**
Experimental evidence for modifying the current physical model for ice accretion on aircraft surfaces
[NASA-TM-87184] p 15 N88-12473
- WALKER, J. D. A.**
Evolution of hairpin vortices in a shear flow
[NASA-TM-100858] p 211 N88-26885
- WALKER, K. P.**
Unified constitutive models for high-temperature structural applications p 190 N88-21523
Unified constitutive model for single crystal deformation behavior with applications p 191 N88-22388
- WALKER, KEVIN P.**
Constitutive modeling of superalloy single crystals with verification testing p 91 N88-11169
- WALKER, R. J.**
Voids in Jovian magnetosphere revisited - Evidence of spacecraft charging p 226 A88-22879
- WALLACE, J. F.**
Gravitational macrosegregation in binary Pb-Sn alloy ingots p 111 A88-41211
- WALLACE, JOHN F.**
Stress rupture behavior of silicon carbide coated, low modulus carbon/carbon composites
[NASA-CR-180863] p 72 N88-14150
- WALLET, T. M.**
Submillimeter backward wave oscillators p 122 A88-19659
- WALLIN, WAYNE E.**
Advanced space solar dynamic power systems beyond IOC Space Station p 50 A88-11798
Solar dynamic power system definition study
[NASA-CR-180877] p 59 N88-20361
- WALTON, E. K.**
Engineering calculations for the Delta S method of solving the orbital allotment problem
[NASA-CR-182372] p 42 N88-14110
- WANG, C. R.**
Turbulence modeling and surface heat transfer in a stagnation flow region p 141 A88-43871
- WANG, CHI R.**
Correlations of velocity and temperature fluctuations in the stagnation-point flow of circular cylinder in turbulent flow
[NASA-TM-100930] p 13 N88-25435
- WANG, CHUNG-HSIEN**
Performance limitations in parallel processor simulations p 208 A88-49101
- WANG, L.**
Gravitational macrosegregation in binary Pb-Sn alloy ingots p 111 A88-41211
- WANG, L. W.**
Fingering flow patterns of thermosolutal convection in rectangular enclosures
[AIAA PAPER 88-3823] p 144 A88-49000
Thermosolutal convection in high-aspect-ratio enclosures
[NASA-TM-100803] p 151 N88-18871

- Fingering flow patterns of thermosolutal convection in rectangular enclosures [NASA-TM-100854] p 152 N88-21417
- WANG, REN-HONG**
Computer-aided modeling and prediction of performance of the modified Lundell class of alternators in space station solar dynamic power systems [NASA-CR-182538] p 201 N88-19000
- WANG, T.**
Development of a special-purpose test surface guided by uncertainty analysis - Introduction of a new uncertainty analysis step [AIAA PAPER 88-0169] p 39 A88-22121
- WARFIELD, M.**
Comparison of computational methods for three-dimensional turbulent turbomachinery flows p 6 A88-42452
- WARNER, J. D.**
Advantages of barium peroxide in the powder synthesis of perovskite superconductors p 221 A88-41496
- WARNER, JOSEPH D.**
Plasma deposition of amorphous hydrogenated carbon films on III-V semiconductors p 220 A88-32862
Laser induced OMCVD growth of AlGaAs on GaAs p 125 A88-34286
Boron nitride - Composition, optical properties, and mechanical behavior p 99 A88-40794
- WARSHAY, MARVIN**
Status of commercial fuel cell powerplant system development p 198 A88-11925
- WATKINS, PIA M.**
Breadboard RL10-2B low-thrust operating mode (second iteration) test report [NASA-CR-182160] p 66 N88-29867
- WATKINS, W. B.**
Further development of the dynamic gas temperature measurement system p 160 N88-11141
- WEBER, R. M.**
Unified constitutive models for high-temperature structural applications p 190 N88-21523
- WEDE, GILBERT J.**
An overview of rotorcraft propulsion research at Lewis Research Center p 22 A88-40554
- WEEKS, DAVID J.**
LERC power system autonomy program 1990 demonstration p 52 A88-11861
- WEILAND, KENNETH E.**
Sources of error in heterodyne moire deflectometry p 158 A88-35004
- WEIMER, DAVID**
Sources of error in heterodyne moire deflectometry p 158 A88-35004
- WEINBERG, I.**
Comparative radiation resistance, temperature dependence and performance of diffused junction indium phosphide solar cells p 198 A88-18580
Radiation and temperature effects in gallium arsenide, indium phosphide, and silicon solar cells p 125 A88-34321
- WEINBERG, IRVING**
Recent developments in indium phosphide space solar cell research p 50 A88-11785
Radiation damage and defect behavior in proton irradiated lithium-counterdoped n+p silicon solar cells p 125 A88-34340
Modelling and design of high efficiency radiation tolerant indium phosphide space solar cells p 200 A88-34394
Effects of electron and proton irradiations on n/p and p/n GaAs cells grown by MOCVD [NASA-TM-100199] p 127 N88-10266
Recent progress in space photovoltaic systems [NASA-TM-100208] p 128 N88-11966
Progress in InP solar cell research [NASA-TM-100914] p 130 N88-24870
- WEIZER, VICTOR G.**
Piezoresistance and solar cell efficiency p 125 A88-34298
- WELSH, P. E.**
Solar energy conversion through the interaction of plasmons with tunnel junctions. Part A: Solar cell analysis. Part B: Photoconductor analysis [NASA-CR-183044] p 203 N88-27621
- WERNET, MARK P.**
Laser anemometry techniques for turbine applications [ASME PAPER 87-GT-241] p 157 A88-11129
Zoom lens compensator for a cylindrical window in laser anemometer uses p 217 A88-17221
Four spot laser anemometer and optical access techniques for turbine applications p 159 A88-36513
Real time optical correlator using a magneto-optic device applied to particle imaging velocimetry p 159 A88-40700
The four spot time-of-flight laser anemometer p 164 N88-11145
- Application of optical correlation techniques to particle imaging velocimetry [NASA-TM-101306] p 163 N88-29152
- WESSEL, F. J.**
An 8-cm ion thruster characterization [NASA-CR-180819] p 56 N88-10106
- WESTFALL, LEONARD J.**
Thermal cycling of tungsten-fibre-reinforced superalloy composites p 70 A88-31770
Composite monolayer fabrication by an arc-spray process p 169 A88-53581
- WETHERHOLD, ROBERT C.**
Thermal cycling of tungsten-fibre-reinforced superalloy composites p 70 A88-31770
- WEYANDT, C.**
Communications satellite systems operations with the space station. Volume 3: Supplementary technical report [NASA-CR-180875] p 48 N88-16794
- WEYANDT, CHARLES**
Communications satellites in non-geostationary orbits [AIAA PAPER 88-0842] p 46 A88-27583
- WEYANDT, CHARLES J.**
Economic benefits of the Space Station to commercial communication satellite operators [IAF PAPER 87-622] p 41 A88-16215
- WHALEN, MARGARET V.**
Compatibility of dispersion-strengthened platinum with resistojel propellants [NASA-TP-2765] p 58 N88-12538
- WHALEN, THOMAS J.**
Improved silicon carbide for advanced heat engines p 106 N88-23879
- WHEELER, D. K.**
Characterization of Ba₂YCu₃O_{7-x} prepared in an inert atmosphere p 221 A88-49376
- WHEELER, D. R.**
Thermal desorption study of physical forces at the PTFE surface p 77 A88-10963
Preliminary study of niobium alloy contamination by transport through helium p 94 N88-24279
- WHERLEY, BRIAN L.**
The effect of gravity on premixed flame propagation and extinction in a vertical standard flammability tube p 78 A88-38532
- WHIPPLE, E. C.**
An unusual charging event on ISEE 1 p 47 A88-40013
- WHITE, C.**
A numerical study of the effects of curvature and convergence on dilution jet mixing [AIAA PAPER 87-1953] p 137 A88-23312
Dilution jet mixing program, phase 3 p 147 N88-11153
A numerical study of the effects of curvature and convergence on dilution jet mixing [NASA-TM-89878] p 26 N88-13347
Transition mixing study empirical model report [NASA-CR-182139] p 155 N88-30076
- WHITE, CRAIG D.**
An empirical model of the effects of curvature and convergence on dilution jet mixing [NASA-TM-100896] p 34 N88-24640
- WHITE, GRAIG D.**
An empirical model of the effects of curvature and convergence on dilution jet mixing [AIAA PAPER 88-3180] p 23 A88-50783
- WHITE, JAMES W.**
A mapped finite difference study of noise propagation in nonuniform ducts with mean flow p 214 A88-18541
- WHITE, K. ALAN**
Moving belt radiator development status [NASA-TM-100909] p 64 N88-25477
- WHITLOW, JOHN B., JR.**
NASA advanced turboprop research and concept validation program [NASA-TM-100891] p 34 N88-22902
NASA/industry advanced turboprop technology program [NASA-TM-100929] p 35 N88-24641
- WHITTENBERGER, D.**
Effect of the microstructure on the thermoelectric properties of polycrystalline lanthanum chalcogenides p 221 A88-40797
- WHITTENBERGER, J. D.**
Identification of salt-alloy combinations for thermal energy storage applications in advanced solar dynamic power systems p 199 A88-24072
- WHITTENBERGER, J. DANIEL**
Fluoride salts and container materials for thermal energy storage applications in the temperature range 973 - 1400 K p 196 A88-11804
Preliminary investigation of inertia friction welding B2 aluminides p 82 A88-14567
The influence of grain size and composition on 1000 to 1400 K slow plastic flow properties of NiAl p 85 A88-29098
- WHYTE, W. A.**
Numerical arc segmentation algorithm for a radio conference - A software tool for communication satellite systems planning [AIAA PAPER 88-0788] p 212 A88-27531
Numerical arc segmentation algorithm for a radio conference: A software tool for communication satellite systems planning [NASA-TM-100789] p 46 N88-22919
- WHYTE, WAYNE A., JR.**
An allotment planning concept and related computer software for planning the fixed satellite service at the 1988 space WARC p 116 A88-36482
An allotment planning concept and related computer software for planning the fixed satellite service at the 1988 space WARC [NASA-TM-100244] p 117 N88-11944
Numerical arc segmentation algorithm for a radio conference-NASARC (version 2.0) technical manual [NASA-TM-100160] p 118 N88-15910
Numerical arc segmentation algorithm for a radio conference-NASARC, version 2.0: User's manual [NASA-TM-100161] p 119 N88-16928
- WILBUR, PAUL J.**
Space plasma contactor research, 1987 [NASA-CR-182148] p 219 N88-23649
- WILKINSON, R. A.**
Electrohydrodynamic migration of charged droplets in an insulating fluid [AIAA PAPER 88-3557] p 143 A88-48946
Electrohydrodynamic migration of charged droplets in an insulating fluid [NASA-TM-100849] p 152 N88-21424
- WILL, HERBERT A.**
The Lewis Strain Gauge Laboratory: Status and plans p 160 N88-11146
- WILLIAMS, ANTHONY D.**
The development of an intelligent interface to a computational fluid dynamics flow-solver code [NASA-TM-100908] p 207 N88-26127
- WILLIAMS, F. A.**
Sooting and disruption in spherically symmetrical combustion of decane droplets in air [IAF PAPER 87-403] p 77 A88-16076
- WILLIAMS, JAMES H., JR.**
Acousto-ultrasonic input-output characterization of unidirectional fiber composite plate by SV waves [NASA-CR-4152] p 178 N88-23224
Input-output characterization of fiber composites by SH waves [NASA-CR-4153] p 179 N88-23986
Characterization of noncontact piezoelectric transducer with conically shaped piezoelement [NASA-CR-4151] p 179 N88-23987
Acousto-ultrasonic input-output characterization of unidirectional fiber composite plate by P waves [NASA-CR-4162] p 180 N88-25923
- WILLIAMS, M. CARLSON**
Inter and intra blade row laser velocimetry studies of gas turbine compressor flows [ASME PAPER 87-GT-235] p 2 A88-11126
- WILLIAMS, MARC H.**
Aeroelastic effects of alternate blade sweep on advanced propfan rotor [ASME PAPER 87-WA/AERO-8] p 184 A88-51328
The 2-D and 3-D time marching transonic potential flow method for propfans p 11 N88-23245
Aeroelastic response of metallic and composite propfan models in yawed flow [NASA-TM-100964] p 37 N88-29807
- WILLIAMS, W. D.**
Rapid thermal annealing of indium phosphide compound semiconductors p 220 A88-26196
- WILLIAMSON, W. S.**
An 8-cm ion thruster characterization [NASA-CR-180819] p 56 N88-10106
Spacecraft dielectric surface charging property determination [NASA-CR-180879] p 49 N88-21243
- WILLOUGHBY, A. J.**
Technology requirements for an orbiting fuel depot: A necessary element of a space infrastructure [NASA-TM-101370] p 49 N88-29845
- WILSON, D.**
A millimeter-wave tunnel Ladder TWT [NASA-CR-182184] p 130 N88-28239
- WILT, DAVID M.**
Laser induced OMCVD growth of AlGaAs on GaAs p 125 A88-34286
- WILT, T. E.**
Fracture toughness computational simulation of general delaminations in fiber composites [AIAA PAPER 88-2261] p 181 A88-32219
- WIMMER, J. M.**
Improved silicon nitride for advanced heat engines [NASA-CR-175006] p 102 N88-15886

- WINER, WARD O.**
Shear rheological characterization of motor oils
p 100 A88-47562
- WINSA, E.**
Dendritic solidification under microgravity conditions
[AIAA PAPER 88-0248] p 110 A88-22186
Isothermal dendritic growth - A low gravity experiment
p 110 A88-28556
Solidification under microgravity conditions - Dendritic growth
[AAS PAPER 86-380] p 110 A88-35130
Isothermal dendritic growth - A proposed microgravity experiment
p 112 A88-49095
- WINSA, E. A.**
Solidification of undercooled Ni-Sn eutectic alloy under microgravity conditions in the Space Shuttle
p 110 A88-28557
Gravitational macrosegregation in binary Pb-Sn alloy ingots
p 111 A88-41211
- WINTUCKY, EDWIN G.**
Ion beam deposition of amorphous carbon films with diamond like properties
p 97 A88-20300
- WINTUCKY, WILLIAM T.**
Technology developments for a compound cycle engine
p 30 N88-16637
- WIRTZ, G. P.**
Hafnia-rich mixed oxide ceramics of the system $\text{HfO}_2\text{-ZrO}_2\text{-TiO}_2$ for heaters and heat exchangers in electrothermal thrusters: The effects of titania on selected electrical and mechanical properties of Hafnia-rich mixed oxides in the system Hafnia-Zirconia-Titania, volume 1
[NASA-CR-182800-VOL-1] p 105 N88-22197
- WITKOWSKI, DAVID**
Aerodynamic interaction between propellers and wings
[AIAA PAPER 88-0665] p 5 A88-22495
- WITTER, STEWART L.**
Cast iron-base alloy for cylinder/regenerator housing
[NASA-CR-182116] p 92 N88-19613
- WLEZIEN, R. W.**
Unsteady features of jets in lift and cruise modes for VTOL aircraft
[SAE PAPER 872359] p 6 A88-37220
- WOJTCZUK, S.**
Detection of radio-frequency modulated optical signals by two and three terminal microwave devices
p 117 A88-50305
- WOLFF, F.**
Control considerations for high frequency, resonant, power processing equipment used in large systems
p 51 A88-11829
- WONG, YAU SHU**
Approximate polynomial preconditioning applied to biharmonic equations on vector supercomputers
[NASA-TM-100217] p 210 N88-10563
- WOOD, C.**
Effect of the microstructure on the thermoelectric properties of polycrystalline lanthanum chalcogenides
p 221 A88-40797
- WOOD, CHARLES**
Effect of high temperature annealing on the thermoelectric properties of GaP doped SiGe
p 220 A88-40796
- WOOD, J. GARY**
Description of an oscillating flow pressure drop test rig
[NASA-TM-100905] p 61 N88-22933
- WOOD, JERRY R.**
Application of advanced computational codes in the design of an experiment for a supersonic throughflow fan rotor
[ASME PAPER 87-GT-160] p 2 A88-11072
- WOODS, CLAUDIA M.**
The use of multigrid techniques in the solution of the Elrod algorithm for a dynamically loaded journal bearing
[NASA-CR-180873] p 151 N88-17954
The solution of the Elrod algorithm for a dynamically loaded journal bearing using multigrid techniques
[NASA-TM-100941] p 154 N88-25854
- WOODWARD, R. P.**
High speed propeller performance and noise predictions at takeoff/landing conditions
[AIAA PAPER 88-0264] p 215 A88-22193
High speed propeller performance and noise predictions at takeoff/landing conditions
[NASA-TM-100267] p 216 N88-13960
- WOODWARD, RICHARD P.**
Advanced turboprop wing installation effects measured by unsteady blade pressure and noise
[AIAA PAPER 87-2719] p 3 A88-18655
Noise of a model high speed counterrotation propeller at simulated takeoff/approach conditions (F7/A7)
[AIAA PAPER 87-2657] p 214 A88-20176
Noise of a model counterrotation propeller with reduced aft rotor diameter at simulated takeoff/approach conditions (F7/A3)
[AIAA PAPER 88-0263] p 214 A88-22192
- Advanced turboprop wing installation effects measured by unsteady blade pressure and noise
[NASA-TM-100200] p 9 N88-10008
Noise of a model high speed counterrotation propeller at simulated takeoff/approach conditions (F7/A7)
[NASA-TM-100206] p 216 N88-10592
Noise of a model counterrotation propeller with reduced aft rotor diameter at simulated takeoff/approach conditions (F7/A3)
[NASA-TM-100254] p 216 N88-13961
- WOODWARD, S. H.**
Phase-resolved heat-flux measurements on the blade of a full-scale rotating turbine
[ASME PAPER 88-GT-173] p 145 A88-54267
- WOOLLAM, JOHN A.**
Electrical resistivity (4K to 2100K) of annealed vapor growth carbon fibers
p 96 A88-17214
Variable angle spectroscopic ellipsometry - Application to GaAs-AlGaAs multilayer homogeneity characterization
p 220 A88-40139
- WOULDS, MICHAEL J.**
Cast iron-base alloy for cylinder/regenerator housing
[NASA-CR-182116] p 92 N88-19613
- WRIGHT, K. H., JR.**
Comment on 'Ram ion scattering caused by Space Shuttle v x B induced differential charging' by I. Katz and V. A. Davis
p 204 A88-35775
- WU, J. C.**
Application of Navier-Stokes analysis to stall flutter
p 38 N88-23249
- WU, X.**
InP based solar cells for space application: Reduction of external losses
p 199 A88-34250
Direct-current magnetron fabrication of indium tin oxide/InP solar cells
p 200 A88-51289
- WU, Y.**
Solidification of undercooled Ni-Sn eutectic alloy under microgravity conditions in the Space Shuttle
p 110 A88-28557
Dendritic growth of undercooled nickel-tin. III
p 86 A88-32887
- WU, Y.-T.**
Efficient probabilistic fracture mechanics analysis
p 180 A88-16933
Validation of the NESSUS probabilistic finite element analysis computer program
[AIAA PAPER 88-2372] p 205 A88-32309
Probabilistic Structural Analysis Methods for select space propulsion system structural components (PSAM)
p 56 A88-49659
- WYETT, L.**
Reusable rocket engine optical condition monitoring
p 158 A88-29817

X

Y

Z

- ZAMAN, A.**
Array trade-off study using multilayer parasitic subarrays
[NASA-TM-101321] p 121 N88-28222
- ZAMAN, A. J. M.**
Case study of active array feed compensation with sidelobe control for reflector surface distortion
[NASA-TM-100287] p 120 N88-23073
- ZAMAN, AFROZ A.**
Analytical approximation of a distorted reflector surface defined by a discrete set of points
[NASA-TM-101323] p 121 N88-27424
- ZAMAN, K. B. M. Q.**
Transition and separation control on a low-Reynolds number airfoil
p 2 A88-11186
Effect of acoustic excitation on the flow over a low-Re airfoil
p 3 A88-14459
Control of shear flows by artificial excitation
[AIAA PAPER 87-2722] p 3 A88-16567
Initial turbulence effect on jet evolution with and without tonal excitation
[AIAA PAPER 87-2725] p 4 A88-20184
A natural low frequency oscillation in the wake of an airfoil near stalling conditions
[AIAA PAPER 88-0131] p 4 A88-22093
A natural low frequency oscillation in the wake of an airfoil near stalling conditions
[NASA-TM-100213] p 9 N88-10779
- ZAMRIK, S. Y.**
Effect of temperature, microstructure, and stress state on the low cycle fatigue behavior of Waspaloy
p 87 A88-35922
- ZARETSKY, ERWIN V.**
Ceramic bearings for use in gas turbine engines
[NASA-TM-100288] p 172 N88-18007
Life and reliability of rotating disks
p 178 N88-22428
- ZHANG, JIAO**
Spur gears: Optimal geometry, methods for generation and Tooth Contact Analysis (TCA) program
[NASA-CR-4135] p 173 N88-23216

ZHANG, Y.

Determination of settings of a tilted head-cutter for generation of hypoid and spiral bevel gears
[NASA-CR-182138] p 174 N88-24976

ZIEMIANSKI, JOSEPH A.

NASA/industry advanced turboprop technology program
[NASA-TM-100929] p 35 N88-24641

ZIERKE, WILLIAM C.

The measurement of boundary layers on a compressor blade in cascade. I - A unique experimental facility
[ASME PAPER 87-GT-248] p 131 A88-11130

The measurement of boundary layers on a compressor blade in cascade. II - Suction surface boundary layers
[ASME PAPER 87-GT-249] p 132 A88-11131

The measurement of boundary layers on a compressor blade in cascade. III - Pressure surface boundary layers and the near wake
[ASME PAPER 87-GT-250] p 132 A88-11132

ZIPF, MARK E.

Computer simulation of a single pilot flying a modern high-performance helicopter
[NASA-TM-100182] p 39 N88-26376

Computer simulation of multiple pilots flying a modern high performance helicopter
[NASA-TM-100183] p 39 N88-26377

ZOLTAN, A.

Effect of the microstructure on the thermoelectric properties of polycrystalline lanthanum chalcogenides
p 221 A88-40797

ZUMWALT, G. W.

Electro-impulse de-icing - A status report
[AIAA PAPER 88-0019] p 17 A88-22017

ZURAWSKI, ROBERT L.

Characterization of aluminum/RP-1 gel propellant properties
[AIAA PAPER 88-2821] p 109 A88-48751

Catalytic ignition of hydrogen and oxygen propellants
[AIAA PAPER 88-3300] p 109 A88-48764

The effect of eddy distribution on momentum and heat transfer near the wall in turbulent pipe flow
[NASA-TM-100257] p 150 N88-15984

Catalytic ignition of hydrogen and oxygen propellants
[NASA-TM-100957] p 63 N88-24689

Characterization of aluminum/RP-1 gel propellant properties
[NASA-TM-100951] p 109 N88-24808

ZUZEK, J. E.

Numerical arc segmentation algorithm for a radio conference - A software tool for communication satellite systems planning
[AIAA PAPER 88-0788] p 212 A88-27531

Numerical arc segmentation algorithm for a radio conference: A software tool for communication satellite systems planning
[NASA-TM-100789] p 46 N88-22919

ZUZEK, JOHN E.

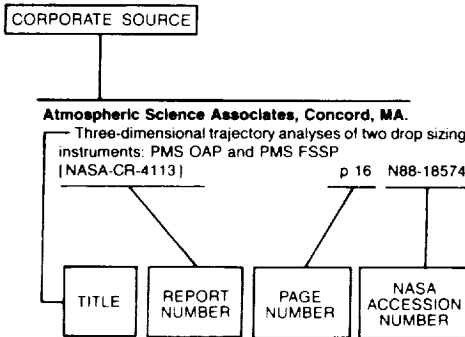
An allotment planning concept and related computer software for planning the fixed satellite service at the 1988 space WARC
[NASA-TM-100244] p 117 N88-11944

Numerical arc segmentation algorithm for a radio conference-NASARC (version 2.0) technical manual
[NASA-TM-100160] p 118 N88-15910

Numerical arc segmentation algorithm for a radio conference-NASARC, version 2.0: User's manual
[NASA-TM-100161] p 119 N88-16928

CORPORATE SOURCE INDEX

Typical Corporate Source Index Listing



Listings in this index are arranged alphabetically by corporate source. The title of the document provides the user with a brief description of the subject matter. The report number helps to indicate the type of document cited (e.g., NASA report, translation, NASA contractor report). The NASA accession number denotes the number by which the citation is identified. The titles are arranged under each corporate source in ascending accession number order.

A

Aerogel TechSystems Co., Sacramento, CA.

Arcjet thruster research and technology [NASA-CR-180865] p 59 N88-17732
Orbital transfer vehicle 3000 LBF thrust chamber assembly hot fire test program [NASA-CR-182145] p 66 N88-29858

Aerometrics, Inc., Mountain View, CA.

Experiments on spray interactions in the wake of a bluff body [ASME PAPER 87-GT-48] p 131 A88-11000

Aerometrics, Inc., Sunnyvale, CA.

Diagnostics development for spray characterization in complex turbulent flows [ASME PAPER 88-GT-241] p 146 A88-54320

Aerostructures, Inc., Arlington, VA.

Aerodynamically forced vibration analysis of turbomachines p 20 A88-31610

Air Force Academy, CO.

Low cost Get-Away-Special (GAS) furnace p 41 A88-28583

Air Force Armament Lab., Eglin AFB, FL.

Production and characterization of CdCl₂ intercalated graphite fibers p 101 A88-51307

AIRResearch Casting Co., Torrance, CA.

Improved silicon nitride for advanced heat engines [NASA-CR-175006] p 102 N88-15886

AIRResearch Mfg. Co., Torrance, CA.

Advanced heat receiver conceptual design study [NASA-CR-180901] p 203 N88-25977

Akron Univ., OH.

Radiation characteristics of microstrip arrays with parasitic elements p 121 A88-10481
Thermomechanical behavior of plasma-sprayed ZrO₂-Y₂O₃ coatings influenced by plasticity, creep, and oxidation p 95 A88-12588

Characteristics of a two-layer electromagnetically coupled rectangular patch antenna p 115 A88-14100
Steady and transient least square solvers for thermal problems p 134 A88-17318

Numerical and analytical study of fluid dynamic forces in seals and bearings p 167 A88-31534

Parametric studies of advanced turboprops [AIAA PAPER 88-2266] p 20 A88-32223
A mixed formulation of C(0)-linear triangular plate/shell element - The role of edge shear constraints p 183 A88-40121

Crosspolarisation characteristics of rectangular patch antennas p 117 A88-47705
Computerized life and reliability modelling for turboprop transmissions

[AIAA PAPER 88-2979] p 100 A88-48031
Gain enhancement of microstrip antennas with overlaying parasitic directors p 117 A88-48653

Hierarchically partitioned nonlinear equation solvers p 210 A88-54980

Input-output-controlled nonlinear equation solvers p 146 A88-55245

SHARP simulation of discontinuities in highly convective steady flow [NASA-TM-100240] p 210 N88-13931

Unified constitutive model development for metal matrix composites at high temperature p 74 N88-22387

An experimental study of biaxial yield in modified 9Cr-1Mo steel at room temperature p 196 N88-30164

[NASA-CR-175012]

Alabama Univ., Huntsville.

Record charging events from Applied Technology Satellite 6 p 46 A88-11737

Comment on 'Ram ion scattering caused by Space Shuttle v x B induced differential charging' by I. Katz and V. A. Davis p 204 A88-35775

Electron beam experiments at high altitudes p 47 A88-46799

Allied-Signal Aerospace Co., Phoenix, AZ.

Elevated temperature durability of ceramic materials [AIAA PAPER 88-3055] p 100 A88-44743

Aluminum Co. of America, Alcoa Center, PA.

Dendritic growth of undercooled nickel-tin. III p 86 A88-32887

Preparation of multistage zone-refined materials for thermochemical standards p 111 A88-43172

Analox Corp., Cleveland, OH.

A statistical rain attenuation prediction model with application to the advanced communication technology satellite project. I: Theoretical development and application to yearly predictions for selected cities in the United States [NASA-CR-179498] p 121 N88-29077

Analytical Services and Materials, Inc., Hampton, VA.

Effect of acoustic excitation on the flow over a low-Re airfoil p 3 A88-14459

Apogee Research Corp., San Diego, CA.

Expert systems for space power supply - Design, analysis, and evaluation p 212 A88-22696

Arizona State Univ., Tempe.

Low Reynolds number modeling of turbulent flows with and without wall transpiration p 136 A88-21983

Performance limitations in parallel processor simulations p 208 A88-49101

Heat transfer in the tip region of a rotor blade simulator p 147 N88-11159

Arizona Univ., Tucson.

A parametric study of mean loading effects on airfoil gust interaction noise [AIAA PAPER 87-2677] p 213 A88-16539

A thermodynamic prediction for microporosity formation in aluminum-rich Al-Cu alloys p 82 A88-18886

Analysis of plasma nitrided steels p 88 A88-38936

Onset of finger convection in a horizontal porous layer underlying a fluid layer p 140 A88-41572

Double-diffusive effects during solidification p 221 A88-43933

Guided-wave approaches to spectrally selective energy absorption [NASA-CR-182532] p 119 N88-17892

Arkansas Univ., Fayetteville.

Study of Staebler-Wronsky degradation effect in a Si:H based P-I-N solar cells [NASA-CR-182564] p 203 N88-25970

Army Aviation Research and Development Command, Cleveland, OH.

Stability of a rigid rotor supported on flexible oil journal bearings [ASME PAPER 87-TRIB-48] p 166 A88-24034

Assessment, development, and application of combustor aerothermal models p 24 A88-54140

Efficiency testing of a helicopter transmission planetary reduction stage [NASA-TP-2795] p 172 N88-15224

Surface fatigue life of CBN and vitreous ground carburized and hardened AISI 9310 spur gears [NASA-TM-100960] p 175 N88-25916

Documentation of the Benson Diesel Engine Simulation Program [NASA-TM-100940] p 36 N88-27201

Army Aviation Research and Development Command, Saint Louis, MO.

Finite-element grid improvement by minimization of stiffness matrix trace [NASA-TM-100255] p 171 N88-13604

Army Aviation Systems Command, Cleveland, OH.

Piezoviscous effects in nonconformal contacts lubricated hydrodynamically p 133 A88-12926

Measurements of the unsteady flow field within the stator row of a transonic axial-flow fan. I - Measurement and analysis technique [ASME PAPER 87-GT-226] p 4 A88-18660

Measurements of the unsteady flow field within the stator row of a transonic axial-flow fan. II - Results and discussion [ASME PAPER 87-GT-227] p 4 A88-18661

Design and performance of controlled-diffusion stator compared with original double-circular-arc stator [SAE PAPER 871783] p 20 A88-30777

Automated acoustic intensity measurements and the effect of gear tooth profile on noise p 168 A88-31623

Development of a thermal and structural analysis procedure for cooled radial turbines [ASME PAPER 88-GT-18] p 145 A88-54164

Parallel computer methods for eigenvalue extraction p 207 N88-23233

Microgravity manipulator demonstration p 173 N88-23242

Aeroelastic forced response analysis of turbomachinery p 34 N88-23247

Impact of ETO propellants on the aerothermodynamic analyses of propulsion components [NASA-TM-101303] p 156 N88-30094

Army Propulsion Lab., Cleveland, OH.

Method for generation of spiral bevel gears with conjugate gear tooth surfaces [ASME PAPER 86-DET-3] p 165 A88-10973

A method for calculating turbulent boundary layers and losses in the flow channels of turbomachines [ASME PAPER 87-GT-225] p 2 A88-11121

An overview of rotorcraft propulsion research at Lewis Research Center p 22 A88-40554

Computerized life and reliability modelling for turboprop transmissions [AIAA PAPER 88-2979] p 100 A88-48031

AS&M, Inc., Hampton, VA.

Transition and separation control on a low-Reynolds number airfoil p 2 A88-11186

Atmospheric Science Associates, Concord, MA.

Three-dimensional trajectory analyses of two drop sizing instruments: PMS OAP and PMS FSSP [NASA-CR-4113] p 16 N88-18574

Avco-Everett Research Lab., MA.

Improved numerical methods for turbulent viscous recirculating flows p 146 N88-11148

Improved numerical methods for turbulent viscous recirculating flows [NASA-CR-180852] p 13 N88-25445

B

Babcock and Wilcox Co., Alliance, OH.

Calibration of high-temperature, fiber-optic, microbend, pressure transducers p 157 A88-22942

Ball Aerospace Systems Div., Boulder, CO.

Optical technologies for space communication systems;
Proceedings of the Meeting, Los Angeles, CA, Jan. 15,
1987
[SPIE-756] p 45 A88-35251

Battelle Columbus Labs., OH.

Low cycle fatigue p 86 A88-35901
[ASTM STP-942]
A nonlinear history-dependent damage model for low
cycle fatigue p 86 A88-35905

Bell Communications Research, Inc., Red Bank, NJ.

Implementation of a fast digital optical matrix-vector
multiplier using a holographic look-up table and residue
arithmetic p 205 A88-17223

Bentley Rotor Dynamics Research Corp., Minden, NV.

Numerical and analytical study of fluid dynamic forces
in seals and bearings p 167 A88-31534

Boeing Military Airplane Development, Wichita, KS.

Multiple-Purpose Subsonic Naval Aircraft (MPSNA):
Multiple Application Propfan Study (MAPS)
[NASA-CR-175104] p 18 A88-28917

Bolt, Beranek, and Newman, Inc., Cambridge, MA.

The generalized transmission error of spiral bevel
gears p 168 A88-49409
Use of the generalized transmission error in the
equations of motion of gear systems p 168 A88-49410

Bowling Green State Univ., OH.

Evaluation studies on carbon supported catalysts for
oxygen reduction in alkaline medium p 77 A88-16643

Brown Univ., Providence, RI.

Control of free shear layers p 134 A88-16545
[AIAA PAPER 87-2689]
Saturation and the limit of jet mixing enhancement by
single frequency plane wave excitation - Experiment and
theory p 8 A88-48899
[AIAA PAPER 88-3613]

C**California State Univ., Long Beach.**

The calculation of flow over iced airfoils
[AIAA PAPER 88-0112] p 4 A88-22078

California Univ., Berkeley.

The structure and dynamics of reacting plane mixing
layers p 136 A88-20871
Unsteady motion and transition to turbulence in
developing curved duct flow p 140 A88-39010
Temperature and velocity profiles in sooting free
convection diffusion flames p 78 A88-43018

California Univ., Irvine.

K-epsilon turbulence model assessment with reduced
numerical diffusion for coaxial jets
[AIAA PAPER 88-0342] p 137 A88-22251

California Univ., La Jolla.

An unusual charging event on ISEE 1 p 47 A88-40013

California Univ., Los Angeles.

Voids in Jovian magnetosphere revisited - Evidence of
spacecraft charging p 226 A88-22879
Experimental studies in vortex pair motion coincident
with a liquid reaction p 142 A88-46316

Calspan Advanced Technology Center, Buffalo, NY.

Phase-resolved heat-flux measurements on the blade
of a full-scale rotating turbine
[ASME PAPER 88-GT-173] p 145 A88-54267

A hybrid numerical technique for predicting the
aerodynamic and acoustic fields of advanced turboprops
[NASA-CR-174926] p 216 A88-12352

Calspan Corp., Arnold AFS, TN.

In-flight measurement of airfoil icing using an array of
ultrasonic transducers p 15 A88-50910

Carnegie-Mellon Univ., Pittsburgh, PA.

Wilson-loop instantons p 212 A88-10410
Numerical methods for one-dimensional
reaction-diffusion equations arising in combustion theory
p 135 A88-18975

An integrated approach for friction damper design
p 167 A88-31598

Evaluation of a turbine blade damper using an integral
approach [AIAA PAPER 88-2400] p 20 A88-32332

Base reaction optimization of manipulators with
redundant kinematics p 173 A88-23238

Case Western Reserve Univ., Cleveland, OH.

Compressive creep behavior of alloys based on B2
FeAl p 82 A88-10043

Improved beta-SiC heteroepitaxial films using off-axis
Si substrates p 219 A88-10431

Interface roughness effect on stresses in ceramic
coatings p 95 A88-12587

Some adhesion/cohesion characteristics of
plasma-sprayed ZrO₂-Y₂O₃ under tensile loading
p 95 A88-12589

Oil film thickness measurement and analysis for an
angular contact ball bearing operating in parched
elastohydrodynamic lubrication p 165 A88-14115

Curvilinear crack layer propagation p 96 A88-14568
The effects of crack surface friction and roughness on
crack tip stress fields p 180 A88-14579

Behavior of ion-implanted junction diodes in 3C SiC
p 122 A88-15423

A theoretical analysis of the extinction limits of a
methane-air opposed-jet diffusion flame p 77 A88-16497

Weak-field magnetization of superconducting
Y1Ba2Cu3O(x) - Relationship to microstructure p 219 A88-18814

Crystallization behavior of a melt-spun Fe-Ni based
steel p 83 A88-19958

Dendritic growth in a supercooled alloy melt
p 83 A88-19966

Sodium sulfate-induced corrosion of pure nickel and
superalloy Udmet 700 in a high velocity burner rig at 900
C p 83 A88-20266

Ion beam deposition of amorphous carbon films with
diamond like properties p 97 A88-20300

Navier-Stokes cascade analysis with a stiff k-epsilon
turbulence solver [AIAA PAPER 88-0594] p 5 A88-22444

Identification of salt-alloy combinations for thermal
energy storage applications in advanced solar dynamic
power systems p 199 A88-24072

Glancing shock wave-turbulent boundary layer
interaction with boundary layer suction
[AIAA PAPER 88-0308] p 6 A88-27718

I-BIEM, an iterative boundary integral equation method
for computer solutions of current distribution problems with
complex boundaries: A new algorithm. I - Theoretical
p 205 A88-27795

Lattice defects in beta-SiC grown epitaxially on silicon
substrates p 220 A88-28711

Effect of fluoride doping on the transition temperature
of YBa2Cu3O(6.5+delta) p 220 A88-29297

Microscopy of epitaxially grown beta-SiC on 001-plane
silicon p 98 A88-31023

Identification of structural interface characteristics using
component mode synthesis p 181 A88-31561

B2 aluminides for high temperature applications
p 85 A88-31684

Room temperature tensile ductility in powder processed
B2 FeAl alloys p 85 A88-31694

Mechanical strength and tribological behavior of
ion-beam-deposited boron nitride films on non-metallic
substrates p 98 A88-32866

Crack diffusion coefficient - A candidate fracture
toughness parameter for short fiber composites
p 70 A88-36945

Powder processing of nickel and other aluminides by
hot consolidation p 87 A88-37158

Analysis of plasma nitrided steels p 88 A88-38936

Real time optical correlator using a magneto-optic device
applied to particle imaging velocimetry p 159 A88-40700

Gravitational macrosegregation in binary Pb-Sn alloy
ingots p 111 A88-41211

On producing an alloy of uniform composition during
rapid solidification processing p 89 A88-41654

Measurements of natural circulation flow in a scale
model PWR reactor system during postulated degraded
core accidents using laser anemometry p 159 A88-43917

Nonlinear roll-up of externally excited free shear
layers p 141 A88-44445

Modelling ignition characteristics of rich H₂/O₂ mixture
in a monolithic catalytic reactor [AIAA PAPER 88-3224] p 78 A88-46499

Semi-empirical crack tip analysis p 183 A88-47681

High T_c screen-printed YBa₂Cu₃O(7-x) films - Effect of
the substrate material p 127 A88-49760

Redundant manipulators for momentum compensation
in a micro-gravity environment p 204 A88-50223

Parched elastohydrodynamic lubrication film thickness
measurement in an instrument ball bearing
[STLE PREPRINT 88-AM-6G-1] p 169 A88-51082

Degradation mechanisms of materials for large space
systems in low Earth orbit [NASA-CR-181472] p 71 A88-10896

Stress rupture behavior of silicon carbide coated, low
modulus carbon/carbon composites [NASA-CR-180863] p 72 A88-14150

The use of multigrid techniques in the solution of the
Eirod algorithm for a dynamically loaded journal bearing
[NASA-CR-180873] p 151 A88-17954

Processing, physical metallurgy and creep of NiAl +
Ta and NiAl + Nb alloys [NASA-CR-182113] p 92 A88-21295

Colloidal characterization of silicon nitride and silicon
carbide p 107 A88-23883

Fraction eutectic measurements in slowly cooled Pb -
15 wt percent Sn alloys [NASA-CR-180830] p 94 A88-25531

Diamond like carbon coatings: Categorization by atomic
number density [NASA-CR-174895] p 108 A88-28151

Optoelectronic gain control of a microwave single stage
GaAs MESFET amplifier [NASA-CR-182201] p 131 A88-30055

Caterpillar Tractor Co., Peoria, IL.

Porosity determination of thermal barrier coatings
[ASME PAPER 88-GT-278] p 68 A88-54350

Cellulose Conversion Enterprises, Berkeley, CA.

Accurate positioning of long, flexible ARM's (Articulated
Robotic Manipulator) p 174 A88-23243

CHAM of North America, Inc., Huntsville, AL.

Numerical and analytical study of fluid dynamic forces
in seals and bearings p 167 A88-31534

Chicago Univ., IL.

Cosmic string induced peculiar velocities p 226 A88-28762

Primordial lithium - New reaction rates, new abundances,
new constraints p 226 A88-31145

Axions from 1987A p 226 A88-35586

Cosmology and particle physics p 226 A88-39734

Primordial nucleosynthesis with decaying particles. I -
Entropy-producing decays. II - Inert decays p 217 A88-47477

Calculations of rates for direct detection of neutralino
dark matter p 227 A88-48463

Cincinnati Univ., OH.

Ohmic contact formation in semi-insulating GaAs using
shallow heavily doped p-type layers p 219 A88-11150

Rapid thermal annealing of indium phosphide compound
semiconductors p 220 A88-26196

Consistent boundary conditions for reduced
Navier-Stokes (RNS) scheme applied to three-dimensional
internal viscous flows [AIAA PAPER 88-0714] p 139 A88-27723

Anisotropic constitutive modeling for nickel base single
crystal superalloys using a crystallographic approach
[AIAA PAPER 88-2440] p 85 A88-32357

A crystallographic model for nickel base single crystal
alloys p 89 A88-48182

Solution of the Neumann pressure problem in general
orthogonal coordinates using the multigrid technique
p 144 A88-50330

Constitutive modeling for single crystal superalloys
p 90 A88-11168

Consistent boundary conditions for Reduced
Navier-Stokes (RNS) scheme applied to 3-dimensional
internal viscous flows [NASA-CR-180874] p 10 A88-15762

A constitutive model with damage for high temperature
superalloys p 93 A88-21510

Anisotropic constitutive modeling for nickel-base single
crystal superalloys [NASA-CR-182157] p 95 A88-29961

City Coll. of the City Univ. of New York.

Wall shear stress measurement in blade end-wall corner
region [ASME PAPER 87-GT-181] p 131 A88-11089

Clarkson Univ., Potsdam, NY.

Soot loading in a generic gas turbine combustor
p 19 A88-27296

Computer-aided modeling and prediction of performance
of the modified Lundell class of alternators in space station
solar dynamic power systems [NASA-CR-182538] p 201 A88-19000

Clemson Univ., SC.

Development of a special-purpose test surface guided
by uncertainty analysis - Introduction of a new uncertainty
analysis step [AIAA PAPER 88-0169] p 39 A88-22121

Cleveland State Univ., OH.

A novel photovoltaic power system which uses a large
area concentrator mirror p 197 A88-11811

A heater made from graphite composite material for
potential deicing application p 17 A88-15724

Modelling the performance of the monogroove with
screen heat pipe for use in the radiator of the solar dynamic
power system of the NASA Space Station [IAF PAPER 87-238] p 134 A88-15960

Oxidation-resistant reflective surfaces for solar dynamic
power generation in near earth orbit p 54 A88-18523

Sensitivity study of the monogroove with screen heat
pipe design [AIAA PAPER 88-0470] p 137 A88-22346

Loss-compensation of intensity-modulating fiber-optic
sensors p 158 A88-22943

Synthesis, electrical and thermal conductivities, and
potential applications of graphite fibrous fibers p 97 A88-28963

An ideal clamping analysis for a cross-ply laminate
p 181 A88-31347

- Automated acoustic intensity measurements and the effect of gear tooth profile on noise p 168 A88-31623
- Fracture toughness computational simulation of general delaminations in fiber composites
[AIAA PAPER 88-2261] p 181 A88-32219
- Probabilistic composite micromechanics
[AIAA PAPER 88-2375] p 182 A88-32312
- Specific heat of pristine and brominated graphite fibers, composites and HOPG p 98 A88-32853
- Differential scanning calorimetric survey of brominated PAN, pitch-based and vapor-grown fibers p 98 A88-32854
- Self-consistent calculations and design considerations for a GaAs nipi doping superlattice solar cell p 124 A88-34249
- Radiation damage and defect behavior in proton irradiated lithium-counterdoped n+p silicon solar cells p 125 A88-34340
- Modelling and design of high efficiency radiation tolerant indium phosphide space solar cells p 200 A88-34394
- Primary arm spacing in chill block melt spun Ni-Mo alloys p 89 A88-41655
- Chemical vapor deposited silica coatings for solar mirror protection
[AIAA PAPER 88-0027] p 99 A88-41796
- Universality relationships in condensed matter - Bulk modulus and sound velocity p 213 A88-43950
- Effect of melt spinning on grain size and texture in Ni-Mo alloys p 89 A88-46030
- Accelerated crack growth rate at low Delta K in a single crystal superalloy p 89 A88-47687
- A comparison of ENO and TVD schemes
[AIAA PAPER 88-3707] p 210 A88-48831
- Analysis of crack propagation in roller bearings using the boundary integral equation method - A mixed-mode loading problem p 168 A88-49183
- Stability of the electrical resistivity of bromine, iodine monochloride, copper(II) chloride, and nickel(II) chloride intercalated pitch-based graphite fibers p 100 A88-49403
- Foil bearing lubrication theory including compressibility effects p 170 A88-54964
- Modelling the performance of the tapered artery heat pipe design for use in the radiator of the solar dynamic power system of the NASA Space Station
[IAF PAPER 88-213] p 56 A88-55361
- High temperature tensile testing of ceramic composites
[NASA-CR-180888] p 161 N88-15996
- Reliability based analysis of contact problems
[NASA-CR-182117] p 189 N88-18975
- Whisker-reinforced ceramic composites for heat engine components p 105 N88-22410
- Continuous fiber ceramic matrix composites for heat engine components p 106 N88-22411
- College of Western New England, Springfield, MA.**
- Forced mixer lobes in ejector designs p 141 A88-46222
- Colorado State Univ., Fort Collins.**
- Space plasma contactor research, 1987
[NASA-CR-182148] p 219 N88-23649
- Columbia Univ., New York, NY.**
- Adaptive grid generation p 209 A88-37363
- Communications Satellite Corp., Clarksburg, MD.**
- Cost-effective intersatellite link applications to the fixed satellite services
[AIAA PAPER 88-0770] p 45 A88-27544
- Service offerings and interfaces for the ACTS network of earth stations
[AIAA PAPER 88-0800] p 116 A88-27551
- Future switching satellites
[AIAA PAPER 88-0802] p 46 A88-27553
- A flexible on-board demultiplexer/demodulator
[AIAA PAPER 88-0811] p 123 A88-27558
- Bandwidth-efficient high-speed coded trellis modulation
[AIAA PAPER 88-0813] p 116 A88-27560
- Connecticut Univ., Storrs.**
- High-temperature oxidation/corrosion of iron-based superalloys p 81 A88-10029
- Three-dimensional flow past two cylinders mounted side by side on an endwall
[AIAA PAPER 88-3718] p 143 A88-48974
- Constitutive modelling of superalloy single crystals with verification testing p 91 N88-11169
- Cornell Univ., Ithaca, NY.**
- Interactive computer simulation of fracture processes p 180 A88-16955
- Effects of numerical dissipation on finite-volume solutions of compressible flow problems
[AIAA PAPER 88-0621] p 5 A88-22469
- Variable angle spectroscopic ellipsometry - Application to GaAs-AlGaAs multilayer homogeneity characterization p 220 A88-40139
- A diagonally inverted LU implicit multigrid scheme
[AIAA PAPER 88-3565] p 209 A88-48791

- Detection of radio-frequency modulated optical signals by two and three terminal microwave devices p 117 A88-50305
- Application of bifurcation theory to axial flow compressor instability
[ASME PAPER 88-GT-231] p 169 A88-54313
- Numerical results for axial flow compressor instability
[ASME PAPER 88-GT-252] p 169 A88-54328

D

- Dana Corp., Fort Wayne, IN.**
- Method for generation of spiral bevel gears with conjugate gear tooth surfaces
[ASME PAPER 88-DET-3] p 165 A88-10973
- Dartmouth Coll., Hanover, NH.**
- Plasticity analysis of wear phenomena as an aid in the development of abrasible materials p 164 A88-10938
- Dynamic recrystallization and grain boundary migration in B2 FeAl p 83 A88-20269
- The microstructure and tensile properties of extruded melt-spun ribbons of iron-rich B2 FeAl p 85 A88-31679
- Dayton Univ., OH.**
- Numerical simulation of self-sustained and forced oscillations in jet shear layers p 3 A88-14155
- Navier-Stokes solutions of flowfield characteristics produced by ice accretion
[AIAA PAPER 88-0290] p 137 A88-22210
- A numerical investigation of the influence of heating on the excitation of high and low Mach number jet flows
[ASME PAPER 87-WA/NCA-13] p 144 A88-51343
- Department of the Air Force, Wright-Patterson AFB, OH.**
- In-flight thrust determination
[SAE AIR 1703] p 16 A88-15227
- Uncertainty of in-flight thrust determination
[SAE AIR 1678] p 16 A88-15228
- Deskin Research Group, Santa Clara, CA.**
- How good is the impedance boundary condition? p 115 A88-24863
- Detroit Diesel Allison, MI.**
- Adiabatic diesel engine component development: Reference engine for on-highway applications
[NASA-CR-179531] p 224 N88-12428
- Deutsche Forschungs- und Versuchsanstalt fuer Luft- und Raumfahrt, Berlin (Germany, F.R.).**
- Excitation of instability waves in free shear layers. I - Theory p 138 A88-26338
- Excitation of instability waves in free shear layers. II - Experiments p 138 A88-26339
- Deutsche Forschungs- und Versuchsanstalt fuer Luft- und Raumfahrt, Cologne (Germany, F.R.).**
- Experimental investigation of the performance of a supersonic compressor cascade
[ASME PAPER 88-GT-306] p 9 A88-54375
- Douglas Aircraft Co., Inc., Long Beach, CA.**
- Effects of environmentally imposed roughness on airfoil performance p 15 N88-15778
- Draper (Charles Stark) Lab., Inc., Cambridge, MA.**
- Oil film thickness measurement and analysis for an angular contact ball bearing operating in parched elastohydrodynamic lubrication p 165 A88-14115
- Parched elastohydrodynamic lubrication film thickness measurement in an instrument ball bearing
[STLE PREPRINT 88-AM-6G-1] p 169 A88-51082
- Drexel Univ., Philadelphia, PA.**
- System architecture of MMIC-based large aperture arrays for space applications p 45 A88-35274
- Modified reaction mechanism of aerated n-dodecane liquid flowing over heated metal tubes p 108 A88-44268
- Duke Univ., Durham, NC.**
- Frequency domain solutions to multi-degree-of-freedom, dry friction damped systems p 184 A88-49714
- Reduced order models for nonlinear aerodynamics p 11 N88-23248

E

- Engineering Science Software, Inc., Smithfield, RI.**
- Unified constitutive model for single crystal deformation behavior with applications p 191 N88-22388
- ENTECH Corp., Dallas-Fort Worth Airport, TX.**
- Development of an advanced photovoltaic concentrator system for space applications p 51 A88-11812
- Development of a dome Fresnel lens/gallium arsenide photovoltaic concentrator for space applications p 199 A88-34310
- Exxon Research and Engineering Co., Annandale, NJ.**
- Quantitative characterization of the viscosity of a microemulsion p 77 A88-11167

F

- Fermi National Accelerator Lab., Batavia, IL.**
- Wilson-loop instantons p 212 A88-10410
- String-driven inflation p 225 A88-27446
- Cosmic string induced peculiar velocities p 226 A88-28762
- Axions from 1987A p 226 A88-35586
- Primordial origin of nontopological solitons p 226 A88-39313
- Cosmology and particle physics p 226 A88-39734
- Primordial nucleosynthesis with decaying particles. I - Entropy-producing decays. II - Inert decays p 217 A88-47477
- Calculations of rates for direct detection of neutralino dark matter p 227 A88-48463
- Florida Univ., Gainesville.**
- Mathematical models for the numerical study of turbulent flows p 140 A88-39472
- Flow Application Research, Fremont, CA.**
- Design point variation of 3-D loss and deviation for axial compressor middle stages
[ASME PAPER 88-GT-57] p 8 A88-54189
- Flow Research, Inc., Kent, WA.**
- Optimizing advanced propeller designs by simultaneously updating flow variables and design parameters
[AIAA PAPER 88-2532] p 6 A88-40718
- Direct simulations of chemically reacting turbulent mixing layers, part 2
[NASA-CR-180853] p 154 N88-25857
- Ford Aerospace and Communications Corp., Palo Alto, CA.**
- New non-geosynchronous orbits for communications satellites to off-load daily peaks in geostationary traffic
[AAS PAPER 87-547] p 42 A88-10957
- Economic benefits of the Space Station to commercial communication satellite operators
[IAF PAPER 87-622] p 41 A88-16215
- Bandwidth and power efficient satellite TDMA demodulator and decoder
[AIAA PAPER 88-0812] p 123 A88-27559
- Communications satellites in non-geostationary orbits
[AIAA PAPER 88-0842] p 46 A88-27583
- The economics of satellite retrieval
[AIAA PAPER 88-0843] p 44 A88-27584
- Advanced satellite system architecture for VSATs with ISDN compatibility
[AIAA PAPER 88-0870] p 116 A88-27604
- Communications satellite systems operations with the space station. Volume 3: Supplementary technical report
[NASA-CR-180875] p 48 N88-16794
- Ford Motor Co., Dearborn, MI.**
- Development of the AGT101 regenerator seals
[ASME PAPER 87-GT-173] p 165 A88-11083
- Strength characterization of yttria/alumina-doped sintered silicon nitride p 97 A88-26154
- Improved silicon carbide for advanced heat engines p 106 N88-23679

G

- Garrett Corp., Phoenix, AZ.**
- Advanced Gas Turbine (AGT) technology development project
[NASA-CR-180891] p 225 N88-20230
- Garrett Engine Co., Phoenix, AZ.**
- Transition mixing study empirical model report
[NASA-CR-182139] p 155 N88-30076
- Garrett Processing Co., Torrance, CA.**
- Cast iron-base alloy for cylinder/regenerator housing
[NASA-CR-182116] p 92 N88-19613
- Garrett Turbine Engine Co., Phoenix, AZ.**
- A numerical study of the effects of curvature and convergence on dilution jet mixing
[AIAA PAPER 87-1953] p 137 A88-23312
- Dilution jet mixing program, phase 3 p 147 N88-11153
- Thermal cyclic durability testing of ceramic materials for turbine engines p 179 N88-23886
- Thermal barrier coating life-prediction model development
[NASA-CR-179507] p 107 N88-28142
- General Dynamics/Astronautics, San Diego, CA.**
- Centaur operations at the space station
[NASA-CR-179593] p 49 N88-25473
- General Dynamics Corp., San Diego, CA.**
- Control considerations for high frequency, resonant, power processing equipment used in large systems p 51 A88-11829
- Design, development, and test of Shuttle/Centaur G-prime cryogenic tankage thermal protection systems p 47 A88-53182
- The ac power system testbed
[NASA-CR-175068] p 127 N88-11948

Centaur operations at the space station: Cost and transportation analysis
[NASA-CR-182128] p 44 N88-29835

General Dynamics Corp., Saint Louis, MO.

In-flight thrust determination
[SAE AIR 1703] p 16 A88-15227
Uncertainty of in-flight thrust determination
[SAE AIR 1678] p 16 A88-15228

General Electric Co., Cincinnati, OH.

Oil film thickness measurement and analysis for an angular contact ball bearing operating in parched elastohydrodynamic lubrication p 165 A88-14115
Scale model acoustic testing of counterrotating fans [AIAA PAPER 88-2057] p 22 A88-37947
A review of path-independent integrals in elastic-plastic fracture mechanics p 183 A88-47001
Blade loss transient dynamics analysis, volume 1. Task 2: TETRA 2 theoretical development
[NASA-CR-179632] p 25 N88-10791
Blade loss transient dynamics analysis, volume 2. Task 2: TETRA 2 user's manual
[NASA-CR-179633] p 25 N88-10792
3D inelastic analysis methods for hot section components p 185 N88-11164
Component specific modeling p 206 N88-11166
Constitutive modeling for single crystal superalloys p 90 N88-11168
Constitutive modeling for isotropic materials p 186 N88-11172
Elevated temperature crack growth p 186 N88-11174
Effects of surface chemistry on hot corrosion life p 91 N88-11180
E3 10C compressor test analysis of high-speed post-stall data
[NASA-CR-179521] p 36 N88-28929

General Electric Co., Evendale, OH.

Results of NASA's Energy Efficient Engine Program
p 19 A88-20785
Thermal barrier coating life prediction model development p 170 N88-11184
Elevated temperature crack growth p 193 N88-22421

General Electric Co., Lynn, MA.

The design of a turboshaft speed governor using modern control techniques
[NASA-CR-175046] p 170 N88-10339

General Electric Co., Schenectady, NY.

Oxidation-resistant reflective surfaces for solar dynamic power generation in near earth orbit p 54 A88-18523
Low cycle fatigue
[ASTM STP-942] p 86 A88-35901
Chemical vapor deposited silica coatings for solar mirror protection
[AIAA PAPER 88-0027] p 99 A88-41796

General Motors Corp., Detroit, MI.

Application of several variable-valve-timing concepts to an LHR engine
[ASME PAPER 87-ICE-29] p 19 A88-15119
Aerothermal modeling program, phase 2 p 146 N88-11149

General Motors Corp., Indianapolis, IN.

Correlation between ultrasonic velocity and density of ceramic turbine blades p 176 A88-12581
Dynamic and static fatigue behavior of sintered silicon nitrides p 96 A88-12602
K-epsilon turbulence model assessment with reduced numerical diffusion for coaxial jets
[AIAA PAPER 88-0342] p 137 A88-22251
Design and development of ceramic components
[AIAA PAPER 88-3054] p 168 A88-44742
The design of an air-cooled metallic high temperature radial turbine p 22 A88-45011
Assessment, development, and application of combustor aerothermal models p 24 A88-54140
Film cooling heat transfer on a turbine airfoil p 147 N88-11156

Nondestructive evaluation of structural ceramics by photoacoustic microscopy
[NASA-CR-180858] p 103 N88-16868

Georgia Inst. of Tech., Atlanta.

An ideal clamping analysis for a cross-ply laminate p 181 A88-31347
The effects of rotational flow, viscosity, thickness, and shape on transonic flutter dip phenomena
[AIAA PAPER 88-2348] p 182 A88-32289
A model for life predictions of nickel-base superalloys in high-temperature low cycle fatigue p 87 A88-35913
Effect of temperature, microstructure, and stress state on the low cycle fatigue behavior of Waspaloy p 87 A88-35922
Thermo-elasto-viscoplastic analysis of problems in extension and shear p 183 A88-41042
Shear rheological characterization of motor oils p 100 A88-47562

Frequency domain solutions to multi-degree-of-freedom, dry friction damped systems p 184 A88-49714
Analysis of shell-type structures subjected to time-dependent mechanical and thermal loading
[NASA-CR-181409] p 185 N88-10388

Deformation, fatigue and fracture behavior of two cast anisotropic superalloys p 187 N88-13732
Analysis of shell-type structures subjected to time-dependent mechanical and thermal loading
[NASA-CR-182705] p 189 N88-20668
Non-isothermal elastoviscoplastic analysis of planar curved beams p 190 N88-21526
Application of Navier-Stokes analysis to stall flutter p 38 N88-23249

Grumman Aerospace Corp., Bethpage, NY.

Heat pipe radiators for solar dynamic space power system heat rejection p 132 A88-11807
High thermal-transport capacity heat pipes for space radiators
[SAE PAPER 871509] p 136 A88-21155
Solar dynamic heat rejection technology. Task 2: Heat pipe radiator development
[NASA-CR-182141] p 152 N88-23182

GTE Labs., Inc., Waltham, MA.

A payoff for investigating the influence of convection on GaAs crystal growth p 221 N88-17702

H

Hahn-Meitner-Inst. fuer Kernforschung, Berlin (Germany, F.R.).

On the cyclic stress-strain behaviour of a Ni-base superalloy at room temperature p 84 A88-24521

Hamilton Standard, Windsor Locks, CT.

Analysis and test evaluation of the dynamic stability of three advanced turboprop models at zero forward speed
[NASA-CR-175025] p 26 N88-14095
Analysis and test evaluation of the dynamic response and stability of three advanced turboprop models at low forward speed
[NASA-CR-175026] p 27 N88-14096
Large-Scale Advanced Prop-Fan (LAP) blade design
[NASA-CR-174790] p 27 N88-14097
Large-Scale Advanced Prop-Fan (LAP)
[NASA-CR-182112] p 32 N88-20306
Experimental and analytical evaluation of the effects of simulated engine inlets on the blade vibratory stresses of the SR-3 model prop-fan
[NASA-CR-174959] p 36 N88-28927
SR-7A aerelastic model design report
[NASA-CR-174791] p 36 N88-28928

Hamilton Standard Div., United Aircraft Corp., Windsor Locks, CT.

Noise characteristics of model counter-rotating Prop-Fans
[AIAA PAPER 87-2656] p 213 A88-16526

Hampden-Sydney Coll., VA.

Gigawatt-tolerant power switches and memory elements p 123 A88-22704
Neutron radiation tolerance of Au-activated silicon p 222 N88-24316

Harris Corp., Melbourne, FL.

Solar concentrator advanced development project
p 50 A88-11799
Development of composite facets for the surface of a space-based solar dynamic concentrator p 54 A88-18230

Solar concentrator advanced development program, task 1
[NASA-CR-179489] p 201 N88-18068

Honeywell, Inc., Bloomington, MN.

Two stage dual gate MESFET monolithic gain control amplifier for Ka-band p 124 A88-29821
A 30 GHz monolithic receive module technology assessment
[NASA-CR-180825] p 129 N88-23084

Houston Univ., TX.

Roles of initial condition and vortex pairing in jet noise p 213 A88-13963
Gas liquid flow at microgravity conditions - Flow patterns and their transitions p 141 A88-42839

Hughes Aircraft Co., El Segundo, CA.

A simple circular-polarized antenna: Circular waveguide horn coated with lossy magnetic material p 116 A88-36648

Hughes Aircraft Co., Long Beach, CA.

Design description report for a photovoltaic power system for a remote satellite earth terminal
[NASA-CR-179586] p 200 N88-12875

Hughes Aircraft Co., Los Angeles, CA.

Auxiliary propulsion system flight package
[NASA-CR-180828] p 56 N88-10886

Hughes Research Labs., Malibu, CA.

A prediction model of the depth-of-discharge effect on the cycle life of a storage cell p 197 A88-11896

An 8-cm ion thruster characterization
[NASA-CR-180819] p 56 N88-10106
Spacecraft dielectric surface charging property determination
[NASA-CR-180879] p 49 N88-21243

Illinois Inst. of Tech., Chicago.

Precipitation in a rapidly solidified and aged Ni-Al-Mo alloy p 82 A88-18528
Absolute instability of the Gaussian wake profile p 136 A88-20842

Illinois Univ., Chicago.

Method for generation of spiral bevel gears with conjugate gear tooth surfaces
[ASME PAPER 86-DET-3] p 165 A88-10973
A probabilistic model of brittle crack formation p 180 A88-18696
On self-similarity of crack layer p 181 A88-24054
Semi-empirical crack tip analysis p 183 A88-47681
Spur gears: Optimal geometry, methods for generation and Tooth Contact Analysis (TCA) program
[NASA-CR-4135] p 173 N88-23216
On governing equations for crack layer propagation
[NASA-CR-182120] p 194 N88-23272
Determination of settings of a tilted head-cutter for generation of hypoid and spiral bevel gears
[NASA-CR-182138] p 174 N88-24976

Illinois Univ., Urbana.

How good is the impedance boundary condition? p 115 A88-24863
Macrocrack interaction with transverse array of microcracks p 181 A88-30236
A simple circular-polarized antenna: Circular waveguide horn coated with lossy magnetic material p 116 A88-36648
The effect of gravity on premixed flame propagation and extinction in a vertical standard flammability tube p 78 A88-38532
Slotline fed microstrip antenna array modules p 126 A88-44170
Modal attenuation in multilayered coated waveguides p 126 A88-45755
Polarization determination utilizing two arbitrarily polarized antennas p 116 A88-47424
Optimal cooperative time-fixed impulsive rendezvous
[AIAA PAPER 88-4279] p 42 A88-50406
Deposition of vanadium oxide films by direct-current magnetron reactive sputtering p 221 A88-51286
Cyclic fatigue damage characteristics observed for simple loadings extended to multiaxial life prediction
[NASA-CR-182126] p 195 N88-25016

Illinois Univ., Urbana-Champaign.

Hafnia-rich mixed oxide ceramics of the system HfO₂-ZrO₂-TiO₂ for heaters and heat exchangers in electrothermal thrusters: The effects of titania on selected electrical and mechanical properties of Hafnia-rich mixed oxides in the system Hafnia-Zirconia-Titania, volume 1
[NASA-CR-182800-VOL-1] p 105 N88-22197
Fatigue damage mapping p 193 N88-22423
The relationship between observed fatigue damage and life estimation models
[NASA-CR-182191] p 196 N88-27611

Indian Inst. of Tech., Madras.

Effect of stage loading on endwall flows in an axial flow compressor rotor
[ASME PAPER 88-GT-111] p 145 A88-54229

Induction General, Inc., Pittsburgh, PA.

High frequency power distribution system
[NASA-CR-175071] p 129 N88-23939

Instituto Superior Tecnico, Lisbon (Portugal).

Unsteady motion and transition to turbulence in developing curved duct flow p 140 A88-39010

Integral Technologies, Inc., Westmont, IL.

Application of several variable-valve-timing concepts to an LHR engine
[ASME PAPER 87-ICE-29] p 19 A88-15119
Design, calibration and error analysis of instrumentation for heat transfer measurements in internal combustion engines p 157 A88-18509

Intercal Co., Port Huron, MI.

Stability of the electrical resistivity of bromine, iodine monochloride, copper(II) chloride, and nickel(II) chloride intercalated pitch-based graphite fibers p 100 A88-49403

International Centre for Theoretical Physics, Trieste (Italy).

Primordial origin of nontopological solitons p 226 A88-39313

International Fuel Cells Corp., South Windsor, CT.

Stress-life interrelationships associated with alkaline fuel cells p 197 A88-11903
Regenerative fuel cell study for satellites in GEO orbit p 52 A88-11904

International School for Advanced Studies, Trieste (Italy).

Primordial origin of nontopological solitons p 226 A88-39313

International TechnoGroup, Inc., Milford, OH.

A crystallographic model for nickel base single crystal alloys p 89 A88-48182

Intersonics, Inc., Northbrook, IL.

Program for the feasibility of developing a high pressure acoustic levitator [NASA-CR-182154] p 113 N88-26498

Iowa State Univ. of Science and Technology, Ames.

Measurements of the unsteady flow field within the stator row of a transonic axial-flow fan. I - Measurement and analysis technique [ASME PAPER 87-GT-226] p 4 A88-18660

Measurements of the unsteady flow field within the stator row of a transonic axial-flow fan. II - Results and discussion [ASME PAPER 87-GT-227] p 4 A88-18661

Design point variation of 3-D loss and deviation for axial compressor middle stages [ASME PAPER 88-GT-57] p 8 A88-54189

Iowa Univ., Iowa City.

Plasma wave turbulence around the shuttle - Results from the Spacelab-2 flight p 218 A88-47783
Gaseous environment of the Shuttle early in the Spacelab 2 mission p 47 A88-47972
Double-probe potential measurements near the Spacelab 2 electron beam p 204 A88-53464
Exposed high-voltage source effect on the potential of an ionospheric satellite p 218 A88-54992

J**Jet Propulsion Lab., California Inst. of Tech., Pasadena.**

Research opportunities in microgravity science and applications during Shuttle hiatus p 109 A88-13164
Modal test/analysis correlation for the Centaur G prime launch vehicle p 44 A88-18631
Effect of high temperature annealing on the thermoelectric properties of GaP doped SiGe p 220 A88-40796
Effect of the microstructure on the thermoelectric properties of polycrystalline lanthanum chalcogenides p 221 A88-40797

John Carroll Univ., Cleveland, OH.

Fiber-linked interferometric pressure sensor p 157 A88-11743

Time domain referencing in intensity modulation fiber optic sensing systems p 217 A88-12660

Joint Inst. for Lab. Astrophysics, Boulder, CO.

Magnetic fields interacting with nonlinear compressible convection p 226 A88-31163

K**Kansas Univ., Lawrence.**

A hypermatrix formulation for subspace iteration p 205 A88-15427

voids in Jovian magnetosphere revisited - Evidence of spacecraft charging p 226 A88-22879

Controlled excitation of a cold turbulent swirling free jet [ASME PAPER 87-WA/NCA-18] p 140 A88-41568

Effect of initial tangential velocity distribution on the mean evolution of a swirling turbulent free jet [AIAA PAPER 88-3592] p 7 A88-48893

Kansas Univ. Center for Research, Inc., Lawrence.

Controlled excitation of a cold turbulent swirling free jet [ASME PAPER 87-WA/NCA-18] p 140 A88-41568

Kentucky Univ., Lexington.

Study of free-piston Stirling engine driven linear alternators [NASA-CR-181425] p 170 N88-10355

Kenyon Coll., Gambier, OH.

Thermal conductivity of pristine and brominated highly graphitized pitch based carbon fibers p 97 A88-20257

L**Lawrence Livermore National Lab., CA.**

Feasibility of hydroxyl concentration measurements by laser-saturated fluorescence in high-pressure flames p 77 A88-17218

Liverpool Univ. (England).

Unsteady motion and transition to turbulence in developing curved duct flow p 140 A88-39010

Lockheed Aeronautical Systems Co., Marietta, GA.

Aeroacoustics of advanced STOVL aircraft plumes [SAE PAPER 872358] p 215 A88-37219

Centerline Mach number characteristics of highly heated free jets [AIAA PAPER 88-3612] p 7 A88-48898

Acoustically excited heated jets. 1: Internal excitation [NASA-CR-4129-PT-1] p 12 N88-23751

Acoustically excited heated jets. 2: In search of a better understanding [NASA-CR-4129-PT-2] p 12 N88-23752

Acoustically excited heated jets. 3: Mean flow data [NASA-CR-4129-PT-3] p 12 N88-23753

Propfan test assessment testbed aircraft stability and control/performance 1/9-scale wind tunnel tests [NASA-CR-182121] p 17 N88-26360

Lockheed Aircraft Corp., Marietta, GA.

Aeroacoustics of advanced STOVL aircraft plumes [SAE PAPER 872358] p 215 A88-30998

Lockheed-Georgia Co., Marietta.

Effects of nozzle-exit boundary-layer conditions on excitability of heated free jets [AIAA PAPER 87-2723] p 135 A88-20182

Measurement and prediction of propeller flow field on the PTA aircraft at speeds of up to Mach 0.85 [AIAA PAPER 88-0667] p 19 A88-22497

Lockheed Missiles and Space Co., Sunnyvale, CA.

Polarization determination utilizing two arbitrarily polarized antennas p 116 A88-47424

Los Alamos National Lab., NM.

Integrated heat pipe-thermal storage system performance evaluation p 132 A88-11803

Characteristics of fluid flow in the combustion synthesis of TiC from the elements p 110 A88-28564

Development of an integrated heat pipe-thermal storage system for a solar receiver [AIAA PAPER 88-2683] p 141 A88-43746

Monte Carlo simulation of modulated phases [NASA-TM-89654] p 210 N88-12323

Solid-state combustion synthesis of ceramics and alloys in reduced gravity [NASA-CR-4163] p 75 N88-25479

M**Maine Univ., Orono.**

Three-dimensional flow past two cylinders mounted side by side on an endwall [AIAA PAPER 88-3718] p 143 A88-48974

Manhattan Coll., New York.

Three dimensional thermal analysis of rocket thrust chambers [AIAA PAPER 88-2643] p 54 A88-43721

Manufacturing Technology, Inc., Mishawaka, IN.

Preliminary investigation of inertia friction welding B2 aluminides p 82 A88-14567

MARC Analysis Research Corp., Palo Alto, CA.

Probabilistic Structural Analysis Methods for select space propulsion system structural components (PSAM) p 56 A88-49659

MHOST: An efficient finite element program for inelastic analysis of solids and structures p 33 N88-22394

Marko Materials, Inc., North Billerica, MA.

Dispersion strengthened NIAI alloys produced by rapid solidification processing p 88 A88-40588

Martin Marietta Aerospace, Denver, CO.

Space station onboard propulsion system: Technology study [NASA-CR-179233] p 59 N88-15006

Maryland Univ., College Park.

Critical light light scattering p 158 A88-33003

Massachusetts Inst. of Tech., Cambridge.

Investigation of surface water behavior during glaze ice accretion [AIAA PAPER 88-0115] p 14 A88-22079

Vapor condensation rate at a turbulent liquid interface, for application to cryogenic hydrogen [AIAA PAPER 88-0559] p 137 A88-22419

Solidification of undercooled Ni-Sn eutectic alloy under microgravity conditions in the Space Shuttle p 110 A88-28557

Bladed disk assemblies; Proceedings of the Eleventh Biennial Conference on Mechanical Vibration and Noise, Boston, MA, Sept. 27-30, 1987 p 20 A88-31608

Measurement of ice thickness (icing) in aeronautics p 15 A88-32714

Dendritic growth of undercooled nickel-tin. III p 86 A88-32887

A model for life predictions of nickel-base superalloys in high-temperature low cycle fatigue p 87 A88-35913

Thermal-mechanical cyclic stress-strain responses of cast B-1900 + Hf p 87 A88-35919

In-flight measurement of airfoil icing using an array of ultrasonic transducers p 15 A88-50910

Ultrasonic techniques for aircraft ice accretion measurement [AIAA PAPER 88-4656] p 18 A88-51910

Vapor condensation on a turbulent liquid interface p 150 N88-15939

An experimental and theoretical study of the ice accretion process during artificial and natural icing conditions [NASA-CR-182119] p 16 N88-21143

Acousto-ultrasonic input-output characterization of unidirectional fiber composite plate by SV waves [NASA-CR-4152] p 178 N88-23224

Experimental measurements of heat transfer from an iced surface during artificial and natural cloud icing conditions [AIAA-86-1352] p 153 N88-23718

Input-output characterization of fiber composites by SH waves [NASA-CR-4153] p 179 N88-23986

Characterization of noncontact piezoelectric transducer with conically shaped piezoelement [NASA-CR-4151] p 179 N88-23987

Acousto-ultrasonic input-output characterization of unidirectional fiber composite plate by P waves [NASA-CR-4162] p 180 N88-25923

Massachusetts Univ., Amherst.

Temperature stability of Al(x)Ga(1-x)As (x = 0-1) thermal oxide masks for selective-area optaxy p 221 A88-45858

Max-Planck-Inst. fuer Metallforschung, Stuttgart (Germany, F.R.).

Cyclic hardening mechanisms in Nimonic 80A p 84 A88-24490

Max-Planck-Institut fuer Stromungsforschung, Goettingen (Germany, F.R.).

A model of the wall boundary layer for ducted propellers [AIAA PAPER 87-2742] p 214 A88-16578

Maxwell Labs., La Jolla, CA.

Electron collection by multiple objects within a single sheath p 219 A88-54999

Maxwell Labs., Inc., San Diego, CA.

Hollow cathodes as electron emitting plasma contactors - Theory and computer modeling p 218 A88-47973

McDonnell Aircraft Co., Saint Louis, MO.

STOVL acoustic fatigue technologies [SAE PAPER 872360] p 215 A88-37221

McDonnell-Douglas Corp., Saint Louis, MO.

Uncertainty of in-flight thrust determination [SAE AIR 1678] p 16 A88-15228

Acoustics technologies for STOVL aircraft [AIAA PAPER 88-2238] p 215 A88-35939

McDonnell-Douglas Research Labs., Saint Louis, MO. Unsteady features of jets in lift and cruise modes for VTOL aircraft [SAE PAPER 872359] p 6 A88-37220

Mechanical Technology, Inc., Latham, NY.

Mod II engine development p 165 A88-11972

Analysis and design of a gas-lubricated, sectored, floating ring seal [ASME PAPER 87-TRIB-55] p 166 A88-23310

Automotive Stirling engine: Mod 2 design report [NASA-CR-175106] p 223 N88-11578

Seal technology for liquid oxygen (LOX) turbopumps [NASA-CR-174866] p 171 N88-13603

Michigan State Univ., East Lansing.

Coherent motion induced fluctuations in the primary transition region of a plane shear layer p 133 A88-14125

Gravitationally defined velocities for a low speed hot-wire calibration p 133 A88-14170

Electrothermal propulsion of spacecraft with millimeter and submillimeter electromagnetic energy p 54 A88-46220

Michigan Technological Univ., Houghton.

Local convective flows in partly solidified alloys p 219 A88-18467

Interdiffusion in Ni-rich, Ni-Cr-Al alloys at 1100 and 1200 C. I - Diffusion paths and microstructures. II - Diffusion coefficients and predicted concentration profiles p 84 A88-24485

Predicting diffusion paths and interface motion in gamma/gamma + beta, Ni-Cr-Al diffusion couples p 84 A88-24486

Time-accurate simulations of a shear layer forced at a single frequency [AIAA PAPER 88-0061] p 138 A88-27716

Diffusional transport during the cyclic oxidation of gamma + beta, Ni-Cr-Al(Y, Zr) alloys p 85 A88-28902

Channel formation in Pb-Sn, Pb-Sb, and Pb-Sn-Sb alloy ingots and comparison with the system NH4Cl-H2O p 89 A88-46038

Michigan Univ., Ann Arbor.

Choice of implicit and explicit operators for the upwind differencing method [AIAA PAPER 88-0624] p 209 A88-22472

Mixing, transport and combustion in sprays p 138 A88-25828

Comment on 'Ram ion scattering caused by Space Shuttle v x B induced differential charging' by I. Katz and V. A. Davis p 204 A88-35775

Microwave and millimeter-wave power generation in silicon carbide avalanche devices p 126 A88-47599
Particle-laden weakly swirling free jets - Measurements and predictions

[AIAA PAPER 88-3138] p 142 A88-48757
Splitting of inviscid fluxes for real gases

[AIAA PAPER 88-3526] p 142 A88-48782
Monte Carlo simulation of modulated phases

[NASA-TM-89654] p 210 N88-12323
Nucleate pool boiling: High gravity to reduced gravity;

liquid metals to cryogenics p 113 N88-24464

Midwest Research Inst., Golden, CO.

Direct-current magnetron fabrication of indium tin oxide/InP solar cells p 200 A88-51289

Minnesota Mining and Mfg. Co., Saint Paul.

Design and demonstration of a system for the deposition of atomic-oxygen durable coatings for reflective solar dynamic power system concentrators
[NASA-CR-4158] p 64 N88-25474

Minnesota Univ., Minneapolis.

Measurements of the turbulent transport of heat and momentum in convexly curved boundary layers - Effects of curvature, recovery and free-stream turbulence

[ASME PAPER 87-GT-199] p 131 A88-11103
Description of an oscillating flow test program

p 133 A88-11963
Development of a special-purpose test surface guided by uncertainty analysis - Introduction of a new uncertainty analysis step

[AIAA PAPER 88-0169] p 39 A88-22121
Efficient numerical techniques for complex fluid flows

p 146 N88-11151
Prediction of turbine blade heat transfer

p 148 N88-11162
A survey of oscillating flow in Stirling engine heat exchangers

[NASA-CR-182108] p 152 N88-22322
Two-equation low-Reynolds-number turbulence modeling of transitional boundary layer flows characteristic of gas turbine blades

[NASA-CR-4145] p 153 N88-23185

Missouri Univ., Rolla.

A model of the wall boundary layer for ducted propellers

[AIAA PAPER 87-2742] p 214 A88-16578
Glass properties in the yttria-alumina-silica system

p 96 A88-18361

Montreal Univ. (Quebec).

Thermal-mechanical cyclic stress-strain responses of cast B-1900 + Hf p 87 A88-35919

Motorola, Inc., Chandler, AZ.

Hardware realization of a baseband processor for a SS-FDMA/TDMA/DAMA system

[AIAA PAPER 88-0830] p 124 A88-27575

N

National Aeronautics and Space Administration, Washington, DC.

Application of a semianalytical technique for sensitivity analysis of unsteady aerodynamic computations

[AIAA PAPER 88-2377] p 6 A88-32314
Plasma wave turbulence around the shuttle - Results from the Spacelab-2 flight

p 218 A88-47783

National Aeronautics and Space Administration, Ames Research Center, Moffett Field, CA.

Ground tests confirm the promise of hypersonic propulsion p 2 A88-10369

Hypersonic structures and materials - A progress report p 17 A88-16748

Retooling CFD for hypersonic aircraft p 1 A88-16749

Numerical study of chemically reacting flows using an LU scheme

[AIAA PAPER 88-0436] p 5 A88-24825
Multielement mapping of alpha-SiC by scanning Auger microscopy

p 158 A88-27617
Numerical study of chemically reacting flows using an LU scheme

[NASA-CR-180882] p 26 N88-14094

National Aeronautics and Space Administration, Flight Research Center, Edwards, CA.

In-flight thrust determination

[SAE AIR 1703] p 16 A88-15227
Uncertainty of in-flight thrust determination

[SAE AIR 1678] p 16 A88-15228

National Aeronautics and Space Administration, Langley Research Center, Hampton, VA.

Ground tests confirm the promise of hypersonic propulsion p 2 A88-10369

Transition and separation control on a low-Reynolds number airfoil p 2 A88-11186

Effect of acoustic excitation on the flow over a low-Re airfoil p 3 A88-14459

Hypersonic structures and materials - A progress report p 17 A88-16748

Retooling CFD for hypersonic aircraft p 1 A88-16749

The challenges and opportunities of supersonic transport propulsion technology

[AIAA PAPER 88-2985] p 23 A88-48032

National Aeronautics and Space Administration, Marshall Space Flight Center, Huntsville, AL.

LERC power system autonomy program 1990 demonstration p 52 A88-11861

Simulation of fluid flows during growth of organic crystals in microgravity p 109 A88-13163

Research opportunities in microgravity science and applications during Shuttle hiatus p 109 A88-13164

Comment on 'Ram ion scattering caused by Space Shuttle v x B induced differential charging' by I. Katz and V. A. Davis p 204 A88-35775

Impact of ETO propellants on the aerothermodynamic analyses of propulsion components

[NASA-TM-101303] p 156 N88-30094

National Bureau of Standards, Gaithersburg, MD.

Quantitative characterization of the viscosity of a microemulsion p 77 A88-11167

Preparation of multistage zone-refined materials for thermochemical standards p 111 A88-43172

Critical exponent for the viscosity of four binary liquids p 222 A88-53050

Spacecraft fire detection and extinguishment: A bibliography

[NASA-CR-180880] p 45 N88-18612

National Cheng Kung Univ., Tainan (Taiwan).

Fingering flow patterns of thermosolutal convection in rectangular enclosures

[AIAA PAPER 88-3823] p 144 A88-49000

National Taiwan Univ., Taipei.

Experimental study of thermocapillary flows in a thin liquid layer with heat fluxes imposed on the free surface

p 144 A88-49087

Naval Air Propulsion Test Center, Trenton, NJ.

Conceptual design of an optic based engine control system

[ASME PAPER 87-GT-168] p 18 A88-11079

Naval Coastal Systems Center, Panama City, FL.

Production and characterization of CdCl₂ intercalated graphite fibers p 101 A88-51307

Naval Postgraduate School, Monterey, CA.

An unusual charging event on ISEE 1 p 47 A88-40013

Naval Research Lab., Washington, DC.

Radiation and temperature effects in gallium arsenide, indium phosphide, and silicon solar cells

p 125 A88-34321

Nebraska Univ., Lincoln.

Electrical resistivity (4K to 2100K) of annealed vapor growth carbon fibers p 96 A88-17214

Electron-spin-resonance studies of vapor-grown carbon fibers p 96 A88-17368

Variable angle spectroscopic ellipsometry - Application to GaAs-AlGaAs multilayer homogeneity characterization p 220 A88-40139

Comparison of UNL laser imaging and sizing system and a phase/Doppler system for analyzing sprays from a NASA nozzle

[NASA-CR-182437] p 150 N88-16956

Nielsen Engineering and Research, Inc., Mountain View, CA.

Investigation of the validity of Reynolds averaged turbulence models at the frequencies that occur in turbomachinery

[NASA-CR-182162] p 65 N88-28087

North Carolina State Univ., Raleigh.

Transfer matrix modeling of geared system vibration p 168 A88-39703

Northwestern Univ., Evanston, IL.

Finite element methods in probabilistic mechanics p 212 A88-29060

Elevated temperature strain gages p 160 N88-11144

Electrical properties of materials for elevated temperature resistance strain gage application

[NASA-CR-182214] p 164 N88-30106

Notre Dame Univ., IN.

An expert system for probabilistic description of loads on space propulsion system structural components

[AIAA PAPER 88-2371] p 182 A88-32308

O

Ohio Northern Univ., Ada.

Sources of error in heterodyne moiré deflectometry p 158 A88-35004

Ohio State Univ., Columbus.

Implementation of a fast digital optical matrix-vector multiplier using a holographic look-up table and residue arithmetic p 205 A88-17223

Performance of laser Doppler velocimeter with polydisperse seed particles in high speed flows

[AIAA PAPER 88-0425] p 157 A88-22317

Stability of a rigid rotor supported on flexible oil journal bearings

[ASME PAPER 87-TRIB-48] p 166 A88-24034

Primordial lithium - New reaction rates, new abundances, new constraints p 226 A88-31145

Evaluation of a turbine blade damper using an integral approach

[AIAA PAPER 88-2400] p 20 A88-32332

Direct mass spectrometric identification of silicon oxychloride compounds p 78 A88-44425

Modal attenuation in multilayered coated waveguides p 126 A88-45755

A satellite system synthesis model for orbital arc allotment optimization p 117 A88-48579

Structure of a reattaching supersonic shear flow

[AIAA PAPER 88-3615] p 8 A88-48901

Implementation of a digital optical matrix-vector multiplier using a holographic look-up table and residue arithmetic

[NASA-CR-180431] p 205 N88-10496

Engineering calculations for the Delta S method of solving the orbital allotment problem

[NASA-CR-182372] p 42 N88-14110

A flow visualization study of the leading edge separation bubble on a NACA 0012 airfoil with simulated glaze ice

[NASA-CR-180846] p 10 N88-14966

Electromagnetic fields backscattered from an s-shaped inlet cavity with an absorber coating on its inner walls

[NASA-CR-182401] p 118 N88-15130

An experimental mapping of the flow field behind a glaze ice shape on a NACA 0012 airfoil

[NASA-CR-180847] p 10 N88-15766

Material parameter measurements at high temperatures

[NASA-CR-182707] p 80 N88-20397

Measurement of the properties of lossy materials inside a finite conducting cylinder

[NASA-CR-182664] p 213 N88-20962

The effects of magnetic nozzle configurations on plasma thrusters

[NASA-CR-183096] p 219 N88-26223

A review of gear housing dynamics and acoustics literature

[NASA-CR-183110] p 175 N88-26675

Oklahoma State Univ., Stillwater.

Lateral jet injection into swirling combustor flowfields

[AIAA PAPER 88-3183] p 141 A88-44783

Oregon State Univ., Corvallis.

Assessment of nuclear reactor concepts for low power space applications p 217 N88-24409

Oxford Univ. (England).

High-resolution heat-transfer-coefficient maps applicable to compound-curve surfaces using liquid crystals in a transient wind tunnel p 134 A88-18506

P

Page (R. J.) Co., Santa Ana, CA.

Slip casting and extruding shapes of rhenium with metal oxide additives. Part 2: Development of grain stabilized rhenium parts for resistojets

[NASA-CR-180851] p 57 N88-11749

Pennsylvania State Univ., State College.

The measurement of boundary layers on a compressor blade in cascade. I - A unique experimental facility

[ASME PAPER 87-GT-248] p 131 A88-11130

The measurement of boundary layers on a compressor blade in cascade. II - Suction surface boundary layers

[ASME PAPER 87-GT-249] p 132 A88-11131

The measurement of boundary layers on a compressor blade in cascade. III - Pressure surface boundary layers and the near wake

[ASME PAPER 87-GT-250] p 132 A88-11132

Pennsylvania State Univ., University Park.

Laser Doppler velocimeter measurement of annulus wall boundary layer development in a compressor rotor

[ASME PAPER 87-GT-251] p 132 A88-11133

A space-marching method for the computation of viscous internal flows p 135 A88-20459

Skin friction measurements by laser interferometry in swept shock wave/turbulent boundary-layer interactions

[AIAA PAPER 88-0497] p 5 A88-22364

Velocity-coupled flow oscillations in a simulated solid-propellant rocket environment

[AIAA PAPER 88-0543] p 108 A88-27720

Numerical study of multicomponent droplet vaporization at near critical conditions

- [AIAA PAPER 88-0637] p 108 A88-27721
Effect of temperature, microstructure, and stress state on the low cycle fatigue behavior of Waspaloy p 87 A88-35922
Comparison of computational methods for three-dimensional turbulent turbomachinery flows p 6 A88-42452
Finite-dimensional modeling of network-induced delays for real-time control systems p 208 A88-54537
Pittsburgh Univ., PA.
Low-temperature photoluminescence studies of chemical-vapor-deposition-grown 3C-SiC on Si p 127 A88-53396
Raman scattering studies of chemical-vapor-deposited cubic SiC films of (100)Si p 127 A88-53397
Pratt and Whitney Aircraft, East Hartford, CT.
Inter and intra blade row laser velocimetry studies of gas turbine compressor flows [ASME PAPER 87-GT-235] p 2 A88-11126
In-flight thrust determination [SAE AIR 1703] p 16 A88-15227
Uncertainty of in-flight thrust determination [SAE AIR 1678] p 16 A88-15228
Results of NASA's Energy Efficient Engine Program p 19 A88-20785
Fatigue life prediction modeling for turbine hot section materials p 184 A88-54144
Thermal barrier coating life prediction model development [ASME PAPER 88-GT-284] p 68 A88-54353
Current status and future trends in turbine application of thermal barrier coatings [ASME PAPER 88-GT-286] p 169 A88-54355
Development of heat flux sensors for turbine airfoils p 160 N88-11143
Coolant passage heat transfer with rotation p 147 N88-11160
3-D inelastic analysis methods for hot section components p 206 N88-11165
Creep fatigue life prediction for engine hot section materials (isotropic): Third year progress review p 186 N88-11173
Life prediction and constitutive models for engine hot section anisotropic materials program p 186 N88-11175
Thermal barrier coating life prediction model development p 171 N88-11185
A constitutive model for an overlay coating p 105 N88-21525
On 3-D inelastic analysis methods for hot section components. Volume 1: Special finite element models [NASA-CR-180893] p 190 N88-21535
Aero/structural tailoring of engine blades (AERO/STAEBL) [NASA-CR-180805] p 207 N88-21682
Life prediction modeling based on cyclic damage accumulation p 178 N88-22426
Fatigue damage modeling for coated single crystal superalloys p 93 N88-22427
Structural Tailoring of Advanced Turboprops (STAT) [NASA-CR-180861] p 36 N88-28074
Development of sensors for ceramic components in advanced propulsion systems: Survey and evaluation of measurement techniques for temperature, strain and heat flux for ceramic components in advanced propulsion systems [NASA-CR-182111] p 163 N88-28299
Pratt and Whitney Aircraft, West Palm Beach, FL.
Conceptual design of an optic based engine control system [ASME PAPER 87-GT-168] p 18 A88-11079
Further development of the dynamic gas temperature measurement system p 160 N88-11141
Breadboard RL10-2B low-thrust operating mode (second iteration) test report [NASA-CR-182160] p 66 N88-29867
Oxidizer heat exchanger component test [NASA-CR-182159] p 67 N88-29876
Priem Consultants, Inc., Cleveland, OH.
Study of industry requirements that can be fulfilled by combustion experimentation aboard space station [NASA-CR-180854] p 224 N88-19377
Princeton Synergetics, Inc., NJ.
The economics of satellite retrieval [AIAA PAPER 88-0843] p 44 A88-27584
Princeton Univ., NJ.
Localization of natural modes of vibration in bladed disks [ASME PAPER 87-GT-46] p 18 A88-10998
Sooting and disruption in spherically symmetrical combustion of decane droplets in air [IAF PAPER 87-403] p 77 A88-16076
Time-accurate simulations of a shear layer forced at a single frequency [AIAA PAPER 88-0061] p 138 A88-27716
Recent developments in flutter suppression techniques for turbomachinery rotors p 21 A88-35530
Growth of needle-shaped crystals in the presence of convection p 111 A88-37715
NASA research Program: The roles of fluid motion and other transport phenomena in the morphology of materials [NASA-CR-182801] p 222 N88-25327
Purdue Univ., West Lafayette, IN.
Feasibility of hydroxyl concentration measurements by laser-saturated fluorescence in high-pressure flames p 77 A88-17218
Design, calibration and error analysis of instrumentation for heat transfer measurements in internal combustion engines p 157 A88-18509
Aerodynamic interaction between propellers and wings [AIAA PAPER 88-0665] p 5 A88-22495
Transient engine performance with water ingestion p 19 A88-27295
Dynamic delamination fracture toughness of a graphite/epoxy laminate under impact p 70 A88-29455
Cooperative synthesis of control and display augmentation for a STOL aircraft in the approach and landing task [AIAA PAPER 88-4182] p 37 A88-50272
Aeroelastic effects of alternate blade sweep on advanced propfan rotor [ASME PAPER 87-WA/AERO-8] p 184 A88-51328
Control of rotor aerodynamically forced vibrations by splitters p 23 A88-52684
Spray characteristics of a spill-return airstream atomizer [ASME PAPER 88-GT-7] p 145 A88-54154
A nonlinear viscoelastic constitutive equation - Yield predictions in multiaxial deformations p 185 A88-54912
Linear and nonlinear mechanical properties of a series of epoxy resins p 101 A88-54976
The 2-D and 3-D time marching transonic potential flow method for propfans p 11 N88-23245
Solar energy conversion through the interaction of plasmons with tunnel junctions. Part A: Solar cell analysis. Part B: Photoconductor analysis [NASA-CR-183044] p 203 N88-27621
- R**
- Rensselaer Polytechnic Inst., Troy, NY.**
Some adhesion/cohesion characteristics of plasma-sprayed ZrO₂-Y₂O₃ under tensile loading p 95 A88-12589
Comparative radiation resistance, temperature dependence and performance of diffused junction indium phosphide solar cells p 198 A88-18580
Dendritic solidification under microgravity conditions [AIAA PAPER 88-0248] p 110 A88-22186
Isothermal dendritic growth - A low gravity experiment p 110 A88-28556
Characterization and modelling of open tube diffused n+p bulk InP solar cells p 199 A88-34270
Solidification under microgravity conditions - Dendritic growth [AAS PAPER 86-380] p 110 A88-35130
Investigation of PTFE transfer films by infrared emission spectroscopy and phase-locked ellipsometry p 99 A88-35568
Gravitational contributions to microstructural coarsening in liquid phase sintering p 111 A88-37155
Preparation of multistage zone-refined materials for thermochemical standards p 111 A88-43172
Gravity and configurational energy induced microstructural changes in liquid phase sintering p 112 A88-49089
Isothermal dendritic growth - A proposed microgravity experiment p 112 A88-49095
A simplified orthotropic formulation of the viscoplasticity theory based on overstress p 189 N88-21505
Rocket Research Corp., Redmond, WA.
Arcjet thruster research and technology, phase 1 [NASA-CR-182107] p 62 N88-23830
Rockwell International Corp., Canoga Park, CA.
Advanced space solar dynamic power systems beyond IOC Space Station p 50 A88-11798
Optical measurements pertaining to Space Station solar dynamic power systems [IAF PAPER 87-229] p 42 A88-15954
Reusable rocket engine optical condition monitoring p 158 A88-29817
Noncontacting measurement technologies for space propulsion condition monitoring p 158 A88-29818
Progress toward an advanced condition monitoring system for reusable rocket engines p 54 A88-32868
Improved maintainability of space-based reusable rocket engines [AIAA PAPER 88-3113] p 55 A88-48037
An expert system approach to turbopump health monitoring [AIAA PAPER 88-3117] p 42 A88-48038
25-LBF GO2/GH2 space station thruster [AIAA PAPER 88-2793] p 56 A88-53101
Space station resistojel system requirements and interface definition study [NASA-CR-180832] p 58 N88-12541
Solar dynamic power system definition study [NASA-CR-180877] p 59 N88-20361
Rockwell International Science Center, Thousand Oaks, CA.
Development of 20 GHz monolithic transmit modules [NASA-CR-182134] p 222 N88-24539
Rose-Hulman Inst. of Tech., Terre Haute, IN.
The impact damped harmonic oscillator in free decay p 167 A88-31581
Royal Aircraft Establishment, Farnborough (England).
In-flight thrust determination [SAE AIR 1703] p 16 A88-15227
Uncertainty of in-flight thrust determination [SAE AIR 1678] p 16 A88-15228
RPK Corp., Columbia, MD.
Aerodynamically forced vibration analysis of turbomachines p 20 A88-31610
- S**
- Sanders Associates, Inc., Nashua, NH.**
Advanced solar receiver conceptual design study p 51 A88-11800
Sandia National Labs., Livermore, CA.
The structure and dynamics of reacting plane mixing layers p 136 A88-20871
Schafer (W. J.) Associates, Inc., Arlington, VA.
Electron beam experiments at high altitudes p 47 A88-46799
Science Applications International Corp., Chatsworth, CA.
Laminar diffusion flames under micro-gravity conditions [AIAA PAPER 88-0645] p 78 A88-27722
Scientific Research Associates, Inc., Glastonbury, CT.
Flow in a model turbine stator p 148 N88-11163
Seville Univ. (Spain).
Efficient probabilistic fracture mechanics analysis p 180 A88-16933
Sikorsky Aircraft, Stratford, CT.
Design and evaluation of high contact ratio gearing [NASA-CR-174958] p 175 N88-28319
Simmonds Precision Products, Inc., Vergennes, Vermont.
Ultrasonic techniques for aircraft ice accretion measurement [AIAA PAPER 88-4656] p 18 A88-51910
Solar Turbines, Inc. San Diego, CA.
Porosity determination of thermal barrier coatings [ASME PAPER 88-GT-278] p 68 A88-54350
Southern Methodist Univ., Dallas, TX.
A mapped finite difference study of noise propagation in nonuniform ducts with mean flow p 214 A88-18541
Southwest Research Inst., San Antonio, TX.
Efficient probabilistic fracture mechanics analysis p 180 A88-16933
Phenomenological modeling of hardening and thermal recovery in metals p 84 A88-24037
Bladed disk assemblies: Proceedings of the Eleventh Biennial Conference on Mechanical Vibration and Noise, Boston, MA, Sept. 27-30, 1987 p 20 A88-31608
Validation of the NESSUS probabilistic finite element analysis computer program [AIAA PAPER 88-2372] p 205 A88-32309
NESSUS/EXPERT - An expert system for probabilistic structural analysis methods [AIAA PAPER 88-2374] p 206 A88-32311
Probabilistic Structural Analysis Methods for select space propulsion system structural components (PSAM) p 56 A88-49659
Thermal barrier coating life prediction model development [ASME PAPER 88-GT-284] p 68 A88-54353
Constitutive modeling for isotropic materials p 185 N88-11171
Unified constitutive models for high-temperature structural applications p 190 N88-21523
Constitutive modeling for isotropic materials [NASA-CR-182132] p 37 N88-29811
Spray automated balancing of rotors: Methods and materials [NASA-CR-182151] p 41 N88-29825

Space Industries, Inc., Webster, TX.

Water-propellant resistojets for man-tended platforms
[IAF PAPER 87-259] p 54 A88-15975

Spectrolab, Inc., Sylmar, CA.

Development of 8 cm x 8 cm silicon gridded back solar cell for space station p 200 A88-34312

Standard Oil Engineered Materials Co., Niagara Falls, NY.

Advanced Gas Turbine (AGT) Technology Development Project, ceramic component developments
[NASA-CR-180871] p 224 N88-20229

Stanford Univ., CA.

Primordial origin of nontopological solitons p 226 A88-39313
Low thrust power-limited transfer for a pole squatter [AIAA PAPER 88-4310] p 42 A88-50435
Double-probe potential measurements near the Spacelab 2 electron beam p 204 A88-53464
Heat transfer with very high free stream turbulence p 148 N88-11161

State Univ. of New York, Buffalo.

Thermal cycling of tungsten-fibre-reinforced superalloy composites p 70 A88-31770
Phase-resolved heat-flux measurements on the blade of a full-scale rotating turbine
[ASME PAPER 88-GT-173] p 145 A88-54267

State Univ. of New York at Buffalo, Amherst.

Time-domain transient elastodynamic analysis of 3-D solids by BEM p 183 A88-48638
A new boundary element formulation for two- and three-dimensional thermoelasticity using particular integrals p 184 A88-53088
A new BEM formulation for two- and three-dimensional elastoplasticity using particular integrals p 184 A88-53089

Stuttgart Univ. (Germany, F.R.).

Cyclic hardening mechanisms in Nimonic 80A p 84 A88-24490

Sundstrand Corp., Rockford, IL.

Toluene stability Space Station Rankine power system p 50 A88-11794
Integrated heat pipe-thermal storage system performance evaluation p 132 A88-11803
Solar dynamic organic Rankine cycle heat rejection system simulation p 132 A88-11808
Development of an integrated heat pipe-thermal storage system for a solar receiver
[AIAA PAPER 88-2683] p 141 A88-43746

Sundstrand Energy Systems, Rockford, IL.

Study of toluene stability for an Organic Rankine Cycle (ORC) space-based power system p 66 N88-29863
Study of toluene rotary fluid management device and shear flow condenser performance for a space-based organic Rankine power system p 67 N88-29872
[NASA-CR-180885]

Sverdrup Technology, Inc., Arnold Air Force Station, TN.

Stability relationship for water droplet crystallization with the NASA Lewis icing spray nozzle
[AIAA PAPER 88-0289] p 137 A88-22209
Hypersonic turbulent wall boundary layer computations
[NASA-CR-182147] p 154 N88-24917

Sverdrup Technology, Inc., Middleburg Heights, OH.

Probabilistic structural analysis of aerospace components using NESSUS
[AIAA PAPER 88-2373] p 182 A88-32310
Hypersonic turbulent wall boundary layer computations
[AIAA PAPER 88-2829] p 7 A88-44667
Splitting of inviscid fluxes for real gases p 142 A88-48782
Three-dimensional viscous flow computations of a circular jet in subsonic and supersonic cross flow
[AIAA PAPER 88-3703] p 143 A88-48916
Cooperative synthesis of control and display augmentation for a STOL aircraft in the approach and landing task p 37 A88-50272
A preliminary design study of supersonic through-flow fan inlets p 23 A88-53137
[AIAA PAPER 88-3075]

Sverdrup Technology, Inc., Cleveland, OH.

Real gas properties and Space Shuttle Main Engine fuel turbine performance prediction p 50 A88-11038
Infrared properties of an anisotropically stirred fluid p 134 A88-16354

Advanced Propfan (LAP) propeller, SR-7A

[AIAA PAPER 87-2717] p 214 A88-16565
Analytical determination of propeller performance degradation due to ice accretion p 19 A88-19669
Initial turbulence effect on jet evolution with and without tonal excitation p 4 A88-20184
[AIAA PAPER 87-2725]

Noise of a model counterrotation propeller with reduced aft rotor diameter at simulated takeoff/approach conditions (F7/A3) p 214 A88-22192

High speed propeller performance and noise predictions at takeoff/landing conditions p 215 A88-22193

Operating envelopes of particle sizing instrumentation used for icing research p 157 A88-22211

Numerical study of chemically reacting flows using an LU scheme p 5 A88-24825

Computation of the velocity field of an excited shear layer p 138 A88-26206

Numerical simulation of hypersonic inlet flows with equilibrium or finite rate chemistry p 5 A88-27717

Glancing shock wave-turbulent boundary layer interaction with boundary layer suction p 6 A88-27718

Velocity-coupled flow oscillations in a simulated solid-propellant rocket environment p 108 A88-27720

Numerical study of multicomponent droplet vaporization at near critical conditions p 108 A88-27721

Consistent boundary conditions for reduced Navier-Stokes (RNS) scheme applied to three-dimensional internal viscous flows p 139 A88-27723

A Navier-Stokes solver using the LU-SSOR TVD algorithm p 6 A88-30560

Developing fluid flow in a curved duct of square cross-section and its fully developed dual solutions p 139 A88-30957

Structural assessment of a Space Station solar dynamic heat receiver thermal energy storage canister p 47 A88-31396

Application of structural tailoring to spar/shell turboprops p 20 A88-32277

High-speed propeller noise predictions - Effects of boundary conditions used in blade loading calculations p 215 A88-36270

An experimental investigation of the effect of test-cell pressure on the performance of resistojets p 40 A88-44820

Characterization of aluminum/RP-1 gel propellant properties p 109 A88-48751

Particle-laden weakly swirling free jets - Measurements and predictions p 142 A88-48757

Summary of low-speed wind tunnel results of several high-speed counterrotation propeller configurations p 7 A88-48758

Catalytic ignition of hydrogen and oxygen propellants p 109 A88-48764

Numerical analysis of three-dimensional viscous internal flows p 142 A88-48779

A diagonally inverted LU implicit multigrid scheme p 209 A88-48791

Saturation and the limit of jet mixing enhancement by single frequency plane wave excitation - Experiment and theory p 8 A88-48899

Initial conditional effect on pressure waves in an axisymmetric jet p 143 A88-48915

Two-dimensional viscous flow computations of hypersonic scramjet nozzle flowfields at design and off-design conditions p 23 A88-50785

Optical strain measurement system development p 159 A88-52557

Views on the impact of HOST p 24 A88-54146

Development of a thermal and structural analysis procedure for cooled radial turbines p 145 A88-54164

Performance and operating envelope of imaging and scattering particle sizing instruments p 161 N88-12042

Operating envelopes of particle sizing instrumentation used for icing research p 161 N88-13573

Consistent boundary conditions for Reduced Navier-Stokes (RNS) scheme applied to 3-dimensional internal viscous flows p 10 N88-15762

A multistage mesh generator for solving the average-passage equation system p 10 N88-15769

Component data base for space station resistojets auxiliary propulsion p 59 N88-17731

Probabilistic structural analysis computer code (NESSUS) p 191 N88-22397

Two-dimensional viscous flow computations of hypersonic scramjet nozzle flowfields at design and off-design conditions p 35 N88-25459

Aging behavior of Au-based ohmic contacts to GaAs [NASA-CR-182146] p 130 N88-25831

Characterization of fatigue crack initiation and propagation in Ti-6Al-4V with electrical potential drop technique p 195 N88-25937

High speed inlet calculations with real gas effects [NASA-CR-182167] p 13 N88-26336

Three-dimensional viscous flow computations of a circular jet in subsonic and supersonic cross flow p 155 N88-26616

Three-dimensional adaptive grid generation for body-fitted coordinate system p 155 N88-27520

Syracuse Univ., NY.

Grain boundary oxidation and an analysis of the effects of oxidation on fatigue crack nucleation life p 87 A88-35938

An isentropic compression heated Ludwig tube transient wind tunnel p 40 A88-37926

Grain boundary oxidation and low-cycle fatigue at elevated temperatures p 193 N88-22420

The analysis of fatigue crack growth mechanism and oxidation and fatigue life at elevated temperatures [NASA-CR-182129] p 94 N88-22987

Resolved shear stress intensity coefficient and fatigue crack growth in large crystals p 195 N88-24997

System Science and Software, San Diego, CA.

Threshold-determining mechanisms for discharges in high-voltage solar arrays p 50 A88-11738

T**Technion - Israel Inst. of Tech., Haifa.**

Phenomenological modeling of hardening and thermal recovery in metals p 84 A88-24037

An algorithm for a generalization of the Richardson extrapolation process p 209 A88-32840

Sources of error in heterodyne moire deflectometry p 158 A88-35004

Finite-dimensional modeling of network-induced delays for real-time control systems p 208 A88-54537

Technische Univ., Berlin (Germany, F.R.).

On the cyclic stress-strain behaviour of a Ni-base superalloy at room temperature p 84 A88-24521

Tel-Aviv Univ. (Israel).

Effects of numerical dissipation on finite-volume solutions of compressible flow problems p 5 A88-22469

Comment on 'Ram ion scattering caused by Space Shuttle v x B induced differential charging' by I. Katz and V. A. Davis p 204 A88-35775

Teledyne CAE, Toledo, OH.

Design and experimental evaluation of a high temperature radial turbine with a moveable sidewall nozzle p 19 A88-30776

Phase-resolved heat-flux measurements on the blade of a full-scale rotating turbine p 145 A88-54267

Teledyne Ryan Electronics, San Diego, CA.

Calibration of high-temperature, fiber-optic, microbend, pressure transducers p 157 A88-22942

Temple Univ. Research Inst., Philadelphia, PA.

Modified reaction mechanism of aerated n-dodecane liquid flowing over heated metal tubes p 108 A88-44268

Tennessee Univ., Knoxville.

A mapped finite difference study of noise propagation in nonuniform ducts with mean flow p 214 A88-18541

Tennessee Univ. Space Inst., Tullahoma.

Flow field measurements in a 90 degree turning duct p 147 N88-11157

Texas A&M Univ., College Station.

Effect of rib angle on local heat/mass transfer distribution in a two-pass rib-roughened channel p 131 A88-11033

Analytical determination of propeller performance degradation due to ice accretion p 19 A88-19669

Model helicopter performance degradation with simulated ice shapes p 17 A88-22783

Analysis of eccentric annular incompressible seals. I - A new solution using fast Fourier transforms for determining hydrodynamic force

- [ASME PAPER 87-TRIB-52] p 166 A88-23308
Analysis of eccentric annular incompressible seals. II - Effects of eccentricity on rotordynamic coefficients
- [ASME PAPER 87-TRIB-53] p 166 A88-23309
Local heat/mass transfer distributions around sharp 180 deg turns in two-pass smooth and rib-roughened channels
- [ASME PAPER 86-GT-114] p 139 A88-28516
Theory versus experiment for the rotordynamic coefficients of labyrinth gas seals. I - A two control volume model p 167 A88-31535
Theory versus experiment for the rotordynamic coefficients of labyrinth gas seals. II - A comparison to experiment p 167 A88-31536
Transient rotor dynamic rub phenomena - Theory and test p 167 A88-31539
Experimental verification of a secondary recirculation zone in a labyrinth seal
[AIAA PAPER 88-3692] p 168 A88-48971
3-D laser anemometer measurements in a labyrinth seal
[ASME PAPER 88-GT-63] p 169 A88-54195
3-D laser anemometer measurements in an annular seal
[ASME PAPER 88-GT-64] p 169 A88-54196
Active control of transient rotordynamic vibration by optimal control methods
[ASME PAPER 88-GT-73] p 208 A88-54202
Local heat/mass transfer and pressure drop in a two-pass rib-roughened channel for turbine airfoil cooling
[NASA-CR-179635] p 148 A88-12039
A comparison of experimental and theoretical results for labyrinth gas seals with honeycomb stators
[NASA-CR-182441] p 172 A88-16006
Experimental rotordynamic coefficient results for honeycomb seals
[NASA-CR-182440] p 172 A88-16007
Entrance and exit region friction factor models for annular seal analysis
[NASA-CR-183084] p 175 A88-25921
- Texas Univ., Austin.**
Polarization determination utilizing two arbitrarily polarized antennas p 116 A88-47424
Investigation of surface tension driven convection as a feasibility study for a micro-gravity experiment
[NASA-CR-182504] p 112 A88-18739
- Texas Univ., San Antonio.**
Probabilistic constitutive relationships for cyclic material strength models p 182 A88-32313
- Thermo Electron Corp., Waltham, MA.**
Effect of the microstructure on the thermoelectric properties of polycrystalline lanthanum chalcogenides p 221 A88-40797
- Timken Co., Canton, OH.**
Improved oil-off survivability of tapered roller bearings
[NASA-CR-180804] p 170 A88-11135
- Toledo Univ., OH.**
A study of Schwarz converters for nuclear powered spacecraft p 51 A88-11823
Fast simulation techniques for switching converters p 122 A88-11878
Thermal stresses of a wind turbine blade made of orthotropic material p 180 A88-18380
Measurement of local convective heat transfer coefficients from a smooth and roughened NACA-0012 airfoil - Flight test data p 136 A88-22207
Mass transport phenomena between bubbles and dissolved gases in liquids under reduced gravity conditions p 138 A88-27719
The effects of rotational flow, viscosity, thickness, and shape on transonic flutter dip phenomena
[AIAA PAPER 88-2348] p 182 A88-32289
Application of a semianalytical technique for sensitivity analysis of unsteady aerodynamic computations
[AIAA PAPER 88-2377] p 6 A88-32314
An experimental investigation of the effect of test-cell pressure on the performance of resistojets
[AIAA PAPER 88-3286] p 40 A88-44820
A cascaded Schwarz converter for high frequency power distribution p 127 A88-54713
Numerical simulation of axisymmetric turbulent flow in combustors and diffusers p 11 A88-17582
[NASA-CR-4115] p 11 A88-17582
Adapting high-level language programs for parallel processing using data flow p 207 A88-23234
- Transmission Technology Co., Inc., Fairfield, NJ.**
Design, manufacture and spin test of high contact ratio helicopter transmission utilizing Self-Aligning Bearingless Planetary (SABP)
[NASA-CR-4155] p 174 A88-24975
- TRW Space Technology Labs., Redondo Beach, CA.**
30-cm electron cyclotron plasma generator p 122 A88-18633

Tulane Univ., New Orleans, LA.
Macrocrack interaction with transverse array of microcracks p 181 A88-30236

U

- Ultrasystems, Inc., Irvine, CA.**
Improved perfluoroalkyl ether fluid development p 68 A88-28624
Improved perfluoroalkylether fluid development
[NASA-CR-180872] p 80 A88-15851
- Union Carbide Corp., South Charleston, WV.**
Mass transport phenomena between bubbles and dissolved gases in liquids under reduced gravity conditions p 138 A88-27719
[AIAA PAPER 88-0450] p 138 A88-27719
- United Technologies Corp., East Hartford, CT.**
Fuel-injector/air-swirl characterization
[NASA-CR-180664] p 27 A88-14985
The effects of inlet turbulence and rotor/stator interactions on the aerodynamics and heat transfer of a large-scale rotating turbine model. Volume 2: Heat transfer data tabulation 65 percent axial spacing p 37 A88-28930
[NASA-CR-179468] p 37 A88-28930
The effects of inlet turbulence and rotor/stator interactions on the aerodynamics and heat transfer of a large-scale rotating turbine model. Volume 2: Heat transfer data tabulation. 15 percent axial spacing p 37 A88-29804
[NASA-CR-179467] p 37 A88-29804
- United Technologies Corp., South Windsor, CT.**
Regenerative fuel cell energy storage system for a low earth orbit space station p 204 A88-30184
[NASA-CR-174802] p 204 A88-30184
- United Technologies Research Center, East Hartford, CT.**
High-temperature oxidation/corrosion of iron-based superalloys p 81 A88-10029
Soot loading in a generic gas turbine combustor p 19 A88-27296
Forced mixer lobes in ejector designs p 141 A88-46222
The effects of turbulence and stator/rotor interactions on turbine heat transfer. II - Effects of Reynolds number and incidence p 145 A88-54152
[ASME PAPER 88-GT-5] p 145 A88-54152
Application of advanced diagnostics to airblast injector flows p 159 A88-54159
[ASME PAPER 88-GT-12] p 159 A88-54159
The effects of turbulence and stator/rotor interactions on turbine heat transfer. I - Design operating conditions p 145 A88-54236
[ASME PAPER 88-GT-125] p 145 A88-54236
The development of a high temperature static strain gage system p 160 A88-11142
Fuel-injector/air-swirl characterization p 146 A88-11150
Measurement of airfoil heat transfer coefficients on a turbine stage p 147 A88-11158
The effects of inlet turbulence and rotor/stator interactions on the aerodynamics and heat transfer of a large-scale rotating turbine model. Part 4: Aerodynamic data tabulation p 153 A88-23956
[NASA-CR-179469] p 153 A88-23956
User's manual for three dimensional boundary layer (BL3-D) code p 155 A88-30063
[NASA-CR-174899] p 155 A88-30063
Assessment of a 3-D boundary layer analysis to predict heat transfer and flow field in a turbine passage p 155 A88-30066
[NASA-CR-174894] p 155 A88-30066
- University of Southern California, Los Angeles.**
The high temperature creep deformation of Si3N4-6Y2O3-2Al2O3 p 76 A88-28981
[NASA-CR-183204] p 76 A88-28981
- Utah State Univ., Logan.**
Double-probe potential measurements near the Spacelab 2 electron beam p 204 A88-53464
- Utah Univ., Salt Lake City.**
Effects of subcritical crack growth on fracture toughness of ceramics assessed in chevron-notched three-point bend tests p 185 A88-54276
[ASME PAPER 88-GT-185] p 185 A88-54276
Microstructural effects on fracture toughness of polycrystalline ceramics in combined mode I and mode II loading p 101 A88-54294
[ASME PAPER 88-GT-208] p 101 A88-54294

V

- Vanderbilt Univ., Nashville, TN.**
The structure and dynamics of reacting plane mixing layers p 136 A88-20871
- Varian Associates, Palo Alto, CA.**
A millimeter-wave tunnel diode TWT p 130 A88-28239
[NASA-CR-182184] p 130 A88-28239

- Virginia Polytechnic Inst. and State Univ., Blacksburg.**
Computer modeling and simulation of a 20kHz ac distribution system for Space Station p 51 A88-11827
VSAT networks - An overview p 115 A88-14091
Spread-spectrum multiple access using wideband noncoherent MFSK p 115 A88-26672
Derivatives of eigenvalues and eigenvectors of a general complex matrix p 209 A88-29269
Explicit finite-volume time-marching calculations of total temperature distributions in turbulent flow p 139 A88-30517
An explicit finite-volume time-marching procedure for turbulent flow calculations p 139 A88-30518
Implementation of optimal trajectory control of series resonant converter p 126 A88-38796
Turbulence modeling in hypersonic inlets p 7 A88-44705
[AIAA PAPER 88-2957] p 7 A88-44705
Acousto-ultrasonics as a monitor of material anisotropy p 176 A88-46828

W

- Washington Univ., Saint Louis, MO.**
Computational prediction of propellant reorientation p 109 A88-15940
- Watkins-Johnson Co., Palo Alto, CA.**
High-efficiency helical traveling-wave tube with dynamic velocity taper and advanced multistage depressed collector p 124 A88-32836
- Westinghouse Electric Corp., Pittsburgh, PA.**
Measurements of natural circulation flow in a scale model PWR reactor system during postulated degraded core accidents using laser anemometry p 159 A88-43917
- Westinghouse Research and Development Center, Pittsburgh, PA.**
Characterization of directionally solidified lead chloride p 111 A88-43170
Preparation of multistage zone-refined materials for thermochemical standards p 111 A88-43172
Low-temperature photoluminescence studies of chemical-vapor-deposition-grown 3C-SiC on Si p 127 A88-53396
Raman scattering studies of chemical-vapor-deposited cubic SiC films of (100)Si p 127 A88-53397
Advanced development of double-injection, deep-impurity semiconductor switches p 222 A88-25346
[NASA-CR-182118] p 222 A88-25346
- Wichita State Univ., KS.**
Electro-impulse de-icing electrodynamic solution by discrete elements p 17 A88-22016
[AIAA PAPER 88-0018] p 17 A88-22016
Electro-impulse de-icing - A status report p 17 A88-22017
[AIAA PAPER 88-0019] p 17 A88-22017
Theoretical analysis of the electrical aspects of the basic electro-impulse problem in aircraft de-icing applications p 15 A88-13310
[NASA-CR-180845] p 15 A88-13310
- Wien Univ. (Austria).**
High-temperature oxidation/corrosion of iron-based superalloys p 81 A88-10029
- Wisconsin Univ., Madison.**
The effects of crack surface friction and roughness on crack tip stress fields p 180 A88-14579
Droplet vaporization in a supercritical microgravity environment p 134 A88-16055
[IAF PAPER 87-384] p 134 A88-16055
The structure and dynamics of reacting plane mixing layers p 136 A88-20871
Containerless processing of undercooled melts p 110 A88-28554
Rapid solidification of highly undercooled liquids p 88 A88-41653
Field oriented control of an induction machine in a high frequency link power system p 127 A88-54711
Noncontact temperature measurement: Requirements and applications for metals and alloys research p 112 A88-23899
- Wisconsin Univ., Milwaukee.**
Investigation of third-order closure model of turbulence for the computation of incompressible flows in a channel with a backward-facing step p 136 A88-21273
Turbulence energy and diffusion transport of third-moments in a separating and reattaching flow p 141 A88-43011
- Wyle Labs., Inc., Huntsville, AL.**
Experiments to ensure Space Station fire safety - A challenge p 41 A88-22405
[AIAA PAPER 88-0540] p 41 A88-22405
Spacecraft fire-safety experiments for space station: Technology development mission p 48 A88-20353
[NASA-CR-182114] p 48 A88-20353
- Wyoming Univ., Laramie.**
A hypermatrix formulation for subspace iteration p 205 A88-15427

Yale Univ.

CORPORATE SOURCE

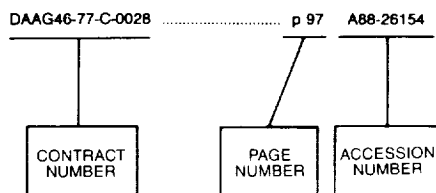
Y

Yale Univ., New Haven, CT.

Turbine airfoil deposition models and their hot corrosion
implications p 91 N88-11178

CONTRACT NUMBER INDEX

Typical Contract Number Index Listing



Listings in this index are arranged alphanumerically by contract number. Under each contract number the NASA accession numbers denoting documents that have been produced as a result of research done under that contract are arranged in ascending order. The NASA accession number denotes the number by which the citation is identified.

AF-AFOSR-80-0160 p 144 A88-50330
 AF-AFOSR-83-0346 p 184 A88-49714
 AF-AFOSR-84-0202 p 135 A88-18975
 AF-AFOSR-85-0244 p 138 A88-25828
 AF-AFOSR-86-0082 p 5 A88-22364
 AF-AFOSR-86-0307 p 209 A88-37363
 AFOSR-ISSA-86-0030 p 65 N88-28087
 DA PROJ. 1L1-61102-AH-45 p 170 N88-11135
 p 172 N88-15224
 p 173 N88-23220
 p 36 N88-27201
 DA PROJ. 1L1-62209-A-47-A p 175 N88-25916
 p 175 N88-30128
 DA PROJ. 1L1-62209-AH-76 p 148 N88-12039
 p 173 N88-21454
 p 174 N88-24975
 p 41 N88-29825
 DAAG29-82-K-0149 p 78 A88-44425
 DAAG46-77-C-0028 p 97 A88-26154
 DAAL03-86-K-0042 p 99 A88-35568
 DAAL03-86-K-0076 p 99 A88-35568
 DAAL03-86-K-0114 p 88 A88-41653
 DAAL03-86-K-0134 p 180 A88-14579
 DAAL03-86-K-0154 p 138 A88-25828
 DE-AC02-80ER-10773 p 217 A88-47477
 DE-AC02-83CH-10093 p 199 A88-34250
 p 200 A88-51289
 DE-AC03-76SF-00515 p 226 A88-39313
 DE-AC04-76DP-00789 p 203 N88-27624
 DE-AI01-76ET-10320 p 201 N88-19014
 DE-AI01-76ET-20320 p 201 N88-21593
 DE-AI01-85CE-50111 p 25 N88-13338
 DE-AI01-85CE-50112 p 223 N88-11578
 p 102 N88-13453
 p 201 N88-14486
 p 102 N88-15872
 p 201 N88-19013
 p 92 N88-19613
 DE-AI01-86CE-50162 p 104 N88-18726
 p 162 N88-18892
 DE-AI03-86SF-16310 p 92 N88-18707
 p 93 N88-22981
 DE-AI05-82OR-1005 p 223 N88-12427
 DE-AL01-86CE-50162 p 224 N88-12428
 DEN3-167 p 165 A88-11083
 p 97 A88-26154
 p 100 A88-44743
 p 224 N88-20229
 p 225 N88-20230
 DEN3-168 p 176 A88-12581
 p 96 A88-12602

DEN3-17 p 168 A88-44742
 DEN3-234 p 176 A88-12581
 DEN3-27 p 92 N88-19613
 p 100 A88-44743
 p 179 N88-23886
 DEN3-282 p 81 A88-10029
 DEN3-329 p 19 A88-15119
 p 224 N88-12428
 DEN3-32 p 165 A88-11972
 p 223 N88-11578
 p 68 A88-54350
 DEN3-332 p 168 A88-44742
 DEN3-336 p 157 A88-18509
 DEN3-342 p 138 A88-26338
 DFG-BE-889/1-1 p 138 A88-26339
 p 17 A88-22017
 DOT-FA03-86-C-00041 p 100 A88-47562
 DOT-RS56-80-C-00015 p 108 A88-27720
 F04611-86-K-0082 p 37 A88-50272
 F33615-86-C-3615 p 167 A88-31535
 F49620-82-K-0033 p 167 A88-31536
 p 131 A88-11103
 F49620-83-C-0062 p 226 A88-22879
 JPL-955232 p 226 A88-31163
 NAGW-91 p 158 A88-35004
 NAGW-933 p 209 A88-29269
 NAG1-224 p 5 A88-22469
 NAG2-373 p 208 A88-49101
 NAG3-113 p 116 A88-47424
 NAG3-149 p 220 A88-40139
 NAG3-154 p 117 A88-48579
 NAG3-159 p 42 N88-14110
 p 136 A88-21983
 NAG3-167 p 176 A88-46828
 NAG3-172 p 214 A88-16578
 NAG3-178 p 168 A88-48971
 NAG3-181 p 169 A88-54195
 p 169 A88-54196
 p 172 N88-16006
 p 172 N88-16007
 p 175 N88-25921
 NAG3-183 p 108 A88-44268
 NAG3-18 p 214 A88-18541
 NAG3-190 p 138 A88-25828
 NAG3-198 p 138 A88-26338
 p 138 A88-26339
 NAG3-211 p 70 A88-29455
 NAG3-21 p 135 A88-18975
 NAG3-24105 p 191 N88-22397
 NAG3-244 p 84 A88-24485
 p 84 A88-24486
 NAG3-262 p 189 N88-21505
 NAG3-264 p 87 A88-35922
 NAG3-280 p 87 A88-35919
 NAG3-284 p 17 A88-22016
 p 17 A88-22017
 p 15 N88-13310
 NAG3-286 p 131 A88-11103
 p 39 A88-22121
 p 42 A88-50435
 NAG3-28 p 10 N88-14966
 p 10 N88-15766
 NAG3-294 p 78 A88-19233
 NAG3-297 p 219 A88-11150
 NAG3-305 p 54 A88-46220
 NAG3-307 p 183 A88-40121
 NAG3-308 p 18 A88-10998
 p 21 A88-35530
 NAG3-315 p 168 A88-31623
 NAG3-328 p 178 N88-23224
 p 179 N88-23986
 p 179 N88-23987
 p 180 N88-25923
 p 205 A88-15427
 NAG3-32 p 110 A88-22186
 NAG3-333 p 110 A88-28556
 p 111 A88-43172
 p 112 A88-49095
 NAG3-33 p 110 A88-35130
 NAG3-347 p 209 A88-29269
 NAG3-348 p 87 A88-35938
 p 193 N88-22420
 p 94 N88-22987
 NAG3-349 p 195 N88-24997
 p 169 A88-54313
 p 169 A88-54328
 NAG3-351 p 77 A88-17218
 NAG3-352 p 71 N88-10896
 NAG3-355 p 11 N88-17582
 NAG3-357 p 213 A88-16539
 NAG3-363 p 140 A88-39472
 NAG3-366 p 217 A88-12660
 NAG3-367 p 167 A88-31598
 NAG3-370 p 188 N88-18969
 NAG3-373 p 180 A88-18380
 NAG3-379 p 74 N88-22387
 p 196 N88-30164
 NAG3-387 p 92 N88-21295
 NAG3-389 p 122 A88-15423
 NAG3-392 p 119 N88-17892
 NAG3-393 p 112 N88-18739
 NAG3-395 p 180 A88-16955
 NAG3-419 p 119 N88-18805
 NAG3-433 p 203 N88-27621
 NAG3-436 p 110 A88-28554
 p 88 A88-41653
 p 112 N88-23899
 NAG3-447 p 111 A88-37715
 p 222 N88-25327
 NAG3-449 p 218 A88-47783
 p 47 A88-47972
 p 204 A88-53464
 p 218 A88-54992
 NAG3-464 p 72 N88-14150
 NAG3-465 p 193 N88-22423
 p 195 N88-25016
 p 196 N88-27611
 NAG3-468 p 107 N88-23883
 NAG3-473 p 115 A88-24863
 NAG3-475 p 116 A88-36648
 p 126 A88-45755
 NAG3-476 p 118 N88-15130
 NAG3-481 p 19 A88-27295
 NAG3-490 p 122 A88-15423
 NAG3-495 p 105 N88-22197
 NAG3-499 p 184 A88-51328
 p 11 N88-23245
 NAG3-501 p 160 N88-11144
 p 164 N88-30106
 NAG3-503 p 187 N88-13732
 NAG3-505 p 108 N88-28151
 NAG3-510 p 141 A88-42839
 NAG3-511 p 85 A88-32357
 p 89 A88-48182
 p 90 N88-11168
 p 93 N88-21510
 p 95 N88-29961
 NAG3-512 p 91 N88-11169
 p 191 N88-22388
 NAG3-516 p 184 A88-49714
 NAG3-521 p 8 A88-54189
 NAG3-522 p 148 N88-11161
 NAG3-526 p 3 A88-14155
 p 144 A88-51343
 p 5 A88-22364
 NAG3-527 p 183 A88-41042
 NAG3-534 p 185 N88-10388
 p 189 N88-20668
 NAG3-535 p 212 A88-29060
 NAG3-542 p 47 A88-40013
 NAG3-543 p 142 A88-46316
 NAG3-546 p 136 A88-21273
 p 141 A88-43011
 NAG3-549 p 141 A88-44783
 NAG3-54 p 134 A88-17318
 p 146 A88-55245
 p 190 N88-21526
 NAG3-550 p 74 N88-22395
 NAG3-551 p 51 A88-11827
 p 126 A88-38796
 NAG3-560 p 219 A88-18467
 p 89 A88-46038
 NAG3-571 p 157 A88-11743
 NAG3-578 p 109 N88-15940
 NAG3-579 p 148 N88-11162
 p 153 N88-23185

NAG3-581

NAG3-581	p 145	A88-54267
NAG3-585-2	p 70	A88-36945
NAG3-5852	p 96	A88-14568
NAG3-589	p 113	N88-24464
NAG3-590	p 91	N88-11178
NAG3-591	p 221	A88-51286
NAG3-593	p 139	A88-30517
	p 139	A88-30518
NAG3-597	p 110	A88-28557
	p 86	A88-32887
NAG3-598	p 133	A88-11963
	p 152	N88-22322
NAG3-599	p 185	A88-54912
	p 101	A88-54976
NAG3-601	p 4	A88-22078
	p 15	N88-15778
NAG3-603	p 127	A88-53396
	p 127	A88-53397
NAG3-604	p 199	A88-34270
NAG3-605	p 123	A88-22704
	p 222	N88-24316
NAG3-610	p 141	A88-46222
NAG3-611	p 168	A88-39703
NAG3-617	p 147	N88-11157
NAG3-618	p 126	A88-47599
NAG3-61	p 156	N88-30084
NAG3-620	p 46	A88-11737
	p 47	A88-40013
	p 47	A88-46799
NAG3-621	p 40	A88-37926
NAG3-623	p 147	N88-11159
NAG3-626	p 17	A88-22783
NAG3-633	p 113	N88-24464
NAG3-634	p 150	N88-16956
NAG3-639	p 213	A88-13963
NAG3-645	p 5	A88-22469
NAG3-655	p 173	N88-23216
NAG3-664	p 210	A88-54980
NAG3-665	p 137	A88-22210
NAG3-666	p 14	A88-22079
	p 15	A88-32714
	p 15	A88-50910
	p 18	A88-51910
	p 16	N88-21143
	p 16	N88-23717
	p 153	N88-23718
NAG3-671	p 133	A88-14125
	p 133	A88-14170
NAG3-672	p 58	N88-12539
NAG3-673	p 134	A88-16545
	p 8	A88-48899
NAG3-676	p 7	A88-44705
NAG3-685	p 76	N88-28981
NAG3-693	p 133	A88-11963
NAG3-699	p 207	N88-23234
NAG3-708	p 51	A88-11823
	p 122	A88-11878
	p 127	A88-54713
NAG3-715	p 209	A88-37363
NAG3-718	p 134	A88-16055
NAG3-722	p 170	N88-10355
NAG3-723	p 82	A88-18886
	p 140	A88-41572
	p 221	A88-43933
NAG3-724	p 11	N88-23248
NAG3-727	p 158	A88-33003
NAG3-729	p 39	N88-26376
	p 39	N88-26377
NAG3-730	p 182	A88-32289
	p 38	N88-23249
NAG3-731	p 137	A88-22419
	p 150	N88-15939
NAG3-735	p 140	A88-39010
NAG3-744	p 111	A88-37155
	p 112	A88-49089
NAG3-749	p 161	N88-15996
NAG3-751	p 181	A88-30236
NAG3-752	p 217	N88-24409
NAG3-754	p 180	A88-18696
	p 181	A88-24054
	p 183	A88-47681
	p 194	N88-23272
NAG3-758	p 220	A88-28711
NAG3-759	p 54	A88-43721
NAG3-762	p 207	N88-23233
NAG3-763	p 208	A88-54202
NAG3-764	p 157	A88-22317
	p 8	A88-48901
NAG3-773	p 175	N88-26675
NAG3-776	p 219	N88-23649
NAG3-783	p 174	N88-24976
NAG3-784	p 80	N88-20397
	p 213	N88-20962
NAG3-786	p 127	A88-54711
NAG3-789	p 185	A88-54276
	p 101	A88-54294

NAG3-797	p 204	A88-50223
NAG3-802	p 203	N88-25970
NAG3-805	p 42	A88-50406
NAG3-809	p 78	A88-46499
NAG3-811	p 173	N88-23238
NAG3-816	p 131	N88-30055
NAG3-818	p 201	N88-19000
NAG3-823	p 208	A88-54537
NAG3-843	p 219	N88-26223
NAG3-95	p 96	A88-17214
	p 96	A88-17368
NAG4-1	p 37	A88-50272
NAG8-058	p 204	A88-35775
NASA ORDER C-300020-J	p 199	A88-34250
	p 200	A88-51289
NASA ORDER C-32000-J	p 45	N88-18612
NASA ORDER C-80011-F	p 110	A88-28564
	p 75	N88-25479
NASA ORDER C-86129-D	p 77	A88-11167
	p 222	A88-53050
NASA ORDER C-99066-G	p 211	N88-26885
	p 207	N88-27799
	p 196	N88-29195
NAS1-17670	p 2	A88-11186
	p 3	A88-14459
NAS1-17683	p 2	A88-11186
	p 3	A88-14459
NAS1-18235	p 2	A88-11186
NAS3-17859	p 175	N88-28319
NAS3-181	p 166	A88-23308
	p 166	A88-23309
	p 167	A88-31535
	p 167	A88-31536
NAS3-20646	p 2	A88-11126
NAS3-21055	p 56	N88-10886
NAS3-21930	p 130	N88-28239
NAS3-22110	p 147	N88-11153
NAS3-22234	p 204	N88-30184
NAS3-22238	p 197	A88-11896
NAS3-22445	p 130	N88-28239
NAS3-22447	p 56	N88-10106
NAS3-22466	p 130	N88-28239
NAS3-22473	p 122	A88-18633
NAS3-22525	p 207	N88-21682
NAS3-22540	p 49	N88-21243
NAS3-22755	p 26	N88-14095
	p 27	N88-14096
	p 170	N88-10339
NAS3-22763	p 78	A88-27722
NAS3-22822	p 86	A88-35905
NAS3-22825	p 27	N88-14097
NAS3-23051	p 32	N88-20306
	p 36	N88-28928
NAS3-23247	p 222	N88-24539
NAS3-23260	p 171	N88-13603
NAS3-23288	p 186	N88-11173
	p 178	N88-22426
NAS3-23349	p 158	A88-29818
	p 54	A88-32868
NAS3-23356	p 124	A88-29821
	p 129	N88-23084
NAS3-23529	p 160	N88-11143
NAS3-23687	p 206	N88-11166
NAS3-23689	p 170	N88-11135
NAS3-23691	p 147	N88-11160
NAS3-23697	p 183	A88-48638
	p 184	A88-53088
	p 184	A88-53089
	p 206	N88-11165
	p 190	N88-21535
NAS3-23698	p 185	N88-11164
	p 33	N88-22394
NAS3-23699	p 216	N88-12352
NAS3-23703	p 168	A88-49409
	p 168	A88-49410
NAS3-23708	p 135	A88-20182
	p 215	A88-30998
	p 215	A88-37219
	p 7	A88-48898
	p 12	N88-23751
	p 12	N88-23752
	p 12	N88-23753
NAS3-23712	p 157	A88-22942
NAS3-23716	p 155	N88-30063
	p 155	N88-30066
NAS3-23717	p 145	A88-54152
	p 145	A88-54236
	p 147	N88-11158
	p 153	N88-23956
	p 37	N88-28930
	p 37	N88-29804
NAS3-23722	p 160	N88-11142
NAS3-23772	p 66	N88-29858
NAS3-23773	p 158	A88-29817
	p 55	A88-48037
NAS3-23790	p 124	A88-27575

NAS3-23862	p 200	N88-12875
NAS3-23881	p 50	A88-11738
	p 204	A88-35775
	p 218	A88-47973
	p 219	A88-54999
NAS3-23893	p 59	N88-15006
NAS3-23894	p 129	N88-23939
NAS3-23900	p 212	A88-22696
NAS3-23925	p 84	A88-24037
	p 185	N88-11171
	p 190	N88-21523
	p 37	N88-29811
	p 91	N88-11180
NAS3-23926	p 186	N88-11172
NAS3-23927	p 186	N88-11175
NAS3-23939	p 105	N88-21525
	p 191	N88-22388
	p 93	N88-22427
NAS3-23940	p 183	A88-47001
	p 186	N88-11174
	p 193	N88-22421
NAS3-23941	p 192	N88-22400
	p 36	N88-28074
NAS3-23943	p 170	N88-11184
NAS3-23944	p 68	A88-54353
	p 169	A88-54355
	p 171	N88-11185
NAS3-23945	p 107	N88-28142
NAS3-24080	p 22	A88-37947
NAS3-2410S	p 177	N88-22414
NAS3-24105	p 50	A88-11038
	p 134	A88-16354
	p 78	A88-19233
	p 143	A88-48916
	p 23	A88-53137
	p 161	N88-12042
	p 161	N88-13573
	p 26	N88-14094
	p 10	N88-15762
	p 10	N88-15769
	p 59	N88-17731
	p 224	N88-19377
	p 33	N88-22384
	p 178	N88-22428
	p 173	N88-23242
	p 34	N88-23247
	p 130	N88-25831
	p 13	N88-26336
	p 155	N88-27520
NAS3-24211	p 36	N88-28929
NAS3-24222	p 213	A88-16526
	p 36	N88-28927
NAS3-24223	p 19	A88-27296
NAS3-24227	p 131	A88-11033
	p 139	A88-28516
	p 148	N88-12039
NAS3-24228	p 160	N88-11141
NAS3-24229	p 154	N88-25857
NAS3-24231	p 209	A88-32840
NAS3-24253	p 41	A88-16215
	p 44	A88-27584
	p 48	N88-16794
NAS3-24339	p 19	A88-22487
	p 17	N88-26360
NAS3-24340	p 155	N88-30076
NAS3-24350	p 137	A88-22251
	p 146	N88-11149
NAS3-24351	p 146	N88-11148
	p 13	N88-25445
NAS3-24352	p 159	A88-54159
	p 146	N88-11150
	p 27	N88-14985
NAS3-24358	p 148	N88-11163
NAS3-24381	p 25	N88-10791
	p 25	N88-10792
NAS3-24383	p 110	A88-28557
NAS3-24384	p 106	N88-23879
NAS3-24385	p 102	N88-15886
NAS3-24387	p 20	A88-31610
NAS3-24389	p 180	A88-16933
	p 205	A88-32309
	p 206	A88-32311
	p 56	A88-49659
NAS3-24390	p 103	N88-16868
NAS3-24399	p 127	N88-11948
NAS3-24529	p 18	N88-28917
NAS3-24539	p 174	N88-24975
NAS3-24564	p 121	N88-29077
NAS3-24618	p 65	N88-28087
NAS3-24619	p 147	N88-11156
NAS3-24621	p 215	A88-35939
	p 6	A88-37220
	p 215	A88-37221
NAS3-24630	p 16	N88-18574
NAS3-24631	p 62	N88-23830
NAS3-24632	p 80	N88-15851

CONTRACT NUMBER INDEX

505-62-81

D-3

505-62-91

CONTRACT NUMBER INDEX

505-62-91	p 11	N88-16681	p 200	N88-12878	510-01-01	p 94	N88-24749
	p 12	N88-23751	p 61	N88-22839	533-04-1A	p 190	N88-21535
	p 12	N88-23752	p 130	N88-24870		p 37	N88-29811
505-63-01	p 12	N88-23753	p 130	N88-25831	533-04-11	p 188	N88-18967
	p 90	N88-10938	p 65	N88-26402		p 153	N88-23956
	p 90	N88-10940	p 79	N88-10132		p 13	N88-25445
	p 101	N88-11838	p 69	N88-13385		p 37	N88-28930
	p 68	N88-12543	p 202	N88-25059	533-04-12	p 37	N88-29804
	p 72	N88-14150	p 203	N88-25978		p 185	N88-11140
	p 102	N88-15885	p 80	N88-26430		p 187	N88-13745
	p 103	N88-17796	p 81	N88-27267		p 155	N88-30063
	p 92	N88-19610	p 81	N88-28109	533-05-01	p 155	N88-30066
	p 208	N88-21697	p 227	N88-28853		p 106	N88-23872
	p 76	N88-28980	p 81	N88-29952	533-05-11	p 177	N88-12106
505-63-1A	p 80	N88-15851	p 223	N88-12427	533-07-01	p 179	N88-23985
	p 150	N88-15983	p 93	N88-22981	535-03-01	p 216	N88-10592
	p 151	N88-17954	p 60	N88-21254		p 26	N88-13346
	p 104	N88-18726	p 223	N88-10700		p 216	N88-13960
	p 154	N88-25854	p 101	N88-10188		p 216	N88-13961
505-63-1B	p 102	N88-14206	p 57	N88-11747		p 40	N88-15814
	p 172	N88-18007	p 227	N88-13209		p 188	N88-18036
	p 188	N88-18968	p 224	N88-14046		p 217	N88-18379
	p 188	N88-18969	p 227	N88-14054		p 34	N88-22902
	p 189	N88-18974	p 224	N88-17561		p 13	N88-24597
	p 189	N88-18976	p 59	N88-20361		p 35	N88-24641
	p 206	N88-19147	p 59	N88-21249		p 14	N88-28041
	p 189	N88-21497	p 60	N88-21250		p 163	N88-28286
	p 190	N88-21534	p 105	N88-21306		p 18	N88-28917
	p 190	N88-22382	p 61	N88-22934		p 36	N88-28929
	p 192	N88-22408	p 222	N88-25346		p 163	N88-29142
	p 194	N88-22446	p 64	N88-25477		p 14	N88-29771
	p 93	N88-22986	p 69	N88-28966	535-03	p 9	N88-10008
	p 94	N88-22987	p 72	N88-10899	535-05-01	p 26	N88-13347
	p 194	N88-23226	p 150	N88-15984		p 35	N88-24642
	p 174	N88-23977	p 109	N88-24808	535-07-01	p 72	N88-11758
	p 194	N88-23994	p 65	N88-28087		p 103	N88-16868
	p 195	N88-24997	p 58	N88-12539		p 103	N88-16877
	p 195	N88-25937	p 60	N88-21252		p 92	N88-21295
	p 95	N88-26436	p 63	N88-24689		p 194	N88-23272
	p 107	N88-26482	p 154	N88-25841		p 76	N88-25483
	p 196	N88-27611	p 66	N88-29858		p 76	N88-25487
	p 207	N88-27796	p 57	N88-11748		p 76	N88-28085
	p 207	N88-27799	p 57	N88-11749		p 163	N88-28299
	p 37	N88-29807	p 57	N88-11750		p 180	N88-28323
505-63-11	p 90	N88-10939	p 58	N88-12538		p 196	N88-28332
	p 72	N88-12551	p 58	N88-12542		p 196	N88-29195
	p 72	N88-12552	p 60	N88-21253	545-03-01	p 11	N88-22019
	p 72	N88-13409	p 62	N88-24295	553-04-12	p 196	N88-30164
	p 73	N88-15020	p 62	N88-24296	553-13-00	p 187	N88-15263
	p 73	N88-16828	p 63	N88-24682	582-01-11	p 172	N88-18933
	p 73	N88-17744	p 63	N88-24688		p 64	N88-24690
	p 73	N88-17745	p 174	N88-24968		p 162	N88-26641
	p 74	N88-21257	p 213	N88-25260		p 155	N88-27520
	p 189	N88-21498	p 44	N88-25470		p 155	N88-30078
	p 94	N88-24766	p 65	N88-28088		p 164	N88-30099
	p 175	N88-26679	p 66	N88-29860	582-01-41	p 65	N88-26401
505-63-12	p 92	N88-15060	p 66	N88-29868	586-01-11	p 92	N88-18707
505-63-2A	p 162	N88-23196	p 63	N88-24687		p 60	N88-21251
505-63-21	p 9	N88-13304	p 67	N88-29869		p 152	N88-22322
505-63-31	p 189	N88-18975	p 58	N88-14127		p 61	N88-22933
505-63-51	p 170	N88-11135	p 102	N88-13453		p 94	N88-24754
	p 171	N88-12797	p 102	N88-15872		p 64	N88-25476
	p 171	N88-12798	p 91	N88-11817		p 203	N88-26732
	p 171	N88-13604	p 177	N88-15257		p 95	N88-27310
	p 172	N88-15224	p 161	N88-15996		p 44	N88-29833
	p 38	N88-19475	p 104	N88-17801	643-10-01	p 117	N88-11944
	p 173	N88-21454	p 73	N88-18640		p 118	N88-15910
	p 173	N88-23216	p 178	N88-23224		p 119	N88-16928
	p 174	N88-24975	p 179	N88-23986		p 46	N88-22919
	p 174	N88-24976	p 179	N88-23987	643-10-05	p 119	N88-17899
	p 175	N88-25916	p 119	N88-18809	650-60-20	p 119	N88-18805
	p 175	N88-28312	p 128	N88-20555		p 120	N88-23073
	p 175	N88-30128	p 119	N88-17880		p 120	N88-25762
505-63-71	p 173	N88-23220	p 130	N88-28240		p 121	N88-27424
505-63-81	p 71	N88-10120	p 128	N88-18835		p 121	N88-28222
	p 188	N88-17095	p 128	N88-21400	650-60-23	p 118	N88-14260
	p 194	N88-23278	p 128	N88-15146		p 164	N88-18910
	p 171	N88-12796	p 120	N88-21389		p 46	N88-22920
505-65-11	p 161	N88-12042	p 129	N88-23084		p 120	N88-24847
505-68-11	p 161	N88-12043	p 222	N88-24539	650-60-26	p 118	N88-13513
	p 15	N88-12473	p 130	N88-30048	669-00-00	p 121	N88-26566
	p 15	N88-13310	p 131	N88-30055	674-22-05	p 80	N88-15853
	p 149	N88-13552	p 149	N88-15924	674-24-05	p 151	N88-18871
	p 161	N88-13573	p 63	N88-24686		p 151	N88-19739
	p 10	N88-15766	p 62	N88-23829		p 152	N88-21417
	p 16	N88-18574	p 67	N88-29873		p 152	N88-21424
	p 16	N88-21143	p 48	N88-10084	674-24-06	p 80	N88-18672
505-69-61	p 32	N88-21161	p 45	N88-12520	674-25-05	p 148	N88-12763
505-80-21	p 218	N88-28760	p 49	N88-29845		p 94	N88-25531
505-90-01	p 92	N88-20417	p 49	N88-21243	674-27-05	p 113	N88-24811
	p 32	N88-21160	p 195	N88-25016	679-10-00	p 46	N88-24683
	p 39	N88-26376	p 130	N88-28239	679-40-00	p 118	N88-11945
	p 39	N88-26377	p 186	N88-12825		p 128	N88-12727
506-41-11	p 127	N88-10266	p 187	N88-14453		p 120	N88-23070
	p 128	N88-11966	p 188	N88-18040		p 49	N88-28082
	p 200	N88-12877	p 195	N88-24002	679-40	p 121	N88-29077

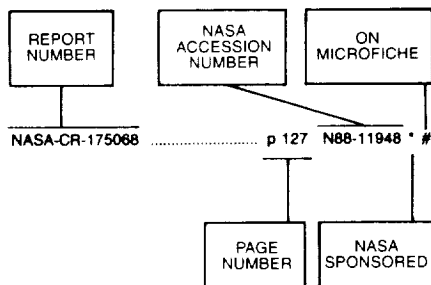
CONTRACT NUMBER INDEX

917-60-00

694-00-03	p 114	N88-26539
694-03-03	p 173	N88-23219
	p 155	N88-30072
694-24-00	p 43	N88-21186
776-33-41	p 201	N88-19014
	p 201	N88-21593
778-32-11	p 25	N88-13338
778-34-22	p 162	N88-18892
778-35-13	p 201	N88-14486
	p 201	N88-19013
	p 225	N88-27980
	p 225	N88-30472
917-60-00	p 43	N88-12515

REPORT/ACCESSION NUMBER INDEX

Typical Report Number Index Listing



Listings in this index are arranged alphanumerically by report number. The NASA accession number denotes the number by which the citation is identified. An asterisk (*) indicates that the item is a NASA report. A pound sign (#) indicates that the item is available on microfiche.

AAS PAPER 86-380 p 110 A88-35130 *
AAS PAPER 87-547 p 42 A88-10957 * #

ACT-101 p 49 N88-28082 * #

AD-A188714 p 206 N88-12288 * #
AD-A189108 p 171 N88-12797 * #
AD-A189109 p 171 N88-12798 * #
AD-A189359 p 170 N88-11135 * #
AD-A190291 p 171 N88-13604 * #
AD-A191003 p 148 N88-12039 * #
AD-A191884 p 172 N88-15224 * #
AD-A192057 p 150 N88-15983 * #
AD-A193313 p 103 N88-16877 * #
AD-A195935 p 173 N88-23220 * #
AD-A196985 p 174 N88-24976 * #
AD-A197535 p 154 N88-25854 * #
AD-A197797 p 173 N88-21454 * #
AD-A197797 p 173 N88-23216 * #
AD-A199197 p 175 N88-28312 * #
AD-A199405 p 174 N88-24975 * #

AIAA PAPER 87-1953 p 137 A88-23312 * #
AIAA PAPER 87-2656 p 213 A88-16526 * #
AIAA PAPER 87-2657 p 214 A88-20176 * #
AIAA PAPER 87-2677 p 213 A88-16539 * #
AIAA PAPER 87-2689 p 134 A88-16545 * #
AIAA PAPER 87-2692 p 3 A88-18654 * #
AIAA PAPER 87-2717 p 214 A88-16565 * #
AIAA PAPER 87-2719 p 3 A88-18655 * #
AIAA PAPER 87-2722 p 3 A88-16567 * #
AIAA PAPER 87-2723 p 135 A88-20182 * #
AIAA PAPER 87-2725 p 4 A88-20184 * #
AIAA PAPER 87-2731 p 214 A88-16571 * #
AIAA PAPER 87-2741 p 212 A88-16577 * #
AIAA PAPER 87-2742 p 214 A88-16578 * #
AIAA PAPER 88-0018 p 17 A88-22016 * #
AIAA PAPER 88-0019 p 17 A88-22017 * #
AIAA PAPER 88-0027 p 99 A88-41796 * #
AIAA PAPER 88-0049 p 5 A88-27715 * #
AIAA PAPER 88-0061 p 138 A88-27716 * #
AIAA PAPER 88-0112 p 4 A88-22078 * #
AIAA PAPER 88-0115 p 14 A88-22079 * #
AIAA PAPER 88-0131 p 4 A88-22093 * #
AIAA PAPER 88-0169 p 39 A88-22121 * #
AIAA PAPER 88-0248 p 110 A88-22186 * #
AIAA PAPER 88-0263 p 214 A88-22192 * #
AIAA PAPER 88-0264 p 215 A88-22193 * #
AIAA PAPER 88-0273 p 5 A88-27717 * #
AIAA PAPER 88-0287 p 136 A88-22207 * #
AIAA PAPER 88-0289 p 137 A88-22209 * #
AIAA PAPER 88-0290 p 137 A88-22210 * #
AIAA PAPER 88-0291 p 157 A88-22211 * #
AIAA PAPER 88-0308 p 6 A88-27718 * #
AIAA PAPER 88-0342 p 137 A88-22251 * #

AIAA PAPER 88-0425 p 157 A88-22317 * #
AIAA PAPER 88-0436 p 5 A88-24825 * #
AIAA PAPER 88-0450 p 138 A88-27719 * #
AIAA PAPER 88-0470 p 137 A88-22346 * #
AIAA PAPER 88-0497 p 5 A88-22364 * #
AIAA PAPER 88-0540 p 41 A88-22405 * #
AIAA PAPER 88-0543 p 108 A88-27720 * #
AIAA PAPER 88-0559 p 137 A88-22419 * #
AIAA PAPER 88-0594 p 5 A88-22444 * #
AIAA PAPER 88-0621 p 5 A88-22469 * #
AIAA PAPER 88-0624 p 209 A88-22472 * #
AIAA PAPER 88-0637 p 108 A88-27721 * #
AIAA PAPER 88-0645 p 78 A88-27722 * #
AIAA PAPER 88-0665 p 5 A88-22495 * #
AIAA PAPER 88-0667 p 19 A88-22497 * #
AIAA PAPER 88-0714 p 139 A88-27723 * #
AIAA PAPER 88-0770 p 45 A88-27544 * #
AIAA PAPER 88-0788 p 212 A88-27531 * #
AIAA PAPER 88-0800 p 116 A88-27551 * #
AIAA PAPER 88-0802 p 46 A88-27553 * #
AIAA PAPER 88-0811 p 123 A88-27558 * #
AIAA PAPER 88-0812 p 123 A88-27559 * #
AIAA PAPER 88-0813 p 116 A88-27560 * #
AIAA PAPER 88-0826 p 123 A88-27572 * #
AIAA PAPER 88-0830 p 124 A88-27575 * #
AIAA PAPER 88-0835 p 124 A88-27578 * #
AIAA PAPER 88-0842 p 46 A88-27583 * #
AIAA PAPER 88-0843 p 44 A88-27584 * #
AIAA PAPER 88-0870 p 116 A88-27604 * #
AIAA PAPER 88-2019 p 40 A88-37926 * #
AIAA PAPER 88-2055 p 6 A88-44490 * #
AIAA PAPER 88-2057 p 22 A88-37947 * #
AIAA PAPER 88-2222 p 39 A88-32188 * #
AIAA PAPER 88-2238 p 215 A88-35939 * #
AIAA PAPER 88-2261 p 181 A88-32219 * #
AIAA PAPER 88-2266 p 20 A88-32223 * #
AIAA PAPER 88-2333 p 20 A88-32277 * #
AIAA PAPER 88-2348 p 182 A88-32289 * #
AIAA PAPER 88-2371 p 182 A88-32308 * #
AIAA PAPER 88-2372 p 205 A88-32309 * #
AIAA PAPER 88-2373 p 182 A88-32310 * #
AIAA PAPER 88-2374 p 206 A88-32311 * #
AIAA PAPER 88-2375 p 182 A88-32312 * #
AIAA PAPER 88-2376 p 182 A88-32313 * #
AIAA PAPER 88-2377 p 6 A88-32314 * #
AIAA PAPER 88-2390 p 182 A88-32322 * #
AIAA PAPER 88-2400 p 20 A88-32332 * #
AIAA PAPER 88-2440 p 85 A88-32357 * #
AIAA PAPER 88-2440 p 70 A88-35945 * #
AIAA PAPER 88-2475 p 47 A88-31396 * #
AIAA PAPER 88-2532 p 6 A88-40718 * #
AIAA PAPER 88-2643 p 54 A88-43721 * #
AIAA PAPER 88-2683 p 141 A88-43746 * #
AIAA PAPER 88-2793 p 56 A88-53101 * #
AIAA PAPER 88-2821 p 109 A88-48751 * #
AIAA PAPER 88-2829 p 7 A88-44667 * #
AIAA PAPER 88-2872 p 22 A88-45011 * #
AIAA PAPER 88-2882 p 23 A88-48752 * #
AIAA PAPER 88-2912 p 55 A88-48753 * #
AIAA PAPER 88-2957 p 7 A88-44705 * #
AIAA PAPER 88-2962 p 22 A88-44706 * #
AIAA PAPER 88-2979 p 100 A88-48031 * #
AIAA PAPER 88-2985 p 23 A88-48032 * #
AIAA PAPER 88-3016 p 22 A88-44727 * #
AIAA PAPER 88-3054 p 168 A88-44742 * #
AIAA PAPER 88-3055 p 100 A88-44743 * #
AIAA PAPER 88-3059 p 71 A88-44745 * #
AIAA PAPER 88-3075 p 23 A88-53137 * #
AIAA PAPER 88-3105 p 55 A88-48755 * #
AIAA PAPER 88-3106 p 55 A88-48756 * #
AIAA PAPER 88-3113 p 55 A88-48037 * #
AIAA PAPER 88-3117 p 42 A88-48038 * #
AIAA PAPER 88-3138 p 142 A88-48757 * #
AIAA PAPER 88-3149 p 7 A88-48758 * #
AIAA PAPER 88-3180 p 23 A88-50783 * #
AIAA PAPER 88-3183 p 141 A88-44783 * #
AIAA PAPER 88-3224 p 78 A88-46499 * #
AIAA PAPER 88-3229 p 23 A88-48759 * #
AIAA PAPER 88-3280 p 23 A88-50785 * #
AIAA PAPER 88-3283 p 55 A88-48761 * #
AIAA PAPER 88-3286 p 40 A88-44820 * #
AIAA PAPER 88-3288 p 142 A88-48762 * #
AIAA PAPER 88-3300 p 109 A88-48764 * #

AIAA PAPER 88-3301 p 144 A88-50786 * #
AIAA PAPER 88-3403 p 55 A88-48765 * #
AIAA PAPER 88-3510 p 111 A88-42908 * #
AIAA PAPER 88-3522 p 142 A88-48779 * #
AIAA PAPER 88-3526 p 142 A88-48782 * #
AIAA PAPER 88-3557 p 143 A88-48946 * #
AIAA PAPER 88-3565 p 209 A88-48791 * #
AIAA PAPER 88-3592 p 7 A88-48893 * #
AIAA PAPER 88-3612 p 7 A88-48898 * #
AIAA PAPER 88-3613 p 8 A88-48899 * #
AIAA PAPER 88-3615 p 8 A88-48901 * #
AIAA PAPER 88-3645 p 209 A88-48806 * #
AIAA PAPER 88-3692 p 168 A88-48971 * #
AIAA PAPER 88-3702 p 143 A88-48915 * #
AIAA PAPER 88-3703 p 143 A88-48916 * #
AIAA PAPER 88-3707 p 210 A88-48831 * #
AIAA PAPER 88-3718 p 143 A88-48974 * #
AIAA PAPER 88-3728 p 143 A88-48980 * #
AIAA PAPER 88-3823 p 144 A88-49000 * #
AIAA PAPER 88-4121 p 204 A88-50223 * #
AIAA PAPER 88-4182 p 37 A88-50272 * #
AIAA PAPER 88-4279 p 42 A88-50406 * #
AIAA PAPER 88-4310 p 42 A88-50435 * #
AIAA PAPER 88-4361 p 8 A88-50604 * #
AIAA PAPER 88-4656 p 18 A88-51910 * #

AIAA-86-1352 p 153 N88-23718 * #
AIAA-87-0178 p 16 N88-23717 * #
AIAA-87-2657 p 216 N88-10592 * #
AIAA-87-2692 p 11 N88-16681 * #
AIAA-87-2719 p 9 N88-10008 * #
AIAA-88-0027 p 105 N88-21306 * #
AIAA-88-0049 p 10 N88-14967 * #
AIAA-88-0061 p 152 N88-19740 * #
AIAA-88-0131 p 9 N88-10779 * #
AIAA-88-0263 p 216 N88-13961 * #
AIAA-88-0287 p 149 N88-13552 * #
AIAA-88-0289 p 24 N88-10790 * #
AIAA-88-0291 p 161 N88-13573 * #
AIAA-88-0436 p 26 N88-14094 * #
AIAA-88-0450 p 80 N88-18672 * #
AIAA-88-0594 p 9 N88-10778 * #
AIAA-88-0714 p 10 N88-15762 * #
AIAA-88-0788 p 46 N88-22919 * #
AIAA-88-0826 p 46 N88-22920 * #
AIAA-88-2348 p 188 N88-18969 * #
AIAA-88-2377 p 189 N88-18976 * #
AIAA-88-2475 p 74 N88-19592 * #
AIAA-88-2645 p 113 N88-24811 * #
AIAA-88-2815 p 14 N88-28041 * #
AIAA-88-2821 p 109 N88-24808 * #
AIAA-88-2829 p 154 N88-24917 * #
AIAA-88-2882 p 1 N88-23729 * #
AIAA-88-2912 p 63 N88-24688 * #
AIAA-88-2914 p 65 N88-28088 * #
AIAA-88-2963 p 33 N88-22037 * #
AIAA-88-2979 p 173 N88-23220 * #
AIAA-88-2985 p 34 N88-23806 * #
AIAA-88-3016 p 32 N88-21162 * #
AIAA-88-3076 p 13 N88-26336 * #
AIAA-88-3091 p 156 N88-30094 * #
AIAA-88-3105 p 63 N88-24682 * #
AIAA-88-3106 p 63 N88-24687 * #
AIAA-88-3114 p 65 N88-26401 * #
AIAA-88-3138 p 34 N88-24639 * #
AIAA-88-3149 p 13 N88-24597 * #
AIAA-88-3152 p 14 N88-29771 * #
AIAA-88-3153 p 196 N88-28344 * #
AIAA-88-3154 p 37 N88-29907 * #
AIAA-88-3180 p 34 N88-24640 * #
AIAA-88-3211 p 66 N88-29980 * #
AIAA-88-3229 p 35 N88-24642 * #
AIAA-88-3283 p 213 N88-25260 * #
AIAA-88-3288 p 174 N88-24968 * #
AIAA-88-3300 p 63 N88-24689 * #
AIAA-88-3403 p 63 N88-24686 * #
AIAA-88-3567 p 13 N88-26340 * #
AIAA-89-0205 p 14 N88-29780 * #

AIME-A88-23 p 43 N88-21186 * #
AIRESEARCH-87-61069 p 203 N88-25977 * #

ASME PAPER 86-DET-3

REPORT NUMBER INDEX

ASME PAPER 86-DET-3	p 165	A88-10973 *	#	DOE/NASA/0167-13	p 224	N88-20229 *	#	E-3798-SESS-3	p 28	N88-15790 *	#
ASME PAPER 86-GT-114	p 139	A88-28516 *	#	DOE/NASA/0234-1	p 92	N88-19613 *	#	E-3798-SESS-4	p 28	N88-15794 *	#
ASME PAPER 86-TRIB-63	p 133	A88-15124 *	#	DOE/NASA/0329-1	p 224	N88-12428 *	#	E-3798-SESS-5	p 28	N88-15800 *	#
ASME PAPER 87-GT-106	p 50	A88-11038 *	#	DOE/NASA/1005-12	p 223	N88-12427 *	#	E-3798-SESS-6	p 29	N88-15807 *	#
ASME PAPER 87-GT-160	p 2	A88-11072 *	#	DOE/NASA/16310-5	p 92	N88-18707 *	#	E-3800	p 128	N88-15146 *	#
ASME PAPER 87-GT-168	p 18	A88-11079 *	#	DOE/NASA/16310-6	p 93	N88-22981 *	#	E-3802	p 223	N88-10700 *	#
ASME PAPER 87-GT-173	p 165	A88-11083 *	#	DOE/NASA/20320-74	p 201	N88-19014 *	#	E-3803	p 148	N88-12752 *	#
ASME PAPER 87-GT-181	p 131	A88-11089 *	#	DOE/NASA/20320-75	p 201	N88-21593 *	#	E-3807	p 128	N88-11966 *	#
ASME PAPER 87-GT-199	p 131	A88-11103 *	#	DOE/NASA/50111-1	p 25	N88-13338 *	#	E-3808	p 201	N88-14486 *	#
ASME PAPER 87-GT-225	p 2	A88-11121 *	#	DOE/NASA/50112-71	p 102	N88-13453 *	#	E-3812	p 38	N88-19475 *	#
ASME PAPER 87-GT-226	p 4	A88-18660 *	#	DOE/NASA/50112-72	p 201	N88-14486 *	#	E-3814	p 90	N88-10940 *	#
ASME PAPER 87-GT-227	p 4	A88-18661 *	#	DOE/NASA/50112-73	p 102	N88-15872 *	#	E-3819	p 25	N88-11679 *	#
ASME PAPER 87-GT-235	p 2	A88-11126 *	#	DOE/NASA/50112-74	p 201	N88-19013 *	#	E-3820	p 206	N88-12288 *	#
ASME PAPER 87-GT-241	p 157	A88-11129 *	#	DOE/NASA/50112-75	p 225	N88-30472 *	#	E-3821	p 90	N88-10938 *	#
ASME PAPER 87-GT-248	p 131	A88-11130 *	#	DOE/NASA/50112-76	p 225	N88-27980 *	#	E-3822	p 9	N88-10779 *	#
ASME PAPER 87-GT-249	p 132	A88-11131 *	#	DOE/NASA/50162-1	p 162	N88-18892 *	#	E-3823	p 40	N88-15814 *	#
ASME PAPER 87-GT-250	p 132	A88-11132 *	#	DOE/NASA/50162-2	p 104	N88-18726 *	#	E-3824	p 90	N88-10939 *	#
ASME PAPER 87-GT-251	p 132	A88-11133 *	#					E-3825	p 57	N88-11746 *	#
ASME PAPER 87-GT-46	p 18	A88-10998 *	#	DOT/FAA/CT-87/17	p 16	N88-21143 *	#	E-3826	p 210	N88-10563 *	#
ASME PAPER 87-GT-48	p 131	A88-11000 *	#	DOT/FAA/CT-87/30	p 16	N88-18574 *	#	E-3827	p 171	N88-13604 *	#
ASME PAPER 87-GT-78	p 21	A88-36745 *	#					E-3829	p 9	N88-10778 *	#
ASME PAPER 87-GT-94	p 131	A88-11033 *	#	D500-11313-1	p 18	N88-28917 *	#	E-3830	p 26	N88-13346 *	#
ASME PAPER 87-ICE-18	p 96	A88-15120 *	#					E-3831	p 148	N88-12763 *	#
ASME PAPER 87-ICE-29	p 19	A88-15119 *	#	E-2543	p 9	N88-12461 *	#	E-3832	p 24	N88-10790 *	#
ASME PAPER 87-TRIB-48	p 166	A88-24034 *	#	E-2593	p 201	N88-19013 *	#	E-3833	p 224	N88-14046 *	#
ASME PAPER 87-TRIB-52	p 166	A88-23308 *	#	E-2727	p 185	N88-11140 *	#	E-3838	p 151	N88-19739 *	#
ASME PAPER 87-TRIB-53	p 166	A88-23309 *	#	E-2776	p 196	N88-30164 *	#	E-3839	p 227	N88-13209 *	#
ASME PAPER 87-TRIB-55	p 166	A88-23310 *	#	E-3056	p 225	N88-30472 *	#	E-3842-1	p 107	N88-26482 *	#
ASME PAPER 87-WA/AERO-8	p 184	A88-51328 *	#	E-3063	p 106	N88-23872 *	#	E-3843	p 72	N88-11758 *	#
ASME PAPER 87-WA/NCA-13	p 144	A88-51343 *	#	E-3187	p 121	N88-29077 *	#	E-3844	p 210	N88-12330 *	#
ASME PAPER 87-WA/NCA-18	p 140	A88-41568 *	#	E-3191	p 172	N88-17045 *	#	E-3845	p 38	N88-11680 *	#
ASME PAPER 88-GT-111	p 145	A88-54229 *	#	E-3218	p 40	N88-17686 *	#	E-3846	p 26	N88-14093 *	#
ASME PAPER 88-GT-125	p 145	A88-54236 *	#	E-3226	p 43	N88-12515 *	#	E-3847	p 227	N88-14054 *	#
ASME PAPER 88-GT-12	p 159	A88-54159 *	#	E-3251	p 62	N88-23829 *	#	E-3848	p 120	N88-21389 *	#
ASME PAPER 88-GT-173	p 145	A88-54267 *	#	E-3295	p 223	N88-12427 *	#	E-3849	p 161	N88-12042 *	#
ASME PAPER 88-GT-185	p 185	A88-54276 *	#	E-3296	p 73	N88-16828 *	#	E-3850	p 57	N88-11745 *	#
ASME PAPER 88-GT-18	p 145	A88-54164 *	#	E-3310	p 71	N88-10121 *	#	E-3851	p 16	N88-18574 *	#
ASME PAPER 88-GT-208	p 101	A88-54294 *	#	E-3353	p 118	N88-13513 *	#	E-3852	p 225	N88-12429 *	#
ASME PAPER 88-GT-231	p 169	A88-54313 *	#	E-3358	p 48	N88-10084 *	#	E-3853	p 11	N88-17582 *	#
ASME PAPER 88-GT-241	p 146	A88-54320 *	#	E-3395	p 68	N88-12543 *	#	E-3854	p 161	N88-12043 *	#
ASME PAPER 88-GT-252	p 169	A88-54328 *	#	E-3464	p 45	N88-12520 *	#	E-3856	p 59	N88-17731 *	#
ASME PAPER 88-GT-278	p 68	A88-54350 *	#	E-3480	p 73	N88-18640 *	#	E-3857	p 57	N88-11750 *	#
ASME PAPER 88-GT-284	p 68	A88-54353 *	#	E-3489	p 79	N88-15036 *	#	E-3858	p 57	N88-11748 *	#
ASME PAPER 88-GT-286	p 169	A88-54355 *	#	E-3507	p 120	N88-19698 *	#	E-3859	p 118	N88-14260 *	#
ASME PAPER 88-GT-306	p 9	A88-54375 *	#	E-3508	p 32	N88-21160 *	#	E-3860	p 101	N88-11838 *	#
ASME PAPER 88-GT-57	p 8	A88-54189 *	#	E-3535	p 187	N88-13745 *	#	E-3861	p 91	N88-11817 *	#
ASME PAPER 88-GT-5	p 145	A88-54152 *	#	E-3548	p 26	N88-13347 *	#	E-3862	p 72	N88-12551 *	#
ASME PAPER 88-GT-63	p 169	A88-54195 *	#	E-3658	p 15	N88-12473 *	#	E-3863	p 210	N88-13931 *	#
ASME PAPER 88-GT-64	p 169	A88-54196 *	#	E-3661	p 171	N88-12796 *	#	E-3865	p 57	N88-11747 *	#
ASME PAPER 88-GT-73	p 208	A88-54202 *	#	E-3663	p 128	N88-12727 *	#	E-3866	p 118	N88-11945 *	#
ASME PAPER 88-GT-78	p 8	A88-54206 *	#	E-3665-1	p 72	N88-10899 *	#	E-3867	p 186	N88-12825 *	#
ASME PAPER 88-GT-7	p 145	A88-54154 *	#	E-3666	p 160	N88-11100 *	#	E-3868	p 152	N88-19740 *	#
				E-3676	p 58	N88-12542 *	#	E-3869	p 25	N88-13338 *	#
ASTM STP-942	p 86	A88-35901 *	#	E-3680	p 224	N88-17561 *	#	E-3870	p 72	N88-15018 *	#
				E-3684	p 25	N88-12490 *	#	E-3871	p 102	N88-13453 *	#
AVSCOM-TM-87-C-2	p 171	N88-12797 *	#	E-3685	p 31	N88-18594 *	#	E-3873	p 102	N88-14206 *	#
AVSCOM-TM-87-C-3	p 171	N88-12798 *	#	E-3689	p 25	N88-13345 *	#	E-3875	p 26	N88-14094 *	#
AVSCOM-TM-88-C-001	p 32	N88-19469 *	#	E-3696	p 200	N88-12877 *	#	E-3876	p 149	N88-14320 *	#
AVSCOM-TM-88-C-003	p 175	N88-30128 *	#	E-3697	p 200	N88-12878 *	#	E-3877	p 9	N88-13304 *	#
AVSCOM-TM-88-C-004	p 175	N88-28312 *	#	E-3704	p 71	N88-10120 *	#	E-3880	p 216	N88-13961 *	#
				E-3708	p 72	N88-14150 *	#	E-3881	p 151	N88-18871 *	#
AVSCOM-TP-88-C-001	p 156	N88-30094 *	#	E-3710	p 177	N88-15257 *	#	E-3882	p 150	N88-15984 *	#
				E-3722	p 118	N88-15910 *	#	E-3883	p 60	N88-21253 *	#
AVSCOM-TR-87-C-14	p 148	N88-12039 *	#	E-3723	p 119	N88-16928 *	#	E-3886	p 161	N88-13573 *	#
AVSCOM-TR-87-C-27	p 206	N88-12288 *	#	E-3724	p 117	N88-11925 *	#	E-3889	p 79	N88-13428 *	#
AVSCOM-TR-87-C-28	p 172	N88-15224 *	#	E-3725	p 11	N88-20262 *	#	E-3890	p 172	N88-18933 *	#
AVSCOM-TR-87-C-29	p 170	N88-11135 *	#	E-3729	p 101	N88-10188 *	#	E-3891	p 217	N88-18379 *	#
AVSCOM-TR-87-C-37	p 173	N88-23220 *	#	E-3732	p 149	N88-15924 *	#	E-3892	p 118	N88-13515 *	#
AVSCOM-TR-88-C-001	p 150	N88-15983 *	#	E-3737	p 9	N88-10008 *	#	E-3896	p 187	N88-13754 *	#
AVSCOM-TR-88-C-002	p 173	N88-21454 *	#	E-3738	p 58	N88-12538 *	#	E-3897	p 151	N88-17954 *	#
AVSCOM-TR-88-C-002	p 173	N88-23216 *	#	E-3739-1	p 10	N88-15762 *	#	E-3898	p 216	N88-13960 *	#
AVSCOM-TR-88-C-004	p 103	N88-16877 *	#	E-3740	p 227	N88-22851 *	#	E-3901	p 224	N88-19377 *	#
AVSCOM-TR-88-C-006	p 154	N88-25854 *	#	E-3744	p 188	N88-17095 *	#	E-3903	p 151	N88-18867 *	#
AVSCOM-TR-88-C-009	p 174	N88-24975 *	#	E-3750	p 72	N88-12552 *	#	E-3904	p 43	N88-28942 *	#
AVSCOM-TR-88-C-011	p 32	N88-21163 *	#	E-3753	p 177	N88-12106 *	#	E-3908	p 188	N88-18036 *	#
AVSCOM-TR-88-C-016	p 174	N88-24976 *	#	E-3754	p 69	N88-13385 *	#	E-3909	p 150	N88-16988 *	#
AVSCOM-TR-88-C-018	p 41	N88-29825 *	#	E-3755	p 72	N88-13409 *	#	E-3912	p 80	N88-18672 *	#
AVSCOM-TR-88-C-019	p 175	N88-25916 *	#	E-3756	p 171	N88-12797 *	#	E-3914	p 32	N88-19469 *	#
AVSCOM-TR-88-C-025	p 36	N88-27201 *	#	E-3756	p 171	N88-12798 *	#	E-3916	p 201	N88-19014 *	#
				E-3759	p 39	N88-26376 *	#	E-3917	p 102	N88-15872 *	#
CALSPAN-7157-A-1	p 216	N88-12352 *	#	E-3760	p 39	N88-26377 *	#	E-3919	p 76	N88-28094 *	#
				E-3762	p 94	N88-25531 *	#	E-3920	p 194	N88-22446 *	#
CONF-8706254-1	p 202	N88-22458 *	#	E-3766	p 216	N88-10592 *	#	E-3921	p 92	N88-15060 *	#
CONF-8708122-1	p 210	N88-12323 *	#	E-3770	p 172	N88-15224 *	#	E-3922	p 73	N88-15020 *	#
CONF-8804122-1	p 203	N88-27624 *	#	E-3773	p 58	N88-12539 *	#	E-3923	p 161	N88-14339 *	#
CONF-880466-1	p 43	N88-26385 *	#	E-3775	p 92	N88-19610 *	#	E-3924	p 149	N88-13552 *	#
				E-3777	p 117	N88-11944 *	#	E-3925	p 46	N88-22920 *	#
DDA-R01-ADECD-NAS	p 224	N88-12428 *	#	E-3780	p 11	N88-16681 *	#	E-3926	p 188	N88-18967 *	#
				E-3783	p 58	N88-14127 *	#	E-3927	p 187	N88-14453 *	#
DE87-014729	p 210	N88-12323 *	#	E-3785	p 80	N88-15853 *	#	E-3928	p 10	N88-15769 *	#
DE88-003153	p 202	N88-22458 *	#	E-3790	p 79	N88-10132 *	#	E-3929	p 119	N88-18805 *	#
DE88-009468	p 203	N88-27624 *	#	E-3792	p 127	N88-10266 *	#	E-3932	p 120	N88-23073 *	#
DE88-009955	p 43	N88-26385 *	#	E-3795	p 187	N88-15263 *	#	E-3934	p 172	N88-18007 *	#
				E-3797	p 79	N88-11775 *	#	E-3935	p 45	N88-19565 *	#
DOE/NASA/0032-28	p 223	N88-11578 *	#	E-3798-SESS-1	p 31	N88-16697 *	#	E-3936	p 73	N88-17744 *	#
DOE/NASA/0167-12	p 225	N88-20230 *	#	E-3798-SESS-2	p 27	N88-15785 *	#	E-3937	p 149	N88-15188 *	#

REPORT NUMBER INDEX

IEPC-88-035

E-3939	p 150	N88-15983 * #	E-4082	p 114	N88-26539 * #	E-4271	p 35	N88-25460 * #
E-3940	p 173	N88-23216 * #	E-4086	p 75	N88-25479 * #	E-4272	p 65	N88-28088 * #
E-3942	p 103	N88-17796 * #	E-4089	p 173	N88-21454 * #	E-4274	p 66	N88-29860 * #
E-3943	p 43	N88-21186 * #	E-4090	p 64	N88-25475 * #	E-4276	p 1	N88-26328 * #
E-3944-1	p 162	N88-23194 * #	E-4091	p 114	N88-21375 * #	E-4277	p 162	N88-26641 * #
E-3945	p 162	N88-23196 * #	E-4092	p 114	N88-21374 * #	E-4278	p 207	N88-27796 * #
E-3946	p 73	N88-17745 * #	E-4096	p 40	N88-25464 * #	E-4281	p 180	N88-28323 * #
E-3948	p 119	N88-17899 * #	E-4099	p 11	N88-22019 * #	E-4287	p 13	N88-26336 * #
E-3951	p 59	N88-15838 * #	E-4101	p 203	N88-26732 * #	E-4288	p 196	N88-28332 * #
E-3953	p 153	N88-23186 * #	E-4102	p 61	N88-22933 * #	E-4294	p 115	N88-28176 * #
E-3954	p 104	N88-17801 * #	E-4104	p 63	N88-24689 * #	E-4295	p 156	N88-30090 * #
E-3955	p 102	N88-15885 * #	E-4105	p 154	N88-23957 * #	E-4297	p 163	N88-29152 * #
E-3956	p 189	N88-21498 * #	E-4106	p 211	N88-25239 * #	E-4304	p 67	N88-29874 * #
E-3958	p 44	N88-17715 * #	E-4110	p 120	N88-24847 * #	E-4305	p 81	N88-28109 * #
E-3959	p 10	N88-14967 * #	E-4111	p 195	N88-25937 * #	E-4308	p 14	N88-28041 * #
E-3960	p 153	N88-23185 * #	E-4112	p 1	N88-21116 * #	E-4309	p 155	N88-30072 * #
E-3961	p 48	N88-17728 * #	E-4115	p 12	N88-23732 * #	E-4310	p 49	N88-28959 * #
E-3962	p 46	N88-22919 * #	E-4117	p 195	N88-25935 * #	E-4314	p 218	N88-28760 * #
E-3963	p 131	N88-30055 * #	E-4118	p 93	N88-22168 * #	E-4315	p 163	N88-28293 * #
E-3964	p 211	N88-19202 * #	E-4119	p 49	N88-21245 * #	E-4317	p 13	N88-27174 * #
E-3966	p 103	N88-16877 * #	E-4120	p 33	N88-22037 * #	E-4321	p 196	N88-28344 * #
E-3967	p 164	N88-18910 * #	E-4122	p 203	N88-25978 * #	E-4325	p 121	N88-28222 * #
E-3969	p 188	N88-18968 * #	E-4123	p 174	N88-23977 * #	E-4327	p 121	N88-27424 * #
E-3970-VOL-1	p 194	N88-23226 * #	E-4124	p 32	N88-21163 * #	E-4331	p 155	N88-27520 * #
E-3970-VOL-2	p 190	N88-22382 * #	E-4129	p 34	N88-22902 * #	E-4336	p 69	N88-28966 * #
E-3970-VOL-3	p 192	N88-22408 * #	E-4130	p 76	N88-25487 * #	E-4337	p 67	N88-29869 * #
E-3971	p 61	N88-22934 * #	E-4131-1	p 163	N88-29142 * #	E-4338	p 212	N88-30377 * #
E-3972	p 188	N88-18040 * #	E-4131	p 163	N88-28286 * #	E-4339	p 130	N88-30048 * #
E-3973	p 10	N88-16679 * #	E-4134	p 162	N88-26644 * #	E-4342	p 155	N88-30078 * #
E-3975	p 60	N88-21252 * #	E-4135	p 94	N88-24754 * #	E-4344	p 18	N88-28062 * #
E-3976	p 162	N88-18892 * #	E-4138	p 1	N88-23729 * #	E-4345	p 81	N88-29952 * #
E-3977	p 104	N88-20454 * #	E-4140	p 64	N88-25477 * #	E-4349	p 156	N88-30084 * #
E-3978	p 190	N88-21534 * #	E-4143	p 34	N88-24640 * #	E-4356	p 66	N88-29888 * #
E-3980	p 189	N88-18974 * #	E-4146	p 14	N88-29746 * #	E-4363	p 115	N88-29997 * #
E-3981	p 119	N88-17880 * #	E-4148	p 173	N88-23219 * #	E-4373	p 14	N88-29780 * #
E-3982	p 201	N88-21593 * #	E-4150	p 64	N88-25474 * #	E-4378	p 67	N88-29873 * #
E-3984	p 92	N88-18707 * #	E-4153	p 61	N88-22939 * #	E-4387	p 14	N88-29771 * #
E-3986	p 104	N88-18726 * #	E-4154	p 94	N88-24749 * #	E-4414	p 49	N88-29845 * #
E-3987	p 152	N88-20599 * #	E-4155	p 61	N88-22935 * #			
E-3988	p 210	N88-19182 * #	E-4156	p 35	N88-25458 * #	EDR-12815	p 103	N88-18688 * #
E-3989	p 46	N88-24663 * #	E-4157	p 113	N88-24811 * #			
E-3990	p 189	N88-18976 * #	E-4160	p 207	N88-26127 * #	ESL-TR-718688-6	p 42	N88-14110 * #
E-3993	p 188	N88-18969 * #	E-4162	p 223	N88-28832 * #			
E-3994	p 194	N88-23994 * #	E-4163	p 13	N88-26340 * #	ESL-718300-1	p 213	N88-20962 * #
E-3995	p 179	N88-23987 * #	E-4166	p 130	N88-24870 * #			
E-3996	p 178	N88-23224 * #	E-4171	p 130	N88-25831 * #	FCR-6128	p 204	N88-30184 * #
E-3999	p 206	N88-19147 * #	E-4172	p 154	N88-24917 * #			
E-4000	p 151	N88-18670 * #	E-4173	p 173	N88-23220 * #	FLOW-RR-425	p 154	N88-25857 * #
E-4001	p 12	N88-23751 * #	E-4176	p 34	N88-24639 * #			
E-4002	p 12	N88-23752 * #	E-4178	p 34	N88-23806 * #	FR-20311-1	p 66	N88-29867 * #
E-4003	p 12	N88-23753 * #	E-4179	p 63	N88-24682 * #	FR-715723-2	p 118	N88-15130 * #
E-4005	p 74	N88-19592 * #	E-4181	p 175	N88-30128 * #			
E-4006	p 175	N88-28312 * #	E-4182	p 76	N88-25483 * #	GARRETT-21-6689	p 155	N88-30076 * #
E-4007	p 189	N88-18975 * #	E-4185	p 175	N88-25916 * #	GARRETT-31-3725(13)	p 224	N88-20229 * #
E-4008	p 59	N88-21249 * #	E-4186	p 75	N88-24712 * #			
E-4009	p 128	N88-18835 * #	E-4190	p 35	N88-25459 * #	GDSS-SP-87-003	p 49	N88-25473 * #
E-4010	p 207	N88-22591 * #	E-4192	p 174	N88-24968 * #	GDSS-SP-88-006	p 44	N88-29835 * #
E-4011	p 104	N88-20455 * #	E-4194	p 196	N88-29195 * #			
E-4012	p 43	N88-24659 * #	E-4198	p 35	N88-24641 * #	GTEC-21-5988	p 107	N88-28142 * #
E-4013	p 179	N88-23985 * #	E-4200	p 164	N88-30099 * #			
E-4015	p 120	N88-25762 * #	E-4201	p 13	N88-25435 * #	HAC-E7324	p 56	N88-10106 * #
E-4019	p 92	N88-20417 * #	E-4204	p 64	N88-24690 * #			
E-4020	p 189	N88-21497 * #	E-4206	p 63	N88-24686 * #	HSER-11054	p 26	N88-14095 * #
E-4023	p 105	N88-21306 * #	E-4208	p 180	N88-25923 * #	HSER-11055	p 27	N88-14096 * #
E-4024	p 208	N88-21697 * #	E-4211	p 12	N88-24592 * #	HSER-9246	p 27	N88-14097 * #
E-4026	p 60	N88-21254 * #	E-4212	p 194	N88-23278 * #	HSER-9251	p 36	N88-28928 * #
E-4027	p 104	N88-18734 * #	E-4216	p 202	N88-25059 * #			
E-4029	p 74	N88-21257 * #	E-4217	p 81	N88-27267 * #	IAF PAPER 87-229	p 42	A88-15954 * #
E-4031	p 128	N88-20555 * #	E-4218	p 76	N88-28095 * #	IAF PAPER 87-234	p 53	A88-15958 * #
E-4033	p 195	N88-24002 * #	E-4221	p 36	N88-27201 * #	IAF PAPER 87-238	p 134	A88-15960 * #
E-4034	p 204	N88-19102 * #	E-4222	p 154	N88-25854 * #	IAF PAPER 87-259	p 54	A88-15975 * #
E-4035	p 175	N88-26679 * #	E-4223	p 155	N88-26616 * #	IAF PAPER 87-384	p 134	A88-16055 * #
E-4040	p 211	N88-22652 * #	E-4228	p 63	N88-24688 * #	IAF PAPER 87-403	p 77	A88-16076 * #
E-4041	p 93	N88-22981 * #	E-4229	p 37	N88-29807 * #	IAF PAPER 87-491	p 122	A88-16133 * #
E-4043	p 179	N88-23986 * #	E-4230	p 63	N88-24687 * #	IAF PAPER 87-622	p 41	A88-16215 * #
E-4046	p 152	N88-21424 * #	E-4231	p 95	N88-26436 * #	IAF PAPER 88-213	p 56	A88-55361 * #
E-4047	p 32	N88-21162 * #	E-4233	p 44	N88-29833 * #			
E-4049	p 174	N88-24975 * #	E-4234	p 13	N88-24597 * #	ICOMP-87-5	p 210	N88-10563 * #
E-4050	p 32	N88-21161 * #	E-4236	p 163	N88-26645 * #	ICOMP-87-6	p 9	N88-10778 * #
E-4055	p 119	N88-18809 * #	E-4237	p 95	N88-27310 * #	ICOMP-87-7	p 148	N88-12752 * #
E-4056	p 60	N88-22080 * #	E-4240	p 35	N88-24642 * #	ICOMP-87-8	p 210	N88-12330 * #
E-4057	p 152	N88-21417 * #	E-4242	p 109	N88-24808 * #	ICOMP-87-9	p 210	N88-13931 * #
E-4058	p 128	N88-21400 * #	E-4243	p 64	N88-25476 * #	ICOMP-88-12	p 196	N88-29195 * #
E-4059	p 211	N88-21717 * #	E-4245	p 213	N88-25260 * #	ICOMP-88-13	p 207	N88-27799 * #
E-4061	p 211	N88-21718 * #	E-4252	p 80	N88-26430 * #	ICOMP-88-14	p 207	N88-27796 * #
E-4062	p 211	N88-26885 * #	E-4253	p 76	N88-28980 * #	ICOMP-88-17	p 212	N88-30377 * #
E-4064	p 121	N88-26566 * #	E-4256	p 65	N88-26401 * #	ICOMP-88-1	p 211	N88-19202 * #
E-4069	p 222	N88-22805 * #	E-4258	p 65	N88-26402 * #	ICOMP-88-2	p 210	N88-19182 * #
E-4073	p 120	N88-23070 * #	E-4259	p 227	N88-28853 * #	ICOMP-88-3	p 206	N88-19147 * #
E-4074	p 60	N88-21250 * #	E-4261	p 130	N88-28240 * #	ICOMP-88-4	p 207	N88-22591 * #
E-4076	p 153	N88-23184 * #	E-4262	p 156	N88-30094 * #	ICOMP-88-6	p 211	N88-22652 * #
E-4077	p 94	N88-24766 * #	E-4264	p 130	N88-25830 * #	ICOMP-88-7	p 211	N88-21717 * #
E-4078	p 154	N88-25841 * #	E-4266	p 207	N88-27799 * #	ICOMP-88-8	p 211	N88-21718 * #
E-4079	p 44	N88-25470 * #	E-4267	p 35	N88-27200 * #	ICOMP-88-9	p 211	N88-26885 * #
E-4080	p 93	N88-22986 * #	E-4268	p 66	N88-28090 * #			
E-4081	p 60	N88-21251 * #	E-4270	p 225	N88-27980 * #	IEPC-88-035	p 67	N88-29873 * #

IEPC-88-045

REPORT NUMBER INDEX

IEPC-88-045	p 67	N88-29869 * #	NAS 1.15:100255	p 171	N88-13604 * #	NAS 1.15:100848	p 93	N88-22981 * #
IEPC-88-091	p 66	N88-29868 * #	NAS 1.15:100256	p 201	N88-14486 * #	NAS 1.15:100849	p 152	N88-21424 * #
			NAS 1.15:100257	p 150	N88-15984 * #	NAS 1.15:100850	p 32	N88-21162 * #
LA-UR-87-2702	p 210	N88-12323 * #	NAS 1.15:100258	p 60	N88-21253 * #	NAS 1.15:100851	p 32	N88-21161 * #
LA-UR-87-3950	p 202	N88-22458 * #	NAS 1.15:100261	p 79	N88-13428 * #	NAS 1.15:100852	p 119	N88-18809 * #
			NAS 1.15:100262	p 217	N88-18379 * #	NAS 1.15:100853	p 60	N88-22080 * #
LG88ER0022-PT-1	p 12	N88-23751 * #	NAS 1.15:100263	p 118	N88-13515 * #	NAS 1.15:100854	p 152	N88-21417 * #
LG88ER0022-PT-2	p 12	N88-23752 * #	NAS 1.15:100265	p 49	N88-28082 * #	NAS 1.15:100855	p 128	N88-21400 * #
LG88ER0022-PT-3	p 12	N88-23753 * #	NAS 1.15:100266	p 187	N88-13754 * #	NAS 1.15:100856	p 211	N88-21717 * #
LG88ER0056	p 17	N88-26360 * #	NAS 1.15:100267	p 216	N88-13960 * #	NAS 1.15:100857	p 211	N88-21718 * #
			NAS 1.15:100268	p 151	N88-18867 * #	NAS 1.15:100858	p 211	N88-26885 * #
MCR-87-500	p 59	N88-15006 * #	NAS 1.15:100269	p 92	N88-19610 * #	NAS 1.15:100859	p 121	N88-26566 * #
			NAS 1.15:100272	p 188	N88-18036 * #	NAS 1.15:100860	p 222	N88-22805 * #
MT186ASE58SRI	p 223	N88-11578 * #	NAS 1.15:100273	p 80	N88-18672 * #	NAS 1.15:100861	p 120	N88-23070 * #
			NAS 1.15:100274	p 201	N88-19014 * #	NAS 1.15:100862	p 60	N88-21250 * #
NAS 1.15:100116	p 171	N88-12796 * #	NAS 1.15:100276	p 102	N88-15872 * #	NAS 1.15:100863	p 93	N88-22986 * #
NAS 1.15:100117	p 187	N88-13745 * #	NAS 1.15:100277	p 151	N88-19739 * #	NAS 1.15:100864	p 60	N88-21251 * #
NAS 1.15:100119	p 128	N88-12727 * #	NAS 1.15:100278	p 76	N88-28084 * #	NAS 1.15:100865	p 114	N88-21375 * #
NAS 1.15:100124	p 25	N88-13345 * #	NAS 1.15:100279	p 194	N88-22446 * #	NAS 1.15:100866	p 114	N88-21374 * #
NAS 1.15:100125	p 79	N88-15036 * #	NAS 1.15:100280	p 149	N88-14320 * #	NAS 1.15:100867	p 173	N88-21454 * #
NAS 1.15:100127	p 58	N88-12542 * #	NAS 1.15:100281	p 73	N88-15020 * #	NAS 1.15:100868	p 64	N88-25475 * #
NAS 1.15:100129	p 177	N88-15257 * #	NAS 1.15:100282	p 161	N88-14339 * #	NAS 1.15:100870	p 62	N88-23829 * #
NAS 1.15:100131	p 224	N88-17561 * #	NAS 1.15:100283	p 92	N88-15060 * #	NAS 1.15:100872	p 40	N88-25464 * #
NAS 1.15:100134	p 25	N88-12490 * #	NAS 1.15:100284	p 149	N88-13552 * #	NAS 1.15:100873	p 11	N88-22019 * #
NAS 1.15:100135	p 31	N88-18594 * #	NAS 1.15:100285	p 46	N88-22920 * #	NAS 1.15:100874	p 154	N88-23957 * #
NAS 1.15:100144	p 200	N88-12877 * #	NAS 1.15:100286	p 119	N88-18805 * #	NAS 1.15:100875	p 211	N88-25239 * #
NAS 1.15:100145	p 200	N88-12878 * #	NAS 1.15:100287	p 120	N88-23073 * #	NAS 1.15:100876	p 120	N88-24847 * #
NAS 1.15:100146	p 71	N88-10120 * #	NAS 1.15:100288	p 172	N88-18007 * #	NAS 1.15:100877	p 195	N88-25937 * #
NAS 1.15:100154	p 118	N88-13513 * #	NAS 1.15:100289	p 149	N88-15188 * #	NAS 1.15:100878	p 1	N88-21116 * #
NAS 1.15:100160	p 118	N88-15810 * #	NAS 1.15:100290	p 32	N88-19469 * #	NAS 1.15:100882	p 12	N88-23732 * #
NAS 1.15:100161	p 119	N88-16928 * #	NAS 1.15:100291	p 187	N88-14453 * #	NAS 1.15:100884	p 195	N88-25935 * #
NAS 1.15:100162	p 117	N88-11925 * #	NAS 1.15:100293	p 150	N88-15983 * #	NAS 1.15:100885	p 93	N88-22168 * #
NAS 1.15:100163	p 11	N88-20262 * #	NAS 1.15:100294	p 103	N88-17796 * #	NAS 1.15:100886	p 49	N88-21245 * #
NAS 1.15:100164	p 101	N88-10188 * #	NAS 1.15:100295	p 43	N88-21186 * #	NAS 1.15:100887	p 33	N88-22037 * #
NAS 1.15:100172	p 227	N88-22851 * #	NAS 1.15:100296	p 73	N88-16828 * #	NAS 1.15:100888	p 174	N88-23977 * #
NAS 1.15:100176	p 72	N88-12552 * #	NAS 1.15:100297	p 73	N88-17745 * #	NAS 1.15:100889	p 32	N88-21163 * #
NAS 1.15:100177	p 177	N88-12106 * #	NAS 1.15:100298	p 188	N88-18967 * #	NAS 1.15:100891	p 34	N88-22902 * #
NAS 1.15:100179	p 72	N88-13409 * #	NAS 1.15:100299	p 162	N88-23196 * #	NAS 1.15:100892	p 76	N88-25487 * #
NAS 1.15:100180	p 171	N88-12797 * #	NAS 1.15:100300	p 119	N88-17899 * #	NAS 1.15:100893	p 162	N88-26644 * #
NAS 1.15:100181	p 171	N88-12798 * #	NAS 1.15:100779	p 150	N88-16988 * #	NAS 1.15:100894	p 94	N88-24754 * #
NAS 1.15:100182	p 39	N88-26376 * #	NAS 1.15:100781	p 59	N88-15838 * #	NAS 1.15:100895	p 1	N88-23729 * #
NAS 1.15:100183	p 39	N88-26377 * #	NAS 1.15:100782	p 104	N88-17801 * #	NAS 1.15:100896	p 34	N88-24640 * #
NAS 1.15:100185	p 223	N88-10700 * #	NAS 1.15:100783	p 102	N88-15885 * #	NAS 1.15:100898	p 173	N88-23219 * #
NAS 1.15:100191	p 58	N88-12539 * #	NAS 1.15:100785	p 60	N88-21252 * #	NAS 1.15:100899	p 225	N88-30472 * #
NAS 1.15:100195	p 80	N88-15853 * #	NAS 1.15:100786	p 44	N88-17715 * #	NAS 1.15:100900	p 44	N88-25470 * #
NAS 1.15:100197	p 79	N88-10132 * #	NAS 1.15:100787	p 10	N88-14967 * #	NAS 1.15:100901	p 61	N88-22939 * #
NAS 1.15:100199	p 127	N88-10266 * #	NAS 1.15:100788	p 48	N88-17728 * #	NAS 1.15:100902	p 114	N88-26539 * #
NAS 1.15:100200	p 9	N88-10008 * #	NAS 1.15:100789	p 46	N88-22919 * #	NAS 1.15:100903	p 94	N88-24749 * #
NAS 1.15:100202	p 79	N88-11775 * #	NAS 1.15:100790	p 211	N88-19202 * #	NAS 1.15:100904	p 61	N88-22935 * #
NAS 1.15:100205	p 148	N88-12752 * #	NAS 1.15:100791	p 103	N88-16877 * #	NAS 1.15:100905	p 61	N88-22933 * #
NAS 1.15:100206	p 216	N88-10592 * #	NAS 1.15:100792	p 164	N88-18910 * #	NAS 1.15:100906	p 113	N88-24811 * #
NAS 1.15:100208	p 128	N88-11966 * #	NAS 1.15:100793	p 73	N88-17744 * #	NAS 1.15:100907	p 94	N88-24766 * #
NAS 1.15:100209	p 90	N88-10940 * #	NAS 1.15:100794	p 188	N88-18968 * #	NAS 1.15:100908	p 207	N88-26127 * #
NAS 1.15:100210	p 206	N88-12288 * #	NAS 1.15:100795	p 61	N88-22934 * #	NAS 1.15:100909	p 64	N88-25477 * #
NAS 1.15:100211	p 25	N88-11679 * #	NAS 1.15:100796	p 188	N88-18040 * #	NAS 1.15:100910	p 223	N88-28832 * #
NAS 1.15:100212	p 90	N88-10938 * #	NAS 1.15:100797	p 10	N88-16679 * #	NAS 1.15:100911	p 13	N88-26340 * #
NAS 1.15:100213	p 9	N88-10779 * #	NAS 1.15:100798	p 162	N88-18892 * #	NAS 1.15:100913	p 153	N88-23186 * #
NAS 1.15:100214	p 40	N88-15814 * #	NAS 1.15:100799	p 104	N88-20454 * #	NAS 1.15:100914	p 130	N88-24870 * #
NAS 1.15:100215	p 90	N88-10939 * #	NAS 1.15:100800	p 190	N88-21534 * #	NAS 1.15:100915	p 153	N88-23184 * #
NAS 1.15:100216	p 57	N88-11746 * #	NAS 1.15:100801	p 189	N88-18974 * #	NAS 1.15:100917	p 154	N88-25841 * #
NAS 1.15:100217	p 210	N88-10563 * #	NAS 1.15:100802	p 201	N88-21593 * #	NAS 1.15:100918	p 173	N88-23220 * #
NAS 1.15:100218	p 9	N88-10778 * #	NAS 1.15:100803	p 151	N88-18871 * #	NAS 1.15:100919	p 35	N88-25458 * #
NAS 1.15:100219	p 26	N88-13346 * #	NAS 1.15:100804	p 92	N88-18707 * #	NAS 1.15:100920	p 34	N88-24639 * #
NAS 1.15:100220	p 24	N88-10790 * #	NAS 1.15:100806	p 104	N88-18726 * #	NAS 1.15:100921	p 34	N88-23806 * #
NAS 1.15:100221	p 224	N88-14046 * #	NAS 1.15:100807	p 210	N88-19182 * #	NAS 1.15:100922	p 76	N88-25483 * #
NAS 1.15:100222	p 160	N88-11100 * #	NAS 1.15:100808	p 119	N88-17880 * #	NAS 1.15:100923	p 75	N88-24712 * #
NAS 1.15:100223	p 227	N88-13209 * #	NAS 1.15:100809	p 46	N88-24663 * #	NAS 1.15:100924	p 43	N88-28942 * #
NAS 1.15:100224	p 72	N88-11758 * #	NAS 1.15:100810	p 189	N88-18976 * #	NAS 1.15:100926	p 63	N88-24682 * #
NAS 1.15:100225	p 210	N88-12330 * #	NAS 1.15:100811	p 188	N88-18969 * #	NAS 1.15:100927	p 174	N88-24968 * #
NAS 1.15:100226	p 38	N88-11680 * #	NAS 1.15:100812	p 194	N88-23994 * #	NAS 1.15:100928	p 196	N88-29195 * #
NAS 1.15:100227	p 26	N88-14093 * #	NAS 1.15:100813	p 162	N88-23194 * #	NAS 1.15:100929	p 35	N88-24641 * #
NAS 1.15:100228	p 227	N88-14054 * #	NAS 1.15:100814	p 206	N88-19147 * #	NAS 1.15:100930	p 13	N88-25435 * #
NAS 1.15:100229	p 57	N88-11745 * #	NAS 1.15:100815	p 151	N88-18870 * #	NAS 1.15:100932	p 63	N88-24686 * #
NAS 1.15:100230	p 225	N88-12429 * #	NAS 1.15:100819	p 126	N88-18835 * #	NAS 1.15:100933	p 64	N88-24690 * #
NAS 1.15:100231	p 161	N88-12043 * #	NAS 1.15:100820	p 207	N88-22591 * #	NAS 1.15:100934	p 12	N88-24592 * #
NAS 1.15:100232	p 57	N88-11750 * #	NAS 1.15:100821	p 74	N88-19592 * #	NAS 1.15:100935	p 194	N88-23278 * #
NAS 1.15:100233	p 57	N88-11748 * #	NAS 1.15:100823	p 104	N88-20455 * #	NAS 1.15:100936	p 202	N88-25059 * #
NAS 1.15:100234	p 118	N88-14260 * #	NAS 1.15:100824	p 43	N88-24659 * #	NAS 1.15:100937	p 81	N88-27267 * #
NAS 1.15:100235	p 101	N88-11838 * #	NAS 1.15:100825	p 179	N88-23985 * #	NAS 1.15:100938	p 76	N88-28095 * #
NAS 1.15:100236	p 72	N88-10899 * #	NAS 1.15:100826	p 120	N88-25762 * #	NAS 1.15:100939	p 175	N88-28312 * #
NAS 1.15:100237	p 58	N88-14127 * #	NAS 1.15:100829	p 120	N88-21389 * #	NAS 1.15:100940	p 36	N88-27201 * #
NAS 1.15:100238	p 72	N88-12551 * #	NAS 1.15:100830	p 92	N88-20417 * #	NAS 1.15:100941	p 154	N88-25854 * #
NAS 1.15:100239	p 69	N88-13385 * #	NAS 1.15:100831	p 189	N88-21497 * #	NAS 1.15:100942	p 63	N88-24687 * #
NAS 1.15:100240	p 210	N88-13931 * #	NAS 1.15:100833	p 120	N88-19698 * #	NAS 1.15:100943	p 95	N88-26436 * #
NAS 1.15:100241	p 57	N88-11747 * #	NAS 1.15:100834	p 105	N88-21306 * #	NAS 1.15:100945	p 13	N88-24597 * #
NAS 1.15:100242	p 118	N88-11945 * #	NAS 1.15:100835	p 208	N88-21697 * #	NAS 1.15:100946	p 95	N88-27310 * #
NAS 1.15:100244	p 117	N88-11944 * #	NAS 1.15:100836	p 152	N88-19740 * #	NAS 1.15:100948	p 35	N88-24642 * #
NAS 1.15:100245	p 186	N88-12825 * #	NAS 1.15:100837	p 45	N88-19565 * #	NAS 1.15:100950	p 64	N88-25476 * #
NAS 1.15:100246	p 91	N88-11817 * #	NAS 1.15:100838	p 60	N88-21254 * #	NAS 1.15:100951	p 109	N88-24808 * #
NAS 1.15:100247	p 25	N88-13338 * #	NAS 1.15:100839	p 104	N88-18734 * #	NAS 1.15:100953	p 35	N88-27200 * #
NAS 1.15:100248	p 72	N88-15018 * #	NAS 1.15:100840	p 74	N88-21257 * #	NAS 1.15:100954	p 63	N88-24688 * #
NAS 1.15:100249	p 102	N88-13453 * #	NAS 1.15:100841	p 128	N88-20555 * #	NAS 1.15:100955	p 14	N88-29746 * #
NAS 1.15:100250	p 102	N88-14206 * #	NAS 1.15:100842	p 195	N88-24002 * #	NAS 1.15:100956	p 76	N88-28980 * #
NAS 1.15:100251	p 9	N88-13304 * #	NAS 1.15:100843	p 204	N88-19102 * #	NAS 1.15:100957	p 63	N88-24689 * #
NAS 1.15:100252	p 148	N88-12763 * #	NAS 1.15:100846	p 211	N88-22652 * #	NAS 1.15:100958	p 80	N88-26430 * #
NAS 1.15:100254	p 216	N88-13961 * #	NAS 1.15:100847	p				

REPORT NUMBER INDEX

NASA-CR-175046

NAS 1.15:100960	p 175	N88-25916 * #	NAS 1.26:179531	p 224	N88-12428 * #	NAS 1.26:182664	p 213	N88-20962 * #
NAS 1.15:100961	p 175	N88-26679 * #	NAS 1.26:179539	p 10	N88-15769 * #	NAS 1.26:182705	p 189	N88-20668 * #
NAS 1.15:100962	p 175	N88-30128 * #	NAS 1.26:179586	p 200	N88-12875 * #	NAS 1.26:182707	p 80	N88-20397 * #
NAS 1.15:100963	p 65	N88-26401 * #	NAS 1.26:179593	p 49	N88-25473 * #	NAS 1.26:182800-VOL-1	p 105	N88-22197 * #
NAS 1.15:100964	p 37	N88-29807 * #	NAS 1.26:179632	p 25	N88-10791 * #	NAS 1.26:182801	p 222	N88-25327 * #
NAS 1.15:100965	p 65	N88-26402 * #	NAS 1.26:179633	p 25	N88-10792 * #	NAS 1.26:183044	p 203	N88-27621 * #
NAS 1.15:100966	p 163	N88-29142 * #	NAS 1.26:179635	p 148	N88-12039 * #	NAS 1.26:183084	p 175	N88-25921 * #
NAS 1.15:100967	p 107	N88-26482 * #	NAS 1.26:180431	p 205	N88-10496 * #	NAS 1.26:183096	p 219	N88-26223 * #
NAS 1.15:100969	p 227	N88-28853 * #	NAS 1.26:180804	p 170	N88-11135 * #	NAS 1.26:183110	p 175	N88-26675 * #
NAS 1.15:100970	p 130	N88-28240 * #	NAS 1.26:180805	p 207	N88-21682 * #	NAS 1.26:183204	p 76	N88-28981 * #
NAS 1.15:100971	p 130	N88-25830 * #	NAS 1.26:180819	p 56	N88-10106 * #	NAS 1.26:4113	p 16	N88-18574 * #
NAS 1.15:100972	p 163	N88-26645 * #	NAS 1.26:180825	p 129	N88-23084 * #	NAS 1.26:4115	p 11	N88-17582 * #
NAS 1.15:100973	p 207	N88-27799 * #	NAS 1.26:180828	p 56	N88-10886 * #	NAS 1.26:4129-PT-1	p 12	N88-23751 * #
NAS 1.15:100974	p 66	N88-28090 * #	NAS 1.26:180830	p 94	N88-25531 * #	NAS 1.26:4129-PT-2	p 12	N88-23752 * #
NAS 1.15:100975	p 225	N88-27980 * #	NAS 1.26:180832	p 58	N88-12541 * #	NAS 1.26:4129-PT-3	p 12	N88-23753 * #
NAS 1.15:100976	p 202	N88-22458 * #	NAS 1.26:180834	p 59	N88-17731 * #	NAS 1.26:4135	p 173	N88-23216 * #
NAS 1.15:100977	p 43	N88-26365 * #	NAS 1.26:180845	p 15	N88-13310 * #	NAS 1.26:4145	p 153	N88-23185 * #
NAS 1.15:101134	p 203	N88-27624 * #	NAS 1.26:180846	p 10	N88-14966 * #	NAS 1.26:4151	p 179	N88-23987 * #
NAS 1.15:101177	p 35	N88-25460 * #	NAS 1.26:180847	p 10	N88-15766 * #	NAS 1.26:4152	p 178	N88-23224 * #
NAS 1.15:101291	p 65	N88-28088 * #	NAS 1.26:180851	p 57	N88-11749 * #	NAS 1.26:4153	p 179	N88-23986 * #
NAS 1.15:101292	p 66	N88-29860 * #	NAS 1.26:180852	p 13	N88-25445 * #	NAS 1.26:4155	p 174	N88-24975 * #
NAS 1.15:101293	p 1	N88-26328 * #	NAS 1.26:180853	p 154	N88-25857 * #	NAS 1.26:4158	p 64	N88-25474 * #
NAS 1.15:101294	p 162	N88-26641 * #	NAS 1.26:180854	p 224	N88-19377 * #	NAS 1.26:4162	p 180	N88-25923 * #
NAS 1.15:101295	p 203	N88-26732 * #	NAS 1.26:180858	p 103	N88-16668 * #	NAS 1.26:4163	p 75	N88-25479 * #
NAS 1.15:101296	p 207	N88-27796 * #	NAS 1.26:180859	p 161	N88-12042 * #	NAS 1.55:10001	p 149	N88-15924 * #
NAS 1.15:101297	p 180	N88-28323 * #	NAS 1.26:180861	p 36	N88-28074 * #	NAS 1.55:10003-SESS-1	p 31	N88-16697 * #
NAS 1.15:101299	p 203	N88-25978 * #	NAS 1.26:180863	p 72	N88-14150 * #	NAS 1.55:10003-SESS-2	p 27	N88-15785 * #
NAS 1.15:101300	p 196	N88-28332 * #	NAS 1.26:180864	p 27	N88-14985 * #	NAS 1.55:10003-SESS-3	p 28	N88-15790 * #
NAS 1.15:101302	p 156	N88-30094 * #	NAS 1.26:180865	p 59	N88-17732 * #	NAS 1.55:10003-SESS-4	p 28	N88-15794 * #
NAS 1.15:101303	p 115	N88-28176 * #	NAS 1.26:180870	p 161	N88-13573 * #	NAS 1.55:10003-SESS-5	p 28	N88-15800 * #
NAS 1.15:101304	p 156	N88-30090 * #	NAS 1.26:180871	p 224	N88-20229 * #	NAS 1.55:10003-SESS-6	p 29	N88-15807 * #
NAS 1.15:101305	p 163	N88-29152 * #	NAS 1.26:180872	p 80	N88-15851 * #	NAS 1.55:10009	p 152	N88-20599 * #
NAS 1.15:101306	p 44	N88-29833 * #	NAS 1.26:180873	p 151	N88-17954 * #	NAS 1.55:10010	p 189	N88-21498 * #
NAS 1.15:101307	p 67	N88-29874 * #	NAS 1.26:180874	p 10	N88-15762 * #	NAS 1.55:2405	p 185	N88-11140 * #
NAS 1.15:101309	p 81	N88-28109 * #	NAS 1.26:180875	p 48	N88-16794 * #	NAS 1.55:2427	p 106	N88-23872 * #
NAS 1.15:101312	p 14	N88-28041 * #	NAS 1.26:180877	p 59	N88-20361 * #	NAS 1.55:2473	p 48	N88-10084 * #
NAS 1.15:101313	p 155	N88-30072 * #	NAS 1.26:180879	p 49	N88-21243 * #	NAS 1.55:2476	p 45	N88-12520 * #
NAS 1.15:101314	p 49	N88-28959 * #	NAS 1.26:180880	p 45	N88-18612 * #	NAS 1.55:3003-VOL-1	p 194	N88-23226 * #
NAS 1.15:101315	p 218	N88-28760 * #	NAS 1.26:180882	p 26	N88-14094 * #	NAS 1.55:3003-VOL-2	p 190	N88-22382 * #
NAS 1.15:101317	p 163	N88-28293 * #	NAS 1.26:180884	p 66	N88-29863 * #	NAS 1.55:3003-VOL-3	p 192	N88-22408 * #
NAS 1.15:101318	p 13	N88-27174 * #	NAS 1.26:180885	p 67	N88-29872 * #	NAS 1.60:2681	p 40	N88-17686 * #
NAS 1.15:101319	p 196	N88-28344 * #	NAS 1.26:180888	p 161	N88-15996 * #	NAS 1.60:2765	p 58	N88-12538 * #
NAS 1.15:101321	p 121	N88-28222 * #	NAS 1.26:180891	p 225	N88-20230 * #	NAS 1.60:2774	p 68	N88-12543 * #
NAS 1.15:101323	p 121	N88-27424 * #	NAS 1.26:180893	p 190	N88-21535 * #	NAS 1.60:2779	p 187	N88-15263 * #
NAS 1.15:101325	p 69	N88-28966 * #	NAS 1.26:180901	p 203	N88-25977 * #	NAS 1.60:2788	p 128	N88-15146 * #
NAS 1.15:101326	p 67	N88-29869 * #	NAS 1.26:181409	p 185	N88-10388 * #	NAS 1.60:2789	p 172	N88-15785 * #
NAS 1.15:101327	p 212	N88-30377 * #	NAS 1.26:181425	p 170	N88-10355 * #	NAS 1.60:2795	p 172	N88-15224 * #
NAS 1.15:101328	p 130	N88-30048 * #	NAS 1.26:181472	p 71	N88-10896 * #	NAS 1.60:2801	p 188	N88-17095 * #
NAS 1.15:101330	p 155	N88-30078 * #	NAS 1.26:182107	p 62	N88-23830 * #	NAS 1.60:2815	p 38	N88-19475 * #
NAS 1.15:101332	p 18	N88-28062 * #	NAS 1.26:182108	p 152	N88-22322 * #	NAS 1.60:2816	p 172	N88-18933 * #
NAS 1.15:101333	p 81	N88-29952 * #	NAS 1.26:182111	p 163	N88-28299 * #	NAS 1.60:2840	p 164	N88-30099 * #
NAS 1.15:101334	p 156	N88-30084 * #	NAS 1.26:182112	p 32	N88-20306 * #	NAS 1.60:2841	p 163	N88-28296 * #
NAS 1.15:101335	p 115	N88-29997 * #	NAS 1.26:182113	p 92	N88-21295 * #	NAS 1.71:LEW-14203-1	p 108	N88-29984 * #
NAS 1.15:101336	p 14	N88-29780 * #	NAS 1.26:182114	p 48	N88-20353 * #	NAS 1.71:LEW-14520-1	p 129	N88-23936 * #
NAS 1.15:101343	p 67	N88-29873 * #	NAS 1.26:182116	p 92	N88-19613 * #	NAS 1.71:LEW-14698-1	p 76	N88-29888 * #
NAS 1.15:101347	p 14	N88-29771 * #	NAS 1.26:182117	p 189	N88-18975 * #			
NAS 1.15:101351	p 67	N88-29771 * #	NAS 1.26:182118	p 222	N88-25346 * #			
NAS 1.15:101357	p 66	N88-29868 * #	NAS 1.26:182119	p 16	N88-21143 * #	NASA-CASE-LEW-14104-2	p 91	N88-14179 * #
NAS 1.15:101370	p 49	N88-29845 * #	NAS 1.26:182120	p 194	N88-23272 * #	NASA-CASE-LEW-14203-1	p 108	N88-29984 * #
NAS 1.15:86997	p 9	N88-12461 * #	NAS 1.26:182121	p 17	N88-26360 * #	NASA-CASE-LEW-14212-1	p 174	N88-23978 * #
NAS 1.15:87050	p 201	N88-19013 * #	NAS 1.26:182122	p 195	N88-25016 * #	NASA-CASE-LEW-14345-1	p 69	N88-26404 * #
NAS 1.15:87184	p 15	N88-12473 * #	NAS 1.26:182126	p 44	N88-29835 * #	NASA-CASE-LEW-14374-1	p 41	N88-28939 * #
NAS 1.15:88844	p 43	N88-12515 * #	NAS 1.26:182128	p 44	N88-29835 * #	NASA-CASE-LEW-14520-1	p 129	N88-23936 * #
NAS 1.15:88886	p 223	N88-12427 * #	NAS 1.26:182129	p 94	N88-22987 * #	NASA-CASE-LEW-14698-1	p 76	N88-29888 * #
NAS 1.15:88893	p 71	N88-10121 * #	NAS 1.26:182132	p 37	N88-29811 * #			
NAS 1.15:89654	p 210	N88-12323 * #	NAS 1.26:182134	p 222	N88-24539 * #	NASA-CP-10001	p 149	N88-15924 * #
NAS 1.15:89829	p 73	N88-18640 * #	NAS 1.26:182137	p 195	N88-24997 * #	NASA-CP-10003-SESS-1	p 31	N88-16697 * #
NAS 1.15:89845	p 32	N88-21160 * #	NAS 1.26:182138	p 174	N88-24976 * #	NASA-CP-10003-SESS-2	p 27	N88-15785 * #
NAS 1.15:89878	p 26	N88-13347 * #	NAS 1.26:182139	p 155	N88-30076 * #	NASA-CP-10003-SESS-3	p 28	N88-15790 * #
NAS 1.26:100193	p 11	N88-16681 * #	NAS 1.26:182141	p 152	N88-23182 * #	NASA-CP-10003-SESS-4	p 28	N88-15794 * #
NAS 1.26:174790	p 27	N88-14097 * #	NAS 1.26:182145	p 66	N88-29858 * #	NASA-CP-10003-SESS-5	p 28	N88-15800 * #
NAS 1.26:174791	p 36	N88-28928 * #	NAS 1.26:182146	p 130	N88-25831 * #	NASA-CP-10003-SESS-6	p 29	N88-15807 * #
NAS 1.26:174802	p 204	N88-30184 * #	NAS 1.26:182147	p 154	N88-24917 * #	NASA-CP-10009	p 152	N88-20599 * #
NAS 1.26:174866	p 171	N88-13603 * #	NAS 1.26:182148	p 219	N88-23649 * #	NASA-CP-10010	p 189	N88-21498 * #
NAS 1.26:174894	p 155	N88-30066 * #	NAS 1.26:182150	p 35	N88-25459 * #	NASA-CP-2405	p 185	N88-11140 * #
NAS 1.26:174895	p 108	N88-28151 * #	NAS 1.26:182151	p 41	N88-29825 * #	NASA-CP-2427	p 106	N88-23872 * #
NAS 1.26:174899	p 155	N88-30063 * #	NAS 1.26:182153	p 155	N88-26616 * #	NASA-CP-2473	p 48	N88-10084 * #
NAS 1.26:174926	p 216	N88-12352 * #	NAS 1.26:182154	p 113	N88-26498 * #	NASA-CP-2476	p 45	N88-12520 * #
NAS 1.26:174958	p 175	N88-28319 * #	NAS 1.26:182157	p 95	N88-29961 * #	NASA-CP-3003-VOL-1	p 194	N88-23226 * #
NAS 1.26:174959	p 36	N88-28927 * #	NAS 1.26:182159	p 67	N88-29876 * #	NASA-CP-3003-VOL-2	p 190	N88-22382 * #
NAS 1.26:175006	p 102	N88-15866 * #	NAS 1.26:182160	p 66	N88-29867 * #	NASA-CP-3003-VOL-3	p 192	N88-22408 * #
NAS 1.26:175012	p 196	N88-30164 * #	NAS 1.26:182162	p 65	N88-28087 * #			
NAS 1.26:175025	p 26	N88-14095 * #	NAS 1.26:182167	p 13	N88-26336 * #	NASA-CR-174790	p 27	N88-14097 * #
NAS 1.26:175026	p 27	N88-14096 * #	NAS 1.26:182168	p 130	N88-28239 * #	NASA-CR-174791	p 36	N88-28928 * #
NAS 1.26:175046	p 170	N88-10339 * #	NAS 1.26:182191	p 196	N88-27611 * #	NASA-CR-174802	p 204	N88-30184 * #
NAS 1.26:175068	p 127	N88-11948 * #	NAS 1.26:182192	p 155	N88-27520 * #	NASA-CR-174866	p 171	N88-13603 * #
NAS 1.26:175071	p 129	N88-23939 * #	NAS 1.26:182201	p 131	N88-30055 * #	NASA-CR-174894	p 155	N88-30066 * #
NAS 1.26:175104	p 18	N88-28917 * #	NAS 1.26:182214	p 164	N88-30106 * #	NASA-CR-174895	p 108	N88-28151 * #
NAS 1.26:175106	p 223	N88-11578 * #	NAS 1.26:182232	p 42	N88-14110 * #	NASA-CR-174899	p 155	N88-30063 * #
NAS 1.26:179233	p 59	N88-15006 * #	NAS 1.26:182401	p 118	N88-15130 * #	NASA-CR-174926	p 216	N88-12352 * #
NAS 1.26:179467	p 37	N88-29804 * #	NAS 1.26:182437	p 150	N88-16956 * #	NASA-CR-174958	p 175	N88-28319 * #
NAS 1.26:179468	p 37	N88-28930 * #	NAS 1.26:182440	p 172	N88-16007 * #	NASA-CR-174959	p 36	N88-28927 * #
NAS 1.26:179469	p 153	N88-23956 * #	NAS 1.26:182441	p 172	N88-16006 * #	NASA-CR-175006	p 102	N88-15866 * #
NAS 1.26:179489	p 201	N88-18068 * #	NAS 1.26:182504	p 112	N88-18739 * #	NASA-CR-175012	p 196	N88-30164 * #
NAS 1.26:179498	p 121	N88-29077 * #	NAS 1.26:182532	p 119	N88-17892 * #	NASA-CR-175025	p 26	N88-14095 * #
NAS 1.26:179507	p 107	N88-28142 * #	NAS 1.26:182538	p 201				

NASA-CR-175068

REPORT NUMBER INDEX

NASA-CR-175068	p 127	N88-11948 * #	NASA-CR-182192	p 155	N88-27520 * #	NASA-TM-100228	p 227	N88-14054 * #
NASA-CR-175071	p 129	N88-23939 * #	NASA-CR-182201	p 131	N88-30055 * #	NASA-TM-100229	p 57	N88-11745 * #
NASA-CR-175104	p 18	N88-28917 * #	NASA-CR-182214	p 164	N88-30106 * #	NASA-TM-100230	p 225	N88-12429 * #
NASA-CR-175106	p 223	N88-11578 * #	NASA-CR-182372	p 42	N88-14110 * #	NASA-TM-100231	p 161	N88-12043 * #
NASA-CR-179233	p 59	N88-15006 * #	NASA-CR-182401	p 118	N88-15130 * #	NASA-TM-100232	p 57	N88-11750 * #
NASA-CR-179467	p 37	N88-29804 * #	NASA-CR-182437	p 150	N88-16956 * #	NASA-TM-100233	p 57	N88-11748 * #
NASA-CR-179468	p 37	N88-28930 * #	NASA-CR-182440	p 172	N88-16007 * #	NASA-TM-100234	p 118	N88-14260 * #
NASA-CR-179469	p 153	N88-23956 * #	NASA-CR-182441	p 172	N88-16006 * #	NASA-TM-100235	p 101	N88-11838 * #
NASA-CR-179489	p 201	N88-18068 * #	NASA-CR-182504	p 112	N88-18739 * #	NASA-TM-100236	p 72	N88-10899 * #
NASA-CR-179496	p 121	N88-29077 * #	NASA-CR-182532	p 119	N88-17892 * #	NASA-TM-100237	p 58	N88-14127 * #
NASA-CR-179507	p 107	N88-28142 * #	NASA-CR-182538	p 201	N88-19000 * #	NASA-TM-100238	p 72	N88-12551 * #
NASA-CR-179521	p 36	N88-28929 * #	NASA-CR-182564	p 203	N88-25970 * #	NASA-TM-100239	p 69	N88-13385 * #
NASA-CR-179531	p 224	N88-14248 * #	NASA-CR-182664	p 213	N88-20962 * #	NASA-TM-100240	p 210	N88-13931 * #
NASA-CR-179539	p 10	N88-15769 * #	NASA-CR-182705	p 189	N88-20668 * #	NASA-TM-100241	p 57	N88-11747 * #
NASA-CR-179586	p 200	N88-12875 * #	NASA-CR-182707	p 80	N88-20397 * #	NASA-TM-100242	p 118	N88-11945 * #
NASA-CR-179593	p 49	N88-25473 * #	NASA-CR-182800	p 105	N88-22197 * #	NASA-TM-100244	p 117	N88-11944 * #
NASA-CR-179632	p 25	N88-10791 * #	NASA-CR-182801	p 222	N88-25327 * #	NASA-TM-100245	p 186	N88-12825 * #
NASA-CR-179633	p 25	N88-10792 * #	NASA-CR-183044	p 203	N88-27621 * #	NASA-TM-100246	p 91	N88-11817 * #
NASA-CR-179635	p 148	N88-12039 * #	NASA-CR-183084	p 175	N88-25921 * #	NASA-TM-100247	p 25	N88-13338 * #
NASA-CR-180431	p 205	N88-10496 * #	NASA-CR-183096	p 219	N88-26223 * #	NASA-TM-100248	p 72	N88-15018 * #
NASA-CR-180804	p 170	N88-11135 * #	NASA-CR-183110	p 175	N88-26675 * #	NASA-TM-100249	p 102	N88-13453 * #
NASA-CR-180805	p 207	N88-21682 * #	NASA-CR-183204	p 76	N88-28981 * #	NASA-TM-100250	p 102	N88-14206 * #
NASA-CR-180819	p 56	N88-10106 * #	NASA-CR-4113	p 16	N88-18574 * #	NASA-TM-100251	p 9	N88-13304 * #
NASA-CR-180825	p 129	N88-23084 * #	NASA-CR-4115	p 11	N88-17582 * #	NASA-TM-100252	p 148	N88-12783 * #
NASA-CR-180828	p 56	N88-10886 * #	NASA-CR-4129-PT-1	p 12	N88-23751 * #	NASA-TM-100254	p 216	N88-13961 * #
NASA-CR-180830	p 94	N88-25531 * #	NASA-CR-4129-PT-2	p 12	N88-23752 * #	NASA-TM-100255	p 171	N88-13604 * #
NASA-CR-180832	p 58	N88-12541 * #	NASA-CR-4129-PT-3	p 12	N88-23753 * #	NASA-TM-100256	p 201	N88-14486 * #
NASA-CR-180834	p 59	N88-17731 * #	NASA-CR-4135	p 173	N88-23216 * #	NASA-TM-100257	p 150	N88-15984 * #
NASA-CR-180845	p 15	N88-13310 * #	NASA-CR-4145	p 153	N88-23185 * #	NASA-TM-100258	p 60	N88-21253 * #
NASA-CR-180846	p 10	N88-14966 * #	NASA-CR-4151	p 179	N88-23987 * #	NASA-TM-100261	p 79	N88-13428 * #
NASA-CR-180847	p 10	N88-15766 * #	NASA-CR-4152	p 178	N88-23224 * #	NASA-TM-100262	p 217	N88-18379 * #
NASA-CR-180851	p 57	N88-11749 * #	NASA-CR-4153	p 179	N88-23986 * #	NASA-TM-100263	p 118	N88-13515 * #
NASA-CR-180852	p 13	N88-25445 * #	NASA-CR-4155	p 174	N88-24975 * #	NASA-TM-100265	p 49	N88-28082 * #
NASA-CR-180853	p 154	N88-25857 * #	NASA-CR-4158	p 64	N88-25474 * #	NASA-TM-100266	p 187	N88-13754 * #
NASA-CR-180854	p 224	N88-19377 * #	NASA-CR-4162	p 180	N88-25923 * #	NASA-TM-100267	p 216	N88-13960 * #
NASA-CR-180858	p 103	N88-16868 * #	NASA-CR-4163	p 75	N88-25479 * #	NASA-TM-100268	p 151	N88-18867 * #
NASA-CR-180859	p 161	N88-12042 * #	NASA-MPD-1683	p 15	N88-12473 * #	NASA-TM-100269	p 92	N88-19610 * #
NASA-CR-180861	p 36	N88-28074 * #	NASA-TM-100116	p 171	N88-12796 * #	NASA-TM-100272	p 188	N88-18036 * #
NASA-CR-180863	p 72	N88-14150 * #	NASA-TM-100117	p 187	N88-13745 * #	NASA-TM-100273	p 80	N88-18672 * #
NASA-CR-180864	p 27	N88-14985 * #	NASA-TM-100119	p 128	N88-12727 * #	NASA-TM-100274	p 201	N88-19014 * #
NASA-CR-180865	p 59	N88-17732 * #	NASA-TM-100124	p 25	N88-13345 * #	NASA-TM-100276	p 102	N88-15872 * #
NASA-CR-180870	p 161	N88-13573 * #	NASA-TM-100125	p 79	N88-15036 * #	NASA-TM-100277	p 151	N88-19739 * #
NASA-CR-180871	p 224	N88-20229 * #	NASA-TM-100127	p 58	N88-12542 * #	NASA-TM-100278	p 76	N88-28094 * #
NASA-CR-180872	p 80	N88-15851 * #	NASA-TM-100129	p 78	N88-15257 * #	NASA-TM-100279	p 194	N88-22446 * #
NASA-CR-180873	p 151	N88-17954 * #	NASA-TM-100131	p 177	N88-15257 * #	NASA-TM-100280	p 149	N88-14320 * #
NASA-CR-180874	p 10	N88-15762 * #	NASA-TM-100133	p 224	N88-17561 * #	NASA-TM-100281	p 73	N88-15020 * #
NASA-CR-180875	p 48	N88-16794 * #	NASA-TM-100134	p 178	N88-15257 * #	NASA-TM-100282	p 161	N88-14339 * #
NASA-CR-180877	p 59	N88-20361 * #	NASA-TM-100135	p 25	N88-12490 * #	NASA-TM-100283	p 92	N88-15060 * #
NASA-CR-180879	p 49	N88-21243 * #	NASA-TM-100144	p 31	N88-18594 * #	NASA-TM-100284	p 149	N88-13552 * #
NASA-CR-180880	p 45	N88-18612 * #	NASA-TM-100145	p 200	N88-12877 * #	NASA-TM-100285	p 46	N88-22920 * #
NASA-CR-180882	p 26	N88-14094 * #	NASA-TM-100146	p 200	N88-12878 * #	NASA-TM-100286	p 119	N88-18805 * #
NASA-CR-180884	p 66	N88-29863 * #	NASA-TM-100154	p 71	N88-10120 * #	NASA-TM-100287	p 120	N88-23073 * #
NASA-CR-180885	p 67	N88-29872 * #	NASA-TM-100160	p 118	N88-13513 * #	NASA-TM-100288	p 172	N88-18007 * #
NASA-CR-180888	p 161	N88-15996 * #	NASA-TM-100161	p 118	N88-15910 * #	NASA-TM-100289	p 149	N88-15188 * #
NASA-CR-180891	p 225	N88-20230 * #	NASA-TM-100162	p 119	N88-16928 * #	NASA-TM-100290	p 32	N88-19469 * #
NASA-CR-180893	p 190	N88-21535 * #	NASA-TM-100163	p 117	N88-11925 * #	NASA-TM-100291	p 187	N88-14453 * #
NASA-CR-180901	p 203	N88-25977 * #	NASA-TM-100172	p 11	N88-20262 * #	NASA-TM-100293	p 150	N88-15983 * #
NASA-CR-181409	p 185	N88-10388 * #	NASA-TM-100176	p 101	N88-10188 * #	NASA-TM-100294	p 103	N88-17796 * #
NASA-CR-181425	p 170	N88-10355 * #	NASA-TM-100177	p 227	N88-22851 * #	NASA-TM-100295	p 43	N88-21186 * #
NASA-CR-181472	p 71	N88-10896 * #	NASA-TM-100179	p 72	N88-12552 * #	NASA-TM-100296	p 73	N88-16828 * #
NASA-CR-182107	p 62	N88-23830 * #	NASA-TM-100180	p 177	N88-12106 * #	NASA-TM-100297	p 73	N88-17745 * #
NASA-CR-182108	p 152	N88-22322 * #	NASA-TM-100181	p 72	N88-13409 * #	NASA-TM-100298	p 188	N88-18967 * #
NASA-CR-182111	p 163	N88-28299 * #	NASA-TM-100182	p 171	N88-12797 * #	NASA-TM-100299	p 162	N88-23196 * #
NASA-CR-182112	p 32	N88-20306 * #	NASA-TM-100183	p 171	N88-12798 * #	NASA-TM-100300	p 119	N88-17899 * #
NASA-CR-182113	p 92	N88-21295 * #	NASA-TM-100185	p 39	N88-26376 * #	NASA-TM-100779	p 150	N88-16988 * #
NASA-CR-182114	p 48	N88-20353 * #	NASA-TM-100189	p 39	N88-26377 * #	NASA-TM-100781	p 59	N88-15838 * #
NASA-CR-182116	p 92	N88-19613 * #	NASA-TM-100191	p 223	N88-10700 * #	NASA-TM-100782	p 104	N88-17801 * #
NASA-CR-182117	p 189	N88-18975 * #	NASA-TM-100193	p 58	N88-12539 * #	NASA-TM-100783	p 102	N88-15885 * #
NASA-CR-182118	p 222	N88-25346 * #	NASA-TM-100195	p 11	N88-16681 * #	NASA-TM-100785	p 60	N88-21252 * #
NASA-CR-182119	p 16	N88-21143 * #	NASA-TM-100197	p 80	N88-15853 * #	NASA-TM-100786	p 44	N88-17715 * #
NASA-CR-182120	p 194	N88-23272 * #	NASA-TM-100199	p 79	N88-10132 * #	NASA-TM-100787	p 10	N88-14967 * #
NASA-CR-182121	p 17	N88-26360 * #	NASA-TM-100200	p 127	N88-10266 * #	NASA-TM-100788	p 48	N88-17728 * #
NASA-CR-182126	p 195	N88-25016 * #	NASA-TM-100202	p 9	N88-10008 * #	NASA-TM-100789	p 46	N88-22919 * #
NASA-CR-182128	p 44	N88-29835 * #	NASA-TM-100205	p 79	N88-11775 * #	NASA-TM-100790	p 211	N88-19202 * #
NASA-CR-182129	p 94	N88-22987 * #	NASA-TM-100206	p 148	N88-12752 * #	NASA-TM-100791	p 103	N88-16877 * #
NASA-CR-182132	p 37	N88-29811 * #	NASA-TM-100208	p 216	N88-10592 * #	NASA-TM-100792	p 164	N88-18910 * #
NASA-CR-182134	p 222	N88-24539 * #	NASA-TM-100211	p 128	N88-11966 * #	NASA-TM-100793	p 73	N88-17744 * #
NASA-CR-182137	p 195	N88-24997 * #	NASA-TM-100212	p 90	N88-10940 * #	NASA-TM-100794	p 188	N88-18968 * #
NASA-CR-182138	p 174	N88-24976 * #	NASA-TM-100213	p 206	N88-12288 * #	NASA-TM-100795	p 61	N88-22934 * #
NASA-CR-182139	p 155	N88-30076 * #	NASA-TM-100214	p 25	N88-11679 * #	NASA-TM-100796	p 188	N88-18040 * #
NASA-CR-182141	p 152	N88-23182 * #	NASA-TM-100215	p 90	N88-10938 * #	NASA-TM-100797	p 10	N88-16679 * #
NASA-CR-182145	p 66	N88-29858 * #	NASA-TM-100216	p 9	N88-10779 * #	NASA-TM-100798	p 162	N88-18892 * #
NASA-CR-182146	p 130	N88-25831 * #	NASA-TM-100217	p 40	N88-15814 * #	NASA-TM-100799	p 104	N88-20454 * #
NASA-CR-182147	p 154	N88-24917 * #	NASA-TM-100218	p 90	N88-10939 * #	NASA-TM-100800	p 190	N88-21534 * #
NASA-CR-182148	p 219	N88-29649 * #	NASA-TM-100219	p 57	N88-11746 * #	NASA-TM-100801	p 189	N88-18974 * #
NASA-CR-182150	p 35	N88-25459 * #	NASA-TM-100220	p 210	N88-10563 * #	NASA-TM-100802	p 201	N88-21593 * #
NASA-CR-182151	p 41	N88-29825 * #	NASA-TM-100221	p 9	N88-10778 * #	NASA-TM-100803	p 151	N88-18871 * #
NASA-CR-182153	p 155	N88-26616 * #	NASA-TM-100222	p 26	N88-13346 * #	NASA-TM-100804	p 92	N88-18707 * #
NASA-CR-182154	p 113	N88-26498 * #	NASA-TM-100223	p 24	N88-10790 * #	NASA-TM-100806	p 104	N88-18726 * #
NASA-CR-182157	p 95	N88-29961 * #	NASA-TM-100224	p 224	N88-14046 * #	NASA-TM-100807	p 210	N88-19182 * #
NASA-CR-182159	p 67	N88-29876 * #	NASA-TM-100225	p 160	N88-11100 * #	NASA-TM-100808	p 119	N88-17880 * #
NASA-CR-182160	p 66	N88-29867 * #	NASA-TM-100226	p 227	N88-13209 * #	NASA-TM-100809	p 46	N88-24663 * #
NASA-CR-182162	p 65	N88-28087 * #	NASA-TM-100227	p 72	N88-11758 * #	NASA-TM-100810	p 189	N88-18976 * #
NASA-CR-182167	p 13	N88-26336 * #	NASA-TM-100228	p 210	N88-12330 * #	NASA-TM-100811	p 188	N88-18969 * #
NASA-CR-182184	p 130	N88-28239 * #	NASA-TM-100229	p 38	N88-11680 * #	NASA-TM-100812	p 194	N88-23994 * #
NASA-CR-182191	p 196	N88-27611 * #	NASA-TM-100230	p 26	N88-14093 * #	NASA-TM-100813	p 162	N88-23194 * #

REPORT NUMBER INDEX

US-PATENT-CLASS-260-389

NASA-TM-100814	p 206	N88-19147 *	NASA-TM-100930	p 13	N88-25435 *	NASA-TP-2774	p 68	N88-12543 *
NASA-TM-100815	p 151	N88-18870 *	NASA-TM-100932	p 63	N88-24686 *	NASA-TP-2779	p 187	N88-15263 *
NASA-TM-100819	p 128	N88-18835 *	NASA-TM-100933	p 64	N88-24690 *	NASA-TP-2788	p 128	N88-15146 *
NASA-TM-100820	p 207	N88-22591 *	NASA-TM-100934	p 12	N88-24592 *	NASA-TP-2789	p 172	N88-17045 *
NASA-TM-100821	p 74	N88-19592 *	NASA-TM-100935	p 194	N88-23278 *	NASA-TP-2795	p 172	N88-15224 *
NASA-TM-100823	p 104	N88-20455 *	NASA-TM-100936	p 202	N88-25059 *	NASA-TP-2801	p 188	N88-17095 *
NASA-TM-100824	p 43	N88-24659 *	NASA-TM-100937	p 81	N88-27267 *	NASA-TP-2815	p 38	N88-19475 *
NASA-TM-100825	p 179	N88-23965 *	NASA-TM-100938	p 76	N88-28095 *	NASA-TP-2816	p 172	N88-18933 *
NASA-TM-100826	p 120	N88-25762 *	NASA-TM-100939	p 175	N88-28312 *	NASA-TP-2840	p 164	N88-30099 *
NASA-TM-100829	p 120	N88-21389 *	NASA-TM-100940	p 36	N88-27201 *	NASA-TP-2841	p 163	N88-28286 *
NASA-TM-100830	p 92	N88-20417 *	NASA-TM-100941	p 154	N88-25854 *			
NASA-TM-100831	p 189	N88-21497 *	NASA-TM-100942	p 63	N88-24687 *	NBSIR-88/3712	p 45	N88-18612 *
NASA-TM-100833	p 120	N88-19698 *	NASA-TM-100943	p 95	N88-26436 *			
NASA-TM-100834	p 105	N88-21306 *	NASA-TM-100945	p 13	N88-24597 *	NEAR-TR-381	p 65	N88-28087 *
NASA-TM-100835	p 208	N88-21697 *	NASA-TM-100946	p 95	N88-27310 *			
NASA-TM-100836	p 152	N88-19740 *	NASA-TM-100948	p 35	N88-24642 *	OS-TR-719300-2	p 80	N88-20397 *
NASA-TM-100837	p 45	N88-19565 *	NASA-TM-100950	p 64	N88-25476 *			
NASA-TM-100838	p 60	N88-21254 *	NASA-TM-100951	p 109	N88-24808 *	PB88-178553	p 45	N88-18612 *
NASA-TM-100839	p 104	N88-18734 *	NASA-TM-100953	p 35	N88-27200 *			
NASA-TM-100840	p 74	N88-21257 *	NASA-TM-100954	p 63	N88-24688 *	PW-FR-19602	p 67	N88-29876 *
NASA-TM-100841	p 128	N88-20555 *	NASA-TM-100955	p 14	N88-29746 *			
NASA-TM-100842	p 195	N88-24002 *	NASA-TM-100956	p 76	N88-28980 *	PWA-5774-82	p 207	N88-21682 *
NASA-TM-100843	p 204	N88-19102 *	NASA-TM-100957	p 63	N88-24689 *	PWA-5940-62-VOL-1	p 190	N88-21535 *
NASA-TM-100846	p 211	N88-22652 *	NASA-TM-100958	p 80	N88-26430 *	PWA-5967-46	p 36	N88-28074 *
NASA-TM-100847	p 59	N88-21249 *	NASA-TM-100959	p 213	N88-25260 *	PWA-6113-12	p 163	N88-28299 *
NASA-TM-100848	p 93	N88-22981 *	NASA-TM-100960	p 175	N88-25916 *			
NASA-TM-100849	p 152	N88-21424 *	NASA-TM-100961	p 175	N88-26679 *	REPT-167-B-87	p 102	N88-14206 *
NASA-TM-100850	p 32	N88-21162 *	NASA-TM-100962	p 175	N88-30128 *	REPT-31-3725(12)	p 225	N88-20230 *
NASA-TM-100851	p 32	N88-21161 *	NASA-TM-100963	p 65	N88-26401 *	REPT-85-22592	p 102	N88-15886 *
NASA-TM-100852	p 119	N88-18809 *	NASA-TM-100964	p 37	N88-29807 *	REPT-85TR20	p 171	N88-13603 *
NASA-TM-100853	p 60	N88-22080 *	NASA-TM-100965	p 65	N88-26402 *	REPT-87-R-1175	p 62	N88-23830 *
NASA-TM-100854	p 152	N88-21417 *	NASA-TM-100966	p 163	N88-29142 *			
NASA-TM-100855	p 128	N88-21400 *	NASA-TM-100967	p 107	N88-26482 *	RI/RD-87-211	p 58	N88-12541 *
NASA-TM-100856	p 211	N88-21717 *	NASA-TM-100969	p 227	N88-28853 *			
NASA-TM-100857	p 211	N88-21718 *	NASA-TM-100970	p 130	N88-28240 *	RI/RD87-250	p 59	N88-20361 *
NASA-TM-100858	p 211	N88-26885 *	NASA-TM-100971	p 130	N88-26830 *			
NASA-TM-100859	p 121	N88-26566 *	NASA-TM-100972	p 163	N88-26645 *	RPT/BB0642	p 59	N88-17732 *
NASA-TM-100860	p 222	N88-22805 *	NASA-TM-100973	p 207	N88-27799 *			
NASA-TM-100861	p 120	N88-23070 *	NASA-TM-100974	p 66	N88-28090 *	R85-956834-1	p 155	N88-30063 *
NASA-TM-100862	p 60	N88-21250 *	NASA-TM-100977	p 225	N88-27980 *	R85-956834	p 155	N88-30066 *
NASA-TM-100863	p 93	N88-22986 *	NASA-TM-100978	p 202	N88-22458 *	R86AEB564	p 36	N88-28929 *
NASA-TM-100864	p 60	N88-21251 *	NASA-TM-101009	p 43	N88-26385 *			
NASA-TM-100865	p 114	N88-21375 *	NASA-TM-101134	p 203	N88-27624 *	SAE AIR 1678	p 16	A88-15228 *
NASA-TM-100866	p 114	N88-21374 *	NASA-TM-101177	p 35	N88-25460 *	SAE AIR 1703	p 16	A88-15227 *
NASA-TM-100867	p 173	N88-21454 *	NASA-TM-101291	p 65	N88-28088 *			
NASA-TM-100868	p 64	N88-25475 *	NASA-TM-101292	p 66	N88-29860 *	SAE PAPER 870445	p 166	A88-23313 *
NASA-TM-100870	p 62	N88-23829 *	NASA-TM-101293	p 1	N88-26328 *	SAE PAPER 871509	p 136	A88-21155 *
NASA-TM-100872	p 40	N88-25464 *	NASA-TM-101294	p 162	N88-26641 *	SAE PAPER 871782	p 19	A88-30776 *
NASA-TM-100873	p 11	N88-22019 *	NASA-TM-101295	p 203	N88-26732 *	SAE PAPER 871783	p 20	A88-30777 *
NASA-TM-100874	p 154	N88-23957 *	NASA-TM-101296	p 207	N88-27796 *	SAE PAPER 871784	p 39	A88-30778 *
NASA-TM-100875	p 211	N88-25239 *	NASA-TM-101297	p 180	N88-28323 *	SAE PAPER 872300	p 21	A88-37199 *
NASA-TM-100876	p 120	N88-24847 *	NASA-TM-101299	p 203	N88-25978 *	SAE PAPER 872332	p 21	A88-37215 *
NASA-TM-100877	p 195	N88-25937 *	NASA-TM-101300	p 196	N88-28332 *	SAE PAPER 872355	p 21	A88-37217 *
NASA-TM-100878	p 1	N88-21116 *	NASA-TM-101303	p 156	N88-30094 *	SAE PAPER 872358	p 215	A88-30998 *
NASA-TM-100882	p 12	N88-23732 *	NASA-TM-101304	p 115	N88-28176 *	SAE PAPER 872358	p 215	A88-37219 *
NASA-TM-100884	p 195	N88-25935 *	NASA-TM-101305	p 156	N88-30090 *	SAE PAPER 872359	p 6	A88-37220 *
NASA-TM-100885	p 93	N88-22168 *	NASA-TM-101306	p 163	N88-29152 *	SAE PAPER 872360	p 215	A88-37221 *
NASA-TM-100886	p 49	N88-21245 *	NASA-TM-101307	p 44	N88-29833 *			
NASA-TM-100887	p 33	N88-22037 *	NASA-TM-101309	p 67	N88-29874 *	SAND-88-0865C	p 203	N88-27624 *
NASA-TM-100888	p 174	N88-23977 *	NASA-TM-101312	p 81	N88-28109 *			
NASA-TM-100889	p 32	N88-21163 *	NASA-TM-101313	p 14	N88-28041 *	SAWE-1818	p 44	N88-25470 *
NASA-TM-100891	p 34	N88-22902 *	NASA-TM-101314	p 155	N88-30072 *			
NASA-TM-100892	p 76	N88-25487 *	NASA-TM-101315	p 49	N88-28959 *	SC5492.FR	p 222	N88-24539 *
NASA-TM-100893	p 162	N88-26644 *	NASA-TM-101317	p 218	N88-28760 *			
NASA-TM-100894	p 94	N88-24754 *	NASA-TM-101318	p 163	N88-28293 *	SN-3504-F	p 80	N88-15851 *
NASA-TM-100895	p 1	N88-23729 *	NASA-TM-101319	p 13	N88-27174 *			
NASA-TM-100896	p 34	N88-24640 *	NASA-TM-101320	p 196	N88-28344 *	SPIE-756	p 45	A88-35251 *
NASA-TM-100898	p 173	N88-23219 *	NASA-TM-101321	p 121	N88-28222 *			
NASA-TM-100899	p 225	N88-30472 *	NASA-TM-101323	p 121	N88-27424 *	STLE PREPRINT 88-AM-6G-1	p 169	A88-51082 *
NASA-TM-100900	p 44	N88-25470 *	NASA-TM-101325	p 69	N88-28966 *	STLE PREPRINT 88-AM-7F-1	p 100	A88-51300 *
NASA-TM-100901	p 61	N88-22939 *	NASA-TM-101326	p 67	N88-29869 *			
NASA-TM-100902	p 114	N88-26539 *	NASA-TM-101327	p 212	N88-30377 *	TL-SEAL-2-88	p 172	N88-16006 *
NASA-TM-100903	p 94	N88-24749 *	NASA-TM-101328	p 130	N88-30048 *	TL-SEAL-5-88	p 175	N88-25921 *
NASA-TM-100904	p 61	N88-22935 *	NASA-TM-101330	p 155	N88-30078 *			
NASA-TM-100905	p 61	N88-22933 *	NASA-TM-101332	p 18	N88-28062 *	TR-EE-88-37	p 203	N88-27621 *
NASA-TM-100906	p 113	N88-24811 *	NASA-TM-101333	p 81	N88-29952 *			
NASA-TM-100907	p 94	N88-24766 *	NASA-TM-101334	p 156	N88-30084 *	TR-712257-6	p 205	N88-10496 *
NASA-TM-100908	p 207	N88-26127 *	NASA-TM-101343	p 115	N88-29997 *			
NASA-TM-100909	p 64	N88-25477 *	NASA-TM-101347	p 14	N88-29780 *	TRC-SEAL-1-88	p 172	N88-16007 *
NASA-TM-100910	p 223	N88-28832 *	NASA-TM-101351	p 67	N88-29873 *			
NASA-TM-100911	p 13	N88-26340 *	NASA-TM-101357	p 14	N88-29771 *	TTC-87-07R	p 174	N88-24975 *
NASA-TM-100913	p 153	N88-23186 *	NASA-TM-101363	p 66	N88-29868 *			
NASA-TM-100914	p 130	N88-24870 *	NASA-TM-101370	p 49	N88-29845 *	US-PATENT-APPL-SN-060200	p 41	N88-28939 *
NASA-TM-100915	p 153	N88-23184 *	NASA-TM-86997	p 9	N88-12461 *	US-PATENT-APPL-SN-130058	p 129	N88-23936 *
NASA-TM-100917	p 154	N88-25841 *	NASA-TM-87050	p 201	N88-19013 *	US-PATENT-APPL-SN-219016	p 76	N88-29888 *
NASA-TM-100918	p 173	N88-23220 *	NASA-TM-87184	p 15	N88-12473 *	US-PATENT-APPL-SN-231026	p 108	N88-29984 *
NASA-TM-100919	p 35	N88-25458 *	NASA-TM-88844	p 43	N88-12515 *	US-PATENT-APPL-SN-661481	p 91	N88-14179 *
NASA-TM-100920	p 34	N88-24639 *	NASA-TM-88886	p 223	N88-12427 *	US-PATENT-APPL-SN-823713	p 91	N88-14179 *
NASA-TM-100921	p 34	N88-23806 *	NASA-TM-88893	p 71	N88-10121 *	US-PATENT-APPL-SN-875798	p 174	N88-23978 *
NASA-TM-100922	p 75	N88-24712 *	NASA-TM-89654	p 210	N88-12323 *	US-PATENT-APPL-SN-924474	p 69	N88-26404 *
NASA-TM-100923	p 43	N88-28942 *	NASA-TM-89829	p 73	N88-18640 *			
NASA-TM-100924	p 63	N88-24682 *	NASA-TM-89845	p 32	N88-21160 *	US-PATENT-CLASS-148-16.6	p 91	N88-14179 *
NASA-TM-100926	p 174	N88-24968 *	NASA-TM-89878	p 26	N88-13347 *	US-PATENT-CLASS-204-192.31	p 91	N88-14179 *
NASA-TM-100927	p 196	N88-29195 *	NASA-TP-2681	p 40	N88-17686 *	US-PATENT-CLASS-219-383	p 41	N88-28939 *
NASA-TM-100928	p 35	N88-24641 *	NASA-TP-2765	p 58	N88-12538 *	US-PATENT-CLASS-260-386	p 69	N88-25404 *
NASA-TM-100929						US-PATENT-CLASS-260-389	p 69	N88-26404 *

US-PATENT-CLASS-260-395*REPORT NUMBER INDEX*

US-PATENT-CLASS-260-395	p 69	N88-26404 *
US-PATENT-CLASS-363-97	p 41	N88-28939 *
US-PATENT-CLASS-415-136	p 174	N88-23978 *
US-PATENT-CLASS-415-170-R ...	p 174	N88-23978 *
US-PATENT-CLASS-427-38	p 91	N88-14179 *
US-PATENT-CLASS-549-241	p 69	N88-26404 *
US-PATENT-CLASS-60-203.1	p 41	N88-28939 *
US-PATENT-4,704,168	p 91	N88-14179 *
US-PATENT-4,728,257	p 174	N88-23978 *
US-PATENT-4,758,380	p 69	N88-26404 *
US-PATENT-4,766,724	p 41	N88-28939 *
UTRC-R86-956480-VOL-2	p 37	N88-29804 * #
UTRC/R86-956480-VOL-3	p 37	N88-28930 * #
UTRC/R86-956480-4	p 153	N88-23956 * #
WYLE-68300-1	p 48	N88-20353 * #

Report Documentation Page

1. Report No. NASA TM-102034		2. Government Accession No.		3. Recipient's Catalog No.	
4. Title and Subtitle Bibliography of Lewis Research Center Technical Publications Announced in 1988				5. Report Date July 1989	
				6. Performing Organization Code	
7. Author(s)				8. Performing Organization Report No. E-4780	
				10. Work Unit No. None	
9. Performing Organization Name and Address National Aeronautics and Space Administration Lewis Research Center Cleveland, Ohio 44135-3191				11. Contract or Grant No.	
				13. Type of Report and Period Covered Technical Memorandum	
12. Sponsoring Agency Name and Address National Aeronautics and Space Administration Washington, D.C. 20546-0001				14. Sponsoring Agency Code	
15. Supplementary Notes Compiled by Technical Information Services Division, Lewis Research Center.					
16. Abstract This compilation of abstracts describes and indexes the technical reporting that resulted from the scientific and engineering work performed and managed by the Lewis Research Center in 1988. All the publications were announced in the 1988 issues of STAR (Scientific and Technical Aerospace Reports) and/or IAA (International Aerospace Abstracts). Included are research reports, journal articles, conference presentations, patents and patent applications, and theses.					
17. Key Words (Suggested by Author(s)) Bibliographies Abstracts Documentation Indexes (Documentation)			18. Distribution Statement Unclassified - Unlimited Subject Category 82		
19. Security Classif. (of this report) Unclassified	20. Security Classif. (of this page) Unclassified	21. No of pages 368	22. Price* A16		

National Aeronautics and
Space Administration

Lewis Research Center
Cleveland, Ohio 44135

Official Business
Penalty for Private Use \$300

FOURTH CLASS MAIL

ADDRESS CORRECTION REQUESTED



Postage and Fees Paid
National Aeronautics and
Space Administration
NASA 451

NASA
